THE PHYSICAL REVIEW

VOLUME 91 *Second Series* NUMBER 6

SEPTEMBER 15, 1953

Published for the

AMERICAN PHYSICAL SOCIETY

by the

AMERICAN INSTITUTE OF PHYSICS

LANCASTER, PA., AND NEW YORK, N. Y.

[illegible]

THE
PHYSICAL REVIEW

A journal of experimental and theoretical physics established by E. L. Nichols in 1893

SECOND SERIES, VOL. 91, NO. 6 SEPTEMBER 15, 1953

Atomic Theory of the λ Transition in Helium

R. P. FEYNMAN
California Institute of Technology, Pasadena, California
(Received May 15, 1953)

It is shown from first principles that, in spite of the large interatomic forces, liquid He^4 should exhibit a transition analogous to the transition in an ideal Bose-Einstein gas. The exact partition function is written as an integral over trajectories, using the space-time approach to quantum mechanics. It is next argued that the motion of one atom through the others is not opposed by a potential barrier because the others may move out of the way. This just increases the effective inertia of the moving atom. This permits a simpler form to be written for the partition function. A rough analysis of this form shows the existence of a transition, but of the third order. It is possible that a more complete analysis would show that the transition implied by the simplified partition function is actually like the experimental one.

INTRODUCTION

THE behavior of liquid helium, especially below the λ transition, is very curious.[1] The most successful theoretical interpretations,[2] so far, have been largely phenomenological. In this paper and one or two to follow, the problem will be studied entirely from first principles. We study the quantum-mechanical behavior of strongly interacting atoms of He^4. We shall try to show that the main features of these curious phenomena can, in fact, be understood from this point of view. Because of the enormous geometrical complexity involved, we shall not attempt to obtain useful quantitative results. The quantum mechanics will not supplant the phenomenological theories. It turns out to support them.

In this paper we begin the study of the statistical mechanics of the liquid.[3]

London[4] has proposed that the transition between liquid He I and liquid He II is a result of the same process which causes the condensation of an ideal Bose-Einstein gas. This idea could be criticized on the grounds that the strong forces of interaction between the He atoms might make the ideal gas approximation (in which these forces are neglected) even qualitatively incorrect. We shall argue that London's view is essentially correct. The inclusion of large interatomic forces will not alter the central features of Bose condensation.

The principal point is an argument which shows that in a liquid-like quantum-mechanical system the strong interactions between particles do not prevent these particles from behaving very much as though they move freely among each other.

The exact partition function is first written down as an integral over trajectories, by using the space-time approach to quantum mechanics.[5] The observation that the atoms move very freely among each other is then made. This permits one to write a simpler form [Eq. (7)] for the partition function. This form should be fairly accurate, at least qualitatively. It becomes clear that a transition is to be expected, and that it involves the symmetrical statistics in an essential way.

On the other hand, the geometrical complexity of the problem still prevents us, so far, from giving a very good estimate of the free energy behavior near the transition point and below. A relatively crude approach gives a transition like that of the ideal gas. That is, the specific heat is continuous, contrary to the experimental observation that it appears to be discontinuous. Some of the geometrical problems which might have to be solved to obtain a more satisfactory solution are discussed in an appendix (see also reference 3).

The crude approach should, however, be quite satisfactory a little above the transition point. So there is

[1] W. H. Keesom, *Helium* (Elsevier Publishing Company, Inc., Amsterdam, 1942).
[2] An excellent summary of the theories of helium II is to be found in R. B. Dingle, Advances in Phys. **1**, 112 (1952).
[3] A preliminary report on this work has been published. R. P. Feynman, Phys. Rev. **90**, 1116 (1953).
[4] F. London, Phys. Rev. **54**, 947 (1938).
[5] R. P. Feynman, Revs. Modern Phys. **20**, 367 (1948).

no doubt that at least the existence of the rise of specific heat[1] of He I on cooling toward the λ point can be understood from first principles.

At the opposite extreme of very low temperatures (say below 0.5°K), the situation again can be partially analyzed. This is done in the next paper.[6]

EXACT EXPRESSION FOR THE PARTITION FUNCTION

To study the thermodynamic properties we must calculate the partition function

$$Q=\sum_i \exp(-\beta E_i), \tag{1}$$

where $\beta=1/kT$ and E_i are the energy levels of the system. In this form the calculation appears hopelessly difficult because the energies E_i are eigenvalues of such a complex Hamiltonian H. The expression for Q is equivalent to the trace of the operator $\exp(-\beta H)$. In Eq. (1) the trace is written in a representation in which H is diagonal. We shall prefer to use the coordinate representation to describe the trace.

To illustrate how this is done, we take the example of a one-dimensional system, of coordinate x and Hamiltonian $p^2/2m+V(x)=H$. The trace of $\exp(-\beta H)$ is then $Q=\int dz(z|e^{-\beta H}|z)$. The matrix element $(z|e^{-\beta H}|z)$ is similar in form to the matrix element $(z|\exp(-itH/\hbar)|z)$ which represents the amplitude that the system initially at $x=z$, is at time t also at the point $x=z$. This latter is[5] the sum over all paths [signified by $\int\cdots\mathfrak{D}x(t)$] which go from z to z of $\exp(iS/\hbar)$, where S is the action $\int_0^t[\frac{1}{2}m\dot{x}^2-V(x(t))]dt$. If we replace $it/\hbar$ by β, we are lead to expect

$$(z|e^{-\beta H}|z)=\int_{tr}\exp\left\{-\int_0^\beta\left[\frac{m}{2\hbar^2}\left(\frac{dx}{du}\right)^2+V(x(u))\right]du\right\}\mathfrak{D}x(u), \tag{2}$$

the variable $u=it/\hbar$ replacing t, and the various signs adjusted accordingly. The integral $\int_{tr}$ is to be taken on all trajectories such that $x(0)=z$ and $x(\beta)=z$. It is easily verified that Eq. (2) is exactly correct. The normalization of the path integral is to be such that

$$\int_{tr'}\exp\left[-\int_0^\beta\frac{m}{2\hbar^2}\left(\frac{dx}{du}\right)^2du\right]\mathfrak{D}x(u)=(m/2\pi\beta\hbar^2)^{\frac{1}{2}}\exp\left[-\frac{m}{2\beta\hbar^2}(z-z')^2\right], \tag{3}$$

where the trajectory tr' runs from $x(0)=z$ to $x(\beta)=z'$. The integral of (2) with respect to z then gives the partition function.

To apply this to liquid helium two modifications are necessary. First, instead of one variable, we have $3N$ variables which we take as the N three-space coordinate vectors $\mathbf{x}_i$ of each of the N atoms ($i=1$ to N). We designate the entire set of coordinates by $\mathbf{x}^N$ and the integral over them all by $d^N\mathbf{x}_i=d\mathbf{x}_1d\mathbf{x}_2\cdots d\mathbf{x}_N$. The initial and final values of these we call $\mathbf{z}_i$. Secondly, He^4 atoms obey symmetrical statistics. The trace of $\exp(-\beta H)$ is to be taken only over symmetrical wave functions. This means that if the initial coordinates are $\mathbf{x}_i(0)=\mathbf{z}_i$, the final coordinates need not be the same, but may be some permutation of these (signified by $P\mathbf{z}_i$). That is,

$$Q=N!^{-1}\sum_P\int d^N\mathbf{z}_i\int_{trP}\exp\left\{-\int_0^\beta\left[\frac{m}{2\hbar^2}\sum_i\left(\frac{d\mathbf{x}_i}{du}\right)^2+\sum_{ij}V(\mathbf{x}_i-\mathbf{x}_j)\right]du\right\}\mathfrak{D}^N\mathbf{x}_i(u), \tag{5}$$

where the integral $\int_{trP}$ is taken over all trajectories $\mathbf{x}_i(u)$ of all the particles such that $\mathbf{x}_i(0)=\mathbf{z}_i$, $\mathbf{x}_i(\beta)=P\mathbf{z}_i$. That is, the final coordinates $\mathbf{x}_i(\beta)$ may now be some permutation P of the initial coordinates $\mathbf{z}_i$. The sum is taken over all permutations P and the integral over all configurations $\mathbf{z}_i$.

In Eq. (5), m is the mass of a helium atom, and $V(\mathbf{R})$ is the mutual potential of a pair of He atoms separated by $\mathbf{R}$. The forces between He atoms are, very likely, fairly accurately two-body forces. This potential is given by Slater and Kirkwood.[7] There is a weak attraction of maximum depth (of energy equivalent to kT at $T=7$°K) at radius about 3.0A. The atomic volume at the transition is $(3.6\text{A})^3$. At 3.6A, $V(\mathbf{R})$ is about equivalent to kT for $T=3$°K. There is, therefore, a weak attraction at the average atomic distance. There is a violent repulsion if the atoms approach more closely than 2.6A ($V=0$ at 2.6A).

The expression (5) is an exact[8] quantum-mechanical expression for the partition function (even though no imaginary unit i appears). We shall use it to develop a qualitative understanding of this function for liquid helium.

The quality u is of course not the time. However, we shall obtain a vivid representation of (5) by imagining that it is the time. We can say that at one time 0 the coordinates $\mathbf{x}_i(0)$ of all the atoms form an initial configuration $\mathbf{z}_i$, and that as time u proceeds the particles move about $[\mathbf{x}_i(u)]$ in such a manner that at the time β the configuration of atoms appears to be the same (although in fact some of the atoms may have been interchanged). Each mode of motion is weighed by the negative exponential of the time integral of the energy required for the motion, and the sum is taken for all such motions. Finally an average (or rather integral) is taken over all possible initial configurations $\mathbf{z}_i$.

We can see immediately that motions which require too large a displacement in the time β have little weight

[6] R. P. Feynman, Phys. Rev. **91**, 1301 (1953).

[7] J. C. Slater and J. G. Kirkwood, Phys. Rev. **37**, 682 (1931).

[8] In so far as the forces can be represented as two-body forces.

because of the high kinetic energy required. Likewise, motions in which the atoms come so close as to appreciably penetrate the radius of their repulsion are of small importance because of the large potential energy which would result. For this reason, also, initial configurations for which the atoms overlap, that is, have centers so close that they would repel, contribute only a small amount. The method of approximation which we shall apply to (5) is to neglect the contributions from motions $\mathbf{x}_i(u)$ and configurations $\mathbf{z}_i$ which give small contributions, and to study more carefully only those motions which give the larger contributions to the total in (5). That is, we shall have motions in which the atoms do not move too fast or far in the time β and in which the atoms never overlap.

We emphasize again that these "motions" must not be construed as a real description of what the atoms are doing. It is simply a formal description of the expression for the partition function. An expression "the atom does not move too far in the time β" does not refer to a real motion as u is not time, but is iu/h. The true behavior of the atoms may have some analogy to the description of the formula (5), but such an analogy need not concern us here. Our reason to continue to call u and β "time" is to help to make our arguments as vivid as possible so that intuition will be most effective.

THE CHARACTER OF THE IMPORTANT TRAJECTORIES

Consider a particular motion in (5) in which some atom i moves to the site initially occupied by atom j. Call the displacement $\mathbf{a}=\mathbf{z}_j-\mathbf{z}_i$. The atom j must, of course, move to some other site to leave room for i. The effect of the motion of j we will associate with atom j. We study here the contribution to be expected just from the displacement of the single atom i by a distance $\mathbf{a}$.

Near the transition temperature displacements larger than about d, the atomic spacing (cube root of atomic volume 3.6A) are not very important [$\exp(-md^2/2\beta h^2)=0.3$ at 2.2°K]. Nevertheless we will try to get an idea of the behavior for larger displacements. These will be useful at lower temperatures. Actually our considerations apply to displacements of any size.

Suppose, then, atom i must make a translation $\mathbf{a}$ of length a. We make this, for example, to be nearly along a straight line. Our arguments will apply for any other route.

The central problem is, what is the effect of the potentials of interaction on this translation? As a simple model which retains the essential features imagine the atoms as hard impenetrable spheres. We are, during a time β, to move atom i from $\mathbf{z}_i$ to $\mathbf{z}_j=\mathbf{z}_i+\mathbf{a}$ and at the end to leave all the other atoms in their original positions. The atoms may not overlap at any time.

There may be atoms in the direct line from $\mathbf{z}_i$ to $\mathbf{z}_j$. Nevertheless, a moment's reflection shows that they will not offer a real potential barrier to the translation of atom i.

It is evident that it is possible to place atom i at any position on the route from $\mathbf{z}_i$ to $\mathbf{z}_j$, provided we readjust the positions of the other atoms to make room for it. In the readjusted positions the total potential energy of all the atoms can be made to be very nearly equal to the potential energy of the original configuration. Therefore, atom i can be moved to any intermediate position without violating any repulsive potential, in fact, without any appreciable modifications of potential energy at all. It is only necessary to move the other atoms around out of the way as atom i moves along. When i reaches the final destination $\mathbf{z}_j$, the other atoms (except j of course, as noted above) may all come back to their original positions (or to some permutation thereof[9]).

The readjustment of the other atoms means that their coordinates $\mathbf{x}_k(u)$ change with time. They contribute just kinetic energy in the exponent in Q. Beside the kinetic energy $\frac{1}{2}m(a/\beta)^2$ needed to move atom i a distance a in time β, we have also to add the kinetic energy of the readjusting atoms. This we can expect will also vary directly as the square of the velocity of atom i. The net effect is an energy of the form $\frac{1}{2}m'(a/\beta)^2$, where m' is an effective mass, somewhat larger than the mass of a single atom m. The difference represents the effective inertia of the atoms which are readjusting.

The time integral of the energy needed for readjustment varies with a and β, as a^2/β. This is clear for small displacements of i, for then only a few atoms shift, and they do this with a velocity proportional to that of i. For large displacements ($a\gg d$) the same form, of course, results. To verify this, imagine that as atom i moves at velocity $v(=a/\beta)$ the time it passes near a particular atom is of order d/v. This atom must adjust through distances of order d in this time, or move at speed about v. The time integral of energy needed for this passage is about $mv^2(d/v)=mdv$. The number of such atoms which must be jostled to move a total distance a is of order a/d. Thus the total time integral of energy of readjustment for all these a/d atoms varies as $mdv\cdot a/d=mva=ma^2/\beta$. It varies with a and b in the required manner.

The effect of the other atoms is not to offer a potential barrier (time integral varying as $a\beta$) but a kind of kinetic energy barrier (time integral varying as a^2/β). The effect of the interactions is taken into account by changing the effective mass of a given moving atom.

To get some idea of the order of m', we recall that the effective mass of a sphere moving through an ideal fluid of the same density is classically $(\frac{3}{2})m$, the extra $\frac{1}{2}$ being the energy of motion of the fluid making way for the sphere. The effect of the attractive forces may in-

[9] The effect of a moving atom in permuting other atoms might have to be considered in more detail if we were to apply these ideas to the case of Fermi-Dirac statistics. It may mean that the m' (discussed further on) is somewhat larger in that case.

crease this somewhat. We may expect m' not to be very much greater than m—perhaps not more than 2 or 3 m.

The effect of the relatively weak attractive potentials may be to alter the motions a bit, in that adjacent atoms tend to stick together a little. Thus the atom i may have a tendency to drag some atoms with it from time to time, possibly increasing m' a little more. On the other hand, in He the zero-point energy[10] is high enough to shake these others loose readily. If the potential were much stronger the group attraction might become accululative, raising m' very much. It is possible that this would result in solidification.

For short displacements a of order d, proportionately less adjustment need be made, so that it is likely that m' may be somewhat less. For high velocities, it may represent less energy to violate the real potential restrictions a little. Thus the readjustments need not be complete, so that m' again may decrease a little with velocity a/β, approaching m as $a/\beta\rightarrow\infty$.

As this is meant to be a first approach to the problem, we shall not attempt to calculate the m'. The geometrical complexity is very great. Further, we shall neglect the variation of m' with a and velocity. It is to be expected that this neglect may not alter our conclusions qualitatively. It is always possible, later, to include such finer details. Nor shall we discuss the variation (expected rise) of m' with increasing density of the fluid.

For every trajectory the atom acts like a free particle of effective mass m'. Hence we may take the integral over all paths $\mathbf{x}_i$ for atom i to go a distance a to be proportional to

$$(m'/2\pi\beta\hbar^2)^{\frac{1}{2}}\exp(-m'a^2/2\beta\hbar^2). \tag{6}$$

The normalization factor has been written as $(m'/2\pi\beta\hbar^2)^{\frac{1}{2}}$ for convenience. That it varies as $\beta^{-\frac{1}{2}}$ may be shown by dimensional analysis [compare Eq. (3)]. Actually a change in this factor will just change the partition function by a factor. It will be easiest to discuss the normalization of the entire partition function.

Therefore, we can approximate Q by

$$Q=\frac{K_\beta}{N!}\left(\frac{m'}{2\pi\beta\hbar^2}\right)^{3N/2}\int\sum_P\exp\left[-\frac{m'}{2\beta\hbar^2}\sum_i(\mathbf{z}_i-P\mathbf{z}_i)^2\right]\times\rho(\mathbf{z}_1,\mathbf{z}_2,\cdots\mathbf{z}_N)d^N\mathbf{z}_i. \tag{7}$$

The factor K_β we shall estimate later. The function $\rho(\mathbf{z}_1,\cdots\mathbf{z}_N)=\rho(\mathbf{z}^N)$ represents a density associated with each configuration. It is discussed in the next section. This expression (7) for Q may be rewritten, using Fourier transforms as

$$Q=\int F(\mathbf{k}^N)\exp[-(\beta\hbar^2/2m')\sum_i\mathbf{k}_i^2]d^N\mathbf{k}_i(2\pi)^{-3N}, \tag{7a}$$

where

$$F(\mathbf{k}^N)=K_\beta(N!)^{-1}\int\sum_P\exp[i\sum_i\mathbf{k}_i\cdot(\mathbf{z}_i-P\mathbf{z}_i)]\times\rho(\mathbf{z}^N)d^N\mathbf{z}_i.$$

This form is especially useful near absolute zero, but we will not need it in this paper.

It should be emphasized that the argument which leads to the free particle approximation for the motion of an atom is of greater generality. The argument results simply from a consideration of the limitations to the true trajectories which result from the interatomic potentials. They therefore apply as well to the nondiagonal element of $\exp(-\beta H)$, as to the diagonal element which appears in Q. Likewise, they are applicable to the true quantum-mechanical kernel, which is the nondiagonal element of $\exp(-itH/\hbar)$. The imaginary weights in this case also restrict the atoms not to overlap at low energy, etc.

This principle may have uses in other branches of physics, for example, in nuclear physics. Here there is the puzzling fact that single nucleons often act like independent particles in spite of strong interactions. The arguments we have made for helium may apply to this case also.[9]

THE CONFIGURATIONS OF IMPORTANCE

Not all configurations $\mathbf{z}_N$ are to be weighed equally. If $\mathbf{z}_i$ and $\mathbf{z}_j$ are closer than the distance at which strong repulsion sets in (2.6A) the configuration should be given very little weight [i.e., ρ in (7) is nearly zero if atoms overlap]. We shall discuss this effect first for the case of low temperature (β large).

Suppose initially in (5) two atoms overlap, say by a distance x, and suppose that this results in an extremely high (relative to $1/\beta$) potential V. If they move a distance x further apart, suppose V goes to 0, and take V independent of x for simplicity. During the interval $u=0$ to β, if the atoms remain overlapped for a time τ, the contribution is the negative exponential of $V\tau$. This contribution is extremely small unless τ is very short (if $V\beta\gg1$ then $\tau\ll\beta$). The most important trajectories are then those that release V as quickly as possible. This can only be done by a high kinetic energy $m'x^2/2\tau^2$. Thus the integral of energy has the value $m'x^2/2\tau\hbar^2+V\tau$, which is least if $\tau=(m'x^2/2V\hbar^2)^{\frac{1}{2}}$, in which case it has the value $(2m'V)^{\frac{1}{2}}x/\hbar$. The contribution varies as $\exp[-(2m'V)^{\frac{1}{2}}x/\hbar]$. This is just the quantum-mechanical penetration factor. In ρ it appears twice, for again we must get into the overlapped condition at the end of the interval β. This argument fails if β does not exceed

[10] The zero-point energy referred to appears in the integral for Q in the following guise. Suppose we restrict the motion of a certain atom k so that, for example, it tries to move along close to i to take advantage of some extra attractive potential between k and i. Then the trajectories of k are restricted, and we lose a great deal in the integral over possible paths of k because we are not adding contributions from very many paths. We lose "volume in path-space." This will suffice to offset the attraction if, in the conventional language, the zero-point motion is sufficiently large.

2τ. In that case a larger penetration results. It is due, of course, to the high kinetic energy that such a small β implies. For the large repulsions V at low temperatures involved here this penetration is very small.

In addition, ρ would not be quite uniform even if there is no overlap of the atoms, and even if they are considered as impenetrable spheres. In fact, ρ would be larger if atoms are well spaced than if they are nearly adjacent (for large β). If two atoms are adjacent initially, the available paths are limited to those which move them apart—for they must not come to overlap. This decreases the effective volume of path space for a short time. Actually this effect is offset partly by the actual attractive potential which results upon the closer approach of the two atoms. Thus ρ represents the effects of short-time adjustments (times$\ll\beta$) while the longer-time effects[11] are contained in the exponential factor in (7) [that is, expression (12) below]. For large β, low T, ρ can be taken as nearly temperature independent, and the main temperature dependence comes from the other factor (12). This ρ as $\beta\to 0$ is the density corresponding to the ground-state wave function. For approximate purposes we can take it to be simply the density function ρ for a classical gas of impenetrable atoms of diameter b. That is, $\rho=0$ if any two $\mathbf{z}_i$'s are closer to each other than b, and is 1 otherwise. This neglects the variations with distance due to the quantum-mechanical effect discussed above of restricted path-space volume, and due to the attractive part of the potential.

For high temperatures, the exponential terms in (7), representing diffusion, are unimportant, and ρ should approach the classical distribution function. Now the attractive forces are weak and unimportant so again can be roughly represented by an impenetrable sphere model. The radius b should be somewhat smaller. We shall neglect this variation of b with temperature.

To summarize, ρ is qualitatively similar to the density distribution of a classical gas. It changes somewhat with temperature.

PROPERTIES OF THE PARTITION FUNCTION

A partition function has several formal properties, and we may test our approximate expression (7) to see how well it satisfies these conditions. Another imimportant function is the nondiagonal element of $\exp(-\beta H)$. That is, $G_\beta(z',z)=(z'|\exp(-\beta H)|z)$, or

$$G_\beta(\mathbf{z}'^N,\mathbf{z}^N)=(N!)^{-1}\sum_P\int_{tr_{P'}}\exp\Big[-\int_0^\beta\Big(\frac{m}{2\hbar^2}\sum_i\Big(\frac{d\mathbf{x}_i}{du}\Big)^2+\sum_{ij}V(\mathbf{x}_i-\mathbf{x}_j)\Big)du\Big]\mathfrak{D}^N\mathbf{x}_i(u),\quad(8)$$

the integral being taken over all trajectories $tr_{P'}$ such that $\mathbf{x}_i(0)=\mathbf{z}_i$, $\mathbf{x}_i(\beta)=P\mathbf{z}_i'$. The final configuration $\mathbf{z}_i'$ may differ from the initial configuration. Of course, $Q=\int G_\beta(\mathbf{z}^N,\mathbf{z}^N)d^N\mathbf{z}_i$.

For large β we have given an argument for behavior of the function $\rho(\mathbf{z}^N)$, which represented it as the square of a function, say $\phi(\mathbf{z}^N)$. One factor was for leaving an unfavorable (say overlappping) configuration. The second was for entering it again. At low temperature $\phi(\mathbf{z}^N)$ is the ground-state wave function. The same arguments give for $G_\beta(\mathbf{z}'^N,\mathbf{z}^N)$ the approximate expression,

$$G_\beta(\mathbf{z}'^N,\mathbf{z}^N)=K_\beta(N!)^{-1}\sum_P\phi(\mathbf{z}'^N)\phi(\mathbf{z}^N)\times\exp\Big[-\frac{m'}{2\beta\hbar^2}\sum_i(\mathbf{z}_i-P\mathbf{z}_i')^2\Big]\Big(\frac{m'}{2\pi\beta\hbar^2}\Big)^{3N/2}.\quad(9)$$

Since $\exp(-\beta_1 H)\exp(-\beta_2 H)=\exp[-(\beta_1+\beta_2)H]$, we have the condition of matrix multiplication, namely, that

$$G_{\beta_1+\beta_2}(\mathbf{z}'^N,\mathbf{z}^N)=\int G_{\beta_1}(\mathbf{z}'^N,\mathbf{z}''^N)G_{\beta_2}(\mathbf{z}''^N,\mathbf{z}^N)d^N\mathbf{z}_i''.$$

This requires that $(\beta=\beta_1+\beta_2)$

$$K_\beta\Big(\frac{m'}{2\pi\beta\hbar^2}\Big)^{3N/2}\sum_P\exp\Big[-\frac{m'}{2\beta\hbar^2}\sum_i(\mathbf{z}_i-P\mathbf{z}_i')^2\Big]=K_{\beta_1}K_{\beta_2}\Big(\frac{m'}{2\pi\beta_1\hbar^2}\Big)^{3N/2}\Big(\frac{m'}{2\pi\beta_2\hbar^2}\Big)^{3N/2}\int N!^{-1}\sum_P\sum_{P'}\times\exp\Big[-\frac{m'}{2\beta_1\hbar^2}\sum_i(P\mathbf{z}_i'-\mathbf{z}_i'')^2-\frac{m'}{2\beta_2\hbar^2}\sum_i(P'\mathbf{z}_j''-\mathbf{z}_j)^2\Big]\times[\phi(\mathbf{z}''^N)]^2d^N\mathbf{z}_i''.$$

Now, in the exponent we can relable i (by permuting the names) as $P'i$, since the sum in on all i. That is, $\sum_i(P\mathbf{z}_i'-\mathbf{z}_i'')^2=\sum_i(PP'\mathbf{z}_i-P'\mathbf{z}_i'')^2$. Now call $PP'=P''$, and the sum on all P is equivalent to a sum on all P''. Finally, since $\mathbf{z}_i''$ are variables of integration in a symmetrical factor $[(\phi(\mathbf{z}''^N)]^2=\rho(\mathbf{z}''^N)=\rho(P'\mathbf{z}''^N)$ for any P', the $\mathbf{z}''^N$ integral does not depend on P', and $\sum_{P'}$ just gives a factor $N!$.

Now the weight function $\rho(\mathbf{z}''^N)$ prevents various $\mathbf{z}_i''$ from being too close together. If, however, β_1 and β_2 are so low that $\exp(-m'd^2/2\beta_1\hbar^2)$ is fairly close to 1, the variations in the exponents due to this restriction

[11] There is a kind of distortion that takes a long time τ to release, namely, a general increase in density over a large area. This restricts the path-space volume for each atom in the area and results in a factor $e^{-\beta E}$ for each particle, where E is the excess energy per particle induced by compression. The energy E can only be released by moving many particles, distributed over the area. These density fluctuations are sound waves. If the wavelength of the fluctuation is $\lambda=2\pi/K$, the time needed to release it is $\tau=1/\hbar\omega=1/\hbar cK$, where c is the speed of sound. This exceeds β if $\lambda>2\pi k T/\hbar c$ or $\lambda>2\pi\cdot 8\text{A}$ for 2.2°K. (This exceeds the diffusion distance $d\approx 3.6\text{A}$ even at 2.2°K, so will not be of concern to us near the transition.) Thus (7) is incomplete in that it does not correctly describe long wave-sound fluctuations. This matter is discussed in a subsequent paper.

is very small. [That is, in the integrand, $\rho(\mathbf{z}''^N)$ varies rapidly while the other factor is smooth.] Therefore, we replace $\rho(\mathbf{z}''^N)$ by an average value and integrate over all $\mathbf{z}''^N$. The effect of $\rho(\mathbf{z}''^N)$ just restricts the volume available to the configuration variables. Let us call

$$V_N=\int\rho(\mathbf{z}^N)d^N\mathbf{z}_i, \tag{10}$$

so that the average value of ρ is V_N/V^N. The integral on $\mathbf{z}_i''$ is now easy, and we find

$$K_{\beta_1+\beta_2}=K_{\beta_1}K_{\beta_2}V_N/V^N.$$

[This verifies our choice of the $\beta^{-\frac{1}{2}}$ dependence in (6).] This means that K_β must have the form

$$K_\beta=V^NV_N^{-1}e^{-\beta E_0}, \tag{11}$$

where E_0 is a constant. Such a constant means, in Q, a constant energy (the energy at absolute zero). We will not try to determine this energy. Let us measure energies above this as a zero level. Then it can be ignored. Our final partition function is then (17) with $K_\beta=V^N/V_N$.

For extremely large β, Q should approach 1 from its original definition as $\sum_i e^{-\beta E_i}$ and the choice $E_0=0$. For such large β, the sum on permutations P means that $P\mathbf{z}_i$ goes successively over every site, while the exponential $\exp[-(m'/2\beta\hbar^2)(\mathbf{z}_i-P\mathbf{z}_i)^2]$ varies smoothly. It is approximated by writing it as $\exp[-(m'/2\beta\hbar^2)\times(\mathbf{z}_i-\mathbf{z}_i')^2]$ and integrating over all $\mathbf{z}_i'$ but dividing by the atomic volume $V_A=V/N$ for each $\mathbf{z}_i'$. However, this does not take into account the restriction that all the $\mathbf{z}_i'$ are on different sites. So an additional $N!/N^N$ is needed. Thus the total factor is $N!/(NV_A)^N$ or $N!/V^N$. The integrals give $(2\pi\beta\hbar^2/m')^{\frac{1}{2}}$ per degree of freedom, so we see that Q approaches

$$Q\sim(K_\beta/V^N)\int\rho(\mathbf{z}^N)d^N\mathbf{z}_i=1$$

as $\beta\to\infty$, as required.

This value of K_β was obtained by an argument involving large β. Let us study its behavior for small values of β. For small β (high T) no permutation is important in (17) except the identity. For no atoms are closer than $b=2.6$A, and $(m'/2\beta\hbar^2)(\mathbf{z}_i-P\mathbf{z}_i)^2$ would be at least $b^2m'/2\beta\hbar^2$, if $P\mathbf{z}_i\neq\mathbf{z}_i$. For small β this results in a large negative exponent. Thus Q approaches the value

$$Q=K_\beta(N!)^{-1}(m'/2\pi\beta\hbar^2)^{3N/2}\int\rho(\mathbf{z}^N)d^N\mathbf{z}_i.$$

The correct limit, according to the classical theory, should be

$$Q=N!^{-1}(m/2\pi\beta\hbar^2)^{3N/2}\int\rho(\mathbf{z}^N)d^N\mathbf{z}_i.$$

Since m' approaches m, K_β must approach 1 as $\beta\to0$.

This means that K_β must be a function of β which varies from V^N/V_N to 1 as β varies from large to small values.

An accurate quantitative analysis of this problem would require close attention to the variation with temperature and density of m', of K and of b (or, more completely, of ρ).

EXISTENCE OF THE TRANSITION

We can use this partition function (7) and the ideas associated with it to understand many of the properties of liquid helium. The behavior of the liquid at very low temperature (below 0.5°K) will concern us in the following paper.[6] Here we will study the behavior in the region of a few degrees and shall show that a transition should occur.

In the qualitative study of such a transition we need not concern ourselves with the continuous variations in the effective constants m', K_β, b. It might be well to remark, however, that 2.2°K the expression $mx^2/2\beta\hbar^2$ is unity for $x=3.4$A. This is just the order of the average spacing of the atoms. Therefore, we are not going to be involved in very long displacements, and it may be that m' does not differ too much from m.

It is not hard to understand that (17) gives a transition. If ρ were a constant it would be the same as the partition function for an ideal gas. The fact that ρ is not perfectly uniform cannot change this much.

To see in more detail how this transition arises, consider the factor

$$\sum_P\exp[-(m'/2\beta\hbar^2)\textstyle\sum_i(\mathbf{z}_i-P\mathbf{z}_i)^2] \tag{12}$$

in the partition function (7).

Each permutation may be divided into cycles. A cycle of length s is a chain of permutations, such as 1 goes to 2, 2 goes to 3, 3 goes to 4, etc. until $s-1$ goes to s and finally s goes to 1. Such a cycle contributes to a term in (12) the factor

$$\exp[-(m'/2\beta\hbar^2)(\mathbf{z}_{12}^2+\mathbf{z}_{23}^2+\cdots+\mathbf{z}_{s1}^2)], \tag{13}$$

where $\mathbf{z}_{ij}=\mathbf{z}_i-\mathbf{z}_j$ and $\mathbf{z}_1$, $\mathbf{z}_2$, etc., are the positions of the particular atoms in the cycle. The total contribution from a given permutation is the product of all these factors, one from each of its cycles. For a given configuration we are to sum such a product over all permutations, that is, over all possible ways of laying out cycles on the configuration.

Consider a permutation of a certain "type," that is, having a certain number of each kind of cycle. That is, P has n_1 cycles of length 1 (i.e., n_1 atoms are not permuted), n_2 cycles of length 2, $\cdots n_s$ of length s, etc. The total number of atoms is N, so that

$$N=\textstyle\sum_s sn_s. \tag{14}$$

To these cycles there correspond n_1 atoms, n_2 polygons of 2 sides, n_3 triangles, $\cdots$, etc. drawn on the configuration, and each contributes its factor (13).

Next we may sum over all permutations of the same type. This means that each polygon will change its shape and location (but not its number of sides) as we go from one permutation to another in the sum. Eventually a given polygon can be considered as taking up all possible forms—that is, a polygon of s sides will have had every possible set of s atom sites for its vertices.[12] As a given polygon changes, of course, the others must change too, for no atom may be a member of more than one polygon in any given permutation P. This presents an enormously complicated mathematical problem.

We shall try to simplify it by an assumption that the various geometrical forms that a given polygon can take are roughly independent of the shapes of the other polygons. That is, we shall assume that the contribution of a polygon of a given size is the average for such a polygon over all possible forms the polygons can take without restriction. That is, *we assume the average factor contributed by a given polygon does not depend on what type the other polygons are.* This assumption is probably not sufficiently accurate to give an exact description of the order of the transition.

We shall actually use, for the contribution of a polygon, the total effect it would have if it were alone. In the various integrations over many polygons, the fact that no atom may be used twice actually restricts the volume of configuration space. It is V_N [Eq. (10)]. To include this effect we will have an additional factor V_N/V^N.

Making these assumptions the total contribution to (12) of all permutations of a given type is

$$V_N V^{-N} C(n_1, n_2 \cdots) f_1^{n_1} f_2^{n_2} \cdots f_s^{n_s} \cdots, \tag{15}$$

where $C(n_1, n_2 \cdots) = N!/\prod_s n_s! s^{n_s}$ is the total number of permutations of a given type, and f_s is the contribution of a polygon of type s, for a given configuration calculated as though it were alone. We may average this over the possible configurations also. That is,

$$f_s = V \int \exp\left[-\frac{m'}{2\beta h^2}(\mathbf{z}_{12}^2 + \mathbf{z}_{23}^2 + \cdots + \mathbf{z}_{s1}^2)\right] \times \rho^{(s)}(\mathbf{z}_1, \mathbf{z}_2 \cdots \mathbf{z}_s) d\mathbf{z}_2 \cdots d\mathbf{z}_s, \tag{16}$$

where $\rho^{(s)}(\mathbf{z}_1 \cdots \mathbf{z}_s)$ is the chance of finding s atoms with their centers at $\mathbf{z}_1, \mathbf{z}_2, \cdots \mathbf{z}_s$. That is,

$$\rho^{(s)}(\mathbf{z}_1 \cdots \mathbf{z}_s) = \int \rho(\mathbf{z}_1, \mathbf{z}_2, \cdots \mathbf{z}_s, \mathbf{z}_{s+1} \cdots \mathbf{z}_N) d\mathbf{z}_{s+1} \cdots d\mathbf{z}_N,$$

where $\rho(\mathbf{z}^N)$ is the configuration density of (7). The factor V comes in (16) from the fact that $\mathbf{z}_1$ can be anywhere and has been integrated out.

[12] Actually the only contributions (near 2°K) come from polygons formed from nearly adjacent atoms. The factor (13) is very small if any of the sides are very long. The polygons of importance may be of any total perimeter (for large s), of course. It is only their individual sides which are limited.

Next we must sum over all permutation types. That is, over all values of $n_1, n_2, \cdots$ subject to (14). Signifying this by $\sum'$ and substituting into (7) we find

$$Q = (K_\beta V_N / V^N)(m'/2\pi\beta h^2)^{3N/2} \sum{}' \prod_s (f_s^{n_s}/n_s! s^{n_s}).$$

The factor $K_\beta V_N / V^N$ presumably varies exponentially with N. We could write it as $\exp(N\alpha)$ where α is independent of N and varies slowly with temperature, vanishing as $T \to 0$. It will make no essential difference in our study of the transition (it just adds $NkT\alpha$ to the free energy A) so we will not bother to carry it along.

The sum is very difficult because of the restriction (14). However, we may use the usual methods of steepest descents. We multiply Q by a factor of the form $\exp(\mu N/kT)$ (μ is the chemical potential) and sum over N. If we then put $N = \sum_s s n_s$, we can sum on all n_s without restriction. Further, if the free energy A is

$$A = -kT \ln Q$$

and the sum is written $\exp(-B/kT)$, we can determine A from

$$A = B + \mu N \tag{18}$$

and

$$\bar{N} = -\partial B/\partial \mu \tag{19}$$

in the usual way. ($\bar{N}$ is the mean number of atoms.) Hence, putting

$$x = (m'/2\pi\beta h^2)^{\frac{1}{2}} \exp(\mu/kT), \tag{20}$$

we can write

$$\exp(-B/kT) = \sum_{\text{all } n_s\text{'s}} x^N \prod_s (f_s^{n_s}/n_s! s^{n_s}) = \prod_s \sum_{n_s} (f_s^{n_s} x^{s n_s}/n_s! s^{n_s}) = \prod_s \exp(f_s x^s/s),$$

or

$$-B = kT \sum_s f_s x^s/s; \tag{21}$$

and (19) gives

$$N = \sum_s f_s x^s. \tag{22}$$

This pair of equations together with (20), (18) determines A and thereby all the thermodynamic functions. The x is determined from the second Eq. (22), by the condition that $\bar{N}$ equal N, the actual number of atoms.

To proceed further we shall have to evaluate f_s. This we do approximately, for the calculation f_s from (16) is difficult. The distribution $\rho^{(s)}$ does not permit atoms to be too close together. This is important for atoms adjacent in the polygon, such as 1 and 2. On the other hand, it is not of great geometrical importance for links much further apart (like 1 and 5). The important polygons correspond to random walks of s steps from each atom to a neighbor, finally returning to the origin. In three dimensions the chance, after a few steps, of coming back to the origin before the final step is not large. In averaging (16) over the polygons, if we include self-crossing polygons in the average we may not be

far off. There are not many of them so they probably do not alter the average very much. This is a second assumption. It is similar to the first. To be more explicit we shall approximate $\rho^{(s)}$ in (16) by

$$\rho^{(s)}(\mathbf{z}_1, \mathbf{z}_2, \cdots \mathbf{z}_s) = p(\mathbf{z}_{12})p(\mathbf{z}_{23})\cdots p(\mathbf{z}_{s1}), \quad (23)$$

where $p(\mathbf{z}_{12})$ is the probability per unit atomic volume, of finding an atom located at $\mathbf{z}_2$ if one is known to be at $\mathbf{z}_1$ (and $\mathbf{z}_{12}=\mathbf{z}_1-\mathbf{z}_2$). It is a function only of the radial distance $p(r)$, $r^2=\mathbf{z}_{12}^2$, which approaches unity as r gets beyond a few times the atomic spacing d [$p(\mathbf{z}_{12})$ is proportional to $\rho^{(2)}(\mathbf{z}_1, \mathbf{z}_2)$.]

Thus, approximately,

$$f_s = V\int \exp[-(m'/2\beta h^2)(\mathbf{z}_{12}^2+\mathbf{z}_{23}^2+\cdots+\mathbf{z}_{s1}^2)] \times p(\mathbf{z}_{12})p(\mathbf{z}_{23})\cdots p(\mathbf{z}_{s1})d\mathbf{z}_2\cdots d\mathbf{z}_s. \quad (24)$$

This formula is wrong for $s=1$, for, of course, $f_1=V$. For $s=2$, (24) is not very good, for (24) averages with weight $p(\mathbf{z}_{12})^2$ while the correct weight in (16) should be $p(\mathbf{z}_{12})$. Short rings are not important in determining the existence nor order of the transition, however.

The expression (24) is nearly in the form of a convolution and can therefore easily be simplified. If the last point of the polygon were not 1 but some other location, say $\mathbf{z}_0$ [i.e., replace $\mathbf{z}_{s1}$ by $\mathbf{z}_{s0}$ in (24)], the expression ($\div V$) would depend on $\mathbf{z}_1-\mathbf{z}_0$ or $\mathbf{z}_{10}$. Call it $g_s(\mathbf{z}_{10})$. Its Fourier transform, $\int g_s(\mathbf{z}_{10})\exp(i\mathbf{K}\cdot\mathbf{z}_{10}) \times d\mathbf{z}_{10}$, is the s power of the Fourier transform,

$$\Gamma(\mathbf{K}) = \int \exp(-m'\mathbf{z}^2/2\beta h^2)p(\mathbf{z})\exp(i\mathbf{K}\cdot\mathbf{z})d\mathbf{z}. \quad (25)$$

Therefore $g_s(\mathbf{z}) = \int \exp(-i\mathbf{K}\cdot\mathbf{z})(\Gamma(\mathbf{K}))^s d\mathbf{K}(2\pi)^{-3}$, and since $f_s = g_s(0)$, we find

$$f_s = V\int \Gamma(\mathbf{K})^s d\mathbf{K}(2\pi)^{-3}. \quad (26)$$

This is not true for $s=1$. For $s=1$ the true f_1 is V, while this gives $f_1 = V\int\Gamma(\mathbf{K})d\mathbf{K}(2\pi)^{-3} = Vp(0)$ from (25). This $p(0)$ should be practically 0, but for generality we retain it. Substitution of this into (21) we get ($f_1=V$)

$$-B = kTV\sum_{s=2}\int (x^s\Gamma(\mathbf{K})^s/s)d\mathbf{K}(2\pi)^{-3} + kTVx,$$

or

$$-B = kTV\int \ln(1-x\Gamma(\mathbf{K}))d\mathbf{K}(2\pi)^{-3} + kTV[1-p(0)]x; \quad (27)$$

and, similarly,

$$\bar{N}/V = \int [1-x\Gamma(\mathbf{K})]^{-1}d\mathbf{K}(2\pi)^{-3} + [1-p(0)]x. \quad (28)$$

To study the transition more closely, we study the effects of the longer cycles. We need f_s for very large s. Since $\Gamma(\mathbf{K})$ in (25) falls as $\mathbf{K}$ rises and is maximum for $\mathbf{K}=0$, we expand $\ln\Gamma(\mathbf{K})$ in powers of $\mathbf{K}^2$ and carry only the first two terms in the form

$$\ln\Gamma(\mathbf{K}) \sim \ln\delta - \tfrac{1}{2}w^2K^2. \quad (29)$$

Here

$$\delta = \int \exp(-m'r^2/2\beta h^2)p(r)4\pi r^2 dr, \quad (30)$$

and

$$w^2\delta = \frac{1}{3}\int r^2\exp(-m'r^2/2\beta h^2)p(r)4\pi r^2 dr. \quad (31)$$

Then for large s, asymptotically,

$$f_s \sim V\delta^s\int \exp(-\tfrac{1}{2}sw^2\mathbf{K}^2)d\mathbf{K}(2\pi)^{-3} = V\Delta\delta^s/s^{\frac{3}{2}}, \quad (32)$$

with $\Delta = (2\pi w^2)^{-\frac{3}{2}}$. If we use this asymptotic form for all $s>1$, we make errors for the first few terms. But the transition occurs because of the character of the convergence of the series for large s. Therefore the predicted character of the transition may be found by studying the sums (21), (22) with the asymptotic form (32) for f_s. For example, the $\bar{N}/V$ sum is [putting $p(0)=0$]

$$\bar{N}/V = \Delta\sum_{s=1}(\delta x)^s/s^{\frac{3}{2}} + (1-\Delta\delta)x, \quad (33)$$

and the expression for B is

$$-B = kTV[\Delta\sum_{s=1}(\delta x)^s/s^{5/2} + (1-\Delta\delta)x]. \quad (34)$$

The same situation exists here as for the ideal gas case. The sum in (33) cannot exceed 2.612 (for $x=1/\delta$) and $2.612\Delta+(1-\Delta\delta)/\delta$ may be less than the actual N/V desired. This will not occur for high temperature (δ small), but on lowering T the difficulty suddenly sets in.

What one must do, as is well known,[4] is to note that the $d\mathbf{K}$ integral in (32) is really a sum over the values of $\mathbf{K}$ which fit in the box of volume V. The lowest state ($\mathbf{K}=0$, using running waves) is distant $d\mathbf{K}=(2\pi)^3/V$ from the next. It suffices to sum on this one and integrate the others. Thus we should add a factor $1+(2\pi)^3V^{-1}\delta(\mathbf{K})$ to the integrand of (32),[13] so that the sum is more closely

$$f_s = V\Delta\delta^s s^{-\frac{3}{2}} + \delta^s, \quad (32a)$$

and (33) becomes

$$\bar{N}/V = \Delta\sum_{s=1}(\delta x)^s s^{-\frac{3}{2}} + (1-\Delta\delta)x + V^{-1}(1-\delta x)^{-1}. \quad (33a)$$

Now δx can become very nearly 1, to order $1/V$ (e.g., put $\delta x = 1-1/gV$) and the sum in this region is $\bar{N}/V = 2.612\Delta+(1-\Delta\delta)\delta^{-1}+g$ which can be satisfied for proper choice of g. For higher temperatures (smaller δ) we can use the original expansion (33). This change in

[13] The validity of this procedure has sometimes been questioned. A method of arriving at the result (32′) which avoids the use of this procedure is given in the Appendix.

behavior for the two regions of T reflects in B (34) as a phase transition. This shows the existence of the transition. As temperature falls δ in (30) rises without limit. Since $p(r)\sim 1$ for large r, as β rises δ eventually behaves as $(2\pi\beta\hbar^2/m')^{\frac{1}{2}}$. Likewise, eventually w^2 becomes $\beta\hbar^2/m'$, so that $\Delta=(2\pi w^2)^{-\frac{1}{2}}$ approaches δ^{-1}. Therefore $2.612\Delta+(1-\Delta\delta)\delta^{-1}$ tends toward zero (as $T^{\frac{1}{2}}$) and must eventually fall below N/V. Actually by putting in very reasonable values for the parameters, it is easy to obtain a transition at about the right place.

If we do not use the asymptotic form (29) for Γ, nothing is fundamentally changed. In (28) the integral on $\mathbf{K}$ should have its factor $1+(2\pi)^3V^{-1}\delta(\mathbf{K})$ as explained, and the equation to determine x becomes (calling $\Gamma(0)=\delta$)

$$\bar{N}/V=\int[1-x\Gamma(\mathbf{K})]^{-1}d\mathbf{K}(2\pi)^{-3}+[1-p(0)]x+V^{-1}(1-\delta x)^{-1}. \quad (36)$$

Above the transition the last term is not required. Below, $\delta x=1-1/gV$ and $\bar{N}/V=\int[1-\delta^{-1}\Gamma(\mathbf{K})]^{-1}d\mathbf{K}\times(2\pi)^{-3}+[1-p(0)]\delta^{-1}+g$, with analogous expressions for B.

RELATION TO EXPERIMENT

It would not be worth while to substitute numbers in these expressions as too many small approximations have been made. In addition, it is difficult to estimate m'. The function $p(r)$ might be calculated roughly for the smaller r by using the corresponding function required for the quantum-mechanical second virial coefficient. This assumed that any two colliding atoms are independent of the others. Alternatively, $p(r)$ could be taken experimentally from x-ray or neutron scattering data.

On the other hand, the formulas (27), (28) have even qualitative faults when compared to experiment. They predict that helium, like the ideal Bose gas, would show a third-order transition (specific heat continuous but discontinuous slope). The experimental data[1] do not agree (apparently the specific heat is discontinuous). This disagreement probably stems from the neglected geometrical correlations among the rings.[14]

In order to study this in greater detail, it was thought that a careful study of the situation at extremely low temperature would be of value. The character of the transition must depend on an accurate description of the phase into which the liquid changes as it cools past the λ point. This phase is represented in an extreme form near absolute zero. In this region Eqs. (27), (28) fail very badly. They predict a specific heat varying as $T^{\frac{1}{2}}$ while experimentally it varies as T^3. In the following paper[6] we shall see that this discrepancy is a result of the error produced by the geometrical approximations made in passing from (7) to (27), (28). The approximations here permit much larger fluctuations in density than is available to the true liquid, and this qualitatively alters the behavior of the specific heat at low temperature.

The experimental specific heat curve shows[1] a slight rise in the He I region as the λ point is approached from above. This is also a property of our expression (34). In this region only a few chains are starting to form. The restriction that no atom may be in more than one chain is not yet of importance. Therefore, in this region our geometrical approximations should be valid. The very least we can say, then, is that the rapid rise in specific heat of He I with falling temperature is completely explained.

SUMMARY

Starting with an exact quantum-mechanical partition function, we have derived an approximate expression [Eq. (7)] which should be qualitatively accurate. It has been shown to be in agreement with experiment in predicting a transition which depends in an essential manner on the statistics.

Further mathematical approximations have not been accurate enough to show whether (7) will correctly predict the order of the transition and the temperature dependence of the specific heat near absolute zero. They do suffice at high temperatures to show the rise in specific heat of He I as the transition is approached.

It is proposed that a more careful analysis of (7) would show more complete agreement with the experimental facts.[1] In the next paper[6] the situation near absolute zero is studied in detail, and it is found that (7) (corrected for the effect mentioned in footnote 11) very likely does predict the correct behavior in this region.

The physical idea which plays a central role is that in a quantum-mechanical Bose liquid the atoms behave in some respects like free particles.

The author appreciates conversations with Edward Kerner and with M. Kac, as a result of which he became interested in the problem. He also is grateful for discussions with E. Wigner, H. Bethe, and R. F. Christy.

APPENDIX

We give here another derivation of the approximate partition function (33a), (34). It has the advantage of showing more clearly the origin of the transition. We will treat it in a very approximate manner as we have already given more complete formulas. (It is the first derivation that the author made.)

Near the transition only permutations involving shifts of each atom to the position of its neighbor, at some mean distance d, are important. The exponential factor from such a shift is $y=\exp(-m'd^2/2\beta\hbar^2)$.

Each permutation can be broken into cycles. We now only count those cycles for which all atoms are adjacent,

[14] Assumptions about the temperature variation of the parameters m, $p(r)$, K_B cannot alter the order of the predicted transition. The effect of modifying (7) in the manner indicated in footnote 11 is discussed in the paper to follow. The change, if anything, is in the wrong direction.

forming a closed chain or ring. If a ring contains s atoms, its contribution is y^s. If we have n_2 rings of 2 atoms, n_3 of 3 atoms, etc., the contribution is $y^{2n_2+3n_3+\cdots}$. The part of the partition function which determines the transition is then

$$q=\sum G(n_2, n_3, \cdots)y^{\sum_s sn_s}, \tag{1-A}$$

where $G(n_2, n_3, \cdots)$ is the number of ways we can lay out polygons, n_2 of 2 sides, n_3 triangles, etc., on the configuration—the sides of the polygons consisting of lines joining nearest neighbors (length d). The sum is restricted for the number of single atoms $n_1=N-\sum_{s=2}sn_s$ must not be negative.

Here again we shall make the error of neglecting the geometrical interference of polygons due to the restriction that each atom be a vertex of only one polygon. We shall include the competition among the polygons for the total number of available atoms by saying that there is an average probability t that any site is unoccupied. This t will later be determined so that the average number of atoms occupied is $\bar{N}=N$. (This can be done in detail by steepest descents, but it amounts to the same thing.) Therefore, instead of q we calculate t^Nq and call it $\exp(-B/kT)$.

The polygons can now be considered as independent. If R_s is the total number of s gons that can be drawn on the configuration, each s gon can be chosen in R_s ways, and all n_s of them in $R_s^{n_s}/n_s!$ ways. The n_1 single atoms can be chosen in $N^{n_1}/n_1!$ ways. Thus

$$\exp(-B/kT)=\sum_{n_1}\sum_{n_2}\cdots\prod_{s=2}R_s^{n_s}(n_s!)^{-1}y^{sn_s}t^{sn_s}t^{n_1}N^{n_1}(n_1!)^{-1}$$

$$=\exp[Nt+\sum_{s=2}R_s(ty)^s],$$

or

$$-B=kT[Nt+\sum_{s=2}R_s(ty)^s]. \tag{2-A}$$

The average number of atoms $\bar{N}$ used in sites is $t(\partial q/\partial t)q^{-1}$, so we have

$$\bar{N}=Nt+\sum_{s=2}sR_s(ty)^s. \tag{3-A}$$

Now we calculate R_s. We call h_s the total number of ways that we can, starting at an atom and making successive steps to adjacent atoms, return after exactly s steps. This forms a closed s gon. We may start at any of the N atoms. The total Nh_s measure the total number of s gons, but counts each s times (for you could start at any of the s atoms as the "first"). Hence we have, $R_s=Nh_s/s$, and

$$-B=kTN[t+\sum_{s=2}h_s(ty)^s/s], \tag{4-A}$$

where t is a parameter determined from $\bar{N}=N$, in (3-A), or

$$1=t+\sum_{s=2}h_s(ty)^s. \tag{5-A}$$

We shall bother to determine the form of h_s for large s only. In the random walk, each step is length d, and may be made to any of the adjacent atoms, which we shall say are l in number, on the average. Each step can be made in l ways, the entire s steps in l^s ways. There are l^s walks in total but only a certain number return to the origin. As is well known, the probability of being at a given point, per unit volume, radius r from the starting point is

$$(2\pi d^2s/3)^{-\frac{3}{2}}\exp(-3r^2/2sd^2)=\Delta s^{-\frac{3}{2}}\exp(-r^2/2sw^2),$$

putting $w^2=d^2/3$ and $\Delta=(2\pi w^2)^{-\frac{3}{2}}$. The chance we are back at the original atom (that is, within a space of one atomic volume $V_A=V/N$ near the origin) is $V_A\Delta s^{-\frac{3}{2}}$, so that

$$h_s=V_A\Delta s^{-\frac{3}{2}}l^s.$$

The reason for the dependence on the $s^{-\frac{3}{2}}$ is easy to see. After s steps we have wandered out to a mean radius of order $s^{\frac{1}{2}}$, or over a volume $s^{\frac{3}{2}}$. Hence, the chance that in this volume we are back at the original atom varies as $s^{-\frac{3}{2}}$. This is correct except for enormous chains $s\gtrsim N^{\frac{2}{3}}$, which are long enough to wander all over the liquid. Then the available volume no longer increases. The chance that one is back at the original atom instead of one of the other roughly equally likely atoms is $1/N$. For such large s, then, $h_s=l^s/N$. The formula,

$$h_s=(V_A\Delta s^{-\frac{3}{2}}+1/N)l^s, \tag{6-A}$$

takes care of both cases, because for small s the first term dominates, and for large s the second takes over, as it should.[15] Substitution into (3-A) gives

$$1=t+V_A\Delta\sum_{s=2}(lyt)^s s^{-\frac{3}{2}}+N^{-1}(1-lyt)^{-1}. \tag{7-A}$$

This may be compared to (33a). To do so, note that our interpretation of $3w^2$ as the mean square length of a step agrees with (31). Further ly is the number of atoms available per step, l, multiplied by the weight $y=\exp(-m'd^2/2\beta\hbar^2)$. In the more general case it becomes δ/V_A as an inspection of (30), the expression for δ, shows. Finally, the parameter t can as well be called V_Ax, and Eq. (7-A) is seen to be identical to (33a) (times V_A). Likewise, substitution of (6-A) into (4-A) gives the corresponding equation (34) for B.

This derivation throws some light on the mathe-

[15] According to (6-A) the chance to return is higher than for an infinite medium. It might be objected that there should be fewer paths available when there are a finite number of atoms in an enclosed space. What we have done corresponds to working with a periodic boundary condition, and the excess arises from the chance to return to one of the images of the origin, instead of to the origin itself. With the more physical boundary condition—that paths cannot cross the liquid surface—the total number of paths for high s is not l^s, but is reduced. It becomes eventually proportional to $e^{-\epsilon^2 l^2}$, where ϵ is a very small number of order $N^{-\frac{1}{3}}$. It makes no essential difference in the result. In the momentum representation of the text it corresponds to taking the lowest state to have a wavelength controlled by the size of the box. I am indebted to Herman Kahn for pointing out this possible objection to (6-A).

matical "cause" of the transition. As T falls y rises, until the enormous number of possible orientations of a very long ring more than compensates for the small contribution of each ($y^l \ll 1$, for l large).

There is no doubt of the geometrical fact of large numbers of orientations for long rings, even if these rings may never use the same atom twice (i.e., cannot cross themselves).[16] Therefore there can be no doubt that (1–A), and its more complete expression (17), will show a transition from this cause. But the order of the transition need not be the same as that of the approximate evaluations we have made. They neglect the geometrical correlations. For example, if a large chain of K atoms is already formed, are the remaining $N-K$ atoms more (or perhaps less) likely to be contiguous and therefore more easily able to make other chains, than if these $N-K$ atoms were chosen at random from among the N? Our assumption in deriving (5–A) was that it was equally likely either way.

[16] For example, the number of ways in which a single polygon which does not cross itself can still be oriented in an infinite medium = constant $\times l^5 s^{-1}$, but the value of l is reduced.

PHYSICAL REVIEW VOLUME 91, NUMBER 6 SEPTEMBER 15, 1953

Atomic Theory of Liquid Helium Near Absolute Zero

R. P. FEYNMAN
California Institute of Technology, Pasadena, California

(Received June 1, 1953)

The properties of liquid helium at very low temperatures (below 0.5°K) are discussed from the atomic point of view. It is argued that the lowest states are compressional waves (phonons). Long-range motions which leave density unaltered (stirrings) are impossible for Bose statistics since they simply permute the atoms. Motions on an atomic scale are possible, but require a minimum energy of excitation. Therefore at low temperature the specific heat varies as T^3 and the flow resistance of the fluid is small. The arguments are entirely qualitative—no calculation of the energy of excitation nor of the low-temperature viscosity is given. In an appendix an expression, previously given, for the partition function is modified to include the effects of phonons.

INTRODUCTION

TISZA[1] has suggested the very fruitful concept that He II might be thought of as a mixture of two fluids, "superfluid" and "normal." At zero temperature the helium is pure superfluid. With rising temperature some sort of "excited molecules" form. These constitute the "normal fluid" which behaves very much like a gas. The proportion of normal fluid increases at first slowly, and then rapidly, with temperature until at the transition temperature of 2.19°K (λ point) the liquid, now He I, contains no more superfluid.

Landau[2] has made even more detailed suggestions. He suggests that there are two kinds of "excited molecules," phonons or quanta of longitudinal compressional waves (sound) and "rotons." The latter are not well understood. It is suggested that they have a minimum energy Δ needed to excite them. For this reason below 0.5°K there are practically only phonons. The rotons can become excited when more energy is available; i.e., at higher temperature. This idea is in agreement with the fact that below 0.5°K the specific heat varies as T^3 in just the manner (and with the correct coefficient) to be expected if only longitudinal sound waves could be excited.

Tisza's view is frankly phenomenological. No serious attempt is made to justify the description from first principles. Landau has made such an attempt by studying the quantum mechanics of a continuous liquid medium. The role of the statistics is not clear in his arguments, however. Furthermore, the magnitudes of energy and inertia that the "rotons" appear to have correspond to a few atoms. A complete understanding of the "roton" state can therefore only be achieved by way of an atomic viewpoint.

A more complete study of liquid helium from first principles might attempt to answer at least three important questions:

(a) Why does the liquid make a transition between two forms, He I and He II?

(b) Why are there no states of very low energy, other than phonons, which can be excited in helium II (i.e., below 0.5°K)?

(c) What is the nature of the excitations which constitute the "normal fluid component" at higher temperatures, say from 1 to 2.2°K?

The first question was answered in a preceding paper.[3] We showed that London's suggestion, that it is the analog of the transition in an ideal Bose gas, is correct.

In this note we hope to make a qualitative argument from first principles to answer the second question.

[1] L. Tisza, Phys. Rev. **72**, 838 (1947). An excellent summary of the theories of helium II is to be found in R. B. Dingle, Supplement to Phil. Mag. **1**, 112 (1952).

[2] L. Landau, J. Phys. U.S.S.R. **5**, 71 (1941).

[3] R. P. Feynman, Phys. Rev. **91**, 1291 (1953), hereafter called I.

(We have not yet found the answer to the third.*) It is to be understood, therefore, that we are aiming here to explain the properties of the liquid only at extremely low temperatures.

We take, as a model, helium atoms obeying the Schrödinger equation and the symmetrical Einstein-Bose statistics with forces between pairs similar to that worked out by Slater and Kirkwood,[4] an attraction at large distances and a strong repulsion at small.[5] (It is sufficient for qualitative purposes, if one wishes, to imagine impenetrable spheres of radius about 2.7A packed into a space so the mean spacing (cube root of atomic volume) is about 3.6A.

At absolute zero the system is in the ground state. Why this is not a solid has been explained by London.[6] The large zero-point motions of the atoms are capable of "melting" any ordered crystalline arrangement that may be temporarily set up. We begin by describing the wave function for this ground state.

DESCRIPTION OF THE GROUND-STATE WAVE FUNCTION

Wave functions can be described qualitatively in words by giving the amplitude for every configuration of the atoms. The ground state has a positive amplitude for any configuration since the lowest state has no nodes. The amplitude is negligible if any two atoms are so close together that they overlap—that is, that a large negative potential has set in. Thus for any atom surrounded by neighbors, considered for a moment fixed, the amplitude falls to zero when the atom moves over to touch any of the neighbors and is probably bound in such a way that it is maximum when the atom is near the center of its "cage." (This curvature makes a strong kinetic energy tending to blow apart the cage, an energy effect canceled by the long-range attraction of the atoms.) Compressing the atom into a smaller cage requires more kinetic energy, and expansion works against the attractive potential so there is some mean density of equilibrium. Fluctuations away from that mean density are of amplitude distributed in a Gaussian manner. For wavelengths exceeding the atomic spacing they are analogous to zero-point fluctuations of the vacuum electromagnetic field (but are wholly longitudinal, scalar waves, of course).

There are a large number of configurations with densities near the most likely density, in all of which the atoms tend to keep separate from one another. They differ from one another mainly in the location of the atoms. The various configurations differ only in that one may be "stirred" into another with a little reshuffling or stirring of the atoms. We may take it that all configurations which have nearly the same type of density fluctuations and which can be essentially just stirred from one to another have the same amplitude in the ground state.

THE CHARACTER OF LOW-ENERGY STATES

We must next determine the character of the low-energy states near the ground state. We aim to show that the only states which differ from the ground state by an infinitesimal energy are the phonons.

First we can take it that the lowest states are those involving large numbers of atoms or large distances. Consider, for example, a tiny region of the liquid, say a cube 3 or 4 atomic spacings on a side. If the atoms in this region are confined in this region (so we have a submicroscopic sample of liquid He) the excitations above the ground state will all involve one node somewhere among the configurations and hence a wavelength of order of a. This must mean an excess kinetic energy of the order $\hbar^2/a^2m$, or at least of order $\hbar^2/Na^2m$, where N is the number of atoms and m is the mass of each—leaving an appreciable gap from the ground state.

This argument fails if in the ground state there are two (or more) regions of configuration space in both of which the amplitude is large and which are completely separated by a region of very small amplitude. (Analogous to a particle in a potential with two wells separated by a barrier.) If the nodal surface is passed through the region of small amplitude (the barrier) very little change in energy results. But we have seen that the states of large amplitude are just all those in which the atoms are reasonably well separated. We can assume that we can get from one to any other without crossing any high potential barrier. We suppose all possible rearrangements may be achieved without the atoms coming too close together at any time. That this is reasonable can be seen by comparing the size of the atoms to their spacing. For example, if at some point they are locally roughly on a cubic close-packed lattice, the nearest neighbors are 4.0A apart (corresponding to the observed atomic volume[5] of 45A³). The diameter of the atoms is 2.7A, the radius at which Slater and Kirkwood's potential passes from minus to plus. The cube edge of the lattice is 5.6A, so a face-centered atom could even pass between those at the corners of the cube! Clearly, if they are allowed to vary their mutual distances a little, all kinds of rearrangements can be made. It is likely that the condition that there be no effective barrier between configurations is equivalent to the condition that the He II is liquid in the lowest state. We assume it valid for He II.

If we are to find extremely low-energy states we must therefore look to excitations involving large groups of atoms or long wavelengths. One possibility is in the compression waves. Suppose the atoms are compressed to a small excess density over a large volume and a rarefaction left adjacently. The only way this fluctuation could even out is for a considerable number of atoms to move, each a little bit. This involves, effectively, the motion of a large mass and can have low kinetic energy. There is, therefore, little doubt that such compressional waves represent a true mode of excitation in the helium, and a mode of very low energy. If the speed of sound is called c and the wave number of the waves K, the frequency $\omega = cK$ and quantum

* *Note added in proof:*—This problem has now been solved. Its solution will appear in a forthcoming publication.

[4] J. C. Slater and J. G. Kirkwood, Phys. Rev. **37**, 682 (1931).

[5] For a detailed account of the properties of helium see W. H. Keeson, *Helium* (Elsevier Publishing Company, Inc., Amsterdam, 1942).

[6] F. London, Nature **141**, 643 (1938).

energy $\hbar cK$ can be as small as desired. Thus there is no reason why we should not expect the specific heat, varying as T^3, from these modes.[7]

We have assumed that the way to release a density fluctuation in a given time which requires the least kinetic energy is to move many atoms a short distance. If only a fraction f of the atoms move, the velocity required is $1/f$ times higher. This means a higher kinetic energy if the kinetic energy varies as the velocity squared.

There are cases, however, in which the kinetic energy does not vary in this way. In a degenerate Fermi gas a single atom excited by a small excess momentum p above the Fermi surface of momentum p_0 has an energy $((p_0+p)^2-p_0^2)/2m$ or $(p_0/m)p$. This linear dependence of energy on momentum means that the group velocity of such waves is energy independent. It is p_0/m. The speed of sound calculated from the compressibility and density of the ideal gas is $3^{-\frac{1}{2}}p_0/m$. The single atoms will run ahead of the sound. Fluctuations are reduced by a process more like diffusion than sound. The specific heat near $T=0$ varies as T instead of T^3 because the density of states for exciting single atoms exceeds that for sound. As we shall see, for Bose helium there are no states, except phonons, whose energy approaches zero as their momentum approaches zero. The sound has no competitor capable of discharging pressure.[8]

LOW-ENERGY STATES DISREGARDING STATISTICS

The Bose statistics play an essential part in the discussion of other possible states of very low-excitation energy. To make this role clear by contrast, we shall first analyze the situation, disregarding the statistics. More precisely we consider in this section an imaginary quantum liquid made of atoms which are, in principle, distinguishable ("Bolzman" statistics). The ground state for Bolzman statistics is the same as for Bose statistics, since the lowest state is, in either case, symmetrical.

We must try to find modes of excitation involving long wavelengths which do not involve changes in mean density. The density fluctuation modes have already been considered. To simplify the argument consider first the following crude model. We consider a set of cells, each of which contains one atom. Each atom is free to wander in its cell and may occupy therefore some ground-state wave function, say constant amplitude in the cell. We are to consider states which can be made solely by rearranging the atoms among the cells. No two atoms may go into the same cell, for that corresponds to a density fluctuation, and we do not wish to consider those.

In the ground state, the amplitude is the same for any rearrangement of the atoms among the cells. The lowest states can now be analyzed as follows. We neglect the statistics, that is, we assume Boltzmann statistics to apply. We can describe a wave function which corresponds to a very low excitation as follows: Pick out a certain atom, A, say. Put it in a given cell. Then all rearrangements of the other atoms among the other cells can be taken to have the same amplitude. If atom A is in a different cell, the amplitude may be different, but again independent of the arrangement of the other atoms. We thus can specify this wave function by giving just the amplitude for various positions of atom A. The function is independent of the position of the others. We may take this as $\exp(iK\cdot R_A)$, where R_A is the position of the center of the cell in which atom A is. We may, with enough accuracy, let R_A be just the position of atom A. The K can be a long wave fitting into the volume V in which the helium is contained. The energy of this state is $\hbar^2K^2/2m'$ where m' is the effective mass needed to move atom A. This energy can be very small, for K can be small.

This effective mass is not far from the mass of one helium atom. It is discussed in a previous paper.[3] We summarize the argument here. To push a single atom along, we need not go over any potential barriers. The other atoms may move out of the way. No matter where atom A is located the other atoms can arrange themselves into a state of minimum energy and this minimum energy is independent of the location of atom A. However, as A moves, the others must readjust themselves into the state of minimum energy for the new position of A. That is, in addition to the kinetic energy of A there is a kinetic energy of the other atoms which must move away to make room for A.

Thus there would be low-lying states, of energy $\hbar K^2/2m'$. The number of such states would be very large, for the wave function could depend in similar ways on the coordinates of other atoms also. [For example, we could choose two atoms A, B and have the wave function vary with their location as $\exp(iK_1\cdot R_A)\exp(iK_2\cdot R_B)$ and be otherwise independent of the distribution of the others in the cells, etc.] The large density of low-lying states would result in a large specific heat near absolute zero.

LOW STATES WITH SYMMETRICAL STATISTICS

However, if the atoms obey Bose statistics none of these states can exist. For in our model, whether atom A is at one location or another is merely an interchange of which atom is which. This cannot change the wave function. In fact, for the model of one atom in a cell no excited state at all can exist for Bose particles without excitation of the atom within the cell.

For the real liquid a similar situation holds—aside from the phonons, there can be no low-lying state. The wave function must have the property that any change, that just means an interchange among the atoms, must not alter the wave function. The excited state must be orthogonal to the ground state, of course. Starting at any configuration and supposing the amplitude is

[7] The partition function discussed previously (reference 3) is extended to include a description of the phonons in the Appendix to this paper.

[8] For an *ideal* Bose gas, as $T\to 0$, the sound velocity approaches zero, so that the expected T^3 specific heat does not appear. It is replaced by T^4. Density fluctuations are much more restricted in liquid helium than they are in the ideal gas. This is the origin of many differences in behavior for the two cases.

the same as for the ground state, we must find a new configuration that represents a kind of stirring of the old configuration (to omit phonon states) such that the amplitude is now reversed in sign. It is clear that *every* configuration is close to the original one, albeit with some atoms interchanged. So it is hard to find a configuration to give the minus amplitude which is sufficiently far (in configuration space) from the original positive amplitude configuration to have a slow rate of decay and thus a low energy.

There are some possibilities of this kind which might at first sight seem allowable. Consider among the atoms a set of adjacent ones forming a large ring. Suppose l atoms are in the ring and let us imagine the wave function is such that, if all move together half an atomic spacing a, the phase changes by π, so when they turn about another $a/2$ the phase changes by 2π, as required by the Bose statistics. (For a shift of a just changes each atom for the one behind.) The mass moving is $m'l$, and the momentum is $\hbar/a$ (for the wavelength is a) so that the energy is $\frac{1}{2}(m'l)^{-1}(\hbar/a)^2$. This may be made low by choosing l very large. (If it were not for the Bose statistics we could have taken the wavelength to be la and the energy would be even lower, varying as $1/l^3$.)

The argument for calculating this energy is incorrect, however. By assuming that all the atoms must move together, degrees of freedom (in which parts of the ring turn by themselves) have been restricted. This tacitly adds a considerable energy by the uncertainty principle.

To understand better the failure of the argument, consider by the same reasoning the case that one had two equal rings parallel to each other. We may argue as before that now the entire mass $2m'l$ moves together with momentum $\hbar/a$ and thus expect an energy $\frac{1}{2}(2m'l)^{-1}(\hbar/a)^2$ for the energy of the lowest state. But this is certainly wrong, for if we consider the rings as independent, the lowest state but one is surely that one for which one of the rings is excited and the other not (momentum O), an energy $\frac{1}{2}(m'l)^{-1}(\hbar/a)^2$, larger than our previous lowest estimate! The error for the first figure of $\frac{1}{2}(2m'l)^{-1}(\hbar/a)^2$ consisted in this. In describing the wave function, the possibility that the two rings could turn independently was omitted. To force the rings to move together would be to force the difference between their displacements to be fixed at zero. Thus the momentum conjugate to this difference coordinate would be very high, and the energy associated with this coordinate very large. Thus the system does not have just the energy estimated but, in fact, a very much higher one. We have not completely specified the wave function. We have not said what the amplitude is to be for configurations in which only one of the rings moves.

In an analogous way, the estimate of energy for the single ring, $\frac{1}{2}(m'l)^{-1}(\hbar/a)^2$, is incorrect. We have specified the amplitude for the case that *all* of the atoms are simultaneously in the mid positions. What is to be the amplitude if only a few move to mid positions? (This may be accomplished without doing violence to the potentials by using the atoms adjacent to the ring and by turning on smaller rings of 4 or 5 atoms.) If the motion (all to $\frac{1}{2}$ position) can be made up of smaller parts moving in concert, and if these smaller parts could also have moved independently, the energy cannot be lower than that corresponding to just one of independent parts being excited.

Since we may well imagine that any motion of the atoms could be made up of combinations of motions of small groups (say 3 or 4 revolving about each other) the lowest energy is the excitation of one of these small groups. These we can identify with Tisza's excited molecules or Landau's rotons (but see next paragraph). Any such small ring of r atoms must, of course, have its first state of excitation of angular momentum $r\hbar$ (or $p=\hbar/a$) because of the statistics. Landau's arguments[2] that such angular momentum must have an excitation energy was made in a way that does not involve the statistics of the atoms. It is possibly equivalent to our argument that large rings need not be considered if their motion is analyzable in smaller parts. The central importance of the statistics would not seem to be here, but rather in the previous argument which shows that no states corresponding to the slow linear motion of a single atom are permitted.

It is not obvious whether the lowest excited state, excluding the phonons, is actually a small ring of atoms turning. The arguments do not exclude the possibility that these are all higher than another type of mode; namely, the rapid motion of a single atom. In our cell model a state which depends on atom A as $\exp iK\cdot R_A$ with $Ka=2\pi$ is, of course, possible. Another possibility is the analog of the excitation of a single atom in a cell. (This may be the same as the single atom motion.) All of these states differ from the ground state by a finite energy. But which is lowest is hard to determine.

Any such excitation can, of course, move through the fluid. (In fact, the lowest state is that in which it has equal amplitude of being anywhere in the fluid.) That is, the wave function could vary as $\exp(iK\cdot R)$, where R is the location of the center of excitation. Then the energy of these excitations might have the form, suggested by Landau,[2] $\Delta+K^2/2\mu$, where Δ is the energy needed to excite the ring or other excitation, and μ is a sort of effective mass.

Our primary purpose was to show that no states close to the ground state exist, exclusive of the phonons. We are not yet able to calculate the energy, nor to give a clear picture of the other modes of excitation.

DESCRIPTION OF SOME PROPERTIES OF THE LIQUID

In concluding that only phonons exist at low temperature, we concur with the opinion of the phenomenological theories. Therefore, a description of how some of the properties of helium arise, according to this model, will repeat much that has already been pointed out by others.[1,2] We limit ourselves, therefore, to a very brief summary from a kinetic theory point of view.

First, consider the motion of an object, such as a small sphere through the liquid. If the object is stationary at a fixed position R, the liquid may get into a certain state which, omitting phonons for a moment, is like the ground state (except that now part of the space occupied by the object is not available to the helium). Let the wave function of the helium be ψ_R. It is a function of all the helium atoms and depends, say parametrically, on R. If R is changed, ψ is also, but the energy of the fluid is not changed. For, rearranging the fluid to a new shape at the same density does not alter the energy. Now if we alter the R from R_1 to R_2 nearby, we will only need to add a little kinetic energy to push the helium atoms out of the

way. The overlap of ψ_{R_1} and ψ_{R_2} will be nearly perfect (except near the surface of the object which is a different volume of space in the two cases, $R=R_1$ and $R=R_2$). The object can move therefore with an *energy* equal to just the kinetic energy of itself and the liquid which flows around it. The fluid will move so that the curl of the velocity is zero, because circulation corresponds to permutation of atoms, and the Bose statistics will not permit such motions, as we have seen.[9]

What will be the losses of energy suffered by such an object? If it loses energy it can do so only by exciting the helium. First, can it excite the molecular excitations? These take a certain energy Δ to excite, but a massive object even moving very slowly may have sufficient energy. On the other hand, for such an object to change energy by Δ its momentum must change by an enormous amount. To create an excitation of very high momentum may take much more energy than Δ. As Landau has shown,[2] if the energy to excite a roton of momentum p is taken to be of the form $\Delta+p^2/2\mu$, the laws of conservation of energy and momentum show that slowly moving objects [velocity less than $(2\mu\Delta)^{\frac{1}{2}}$] can produce no excitations. Likewise, objects moving at velocities below that of sound cannot lose energy by creating phonons. Therefore, at absolute zero and for not too high velocity, a moving object will suffer no viscous drag.

At low temperatures, there are, however, some phonons already existing in the liquid. They can scatter off of the object (changing their energy by the Doppler effect) and in this way the object can lose a little energy. A phonon of energy $\hbar\omega$ carries momentum $\hbar\omega/c$ and behaves very much like a particle of mass $\hbar\omega/c^2$ moving at velocity c. The phonons act in most respects like a gas of such particles, and the resistance suffered by our object is just like the viscosity that would be suffered by an object moving through such a gas.

The actual calculation of this energy loss means a calculation of the viscous drag of such a gas. This requires a knowledge of the mean free path for collision among the phonons. The phonons scatter from one another because the medium is not linear. The speed of sound depends a little on the density. Therefore speaking classically, if a wave is present, another wave impinging finds the index of refraction varying sinusoidally and is thereby scattered. The same thing happens in the quantum mechanical system.

The mean free path should rise rapidly as the temperature falls, because the density of phonons decreases (the scattering cross section also decreases). Interesting phenomena should result when this free path becomes comparable to the dimensions of the apparatus.

If the viscosity is measured by connecting two vessels with a capillary, a different situation arises. The phonons cannot readily work their way through the long capillary, but the bulk liquid can move through it. There is work done on the phonons as the piston moves down in one of the vessels, again by the Doppler effect on the phonons bouncing off of the moving piston. But this work just goes into increasing the phonon energy—that is, the liquid in one vessel is heated, in the other cooled. If isothermal conditions are maintained it goes as heat to the walls of the first container and from the walls of the second. No net work is done in this case and the viscosity appears to vanish. There is essentially no energy loss because there is no real viscous flow of our phonon "gas" through the capillary. The reason that, experimentally, resistance appears[5] if the flow velocity exceeds a certain critical velocity is not clear. Perhaps in passing sharp protuberances in the capillary wall the velocity locally exceeds that needed to create excitations or new phonons. It cannot very well be a kind of turbulence because presumably the velocity field should be always free of circulation.

In two volumes of liquid helium connected by a capillary, the hotter one will exert the higher pressure (fountain effect). The larger number and higher average momentum of phonons in the hotter region results, from wall bombardment, in a higher pressure there. The pressure can only be released slowly by phonons passing through the long capillary. This would be the mechanism of heat conductivity through capillaries. The rate of such conduction would depend on the relative size of the capillaries and the phonon mean free path.

If temperature varies from one point to another in the bulk liquid, then the phonon density varies. What happens depends on the mean free path. If it is long compared to the distances over which the variations occur, the variations are almost immediately evened out by the diffusion of phonons rushing from one place to another (at the speed c). If the mean free path is shorter than the distances involved in the variation, no single photon can go directly from a high- to low-density region. Instead, a cooperative movement sets in. If we consider the analogy to a gas of phonon "particles," a pressure variation is released by body motion—that is, by sound waves. The speed of this sound is $3^{-\frac{1}{2}}$ times the individual particle velocities. In our case, this "second sound" representing waves of phonon density (i.e., temperature) should travel at a velocity $3^{-\frac{1}{2}}c$. At low temperatures it will be experimentally hard to keep the mean free path very small compared to the wave-

[9] For a liquid contained in a simply connected region, the circulation vanishes everywhere if it vanishes locally. But in a region of connectivity like the inside of a torus, although the curl is everywhere zero, the circulation around the ring may not be zero. Such a circulation cannot be compounded of smaller independent units. Therefore, it should be possible to demonstrate circulatory motions in such a vessel which will maintain themselves for a long time. Circulation may be created by rotating the vessel containing He I and cooling to the temperature desired below the λ point. Stopping the rotating vessel should leave the interior liquid with a nearly permanent angular momentum, which could be demonstrated, for example, by its gyroscopic effects. The liquid must be completely confined with no free surface because the exchange of atoms between the rotating liquid and the stationary gas above it might cause a rapid damping of the angular momentum.

length, so that second sound would show appreciable damping and dispersion. At extremely low temperatures the free path may be larger than the apparatus. Then, if a pulse of heat at one point creates extra phonons, these will rush away at speed c so that temperature rise will begin at a distant point delayed only by the time required for *first* sound to traverse the apparatus.[10]

EFFECTS OF He^3 ATOMS AT LOW CONCENTRATIONS

If a foreign atom, say an atom of He^3, is in the liquid, our arguments indicate that it will move about essentially as a free particle, albeit with an effective mass m'' larger than its true mass. (This m'' should be about one atomic mass unit less than the effective mass m' of a He^4 atom.) Such He^3 atoms put into He^4 at low concentration should behave as a perfect gas. Consider, as an example, a concentration of 0.1 percent. The mean spacing of the atoms is so large that the gas is not degenerate, except at a few hundredths of a degree. (The statistics can only be of importance if the atoms can permute. This occurs only if $\exp(-m''D^2kT/2\hbar^2)$ is not too small. Here, D is the mean spacing of the atoms, which is 36A in our example.) The specific heat contributed by the He^3 is then k per atom. This can exceed the specific heat of the phonons (below 0.4° in our example). A temperature pulse would then go mainly into increasing the energy of the He^3 gas. The speed of sound in this gas is of the order of the He^3 atom velocity, and therefore the observed second sound velocity should vary as $(kT/m'')^{\frac{1}{2}}$ in this region.[10] A more detailed analysis of the intermediate region in which both He^3 and phonons contribute requires a study of the collision cross sections for phonon-phonon, phonon-He^3, and He^3-He^3 collisions. Higher concentrations of He^3 require a study of the degenerate Fermi gas. The entire analysis of this paper fails to apply to pure He^3, because the ground state from which we begin is different.

An atom of He^3 should show an appreciably higher free energy when dissolved in He^4, than if that atom is replaced by He^4. This is because, as discussed in a previous paper,[3] for pure He^4 the partition function is the sum on all trajectories which start at some configuration of the atoms $\mathbf{z}_i$ and return to *any* permutation of the original configuration $P\mathbf{z}_i$. With a He^3 atom at $\mathbf{z}_1$ say (and no others nearby), the final configuration is limited to only those permutations for which this atom returns to $\mathbf{z}_1$. We can estimate the effect as follows: Neglect the mass difference of He^3 and He^4. Consider the nondiagonal matrix element $(z'|e^{-\beta H}|z)$ in which the final state differs from the initial state only in that the atom $\mathbf{z}_1$ is moved to another site $\mathbf{z}'_1$. All the other atoms may go to some permutation of the original positions. From what we have said in I, this should depend upon $\mathbf{z}_1$ and $\mathbf{z}'_1$ approximately through a factor $(\beta=1/kT)$,

$$(m'/2\pi\beta\hbar^2)^{\frac{1}{2}}\exp[-m'(\mathbf{z}_1-\mathbf{z}'_1)^2/2\beta\hbar^2], \qquad (1)$$

since the atom acts essentially as a free particle of mass m'. To get the partition function if the atom 1 is He^4, we must sum this over all possible sites $\mathbf{z}'_1$. At low temperatures, where the diffusion distance $(2\beta\hbar^2/m')^{\frac{1}{2}}$ exceeds the atomic spacing $d=(V_A)^{\frac{1}{3}}$, this is approximately the integral of (1) over all $\mathbf{z}'_1$ divided by V_A, the atomic volume. This gives $V_A{}^{-1}$ for He^4. For He^3, $\mathbf{z}'_1$ must coincide with $\mathbf{z}_1$ so (1) gives $(m'/2\pi\beta\hbar^2)^{\frac{1}{2}}$. The ratio of the partition function for He^4 to that in which a He^4 atom is replaced by He^3 is therefore $(m'kT/2\pi\hbar^2)^{-\frac{1}{2}}V_A{}^{-1}$ (at low concentration). The extra free energy per atom of He^3 is therefore $(3/2)kT\ln(2\pi\hbar^2/m''kTV_A{}^{\frac{1}{3}})$ at low temperatures. (Since He^3 is lighter than He^4, m' is replaced by m''.)[11]

DISCUSSION

A number of problems are suggested by this work.

First, a detailed quantitative analysis of all of the properties of liquid He^4 below 0.5°K should be undertaken with the confidence that the problem is relatively simple. Only the phonons should be involved. Their wavelengths are long compared to atomic dimensions, and we have to do essentially with a continuous medium. The statistical mechanical aspects are considered in the appendix. The mean free path for phonon collisions could be computed if the nonlinearity of the medium is included. Work in this direction has been done by Landau and Khalatnikov.[12] An extension could be made to include the effects of small concentrations of He^3.

A more difficult class of problem, and one which we have left completely untouched, is the answer to question (c) of the introduction. Namely, what is the detailed nature of the excitations involved at the higher temperatures of 1 to 2.2°K? Most of the experimental work has been done in this region. The atomic viewpoint cannot claim a real understanding of the situation in liquid He II until this problem is solved. (See note added in proof.)*

There is a third group of problems which has not been touched upon. They involve the question,

(d) What is the mechanism of the Rollin film?[5]

This seems to be a problem of the very low-temperature behavior and should properly have been discussed in this paper. A suggestion of Bijl, de Boer, and Michels[13] involves the idea that the energy of a layer of the

[10] I am indebted to F. G. Brickwedde for calling my attention to this phenomenon.

[11] To the effect considered in the text, there must be added the large free-energy difference at absolute zero, which arises from the difference in zero-point energy occasioned by the difference in atomic mass. In first approximation, the wave function is unaltered but the kinetic energy, $-(\hbar^2/2m)\nabla^2$, is higher, for m is 3 instead of 4. This difference is, therefore, close to $\frac{1}{3}$ of the mean kinetic energy, per He^4 atom, in the ground state.

[12] L. D. Landau and I. M. Khalatnikov, J. Exptl. Theoret. Physik (U.S.S.R.) **19**, 637, 709 (1949).

[13] Bijl, de Boer, and Michels, Physica **8**, 655 (1941).

liquid depends strongly on the thickness of the layer, decreasing for thicker layers, even up to 100 atoms thick. If this view is correct, we should look for the answer by studying the energy of the ground state, to see if it is dependent on the shape of the container. It is possible that such a dependence exists, even for thick layers, because of the very long permutation rings involved at low temperatures in the condensed phase. These rings are long enough to wander over the entire volume of the liquid, so that the energy may be sensitive to the shape. We have not yet been able to verify quantitatively the correctness of this idea.

Finally, the problem of critical flow velocities, and the resistance to high-speed motions, remains unsolved.

The analysis of pure liquid He^3 requires a new start because our physical arguments so far have depended so strongly on the Bose statistics.

The author has profited from conversations with E. Wigner, H. A. Bethe, and R. F. Christy.

APPENDIX

In a previous paper,[3] I, an approximate partition function was proposed for liquid helium. Without modification it will not describe the phonon states correctly. The necessary modifications are discussed here.

In I, it was noted that the partition function of helium is the integral over all configurations $\mathbf{z}_i$ of the quantity

$$W(\mathbf{z}^N)=N!^{-1}\sum_P\int_{\mathrm{tr}P}\exp\left\{-\int_0^\beta\left[\frac{m}{2\hbar^2}\sum_i\left(\frac{d\mathbf{x}_i}{du}\right)^2+\sum_{ij}V(\mathbf{x}_i-\mathbf{x}_j)\right]du\right\}\mathfrak{D}^N\mathbf{x}_i(u), \quad (2)$$

using the notation of that paper [I, Eq. (5)]. The integral $\int_{\mathrm{tr}P}$ is taken over all trajectories $\mathbf{x}_i(u)$ of the atoms which start from the positions $\mathbf{x}_i(0)=\mathbf{z}_i$ and end up at some permutation $\mathbf{x}_i(\beta)=P\mathbf{z}_i$ of $\mathbf{z}_i$. The sum is taken on all permutations P. It was pointed out that if a configuration $\mathbf{z}_i$ contained atoms nearly overlapping, or in some other unfavorable arrangement, the important trajectories $\mathbf{x}_i(u)$ would almost immediately move to release the energy of the unfavorable arrangement (for example, overlapping atoms would spring apart). The time for this was generally much less than β. Thus the various configurations could be given a weight $\rho(\mathbf{z}_1, \mathbf{z}_2\cdots\mathbf{z}_N)=\rho(\mathbf{z}^N)$. The slower motions of atomic diffusion contributed an additional exponential factor, so an approximate expression [I Eq. (7)],

$$W(\mathbf{z}^N)=N!^{-1}K_\beta\left(\frac{m'}{2\pi\beta\hbar^2}\right)^{3N/2}\times\sum_P\exp\left[-\frac{m'}{2\beta\hbar^2}\sum_i(\mathbf{z}_i-P\mathbf{z}_i)^2\right]\rho(\mathbf{z}^N), \quad (3)$$

was proposed. The factor ρ was to be (for low temperatures, large β) nearly independent of β, as it represents the effect of rapid local motions. It is $\phi(\mathbf{z}^N)^2$, where ϕ is the ground-state wave-function.

On the other hand, it was remarked (footnote 11 of I) that general variations in density over large distances would not be so rapidly released. We now consider in detail the effect of these compressional waves.

To a sound wave of wave number K, and frequency $\omega=cK$, where c is the speed of sound, correspond phonons of energy $\hbar\omega$. A density fluctuation of this wavelength $\lambda=2\pi K^{-1}$ would take a time τ of order $1/\hbar\omega$ to decay (calling u "time" as in I). This time will exceed β, for wavelengths $\lambda>2\pi\hbar c/kT=2\pi\cdot 17\mathrm{A}/T^\circ K$. Since this distance exceeds the atomic spacing 3.6A and the diffusion distance $(2\beta\hbar^2/m)^{\frac{1}{2}}=4.8\mathrm{A}/(T^\circ K)^{\frac{1}{2}}$, there is clear separation of these waves from local atomic motions. Therefore, an expression like (3) is correct locally, for a density fluctuation over a small region is rapidly released so that its effect can be contained in ρ (by having ρ smaller for such fluctuations). But a fluctuation over long distances will not even out in a time β and is not correctly described in (3).

Choose a length $1/K_0$ exceeding the atomic spacing, but below the wavelength of sound excited at the given temperature ($\hbar cK_0\beta\gg 1$). For distances inside $1/K_0$ no new considerations are necessary, and (3) is locally correct. For long distances it must be altered. Let $n(\mathbf{R})$ be the average number density at $\mathbf{R}$ in the configuration $\mathbf{z}_i$—the average being taken over a region of volume $1/K_0^3$. We shall determine how the probability of this configuration depends on $n(\mathbf{R})$ [the result is (9) below].

We may describe the motions $\mathbf{x}_i(u)$ as local atomic movements (within distances K_0^{-1}) and general drift motions of the center of gravity of the atoms in a volume K_0^{-3}. It is convenient to describe the initial density distribution by imagining that it arose from an initially uniform distribution of density n_0 by a displacement. If the atoms originally at $\mathbf{R}$ were displaced by $\mathbf{D}_0(\mathbf{R})$, the density is $n(\mathbf{R})=n_0(1+\nabla\cdot\mathbf{D}_0)$, where $n_0=V_A^{-1}$ is the density averaged over the entire fluid. As the trajectories in (2) move, there is a general drift which we will describe by giving the displacement $\mathbf{D}(\mathbf{R}, u)$ as a function of u. What is the energy associated with this drift? First, to the kinetic energy of the atoms due to local motion there is an extra contribution from the general drift $(m/2V_A)(\partial\mathbf{D}/\partial u)^2$ per unit volume. Further, suppose a region temporarily has an extra high local density. This will limit the path-space volume available (and also change the average mutual potential energies). Therefore there will be an extra factor accumulated in each little interval of time. This we can write as a factor $e^{-E\,du\,dV}$ for the volume dV in time du. This E (the energy resulting from the compression) depends just on the density, hence on $\nabla\cdot\mathbf{D}$. We expand it in powers of $\nabla\cdot\mathbf{D}$. The constant term may be omitted by changing the zero from which we

measure energy. The linear term gives nothing for its integral over all the liquid vanishes $\int \nabla\cdot\mathbf{D}dV=0$ from the conservation of mass. The quadratic term is written conveniently as $(1/2)mc^2V_A^{-1}(\nabla\cdot\mathbf{D})^2$, for c defined this way becomes the speed of sound. Higher-order terms produce phonon-phonon scattering, but we neglect them here. Thus, in addition to the features which go to make up (3) locally, there is a factor controlling the large scale motions,

$$\exp\left[-\frac{m}{2V_Ah^2}\int_0^\beta\int\left(\left(\frac{\partial\mathbf{D}}{\partial u}\right)^2+h^2c^2(\nabla\cdot\mathbf{D})^2\right)dVdu\right]\mathfrak{D}\mathbf{D}(\mathbf{R},u), \quad (4)$$

where the $\mathbf{D}$ are to be summed over all displacement fields such that[14] $\mathbf{D}(\mathbf{R},0)=\mathbf{D}_0=\mathbf{D}(\mathbf{R},\beta)$, with

$$\nabla\cdot\mathbf{D}_0=V_An(\mathbf{R})-1.$$

This is best analyzed in momentum space. We put

$$\mathbf{D}(\mathbf{R},u)=\int\mathbf{A}(\mathbf{K},u)\exp(i\mathbf{K}\cdot\mathbf{R})d^3\mathbf{K}(2\pi)^{-3}.$$

The $\mathbf{A}$ field can be separated into transverse components $\mathbf{A}_1$ and $\mathbf{A}_2$ and a longitudinal component $B=\mathbf{A}\cdot\mathbf{K}/K$. Thus

$$\nabla\cdot\mathbf{D}=\int KB(\mathbf{K},u)e^{i\mathbf{K}\cdot\mathbf{R}}d^3\mathbf{K}(2\pi)^{-3}, \quad (5)$$

and (4) becomes

$$\exp\left[-\frac{m}{2V_Ah^2}\int_0^\beta\int\left[\left(\frac{\partial B}{\partial u}\right)^2+h^2c^2\mathbf{K}^2B^2+\left(\frac{\partial\mathbf{A}_1}{\partial u}\right)^2+\left(\frac{\partial\mathbf{A}_2}{\partial u}\right)^2\right]d^3\mathbf{K}(2\pi)^{-3}du\right]\mathfrak{D}\mathbf{A}_1(\mathbf{K},u)\mathfrak{D}\mathbf{A}_2\mathfrak{D}B. \quad (6)$$

The transverse displacements act as free particle motions, for there is no restoring force. They contribute a factor $(m/2\pi\beta\hbar)^{\frac{1}{2}}$ per mode. This is already contained in (3) (but with m' for m, which makes little difference for the small fraction $V_AK_0^3$ of modes involved). We need not count them again in (6).

For each longitudinal mode, we must integrate an expression of the form

$$\exp\left\{-\frac{m\delta}{2V_Ah^2}\int_0^\beta\left[\left(\frac{dB}{du}\right)^2+h^2c^2K^2B^2\right]du\right\}\mathfrak{D}B(u),$$

where δ is the K-space volume per mode for all $B(u)$ which begin and end at B_0. This may be easily done by a method explained in another connection by the author.[15] There results ($\omega=cK$),

$$\left(\frac{m\delta\omega}{2\pi V_Ah\sinh(\omega\beta\hbar)}\right)^{\frac{1}{2}}\exp\left[-\frac{m\delta\omega}{V_Ah}B_0^2\tanh\left(\frac{\omega\beta\hbar}{2}\right)\right]. \quad (7)$$

The complete partition function is the integral (2) over all initial configurations. We therefore integrate (7) over B_0 to get the contribution from this mode. The integral yields

$$[2\sinh(\omega\beta\hbar)\tanh(\tfrac{1}{2}\omega\beta\hbar)]^{-1}=[2\sinh(\tfrac{1}{2}\omega\beta\hbar)]^{-1}=\exp(-\tfrac{1}{2}\omega\beta\hbar)[1-\exp(-\omega\beta\hbar)]^{-1},$$

the usual partition function from such a mode. All the modes together contribute

$$\exp\left\{-\int\ln[2\sinh(\tfrac{1}{2}\omega\beta\hbar)]d^3\mathbf{K}(2\pi)^{-3}V\right\}, \quad (8)$$

the integral extending over all modes of wave number less than K_0. This factor in the partition function gives the usual Debye specific heat, varying as T^3 as long as our temperatures are, as we have assumed, small enough that $K_0c\hbar\beta\gg1$.

Multiplication of the factors (7) for all modes tells us that density fluctuations have a probability proportional to

$$\exp\left\{-\frac{mc^2}{V_Ah}\int[KB_0(\mathbf{K})]^2\tanh\left(\frac{\omega\beta\hbar}{2}\right)\frac{d^3\mathbf{K}}{(2\pi)^3\omega}\right\}, \quad (9)$$

where KB_0 is the Fourier transform of the density fluctuation [from (5)],

$$KB_0(\mathbf{K})=V_A\int(n(\mathbf{R})-n_0)e^{i\mathbf{K}\cdot\mathbf{R}}d^3\mathbf{R}. \quad (10)$$

Since, for large $\omega\beta\hbar$, $\tanh(\frac{1}{2}\omega\beta\hbar)$ is nearly 1, the density fluctuations of short wavelength are independent of the temperature. For these the factor (9) could just as well be combined with the temperature independent factor ρ to make a new effective ρ. This shows that the results do not depend on the exact choice of K_0. For long waves $\tanh(\frac{1}{2}\omega\beta\hbar)$ falls below 1 and wider fluctuations are permitted than would be expected from (3). A more accurate representation of (2) is then (3) with ρ containing general variations in density, these variations being weighed by multiplying by the factor (9), normalized. A factor $(m'/2\pi\beta\hbar^2)^{N/2}$ should be replaced by (8).

The purpose of this appendix is just to note that (3) does not automatically contain the phonon effects, but must be modified to include them. The study of such questions as the nature of higher-energy excitations and the character of the transition can presumably be made using (3) without modification. It is convenient that the sound wavelengths are so long that a nearly complete separation can be made of the local behavior and the behavior of the overlying compressional waves.

[14] In principle the final displacements could differ from the initial by an atomic spacing d (because atoms may be permuted). But the actual displacements permitted by (4) are very much smaller than d, so that the only important term from (4) is that for which the configuration is restored atom by atom.

[15] R. P. Feynman, Phys. Rev. **84**, 108 (1951) Appendix C. The explicit answer is given in R. P. Feynman, Revs. Modern Phys. **20**, 367 (1948) on page 386, by substituting $\gamma=0$, $q_j=q_0=B_0$, $\hbar=-iV_A\hbar^2/m\delta$, $\omega=i\omega\hbar$. $T=\beta$.

Interaction between Classical Electron and Quantized Electromagnetic Field*

I. R. SENITZKY
Signal Corps Engineering Laboratories, Fort Monmouth, New Jersey

(Received May 14, 1953)

The equations of motion for a quantized electromagnetic field subject to the influence of a classical electron of arbitrarily prescribed velocity are solved by a simple method involving the corresponding difference equations. The solution yields some results which are contrary to those of an earlier theory. An expression for the transition probabilities between a high-energy state and neighboring states of the field inside a resonant cavity is obtained.

THE behavior of a quantized field which is subjected to the influence of a classical electron with prescribed motion has been discussed by several authors.[1–4] One of the treatments[2] is not correct, and contradicting results are obtained below. Two of the other treatments[1,3] are mainly concerned with the case in which the electron velocity is independent of the time and also are not very suitable for calculating transition probabilities between quantum states of the field. Another treatment[4] makes use of methods developed by Schwinger[5] to obtain an expression for the state of the field in terms of the initial state. This expression is then used to derive transition probabilities between the lowest-energy state and higher states of an unconfined free space field. In the present note, the above-mentioned expression is derived briefly by elementary methods and is then used to obtain transition probabilities between a high-energy state and neighboring states of the field inside a resonant cavity.

The system under consideration is the radiation field inside a cavity resonator described by the vector potential operator $\mathbf{A}$ and its conjugate $\mathbf{P}$. In the usual way,[6] we expand

$$\mathbf{A}=\sum_k q_k(t)\mathbf{u}_k(\mathbf{r}), \quad \mathbf{P}=\sum_k p_k(t)\mathbf{u}_k(\mathbf{r}),$$

where the subscript k refers to the kth normal mode of the cavity, $\mathbf{u}_k(\mathbf{r})$ is a normalized function describing the spatial dependence of the field, and q and p are the coordinate and momentum operators of the radiation oscillators satisfying the commutation relationship $[q_k, p_k]=ih$, all other commutator pairs vanishing.

Considering the effect of the electron as an external influence, the nonrelativistic Hamiltonian for the field is

$$H=H_0+(e/c)\mathbf{v}\cdot\mathbf{A}(\mathbf{r}_0),$$

where

$$H_0=\sum_k[2\pi c^2 p_k^2+(\omega_k^2/8\pi c^2)q_k^2],$$

ω_k is the angular frequency of the kth mode, $\mathbf{r}_0$ is the position of the electron, and the components of $\mathbf{v}$ are ordinary numbers, since the electron is treated classically. In a representation in which H_0 is diagonal, the vector with components $a(t)_{n_1, n_2\cdots}$, which describes the state of the radiation field at time t (with the ith index referring to the ith mode), is given by the equation of motion,

$$\dot{a}(t)=S(t)a(0), \tag{1}$$

where $S(t)$ is a matrix with elements

$$S(t)_{n_1, n_2\cdots; n_1', n_2'\cdots}.$$

The only nonvanishing elements of S are

$$S_{n_1\cdots n_j\cdots; n_1\cdots n_j\pm 1\cdots}=(e/ihc)[q_j]_{n, n\pm 1}\mathbf{v}\cdot\mathbf{u}_j(\mathbf{r}_0)e^{\mp i\omega_j t}$$

and

$$[q_j]_{n, n+1}=i[2\pi h(n+1)/\omega_j]^{\frac{1}{2}}=[q_j]_{n+1, n}.$$

It can be seen by a straightforward calculation that the commutator $[S(t_1), S(t_2)]$ is a pure imaginary multiple of the unit matrix.

In order to solve Eq. (1), we consider the following difference equation:

$$[a(t_{i+1})-a(t_i)]/\Delta t_i=S(t_i)a(t_i), \tag{2}$$

where

$$\Delta t_i=t_{i+1}-t_i.$$

A solution of Eq. (2), to the first order in Δt, is

$$a(t_i)=e^{S(t_{i-1})\Delta t_{i-1}}e^{S(t_{i-2})\Delta t_{i-2}}\cdots e^{S(t_0)\Delta t_0}a(0). \tag{3}$$

Using the fact that if the commutator of two matrices, A_1 and A_2, is a multiple of the unit matrix, then

$$e^{A_1}e^{A_2}=e^{A_1+A_2}e^{\frac{1}{2}[A_1, A_2]}, \tag{4}$$

and applying it successively to the right side of Eq. (3) (and bearing in mind that all commutators may be treated as numbers) we obtain

$$a(t_i)=\{\exp\sum_{r=0}^{i-1}S(t_r)\Delta t_r\}\times\{\exp\sum_{p=1}^{i-1}\sum_{q=0}^{p-1}[S(t_p), S(t_q)]\Delta t_p\Delta t_q\}a(0).$$

* Parts of this paper were presented before the 1952 Annual Meeting of the American Physical Society.

[1] F. Bloch and A. Nordsieck, Phys. Rev. **52**, 54 (1937).
[2] L. P. Smith, Phys. Rev. **69**, 195 (1946).
[3] W. Thirring and B. Touschek, Phil. Mag. **42**, 244 (1951).
[4] R. R. Glauber, Phys. Rev. **84**, 395 (1951).
[5] J. Schwinger, Phys. Rev. **75**, 651 (1949).
[6] See, for instance, Schiff, *Quantum Mechanics* (McGraw-Hill Book Company, Inc., New York, 1949), Sec. 50.

Taking the limit as $\Delta t \to 0$, we have

$$a(t)=\left\{\exp\int_0^t S(t_1)dt_1\right\} \times\left\{\exp\int_0^t dt_1\int_0^{t_1} dt_2[S(t_1),S(t_2)]\right\}a(0). \quad (5)$$

This is the solution of Eq. (1). A simple check of this solution may be obtained by evaluating the expression $[a(t+\Delta t)-a(t)]/\Delta t$, using Eq. (4). The limit of this expression, as $\Delta t \to 0$, reduces to the right side of Eq. (1).

We apply the above theory to the problem examined by Smith.[2] He considers the effect of only one mode of oscillation, of angular frequency ω, and takes $\mathbf{u}(\mathbf{r}_0)$ as constant inside the cavity along the path of the electron. We ask for the probability of the emission or absorption of a given number of photons by the field when the transit time of the electron is an integral number of cycles of the frequency of oscillation, and the electron velocity is constant. For $t=2\pi m/\omega$, m being any integer, all the matrix elements of $\int_0^t S(t_1)dt_1$ vanish, and $\exp\int_0^t S(t_1)dt_1$ is the unit matrix. Since $[S(t_1),S(t_2)]$ is a pure imaginary number, the absolute values of the elements of $a(t)$ are the same as the absolute values of the corresponding elements of $a(0)$. Thus the probability that the state of the field will be changed is zero. This contradicts the results of Smith, and necessitates a different interpretation of the experimental work of Shulman.[7]

We consider, finally, the situation where a mode of the field is initially in a high-energy state, that is, the cavity contains a large number of photons, and ask for the probability of absorption or emission of a number of photons, small compared to the initial value. We neglect all but the oscillating mode, assuming that all the other modes are in their lowest-energy state, and that the probability of their absorption of quanta (virtual or real) is negligibly small.[8] We write only the index referring to the oscillating mode, considering all the others to be zero. We take $a(0)_m=\delta_{mp}$. Then, from Eq. (5) we obtain

$$|a_k(t)|=|\sum_{n=0}^{\infty}(1/n!)(B^n)_{kp}|, \quad (6)$$

where

$$B=\int_0^t S(t_1)dt_1.$$

Now,

$$(B^n)_{kp}=\sum_{i_1,i_2\cdots} B_{ki_1}B_{i_1i_2}\cdots B_{i_{n-1}p}, \quad (7)$$

and since the only nonvanishing elements of B are $B_{m,m-1}$ and $B_{m-1,m}$, m being any positive integer, we have, setting $r=|k-p|$, $(B^n)_{kp}=0$ for $n<r$, or for $n-r$ being odd. For $n\geq r$ and $n-r$ even, the number of nonvanishing terms on the right side of Eq. (7) is equal to the number of possibilities of going from k to p in n steps, each step being ± 1, namely,

$$n!\left[\left(\tfrac{1}{2}n+\tfrac{1}{2}r\right)!\left(\tfrac{1}{2}n-\tfrac{1}{2}r\right)!\right]^{-1}.$$

Each of these terms has a common factor, corresponding to the creation (if $k>p$) or destruction (if $k<p$) of r real photons. The remaining factor in each term corresponds to the creation and destruction of $\frac{1}{2}(n-r)$ virtual photons. Because of the convergence of the right side of Eq. (6), we can neglect all terms in it with $n>N(r)$, say.

We consider the case $p\gg r$ and $p\gg N(r)$. This means that the initial number of photons is large, and that the change in the number of photons is small compared to the initial number. Then, the $B_{i,i\pm1}$'s occurring in the sum of Eq. (7) do not differ much from $B_{p,p\pm1}$, since $p-r<i<p+r$ in the common factor (corresponding to emission or absorption of real quanta), and $p-\frac{1}{2}(N-r)<i<p+\frac{1}{2}(N+r)$ in the remaining factors (corresponding to emission and absorption of virtual quanta). The common factor is, therefore, approximately $(B_{p,p\pm1})^r$, the upper sign holding for $p>k$ and the lower sign for $p<k$. The remaining $B_{i,i\pm1}$'s in each term of the sum in Eq. (11) can be considered in pairs. For each $B_{i,i+1}$ there is a $B_{i+1,i}$ in the same term, and their product is $-|B_{i,i+1}|^2$. We therefore have

$$(B^n)_{kp}\cong(-1)^{\frac{1}{2}(n-r)}n! \times\left[\left(\frac{n+r}{2}\right)!\left(\frac{n-r}{2}\right)!\right]^{-1}(B_{p,p\pm1})^r|B_{p,p+1}|^{n-r}$$

for $n-r$ even and positive, and zero otherwise. Substituting in Eq. (6) we obtain as the probability that the field absorb or emit r quanta,

$$|a(t)_{p\pm r}|^2\cong|J_r(2|B_{p,p+1}|)|^2, \quad (12)$$

where J_r is the Bessel function of the rth order. If we take $\mathbf{u}(\mathbf{r}_0)=\mathbf{u}_0$, a constant, along the electron path inside the cavity and zero outside the cavity, and if we

[7] C. Shulman, Phys. Rev. **82**, 116 (1951). Smith's results imply that transitions are produced when the electron transit time is an integral number of cycles, and Shulman measured this supposed effect, interpreting his results by Smith's theory. The main error in Smith's paper is the use of ordinary probability theory instead of quantum theory to obtain the probability of a transition involving more than one quantum. Another aspect of Smith's treatment has been criticized by D. Gabor, Phil. Mag. **41**, 1180 (1950). However, Gabor's own quantum-mechanical analysis does not seem to be correct.

[8] This is the case if the coupling between the electron and the nonoscillating modes is negligible. However, irrespective of the coupling, our interest is in the transition probabilities of the oscillating mode, regardless of the transitions made by the other modes. We can therefore sum over all the quantum states of the other modes. Setting

$$S_{n_1}\cdots{}_{n_i}\cdots;{}_{m_1}\cdots{}_{m_i}\cdots=\sum_i S_{n_i m_i}{}^{(i)}\prod_{j\neq i}\delta_{n_j m_j},$$

we have S expressed as a sum of commuting matrices. Then, $\exp(\int_0^t S(t_1)dt_1)$ becomes a product of terms, each one of which refers essentially to one mode. Summing over all the quantum states of the initially nonoscillating modes makes all the factors referring to these modes equal to unity. The subsequent treatment is applicable, therefore, even when the absorption probabilities for the nonoscillating modes are not negligible, provided the notation is understood to mean that a summation is taken over all the quantum states of these modes.

take the electron velocity to be constant, then

$$|B_{p,p+1}| = edu_0\left(\frac{2\pi p}{h\omega}\right)^{\frac{1}{2}}\frac{\sin(\omega t/2)}{(\omega t/2)},$$

where d is the distance of electron path in the cavity. If we set

$$\mathbf{E}_0 = 2\mathbf{u}_0(2\pi p h\omega)^{\frac{1}{2}}$$

(this may be considered the amplitude of the corresponding classical field), Eq. (8) becomes

$$|a(t)_{p\pm r}|^2 = \left|J_r\left(\frac{edE_0}{h\omega}\frac{\sin(\omega t/2)}{(\omega t/2)}\right)\right|^2. \qquad (9)$$

Equation (9) is identical with one obtained by Ward,[9] as the approximate probability that a quantum-mechanical electron will absorb or emit r quanta in passing through a cavity containing a classical field of amplitude E_0. The similarity of the two results is due to the fact that the approximations made in going from Eq. (5) to Eq. (9), as well as Ward's approximations, reduce the problem to one of the absorption or emission of energy according to essentially classical rules except that the change takes place in discrete quanta.

The author is indebted to Professor Julian Schwinger for enlightening discussions related to the foregoing subject matter.

[9] J. C. Ward, Phys. Rev. **80**, 119 (1950).

PHYSICAL REVIEW VOLUME 91, NUMBER 6 SEPTEMBER 15, 1953

Optical Studies of Injected Carriers. I. Infrared Absorption in Germanium

ROGER NEWMAN
General Electric Research Laboratory, Schenectady, New York
(Received June 3, 1953)

The infrared absorption of injected carriers in germanium has been observed by a modulation technique. For injection into low-resistivity material, the data indicate a linear relationship between injected carrier density and injection current. For injection into high-resistivity material, departure from a linear relationship is indicated. The absorption spectrum of injected carriers resembles that of extrinsic carriers.

THIS note describes some preliminary observations on the infrared absorption of injected carriers in germanium.[1] The process was studied for two cases: injection into almost intrinsic material (40 ohm cm, n type) and injection into doped material (0.5 ohm cm, p type).

The experimental technique was as follows: A dc light source was focused on a small region of a grown p-n junction diode cut with plane parallel faces. The diode was masked by a slit so that only a 15-mil region immediately adjacent to the barrier on the low-conductivity side was exposed. A 50 percent on-off square-wave generator pulsed the diode at about 360 cps and injected carriers. The latter modulated the transmission of the light through the germanium. After dispersal by a monochromator (Perkin-Elmer) the modulated portion of the dispersed light was detected by a dry-ice-cooled PbS cell used in conjunction with an L-C tuned regenerative feedback amplifier and recording potentiometer.

Where extreme sensitivity was not important, an ac thermocouple was employed as a detector. The diode current was then modulated at 13 cps by a mechanical switch operating in conjunction with the synchronous rectifier of the thermocouple amplifier.

If the dimensions of the region of the diode that is studied are small, compared to characteristic decay lengths for injection, then the modulation in light level at some particular wavelength is

$$\Delta I = I_0 T_0(1-e^{-k(i)d}).$$

Here I_0 is the incident light intensity, T_0 is the trans-

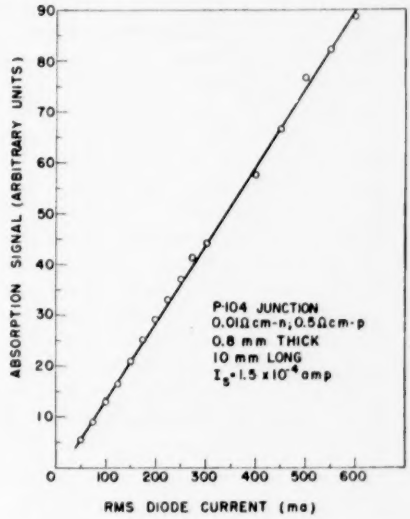

FIG. 1. Absorption signal at 2.3μ as a function of diode current at 25°C for injection into 0.5-ohm cm material.

[1] K. Lehovec, Proc. Inst. Radio Engrs. **40**, 1407 (1952).

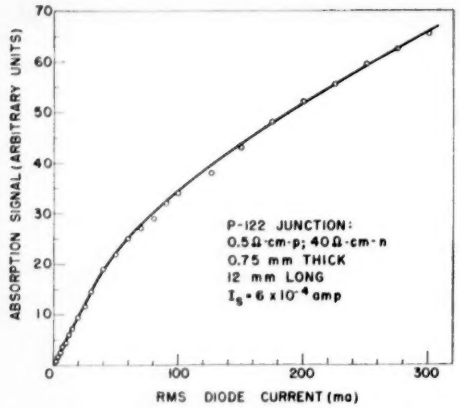

FIG. 2. Absorption signal at 2.3μ as a function of diode current at 25°C for injection into 40-ohm cm material.

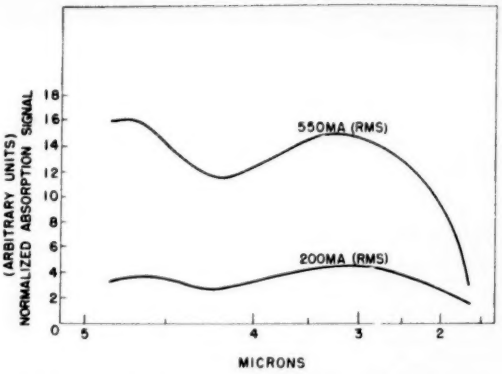

FIG. 3. Normalized absorption signal (M/C) at 25°C as a function of wavelength for two injection levels. Thermocouple detector.

mission of the germanium without injection, $k(i)$ is an absorption constant characteristic of a certain uniform current density i, and d is the thickness of the sample. If the light detector is linear, then the normalization factor I_0T_0 can be evaluated by observing the signal obtained by full modulation of the light, as for example, by on-off mechanical chopping. The ratio of the current modulation signal M to the chopped beam signal C is

$$M/C = 1 - e^{-kd} \approx kd \text{ (for small } kd).$$

Before proceeding it is of interest to note that currents of the order of 200 microamperes were observable (signal/noise$\sim$2) which, as is implied below, amounted to a change in light level of about 1 part in 10^5. This is not the lower limit of sensitivity.

Figures 1 and 2 show typical plots of M *versus* diode current at a fixed wavelength for the two types of injection considered. Since the highest signal level shown amounted to less than 1 percent of full modulation, as indicated by mechanical light chopping, M should be proportional to $k(i)$ for a given sample. Since it is further to be expected that k should be proportional to injected carrier density, M should likewise be proportional to the injected carrier density.

Thus, the linearity of the M *vs* current curve, Fig. 1, for the injection into doped material seems in accord with simple p-n junction theory. The nonlinearity of the M *vs* current curve, Fig. 2, for injection into high-resistivity material seems at first surprising. However, this particular situation is complex in that for the particular range of current used majority and minority carrier densities are comparable and simple diode theory cannot be expected to apply. As some confirmation of the optical results for this case, the conductance between two tin probe points soldered to the high-resistivity material was measured as a function of diode current. The conductance showed a characteristic, at least qualitatively, similar to the M *vs* current curve. It is of further interest to note, in connection with the paper which follows, that M^2 for the high-resistivity injection is, to an excellent approximation, linear in current for currents greater than about 10 milliamperes.

In Fig. 3 plots of M/C against wavelength are shown. If the absorption for injected carriers is essentially like that for extrinsic carriers, then its wavelength dependence should be essentially like that of free holes. This conclusion arises from consideration of the respective absorption cross sections for holes and electrons.[2] The conclusion is born out by the curves of Fig. 3. Notably, the fine structure reported by Briggs and Fletcher for p-type germanium seems in evidence in the curve. We believe that this provides conclusive evidence that the presence of the structure is independent of the source of the holes. The question still remains as to whether structure is an intrinsic property of the spectrum of free holes or results from some more or less constant defect characteristic of real germanium.

Kaiser and co-workers[3] have reported that when p-type material is cooled to 77°K or below, profound changes in the free hole absorption occurred. It is of interest to see whether the corresponding changes occur in the spectrum of injected holes. Our results in this connection will be presented in the near future.

[2] H. B. Briggs and R. C. Fletcher, Phys. Rev. **87**, 1130 (1952).
[3] Kaiser, Collins, and Fan, Bull. Am. Phys. Soc. **28**, No. 2, 32 (1953).

Optical Studies of Injected Carriers. II. Recombination Radiation in Germanium

ROGER NEWMAN
General Electric Research Laboratory, Schenectady, New York
(Received June 3, 1953)

The radiation produced by the direct recombination of electrons and holes in germanium is studied. The observed spectral distribution is in fair agreement with theory. For injection into high resistivity, as well as into doped material, the radiation is observed to be a linear function of injection current. Possible explanations for this are discussed. Magnetic concentration of carriers produced changes in the radiation intensity. Polarization of the radiation at oblique angles of emergence is observed.

THE radiation produced by the direct recombination of electrons and holes in germanium was observed by Haynes and Briggs.[1] The present work extends the study of this radiation. As in the preceding paper,[2] studies were made on two types of grown $p-n$ junction diodes cut with plane parallel faces; one in which the injection took place in high-resistivity material (40 ohm cm, n type), the other in which the injection took place in doped material (0.5 ohm cm, p type).

The experimental technique was as follows: The diodes were attached to water-cooled metal blocks which limited temperature rises to less than 10°C for the data quoted in this report. The diodes were pulsed by a 50 percent on-off square-wave generator operating in the vicinity of 350 cps. The radiation from the diodes was detected by a dry-ice-cooled PbS cell used in conjunction with an L–C tuned regenerative feedback amplifier and recording potentiometer. The spectral distribution curves were obtained using a Perkin-Elmer monochromator with a fused quartz prism.

Application of standard radiation theory indicates that the spectral distribution function $I(\nu)$ of recombination radiation from intrinsic material should obey the following relation:

$$I(\nu) \propto \nu^3 e^{-h\nu/kT}[1-e^{-\alpha_\nu d}].$$

Here α_ν is the absorption constant at frequency ν and d, the thickness of the material. Figure 1, shows the observed spectral distribution obtained for a diode and a curve calculated from the above relationship. The absorption data were taken from Briggs.[3] The agreement of observed and calculated curves is probably as good as can be expected. The discrepancy that exists might arise from a spectrometer calibration difference or from errors in the longer-wavelength absorption coefficients. The radiation from thicker diodes than that employed for the figure showed very slight displacements of the distribution curve toward lower frequencies as is to be expected.

If the radiation arises from the direct recombination of electrons and holes, then the intensity of total radiation from a small volume would be expected to be proportional to the $n-p$ product. It was of interest to test this hypothesis by variation of the diode injection current. Before discussing the results in detail, it is worth noting that currents as small as 1 milliampere ($\sim$0.03 amp/cm^2) produced detectable radiation (signal/noise$\sim$4) using an $f/4$ optical system. Presumably, by using larger apertures even smaller currents could be detected.

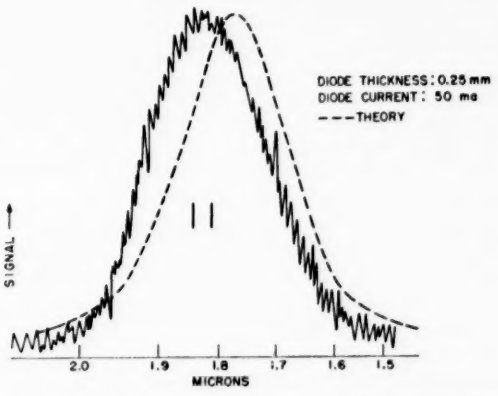

FIG. 1. Spectral distribution of recombination radiation in germanium at 25°C. The theoretical curve was normalized to have the same area under the curve as the experimental curve.

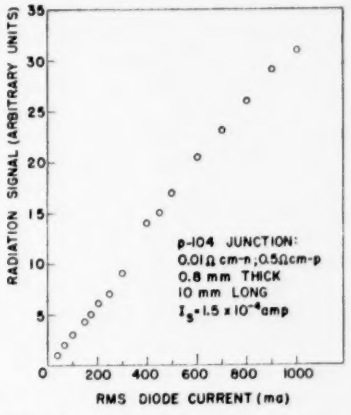

FIG. 2. Radiation signal as a function of diode current for injection into 0.5-ohm cm material.

[1] J. R. Haynes and H. B. Briggs, Phys. Rev. **86**, 647 (1952).
[2] R. Newman, preceding paper [Phys. Rev. **91**, 1311 (1953)]; referred to hereafter as I.
[3] H. B. Briggs, J. Opt. Soc. Am. **42**, 686 (1952).

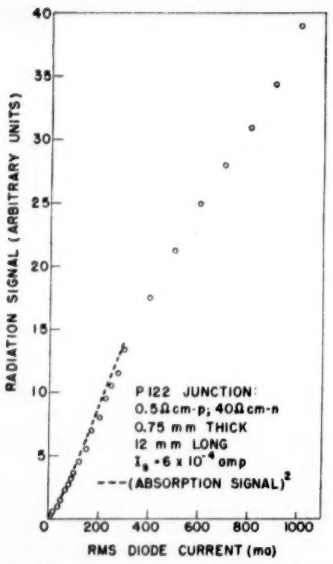

FIG. 3. Radiation signal as a function of diode current for injection into 40-ohm cm material. The dotted curve is the normalized square of the absorption signal obtained from the same diode.

Figure 2 shows typical radiation signal *vs* current data for a diode in which injection took place into doped material. It is essentially a linear relationship. This is understandable on the basis of simple diode theory. A calculation based on the observed reverse saturation current indicates that for forward currents up to the order of 1.5 amperes (rms) the majority carrier density will remain essentially constant. In other words, using the language of chemical kinetics, the expected bimolecular reaction, which produces the radiation, will operationally appear as first order in the minority carrier density, which is indeed what is observed.

In contrast to this case, it was anticipated that a study of the radiation *vs* current curve for injection into almost intrinsic material might yield more direct evidence for the bimolecular process. However, as Fig. 3 shows, the radiation *vs* current data for this case again gives an essentially linear relationship. As pointed out in I, simple diode theory can not be expected to apply for the range of currents used here. If the interpretation of the data for the absorption of injected carriers is correct, then a nonlinear relationship between injected carrier density (equals total carrier density for regions of interest) and current is indicated. As was suggested in I, empirically, the square of the carrier density, as observed by optical absorption, is linear with current. This is shown as the dotted curve of Fig. 3. In consequence, the radiation would then be expected to be also linear with current if it arises from the bimolecular process. For both classes of injection, negative departures from linearity would be expected at higher-current levels.

As an interesting sidelight to the recombination problem, it has been observed that changes in the radiation signal could be produced by introducing a large magnetic field (20 kilogauss) perpendicular to the direction of current flow. When the magnetic field deflected carriers away from the surface seen by the detector, increases in radiation signal as large as 30 percent could be observed. Conversely, when the field deflected carriers toward the surface seen by the detector, decreases as large as 40 percent could be observed. The percent changes in signal showed a dependence on the current level. However, because the effect was rather poorly reproducible in its quantitative detail, this dependence was not studied as fully as would have been desirable. The experiment may be considered an optical analog of the Suhl effect. The changes in signal level presumably result from changes in the ratio of radiative to nonradiative recombinations.

Germanium has a refractive index of approximately 4. This implies that all radiation seen external to a plane surface was originally directed within a cone whose axis is the surface normal and with a 14.5° half-angle. All other radiation is totally reflected. Using Snell's Law, one can calculate how the radiation within the cone is dispersed on passing through the surface. The intensity of radiation in a given plane of refraction and at a fixed distance from the radiating diode should be proportional to $\cos\psi/\cos\phi(T_p+T_s)$, where ψ is the angle of external refraction, ϕ the angle of interior incidence, and T_p and T_s are the transmission coefficients for light polarized, respectively, parallel and perpendicular to the plane of incidence. The experimental data are satisfactorily fitted by this relationship.

Radiation emerging from the germanium at angles of refraction differing from 0° is polarized by the refraction. At the Brewster angle (~75°) the ratio T_p/T_s is calculated to be 4.5. For a diode which, just prior to measurement had received a metallographic polish, the value 3.3 was observed as the ratio of the intensities of parallel and perpendicular components at the Brewster angle. The discrepancy between the observed and calculated ratio is perhaps the result of the visible slight imperfections which remained in the surface after the polishing. No great pains were taken to see how high a ratio could be obtained. It is of interest to note that the polarization ratio for a diode that had been lying around the laboratory for several weeks could be raised from 1.3 to 2.5 by chemical etching. This implies the presence of a surface film of at least 1000A thickness prior to the etch. The film may have been accidentally acquired. Rank and Cronemeyer[4] report a related phenomenon.

It is a pleasure to acknowledge the assistance of R. L. Watters, who designed the amplifier used in this work and that of the preceding paper. Dr. R. N. Hall was an agreeable source of samples and ideas, both of high quality.

[4] D. H. Rank and D. C. Cronemeyer, Phys. Rev. **90**, 204 (1953).

Current Carrier Lifetimes Deduced from Hall Coefficient and Resistivity Measurements

L. P. HUNTER, E. J. HUIBREGTSE, AND R. L. ANDERSON
Research Department, International Business Machines Corporation, Poughkeepsie, New York

(Received June 9, 1953)

The conventional expression for the Hall coefficient in semiconductors is based on the assumption of an infinite rate of carrier recombination. If the latter assumption is not made, diffusion currents are present which change the value of the Hall coefficient. It is this change in the Hall coefficient which forms a basis for an independent measurement of carrier lifetime. Methods for obtaining the value of a parameter m which contains the bulk lifetime τ and the surface recombination velocity s are described. Lifetimes, as deduced from Hall measurements, compare reasonably well to lifetimes obtained on the same samples by injection methods.

THE theory of Landauer and Swanson[1] provides a basis for the deduction of current carrier lifetimes from Hall coefficient and resistivity measurements. The essential effect given by this theory is the shifting of the intrinsic value of the Hall coefficient with lifetime. In the conventional plot of the logarithm of the Hall coefficient against the reciprocal of the absolute temperature, this shows up as a shifting of the intrinsic Hall coefficient line with the change in lifetime. The maximum shift permissible in the Hall coefficient for infinitesimal and infinite lifetimes is shown in Fig. 1, which has been drawn for the particular case of 10^{14} donor impurities per cm^3.

The theory[1] expresses the Hall coefficient R as $R=R_L+R_D$, where R_L is the usual Hall coefficient and R_D is that portion of the true Hall coefficient due to the diffusion of carriers having finite lifetime. R_D may be expressed as the product of a coefficient m containing the surface recombination velocity s and bulk lifetime τ as parameters, and an expression $\mathfrak{R}$ which is a function only of the mobilities and carrier concentrations. The coefficient m lies between zero and one for any combination of surface recombination velocity and bulk lifetime. For $m=0$, either the surface recombination velocity is infinite or the bulk lifetime is zero. For $m=1$, s must be zero and τ infinite.

In the intrinsic range ($n=p=n_i$) the usual Hall coefficient R_{Li} is given by

$$R_{Li}=\frac{1}{en_i}\frac{1-b_Hb}{(b+1)^2}\frac{\mu_{Hp}}{\mu_p}, \tag{1}$$

and the diffusion term is given by

$$\mathfrak{R}_i=\frac{1}{en_i}\frac{(b-1)(b_H+1)}{2(b+1)^2}\frac{\mu_{Hp}}{\mu_p}, \tag{2}$$

which combined give the total Hall coefficient,

$$R_i=\frac{1}{en_i}\frac{\mu_{Hp}}{\mu_p}\left[\frac{(1-b_Hb)}{(b+1)^2}+\frac{m}{2}\frac{(b_H+1)(b-1)}{(b+1)^2}\right], \tag{3}$$

where b and b_H are, respectively, the drift and Hall electron-to-hole mobility ratios, μ_p and μ_{Hp} are the drift and Hall hole mobilities, n_i is the number of either holes or electrons, and e is the electronic charge in coulombs. To illustrate the importance of the effect of lifetime on the intrinsic Hall coefficient, we will form the ratio $R_{i\epsilon}/R_{i\infty}$ where $R_{i\epsilon}$ represents the Hall coefficient for infinitesimal total lifetime [$m=0$, in Eq. (3)], and $R_{i\infty}$ represents the Hall coefficient for infinite total lifetime [$m=1$, in Eq. (3)]. This ratio becomes

$$\frac{R_{i\epsilon}}{R_{i\infty}}=\frac{2(1-b_Hb)}{(b+1)(1-b_H)}. \tag{4}$$

At 300°K our best values for germanium for b and b_H are, respectively, 2.0 and 1.3, substituting these in Eq. (4) gives a ratio of 3.5. Since b and b_H are functions of temperature, the ratio $R_{i\epsilon}/R_{i\infty}$ is also a function of temperature. This effect may be used directly to determine the lifetime of the current carriers in a given semiconductor specimen provided the Hall and drift mobility ratios are known. The drift mobility ratio may be obtained directly from the resistivity curve,[2] and the Hall mobility ratio may be obtained from the infinitesimal lifetime Hall coefficient curve in combination with the resistivity curve, as will be shown later.

One convenient way of using this shift directly is to form the ratio of the intrinsic Hall mobility to the extrinsic Hall mobility extrapolated to a common temperature. The intrinsic Hall mobility μ_{Hi} is given by

$$\mu_{Hi}=R_i/\rho_i=\mu_{Hp}\left[\frac{1-b_Hb}{b+1}+\frac{m}{2}\frac{(b_H+1)(b-1)}{b+1}\right]. \tag{5}$$

Here $\mu_{Hp}=R_p/\rho_p$ is the extrinsic Hall mobility for a P-type sample. The desired ratio for a P-type sample is then

$$r_p=\frac{\mu_{Hi}}{\mu_{Hp}}=\frac{R_i\rho_p}{\rho_iR_p}=\frac{1-b_Hb}{b+1}+\frac{m}{2}\frac{(b_H+1)(b-1)}{b+1}. \tag{6}$$

For an N-type sample the extrinsic Hall mobility is given by

$$\mu_{Hn}=R_n/\rho_n=b_H\mu_{Hp}. \tag{7}$$

[1] R. Landauer and J. Swanson, Phys. Rev. **91**, 555 (1953).

[2] L. P. Hunter, Phys. Rev. **91**, 579 (1953).

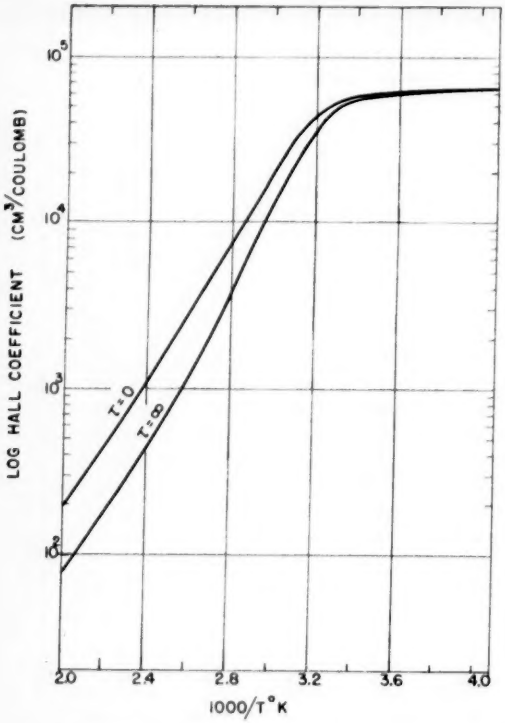

FIG. 1. The extreme positions permissible for the Hall coefficients as functions of temperature are plotted from the theoretical equations corresponding to infinitesimal and infinite lifetimes, using an impurity concentration of 10^{14} donors per cm³.

The desired ratio for an N-type sample is then

$$r_n=\frac{\mu_{Hi}}{\mu_{Hn}}=\frac{R_i\rho_n}{\rho_i R_n}=\frac{1}{b_H}\left[\frac{1-b_H b}{b+1}+\frac{m}{2}\,\frac{(b_H+1)(b-1)}{b+1}\right]. \quad (8)$$

In Fig. 2 is shown the method of measuring the ratio μ_{Hi}/μ_{Hn}. The quantities R_n and ρ_n are extrapolated from the extrinsic range, and the R_i and ρ_i are extrapolated from the intrinsic range. At any temperature in the range where these extrapolations are sufficiently accurate, the ratio may be computed.

In Fig. 3 is given a chart from which the coefficient m may be determined if the temperature and the mobility ratio r_p or r_n are known. The chart of Fig. 3 was prepared using $b_H=1.30$ and $b=2.0$ at 300°K. The temperature dependences of b and b_H were taken as $T^{0.8}$ since the best data to date indicate a $T^{-1.5}$ dependence for both μ_{Hn} and μ_n, and a $T^{-2.3}$ dependence for both μ_{Hp} and μ_p.[3] After m is found the problem still remains to determine the contributions of surface recombination and bulk recombination to m. If it is known that surface recombination is negligible then m depends on the bulk lifetime τ through the equations,

$$m=\frac{2}{\beta w}\tanh\left(\frac{\beta w}{2}\right), \quad (9)$$

where

$$\beta^2=\frac{1}{\tau}\,\frac{e}{kT}\,\frac{bn+p}{b(n+p)}\,\frac{1}{\mu_p}=\frac{1}{\tau D}.$$

If the bulk recombination is negligible,

$$m=2D/sw, \quad (10)$$

under the approximations $2D<st$ and $t<w$, where t is sample thickness and w the width. If the coefficient m is determined by both s and τ and if the sample is rectangular, there is no way of distinguishing s and τ without auxiliary experiments.

Using the ratio r_n or r_p as a measure of the intrinsic-line displacement requires data taken to sufficiently high temperatures to fix the position and slope of the intrinsic line well enough for extrapolation. Going to such temperatures is sometimes inconvenient and at best gives inaccurate values of τ in the one-microsecond range. In Table I is shown some data taken on an N-type sample.

The values of m shown in this table show a smooth trend. This is to be expected since they are the results of three smooth extrapolations. The accuracy of R_n

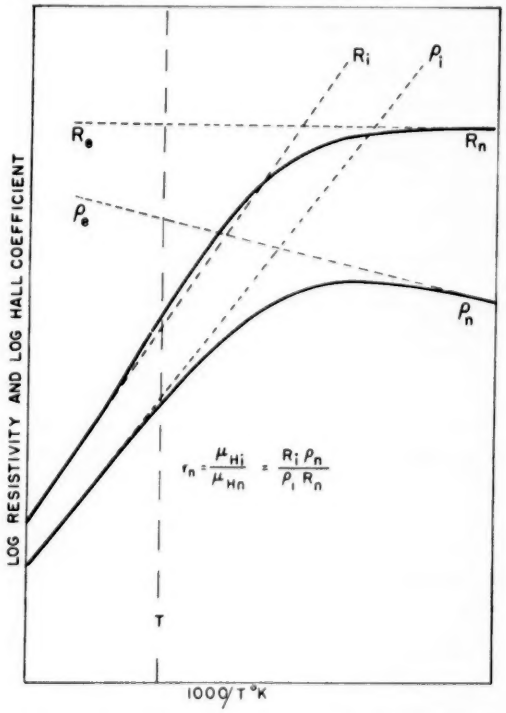

FIG. 2. Extrapolation method used to determine the Hall mobility ratio r_n. $r_n=\mu_{Hi}/\mu_{Hn}$.

[3] M. B. Prince, Bull. Am. Phys. Soc. **28**, No. 2, 10 (1953).

and R_i individually rest upon the accuracy of the magnetic field measurement, but their quotient is independent of the field measurement. The ρ_i extrapolation is very well established since it is the average of many samples. Therefore, the final accuracy is limited by the ρ_n and R_i extrapolations. These would seem to give no better than ± 0.1 to the value of m. Such an uncertainty in m still yields reasonably good values for τ in the 10-to-100-microsecond range.

In order to get away from these relatively inaccurate extrapolations, it will be shown that the shift in the temperature of the Hall coefficient taken at some arbitrary factor c, below the extrinsic value can be related to the coefficient m. Also, it will be shown that if a sample is prepared for which $m=0$, the Hall mobility ratio b_H can be found by measuring the ratio of the extrapolated extrinsic resistivity to the measured resistivity at the temperature where $R=R_n/c$.

First, considering an N-type sample, we will derive a formula for b_H. The defining equations are

$$\left.\begin{aligned} -R_n &= \frac{\mu_{Hn}}{\mu_n}\frac{1}{eN}, \\ \sigma_n &= eNb\mu_p, \\ R_0 &= \frac{\mu_{Hp}}{\mu_p}\frac{1}{e}\frac{p-nbb_H}{(p+nb)^2}, \quad (m=0), \\ \sigma &= e(p+nb)\mu_p, \end{aligned}\right\} \tag{11}$$

The ratio of resistivities r_c is defined as

$$r_c=\rho_n/\rho=\sigma/\sigma_n=(p+nb)/Nb, \tag{12}$$

and the factor c is defined by

$$c=\frac{R_n}{R_0}=-\frac{\mu_p}{\mu_{Hp}}\frac{\mu_{Hn}}{\mu_n}\frac{(p+nb)^2}{N(p-nbb_H)}, \tag{13}$$

or

$$-\frac{c}{br_c}=\frac{b_H}{b}\frac{(p+nb)}{(p-nbb_H)}, \tag{14}$$

by eliminating N between (12) and (13). Solving (14) for b_H we get

$$b_H=\frac{p}{nb-(r_c/c)(p+nb)}. \tag{15}$$

From the defining Eqs. (11) and (12) and the relation

TABLE I. Data and results of r_n and m for an N-type sample from extrapolation method.

$T°K$	$1000/T$	$10^{-4}R_i$	ρ_i	$R_n\times10^{-4}$	ρ_n	r_n	m
312	3.2	3.70	26.2	4.20	12.8	0.43	0.00
322	3.1	2.28	17.0	4.20	13.5	0.43	0.04
333	3.0	1.39	11.0	4.20	14.1	0.43	0.12
345	2.9	0.86	7.05	4.20	14.9	0.43	0.16
357	2.8	0.53	4.55	4.20	15.7	0.44	0.20
370	2.7	0.32	2.92	4.20	16.6	0.44	0.28

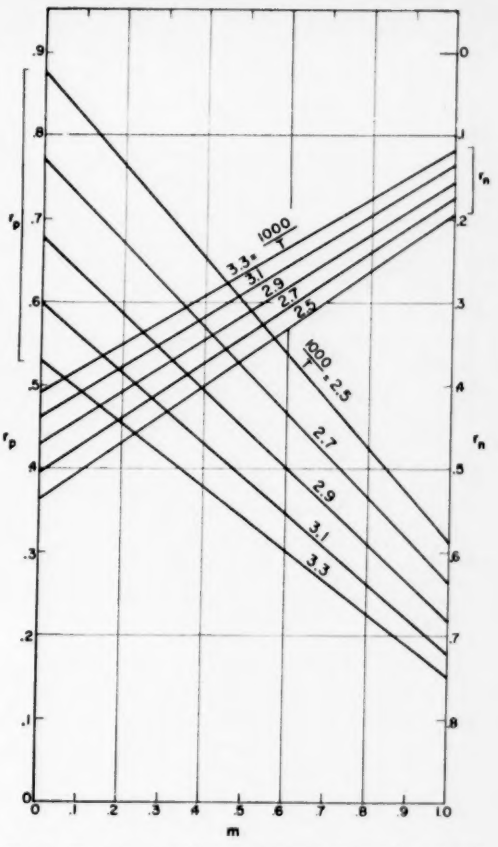

FIG. 3. Chart from which m is obtained after r_n (or r_p) and the temperature have been determined.

$n=N+p$, we find

$$p=\frac{Nb(r_c-1)}{b+1}, \quad n=\frac{N(br_c+1)}{b+1}. \tag{16}$$

When Eqs. (16) into (15) are substituted, we get the desired equation for b_H,

$$b_H=\frac{r_c-1}{br_c+1-(r_c^2/c)(b+1)}. \tag{17}$$

In the case of a P-type sample, the equation for b_H is

$$b_H=\frac{b+r_c-(r_c^2/c)(b+1)}{b(r_c-1)}. \tag{18}$$

For a P-type sample at the Hall zero, c can become infinite while r_c remains finite. In this case the equation for b_H becomes[4]

$$b_H=\frac{b+r_\infty}{b(r_\infty-1)}. \tag{19}$$

[4] For comparison see W. Shockley, *Electrons and Holes in Semiconductors* (D. Van Nostrand and Company, New York, 1950). Problem 7, page 218.

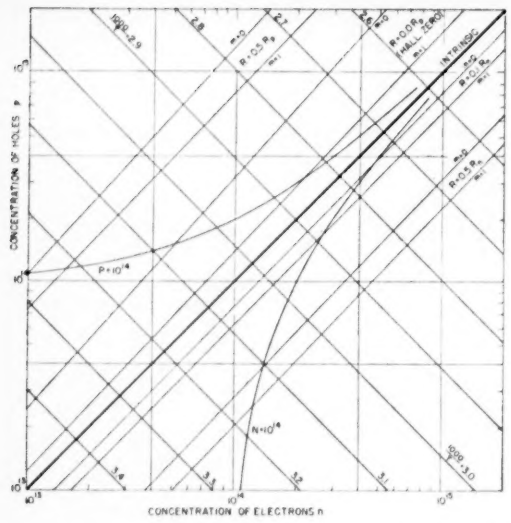

FIG. 4. Chart used to determine m from the extrinsic Hall coefficient R_n and the temperature at which the Hall coefficient R is a desired fraction c of R_n. ($c=R_n/R$) Curves for $m=0$ and $m=1$ are shown for $c=2$ and $c=10$ for N-type samples, and for $c=2$ and $c=\infty$ for P-type samples.

When Eqs. (17), (18), or (19) are used for determining b_H, it is essential that they be applied only to data taken on samples for which m is substantially zero. This may be accomplished by grinding the surfaces so that the surface recombination velocity exceeds 20 000 cm per second. Under such conditions the error in r_c, due to the nonzero value of m, will be less than 3 percent. Some values of b_H determined in this manner are given in Table II. It was found that higher values of c gave progressively lower values of b_H. This might be an indication that m increases as one approaches the intrinsic range. The results of Table I seem also to bear this out. If such is the case, it provides an additional source of error in extrapolating the intrinsic range and gives us a strong reason for using a nonextrapolation method for determining m.

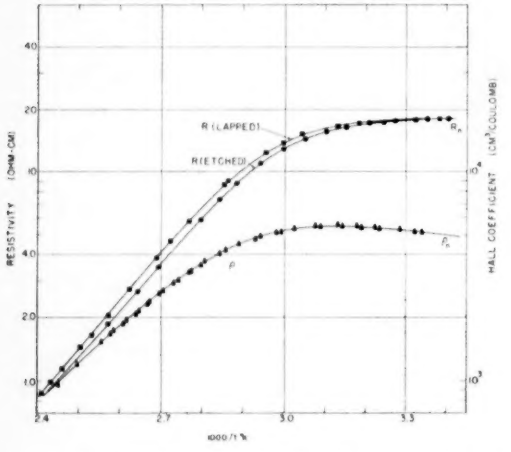

FIG. 5. The resistivity and Hall coefficients of a typical sample (W7-E) showing the shift in the Hall coefficient due to surface treatment.

We will now consider the variation with m of the temperature of the Hall coefficient taken at the arbitrary factor c below the extrinsic value. The general equation for the Hall coefficient is

$$R=\frac{1}{e}\frac{\mu_H}{\mu_p}\left[\frac{p-nbb_H}{(p+nb)^2}+m\frac{(b-1)(b_H+1)np}{(p+nb)^2(n+p)}\right]. \quad (20)$$

For an N-type sample, and $c=R_n/R$ as before, we find

$$\frac{b_H}{bc}=\frac{n-p}{(nb+p)^2}\left[(nbb_H-p)-m\frac{(b-1)(b_H+1)np}{n+p}\right]. \quad (21)$$

Substituting $n_i^2=np$ and solving for n, we get

$$n=\frac{cb}{b_H}\frac{n_i^2(n_i^2-p^2)}{(n_i^2b+p^2)^2}\left[\frac{n_i^2bb_H-p^2}{p}-m\frac{(b-1)(b_H+1)n_i^2p}{n_i^2+p^2}\right]. \quad (22)$$

A plot of Eq. (22) is given in the chart of Fig. 4. Since

$$n_i^2=(2\pi mkT/h)^3e^{\Delta E/kT}, \quad (23)$$

we may associate a given value of $1/T$ with a given n_i^2 using the intrinsic-resistivity curve. The lines of constant $1/T$ are also lines of constant n_i^2. To the right of the intrinsic line are shown two sets of m-parameter lines. One set for $c=2$, the other for $c=10$. Cutting across these lines is a line representing an N-type sample with 10^{14} donors per cc. It is seen that $0.1R_n$ Hall coefficient shifts $1000/T$ from 2.750 to 2.882 (16.5°C) for a change from zero to infinite lifetime. The $0.5R_n$ Hall coefficient changes 5.8°C for the same range of lifetime. Since the 0.1 factor coefficient lies much nearer to intrinsic than does the 0.5 factor coefficient, it is safer to use the latter for lifetime determination.

An equation similar to (22) can be plotted for the P-type side of the chart and the lines at the upper left of Fig. 4 represent $R=0.5R_p$. It was felt to be advantageous also to plot the conditions for the zero of the Hall coefficient. Accordingly, the equations

$$nbb_H=p \quad \text{or} \quad n=n_i/(bb_H)^{\frac{1}{2}}$$

for $m=0$, and

$$nb_H=p \quad \text{or} \quad n=n_i/(b_H)^{\frac{1}{2}} \quad (24)$$

for $m=1$, are plotted to the left of the intrinsic line in Fig. 4. Cutting across these lines is the curve of a P-type sample with 10^{14} acceptors per cm³. The $(1000/T)$ shift of the Hall zero for the complete lifetime range is seen

to be 0.221 corresponding to the temperature shift of 25.3°C.

In principle, the m value of a particular sample may be obtained from the chart of Fig. 4 by measuring the temperature of the Hall coefficient at some appropriate c factor and marking it off on the curve of that particular sample plotted on the chart. A specific sample curve may be plotted by determining, for example, the N from the extrinsic R_n and ρ_n, and using the condition of space-charge neutrality, $n=N+p$. The absolute value of m, so determined, has been found to be good to about ± 0.1. If it is desired to measure m with greater accuracy, it is necessary to measure the temperature shift of the appropriate c-factor Hall coefficient between a sample condition of known $m=0$ and the unknown condition. Such a shift is shown in the data of Fig. 5.

The sample represented by the data of Fig. 5 was measured in both a lapped and etched condition. In the lapped condition the recombination velocity on the edge surfaces was sufficient to keep the $m=0$.[5] The $\Delta(1000/T)$ between the lapped and etched conditions is found to be 0.0274 at $R=0.5R_n$. In order to determine precisely the values of m corresponding to the measured $\Delta(1000/T)$ values, the following approximate relations have been worked out for germanium in the temperature range 300°K to 400°K. For

$$\begin{aligned} &R=0.5R_n, \quad m=3.47(1000/T+2.00)\Delta(1000/T);\\ &R=0.1R_n, \quad m=4.47(1000/T-1.10)\Delta(1000/T);\\ &R=0.5R_p, \quad m=7.70(1000/T-0.487)\Delta(1000/T);\\ &R=0.0R_p, \quad m=0.531(11.50-1000/T)\Delta(1000/T). \end{aligned} \tag{25}$$

From the measured temperature and $\Delta(1000/T)$ values and the use of the equation for $R=0.5R_n$, we find $m=0.44$. The value of the surface recombination rate s computed from Fig. 6 is 370 cm/sec. This checks very closely the value obtained by drift measurements on the same sample.

For convenience curves of sw and τ/w^2 against m are plotted in Fig. 6. The approximation involved in the sw curve is that the effects of the recombination on the Hall probe surfaces predominates over all other recombination effects either surface or bulk. Careful consideration will show that this is true over a wide range of conditions of normal samples. The approximation involved in the τ/w^2 curve is that all surface recombination effects are negligible compared to the bulk recombination effect.

In Table III a comparison is given between results calculated from Hall measurements and drift-lifetime measurements made on several samples. A temperature dependence of the drift lifetime was noted, and the values compared with the Hall measurements are obtained by extrapolation to the temperature of the Hall measurement. This was always a short extrapolation.

[5] In this measurement (unlike a drift measurement) there can be no deviation from equlibrium conditions within the sample if the s on the Hall probe surfaces is large enough.

TABLE II. Values of b_H, calculated at the temperature indicated, for four samples of different resistivity and conductivity type.

Sample	Type	T°K	$1000/T$	c	r_c	b	b_H
W9-B	N	356	2.81	1.5	1.31	2.25	1.35
W2-3	N	322	3.11	1.5	1.31	2.10	1.41
W3-3	P	347	2.88	1.5	1.165	2.22	1.39
W7-E	N	340	2.94	1.5	1.31	2.18	1.35

In general, if there is a barrier under the Hall probes, one expects a floating potential in addition to the voltage due to the diffusion currents under consideration. If there is no barrier, the diffusion current voltage should be zero. These effects might be expected to be appreciable,[6] but the agreement shown in Table III seems to indicate that for normal point contact probes they are not very large.

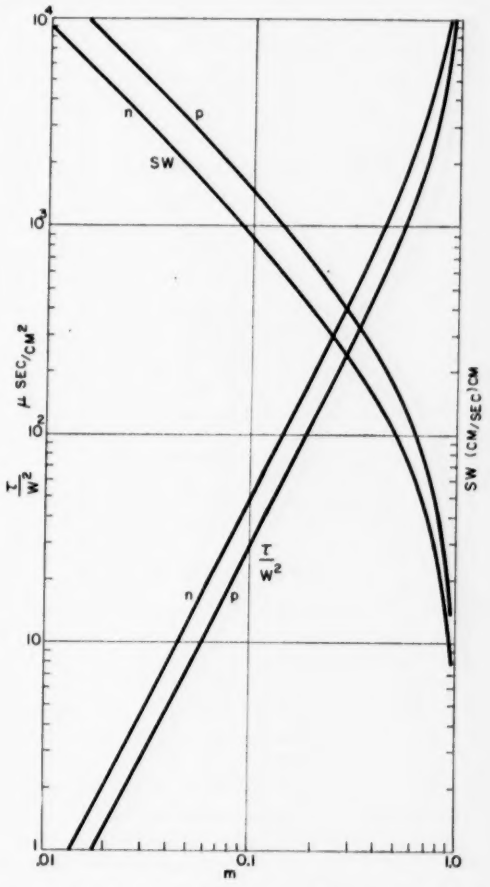

FIG. 6. Chart used to determine bulk lifetime τ or surface recombination velocity s from the previously determined value of m and the width w of the sample.

[6] J. Swanson (private communication).

TABLE III. Comparison of lifetimes as obtained from Hall and drift measurements on four representative samples.

Sample	Type	Measurement	$\Delta(1000/T)$	m	τ μsec	s cm/sec	Drift measurement τ μsec	Drift measurement s cm/sec
W3-3	P	$R=0.0R_p$	0.0075±0.001	0.036±0.005	0.48±0.1		<1	
W7-E	N	$R=0.5R_n$	0.025 ±0.003	0.44 ±0.05		370±70		450±30
W3-5	P	$R=0.5R_p$	0.0055±0.001	0.10 ±0.01	2.0 ±0.3		~2	
W12B-4	N	$R=0.5R_n$	0.020 ±0.003	0.35 ±0.05	35±5		32±5	

CONCLUSIONS

Current carrier lifetime can be deduced from Hall coefficient and resistivity measurements without recourse to the injection of excess minority carriers or the measurement of short time intervals. For reasonable sizes of samples this method allows the measurement of lifetimes in the 0.1μsec range, and will detect changes in lifetime of the order of 0.01μsec. On the other end of the range it will measure a 1000μsec lifetime to about 10 percent and will just distinguish the difference between ∞ life and 10^4μsec. Its chief advantage lies in the measurement of very short lifetimes.

In using this method the best procedure is to use a c factor as small as possible, so that any changes in lifetime associated with the intrinsic region will be minimized.

The authors wish to acknowledge their indebtedness to J. A. Swanson and R. W. Landauer for many helpful discussions, to H. Fleisher for drift-lifetime measurements, and to B. E. Montgomery and V. M. Palmer for many of the accurate measurements involved.

PHYSICAL REVIEW VOLUME 91, NUMBER 6 SEPTEMBER 15, 1953

Brillouin Zone Investigation of Mg Alloys. I. Hall Effect and Conductivity

A. I. SCHINDLER AND E. I. SALKOVITZ
Naval Research Laboratory, Washington, D. C.

(Received April 23, 1953)

The Brillouin zone structure of hexagonal metal, in particular magnesium as calculated by Jones, has been examined by Hall measurements. The theory predicts a strong dependence on alloying, and the Hall data obtained on alloys of magnesium with aluminum or silver seem to corroborate Jones' theory. In the case of the silver alloys, the absolute value of the Hall constant decreases linearly as a function of alloying addition (0.1 at percent silver decreases the Hall constant by 5 percent). In the aluminum alloys the effect is not so great (0.1 at percent aluminum decreases the Hall constant by ~2 percent) and a break in the Hall constant *versus* composition curve is detected. This break can be interpreted as being due to Brillouin zone overlap in the c direction.

Familiar conductivity rules for alloys are examined in the light of Jones' theory and it is shown that deviations from these rules are to be expected for the alloys of divalent hexagonal metals. A broad experimental program is outlined.

I. INTRODUCTION

ALTHOUGH the electronic structure of the metals in the first column of the periodic table may be regarded as rather satisfactorily established, this is not the case for the divalent hexagonal metals of the second column. More data on the properties of these metals and their alloys are necessary to develop theories concerning their general behavior.

Figure 1 shows the first Brillouin zone for pure close-packed hexagonal magnesium as deduced by Jones.[1] The density of states as suggested by Mott[2] is given in Fig. 2. The Brillouin zone is bounded by {0002}, {1100}, and {1101} faces. Since this prism can contain only 1.743 states/atom, Jones has added the 6 truncated prisms to the A faces such that 2 states/atom are available. Consequently in pure magnesium, overlap takes place in the a direction into these prisms but not in the c direction. The calculations show that there is no energy discontinuity at the edges labeled Q.

Jones has also shown that small overlap across the boundary surface of a Brillouin zone compresses the zone in the direction perpendicular to the surface concerned, resulting in an expansion in this direction in the real lattice. When silver is added to magnesium, the average electron-atom ratio for the alloy is reduced and there is less overlap in the a direction relative to pure magnesium. Consequently a contraction in this direction should occur in the real lattice in addition to any contraction due only to the size effect of the ions. This has been found to be the case by actual x-ray

[1] H. Jones, Proc. Roy. Soc. (London) **A147**, 400 (1934); Physica **15**, 13 (1949); Phil. Mag. **41**, 663 (1950).
[2] W. Hume-Rothery, *Atomic Theory for Students of Metallurgy* (Institute of Metals, London, 1948), Chap. XXVIII.

measurements.[3] Raynor has also found that when indium which has 3 outer electrons is added to pure magnesium, the c parameter decreases (due to size effect) up to 0.75 atomic precent addition. Beyond 0.75 percent the c parameter increases. The explanation appears to be that at an electron-to-atom ratio of 2.0075 the truncated prisms have been filled and overlap begins to occur in the c direction in the Brillouin zone.

II. HALL EFFECT

The experimental corroboration of the Brillouin zone theory for magnesium so far has come from x-ray data alone. A more direct approach to the study of Brillouin zone overlap can be achieved by examining the effect of alloying on the Hall constant. The effects that should be observed are outlined below and preliminary results on dilute magnesium alloys containing silver and aluminum are presented.

One can write

$$R=-\left|\frac{1}{e}\right|\left\{\frac{n_1\mu_1{}^2-n_2\mu_2{}^2}{(n_1\mu_1+n_2\mu_2)^2}\right\}, \qquad (1)$$

where R is the Hall constant, μ is the mobility, and n is the number of charge carriers per cc, and subscripts 1 and 2 refer to electrons and holes, respectively.

In pure magnesium because of the overlapping Brillouin zone, the configuration of the 3*s* electrons is such that conduction must be considered a two-zone process. Further, since pure magnesium has a negative Hall constant the process is one in which electron conduction predominates. In such a two-zone system, the effect of changing the relative number of electrons to holes upon the Hall constant will depend on the relative values of their mobilities.Without the latter information, it is impossible to separate the effects due to either electrons or holes.

If magnesium is alloyed with elements of Column I, the effect would be to reduce the size of the Fermi sphere, and should cause a decrease in the number of overlap electrons and an increase in the number of holes. Alloying magnesium with elements of Column III or IV should have an opposite effect. As stated above, the sign of the change of the Hall constant in magnesium resulting from alloying cannot be predicted without prior knowledge of the charge carrier mobilities. However, as elements of Column III or IV are added to magnesium a point will be reached where overlap will take place across the B faces in the c direction (see Fig. 1). At this composition, some abrupt change in the Hall constant *versus* composition curve would be expected, since the effect resulting from holes would change abruptly.

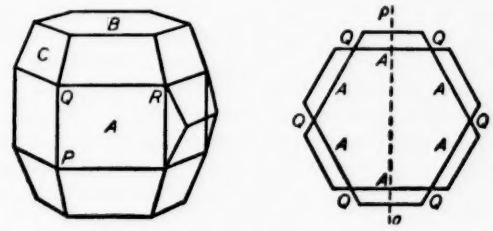

FIG. 1. (a) First Brillouin zone of magnesium as proposed by H. Jones. (b) Equatorial section of (a).

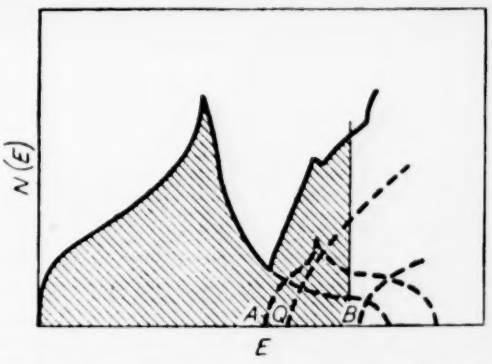

FIG. 2. Density of states for magnesium as proposed by N. F. Mott.

Preliminary measurements have been made on pure magnesium and on magnesium alloys containing small amounts of aluminum or silver. They were kindly supplied to us by Professor Dorn of the University of California who had obtained them from the Dow Chemical Company. The measurements were carried out at room temperature using a technique described elsewhere.[4] The results are plotted in Fig. 3. The absolute value of the Hall constant is reduced by additions of either silver or aluminum. The magnitude of the changes (an addition of 0.1 at percent of silver changes the Hall constant by 5 percent) seems to verify the assumption that alloying changes the electronic configuration of magnesium rather radically, although the exact interpretation of the experimental results is not clear. The slope of the Hall constant curve *versus* composition for aluminum is not as steep as that for silver; the ratio of slopes is 2.4 to 1. The curve of the Hall constant for aluminum additions indicates a break between 1.3 and 1.8 at percent aluminum; but the break in the x-ray c/a curve is at 0.75 at percent as reported by Raynor.[3] Therefore the Hall measurements were repeated. The last point was reproducible to within 1 percent but the point for 1.3 percent aluminum was less reproducible and seemed to be temperature dependent which may be the result of overlap occurring as a result of thermal heating.[5]

[3] W. Hume-Rothery and G. V. Raynor, Proc. Roy. Soc. (London) **A177**, 27 (1940); G. V. Raynor, Proc. Roy. Soc. (London) **180**, 107 (1942); R. S. Busk, Trans. Am. Inst. Mining Met. Engrs. **188**, 1460 (1950).

[4] Albert I. Schindler and Emerson M. Pugh, Phys. Rev. **89**, 295 (1953).

[5] It should be noted that Raynor did not make x-ray measurements between 0.75 and 2 at percent.

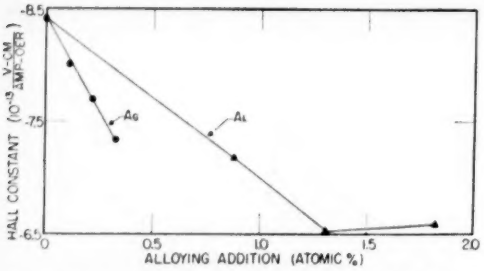

FIG. 3. Hall constant as a function of alloying additions.

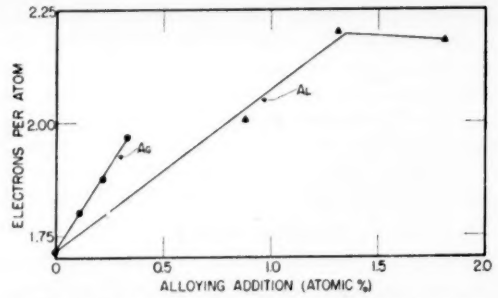

FIG. 4. The number of electrons per atom as a function of alloying additions.

In Fig. 4, the number of electrons per atom is calculated assuming a one-zone system (in which only the electrons are conducting). The calculations then show magnesium to have 1.74 electrons per atom. The correct calculations for the number of holes as well as the number of electrons requires a knowledge of their respective mobilities.

III. CONSIDERATIONS OF CONDUCTIVITY RULES

Speculations may be made concerning the electrical resistivity of dilute magnesium alloys. Linde's rule states that the increase in resistivity of a metal per atomic percent addition of a second metal, aside from an additive constant, is proportional to $(\Delta Z)^2$, the square of the difference in valences of the two metals concerned. This rule was based on experiments with monovalent metal solvents. It received theoretical justification by Mott[6] whose theory treated the conduction electrons as though they were free and assumed only non-overlapping solvents. The validity of Linde's rule in the vicinity of Brillouin zone overlap is questionable and should be checked for divalent hexagonal metals.

For a dilute solid solution one usually writes the resistivity ρ as

$$\rho = m^*/Ne^2(p_t + p_0),$$

where m^*, N, and e are the effective mass, the number per unit volume, and the charge of the electron, respectively. p_t is the scattering probability in a pure metal arising from displacement of the atoms from their mean position due to thermal vibration and is therefore temperature dependent. p_0 is the scattering probability arising from perturbation to the periodic field when foreign atoms are introduced and is usually considered temperature independent. Normally the increase in resistivity due to the presence of a second metal is said to be due to p_0 which is proportional to $(\Delta Z)^2$.

An implicit assumption exists that the effect of temperature and alloying addition on the resistivity are separable and additive (p_0 is not temperature dependent and p_t is not dependent upon solute concentration). This may not be valid when the solvent is such that alloying additions change the amount of overlap and consequently the temperature dependence of the overlap. To our knowledge the dependence of scattering probability upon alloying addition as a function of c/a has not been studied. One would expect.

(1) p_t to be dependent upon c/a, and upon Brillouin zone overlap.

(2) p_0 to be temperature *dependent* near an overlap.

A corollary of Linde's rule is Matthiessen's rule, which states that the increase in resistance of a metal due to a small concentration of another metal in solid solution is independent of the temperature, or that $\partial\rho/\partial t$ (where t is temperature) is independent of concentration. By the above arguments p_t for hexagonal metals depends upon c/a and upon Brillouin zone overlap. Consequently $\partial\rho/\partial t$ should depend upon concentration in magnesium alloys.

In view of the results of the Hall measurements and in order to examine the validity of the conductivity rules, a broad experimental program has been outlined and is being undertaken. Hall and conductivity measurements are being made on an extended series of these alloys as a function of temperature. Measurements on single crystals will give the properties as functions of crystal orientation. If a similar program is conducted on alloys of other hexagonal metal, x-ray studies will be necessary to determine how the Jones theory applies when the anisotropy is different from that in magnesium.

[6] N. F. Mott, Proc. Cambridge Phil. Soc. **32**, 281 (1936).

A Two-Electron Example of Ferromagnetism*

J. C. SLATER, H. STATZ, AND G. F. KOSTER†
Massachusetts Institute of Technology, Cambridge, Massachusetts

(Received June 3, 1953)

We examine the problem of two holes in an otherwise filled band, or two electrons in an empty band, by the method of configuration interaction, using Wannier functions, asking which state lies lower, the triplet or singlet. If the triplet lies lower, it would indicate that the spins set themselves parallel, favoring ferromagnetism. We find that if the band is nondegenerate, the singlet will always lie lower, so that ferromagnetism requires a degenerate band, such as the fivefold degenerate *d* band. With a degenerate band ferromagnetism can arise under some circumstances, provided the band is not too broad. The cause of the ferromagnetism is an intra-atomic exchange effect, causing the two electrons or holes to prefer to align themselves with parallel spin when they happen to lie on the same atom. The model leads to a treatment of correlation, showing that with increasing interatomic distance the likelihood of finding the two electrons or holes on the same atom decreases, vanishing at infinite internuclear distance. The ferromagnetic interaction depends both on an intra-atomic exchange integral, which persists to infinite distance, and the probability of finding the electrons or holes on the same atom, which vanishes in the limit.

IN a recent paper,[1] one of the authors has outlined a general procedure for attacking problems in ferromagnetism from the point of view of the energy band theory. It is the purpose of the present paper to make a specific application of this method to a case simple enough to handle in detail, and yet close enough to physical reality to furnish useful information. First let us remind the reader of the essential features of the energy band theory of ferromagnetism. We start with an energy band partly filled with equal numbers of electrons of each spin, so that it is not magnetic, and ask whether the energy is increased or decreased if we reverse the spins of some electrons, so as to magnetize the system. If the energy increases, we assume that the system is nonmagnetic, while if it decreases it is ferromagnetic.

The energy will change for two reasons when we reverse the spin, according to the simple energy band theory. First, we shall have to increase the one-electron or Fermi energy of those electrons whose spins we reverse, for we lift them from the lower part of the band to previously unoccupied levels, which they must occupy on account of the exclusion principle when their spins are reversed. This increase of energy is proportional to the breadth of the energy band. Secondly, we decrease the exchange energy when we reverse the spins, for when we use a single determinantal wave function, as we do with the naive energy band theory, we have a sum of exchange integrals coming in with negative signs, between all pairs of electrons with parallel spins, and we increase the number of such pairs when we magnetize the crystal. The leading term in these exchange integrals is an intra-atomic integral, of the nature of the exchange integral between two electrons in a single atom in complex spectrum theory, and this does not depend greatly on interatomic distance. We then can draw two conclusions, one correct and the other incorrect, regarding the dependence on internuclear distance of the tendency toward ferromagnetism.

In the first place, at small enough internuclear distances, the energy bands will broaden so much that the increase in Fermi energy will more than balance the decrease in exchange energy, and the magnetized state will always lie above the nonmagnetized state. Thus, as pointed out by one of the authors previously,[2] we shall never be able to have ferromagnetism except for rather narrow energy bands, such as we have for the *d* electrons in the ferromagnetic elements. This conclusion from the simple energy band theory seems reliable. On the other hand, as the internuclear distance is increased, and the energy bands decrease to zero in width, the simple energy band theory would tell us that the magnetized state should have a lower energy than the nonmagnetized state by the amount of the exchange integrals, which as we have seen remain finite at infinite internuclear distance. This is clearly wrong, for it is obvious physically that at infinite internuclear distance it cannot make any difference to the energy whether the spins on the various atoms are parallel or not.

It is this error in the simple energy band theory which was discussed in reference 1, and it was shown there that to correct it it is necessary to carry out a configuration interaction between many states set up from energy band functions in the form of determinantal wave functions. This configuration interaction is similar to the one used in the hydrogen molecule, where we start by formulating the problem in terms of molecular orbitals, which disregard the correlation between electrons, but end up by superposing configurations in order

* Supported in part by the U. S. Office of Naval Research, in part by the Army, Navy, and Air Force.

† Staff member, Lincoln Laboratory, Massachusetts Institute of Technology, Cambridge, Massachusetts.

[1] J. C. Slater, Revs. Modern Phys. **25**, 199 (1953). See also Solid-State and Molecular Theory Group, Massachusetts Institute of Technology, Quarterly Progress Report, p. 17, July 15, 1952 (unpublished).

[2] J. C. Slater, Phys. Rev. **49**, 537, 931 (1936).

to build up a Heitler-London-like solution at infinite separation, with each atom electrically neutral, and no ionic character in the wave function. In other words, the configuration interaction must correct for the correlation energy effect. No detailed calculations of correlation energy were made in reference 1, but the object of the present paper is to carry through a special case, and to show that in fact we verify the conclusions of reference 1, removing the difficulties in the elementary energy band theory.

A similar calculation was carried out by one of the authors[3] for a special case rather far from the actual problem met in ferromagnetic materials, but the method employed there can be used in other cases as well, and is employed in the present paper. The problem considered in reference 3 was the following. We start with a band filled with electrons of positive spin, containing no electrons of negative spin, and then ask whether the energy is increased or decreased when the spin of one electron is reversed. The same features come into this problem which we have already mentioned: when the spin is reversed, the electron of reversed spin can fall from the highest energy level of the band of plus spin to the lowest energy level of the band of reversed spin, thus decreasing its Fermi energy, but at the same time the exchange energy is increased. The configuration interaction problem, however, is now simple enough so that we can handle it in detail. The initial state, of maximum multiplicity, must be handled by a single determinant, since there is no other way of arranging the electronic spins to give the same multiplicity, provided we use only the one-electron wave functions in the original energy band. The other state, with one reversed spin, must be treated by configuration interaction, but this can be done completely. This problem can be considered to consist of an electron, with negative spin, interacting with a hole of positive spin. The ordinary energy band solutions correspond to the case where the electron and hole separately wander through the crystal. There are special states, however, analogous to the states of an exciton, in which the electron and hole execute orbits around each other. The lowest of these exciton-like states is the lowest state of the problem of reversed spin, and its energy was shown in reference 3 to approach the energy of the state of maximum multiplicity, in the limit of infinite interatomic distance. The correlation takes the form, in this case, of the tendency of the electron and hole to associate into the bound orbital structure.

The actual calculation of reference 3 was carried out by means of Wannier functions.[4] These, as is well known, are localized atomic orbitals, located on the various atoms, orthogonal to each other, and each determined from one energy band. They form a complete orthogonal set of functions, so that any function of the coordinates of one electron can be expanded in terms of them. If $a_i(\mathbf{r}-\mathbf{R}_m)$ represents the Wannier function related to the ith energy band, located on the atom at $\mathbf{R}_m$, then any function of the coordinates of one electron can be written as $\sum(i, m)U_i(\mathbf{R}_m)a_i(\mathbf{r}-\mathbf{R}_m)$, where the U's are coefficients. If, as in reference 3, we assume that we need only consider electrons in a given band, we do not need to sum over i, and can use the a's only for the band concerned, so that the function reduces to $\sum(m)U(\mathbf{R}_m)a(\mathbf{r}-\mathbf{R}_m)$. Similarly if we have a function involving two electrons, or an electron and a hole as in reference 3, we can write the wave function in the form $\sum(i, j, m, n)U_{ij}(\mathbf{R}_m, \mathbf{R}_n)a_i(\mathbf{r}_1-\mathbf{R}_m)a_j(\mathbf{r}_2-\mathbf{R}_n)$, where $\mathbf{r}_1$, $\mathbf{r}_2$ represent the coordinates of the two electrons, and where again the summation over i and j drops out if both electrons are in the same band. The essence of the calculation involving Wannier functions is the fact that the coefficients $U(\mathbf{R}_m)$, or $U(\mathbf{R}_m, \mathbf{R}_n)$, behave very much like continuous functions of the variables $\mathbf{R}_m$, or $\mathbf{R}_m$, $\mathbf{R}_n$, though we are interested only in discrete values of these variables. The equations giving the U's are difference equations, which resemble differential equations and in some circumstances can be reduced to them, and these differential equations resemble Schrödinger's equations for free particles.

Using these methods, the solution of the configuration interaction problem for the case of reference 3 reduced essentially to a hydrogen-like problem of the stable states of a two-particle system consisting of an electron and a hole attracting each other. A separation of variables was possible, into coordinates of the center of mass and relative coordinates of the two particles. The separation of the motion of the center of mass corresponds to the conservation of the sum of the $\mathbf{k}$ vectors, or propagation vectors, of the particles. The motion of the relative coordinates reduces to the problem of a single particle in an attractive center of force, whose resemblance to the hydrogen problem is obvious. In reference 3, the problem was discussed both by means of the difference equation and the differential equation, similar results being obtained by both methods, but in the case of narrow bands, or large internuclear distances, the method of difference equations becomes more appropriate, and leads to exact results in the limit of infinite internuclear distances. It was in this way that rigorous proofs could be given that the energies of the lowest states of different multiplicity coincide at infinite separation. At smaller distances, it was shown in reference 3 that ferromagnetism was not excluded, until the distance became so small that the energy bands broadened to the extent where the elementary energy band theory indicated that ferromagnetism was impossible. In reference 3, however, it was not possible to state positively whether ferromagnetism would or would not occur in any definite case.

We now are ready to state the problem which is discussed in the present paper. This is one in which we have a crystal lacking just two electrons from an

[3] J. C. Slater, Phys. Rev. **52**, 198 (1937).
[4] G. H. Wannier, Phys. Rev. **52**, 191 (1937); see also J. C. Slater, Phys. Rev. **76**, 1592 (1949).

otherwise filled band. This could, for instance, represent in a simplified way a copper-nickel alloy of such composition that the d band was filled except for two electrons, the remaining electrons being in the $4s$ states, which we disregard. We ask a simple question: would the system have lower energy if the two holes set themselves with their spins parallel, as we should expect in a ferromagnetic case, or antiparallel? This problem, being again a two-particle problem, can be handled by Wannier functions in a convenient way. We again can separate variables into the coordinates of the center of mass of the two holes, and the relative coordinates. Now, however, the two holes will repel each other, unlike the hole and electron which attracted each other in the case of reference 3, and they will not form a stable "atom." This avoidance of like charges on account of Coulomb repulsion is the way in which correlation comes into the present problem, just as the attraction of unlike charges to form bound "atomic" states was a manifestation of correlation in the case treated in reference 3. Fortunately in the present case, in contrast to that of reference 3, the sign of the energy difference between the magnetic and nonmagnetic states can sometimes be found by fundamental methods, and is not dependent on the evaluation of any exchange integrals or other numerical calculations.

We find in the first place that if the band under consideration is not degenerate, the lowest state will always be one in which the spins of the two holes are opposite to each other, so that we shall always expect a nonmagnetic system. The argument behind this conclusion is simple. In a problem involving two electrons, or two holes, the system will form singlets when the spins are antiparallel, triplets when they are parallel. The part of the wave function involving coordinates will be symmetric in the two electrons for singlets, antisymmetric for triplets. When we separate off the problem involving the relative coordinates, so that we have the analog of a particle moving in a repulsive central field, this statement goes into the requirement that the wave function involving the relative coordinates must be an even function, or have even parity, for the singlets, and have odd parity for the triplets. The wave functions resemble those of a particle in a central field, so that the functions of even parity resemble atomic $s, d, \cdots$ states, and those of odd parity resemble atomic $p, f, \cdots$ states. We naturally find that the lowest state of the problem is an s-like state, which corresponds to a singlet, or to the nonmagnetic case. Thus we conclude that ferromagnetism will never result from holes in a nondegenerate band, even if the band is narrow enough not to have trouble with the Fermi energy.

We therefore conclude that a degenerate band, such as the fivefold degenerate d band in the iron group, is an essential feature in the existence of ferromagnetism. When we analyze this problem of the degenerate band by means of Wannier functions, we find that we can no longer conclude that the singlet state must lie lower, and in fact the triplet will often lie lower, though this is not always necessary, so that ferromagnetism is definitely possible, though not required, in such a case. We can see clearly, from our calculation, the origin of the preference for parallel spins in the case of degenerate bands. It comes from those cases in which both holes happen in the course of their wanderings to be simultaneously on the same atom. Then, by Hund's rule, they will have lower energy if their spins are parallel. As they wander apart from each other, they naturally retain their magnetic moments. The reason why we cannot have this situation except with a degenerate band is obvious: with a nondegenerate band, formed from a single atomic orbital, the two holes cannot be on the same atom, unless they have opposite spins, on account of the exclusion principle. Our explanation of ferromagnetism is thus what Van Vleck[5] terms an intramolecular theory, and in fact many of the aspects of the present treatment are similar to the viewpoint of Van Vleck as expressed in reference 5.

From the nature of our solution, we can see why it is that the energy difference between magnetic and nonmagnetic states goes to zero at infinite internuclear distance, even though it depends on an intra-atomic exchange integral which does not go to zero at infinite distance. The way in which this comes about is simple. The wave function in the ferromagnetic case may be considered to be a mixture of non-ionic states, in which the two holes are on different atoms, and in which there is no tendency toward parallel alignment of the spins, and ionic states, in which both holes are on the same atom, and the spins tend to be aligned on account of Hund's rule. The energy difference between magnetic and nonmagnetic states in some simple cases proves to be the product of two things: the intra-atomic exchange integral tending to align the spins, which remains finite out to infinite internuclear distance, and the square of the coefficient of the ionic term in the linear combination representing the wave function, which expresses the probability that both holes are found on the same atom. This probability goes to zero at infinite internuclear distance, since the ionic state, with both holes on the same atom, has a higher energy in that limit than the other states in which the holes are on different atoms. Thus the energy difference between magnetized and nonmagnetized states of the whole crystal goes to zero at infinite separation simply because the probability of finding the two holes on the same atom vanishes, and it is only when they are on the same atom that the intra-atomic exchange is effective in lining up the spins.

The correlation effect, in other words, is taken into account most naturally in the present case, not by subtracting a correlation energy from the exchange energy as given by the energy band theory, but by

[5] J. H. Van Vleck, Revs. Modern Phys. **25**, 220 (1953).

multiplying the exchange integral of that theory by a factor which measures the probability of finding an ionic state. This factor goes to zero at infinite internuclear distance, but at the actual interatomic distance in a ferromagnetic crystal, it seems not unlikely that it has not decreased very much as compared to its value on the simple energy band theory, so that while the tendency to ferromagnetism is decreased somewhat on account of this correlation effect, it still remains of the same order of magnitude as found in the simple energy band theory. A similar conclusion was reached in reference 3. If we make this modification, the energy band theory should be approximately valid. In particular, the increase in Fermi energy when we magnetize the system remains approximately as in that theory, so that the conclusion that ferromagnetism is impossible with broad bands remains unchanged. For a trivial reason, however, this increase in Fermi energy does not appear in the present calculations. The reason is that we are dealing with only two electrons, which must be in the bottom of the Fermi band in the lowest energy level of the system, which alone we have considered; and we are dealing with at least a twofold degenerate band in the ferromagnetic case. Thus the two electrons can have their spins parallel, and yet one can be in the lowest state of one band, the other in the lowest state of the other, so that in this special case it does not increase the Fermi energy to set their spins parallel. This is a special case arising from our two-electron problem, and does not in any way affect the validity of the general argument.

2. WANNIER FUNCTION FORMULATION OF THE PERIODIC POTENTIAL PROBLEM

We shall now proceed with the more quantitative treatment of the ideas which have been presented in the introductory section. Our problem of the motion of two holes is very similar to the motion of two electrons. Furthermore, though the holes really move in the field of all particles, still we can approximate their motion as if they moved in a periodic potential. We shall accordingly treat in the present section, and in the larger part of this paper, the problem of two electrons moving in a periodic potential, subject to a simple Coulomb repulsion, or a screened Coulomb repulsion. In a later section we shall discuss the extent to which this simple case forms an approximation to the real problem of two holes acted on by all electrons.

We assume, then, that the Hamiltonian of our problem is given by

$$H=H_1+H_2+g_{12}, \tag{1}$$

where H_1, H_2 are one-electron Hamiltonians of the two electrons in a periodic crystalline field, and where g_{12} is the repulsion between the two electrons. We shall now set up the Schrödinger problem connected with the Hamiltonian (1) in terms of the Wannier functions defined by the periodic potential H_1. In order to have our mathematical machinery clearly in mind, let us remind the reader of the nature of these Wannier functions. Many of these properties are given in references 3 and 4, and others in another paper by one of the authors.[6] We start with the one-electron Hamiltonian H_1. We know that it has solutions $\psi_i(\mathbf{k}, \mathbf{r})$, where $\mathbf{k}$ is a propagation vector, and i refers to the various energy bands. That is, these functions satisfy the differential equation $H_1\psi_i(\mathbf{k}, \mathbf{r})=E_i(\mathbf{k})\psi_i(\mathbf{k}, \mathbf{r})$, where $E_i(\mathbf{k})$ gives the one-electron energy, as it depends on the index i defining the energy band, and on the value of $\mathbf{k}$. As Bloch has shown, these solutions satisfy the equation $\psi_i(\mathbf{k}, \mathbf{r}+\mathbf{R}_n)=\exp(i\mathbf{k}\cdot\mathbf{R}_n)\psi_i(\mathbf{k}, \mathbf{r})$, where $\mathbf{R}_n$ is one of the translation vectors of the lattice.

In terms of these energy-band functions ψ, the Wannier functions are defined as

$$a_i(\mathbf{r}-\mathbf{R}_m)=N^{-1}\sum(\mathbf{k})\exp(-i\mathbf{k}\cdot\mathbf{R}_m)\psi_i(\mathbf{k}, \mathbf{r}), \tag{2}$$

where N is the number of unit cells in the volume of the crystal over which we apply periodic boundary conditions, and the ψ's are normalized over this volume. The summation extends over all $\mathbf{k}$ values in the unit cell of reciprocal space, there being just N such $\mathbf{k}$ values. Equivalent to Eq. (2) is the relation

$$\psi_i(\mathbf{k}, \mathbf{r})=N^{-1}\sum(\mathbf{R}_m)\exp(i\mathbf{k}\cdot\mathbf{R}_m)a_i(\mathbf{r}-\mathbf{R}_m). \tag{3}$$

We can then show that the a's as defined above are normalized and orthogonal, in the sense that the integral over all space of two a's connected with different i's, or different $\mathbf{R}_m$'s, is zero. The a's form a complete orthogonal set of functions, as we have stated earlier, in terms of which any function of the coordinates of a single electron may be expanded.

In order to work with the Wannier functions, we must know the matrix components of the one-electron Hamiltonian between different Wannier functions. To state these matrix components in the most concise way, it is first desirable to express the one-electron energy $E_i(\mathbf{k})$ of the energy-band functions in a different form. Since it is a periodic function of position in the reciprocal lattice, it can be expanded in the form

$$E_i(\mathbf{k})=\sum(\mathbf{R}_m)\mathcal{E}_i(\mathbf{R}_m)\exp(-i\mathbf{k}\cdot\mathbf{R}_m). \tag{4}$$

Then we can show that the matrix components of H_1 between the various Wannier functions are

$$\int a_i^*(\mathbf{r})H_1a_j(\mathbf{r}-\mathbf{R}_m)d\tau=\delta_{ij}\mathcal{E}_i(-\mathbf{R}_m). \tag{5}$$

We can use the expansion (4) for $E_i(\mathbf{k})$ to prove another valuable result. Let us replace $\mathbf{k}$ by $\mathbf{p}/\hbar$, where $\mathbf{p}$ is a pseudo-momentum, and let the $\mathbf{p}$ in this be replaced by the operator $-i\hbar/\nabla$, in the usual manner employed in quantum mechanics. Let the gradient ∇ operate on a variable $\mathbf{R}$, and let us form the expression

[6] G. F. Koster, Phys. Rev. **89**, 67 (1953).

$E_i(\mathbf{p}/h)f(\mathbf{R})$, where f is any function. Then we find

$$E_i(\mathbf{p}/h)f(\mathbf{R})=\sum(\mathbf{R}_m)\mathcal{E}_i(\mathbf{R}_m)f(\mathbf{R}-\mathbf{R}_m). \quad (6)$$

We have now assembled the necessary properties of the Wannier functions and the energy operators, and can proceed with the formulation of our problem. We have already stated in Sec. 1 that on account of the complete orthogonal nature of the Wannier functions, we can write any function of the coordinates $\mathbf{r}_1$ and $\mathbf{r}_2$ of the two electrons, and in particular the wave function $\psi(\mathbf{r}_1, \mathbf{r}_2)$, in the form

$$\psi(\mathbf{r}_1, \mathbf{r}_2)=\sum(i, j, m, n)U_{ij}(\mathbf{R}_m, \mathbf{R}_n) \times a_i(\mathbf{r}_1-\mathbf{R}_m)a_j(\mathbf{r}_2-\mathbf{R}_n). \quad (7)$$

In a later section, we shall set up determinantal functions of the coordinates and spins of many electrons by such a method, but our two-electron problem is so simple that we may take account of the spin degeneracy at the outset by noticing that $\psi(\mathbf{r}_1, \mathbf{r}_2)$ must be symmetric in the coordinates $\mathbf{r}_1$, $\mathbf{r}_2$ for a singlet state, antisymmetric for a triplet. These conditions are fulfilled if the U_{ij}'s satisfy the condition

$$U_{ji}(\mathbf{R}_n, \mathbf{R}_m)=\pm U_{ij}(\mathbf{R}_m, \mathbf{R}_n), \quad (8)$$

where the + sign refers to the singlet, the − to the triplet.

We can now find the matrix components of the Hamiltonian (1) between the various products of Wannier functions included in (7), and thus set up the general equations for the U_{ij}'s. These equations may be expressed in either of the equivalent forms

$$\begin{aligned}&\sum(\mathbf{R}_s)[\mathcal{E}_i(\mathbf{R}_s)U_{ij}(\mathbf{R}_m-\mathbf{R}_s, \mathbf{R}_n) \\ &\quad+\mathcal{E}_j(\mathbf{R}_s)U_{ij}(\mathbf{R}_m, \mathbf{R}_n-\mathbf{R}_s)] \\ &\quad+\sum(k, l, \mathbf{R}_r, \mathbf{R}_s)U_{kl}(\mathbf{R}_m-\mathbf{R}_r, \mathbf{R}_n-\mathbf{R}_s) \\ &\quad\times\int a_i^*(\mathbf{R}_1-\mathbf{R}_m)a_j^*(\mathbf{r}_2-\mathbf{R}_n)g_{12} \\ &\quad\times a_k(\mathbf{r}_1-\mathbf{R}_m+\mathbf{R}_r)a_l(\mathbf{r}_2-\mathbf{R}_n+\mathbf{R}_s)dv_1dv_2 \\ &\qquad=EU_{ij}(\mathbf{R}_m, \mathbf{R}_n), \quad (9)\end{aligned}$$

or

$$\begin{aligned}&[E_i(\mathbf{p}_1/h)+E_j(\mathbf{p}_2/h)]U_{ij}(\mathbf{R}_m, \mathbf{R}_n) \\ &\quad+\sum(k, l, \mathbf{R}_r, \mathbf{R}_s)U_{kl}(\mathbf{R}_m-\mathbf{R}_r, \mathbf{R}_n-\mathbf{R}_s) \\ &\quad\times\int a_i^*(\mathbf{R}_1-\mathbf{R}_m)a_j^*(\mathbf{r}_2-\mathbf{R}_n)g_{12}a_k(\mathbf{r}_1-\mathbf{R}_m+\mathbf{R}_r) \\ &\quad\times a_l(\mathbf{r}_2-\mathbf{R}_n+\mathbf{R}_s)dv_1dv_2=EU_{ij}(\mathbf{R}_m, \mathbf{R}_n). \quad (10)\end{aligned}$$

Here the notation $E_i(\mathbf{p}_1/h)$ means that $\mathbf{p}_1$ is to be a differential operator operating on the first argument, $\mathbf{R}_m$, of the expression $U_{ij}(\mathbf{R}_m, \mathbf{R}_n)$, while $E_j(\mathbf{p}_2/h)$ operates on the second argument $\mathbf{R}_n$.

We shall now show that a separation of variables can be carried out in Eqs. (9) and (10), into the coordinates of the center of mass of the two electrons, and the relative coordinates. We have already mentioned that this separation of variables is connected with the fact that the total $\mathbf{k}$ vector of the system is a constant of the motion. The reason for this of course goes back to the group theory. The Hamiltonian function of Eq. (1) commutes with an operation in which both $\mathbf{r}_1$ and $\mathbf{r}_2$ are translated by one of the lattice vectors $\mathbf{R}_s$. We can then choose two-electron wave functions which diagonalize this operation, in such a way that the wave function is multiplied by $\exp(i\mathbf{K}\cdot\mathbf{R}_s)$ when we make such a translation, where $\mathbf{K}$ is a constant vector. If we build up our wave functions out of Bloch waves instead of from Wannier functions, we can set up a wave function having the required properties by using only those Bloch waves for which the sum of the $\mathbf{k}$'s of the waves for the two electrons equals $\mathbf{K}$. If we use a wave function like (7), constructed from Wannier functions, our condition reduces to the statement that

$$U_{ij}(\mathbf{R}_m+\mathbf{R}_s, \mathbf{R}_n+\mathbf{R}_s)=\exp(i\mathbf{K}\cdot\mathbf{R}_s)U_{ij}(\mathbf{R}_m, \mathbf{R}_n). \quad (11)$$

We may now regard U_{ij} as depending on the two quantities $(\mathbf{R}_m+\mathbf{R}_n)/2$, which would be the coordinate of the center of mass if $\mathbf{R}_m$ and $\mathbf{R}_n$ were regarded as the coordinates of two particles, and $(\mathbf{R}_m-\mathbf{R}_n)$, rather than on $\mathbf{R}_m$ and $\mathbf{R}_n$. From (11) we see that a change in the quantity $(\mathbf{R}_m+\mathbf{R}_n)/2$, keeping $(\mathbf{R}_m-\mathbf{R}_n)$ constant, merely multiplies $U_{ij}(\mathbf{R}_m, \mathbf{R}_n)$ by a constant. Thus the variable $(\mathbf{R}_m+\mathbf{R}_n)/2$ must enter the function $U_{ij}(\mathbf{R}_m, \mathbf{R}_n)$ only in an exponential factor, and we may write $U_{ij}(\mathbf{R}_m, \mathbf{R}_n)$ in the form

$$U_{ij}(\mathbf{R}_m, \mathbf{R}_n)=\exp(i\mathbf{K}\cdot(\mathbf{R}_m+\mathbf{R}_n)/2)F_{ij}(\mathbf{R}_m-\mathbf{R}_n). \quad (12)$$

We expect, then, that if we make the substitution (12) in Eqs. (9) and (10), these equations will reduce to equations for the function $F_{ij}(\mathbf{R}_m-\mathbf{R}_n)$, the function depending on the relative coordinates, independent of $(\mathbf{R}_m+\mathbf{R}_n)/2$. If we substitute (12) in (9) and replace $\mathbf{R}_m-\mathbf{R}_n$ by the single quantity $\mathbf{R}_p$, the resulting equation reduces to

$$\begin{aligned}&\sum(\mathbf{R}_s)[\mathcal{E}_i(\mathbf{R}_s)\exp(-i\mathbf{K}\cdot\mathbf{R}_s/2) \\ &\quad+\mathcal{E}_j(\mathbf{R}_s)\exp(i\mathbf{K}\cdot\mathbf{R}_s/2)]F_{ij}(\mathbf{R}_p-\mathbf{R}_s) \\ &\quad+\sum(k, l, \mathbf{R}_r, \mathbf{R}_s)\exp(-i\mathbf{K}\cdot(\mathbf{R}_r+\mathbf{R}_s)/2) \\ &\quad\times F_{kl}(\mathbf{R}_p-\mathbf{R}_r+\mathbf{R}_s)\int a_i^*(\mathbf{r}_1-\mathbf{R}_p)a_j^*(\mathbf{r}_2)g_{12} \\ &\quad\times a_k(\mathbf{r}_1-\mathbf{R}_p+\mathbf{R}_r)a_l(\mathbf{r}_2+\mathbf{R}_s)dv_1dv_2=EF_{ij}(\mathbf{R}_p). \quad (13)\end{aligned}$$

In deriving Eq. (13), we have used the relation $\mathcal{E}_i(-\mathbf{R}_s)=\mathcal{E}_i(\mathbf{R}_s)$, which must hold since the energy is always an even function of $\mathbf{k}$. Similarly if we substitute (12)

in (10), we find

$$\{\exp(-i\mathbf{K}\cdot\mathbf{R}_p/2)E_i(\mathbf{p}/\hbar)\exp(i\mathbf{K}\cdot\mathbf{R}_p/2)$$
$$+\exp(i\mathbf{K}\cdot\mathbf{R}_p/2)E_j(\mathbf{p}/\hbar)\exp(-i\mathbf{K}\cdot\mathbf{R}_p/2)\}F_{ij}(\mathbf{R}_p)$$
$$+\sum(k,l,\mathbf{R}_r,\mathbf{R}_s)\exp(-i\mathbf{K}\cdot(\mathbf{R}_r+\mathbf{R}_s)/2)$$
$$\times F_{kl}(\mathbf{R}_p-\mathbf{R}_r+\mathbf{R}_s)\int a_i^*(\mathbf{r}_1-\mathbf{R}_p)a_j^*(\mathbf{r}_2)g_{12}$$
$$\times a_k(\mathbf{r}_1-\mathbf{R}_p+\mathbf{R}_r)a_l(\mathbf{r}_2+\mathbf{R}_s)dv_1dv_2=EF_{ij}(\mathbf{R}_p). \quad (14)$$

In Eq. (14), the operator $\mathbf{p}$ is assumed to operate on the quantity $\mathbf{R}_p$ which follows it, both in the exponential and in $F_{ij}(\mathbf{R}_p)$.

In Eqs. (13) and (14) we have derived the equations for the quantities $F_{ij}(\mathbf{R}_p)$, expressing the function of the relative coordinates. These quantities of course depend on the assumed value of $\mathbf{K}$, the combined propagation vector of the two particles. In our case, we shall be looking for the lowest energy states of the system, and ordinarily these will come for $\mathbf{K}=0$, so that we shall set $\mathbf{K}=0$ in these equations for our further application. The quantity $F_{ij}(\mathbf{R}_p)$ must have certain symmetry properties for the singlet and triplet states, to assure that the function $U_{ij}(\mathbf{R}_m,\mathbf{R}_n)$ shall have the properties given in Eq. (8). We readily see that this requires that

$$F_{ji}(-\mathbf{R}_p)=\pm F_{ij}(\mathbf{R}_p), \quad (15)$$

where as before the + sign refers to the singlet, the − to the triplet.

In Eqs. (13) and (14), we have matrix components involving the integrals

$$\int a_i^*(\mathbf{r}_1-\mathbf{R}_p)a_j^*(\mathbf{r}_2)g_{12}a_k(\mathbf{r}_1-\mathbf{R}_p+\mathbf{R}_r)a_l(\mathbf{r}_2+\mathbf{R}_s)dv_1dv_2.$$

Such an integral is the Coulomb repulsion between one electron whose distribution is given by $a_i^*(\mathbf{r}_1-\mathbf{R}_p)\times a_k(\mathbf{r}_1-\mathbf{R}_p+\mathbf{R}_r)$ and a second electron with distribution $a_j^*(\mathbf{r}_2)a_l(\mathbf{r}_2+\mathbf{R}_s)$. Each of these distributions will integrate to zero, on account of the orthogonality of the a's, unless the two Wannier functions are identical. Thus each one will correspond to a multipole, and the Coulomb interactions between them will be relatively small. In our present qualitative discussion, we shall consider only the largest integrals, and shall disregard the smaller ones, though this would by no means be justified in later more quantitative attempts to discuss ferromagnetism. The largest terms will come if $\mathbf{R}_p=\mathbf{R}_r=\mathbf{R}_s=0$, so that all four Wannier functions are located on the same atom. We shall denote such terms by the abbreviation

$$\int a_i^*(\mathbf{r}_1)a_j^*(\mathbf{r}_2)g_{12}a_k(\mathbf{r}_1)a_l(\mathbf{r}_2)dv_1dv_2=(ij/g/kl). \quad (16)$$

These terms are similar to the intra-atomic exchange integrals met in the theory of complex spectra; if the Wannier functions were identical with atomic orbitals, as they are in the limit of infinite internuclear distance, they would become exactly such exchange integrals, and hence approach finite values at infinite separation. We shall retain all such integrals in our discussion. In case any one of the quantities $\mathbf{R}_p$, $\mathbf{R}_r$, $\mathbf{R}_s$ is different from zero, however, the integral will involve the interaction of a multipole with a charge or another multipole, and will vanish in the limit of infinite separation. We shall disregard all such integrals. This is particularly reasonable, in that in a real ferromagnetic substance, the 4s electrons will shield one atom from another, so that g_{12} should really be chosen as a screened Coulomb potential, which will rapidly make all such integrals drop to zero as the multipoles are found on different atoms. Such terms would be much less important here than, for instance, in the study of impurity levels in a semiconductor, or exciton levels in an insulator.

When we make these assumptions, and set $\mathbf{K}=0$, Eqs. (13) and (14) become simplified to the form

$$\sum(\mathbf{R}_s)[\mathcal{E}_i(\mathbf{R}_s)+\mathcal{E}_j(\mathbf{R}_s)]F_{ij}(\mathbf{R}_p-\mathbf{R}_s)$$
$$+\sum(k,l)(ij/g/kl)\delta(\mathbf{R}_p,0)F_{kl}(\mathbf{R}_p)=EF_{ij}(\mathbf{R}_p), \quad (17)$$

$$[E_i(\mathbf{p}/h)+E_j(\mathbf{p}/h)]F_{ij}(\mathbf{R}_p)$$
$$+\sum(k,l)(ij/g/kl)\delta(\mathbf{R}_p,0)F_{kl}(\mathbf{R}_p)=EF_{ij}(\mathbf{R}_p). \quad (18)$$

We are now ready to start the discussion of the solution of these equations. The first case we shall take up is that of a nondegenerate band; that is, the case where we can get a good approximation by assuming that the wave function can be expanded to an adequate approximation in terms of the Wannier functions of only one band, say the ath band. In this case, Eqs. (17) and (18) reduce to the simple forms

$$\sum(\mathbf{R}_s)2\mathcal{E}_a(\mathbf{R}_s)F_{aa}(\mathbf{R}_p-\mathbf{R}_s)$$
$$+(aa/g/aa)\delta(\mathbf{R}_p,0)F_{aa}(\mathbf{R}_p)=EF_{aa}(\mathbf{R}_p), \quad (19)$$

$$2E_a(\mathbf{p}/h)F_{aa}(\mathbf{R}_p)$$
$$+(aa/g/aa)\delta(\mathbf{R}_p,0)F_{aa}(\mathbf{R}_p)=EF_{aa}(\mathbf{R}_p). \quad (20)$$

3. THE SINGLE NONDEGENERATE BAND

We can discuss the single nondegenerate band either from the point of view of the difference equation (19), or the differential equation (20). The former is more adequate, particularly at large internuclear distances, but the latter is somewhat simpler to understand, and we shall therefore start our discussion with this differential equation. Since we are considering two electrons in an empty band, and are looking for the lowest-energy levels of these electrons, it is reasonable to suppose that we are dealing mostly with the bottom of the band, so that we can expand the energy operator $E_a(\mathbf{p}/h)$ in the standard way as $-h^2\nabla^2/2m_e$, where m_e is an effective mass, and where the Laplacian operates on the appropriate variable. We shall first consider the form which Eq. (10) takes, in which the coordinates of the two

electrons are considered separately, and then we shall come to the corresponding form of Eq. (20), where we have introduced the relative coordinates. The suitable form of (10) is

$$[(-h^2/2m_e)(\nabla_m^2+\nabla_n^2)+(aa/g/aa)\delta(\mathbf{R}_m, \mathbf{R}_n)] \times U_{aa}(\mathbf{R}_m, \mathbf{R}_n)=EU_{aa}(\mathbf{R}_m, \mathbf{R}_n), \quad (21)$$

where the Laplacians ∇_m^2 and ∇_n^2 operate on $\mathbf{R}_m$ and $\mathbf{R}_n$, respectively.

In Eq. (21), we have an ordinary Schrödinger equation for the motion of two particles, each of mass m_e, subject to a potential energy which is a delta function, equal to zero when the coordinates of the two electrons are different, but positive, equal to the repulsive Coulomb interaction $(aa/g/aa)$, when they are the same. We can solve (21) for $U_{aa}(\mathbf{R}_m, \mathbf{R}_n)$ as a function of continuous variables $\mathbf{R}_m$, $\mathbf{R}_n$, but must remember that we are interested in only discrete values of these variables. The reason why the differential equation is not as satisfactory as the rigorous difference equation for handling this problem comes from the delta function, which is a little hard to interpret with the differential equation, but which becomes perfectly simple to understand in the case of the difference equation, which we shall take up later.

For a first orientation regarding the solutions of (21), let us take a one-dimensional case, in which the atoms are arranged along a line. We must now consider the boundary conditions to be applied, which we have been omitting previously. To be specific, let us require that our wave function vanish on the boundary of a finite crystal. In the present one-dimensional case, if we replace our discrete variables by a continuous variable x_1 for the coordinate of the first electron, x_2 for the second, this means that both x_1 and x_2 are to be confined to a region between 0 and X, the wave function vanishing at these values. The differential equation which we must then solve is

$$(-h^2/2m_e)(\partial^2/\partial x_1^2+\partial^2/\partial x_2^2)U(x_1, x_2) + (aa/g/aa)\delta(x_1, x_2)U(x_1, x_2)=EU(x_1, x_2), \quad (22)$$

where we have omitted the subscripts on U for convenience. This equation is to be solved in the square region $0<x_1<X$, $0<x_2<X$, subject to the condition that U vanish on the boundaries of the square.

If we first disregard the repulsive interaction between the particles, the problem of solving Schrödinger's equation for the two particles is just like the wave equation for the vibration of a square membrane held at its edges. The wave functions will be of the form $\sin(n_1\pi x_1/X)\sin(n_2\pi x_2/X)$. If n_1 and n_2 are different, there will be two degenerate states, the one given above and that with n_1 and n_2 interchanged, and we may take sums and differences, obtaining the functions

$$\sin(n_1\pi x_1/X)\sin(n_2\pi x_2/X) \pm\sin(n_2\pi x_1/X)\sin(n_1\pi x_2/X), \quad (23)$$

the sum being symmetric, the difference antisymmetric, on interchange of x_1 and x_2. For $n_1=n_2$, only the symmetric function exists, the expression of the exclusion principle. In accordance with the discussion of Sec. 1, we see that the lowest state, that for $n_1=n_2=1$, is symmetric, and is therefore a singlet state, while the lowest triplet state, for $n_1=1$, $n_2=2$, using the combination with the minus sign from (23), lies higher.

We now ask for the effect of the repulsion between the two electrons. In our two-dimensional representation of the problem, this means that in the square region in which we are solving Schrödinger's equation, there will be a region along the 45° diagonal, $x_1=x_2$, in which the potential energy is a large positive quantity, and the kinetic energy negative. This perturbation will have no effect on the triplet wave functions or energy levels, for these wave functions on account of antisymmetry are zero along the 45° diagonal. It will have a profound effect on the singlet wave functions and energy levels, however, increasing the energy of the singlets since the perturbative potential is everywhere positive. If the repulsive energy is large, the perturbed wave function will be reduced almost to zero in the neighborhood of the 45° line. That is, a correlation effect will be introduced into the wave function, keeping the electrons apart on account of the repulsion, modifying both wave function and energy of the singlet states.

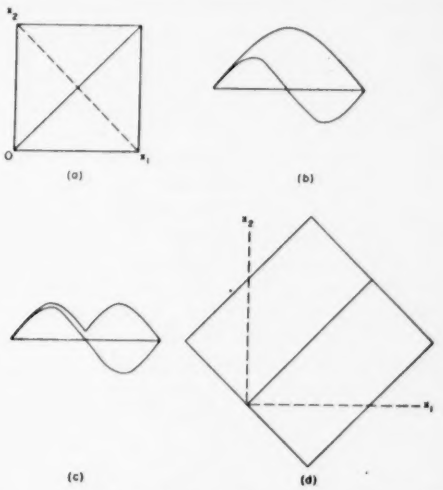

FIG. 1. (a) Square within which wave function is defined. (b) Symmetric and antisymmetric wave functions along line x_1-x_2 of Fig. 1(a), no repulsive potential. (c) Same as 1(b), with repulsive potential. (d) Square for use with modified boundary conditions.

The nature of the resulting wave functions is shown in Fig. 1. Here, first, in Fig. 1(a), we show the square in which the wave function is different from zero, with the 45° diagonal with respect to which the function is even (for singlets) or odd (for triplets). In Fig. 1(b),

we show how the wave functions look as a function of position along the dotted line of Fig. 1(a), for the case without repulsive potentials; this gives a good indication of the behavior of the wave function. The symmetric function represents the lowest singlet, with $n_1=n_2=1$, and the antisymmetric function represents the lowest triplet. In Fig. 1(c), we show how the wave functions of the same two states may well look in the presence of a repulsive potential represented by a delta function along the 45° diagonal. The wave function of the singlet state has become very small near the diagonal, so that it is almost identical with the triplet, except close to the barrier, where it behaves in such a way as to lead to a symmetric rather than an antisymmetric combination. Since the wave functions are nearly identical, the energy levels must also be almost identical. Yet the energy of the singlet state, corresponding to the wave function without the node, must still lie below that of the triplet state, which has a node, though now they will lie very close together. The proof of this would be obvious if we had a one-dimensional problem, for we know that in a one-dimensional problem the eigenvalue of a state with more nodes is always greater than that of one with fewer nodes. This theorem does not always hold in more than one dimension; but this is a case where it does. For instance, we can build up approximate solutions of the form of that given in Fig. 1(c) by perturbation theory, from solutions of the problem with an infinitely high barrier along the 45° line, on one side or the other of this diagonal. We shall find straightforwardly that the energy of the symmetric combination is always lower than that of the antisymmetric combination, though they will approach each other for the infinitely great repulsive barrier.

Another way in which we can make sure that the lowest state of this problem will be a singlet is to replace it by a problem with slightly different boundary conditions, as shown in Fig. 1(d). The potential energy of interaction between the two particles is the same as in the case we have just considered, but we require that the wave function vanish along the boundaries of the square tilted up at an angle of 45°, rather than along the boundaries of the square shown in Fig. 1(a). In this case Schrödinger's equation can be separated, using coordinates $u=x_1+x_2$, $v=x_1-x_2$, and the boundary conditions can be stated in the form that the wave function must go to zero at certain values of u and of v. The repulsive interaction potential depends only on v, so that we are interested in comparing two different wave functions, one symmetric and one antisymmetric as far as their dependence on v is concerned, but both having the same dependence on u. In this case we really have a one-dimensional problem, so that we can use the rigorous theorem telling us that the lowest symmetric state will lie lower than the lowest antisymmetric state.

The boundary conditions in this rotated frame no longer have the simple meaning that each electron can move between 0 and X along the x axis. Instead, the center of gravity of the two electrons can move within fixed limits, and the distance between the two electrons has a maximum value which it cannot exceed, but below which the electrons can move unrestrictedly. With the original boundary conditions, on the contrary, if the center of gravity is near the wall of the box the two electrons cannot get more than a relatively small distance apart because they are hindered by the box. In the case of either set of boundary conditions, the differential equation itself can be separated into the motion of the center of gravity and the relative coordinates, and the difference between the two boundary conditions comes only in the regions where the electrons are far apart. In the one-dimensional case which we have described, it is clear that either type of boundary conditions leads to the same qualitative results. It seems almost inconceivable that they should lead to different types of results in more complicated cases, and we shall use boundary conditions of the type illustrated in Fig. 1(d) in our further development. By this means we not only separate variables in the differential equation, into the coordinates of the center of gravity and the relative coordinates, but we also separate variables in the treatment of the boundary conditions. In this problem, where we are dealing with wave functions in the continuum, this matter of boundary conditions at large values of the coordinates is an important question, contrary to the case of reference 3, where we were dealing with bound states, whose wave functions fell off rapidly at large distances.

We have now shown in our simple one-dimensional case that as the repulsive interaction between the two electrons increases, it is true that the energy of the lowest singlet state rises toward that of the lowest triplet, but never enough to make the two levels cross. The singlet state always lies lower, so that the two electrons always tend to set their spins antiparallel. The three-dimensional case follows almost as simply. For the three-dimensional problem we can again separate variables, obtaining separate equations for the center of gravity and the relative coordinates. We may use the same kind of simplified boundary conditions that we did in Fig. 1(d). That is, for the relative coordinates, we allow the particles to move freely so long as the distance between them does not exceed a fixed maximum. In other words, as far as the relative coordinates are concerned, the problem is like that of a single particle moving in a spherical box, subject to a repulsive center of force at the center of the box. On account of the antisymmetry principle, the wave function of coordinates only must again be symmetric or antisymmetric with respect to interchange of the coordinates of the two electrons, which means with respect to inversion of the relative coordinates. The spherical symmetry of the problem leads to a solution in which we have a function of r, multiplied by a spherical harmonic of angle. The inversion symmetry corresponds to the parity. That is, the singlets corre-

spond to functions of even parity, or even l value, where l is the ordinary azimuthal quantum number, while the triplets correspond to odd parity. Thus the lowest singlet state corresponds to the lowest s state, or state of $l=0$, while the lowest triplet corresponds to the lowest p state, or state of $l=1$. One can now prove quite generally that the lowest s state must lie lower than the lowest p state. We may, without the formality of this proof, satisfy ourselves in an elementary way that the theorem must be true. We know that when we separate variables, the radial wave function is given by a one-dimensional Schrödinger equation, which differs from one l value to another only by the presence of the effective potential energy $l(l+1)/r^2$, in atomic units, representing the centrifugal effect. An increase of l then increases the effective potential energy everywhere. It must therefore certainly be true that the lowest energy level of the state for $l=1$ must lie higher than the lowest level for $l=0$, since the effective potential energy is increased everywhere in going from the state $l=0$ to $l=1$. The three-dimensional case, then, behaves like the one-dimensional case, and we see here too that the lowest state must be a singlet.

We shall now give a similar and more quantitative discussion based on the difference equation (19), rather than on the differential equation. We assume again the type of boundary conditions illustrated in Fig. 1(d), by which we separate variables, assume that the boundary conditions can also be stated in terms of separate limits on the coordinates of the center of mass and the relative coordinates, and use Eq. (19), together with appropriate boundary conditions on $\mathbf{R}_p$. A three-dimensional difference equation of the type (19) cannot be easily solved; the relaxation method, used for the approximate solution of two- and three-dimensional differential equations when approximated by difference equations, is probably the best method of handling it. The one-dimensional case, however, is easy to treat, and as we have just seen it shows all the essential features of the three-dimensional problem. Even the one-dimensional case is rather complicated if we have interactions between other than nearest neighbors; that is, if $\mathcal{E}_a(R_s)$ is appreciable except for R_s equal to the distance between nearest neighbors. We recall, from Eq. (4), that a restriction to nearest-neighbor interactions is another way of saying that the energy is a sinusoidal function of k, the propagation vector, an approximation which holds well for narrow bands. We shall then set up the special case of Eq. (19) in which R_p is restricted to an equally spaced set of points on a line, and R_s refers only to a unit displacement. Essentially this same problem was discussed by one of the authors and Shockley[7] in treating the similar problem of the exciton.

To simplify notation, let the various lattice points be denoted by an index n. Here $n=0$ refers to $R_p=0$, positive and negative values of n to positive and negative R_p's (that is, to the case where the first particle is to the right or left of the second), and in accordance with our previous discussion, we shall impose the boundary condition that our function is to vanish for given limits of R_p, or of the relative coordinates; in particular, we assume that the function will vanish for $n=\pm N$. Let the F_{aa}'s be denoted by $F_{aa}(n)$. Then Eqs. (19) become

$$\begin{aligned} &2\mathcal{E}_a[F_{aa}(n+1)+F_{aa}(n-1)]=EF_{aa}(n) \quad \text{if} \quad n\neq 0 \\ &2\mathcal{E}_a[F_{aa}(1)+F_{aa}(-1)] \\ &\qquad +(aa/g/aa)F_{aa}(0)=EF_{aa}(0). \end{aligned} \tag{24}$$

We can at once solve all of Eqs. (24) except that for $n=0$ by the assumption

$$\begin{aligned} &F_{aa}(n)=\sin(\alpha(N-n)) \quad \text{if} \quad 0\geq n\geq N \\ &F_{aa}(-n)=\pm F_{aa}(n), \end{aligned} \tag{25}$$

where the $\pm$ sign refers to singlets or triplets. The solution (25) is chosen so that it automatically satisfies the boundary conditions when $n=\pm N$. Substitution of (25) in the first equation of (24) shows that that equation is satisfied if

$$E=4\mathcal{E}_a\cos\alpha, \tag{26}$$

which is what we expect from Eq. (4), when we remember that we are dealing with the energy of two electrons. We note, incidentally, that to have the energy a minimum for $\alpha=0$ [or for $k=0$ in Eq. (4)], which is the convenient assumption to make, $\mathcal{E}_a$ must be negative.

We must now substitute in Eq. (24) for $n=0$, to determine the propagation constant α, and hence the energy of each state. For the triplet states, this is trivial. We must have $F_{aa}(0)=0$, which demands at once $\sin(\alpha N)=0$, $\alpha=m\pi/N$, where $m=1, 2\cdots N-1$, so that we have $N-1$ triplet states. For the singlets, we have $-4\mathcal{E}_a\cos(\alpha N)\sin\alpha+(aa/g/aa)\sin(\alpha N)=0$, or

$$4\mathcal{E}_a\cot(\alpha N)\sin\alpha=(aa/g/aa). \tag{27}$$

We can solve this transcendental equation by plotting the quantity $-\cot(\alpha N)\sin\alpha$ as a function of α, and finding the values of α for which it equals $-(aa/g/aa)/4\mathcal{E}_a$, which we remember is a positive quantity, since $\mathcal{E}_a$ is chosen to be negative. In Fig. 2 we show the function $-\cot\alpha N\sin\alpha$, as a function of α, for $N=4$. At $\alpha=0$ the function equals $-1/N$. It goes through zero when $\alpha N=\pi/2, 3\pi/2, \cdots$, or in general for $\alpha=m\pi/2N$ where m is an odd integer, so that it goes through zero N times for α between zero and π. At $\alpha=\pi$, the function equals $1/N$. The function becomes infinite when $\alpha=m\pi/N$ where m is any integer from 1 to $N-1$; that is, it becomes infinite at the same values of α for which we have triplet states.

We now see that if $(aa/g/aa)=0$, so that we have the problem of the free particles, we have N singlet states, corresponding to the values of g where this curve is zero. The lowest singlet state, corresponding

[7] J. C. Slater and W. Shockley, Phys. Rev. **50**, 705 (1936).

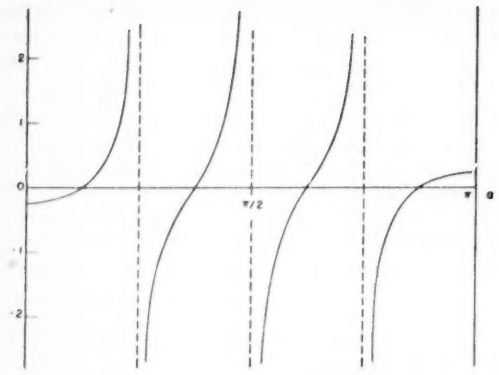

FIG. 2. Function $-\cot\alpha N \sin\alpha$, for $N=4$.

to $\alpha=\pi/2N$, is the lowest state of the problem, below the lowest triplet, which has $\alpha=\pi/N$, as indicated previously. To visualize the energies, we remember that the energy is given by $4\mathcal{E}_a\cos\alpha$, where $\mathcal{E}_a$ is negative, so that $\alpha=0$ corresponds to the center of the Brillouin zone, $\alpha=\pm\pi$ to its edges, and the energy has its minimum at the center of the zone, its maximum at the edges. Thus increasing α increases the energy. Now as $(aa/g/aa)$ increases from zero, or as the repulsive effect between electrons is introduced, we find the singlet values of α from Fig. 2 by finding the intersections of the curve with the horizontal line at height $-(aa/g/aa)/4\mathcal{E}_a$, depending on the magnitude of the repulsive interaction in terms of the band width. As this line rises, it is clear that the α's of all singlet levels increase, so that their energies rise, a consequence of the positive repulsive energy. These α's, however, approach the asymptotic values which give the triplet energies, as the repulsive interaction is indefinitely increased; so that no matter how great the repulsion, or how narrow the band width, the lowest singlet will never rise above the lowest triplet.

For small values of $(aa/g/aa)$, there are N intersections of a horizontal line with the curve of Fig. 2. That is, there are N singlet states, and taken together with the $N-1$ triplets, we have $2N-1$ states in all, which is as it must be, since there are $2N-1$ values of n, between $n=-N$ and $+N$, for each of which a quantity $F_{aa}(n)$ is defined, and there must be as many states as values of this quantity. At a certain height, however, the intersection in Fig. 2 corresponding to the largest α value becomes lost, and we must investigate what happens to this solution, though it is not the one that concerns us directly, since it corresponds to the highest singlet, and we are principally interested in the lowest singlet. It is interesting first to see for what value of $(aa/g/aa)$ this occurs. From what we have seen before, it comes when $-(aa/g/aa)/4\mathcal{E}_a=1/N$. This has a simple meaning. The quantity $-4\mathcal{E}_a/N$ is the total band width, $-8\mathcal{E}_a$, divided by $2N$, the number of lattice points plus one, or is approximately the one-electron energy per lattice point at the top of the energy band. Our limiting condition comes when the repulsive interaction $(aa/g/aa)$ equals this band energy per lattice point. We shall now show that for larger values of $(aa/g/aa)$, this solution emerges from the top of the band, and becomes a higher and isolated energy level, equal in energy approximately to $(aa/g/aa)$ in the limit of very high repulsive energy, and corresponding to a wave function in which the two electrons are attached permanently to the same atom, never wandering through the lattice. This special solution can be at once identified from Eq. (24). In case $(aa/g/aa)$ is very large compared to $\mathcal{E}_a$, we can almost disregard $\mathcal{E}_a$ in Eq. (24). Then we have a limiting solution in which $F_{aa}(n)=0$ except for $n=0$, in which case of course $F_{aa}(0)$ must be unity by normalization (it is to be noticed that we have not so far normalized our wave functions). Equation (24) then tells us that $E=(aa/g/aa)$.

The physical meaning of this special solution is clear. In the limit of narrow bands, where $\mathcal{E}_a$ is negligible, Eq. (24) leads to no nondiagonal matrix components, which means that electrons are not likely to wander from one atom to another. In our problem of the relative motion of the electrons, there is one lattice point, $R_p=0$ or $n=0$, corresponding to an ionic state; all remaining $2N-2$ lattice points correspond to non-ionic states, with the two electrons on different atoms. These $2N-2$ states will be degenerate with each other, and as soon as the nondiagonal matrix components $\mathcal{E}_a$ become different from zero, linear combinations will be introduced corresponding to the wandering of electrons from one lattice point to another to remove this degeneracy. The one ionic state, however, will have a much higher energy, and it will remain as an isolated state until the $\mathcal{E}_a$'s become great enough so that there is an appreciable probability of mixing ionic states with the non-ionic ones arising from the $2N-2$ remaining states.

The importance of this special ionic state arises from its effect on the other states in the limit of narrow bands. If our wave functions are all normalized, then the completeness theorem demands that the sum of the squares of the $F_{aa}(n)$'s, for a given n, for all the states in the band, must equal unity. We have just seen that in the limit of narrow bands, the single ionic state will have $F_{aa}(0)$ equal approximately to unity, so that this means that in this limit, all the other states must have $F_{aa}(0)$ approximately zero. In other words, all the states, singlets as well as triplets, must lead to a vanishing probability of ionic arrangements of two electrons on the same atom, in the limit of narrow bands, or infinite internuclear distance. This is the origin of the correlation effect, tending to keep electrons from occupying the same atom in the limit of widely separated atoms. We can investigate this correlation effect directly, through our exact solution for $F_{aa}(0)$ for the various states, and we shall do this presently. But it is very important that we can deduce the

correlation effect as well by use of the completeness theorem, for this can be used in the three-dimensional case, where we cannot get an exact solution of the difference equations, just as well as in this soluble one-dimensional case. The completeness relation holds equally well there, and inspection of the difference equation will show that this special ionic state occurs perfectly generally, and is not limited to the one-dimensional problem.

Let us now see analytically how these results come about. First we shall investigate the ionic state, when $(aa/g/aa)$ is great enough so that it no longer can be described in terms of the solution we have set up already. In this case, we easily find that the substitute for Eq. (25) is

$$F_{aa}(n)=(-1)^n \sinh(\gamma(N-n)),$$
$$F_{aa}(-n)=F_{aa}(n), \tag{28}$$

where we use only the + sign in the relation between $F_{aa}(-n)$ and $F_{aa}(n)$, since this special solution occurs only for the singlets. The energy equation, corresponding to (26), is then

$$E=-4\mathcal{E}_a \cosh\gamma. \tag{29}$$

When we substitute in the equation for $n=0$, to determine the value of γ, we find

$$-4\mathcal{E}_a \coth(\gamma N) \sinh\gamma=(aa/g/aa). \tag{30}$$

We may plot $\coth(\gamma N)\sinh\gamma$ as a function of γ, in a way similar to Fig. 2, to determine the value of γ graphically. When $\gamma=0$, $\coth\gamma N \sinh\gamma$ equals $1/N$, so that the limiting case $-(aa/g/aa)/4\mathcal{E}_a=1/N$ corresponds to $\gamma=0$, just as it corresponds to $\alpha=\pi$. As $(aa/g/aa)$ increases from this value, γ increases without limit. If N is large, the quantity $\coth\gamma N$ very rapidly approaches unity, so that Eq. (30) can be solved directly. For large γ, Eq. (28) shows that $F_{aa}(n)$ decreases very rapidly with increasing n, so that $F_{aa}(0)$ is much larger than any of the other values. This verifies our earlier statement that this state is one in which practically the entire function is concentrated at $R_p=0$, corresponding to the ionic states. Furthermore, for large γ, $\sinh\gamma$ and $\cosh\gamma$ approach each other, so that by comparing (29) and (30), we see that the energy approaches $(aa/g/aa)$, as we previously stated.

It helps one's understanding of the nature of this special state if one sees how the quantities $F_{aa}(n)$ depend on n, for increasing values of the ratio $-(aa/g/aa)/4\mathcal{E}_a$ of the repulsive interaction to the band width. In Fig. 3, we show these functions, for a series of increasing values of this ratio. The actual values of $F_{aa}(n)$ alternate in sign from one value of n to the next, and in the interest of clarity, this alternation is not shown, but only the magnitude of the F's. For no repulsive interaction, the curve is the simple sine curve, reducing to zero for $n=\pm N$, and having a maximum for $n=0$. As the repulsion increases in proportion to the band width, the curves become flatter, being made up of sine curves of longer and longer wavelength, until finally they become straight lines, and the case of an infinitely long wavelength, which is the limiting case $\alpha=\pi$ or $\gamma=0$. Then as γ builds up, they start to fall off exponentially as we go away from the origin, this falling off becoming steeper as the repulsion increases, or the band width decreases. For infinite repulsion, or zero band width, the falling off is infinitely rapid, only the case of $R_p=0$ giving a nonvanishing contribution. The curves of Fig. 3 are of course not normalized, but are adjusted to give the same values for $R_p=0$, in order to make a clear picture of what is going on.

Let us next consider the values of the quantities $F_{aa}(0)$ for the other singlet states; we have seen that as the detached ionic state builds up, these other singlets will approach zero at $R_p=0$. We can investigate this at once from Eq. (24). From that equation we see that

$$F_{aa}(0)/F_{aa}(1)=-4\mathcal{E}_a/(aa/g/aa)-E. \tag{31}$$

Since E approaches zero as $\mathcal{E}_a$ approaches zero, for these states, we see that the ratio $F_{aa}(0)/F_{aa}(1)$ goes to zero according to the quantity $-4\mathcal{E}_a/(aa/g/aa)$, or proportionally to the band width.

In the limit of narrow band width, we can easily get analytic formulas for the energy of the various levels, by making suitable approximations using Eqs. (27) and (30), for the case of large α. We find in this way that the energies of the $N-1$ singlet states which coincide at zero band width are

$$E_m=4\mathcal{E}_a\cos(m\pi/N)$$
$$-(16/N)(\mathcal{E}_a^2/(aa/g/aa))\sin^2(m\pi/N)\cdots, \tag{32}$$

where $m=1, 2, \cdots N-1$. For the one singlet going to the ionic state at zero band width we have

$$E=(aa/g/aa)+8\mathcal{E}_a^2/(aa/g/aa)\cdots. \tag{33}$$

From Eqs. (31) and (32) we can immediately get a verification of our earlier statement that the energy separation between singlet and triplet, for large internuclear distances, is sometimes given by a product of an intra-atomic exchange integral, and the probability of finding two electrons on the same atom. In our case, the triplet energies are given by the first term of Eq. (32), $4\mathcal{E}_a\cos(m\pi/N)$. Thus the second term, $(16/N)(\mathcal{E}_a^2/(aa/g/aa))\sin^2(m\pi/N)$, gives the singlet-triplet separation. The intra-atomic exchange integral

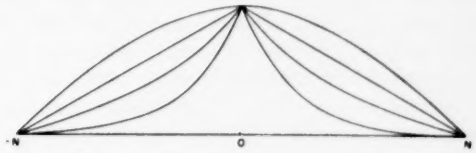

FIG. 3. $F_{aa}(n)$ as a function of n, for highest singlet level, different values of repulsive interaction.

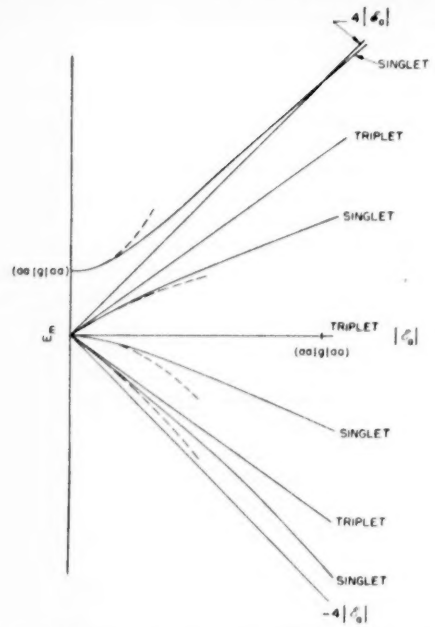

FIG. 4. Energy E_m as function of band width $|\mathcal{E}_a|$, for one-dimensional model. Dotted lines represent approximations of Eqs. (32), (33).

is $(aa/g/aa)$, and the probability of finding two electrons on the same atom is $F_{aa}(0)^2$. To get this, from Eq. (31), we must know $F_{aa}(1)$, which we can find by normalization. The values of $F_{aa}(n)$ are given in Eq. (25), and for all values of n except $n=0$ we can assume to our present approximation that $\alpha=m\pi/N$. Since the sum of the squares of the F_{aa}'s must add to unity, by normalization, we see that the normalized F_{aa}'s must be given by $F_{aa}(n)=N^{-\frac{1}{2}}\sin(m\pi/N)(N-n)$. Hence $F_{aa}(1)=\pm N^{-\frac{1}{2}}\sin(m\pi/N)$. When we combine this value with Eq. (31), we find $F_{aa}(0)$, and it is then obvious that the energy difference between singlet and triplet is in fact given precisely by $(aa/g/aa)F_{aa}(0)^2$, as we expected to find.

We can now illustrate the applicability of our approximations, by showing in Fig. 4 the seven energy levels for the case $N=4$, as a function of the band width, computed exactly by our numerical method, and compare them with the parabolic expressions of Eqs. (32) and (33). In Fig. 4 we plot the dimensionless quantity $E/(aa/g/aa)$ as a function of the other dimensionless quantity $-\mathcal{E}_a/(aa/g/aa)$. We see clearly the way in which the ionic state, which is separated from the other states at zero band width, becomes absorbed into the energy band at large enough band width. We also see the way in which the lowest state is a singlet, though the singlets and triplets approach each other in the limit of zero band width. We recall that in the real crystal, where the band width goes to zero at infinite internuclear separation, the situation shown in Fig. 4 at the origin would correspond to the situation in the crystal at infinite internuclear distance.

We have now followed our case of a one-dimensional model, as handled by the exact difference equation method, about as far as is profitable. We have already stated that a comparable treatment of the two- or three-dimensional case is not easy in any simple way. However, we have carried through a simplified treatment of a two-dimensional case, which goes far enough so that we can see the general method of treatment which can be used, and the general type of results to be expected. We consider a two-dimensional square lattice in the relative coordinate space, and assume that there are only nine nonvanishing values of the quantity $F_{aa}(\mathbf{R}_p)$: those for which the x and y components of $\mathbf{R}_p$ are equal to 0, ±1 times the lattice spacing, while we assume that $F_{aa}(\mathbf{R}_p)$ vanishes for the x and y components of $\mathbf{R}_p$ equal to ±2 times the lattice spacing. In this way, we can convert the difference equation, Eq. (19), into a secular equation, which will have nine rows and columns, and can solve this secular equation directly. As we shall see in a moment, crystal symmetry reduces these secular equations from nine by nine to not more than cubic equations, so that they are not hard to discuss. We make the same type of assumption regarding the $\mathcal{E}_a$'s which we used in the one-dimensional case, namely that the only nonvanishing components were those in which either the x or the y component of $\mathbf{R}_p$ equals one unit, the other component being zero; that is, we consider interactions only between nearest neighbors. Furthermore, we assume the $\mathcal{E}_a$ to be the same for interactions along the x and y axes.

The Hamiltonian of Eq. (19), under these circumstances, shows the symmetry of the point group of the square, so that the quantities $F_{aa}(\mathbf{R}_p)$ must transform according to irreducible representations of this point group. First we have the A_1 type of symmetry, in which the wave function transforms into itself under each of the eight symmetry operations of the group. This is the analog of an atomic s state. We find three such states, and the cubic secular equation is

$$E^3-(aa/g/aa)E^2-32\mathcal{E}_a^2E+16\mathcal{E}_a^2(aa/g/aa)=0. \quad (34)$$

The first terms in the expansion of the roots, for small band width, are

$$\begin{aligned} E&=(aa/g/aa)+16\mathcal{E}_a^2/(aa/g/aa)\cdots, \\ E&=\pm4\mathcal{E}_a-8\mathcal{E}_a^2/(aa/g/aa)\cdots. \end{aligned} \quad (35)$$

The first root is the ionic state, and the lower of the other two gives the lowest energy level of the problem, a singlet of s-like symmetry, as we should expect.

We find no solutions of symmetry of type A_2, functions transforming like the quantity $xy(x^2-y^2)$. We have one singlet of symmetry type B_1, which transforms like (x^2-y^2), and one of symmetry type B_2, which transforms like xy. These singlets both have energy of

zero. They are analogs of atomic d states, and are naturally expected to have energies well above the lowest state.

The triplet levels correspond to the two-dimensional irreducible representation of type E, transforming like x and y, or like atomic p functions. There are two such levels, corresponding to energies $E=\pm 2_s \mathcal{E}_a$. The lowest of these triplets, therefore, lies above the lowest singlet as given in Eq. (35). In Fig. 5 we show the way in which these energy levels start off as a function of the band width. The resemblance to Fig. 4, where we plotted the energies in the one-dimensional case, is obvious. We find here, again, as we expected, that the lowest singlet would lie below the lowest triplet, though the energy difference between singlet and triplet is here linear in $\mathcal{E}_a$, rather than quadratic as before. While we have not carried through any more complicated problems, it seems very obvious that we should have the same situation quite generally in this problem of a nondegenerate band. Furthermore, we see that we could handle a more general case to this same approximation without very serious difficulty, taking advantage of the symmetry of the point group of the crystal, setting up secular equations for the energy, and solving to the second power in $\mathcal{E}_a$.

4. THE CASE OF OVERLAPPING BANDS

We have now investigated the case where both electrons are in the same nondegenerate band, and have concluded, as in Sec. 1, that it does not lead to ferromagnetism. Fortunately much of the analysis can be used again in considering the degenerate band, to which we now proceed. Let us assume that there are two bands, a and b, which must both be used in the expansion of the wave function. Thus we must consider F_{aa}, F_{ab}, F_{ba}, and F_{bb}; but we can eliminate F_{ba} by use of Eq. (15). Let us set up the equation similar to Eq. (17) for this case, making the same assumption as before that the integrals involving the g's are to be disregarded unless all four Wannier functions are on the same atom. We find, for the singlets,

$$\sum_s 2\mathcal{E}_a(\mathbf{R}_s)F_{aa}(\mathbf{R}_p-\mathbf{R}_s) +\delta(\mathbf{R}_p,0)[(aa/g/aa)F_{aa}(\mathbf{R}_p)+2(aa/g/ab)F_{ab}(\mathbf{R}_p) +(aa/g/bb)F_{bb}(\mathbf{R}_p)]=EF_{aa}(\mathbf{R}_p), \quad (36)$$

$$\sum_s[\mathcal{E}_a(\mathbf{R}_s)+\mathcal{E}_b(-\mathbf{R}_s)]F_{ab}(\mathbf{R}_p-\mathbf{R}_s) +\delta(\mathbf{R}_p,0)[(ab/g/aa)F_{aa}(\mathbf{R}_p) +\{(ab/g/ab)+(ab/g/ba)\}F_{ab}(\mathbf{R}_p) +(ab/g/bb)F_{bb}(\mathbf{R}_r)]=EF_{ab}(\mathbf{R}_p), \quad (37)$$

$$\sum_s 2\mathcal{E}_b(\mathbf{R}_s)F_{bb}(\mathbf{R}_p-\mathbf{R}_s) +\delta(\mathbf{R}_p,0)[(bb/g/aa)F_{aa}(\mathbf{R}_p)+2(bb/g/ab)F_{ab}(\mathbf{R}_p) +(bb/g/bb)F_{bb}(\mathbf{R}_p)]=EF_{bb}(\mathbf{R}_p), \quad (38)$$

and for the triplets:

$$\sum_s 2\mathcal{E}_a(\mathbf{R}_s)F_{aa}(\mathbf{R}_p-\mathbf{R}_s)=EF_{aa}(\mathbf{R}_p), \quad (39)$$

$$\sum_s[\mathcal{E}_a(\mathbf{R}_s)+\mathcal{E}_b(-\mathbf{R}_s)]F_{ab}(\mathbf{R}_p-\mathbf{R}_s) +\delta(\mathbf{R}_p,0)[(ab/g/ab)-(ab/g/ba)]F_{ab}(\mathbf{R}_p) =EF_{ab}(\mathbf{R}_p), \quad (40)$$

$$\sum_s 2\mathcal{E}_b(\mathbf{R}_s)F_{bb}(\mathbf{R}_p-\mathbf{R}_s)=EF_{bb}(\mathbf{R}_p). \quad (41)$$

The equations for the triplets are separated from each other, but those for the singlets are not. Let us first inquire what can be done about this. To see how to proceed, we must look a little more carefully at the type of overlapping bands which we are likely to have. A case of accidental degeneracy is so unlikely as to be unimportant. The cases which are significant are those where, at the bottom of the band, there are two or more degenerate levels, arising from crystal symmetry. A simple example in the two-dimensional Mathieu problem has been discussed[8] earlier by one of the authors; this is the case of degeneracy arising from an atomic p_x and p_y function, and is typical of the sort of degeneracy which we shall really encounter in the ferromagnetic metals, though of course the problem there, arising from d-electron degeneracy in three dimensions, is more complicated. In reference 8, it was shown that in defining the Wannier functions in such a case, we may if we choose consider one band to consist of the lower energy state for each point in the Brillouin zone, the other band to consist of the higher-energy state at each point. In such a case the resulting Wannier functions, as well as the energies as functions of $\mathbf{k}$, show the complete symmetry of the lattice. However, another of the authors (see reference 6) has pointed out that it is not necessary to proceed in this way, and in fact it

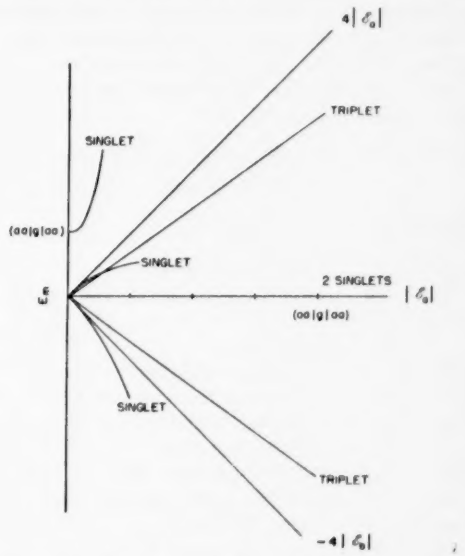

FIG. 5. Energy E_m as function of band width, $|\mathcal{E}_a|$, for two-dimensional model, nondegenerate band.

[8] J. C. Slater, Phys. Rev. **87**, 807 (1952); see particularly pp. 827–831.

is not always desirable. We can instead set up energy surfaces which are discontinuous along certain 45° lines (in a two-dimensional Brillouin zone) or certain planes (in a three-dimensional case), combining the lower of the two energy surfaces on one side of this line with the higher one on the other, in such a way that the resulting energy surfaces transform into each other in the same way as the atomic p_x and p_y functions, under the various symmetry operations of the crystal. If we choose the energy bands in this way, the resulting Wannier functions also transform like p_x and p_y functions, and in fact reduce to those functions in the limit of infinite interatomic distance. For the present purpose, this second type of treatment is more appropriate, since it exhibits the degeneracy in an obvious way.

If we suppose, then, that the band a corresponds to that generated by atomic p_x-like functions, and b to that generated by p_y-like functions, we can at once draw certain conclusions about some of the matrix components on grounds of symmetry. Thus the components like $(ab/g/aa)$ contain just one factor, the function symbolized by b, which changes sign on reflection in the plane $y=0$, so that the integrals must change sign when the sign of y is changed. On the other hand, this merely changes the name of one of the variables of integration, so that it cannot change the value of the integral, which consequently must equal zero. The same is true, as we see by inspection of Eqs. (36), (37), (38), of each component connecting an F_{ab} with either F_{aa} or F_{bb}. Consequently we see that (36) and (38) become equations for F_{aa} and F_{bb} only, while (37) is an equation for F_{ab} only. Furthermore, since the states a and b differ only by a rotation, there will be a degeneracy between Eqs. (36) and (38). We find easily that this degeneracy is to be removed by assuming that $F_{bb}(\mathbf{R}_p) = \pm F_{aa}(\mathbf{R}_p)$. When we insert these assumptions, Eqs. (36) and (38) reduce to

$$\sum_s 2\mathcal{E}_a(\mathbf{R}_s)F_{aa}(\mathbf{R}_p-\mathbf{R}_s)+\delta(\mathbf{R}_p,0)[(aa/g/aa) \pm (aa/g/bb)]F_{aa}(\mathbf{R}_p)=EF_{aa}(\mathbf{R}_p). \quad (42)$$

Furthermore, Eq. (37) reduces to

$$\sum_s[\mathcal{E}_a(\mathbf{R}_s)+\mathcal{E}_b(-\mathbf{R}_s)]F_{ab}(\mathbf{R}_p-\mathbf{R}_s) +\delta(\mathbf{R}_p,0)[(ab/g/ab)+(ab/g/ba)]F_{ab}(\mathbf{R}_p) =EF_{ab}(\mathbf{R}_p). \quad (43)$$

We now see that all the equations which we finally must solve are of the same form as that for the single band, which we discussed earlier. As in that case, we may use the one-dimensional case as a guide in understanding the solution; a problem with p_x- and p_y-like functions on atoms arranged along the z axis would show the desired behavior. In such a case the quantities $\mathcal{E}_a(\mathbf{R}_s)$ and $\mathcal{E}_b(\mathbf{R}_s)$ will be equal, so that Eqs. (42) and (43) will have the same nondiagonal matrix components. In discussing our solutions, let us first take the case where one electron is in each band, so that we are finding F_{ab}, from Eq. (40) for the triplet, (43) for the singlet. We remember that for this case, no symmetry requirements are imposed on F_{ab} on account of the symmetry or antisymmetry of the wave function ψ. The nature of the equations (40) and (43), which have inversion symmetry, demands that the solutions be either symmetric or antisymmetric on inversion, and we can have symmetric solutions for both the singlet and triplet, so that from our earlier discussion we know that the lowest symmetric solution will represent the lowest energy level of the problem. We now notice that the repulsive interaction in the singlet case is $(ab/g/ab)+(ab/g/ba)$, and in the triplet case $(ab/g/ab)-(ab/g/ba)$. Since the exchange integral $(ab/g/ba)$ is positive, this means a smaller repulsive interaction in the triplet. The main consequence of our study of the one-dimensional case was the result that the energy increased as the repulsive interaction increased (since this increased the value of α), so that we conclude unambiguously that of these two states, the triplet lies lower. We cannot conclude that it is the lowest-energy level of the problem, however, until we have examined the other singlets, arising from the case where both electrons are in the same state a, to be sure that they do not lie even lower than this triplet.

These other two singlets are given by Eq. (42), and correspond again to symmetric solutions, with the repulsive interaction $(aa/g/aa)\pm(aa/g/bb)$. We can now see easily that these repulsive interactions are greater than with the solutions we have just considered, in which the repulsive interactions were $(ab/g/ab) \pm (ab/g/ba)$. In the first place, as we can see from the definitions, $(aa/g/bb)=(ab/g/ba)$, so that the separation of levels in either case is the same, and the order of levels will be determined by the two repulsive interactions $(aa/g/aa)$ and $(ab/g/ab)$. The first of these is the interaction of a charge distributed on orbital a, with itself; the second, the interaction of a charge distributed on orbital a with another on orbital b. It seems plausible that the second would be smaller than the first, and calculation in special cases shows that this is indeed the case. Thus, if the two functions a and b are atomic p_x and p_y functions, we can find these various quantities in terms of the well-known F integrals. We find that $(aa/g/aa)$ equals $F^0+(4/25)F^2$, $(ab/g/ab)$ equals $F^0-(2/25)F^2$, so that in fact the second is smaller than the first in this case. Furthermore we find in this special case that $(aa/g/bb)=(ab/g/ba) =(3/25)F^2$, so that the repulsive interactions for the three singlets are $F^0+(7/25)F^2$, $F^0+(1/25)F^2$, and $F^0+(1/25)F^2$; for the triplet, it is $F^0-(5/25)F^2$. On the basis of the magnitudes of the repulsive interactions, we should certainly say in this case that the triplet state was the lowest, and that we should have ferromagnetism.

We have just been discussing a one-dimensional case of the two overlapping bands. Two- and three-dimensional cases can also be handled, by means of difference equations, as in Sec. 3, but here the problem becomes

a good deal more complicated. The reason is that the Wannier functions, instead of transforming into themselves under all operations of the point group, as we tacitly assumed in the case of the nondegenerate band, can under some operations transform into each other, as the p_x- and p_y-like functions do. The wave function of the whole problem, made of a linear combination of these Wannier functions with the coefficients $F_{aa}(\mathbf{R}_p)$, $F_{ab}(\mathbf{R}_p)$, etc., must transform according to an irreducible representation of the point group, but this imposes somewhat complicated requirements on the transformation properties of the F's. We have analyzed a two-dimensional problem, involving the same network of nine points as in the case considered in Sec. 3, but now making wave functions out of the p_x- and p_y-like Wannier functions. Since the results are rather complicated, and not very clearcut, we shall not reproduce the calculations, but shall state the general results. The complications arise because now there are a number of different parameters entering the problem, both different integrals of the nature of $(aa/g/aa)$, etc., and also two quantities of the nature of $\mathcal{E}_a$. One of these arises from the interaction of two p_x-like Wannier functions spaced along the x axis, and the other from two p_x-like functions spaced along the y axis. There is no necessary requirement concerning the relative sizes of these parameters, and the result is that we find that we can choose values of the parameters for which the lowest state is a triplet, but also other values for which a singlet lies lowest.

We find, as in the one-dimensional case, that we can separate the problems for F_{aa} and F_{ab}; that is, the case where both electrons are in one band, and the case where one is in each. As in the one-dimensional case, we find that the lowest state for the case where they are both in one band is a singlet, and the lowest state for the case where there is one in each is a triplet. The ambiguity arises, however, in determining whether the lowest singlet coming for the case where both are in one band lies lower or higher than the lowest triplet. As we have stated above, values of the parameters can be chosen which lead to either of the situations. If we take this as a fair indication of what would be found in a more complete treatment of the three-dimensional problem with overlapping bands, we should conclude that cases can certainly arise where the triplet level lies lowest, and where our two-electron problem leads to ferromagnetism. On the other hand, there can also probably be cases where it does not, and where we should have a nonmagnetic situation. It will take further work, with a model closer to that actually found in the iron group elements, to find which case actually exists in the elements known to be ferromagnetic. The general lines of the approach would probably be similar to those which we have just outlined, using Wannier functions having symmetry properties appropriate to the crystal symmetry, making linear combinations of them having the proper symmetry behavior, and approximately solving the difference equations to get the energies of the various states.

5. DETERMINANTAL FORMULATION OF THE PROBLEM

We have now completed our general argument, so far as it relates to two electrons in a periodic potential, governed by a Hamiltonian $H_1+H_2+g_{12}$. We next wish to show that the real problem, in which the Hamiltonian comes from attractions between the various electrons and the nuclei, and repulsions between the electrons, and in which the two electrons we are considering are in atoms containing closed inner shells, leads to the same sort of results. This is of course to be expected, since we know that closed inner shells act on outer electrons like potential fields. We also wish to show that the problem of two holes in an otherwise filled band, which is the case which is close to the real ferromagnetic problem, acts like that of two electrons. This also is to be expected, on account of Heisenberg's[9] well-known proof of the equivalence of holes and electrons. The proofs of these results are not stated in language very well suited to the present problem, and on account of the importance of these results, not only in the present problem, but in the theory of solids in general, it seems worth while giving a general discussion of these questions. We shall set up this discussion by formulating the problem of holes and electrons in terms of determinantal combinations of Wannier functions (or of Bloch functions), setting up the matrix components of the real Hamiltonian of the problem between such determinantal functions, and showing that they take the same form as the matrix components of Hamiltonians like $H_1+H_2+g_{12}$.

As a preliminary, let us ask how we should formulate the two-electron problem which we have just been considering, in terms of determinantal functions. Instead of starting with the products $a_i(\mathbf{r}_1-\mathbf{R}_m)a_j(\mathbf{r}_2-\mathbf{R}_n)$, we should form spin-orbital one-electron functions, by multiplying the a's by spin functions in the usual way, and forming antisymmetric determinants from them. These two-dimensional determinants would form a complete orthogonal set for expanding any two-electron antisymmetric function of coordinates and spins, so that we should express our wave function as a linear combination of such determinants, the coefficients of this expansion having many similarities to the quantities $U_{ij}(\mathbf{R}_m, \mathbf{R}_n)$ which we have been discussing. We should then have a problem of spin degeneracy. For every pair of orbital functions, such as $a_i(\mathbf{r}-\mathbf{R}_m)$ and $a_j(\mathbf{r}-\mathbf{R}_n)$, there would be four assignments of spin: each orbital could be associated with either a $+$ or $-$ spin. The first step in our problem would be to make the correct combinations of these determinants to describe the resulting single or triplet state. When we had done this, we should end up with wave functions

[9] W. Heisenberg, Z. Physik **10**, 888 (1931).

which were products of functions of coordinates, which would be symmetric for the singlet, antisymmetric for the triplet, and functions of spins. The functions of coordinates would be the same ones which would be built up, according to our previous method of discussion, by combining the two product functions $a_i(\mathbf{r}_1-\mathbf{R}_m)\times a_j(\mathbf{r}_2-\mathbf{R}_n)$ and $a_j(\mathbf{r}_1-\mathbf{R}_m)a_i(\mathbf{r}_2-\mathbf{R}_n)$, with plus or minus sign. Thus we should be led back to the method of discussion which we have already used, but since that is limited to the two-electron problem, we prefer to state our present discussion in terms of the determinantal method, which is quite general.

We wish now to investigate the equivalence of two problems: first, that in which a certain number of electrons (two in the present case) are moving in a self-consistent field determined from other electrons in inner shells, and secondly, that in which all the electrons, including those in inner shells as well as the outer electrons, are moving in the field of the nuclei. Let there be n_0 electrons in inner shells, n_1 outside the inner shells. Let the orbitals corresponding to these inner shells be filled in all configurations which we consider in a problem of configuration interaction, and let these same electrons in filled orbitals be the ones which we consider in setting up a self-consistent field. The Hamiltonian for the self-consistent problem will be $H_0(r_1)+\cdots+H_0(r_{n_1})+\sum(\text{pairs of outer electrons})g_{ij}$, where H_0 represents the one-electron Hamiltonian of an outer electron in the field of the nuclei and the electrons in closed shells, where $r_1\cdots r_{n_1}$ refer to the n_1 outer electrons only, and where the g_{ij} terms represent the Coulomb repulsion of outer electrons. We realize of course at the outset that the eigenvalues of this self-consistent Hamiltonian will not agree at all with the eigenvalues of the true problem, for the eigenvalues of the self-consistent Hamiltonian will include the sum of the one-electron energies of all electrons in closed shells, and it is well known that this sum counts the repulsive interactions between electrons in closed shells twice. Nevertheless this correction term, though large, will be common to each configuration obtained by allowing the outer electrons to be located in different outer orbitals, so that it will appear as a constant correction in the final answer, and will not affect questions relating to the relative position of multiplet levels.

The true Hamiltonian of the complete problem will be the sum of one-electron operators, $f(r_s)$, for all n_0+n_1 electrons, where f includes the kinetic energy operator and the potential energy in the field of the nuclei, and a sum of two-electron operators g_{ij} over all pairs of electrons, the g_{ij}'s again representing Coulomb repulsions. To expand the solutions of this problem, we set up a self-consistent field involving all the electrons, assume that we have energy band solutions of this self-consistent problem, and use either the energy band functions, or the related Wannier functions, as a complete orthogonal set of one-electron functions. We set up all the (n_0+n_1)-dimensional determinants formed from these one-electron functions, when supplemented by spin. Since however we are assuming that the inner shells are always kept filled, we shall consider only those determinants in which all n_0 inner spin-orbital one-electron functions appear, in expanding the true wave function; we explicitly disregard those determinants corresponding to electrons being excited from the inner closed shells. We now wish to compare the diagonal and nondiagonal matrix components of the true Hamiltonian operator, between determinants differing in the orbital or spin configuration of the n_1 electrons outside the closed shells, with the corresponding matrix components of the self-consistent Hamiltonian operator between corresponding determinantal functions formed just from the n_1 spin-orbital functions of the outer electrons. If the two sets of matrix components agree (except for the constant additive correction in the diagonal matrix components, which we have already mentioned), we shall then see that either method of treatment will lead to the same configuration interaction problem.

We need the formulas for matrix components of the true Hamiltonian operator between determinantal wave functions. These well-known formulas[10] can be expressed in terms of certain integrals defined as

$$(i/f/j)=\sum(\text{spin }1)\int u_i^*(x_1s_1)f_1u_j(x_1s_1)dv_1$$

$$(ij/g/kl)=\sum(\text{spin }1)\sum(\text{spin }2)\int u_i^*(x_1s_1)\times u_j^*(x_2s_2)g_{12}u_k(x_1s_1)u_l(x_2s_2)dv_{12},$$

where x_1s_1 stands for the coordinates and spin of the first electron, and so on. The u's are the one-electron functions of coordinates and spin. We note that $(ij/g/kl)$ is zero unless the spins of u_i and u_k are the same and the spins of u_j and u_l are the same. In terms of these symbols, we find that the diagonal matrix component of energy with respect to a determinantal wave function equals

$$\sum(i)(i/f/i)+\sum(\text{pairs } i,j)[(ij/g/ij)-(ij/g/ji)], \quad (44)$$

where the sums are to extend over all one-electron orbitals occupied in the determinant, and where the exchange integral $(ij/g/ji)$ is zero unless u_i and u_j correspond to the same spin. The nondiagonal matrix component between two determinantal wave functions will be zero if the two determinants differ in more than two orbitals. If they differ in just two, say by having orbitals u_i and u_j replaced by u_i', u_j', all others being common to both determinants, the nondiagonal matrix

[10] For diagonal components, see J. C. Slater, Phys. Rev. **34**, 1293 (1929); for nondiagonal components, J. C. Slater, Phys. Rev. **38**, 1109 (1931); note a typographical error there in the formula for a quantity called $(U/G/U')$. For the nondiagonal components, see also E. U. Condon, Phys. Rev. **36**, 1121 (1930).

component is

$$(ij/g/i'j')-(ij/g/j'i'). \tag{45}$$

If they differ in one orbital, u_i being replaced by u_i', all others being common to both determinants, the nondiagonal matrix component is

$$(i/f/i')+\sum(k\neq i)[(ik/g/i'k)-(ik/g/ki')]. \tag{46}$$

The formulas which we have just written are correct for the true Hamiltonian, and the determinantal wave functions formed from one-electron orbitals of all electrons in the system. Let us now consider the corresponding formulas when we use the self-consistent Hamiltonian, and determinantal wave functions formed from the n_1 one-electron orbitals for the electrons outside closed shells only. The formulas are unchanged, provided we make several changes in interpretation. First, all summations are to extend only over the orbitals representing electrons outside closed shells. Secondly, the one-electron operator f, instead of being kinetic energy and the potential energy in the field of the nuclei, is to be the self-consistent one-electron operator H_0 previously mentioned. Let us now examine the exact formulas (44), (45), (46) for matrix components, and see to what extent they can be thrown into this alternative form to represent the self-consistent problem.

First we consider the diagonal matrix component (44). In the term $\sum(i)(i/f/i)$, we first have the sum over the outer electrons, which we shall consider in a moment, and then the sum over the inner electrons, which is merely a constant as far as our present problem is concerned, identical for all configurations which we must consider, and therefore which we may disregard. In the double sum over pairs, we have three sorts of terms: those in which both electrons of the pair are in closed shells, which again contribute only to a constant energy, and may be disregarded; those in which one electron is in a closed shell, the other outside; and those in which both electrons are outside closed shells. These latter terms are identical for the true problem and the self-consistent problem, so that we do not have to consider them further. We must then show that the sum of terms $(i/f/i)$ over the outer electrons, plus the sum of quantities $(ij/g/ij)-(ij/g/ji)$ in which one of the electrons is in an orbital u_j in a closed shell, the other in an orbital u_i outside closed shells, is equivalent to the sum of terms $(i/H_0/i)$ over the electrons outside closed shells, where the symbol $(i/H_0/i)$ stands for $\int u_i^*(x_1)H_0u_i(x_1)dv_1$.

We now notice that the sum of quantities $(ij/g/ij)$, where j is summed over the orbitals in the closed shells, is the total Coulomb interaction of an outer electron in orbital u_i, with the charge density of all electrons in the closed shells. Thus this sum, plus the quantity $(i/f/i)$ is the diagonal matrix component of the kinetic energy of the electron in orbital u_i, plus its potential energy in the field of the nuclei, and of all electrons in closed shells. If our self-consistent Hamiltonian H_0 consisted just of these terms, and if the exchange integrals $(ij/g/ji)$ were not present, we should have demonstrated the equivalence of the two problems. Let us consider these exchange integrals more in detail.

We may rewrite the integral $(ij/g/ji)$ in the form

$$\int u_i^*(x_1)u_i(x_1)\left[\frac{u_i^*(x_1)u_j^*(x_2)g_{12}u_j(x_1)u_i(x_2)}{u_i^*(x_1)u_i(x_1)}dv_2\right]dv_1, \tag{47}$$

provided the spins of u_i and u_j are the same, a form suggested by the method of treating the Hartree-Fock equation discussed by one of the present authors.[11] This represents the Coulomb interaction between the electron in orbital u_i, and a charge density $[u_i^*(x_1)u_j^*(x_2)u_j(x_1)u_i(x_2)]/[u_i^*(x_1)u_i(x_1)]$, a charge density at point x_2, depending parametrically on the position x_1 of the electron in question. In reference 11, it was pointed out that the sum of such charges, summed over all values of j, both in closed shells and for the electrons outside closed shells, has interesting properties. It represents a total charge distribution amounting to one electronic charge, whose maximum density comes at the position x_1 of the electron in question, where it equals the density of all electrons of the appropriate spin at that point of space. This sum was called the exchange charge density in the reference just quoted.

Our present summation, however, is only over the electrons in the closed shells, and has a different significance. We readily find, by integrating over x_2, that this total charge density is zero. When x_2 equals x_1, it reduces to the total charge density of electrons in closed shells, having the same spin as u_i, at the point x_1. Since the total charge density is zero, it must have opposite sign at some other positions. In other words, we have found that the diagonal matrix component of energy in the exact problem includes a sum of one-electron energies of all electrons outside closed shells, consisting of the kinetic energy of the electrons, their potential energy in the field of the nuclei and of all electrons in closed shells, and their potential energy in the field of these exchange charges whose total charge densities integrate to zero. These exchange charges are different for each u_i, so that we cannot say that the true diagonal matrix components are just as if we had a self-consistent problem, but if we disregard these exchange charges, we can make that statement, and we should then conclude that the self-consistent field to use in the present problem is that arising from the nuclei, and all electrons in inner shells, with no correction at all for exchange. Since the important exchange effects are between electrons in the same shell, which we are taking into account explicitly in our present treatment of configuration interaction of the outer

[11] J. C. Slater, Phys. Rev. **81**, 385 (1951); see Eqs. (4), (5).

electrons, we feel that we shall not make a serious error if we disregard these exchange effects between the outer electrons and those in the closed shells. It is only to the extent to which we are justified in doing so that our replacement of the true problem by a self-consistent treatment of the inner shells is justified.

Let us now consider the same sort of question for the nondiagonal matrix components of energy. The non diagonal matrix components of the form (45), involving changes in two outer electrons, are just the same whether we use the exact method or the self-consistent method, and hence need not be further discussed. As for the components of form (46), encountered when only one outer electron shifts from one orbital to another, the terms in the summation for which k refers to an outer electron are the same in the exact and the self-consistent method, and need not be further discussed. The summation of the terms $(ik/g/i'k)$ over orbitals u_k in the closed shell gives us just the nondiagonal matrix component of the Coulomb interaction between the outer electron, and all electrons in inner shells. Thus, if we are using for H_0 the kinetic energy, the potential energy in the field of the nuclei, and in the field of all inner electrons, these terms give just the contribution to the nondiagonal matrix components of H_0 required to take account of the Coulomb interactions with the inner electrons. Finally, the sum of terms $(ik/g/ki')$ in which u_k goes over the inner shells yields nondiagonal matrix components of the interaction with the same type of exchange charge, whose total integral vanishes, which we have already decided to disregard in considering the diagonal matrix components.

We see finally, then, that if we take the self-consistent operator H_0 as representing the kinetic energy of an electron, and its potential energy in the field of the nuclei and of the charge of all electrons in closed shells, without any exchange correction, then the self-consistent problem for the outer electrons, and the true problem, will have the same matrix components of energy for the configuration interaction problem, provided we disregard exchange interactions between the outer and the inner electrons. We have seen furthermore that these neglected exchange interactions are not the major ones involved in the problem, since those are exchanges between the outer electrons, which of course we are retaining in our configuration problem. Thus we feel that this procedure of replacing inner shells by a potential field is justified well enough to make it useful, and in particular well enough so that we can trust the results of earlier sections, in which we have discussed the configuration interaction problem of two electrons in such a potential field.

One word of caution should be spoken here, as a warning to those who may use this method of replacing inner shells by a potential field. As we have set up the method, the wave functions of the outer electrons are to be expressed as linear combinations of Bloch or Wannier functions of the outer bands, as derived from a self-consistent field problem in which all electrons of the system are taken into account (and which therefore, in general, is quite a different self-consistent field from that involved in our one-electron Hamiltonian H_0, though in our present problem of two electrons only in outer shells the two are indistinguishable). This means that the wave functions of the outer electrons are automatically kept orthogonal to those of the electrons in closed shells. We must remember that unless some such means is adopted for keeping the wave functions of outer electrons orthogonal to those of inner closed shells, we may run into grave errors in treating the outer electrons as a problem by themselves, merely in a periodic potential field. For we are likely to end up with some sort of wave function for the outer electrons which is not orthogonal to the inner shells, and in such a case the energy can appear to decrease greatly, in a way which has no physical significance. In other words, we are running into the fact that a variation method may not be used for the wave functions of the outer electrons of an atomic system, unless we impose an additional condition that the wave functions are kept orthogonal to all lower wave functions of the system.

We have now discussed the determinantal formulation of our problem enough to justify our use of the self-consistent method. It remains only to show that the problem of a certain number (in our case two) of holes in otherwise filled bands will behave in many ways like an equal number of electrons in an empty band. In finding each matrix component of energy, we first find the component as if all holes were filled, and then subtract out those terms coming from the missing electrons. Thus, in the terms $(i/f/i)$ in Eq. (44), from the diagonal matrix component, we include terms for all electrons in the band (which then will drop out of our problem as an additive constant, when we compare with the self-consistent problem), and subtract from this the terms relating to the holes, or missing orbitals. These terms then appear with negative sign in the final energy. Similarly in the Coulomb integrals $(ij/g/ij)$ from Eq. (44), we include terms between all pairs of electrons in all bands, with the holes filled; we subtract the terms between each hole and all other orbitals (including those which actually are not occupied on account of the holes); and finally we add terms between pairs of unoccupied orbitals, or pairs of holes. The terms which we have subtracted amount to the Coulomb interaction between each hole and the complete electronic charge of all bands, aside from its own charge. In the exchange terms $(ij/g/ji)$, we similarly include all terms between all pairs of orbitals, whether occupied or not; subtract those between each hole and all other orbitals; and add those for interaction between holes. In other words, the diagonal matrix component of energy equals a constant, minus the diagonal matrix components of one-electron energy for the various holes, in self-consistent fields determined from the nuclei, the complete charge of all electrons, but di-

minished by an exchange correction which is just like that met in the Hartree-Fock method, and which is discussed in reference 11; and finally, plus the Coulomb and exchange corrections between pairs of holes, appearing with the same sign as if they were pairs of electrons. As for the one-electron energies, it was shown in reference 11 that we do no great violence to the problem to replace the Hartree-Fock self-consistent field, which is slightly different for each orbital, by an averaged self-consistent field, as given in Eq. (7) of that reference, and this is the type of self-consistent field which we should use here.

Before passing on to the nondiagonal matrix components, let us see that these diagonal components are consistent with the usual interpretation of holes as being particles of positive charge. If our one-electron orbitals are Bloch functions, the one-electron energy will appear in the diagonal matrix component, and the usual energy band interpretation of the behavior of holes assumes that the energy of the whole crystal is a constant, minus the one-electron energy of the holes, which agrees with our present findings. In the usual energy band treatment, we do not consider the interaction energy between electrons, unless we are dealing with a correlation or ferromagnetic problem, but if we consider such terms, we assume that these represent Coulomb repulsions and exchange integrals just as if the particles were positive electrons. The Coulomb and exchange integrals, depending on the products of the charges of the two particles, should have the same sign whether we are dealing with holes or electrons, and this is what we find.

We have a similar situation for the nondiagonal matrix components. Thus, if two holes u_i and u_j are replaced by holes u_i' and u_j', the problem is just like that if electrons in orbitals u_i' and u_j' changed to u_i and u_j, so that the nondiagonal matrix component is just that given by Eq. (45), exactly like the matrix component between the corresponding electrons. In the case where one hole only changes from orbital u_i to u_i', and we are using Eq. (46), the same sort of consideration shows that there will be one-electron terms of opposite sign to those for an electron, and representing the one-electron nondiagonal matrix component of energy in a self-consistent field which may again be replaced by the averaged self-consistent field of reference 11; plus two-electron terms of the same sign as those found for electrons. If we are using Bloch functions, there will be no nondiagonal one-electron matrix components of energy, but with Wannier functions these components are what result in the one-electron energy, as we see from Eq. (5), for instance. It is then clear, for instance from Eq. (10), that it is right for these terms to come in with negative sign for the holes. For when we are using the operator form of these nondiagonal matrix components, if we are dealing with the top of a band, as we usually are with holes, the one-electron energy E_k for a nondegenerate band will be a constant, minus a term in the square of k. When we use the negative of this, we find that the correct energy of the band lacking a hole will be a constant, plus a term in the square of the k of the hole, which is as it should be, the lowest energy coming when the hole is at the top of the band.

The net effect of our calculations of the present section, then, is that we are justified in treating a simplified problem of electrons or holes in a self-consistent field, to the same extent that we are justified in using a single self-consistent field according to the methods of reference 11. Furthermore, we find that the exchange integral terms come in with the same sign, whether we are dealing with electrons or holes. In other words, whichever case we are considering, Hund's rule will still lead to the triplet states of a two-electron atomic system lying lowest, and the conclusions of the present paper regarding the relative order of levels will hold whether we are dealing with electrons or holes. This of course agrees with the well-known case of atomic spectra, in which the energy separations of a shell of equivalent electrons containing two electrons (say a p^2 configuration) are given by the same F and G integrals as the separation of a complete shell with the same number of holes (as in a p^4 configuration).

Absorption of Infrared Light by Free Carriers in Germanium

H. B. Briggs and R. C. Fletcher
Bell Telephone Laboratories, Murray Hill, New Jersey
(Received June 3, 1953)

The absorption of infrared light associated with the presence of free carriers in germanium has been measured by injecting these carriers across a $p-n$ junction at room temperature. The absorption is found to be proportional to the concentration of carriers. The absorption as a function of wavelength shows the same rather sharp maxima previously observed in normal p-type germanium. These bands are found to change with temperature. An explanation of this absorption is offered in terms of a degenerate energy band scheme.

THE presence of donor or acceptor impurities in germanium has been found to cause additional absorption of infrared light of wavelengths greater than the fundamental absorption limit of two microns.[1-3] Some such absorption would be expected according to the classical Drude-Zener[4] theory of the optical properties of the free carriers, which in this case are the holes and electrons released by the ionized impurities. However, the observed absorption is two to three orders of magnitude higher than the Drude-Zener theory would predict.[1-3] In addition for p-type germanium, the absorption has structure[3] instead of increasing uniformly with the square of the wavelength as the Drude-Zener theory predicts for this wavelength range. These observations have led us to perform two additional types of experiments. First, in order to show that the additional absorption, particularly in p-type germanium, is really caused by the free carriers, we have measured the excess absorption caused by free carriers which have been *injected* into the germanium. Second, the absorption by p-type germanium in thermal equilibrium has been measured as a function of temperature.

EXPERIMENTAL METHOD

The first experiment depends upon the injection of free carriers across a $p-n$ junction when the junction is biased in the forward, or low resistance, direction.[5] If the light, whose absorption is to be measured is allowed to pass through the sample in a narrow beam parallel and near to the junction, the injected carriers will cause an increase in absorption which can be measured.[6]

A single crystal of germanium containing a junction between 2.0 ohm-cm, p-type (gallium doped) and 5.5 ohm-cm, n-type (arsenic doped) was finished in a rectangular block $1.5\times1.0\times0.4$ cm, the plane of the junction being perpendicular to the long dimension. The sides exposed to the light were finished plane parallel and polished.

The germanium block fitted in a groove in a Bakelite mount (Fig. 1). The attachments S_1S_2 are opaque shields with 0.5-mm apertures which limited the light beam to a narrow region in the germanium. The germanium block could be moved with respect to the apertures with a calibrated screw. P_1 and P_2 are voltage probes positioned 0.75 mm apart at each edge of the aperture in S_1 and making contact with the germanium, and I_1I_2 are current leads making pressure contacts with the gold-plated ends of the germanium block. Sample and mount were supported in front of the entrance slit of a Perkin-Elmer spectrometer, the plane of the junction being parallel to the slit.

The increased absorption caused by the injected carriers was determined by modulating the voltage applied across the junction with a 10 cps rectangular wave obtained from a motor driven commutator and detecting the rectangular wave of transmitted light with either a lead sulfide photocell or a thermocouple followed by an amplifier and rectifier. This signal was compared with the signal obtained by eliminating the modulation voltage across the junction and inserting a light chopper, driven by the same motor as the commutator at the same frequency, and using the same

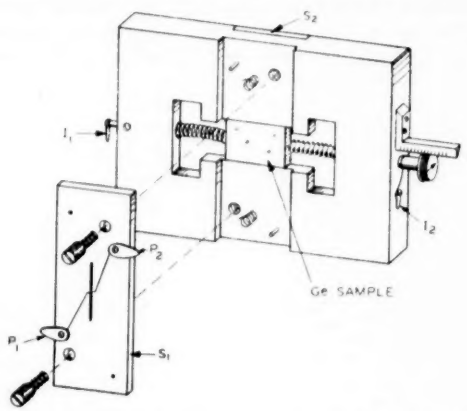

FIG. 1. Experimental arrangement for measuring infrared light absorption by injected carriers; I_1I_2 are the current leads to the $p-n$ junction, P_1P_2 are the voltage probes, and S_1S_2 is the light shield in which the illuminating slit is cut.

[1] H. Y. Fan and M. Becker, *Proceedings of Reading Conference* (Butterworths Scientific Publications, London, 1951), pp. 132–147.
[2] H. B. Briggs, Phys. Rev. **77**, 727 (1950); M. Becker and H. Y. Fan, Phys. Rev. **76**, 1531 (1949).
[3] H. B. Briggs and R. C. Fletcher, Phys. Rev. **87**, 1130 (1952).
[4] E.g., see F. Seitz, *Modern Theory of Solids* (McGraw-Hill Book Company, Inc., New York, 1940), p. 639.
[5] W. Shockley, Bell System Tech. J. **28**, 435–489 (1949).
[6] This type of absorption was first suggested to one of us by R. L. Wallace, August 30, 1949. Similar suggestions have been published: K. Lehovec, Proc. Inst. Radio Engrs. **40**, 1407 (1952).

detection scheme. If the ratio of the first signal (voltage modulation) to the second signal (light modulation) is called r, the absorption coefficient attributable to the injected carriers, α_i, is given by

$$\alpha_i = \frac{1}{d} \ln\left(\frac{1}{1-r}\right),$$

where d is the thickness of the sample traversed by the light. This formula neglects changes in multiple reflections caused by α_i, an approximation which introduces an error of less than 4 percent in the experiments to be described. This method of measuring α_i is not subject to errors in determining the reflection coefficient or to the errors introduced by changed light paths which are normally encountered in measuring absorption coefficients.

The concentration of added carriers attributable to hole or electron injection was determined from measurements of voltage across the probes P_1P_2 and current

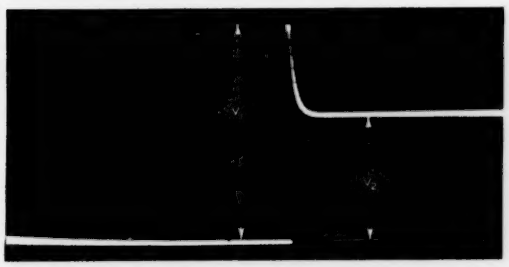

FIG. 2. A photograph of the oscilloscope trace of the voltage across the probes P_1P_2 as a function of time after the forward voltage is applied across the $p-n$ junction. The initial deflection V_1 is associated with the conductivity of normal germanium before the injected carriers arrive. The steady-state value of V_2 is associated with the increased conductivity of the injected carriers added to the normal conductivity.

through the sample. The voltage across P_1P_2 was displayed on an oscilloscope screen through a balanced input amplifier. A photograph of a typical oscilloscope pattern is shown in Fig. 2. The initial rise V_1, arises from the conductivity of normal germanium before the injected carriers arrive at the probes. The sharp drop to an intermediate position is caused by the arrival of the injected carriers, so that V_2 arises from the combination of the conductivity of the normal germanium plus that associated with the injected carriers. For every injected carrier added, there must also be an extra carrier added of the type normally present in order to preserve neutrality. Thus, for an n-type sample, if σ_n and σ_i represent the normal and increased conductivities, respectively, and n and p_i equal the concentrations of the normal and injected carriers, respectively,

$$\sigma_n = ne\mu_n,$$
$$\sigma_i = ne\mu_n + p_i e(\mu_n + \mu_p),$$

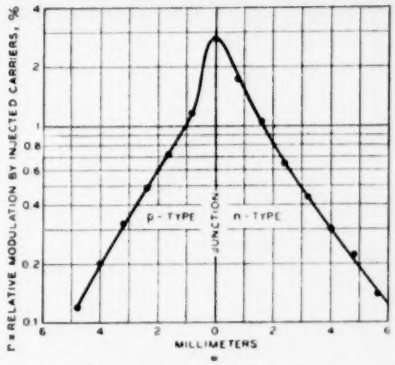

FIG. 3. Modulation of infrared light by carrier injection versus distance from the $p-n$ junction: $\lambda = 2.4\mu$, injection current = 100 ma.

so that

$$p_i = \frac{\sigma_i - \sigma_n}{e(\mu_p + \mu_n)}.$$

Here μ_n and μ_p are the mobilities of electrons and holes, respectively, and e is the electronic charge. Heating effects in the germanium sample containing the $p-n$ junction restricted the injection currents to values not greater than 1 ampere per cm^2 for which value the maximum calculated carrier density was 2×10^{15} per cm^3.

Measurements have also been made on p-type and n-type samples in thermal equilibrium (hereinafter called normal to distinguish them from the injection experiments). Extinction coefficients for these samples were obtained by the conventional means of measuring the ratio of incident to transmitted light, and using a value for the reflectivity obtained from a separate experiment. The carrier densities were calculated from resistivity measurements using the drift mobilities measured at room temperature for lattice scattering[7] and corrected for impurity scattering according to the Conwell-Weisskopf[8] formula. This method was checked by using two p-type samples in which J. D. Struthers of these Laboratories had measured the impurity concentration by using radioactive gallium for the impurity. The temperature dependence of the absorption of the several p-type samples was measured by putting the sample in contact with a copper block, which was cooled by an appropriate refrigerant. Higher temperatures were obtained by passing heavy currents through the samples. Temperatures were measured with an iron-constantan thermocouple attached to the pressure contacts to the samples.

RESULTS

The relative modulation of light by injected carriers, $r = \alpha_i d$, is shown in Fig. 3 as a function of distance from

[7] J. R. Haynes and W. Shockley, Phys. Rev. **81**, 835–843 (1951).
[8] E. M. Conwell, Proc. Inst. Radio Engrs. **40**, 1330 (1952).

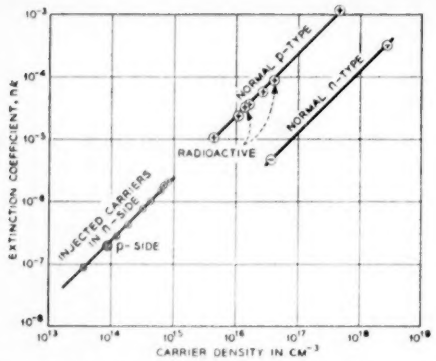

FIG. 4. The extinction coefficient due to injected carriers plotted *vs* carrier density at a wavelength of 2.5μ. To compare with this the extinction coefficient of several normal germanium samples are plotted *vs* their carrier densities. The heavy straight lines are drawn at 45° on the log-log plot indicating a direct proportionality. The carrier densities of the two samples indicated by arrows were determined by radioactive methods.

the $p-n$ junction. To obtain these points the crystal was moved with respect to the illuminating slit. The resulting straight lines on this semilog plot indicate approximately an exponential dependence of α_i on distance. Because of the high current densities used in these experiments, the current is mainly carried by field drift rather than diffusion. Thus, the slopes of the two exponentials determine the distance the minority carriers drift in a lifetime. This distance is approximately 0.19 cm on both sides of the junction for the current used in Fig. 3. In the experimental results to follow, the slit was maintained from 1.5 to 4 mm from the junctions.

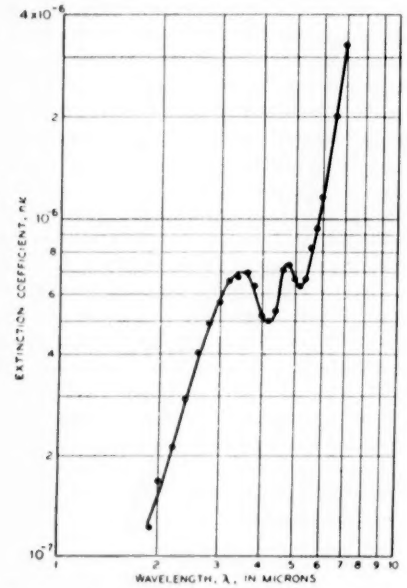

FIG. 5. The extinction coefficient for injected carriers plotted *vs* wavelength of the incident light (total carrier density $=3\times10^{14}$ cm^{-3}). The absorption maxima at 3.4μ and 4.7μ previously observed in normal p-type germanium (see reference 3) are clearly evident here also.

The dependence of the absorption on carrier density as obtained by injection methods is compared with that obtained by conventional methods in Fig. 4. The circled points are values of the extinction coefficient ($\lambda\alpha_i/4\pi$) measured for injected carriers as a function of the added carrier density (p_i). Light of 2.5μ wavelength was used, with the light slit located on the n side of the junction. Essentially the same results were obtained by injection into the p side of the junction, as is indicated by the doubled-circle point. The circled crosses represent the values of the extinction coefficient at the same wavelength for normal p-type germanium (Ga-doped) as a function of hole density. Likewise the circled bars indicate the extinction coefficients for some n-type germanium (As-doped). The straight lines on this log-log plot are drawn at a 45° angle indicating that the extinction coefficient is proportional to the carrier concentration. This same proportionality was found using wavelengths of 3.4μ, 4.2μ, and 4.8μ. This proportionality can be expressed as a cross section by dividing the absorption coefficient by the carrier concentration. For the injected carriers the cross section at 2.5μ as determined from Fig. 4 is thus 1.2A^2. For the p-type samples the cross section is 1.2A^2 and for n-type samples it is 0.07A^2. It can be observed that the cross section for injected carriers is very nearly the sum of the cross sections of the n- and p-type samples, as it should be if the absorption in both instances is by the free carriers.

Figure 5 shows the extinction coefficient as a function of wavelength for injection into the n-type side of the junction for a total injection carrier density (holes plus electrons) of 3×10^{14} cm^{-3}. The absorption maxima at 3.4μ and 4.7μ previously reported for normal p-type germanium[3] are clearly present also in the absorption by injected carriers into n-type germanium.

Finally the absorption by normal p-type germanium for several different temperatures is plotted in Fig. 6.[9] This absorption is plotted as a cross section, by subtracting from the observed absorption the absorption in a pure sample, which is presumably caused by lattice interactions, and dividing by the carrier density. Also, for convenience of theoretical interpretation the wavelength has been converted to photon energy. It is observed that the cross section of the 0.39 ev ($\lambda=3.2\mu$) absorption maximum increases, sharpens, and moves to lower energies as the temperature is decreased. The absorption of the 0.26 ev ($\lambda=4.7\mu$) maximum decreases until it practically disappears at low temperatures. The broad maximum at low photon energies (0.06 ev or 20μ) increases and sharpens as the temperature is lowered.

[9] Reports of similar work have been made by Kaiser, Collins, and Fan, Bull. Am. Phys. Soc. **28**, No. 2, 32 (1953).

DISCUSSION

The simplest way to explain the direct proportionality between the absorption and the concentration of the carriers is to assume that the extra absorption observed in the infrared is caused by the free carriers, whether they be introduced by ionization of chemical impurities or whether they are injected across junctions.

We have considered two other possibilities to explain the observed proportionality. First, the absorption might be associated with the normal ionized acceptor and donor impurities. This absorption would be proportional to the number of such impurities present and would thus explain the observed proportionalities in normal samples. However, the fact that injected carriers have the same absorption eliminates this as a possibility. In addition, experiments have been carried out with compensated samples in which the carrier density was not proportional to the impurities.[8] In these the absorption was found to be proportional to the carrier concentration and not to the impurity concentration.

A second possibility is that the absorption is associated with impurities other than the impurities governing the electrical resistivity or with crystal imperfections. These are assumed to introduce an energy level into the forbidden band from which either electrons or holes can be excited by absorbing light. This possibility is suggested particularly by the absorption bands observed in p-type germanium. In order that this absorption be proportional to the carrier concentration we must assume that the carriers change the population of these levels. For instance, consider the absorption caused by ionizing a hole trapped on an impurity level (Fig. 7). In this case the absorption will be proportional to the number of empty impurity levels. If the Fermi level is above the impurity level, as shown in Fig. 7, the relative population of levels in the impurity level and in the valence band will be governed by a Boltzmann distribution. That is, the number of empty impurity levels in thermal equilibrium will be proportional to the number of free holes. This would thus explain the observed proportionality between absorption constant and free holes.

When carriers are introduced by injection, however, the holes are not in thermal equilibrium, and we would expect that the ratio of empty impurity levels to free holes would be considerably different. The fact that the cross section for injected carriers is the same as that for carriers in thermal equilibrium strongly suggests that the absorption is not caused by impurities or imperfections.

Moreover it should be pointed out that in order for the cross section to remain constant from sample to sample, the concentration of impurity levels must remain constant. Every sample tried had essentially the same cross section. This same cross section has also been measured on samples prepared in other laboratories with different doping materials.[10] It seems most unlikely that an uncontrolled impurity or imperfection would remain as constant under such a variety of situations.

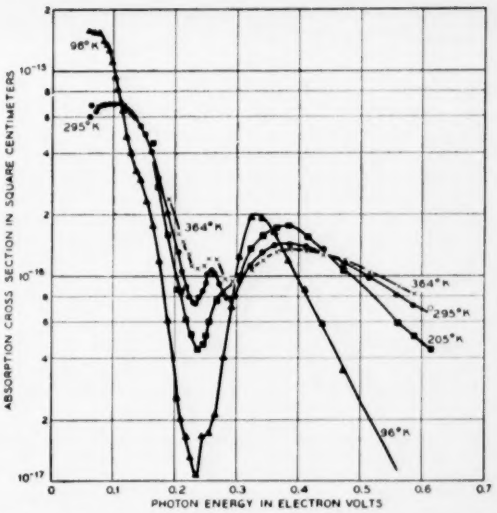

FIG. 6. The absorption cross section for free holes measured in normal p-type germanium plotted *vs* the energy of the incident light for four different temperatures. The lattice absorption at long wavelengths (energies less than 0.1 ev) has been subtracted from the normal absorption in order to get the cross section.

Finally, it should be observed that in order for the absorption to be ascribed to empty energy levels in the forbidden band, the cross section for capture of photons by these empty levels is required to be extremely large. If the number of impurity levels is so small that it does not affect the resistivity in fairly pure samples where the concentration of donors and acceptors are lower than 10^{14} cm^{-3}, the impurities must be present in concentrations smaller than this. At the same time the extinction coefficient for the heaviest concentration of

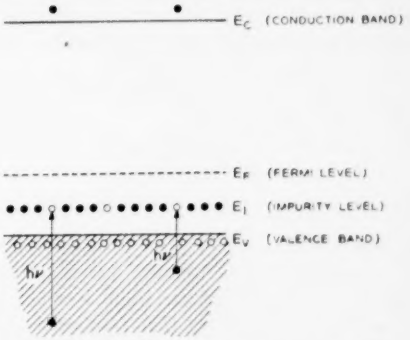

FIG. 7. An energy scheme for impurities or imperfections (E_I) which could explain how an impurity absorption could be proportional to the concentration of free holes as long as the Fermi level is above the impurity level. This is probably not the explanation of the observed absorption, however.

[10] D. Cronemeyer (private communication).

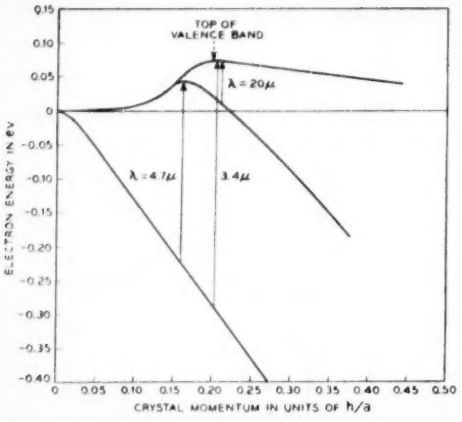

FIG. 8. A proposed energy scheme for the degenerate bands within the valence band plotted *vs* the crystal momentum of an electron along the direction in which the valence band has its maximum energy. The absorption maxima in *p*-type germanium are indicated by the arrows. This scheme is consistent with the observed dependence of the absorption cross section of free holes on wavelength and temperature. (Here h is Planck's constant and a is the edge length of the unit cube.)

holes (Fig. 4) is observed to reach values of 10^{-3} (corresponding to an absorption constant of 50 cm^{-1}). Even if all of the impurity levels were empty, this would require a cross section for capture of photons by empty impurity levels in excess of 5000A², an unreasonably large value.

Thus to summarize we do not believe the extra absorption beyond the fundamental absorption edge can be associated with the normal acceptors or donors because the cross section measured in normal samples is the same for (1) injected carriers and (2) compensated samples. We do not believe it is associated with impurities or imperfections because (1) the cross section is the same for injected carriers, (2) the concentration of such uncontrolled impurities is required to be the same for different samples and (3) too large a cross section is required. We feel that the most reasonable explanation of the extra absorption is that the free carriers themselves are absorbing the light by some mechanism other than that proposed by the simple Drude-Zener theory.

Bardeen has proposed a modification of the Drude-Zener theory[11] which predicts a higher absorption cross section. He points out that the optical modes of vibration may contribute to the scattering of the excited carriers whereas these modes have only a small influence on the scattering of the unexcited carriers. Thus the mean free time between collisions would be much smaller for the excited carriers than that estimated from the mobility of the thermal carriers, and a larger cross section for capture of a photon would be expected. This may explain the absorption observed in *n*-type germanium, where the dependence on wavelength is approximately that predicted by the Drude-Zener theory.[1] In *p*-type germanium the appearance of absorption bands with an unpredicted temperature dependence suggests that an entirely new explanation needs to be found.

[11] J. Bardeen, Phys. Rev. **79**, p. 216 (1950).

POSSIBLE EXPLANATION OF ABSORPTION BY FREE HOLES

A possible explanation of the absorption by free holes might be that the light induces transitions between the various branches of the degenerate bands.[12,13] The feature of such degenerate bands which is essential for explaining the observed absorption is that there be two energy maxima, associated with different bands and/or directions, which are within approximately 0.03 ev of each other. One possible energy scheme is shown in Fig. 8. Here the electron energy of the three degenerate bands within the valence band is plotted against the crystal momentum in such a way as to be approximately consistent with the observations. The scale of the momentum axis was chosen so that the effective mass associated with the curvature at the top of the valence band be made equal to the free electron mass. The absorption bands arise because two of the bands are assumed to have maxima at values of momentum greater than zero. The holes will be concentrated within $\approx kT$ of the highest maximum, so that if the next highest maximum is within kT of the first, it will have an appreciable population. Transitions may thus occur from both maxima to the lower band, giving rise to the two absorption bands. The long wavelength (low-energy) absorption may be caused by transitions between the two upper bands. As the temperature is lowered, the lower-energy maximum will become depopulated and the associated absorption maximum will disappear. The other absorption band will increase and narrow. Finally, the long wavelength absorption will also tend to increase and its cutoff will shrink to lower photon energies. These effects are just what are observed.

There are, however, theoretical objections to the above explanation. Calculations[13] which have been made of the energy band structure indicate that the valence band is of the order of 10 ev wide. The detail shown in Fig. 8 covers only 0.3 ev. This suggests that all of this detail occurs near the center of the Brillouin zone, ca, $P<h/20a$. Such detail does not seem to be within the framework of the theoretical calculations.[13] In addition it requires a rather small effective mass (ca, $\frac{1}{10}$ of the free electron mass). These objections have not yet been resolved.

The authors are glad to acknowledge their indebtedness to J. R. Haynes, who suggested the techniques used in the measurement of absorption by injected carriers, to Conyers Herring for stimulating discussions, and to H. R. Moore who designed and built the detector amplifier system used in the measurements.

[12] W. Shockley, Phys. Rev. **78**, 173 (1950).
[13] F. Hermann and J. Callaway, Phys. Rev. **89**, 518–19 (1953).

The Atomic Heat of Germanium below 4°K*

P. H. KEESOM AND N. PEARLMAN
Department of Physics, Purdue University, Lafayette, Indiana
(Received May 25, 1953)

The atomic heat of germanium below 4°K has been measured with pure polycrystalline and single crystal ingots, indium and antimony doped single crystal ingots, and pure crushed material. The lattice contribution is in all cases proportional to T^3 and corresponds to a Debye temperature of (362±6)°K, which agrees with the value calculated from elastic constants. From the degree to which this cubic term represents the total measured atomic heat, the estimated upper limit for the ratio of the effective carrier mass to that of free electrons is found to be in the neighborhood of unity.

I. INTRODUCTION

THE atomic heat of germanium has been of special interest since Critescu and Simon[1] reported an anomalous peak in the atomic heat curve around liquid nitrogen temperatures. Recently, two measurements in the liquid hydrogen range and higher, which do not reproduce this anomaly, have been reported.[2,3] Detailed information on the vibration spectrum, such as has been obtained by Smith[4] for diamond and by Hsieh[5] for germanium (which also crystallizes in the diamond lattice) is necessary for calculation of the atomic heat in this temperature range. Blackman has shown,[6] however, that below about $\theta/50$ or $\theta/100$ (true T^3 region), where θ is the Debye temperature, it should be possible to apply the Debye theory[7] and thereby calculate θ from elastic constants. This has been done for silicon,[8] but no heat capacity data at very low temperatures have been reported for other elements which crystallize in the diamond lattice, except for two preliminary communications[9–11] of measurements on germanium in the liquid helium region. There was a large discrepancy, however, between the two results, amounting to a factor of over two in the atomic heat. Since Estermann and Friedberg[9,10] used crushed germanium in a copper calorimeter containing helium exchange gas whereas we used ingots suspended in vacuum, we have also measured crushed germanium in an effort to determine the cause of the disagreement.

We were also interested in seeing if the linear term in the atomic heat below 4°K also reported by Estermann and Friedberg[9] in one of their specimens was real. They attributed this term to the heat capacity of holes with effective mass about seven times that of free electrons, the holes being contributed by impurity atoms. We found a term corresponding to electronic specific heat in our measurements on silicon,[8,11,12] but from those results and our earlier measurements on germanium it appeared unlikely that such a term would be detectable in the latter element, because of its much larger lattice atomic heat.

II. EXPERIMENT

A. Samples

Six ingots, described in Table I, were used in these measurements. All of the ingots were prepared by Miss L. Roth of this department. The starting material was pure germanium dioxide obtained from the Eagle-Picher Company, which was reduced to the metal and then purified further. This material was then cast in vacuum to form the polycrystalline ingots. The single crystals were grown by seeding the melt (doped with Sb and In for SX III and SX IV, respectively), also in vacuum. X-ray analysis of the SX ingots performed by I. Geib of this department showed them to be single crystals. Neither of the last two ingots showed any evidence in this analysis of segregation of the impurities which had been added to the melt.

The resistivity of small samples cut from the ends of the ingots was measured, and is also given in Table I. Carrier concentrations were obtained in two ways: (a) by use of empirical relations obtained by Taylor[13] between Hall constant and resistivity of germanium at room temperature,

$$\log n_h = 15.77 - 1.23 \log \rho \quad (1)$$

$$\log n_e = 15.54 - 1.16 \log \rho, \quad (2)$$

where n_h is the number of holes per cm³ in P-type germanium, n_e is the number of electrons per cm³ in N-type, and ρ is the resistivity in ohm-cm: (b) by measurement of the Hall constant on the same samples on which the resistivity was measured. In the cases where both methods were used, the two estimates agreed fairly well.

* Work assisted by contract between the U. S. Signal Corps and the Purdue Research Foundation.

[1] S. Critescu and F. Simon, Z. physik. Chem. **25b**, 273 (1934).
[2] R. W. Hill and D. H. Parkinson, Phil. Mag. **43**, 309 (1952).
[3] I. Estermann and J. R. Weertman, J. Chem. Phys. **20**, 972 (1952).
[4] H. M. J. Smith, Trans. Roy. Soc. (London) **A241**, 105 (1948).
[5] Y. C. Hsieh, Phys. Rev. **85**, 730 (1952).
[6] M. Blackman, Repts. Progr. Phys. **8**, 11 (1941).
[7] P. Debye, Ann. Physik **39**, 789 (1912).
[8] N. Pearlman and P. H. Keesom, Phys. Rev. **88**, 398 (1952).
[9] I. Estermann and S. A. Friedberg, Phys. Rev. **85**, 715 (1952).
[10] See reference 3, footnote on p. 976.
[11] P. H. Keesom and N. Pearlman, Phys. Rev. **85**, 730 (1952).
[12] Keesom, Lark-Horovitz, and Pearlman, Science **116**, 630 (1952).
[13] W. E. Taylor, thesis, Purdue University, June, 1950 (unpublished).

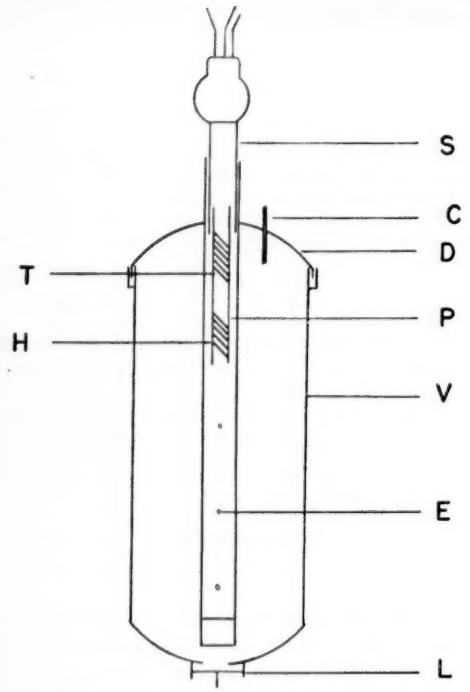

FIG. 1. Schematic drawing of container for crushed germanium.

The crushed material was prepared in a silicon carbide mortar from pure Eagle-Picher germanium. The dust was discarded and pieces from 0.1 to 3 mm were used.

B. Apparatus

The apparatus in which the heat capacity of the ingots was measured has been described previously.[8] For the second series of measurements, about 4 moles of crushed germanium was poured into a copper container (see Fig. 1). The container had a volume of 110 cm³ and weighed 93 grams, about 3 grams of which were solder. The pouring hole was later sealed with a small lid, *L*. Into the other end, *D*, of the container, *V*, was soldered a central tube pierced with holes, *E*. Into this tube was soldered a Kovar-to-glass seal, *S*, on the wires of which was wrapped a piece of cigarette paper, *P*. The phosphor-bronze thermometer wire, *T*, and the noninductively wound heater wire, *H*, were both wound on *P*. A 1 mm o.d. monel capillary tube, *C*, was also soldered into a hole in *D*. The container was pumped out through *C*, and its volume measured before and after filling with the crushed germanium. Volume measurements were made by comparison with a calibrated volume, using a manometer. After these measurements, this arrangement was used to fill the container with a known amount of helium gas. The capillary was then pinched off near the can, and the end tinned. Cerroseal solder (50 percent Sn, 50 percent In) was used throughout.

After filling with crushed germanium and helium exchange gas, the copper container was hung in the same vacuum can previously used to contain the ingots. The measuring procedure was then the same as has been described earlier.[8]

III. RESULTS

The results of measurements on the ingots are collected in Table II. No corrections were necessary for the heat capacity of wires and Glyptal. The method of least squares was applied to these data to calculate the coefficients in the relation,

$$C_v = \alpha T^3 + \gamma T. \tag{3}$$

These coefficients are listed in Table III together with their standard errors, S_α and S_γ. The series of measurements with the largest standard error, those on SX II, are plotted in Fig. 2 in the form C_v/T *vs* T^2, to indicate the extent to which Eq. (3) represents the data. The line drawn is that with the coefficients given in Table III for this ingot, the solid portion covering those points which were used in calculating the coefficients.

The results of measurements on the crushed material are given in Table IV. Three separate runs were made: *A* container filled with 3.15×10^{-5} mole of helium gas (5.5 mm Hg at room temperature); *B* container filled

TABLE I. Germanium ingots.

Sample	Material	Weight (g)	Resistivity at room temperature (ohm-cm)	Carrier type and concentration, n (cm^{-3})
PX I	Pure Ge—polycrystalline	488	7.5	[a] $5\times10^{14}(P)$
PX II	Pure Ge—polycrystalline	108		[b] $1\times10^{15}(P)$
SX I	Pure Ge—single crystal	108	2.5–7	[a] $1\times10^{15}-4\times10^{14}(N)$
SX II	Pure Ge—single crystal	101	0.5–13	[a] $8\times10^{15}(N)-2\times10^{14}(P)$ [b] $4\times10^{15}(N)-2\times10^{14}(P)$
SX III	Sb-doped single crystal	128	0.003–0.05	[a] 3×10^{18} to $1\times10^{17}(N)$
SX IV	In-doped single crystal	110	0.037–0.2	[a] 3×10^{17} to $4\times10^{16}(P)$

[a] From Eqs. (1) and (2).
[b] From Hall constant.

TABLE II. Data on atomic heat of germanium ingots.

PX I: 10/4/51
Points 10 through 33 used for least squares fit

Point	T (°K)	ΔT (°K)	C_v millijoules / mole degree
1	4.240	1.781×10^{-2}	3.169
2	4.256	1.771	3.187
3	4.267	1.735	3.254
4	3.927	2.162	2.610
5	3.943	2.091	2.698
6	3.959	2.054	2.748
7	3.654	2.677	2.107
8	3.675	2.583	2.184
9	3.695	2.536	2.225
10	3.259	3.807	1.486
11	3.298	3.661	1.545
12	3.329	3.600	1.571
13	2.893	2.416	1.072
14	2.916	2.436	1.063
15	2.937	2.360	1.098
16	2.673	3.162	0.819
17	2.730	2.990	0.866
18	2.762	2.864	0.904
19	2.441	4.091	0.633
20	2.474	3.250	0.666
21	2.484	1.631	0.664
22	2.053	2.970	0.364
23	2.090	2.847	0.380
24	2.116	2.762	0.392
25	1.883	3.720	0.291
26	1.906	1.814	0.289
27	1.920	1.708	0.307
28	1.750	2.210	0.237
29	1.770	2.136	0.245
30	1.787	2.098	0.250
31	1.541	2.804	0.187
32	1.554	2.705	0.194
33	1.582	2.748	0.191

PX I: 10/9/51
Points 1 through 21 used for least squares fit

1	2.505	1.671×10^{-2}	0.645
2	2.510	1.629	0.662
3	2.372	1.925	0.560
4	2.380	1.920	0.561
5	2.311	2.077	0.519
6	2.324	2.085	0.517
7	1.901	3.883	0.277
8	1.921	3.747	0.287
9	1.755	4.735	0.227
10	1.791	4.549	0.237
11	1.815	4.519	0.238
12	1.638	2.920	0.182
13	1.658	2.852	0.187
14	1.675	2.698	0.197
15	1.464	4.216	0.126
16	1.491	3.864	0.138
17	1.508	3.932	0.136
18	2.728	2.417	0.860
19	2.731	2.406	0.864
20	3.150	1.614	1.288
21	3.157	1.597	1.301
22	3.627	1.110	1.873
23	3.635	1.051	1.979
24	3.645	2.086	1.994
25	3.979	0.796	2.616
26	3.989	0.798	2.608
27	4.227	1.454	2.867
28	4.239	1.440	2.896
29	4.247	1.402	2.975

PX II: 9/24/51
Points 1 through 58 used for least squares fit

1	3.796	1.737×10^{-2}	2.419
2	3.801	1.704	2.465
3	3.903	1.592	2.639

PX II: 9/24/51—*Continued*
Points 1 through 58 used for least squares fit

Point	T (°K)	ΔT (°K)	C_v millijoules / mole degree
4	3.929	1.545×10^{-2}	2.719
5	3.952	1.545	2.720
6	4.083	1.504	2.795
7	4.108	1.459	2.880
8	4.137	2.932	2.867
9	4.241	1.340	3.137
10	4.253	1.300	3.234
11	4.263	1.330	3.161
12	3.875	1.631	2.576
13	3.886	1.620	2.594
14	3.894	1.602	2.623
15	3.542	2.304	1.823
16	3.558	2.337	1.797
17	3.570	2.298	1.827
18	3.250	1.428	1.439
19	3.261	1.390	1.479
20	3.270	1.404	1.464
21	2.973	1.902	1.081
22	3.003	1.826	1.126
23	3.034	1.746	1.177
24	2.713	2.419	0.850
25	2.728	2.423	0.848
26	2.741	2.399	0.856
27	2.476	3.190	0.644
28	2.500	3.068	0.670
29	2.512	3.053	0.673
30	2.327	3.858	0.532
31	2.354	3.724	0.552
32	2.360	0.915	0.566
33	2.357	0.927	0.559
34	2.194	1.220	0.425
35	2.211	2.358	0.440
36	2.227	2.310	0.449
37	2.110	2.719	0.369
38	2.018	3.183	0.326
39	1.818	4.070	0.255
40	1.652	2.304	0.225
41	1.528	3.354	0.155
42	1.523	3.405	0.152
43	3.125	1.645	1.250
44	3.149	1.605	1.281
45	3.315	2.712	1.549
46	3.452	2.390	1.758
47	3.527	2.288	1.835
48	3.704	1.920	2.188
49	3.798	1.783	2.357
50	3.823	1.743	2.410
51	3.878	1.672	2.512
52	3.880	1.607	2.615
53	3.949	1.568	2.680
54	3.971	1.546	2.718
55	3.993	1.532	2.743
56	4.011	1.530	2.748
57	4.106	3.082	2.728
58	4.226	1.343	3.130

SX I: 8/27/51
Points 1 through 4 and 8 through 44 used for least squares fit

1	2.746	3.550×10^{-2}	0.979
2	4.153	2.079	3.226
3	4.182	2.066	3.246
4	4.193	2.071	3.239
5	4.508	1.747	3.882
6	4.537	1.709	3.969
7	4.553	1.753	3.869
8	3.808	3.013	2.249
9	3.824	2.923	2.318
10	3.836	2.907	2.311
11	3.682	3.285	2.063
12	3.694	3.286	2.062

TABLE II.—*Continued.*

SX I: 8/27/51—*Continued*
Points 1 through 4 and 8 through 44 used for least squares fit

Point	T (°K)	ΔT (°K)	C_v millijoules / mole degree
13	3.696	3.297×10^{-2}	2.055
14	3.537	3.735	1.814
15	3.541	3.671	1.846
16	3.537	3.688	1.837
17	3.261	4.730	1.432
18	3.271	4.639	1.460
19	3.270	4.646	1.458
20	3.002	6.138	1.031
21	3.005	6.059	1.118
22	2.995	6.223	1.088
23	2.770	4.073	0.854
24	2.744	4.162	0.835
25	2.695	4.420	0.786
26	2.538	5.167	0.673
27	2.535	5.189	0.670
28	2.371	3.207	0.541
29	2.332	3.339	0.519
30	2.163	4.280	0.405
31	2.104	4.659	0.372
32	1.995	6.307	0.275
33	1.878	6.411	0.270
34	1.806	7.276	0.238
35	1.692	9.018	0.192
36	1.463	12.57	0.138
37	1.443	13.24	0.131
38	1.547	10.98	0.158
39	3.872	2.774	2.444
40	3.895	2.715	2.496
41	3.913	2.700	2.510
42	4.065	2.364	2.867
43	4.081	2.318	2.924
44	4.095	2.307	2.938
46	4.382	3.929	3.451
47	4.422	5.382	3.780
48	4.449	3.643	3.724
49	4.685	3.079	4.406
50	4.710	1.501	4.520
51	4.977	1.250	5.428
52	4.980	1.293	5.248

SX II: 9/12/51
Points 8 through 28 used for least squares fit

1	3.491	2.223×10^{-2}	1.826
2	3.598	2.101	1.933
3	3.621	2.091	1.942
4	3.631	2.070	1.961
5	3.335	2.776	1.462
6	3.288	1.417	1.429
7	3.282	1.440	1.406
8	2.985	1.918	1.055
9	2.991	1.886	1.073
10	2.999	1.863	1.086
11	2.608	2.888	0.701
12	2.622	2.795	0.724
13	2.614	2.830	0.715
14	2.297	4.267	0.474
15	2.323	4.130	0.490
16	2.339	3.916	0.517
17	2.002	6.02	0.336
18	2.023	5.98	0.338
19	2.015	5.94	0.340
20	1.815	8.17	0.248
21	1.837	8.01	0.252
22	1.723	2.43	0.206
23	1.728	2.37	0.211
24	1.664	2.66	0.188
25	1.661	2.69	0.186
26	1.554	3.19	0.157
27	1.554	3.30	0.152
28	1.488	3.80	0.132

SX II: 9/12/51—*Continued*
Points 8 through 28 used for least squares fit

Point	T (°K)	ΔT (°K)	C_v millijoules / mole degree
29	1.484	3.82×10^{-2}	0.131
30	4.505	0.988	4.107
31	4.516	1.577	3.860
32	4.555	2.122	3.831
33	4.388	1.243	3.270
34	4.158	1.415	2.871
35	4.237	1.296	3.153

SX III: 9/19/51
Points 14 through 43 used for least squares fit

1	4.236	2.280×10^{-2}	3.259
2	4.240	2.272	3.270
3	4.253	2.268	3.276
4	4.514	1.684	4.415
5	4.240	2.292	3.242
6	3.839	1.604	2.391
7	3.841	1.697	2.260
8	3.513	2.176	1.761
9	3.522	2.171	1.766
10	3.527	2.076	1.847
11	3.198	3.069	1.248
12	3.216	2.914	1.315
13	3.215	1.429	1.318
14	2.806	2.208	0.852
15	2.812	2.090	0.901
16	2.819	2.086	0.902
17	2.448	3.400	0.553
18	2.462	3.200	0.588
19	2.485	3.014	0.624
20	2.228	4.518	0.416
21	2.239	4.361	0.431
22	2.064	1.429	0.336
23	2.078	1.435	0.334
24	2.089	1.391	0.345
25	1.936	1.716	0.279
26	1.941	1.622	0.300
27	1.938	1.684	0.285
28	1.776	2.021	0.237
29	1.776	2.133	0.225
30	1.780	2.152	0.223
31	1.716	2.296	0.209
32	1.729	2.333	0.205
33	1.738	2.289	0.209
34	1.640	2.514	0.191
35	1.642	2.458	0.195
36	1.547	2.969	0.161
37	1.534	2.994	0.160
38	1.415	3.799	0.126
39	1.427	3.780	0.127
40	1.434	3.743	0.128
41	1.457	3.686	0.130
42	1.495	3.312	0.145
43	1.648	2.508	0.191

SX IV: 11/13/51
Points 1 through 29 used for least squares fit

1	4.196	1.149×10^{-2}	3.143
2	4.200	1.222	2.955
3	4.205	1.217	2.968
4	3.749	1.712	2.109
5	3.754	1.714	2.106
6	3.756	1.721	2.098
7	3.548	2.046	1.764
8	3.558	2.070	1.743
9	3.562	2.093	1.724
10	3.201	2.841	1.270
11	3.223	2.719	1.327
12	3.236	2.670	1.351
13	2.869	3.863	0.934
14	2.875	3.777	0.955

TABLE II.—*Continued.*

SX IV: 11/13/51—*Continued*
Points 1 through 29 used for least squares fit

Point	T (°K)	ΔT (°K)	C_v millijoules / mole degree
15	2.874	2.730×10^{-2}	0.911
16	2.606	3.561	0.698
17	2.619	3.477	0.715
18	2.620	3.509	0.708
19	2.117	5.414	0.459
20	2.124	5.402	0.460
21	1.990	5.319	0.317
22	2.005	5.187	0.325
23	1.773	7.084	0.238
24	1.752	2.157	0.237
25	1.757	2.075	0.246
26	1.346	4.623	0.110
27	1.346	4.586	0.111
28	1.486	3.561	0.143
29	1.488	3.669	0.139

with the same amount of gas (11.25 mm Hg at room temperature) and 239.5 g crushed germanium; C container filled with 8.27×10^{-7} mole of helium gas (0.38 mm Hg at room temperature) and the same amount of germanium. A smooth curve was drawn through the points of set A (see Fig. 3), and this curve was then used to correct the values of sets B and C, also plotted in Fig. 3, for the heat capacity of the calorimeter and exchange gas. A further correction was made to set C to take into account the difference in amount of exchange gas for this run. The atomic heat values calculated from runs B and C are plotted in Fig. 4, together with a smooth curve representing the measurements on the ingots. It is evident that above about 3°K, there is

TABLE III. Atomic heat of germanium ingots. $C_v=\alpha T^3+\gamma T$. S_α and S_γ are the standard errors in α and γ.

Sample	Date	α joules/mole deg^4	S_α	γ joules/mole deg^2	S_γ
PX I	10/ 4/51	4.21×10^{-5}	0.05×10^{-5}	0.79×10^{-3}	0.32×10^{-3}
PX I	10/11/51	4.02	0.11	−0.19	0.62
PX II	9/24/51	4.26	0.05	−0.28	0.62
SX I	8/27/51	4.33	0.05	−0.15	0.55
SX II	9/12/51	3.95	0.17	0.39	0.92
SX III	9/15/51	3.78	0.06	0.92	0.29
SX IV	11/13/51	3.92	0.05	0.97	0.54

TABLE IV. Data on atomic heat of crushed germanium.

Set A: Cu calorimeter
December 3, 1952

Point	T (°K)	ΔT (°K)	C millijoules / degree
1	4.270	3.353×10^{-2}	14.92
2	4.292	3.758	15.11
3	3.812	1.248	10.01
4	3.819	1.226	10.19
5	3.355	1.507	8.082
6	3.367	1.505	8.077
7	2.689	1.064	5.487
8	2.693	1.047	5.582
9	1.736	1.716	3.384
10	1.716	1.727	3.357

December 5, 1952

1	2.241	1.270×10^{-2}	4.440
2	2.249	1.246	4.518
3	1.751	1.654	3.379
4	1.743	1.635	3.401
5	2.686	1.488	5.684
6	2.695	1.464	5.771
7	3.011	2.053	6.881
8	3.023	2.030	6.953
9	3.512	1.587	8.879
10	3.529	1.626	8.644
11	3.956	2.459	11.43
12	3.975	2.437	11.54
13	4.147	2.083	13.52
14	4.163	2.108	13.34
15	4.274	1.946	14.45
16	4.281	1.930	14.57

Set B: Cu+Ge
December 11, 1952

Point	T (°K)	ΔT (°K)	C millijoules	C_{ex} millijoules/degree	C_v millijoules / mole degree
1	2.287	1.704×10^{-2}	7.216	4.57	0.655
2	2.300	1.695	7.254	4.62	0.650
3	1.817	1.377	5.256	3.54	0.425
4	1.825	1.391	5.203	3.55	0.408
5	2.039	1.950	6.086	4.00	0.517
6	2.053	1.919	6.185	4.04	0.532
7	2.137	1.847	6.431	4.23	0.544
8	2.565	1.406	8.447	5.30	0.779
9	2.570	1.446	8.214	5.32	0.715
10	2.856	2.184	10.89	6.17	1.167
11	2.865	2.428	10.23	6.20	0.997
12	3.160	1.965	12.64	7.24	1.335
13	3.170	1.962	12.66	7.26	1.335
14	3.429	1.696	14.66	8.35	1.560
15	3.439	1.682	14.78	8.39	1.580
16	3.722	1.841	18.34	9.86	2.097
17	3.737	1.841	18.34	9.93	2.080
18	3.980	1.512	22.37	11.57	2.671
19	3.992	1.508	22.42	11.65	2.663
20	4.212	2.535	26.67	13.83	3.175
21	4.238	2.477	27.30	14.22	3.234

Set C: Cu+Ge+reduced He pressure
December 19, 1952

1	2.183	1.847×10^{-2}	6.298	3.96	0.554
2	2.190	1.884	6.179	3.96	0.549
3	1.800	1.671	4.210	3.09	0.277
4	1.792	1.690	4.170	3.08	0.270
5	1.985	2.249	5.167	3.47	0.415
6	1.993	2.204	5.276	3.49	0.425
7	2.185	1.851	6.284	3.94	0.579
8	2.185	1.932	6.020	3.94	0.539
9	2.185	1.932	6.020	3.94	0.539
10	2.466	2.051	7.566	4.69	0.707
11	2.472	2.111	7.351	4.71	0.653
12	2.472	2.111	7.351	4.71	0.653
13	2.857	1.533	10.13	5.87	1.053
14	2.863	1.533	10.13	5.90	1.046
15	3.205	1.773	12.64	7.06	1.380
16	3.207	1.770	12.66	7.08	1.380
17	3.488	2.099	15.73	8.23	1.855
18	3.490	2.097	15.73	8.24	1.852
19	3.815	3.391	19.48	10.07	2.327
20	3.808	1.709	19.33	10.01	2.305
21	4.140	2.655	24.86	12.82	2.977
22	4.141	2.642	24.98	12.83	3.005

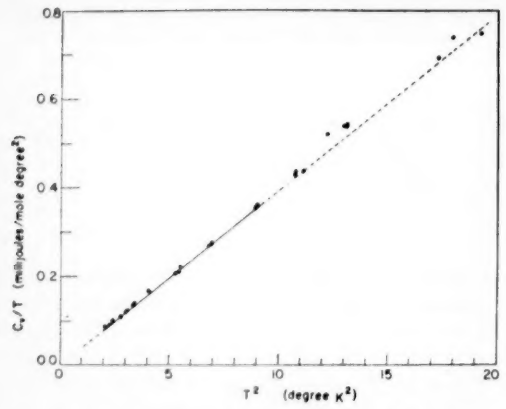

FIG. 2. Plot of C_v/T *vs* T^2 for ingot SX II. The line has the equation given in Table III: the solid portion covers the region in which points were used for the least-squares analysis.

no difference between the ingot and our crushed germanium results. Below this temperature, the points of set *B* are increasingly high with respect to the curve as *T* decreases. When the amount of helium exchange gas is decreased by a factor of 30, as was done for run *C*, the points again lie above the curve, but consistently below those of the run with the larger amount of exchange gas.

The difference between runs *B* and *C* and the curve representing measurements on the ingots is of the order of magnitude which would be expected if it were due to exchange gas desorbed from the small pieces of germanium during the heating periods. We estimate the area of the germanium as about 3000 cm^2 (particles approximated as 1-mm cubes). From the results of Dana and Kamerlingh Onnes,[14] and Keesom and Schweers,[15] respectively, we estimate 100 joules/mole for the heat of desorption and 10^{-9} mole/cm^2 degree for the amount desorbed. These values lead to the estimate of 10^{-5} to 10^{-4} joule/degree per mole of germanium for the heat of desorption. It thus appears that the excess heat capacity we observe below 3°K in the measurements on crushed germanium is due to desorption of exchange gas. Furthermore, as can be seen from Fig. 3 and Table IV, at the lowest temperatures about $\frac{2}{3}$ of the total heat capacity in these measurements is due to the calorimeter, so the accuracy of the crushed material measurements is not very high below 3°K. We therefore conclude that there is no significant difference between the results on the ingots and those on the crushed material.

It has been pointed out[16] that the low heat conductivity of germanium at very low temperatures might lead to the measurement of erroneously low values of the heat capacity of solid ingots, due to imperfect distribution of the heat input over the specimen. For several reasons, this does not appear to have been the case in our measurements. In the first place, the maximum diameter of our smallest ingot was 15 mm, while that of the largest was about 40 mm; the lengths varied from 60 to 100 mm. Despite this variation in size (and in shape as well, since although the single crystals were solids of revolution, their elevations were in general irregular), the measured atomic heat did not vary significantly from sample to sample, so there was no detectable dependence on size or shape. A rough calculation of the thermal relaxation time using the thermal conductivity measured by Estermann and Zimmerman[17] gives values ranging down from about 1 second at 4°K for the most unfavorable case of our largest ingot and impure material. It is therefore to be expected that good thermal equilibrium was achieved in the ingots before the first observation in the after-period, ten seconds after the end of the heating period. Finally, this was certainly not a problem in the measurements on the crushed germanium, but above about 3°K there is no significant difference between these results and those on the ingots. Since the heat capacity falls as rapidly as the thermal conductivity, it is unlikely that the deviations at the lowest temperatures are due to this phenomenon.

IV. DISCUSSION

The average for α, weighted by standard errors, is $(4.08\pm0.22)\times10^{-5}$ joule/mole degree^4, which corresponds to (362 ± 6)°K for θ. This agrees well with the value 375°K, calculated by a modification[18,19] of the

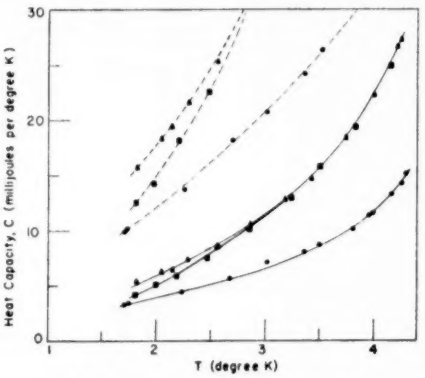

FIG. 3. Heat capacity measurements: ●—run *A* (container plus exchange gas); ▲—run *B* (container plus exchange gas and crushed germanium); ■—run *C* (same as *B*, with reduced exchange gas pressure). Solid lines refer to scale at left; dashed lines to heat capacity values multiplied by three.

[14] L. I. Dana and H. Kamerlingh Onnes, Communs. Kamerlingh Onnes Lab., Univ. Leiden, No. 179c; Proc. Koninkl. Ned. Akad. Wet. **29**, 1051 (1926).
[15] W. H. Keesom and J. Schweers, Communs. Kamerlingh Onnes Lab., Univ. Leiden, No. 264c; Physica **8**, 1020 (1941).
[16] I. Estermann (private communication).
[17] I. Estermann and J. E. Zimmerman, Technical Report No. 6, Department of Physics, Carnegie Institute of Technology, June, 1951 (unpublished).
[18] M. Durand, Phys. Rev. **50**, 449 (1936).
[19] See reference 8, Appendix II.

Hopf-Lechner method,[20] using the elastic constants of germanium recently measured by Bond and collaborators.[21] It can be seen from Fig. 2 that the true T^3 region, in which θ is constant, extends to about 4°K. This is about $\theta/100$, in agreement with Blackman's calculations.[6]

The standard error given above for $\langle\alpha\rangle_{Av}$ is larger than any listed in Table III because the latter, being calculated by the method of least squares, involve the assumption that only random errors are present. We therefore estimated our total experimental error from the observed spread of the α values of all the ingots around their average. In doing this we make the assumption that the Debye temperature of pure germanium is not changed by the addition of small amounts of impurities. On the other hand, if our estimate of the experimental error is too large, our results would indicate the presence of such an effect. The possible difference in θ values, however, is not more than a few degrees.

For a degenerate carrier gas in germanium, γ, the coefficient of the linear term in Eq. (3) will be given by

$$\gamma = 2.15\times10^{-11}\mu n^{\frac{1}{3}} \text{ joule/mole degree}^2, \qquad (4)$$

where μ is the ratio of effective carrier mass to that of free electrons and n is the number of carriers per cm^3. Hung and Gliessman[22,23] have found that for n less than about 10^{18} cm^{-3} the carrier gas will not be degenerate, so only for SX III would one expect to find a linear term in the low temperature atomic heat. Debye and Conwell[24] have shown that Hall constant and resistivity data in N-type germanium with n less than 10^{18} cm^{-3} correspond well to a value of $\frac{1}{4}$ for μ. Recently

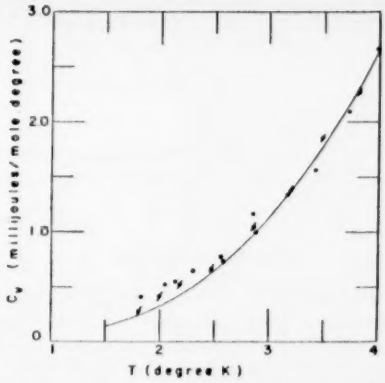

FIG. 4. Atomic heat of germanium: solid line represents results on measurements on ingots; ● —calculated from run B with crushed germanium; ● —calculated from run C with crushed germanium (reduced exchange gas pressure).

Benedict and Shockley[25] have derived the value 0.6 for μ in N-type germanium with n less than 10^{15} cm^{-3} on the basis of dielectric constant measurements in the microwave region. Since μ should be roughly independent of n, it is possible to find at least a rough estimate of γ from Eq. (4). This is 0.6–1.4×10^{-5} for SX III so that there is good agreement with our observed value, whereas values of μ much larger than unity would seem to be excluded.[26]

We would like to express our appreciation of the support of Dr. K. Lark-Horovitz, who suggested the problem and provided valuable guidance in its execution.

[20] L. Hopf and G. Lechner, Verhandl. deut. physik. Ges. **16**, 643 (1914).
[21] Bond, Mason, McSkimin, Olsen, and Teal, Phys. Rev. **78**, 176 (1950).
[22] C. S. Hung and J. R. Gliessman, Phys. Rev. **79**, 726 (1950).
[23] J. R. Gliessman, thesis, Purdue University, August, 1950 (unpublished).
[24] P. P. Debye and E. M. Conwell, Phys. Rev. **87**, 1131 (1952).
[25] T. S. Benedict and W. Shockley, Bull. Am. Phys. Soc. **28**, No. 2, 9 (1953).
[26] If the data of I. Estermann and S. A. Friedberg [Technical Report No. 4, Department of Physics, Carnegie Institute of Technology, June, 1951 (unpublished)] are analyzed by least squares, one obtains $(6.57\pm1.21)\times10^{-5}$ and $(5.88\pm0.9)\times10^{-5}$ joule/mole degree^4 for α for their pure and impure samples, respectively, and $(19.5\pm10.3)\times10^{-5}$ and $(75.9\pm9.7)\times10^{-5}$ joule/mole degree^3 for γ for the two samples. There is thus no significant difference between their values of α and ours, while an even higher value of μ than they report is required to account for the value of γ in their impure sample, if it is taken to be significant.

The Heat Capacity of KCl below 4°K*

P. H. KEESOM AND N. PEARLMAN
Department of Physics, Purdue University, West Lafayette, Indiana
(Received June 10, 1953)

The heat capacity of KCl has been found to be proportional to T^3 below 4°K, with a Debye θ of 233°K. This agrees with values calculated from elastic constants and also from the vibration spectrum.

I. INTRODUCTION

THE heat capacity of KCl at liquid helium temperatures was first measured by Keesom and Clark[1] shortly after linear terms were found in the low-temperature atomic heats of silver and zinc.[2] Since these linear terms were attributed to the heat capacity of the degenerate electron gas in metals,[3] it was expected that such a term would be absent in the insulator KCl, and this expectation was borne out. Keesom and Clark[1] made their measurements with powered KCl in a calorimeter which also contained a small amount of He gas for heat exchange. As a result they found it difficult, at their lowest temperatures (about 2°K), to separate the heat capacity of the KCl from the desorption heat of that part of the exchange gas which had been adsorbed on the powder. In particular, it was impossible to ascertain if the heat capacity of the KCl was proportional to T^3.

Blackman and others have shown[4] that independently of crystal structure, the lattice contribution to heat capacity should be proportional to T^3 for T less than $\theta/50$ or $\theta/100$, where θ is the Debye temperature at very low temperatures. Since θ is about 230°K for KCl,[1] this "true T^3 region" should be found at liquid helium temperatures. Despite the fact that Keesom and Clark themselves pointed out the limited accuracy of their results, various authors[5] have since concluded from these data that the low-temperature heat capacity of KCl shows no T^3 dependence, even at the lowest temperatures.

We have also experienced difficulty due to adsorption in measurements on crushed germanium.[6] Since our results on ingots of germanium were much more reliable, we considered it worth while to remeasure the heat capacity of KCl at liquid helium temperatures using a large single crystal, as had already been suggested by Keesom and Clark.[1] As they pointed out, this would be feasible if the thermal conductivity, k, is high enough at low temperatures. Measurements by De Haas and Biermasz[7] show that the thermal conductivity of KCl decreases from about 2 watt (cm degree)$^{-1}$ at 4°K to 0.6 at 2°K. This is considerably larger than the thermal conductivity of germanium in the same temperature range.[8] When the larger specific heat c, and smaller density, ρ, of KCl compared to Ge are also taken into account, the thermal diffusivity $k/\rho c$, on which the rate of approach to thermal equilibrium depends, is seen to be somewhat larger for KCl than for Ge at liquid helium temperatures. Since we experienced no difficulty from this source in our measurements on Ge, we anticipated that KCl would also be suitable for this type of measurement.

TABLE I. Data for heat capacity of KCl.

Point	T (°K)	ΔT (°K)	C_v millijoules / half-mole °K
		February 4, 1953	
1	4.231	3.106×10^{-2}	11.52
2	4.230	3.106	11.52
3	3.912	3.912	9.142
4	3.929	3.858	9.270
5	3.567	2.404	7.093
6	3.567	2.394	7.123
7	3.312	3.096	5.507
8	3.316	2.987	5.709
9	2.924	4.419	3.856
10	2.925	4.419	3.856
		March 9, 1953	
1	1.466	3.107×10^{-2}	0.4678
2	1.434	3.480	0.4277
3	1.441	3.553	0.4253
4	1.656	4.379	0.6903
5	1.667	4.422	0.6855
6	1.670	4.415	0.6861
7	1.985	3.823	1.221
9	2.012	3.721	1.259
10	2.324	3.957	2.006
11	2.322	4.105	1.935
12	2.335	4.015	1.962
13	4.247	1.333	12.07
14	4.293	2.883	12.02

II. EXPERIMENT

A single crystal of KCl, diameter 37 mm, length 88 mm, weight 189 g, was procured from the Harshaw

* This work was supported by the Signal Corps Contract.
[1] W. H. Keesom and C. W. Clark, Commun. Kamerlingh Onnes Lab., Leiden, No. 238c; Physica **2**, 698 (1935).
[2] W. H. Keesom and J. A. Kok, Commun. Kamerlingh Onnes Lab., Leiden, No. 232d; Physica **1**, 770 (1933–34).
[3] A. Sommerfeld, Z. Physik **47**, 1 (1928).
[4] M. Blackman, Repts. Progr. Phys. **8**, 11 (1941).
[5] See, e.g., F. Seitz, *The Modern Theory of Solids* (McGraw-Hill Book Company, Inc., New York, 1940), p. 114; R. B. Leighton, Revs. Modern Phys. **20**, 165 (1948).
[6] P. H. Keesom and N. Pearlman, Phys. Rev. **91**, 1347 (1953).
[7] W. J. De Haas and Th. Biermasz, Commun. Kamerlingh Onnes Lab., Leiden, No. 249a; Physica **4**, 752 (1937).
[8] I. Estermann and J. E. Zimmerman, Technical Report No. 6, Department of Physics, Carnegie Institute of Technology, June 1951 (unpublished).

Chemical Company. Constantan heater wire and phosphor-bronze thermometer wire were secured to the crystal with Glyptal lacquer. No correction was necessary for the heat capacity of the wires and the lacquer. The crystal was hung with Nylon thread in a vacuum can, and the measurements were carried out in the manner described earlier.[9]

III. RESULTS

The results of our measurements are collected in Table I. These data are plotted in the form C_v/T *versus* T^2 in Fig. 1, where C_v is the heat capacity of one-half mole of KCl. The method of least squares applied to the data gives for the equation of the line in Fig. 1

$$C_v/T=(15.37\pm0.09)\times10^{-5}T^2-(0.37\pm0.39)10^{-5}\times\text{joules/mole degree}^2. \quad (1)$$

The coefficient of the quadratic term corresponds to a value for θ of $(233\pm3)°$K, and it is evident that there is no other significant contribution to the heat capacity. The results of Keesom and Clark[1] are also plotted in Fig. 1 for comparison.

IV. DISCUSSION

It appears from Fig. 1 that the data of Keesom and Clark[1] agree well with ours above about 3.6°K. They found larger values of the molar heat at lower temperatures, which would be expected if, as they suspected, some of their helium exchange gas was being desorbed from their KCl powder during the heating periods. This effect would not be noticeable in the case of our single crystal of KCl.

The excellent agreement of our data with the calculated straight line drawn in Fig. 1 leads us to the conclusion that below about 4°K (about $\theta/50$), the molar heat is proportional to T^3, as predicted by Blackman.[4] The reported deviations from this relation[5] would appear to be nonexistent. They apparently were based on attributing higher accuracy to the original measurements of Keesom and Clark[1] than the authors themselves claimed. Our value of θ, 233°K, agrees fairly well with that of Durand,[10] 246°K, calculated from his estimates of the elastic constants at 0°K, based on measurements down to liquid nitrogen temperatures, and also with Iona's value, 230°K, found from his calculation of the elastic frequency spectrum.[11]

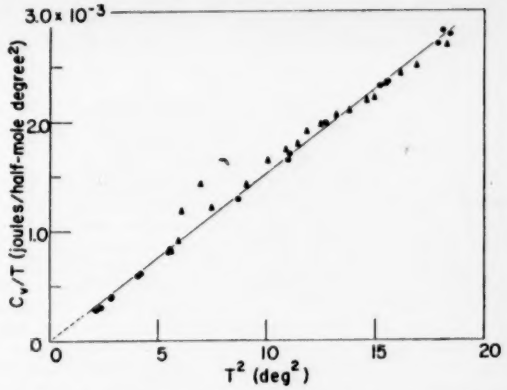

FIG. 1. C_v/T *vs* T^2 for KCl. ●—Our results. ▲—Keesom and Clark.

We would like to express our appreciation of the support of Dr. K. Lark-Horovitz, who suggested the problem and provided valuable guidance in its execution.

[9] N. Pearlman and P. H. Keesom, Phys. Rev. **88**, 398 (1952).

[10] M. Durand, Phys. Rev. **50**, 449 (1936).

[11] M. Iona, Phys. Rev. **60**, 822 (1941).

Fluorescence, Phosphorescence, and Photostimulation of NaCl(AgCl) with High-Energy Irradiation*

MILTON FURST AND HARTMUT KALLMANN
Physics Department, New York University, Washington Square, New York, New York

(Received July 18, 1952)

Quantitative results are presented on the light-emitting and storage properties of silver chloride activated sodium chloride crystals excited with high-energy radiation. The characteristic of the strong light emission, mostly in the ultraviolet range, upon stimulation by longer wavelength light after pre-excitation with high-energy radiation, is extensively investigated, as well as the fluorescence and phosphorescence. A practically linear stimulated light response as a function of the roentgen dose over a range from about 10^{-2} to 10^{4} roentgens is found. Such a measurement of stimulated light can be performed a considerable time after the exposure to the high-energy radiation and still provide a determination of the dose. Both the ordinary phosphorescence and the stimulated light phosphorescence under suitable conditions may decay very slowly and show many other similarities. The measurements show that the amount of energy stored by the crystal which can later be released as emitted light is greater than 3 percent of the energy totally absorbed. After a sufficiently long stimulation by visible light the rate of de-excitation becomes very small; further stimulation with light of shorter wavelengths produces a rise in the amount of stimulated light and an increase in the de-excitation rate. The amount of stored energy which can be stimulated as light decays slowly with storage time. This effect is closely correlated with the coloration well known with pure NaCl crystals; bleaching a crystal results in a reduced stimulation. Most of the experiments were carried out with a radium gamma-ray source, but measurements with x-rays and fast electrons show very similar results. Experiments with fast electrons were performed with doses up to 500 000 rep; saturation then occurs, but after de-excitation (bleaching) the crystal could be re-excited and be used again with no appreciable change in properties. The counting properties of these crystals are rather poor because of small peak heights. A rather complete explanation of these properties can be given by a model assuming a continuous distribution of traps over a small range. The energy released from these traps goes to the activator, from which the energy is emitted as light.

I. INTRODUCTION

THE more qualitative aspects of the fluorescence, phosphorescence, energy storage, and release of the stored energy as light in AgCl-activated NaCl crystals when excited by high-energy radiation have been presented in two letters.[1,2] Here quantitative results of more complete experiments and some further findings with such crystals will be given. Alkali-halide crystals with and without special activation have been previously investigated and found to exhibit long-time phosphorescence, and energy storage and release by light,[3–8] though very little quantitative data on stimulation properties has been published. The emitted light intensities of activated crystals were found to be very much greater than for pure NaCl; in fact NaCl(AgCl) is one of the most efficient stimulable phosphors, which has not been fully recognized and investigated previously. It is the large amount of light (see Sec. IV), which can be released by stimulation which makes these systems particularly interesting.

The present investigation has been carried out with NaCl crystals activated with 1 percent of AgCl[9] since, of the crystals so far studied, these were found to have the best energy storage properties. The fluorescence (integrated intensity) of these crystals under gamma-ray excitation was found to be about the same as that of an anthracene crystal of the same mass. Upon removal of the excitation source the crystal showed a rather long-time phosphorescence, especially if the excitation time was sufficiently extended. After the decay of the phosphorescence to a low level and subsequent irradiation of the crystal with light in a range from the near ultraviolet to the near infrared (designated below as stimulating light), the crystal exhibited a strong light emission mostly in the ultraviolet region (stimulated light). No such stimulation occurs if the crystal is not previously excited with high-energy radiation. This shows that a portion of the energy absorbed from the gamma radiation can be stored in the crystal and be released by light. This storage of energy is found to be associated with the presence of color centers which have been so extensively studied by Pohl[3] and many

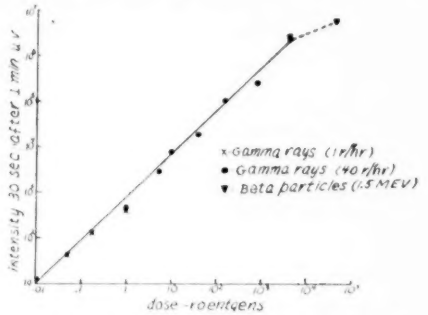

FIG. 1. Light-stimulated intensities for various doses.

* This work was supported by the U. S. Signal Corps Engineering Laboratories, Evans Signal Laboratory, Belmar, New Jersey.

[1] M. Furst and H. Kallmann, Phys. Rev. **82**, 964 (1951).
[2] H. Kallmann and M. Furst, Phys. Rev. **83**, 674 (1951).
[3] R. W. Pohl, Proc. Phys. Soc. (London) **49**, extra part, 3 (1937).
[4] K. Przibram, Z. Physik **20**, 196 (1924); **107**, 709 (1937).
[5] D. Glasser and I. E. Beasely, Phys. Rev. **47**, 570, 789 (1935).
[6] M. Kato, Sci. Papers Inst. Phys. Chem. Research Tokyo **41**, 113 (1943); **42**, 35, 95 (1944).
[7] Weyl, Schulman, Ginther, and Evans, J. Electrochem. Soc. **95**, 70 (1949); Schulman, Ginther, and Klick, J. Appl. Phys. **22**, 1479 (1951).
[8] F. Seitz, Revs. Modern Phys. **18**, 384 (1946).
[9] Most of them provided by the courtesy of Harshaw Chemical Company.

other investigators. We have not attempted to work out the full relationship between these two effects since more careful study of the influence of the activators on the behavior of the color centers must first be made. The stimulated light also exhibits a fairly slow decrease after removal of the stimulating source, similar to the phosphorescence after gamma excitation. The initial intensity of the stimulated light after sufficient excitation was many times greater than the fluorescent intensity with the identical gamma-ray source.

Of practical interest is the essentially linear light stimulation with high-energy radiation doses (Fig. 1) within the range of 10^{-2} to about 10^{4} roentgens (see Sec. IV). Also the amount of high-energy radiation absorbed by a crystal can be measured at a considerably later time.

II. FLUORESCENCE AND SPECTRAL DISTRIBUTION

The measuring arrangement was essentially the same as that used in previous measurements with solutions and crystals.[10]

Since the total fluorescent light output of these activated NaCl crystals is of the order of 10 percent of the total absorbed energy,[11] their fluorescence cannot stem from the direct excitation of the activators alone because their concentration is not more than 1 percent; instead the fluorescence must at least partly originate in a transport of energy from the bulk material to the activators (see Theoretical Section).

The fluorescent spectral distribution under gamma-ray excitation is depicted in Fig. 2. Two bands occur, one ranging from about 2300A to 2600A and a somewhat weaker band ranging from about 3200A to 4500A, essentially the same as those found with light excitation.[6] With the use of filters, it was found that more than 75 percent of the fluorescent emission lies in the ultraviolet below 4000A. The stimulated light emission also occurs in practically the same spectral regions, but the far ultraviolet band is relatively weaker. The gamma-ray-excited emission spectra of crystals from different portions of a large crystal from the melt show characteristic differences; those portions from the bottom (cone portion) having a greater relative intensity in the shorter ultraviolet band. Figure 2 also shows the stimulating light spectrum that was most often used; this source is designated as a 3600A source. The spectrum of the stimulated light is essentially independent of that of the stimulating light; thus the stimulated band below 4000A also appears under stimulation with longer wavelengths. The stimulation band is found to be broader, especially toward the ultraviolet, than the absorption band of the color centers of the pure NaCl crystal.[12]

[10] H. Kallmann and M. Furst, Phys. Rev. **79**, 857 (1950); Broser, Kallmann, and Martius, Z. Naturforsch. **4a**, 204 (1949).
[11] Furst, Kallmann, and Kramer, Phys. Rev. **89**, 416 (1953).
[12] N. F. Mott and R. W. Gurney, *Electronic Processes in Ionic Crystals* (Oxford University Press, London, 1948), p. 111.

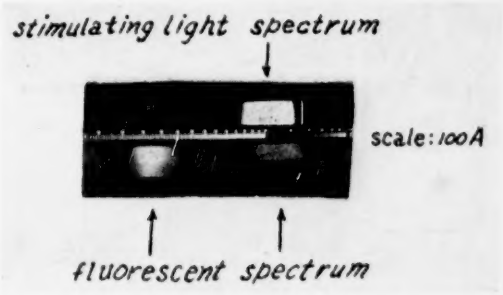

FIG. 2. Fluorescent spectrum of NaCl activated with 1 percent AgCl under gamma-ray excitation.

III. PHOSPHORESCENCE AFTER HIGH-ENERGY EXCITATION

Starting with a de-excited crystal (see below), it was observed that the fluorescent light emission under gamma excitation did not rise almost instantaneously as with organic crystals; instead a continuous rise was found which became more and more gradual (see Fig. 3). The rise time is independent of the excitation intensity in the range 0.05 r/hr to 3.7 r/hr. Upon the removal of the exciting source an almost immediate drop to about one-third of the fluorescence occurs; then there is a more gradual decrease in phosphorescent intensity. Figures 4 and 5 show the decay of phosphorescence after various doses of gamma radiation. The values there are referred to the reading 1 minute after removal of the exciting source; this period is considerably longer than the time of the initial very fast decay. The essential results are that the decrease in phosphorescent light is slower than exponential. However, the shape of the curve is practically the same for different doses when applied for equal periods of time; thus it is the duration of excitation which mainly determines the shape of these curves. These results cannot be correlated to those found by Kato.[6] Explanations for these effects will be given in the Theoretical Section.

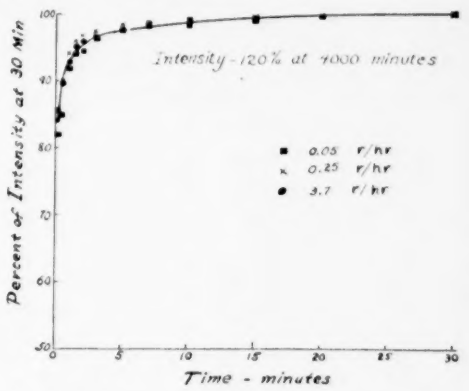

FIG. 3. Rise in fluorescent intensity for gamma-ray excitation—dose rate 1 roentgen per hour.

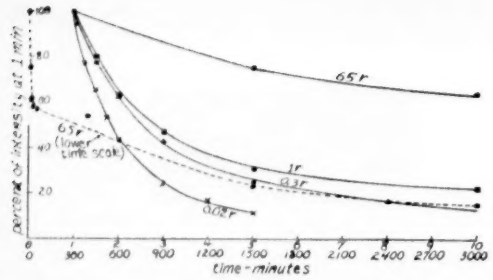

FIG. 4. Phosphorescent decay for various doses after excitation, at rate of 1 roentgen per hour.

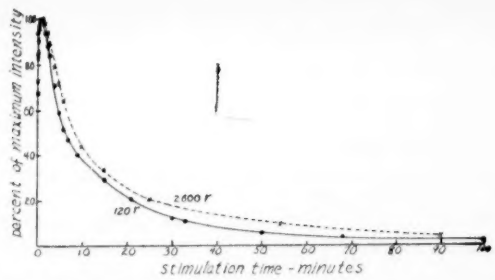

FIG. 6. Stimulated intensity under continuous visible stimulation.

IV. ENERGY STORAGE AND RELEASE BY LIGHT

The amount of light which can be released by stimulation is considerably larger than the total amount of light which is emitted as phosphorescence in several days at room temperature. The band of stimulating light lies in the range from about 3000A to about 5000A, though light outside of this range is also somewhat effective for stimulation (see also Sec. VI). With light of about 2500A, however, direct excitation already occurs.

In determinations of the intensity of the stimulated light it is not necessary to observe the stimulated light while the stimulating light is acting, since the light emitted after removal of the stimulating source also decays slowly; thus two types of experiments were performed. In one series the excited crystal was illuminated with the stimulating light (usually a 3600A source) for a definite time period; then the crystal was placed in the instrument and measurements were begun within 30 seconds. In the other series of experiments the crystal was irradiated with visible light and its light emission was measured simultaneously by screening of the stimulating light by suitable filters. This could not be accomplished for the ultraviolet, which is one of the reasons for always using intermittent stimulation for these wavelengths.

A maximum in the stimulated light emission was not immediately reached upon the application of the stimulating light, a behavior similar to that with the fluorescent light. Figure 6 shows as examples the relative stimulated light intensities under continuous visible irradiation after 120 and 2600 roentgen doses were applied; these curves are remarkably similar (see Theoretical Section). The time when the maximum is reached depends on the intensity of the stimulating source, so that, for example, with the stimulating ultraviolet intensity reduced by a factor of 10, the time for maximum stimulated intensity was increased from 3 minutes to 20 minutes. A similar shift was found with visible stimulation.

The curves of Fig. 6 further show that the stimulated light intensity does not decrease exponentially, but at a much smaller rate.[13] A similar effect is found with ZnS phosphors. This may also be seen from Table I, which presents the stimulated intensities for intermittent stimulation with varying dark periods in between.

From these continuous-stimulation curves, a lower limit for the entire stimulated light (light intensity multiplied by time) can be calculated by integrating the curve. This can then be compared to the total amount of fluorescent light emitted under simultaneous gamma excitation, which is essentially given by the maximum fluorescent intensity multiplied by the time

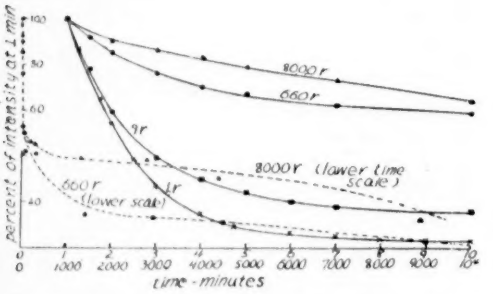

FIG. 5. Phosphorescent decay for various doses after excitation, at rate of 40 roentgens per hour.

TABLE I. Decrease of stimulated intensity with ultraviolet stimulation dose 8000 roentgens.

Irradiation	Time	Intensity 30 sec after irradiation
Gamma, at rate of 40 r/hr	200 hr[a]	5000[b]
No irradiation	503 hr	170[b]
Ultraviolet	1 min	185 000
No irradiation	25 hr	130[c]
Ultraviolet	1 min	47 500
No irradiation	4.5 hr	550[c]
Ultraviolet	1 min	32 000
No irradiation	65 hr	29[c]
Ultraviolet	1 min	26 500
No irradiation	36 min	330[c]
Ultraviolet	1 min	21 000
No irradiation	24 hr	...
Ultraviolet	2 min	7000
No irradiation	17 hr	24[c]
Ultraviolet	1 min	5700

[a] Excitation time.
[b] Remaining phosphorescence after high-energy excitation.
[c] Remaining phosphorescence from previous stimulation.

[13] It may be noted that these curves do not represent a spontaneous decay but a decrease while the stimulating light acts.

for long exposures. These calculations show that the total amount of stimulated light (released by visible light) is about 30 percent of the total fluorescent light. However, since there is considerable additional stimulation possible by means of light in the near ultraviolet, the total amount of stored energy which can be emitted as light may still lie above this figure. Since about 10 percent of the absorbed gamma-ray energy is emitted as light as shown by comparing with anthracene,[11] the portion of absorbed energy which is stored and can later be emitted as light in NaCl(AgCl) turns out to be greater than 3 percent.

TABLE II. Stimulated light intensities.

Irradiation	Time	Intensity[a]	Percent of first ultraviolet reading
Gamma, at rate of 40 r/hr	20 hr	...	...
Ultraviolet	1 min	210 000	100
Ultraviolet	2 min	84 000	41
No irradiation	30 hr		
Ultraviolet	1 min	36 600	18
No irradiation	72 hr	...	...
Ultraviolet	1 min	20 000	10
Gamma, at rate of 1 r/hr	1 min	440[b]	...
Ultraviolet	1 min	12	100
Ultraviolet	1 min	7	60
Gamma, at rate of 1 r/hr	5 min	530[b]	...
Ultraviolet	1 min	17	37
Gamma, at rate of 1 r/hr	18 min	630[b]	...
Ultraviolet	1 min	130	100
Ultraviolet	1 min	130	100
Ultraviolet	1 min	65	50
Gamma, at rate of 40 r/hr	8 min	...	...
Ultraviolet	1 min	2600	100
Ultraviolet	1 min	1200	46
Gamma, at rate of 40 r/hr	15 min	...	...
Ultraviolet	1 min	5500	100
Ultraviolet	1 min	1900	35
Ultraviolet	1 min	1050	19
Gamma, at rate of 40 r/hr	60 min	...	...
Ultraviolet	1 min	19 500	100
Ultraviolet	1 min	9000	46

[a] Stimulated readings were obtained 30 seconds after stimulation.
[b] Fluorescent value.

After application of the stimulating light for a short interval and its subsequent removal, the light does not completely decay instantaneously; instead a decrease in intensity similar to that of the phosphorescence after high-energy excitation is found. Examples of such curves under various conditions are given in Figs. 7 and 8. All of the curves in the figures are similar in shape to each other (percentage curves) if the same light stimulation is used, though the high-energy excitation conditions are considerably different. However, an increase in the length of the stimulation period (with a weaker light source) produced a considerable slowing down of the phosphorescent decay of the stimulated light (see Fig. 8); this is analogous to the slowing down after prolonged gamma-ray excitation (Figs. 4 and 5).

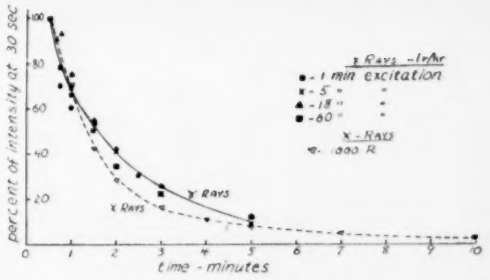

FIG. 7. Decay after 1 minute of ultraviolet stimulation with gamma-ray and x-ray excitations.

The stimulated light intensities produced during short stimulation periods using the 3600A source after various intervals without stimulation are shown in Tables I and II. The crystal used for the measurements in Table I was cut from the edge of a large crystal grown from the melt and shows poorer storage qualities than other pieces of the same large crystal (see Sec. IX). Table II shows results with more efficient crystals under different excitation and stimulation periods. The periods of darkness were usually long enough for the phosphorescence of the stimulated light to decay to a relatively small portion (about 1 percent) of its value at 30 sec. The ratio of the stimulated intensity after the first stimulation to that after the second one was usually between 2 and 3 (except with long periods of darkness, when the factor was about 4). The ratio between successive stimulations then usually decreases and approaches nearly one after a large number of stimulations are applied. This behavior is similar to that observed with continuous stimulation by visible light, where the slowing down of the decrease in the stimulated light intensities with increasing stimulation time was still more pronounced.

The dependence of the amount of stimulated light on the applied dose and dose rate of excitation are described in Table III; similar doses were applied but at different rates, corresponding to different periods of

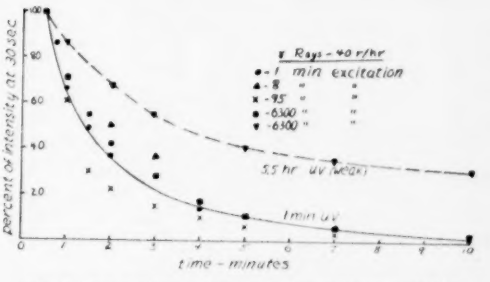

FIG. 8. Decay after 1 minute of ultraviolet stimulation with gamma-ray excitation.

TABLE III. Intensities for different excitation rates after ultraviolet stimulation.

Rate r/hr	γ irradiation Time	Dose, roentgens[a]	Intensity 30 sec after 1 min of uv stimulation
0.01	2 hr	0.020	24
1	1 min	0.017	22
1	60 min	1	380
60	1 min	1	420

[a] Different crystals were used with the two doses.

excitation. The results show that the intensity of the stimulated light depends essentially only on the total dose of radiation rather than on the length of excitation time for a given dose. For very much larger differences in exposure time than described in the table, the effect of the decay of the stored energy becomes noticeable (see Sec. V).

In Fig. 1 the relationship between stimulated light intensities and dose are described. The smallest dose of gamma radiation measurable with accuracy by stimulated light was about 10 milliroentgens; somewhat smaller doses could be detected, but the readings were close to the small residual stimulated intensities present even with unexcited crystals. For softer high-energy radiations, especially x-rays, the minimum detectable dose would be smaller because of the greater amount of energy absorbed by the same crystal volume for the same roentgen dose. The curve of Fig. 1 shows that from about 0.01 to 4200 roentgens, a factor greater than 10^5 in dosage range, the intensity of the stimulated light was essentially proportional to the dosage. There are fluctuations in the curve, possibly due in some cases to the differences in the periods of excitation (see also next section); however, no systematic deviations were found. High-energy electrons ($\sim$1.5 Mev)[14] were also used as an excitation source, and the point corresponding to 4000 r with this source fits rather well in the curve obtained for gamma rays. With 40 000 r, a deviation from linearity becomes noticeable, and at 5×10^5 roentgens definite saturation was observed. (Part of this saturation effect may be due to the increased opacity of the crystal due to the strong coloration.) An extensive check of the relation between the stimulated light intensity and the previous roentgen dose shows that these crystals can be used for quantitative dose measurements, especially if the relatively small decay of the stimulated light intensity with storage time is taken into account. A crystal which has been highly excited and then de-excited can be re-excited with no noticeable change in its properties even after having received a total dosage of millions of roentgens.

TABLE IV. Stimulated intensities with various doses and periods of darkness.

Dose, roentgens	Rate, r/hr	Excitation time, min	Dark period	Intensity 30 sec after 1 min uv
		Crystal No. 1		
0.13	0.53	15	2 min	49
0.14	0.53	16	80 min	51
0.14	0.53	16	17.5 hr	37
0.13	0.53	15	162 hr	17
0.53	0.53	60	5 min	190
0.55	0.53	62	75 min	160
0.53	0.53	60	16.5 hr	120
11	44	15	2 min	4200
11	44	15	80 min	3750
12	44	16.5	18.5 hr	2700
11	44	15	64 hr	1800
11	44	15	960 hr	800
44	44	60	5 min	15 000
44	44	60	80 min	11 000
44	44	60	16 hr	10 500
		Crystal No. 3		
0.13	0.53	15	2 min	46
0.15	0.53	17	90 min	28
0.14	0.53	16	17.5 hr	10
0.13	0.53	15	162 hr	3
0.53	0.55	62	5 min	165
0.53	0.53	60	5 min	180
0.55	0.53	62	65 min	130
0.53	0.53	60	15.5 hr	34
0.54	0.53	60	64 hr	13
11	44	15	2 min	1400
11	44	15	17.5 hr	600
56	44	77	2 min	9600
44	44	60	17 hr	1600

V. DECAY OF STIMULATED LIGHT INTENSITY WITH STORAGE TIME

The stimulated light intensities are only comparatively slightly diminished if the energy is stored in the crystal for a considerable length of time. Results using two different crystals are given in Table IV. Crystal No. 1, typical of crystals from the center of a large crystal grown from the melt, exhibits a decrease of stimulated light intensity with a storage time of 160 hours by a factor of at most 3. Crystal No. 3, which was obtained from the edge of the same large crystal grown from the melt as was crystal No. 1, exhibits a somewhat faster decrease in stimulated intensity with storage time for these doses. Experiments with other crystals bear out the somewhat faster decay with crystals near the edge (see below).

The slow decrease of energy storage and its localization are also shown by an experiment using fast electrons (beta particles) for exciting a small area of the crystal. Subsequent stimulation produced a sharp luminescent spot which gave no visual evidence of any broadening when the stimulation was repeated after the lapse of two weeks.

[14] The fast electron generator of the Electronized Chemical Company, Brooklyn, New York, was used (see Sec. VII).

VI. DE-EXCITATION

De-excitation of the crystal is shown by the decrease in stimulability.[15] Figure 6 and Tables I and V represent also such de-excitation. With increasing de-excitation, further de-excitation becomes increasingly difficult.

This decrease in the rate of de-excitation is not determined by the absolute amount of residual stored energy but rather by the percentage of the initial stored energy that remains (Fig. 6); it occurs with near-ultraviolet light (~3600A) stimulation as well as with visible stimulation, but the slowing down occurs with a different degree of stimulability. With shorter wavelengths, of about 2500A, the de-excitation process is somewhat faster, but with such wavelengths there is also some direct excitation, and an equilibrium is reached under prolonged irradiation. As a result of these measurements, the method of de-exciting strongly excited crystals usually consisted of exposing the crystal to ultraviolet light in the region of 2500A and then to light with longer wavelengths for final de-excitation.

Even after such a procedure the crystals still retain a small amount of residual excitation equivalent to about an exposure of the order of 1 milliroentgen (a reading of about 5 in Tables I and IV) which could not be removed by this method. This small excitation was present even with crystals that were not previously exposed to high-energy radiation except cosmic rays. Preliminary experiments with cosmic rays have been inconclusive in deciding whether the residual effect is due to them or to a small direct excitation with the stimulating source. This will be investigated further.

Experiments carried out alternately with different wavelengths of stimulating light have shown that they influence each other in producing stimulation. Typical results with intermittent stimulation are shown in Table V. The light sources used for quenching did not all have the same total energy; thus the source of visible light had an energy greater by a factor of 50 than the 3600A source, while the source in the region of 2800A was the weakest. This table shows that in spite of these different strengths the shorter wavelengths de-excite more efficiently. Initially, with the above-mentioned sources, the stimulated light intensity decreases for each consecutive shot of stimulating light from the same source. Periods of darkness of the order of a day do not appreciably accelerate the decrease in stimulated intensity. If a partially de-excited crystal is stimulated for a longer period of time (e.g., 10 min or longer) and then followed by a dark period of the same duration, a subsequent short stimulation (30 sec) of the same wavelength (for visible and ultraviolet) produces a greater stimulated intensity than the preceding long stimulation. This is due to a heating of the crystal during the prolonged stimulation and a consequent faster decay of the emitted light (see below).

Once the crystal is considerably de-excited, an

TABLE V. Stimulation and de-excitation with different light sources.

Stimulation			Emission intensity after 30 sec		
Visible	uv, region of 3600A	uv, region of 2800A	Visible	uv, region of 3600A	uv, region of 2800A
30 sec	...	...	2 030 000	...	...
...	30 sec	...	...	3 330 000	...
...	...	30 sec	...	...	1 530 000
30 sec	...	...	850 000	...	...
30 sec	...	...	535 000	...	...
...	30 sec	...	...	1 000 000	...
...	30 sec	...	...	900 000	...
...	30 sec	...	...	775 000	...
...	...	30 sec	...	...	450 000
...	...	30 sec	...	...	370 000
...	...	30 sec[a]	...	...	280 000
...	30 sec	...	...	370 000	...
30 sec	...	...	170 000	...	...
30 sec	...	...	124 000	...	...
2 min	...	...	40 000	...	...
2 min	...	...	12 000	...	...
30 sec	...	...	13 500	...	...
...	2 min	...	...	125 000	...
...	2 min	...	...	100 000	...
30 sec	...	...	36 500	...	...
...	...	30 sec	...	...	32 000
...	...	2 min	...	...	33 000
...	...	2 min	...	...	29 000
...	...	30 sec	...	...	25 000
30 sec	...	...	14 000	...	...
...	30 sec	...	...	44 000	...
10 min	...	...	750	...	...
30 sec	...	...	1250	...	...
...	10 min	...	...	8700	...
...	30 sec	...	...	15 000	...
30 sec	...	...	4000	...	...
...	...	14 min	...	...	2900
...	...	30 sec	...	...	3100
30 sec	...	...	2200	...	...
...	30 sec	...	...	6800	...
...	30 sec	...	...	7700	...
...	30 sec[a]	...	...	7100	...
30 sec	...	...	2600	...	...
45 min	...	...	170	...	...
30 sec	...	...	180	...	...
30 sec	...	...	165	...	...
...	30 sec	...	...	2400	...
30 sec	...	...	980	...	...
30 sec	...	...	680	...	...
30 sec	70 min[b]	...	180	...	...
30 sec	...	...	130	...	...
...	30 sec	...	...	390	...
...	30 sec	...	...	470	...
...	30 sec	...	...	480	...
30 sec	...	...	250	...	...
30 sec	...	...	145	...	...
8.5 min	...	...	9	...	...
30 sec	...	...	19	...	...
30 sec	...	...	22	...	...
...	...	30 sec	...	...	72
...	...	30 sec	...	...	82
30 sec	...	...	39	...	...
30 sec[c]	...	...	33	...	...
...	30 sec	...	...	260	...
...	30 sec	...	...	380	...
...	30 sec	...	...	430	...

[a] The crystal had been in the dark for 16 hours.
[b] Visible light was applied directly after 70 minutes of ultraviolet.
[c] The crystal had been in the dark for 64 hours; the decay after stimulation was slower than with the previous shot.

[15] By stimulability we mean the capability of the crystal to emit light induced by irradiation of the crystal with a visible or near-ultraviolet light source. It depends mainly on the previous excitation of the crystal, for instance by gamma radiation. It is essentially zero if the crystal is completely de-excited and not again excited by high-energy radiation.

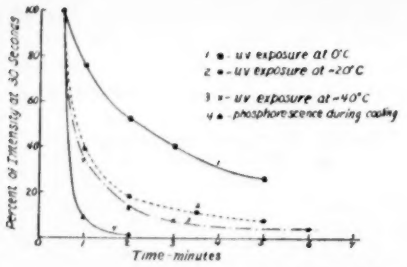
Percent of Intensity at 30 Seconds
1 ● - uv exposure at 0°C
2 ● - uv exposure at -20°C
3 × - uv exposure at -40°C
4 ▲ - phosphorescence during cooling
Time - minutes

FIG. 9. Effect of temperature on stimulated emission.

interaction in the de-excitation by different wavelengths occurs which can be seen in Table V. After ultraviolet stimulation (3600A) the succeeding stimulation by visible light produces a considerably higher value than the previous similar visible stimulation. There are also indications, not shown in this table, that in a similar manner stimulation with shorter ultraviolet wavelengths induces an increase in stimulation with longer ultraviolet wavelengths. The effect is due to the presence of electron traps of different depths (see Theoretical Section).

In order to provide more information about the phosphorescent properties of these crystals a small number of experiments at different temperatures were performed. Figure 9 presents curves of phosphorescent decay after stimulation is removed for different temperatures (curves 1–3), while curve 4 gives the light emission as function of time for a warm crystal during its period of cooling off towards room temperature. The curves show how the decay of light emission becomes more rapid with increasing temperature. Figure 10 depicts something like a glow curve: an excited crystal cooled down to −78°C was stimulated by ultraviolet at this temperature and then slowly warmed up. The first part of the curve shows the phosphorescent decay at the low temperature; after about two minutes the warming up prevents the further decrease of the phosphorescent emission and the light emission increases to a maximum followed by another decrease as a consequence of a depletion of the phosphorescent traps (see Theoretical Section). However, no effort to obtain accurate glow curves was made because of appreciable retrapping and the lack of saturation of the traps; both of these conditions are necessary for the usual interpretation given to glow curves.

VII. OTHER EXCITATION SOURCES

The experiments described above are concerned almost entirely with excitation by gamma rays. Fast electrons (beta particles) also produce a similar excitation of the crystal, and the results described above are also valid with this type of excitation (see also Fig. 1). Though some experiments with fast electrons were performed using a 10-millicurie strontium 90 source, most of the quantitative results with fast electrons were obtained by using pulses from a discharge tube.[16] The equipment provided a pulse of 1.5-Mev electrons for a period of about 10^{-5} second. The radiation intensity transferred in one pulse to the crystal was of the order of 7×10^{5} erg/cm^2 [10 000 rep (roentgen-equivalent-physical)] at about 120 cm from the source as determined by calorimetric measurements.

The amount of light stimulated after the electron excitation was essentially the same as that with gamma-ray excitation for the same amount of absorbed energy if the decay of the stored energy in the interval between excitation and stimulation was taken into consideration. The decay of the light emitted after stimulation followed practically the same curves for both types of excitation; also the same type of variability among the different crystals was obtained, although in the case of the electron pulse the density of excitation is 10^{10} times larger than in the case of gamma-ray excitation. With large doses (500 000 rep) either obtained by changing the position of the crystal with respect to the discharge tube or increasing the number of pulses, a definite saturation of the light emitted after stimulation was obtained; thus the light emitted after 30 seconds of ultraviolet stimulation with 500 000 rep and 30 000 rep were found to be about equal. However, de-excitation of the more excited crystals occurred at a slower rate.

With alpha particles[17] the main features of the phenomenon were the same, but the observed fluorescent and stimulated light intensity was smaller for the same amount of absorbed energy for alpha-particle excitation than it is for gamma-ray and fast-electron excitation. Because of the observed deterioration of crystals under alpha-particle excitation,[18] extensive experiments with the alpha-particle source were not carried out.

X-ray excitation also produces results similar to gamma-ray excitation, as can be seen from Fig. 7; also the stimulated light intensity for a 1000-r x-ray dose fits rather well with the results shown in the curve of Fig. 1. The tremendous storage and stimulation properties of these crystals can be demonstrated by the ability

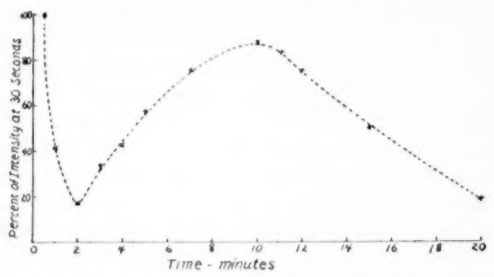

FIG. 10. Light emission of warming crystal, stimulated at −78°C.

[16] Electronized Chemical Company.
[17] C. E. Mandeville and H. O. Albrecht, Phys. Rev. **90**, 25 (1953).
[18] I. Broser and H. Kallmann, Z. Naturforsch. **5a**, 381 (1950).

to depict an object by means of x-rays. The latent image of the object in a crystal can later be photographically recorded by first stimulating the crystal and then placing it directly on a photographic plate. Such a picture was made with as little as 0.1 r from a 60-kv x-ray source. The resolution on these photographs was good. Using a 1-r dose, two clear pictures of the same latent image were made after a lapse of about 30 minutes after the x-ray exposure, during which time the crystal was exposed to sunlight for several minutes. With about 100 r, even after a lapse of 5 days, the latent image was still made visually observable on the crystal by stimulation with an ultraviolet lamp, although by far the greater portion of the emitted light is in the invisible ultraviolet.

VIII. COUNTING PROPERTIES

Some experiments on the counting properties of these crystals have been carried out by L. Bittman and N. Linson at this laboratory. The peak heights of the fluorescent light flashes emitted under gamma-ray excitation were found to be smaller than those of anthracene when measured with a circuit with short time constant, in spite of the high fluorescent efficiency of these crystals. An explanation will be given in the Theoretical Section.

IX. ENERGY STORAGE WITH DIFFERENT CRYSTALS[19]

As previously remarked, the light emission properties of these crystals depend on the degree of activation and on the location in the original melt. Investigation has yielded the following results: Crystals with activations of 0.1 percent and 0.2 percent AgCl were found to be inferior to those with 1 percent activation with respect to fluorescent, phosphorescent, and stimulation efficiencies; but their fluorescence is not weakened as much as the storage efficiency. Those with 5 and 10 percent activation showed a slightly smaller fluorescent and storage efficiency than the 1 percent crystal, but the peak heights of the 5 percent activated crystals have been found to be slightly higher than the 1 percent activated crystals.[20] Investigation of specimens taken from different portions of a quite large crystal grown from the melt made by Harshaw Chemical Company has revealed characteristic differences in the storage and fluorescent properties of the various sections of the large crystal. Table VI indicates the type of variation for the various portions of this large crystal. Specimens from the bottom (cone portion) of the large crystal have smaller stimulabilities than those from the central portion, but the phosphorescence of the stimulated light decreases more slowly with the crystals from the cone portion. The fluorescence of specimens from the cone portion are, however, somewhat higher than those from the top section. Similar results were obtained with portions from other large crystals grown from the melt. These results indicate—and this is the reason for their presentation—that the different traps which are so important for all the light-emitting phenomena of these crystals are not purely a function of the activator (its concentration) but depend considerably on the way the crystal is grown. This indicates that the fluorescent and storage effects are not completely correlated to each other. Crystals with higher concentrations of silver chloride (5 percent and 10 percent) seem to be inferior to the 1 percent crystals in both fluorescent and stimulation properties.

TABLE VI. Response of specimens from different portions of a large NaCl(AgCl 1 percent) crystal.

Crystal No.	Section	Thickness	I_{f160}[a]	$I_{f160}/I_{f\frac{1}{4}}$[b]	I_{s120}[c]	I_{s120}/I_{s300}[d]	I_{f160}/I_{s}
20	Bottom	0.75 cm	235	1.25	80	3.1	0.34
21	Bottom	0.8 cm	310	1.1	120	4.6	0.39
22	Center	0.85 cm	300↑	1.3	240	8	0.8
23	Top	1 cm	215	1.07	270	68	1.3
24	Top	0.8 cm	195	1.2	190	21	1

[a] I_{f160} = fluorescent intensity after 60 minutes of irradiation.
[b] $I_{f\frac{1}{4}}$ = fluorescent intensity after ¼ minute of irradiation.
[c] I_{s120} = stimulated intensity 30 seconds after termination of stimulation.
[d] I_{s300} = stimulated intensity 300 seconds after termination of stimulation.

X. COLORATION AND BLEACHING

In experiments with considerable excitation, the NaCl(AgCl) crystal became colored, as is well known for alkali halide crystals;[3,21] the stimulation was found to be fairly closely correlated with the coloration. Those crystals which exhibited high fluorescence but smaller stimulation capabilities were also found to have less coloration for the same dosage than crystals with better stimulation qualities. These experiments show further that the fluorescent efficiency is partially independent of the storage and stimulation efficiencies.

Coloration and stimulability have the following properties in common: (1) Both proceed parallel to each other until the crystal becomes quite opaque and saturation sets in. Considerable stimulability remains, however, when the crystal appears transparent, most likely because the stimulability measurements are more sensitive than those of coloration. (2) As with color centers, where the action of light in any part of the F band bleaches all the rest of the band, de-excitation with one wavelength also decreases the stimulability by other wavelengths; however, it is not completely removed. (3) The growing of the crystal appears to be important for both the coloration of the crystal and the storage and stimulation qualities, as indicated by the influence of position of the specimens in the crystal grown from the melt. (4) The decay of the stored energy as determined by the amount of stimulation is similar to the decay of the degree of coloration as reported by Alger.[21] The number of trapped electrons as determined

[19] Some of the crystals were supplied by the courtesy of Squier Laboratory, Signal Corps.
[20] Bittman, Furst, and Kallmann, Phys. Rev. **87**, 83 (1952).
[21] R. S. Alger, J. Appl. Phys. **21**, 30 (1950).

from the saturation of light emission ($\sim 10^{17}$ per gram) is about the same as the number of vacancies associated with the color centers.[3] There are, however, features occurring with color centers and stimulable energy storage which are not correlated with each other (see Theoretical Section).

XI. THEORETICAL CONSIDERATIONS (DYNAMICS OF PHOSPHORESCENCE, STIMULATION, AND DE-EXCITATION)

The experiments described above on the slow rise of the fluorescent light emission, on the phosphorescent decays after excitation and stimulation, and on the stimulability and the de-excitation of the crystal can all be explained by using the relatively simple model depicted in Fig. 11. The valence band and the lowest excited band of the bulk material are shown, and it is assumed that practically the entire excitation of the crystal by high-energy radiation takes place from the valence band to various higher excitation bands of the bulk material. The electrons excited to these bands will return to the valence band mostly by means of passing through the band of lowest excitation energy shown in the figure. In the energy gap between these two bands there are a number of trap levels distributed over a range of energy; these traps are assumed to be much less numerous than the number of atoms of the bulk material. These are divided into two types, designated by p and s for reasons discussed below. In addition there are levels of the activator atoms. It is assumed that most of the deep traps are not directly associated with the activators, since strong trapping also occurs without activators being present. The amount of direct excitation from the valence band to activator or trap levels is assumed to be negligible. The electrons or excitation energy which reach the excited band of the bulk material will go either to the traps or to the activators from which light may be emitted. From the curve of fluorescent light as a function of time, it can be concluded that a considerable amount of excitation energy goes to the traps.

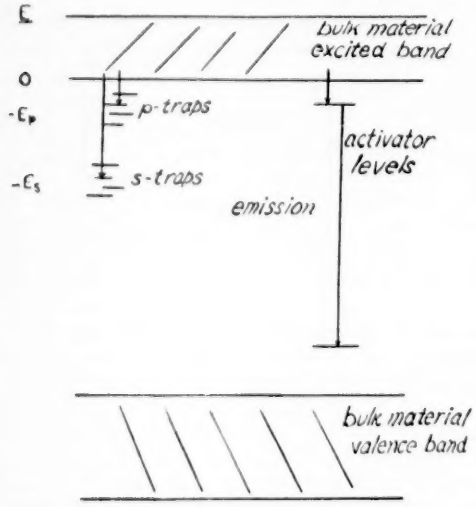

FIG. 11. Energy level scheme for emission and storage with activated NaCl crystals.

The less deep traps, p, are assumed to be responsible for the phosphorescence, whereas the deeper traps, s, are associated with the storage phenomenon. The number of s traps is calculated from the saturation of stimulation at about 5×10^5 roentgens to be about 10^{17} per gram of the bulk material. Two types of traps are assumed because it was found that the energy storage exhibits only a very small short time component, smaller than expected from the appreciable intensity of the short time component found in the phosphorescence even after prolonged periods of high-energy excitation. The stimulable stored energy, on the other hand, decays only very slowly with time and is still considerable after 1000 hours. Nevertheless, it is not completely certain that it is necessary to discriminate between two different types of traps. The experiments are not conclusive enough to exclude the possibility of postulating a continuous distribution of similar traps from the highest p traps to the deepest s traps. Certainly some of the observed long time phosphorescence is due to the spontaneous release from s traps.

It was indicated in Fig. 3 that the fluorescent light emission reaches a rather steady value after about 20 minutes and then rises only very slowly within days. This rise of the fluorescent radiation is due to the fact that not all of the electrons in the excited level of the bulk material reach the emission centers; instead a considerable portion are trapped in the p and s levels. Only if the number of electrons released from these traps by collisions with the lattice becomes equal to the number of electrons falling from the excited state into these traps, will the net consumption of electrons by the traps stop and the light emission increase. For an energy level i lying below the excitation band by an amount E_i, the time τ_i when equilibrium (between filling and release) will be reached for this level (τ_i also gives the decay time of the trap) is given by the following well-known equation:

$$1/\tau_i = \gamma_i \exp(-E_i/kT), \tag{1}$$

where $\gamma_i = \epsilon_i \nu_i$, ν_i is the frequency factor of the average number of vibrations made per second by the electrons occupying these traps, ϵ_i is a factor which is a measure of the retrapping and structure, and the exponential is the Boltzmann factor.

A rise in the fluorescent curve and its practical leveling off after a certain time could perhaps also be explained by the assumption that the saturation occurs not because of an equilibrium between the number of electrons trapped and those released by heat, but rather because all of the available traps are filled to capacity (saturated). This is very often observed in ZnS phosphor but is not observed for these crystals under the condi-

tions of the investigation, since it was found that the rise time curve of the fluorescent light is practically independent of the intensity of the exciting radiation (Fig. 3), clearly indicating an equilibrium between filling and emptying of the traps but no trap saturation.[22] According to Eq. (1), the rise with time t of the fluorescent intensity I should be given by

$$I = A + B \ln t, \tag{2}$$

where the constants A and B are dependent upon the special model which is chosen for the light emitting processes. Equation (2) holds as long as equilibrium is not reached for all traps. It is valid for a time period extending between a time equal to the time constant of the shallowest trap to that of the longest living traps. After a time τ_m given by Eq. (1), where E_i is replaced by the energy of the deepest trap, no further rise occurs. The experimental curve (Fig. 3) rises over a period of days and can be represented rather well by Eq. (2). This formula is derived under the assumptions that the number of electrons in the excitation levels are proportional to the excitation intensity, and that they contribute either to light emission or filling the traps. The filling of the traps is assumed to be proportional to the number of traps, and the trapping cross section to be the same for all depths of traps. It is further assumed that the retrapping probability does not vary considerably during the period of observation; this is borne out by the similarity of curve shapes in Fig. 3 for different dose rates. Finally, the crude simplification is made that for a given time of excitation t, all traps of an energy E_p, where $E_p/kT = \log(\gamma_p t)$, are filled to equilibrium while all others of greater energy are not filled at all.

If the factor γ_p is assumed to be of the order of 10^{10} per second, a value of $\frac{3}{4}$ ev for the center of the E_p band can be obtained from the phosphorescence experiments. This value is only a crude estimate, since γ is not known accurately enough. Without retrapping and with strong coupling of the traps with the lattice, a factor of 10^{12} per second is usually assumed. For the energy levels involved here, a change of γ from 10^{10} to 10^{12} produces a change of only 15 percent in the calculated energy. A more accurate determination of the trap-level energies can be made if the experiments are performed at a series of different temperatures; this is contemplated for the future.

The strong probability of trapping by these levels can be concluded from various experiments. It was observed that the fluorescent efficiency of these substances is of the order of that of anthracene (10 percent absolute yield). At the same time, in counting experiments the peak heights of light flashes produced by single gamma quanta or alpha particles are found to be smaller than in anthracene. This indicates that a considerable portion of the excited electrons do not immediately lead to light emission but first fill traps. Investigations are under way to show this effect more directly. The very large number of available traps is further shown by the small peak heights from alpha particles, since even the strong excitation density produced by alpha particles is not enough to *saturate* the available traps around an alpha-particle track. In ZnS the situation is mostly reversed.

The experiments show that the phosphorescent effects both after excitation as well as after stimulation are quite similar. It is, therefore, probable that the directly excited electrons and those released by stimulation populate the same excited band since they are subject to being trapped by the same trap levels. If the shapes of the decay curves in Figs. 4 and 5 are considered, it is seen that they deviate considerably from being exponential and that their "decay times" vary with the time of excitation and extend from minutes to hours. This dependence of the decay time on the period of excitation can be explained as follows. According to Eq. (1) the lifetime of the electrons trapped in these levels depend strongly on their energy; thus, if this energy covers a range of about 0.2 ev, the lifetime of these traps would vary from minutes to more than a day. If now the excitation is extended over a certain period T_R, all traps which have a lifetime τ_i smaller than T_R are filled practically to equilibrium; a further extension of the excitation will not increase the population of these traps, but only those traps with lifetimes greater than T_R will have their population increased. Thus, if the same dose is given once within a very short period of excitation and then with a very long time of excitation, the percentage decay such as shown in Figs. 4 and 5 should be more gradual with long excitation time than with short excitation time, since with short excitation time the trap levels with longer lifetimes have the same population as those with shorter lifetimes but contribute less to emission. This is precisely what was found under both excitation and stimulation.

To account for these effects it is sufficient to assume a relative small energy range (of the order of 0.2 ev) with a rather uniform and continuous distribution. This does not necessarily include the deeper s traps (see below). With this assumption and simplifications such as those used with Eq. (2), one obtains an expression for the light intensity I as a function of time t of the type

$$I = K \int_{\delta_R}^{\infty} \frac{e^{-t\delta}}{\delta} d\delta, \tag{3}$$

where $\delta = 1/\tau$ of Eq. (1), δ_R is the reciprocal of the irradiation time T_R, and K is a constant.

This equation can be used to compare the amount of light emission obtained after removal of the source for different times of T_R and to compute the relative decay curves. Such comparisons are shown in Table VII, and a fair agreement is found. The largest deviations occur

[22] The possibility still remains that local saturation occurs in the "channel" of the electron; however, pulse measurements appear to show that this is not the case.

TABLE VII. Comparison of phosphorescent intensities with those calculated from Eq. (3).

Irradiation time T_R minutes	Phosphorescent intensity $t=1$ minute[a] Measured	Calculated	$t=5$ minutes Measured	Calculated
1	0.04	0.02	0.002	0.001
13	0.39	0.25	0.09	0.08
1000	0.71	0.72	0.48	0.53
12 000	1	1	0.79	0.81

t,[a] minutes	Phosphorescent decay[b] Measured	Calculated
1	1.0	1.0
5	0.79	0.82
10	0.64	0.74
200	0.46	0.40
1000	0.39	0.23
9000	0.12	0.03

[a] t is the time after removal of the exciting source.
[b] $T_R = 12\,000$ minutes.

when the decay time approaches the irradiation time; the values calculated from the equations are then too small. This is expected from the complete neglect of the filling of traps with lifetimes greater than the irradiation time. It may be noted that the same reasoning would give an hyperbolic decay law if the traps were filled to saturation rather than equilibrium.[23] Equations (2) and (3) are derived from the basic equations of trap dynamics.[24]

The light emission stimulated by visible or ultraviolet light reaches a maximum only several minutes (up to 20 minutes in the experiments performed) after the stimulation is initiated. This rise comes about because some electrons released from the s traps are first utilized for filling p traps instead of going to the emission level. Thus the stimulated light intensity would be expected to show a rise similar to that of the fluorescent light intensity if depletion of the electrons in the s traps by the stimulating light did not take place. If the stimulating light is very weak, the depletion in the s traps is small and a rise curve for the stimulated light rather similar to that of the exciting light is obtained. If the stimulating light intensity is strong, the s traps are rather quickly depleted and the light emission decreases long before the nearly steady value of the emission curve can be measured.

Since the stored energy which can be stimulated has a long lifetime and still amounts to 20 percent after 60 000 minutes, the s levels associated with the stimulation must have [from Eq. (1)] a depth below the excitation level of at least 1 ev. The long lifetime explains the linearity of the stimulated light with dose for quite different dose rates. From the preferable stimulation by light of energy greater than 5000A, one might be inclined to assume that the energy E_s of these traps is considerably more than 1 ev; the noticeable decay of the stored energy, however, indicates that this is not the case.

To explain this difference in the energy required by the stimulating light and the thermal release, one resorts to the often assumed shift in the curves of potential *vs* configurational coordinates between the s trap levels and the first excited band (Franck-Condon principle).[25] A similar effect occurs also in ZnS phosphors, but here for similar trap depths the wavelength of the stimulating light lies in the infrared.

Although this assumption not only explains the difference between the energy $h\nu$ of the observed stimulation band and the thermal de-excitation energy, but additionally explains the stimulation and de-excitation curves as functions of time (see below), it is felt that this explanation needs considerably more exploration. It is noteworthy that such a difference between the energy associated with the stimulation frequency and the thermal de-excitation energy occurs for trapped and stimulable electrons of many other materials. However, it is rather surprising that this effect is so marked in the NaCl(AgCl), where one assumes that the electrons are relatively free in the excited level, which would indicate a flat rather than a steep potential curve. A similar assumption about the potential curves also explains the shape of the de-excitation curves of Fig. 6 and the de-excitation shown in Tables I and V for visible and ultraviolet light. With progressing de-excitation the decrease is more gradual than exponential and is slower with visible than with ultraviolet light. If the energy range of the s levels were very narrow, an exponential de-excitation curve would be expected since all electrons absorb the stimulating light equally strongly. A deviation from an exponential law such as found would also be expected if retrapping decreased with increasing excitation of the crystal. Since, however, it was found that these de-excitation curves are essentially independent of the dose (Sec. IV), one must assume that retrapping is constant to a first approximation. If the s traps cover a wider energy range, light of frequency ν can empty only those traps with energies larger than a certain energy E_i with maximum efficiencies. The release of electrons from trap levels deeper than E_i will be much less probable, since the $h\nu$ of the stimulating light is not large enough to raise the electrons above the upper potential curve. On account of the space extension of the wave function, some releasing will still take place but with a very small probability. Thus one finds that at the beginning of stimulation de-excitation is rapid, but that it slows down considerably as soon as the electrons in the favorable energy range are exhausted; however, it does not stop completely since also the electrons in deeper traps are still released. This explanation also makes understandable the more pronounced slowing down with visible light.

From Table IV, which shows that after 40 days a

[23] H. W. Leverenz, *An Introduction to Luminescence of Solids* (John Wiley and Sons, Inc., New York, 1950), p. 269 ff.
[24] H. Kallmann and B. Kramer, Phys. Rev. **87**, 91 (1952).
[25] P. Pringsheim, *Fluorescence and Phosphorescence* (Interscience Publishers, Inc., New York, 1949), p. 147.

major portion of the stored energy has decayed thermally, it can be estimated that the *s* traps have an energy depth around 1 ev and a width of not more than several tenths of an ev. On the other hand, conclusions about the range of the *s* trap band cannot be made from the width of the stimulation band, since the decay of the storage energy indicates that the *s* traps have a considerably smaller range than the width of the stimulation band. The width of the stimulation band must already be inherent to a single *s* level; this can also be understood from the potential curve picture and the considerable space extension of the wave function.

If the stored energy is already depleted to a certain extent by stimulation, it is observed that stimulation by visible light following one with ultraviolet light exhibits a larger stimulated intensity than a similar stimulation with visible light before the ultraviolet stimulation (Table V); these effects together with the arguments expressed previously in this section also indicate that considerable retrapping occurs. The traps easily emptied by visible light are depleted first. If then ultraviolet stimulation is applied, electrons in deeper traps are raised to the excitation level, and some are retrapped in those levels easily emptied by visible light, especially during the period of phosphorescence after the ultraviolet stimulation is discontinued. In this way the traps which are easily emptied by visible light are partially refilled, so that stimulability by such light is increased. An analogous argument explains the increase in ultraviolet stimulability after different short shots of ultraviolet stimulation (see Table V). It also makes understandable the observation with certain crystal specimens that after a long period of stimulation, a long dark period increases the stimulability with the same light.

The *s* traps are associated with the traps responsible for the coloration of the crystal, as was shown in Sec. X. We have, however, not investigated this relationship precisely enough to determine how the introduction of the activators modify the properties of the traps responsible for the coloration.

Another problem which we would like to mention is the following: It is generally assumed that the electrons in the excited band behave like free electrons hampered in their motion by traps. This would imply that the probability of recombination of the electrons with the positive charges accompanied by light emission should depend on the total strength of the excitation as is also assumed in ZnS. (Light emission there is proportional to the number of electrons in the conduction band multiplied by the number of positive charges.) Thus, as a consequence, the light emission curves (both fluorescent and phosphorescent) should depend on the degree of excitation. However, the experiments described above show no pronounced effect of this kind. This may be due to the production of excitons rather than free electrons.

The results derived from the small number of heating and cooling experiments are also in agreement with the presented model. Since the *s* traps are considerably deeper than the *p* traps, it was found that the phosphorescence was completely altered by changing the temperature, whereas heating up to about 70°C had only slight effects on the storage capability of the crystal. The rapid decrease in phosphorescent light emission, while the crystal was being cooled, is due to the fact that the *p* traps release much fewer electrons per unit time at lower temperatures.

The above considerations deal mostly with the dynamics of trap filling, emptying, and refilling, and with only roughly determined positions of the energy levels of the traps. They are sufficient to show that the situation is quite different from those found discussed in the theoretical papers of Williams and Johnson which deal mainly with thallium-activated potassium chloride.[26]

[26] F. E. Williams, J. Chem. Phys. **19**, 457 (1951); P. D. Johnson and F. E. Williams, J. Chem. Phys. **20**, 124 (1952).

Inelastic Scattering of Thermal Neutrons in Lead

ANDREW W. MCREYNOLDS*
Brookhaven National Laboratory, Upton, New York
(Received May 22, 1953)

The total thermal inelastic scattering cross section of lead has been measured from transmission of a single crystal, from 2–8 angstroms (0.02–0.0013 ev) at 80°K and 295°K, and is found to be in quantitative agreement with current theory of one-phonon process of energy exchange with the lattice. Measurements of differential cross section at 1.08 angstrom (0.07 ev) are in agreement with Debye-Waller theory. Thus inelastic cross section through the thermal range is found to fit the two theories in their ranges of validity.

NEUTRONS of thermal energies may be scattered in a crystal either elastically or by an inelastic process in which energy is exchanged between the neutron and lattice thermal vibrations. The total scattering cross section is the sum of a coherent part and an incoherent part arising from spin dependence of cross section or random isotopic distribution. The latter component is isotropic and practically independent of temperature and neutron energy, and in lead is also negligibly small. The total scattering may therefore be considered as the sum of elastic Bragg diffraction and of inelastic, or thermal diffuse scattering. Figure 1 shows qualitatively the variation with wavelength of the cross section for the various processes, which add to give the total scattering plus capture cross section. The shaded region represents the thermal inelastic process by which the neutrons are thermalized to temperature equilibrium with the surrounding lattice. It has been considered theoretically by Weinstock[1] and by Kleinman.[2] Qualitatively, at long wavelengths where energy is much less than thermal, the most probable result of scattering is a gain of energy (curve 1 in Fig. 1). The cross section decreases linearly with decreasing wavelength, reaching a minimum in the vicinity of the Bragg cutoff. With further decreasing wavelength, the cross section again increases, and, as energy-loss processes (curve 2) become more probable, the total inelastic approaches the total free cross section. In the region $\lambda > \lambda_c$, where all scattering is inelastic, Bragg diffraction is no longer possible and the cross section may be determined directly from the transmission. Measurements by Palevsky, Hughes and Smith[3–5] in this region ($\lambda > 4A$, $E = 0.0002 - 0.003$ ev) on Fe, Be, and graphite verify the linear dependence on temperature[6] and wavelength and are in good quantitative agreement with the theory. In the present experiments, measurements at 80°K and 295°K have been extended from 8A through the 1–5.7-angstrom (0.08–0.0025) ev region of Bragg diffraction to check validity of the theory in that range. Inelastic scattering can be distinguished from elastic through the angular and wavelength dependence of the latter. Total inelastic cross section as a function of wavelength was measured by transmission of a high resolution monochromatic beam through single crystals at wavelength for which no elastic scattering was possible. At one wavelength, 1.08A, the differential inelastic cross section *vs* angle was observed by measuring scattered neutron intensity in non-Bragg directions.

NEUTRON BEAMS

The Brookhaven reactor was used as a thermal neutron source, with maximum of its Maxwellian

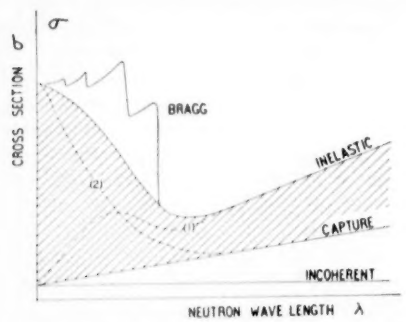

FIG. 1. Qualitative features of the cross section for scattering and capture of thermal neutrons in crystals. Curves 1 and 2 are components of inelastic cross section for energy gained and lost.

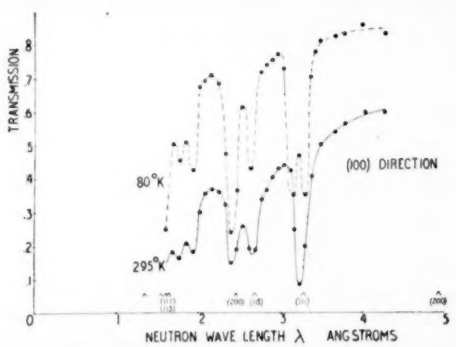

FIG. 2. Neutron transmission of 9.35-cm Pb crystal in (100) direction. Computed positions of Bragg peaks are as shown.

* Present address: Joint Establishment for Nuclear Energy Research, Kjeller, Norway.

[1] R. Weinstock, Phys. Rev. **65**, 1 (1944).
[2] D. Kleinman, Phys. Rev. **81**, 326 (1951).
[3] Johnson, Palevsky and Hughes, Phys. Rev. **82**, 345 (1951).
[4] H. Palevsky and R. R. Smith, Phys. Rev. **86**, 604 (1952).
[5] Palevsky, Hughes, and Smith, Phys. Rev. **87**, 221 (1952).
[6] Except for anomalous temperature dependence in graphite.

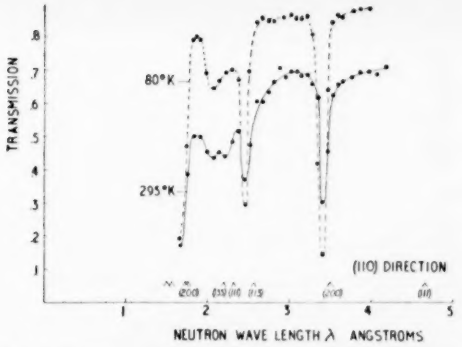

FIG. 3. Neutron transmission through 5.08 cm of same Pb crystal as Fig. 2 but in (110) direction.

distribution near 1 angstrom. Selection of high-resolution monochromatic beams over the range 2–8 angstroms required different techniques in different wavelength ranges, and a combination of crystal diffraction and mechanical choppers. From 2–5 angstroms, a 15′ half-width beam from a $\frac{1}{4}$ in.$\times$2 in. graphite collimator was reflected from the (200) or (111) planes of a lead crystal at incident angles of 25° to 90°. Since the diffraction rocking curve due to mosaic spread of the lead crystal was about 15′, wavelength resolution was from 0.003 to 0.01. At the same angles, however, second- and higher-order reflections of the much more abundant neutrons of $\sim$1A are also present and had to be eliminated. Beryllium, with Bragg cutoffs of 3.6 and 3.9 angstroms, was satisfactory as a filter to transmit only neutrons of $\lambda > 3.6$A. For shorter wavelengths, a mechanical velocity selector was used.

The mechanical selector consists of a series of four cadmium disks, each with 36 radial slots, mounted on the same rotating shaft. Disks are 12 in. in diameter, 0.030 in. thick, with 2-in. long slots 2 degrees wide and spaced 8 degrees apart. They were located 33.3 cm apart along the shaft, and adjacent disks rotated slightly, defining a series of helical paths of 0.07–0.35 radian/meter. The resolution $\Delta\lambda/\lambda$ is constant for all velocities, being determined by the angular displacement of the disks. The velocity of the neutrons transmitted is proportional to the rotational speed, 3600 rpm, corresponding to 2700 meters/second ($\lambda = 1.46$ angstroms) when set at 25 percent resolution, or 1080 meters/second (3.6 angstroms) when set at 10 percent resolution. In contrast to velocity selection by diffraction, the transmitted beam contains no shorter wavelength harmonics. The reactor neutron beam was therefore first passed through the velocity selector to select a broad wavelength spread, then diffracted from the lead crystal to obtain higher resolution.

For $\lambda > 5.7$A, the Bragg cutoff for lead, the crystal monochromator could no longer be used. In this region, however, diffraction effects no longer occur in the transmission sample, so high-wavelength resolution of

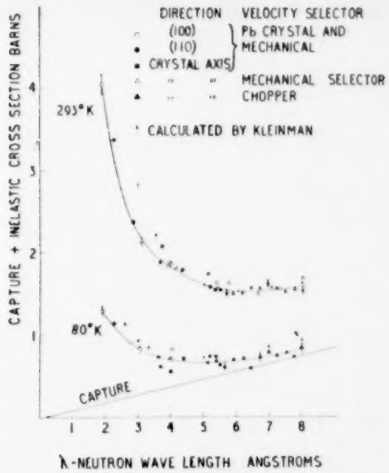

FIG. 4. Thermal inelastic scattering cross section for neutrons in lead as determined by total transmission measurements. Direction of beam and velocity selector used are indicated by points.

the neutron beam is not required. The velocity selector was set for a 10 percent resolution and used for the 5.7–8-angstrom region, with a 6-in. filter of BeO placed in the beam to eliminate fast neutrons not stopped by the Cd disks and further to reduce the background from neutrons below the BeO cut-off wavelength of 4.7 angstroms. Transmission measurements in this range were duplicated using the chopper time-of-flight apparatus also.

Sample

The transmission sample used was a single crystal grown in a graphite mold by lowering a melt of 99.99 percent Pb at about 0.5 in./hr through an electric tube furnace about 20°C above the melting point. From this 2-in. diameter ingot a 3.60-in. length was cut. Since lead recrystallizes at room temperature, the end faces were machined carefully and chemically etched to remove surface grains formed by the cutting process.

TRANSMISSION MEASUREMENTS

For room temperature measurement beam intensities and backgrounds were measured with and without the sample in the beam, with results as shown in Fig. 2. For 80°K measurements, the sample was placed inside a soft glass Dewar flask and in contact through a metal support trough with liquid nitrogen below the beam level. Attenuation in the soft glass walls of the Dewar was relatively small. Figure 2 shows curves of transmission *versus* wavelength. Near the cut-off region it is smooth, representing only inelastic scattering, but with decreasing wavelength, more Bragg reflections become possible and the curve is accordingly irregular. Diffraction has been minimized by choosing the direction of

transmission as a major crystallographic direction of symmetry. The wavelength for which many planes satisfy the Bragg condition, $\lambda = 2d \sin\theta$, then coincide in a number of cases, as indicated, leaving regions in which no elastic scattering occurs. Figure 3 represents similar curves for a different crystallographic direction. Even in these favorable directions, for $\lambda < 2$ angstroms the Bragg peaks become so numerous and close together that they begin to overlap, preventing inelastic scattering measurements in the intervals between. The inelastic component of the total cross section, which varies smoothly with λ, corresponds to a transmission curve which is the upper envelope of those shown in Figs. 2 and 3. For each of these latter curves there are gaps between the Bragg wavelengths, at which the inelastic cross section can be calculated. Figure 4 shows points thus determined, together with cross sections calculated from measurements with the velocity selector and chopper in the longer wavelength region.

The dashed line shown in Fig. 4 represents the inelastic cross section as calculated by Kleinman on the basis of one-phonon theory, plus capture cross section calculated from the latest value 0.18 barn at 2200 m/sec. The agreement between calculated curves and measured values is very good with regard to dependence on both wavelength and temperature.

For wavelengths shorter than about 2 angstroms, the cross section should continue to increase, but is no longer represented by the single phonon calculation which begins to decrease as the proportion of multiple-phonon processes becomes appreciable. Also, the measurement of total inelastic cross section by transmission becomes impossible to do with accuracy because of the profusion of Bragg reflections.

DIFFERENTIAL SCATTERING MEASUREMENTS

In this region, however, as the neutron energy becomes comparable to the Debye temperature of the crystal, the scattering is no longer isotropic but should follow the Debye-Waller dependence on direction. Measurements of the differential cross sections *versus* angle have been made using a monochromatic beam of 1.08A neutrons from the (200) plane of a Pb monochromator crystal. Scattered intensity *versus* angle from a large-grained 0.350-in. polycrystalline Pb slab, as measured with a neutron spectrometer, is shown in Fig. 5. The diffraction peaks are broadened by a wide counter aperture used to increase intensity of the diffuse scattering. Between the peaks intensity is attributable to thermal inelastic plus multiple elastic scattering. Measurements were therefore made at 16°, 31°, 49°, and 63°, between the successive peaks. Poor geometrical conditions make the solid angle subtended by the counter difficult to determine. Therefore, as a calibration, similar intensity *vs* angle curves were measured for 0.250-in. and 0.114-in. slabs of vanadium, for which the cross section is entirely incoherent, therefore isotropic. From the ratio of intensity for Pb and V,

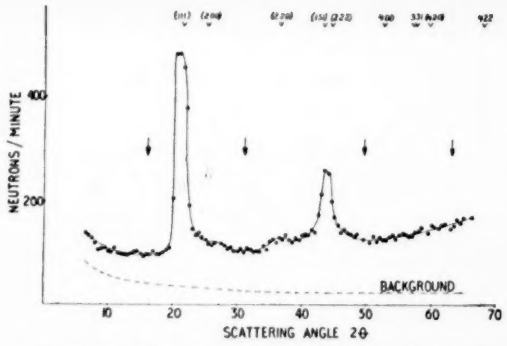

FIG. 5. Scattered intensity of 1.08A neutrons from 0.350-in. polycrystalline Pb slab. Arrows indicate points between Bragg peaks where differential inelastic cross section was measured.

with corrections for background, the differential cross section can be determined.

Although the counter was placed between diffraction peaks, neutrons scattered two or more times could strike it, and must be included in the calculations. Making the reasonable assumption that such multiple scattering is isotropic, its probability can fairly easily be calculated for the case of an infinite slab sample from the known capture and scattering cross sections, and we find

$$\frac{I_{\mathrm{Pb}}-B}{I_{\mathrm{V}}-B}=\frac{[(\sigma_{in}/\sigma)(1-T)T+(\sigma_s/\sigma)^2(1-T)(1-T')T'']_{\mathrm{Pb}}}{[(\sigma_s/\sigma)(1-T)T+(\sigma_s/\sigma)^2(1-T)(1-T')T'']_{\mathrm{V}}},$$

where I_{Pb}, I_{V} = scattered intensities from Pb, V; B = background; σ_{in}, σ_s, σ = inelastic, total scattering, and total cross sections; $T=\exp(-n\sigma x)$ = transmission through slab; T' = fraction of primary scattered neutrons which emerge from the sample without secondary scattering or capture; and T'' = factor (≈ 1) for absorption in multiple scattering. Since defining slits allowed the counter to view only a 2 cm×5 cm area of the sample, however, the calculation of $1-T'$ and T'' was more complex and required numerical integration of a function of the form $\exp(-n\sigma x)$ over all directions and the volume of the sample. For the two cases used, 0.350-in. Pb compared to 0.250 in. V, and 0.163-in. Pb compared to 0.114-in. V, the relations derived by this process were

$$\left(\frac{\sigma_{in}}{\sigma}\right)_{\mathrm{Pb}}=0.83\left(\frac{I_{\mathrm{Pb}}-B}{I_{\mathrm{V}}-B}\right)-0.31,$$

and

$$\left(\frac{\sigma_{in}}{\sigma}\right)_{\mathrm{Pb}}=0.78\left(\frac{I_{\mathrm{Pb}}-B}{I_{\mathrm{V}}-B}\right)-0.18,$$

respectively, the last terms in each case representing corrections for multiple scattering of 3.25 and 1.9 barns. Since this multiple scattering correction is uncertain to perhaps 0.5 barn and since at small angles it considerably exceeds the primary diffuse scattering,

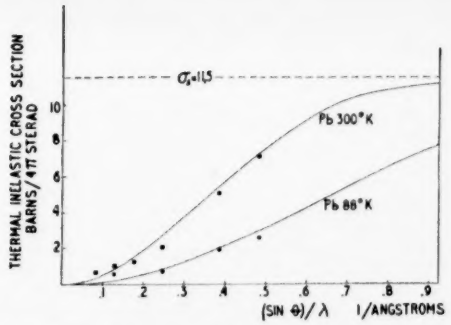

FIG. 6. Differential cross section for thermal inelastic scattering of neutrons in Pb: Points are measured values for 1.08-angstrom neutrons, and curves are computed Debye-Waller factors assuming Debye temperature of 88°K for Pb.

the expected error is relatively large. In Fig. 6 are shown the measured cross sections at four values of $\sin\theta/\lambda$ for 295°K and 80°K (where $\theta=\frac{1}{2}$ scattering angle). The curves shown are computed from the Debye-Waller relation $1-e^{-2w}$ on the basis of an 88° Debye temperature. Agreement between experiment and theory is at least as good as can be expected from the accuracy of the data.

CONCLUSIONS

The direct transmission experiments show that the total inelastic scattering cross section is well represented by one-phonon theory both beyond the cutoff and throughout the lower-energy part of the diffraction region, to wavelengths of 2 angstroms (0.02 ev). At shorter wavelengths, where the neutron temperature is comparable to the crystal Debye-temperature, the one-phonon theory is not expected to apply and direct measurement was not possible. Here, however, the differential scattering cross section was confirmed to be represented by the Debye-Waller factor $(1-e^{-2w})$ and the total cross section may be determined by integration over all angles. Thus the total thermal inelastic cross section as a function of temperature and wavelength may be computed from theory at least over the range $\lambda>1$ angstrom ($E=0$ to 0.08 ev), and probably to higher energies, covering the thermal region.

The author is indebted to D. Kleinman for many suggestions and discussions, D. Fishbach for collaboration in differential scattering measurements, W. Augustyniak for development work on the mechanical selector and spectrometer, and R. R. Smith for assistance in the chopper measurements.

The Hall Effect in Yttrium, Lanthanum, Cerium, Praseodymium, Neodymium, Gadolinium, Dysprosium, and Erbium*

C. J. KEVANE,† S. LEGVOLD, AND F. H. SPEDDING
Institute for Atomic Research and Department of Physics, Iowa State College, Ames, Iowa
(Received May 25, 1953)

The Hall effect has been studied from 300°K to 20.3°K in metallic yttrium, lanthanum, cerium, praseodymium, and neodymium. The ferromagnetic rare earth metals, gadolinium, dysprosium, and erbium have been studied quantitatively only above their respective Curie temperatures with gadolinium being measured to 350°C. The measurements have been made at many temperatures using an alternating current method. Yttrium, lanthanum, gadolinium, and erbium are found to have negative Hall effects at all temperatures studied. Cerium, praseodymium, and neodymium show positive Hall effects throughout the temperature range investigated. Dysprosium metal exhibits a negative Hall effect from 300°K down to about 130°K, but below that temperature the effect is positive. This reversal is interpreted as being due to a change in the sign of the extraordinary Hall effect. The Hall coefficient of cerium is found to go through a thermal hysteresis loop in a manner similar to the electrical resistivity and other properties. Values for the ordinary Hall coefficients are obtained where necessary from the temperature variation of the Hall effect. The Hall coefficients are used to calculate for each metal the effective number of carriers, n^*, ($n^*=1/NeR_0$), on a simple one-band model. In addition, the two-band model, assuming electron conduction in the 5*d* band and hole conduction in the 6*s* band, is used to understand the positive effect in three of the metals and to obtain curves for the number of holes in the 6*s* band as a function of the ratio of *d*-electron mobility to *s*-hole mobility. No ordered change in the magnitude and sign of the effect along the rare earth series is observed.

I. INTRODUCTION

THE development of methods for preparing highly pure rare earth salts[1] and metals[2] has made possible the study of the properties of many of the rare earth metals of high purity.

The study of the Hall effect in rare earth elements is of interest because of their electronic structures, which differ principally in the occupation of 4*f* states and not in the occupation of valence states which are ordinarily considered to be the ones which become of importance in electrical conduction. It has been found[3] that there is a regular change in the magnitude and sign of the Hall coefficients of the transition metals of the fifth and sixth periods as electrons fill 5*d* and 6*d* states. This investigation was initiated to determine what effect the filling of 4*f* states has on the Hall effect in the rare earth elements. Because of its similarity in electronic structure to the rare earths, the Hall effect in metallic yttrium was also studied.

The temperature range below room temperature was of special interest because many of the metals show abnormal properties in this range. For cerium, in particular, the electrical resistivity,[4] magnetic susceptibility,[5] crystal structure,[6] and thermal expansion[7] show remarkable behavior in this temperature range. It has been suggested[6] that this behavior is associated with a shift of an electron between 4*f* and 5*d* states. Since the Hall effect gives information about the numbers and types of carriers of electrical current, it was thought that this study might give evidence supporting or contradicting the hypothesis of a $4f \leftrightarrow 5d$ shift.

Some of the rare earth metals have been reported to show more than one crystal structure. Lanthanum,[8,9] cerium,[6,9,10] and praseodymium[9,11,12] have been reported to exist with both the face-centered cubic (f.c.c.) and hexagonal close-packed (h.c.p.) structures or in mixtures of the two. Because crystal structure may be important to the Hall effect, an attempt was made to determine the crystal structures of the Hall sample metals and to correlate changes in the Hall effect with changes in structure.

Besides allotropy, another property of these metals which affects interpretation of the results of Hall effect measurements is the magnetic property. Several of the metals are ferromagnetic[9,13,14] and most are rather highly paramagnetic[5,12,13] in this temperature range. Because magnetization has a strong influence on the Hall effect,[15] one might expect the interpretation of

* Contribution No. 246 from the Institute for Atomic Research and Department of Physics, Iowa State College, Ames, Iowa. Work was performed in the Ames Laboratory of the U. S. Atomic Energy Commission.

† Now at Motorola Research Laboratory, Phoenix, Arizona. Part of the material reported here appears in the first author's thesis presented to the Graduate Faculty of the Iowa State College in partial fulfillment of the requirements for the Doctor of Philosophy degree.

[1] F. H. Spedding *et al.*, I. J. Am. Chem. Soc. **69**, 2777 (1947); II. J. Am. Chem. Soc. **69**, 2786 (1947); III. J. Am. Chem. Soc. **69**, 2812 (1947).

[2] F. H. Spedding and A. H. Daane, J. Am. Chem. Soc. **74**, 2783 (1952).

[3] E. Justi and M. Kohler, Abhandl. braunschweig. wiss. Ges. **3**, 44 (1951).

[4] James, Legvold, and Spedding, Phys. Rev. **88**, 1092 (1952).

[5] C. La Blanchetais, Compt. rend. **220**, 392 (1945).

[6] A. F. Schuch and J. H. Sturdivant, J. Chem. Phys. **18**, 145 (1950).

[7] F. Trombe and M. Foex, Compt. rend. **217**, 501 (1943).

[8] E. Zintl and S. Neumayr, Z. Electrochem. **39**, 84 (1933).

[9] W. Klemm and H. Bommer, Z. anorg. u. allgem. Chem. **231**, 138 (1937).

[10] A. W. Hull, Phys. Rev. **18**, 88 (1921).

[11] A. Rossi, Nature **133**, 174 (1932).

[12] W. Klemm and H. Bommer, Z. anorg. u. allgem. Chem. **241**, 264 (1939).

[13] F. Trombe, Ann. phys. **7**, 385 (1937).

[14] F. Trombe, Compt. rend. **221**, 19 (1945).

[15] Pugh, Rostoker, and Schindler, Phys. Rev. **80**, 688 (1950).

TABLE I. Spectrographic analyses of metal samples used in Hall effect measurements.

Metal	Analysis
Yttrium	Al, very weak; Ca, weak; Fe, very weak; Dy, 0.5%; Ho, 0.01%; Tb, 0.29%; other rare earths, not detected.
Lanthanum	Si, 0.1%; Ca, 0.05%; Fe, 0.02%; Ta, other rare earths, not detected.
Cerium	Si, 0.02%; Ca, 0.04%; Nd, 0.03%; La, 0.03%; Pr, Ta, not detected.
Praseodymium	Ca, 0.04%; Nd, 0.06%; other rare earths, not detected.
Neodymium	Ca, 0.02%; Fe, other rare earths, not detected.
Gadolinium	Ca, 0.02%; Sm, 0.06%; Fe, Co, not detected.
Dysprosium	Ca, very weak; Ho, 0.05%; Y, 0.02%; Fe, Ta, not detected.
Erbium	Si, trace; Ho, 0.02%; Y, 0.02%; Ca, Fe, very weak; Ta, not detected.

results to be complicated by the extraordinary Hall effect.

Hall effect measurements were made on metallic, polycrystalline yttrium, lanthanum, cerium, praseodymium, and neodymium in the temperature range from 20.3°K to 300°K. The ferromagnetic metals were studied quantitatively only above their respective Curie temperatures where they are paramagnetic.

Sample purities were determined spectrographically and the results are shown in Table I. In Table II are shown the histories of the samples used and the symbols on the graphs reporting results refer to this table.

II. APPARATUS AND MATERIALS

Measurements of the Hall effect were made using an ac method in which the sample is placed in a steady magnetic field and an alternating primary current flows through the sample at right angles to the field.[16–18]

TABLE II. Histories of metal samples used in Hall effect measurements.

Sample	History
Y-0	Cast, unannealed.
Y-1	Cast, annealed 36 hours at 500°C, slow-cooled to room temperature.
La-5	Cast, annealed 97 hours at 370°C, quenched to room temperature.
Ce-1	Cast, annealed 97 hours at 370°C, quenched to room temperature.
Pr-1	Cast, annealed 79 hours at 410°C, quenched to room temperature.
Pr-3	Pr-1, plus: cooled to 20.3°K, annealed 79 hours at 410°C, and quenched to room temperature.
Pr-5	Pr-3, plus: cooled to 20.3°K, annealed 79 hours at 410°C, and quenched to room temperature.
Nd-1	Cast, annealed 37 hours at 400°C, slow-cooled to room temperature.
Gd-0	Cast, unannealed.
Dy-0	Cast, unannealed.
Er-1	Cast, annealed 45 hours at 500°C, slow-cooled to room temperature.

[16] W. F. Leverton and A. J. Dekker, Phys. Rev. **80**, 732 (1950).
[17] A. W. Smith, Phys. Rev. **35**, 81 (1912).
[18] L. A. Wood, Phys. Rev. **41**, 231 (1932).

The resulting Hall voltage is alternating with the frequency of the primary current and can be amplified electronically and measured. In this method, if the frequency is high enough,[17] no correction is required for other thermoelectric, thermomagnetic, and galvanomagnetic effects.

A block diagram of the electronic equipment is shown in Fig. 1. The amplifier gain was approximately 4×10^8 with a noise level, referred to the input, of about 5×10^{-9} volt. The band width was 1 cycle per second, this narrow band characteristic being attained through the use of two parallel-tee feedback networks in the amplifier.

The current supply was capable of delivering up to 5 amperes of current to the sample, and in most cases the measurements were made using primary currents of approximately 1 ampere. The magnet provided fields up to 5600 oersteds and the fields were uniform to better than 1 percent over the region occupied by the Hall samples.

Because of the wide temperature range over which measurements were made, it was necessary to provide some means for adjusting the positions of the Hall contacts to equipotentiality. This was done by means of a three-contact method[19] in which this adjustment is made through the use of a potentiometer connected to the double contact (see Fig. 1). By adjusting the movable contact of the potentiometer, one obtains the condition of equipotentiality. Because of the high resistivity of the rare earth metals, this adjustment was very useful since large voltages resulted from slight shifts of the contacts due to temperature changes. After the potentiometer was set for minimum output voltage, with zero magnetic field, the remaining signal was bucked out by means of a small voltage of variable phase and amplitude from a transformer in the current supply circuit.

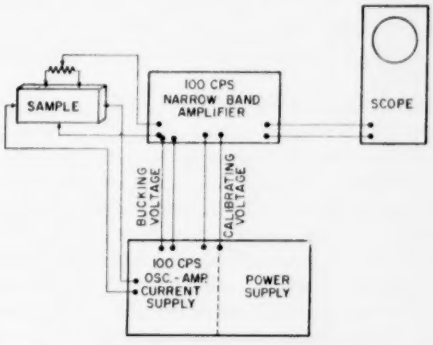

FIG. 1. Block diagram of Hall effect equipment.

The impedance of the amplifier input circuit was high compared to the resistance of the Hall samples. For each Hall coefficient determination, the gain of the

[19] F. Kolacek, Ann. Physik **39**, 1491 (1912).

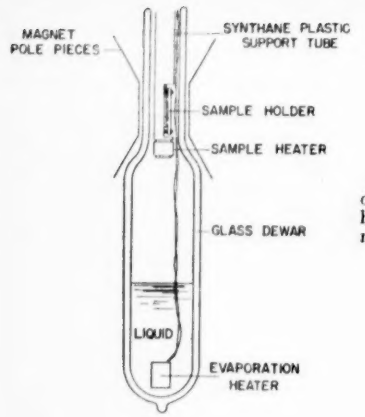

FIG. 2. Schematic diagram of sample holder, Dewar, and magnet.

amplifier was effectively measured by comparing the amplifier output when first the Hall voltage and then the voltage from a standard resistance and voltage divider in the primary current circuit was applied to the amplifier input. The results obtained with this equipment were in agreement with those obtained using a dc potentiometer method and the same sample of gadolinium.

Various temperatures for the sample were obtained by boiling either liquid nitrogen or liquid hydrogen and passing the evaporated gas over the sample (see Fig. 2). By controlling the rate of ebullition and by introducing varying amounts of heat through a heater attached to the sample holder, temperatures between 20.3°K and 300°K could be attained. For the higher temperatures liquid nitrogen was used except in the case of cerium where it was necessary to cause the temperature to change continuously without reversal. The lowest temperatures were obtained by raising the level of liquid hydrogen in the Dewar until the sample was immersed. Temperatures were measured by means of copper-constantan thermocouples fastened to each end of the sample holder. The average of these two was taken to be the temperature of the sample; the greatest temperature difference between the ends of the sample was found to be 4°K. The thermocouples were calibrated at 10°K intervals against a platinum resistance thermometer.

Cancellation of magnetic moment in the primary current circuit and rigid construction of the sample holder and support were used to prevent vibration which would, if it occurred, cause spurious voltages to appear in the Hall voltage circuit. The sample holder was made of copper and brass for rigidity and this was fastened to a supporting piece of Synthane micarta which was, in turn, rigidly supported at the top of the Dewar. The Synthane was chosen for its mechanical strength, low thermal conductivity, and small magnetic susceptibility. Using this type holder and support, the Hall voltage in copper was linear with field up to 15 000 oersteds, the highest field used to test for vibration.

The Hall voltage contacts were tungsten wires with knife edges pressed under bending against the sides of the sample. These contacts provided reliable, low-resistance connections to the sample over long periods of time and throughout the temperature range over which measurements were made. Samples were easily removable for annealing.

Hall samples were cut from the castings and filed to the final dimensions of $2.4\times0.5\times0.1$ cm. Samples to be annealed were wrapped in tantalum foil and sealed under high vacuum in quartz tubes, with lanthanum turnings as a getter. Companion samples accompanied the Hall sample through all heat treatments and needles were filed from the companion samples for x-ray structure analysis.

III. RESULTS AND DISCUSSION

When magnetization is present in a metal sample of the usual form, the Hall coefficient $V_H t/IH_0$ can be expressed[15] by

$$V_H t/IH_0 = R_0(H+4\pi\alpha M); \qquad (1)$$

where V_H = Hall voltage, t = sample thickness, I = primary current, H_0 = applied field, H = magnetizing field, M = intensity of magnetization, R_0 = ordinary Hall coefficient, and α is a parameter which can be interpreted as a measure of the average magnetic field due to magnetization which acts on conduction particles.

In the neighborhood of the Curie point, values of α for nickel have been found to be of the order of 60; above and below the Curie temperature, α was found to be smaller.[15]

In the case of a paramagnetic material, $M=\chi H$, where χ is the magnetic susceptibility, and, for the usual Hall sample, which is a thin plate, $H=H_0-4\pi M$. For this case Eq. (1) becomes[20]

$$V_H t/IH_0 = R_0(1+4\pi\alpha\chi)/(1+4\pi\chi). \qquad (2)$$

When a Curie-Weiss law of paramagnetism is obeyed, the result is

$$V_H t/IH_0 = R_0(T-\theta+4\pi\alpha C)/(T-\theta+4\pi C), \qquad (3)$$

where θ = Curie temperature, C = Curie constant, and T = temperature.

In a paramagnetic, if α and C are sufficiently large, the measured Hall coefficient at some temperature, i.e., $V_H t/IH_0$, would be appreciably different from the ordinary Hall coefficient R_0, while the Hall voltage would still be proportional to the applied field. In the work reported here, high applied fields were not available so that a test for the condition of linearity with applied field could not be made for fields greater than 5600 oersteds. At all the temperatures at which data

[20] N. Rostoker and E. M. Pugh, Phys. Rev. 82, 125 (1951).

were taken, the Hall voltage was proportional to the applied field.

The experimental curves for the ferromagnetics above the Curie temperatures showed the same general temperature dependence described by Eq. (3) so that, for these rare earth metals, α and C must be large enough to give an appreciable extraordinary Hall effect at temperatures where they are paramagnetic. In a truly paramagnetic region, the ordinary and extraordinary effects would be inseparable by the magnetic saturation method.[15] In this work it was assumed that the metals were paramagnetic and Eq. (3) was used to attempt to separate the two effects by choosing R_0 and α to best fit the experimental curve.

Hall effect data may be interpreted on the basis of a simple one-band theory in which the effective number of carriers per atom contributing to conduction n^* is

$$n^*=1/NeR_0, \tag{4}$$

where N is the number of atoms per unit volume, e the charge on the carrier, and R_0 the ordinary Hall coefficient. For each metal n^* is calculated from the observed Hall coefficient.

A two-band theory of Mott[21] developed by Sondheimer[22] has been used to understand the observed Hall effect and magnetic properties in nickel[15] and the observed Hall effect in the transition elements of the fifth and sixth periods.[3] According to the theory, conduction takes place in two overlapping bands, one nearly full and the other nearly empty. The expression for the Hall coefficient according to this theory can be written

$$R_0=\frac{1}{Ne}\left[\frac{n_s-n_d\mu_d^2/\mu_s^2}{(n_s+n_d\mu_d/\mu_s)^2}\right], \tag{5}$$

where N is the number of atoms per unit volume, e the magnitude of the electronic charge, n_s the number of holes per atom in the nearly-full band, n_d the number of electrons per atom in the nearly-empty band, μ_d the mobility of the electrons, and μ_s the mobility of holes.

This relation, with the observed Hall coefficient R_0 and a relation between n_s and n_d, gives n_s as a function of the mobility ratio μ_d/μ_s.

Three of the metals studied were found to have positive Hall coefficients. From the electronic configuration of these elements, it appears that the two-band theory is necessary to explain the result. For each metal, including those having negative Hall coefficients, it was assumed that conduction is by electrons in the $5d$ band, by holes in the $6s$ band, and that there are three electrons available to be distributed between these bands. The $4f$ band is assumed to contribute nothing to conduction. It is to be noted that in the case of the so-called condensed cerium the assumption is made that there are four electrons available for conduction; this is believed to occur because the $4f$ electron has moved to the $5d$ and $6s$ conduction bands. The consequent relations between n_s and n_d are $n_d=1+n_s$ and for condensed cerium $n_d=2+n_s$.

In Fig. 3 are shown graphs of n_s as a function of μ_d/μ_s obtained from the two-band expression for the Hall coefficient, the observed ordinary Hall coefficients, and the above assumed relation between n_s and n_d. For those metals having positive coefficients, n_s has two possible values for some choices of the mobility ratio, and there is a maximum value for the mobility ratio, while in the light of the assumptions listed above for those having negative coefficients, the mobility ratio is limited only by the requirement that the $6s$ band be filled to such a level that conduction in this band is by holes.

It can be seen from Fig. 3 that if one were to assume a fixed mobility ratio for all the metals, a value of 0.1 or less would be satisfactory for all observed Hall coefficients, and then differences in magnitude and sign could be attributed to slight changes in n_s in going from element to element. In every case the $6s$ band would be nearly full. A less likely explanation is that n_s is fixed and a different mobility ratio exists for each metal. In all probability only slight variations in μ_d/μ_s occur for the different metals.

A. Yttrium

The Hall coefficient V_Hl_0/IH_0, where V_H=Hall voltage, l_0=room temperature thickness, I=primary current, and H_0=applied magnetic field, is shown plotted as a function of temperature in Fig. 4. The effect was negative at all temperatures studied, and the Hall voltage was proportional to applied field up to 5600 oersteds at 20.3°K, 78°K, and 300°K. The effect

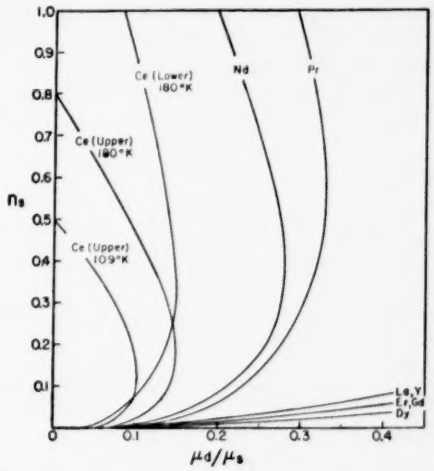

FIG. 3. Number of holes in the $6s$ band as a function of the mobility ratio from the two-band theory of the Hall effect.

[21] N. F. Mott, Proc. Phys. Soc. (London) **47**, 571 (1953).
[22] E. H. Sondheimer, Proc. Roy. Soc. (London) **A193**, 484 (1948).

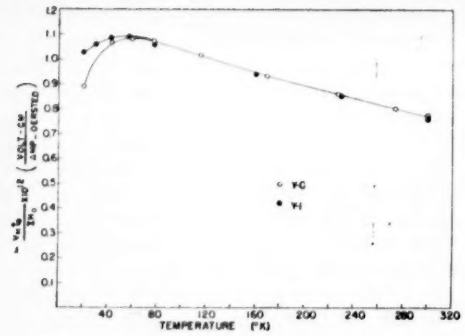

FIG. 4. Hall coefficient of yttrium as a function of temperature.

of annealing (Table II) was to raise the values of the Hall coefficient below 50°K while leaving those above that temperature unchanged.

The room temperature value of the Hall coefficient, -0.770×10^{-12} volt-cm/amp-oersted, corresponds to 2.7 negative carriers per atom effectively contributing to conduction if one assumes the unlikely one-band treatment and uses Eq. (4).

It should be noted that the two-band treatment is capable of accounting qualitatively for the temperature dependence of the Hall coefficient in yttrium since, as the lattice contracts, either the ratio of the number of holes to electrons or the mobility ratio or both, could change.

B. Lanthanum

The Hall effect in lanthanum metal was studied in the temperature range from 20.3°K to 300°K. At all temperatures studied the effect was negative and the Hall voltage was found to be linear with magnetic field at 20.3°K, 78°K, and 300°K.

Measurements made on a cast, unannealed sample resulted in a value of -0.35×10^{-12} volt-cm/amp-oersted for the room temperature Hall coefficient. Annealing at 350°C raised this value to -0.8×10^{-12} volt-cm/amp-oersted, and although further heat treatment resulted in additional changes, the magnitude did not depart by more than 10 percent from this value of -0.8×10^{-12} at room temperature.

In an attempt to get the metal into the face-centered cubic (f.c.c.) structure, it was annealed 97 hours at 370°C and quenched to room temperature. The x-ray diffraction pattern from a filed needle showed h.c.p. lines but the line intensities were not correct for that structure. Coincidence of f.c.c. and h.c.p. lines could not explain the intensity distribution since a non-coinciding cubic line was missing. No correlation could be made between structure changes and Hall coefficient changes resulting from heat treatments.

A typical curve of the observed Hall coefficient as a function of temperature for an annealed sample is shown in Fig. 5. All curves obtained showed the same temperature variation but the magnitudes were different depending on the heat treatments. The curve shown represents the temperature dependence and average magnitude. The sign is negative as in the case of yttrium, and the effective number of carriers contributing to conduction is very nearly the same in the two cases. The temperature variation is more complex in the case of lanthanum, however, showing both a maximum at 170°K and a minimum at 40°K while yttrium shows only a maximum at about 50°K.

The value -0.8×10^{-12} volt-cm/amp-oersted for the Hall coefficient at room temperature corresponds to a contribution to conduction of 2.9 electrons per atom on a simple one-band model.

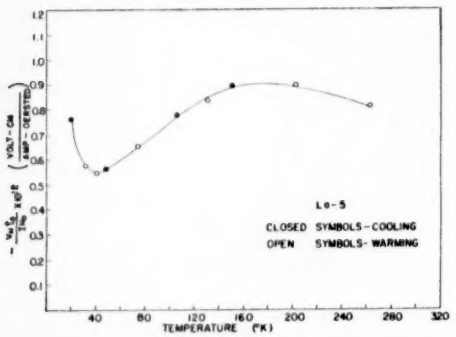

FIG. 5. Hall coefficient of lanthanum as a function of temperature.

C. Cerium

After annealing 97 hours at 370°C and quenching to room temperature, cerium showed only f.c.c. lines and the room temperature Hall coefficient $V_H l_0/IH_0$ was found to be $+1.81\times10^{-12}$ volt-cm/amp-oersted. This was reproducible for several samples within limits of probable error of about 0.5 percent. This result compares favorably with the value $+1.92\times10^{-12}$ volt-cm/amp-oersted found by Smith[23] using a dc method.

The room temperature value after the first and subsequent cycles to 20.3°K was about $+1.4\times10^{-12}$ volt-cm/amp-oersted. X-ray analysis of the companion sample after cycling to low temperatures showed no evidence of the presence of h.c.p. structure. The low room temperature value after cooling may be due to dislocations produced during the transition to and from the condensed state.[6] Reannealing and quenching always raised the room temperature coefficient back to the higher value. The Hall effect was positive at all temperatures at which it was observed and the Hall voltage was found to be linear with magnetic field to 5600 oersteds at 20.3°K, 78°K, 100°K, and 300°K.

A graph of the Hall coefficient as a function of temperature, which is typical of several such curves obtained, is shown in Fig. 6. In every case the first cooling after annealing resulted in a curve which was

[23] A. W. Smith, Phys. Rev. **8**, 79 (1916).

above those observed subsequently without reannealing. The first cooling curve showed the rapid decrease at a slightly lower temperature than did subsequently obtained curves. The details of the first cooling curve were not as reproducible from sample to sample as were those of the second cooling curve.

The large increase in the Hall coefficient as the metal is cooled to 110°K could be the result of the extraordinary effect, but this seems unlikely. The magnetic susceptibility of cerium is reported[5] to obey a Curie law in this temperature range with a Curie temperature of −51°K. To show such a large extraordinary effect so far from the Curie temperature would require α to be of the order of 1000 at 110°K if one assumes $R_0 = +1.0\times10^{-12}$ volt-cm/amp-oersted. Values of α up to 60 have been reported for nickel[15] in the neighborhood of its Curie temperature.

The sudden decrease of the coefficient near 110°K on cooling and the increase near 180°K on warming can be correlated with reported anomalies in resistivity,[4] magnetic susceptibility,[15] specific heat,[24] crystal structure,[6] and thermal expansion.[7] It has been suggested by Pauling[6] that these anomalies are accompanied by a shift of an electron between 4*f* and 5*d* states.

These changes in the Hall coefficient $V_H t_0/IH_0$ could be interpreted in at least three ways. First, they could represent changes in the effective number of carriers accompanying the $4f \leftrightarrow 5d$ shift. Second, if the rise of the upper part of the curve is due to the extraordinary Hall effect, then the sudden decrease at 110°K could be due to the decrease or vanishing of magnetic moment in the metal due to the $4f \leftrightarrow 5d$ transition and a simultaneous change in n_s and n_d which would yield nearly the same R_0. Third, the change in the Hall coefficient may be due to a combination of changes in the magnetic moment and in the effective number of carriers accompanying a $4f \leftrightarrow 5d$ shift. Evidence for the second possibility is that the high temperature limit of the upper branch of the curve seems to be about the same as the high temperature (180°K) limit of the lower branch.

The increase at low temperatures along the lower branch of the loop may be the result of the extraordinary effect. It has been suggested[24] that the transition to the condensed state may be incomplete, and if this were true then there might be an extraordinary effect in the noncondensed phase (which is probably h.c.p.) causing the rise.

The value of the Hall coefficient at 180°K on the lower branch, which is assumed to be the ordinary coefficient R_0, because there seems to be little or no temperature dependence there, corresponds in the one-band model to 1.6 holes per atom effective in conduction. This result assumes an increase in density of 18 percent associated with the transition to the condensed state. Although the work here indicates that the transition may be incomplete at that temperature, these values for the change in density and linear dimension were taken from the x-ray structure findings of Schuch and Sturdivant[6] which were carried out at 78°K.

[24] Parkinson, Simon, and Spedding, Proc. Roy. Soc. (London) **A207**, 137 (1951).

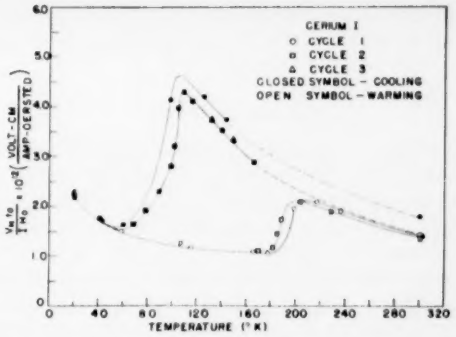

FIG. 6. Hall coefficient of cerium as a function of temperature.

D. Praseodymium

The Hall effect in praseodymium metal was positive at all temperatures studied, and the Hall voltage was linear with applied field to 5600 oersteds at 20.3°K, 78°K, and 300°K. The room temperature value of the Hall coefficient was found to be $+0.709\pm0.008\times10^{-12}$ volt-cm/amp-oersted. This value was not affected by annealing or cooling within the limits of probable error shown.

X-ray crystallographic analysis resulted in h.c.p. lines of incorrect intensity distribution and in extra lines which could not be indexed as either h.c.p. or f.c.c.

The temperature variation of the Hall coefficient is shown in Fig. 7. Investigation of the magnetic properties of praseodymium[12] have indicated a paramagnetic Curie point at 0°K. The increase in the magnitude of the Hall coefficient below 100°K could be associated with an increasing extraordinary Hall effect as a Curie point at 0°K is approached.

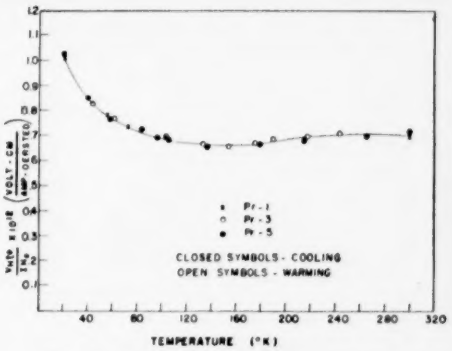

FIG. 7. Hall coefficient of praseodymium as a function of temperature.

The room temperature value corresponds to a contribution to conduction of 3 holes per atom on the basis of a simple one-band model.

E. Neodymium

The room temperature value of the Hall coefficient for neodymium was found to be $+0.971\pm0.006\times10^{-12}$ volt-cm/amp-oersted. This corresponds in the one-band model to 2.1 holes per atom effectively contributing to conduction.

Figure 8 shows the Hall coefficient as a function of temperature. The small maximum at 70°K may be associated with a magnetic effect. It has been reported[13] that an extrapolation of magnetic susceptibility data to temperatures lower than those at which measurements were made indicates a paramagnetic Curie temperature at about 70°K, which is approximately the position of the first minimum in the Hall coefficient. Although no magnetic data exists below 80°K, it is also possible that the rapid rise below 40°K could be associated with the extraordinary effect as a paramagnetic Curie point is approached.

F. Gadolinium

The Hall effect in gadolinium was studied from 30°C to 350°C. These measurements were made with the sample in a vacuum furnace. At all the temperatures indicated, the Hall voltage was proportional to the applied magnetic field H_0, the maximum value of which was 5600 oersteds. According to published data on the magnetic properties above the Curie point,[13] the demagnetizing field was less than 10 percent of the applied field at temperatures above 80°C. The value of the Hall coefficient $V_H t_0/IH_0$ at 350°C is -4.48×10^{-12} volt-cm/amp-oersted. The increase as the temperature is lowered might be attributed to the extraordinary effect in a paramagnetic region.

Using the magnetic data of Trombe,[13] one obtains from Eq. (3) a calculated curve which fits fairly well the experimental curve (Fig. 9) for temperatures above 120°C if one takes $R_0=-0.95\times10^{-12}$ volt-cm/amp-oersted and $\alpha=240$. The calculated values are indicated by the crosses on Fig. 9. The dotted curve is the curve calculated using $R_0=-0.4\times10^{-12}$ volt-cm/amp-oersted and $\alpha=600$. At lower temperatures, the calculated curve falls below the experimental curve, indicating that α is increasing as the temperature is lowered toward the Curie point, if one assumes R_0 constant. One can see that this is not a precise way to determine R_0 and α.

The value -0.95×10^{-12} volt-cm/amp-oersted for the ordinary Hall coefficient corresponds in the one-band analysis to 2.1 negative carriers per atom.

G. Dysprosium

The Hall coefficient $V_H t_0/IH_0$ for dysprosium metal is shown in Fig. 10 plotted as a function of temperature. The effect was negative in the temperature range from 290°K to about 130°K but reversed sign and became positive at lower temperatures. The increase in magnitude followed by the decrease and reversal of sign is believed due to the extraordinary Hall effect. It has been reported that the magnetic susceptibility of dysprosium exhibits a maximum at about 180°K.[14] This may be due to the existence of two magnetic states, and one could understand the behavior of the Hall effect if it were assumed that the parameter α is positive in sign for the high temperature (paramagnetic) state and negative for the state which persists below 180°K.

Below 169°K the Hall voltage was not a linear function of the applied field and evidence of remanence appeared, with the Hall voltage forming a hysteresis loop with applied field. The temperature range in which this occurred is indicated by the dotted portion of the curve.

Because of the limited temperature range over which data were taken, it is difficult even to get an estimate of R_0 and α. Assuming both are constant in the high temperature range, and using Eq. (3), the magnetic data of Trombe, and the experimental values at 290°K and 220°K, one finds $R_0=-1.3\times10^{-12}$ volt-cm/amp-oersted, and $\alpha=18$. Calculated values of $V_H t_0/IH_0$ for intermediate temperatures, using these values for R_0 and α, do not agree well with the observed ones, due

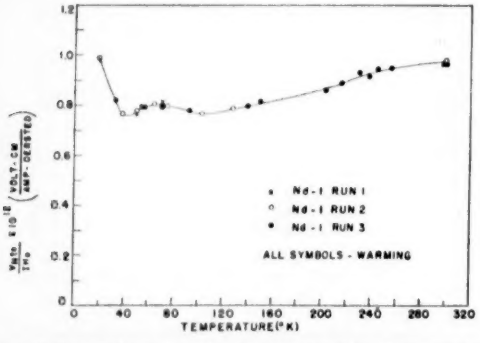

FIG. 8. Hall coefficient of neodymium as a function of temperature.

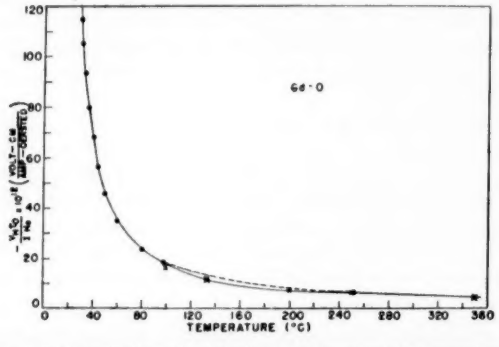

FIG. 9. Hall coefficient of gadolinium as a function of temperature.

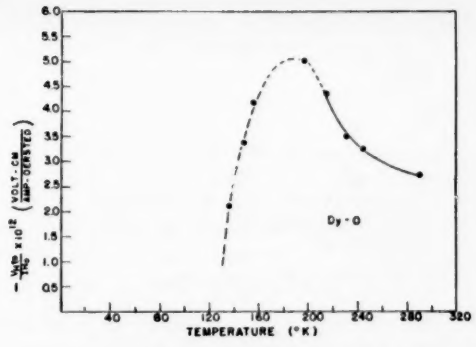

FIG. 10. Hall coefficient of dysprosium as a function of temperature.

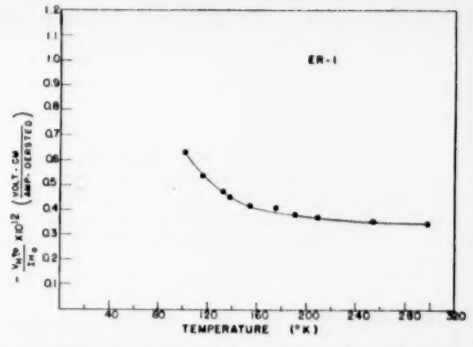

FIG. 11. Hall coefficient of erbium as a function of temperature.

possibly to rapid variation of α with temperature in this range.

The number of negative carriers per atom corresponding to $R_0=-1.3\times10^{-12}$ volt-cm/amp-oersted is 1.5 in the one-band model.

H. Erbium

The Hall effect in erbium was negative in the temperature range from 100°K to 300°K and at 78°K and at 20.3°K. The temperature variation of the Hall coefficient $V_H I_0/IH_0$ is shown in Fig. 11. The increasing magnitude as the temperature decreases appears to be that resulting from the extraordinary effect near a Curie point.

Since the curve is nearly flat at room temperature, the value at this temperature is very nearly R_0. The room temperature Hall coefficient, -0.341×10^{-12} volt-cm/amp-oersted, corresponds to 2.1 negative carriers per atom in the one-band treatment.

ACKNOWLEDGMENTS

The authors wish to thank Dr. J. Powell for preparing the rare earth salts; Mr. D. Dennison and Mr. R. Barton for preparing the metals; Dr. J. Banister and Mr. G. Anderson for the x-ray analysis; Mr. A. Read, Mr. E. Harris, Mr. R. Anderson, and Mr. W. Sylvester for assistance in designing and building equipment; and Dr. G. C. Danielson and Dr. J. M. Keller for many helpful discussions.

Infrared Absorption in *P*-Type Germanium*

W. KAISER, R. J. COLLINS, and H. Y. FAN
Purdue University, Lafayette, Indiana

(Received June 11, 1953)

Infrared absorption in *p*-type germanium was investigated at various temperatures down to 5°K. The absorption coefficient is proportional to the hole concentration and shows band structure, a strong band beyond 10 microns and two weaker bands at shorter wavelengths. The strong band is shown to be caused by excitations within the filled band because of the presence of holes. The relative strengths of the two weaker bands change with temperature, only one being observable at low temperatures.

THE absorption of infrared radiation ($h\nu$ less than the forbidden energy gap) in *p*-type germanium[1] shows spectral structure in contrast to the case of *n* type, where the absorption increases smoothly approximately λ^2. Figure 1 shows the absorption curves reduced to unit carrier concentration, after subtracting the lattice absorption.[2] The *p*-type curve shows two weak bands[3] at 2200 cm^{-1} and 3500 cm^{-1}, followed by a much stronger band beginning around 1800 cm^{-1}. The smoothly rising *n*-type curve is much lower.

Regarding the mechanism of absorption, the following observations are to be noted. (A) Samples having different hole concentrations with either indium or aluminum as acceptor give approximately the same absorption curve reduced to unit hole concentration. (B) The Fermi level in these samples varied from 0.1 ev to 0.24 ev above the valence band, whereas the strong absorption band corresponds to $h\nu<0.1$ ev. (C) *P*-type material with fairly high acceptor concentration after being converted to high-resistivity *n* type by adding donor impurities to the melt showed only weak absorption, characteristic of *n* type. It follows from (B) that the strong absorption band cannot be due to excitation of electrons from the valence band to empty levels within the energy gap. Furthermore, in view of (C) it cannot be due to excitation of electrons from localized states to higher excited states. It could only be caused then by excitations within the valence band due to the presence of holes. This indicates an overlapping of bands and complicated band structure. The evidence is not as conclusive, however, for

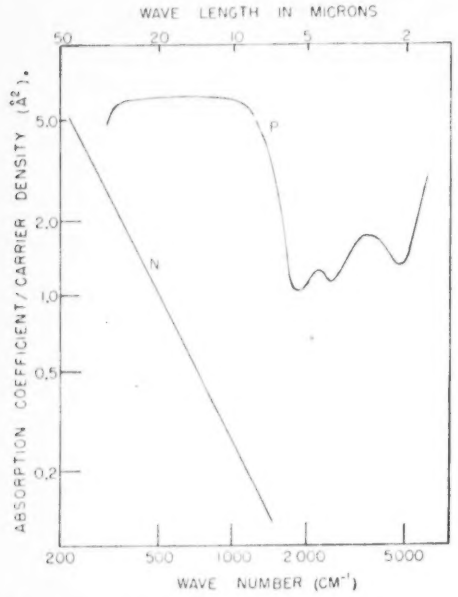

FIG. 1. Absorption coefficient reduced to unit carrier concentration for germanium. The lattice absorption independent of carrier concentration has been subtracted.

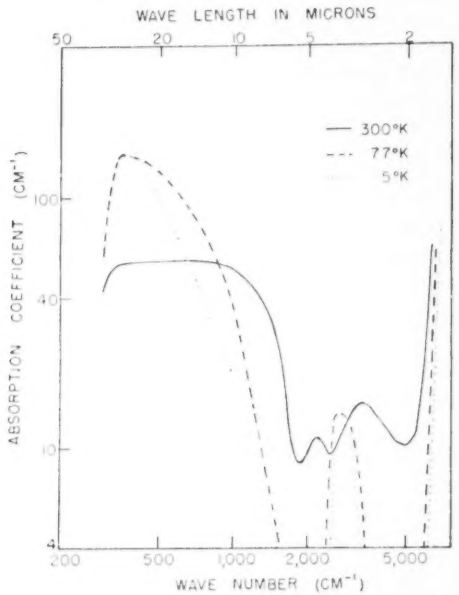

FIG. 2. Absorption coefficient for indium-doped *p*-type germanium with room temperature resistivity 0.07 ohm-cm. The lattice absorption has been subtracted.

* Work supported by a Signal Corps contract.

[1] R. J. Collins and H. Y. Fan, Purdue Semiconductor Progress Report, June 30, 1953 (unpublished); Kaiser, Collins, and Fan, Bull. Am. Phys. Soc. **28**, No. 2, 32 (1953).

[2] R. J. Collins and H. Y. Fan, Phys. Rev. **86**, 648 (1952); R. C. Lord, Phys. Rev. **85**, 140 (1952).

[3] H. B. Briggs and R. C. Fletcher, Phys. Rev. **87**, 1130 (1952).

the two short wavelength peaks, which correspond to $h\nu$ close to one half of the energy gap.

Figure 2 shows typical absorption coefficient curves for indium-doped samples at 300°K, 77°K, and 5°K. For different samples the low temperature curves are also proportional to the room temperature hole concentrations. At 77°K the hole concentration in these samples is the same as at room temperature. Thus, the mechanism for the strong absorption band seems to be the same as at room temperature. This conclusion is supported by the measurement of gold-doped samples.[4] These p-type samples with an acceptor activation energy of 0.23 ev have very few holes at 77°K. At 300°K the measured absorption is the same as in other samples of corresponding carrier concentration, and at 77°K the absorption becomes negligible.

There is some uncertainty about the interpretation of the absorption at 5°K. Within the limit of measurements the long wavelength absorption has not reached a peak. It is, therefore, uncertain whether we have here the same band observed at the higher temperatures. Furthermore, the Hall coefficient of the samples reaches a maximum at some low temperature, the magnitude and temperature depending on the sample purity, and drops again to about the room temperature value by 5°K. The resistivity at 5°K, on the other hand, can be orders of magnitude higher than at 300°K.[5] Consequently, it is not certain that the measured Hall coefficient gives the true hole concentration in the valence band, and we cannot be sure that the long wavelength absorption is due to the presence of free holes.

Figure 3 shows the absorption curves above 1000 cm^{-1} at various temperatures. Of the two peaks observed at room temperature the one at longer wavelength decreases with decreasing temperature, unseen at 77°K, whereas the one at shorter wavelength increases and shows a shift toward longer wavelength.

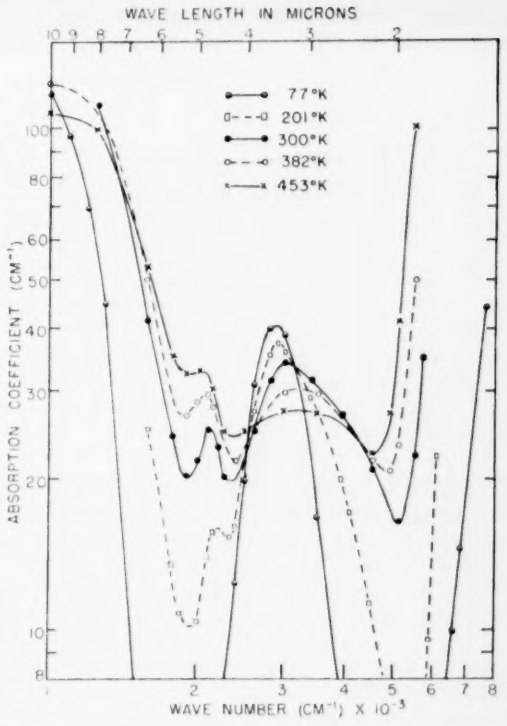

FIG. 3. Absorption coefficient for indium-doped p-type germanium with room temperature resistivity 0.04 ohm-cm.

Up to the highest temperature the sample is in the impurity range, the hole concentration remaining practically constant. A possible explanation for the temperature variation of the two bands might be that the one at longer wavelength is connected with holes of higher energy. It is also possible that the longer wavelength peak involves the absorption of an optical phonon.[6] However, the two peaks are $\sim$0.1 ev apart, whereas the strong lattice band in germanium corresponds to only 0.04 ev.[2]

[4] Benko, Fan, and Lark-Horovitz, Purdue Semiconductor Progress Report, June 30, 1952 (unpublished).

[5] Measurements by H. Fritzsche [see C. S. Hung and J. R. Gliessman, Phys. Rev. **79**, 726 (1950)].

[6] Suggested by Professor J. Bardeen in a private discussion.

Auger Peaks in the Energy Spectra of Secondary Electrons from Various Materials

J. J. LANDER
Bell Telephone Laboratories, Murray Hill, New Jersey
(Received June 5, 1953)

The energy spectra of secondary electrons from carbon, beryllium, aluminum, nickel, copper, barium, platinum, and the oxides of beryllium, aluminum, nickel, copper, and barium have been measured with equipment of high stability and sensitivity. Characteristic peaks due to Auger electrons emitted as a result of absorption of a valence electron by an excited x-ray level were observed for all these materials.

The peaks exhibit structure which is of some theoretical interest. The structure can be related to the distribution in energy of electrons in the valence band, and it complements that observed in soft x-ray emission work. Since the emission of the Auger electron is not subject to the selection rules governing the emission of x-radiation, additional information can be obtained from the Auger electron energy distribution.

Excitation of Auger peaks by a beam of low velocity electrons provides an interesting technique for surface analysis.

"Plasma" peaks of the type reported by Ruthemann, and interpreted by Pines and Bohm, were also observed.

1. INTRODUCTION

CERTAIN discrete maxima in the energy spectra of secondary electrons excited by a primary beam of moderate voltage (roughly from one hundred to a few thousand volts) are the principal subject of this report. "Peaks" or "humps" of this type have been reported by others, but their nature has not been established.[1] The features, observed in distributions obtained by us from a number of materials, are attributed to Auger electrons emitted after excitation of x-ray levels by the primary beam or secondarily by x-radiation excited by the primary beam.

We will be concerned with the following process: an atom which has lost an electron from an inner level (K, L, etc.) returns toward the normal state by absorption of an electron from an upper level (valence, K, etc.) and the energy released in this transition appears in the form of an Auger electron ejected from a nearby upper level. These processes will be described, using the Skinner notation, as $V\rightarrow K$, $V\rightarrow L$, $K\rightarrow L$, etc. They complement those in which the energy balance is restored by emission of x-radiation. The selection rules governing the radiative process limits the information obtainable by the x-ray method. The Auger process is not subject to this limitation. For example, in the soft x-ray spectroscopy of carbon, the distribution of valence p electrons is largely reflected in the radiation distribution curve, whereas the Auger electron distribution curve should reflect the distribution of both p and s electrons.

Unfortunately the Auger electron distribution does not reflect the distribution of valence band electrons in a simple manner. Consider the three processes shown in Fig. 1. These all yield Auger electrons with energy W_K-2W. Energy is here taken relative to that of an electron at rest in free space, $-W_K$ is the energy of the x-ray level involved in the process (here assumed to be a K level), and $-W$ is the average of the initial energies of the two electrons.

To obtain an approximate distribution function for the Auger spectrum, assume that the probability of transitions yielding electrons in the energy range $d(W_K-2W)$ is proportional to the product of the densities in the regions dW' and dW'' of the valence band, equidistant from W, and for which electron densities are given by a distribution function $\rho(W)$. The number of Auger electrons, dN, in the range $d(W_K-2W)$ can be obtained by integration with respect to ΔW. The integration limits are W_a-W and zero if W is in the lower half of the band, or zero and $W-\varphi$ if W is in the

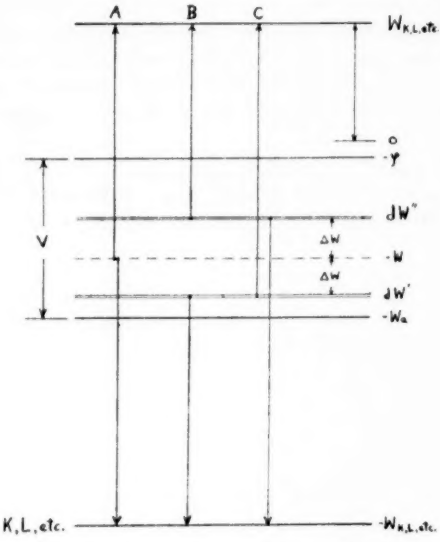

FIG. 1. Auger electron emission resulting from transitions of type $V\rightarrow K$, $V\rightarrow L$, etc. The three processes A, B, and C yield Auger electrons with equal energies.

[1] For a discussion of related work and appropriate references see the review article by K. G. McKay, *Advances in Electronics* (Academic Press, Inc., New York, 1948), pp. 72 and 83.

upper half. Thus,

$$dN(W_K-2W) \sim dW\int_{W_a-W}^{0}\rho(W-\Delta W)\rho(W+\Delta W)d(\Delta W)$$

or

$$dW\int_{0}^{W-\varphi}\rho(W-\Delta W)\rho(W+\Delta W)d(\Delta W).$$

Integrals of the above type might be called Auger transforms. It is expected that more complicated expressions will be required for a generally satisfactory theory. For simply behaved materials it is clear that the energy range of the Auger distribution should be double that of the valence band. Commonly the maximum in ρ is in the upper part of the valence band. In this case the Auger distribution should also peak in the upper part of the spectrum and then fall to zero at a value (in the vacuum) equal to $W_K-2\varphi$. The Auger spectrum will show much less detail than the soft x-ray spectrum.

Excitation of characteristic Auger electrons by x-radiation has been the subject of considerable investigation since the classic work of Auger.[2] A working analytical instrument based on this process has been described recently by Steinhardt and Serfass.[3] Excitation by an electron beam of moderate energy provides an experimental alternative with features of specific interest which will be discussed in the final section of this paper. Excitation of high energy processes by high energy electrons has been described by de Broglie and Thibaud.[4]

The spectra from numerous materials have been re-examined using equipment which was well stabilized and capable of good resolution and high sensitivity. The characteristic peaks observed have, in general, sufficient intensity to make the technique interesting as a means of surface analysis, and they show structure which is of some theoretical interest. Features observed in the low and high voltage regions of the energy distribution curves agree substantially with those reported by others and have not been described in detail. The literature is voluminous and the review of McKay is sufficiently comprehensive.

2. APPARATUS

Desirable features in the required equipment are high stability, high sensitivity, good resolution, and good vacuum conditions. The construction of the spherical electron analyzer used to obtain high sensitivity and of the electron gun used to obtain high stability (see Fig. 2) is somewhat novel. The principal items of apparatus are described briefly below.

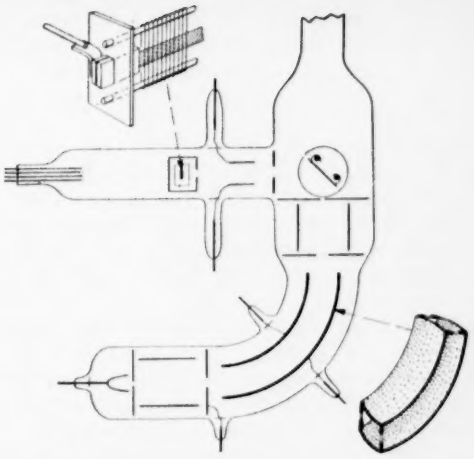

FIG. 2. Spherical electron velocity analyzer, electron gun, and target at 45° to gun and analyzer.

(a) The *beam voltage source* consisted of two 105- and nine 150-voltage regulator tubes in series across a filtered 2500-volt dc supply stabilized by drawing 10 milliamperes.

(b) The *electron gun* (see Fig. 2) was a tungsten ribbon filament 0.040 in. wide, 0.50 in. long, and 0.001 in. thick, welded to nickel leads and on which was floated a flattened 6AK5 grid by means of mica supports. A 0.050-in. hole in the surrounding rectangular plate defined the beam. Deflection, and to some extent focusing, was accomplished by adjusting voltages on the square box array of plates following this hole. Deflection voltages were supplied by a regulated source. The grid over the filament produced a triode with an average transconductance of about 1000 micromhos in the range of operation, which was normally with a cathode bias resistor of 20 000 ohms, a plate current of about 0.2 milliampere and grid at about −4 volts. High beam current stabilization was thus obtained when the filament temperature was sufficiently high.

(c) The *velocity analyzer* (see Fig. 2) consisted of two 90° sections less one-half the gap distance at each end, cut from glass spheres coated with Aquadag, dimensions as shown in the drawing. Ten-mil object and twenty-mil image slits were located at distances from the analyzer plates equal to the average radius of curvature of the analyzer plates. The two-dimensional focusing principle of the spherical analyzer was used to obtain high sensitivity. The resolution of the instrument was better than one percent, as checked by measuring half-breadths of curves from elastically scattered primary electrons. In a preliminary stage of construction the collector and image slit were replaced by a fluorescent screen. It was found that the analyzer produced an excellent image of electrons drawn from a wide tungsten ribbon filament.

[2] P. Auger, Compt. rend. **180**, 65 (1925).
[3] R. G. Steinhardt and E. H. Serfass, Anal. Chem. **23**, 1585 (1951).
[4] M. de Broglie and H. Thibaud, Compt. rend. **180**, 179 (1925).

It is to be noted that the width in energy of the electrons passing through the image slit of this type of analyzer is proportional to their average energy. The curves shown in Figs. 3 and 4 have not been corrected for this effect.

(d) The *electrometer amplifier* has been described elsewhere.[5] Its limiting current sensitivity was about 1×10^{-15} ampere. Distribution curves were normally obtained by operating an Esterline Angus recording milliameter with the output of the amplifier, the time axis being controlled by the recorder gears and the rate of sweep.

(e) The *sweep* voltage was obtained from regulated circuitry which provided for manual selection or automatic sweep at selected rates. A rate of about two volts per second was found convenient for most studies. Sweep voltages were read on a calibrated meter with an accuracy of about 0.2 percent, and were subsequently converted to electron energy using the analyzer constant obtained from measurements of high voltage elastically scattered primary beams of measured voltage.

(f) The *target* (see Fig. 2): One or more targets set at 45° to the primary beam and to the analyzer were supported on a tungsten wire frame. They could be moved into position magnetically along the horizontal axis of the target so that exposure under high vacuum to one of several sources of evaporating material in attached tubes was feasible. They were demagnetized before analysis. In various phases of the work, copper, platinum, and nickel targets were used, either for direct analysis or as substrates for other materials.

It was apparent from tests which were made that space charge distortion affected the distributions obtained in the range below about 15 volts. This distortion is a function of the analyzer construction as well as that of the target and slit system. It is of no importance to the interpretation of results which will be discussed.

(g) The *vacuum system* consisted of Pyrex glassware, mechanical pump, a two-stage mercury pump, and two liquid air traps. Bake-out procedures which produced pressures of about 1×10^{-8} mm of Hg were used.

3. EXPERIMENTAL RESULTS AND INTERPRETATION

The materials investigated were carbon, beryllium, aluminum, nickel, barium, copper, platinum, and the oxides of beryllium, aluminum, nickel, barium, and copper. Quantitative data are given in the summary of measurements in Table I. The measurements and their interpretation are discussed for each material in the following subsections.

3.1 Carbon

Carbon was applied to a nickel target in the form of a sprayed Aquadag coating. It was also unintentionally deposited and observed (with identical results) on several surfaces after primary beam bombardment for many minutes, while the pressure in the vacuum system was in the 10^{-6} and 10^{-7} mm of Hg range. A representative distribution curve is given in Fig. 3 with the carbon feature enlarged and compared with the carbon K x-ray emission curve (due largely to p electrons) given by Skinner.[6]

Note that a curve corrected to give number of electrons per constant energy difference would be nearly flat in the central region, would have a low voltage maximum displaced toward zero, and would have a much lower peak of primary electrons. The shape of the Auger peak would be affected very little.

TABLE I. Summary of measurements of characteristic features.

Material	Test	V_p[a] (volts)	V_1[b]	V_2[b] (volts)	V_3	i(max V_a)[c] (amp $\times10+14$)	i_b[d]	R[e] (percent)	Transition type
Carbon	35	488	276	···	···	1	40	2.5	$V\rightarrow K$
Carbon	36	650	277	···	···	2	36	5.6	$V\rightarrow K$
Carbon	37	771	277	···	···	8	92	8.7	$V\rightarrow K$
Carbon	38	924	277	···	···	14	77	18.2	$V\rightarrow K$
Carbon	39	1210	277	···	···	18	76	23.7	$V\rightarrow K$
Oxygen (NiO)	26	1212	520	···	···	4	85	5	$V\rightarrow K$
Beryllium	59	333	107	···	···	4	16	25	$V\rightarrow K$
Beryllium	61	484	108	···	···	8	24	33	$V\rightarrow K$
Beryllium	62	650	108	···	···	14	34	44	$V\rightarrow K$
Beryllium	63	774	108	···	···	18	34	53	$V\rightarrow K$
Beryllium	64	1070	108	···	···	16	26	62	$V\rightarrow K$
Beryllium oxide	69	775	102	···	···	4	28	14	$V\rightarrow K$
Aluminum	74	640	70	···	···	10	65	16	$V\rightarrow L$
Nickel	13	1075	160	69	···	10	70	14	$V\rightarrow M$
Copper	96	1075	185	63	···	8	57	14	$V\rightarrow M$
Barium	108	1210	94	75	56	20	66	30	$V\rightarrow O$
Platinum	116	1200	91	64	···	8	40	20	$V\rightarrow O$

[a] V_p = primary beam voltage.
[b] V_1, V_2, etc. = high voltage edges of features 1, 2, etc.
[c] i(max V_a) = maximum current of strongest feature. V_1 in the case of C, O, Be, BaO, Al, Ni; V_2 for Cu, Pt; V_3 for Ba.
[d] i_b = Average background current for characteristic feature at V_a.
[e] $R=100[i(\max V_a)-i_b]/i_b$.

[5] W. T. Hughes and J. J. Lander, Rev. Sci. Instr. **24**, 331 (1953).
[6] H. W. B. Skinner, Repts. Progr. Phys. **5**, 257 (1938).

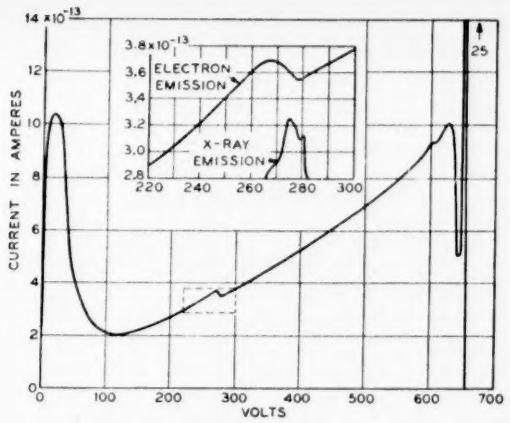

FIG. 3. Secondary electron velocity distribution (not normalized) from carbon. Insert shows Auger peak obtained by amplification, and the soft x-ray emission peak.

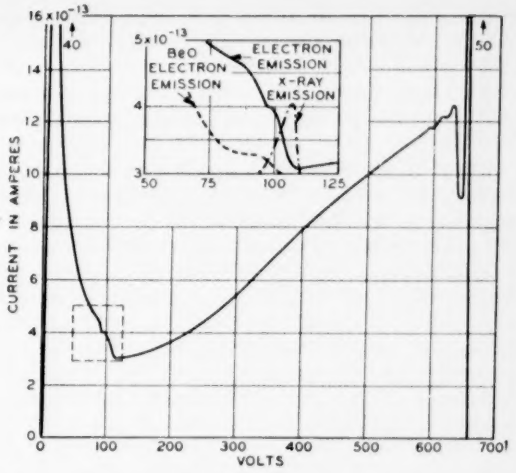

FIG. 4. Secondary electron velocity distribution (not normalized) from beryllium. Insert shows Auger peak obtained by amplification, the soft x-ray emission peak, and the Auger peak obtained from beryllium oxide. The set of peaks near the primary beam (at 660 volts) is the "plasma" feature.

The difference in energy between the high voltage edge at 277 volts and that at 282 volts in the curve given by Skinner is largely the result of the effect of the work function of carbon (about 4.5 volts). This energy is lost by the Auger electron in escaping from the surface. The energy difference between the high voltage edge and the maximum is about 11 volts. The corresponding value for the x-ray emission curve is about 7 volts. The long tail on the low voltage side (asymptotic approach to the background) is partly the result of secondary inelastic collisions by primary Auger electrons within the material, as well as the energy range doubling effect described in the introduction. It is probably the most serious experimental limitation to use of the method for obtaining very accurate distributions in energy.

The dependence of the intensity of the feature on primary beam voltage is given in Table I. The ratio R of the current at the peak maximum $(i_{max}-i_b)$ to the background current i_b is nearly proportional to $(V_p-277)^2$ for low V_p. Absorption corrections would yield a more complicated form for this dependence.

3.2 Oxygen

Oxygen was studied in the form of oxides of several of the metals investigated (Ni, Al, Be, and Ba). The voltage at maximum peak height was about 515, and in all cases the feature was relatively weak (the maximum observed ratio of peak to background was about 0.06, obtained with a primary beam of about 1400 volts). The K x-ray absorption edge for oxygen is 526 volts, which is interpreted as good agreement with the value 515 for maximum peak height. The shape of the feature was not resolved well enough to justify reproduction. This was due in part to the low intensity of the feature and in part to the lower resolving power of the analyzer in the higher voltage range.

3.3 Beryllium

Beryllium produced the strongest of the features observed from different materials. A representative curve is reproduced in Fig. 4. Because of the more complicated nature of this curve, the film of evaporated material (about 100 000A thick) was removed after the experiments and analyzed spectrochemically. The analysts reported that it was 99+ percent pure. Patterns obtained from a second evaporation of beryllium agreed well with that given in Fig. 4. Although the beryllium feature is relatively strong, resolution is somewhat limited by the steeply ascending background due to the low voltage secondaries. Note that again the center section of the curve would be nearly flat if plotted on a constant energy difference basis.

A comparison between the distribution of Auger characteristic electrons (due to s and p electron transitions) and the x-ray K band emission data (due largely to p electron transitions) is also given in Fig. 4. The high voltage edges are in good agreement (108 volts plus the work function, compared with 110 volts). The secondary electron distribution shows a second peak (overlapping band?) with a high voltage edge near 98 volts. The measured variation with primary voltage of the ratio of maximum current of the feature to the average background current is given in Table I.

The double peak in the distribution function is not readily explained as due to overlapping of the s and p bands. The distribution calculated by Herring and Hill[7] has too few electrons in the upper section to give the curve observed unless these electrons are highly favored by the transition probabilities. Other possi-

[7] C. Herring and A. G. Hill, Phys. Rev. **58**, 132 (1940).

bilities may be considered, such as amorphous surface structure or surface alloying with an impurity. Further experimental work is desirable.

Oxidation of beryllium yielded a smooth, much less intense, feature with high voltage edge at 102 volts (see Fig. 4).

In the region near the elastically scattered primary beam, peaks were observed which correspond to those reported by Ruthemann.[8] In a distribution curve for secondary electrons obtained by transmission of a beam of electrons of about 7000 volts through beryllium foil, he observed four maxima corresponding to discrete energy losses of 18 volts. We found that slight oxidation changed the character of this region of the curve considerably. The first maximum moved nearer the elastically scattered primary electron peak and the others tended to disappear.

3.4 Aluminum

Pure aluminum evaporated on a nickel target yielded a fairly strong feature with edge on the high voltage side at about 70 volts and maximum at about 64 volts. No structure appeared. Resolution of the aluminum peak was poorer than that of beryllium because of the steeply ascending background of low voltage secondaries. The peak is the result of a valence band to L transition. The x-ray emission band corresponding to s and d electron densities and reported by Skinner shows two maxima separated by about 7 volts.

As in the case of beryllium, oxidation was observed to reduce the relative intensity of the feature and displace the maximum toward the low voltage region.

3.5 Nickel

A number of features were observed. Two were observed which correspond to transitions of the type $V \rightarrow M$. They were moderately intense, one with high voltage edge at 160 volts and maximum at about 152 volts, the second with high voltage edge at 69 and maximum at about 62. A high voltage primary beam (1420 volts) produced two weak features, one with edge at about 816 volts and the other at about 774. They are apparently $V \rightarrow L$ or $M \rightarrow L$ type transitions.

3.6 Copper

Results similar to nickel were obtained in the $V \rightarrow M$ type transition range. The features had high voltage edges at 185 volts and 63 volts. Features in the expected range of $V \rightarrow L$ transitions were not observed.

3.7 Barium

The features observed were apparently of type $V \rightarrow O$, with edges at 94, 75, and 56 volts.

[8] G. Ruthemann, Ann. Physik **2**, 113 (1948).

3.8 Platinum

Platinum produced one moderately strong feature with edge at 74 and one weak feature with edge at 91. These are apparently $V \rightarrow O$ type transitions.

4. DISCUSSION

4.1 Band Structure Study

The characteristic Auger features observed in the curves for the velocity distributions of secondary electrons have structure analogous in general to that observed in soft x-ray spectra, but differing in detail. A fairly exact theoretical treatment of Auger-type transition probabilities is required in order to interpret this structure in a satisfactory manner. Conversely, the method offers a means of checking a general theory of Auger-type transition probabilities. In addition to the structure of the peaks reported above, it is to be noted that light elements gave the strongest peaks, and this is the theoretically expected result.

The disadvantages more or less inherent to the method are

(a) The complicated nature of the relation between Auger electron distribution and distribution of electrons in the valence band.

(b) A long low voltage tail which is produced by Auger electron secondary energy losses within the material. Some reduction in this tail might be realized by directing the primary beam to the target at a grazing angle of incidence.

(c) Features of interest often occur on a steep background slope produced by low voltage secondaries. Automatic compensation for this slope does not offer a completely satisfactory means of circumventing the difficulty because the exact form of this slope is not readily determinable.

(d) The distribution in velocity of the electrons in the primary beam sets a resolution limit amounting to several tenths of a volt. Beam sources other than tungsten are feasible but much less practical.

Compared with the soft x-ray emission technique, the method has some experimental advantages. Analyses can be made very rapidly, in fact, a feature can conceivably be scanned and displayed on an oscilloscope in a small fraction of a second. The experimental tube is comparatively simple and it can be maintained at extremely low pressures without unusual difficulty. Precision gratings are not needed; measurement is reduced to reading a voltmeter.

4.2 Surface Study

It would appear that when primary beams of moderate velocity are used, the yield of characteristic Auger electrons is high for peaks in the low voltage range and for the lighter elements. Most elements can be relied on to yield one or more useful features in this range.

We are essentially interested in those low velocity electrons which have escaped from the target with little energy loss (aside from that due to the external work function). The absorption coefficients for these electrons are very high, and it is clear that electrons will be observed, on the average, from an outer surface layer of the order of ten atoms thick--thicker for atoms of very low atomic number, thinner for atoms of high atomic number.

The data required for an accurate calculation of the sensitivity of the method to surface contamination are not available (see the review of McKay[1]). It is, therefore, of some interest to turn the problem around. The method may be used as a means for determining absorption coefficients with fair accuracy. Consider a surface which yields characteristic electrons in the velocity range desired. Evaporate on this surface at known rate a material whose absorption coefficient is to be studied and bombard continuously with a primary beam of relatively high energy and constant current. Since absorption of the primary beam will be low relative to absorption of the characteristic secondaries, the decay of the intensity of these secondaries with known thickness of evaporated material should provide a reliable measure of the absorption coefficient desired.

In many problems of applied physics and chemistry, the identification of surface composition is at present impossible but of considerable importance. Where the material of interest is present to a depth of several atomic layers and the high vacuum condition is not prohibitive, the method offers a positive means of analysis. Problems of this type can be of widely varied type.

4.3 Distribution in the Region Near the Primary Beam Voltage

The nature and interpretation of the velocity distribution in the region just below the primary beam has been the subject of considerable study (see McKay,[1] Ruthemann,[8] Rudberg,[9] and Rudberg and Slater[10]). Effects similar to those reported by Ruthemann and interpreted as plasma waves by Pines and Bohm,[11] have been mentioned in Sec. 3.3. Qualitatively similar results were obtained, but the mechanism of discrete energy loss responsible for Ruthemann's results appeared to be much less efficient under the condition of our work (lower beam voltage and reflection rather than transmission). It is, however, of some interest to note that the phenomenon can be observed in the spectrum of reflected electrons. Beryllium gave the strongest features, but comparison of curves obtained with primary beams of 1400 volts and 300 volts showed no significant difference. Aluminum (which, Ruthemann found, gave an excellent series of peaks) yielded two weak peaks. It was observed that superficial oxidation (a monolayer or two) was sufficient to change the character of this region of the curve drastically. Ruthemann also observed peaks at a voltage $V_p - V_f$, where V_f is the voltage of an x-ray type transition (thus $V_p - 278$ for carbon, and $V_p - 525$ for oxygen). Such peaks were not seen in the present work.

Results qualitatively comparable to those obtained by Rudberg[9] for Cu, Ba, and BaO were observed. It is to be emphasized that this region is extremely sensitive to surface impurities and that the interpretation of the wide range of velocity distributions which can be obtained appears unusually difficult.

ACKNOWLEDGMENT

This work has greatly benefited by discussions between the author and C. Herring, G. Wannier, K. G. McKay, H. Hagstrum, and K. H. Storks.

[9] E. Rudberg, Phys. Rev. **50**, 48 (1936).
[10] E. Rudberg and J. C. Slater, Phys. Rev. **50**, 150 (1936).
[11] D. Pines and D. Bohm, Phys. Rev. **83**, 221 (1951); **85**, 338 (1952).

Magnetoresistance of Mg, Cu, Sb, and Al at Liquid Helium Temperatures*†

G. B. YNTEMA‡
Sloane Physics Laboratory, Yale University, New Haven, Connecticut
(Received July 9, 1952)

The resistance of pure samples of magnesium, copper, antimony, and aluminum was measured at temperatures between 1.1°K and 4.22°K in transverse magnetic fields ranging from zero to 22 kg. In a magnesium specimen the dependence of the magnetoresistance on the resistance in zero field was in strict agreement with the Kohler rule, even though the temperature coefficient of the resistance in zero field was negative. The copper samples also showed negative temperature coefficient of resistance, and the temperature dependence of the magnetoresistance was qualitatively in accord with the Kohler rule. The second derivative with respect to temperature of the resistance of the copper samples in zero field was negative in the liquid helium range.

I. INTRODUCTION

THE effect of a magnetic field on the electrical resistance of pure metals becomes very large at low temperatures. The pioneering work by Kapitza,[1] who made measurements with very high fields on samples at the temperature of liquid nitrogen, and the subsequent work at lower temperatures by many experimenters have shown that the magnitude and form of the variation of the resistance with magnetic field strength varies widely among the pure metals. Extensive references may be found in articles by Justi, Kramer, and Schulze[2] and by Mendoza and Thomas.[3]

Attempts to find theoretical relations between the magnetoresistances of different metals have been limited in success, even in the case of the alkalies.[4,5] However, a rule derived by Kohler[6] is often found to describe the variation with temperature of the magnetoresistance of a particular sample, and it likewise often applies to the comparison between magnetoresistances of two samples of the same element. Kohler's rule may be written

$$\frac{\Delta R}{R_{H=0,T}}=f\left(H\times\frac{R_{0°C}}{R_{H=0,T}}\right),$$

where ΔR is the increment to the resistance at temperature T resulting from the application of the field, $R_{H=0,T}$ is the resistance in zero field, and $R_{0°C}$ is the resistance at the ice point. The deduction of this rule is based on a rather general model of the conduction process, and as Justi points out,[4] involves assumptions of (1) Ohm's law, (2) additive scattering mechanisms, (3) an isotropic mean free time of flight of the electrons, and (4) no variation in the number of conduction electrons.

Some of the samples used in the work here reported showed a negative temperature coefficient of resistance in the liquid helium range. References to the many reports of similar behavior in several elements may be found in reference 3. Giauque *et al.*[7] using impure gold found a minimum in the resistance as a function of temperature and also found negative magnetoresistance. In accord with the suggestion[7] that there is a connection between the two anomalies, Gerritsen and Linde[8] produced both effects by addition of a little manganese to silver; and MacDonald suggests that, under certain assumptions, both effects might arise from scattering by internal boundaries. However, lacking theoretical predictions of the magnitude of the negative magnetoresistance and of the temperature range in which it should occur, it is difficult to conclude from experiment whether it is necessarily connected with a minimum in the resistance-temperature curve.

II. EXPERIMENTAL TECHNIQUE

Magnetic fields up to 22 kilogauss were obtained with a large Weiss electromagnet, whose current was regulated through the field excitation of the dc generator, and stabilized by degenerative feedback from the generator output voltage. Throughout the space occupied by the sample in which the resistance was measured the field strength was always within one percent of that at the center of the magnet gap, being calibrated in terms of magnet current by means of a fluxmeter which had been standardized against the proton resonance frequency. In this standardization the mean deviation of the fluxmeter readings from the field strength indicated by the proton resonance was 5 gauss.

The samples were immersed in liquid helium in a Dewar flask, in turn surrounded by liquid nitrogen. The temperature was determined from the vapor

* Assisted by the U. S. Office of Naval Research.
† This forms part of a dissertation presented in candidacy for the degree of Doctor of Philosophy in Yale University.
‡ U. S. Atomic Energy Commission Predoctoral Fellow, 1950–1952. Now at University of Illinois, Urbana, Illinois.
[1] P. Kapitza, Proc. Roy. Soc. (London) **A123**, 292 (1929).
[2] Justi, Kramer, and Schulze, Physik. Z. **41**, 308 (1940).
[3] E. Mendoza and J. G. Thomas, Phil. Mag. **42**, 291 (1951).
[4] E. Justi, Physik. Z. **41**, 563 (1940).
[5] D. K. C. MacDonald, Proc. Phys. Soc. (London) **A63**, 290 (1950).
[6] M. Kohler, Ann. Physik **32**, 211 (1938).
[7] Giauque, Stout, and Clark, Phys. Rev. **51**, 1108 (1937); W. F. Giauque and J. W. Stout, J. Am. Chem Soc. **60**, 388 (1938); and J. W. Stout and R. E. Barieau, J. Am. Chem. Soc. **61**, 238 (1939).
[8] A. N. Gerritsen and J. O. Linde, Physica **17**, 473, 584 (1951).

pressure of the helium bath, using either a mercury or an oil manometer and the Mond vapor pressure tables.[9]

All the samples were between 1.0 mm and 0.9 mm in diameter. For mechanical protection they were mounted, in various ways, inside thin-walled cylindrical metal holders. These fitted inside a narrow section at the bottom of the helium Dewar, so that the samples were held between the magnet poles in a transverse field. The holder used with the copper samples was of brass, and those used with the other samples were of stainless steel. The distortion of the magnetic field by the slightly paramagnetic stainless steel was judged to be negligible, especially in view of the circular symmetry of the holders. All the holders were designed so that, once mounted, the samples were safe from mechanical abuse and could not be strained by differential contraction with the holders on cooling. Current leads were soldered to the copper and antimony samples with Rose metal while potential contacts were made by spot welding. On one of the magnesium samples all electrical contacts were made with a conducting silver paste; to the other, leads were held by small U-shaped phosphor-bronze clips. The aluminum samples were mounted before the final anneal, the potential leads being held against them by manganin springs and asbestos being used for insulation; after the annealing, current leads were soldered with Rose metal to the sample ends, which had previously been plated with copper.

Each sample, except for some of the copper samples as will be mentioned, was cleaned by etching about 0.02 mm off its diameter before each anneal. With the exception of the same copper samples, the copper, magnesium, and antimony were annealed in a vacuum of better than 10^{-5} mm of Hg. The aluminum was annealed in a vacuum maintained by a fore pump at about 50 microns of Hg.

Resistance was measured by the change in the potential drop between two points on the sample when a current through it of known magnitude was reversed. In order to check for drift in the thermal emf's in the potential measuring circuit between the times of the two potential readings, the current was reversed a second time and the potential read again. If the drift was small between the first and third readings, their average was used in the calculation of the change due to the reversal of the measuring current. As a precaution against the production by the Hall effect of spurious increments to the observed resistance, a resistance measurement was made at least once on each sample with the direction of the magnetic field reversed.[10] No significant discrepancy was detected in this way.

The potential to be measured was amplified with a dc amplifier manufactured by the Perkin-Elmer Corporation of Norwalk, Connecticut. Following MacDonald,[11] the input impedance of the amplifier was increased by degenerative feedback to about 3000 ohms so that variations of the resistance in leads and contacts would be insignificant. The output voltage from the circuit consisting of amplifier and feedback network was measured with a Leeds and Northrup Type K potentiometer and a galvanometer. The period of the latter, about two seconds, limited the effective "noise" in the amplifier to a narrow frequency band, with the result that the "noise" level was equivalent to about 10^{-9} volt of input signal. The current through the sample was supplied by a storage battery and regulated by suitable variable resistors and was measured with a set of standard resistors and a potentiometer.

In most of the measurements the scatter of the data was much greater than any of the expected systematic errors. This scatter was caused by changes in the thermal emf's between potential readings and by electromagnetic pickup in the loop formed by the sample and potential leads. This pickup was especially severe at fields greater than 20 kg, so that the measurements at these highest fields are less reliable than the others. Uncertainty in the measuring current, uncertainty in the resistance of the potential leads, and uncertainty in the amplifier gain total one part in 2000 in each resistance measurement. In the helium II range the temperature difference between the sample and the bath could be calculated[12] and was negligible. That convection was adequate in the helium I range is indicated by the absence of anomalies in the resistance-temperature curves at the lambda point and by the fact that the resistances were ohmic for all currents up to a value at which the potential readings became unstable, presumably due to large bubbles in the helium I. In the measurements of the ice point resistance the error due to uncertainty in the temperature of the sample was not greater than 1 part in 1000.

III. SAMPLES AND RESULTS

(a) *Magnesium.*—This was Johnson Matthey and Company magnesium in the form of rods, Lab. No. 1848. They report the following impurities measurable chemically: Fe, 0.013 percent, Mn, 0.0023 percent; Pb, 0.0013 percent. Detected spectrographically were: Mn, Fe, Si, Cu, Ag, Pb, Al, Ca, and Na. Baker and Company of Newark, New Jersey, drew the material cold through clean diamond dies to 0.0395-inch diameter. In an attempt to obtain random crystal orientation sample No. 2 was annealed for one hour at 350°C, work-hardened by flexing, and annealed again for an hour at 365°C. Sample No. 5 was annealed only once, for one hour at 365°C. Microscopic examination of samples prepared in the same way as No. 2 and No. 5

[9] H. van Dijk and D. Shoenberg, Nature **164**, 151 (1949).
[10] C. J. Milner, Proc. Roy. Soc. (London) **A160**, 207 (1937).
[11] D. K. C. MacDonald, J. Sci. Instr. **24**, 232 (1947); and B. Frankenhaeuser and D. K. C. MacDonald, J. Sci. Instr. **26**, 145 (1949).
[12] P. L. Kapitza, J. Phys. (U.S.S.R.) **4**, 181 (1941).

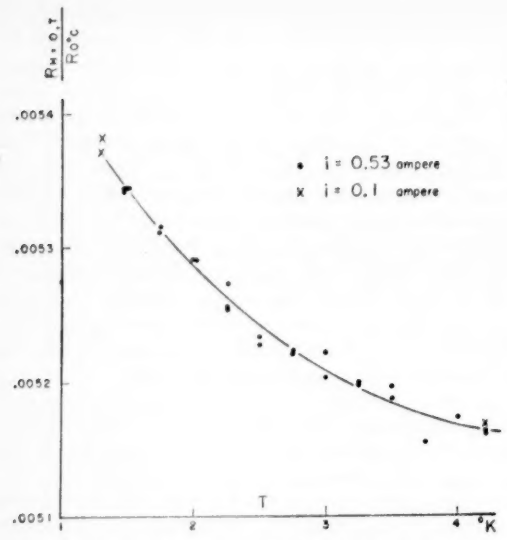

FIG. 1. Resistance of magnesium sample No. 2 at liquid helium temperatures in zero magnetic field.

showed equiaxed grains, those in the sample corresponding to No. 2 being roughly 1/15 the wire diameter in width, those in the sample corresponding to No. 5 being about 1/30 the wire diameter.

The variation of the zero field resistance of sample No. 2 with temperature is shown in Fig. 1. Sample No. 5 had slightly larger residual resistance than sample No. 2 but the same variation with temperature in the helium range. This variation is in accord with the results of previous workers.[13–15] The increase of resistance in magnetic field is shown in a Kohler plot, Fig. 2, where measurements of resistance in the magnetic field were made with a current of 0.1 ampere. In each sample the variation of magnetoresistance with temperature was closely in accord with the Kohler rule. In order to display this on a sufficiently large scale, the following artifice was used. Figure 3 plots differences between the ordinates of the arbitrarily selected line drawn dotted in Fig. 2 and the ordinates of the points for sample No. 2.

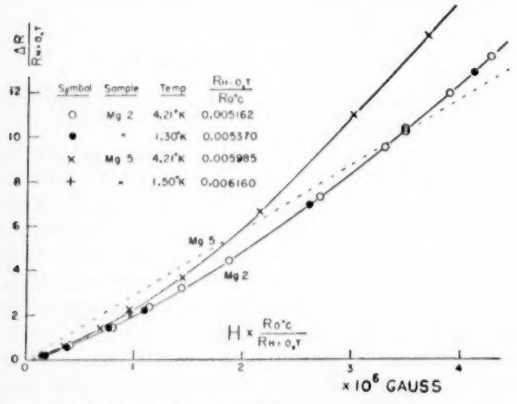

FIG. 2. Kohler plot of magnetoresistance of magnesium samples at liquid helium temperatures. Measuring current 0.1 ampere.

The magnetoresistance was positive even in very small fields, as shown in Fig. 4.

(b) *Copper.*—The copper also was supplied by Johnson Matthey and Company in the form of rods, Lab. No. 1562. They report the following impurities determined spectrographically: Ag, 0.0003 percent; Ni, 0.0005 percent; Pb, 0.0004 percent; Fe, less than 0.0005 percent; Ca, Si, and Mg all faintly detectable. They further report no sign of embrittlement on heating in hydrogen, indicating an absence of oxygen. Baker and Company drew the material cold through clean diamond dies to 0.0394-inch diameter. Sample No. 11 was not annealed but was etched. Samples Nos. 12, 22, and 23 were annealed, each for one hour, at 750°C, 430°C, and 1000°C, respectively. In samples Nos. 5, 6, and 8 the attempt was made to randomize the orientations of the crystal axes by a second recrystalization. They were annealed for one hour at 600°C, worked by bending until hard, and annealed again for one hour, No. 5 at 550°C, No. 6 at 680°C, and No. 8 at 820°C under a vacuum of about 50 microns. These three samples were not etched. Microscopic examination of pieces prepared in the same manner showed that the grain size increased strongly with annealing temperature. Samples Nos. 13 and 14 were prepared in order to investigate further whether the grain size affected the resistance at liquid helium temperatures. They were annealed for one hour at 750°C, bent until hardened

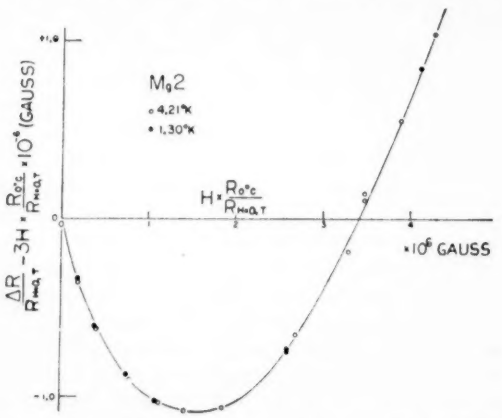

FIG. 3. Magnetoresistance of magnesium sample No. 2 plotted on an expanded scale to show agreement with the Kohler rule. The ordinate of this graph is the difference between the ordinate of Fig. 2 and an arbitrarily chosen term, indicated by the dotted line in Fig. 2, proportional to the abscissa.

[13] W. Meissner and B. Voigt, Ann. Physik **7**, 761 (1930).
[14] Garfunkel, Dunnington, and Serin, Phys. Rev. **79**, 211 (1950).
[15] D. K. C. MacDonald and K. Mendelssohn, Proc. Roy. Soc. (London) **A202**, 523 (1950).

and annealed for one hour at 720°C. Then they were cold worked again, No. 13 being worked lightly, and No. 14 heavily. They were given a final anneal at 550°C. Microscopic examination of pieces prepared in similar fashion showed that the grain size of sample No. 13 was 3 or 4 times that of sample No. 14.

Figure 5 shows the resistance of the copper samples at liquid helium temperatures. They all had a negative temperature coefficient, similar to the spectroscopically pure copper samples of MacDonald,[16] and the "commercial" wire samples of Mendoza and Thomas.[3] Figure 6 is an expanded plot of the resistance of sample No. 12 as a function of temperature; and such plots for the other samples all show the same negative curvature. The slopes of the curves for No. 5, No. 8, No. 11, and No. 22 are the same as for No. 12; that for No. 13 is

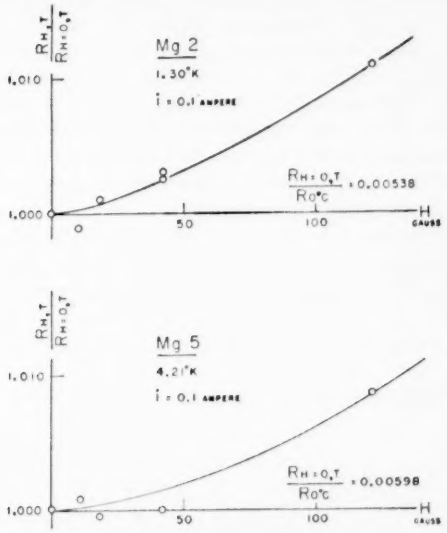

FIG. 4. Magnetoresistance of magnesium samples in low fields. Upper graph, sample No. 2 at 1.30°K. Lower graph, sample No. 5 at 4.21°K. Measuring current 0.1 ampere.

less steep by 0.00002 per degree K. In Fig. 7 is displayed graphically the heat treatment of the samples, and the resistance in liquid helium of each sample in its final form. The resistance appears to depend in a regular fashion only on the temperature of the final anneal. The increase of the resistance with annealing temperature between 550°C and 820°C is similar to the behavior noted in gold samples by de Haas and van den Berg,[17] who found that the value of the minimum resistance increased with the duration of the anneal.

The magnetoresistances of the copper samples at 4.2°K are shown in the Kohler plot, Fig. 8. Measurements with magnetic fields at more than one temperature were made on samples No. 11, 12, and 22, and in each of these the magnetoresistance was smaller at the lower temperature. The data on sample No. 12 are shown in Fig. 9. Figure 10, which is a Kohler plot of

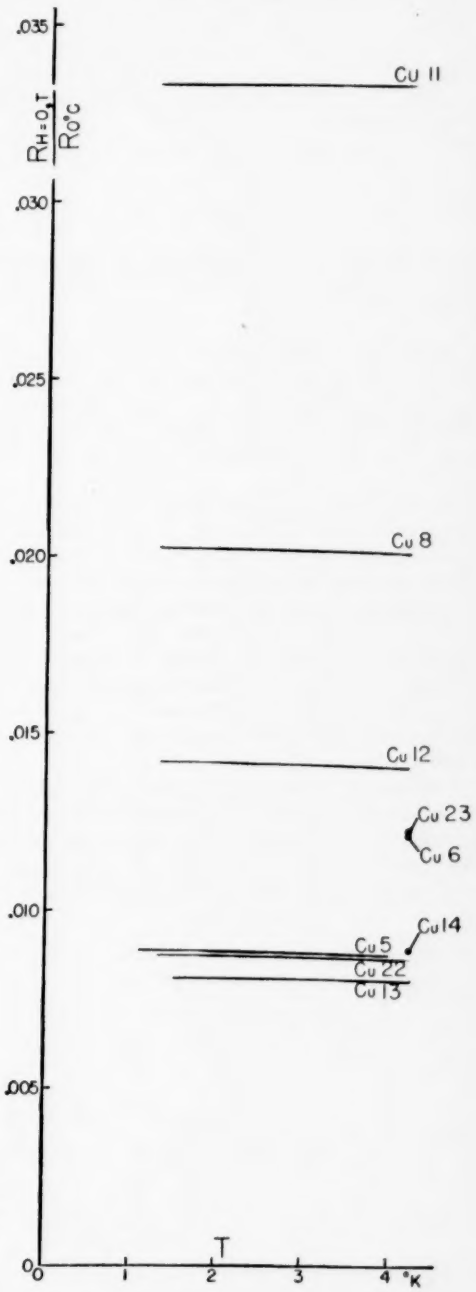

FIG. 5. Resistance of copper samples at liquid helium temperatures in zero magnetic field.

[16] D. K. C. MacDonald, Proceedings of the International Conference on Low-Temperature Physics, Oxford, August (1951).

[17] W. J. de Haas and G. J. van den Berg, Comm. Leiden No. 241d; Physica **3**, 440 (1936); and W. J. de Haas and G. J. van den Berg, Comm. Leiden No. 249b; Physica **4**, 683 (1937).

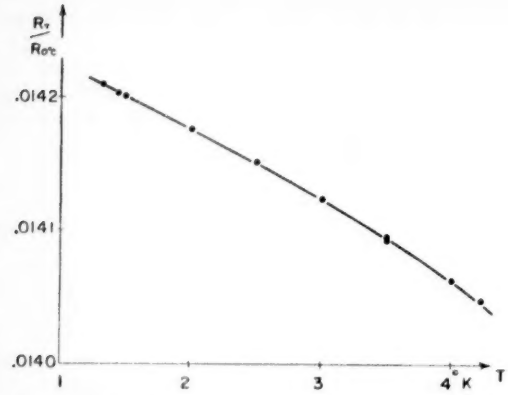

FIG. 6. Resistance of copper sample No. 12 at liquid helium temperatures in zero magnetic field, plotted on expanded scale. Measuring current 2.14 ampere.

the same data, suggests that the temperature dependence of the magnetoresistance is slightly stronger than would be predicted by the Kohler rule, although the discrepancy is not great enough to be conclusive. Samples Nos. 11 and 22 showed better agreement with the rule.

The magnetoresistance at small field strengths was investigated in sample No. 12, and no decrease in resistance could be detected, as is shown in Fig. 11.

Ohm's law was found to hold within the accuracy of measurement for all zero field resistances up to the maximum currents used, which were from 1 to 5 amperes depending on the sample. In sample No. 8 the magnetoresistance at the maximum field was investigated as a function of current and found to be proportional to the latter for currents of 0.1 and 0.05 ampere.

(c) *Antimony.*—This was supplied by Johnson Matthey and Company in the form of ingots, Lab. No. 2696. The manufacturers report impurities totaling 0.0887 percent, including As, Cu, Fe, Ni, S, Pb, Bi, Al, and Si. Baker and Company extruded the metal through iron

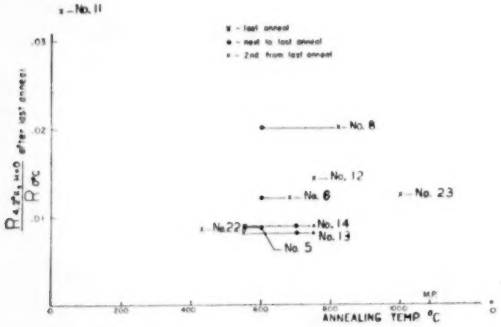

FIG. 7. Heat treatment of copper samples, displayed as resistance of samples in final form at 4.2°K in zero magnetic field. Samples which were annealed more than once were cold worked between anneals. Sample No. 11 was cold drawn wire, unannealed.

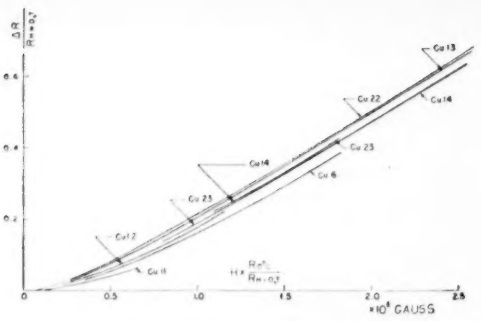

FIG. 8. Kohler plot of magnetoresistance of copper samples at 4.2°K.

dies at approximately 400°C, forming wire 0.0394 inch in diameter. Two samples, Nos. 2 and 3, from this wire were annealed for one hour at 365°C. Sample No. 5 was not annealed but was etched. In microscopic examination of a piece of the unannealed wire individual grains could not be seen, but there were fine striations parallel to the wire axis. Samples annealed like Nos. 2 and 3 showed large grains, of which some were equiaxed and others were longer in the direction of the wire axis than in the direction of its radius.

The variation of the resistance of sample No. 2 with temperature is shown in Fig. 12. A similar plot for sample No. 5 would have an average slope steeper by 0.0003 per °K. The value of $R_{H=0,T}/R_{0°C}$ for sample No. 5 was 0.0353 at 4.19°K and 0.0350 at 1.26°K and

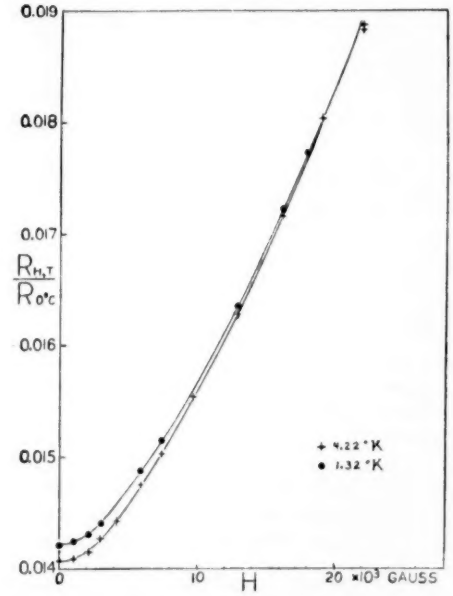

FIG. 9. Magnetoresistance of copper sample No. 12, plotted on expanded scale. Crosses represent measurements at 4.22°K; circles, at 1.32°K. Measuring current 2.14 ampere.

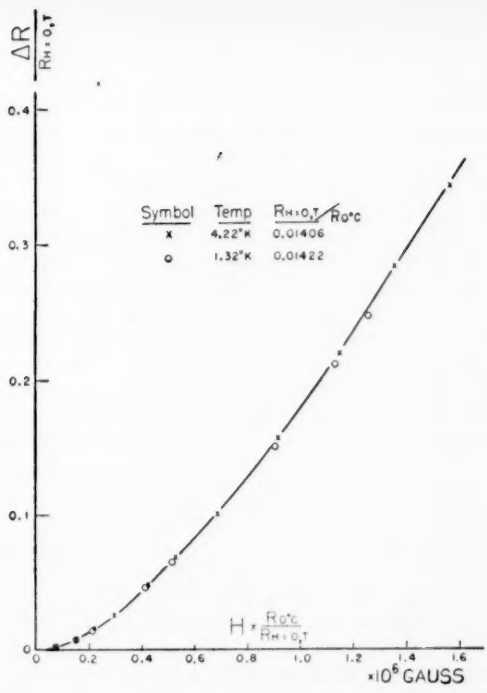

FIG. 10. Kohler plot of magnetoresistance of copper sample No. 12. Crosses represent measurements at 4.22°K; circles, at 1.32°K.

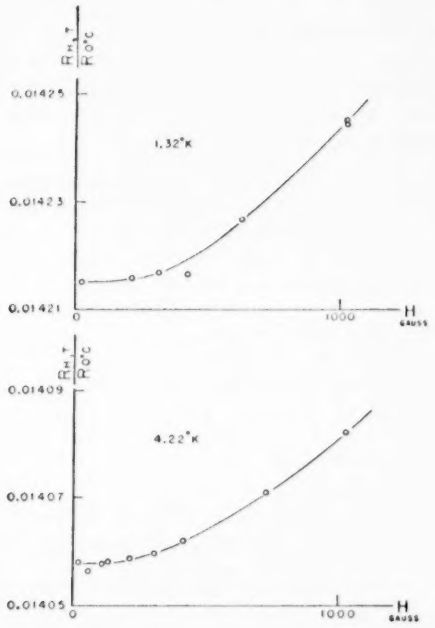

FIG. 11. Magnetoresistance of copper sample No. 12 in small fields. Upper graph, at 1.32°K. Lower graph, at 4.22°K. Measuring current 2.14 ampere.

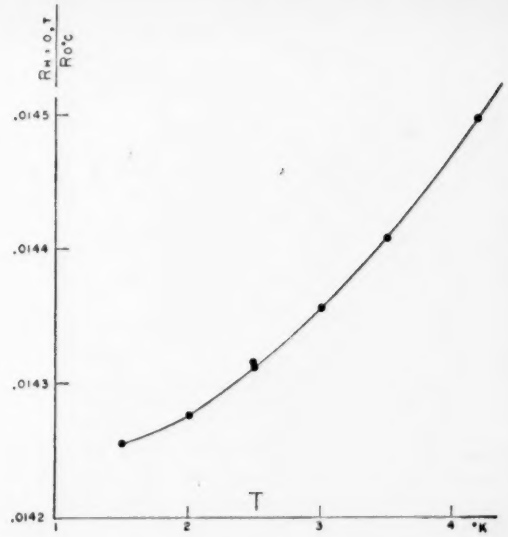

FIG. 12. Resistance of antimony sample No. 2 at liquid helium temperatures in zero magnetic field. Measuring current 0.1 ampere.

for sample No. 3, 0.0142 at 4.19°K. The magnetoresistance of samples Nos. 2 and 5 is shown in a Kohler plot, Fig. 13. Points for No. 3 would lie on the curve for No. 2 in this figure. The resistance in zero field was ohmic for currents from 0.001 to 0.1 ampere. The dependence of magnetoresistance on current was not investigated. The currents used in the magnetoresistance measurements were 0.001 ampere for samples No. 2 and No. 3, and 0.005 ampere for sample No. 5.

(d) *Aluminum.*—Hilger aluminum from Johnson Matthey and Company was supplied in the form of rods, Lab. No. 1011. The manufacturers report impurities totaling a 0.0045 percent, consisting of Mg, Si, Cu, and Fe. The material was cold-drawn through clean diamond dies by Baker and Company to 0.0394-in. diameter. In an

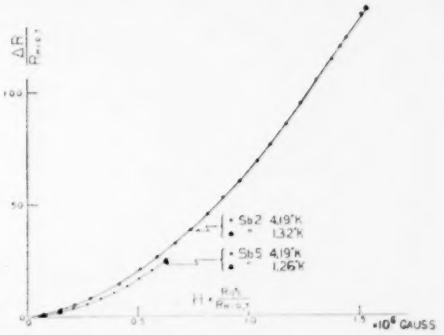

FIG. 13. Kohler plot of magnetoresistance of antimony samples. Upper curve: sample No. 2, measuring current 0.001 ampere, dots for measurements at 4.19°K, triangle for measurement at 1.32°K. Lower curve sample No. 5, measuring current 0.005 ampere, dots at 4.19°K, triangles at 1.26°K.

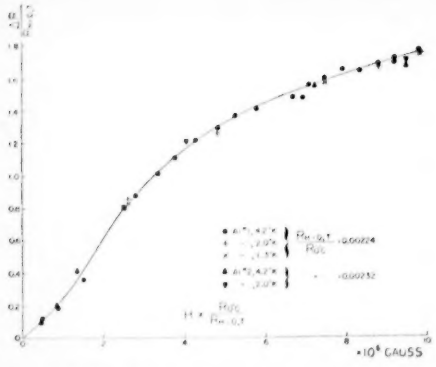

FIG. 14. Kohler plot of magnetoresistance of aluminum samples at liquid helium temperatures.

attempt to make the crystal orientations random the two samples used were annealed for one hour at 320°C, cold worked by bending until hard, and annealed again for an hour at 360°C. Then, in order to find whether grain size was important, they were worked again—sample No. 1 heavily, and sample No. 2 lightly—and annealed for the last time for three hours at 340°C. A piece prepared like sample No. 1 had equiaxed grains of width ranging up to one-tenth the wire diameter; one like sample No. 2 had equiaxed grains about one-fourth the wire diameter in width.

The resistance measurements were made with a current of 0.1 ampere. Within the accuracy of measurement (±0.5 percent), the resistance in zero field was constant throughout the liquid helium temperature range. The results of magnetoresistance measurements are shown in a Kohler plot, Fig. 14. The shape of the curve, with the change in sign of the curvature, is in agreement with the curve compounded by Justi *et al.*[18] from their data at various temperatures.

[18] E. Justi and H. Scheffers, Physik. Z. **39**, 105 (1938); Foroud, Justi, and Kramer, Physik. Z. **41**, 113 (1940).

IV. DISCUSSION

Previous reports of the temperature variation of magnetoresistance as being qualitatively in agreement with the Kohler rule, in cases where the zero field resistance showed negative temperature coefficient, have been made by Nakhimovich[19] on gold samples and by Gerritsen and Linde[8] on silver samples. These reports, together with the present results on samples of copper and magnesium, are of interest in attempting to account for a negative temperature coefficient. For these data would support the hypothesis of a mechanism of scattering which becomes increasingly effective with decreasing temperature, since the assumptions implicit in the Kohler rule would apply to such a case. On the other hand, an explanation of the resistance minimum based on a change in the density of effective conduction electrons or on some sort of change in their acceleration by the electric field would not lead to the observed decrease in magnetoresistance with decrease in temperature.

MacDonald's hypothesis[20] that scattering by impurities in the grain boundaries increases in effectiveness with decreasing temperature could permit a plausible explanation of the effect of annealing observed in the present work on copper and in the work of de Haas and van den Berg on gold.[17] For impurities would presumably collect at the grain boundaries in increasing concentration with increasing time and, within limits, with increasing temperature of annealing.

It is a pleasure to express my appreciation to the members of the Yale low-temperature group, who assisted in the taking of data, to Professor W. D. Robertson and Mr. W. E. Tragert, who gave advice and suggestions regarding the metallurgical aspects of the work, and especially to Professor C. T. Lane, who suggested and directed the research.

[19] N. M. Nakhimovich, J. Phys. (U.S.S.R.) **5**, 141 (1941).
[20] D. K. C. MacDonald, Phil. Mag. **42**, 756 (1951); D. K. C. MacDonald, Phil. Mag. **43**, 124 (1952).

Molecular Beam Investigation of Rotational Transitions. I. The Rotational Levels of KCl and Their Hyperfine Structure*

CHARLES A. LEE,† B. P. FABRICAND, R. O. CARLSON,‡ AND I. I. RABI
Columbia University, New York, New York

(Received May 27, 1953)

The molecular beam electrical resonance method, which has heretofore been confined to the study of transitions between the $m=0$ and $m=\pm 1$ states of diatomic polar molecules in the state $J=1$, has been extended to the study of rotational transitions from $J=0$ to $J=1$. The inhomogeneous electric fields together with a stop wire are so arranged that molecules in the state $J=0$ are selectively refocused on the detector. A transition to the state $J=1$, under the influence of the applied rf field, is observed by a reduction in beam intensity at the detector. The spectra obtained in this way yield more information than with the older method. The hyperfine structure of the state $J=1$ of the molecules $K^{39}Cl^{35}$, $K^{39}Cl^{37}$, and $K^{41}Cl^{35}$ has been investigated at zero field for several vibrational states. The molecular constants obtained for these molecules are:

	$K^{39}Cl^{35}$	$K^{39}Cl^{37}$	$K^{41}Cl^{35}$
ν_{01} (Mc/sec)	3856.370 ± 0.001	3746.583 ± 0.001	3767.394 ± 0.001
$-\nu_{11}\approx\alpha_e$ (Mc/sec)	23.680 ± 0.001	22.676 ± 0.002	22.865 ± 0.001
$\nu_{21}\approx\gamma_e$ (Mc/sec)	0.050 ± 0.001	0.047 ± 0.001	0.048 ± 0.001
B_e (Mc/sec)	3856.399 ± 0.007	3746.611 ± 0.007	3767.421 ± 0.007

$r_e=2.6666\pm0.0001$A.

The structure of the $J=1$ state was attributable to a nuclear quadrupole interaction for each nucleus. The variations of $(eqQ)_K$ and $(eqQ)_{Cl}$ with vibrational state are

	$v=0$	1	2	3
$(eqQ)_K$ ($K^{39}Cl^{35}$) Mc/sec	-5.656 ± 0.006	-5.622 ± 0.006	-5.571 ± 0.008	-5.511 ± 0.008
$(eqQ)_K$ ($K^{39}Cl^{37}$) Mc/sec	-5.660 ± 0.006	-5.628 ± 0.010		
$(eqQ)_K$ ($K^{41}Cl^{35}$) Mc/sec	-6.899 ± 0.006	-6.840 ± 0.010		
$\lvert(eqQ)_{Cl}\rvert$ ($K^{39}Cl^{35}$) (Mc/sec)	<0.040	0.075 ± 0.010	0.237 ± 0.010	0.393 ± 0.010

The ratios of the quadrupole moments of the potassium isotopes is

$$Q_{K^{41}}/Q_{K^{39}}=1.220\pm0.002.$$

From observation of line shifts in a weak electric field, the molecular dipole moment was determined in two vibrational states. For $v=0$, $\mu=10.48\pm0.05$ Debye, and for $v=2$, $\mu=10.69\pm0.05$ Debye. The ratio of the dipole moments is 1.020 ± 0.004. The mass ratios of the chlorine and potassium isotopes calculated from the molecular constants are

$$Cl^{35}/Cl^{37}=0.9459803\pm0.0000015 \quad \text{and} \quad K^{39}/K^{41}=0.9512189\pm0.0000015.$$

INTRODUCTION

PREVIOUS investigations with the molecular beam electrical resonance method (MBER) were confined to the study of transitions from the state $m_J=0$ to $m_J=\pm1$ of the rotational state $J=1$ of diatomic polar molecules. Although these transitions are forbidden, the presence of even a weak static electric field breaks down this selection rule.

The advantage of this method was that the transition could be studied at low frequencies of the oscillating field. In the state of the art when these experiments were first started, this point was important. The chief disadvantage was that the fine structure of the level arising from nuclear quadrupole and other interactions was complicated by the circumstance that these interactions, as well as the effect of the electric field, vary with vibrational state. The spectrum, therefore, becomes very difficult to unravel. In addition, the molecular constants such as B_e and the electrical dipole moment μ could be determined with only poor precision.

The advance of the microwave art in the last decade makes it possible and convenient to study the transitions between states of different rotational quantum numbers. In this paper the transitions which are studied are between the state $J=0$ to $J=1$ of $K^{39}Cl^{35,37}$, and $K^{41}Cl^{35}$. This is, of course, a clear advantage in the simplification of the spectrum, because the different vibrational states overlap only slightly. More importantly, one may obtain very accurate values for the rotational and vibration-rotational constants of the molecule and therefore very accurate values of the mass ratios of isotopes. In addition, one obtains accurate values of the electric dipole moment of the molecule and its variation with vibrational state. None of the other information of the nuclear interactions with the molecule is lost in the process.

There already exists in the literature an electron diffraction measurement of the internuclear separation of the atoms in KCl. Studies made with the MBER

* This research has been supported in part by the U. S. Office of Naval Research.

† Submitted in partial fulfillment of the requirements for the degree of Doctor of Philosophy in the Faculty of Pure Science, Columbia University.

‡ U. S. Atomic Energy Commission Predoctoral Fellow.

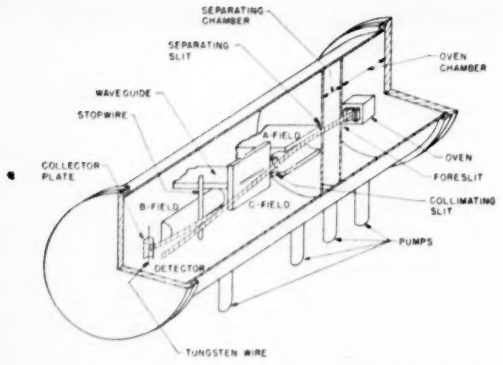

FIG. 1. Schematic of molecular beam electrical resonance apparatus.

method indicate important disagreement with such data in a number of cases. Furthermore, the measurement of Grabner and Hughes[1] on KF made it seem desireable to continue the series with other halide molecules. For these reasons, in addition to the purely technical one that potassium is very easily detected by the hot wire surface ionization detector, it was decided that a careful messurement of KCl would give information of interest and value.

DESCRIPTION OF APPARATUS

The general features of the apparatus used in these experiments are similar to the one described by H. Hughes.[2] The apparatus was originally designed and constructed by V. Hughes of this laboratory and was modified to do the experiments described here.

A cutaway schematic view of the apparatus as modified for these experiments is shown in Fig. 1. The vacuum envelope consisted of a brass cylinder $25\frac{3}{8}$ in. long and $6\frac{3}{4}$ in. in diameter. At approximately the center of this cylinder a cylindrical cross piece of somewhat larger diameter was joined for easy access to the C-field region. Two three-stage DPI fractionating diffusion pumps were used to evacuate the observation chamber, a two-stage pump for the separating chamber, and a two-stage pump for the oven chamber. The forevacuum for these pumps was supplied by a booster diffusion pump and a Welch Duo-Seal mechanical pump.

The cylindrical surfaces of the inhomogeneous deflecting fields corresponded to the flow lines of a two-wire field, to provide fields which were readily calculable. They were milled from rectangular blocks of duraluminum and polished to allow potentials of 10 000 volts to be applied between the two halves of the fields under vacuum. Figure 2 shows an oblique projection of such a field, and the accompanying Table I gives the design constants for the A and B fields. For mounting in the apparatus, the fields were set on heavy brass blocks which rested on a flat tray fixed in the bottom of the cylindrical envelope. These brass blocks had leveling adjustments and were positioned horizontally by screws through the side of the vacuum envelope. Alignment of these fields was facilitated by mounting knife edges at each end of each field. The position of the deflecting fields relative to the other components of the apparatus, such as the oven, the collimator, the stopwire, and the detector, are shown in Fig. 3.

TABLE I. Design constants of the A and B fields.

	A field	B field
a	0.733 cm	0.458 cm
x_0	0.733 cm	0.688 cm
y_0	0.550 cm	0.500 cm
x_1	1.139 cm	1.261 cm
x_2	0.633 cm	0.588 cm
r_1	0.805 cm	0.714 cm
r_2	0.742 cm	0.473 cm
c_1	0.334 cm	0.547 cm
c_2	−0.109 cm	0.115 cm
x_1-x_2	0.506 cm	0.674 cm
$\Delta V/E$	0.419 cm	0.467 cm
$(\partial E/\partial x)/E$	−1.364 cm^{-1}	−2.014 cm^{-1}
$(\partial E/\partial x)/\Delta V$	3.26 cm^{-2}	4.31 cm^{-2}

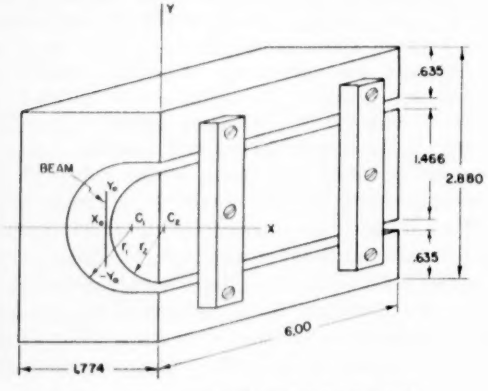

FIG. 2. Oblique projection of deflecting field. (Dimensions in cm.)

Two pairs of slits defined the beam; the slit separation on the iron oven was 1 mil, and the two quartz slits comprising the collimator were 1 mil apart. These quartz slits were waxed to a piece of Micalex which projected into the region between the A field and the C field. The stopwire was a 20-mil tungsten wire which protruded through a hole in the top of the B field into the beam path, and the detector was a heated tungsten filament 3 mils in diameter.

The oven and slit movements on the separating chamber plates were spring loaded pusher devices, with sylphon bellows for vacuum seals. With only a pushing force required, accurate alignment of the internal and external portions of the movement was not necessary. The collimator, stopwire, and detector

[1] L. Grabner and V. Hughes, Phys. Rev. **79**, 819 (1950).
[2] H. Hughes, Phys. Rev. **72**, 614 (1947).

movements had dovetail ways restricting the motion to a line in the plane perpendicular to the path of the beam. Here also a sylphon bellows permitted movement under vacuum. The movement with bellows and ways was mounted in a cup-like structure which was waxed in place on top of the vacuum envelope with Apiezon W40. Dial micrometers enabled the position of these movements to be determined to 0.2 mil.

The C field consisted of two brass plates lapped on each other and polished. These were clamped together with four quartz spacers (0.6100 ± 0.0002 cm) between the plates at each corner. In the center of the plate was a narrow slit through which microwave energy is fed into the C field by a wave guide whose height, in passing through the vacuum envelope to the C field, gradually tapered to the narrow dimension of the slit. Since the wave guide transmitted energy in the TE_{01} mode, the long dimension of the slit determined the cut-off wavelength of the guide, and this dimension was constant as the wave guide passed through the vacuum envelope to the C field (see Fig. 4). At the flange fitting outside the vacuum envelope, a vacuum seal was made with a 5-mil mica sheet and a Neoprene gasket. Around the edges of the parallel plates of the C field a light coating of Aquadag was painted, and across the top and bottom of the plates were clamped sheets of mica with a light coating of Aquadag. We wished by these methods to reduce the amount of energy radiated from the C-field structure into the observation chamber. At no time was any effect due to coupling between the klystron and the detector observed. The termination at the end of the wave guide, which represented a considerable reflection, was essentially independent of frequency, or more precisely, was a slowly varying function of frequency compared to the resolution of the apparatus.

This method provided a simple and satisfactory frequency insensitive way of introducing microwave power into a limited region of an extended homogeneous electric field without disturbing this field to any important extent. These conditions were quite necessary for the accurate measurement of the electric dipole moment of the molecule.

FREQUENCY GENERATION AND MEASUREMENT

A reflex klystron was used as a source of microwave energy in the frequency region of 4000 to 8000 Mc/sec supplying a few hundred milliwatts of power. Very little of this power was necessary to induce transitions in the molecules comprising the beam, except in the case where an absorption was intentionally power broadened to facilitate searching. The power required for optimum transition probability in the C field 5 cm in length was of the order of a microwatt, which introduces the possibility of using harmonic generation in a frequency region where a direct source is not available.

The band width and stability requirements of the source were determined by the resolution of the apparatus, which in this experiment was prescribed by

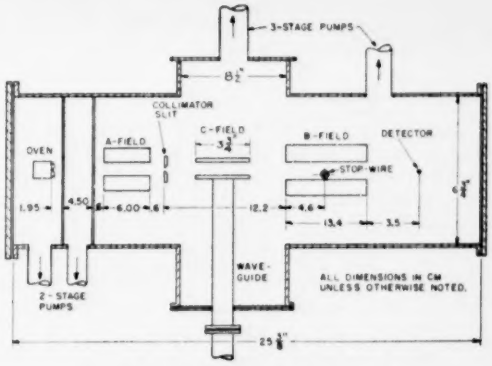

FIG. 3. Dimensions of apparatus.

the length of the C field and the thermal velocities of the molecules in the beam. The frequency width of a resonance line is given by the uncertainty relation,

$$\Delta\nu\Delta\tau=1,$$

where $\Delta\tau$ is the time spent in the radiation field. For KCl this minimum resolution is $\Delta\nu=18$ kc/sec. The contribution to the width of a resonance due to the natural lifetime of a rotational state is negligible. The high resolution obtainable required a frequency stability of 1 part in 10^8, and for the type of reflex klystron used (2K44) was attainable only by automatic frequency regulation. The klystron source was operated in an oil bath from a regulated (5 parts in 10^6) power supply, and as a reference frequency for stabilization, a harmonic of a secondary standard was used.

In Fig. 5, a block diagram of the apparatus shows the stabilizing and frequency measuring circuits. The secondary standard was a 50-kc quartz bar of the type used for Loran in World War II. The 50-kc signal from this crystal was multiplied by conventional vacuum tube multipliers to a frequency of 240 Mc/sec. Harmonics in the frequency range of the klystron were then obtained by feeding the 240-Mc signal into a harmonic generator of a coaxial type employing a silicon crystal diode. The 35th harmonic of 240 Mc/sec was still sufficiently strong to be used for frequency regulation. It should be emphasized here that although a standard circuit was used for the oscillator employing the quartz bar, and standard multiplier circuits were used, extreme

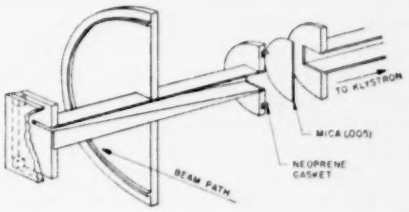

FIG. 4. Isometric section of wave guide which introduces microwave energy into C field.

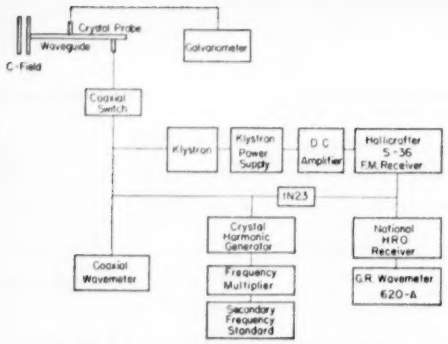

FIG. 5. Schematic of frequency generation and measuring circuit.

care must be used in their construction and operation to keep sideband and hum modulation at a minimum. A signal at 80 Mc/sec may appear to be free of such defects, but a harmonic at several thousand megacycles may show troublesome sidebands and noise modulation.

To obtain an error signal for stabilizing the frequency, the beat frequency between a crystal harmonic and the klystron in the range of 40 to 80 Mc/sec was amplified in an S-36 Hallicrafter receiver. The dc signal from the receiver discriminator was then amplified and used to control the repeller voltage of the klystron. The problem of isolating the high potential of the repeller circuit from the conventional dc amplifiers following the receiver was solved by using, in the last stage of amplification, a cylindrical magnetron diode (GL 2B23) operating in the region of cutoff. The error signal controlled the magnitude of the magnetic field, and the proportional diode current developed a potential across a resistor in series with the repeller lead to the klystron. With the stabilizing circuit in operation, there remained 5 to 10 kc of hum (60, 120) modulation of the klystron signal, but the center frequency was stable to less than 100 cps. The klystron frequency, in addition, was easily varied over a few megacycles by varying the main tuning of the S-36 receiver.

Frequency measurements were made by amplifying the beat frequency between the klystron and a crystal harmonic different from the one used for stabilizing the klystron frequency. By feeding harmonic power from the lower frequency multipliers, in addition to power at 240 Mc, into the crystal multiplier, harmonics in the frequency range of the klystron could be obtained at intervals of 20 mc. This permitted selection of a beat frequency between the klystron and a crystal harmonic in the range 10—30 Mc/sec. Then the signal was amplified by a National HRO receiver, and a zero beat with the radiated signal from a General Radio 620-A heterodyne frequency meter was obtained. The calibration of the receiver did not affect this measurement since the HRO was used only as a selective amplifier for the signal from the klystron (beating against a crystal harmonic), and the signal radiated from the heterodyne frequency meter. A preliminary measurement of the klystron frequency was made with a coaxial wavemeter (0.1 percent accuracy). This helped identify the crystal harmonic with respect to which the beat frequency was measured.

THEORY

A. Molecular Structure

The energy levels of a vibrating rotator have been calculated by Dunham[3] using a WKB method for any potential which can be expanded as a series of powers of $(r-r_e)$ in the neighborhood of the potential minimum, where r_e is defined as the equilibrium internuclear distance.

The equation for the energy levels can be most conveniently written in the following form:

$$F_{v,J}=\sum_{l,j} Y_{lj}(v+\tfrac{1}{2})^l J^j(J+1)^j, \qquad (1)$$

where l and j are summation indices, v and J the vibrational and rotational quantum numbers, respectively, and the Y_{lj} the coefficients.

The connection between some Y's and the ordinary band spectrum constants is shown below:

$$Y_{10}\sim\omega_e, \quad Y_{02}\sim-D_e, \quad Y_{11}\sim-\alpha_e,$$
$$Y_{01}\sim B_e, \quad Y_{20}\sim\omega_e x_e, \quad Y_{21}\sim\gamma_e,$$

where the symbols on the right side refer to the coefficients in the Bohr theory expansion for the molecular energy levels; i.e.,

$$F_{v,J}=\omega_e(v+\tfrac{1}{2})-\omega_e x_e(v+\tfrac{1}{2})^2+\cdots+B_vJ(J+1) -D_vJ^2(J+1)^2+\cdots,$$

and

$$B_v=B_e-\alpha_e(v+\tfrac{1}{2})+\gamma_e(v+\tfrac{1}{2})^2+\cdots.$$

$B_v=\hbar^2/2\mu r_v^2$ is the rotational constant for a given vibrational state;

$B_e=\hbar^2/2\mu r_e^2$; α_e is the vibrational-rotational interaction constant;

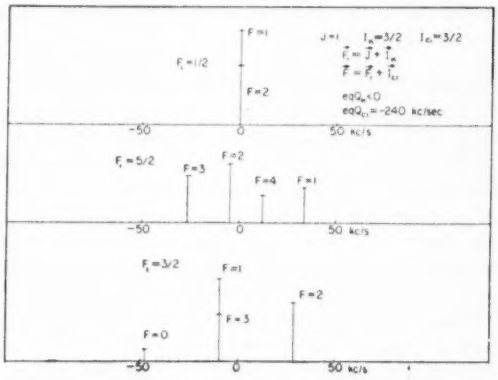

FIG. 6. Theoretical splitting of F_1 levels of the chlorine quadrupole interaction.

[3] J. L. Dunham, Phys. Rev. 41, 721 (1932).

γ_e is a higher order anharmonic vibrational-rotational interaction term; D_v is the first rotational stretching term.

In this experiment we wished to observe the transition $J=0\rightarrow J=1$ for several vibrational levels. If, for the moment, we neglect hyperfine structure, the frequencies of this rotational transition for the first four vibrational states are given by the following expressions:

$$\begin{aligned} f_0&=2Y_{01}+4Y_{02}+Y_{11}+(1/2)Y_{21},\\ f_1&=2Y_{01}+4Y_{02}+3Y_{11}+(9/2)Y_{21},\\ f_2&=2Y_{01}+4Y_{02}+5Y_{11}+(25/2)Y_{21},\\ f_3&=2Y_{01}+4Y_{02}+7Y_{11}+(49/2)Y_{21}, \end{aligned} \tag{2}$$

where the subscript f_v denotes the vibrational state. It is easily seen that from a knowledge of f_0, f_1, f_2, and f_3 three coefficients may be determined. The smallest coefficient Y_{02}, the rotational stretching term, is calculated from the relation

$$Y_{02}=-4B_e^3/\omega_e^2.$$

B_e is calculated from the relation:

$$Y_{01}=B_e\left[1+\frac{B_e^2}{\omega_e^2}\beta_{01}\right], \tag{3}$$

where

$$\beta_{01}=\frac{Y_{10}^2Y_{21}}{4Y_{01}^3}+16a_1\frac{Y_{20}}{3Y_{01}}-8a_1-6a_1^2+4a_1^3$$

and

$$a_1=\frac{Y_{11}Y_{10}}{6Y_{01}^2}-1\approx-\frac{\alpha_e\omega_e}{6Y_{01}^2}-1.$$

B. HYPERFINE STRUCTURE

The nuclear spins of potassium and chlorine are each $\frac{3}{2}$. The ground state $J=0$ has negligible hfs. What splitting of the ground state that may exist would arise from an interaction that mixes in higher rotational states. However, in KCl such effects are still unobservable with the improved resolution and accuracy of the present experiment.

The fine structure of the $J=1$ state of KCl arises entirely from the interaction of the nuclear quadrupole moments with the rest of the molecule. The Hamiltonian for this interaction consists of two terms, one for each nucleus, and is of the form:

$$\begin{aligned} \mathcal{H}=&-\frac{eqQ_K}{2I(2I-1)(2J-1)(2J+3)}\\ &\times[3(\mathbf{I}\cdot\mathbf{J})^2+\tfrac{3}{2}(\mathbf{I}\cdot\mathbf{J})-\mathbf{I}^2\mathbf{J}^2]\\ &-\frac{eqQ_{Cl}}{2I(2I-1)(2J-1)(2J+3)}\\ &\times[3(\mathbf{I}\cdot\mathbf{J})^2+\tfrac{3}{2}(\mathbf{I}\cdot\mathbf{J})-\mathbf{I}^2\mathbf{J}^2]. \end{aligned}$$

The $\mathbf{I}_k\cdot\mathbf{J}$ interaction between the potassium spin and the rotational angular momentum is too small in KCl to be observable. It is known from experiment that $eqQ_K\gg eqQ_{Cl}$; therefore, we may consider that the quantum numbers associated with the three energy levels $\mathbf{F}_1=\mathbf{J}+\mathbf{I}_k$ are good quantum numbers. The first interaction term of the Hamiltonian, the potassium quadrupole interaction, is diagonal in this representation. The splitting of the F_1 levels by the chlorine interaction may then be calculated by second-order perturbation theory using an F representation, where $\mathbf{F}=\mathbf{F}_1+\mathbf{I}_{Cl}$.

$$W(F_1,F)=E_{F_1}+\lambda V_{F_1,F;F_1,F}+\lambda^2\sum_{F_1'\neq F_1}\frac{|V_{F_1F;F_1'F}|^2}{E_{F_1}-E_{F_1'}},$$

where

$$\lambda V_{F_1F;F_1F}=(I_KJF_1I_{Cl}F|\mathcal{H}_{Cl}|I_KJF_1I_{Cl}F),$$

$$F_1'=F_1\pm1,2;$$

and

$$E_{F_1}=(I_KJF_1|\mathcal{H}_K|I_KJF_1),\quad F_1=\tfrac{1}{2},\tfrac{3}{2},\tfrac{5}{2}.$$

The off-diagonal matrix elements of the operator $\mathbf{I}_2\cdot\mathbf{J}$ are given in a paper by Bardeen and Townes.[4] The splitting of the F_1 levels by the chlorine quadrupole interaction is shown in Fig. 6 for an assumed quadrupole interaction constant of $eqQ_{Cl}=-240$ mc/sec.

A very good determination of the mass ratios of the chlorine and potassium isotopes is possible from a measurement of rotational transitions in the three isotopic species $K^{39}Cl^{35}$, $K^{39}Cl^{37}$, and $K^{41}Cl^{35}$. At least two vibrational states must be measured in each of these molecules to obtain sufficiently accurate values of the coefficients Y_{01}, such that the error in the mass ratio is only a few parts per million. The ratio of the reduced masses is obtained from the expression derived by Dunham,[5]

$$\frac{Y_{01}(K^{39}Cl^{37})}{Y_{01}(K^{39}Cl^{35})}=\frac{\mu_{35}}{\mu_{37}}\left[1+\beta_{01}\left(\frac{B_e^2}{\omega_e^2}\right)_{35}\left(\frac{\mu_{35}}{\mu_{37}}-1\right)\right], \tag{4}$$

and the mass ratio from the relation

$$\frac{m_{35}}{m_{37}}=\frac{(\mu_{35}/\mu_{37})(m(K)/m_{37})}{m(K)/m_{37}+1-\mu_{35}/\mu_{37}}, \tag{5}$$

where μ_{35} and μ_{37} are the reduced masses of $K^{39}Cl^{35}$ and $K^{39}Cl^{37}$, respectively. The ratio of the masses of K^{39} to K^{41} are obtained in a similar manner. The ratio of the mass of K^{39} to the mass of Cl^{37}, occurring in expression Eq. (5) for the mass ratio of the chlorine isotopes, and the ratio of the mass of Cl^{35} to the mass of K^{41} used to obtain the potassium isotope mass ratio, were obtained from precision mass spectrographic measurements of these isotopes given by Collins, Nier, and Johnson.[6]

[4] J. Bardeen and C. H. Townes, Phys. Rev. **73**, 97 (1948).
[5] J. L. Dunham, Phys. Rev. **41**, 721 (1932).
[6] Collins, Nier, and Johnson, Phys. Rev. **84**, 717 (1951).

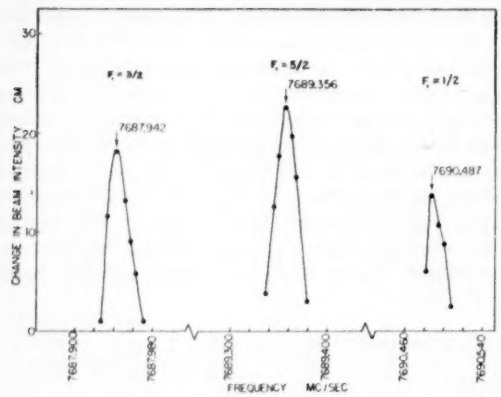

FIG. 7. Observed hfs of $v=0$ state of $K^{39}Cl^{35}$ for the transition $J=0\rightarrow J=1$.

From the frequency shift of the transition $J=0\rightarrow 1$ in a uniform electric field, the electric dipole moment was calculated. A transition from the ground state $J=0$ to an F level of the $J=1$ rotational state which had zero polarizability in very weak fields was observed. Under these circumstances the frequency shift of the line arises only from the relatively large polarizability of the $J=0$ state. The observed frequency shift of the transition, considering only the polarizability of the ground state, is given by

$$f=-\frac{1}{6}\frac{\mu^2E^2}{hh^2/2A},$$

where μ is the permanent dipole moment of the molecule, E the static electric field strength, and A the moment of inertia of the molecule.

The actual transition chosen was from $F=0, 1, 2, 3$ $(J=0)$ to $F=1, 2$ $(J=1, F_1=\frac{1}{2})$. These two F levels of the upper state, in addition to having zero polarizability in very weak fields, are not split by the chlorine quadrupole interaction. The separation is <500 cps in second-order perturbation.

Relative line intensities were calculated approximately by assuming the fraction of molecules making a transition to a particular excited state, while traversing the C field, was proportional to the number of available ground states consistent with the selection rule $F=0, \pm 1$ $(F=0\rightarrow F=0$ forbidden). Due to lack of precise measurement of the rf amplitude in the C field, and knowledge of the composition of the refocused beam, we could only determine a rough agreement between the observed and calculated intensities.

PROCEDURE

Molecular beams of about 1 500 000 to 5 000 000 cm (where 1 cm$\sim 10^{-15}$ ampere of ion current from the detector) were evaporated from a hot oven source. After one had determined that this total beam was properly collimated, the stopwire was 5 mils beyond the beam center as seen in Fig. 1, the residual beam due to gas scattering was approximately 100 cm. To keep the residual beam low requires a very good vacuum (less than 10^{-6} mm of Hg) and a stable vacuum which requires diffusion pumps which are not subject to "kicking."

The B-field voltage was then set at a predetermined value, which with the proper A-field potential would refocus molecules in the $J=0$ state around the stopwire. For molecules of the most probable velocity in the beam, the deflection at the stopwire for these potentials was 5 mils. As the potential of the A field was varied, a maximum of the refocused beam was observed. However, this was not quite a maximum for refocusing of the $J=0$ state because a small percentage of molecules in the $J=1$, $m=\pm 1$ and $J=2$, $m=\pm 2$ states were refocused at slightly higher potentials, but not high enough to be resolved. Experimentally the difference in the total number of molecules in the $J=0$ state was very slight and for reasons of stability the A field was set at the maximum refocusing potential. Out of a total beam of 2 000 000 cm we would refocus 500 cm of which about 40 to 50 percent would consist of molecules in the $J=0$ state.

The exploration for the spectrum was conducted at zero C-field voltage by varying the frequency of the klystron oscillator. As a starting point for this exploration, a value of B_e was calculated from an electron diffraction measurement of the internuclear distance in KCl. The resonances were initially power broadened to several megacycles which facilitated searching by permitting larger frequency intervals between observations and increasing the intensity of resonances by smearing out the hyperfine structure. At these high power levels spurious responses were observed which presumably were caused by radiation from the C-field structure causing transitions to occur in the interfield region where intense electric fields existed. When changes in beam intensity were observed, a more detailed exploration was made at low power levels. Points on a resonance were made by averaging deflections made by opening and closing a coaxial switch located between the klystron and the wave guide carrying energy to the C field. (See Fig. 5.) These points were taken at frequency intervals of 4 to 10 kc/sec. At low rf power levels and maximum resolution no spurious resonances were observed. Absolute power measurements were not made, but relative power indications were obtained by a pickup probe inserted in the wave guide carrying energy to the C field.

The molecular dipole moment was determined through a measurement of the transition frequencies to the states $(F_1=\frac{1}{2}, F=1, 2)$ as a function of the potential across the C field from zero up to 7.5 volts. Beyond this point, which represents an electric field intensity of 12.3 volts/cm, the $\boldsymbol{\mu}\cdot\mathbf{E}$ interaction begins to break up the F_1 representation. There was a contact potential

between the C-field plates of 0.087 volt. This was measured by reversing the polarity of the C-field potential at a given point and then readjusting the potential to bring the peak of the resonance back to the same frequency, i.e.,

$$f=f_0+\alpha(V_++C), \quad f=f_0+\alpha(V_-C),$$

where C is the contact potential, $C=\frac{1}{2}(V_--V_+)$. Measurements of the potential were made with a voltage divider and a Leeds and Northrup type K potentiometer.

DATA AND RESULTS

The spectral patterns of the three isotopic species $K^{39}Cl^{35}$, $K^{39}Cl^{37}$, and $K^{41}Cl^{35}$ are widely separated because of the different moments of inertia. For each molecule the rotational transition $J=0\rightarrow J=1$ consists of a series of lines with a spacing of $\sim 2\alpha_e$ between adjacent vibrational state lines. Since the rotational state zero has negligible hfs, the structure of the rotational transition for a given vibrational state gives directly the hfs of the $J=1$ state. Figure 7 shows the splitting of the rotational transition in the $v=0$ state for $K^{39}Cl^{35}$ due to the potassium quadrupole interaction. In this vibrational state the chlorine quadrupole interaction is negligible. However the chlorine quadrupole interaction increases quite rapidly with vibrational state, and in Fig. 8 for the $v=2$ state, the splitting of the $F_1=\frac{3}{2}$ state by the chlorine interaction is clearly resolved. The theoretical patterns are shown in Fig. 6. In Fig. 9 the progressive splitting of the $F_1=\frac{3}{2}$ state into the various F states by the chlorine interaction for the first four vibrational states is shown. In addition to the increasing chlorine interaction with increasing vibrational state, the potassium quadrupole interaction decreased, but only by 1 percent per vibrational state. These quadrupole interactions are listed in Table II for each molecule, nucleus, and vibrational state.

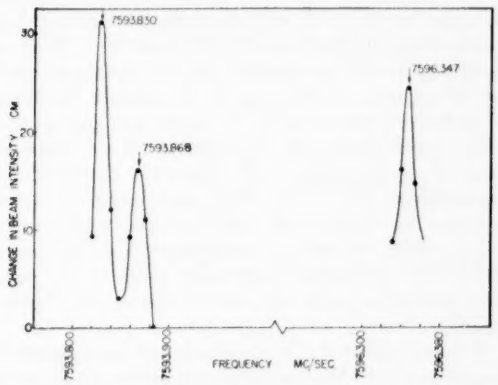

FIG. 8. Observed hfs of $v=2$ state of $K^{39}Cl^{35}$ for the transition $J=0\rightarrow J=1$. (Center line $F_1=5/2$ not shown.)

A considerable body of molecular data was calculable from the observed spectra. Table III shows the Dunham coefficients for the three isotopic species. Here $Y_{02}\approx -D_e$ is calculated from an approximate knowledge of B_e and ω_e. The coefficients Y_{11} and Y_{21} are equal to α_e and γ_e, respectively, within the experimental error. This is not the case for B_e, and the calculation of B_e from Y_{01} must be obtained from Eq. (3). The uncertainty of B_e is considerably greater than Y_{01} because Eq. (3) contains $\omega_e=280$ cm^{-1} and $\omega_e x_e=0.9$ cm^{-1}, which were measured by optical spectroscopic observations of vibrational bands[7] and introduce the additional error. The internuclear distance r_e is simply calculated[8] from the relation:

$$B_e=\hbar^2/2\mu r_e^2.$$

Table IV shows the variation of dipole moment and internuclear distance with vibrational state. The error quoted for the dipole moment is equal to twice the error one computes from the deviations of the observed points from a least squares fit of the data. Table V gives the chlorine and potassium mass ratios as calculated from Eqs. (4) and (5). Finally Table VI gives a complete catalog of the frequencies of all the lines observed in KCl. The numbers in parentheses identify the final upper state of the transition.

DISCUSSION

For nuclear physics, the most interesting experimental result of these measurements is the ratio of the nuclear quadrupole moment of K^{41} to that of K^{39}. This value is 1.220 ± 0.0002, and is the only case in the literature for spin $\frac{3}{2}$ when the isotope heavier by two neutrons has the larger quadrupole moment. The other two cases, for which the heavier isotope has the larger quadrupole moment, $Eu^{151,153}$ and $In^{113,115}$ have spins of 5/2 and 9/2 respectively. It is suggestive that K^{39} has 20 neutrons, a magic number, while K^{41} has 22.

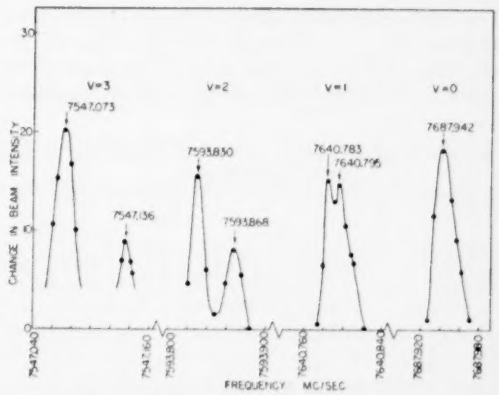

FIG. 9. Variation of hfs due to chlorine quadrupole interaction with with vibrational state. (Upper state $F_1=3/2$.)

[7] H. Levi, dissertation, Berlin, 1934 (unpublished).

[8] J. W. M. Dumond and E. R. Cohen, U. S. Atomic Energy Commission Special Technical Report No. 1, Nov. 1952 (unpublished).

TABLE II. Variation of the potassium and chlorine nuclear quadrupole interactions with vibrational state.

	$v=0$	1	2	3
$(eqQ)_K$ ($K^{39}Cl^{35}$) Mc/sec	-5.656 ± 0.006	-5.622 ± 0.006	-5.571 ± 0.008	-5.511 ± 0.008
$(eqQ)_K$ ($K^{39}Cl^{37}$) Mc/sec	-5.660 ± 0.006	-5.628 ± 0.010		
$(eqQ)_K$ ($K^{41}Cl^{35}$) Mc/sec	-6.899 ± 0.006	-6.840 ± 0.010		
$\lvert(eqQ)_{Cl}\rvert$ ($K^{39}Cl^{35}$) Mc/sec	<0.040	0.075 ± 0.010	0.237 ± 0.010	0.393 ± 0.010

TABLE III. Molecular constants of KCl.

	$K^{39}Cl^{35}$	$K^{39}Cl^{37}$	$K^{41}Cl^{35}$
Y_{01} Mc/sec	3856.370 ± 0.001	3746.583 ± 0.001	3767.394 ± 0.001
$-Y_{02}\approx D_e$ Mc/sec	0.003	0.003	0.003
$Y_{11}\approx\alpha_e$ Mc/sec	23.680 ± 0.001	22.676 ± 0.002	22.865 ± 0.001
$Y_{21}\approx\gamma_e$ Mc/sec	0.050 ± 0.001	0.047 ± 0.001	0.048 ± 0.001
B_e Mc/sec	3856.399 ± 0.007	3746.611 ± 0.007	3767.421 ± 0.007
$r_e=2.6666\pm0.0001$A			

The sign of the interaction constant eqQ for potassium is quite readily determined from the spectral pattern of the $v=0$ state. The sign of the chlorine quadrupole interaction constant may be inferred if the transitions to the states $(F_1=\frac{3}{2}, F=1, 3)$ and $(F_1=\frac{3}{2}, F=2)$ are identified by their relative intensities. The theoretical and experimental plots of these transitions are shown in Figs. 6 and 9. The transition to the state $(F_1=\frac{3}{2}, F=0)$, which should be much weaker and would have been resolved only in higher vibrational states of reduced population, was never clearly observed. Nevertheless the difference in intensities of the two observed transitions was always distinct and easily measured. Further a negative interaction agrees with the measurement of Logan, Coté, and Kusch[9] ($eqQ=-0.420$ Mc/sec for the chlorine nucleus in KCl). The magnitude is also in qualitative agreement if one remembers that in the magnetic method the chlorine quadrupole interaction constant is an average over vibrational and rotational states excited thermally in the oven source. It is interesting to note the very rapid increase of the chlorine interaction and the rather gradual decrease of the potassium interaction with increasing vibrational state.

TABLE IV. Variation of dipole moment and internuclear distance with vibrational state.

	$K^{39}Cl^{35}$	
	$v=0$	$v=2$
r_v A	2.6707 ± 0.0001	2.6872 ± 0.0001
μ_v Debye	10.48 ± 0.05	10.69 ± 0.05
	$\mu_2/\mu_0=1.020\pm0.004$	

TABLE V. Mass ratios of the potassium and chlorine isotopes.

$Cl^{35}/Cl^{37}=0.9459803\pm0.0000015$
$K^{39}/K^{41}=0.9512189\pm0.0000015$

These very precise measurements of the molecular constants given in Table III permit an evaluation of the mass ratios which is presumably better than the theory allows, because no detailed account is taken of the effects of "L" uncoupling and the fractional error due to electron distribution. It is possible for these effects to be several times the experimental error quoted here. Nevertheless, the calculated values given in Table V agree closely with the mass spectroscopic measurements of Collins, Nier, and Johnson[10] which indicates that these errors may be quite small for the alkali halides. A further development of the theory would make it possible to get mass ratios by means of these molecular beam methods to almost any desired accuracy.

It is interesting that the variation of dipole moment is approximately 1 percent per unit increase in v, while the internuclear distance increases by only 0.3 percent. Comparing this change of the dipole moment with

TABLE VI. Catalog of frequencies of all the lines observed in KCl for the rotational transition $J=0\rightarrow J=1$ in Mc/sec.

Vibrational state	$K^{39}Cl^{35}$	$K^{39}Cl^{37}$	$K^{41}Cl^{35}$	Final state
$v=0$	7690.487	7471.917	7513.659	$(F_1=1/2, F=1, 2)$
	7689.356	7470.776	7512.280	$(F_1=5/2, F=1, 2, 3, 4)$
	7687.942	7469.370	7510.555	$(F_1=3/2, F=0, 1, 2, 3)$
$v=1$	7643.316	7426.754	7468.107	$(F_1=1/2, F=1, 2)$
	7642.200			$(F_1=5/2, F=1, 2, 3, 4)$
	7640.783			$(F_1=3/2, F=1, 2, 3)$
	7640.795			
$v=2$	7596.347			$(F_1=1/2, F=1, 2)$
	7593.868			$(F_1=3/2, F=1, 2, 3)$
	7593.830			
$v=3$	7549.569			$(F_1=1/2, F=1, 2)$
	7547.136			$(F_1=3/2, F=1, 2, 3)$
	7547.073			

[9] Logan, Coté, and Kusch, Phys. Rev. **86**, 280 (1952).

[10] Collins, Nier, and Johnson, Phys. Rev. **84**, 717 (1951).

vibrational quantum number and the corresponding changes of the two quadrupole interaction constants, one must conclude that a simple explanation of these variations in terms of potassium and chlorine moving apart as atoms or ions does not seem likely. In addition, it should be noticed that our value of α_e of 23.680 Mc/sec differs greatly from the Morse potential value of 17.5 Mc/sec.

The comparison of our result for the internuclear distance r_e with the electron diffraction value of Maxwell, Hendricks, and Mosley[11] at 1200°K can be made using the measured variation of r with temperature. When r_e is evaluated from the electron diffraction data we find a value of 2.75A, which is approximately 3 percent larger than our directly measured value of 2.667A. It seems that electron diffraction measurements are consistently high by about the same amount for KBr, CsCl, and NaCl.

In view of the data made available by the techniques described in this paper, it would be desirable to reduce the amount of time required to search and take data. The problem of searching might be solved by automatic frequency sweeping and recording of the beam intensity.

[11] Maxwell, Hendricks, and Mosley, Phys. Rev. **52**, 968 (1937).

PHYSICAL REVIEW VOLUME 91, NUMBER 6 SEPTEMBER 15, 1953

Molecular Beam Investigation of Rotational Transitions. II. The Rotational Levels of KBr and Their Hyperfine Structure*

B. P. Fabricand,† R. O. Carlson,‡ C. A. Lee, and I. I. Rabi
Columbia University, New York, New York

(Received May 27, 1953)

The molecular beam electrical resonance method has been used to study the hyperfine structure of the first rotational state in $K^{39}Br^{79}$ and $K^{39}Br^{81}$.

The hyperfine structure arises from the splitting of the $J=1$ state into 10 levels by the quadrupole interactions of potassium and bromine. Molecules in the $J=0$ rotational state were refocused, and transitions to the $J=1$ state were observed by a decrease in beam intensity at the surface ionization detector.

From the structure of the line resulting from the transition $J=0\rightarrow J=1$ in the three lowest vibrational states, the following results were obtained. The molecular constants are

	KBr^{79}	KBr^{81}
Y_{01} Mc/sec	2434.947 ±0.001	2415.075±0.001
$-Y_{02}$ Mc/sec	0.001	0.001
$-Y_{11}$ Mc/sec	12.136 ±0.001	11.987±0.001
Y_{21} Mc/sec	0.023 ±0.001	0.022±0.001
B_e Mc/sec	2434.953 ±0.007	2415.081±0.007
r_e A	2.8207±0.0001	

The quadrupole interactions and dipole moments in $K^{39}Br^{79}$ in the $v=0$, 1, 2 vibrational states are

	$v=0$	1	2
$(eqQ)_K$ Mc/sec	−5.003±0.003	−4.984±0.003	−4.915±0.003
$(eqQ)_{Br}$ Mc/sec	+10.244±0.006	+11.224±0.006	+12.204±0.006
μ Debye	10.41 ±0.05		9.93 ±0.05

The quadrupole interactions in the $v=0$ state of $K^{39}Br^{81}$ are $(eqQ)_K=-5.002\pm0.003$ and $(eqQ)_{Br}=8.555\pm0.006$ Mc/sec.

The mass ratio of the bromine isotopes is $M_{Br^{79}}/M_{Br^{81}}=0.9753088\pm0.0000020$. The ratio of the bromine quadrupole moments is $Q_{Br^{79}}/Q_{Br^{81}}=1.1973\pm0.0006$.

I. INTRODUCTION

THE experiments to be described in this paper deal with measurements of the rotational spectra of $K^{39}Br^{79}$ and $K^{39}Br^{81}$ and form part of a program for a more precise study of the alkali halides by means of the molecular beam electrical resonance method.[1,2] The molecules were studied in the $^1\Sigma$ electronic state and the three lowest vibrational states. All observed resonance lines arise from the rotational transition $J=0\rightarrow J=1$. Each line corresponds to one of the energy levels arising from the hyperfine structure splitting of the first rotational state. The spectrum of these lines is characteristic of a diatomic molecule with two nuclear

* This research has been supported in part by the U. S. Office of Naval Research.

† Submitted in partial fulfillment of the requirements for the degree of Doctor of Philosophy in the Faculty of Pure Science, Columbia University.

‡ Predoctoral Fellow of U. S. Atomic Energy Commission.

[1] H. K. Hughes, Phys. Rev. **72**, 614 (1947).

[2] Lee, Fabricand, Carlson, and Rabi (preceding paper), Phys. Rev. **91**, 1395 (1953). For brevity, this paper will henceforth be referred to as I.

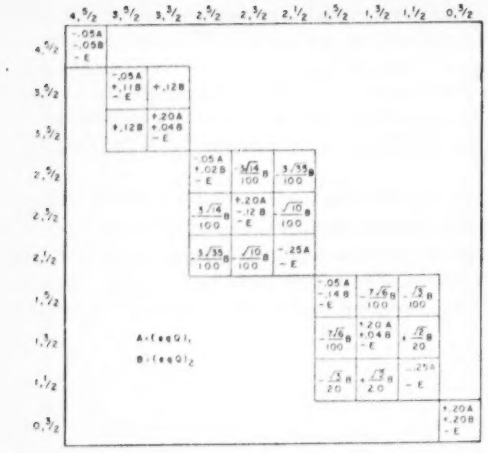

FIG. 1. Matrix of the quadrupole interaction operators in KBr.

electric quadrupole interactions each associated with a nucleus of spin 3/2. In this molecule, as contrasted with KCl, the quadrupole interactions of potassium and of bromine are of comparable magnitudes.

From the experimental data were obtained the molecular constants of the molecules, the electric dipole moment, the quadrupole interactions, the ratios of the quadrupole moments and masses of the bromine isotopes. Of great interest are the variations with vibrational state of the electric dipole moment and the bromine quadrupole interaction in light of the extraordinary variations of these quantities in KCl given in reference I.

The apparatus and the general experimental procedure are described in I. For the molecules used in this experiment, a beam is obtained from a hot oven source at a temperature of approximately 900°K. At this temperature, a large number of rotational states are excited. The molecules in the $J=0$ state, about one part in 8000, are selected for refocusing. Transitions to the $J=1$ state are observed by a decrease in beam intensity at the surface ionization detector. A 2K43 klystron supplied the necessary microwave power for exciting these transitions (around 4800 Mc/sec). The details of frequency measurements, frequency stabilization, and the procedure used in locating and resolving the spectra are given in I.

Since only a small fraction of the molecules are in the $J=0$ state and the number of hyperfine structure and vibrational levels in the $J=1$ state is large, the intensity change for any one transition is small. To obtain the necessary signal-to-noise ratio, very intense molecular beams had to be employed. With a galvanometer sensitivity of 10^{-15} amp/cm, the direct beam was about 10^7 centimeters of which 2000 centimeters were refocused. For the lines arising from the

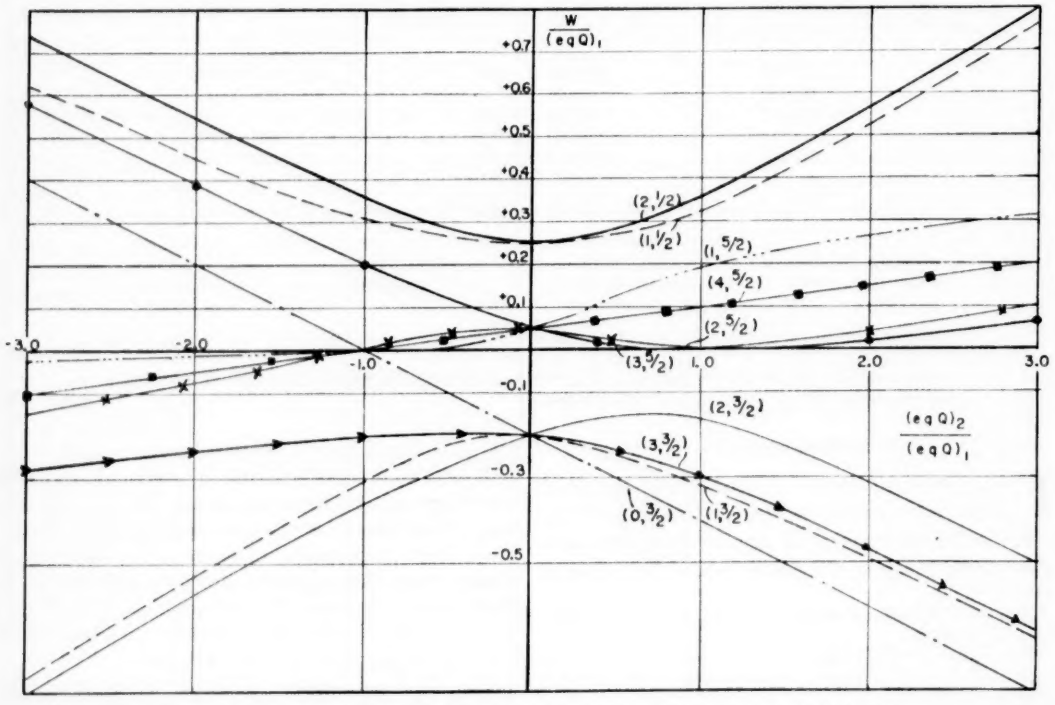

FIG. 2. Plot of the energy levels in the $J=1$ state in units of $(eqQ)_1$ against the ratio $(eqQ)_2/(eqQ)_1$.

zeroth vibrational state, the intensity was approximately 0.7 percent of the refocused beam and 0.2 percent for the second vibrational state. In all cases, the line intensity relative to the refocused beam was half the expected value as calculated from the line intensities observed in KCl.

II. THEORY

In this paper, the energy levels which arise from the splitting of the first rotational state by two nuclear electric quadrupole interactions will be calculated exactly.

The part of the Hamiltonian dealing with the hyperfine structure is

$$-eq_1Q_1\frac{[3(\mathbf{I}_1\cdot\mathbf{J})^2+\frac{3}{2}\mathbf{I}_1\cdot\mathbf{J}-\mathbf{I}_1^2\mathbf{J}^2]}{2I_1(2I_1-1)(2J-1)(2J+3)}$$
$$-eq_2Q_2\frac{[3(\mathbf{I}_2\cdot\mathbf{J})^2+\frac{3}{2}\mathbf{I}_2\cdot\mathbf{J}-\mathbf{I}_2^2\mathbf{J}^2]}{2I_2(2I_2-1)(2J-1)(2J+3)}.$$

The subscripts 1 and 2 refer to the two nuclei. q is the gradient of the electric field at the nucleus along the internuclear axis produced by all charges outside the nucleus, and Q is the nuclear quadrupole moment. In KBr, both nuclei have spins of 3/2. The matrix of the quadrupole operators in the $I_1JF_1I_2FM$ representation is shown in Fig. 1. In this representation, the spin of nucleus 1 is coupled to J through the quadrupole interaction, giving three energy states characterized by $F_1=I_1+J=1/2$, 3/2, and 5/2. The quadrupole interaction of nucleus 2 splits these F_1 states into 10 states labeled by $(F=I_2+F_1, F_1)=(2, 1/2)$, (1, 1/2), (3, 3/2), (2, 3/2), (1, 3/2), (0, 3/2), (4, 5/2), (3, 5/2), (2, 5/2), (1, 5/2). The quadrupole operator of nucleus 1 is diagonal in this representation, but off-diagonal elements occur for the quadrupole operator of nucleus 2. The matrix elements were taken from Bardeen and Townes.[3]

TABLE I. Frequencies of all observed lines in Mc/sec. The numbers in parentheses represent the hyperfine structure levels (F, F_1) of the $J=1$ state to which the transitions take place.

Vibrational state	$K^{39}Br^{79}$		$K^{39}Br^{81}$	
0	4860.523	(2, 1/2)	4820.613	(2, 1/2)
			4820.130	(1, 1/2)
	4859.740	(3, 5/2)	4819.815	(3, 5/2)
			4818.143	(1, 5/2)
	4857.502	(4, 5/2)	4817.992	(4, 5/2)
	4857.383	(2, 5/2)	4817.909	(2, 5/2)
	4856.588	(3, 3/2)	4817.056	(3, 3/2)
			4815.884	(1, 3/2)
	4854.856	(2, 3/2)	4815.635	(2, 3/2)
1	4836.530	(2, 1/2)	4794.062	(2, 1/2)
	4835.743	(3, 5/2)	4793.140	(3, 5/2)
	4833.270	(4, 5/2)		
	4833.143	(2, 5/2)		
	4832.362	(3, 3/2)		
	4830.463	(2, 3/2)		
2	4812.622	(2, 1/2)		
	4811.835	(3, 5/2)		
	4809.129	(4, 5/2)		
	4808.990	(2, 5/2)		
	4808.247	(3, 3/2)		
	4806.153	(2, 3/2)		

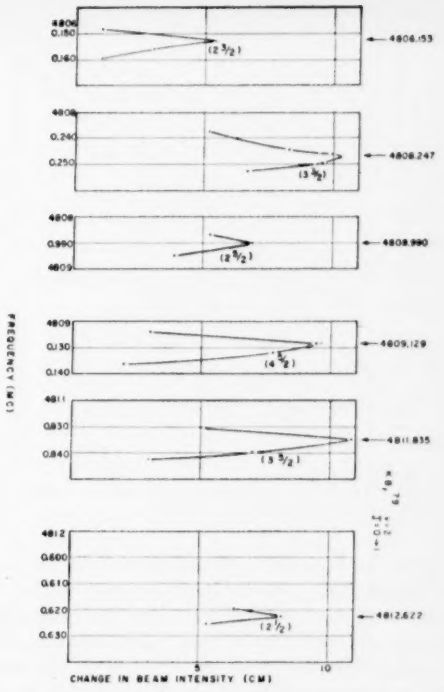

FIG. 3. Spectrum of the rotational transition $J=0\rightarrow J=1$ in the vibrational state $v=2$ in KBr^{79}.

Diagonalization of the matrix yields the 10 energy levels of the first rotational state in terms of the quadrupole interactions of the two nuclei. Figure 2 is a plot of the energy of the levels in units of the quadrupole interaction of nucleus 1 against the ratio $(eqQ)_2/(eqQ)_1$. The right side of Fig. 2 gives the energy levels for a positive ratio, and the left side for a negative ratio.

III. EXPERIMENTAL DATA

The spectrum of KBr differs from that of KCl described in I in that the lines are much further apart in frequency and are, therefore, well resolved. The separations of the lines are of the order of one or two Mc/sec. Because KBr is heavier, the molecules of KBr spend more time in the radiation field, and the theoretical half-width of the lines are less than in KCl. Actual half-widths were about 15 kc/sec, the theoretical about 10 kc/sec.

In the zeroth vibrational state, nine of the ten lines resulting from the rotational transition $J=0\rightarrow J=1$ were observed. Figure 3, which is typical of the spectra

[3] J. Bardeen and C. H. Townes, Phys. Rev. **73**, 97 (1948).

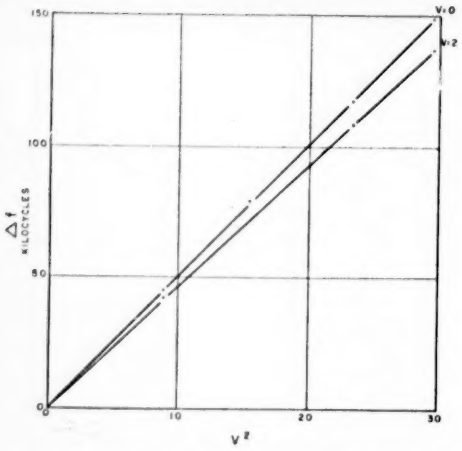

FIG. 4. Frequency shift of the transition $(J=0)\rightarrow(J=1, F_1=1/2, F=2)$ with the square of the applied voltage in the vibrational states $v=0$ and $v=2$ in KBr^{79}.

observed for both $K^{39}Br^{79}$ and $K^{39}Br^{81}$ in the several vibrational states, shows six of the lines in the vibrational state, $v=2$, of $K^{39}Br^{79}$. The line spacings are markedly different for different vibrational states, because of the variation of the quadrupole interactions with internuclear distance. In Table I are listed the frequencies of all observed lines.

The electric dipole moment was obtained by observing the shift in frequency of one of the transitions, $(J=0)\rightarrow(J=1, F_1=1/2, F=2)$, in very small electrostatic fields, of the order of one or two volts per centimeter. For these small fields, the $J=1$ state is unshifted in energy, and the increase in frequency of this transition is due to the energy decrease of the more easily polarized $J=0$ state. This energy decrease is given by $\frac{1}{6}\mu^2E^2/(h^2/2A)$, where μ is the dipole moment and A the moment of inertia. Figure 4 shows a plot of frequency shift *versus* the square of the applied voltage for the zeroth and second vibrational states in $K^{39}Br^{79}$. The slope of the lines is proportional to the product μ^2A. Since A is known from the zero field data, μ is easily calculated.

In addition to the sharp line spectra described above, there appeared in certain frequency regions resonance bands which were approximately ten to twenty Mc/sec wide. These bands appeared in the regions centered, approximately, about the following frequencies: 5230 Mc/sec, 5170 Mc/sec, 4980 Mc/sec, 4780 Mc/sec. The frequency region searched extended from 4400 to 5300 Mc/sec, so that there is the possibility of the occurrence of other bands in other regions. The intensity of the bands depended markedly on the microwave power input. At powers comparable to those used in resolving the sharp line spectra, the band intensity was about 1/5 the line intensity. The origin of these bands is not known. In view of the low intensity of the diatomic lines, it is possible that these bands arise from other forms of molecular aggregates of potassium and bromine, such as polymers of the KBr molecule.[4]

TABLE II. Potassium and bromine quadrupole interaction constants in KBr.

Quantity	$K^{39}Br^{79}$	$K^{39}Br^{81}$
$(eqQ)_K$ $(v=0)$ Mc/sec	-5.003 ± 0.003	-5.002 ± 0.003
$(v=1)$	-4.984 ± 0.003	
$(v=2)$	-4.915 ± 0.003	
$(eqQ)_{Br}$ $(v=0)$ Mc/sec	$+10.244\pm0.006$	$+8.555\pm0.006$
$(v=1)$	$+11.224\pm0.006$	
$(v=2)$	$+12.204\pm0.006$	

IV. RESULTS

By comparing the splitting of the observed lines in each vibrational state with the theoretical energy level pattern shown in Fig. 2, the potassium and bromine quadrupole interactions in each vibrational state were calculated. These values are listed in Table II. The observed line spacings do not correspond to the theoretical pattern for any other values of the quadrupole interactions, so that these values are unique. The uncertainties given for each quantity arise from a 2-kc/sec uncertainty in the determination of the peak of each line. The accuracy of these interactions is greater than for the corresponding quantities in KCl because (1) the splitting of the lines is greater in KBr, and (2) there are more resolved lines.

To calculate the molecular constants one must know the frequencies of the lines arising from the pure rotational transitions $J=0\rightarrow J=1$ for the different vibrational states, apart from the influence of the quadrupole interactions. Since the quadrupole interactions are known from the spectrum, the frequencies of the unperturbed lines are readily calculated from the theory. The constants are listed in Table III. The relationships of the Y's, the Dunham coefficients, to the spectra are discussed in I. All the Y's listed were obtained from the spectra except Y_{02}, which was calculated from the relationship $-Y_{02}=4B_e^3/\omega_e^2$. Table IV gives the internuclear distances and electric dipole moments in the zeroth and second vibrational states.

The mass ratio of the bromine isotopes was calculated from the formula:

$$\frac{M_1}{M_2}=\frac{(M/M_2)(Y_{01}^{81}/Y_{01}^{79})}{1+M/M_2-Y_{01}^{81}/Y_{01}^{79}},$$

where M_1 is the mass of Br^{79}, M_2 the mass of Br^{81}, and M the mass of K^{39}. The result is

$$M_{Br^{79}}/M_{Br^{81}}=0.9753088\pm0.0000020.$$

The ratio of the nuclear quadrupole moments of the bromine isotopes was calculated from the ratio of the

[4] Ochs, Coté, and Kusch, J. Chem. Phys. **21**, 459 (1953).

bromine quadrupole interactions in the zeroth vibrational state in KBr^{79} and KBr^{81}. The result is

$$Q_{Br^{79}}/Q_{Br^{81}}=1.1973\pm0.0006.$$

V. DISCUSSION

A proof that the potassium quadrupole interaction, $(eqQ)_K$, is negative and the bromine interaction, $(eqQ)_{Br}$, is positive follows. The ratio of the quadrupole interactions, $(eqQ)_2/(eqQ)_1$, is negative, since the observed line pattern does not fit the theoretical pattern for positive values. This can be seen from the energy level diagram (Fig. 2), which has been plotted by assigning a negative value to the denominator of the ratio, $(eqQ)_1$. From the experimental data, the values of the ratios of the quadrupole interactions in KBr^{79} and KBr^{81} are -2.048 and -1.170, respectively. These values of the ratios were assigned once the values of the rotational constants for both isotopic species were calculated, since the rotational constant, being inversely proportional to the reduced mass of the molecule, is larger for KBr^{79}. Now,

$$\frac{(eqQ)_{Br^{79}}/(eqQ)_K}{(eqQ)_{Br^{81}}/(eqQ)_K}=\frac{Q^{79}}{Q^{81}}=1.2 \text{ if } (eqQ)_{Br} \text{ is } (eqQ)_2,$$

$$\frac{(eqQ)_K/(eqQ)_{Br^{81}}}{(eqQ)_K/(eqQ)_{Br^{79}}}=\frac{Q^{79}}{Q^{81}}=0.85 \text{ if } (eqQ)_{Br} \text{ is } (eqQ)_1.$$

Here the assumption is apparently made that $(eqQ)_K$ is the same in both molecular species. However, since the ratio of the quadrupole interactions for the bromine isotopes is known to be 1.2, and the spacings of the spectra for the two isotopes fit Fig. 2 with the same scale factor, $(eqQ)_1$, one of the interactions must be constant in both molecular species. The common interaction, $(eqQ)_1$, must therefore be $(eqQ)_K$, and the sign of its interaction negative. The ratio 1.2 for the quadrupole moments of the bromine isotopes is then in agreement with the observations of Townes,[5] Dehmelt and Kruger,[6] and King and Jaccarino.[7]

The signs of the K^{39} quadrupole interactions in KF,[8] KCl, and KBr are also all negative. The absolute magnitudes decrease from 7.938 Mc/sec in KF to 5.656 Mc/sec in KCl to 5.003 Mc/sec in KBr. Similar behavior has been observed for the Na^{23} quadrupole interaction constants in the sodium halides by Logan, Coté, and Kusch.[9]

The change with vibrational state of $(eqQ)_{K^{39}}$ in KBr and KCl does not remain constant, but becomes larger for higher vibrational states. In $K^{39}Cl^{35}$, the change in this interaction increased from 0.8 percent for $v=0\rightarrow v=1$ to 1.1 percent for $v=2\rightarrow v=3$. In KBr^{79}, the decrease in $(eqQ)_K$ for $v=0\rightarrow v=1$ is about 1/3 that for $v=1\rightarrow v=2$. This shift corresponds to percentage decreases of 0.4 percent and 1.4 percent, respectively. In $K^{39}F$, $(eqQ)_K$ decreases by about 1.3 percent for unit change in the vibrational quantum number. The potassium interaction decreases with vibrational state in the potassium halides thus far studied.

In both KCl and KBr the quadrupole interaction constants for the halogen show large changes with vibrational state. The change in the bromine interaction is to larger values and appears to be a constant amount of about one Mc/sec, 10 percent of the interaction, for the lowest vibrational states. This change is in contrast to the erratic changes with vibrational state exhibited by the chlorine interaction in KCl.

The value obtained for the ratio of the quadrupole moments of the bromine isotopes has been corrected to take into account the fact that the gradient of the electric field at the bromine nucleus, which enters into the experimentally measured quadrupole coupling, is not the same for two isotopes in the same molecule because of different zero point vibration for the two isotopic species. This effect amounts to about one part in 6000 in the quadrupole moment ratio.

In calculating the mass ratio of the bromine isotopes from the mass ratio formula, the Y_{01}'s were obtained from the spectra. The mass of Br^{81} used was that given by Ogata,[10] and the mass of K^{39} that given by Collins, Nier, and Johnson.[11] The ratio of the Y_{01}'s was corrected by small terms of the order of B_e^2/ω_e^2 given by Dunham,[12] since Y_{01} is not exactly inversely proportional to the reduced mass of the molecule.

The theory on which the mass ratio formula is based assumes a vibrating rotator model diatomic molecule. Any deviations from this model would result in inaccuracies in the mass ratio. Such deviations can arise

TABLE III. The molecular constants of KBr.

Quantity	$K^{39}Br^{79}$	$K^{39}Br^{81}$
Y_{01} Mc/sec	2434.947 ±0.001	2415.075±0.001
$-Y_{02}$	0.001	0.001
$-Y_{11}$	12.136 ±0.001	11.987±0.001
Y_{21}	0.023 ±0.001	0.022±0.001
B_e	2434.953 ±0.007	2415.081±0.007
r_e A	2.8207±0.0001	

TABLE IV. Internuclear distances and electric dipole moments in the vibrational states $v=0$ and $v=2$ in $K^{39}Br^{79}$.

Quantity	$v=0$	$v=2$
r A	2.8243±0.0001	2.8384±0.0001
μ Debye	10.41±0.05	9.93±0.05
	$\mu_0/\mu_2=1.048\pm0.004$	

[5] C. H. Townes, Phys. Rev. **71**, 909 (1947).
[6] Dehmelt and Kruger, Z. Physik **129**, 401 (1951).
[7] J. G. King and V. Jaccarino (private communication).
[8] L. Grabner and V. Hughes, Phys. Rev. **79**, 819 (1950).
[9] Logan, Coté, and Kusch, Phys. Rev. **86**, 280 (1952).
[10] K. Ogata, Phys. Rev. **75**, 200 (1949).
[11] Collins, Nier, and Johnson, Phys. Rev. **84**, 717 (1951).
[12] J. L. Dunham, Phys. Rev. **41**, 721 (1932).

from the following causes: (1) interaction between electronic and nuclear motions which leads to a mixing of the ground electronic state with the excited II state, and hence a slight change in the rotational energy; (2) the moment of inertia of the electrons which is calculated in the above model on the assumptions that each atom has the proper number of electrons to make it neutral and that the entire mass of the atom is concentrated at the nucleus. These effects cannot be precisely evaluated because the electronic wave functions are not known. The error quoted in the mass ratio is experimental error.

The values of the internuclear distances in KCl and KBr are about 3 percent lower than the values given by electron diffraction methods after correction for the vibrational state distribution has been made. Similar discrepancies have been observed in CsCl by Luce and Trischka,[13] and in NaCl by Stitch, Honig, and Townes.[14]

As can be seen from Table IV, the electric dipole moment of KBr decreases with increasing vibrational quantum number. The percentage decrease in the dipole moment is about 5 percent for the change from the zeroth to the second vibrational state. The percentage increase in the internuclear distance for this change in vibrational state is about 0.5 percent. Hence, a small increase in the internuclear distance causes a large decrease in the dipole moment.

The experimental value of the vibration-rotation interaction constant, $\alpha_e = -Y_{11}$, is 12.136 Mc/sec. The theoretical value, computed on the assumption of a Morse potential for KBr, is 10.0 Mc/sec.

[13] R. G. Luce and J. W. Trischka, Phys. Rev. **83**, 851 (1951).
[14] Stitch, Honig, and Townes, Phys. Rev. **86**, 813 (1952).

PHYSICAL REVIEW VOLUME 91, NUMBER 6 SEPTEMBER 15, 1953

A Self-Consistent Calculation of the Dissociation of Oxygen in the Upper Atmosphere. II. Three-Body Recombinations*

HARRY E. MOSES, *Mathematics Research Group, New York University, New York, New York*

AND

TA-YOU WU, *National Research Council, Ottawa, Canada*

(Received June 2, 1953)

The dissociation region of oxygen molecules is treated in the same "self-consistent" manner described in previous papers, except that now the densities of atomic and molecular oxygen have been calculated as functions of the altitude, on the assumption that the main recombination process between oxygen atoms is a three-body nonradiative process. The result of the present work indicates that dissociation occurs at an altitute about 5 km higher than the corresponding previous calculation. Furthermore, the region of dissociation is broader than in the previous model. The maximum atomic density is 0.5 to 1×10^{13}/cm^3.

I. INTRODUCTION

IN two previous papers[1,2] the densities of atomic and molecular oxygen in the upper atmosphere were calculated in terms of two different models. Both of these models were carried out in a "self-consistent" manner, that is, no *a priori* assumptions were made as to the distribution of molecular or atomic oxygen. (Such assumptions have been made by previous authors in the field.[1,2])

In the first model it was possible to calculate the distribution of temperature as well as the distribution of the atomic and the molecular oxygen densities. In the second model, a temperature distribution was assumed in order to avoid the necessity of imposing a severe assumption, used in the first model, with respect to energy balance.

In both of these models the principal recombination process was assumed to be a two-body radiation process. The present paper is to be regarded as a direct extension of reference 2; the assumption of two-body recombinations is replaced by the assumption that the oxygen atoms recombine in a three-body process. Therefore, instead of repeating the various details of the model of reference 2 and of the method of solution of the equations for the densities, we shall merely indicate the modifications.

II. THE THREE-BODY RECOMBINATION PROCESS

The principal modification of reference 2 which we introduce in the present work is to replace the two-body recombination process (11) there by the three-body recombination process (10). The rate of recombination of the oxygen atoms is taken to be $Cn_M n_P^2$ where C is the three-body recombination coefficient

* This work was performed at Washington Square College of Arts and Science, New York University, and was supported in part by contract with the U. S. Air Force through sponsorship of the Geophysics Research Directorate of the Air Force Cambridge Research Center, Air Research and Development Command.
[1] H. E. Moses and T. Y. Wu, Phys. Rev. **83**, 109 (1951).
[2] H. E. Moses and T. Y. Wu, Phys. Rev. **87**, 628 (1952).

and n_M is the number density of the third body M. Various additional assumptions are now necessary, since the recombination coefficient C and the number density n_M are not known. First of all we shall assume that all atoms or molecules are equally efficient as third bodies. Once one makes this assumption it is clear that it is sufficient to take n_M as the number density of nitrogen molecules, since nitrogen predominates so greatly in the region of interest. We further assume that it obeys its own barometric equation of the usual exponential type when the temperature is taken as constant. We have prescribed that just below the altitude at which dissociation becomes important, the number density of nitrogen molecules will be four times that of oxygen, that is, the oxygen—nitrogen ratio is the same as at sea level.

For C we have taken two values, namely $C=10^{-32}$ and $C=2\times10^{-33}$ cm^6/sec. These are typical values given by chemists for three-body processes and used by previous workers on the present problem.[3]

The formulas and method of procedure are substantially the same as those of reference 2. We need merely replace the two-body recombination coefficient B' by

$$B'=Cn_M,$$

where n_M is a function of the altitude and is given by the barometric equation as described above. (Incidentally there is a misprint in reference 2. The letter B in Eqs. (15) through (17) should be replaced by B'.)

III. RESULTS

The results of the calculation are summarized in Fig. 1. The temperature was taken as 300°K. The altitude x_0 was chosen to correspond to the value $n_2=2\times10^{13}$/cm.[3] Only above this altitude does dissociation become important. If we use the pressure-*vs*-altitude results of the Rocket Panel[4] we find that x_0 is about 90 km. The curves of n_2 and n_p are given in Fig. 1. We have also superposed the curve of n_2 as it would be if no dissociation took place—the values are obtained from the ordinary barometric equation.

It is seen that in the present model dissociation occurs at higher altitudes (about 5 km higher) than in the model of two-body recombination. This result is a consequence of the use in the present work of a greater

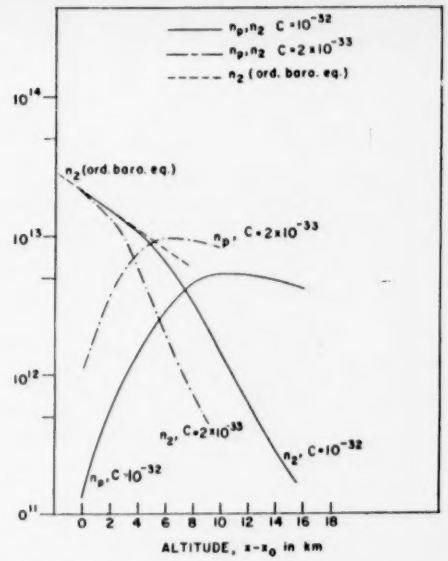

FIG. 1. The number densities of atomic and molecular oxygen as functions of the altitude.

value for the effective two-body recombination coefficient Cn_M. Hence in the present model the oxygen atoms can recombine more readily than in the model of reference 2, and only at higher altitudes are dissociations numerous enough to insure number balance. Another striking difference between the present results and those of reference 2 is the broadness of the region in which dissociation takes place—about 25 km, as opposed to less than 15 km of reference 2.

These differences between the results of the present paper and those of reference 2 (and reference 1) indicate the high degree of sensitivity of the results to the model used. We must conclude that the problem of obtaining really useful numerical results for the dissociation of oxygen in the upper atmosphere cannot be solved until much more reliable data on the various cross sections and information concerning the recombination process are available; then it will be clear which model should be used. This result, though not surprising, indicates that any numerical results which are available at present concerning oxygen dissociation in the upper atmosphere must be accepted only with great reserve.

[3] R. Penndorf, J. Geophys. Research **54**, 7 (1949).
[4] The Rocket Panel, Phys. Rev. **88**, 1027 (1952).

Effective Nuclear Charges for Atoms from Self-Consistent Field Calculations*

A. J. FREEMAN
Physics Department, Massachusetts Institute of Technology, Cambridge, Massachusetts
(Received May 6, 1953)

Results of calculations of $2Z_p$, the effective nuclear charge for the potential in an atom are reported for those atoms treated by self-consistent field methods. Tables of the effective nuclear charges are given for atoms in various degrees of ionization.

FOR many purposes, such as in some molecular calculations, it is necessary to have available tabulated values of $2Z_p(r)$, the effective nuclear charges for the potential in an atom. These are functions found from self-consistent field calculations of the one-electron wave functions, which have not usually been included in the literature. The purpose of this paper is to report calculations of the $2Z_p(r)$ function for those atoms for which the one-electron wave functions are available.[1]

If the wave function for a many-electron atom is expressed as a product of one-electron wave functions, each of these has the form $\Phi(\phi)\Theta(\theta)P_{nl}(r)/r$. The solutions for Φ and Θ are well known. $P_{nl}(r)$ satisfies the differential equation,

$$d^2P_{nl}/dr^2+\{E_{nl}+2Z_{pnl}/r-l(l+1)/r^2\}P_{nl}=0, \quad (1)$$

where E_{nl} is the energy of the nl electron in Rydberg units, and r is the radius expressed in Bohr units. $P_{nl}(r)$ is the radial wave function of the nl type electron, defined so that

$$\int_0^r P_{nl}^2(r)dr, \quad (2)$$

is the charge within a sphere of radius r due to this electron. $2Z_{pnl}$, the effective nuclear charge for the potential of an electron with quantum numbers n and l is given by

$$2Z_{pnl}=2Z-2\sum_{nl}{}'\,2(2l+1)\times\left\{\int_0^r P_{nl}^2dr'+r\int_r^\infty \frac{P_{nl}^2}{r'}dr'\right\}, \quad (3)$$

with Z the atomic number. The prime indicates summation over all nl values other than those of the electron considered, and is necessarily included so as to take into account the fact that an electron does not act electrostatically on itself. The total effective charge $2Z_p(r)$ used in finding the potential due to all electrons is defined by Eq. (3), with the summation extending over the quantum numbers n and l of all the electrons in the atom. $2Z_p(r)$ is conveniently calculated from the total radial wave function $P(r)$ through the use of the Milne predictor-corrector method[2] of numerical integration applied to the differential equation:

$$d^2Z_p(r)/dr^2=P^2(r)/r, \quad (4)$$

where

$$P^2(r)=\sum_{nl}2(2l+1)P_{nl}^2(r). \quad (5)$$

It is the $P_{nl}(r)$'s, the one-electron wave functions, which are usually tabulated in the literature as a result of self-consistent field calculations. Following the procedure outlined here, we have calculated the $2Z_p(r)$ functions. The results are given in Table I for the atoms in various degrees of ionization. The maximum error is given by the difference between twice the value of the atomic number and the value of $2Z_p$ at $r=0.00$. The maximum error is 0.01 for B, O^+, O^{++}, Al^{++}, Ga, Ga^{+++}, and As^{++}; 0.02 for C^{++++}, N, O, O^{+++}, Na^+, K, Cr, As^+, and As^{+++}; 0.03 for C^{++}, Cr^{++}, and As; 0.04 for Si^{+++}, Si^{++++}, Zn, Ge, and Ga^+; 0.05 for Ca^+; and 0.08 for Ge^{++}.

For completeness, we list in Table II the atoms for which $2Z_p$ has been calculated and the results published in the literature.[1]

The author wishes to thank Professor John C. Slater for suggesting the problem and for his help and advice during the course of the calculations.

* Supported by the U. S. Office of Naval Research.

[1] H. H. Landolt and R. Börnstein, *Zahlenwerte und Funktionen aus Physik, Chemie, Astronomie* (J. Springer, Berlin, 1950), sixth edition, Vol. I, page 276 gives a complete tabulation of published work on self-consistent calculations.

[2] W. E. Milne, *Numerical Calculus* (Princeton University Press, Princeton, 1949), p. 140 (without predictor).

TABLE I. Values of the $2Z_p$'s. (The values of $2Z_p$ are rounded off to two decimal places. Where a third decimal is specified to be $\geqslant 5$, the second decimal should be decreased by one. For example, 0.01_8 should be read 0.008.)

r	B[a]
0.00	10.00
0.01	9.78
0.02	9.55
0.03	9.33
0.04	9.12
0.06	8.70
0.08	8.31
0.10	7.94
0.12	7.60
0.14	7.29
0.16	7.00
0.18	6.74
0.20	6.50
0.22	6.27
0.24	6.07
0.26	5.88
0.28	5.71
0.30	5.56
0.35	5.21
0.40	4.92
0.45	4.66
0.50	4.44
0.55	4.23
0.60	4.04
0.65	3.87
0.70	3.69
0.8	3.37
0.9	3.06
1.0	2.78
1.1	2.51
1.2	2.26
1.3	2.03
1.4	1.81
1.5	1.62
1.6	1.44
1.7	1.28
1.8	1.14
1.9	1.01
2.0	0.90
2.2	0.70
2.4	0.55
2.6	0.43
2.8	0.34
3.0	0.26
3.2	0.20
3.4	0.16
3.6	0.13
3.8	0.10
4.0	0.08
4.5	0.04
5.0	0.02
5.5	0.01_4
6.0	0.01_3
6.5	0.00_4
7.0	0.00_2
7.5	0.00_1
8.0	0.00

r	C[b]	C^{++}[b]	C^{++++}[b]
0.00	12.00	12.00	12.00
0.02	11.42	11.47	11.55
0.04	10.85	10.95	11.12
0.06	10.32	10.47	10.71
0.08	9.83	10.03	10.35
0.10	9.37	9.63	10.02
0.12	8.96	9.27	9.73
0.14	8.58	8.94	9.47
0.16	8.23	8.65	9.25
0.18	7.92	8.39	9.06
0.20	7.63	8.16	8.90
0.25	7.02	7.68	8.59
0.30	6.51	7.31	8.38
0.35	6.08	7.01	8.25
0.40	5.70	6.76	8.16
0.45	5.35	6.55	8.10
0.50	5.03	6.35	8.07
0.55	4.73	6.17	8.05
0.60	4.44	6.00	8.03_3
0.65	4.16	5.84	8.02
0.70	3.90	5.69	8.02_8
0.75	3.65	5.54	8.02_6
0.80	3.41	5.41	8.01_4
0.9	2.96	5.16	8.01_6
1.0	2.56	4.95	8.00
1.1	2.20	4.76	
1.2	1.88	4.61	
1.3	1.61	4.48	
1.4	1.37	4.38	
1.5	1.16	4.29	
1.6	0.98	4.23	
1.7	0.83	4.17	
1.8	0.70	4.13	
1.9	0.59	4.10	
2.0	0.50	4.07	
2.1	0.42	4.05	
2.2	0.35	4.04	
2.3	0.30	4.02	
2.4	0.25	4.02_6	
2.6	0.18	4.00_4	
2.8	0.12	4.00	
3.0	0.08		
3.2	0.06		
3.4	0.04		
3.6	0.03		
3.8	0.02		
4.0	0.01_4		
4.5	0.01_6		
5.0	0.00_2		
5.5	0.00_1		
6.0	0.00		

r	N[a]
0.00	14.00
0.01	13.63
0.02	13.27
0.03	12.92
0.04	12.58
0.06	11.93
0.08	11.33
0.10	10.78
0.12	10.29
0.14	9.85
0.16	9.45
0.18	9.08
0.20	8.75
0.25	8.03
0.30	7.42
0.35	6.88
0.40	6.39

[a] Brown, Bartlett, and Dunn, Phys. Rev. **44**, 296 (1933) (without exchange).
[b] A. Jucys, Proc. Roy. Soc. (London) **A173**, 59 (1939) (with exchange).

TABLE I.—*Continued.*

r	N^{a}
0.45	5.94
0.50	5.51
0.6	4.72
0.7	4.00
0.8	3.38
0.9	2.83
1.0	2.35
1.1	1.95
1.2	1.61
1.4	1.09
1.6	0.73
1.8	0.49
2.0	0.33
2.2	0.22
2.4	0.14
2.6	0.09
2.8	0.06
3.0	0.04
3.2	0.03
3.4	0.02
3.6	0.01_2
3.8	0.01_8
4.0	0.01_6
4.5	0.00_2
5.0	0.00

r	O^{a}	O^{+a}	O^{++a}	O^{+++a}
0.00	16.00	16.00	16.00	16.00
0.01	15.56	15.57	15.59	15.61
0.02	15.12	15.15	15.19	15.22
0.03	14.70	14.74	14.79	14.85
0.04	14.28	14.34	14.42	14.49
0.06	13.50	13.60	13.71	13.82
0.08	12.80	12.93	13.07	13.23
0.10	12.17	12.33	12.50	12.71
0.12	11.61	11.79	12.00	12.25
0.14	11.10	11.31	11.56	11.85
0.16	10.64	10.88	11.16	11.50
0.18	10.22	10.49	10.81	11.19
0.20	9.83	10.13	10.49	10.91
0.25	8.99	9.35	9.80	10.34
0.30	8.24	8.69	9.22	9.86
0.35	7.58	8.09	8.71	9.45
0.40	6.96	7.54	8.24	9.08
0.45	6.37	7.02	7.80	8.75
0.50	5.82	6.55	7.40	8.43
0.6	4.84	5.69	6.69	7.88
0.7	3.98	4.95	6.09	7.42
0.8	3.25	4.34	5.60	7.06
0.9	2.64	3.84	5.21	6.77
1.0	2.13	3.43	4.91	6.55
1.1	1.72	3.11	4.67	6.39
1.2	1.38	2.85	4.49	6.27
1.4	0.89	2.50	4.26	6.13
1.6	0.56	2.29	4.14	6.06
1.8	0.36	2.17	4.07	6.02
2.0	0.23	2.10	4.04	6.01_2
2.2	0.15	2.06	4.02	6.01_5
2.4	0.09	2.03	4.01	6.00_3
2.6	0.06	2.02	4.00_4	6.00_1
2.8	0.04	2.01	4.00_2	6.00
3.0	0.03	2.01_6	4.00_1	
3.2	0.02	2.00_4	4.00	
3.4	0.02_6	2.00_2		
3.6	0.01	2.00_1		
3.8	0.01_8	2.00		
4.0	0.00			

r	Na^{+d}
0.00	22.00
0.01	21.30
0.02	20.62
0.03	19.97
0.04	19.35
0.06	18.20
0.08	17.19
0.10	16.30
0.12	15.50
0.14	14.78
0.16	14.12
0.18	13.51
0.20	12.93
0.25	11.62
0.30	10.43
0.35	9.36
0.40	8.39
0.45	7.51
0.50	6.74
0.6	5.46
0.7	4.50
0.8	3.79
0.9	3.27
1.0	2.90
1.1	2.64
1.2	2.45
1.4	2.22
1.6	2.11
1.8	2.06
2.0	2.03
2.2	2.01_4
2.4	2.01_8
2.6	2.01_6
2.8	2.00_4
3.0	2.00_2
3.2	2.00

r	Al^{++a}
0.00	26.00
0.02	24.28
0.04	22.71
0.06	21.34
0.08	20.15
0.10	19.11
0.12	18.18
0.14	17.33
0.16	16.55
0.18	15.82
0.20	15.13
0.22	14.48
0.24	13.86
0.26	13.27
0.28	12.71
0.30	12.17
0.32	11.26
0.34	11.19
0.36	10.74
0.38	10.31
0.40	9.91

[a] Hartree, Hartree, and Swirles, Trans. Roy. Soc. (London) **A238**, 229 (1939) (with exchange).
[d] D. R. Hartree and W. Hartree, Proc. Roy. Soc. (London) **A193**, 299 (1948) (with exchange).
[e] A. Kritschagina and M. Petrashen, J. Exptl. Theoret. Phys. (U.S.S.R.) **8**, 507 (1938) (with exchange).

TABLE I.—*Continued.*

r	Al^{++} [a]
0.45	9.02
0.50	8.27
0.55	7.65
0.60	7.13
0.65	7.11
0.70	6.36
0.75	6.08
0.80	5.85
0.85	5.65
0.90	5.49
0.95	5.36
1.00	5.24
1.1	5.05
1.2	4.91
1.3	4.79
1.4	4.69
1.5	4.60
1.6	4.53
1.7	4.46
1.8	4.40
1.9	4.34
2.0	4.29
2.2	4.22
2.4	4.15
2.6	4.11
2.8	4.07
3.0	4.05
3.2	4.03
3.4	4.02
3.6	4.02_5
3.8	4.01
4.0	4.01_6
4.2	4.00_4
4.4	4.00_3
4.8	4.00

r	Si^{+++} [b]	Si^{++++} [b]
0.00	28.00	28.00
0.01	27.05	27.07
0.02	26.13	26.16
0.03	25.26	25.31
0.04	24.45	24.51
0.06	23.00	23.09
0.08	21.74	21.86
0.10	20.65	20.79
0.12	19.67	19.84
0.14	18.78	18.98
0.16	17.96	18.82
0.18	17.19	17.44
0.20	16.46	16.74
0.25	14.81	15.15
0.30	13.37	13.78
0.35	12.15	12.61
0.40	11.12	11.63
0.45	10.26	10.84
0.50	9.57	10.19
0.6	8.55	9.29
0.7	7.89	8.74
0.8	7.46	8.42
0.9	7.17	8.23
1.0	6.95	8.12
1.1	6.79	8.06
1.2	6.66	8.03

r	Si^{+++} [b]	Si^{++++} [b]
1.4	6.46	8.01
1.6	6.32	8.00
1.8	6.22	
2.0	6.14	
2.2	6.09	
2.4	6.06	
2.6	6.04	
2.8	6.02	
3.0	6.01	
3.2	6.00	

r	K [c]
0.000	38.00
0.005	37.26
0.010	36.54
0.015	35.84
0.020	35.16
0.03	33.86
0.04	32.66
0.05	31.56
0.06	30.56
0.07	29.62
0.08	28.74
0.09	27.92
0.10	27.14
0.12	25.67
0.14	24.32
0.16	23.06
0.18	21.88
0.20	20.78
0.22	19.76
0.24	18.83
0.26	17.96
0.28	17.17
0.30	16.44
0.35	14.87
0.40	13.58
0.45	12.50
0.50	11.58
0.55	10.76
0.60	10.00
0.7	8.65
0.8	7.46
0.9	6.40
1.0	5.47
1.1	4.67
1.2	4.00
1.4	2.97
1.6	2.28
1.8	1.81
2.0	1.49
2.2	1.27
2.4	1.10
2.6	0.97
2.8	0.86
3.0	0.77
3.2	0.69
3.4	0.62
3.6	0.55
3.8	0.49
4.0	0.44
4.5	0.33
5.0	0.24
5.5	0.17
6.0	0.12
6.5	0.08
7.0	0.06

[a] Hartree, Hartree, and Manning, Phys. Rev. **60**, 857 (1941) (with exchange).
[b] D. R. Hartree and W. Hartree, Proc. Cambridge Phil. Soc. **34**, 550 (1938) (with exchange).

TABLE I.—*Continued.*

r	K[a]
8.0	0.03
9.0	0.01
10.0	0.01_6
11.0	0.00_2
12.0	0.00

r	Ca[+ b]
0.00	40.00
0.01	38.42
0.02	36.92
0.03	35.55
0.04	34.29
0.05	33.14
0.06	32.08
0.07	31.11
0.08	30.19
0.10	28.52
0.12	26.99
0.14	25.57
0.16	24.25
0.18	23.03
0.20	21.90
0.22	20.86
0.24	19.90
0.26	19.03
0.28	18.23
0.30	17.51
0.35	15.94
0.40	14.67
0.45	13.59
0.50	12.65
0.55	11.80
0.60	11.02
0.7	9.61
0.8	8.37
0.9	7.31
1.0	6.41
1.1	5.66
1.2	5.05
1.4	4.17
1.6	3.61
1.8	3.24
2.0	2.99
2.2	2.81
2.4	2.67
2.6	2.56
2.8	2.47
3.0	2.39
3.2	2.32
3.4	2.26
3.6	2.21
3.8	2.17
4.0	2.14
4.5	2.08
5.0	2.04
5.5	2.02
6.0	2.01_3
6.5	2.01_6
7.0	2.00_3
8.0	2.00

r	Cr[i]	Cr[++ i]
0.000	48.00	48.00
0.005	46.97	46.99
0.010	45.96	46.00
0.015	44.99	45.05
0.020	44.06	44.14
0.025	43.17	43.27
0.030	42.33	42.45
0.035	41.53	41.67
0.040	40.77	40.93
0.045	40.05	40.22
0.050	39.36	39.55
0.06	38.05	38.29
0.07	36.84	37.11
0.08	35.69	36.01
0.09	34.61	34.96
0.10	33.57	33.96
0.11	32.58	33.01
0.12	31.63	32.09
0.13	30.71	31.22
0.14	29.83	30.38
0.15	28.99	29.57
0.16	28.18	28.80
0.18	26.66	27.37
0.20	25.28	26.06
0.22	24.02	24.87
0.24	22.87	23.80
0.26	21.82	22.83
0.28	20.85	21.94
0.30	19.96	21.13
0.32	19.14	20.38
0.36	17.64	19.02
0.40	16.29	17.81
0.44	15.04	16.71
0.48	13.88	15.69
0.52	12.80	14.73
0.56	11.77	13.83
0.60	10.80	12.98
0.64	9.90	12.19
0.68	9.06	11.45
0.72	8.27	10.77
0.76	7.55	10.14
0.80	6.88	9.56
0.84	6.27	9.04
0.88	5.71	8.56
0.92	5.20	8.12
0.96	4.73	7.73
1.00	4.31	7.37
1.04	3.93	7.05
1.08	3.58	6.76
1.12	3.26	6.50
1.16	2.98	6.26
1.20	2.72	6.05
1.24	2.49	5.87
1.28	2.27	5.69
1.32	2.08	5.54
1.36	1.90	5.40
1.40	1.75	5.28
1.44	1.60	5.17
1.5	1.41	5.02
1.6	1.14	4.82
1.7	0.93	4.66
1.8	0.76	4.53
1.9	0.62	4.43
2.0	0.51	4.35
2.1	0.42	4.29
2.2	0.34	4.23
2.3	0.28	4.19
2.4	0.23	4.16
2.6	0.15	4.11

[h] D. R. Hartree and W. Hartree, Proc. Roy. Soc. (London) **A164**, 167 (1938) (with exchange).
[i] R. L. Mooney, Phys. Rev. **55**, 557 (1939) (without exchange). We take a $(3s)^2(3p)^6(3d)^4$ configuration for Cr.

TABLE I.—*Continued.*

r	Cr[1]	Cr^{++}[1]
2.8	0.10	4.07
3.0	0.07	4.05
3.2	0.05	4.03
3.4	0.03	4.02
3.6	0.02	4.02_5
3.8	0.01_2	4.01_8
4.0	0.01_8	4.01_6
4.4	0.00_2	4.00_2
4.8	0.00	4.00

r	Zn[1]
0.000	60.00
0.005	58.61
0.010	57.26
0.015	55.97
0.020	54.75
0.025	53.60
0.030	52.52
0.035	51.49
0.040	50.51
0.05	48.69
0.06	47.00
0.07	45.42
0.08	43.92
0.09	42.49
0.10	41.13
0.12	38.59
0.14	36.29
0.16	34.22
0.18	32.35
0.20	30.66
0.22	29.13
0.24	27.72
0.26	26.41
0.28	25.19
0.30	24.03
0.35	21.39
0.40	19.01
0.45	16.87
0.50	14.95
0.55	13.24
0.60	11.75
0.7	9.32
0.8	7.51
0.9	6.16
1.0	5.14
1.1	4.36
1.2	3.74
1.3	3.25
1.4	2.84
1.6	2.22
1.8	1.77
2.0	1.42
2.2	1.14
2.4	0.92
2.6	0.74
2.8	0.59
3.0	0.48
3.2	0.38
3.4	0.31
3.6	0.24
3.8	0.19
4.0	0.15
4.5	0.09
5.0	0.05
5.5	0.03
6.0	0.01_6
6.5	0.01_3
7.0	0.00_4
7.5	0.00_1
8.0	0.00

r	Ga[1]	Ga^{+}[1]	Ga^{+++}[1]
0.000	62.00	62.00	62.00
0.005	60.54	60.56	60.56
0.010	59.12	59.16	59.16
0.015	57.78	57.82	57.82
0.020	56.50	56.56	56.56
0.025	55.30	55.38	55.38
0.030	54.17	54.26	54.26
0.035	53.11	53.20	53.20
0.040	52.09	52.20	52.20
0.05	50.20	50.32	50.34
0.06	48.44	48.58	48.62
0.07	46.79	46.94	47.00
0.08	45.22	45.36	45.46
0.09	43.73	43.88	44.00
0.10	42.31	42.46	42.60
0.12	39.67	39.82	40.00
0.14	37.29	37.44	37.66
0.16	35.15	36.30	35.36
0.18	33.22	33.38	33.68
0.20	31.48	31.64	31.98
0.22	29.89	30.06	30.44
0.24	28.43	28.61	29.02
0.26	27.07	27.26	27.70
0.28	25.80	25.99	26.47
0.30	24.59	24.79	25.31
0.35	21.82	22.04	22.64
0.40	19.33	19.58	20.27
0.45	17.11	17.38	18.16
0.50	15.14	15.43	16.30
0.55	13.42	13.73	14.69
0.60	11.92	12.26	13.30
0.7	9.54	9.92	11.13
0.8	7.79	8.22	9.60
0.9	6.50	6.97	8.54
1.0	5.54	6.06	7.79
1.1	4.80	5.37	7.28
1.2	4.21	4.83	6.91
1.3	3.74	4.40	6.65
1.4	3.34	4.06	6.47
1.6	2.71	3.53	6.25
1.8	2.23	3.15	6.13
2.0	1.85	2.86	6.07
2.2	1.55	2.64	6.04
2.4	1.29	2.48	6.02
2.6	1.09	2.36	6.01
2.8	0.91	2.26	6.00_4
3.0	0.77	2.19	6.00_2
3.2	0.65	2.14	6.00_1
3.4	0.55	2.10	6.00
3.6	0.47	2.07	
3.8	0.40	2.05	
4.0	0.34	2.04	
4.5	0.23	2.02	
5.0	0.16	2.01_8	
5.5	0.11	2.00_4	
6.0	0.07	2.00_2	
6.5	0.05	2.00_1	

[1] Hartree, Hartree, and Manning, Phys. Rev. **59**, 299 (1941) (without exchange).

TABLE I.—*Continued.*

r	Ga[j]	Ga^{+} [j]
7.0	0.03	2.00
7.5	0.02	
8.0	0.01_2	
9.0	0.00	

r	Ge[k]	Ge^{++} [k]
0.000	64.00	64.00
0.005	62.48	62.48
0.010	61.00	61.01
0.015	59.60	59.61
0.020	58.27	58.29
0.025	57.03	57.06
0.030	55.86	55.89
0.035	54.75	54.79
0.040	53.69	53.74
0.05	51.71	51.78
0.06	49.89	49.97
0.07	48.17	48.26
0.08	46.54	46.64
0.09	44.99	45.11
0.10	43.51	43.64
0.12	40.77	40.93
0.14	38.31	38.49
0.16	36.10	36.31
0.18	34.11	34.35
0.20	32.31	32.57
0.22	30.67	30.96
0.24	29.16	29.47
0.26	27.74	28.08
0.28	26.41	26.77
0.30	25.16	25.54
0.35	22.26	22.71
0.40	19.68	20.19
0.45	17.40	17.97
0.50	15.40	16.03
0.55	13.66	14.36
0.60	12.18	12.94
0.7	9.84	10.73
0.8	8.16	9.16
0.9	6.92	8.04
1.0	5.98	7.23
1.1	5.24	6.63
1.2	4.64	6.16
1.3	4.14	5.79
1.4	3.72	5.50
1.6	3.04	5.05
1.8	2.48	4.74
2.0	2.04	4.52
2.2	1.68	4.36
2.4	1.38	4.25
2.6	1.12	4.17
2.8	0.92	4.11
3.0	0.76	4.07
3.2	0.62	4.05
3.4	0.52	4.03
3.6	0.42	4.02
3.8	0.34	4.01_2
4.0	0.28	4.01_8
4.5	0.18	4.00
5.0	0.10	
5.5	0.06	
6.0	0.04	
6.5	0.02	
7.0	0.01_4	
7.5	0.01_8	
8.0	0.00_4	
9.0	0.00	

r	As[j]	As^{+} [j]	As^{++} [j]	As^{+++} [j]
0.000	66.00	66.00	66.00	66.00
0.005	64.41	64.41	64.41	64.42
0.010	62.87	62.87	62.88	62.89
0.015	61.40	61.41	61.42	61.44
0.020	60.03	60.03	60.05	60.07
0.025	58.73	58.74	58.77	58.79
0.030	57.52	57.53	57.56	57.58
0.035	56.37	56.38	56.41	56.44
0.040	55.28	55.29	55.33	55.36
0.05	53.23	53.25	53.30	53.34
0.06	51.33	51.35	51.41	51.46
0.07	49.54	49.57	49.63	49.69
0.08	47.85	47.87	47.95	48.02
0.09	46.24	46.27	46.35	46.43
0.10	44.70	44.74	44.83	44.91
0.12	41.87	41.91	42.02	42.12
0.14	39.33	39.38	39.51	39.62
0.16	37.05	37.11	37.26	37.39
0.18	35.00	35.07	35.24	35.39
0.20	33.15	33.23	33.41	33.58
0.22	31.45	31.54	31.74	31.92
0.24	29.88	29.98	30.19	30.39
0.26	28.41	28.52	28.75	28.96
0.28	27.02	27.14	27.39	27.62
0.30	25.71	25.84	26.10	26.36
0.35	22.70	22.85	23.15	23.45
0.40	20.03	20.21	20.55	20.89
0.45	17.68	17.90	18.27	18.66
0.50	15.66	15.90	16.31	16.75
0.55	13.92	14.20	14.65	15.12
0.60	12.45	12.76	13.25	13.76
0.7	10.16	10.54	11.09	11.70
0.8	8.51	8.96	9.58	10.28
0.9	7.30	7.81	8.51	9.29
1.0	6.37	6.95	7.72	8.58
1.1	5.62	6.27	7.11	8.06
1.2	5.00	5.72	6.63	7.66
1.3	4.47	5.25	6.23	7.35
1.4	4.00	4.85	5.90	7.10
1.6	3.22	4.19	5.38	6.72
1.8	2.59	3.68	5.00	6.47
2.0	2.08	3.28	4.71	6.30
2.2	1.67	2.97	4.50	6.19
2.4	1.34	2.73	4.35	6.11
2.6	1.07	2.55	4.25	6.06
2.8	0.85	2.41	4.17	6.03
3.0	0.68	2.30	4.12	6.01_4
3.2	0.54	2.22	4.08	6.00_1
3.4	0.43	2.16	4.05	6.00
3.6	0.35	2.12	4.04	
3.8	0.28	2.09	4.02	
4.0	0.22	2.06	4.02_6	
4.5	0.13	2.03	4.01_6	
5.0	0.07	2.01	4.00_2	
5.5	0.04	2.01_6	4.00	
6.0	0.02	2.00_3		
6.5	0.01	2.00		
7.0	0.01_6			
7.5	0.00_4			
8.0	0.00			

[k] Hartree, Hartree, and Manning, Phys. Rev. **59**, 306 (1941) (without exchange).

TABLE II. Atoms whose $2Z_p$'s are given in the literature.

Atomic number	Element	Atomic number	Element
2	He	19	K^+, K^{++}
3	Li^+	20	Ca, Ca^{++}
4	Be, Be^{++}	26	Fe
9	F	29	Cu^+
10	Ne	37	Rb^+
11	Na	47	Ag^+
13	Al^+, Al^{+++}	55	Cs^+
14	Si^{++}	74	W
18	Ar	80	Hg, Hg^{++}

PHYSICAL REVIEW VOLUME 91, NUMBER 6 SEPTEMBER 15, 1953

Range-Energy Relations of 10- to 250-kev Protons and Helium Ions in Various Gases*

CHARLES J. COOK, EMERSON JONES, JR.,† AND THEODORE JORGENSEN, JR.
University of Nebraska, Lincoln, Nebraska

(Received May 5, 1953)

An analyzed beam of ions was brought through a differential pumping system into a low-pressure gas stopping cell, where the data necessary to plot a Bragg curve were obtained with the aid of a double grid ionization chamber of variable transverse radius. It was found that the resulting ionization extrapolated ranges may be uniquely determined only if the ionization chamber radius is greater than the transverse radius of the ionization envelope of the beam in the stopping gas. The ionization extrapolated range-energy relations for slow protons and alpha particles were determined in various gases. These data are also expressed in terms of an empirical relation. The observed range-energy relations are compared with previous data where they exist.

INTRODUCTION

THE range-energy relations of protons and alpha particles in various gases have been studied intensively in the past.[1] However, there has been a need for further measurements in this field at low energies.[2–5] The purpose of this investigation is to establish experimentally the range-energy relations for low-energy protons and helium ions in various gases. An ionization extrapolated range was determined by bringing a homogeneous beam of ions of known energy through a differential pumping system of negligible stopping power, into a low-pressure gas, where data for a Bragg curve were obtained by using a movable ionization chamber.

EXPERIMENTAL APPARATUS

The ion beam was produced by a Cockcroft-Walton accelerator, and after being magnetically analyzed, was brought to focus on the exit aperture of the differential pumping window leading into the stopping cell as shown in Fig. 1. The ion beam was accurately centered on this aperture by means of electrostatic deflection, which could move the beam both horizontally and vertically.

The differential pumping system consisted of three thin tungsten or tantalum diaphragms with a small aperture in each to pass the beam and to impede the flow of gas from the stopping cell; further details are shown in Fig. 2. Corrections to the ranges caused by the observed gas pressure in the intermediate regions of this window were calculated and were found to be less than 0.3 percent in all cases.

The energy of the ion beam was determined by measuring the potential of the anode of the high-frequency ion source, since the energy of the accelerated ions is known to be only about 100 volts less than this potential. The accelerating potential was measured by accurately determining the potential drop across a known fraction of a 1200-megohm voltmeter stack with a Leeds and Northrup K-2 potentiometer. This fraction was checked frequently and adjusted within 0.1 percent of the desired ratio so that temperature effects were compensated.

This arrangement was checked by means of the $Mg(p,\gamma)$ resonance at 222 kev.[6] A series of daily measurements of this resonance indicated that the voltmeter read 2 percent high with a 2 percent variation. These variations were random and not due to a possible film

* Research performed under contract with the U. S. Atomic Energy Commission.

† Now at the Los Alamos Scientific Laboratory, Los Alamos, New Mexico.

[1] A. E. Taylor, Repts. Progr. Phys. **15**, 49 (1952).
[2] Cornog, Franzen, and Stephens, Phys. Rev. **74**, 1 (1948).
[3] H. A. Bethe, Revs. Modern Phys. **22**, 213 (1950).
[4] A. P. French and F. G. P. Seidl, Phil. Mag. **42**, 537 (1951).
[5] W. A. Wentzel and W. Whaling, Phys. Rev. **87**, 499 (1952).
[6] Hole, Holtsmark, and Tangen, Z. Physik **118**, 48 (1941).

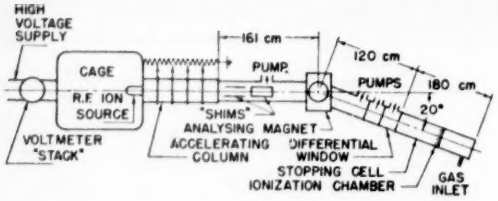

FIG. 1. Schematic diagram of the accelerator and experimental apparatus.

forming on the target. Therefore, the beam energy was considered to be known within 2 percent above 125 kev and 1 percent below. Variations in the accelerating potential detectable by the voltmeter were kept less than 0.015 percent of the desired potential from 20 to 250 kev by means of a galvanometer-phototube-amplifier system used to control a variable impedance transformer in series with the primary of the high voltage transformer.[7] The ripple of the accelerating potential was no greater than 0.15 percent for a well focused beam. The analyzing magnet current regulator maintained the magnet current within 0.2 percent of any selected value.

The gas stopping cell was a brass tube 6 inches in diameter and 200 cm long. The ionization chamber could be moved over most of the length of the stopping cell, and its position was measured to the nearest millimeter. Gas was let into the stopping cell through a manifold of five needle valves. The pressure of the stopping gas was measured with two McLeod gauges especially constructed for precise reading in the pressure range used. There were two traps, cooled with a dry ice-acetone mixture, in series between the gauges and the stopping cell. During the experiment the stopping gas flowed through the stopping cell at a nominal rate of one cc per minute, varying of course with the pressure and kind of gas. The secular equilibrium pressure could be maintained with only slight variation over long periods of time. The pressures were assumed known to ± 0.5 percent. Temperatures were determined to the nearest degree by a mercury thermometer in contact with the wall of the stopping chamber.

The ionization chamber consisted of a collecting plate and two grids, all of brass. The plate was divided into annular rings 1, 2, 3, 4, 5, and 6 cm outside radii.

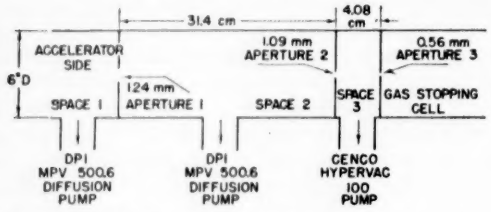

FIG. 2. Schematic diagram of the differential pumping system.

[7] L. N. Ridenour and C. W. Lampson, Rev. Sci. Instr. 8, 162 (1937).

The electrical connections to these rings were such that any one ring or any combination of them could be connected to a single galvanometer for measuring the ionization current, while the rings that were not used in this way served as guard rings. The largest ring always served as a guard ring. The collecting plate was kept at a positive potential, the middle grid was kept at a negative potential to repel electrons which would otherwise arrive at the plate from the region in front of the ion chamber, and the front grid was kept at ground potential. A careful study showed that the range measurements were independent of the ion chamber potentials over wide limits. The grid-grid and grid-plate spacings were 3.0 mm, and corrections for the depth of the chamber were made for all range determinations.

EXPERIMENTAL PROCEDURE

The ionization extrapolated range of an ion beam in a gas was determined by plotting a Bragg curve showing the relative ion chamber currents for various positions of the chamber along the stopping cell and extrapolating the straight portion of this curve to zero current. It is necessary, in order to obtain precise data for such a Bragg curve, that the beam current entering the stopping cell and the pressure of the stopping gas remain constant while the data is being taken. It was found that the major contributions to the instability of the beam were due to slight changes in the position of the focused spot caused by slight variations of the many parameters involved in producing a well-focused beam with this accelerator. These position changes need be very slight since the diameter of the focused beam was about the same as the diameter of the aperture of the window. Rather than attempt to stabilize the accelerator completely, the beam was swept vertically past the window aperture with 60-cycle modulation of large amplitude. The ion beam then passed the window at essentially a constant rate, and as a result, minor vertical changes in position of the beam that would ordinarily decrease the beam current into the stopping cell did not produce a detectable change of the average modulated beam current into the stopping cell. The horizontal changes in position of the focused spot were eliminated by slowly varying the magnet current in order to observe the maximum ionization current. Other factors influencing the average beam current into the stopping cell produced negligible variations. Careful investigations showed that ionization extrapolated ranges do not depend upon beam modulation even when the beam current into the stopping cell is reduced by a factor of 1000 by modulation.

To make sure that a given Bragg curve depended only on the ionizing power of the beam, the data were taken, once for successive positions of the chamber for increasing chamber-window distances, and then again for successive positions for decreasing chamber-window distances. If both curves were essentailly the same,

there could have been no pressure change, beam intensity changes, etc., and the curves were accepted. All other Bragg curves were rejected. The ionization extrapolated ranges can be determined within ±0.5 percent from the original data.

While the apparatus was being developed so that Bragg curves could be obtained with suitable precision, preliminary experiments showed that the extrapolated ranges of protons of a known energy in a gas determined with an ionization chamber of fixed radius, when normalized to standard conditions of pressure and temperature, were not independent of the pressure. This effect is caused by the scattering of the beam by the stopping gas. At lower pressures, the ionization envelope of the beam in the gas is so large that the ionization current collected by the ionization chamber decreased rapidly with the increasing distance along the stopping cell, primarily because the beam is scattered outside the volume swept by the chamber and only partially because of a decrease in the ionizing power of the beam. A set of Bragg curves taken with various sized chambers showing this effect is given in Fig. 3.

If it is assumed that the size of the ionization envelope is inversely proportional to the pressure, it would appear that an increase in pressure should produce the same effect in the normalized range as a corresponding proportional increase in the radius of the ionization chamber. In other words, the normalized range for a given product of pressure and chamber radius Pr should be unique for a given stopping gas and particle energy. Normalized ranges for 60-kev protons in hydrogen are plotted in Fig. 4 against the values of Pr. This curve shows the range to be a function of Pr within experimental error. These curves were obtained for various gases at various energies, and all had similar shapes. They all showed the characteristic "saturation" effect at the higher Pr values. This saturation occurs when the pressure of the gas and the radius of the chamber are such that essentially all of the ionization envelope is contained in the volume swept by the ionization chamber.

To assure that saturation occurred in every range determination, and therefore that a unique range was obtained, it was not necessary to obtain a Pr curve for every energy. It was enough to show that the observed range is the same for ionization chambers of 4- and 5-cm radius. The procedure adopted was to observe the Bragg curves at as low a pressure as possible and yet have a saturated range. This procedure reduced the relative error inherent in observing the position of the ionization chamber as well as the correction due to the finite depth of the ionization chamber.

After the criterion for unique normalized ionization extrapolated ranges was established, it was possible to measure these ranges in gases with good precision. The errors in the high potential determination were reflected into errors in the normalized range amounting

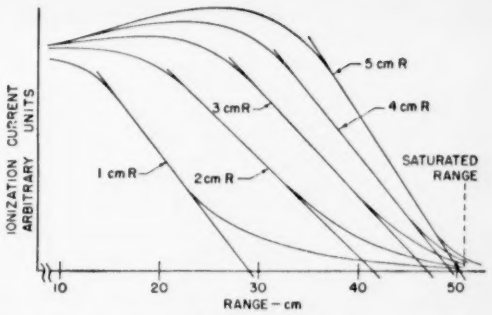

FIG. 3. Bragg curves for 50-kev protons in CO gas at 1.06-mm Hg for 1-, 2-, 3-, 4-, and 5-cm radius ionization chamber.

to 3 percent above 125 kev and 1.5 percent below. These errors, together with errors of ±0.5 percent in the pressure and ±0.3 percent in the temperature of the stopping gas, ±0.5 percent in the measurement of the position of the ion chamber, and ±0.5 percent in the extrapolation of Bragg curves are consistent with actual variations in the range determinations. The root-mean-square deviations for proton ranges were investigated for all stopping gases at various energies from 50 to 200 kev and were always found to be less than 1.4 percent.

Errors introduced into the range determinations by contaminants in the stopping cell were difficult to estimate. The stopping cell was pumped down to a low pressure, as shown on an ionization gauge, and was tested for rate of pressure rise each day before the stopping gas was let into the stopping cell. This was done to insure that no appreciable vapors from within the apparatus nor any air leaking into the stopping cell could contaminate the stopping gas. Gases were admitted to the stopping cell through two dry ice-acetone traps in series to remove water vapor. Hydrogen gas was further purified by removing a trace of oxygen catalytically. All gases were from commercial tanks and were stated to be 99.5 percent pure or better except for nitrous oxide which was stated to be 98 per-

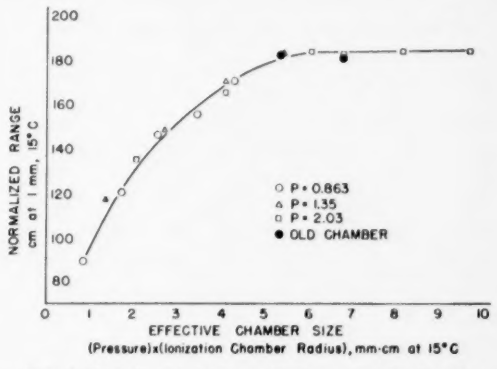

FIG. 4. Variation of the normalized range with effective chamber size for 60-kev protons in hydrogen gas.

TABLE I. Observed ionization extrapolated ranges for protons.

	Ranges—cm at 1-mm Hg, 15°C								
E kev	H_2	O_2	A	Air	N_2	CO	CH_4	N_2O	CO_2
4.00	29.4								
4.90	32.0								
6.66			15.6	12.5	10.3				
8.00						14.4			
10.0			20.9			17.5	18.3		
11.0									14.3
11.5				19.4					
12.0	57.9				19.7	19.4	20.4	14.5	
13.0		23.9							
15.0	68.4				22.8				18.0
16.0						24.4	24.4		
20.0		32.1	31.5	28.9	28.0	28.6	27.8	20.5	22.1
21.5	87.1								
25.0	97.0				32.2				
30.0	109	43.9	42.8	39.2	36.6	37.3	36.3	28.4	30.1
35.0					41.2				
37.5	129								
40.0		54.3	52.0	48.1	45.0	45.8	43.9	34.5	36.3
45.0	146								
46.0	147								
50.0		63.4	58.6	57.2	53.2	53.7	51.1	40.6	42.6
57.0	174								
60.0		71.5	67.2	64.3	62.0	62.3	58.2	46.0	48.2
70.0	203	80.3	73.5	71.9	69.3	71.3	65.0	50.8	53.9
80.0		88.1	82.8	80.0	76.9	78.5	72.3	56.8	59.9
85.0	237								
90.0		97.0	92.7	89.0	85.4	86.1	78.8	62.7	64.6
95.0	266								
100			102	96.3	94.2	95.1	84.8	68.4	70.0
110		114							
120	331								
125		125	124	115	114	115	104	81.0	85.0
140	388								
150		149	147	137	136	137	124	96.7	99.8
170	485								
175		169	172	159	159	158	146	111	114
200		192	200	182	182	182	170	126	131
202	594								
205							175		
225		217		209		207	195	144	
240					219				
241	739								
250		243		232		236	222	164	166
252			259						

cent pure with unknown impurities. Air was drawn from outside the laboratory and carbon dioxide was obtained from the solid form. Since the ranges of protons in all gases except hydrogen are about the same, small amounts of likely impurities would cause insignificant errors in the ranges. Since the ranges in hydrogen from four different tanks from different suppliers were experimentally identical, it was assumed that the nitrogen contaminant was negligible in each. Care was taken that no mercury vapors from the McLeod gauges entered the stopping cell except that which came past the two traps. No evidence could be found of possible mercury contamination.

EXPERIMENTAL RESULTS

Ionization extrapolated ranges of protons and helium ions in the various gases studied, normalized to 1-mm Hg and 15°C, are shown in Tables I and II.

The relation between the normalized range R and the incident energy E can be very closely approximated by empirical relations of the form

$$R=kE^n, \quad E<E_0; \quad R=C(E+E_1)^{1.5}, \quad E>E_0,$$

where k, C, E_1, and n are parameters chosen so that these relations fit the data, and E_0 is the energy for which the rate of energy loss is a maximum. The first equation is suggested by the linear portion of the curves when the data are plotted on log-log paper. The second equation is suggested by Geiger's relation[8] for high energies. The requirement that these two empirical relations must be continuous with their first derivatives at E_0 reduces the number of independent parameters, including E_0, to three. The empirical relations fit the data to within 2 percent except near E_0. Values of the parameters are shown in Tables III and IV.

DISCUSSION OF RESULTS

Since, at the present time, there are no existing theoretical range-energy relations for ions below the energy for which Bethe's equation[9] is valid, here called slow ions, it is only possible to compare the range-energy relations found in this experiment with similar range-energy relations found in previous experiments.

Bethe[3] and Jesse and Sadauskis[10] have constructed the most precise range-energy relation for alpha particles in air previously available in this energy range. It was based on the experiment of Holloway and

TABLE II. Observed ionization extrapolated ranges for alpha-particles in various gases.

	Ranges—cm at 1-mm Hg, 15°C		
E kev	A	Air	H_2
20.0	35.2		125
30.0	45.2	31.5	168
40.0	54.3	40.4	203
50.0	60.7	46.9	234
60.0	68.7		251
70.0	74.3		276
70.5		60.0	
80.0	81.4		302
90.0	86.8	71.0	324
100	91.4	76.1	342
125	105	89.0	391
150	118	101	433
175	129	114	467
200	141	124	506
225	151	131	534
250	161	143	585

[8] H. Geiger, Proc. Roy. Soc. (London) **83**, 492 (1910).
[9] M. S. Livingston and H. A. Bethe, Revs. Modern Phys. **9**, 261 (1937).
[10] W. P. Jesse and J. Sadauskis, Phys. Rev. **78**, 1 (1950).

Livingston[11] in which the specific ionization of a single alpha particle in the air was determined and the mean range of a beam of alpha particles in air was then calculated using W(air), the energy lost by the incident alpha particle per ion pair produced in air. Jesse and Sadauskis found that above about 300 kev, W(air) was not a constant as was assumed for all energies by Holloway and Livingston. They then recalculated the range-energy relation from the specific ionization as observed by Holloway and Livingston for energies greater than 271 kev. However, the work of Jesse and Sadauskis may be extrapolated to lower energies by extending the linear relation that exists from 300 kev to 2 Mev for the ratio of W(argon) to W(air).[10] The range-energy relation that is calculated from the specific ionization curve as found by Holloway and Livingston, using this low energy extrapolation, is shown in Fig. 5 and is labeled the Jesse and Sadauskis (1950) extrapolated range-energy relation.

The range-energy relation for alpha particles in air found in this investigation [the University of Nebraska (U. of N.) 1953 relation)] is also shown in Fig. 5. The Bethe (1950) relation for alpha particles in air was also determined by extrapolating the work of Jesse and Sadauskis and thereby correcting the ranges calculated by Holloway and Livingston. This curve is essentially the same as the U. of N. relation. It is apparent that the agreement between the relations presented so far depend upon fortuitous extrapolations of the work of Jesse and Sadauskis.

The Bethe[9] (1937) range-energy relation for alpha particles in air is also given in Fig. 5. This relation was

TABLE III. Empirical range-energy relation constants for protons in various gases.

Gas	K cm/(kev)^n	C cm/(kev)$^{\frac{1}{2}}$	n	E_0 kev	E_1 kev
Hydrogen	11.2	0.147	0.67	42.5	53
Oxygen	3.90	0.0400	0.71	79.0	88
Argon	4.39	0.0440	0.67	58.4	73
Air	3.26	0.0393	0.73	76,5	80
Nitrogen	3.34	0.0414	0.71	62.9	70
Carbon monoxide	3.35	0.0376	0.71	77.3	86
Methane	3.80	0.0385	0.67	56	70
Nitrous oxide	2.50	0.0251	0.71	73	92
Carbon dioxide	2.64	0.0259	0.71	85	95

TABLE IV. Empirical range-energy relation constants for alpha particles in various gases.

Gas	n	K cm/(kev)^n
Hydrogen	0.558	25.2
Argon	0.596	5.95
Air	0.687	3.23

[11] M. G. Holloway and M. S. Livingston, Phys. Rev. **54**, 18 18 (1938).

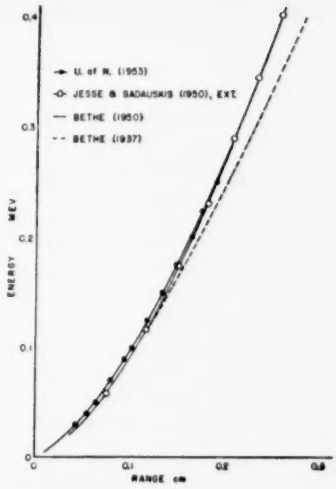

FIG. 5. Range of alpha particles in air at 760-mm Hg and 15°C.

derived from cloud chamber work by Blackett and Lees[12] and is admittedly quite inaccurate.[3,10]

The range-energy relation for protons in air has been previously derived from the range-energy relation for alpha particles in air, at 760-mm Hg, 15°C, by the semi-empirical expression[9]

$$R_H(E)=1.0072R_\alpha(3.971E)-0.20,$$

where $R_H(E)$ is the range in cm of a proton of incident energy E, $R_\alpha(3.971E)$ is the range in cm of an alpha particle of incident energy $3.971E$, and 0.20 = Blackett's empirical constant. This relation is valid in the energy region where Bethe's expression for the rate of energy loss of the ion is valid, that is, for proton energies above 300 kev and alpha-particle energies above 1200 kev. Below this region Blackett's constant becomes a decreasing function of energy.

Jesse and Sadauskis[10] used the above expression to calculate the range-energy relation of protons in air down to an energy of 302 kev (calculations from their table of alpha-particle ranges give 0.40-cm range at 306 kev for protons in air). Bethe[3] used this expression down to a proton energy of only 500 kev. From 0 to 170 kev Bethe calculated the ranges from the rate of energy loss of protons in air as determined by Crenshaw.[13] The region from 170 to 500 kev was fitted by interpolation. Bethe's 1950 relation, as well as Jesse and Sadauskis' range at 306 kev, are shown in Fig. 6. The Bethe 1937 alpha-particle ranges, which are based on the work of Blackett and Lees, appear to be too long, and it would seem that the proton ranges should thus also be too long. In fact, the Bethe ranges at 306 kev are nearly 20 percent longer than that calculated at this energy by Jesse and Sadauskis.

[12] P. M. S. Blackett and D. S. Lees, Proc. Roy. Soc. (London) **134**, 658 (1932).

[13] C. M. Crenshaw, Phys. Rev. **62**, 54 (1942).

The U. of N. ranges of protons in air are also shown in Fig. 6. The U. of N. range at 306 kev found by means of the empirical relation is 0.393 compared to 0.40 cm calculated by Jesse and Sadauskis. These two ranges differ by less than the experimental error and indicate that Blackett's constant is probably not energy-dependent for energies greater than 300 kev.

The U. of N. and the Brookhaven[14] range-energy relations for protons in hydrogen are shown in Fig. 7. The range-energy relation published by the Brookhaven National Laboratory was obtained from the theoretical stopping power of protons in hydrogen as calculated by Hirschfelder and Magee.[15] The range-energy relations determined by Crenshaw[13] and Phillips[16] agree with the U. of N. range-energy relation within experimental error. The agreement found between these various range-energy relations for protons in hydrogen is most gratifying.

In the comparison of present results for the other gases with previous work it is necessary either to integrate the rates of energy loss data to obtain ranges or to differentiate the present data to obtain rates of energy loss. Satisfactory comparisons have not been obtained by either procedure.

Probably the best way of obtaining rates of energy loss from the present data is to differentiate empirical

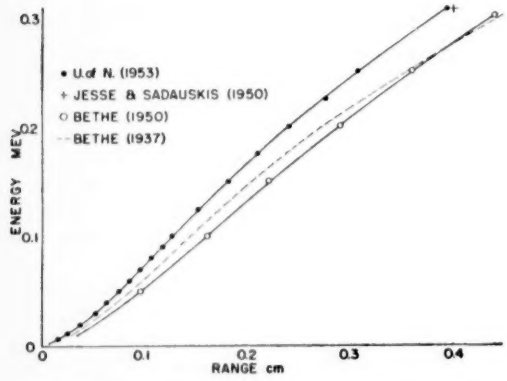

FIG. 6. Range of protons in air at 760 mm Hg and 15°C.

[14] H. Bethe, Brookhaven National Laboratory Report BNL-T-7, 1949 (unpublished).
[15] J. O. Hirschfelder and J. L. Magee, Phys. Rev. **73**, 207 (1948).
[16] James A. Phillips, Phys. Rev. **90**, 532 (1953).

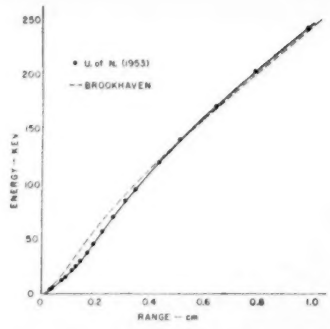

FIG. 7. Range of protons in hydrogen gas at 760 mm Hg and 15°C.

relations suitable for this purpose. The empirical relations previously given have discontinuous second derivatives at E_0. This, of course, creates errors in the rate of energy loss curves obtained from the present data. Mechanical differentiation likewise is subject to errors. Nevertheless, all attempts to find rates of energy loss from the present data give values that are greater than the results given by the differential type experiment. For protons in argon, the present experiment gives rates of energy loss of the order of 20 percent greater than the Los Alamos results.[16] The difference appears to be too large to be accounted for by experimental errors or errors in differentiation.

Although this difference in the rates of energy loss could be caused by a large systematic error, it should probably be attributed to the fundamental difference of the two experiments. The differential type experiment excludes from consideration any particle which has suffered an appreciable angular scattering, while the present integral type of experiment gives a unique result only when essentially all the ions are collected.

ACKNOWLEDGMENTS

We wish to express our appreciation to Mr. J. S. Heiser for his expert assistance in the construction of the accelerator and other apparatus and to Mr. Arthur J. Meyerott and Mr. William A. Barrett, Jr. for their technical assistance. We wish to express our gratitude to the Board of Regents of the University of Nebraska for a special grant which enabled us to start this work and to the U. S. Atomic Energy Commission for its continued support.

Fast Neutron Cross Sections and Nuclear Level Density*

D. J. HUGHES, R. C. GARTH,† AND J. S. LEVIN
Brookhaven National Laboratory, Upton, New York

(Received June 1, 1953)

The capture cross sections for unmoderated fission neutrons, effective energy one Mev, are determined by the average properties of nuclear levels at excitation energies equal to neutron binding plus one Mev. The level spacings determined from measured cross sections for 61 isotopes are discussed in connection with the statistical and shell nuclear models. Whereas the discontinuity in neutron binding energy at magic numbers accounts for most of the abnormality of the cross sections of the magic-N nuclei, the effect of shell structure is evident in level spacing even at high (5–7 Mev) excitation energy. The level spacings obtained for nonmagic-number nuclei, on the other hand, are in reasonable agreement with the statistical nuclear model, and in addition are the same for levels of widely different spin.

THE results of a survey[1,2] of capture cross sections for one-Mev (effective energy) neutrons showed that nuclei containing 50, 82, and 126 neutrons had cross sections lower by a factor of fifty than neighboring nuclei. The low cross sections for these nuclei were explained in terms of the sudden decrease in neutron binding energy that occurs at completed nuclear shells. The fast neutron absorption cross section is proportional to the average level density in the compound nucleus, which density is a rapidly increasing function of excitation energy. As the excitation energy following capture is given by the neutron binding energy plus one Mev, the low cross sections furnished evidence for the occurrence of "magic-number" nuclei with unusually low binding energy. At the present time, however, neutron binding energies are reasonably well fixed by work with (γ, n), (n, γ) and (d, p) reactions,[3] and the fast capture cross sections can be used to determine the nuclear level densities at known excitation energies. The level densities determined in this way can be used to check the validity of the statistical nuclear model with regard to variation of level density with odd-even character, with atomic weight, and with magic numbers. In the present paper we shall discuss the level densities determined from the experimental cross sections, after a brief description of measurements more recent than those already reported.[1,2]

I. EXPERIMENTAL RESULTS

The fast cross sections of references 1 and 2 were measured at the deuterium-moderated pile of the Argonne National Laboratory, using unmoderated fission neutrons of effective energy one Mev for the capture reactions. The fission neutrons were obtained from a U^{235} plate that was placed in a thermal beam with no shielding, and because of the high fast flux produced, irradiations could be performed only when no other experiments were in progress at the pile. A similar "converter plate," now in use at Brookhaven for the same type of measurements, is shielded in such a way that irradiations can take place without interfering with other pile experiments. The shielding of the fission neutrons is difficult because it is necessary to avoid the production of resonance neutrons by slowing down in the shielding blocks, neutrons which have capture cross sections much higher than the unmoderated neutrons.

The purpose of the present design (Fig. 1) is to obtain a high flux of thermal neutrons (which do not need to be collimated) at the U^{235} plate, with as few resonance neutrons as possible, and to shield the plate without production of resonance neutrons in the shield. The plate is placed near the pile reflector in order to obtain a high thermal neutron flux, even though resonance neutrons from the pile lattice are appreciable at that position. Placing the plate at a thermal column would ensure a low resonance flux, but would entail a serious loss of thermal flux.

The cadmium ratio measured in the position of the plate (the plate being absent) with a $1/v$ detector (a BF_3 proportional counter) is about 200, a surprisingly low value considering the amount of graphite reflector between the point of measurement and the pile lattice. Additional experiments showed that the resonance neutrons causing the poor ratio were those leading out of

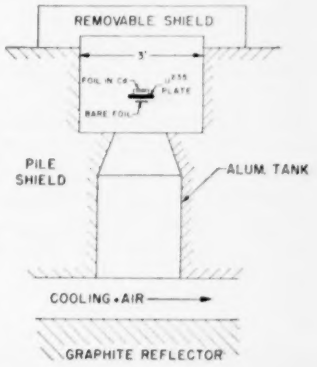

FIG. 1. Experimental arrangement for production of unmoderated fission neutrons inside shield of the Brookhaven pile. The foil inside cadmium is activated by fission neutrons and the bare foil is a monitor of the thermal flux.

* Work carried out under contract with the U. S. Atomic Energy Commission.

† Now at Brooklyn College, Brooklyn, New York.

[1] Hughes, Spatz, and Goldstein, Phys. Rev. **75**, 1781 (1949); this paper contains references to older work.

[2] D. J. Hughes and D. Sherman, Phys. Rev. **78**, 632 (1950).

[3] Summarized by J. A. Harvey, Phys. Rev. **81**, 353 (1951).

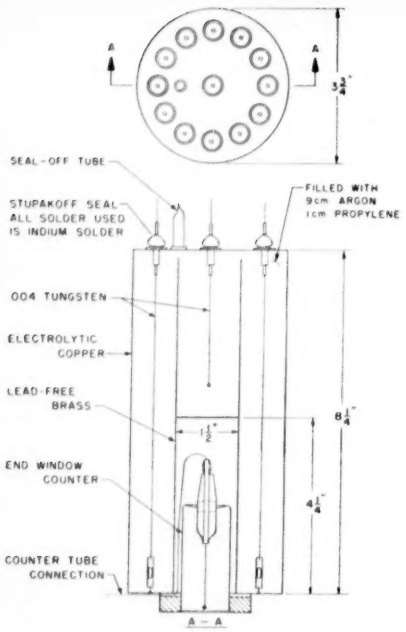

FIG. 2. Anticoincidence counter used for measurement of weak activities. The counter surrounding the central G-M tube removes the cosmic-ray background and thus reduces the background to about 6 counts/min.

the center of the pile through cooling channels (air ducts) and reaching the plate indirectly, rather than coming directly through the graphite itself. In measurements of fast neutron capture cross sections, it has been necessary in many cases to surround the samples by protective layers of the element being irradiated in order to eliminate, by self-protection, the resonance neutrons. Such a "sandwich" arrangement is satisfactory for most isotopes, but for a few with prominent low-lying resonances, such as In and Au, further corrections must be made. It has been found to be quite simple to carry on long irradiations in the arrangement of Fig. 1 without disturbing other experiments at the pile, and this property of the apparatus is very useful for the long-lived activities that have been measured recently.

An anticoincidence counter has been developed[4] for measuring the long-lived samples of low activity often produced in this work. This counter, shown in Fig. 2, removes the cosmic-ray component of the end window counter background, thus lowering the background to about 6 c/m, which is probably contributed by the material of the counter tube itself (lead gaskets, for instance). The reduction in background already obtained is very useful for weak activities, and counters are now being prepared of materials that should have still lower background ratios.

[4] We wish to express our appreciation to H. Palevsky for the design of this counter and to W. Higinbotham for its construction.

The recent work at Brookhaven[5,6] has been devoted mainly to cross sections at and near magic number nuclei, both proton- and neutron-magic. Some of these cross sections have been much more difficult to measure than the earlier ones because of isomeric states and long half-lives. The results of the Brookhaven measurements will be combined with the earlier work in the subsequent discussion.

In order to illustrate the general behavior of the measured cross sections we present in Fig. 3 the isotopic activation values as a function of atomic weight, A. The cross sections are found to increase steadily up to a value of about 100 millibarns at $A=100$, after which there is no great change, with the marked exceptions of those nuclei for which there is a magic or near-magic number of protons or neutrons. All the target nuclei

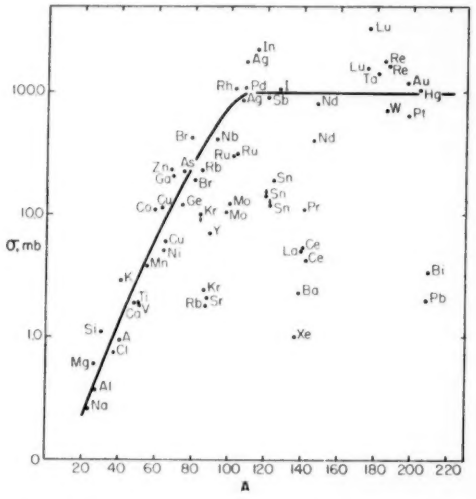

FIG. 3. Isotopic activation cross sections at effective energy one Mev as a function of atomic weight.

investigated have an even number of neutrons, with the single exception of $_{71}Lu^{176}$, which is seen to have a fast cross section over twice as great as that for nuclei of comparable atomic weight. The 61 isotopes studied are approximately equally divided into those of odd and even A. In all cases the residual nuclei after neutron capture are beta emitters, being on the neutron rich side of the valley of stability. The smooth curve is a a graphical average of the experimental points for those isotopes whose cross sections represent what may be called "normal behavior."

The exceptional behavior of nuclei having a magic number of neutrons is brought out more clearly by plotting the cross sections against the number of neutrons as in Fig. 4. Those nuclei containing 50, 82, or 126 neutrons are found to have cross sections that

[5] Hughes, Garth, and Eggler, Phys. Rev. **83**, 234 (1951).
[6] Garth, Hughes, and Levin, Phys. Rev. **87**, 222 (1952).

range from one-hundredth to one-tenth of those of normal nuclei. The two Mo and the two Ru isotopes indicate an anomalously low cross section in the region 56–60 neutrons but the cross sections of Rh and Ag are normal. It is perhaps significant that the latter have even, and the former odd Z. When the cross sections are plotted against the atomic number Z (Fig. 5), it is found that there is a less sensitive dependence upon the number of protons in the target nuclei. The low values of cross section for tin isotopes having 50 protons and for lead having 82 protons are noteworthy, although for $_{82}Pb^{208}$ the magic number of neutrons may obscure the effect of a magic number of protons. For $_{20}Ca^{48}$, however, there is no marked difference in behavior from that of neighboring nuclei. The points are plotted with

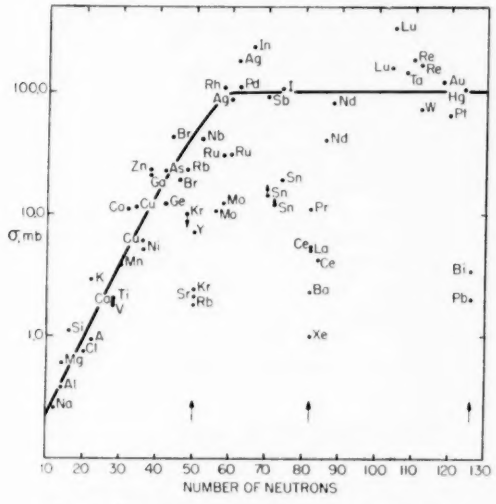

FIG. 4. The cross sections of Fig. 3 as a function of neutron number of target nucleus.

open circles for even Z and solid dots for odd Z to show that there is no obvious regularity in the pattern that may be ascribed to the even-odd character of Z. Quantitatively, it is found that on the average the nuclei of odd Z have a fast cross section that is slightly (35 percent) higher than the nuclei of even Z, if all nuclei that contain magic or near-magic numbers of neutrons or protons are ignored. The 56–60 neutron isotopes just discussed are also omitted in this calculation.

The regular pattern of cross sections as well as the exceptional behavior at magic numbers that is illustrated in Figs. 3, 4, and 5 is directly related to the level densities in the compound nuclei involved. These level densities can be calculated from the observed cross sections and compared with various nuclear models, as well as with other experimental results on level densities.

II. DETERMINATION OF LEVEL DENSITIES FROM CROSS SECTIONS

The fission neutrons have an effective energy[1] for the capture reaction of 1 Mev, and an energy spread sufficiently wide that the cross section is determined by resonance properties averaged over many levels. The cross section in this situation is given[7] by

$$\sigma_l=\pi\lambda^2(2l+1)\frac{2\pi(\Gamma_{nl}\Gamma_{\gamma l})_{Av}}{D_l[(\Gamma_{nl})_{Av}+(\Gamma_{\gamma l})_{Av}]}, \tag{1}$$

where σ_l is the contribution to the cross section of neutrons with angular momentum $l\hbar$ and wavelength λ. Γ_{nl} and $\Gamma_{\gamma l}$ are the neutron and radiation widths respectively of the many levels involved, with "Av" signifying average values, and D_l is the spacing of levels formed by l neutrons.[8] Considering only $l=0$, it is seen that where $\Gamma_n>\Gamma_\gamma$ (neutron energy >10 kev) the variation of cross section with energy will be as $1/E$. As the neutron energy increases further, however, the capture cross section falls off less rapidly as higher l's become important.

The effect of higher l interactions can be illustrated by summing Eq. (1) over all significant l's, remembering that the highest effective l is given by $l\lambda=R$ (the nuclear radius), and that $\sum_0^l(2l+1)=(l+1)^2$. We thus obtain

$$\sigma(n,\gamma)=2\pi^2(\lambda+R)^2\Gamma_\gamma/D, \tag{2}$$

if we assume that D_l (here written as D) is the same for all l's, a form already given by Bethe,[9] which shows that

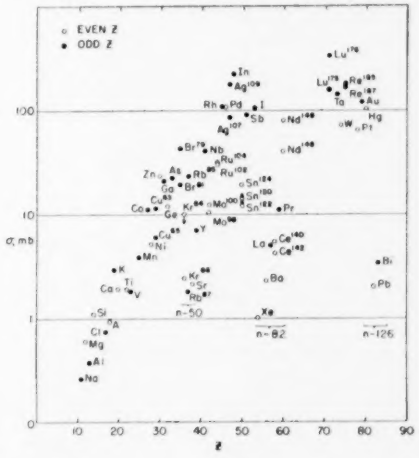

FIG. 5. The cross sections of Fig. 3 as a function of atomic number of target nucleus.

[7] Feshbach, Peaslee, and Weisskopf, Phys. Rev. **71**, 145 (1947).

[8] The spin factor that appears for the cross section of a single resonance becomes unity when averaged over many resonances. The level spacing D_l refers to levels of a single spin and parity value of the compound nucleus, formed by neutrons of angular momentum $l\hbar$.

[9] H. A. Bethe, Phys. Rev. **57**, 1125 (1940).

σ is proportional to $1/E$ if $\lambda > R$, that is, for $l=0$. For this case we have

$$\sigma(n,\gamma) = 2\pi^2\lambda^2\Gamma_\gamma/D_0, \tag{3}$$

which gives the cross section as a simple function of the radiation width and level spacing. Measured cross-section[1] curves near 1 Mev show a definite $1/E$ behavior and hence indicate that $l=0$ interactions predominate, in spite of the fact that λ and R are comparable for 1-Mev neutrons at $A=100$.

When the measured values of the capture cross sections (for the effective energy 1 Mev) are substituted in Eq. (3), together with values of the radiation width, Γ_γ, the average spacing of levels, D_0, can be found. Fortunately the radiation width is known reasonably well, at least for heavy elements. For atomic weights greater than 100, Γ_γ is about 0.1 ev, and is not much affected by changes in excitation energy. Its value increases to several ev for atomic weights near 20. Heidman and Bethe[10] have made an estimate of Γ_γ as a function of A for excitation by neutron capture, and their results are shown in Fig. 6. The level separation thus obtained by use of Eq. (3) refers to levels formed by neutrons for which $l=0$, and to an excitation energy, E^*, of the compound nucleus equal to 1 Mev plus the neutron binding energy, E_B. The neutron binding energies for most nuclei are known to a few hundred kilovolts, and can be computed by means of Fermi's empirical mass formula,[11] with corrections obtained from the summary of experimental data by Harvey.[3]

The values of D_0 calculated from Eq. (3) are listed in Table I, which also includes the isotopic capture cross sections for neutrons of thermal energy that are used in the measurements[1,2,5,6] for neutrons of 1 Mev effective energy. The excitation energy, E^*, the spin of the target nucleus, and the particular activity measured are also tabulated. In a few cases isomeric activities

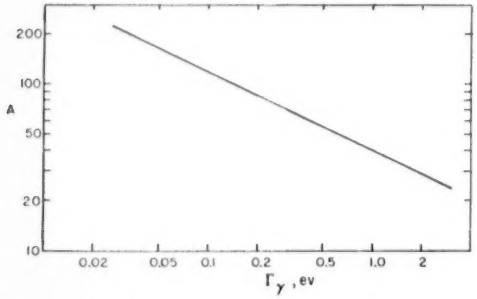

FIG. 6. The radiation width as a function of atomic weight for levels excited by slow neutrons, as given by Heidman and Bethe (see reference 10).

[10] J. Heidman and H. A. Bethe, Phys. Rev. **84**, 274 (1951); our use of the radiation width estimated by these authors is not legitimate for $A<40$ because of their use of the fast capture cross section data itself in that region in determination of the widths.

[11] N. Metropolis and G. Reitwiesner, *Table of Atomic Masses* (Argonne National Laboratory, Lemont, Illinois, 1950).

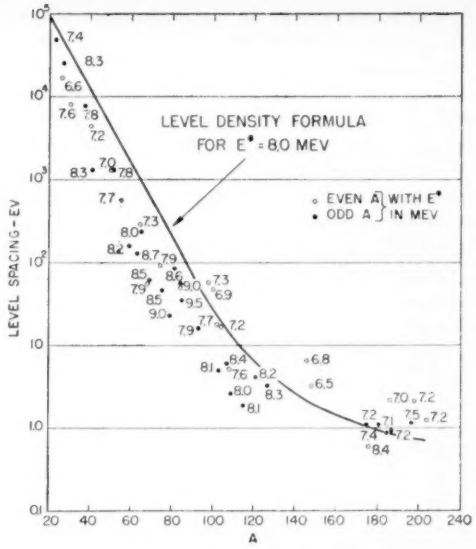

FIG. 7. Level spacings for "normal" (nonmagic-number) nuclei calculated from experimental cross sections, compared with the prediction of the statistical model for 8-Mev excitation. The actual excitation energies of the individual isotopes are also given.

result and it is necessary to add these activities to obtain the complete (n,γ) cross section. For Sn^{120} and Sn^{122} only lower limits for the latter were obtained because the long-lived isomeric states have not been measured, while in several other cases the thermal isomeric ratio was assumed to hold for the fast cross sections.

III. COMPARISON OF LEVEL DENSITIES WITH NUCLEAR MODELS

It is of interest to compare the average level spacings obtained from the measured fast cross section with the predictions of various theoretical models. In particular, it is of great interest to see to what extent the statistical model is evidenced as contrasted to the shell model that seems to be valid for ground and low-lying levels. The statistical model of the excited nucleus leads to the familiar formula:

$$W(E) = c\exp[2(aE^*)^{\frac{1}{2}}] = 10^6/D_0, \tag{4}$$

where $W(E)$ is the level density, or the average number of levels per Mev while a and b are parameters. The parameters, which vary with atomic weight, are determined[12] from experimental values of D_0 for levels excited by neutrons slightly above thermal energy ($E^* = E_B$) and for levels near ground ($E^* \sim 1$ Mev).

The predicted level spacing may be compared with the experimental values for *normal* (nonmagic-number) nuclei very easily because the neutron binding energy of each nucleus measured is about 7 Mev. Using the

[12] J. M. Blatt and V. F. Weisskopf, *Theoretical Nuclear Physics* (John Wiley and Sons, New York, 1952), pp. 371–374.

TABLE I. Measured isotopic activation cross sections for fission neutrons (effective energy 1 Mev). Also listed are the thermal activation cross sections[a] and level spacings (D_0) at excitation energy E^*.

Target nucleus	Neutron number	Spin	Half-life	σ thermal (b)	σ fast (mb)	E^* (Mev)	D_0 (ev)
$_{11}Na^{23}$	12	3/2	15 hr	0.49	0.26	7.39	4.8×10^4
$_{12}Mg^{25}$	14	0	9.6 min	0.049	0.6	6.61	1.7×10^4
$_{13}Al^{27}$	14	5/2	2.3 min	0.215	0.37	8.3	2.5×10^4
$_{14}Si^{30}$	16	0	2.7 hr	0.12	1.1	7.6	8.0×10^3
$_{17}Cl^{37}$	20	3/2	38 min	0.56	0.74	7.8	6.6×10^3
$_{18}A^{40}$	22	0	1.8 hr	1.2	0.93	7.22	4.4×10^3
$_{19}K^{41}$	22	3/2	12.4 hr	1.0	2.9	8.27	1.3×10^3
$_{20}Ca^{48}$	28	0	8.5 min	1.1	1.9	5.35	1.5×10^3
$_{22}Ti^{50}$	28	0	6 min	0.14	1.9	7.01	1.3×10^3
$_{23}V^{51}$	28	7/2	3.9 min	4.5	1.8	7.81	1.3×10^3
$_{25}Mn^{55}$	30	5/2	2.6 hr	12.6	3.82	7.73	5.4×10^2
$_{27}Co^{59}$	32	7/2	11 min	14	4.6	8.22	1.6×10^2
			5 yr	20	... } 11.0[b]		
$_{28}Ni^{64}$	36	0	2.6 hr	2.6	5.1	7.34	2.9×10^2
$_{29}Cu^{63}$	34	3/2	12.9 hr	4.0	11.4	8.74	1.3×10^2
$_{29}Cu^{65}$	36	3/2	4.3 min	2.0	6.0	8.00	2.4×10^2
$_{30}Zn^{68}$	38	0	52 min	1.0	8.0	7.90	56
			14 hr	0.1	15.2 } 23.2		
$_{31}Ga^{69}$	38	3/2	20 min	1.4	20.9	8.51	63
$_{32}Ge^{74}$	42	0	82 min	0.45	12	7.93	92
$_{33}As^{75}$	42	3/2	27 hr	4.1	22.5	8.51	47
$_{35}Br^{79}$	44	3/2	18 min	8.5	29	9.03	23
			4.4 hr	2.9	13.5 } 42.5		
$_{35}Br^{81}$	46	3/2	36 hr	2.5	17	8.62	85
$_{36}Kr^{84}$	48	0	4 hr	0.1	1.9	9.01	>50
			10 yr	0.06	<8 } <10		
$_{36}Kr^{86}$	50	0	78 min	0.06	2.4	6.17	3.1×10^2
$_{37}Rb^{85}$	48	5/2	19.5 day	0.72	23.1	9.50	35
$_{37}Rb^{87}$	50	3/2	17.5 min	0.12	1.8	6.67	4.1×10^2
$_{38}Sr^{88}$	50	0	53 day	0.005	2.1	7.12	3.8×10^2
$_{39}Y^{89}$	50	1/2	61 hr	1.38	7.0	7.63	1.1×10^2
$_{41}Nb^{93}$	52	9/2	6.6 min	1.1	41	7.94	16
$_{42}Mo^{98}$	56	0	67 hr	0.13	10.4	7.32	58
$_{42}Mo^{100}$	58	0	15 min	0.18	12.3	6.87	47
$_{44}Ru^{102}$	58	0	42 day	1.2	30	7.67	18
$_{44}Ru^{104}$	60	0	4 hr	0.7	31	7.21	17
$_{45}Rh^{103}$	58	1/2	44 sec	137	94	8.12	5
			4.2 min	12	15.4 } 109		
$_{46}Pd^{108}$	62	0	13 hr	7.7	108	7.60	5.3
$_{47}Ag^{107}$	60	1/2	2.3 min	32	85	8.41	6
$_{47}Ag^{109}$	62	1/2	25 sec	84	174	8.03	2.7
			225 day	2.2	... } 178*[b]		
$_{49}In^{115}$	66	9/2	13 sec	52	57	8.09	1.9
			54 min	145	166 } 223		
$_{50}Sn^{120}$	70	1/2	27.5 hr	0.13	14	7.82	<29
			>400 day	...	... } >14		
$_{50}Sn^{122}$	72	5/2	40 min	0.16	12	7.63	<32
			126 day	...	... } >12		
$_{50}Sn^{124}$	74	7/2	9.5 min	0.15	15	7.38	19
			9.4 day	0.005	4 } 19		
$_{51}Sb^{121}$	70	5/2	2.8 day	6.8	90	8.18	4.2
$_{53}I^{127}$	74	5/2	27 min	6.7	105	8.33	3.3
$_{54}Xe^{136}$	82	0	3.9 min	0.15	1.0	5.65	3.02×10^2
$_{56}Ba^{138}$	82	0	86 min	0.5	2.3	6.26	1.35×10^2
$_{57}La^{139}$	82	7/2	40 hr	8.4	5.0	6.55	63
$_{58}Ce^{140}$	82	0	28 day	0.27	5.4	6.85	52
$_{58}Ce^{142}$	84	0	33 hr	0.85	4.2	6.54	65
$_{59}Pr^{141}$	82	5/2	19 hr	11.2	11.0	7.15	26
$_{60}Nd^{146}$	86	0	11 day	1.8	40	6.78	6.7
$_{60}Nd^{148}$	88	0	1.7 hr	3.7	80	6.46	3.3
$_{71}Lu^{175}$	104	7/2	3.7 hr	25	158	7.19	1.1
			10^{10} yr	(small)	... } 158[b]		
$_{71}Lu^{176}$	105	7/2	6.7 day	4000	330	8.42	0.5
$_{73}Ta^{181}$	108	7/2	16 min	0.02	... } 142[b]	7.12	1.13
			117 day	21	142	7.01	2.18
$_{74}W^{186}$	112	0	25 hr	40	71	7.40	0.87
$_{75}Re^{185}$	110	5/2	90 hr	101	180	7.23	0.93
$_{75}Re^{187}$	112	5/2	18 hr	75	165	7.16	2.14
$_{78}Pt^{198}$	120	0	31 min	3.9	64	7.52	1.15
$_{79}Au^{197}$	118	3/2	2.7 day	95	120	7.19	1.26
$_{80}Hg^{204}$	124	0	5.5 min	0.43	102	5.06	61
$_{82}Pb^{208}$	126	0	3.3 hr	0.0006	2.0	5.27	35
$_{83}Bi^{209}$	126	9/2	5 day	0.017	3.4		

[a] U. S. Atomic Energy Commission Report AECU-2040 (Office of Technical Services, Dept. of Commerce, Washington, D. C., 1952).
[b] It is assumed that the isomeric ratio is the same for both thermal and fast activations.

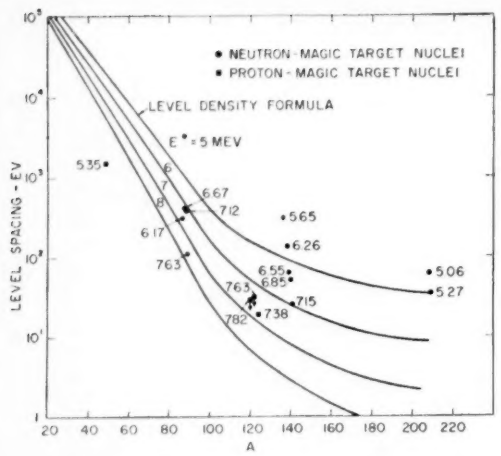

FIG. 8. Level spacings for magic and near-magic number nuclei calculated from experimental cross sections, compared with predictions of statistical model for several excitation energies. Actual excitation energies for individual isotopes are given by number. ●—Magic-N target nuclei. ■—Magic-Z target nuclei.

average value for E^* of $7+1$ Mev in Eq. (4), we obtain a curve that shows the variation of D_0, the average level spacing for this excitation energy, with atomic weight. This curve is shown in Fig. 7, together with the level spacings obtained from Eq. (3) for the individual isotopes. Beside each point is listed its individual excitation energy, which is usually near 8 Mev. The points are seen to follow the pattern of the computed curve with good general agreement, especially when allowance is made for the deviation of the actual values of E^* from the 8-Mev average represented by the curve. As the experimental error is of the order of 50 percent, no significance can be attached to variations of this magnitude for individual cross sections. The theoretical level spacing is about right for $A>150$ but rises above the experimental points with decreasing A, reaching a factor of about five at $A=20$. Actually, considering the approximate nature of the level density formula[12] and the fact that it was adjusted to fit levels in a lower energy region, we see that the agreement exhibited in Fig. 7 is satisfactory, especially at high A.

Before discussing the magic-number nuclei, which were omitted from Fig. 7, it is of value to consider several other characteristics of the spacings of the "normal" nuclei. From the observed cross sections for nuclei of different spins, we can ascertain if the level density increases with spin of the levels. The high-spin target nuclei of Table I however, three of spin 9/2 and seven of spin 7/2, show the same level spacing as the low-spin nuclei. This finding cannot be explained by a large Γ_γ that cancels a large D_0 because slow neutron resonances of these isotopes have normal values of Γ_γ (~ 0.1 ev). The equality of level spacing for different spins is not in agreement with the suggestion[13,14] that the level density is proportional to $(2J+1)$, where J is the spin of the compound nucleus.

As the nuclei of Table I are approximately equally divided between even and odd Z, it is possible to obtain a reasonably accurate estimate of the effect of even-odd Z on level density. The neutron binding energy (hence E^*) is not affected by the odd-even nature of Z, hence any difference in cross section depending on Z would indicate a corresponding difference in level spacing at the same excitation energy. The cross sections of Fig. 5 do not indicate a large difference between even and odd Z, omitting magic-number nuclei, and calculation shows that the odd-Z nuclei are higher on the average by only 35 percent, an amount of doubtful significance. A more sensitive test of Z-dependence of level spacing is furnished by the magic-Z nuclei to be discussed. As the binding energy of a neutron to an odd-*neutron* nucleus is higher than to a even-neutron nucleus, a higher excitation energy and cross section is expected. The only example studied is Lu^{176}, which has a cross section at least twice normal, in agreement with its high neutron binding energy.

In the case of magic-N target nuclei, it is necessary to consider their anomalously low neutron binding energy, which accounts for most of the decrease in cross section for these nuclei relative to their normal neighbors. As magic-Z nuclei exhibit normal neutron binding energies, no cross-section decrease for this reason, analogous to that for magic-N nuclei, is expected. In Fig. 8 are shown curves calculated from Eq. (4) for values of E^* ranging from 5 to 8 Mev, together with experimental level spacings for nuclei resulting from target nuclei containing a magic number of neutrons or protons. In the majority of cases it is noted that the level spacing calculated from the experimental cross sections for nuclei with a magic number of neutrons exceeds the value predicted by the statistical model by as much as a factor of two or three, and in some instances by as much as six. Thus, whereas the low binding energy of magic-N nuclei accounts for a large part of their decrease in cross section, the remaining discrepancy of Fig. 8 implies that the level spacing in the compound nuclei (magic plus one neutron) is larger than predicted by Eq. (4) by a factor of about four. This anomaly would be even larger if the theoretical level spacings were reduced to conform better to the experimental spacing observed for normal nuclei.

The few magic-Z nuclei ($Z=50$) of Fig. 8, with approximately normal values of E^*, have level spacings greater than expected from the theoretical level density formula (again allowing for a reduction in theoretical spacing to conform with normal nuclei). This result indicates that the level spacing in these target magic-Z nuclei is greater than predicted by the statistical model, as for the magic-N case. The spacing for $_{20}Ca^{48}$

[13] L. Wolfenstein, Phys. Rev. **82**, 690 (1951).
[14] W. Hauser and H. Feshbach, Phys. Rev. **87**, 366 (1952).

is actually less than expected; hence $Z=20$ does not seem to exhibit magic behavior. Since the number of neutrons is twenty-eight in this nucleus, it is of interest to note that there is no evidence from this result that twenty-eight is a magic number, as is also shown by $_{22}Ti^{50}$ and $_{23}V^{51}$.

It is thus seen from the results with magic-number nuclei that the level spacing is greater than predicted by the statistical model for those nuclei containing one neutron in addition to a closed shell, whether the shell is composed of protons or neutrons. A wide level spacing also exists for these particular nuclei for excitation energies about one Mev lower, as shown by the sparse resonance level structure measured[15] with slow neutrons. The difference in behavior between these and the normal nuclei is evidence for the effect of shell structure on the level spacing, which spacing we have interpreted in terms of the statistical model for normal nuclei. The simultaneous appearance of features of the statistical and the shell model, which models seem contradictory in their main features, has been the subject of several recent studies that have attempted to correlate the features of the two models.[16–20]

There are several methods, more or less equivalent, of reconciling the shell and statistical models with regard to the level spacing at high excitation that is our concern. Perhaps the simplest approach is to consider that the ground state energy of a nucleus possesses the shell characteristics; this approach explains why the binding energy of a neutron to a magic-N nucleus is low. The anomalous level density at the appropriate excitation energy of the nucleus formed, however, requires additional explanation. The observed low density of levels can be explained by assuming that energy is necessary to break the shell structure, with the result that the normal level density is not reached until several Mev higher excitation energy. This effect can be taken into account crudely by substituting the expression E^*-E_s in the level density formula for E^*, where E_s is the energy that must be added to the nucleus to break the shell. The present results for the magic-Z and magic-N target nuclei make it appear that E_s is very roughly the same for proton and neutron shells, and in magnitude about 1–2 Mev.

Another way of looking at the combination of the shell and statistical models is to assume that at high excitation energy the statistical model is valid, and that all similar weight nuclei will have the same spacing at an energy measured relative to a fictitious ground state energy,[20] whose location corrects for the shell effects, rather than the actual ground state. At first approximation, this energy state would be a smooth function of N and Z and most simply can be considered just the energy value given by the semiempirical mass formula.[11] According to this picture, magic-number nuclei have a lower ground-state energy than the formula predicts because of shell effects. The actual mass formula is somewhat arbitrary, of course, and as usually expressed,[11] individual nuclei are sometimes below and sometimes above the formula prediction; thus certain nuclei would have their ground-state energies raised, others depressed, by shell effects. The two models we have described here of course consist of equivalent views of the interpolation between the first excited states, which exhibit shell properties, to higher excitation energies where the statistical variation of level density with energy seems to be correct.

The view that the ground state is depressed for magic-number nuclei is applied by Blatt and Weisskopf[21] to the level spacings appropriate for neutron capture. The results obtained from their diagram (p. 766), however, differ in several respects from the present experimental level spacings. Thus the high spacing in a compound nucleus consisting of a magic-N nucleus plus one neutron is ascribed to the binding energy shift alone, whereas an additional change in level spacing is indicated by the experimental cross sections. Also, neutron capture in a magic-N *or* magic-Z nucleus is predicted to give the same level spacing (hence cross section); experimentally the former results in a much larger spacing, however.

The level spacings obtained in this work from the fast capture cross sections will be useful in a comparison with the directly measured spacings now becoming available with recently improved velocity selectors. These instruments are able to resolve the individual resonances for slow neutrons in sufficient numbers to give directly measured level spacings at excitation energies one million volts below those used in the present work. The comparison will give a valuable check on the assumed radiation widths in the present study and also help to clarify the effect of higher l's in the Mev work because only $l=0$ collisions are possible at the lower energy. Comparison of the same nuclei at one Mev and low energy will also be useful in the case of certain isotopes that seem to have unusually great spacings as measured with velocity selectors.

We would like to acknowledge the help of W. Kato in some of the recent measurements. Discussions with V. Weisskopf and H. Feshbach have been of great assistance in the interpretation of the results.

[15] *Neutron Cross Sections*, Atomic Energy Commission Report AECU-2040 (Office of Technical Services, Dept. of Commerce, Washington, D. C., 1952).
[16] V. F. Weisskopf, Helv. Phys. Acta **23**, 187 (1950).
[17] I. G. Weinberg and J. M. Blatt, Am. J. Phys. **21**, 124 (1952).
[18] D. L. Hill and J. A. Wheeler, Phys. Rev. **89**, 1102 (1953).
[19] Feshbach, Porter, and Weisskopf, Phys. Rev. **90**, 166 (1953).
[20] H. Hurwitz and H. A. Bethe, Phys. Rev. **81**, 898 (1951).
[21] Reference 10, pp. 763–767.

Application of the *jj*-Coupling Model to Moderately Light Nuclei*

DIETER KURATH†
Department of Physics, University of Chicago, Chicago, Illinois, and Argonne National Laboratory, Lemont, Illinois
(Received June 8, 1953)

An investigation based on the strong spin-orbit coupling model is made for nuclei in the $1d_{3/2}$ and $1f_{7/2}$ shells. Hartree-Fock wave functions and central forces are used in calculating ground state spins and binding energy differences. Coupling rules are found for configurations of identical nucleons and for the simplest odd-odd nuclei. Approximate wave functions are constructed for odd-A and even-even nuclei having both neutrons and protons in the $1f_{7/2}$ shell. Binding energy differences, magnetic moments, and beta decay matrix elements are calculated with these functions. The result of comparing binding energy differences with experiment is interpreted as favoring strong spin-orbit coupling over weak spin-orbit coupling.

I. INTRODUCTION

THE hypothesis of strong spin-orbit coupling,[1] the basis of the *jj* model, has been quite successful in explaining the shell structure of nuclei, and in accounting for observed spins and magnetic moments. For this reason a more detailed investigation has been made to see whether there are other experimental features of nuclear structure contained in the model.

In an earlier paper,[2] the model was applied to the $1p$ shell which is filled in between $_2$He^4 and $_8$O^{16}. The results were compared with those of a previous calculation[3] based on the hypothesis of weak spin-orbit coupling, the *LS* model. Neither model presents a consistently better picture of the experimental results than the other, but there is a tendency for the *LS* model to be preferable for the light nuclei in the shell, while the *jj* model is better for the heavier nuclei.

In going to heavier nuclei, the next region where the filling of shells is unambiguous is the $1d_{3/2}$ shell from $_{16}$S^{32} to $_{20}$Ca^{40} and the $1f_{7/2}$ shell from $_{20}$Ca^{40} to $_{28}$Ni^{56}. The first part of the paper treats the order of nuclear energy levels in this region for configurations of identical nucleons and for odd-odd nuclei involving only two nucleons or a nucleon and a hole in a shell. The latter category contains the interesting nuclei, $_{17}$Cl^{36} and $_{19}$K^{40}, whose spins have been measured.

The second part of the paper treats the ground states of the odd mass number and even Z-even mass number nuclei in the $1f_{7/2}$ shell. Approximate wave functions are constructed for those configurations not consisting of identical nucleons in the shell. Binding energies, magnetic moments, and ft values are computed. In particular, the binding energy differences of isobars are related to the symmetry properties of the wave functions. The symmetry properties depend on the strength of spin-orbit coupling, and the experimental evidence is shown to favor strong coupling.

II. METHOD OF CALCULATION

The calculations are carried out with Hartree-Fock wave functions. While there are objections[4] to the use of such functions, wherein the total wave function is represented by the product of individual nucleon functions, this procedure offers the only feasible means of calculation, and presents reasonable values for spins and magnetic moments.

Two fundamental assumptions are employed in constructing the wave functions:

(1) The Hamiltonian is symmetric to the exchange of any two nucleons, which allows the separation of the wave function into the product of a space spin function and an isotopic spin function. This assumption of the equality of $p-p$, $n-p$, and $n-n$ forces makes the isotopic spin T a good quantum number. The effect of Coulomb forces for determining the wave functions is also assumed to be negligible, which should be a valid approximation since the nuclei treated are rather light.

(2) The intrinsic spin and orbital angular momentum of each individual nucleon are strongly coupled so that the individual particle energy for the state $j=l+\frac{1}{2}$ lies considerably below that for $j=l-\frac{1}{2}$.

The single particle wave functions are taken to be those resulting from a central harmonic oscillator potential. The state of orbital angular momentum l is then represented by the product of a spherical harmonic and a radial wave function. The radial dependence for states encountered in this calculation is given by the functions with no nodes:

$$R_l(r)=N_l r^l \exp[-(r/r_l)^2], \qquad (1)$$

where N_l is a normalization factor. The parameter r_l in the oscillator function can be chosen in such a way as to make the function quite similar to that function resulting from a square-well potential with constants

* Much of this material is contained in a thesis submitted to the University of Chicago in partial fulfillment of the requirements for the degree of Doctor of Philosophy (August 1951).
† Present address: Argonne National Laboratory, Lemont, Illinois.
[1] M. G. Mayer, Phys. Rev. **75**, 1969 (1949); Haxel, Jensen, and Suess, Phys. Rev. **75**, 1766 (1949).
[2] D. Kurath, Phys. Rev. **88**, 804 (1952).
[3] E. Feenberg and E. Wigner, Phys. Rev. **51**, 95 (1937); E. Feenberg and M. Phillips, Phys. Rev. **51**, 597 (1937).
[4] H. A. Bethe and R. F. Bacher, Revs. Modern Phys. **8**, 149 (1936).

TABLE I. Coefficients in the potential energy expressions, $(\alpha_0+\alpha_1x+\alpha_2x^2+\alpha_3x^3)K$ and $(\beta_0+\beta_1x+\beta_2x^2+\beta_3x^3)K$, where $x=\rho^4/4(1+\rho^2)$, $\rho=r_I/r_0$ and $K=(A_0/735)(1+\rho^2)^{-9/2}$.

	α_0	α_1	α_2	α_3	β_0	β_1	β_2	β_3
$(1f_{7/2})^2$								
$I=6$	−525	−2520	−630	2100	735	5040	6930	2100
4	−195	−2124	−1425	4212	735	5040	10 494	4212
2	15	−360	−4950	8580	735	8820	18 810	8580
0	105	2268	12 474	36 036	735	11 340	37 422	36 036
$(1f_{7/2})^3$								
$I=15/2$	−1350	−7290	−2430	7740	2205	15 120	23 220	7740
11/2	−930	−5526	−5958	12 948	2205	18 270	32 796	12 948
9/2	−765	−6120	−4770	12 420	2205	16 290	31 410	12 420
7/2	−630	−2772	5544	36 036	2205	21 420	51 282	36 036
5/2	−525	−3528	−9954	18 564	2205	22 050	43 218	18 564
3/2	−450	−5238	−6534	15 444	2205	17 550	36 828	15 444
$(1f_{7/2})^4$								
$I=8$	−2340	−13 428	−7164	19 224	4410	32 040	53 208	19 224
6	−1890	−10 332	−2016	38 136	4410	36 540	72 072	38 136
5	−1710	−11 664	−10 692	25 272	4410	34 560	64 044	25 272
4	−1560	−9684	−14 652	29 832	4410	39 060	72 864	29 832
4	−1560	−9936	−2808	40 248	4410	36 540	75 636	40 248
2	−1350	−11 448	−11 124	27 144	4410	34 020	67 068	27 144
2	−1350	−8172	−6336	44 616	4410	40 320	83 952	44 616
0	−1260	−5544	11 088	72 072	4410	42 840	102 564	72 072

fitting experimental observations. In this way the differences resulting from the use of these two central potential wells can be minimized.

These orbital functions are then coupled with intrinsic spin functions in linear combinations that have individual particle eigenvalues $j=l\pm\frac{1}{2}$. The individual particle eigenfunctions are multiplied by isotopic spin functions and combined into many-particle Hartree-Fock wave functions having total angular momentum I and isotopic spin T. The procedure is illustrated in Appendix III.

With these wave functions as zero-order functions, the potential energy of two-body interactions can be calculated as a first-order perturbation. If the nuclear interactions are restricted to be charge independent static central forces, the general interaction of two nucleons is[5]

$$[C_0+C_1(\boldsymbol{\sigma}_1\cdot\boldsymbol{\sigma}_2)+C_2(\boldsymbol{\tau}_1\cdot\boldsymbol{\tau}_2)+C_3(\boldsymbol{\sigma}_1\cdot\boldsymbol{\sigma}_2)(\boldsymbol{\tau}_1\cdot\boldsymbol{\tau}_2)]J(r_{12}), \quad (2)$$

where $\boldsymbol{\sigma}$ and $\boldsymbol{\tau}$ are the ordinary spin and isotopic spin vectors, respectively, and $J(r_{12})$ is the spatial dependence. The interaction can be alternatively expressed in the form of exchange interactions

$$[W+MP_{12}+BQ_{12}+HP_{12}Q_{12}]J(r_{12}), \quad (3)$$

where P_{12} and Q_{12} are the operators that exchange the space coordinates and spin coordinates respectively for particles 1 and 2. The coefficients identify the usual name for the interaction, Wigner, Majorana, Bartlett, and Heisenberg. The wave functions are antisymmetric to the complete exchange of two nucleons, so that if one introduces the operator R_{12} which exchanges the charge of two nucleons, all wave functions obey the relationship

$$P_{12}Q_{12}R_{12}\psi=-\psi. \quad (4)$$

The coefficients in (2) and (3) are connected by the relationships for antisymmetric wave functions:

$$\begin{aligned} Q_{12}&=\tfrac{1}{2}(1+\boldsymbol{\sigma}_1\cdot\boldsymbol{\sigma}_2),\\ P_{12}Q_{12}&=-R_{12}=-\tfrac{1}{2}(1+\boldsymbol{\tau}_1\cdot\boldsymbol{\tau}_2),\\ P_{12}&=-\tfrac{1}{4}(1+\boldsymbol{\sigma}_1\cdot\boldsymbol{\sigma}_2)(1+\boldsymbol{\tau}_1\cdot\boldsymbol{\tau}_2). \end{aligned} \quad (5)$$

Therefore, by calculating the energies for the four possible interactions (1, P_{12}, Q_{12}, and $P_{12}Q_{12}$), one can obtain the result for any central-force interaction. The central-force solution of the deuteron, where $P_{12}=1$, requires that $W+M\approx0.8$ and $H+B\approx0.2$ in order to account for the difference of singlet and triplet potentials for low energy neutron-proton scattering. Aside from this restriction, the coefficients are rather uncertain.

For the spatial dependence of the interaction, the negative Gaussian is used:

$$J(r_{12})=A_0\exp[-(r_{12}/r_0)^2]. \quad (6)$$

The parameters A_0 and r_0 are related from the determination of the deuteron binding energy.[6] This function provides easy variation of the range of interaction, r_0, and in the limit as r_0 goes to zero it behaves like a delta function. In this limit the ambiguity in exchange mixture is removed since P_{12} approaches unity, and one can also check results of previous delta function calculations. The method of calculating the interaction integrals plus a tabulation of these integrals is presented in Appendix I.

[5] E. Wigner and L. Eisenbud, Proc. Nat. Acad. Sci. U. S. **27**, 281 (1941).

[6] H. A. Bethe, Revs. Modern Phys. **8**, 111 (1936).

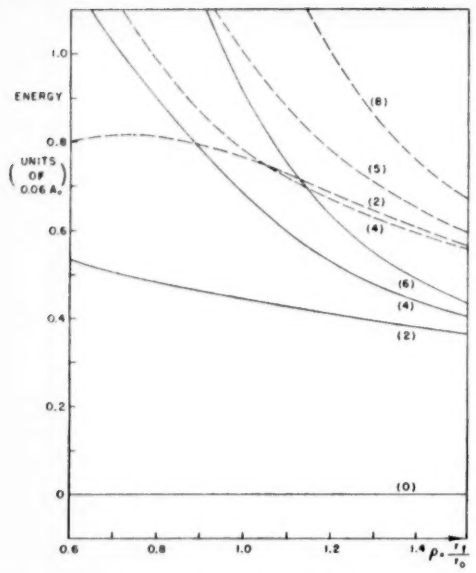

FIG. 1. Order of energy levels of the $(1f_{7/2})^2$ and $(1f_{7/2})^4$ configurations for the interaction (8) as a function of ρ, the ratio of nuclear size parameter to range of nuclear forces. Solid lines are levels appearing in both configurations; broken lines are additional levels for $(1f_{7/2})^4$.

III. DETERMINATION OF GROUND STATES

A. Identical Nucleons

The ordering of energy levels for a given nucleus depends only on the interactions among the nucleons outside closed shells. In configurations where the nucleons in unfilled shells are identical, the predictions of ground state spins have been given for the cases of delta function[7] and infinite range[8] forces. The two approximations give a spin of zero for an even number of identical nucleons or holes, but for an odd number they differ in all but the trivial cases of a single particle or hole in a shell. Since the $1d_{3/2}$ shell contains no configurations where the predictions differ, only the $1f_{7/2}$ shell is treated.

Since the $1f_{7/2}$ shell is filled above $_{20}Ca^{40}$, the nuclei having an unfilled shell of identical $1f_{7/2}$ nucleons are the Ca isotopes, and those nuclei with filled $1f_{7/2}$ neutron shells, $_{21}Sc^{49}$, $_{22}Ti^{50}$, $_{23}V^{51}$, $_{24}Cr^{52}$, $_{25}Mn^{53}$, $_{26}Fe^{54}$, $_{27}Co^{55}$, and $_{28}Ni^{56}$. The potential energy of interaction among $1f_{7/2}$ nucleons is all that splits the levels, so the theory of holes says that the level order for n identical particles is the same as that for n identical holes. Therefore the only configurations one needs in order to study the level splitting are $(1f_{7/2})^2$, $(1f_{7/2})^3$, and $(1f_{7/2})^4$.

For identical nucleons, the charge-exchange operator R_{12} has the eigenvalue one, so from (4) we see that $P_{12}Q_{12}=-1$ or $P_{12}=-Q_{12}$. The level order for the configurations is obtained using the finite range interaction integrals of Appendix I. The general expression of the potential energy of a level is

$$E=(M-B)(\alpha_0+\alpha_1x+\alpha_2x^2+\alpha_3x^3)K + (W-H)(\beta_0+\beta_1x+\beta_2x^2+\beta_3x^3)K, \quad (7)$$

where W, M, B, and H are the strengths of 1, P_{12}, Q_{12}, and $P_{12}Q_{12}$ exchange, respectively. As shown in the appendix, K and x involve the parameters A_0, r_0, of the Gaussian interaction and the oscillator wave function parameter, r_f. The coefficients α_i and β_i are tabulated for the various levels in Table I.

The level order depends on the quantity $\rho=r_f/r_0$, the ratio of the range of a $1f_{7/2}$ nucleon to the range of nuclear forces. Some possible exchange mixtures are:

$$[0.8P_{12}+0.2Q_{12}]J(r_{12}), \text{ Majorana plus Bartlett}; \quad (8)$$

$$P_{12}[0.8+0.2Q_{12}]J(r_{12}), \text{ Majorana plus Heisenberg}; \quad (9)$$

$$\tfrac{1}{2}[1+P_{12}][0.8+0.2Q_{12}]J(r_{12}), \text{ Serber mixture}. \quad (10)$$

The space exchange part of (10) comes from the present interpretation[9] of high-energy neutron-proton scattering, although such a potential violates the saturation requirements for nuclear forces.

The level order of the various configurations is presented as a function of ρ in Figs. 1 and 2 for the interaction (8). For an even number of nucleons, the ground state has $I=0$ and is well separated from the first excited state 2 for all ranges. This is true for any exchange mixture that is not predominantly spin dependent. For three nucleons (or holes) there is a crossing

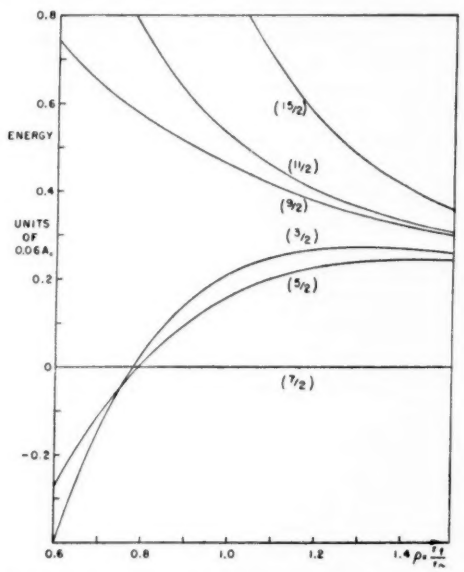

FIG. 2. Order of energy levels of the $(1f_{7/2})^3$ configuration as a function of ρ for the interaction (8).

[7] M. G. Mayer, Phys. Rev. **78**, 22 (1950).
[8] G. Racah, Phys. Rev. **78**, 622 (1950).
[9] R. S. Christian and E. W. Hart, Phys. Rev. **77**, 441 (1950).

of the 7/2 level with those of lower I. The position of crossover depends on the exchange mixture, and the ground state of $(1f_{7/2})^3$ is listed as a function of ρ for several mixtures in Table II.

In order to estimate a value for ρ corresponding to existing nuclei, the parameter r_f is determined by comparing the oscillator wave function with a square-well wave function whose constants are determined from the experimental evidence in this region of masses:

Atomic mass number, $A=43$.
Nuclear radius $=1.48\times10^{-13}A^{\frac{1}{3}}$ cm $=5.19\times10^{-13}$ cm.
Binding energy of last nucleon $=8$ Mev.

For $r_f\approx2.9\times10^{-13}$ cm, the two wave functions are quite similar. If the range of nuclear forces r_0 for a Gaussian potential is assumed to be about 2.8×10^{-13} cm, the ratio $\rho\approx1$. This is near the region of crossing, but would tend to favor $I=7/2$ as ground state. The use of a Yukawa spatial dependence shifts the crossover region so that an I of 7/2 is heavily favored; for the Serber exchange mixture (10), 7/2 would be low for all ranges. The singularity of the Yukawa potential at the origin, which makes it similar to a delta function, accounts for this behavior, as has been pointed out by Talmi,[10] who used a Yukawa dependence with Majorana exchange. Similar level order calculations have recently been published by Flowers and Edmonds,[11] using an elegant group theoretical approach and covering other configurations as well.

The behavior of the levels as given by the Gaussian calculation has some similarity to experimental facts. It presents a possible explanation[12] of the spin of 3/2 observed in the $(1d_{5/2})^3$ configuration of Na^{23}. The fact that the $(1f_{7/2})^3$ configuration of V^{51} has a measured spin of 7/2 while the $(1f_{7/2})^{-3}$ configuration of Mn^{55} is measured as 5/2 can be interpreted as evidence that these nuclei are near the region of level crossing. In the $1g_{9/2}$ shell there is strong experimental evidence that there is a state, 7/2 (even parity), that competes with the 9/2 level in configurations of 3, 5, or 7 nucleons. These are the configurations where a generalization of the calculation results would lead one to expect crossovers with the 7/2+ state being one which drops below 9/2 as one goes from large to small values of r_g/r_0. However, one would also expect the levels 5/2+ and 3/2+ to be low-lying states in configurations $(1g_{9/2})^{3 \text{ or } 7}$, and one would expect 1/2+ in addition to these for $(1g_{9/2})^5$. These have not been observed in any of the numerous nuclei where such configurations occur. Recent explicit calculations of the $(1g_{9/2})^3$ configuration[13] show that 7/2+ is not expected as ground state with the usual central forces, although the level spacing is quite small. Therefore, while the model does contain the possibility of level crossings in those nuclei where such behavior is observed, it does not explain all the observed facts, and further clarification is needed.

TABLE II. Ground state of $(1f_{7/2})^3$ as function of $\rho=r_f/r_0$.

Potential	$I=7/2$	$I=5/2$	$I=3/2$
(8)	$\rho>0.79$	$0.74<\rho<0.79$	$\rho<0.74$
(9)	$\rho>0.90$	...	$\rho<0.90$
(10)	$\rho>0.75$	$0.58<\rho<0.75$	$\rho<0.58$

B. Odd-Odd Nuclei

The question of ground state spins for odd-odd nuclei has been investigated by Nordheim,[14] who found quite good agreement with experimental evidence by using the following hypotheses.

1. The individual configurations of neutrons and protons in odd-odd nuclei are the same as in odd-A nuclei with the same number of nucleons in the odd-particle group.

2. If the odd neutron and proton groups belong to different Schmidt groups, the resultant spin is the difference. $j_1=l_1+\frac{1}{2}$, $j_2=l_2-\frac{1}{2}$ gives $I=|j_1-j_2|$.

3. If the odd neutron and proton groups belong to the same Schmidt group, the resultant spin is high, often the maximum possible.

$j_1=l_1\pm\frac{1}{2}$, $j_2=l_2\pm\frac{1}{2}$ gives I large, often j_1+j_2.

When the odd-odd nucleus has a configuration of a single proton (or proton-hole) in a shell together with a single neutron (or neutron-hole) in a shell, the wave function is determined uniquely by stipulating I. Calculations for such simple configurations in the $1d_{3/2}$ and $1f_{7/2}$ shell were carried out to compare results with the Nordheim rules and with experimental evidence. The energy levels are listed in the tables of Appendix II for the static central force interactions.

The results can be summarized in the following manner. The space-dependent Majorana and Wigner interactions give different predictions for the coupling of two particles (or holes) and the coupling of a particle and a hole. For two particles, the Majorana interaction shows competition between parallel and antiparallel alignment of the j's. It favors antiparallel alignment for vanishing range of nuclear forces but parallel alignment for any reasonable ratio of nuclear size to range of forces. This is shown in Table III where the crossover value of $\rho=r_f/r_0=r_d/r_0$, the ratio of oscillator parameter to nuclear force range, is given. For the nuclei in question it is expected that this ratio is close to unity. Wigner forces would give antiparallel alignment of j's.

However, for the coupling of a particle and a hole, Majorana forces give competition between parallel j alignment and a value of I one unit less. For vanish-

[10] I. Talmi, Phys. Rev. **82**, 101 (1951).
[11] B. H. Flowers, Proc. Roy. Soc. (London) **A212**, 248 (1952); A. R. Edmonds and B. H. Flowers, Proc. Roy. Soc. (London) **A214**, 515; **A215**, 120 (1952).
[12] D. Kurath, Phys. Rev. **80**, 98 (1950).
[13] I. Talmi, Helv. Phys. Acta **25**, 185 (1952); B. H. Flowers, Proc. Roy. Soc. (London) **A215**, 398 (1952).
[14] L. W. Nordheim, Revs. Modern Phys. **23**, 322 (1951).

TABLE III. Coupling of a single neutron with a single proton. The ratio ρ = (nuclear size parameter)/(range of nuclear forces), is expected to be near one in the region of physical interest. $\rho = r_f/r_0 = r_d/r_0$.

Configuration	Nucleus	I_{exp}	Majorana potential I for $\rho=\infty$	Majorana potential I for $\rho=0.1$	Majorana potential Crossover region	Serber potential I
$(1d_{3/2})(1d_{3/2})$	$_{17}Cl^{34}$	...	0	3	$\rho=2.8$	Always 3
$(1d_{3/2})^{-1}(1d_{3/2})^{-1}$	$_{19}K^{38}$	(2 or 3)[a]	0	3	$\rho=2.8$	Always 3
$(1d_{3/2})(1f_{7/2})$	$_{17}Cl^{38}$	(2)[a]	2	5	$\rho=4.3$	5 for $0.4<\rho<1.85$ 2 for $\rho<0.4$, $\rho>1.85$
$(1f_{7/2})(1f_{7/2})$	$_{21}Sc^{42}$	...	0	7	$\rho=2.0$	7 for $\rho<2.5$

[a] Inferred from beta decay.

ing range of nuclear forces ($\rho=\infty$) an I of one unit less than the maximum is favored, while for long-range forces the result is parallel alignment. This behavior is presented in Table IV, and the crossover values of ρ are seen to be considerably smaller than for the particle-particle cases. Wigner forces favor the smaller I, namely the $\rho=\infty$ result. The results for space-dependent interactions do not show any of the dependence on Schmidt line groups postulated by the Nordheim rules.

On the other hand, the spin-exchange Bartlett and Heisenberg interactions do not differentiate between particle-particle and particle-hole couplings. The Bartlett interaction gives results in agreement with the Nordheim rules, and the Heisenberg interaction also gives this agreement but less unequivocally. From the deuteron one expects that space-dependent interaction has a weight of about 0.8 while spin dependence has a weight of about 0.2. So the separation of particle-particle cases from particle-hole cases should be real. The I's expected for an exchange mixture like the Serber potential (10) are given in the last column of Tables III and IV.

In comparing the particle-particle predictions with experimental results Sc^{42} is unknown, and the decay scheme of Cl^{34} cannot be easily interpreted. The allowed decay of K^{38} to the $I=2$ level of A^{38} is consistent with an assignment of 3 for the spin of K^{38}, in agreement with calculation. The spin of Cl^{38} seems to be 2. Here Majorana forces would give 5, but spin-dependent forces favor 2 in agreement with the Nordheim rule. The Serber mixture bring 2 close to 5, but still above it for the region of physical interest $\rho\approx 1$.

For particle-hole coupling there is more certain experimental evidence. The measured I's of Cl^{36} and K^{40} are both one unit less than the maximum for the shell model assignments. These agree with the results of using a Serber potential, although other combinations would give these results also. The spin assignment of 6 for Sc^{48} has been found to be compatible with recent experimental results.[15] A further experimental result of interest[16] is the measured spin of 6 for V^{50}, $[(1f_{7/2})^3 \times (1f_{7/2})^{-1}]$. An extensive calculation[17] of V^{50} also found a spin of 6 for the case of vanishing range of nuclear forces.

The results of this calculation agree with the Nordheim rule for coupling of two $l+\frac{1}{2}$ or two $l-\frac{1}{2}$ particles. For the coupling of an $l+\frac{1}{2}$ particle with an $l-\frac{1}{2}$ particle the Majorana interaction gives parallel and antiparallel j alignment as the low states but favors parallel alignment for expected values of the range parameter ρ. Spin-dependent interactions favor antiparallel alignment, in agreement with Nordheim's rule, but interactions with 20 percent spin dependence still favor parallel alignment. This disagrees with the experimental result for Cl^{38}, which fits the Nordheim rule.

For the coupling of a particle and a hole, the present calculation gives strong evidence for an I of one unit less than that of parallel j alignment regardless of the Schmidt line groups involved. This seems to be in good agreement with experiment and explains K^{40}, an outstanding exception to the Nordheim rule.

The over-all picture for odd-odd nuclei is still obscure. While the calculation of particle-hole coupling seems to fit in well with experimental evidence, the particle-particle results are not well supported. Furthermore, there must be a region of transition from the particle-particle picture to the particle-hole picture as one considers nuclei other than the simple cases treated here, and the calculation becomes formidable. For this reason, odd-odd nuclei are not treated further in this paper.

IV. POTENTIAL ENERGY CONTRIBUTIONS WITHIN THE $1f_{7/2}$ SHELL

When one deals with configurations having both neutrons and protons in unfilled shells, there are generally several states with the same total angular momentum and isotopic spin. The problem of selecting the state presumed to have lowest energy without solving secular determinants is decided as follows.

The ground-state I's are presumed to be 7/2 for odd-A nuclei and 0 for even-even nuclei together with $T=T_z$. Those magnetic moments that have been measured are found to lie near the Schmidt line. The configurations of identical nucleons have calculated magnetic moments on the Schmidt lines, and also have the property that for an $I=7/2$, $M=7/2$ state the configurations consist of an individual particle with $m=7/2$

[15] Hamermesh, Hummel, Goodman, and Engelkemeir, Phys. Rev. **87**, 528 (1952); D. Kurath, Phys. Rev. **87**, 528 (1952).
[16] Kikuchi, Sirvetz, and Cohen, Phys. Rev. **88**, 142 (1952).
[17] A. Hitchcock, Phys. Rev. **87**, 664 (1952).

while the m's of the remaining particles cancel in pairs, (i.e., for every particle in a $+m$ state there is one in a $-m$ state). Similarly the $I=0, M=0$ states are made up of configurations wherein the individual particle m's cancel in pairs. The property that only such configurations occur is assumed to carry over to the ground states of nuclei with both neutrons and protons in the unfilled $1f_{7/2}$ shell. As a result of restriction to such configurations,[18] the quantum numbers I and T serve to determine a wave function uniquely. The validity of this assumption is tested in Appendix III for the case of three $1f_{7/2}$ nucleons where three states with $I=7/2$, $T=1/2$ are possible. Solution of the secular determinant shows that the lowest energy eigenvalue is quite close to that found by calculating the diagonal matrix element with the approximate wave function formed using the procedure stated above.

By constructing the approximate wave functions for all odd-A and even-even nuclei in the $1f_{7/2}$ shell in accordance with these assumptions, as illustrated in Appendix III, one can then calculate diagonal energy matrix elements for the various static central force interactions. The resulting potential energy contributions from within the $1f_{7/2}$ shell can be summarized in the expression:

$$V_n=\left[\frac{n(n+2)-4T(T+1)}{4}\right]b(\rho)+\left[\frac{n-I/(7/2)}{2}\right]D(\rho)+\left[\frac{n(n-2)+I/(7/2)}{4}\right]d(\rho). \quad (11)$$

Here T is the isotopic spin, I the total angular momentum, and n is the number of nucleons in the $1f_{7/2}$ shell. In this expression $b(\rho)$, $D(\rho)$, and $d(\rho)$ are quantities which depend on the interaction potential used and the nuclear size through the ratio of oscillator parameter to range of nuclear forces, $\rho=r_f/r_0$ introduced in Sec. I. Explicit expressions for these quantities are given in Eq. (A8) of Appendix I, but considerable information can be obtained without them. In order to obtain an idea of the physical meaning of the quantities b, d, and D, we notice that for identical particles $T=n/2$, so that b is not present. For two neutrons, $V_2=D$, and for three neutrons, $V_3=D+d$ so that D is the binding of two identical nucleons and d is the amount added when another identical one is present. On the other hand, b arises when both neutrons and protons are present; its coefficient depends on the isotopic spin T, that is, the symmetry properties of the wave functions. It is the only term of V_n that is involved when the difference in binding energy for isobars with the same I is evaluated.

ISOBAR DIFFERENCES

A. Comparison of Calculation and Experiment

The experimentally measured odd-A beta decays in the $1f_{7/2}$ shell consist of one mirror decay, and ten others which have $\log ft$ values around five and are thus allowed transitions. These provide the most accurate experimental data for comparing energy differences with the calculated values. In addition, there are three isobar pairs of even-even nuclei whose mass differences have been measured.

The theoretical binding energy difference consists of two parts:

1. the Coulomb energy difference;
2. the difference in that part of the potential energy term due to interactions of the $1f_{7/2}$ nucleons with themselves.

The Coulomb difference has two contributions, one arising from the repulsion of a $1f_{7/2}$ proton by the protons in the closed shells, and the other coming from the Coulomb interaction of the $1f_{7/2}$ protons with each other. The interaction with the core can be estimated by the change in electrostatic energy of a uniformly charged sphere of nuclear dimensions upon adding a proton

$$\epsilon=(6/5)Ze^2/R. \quad (12)$$

At $_{20}Ca^{41}$, $Z=20$, $R=(1.48\times10^{-13})(41)^{\frac{1}{3}}=5.10\times10^{-13}$ cm; these give a value of $\epsilon=6.75$ Mev. This value is in good agreement with the experimental difference obtained from the mirror decay, $Sc^{41}(\beta^+)Ca^{41}$, where the binding energy difference is the sum of the kinetic energy of the beta particle, the neutron-proton mass difference, and two electron masses. Numerically this is $4.94\pm0.07+0.78+1.02=6.74\pm0.07$ Mev. Therefore, this part of the Coulomb difference is included in the calculation as $\epsilon=6.75(41/A)^{\frac{1}{3}}$ Mev to provide for the dependence on nuclear radius. The electrostatic interaction of the $1f_{7/2}$ protons is calculated in the same way

TABLE IV. Coupling of a single nucleon with a single hole for odd-odd nuclei. The ratio $\rho=$ (nuclear size parameter)/(range of nuclear forces) is expected to be near one in the region of physical interest. $\rho=r_f/r_0=r_d/r_0$.

Configuration	Nucleus	I_{exp}	Majorana potential: I for $\rho=\infty$	Majorana potential: I for $\rho=0.1$	Majorana potential: Crossover region	Serber potential I
$(1d_{3/2})(1d_{3/2})^{-1}$	$_{17}Cl^{36}$	(2)	2	3	$\rho=1.5$	2 for $\rho>0.85$
$(1d_{3/2})^{-1}(1f_{7/2})$	$_{19}K^{40}$	(4)	4	5	$\rho=1.3$	4 for $\rho>0.6$
$(1f_{7/2})(1f_{7/2})^{-1}$	$_{21}Sc^{48}$	...	6	6	6, 7 degenerate at $\rho=0$	6 for $\rho>0.5$ 7 for $\rho<0.5$

[18] These ground states are believed to be identical with those found by B. H. Flowers using the symplectic group. See reference 11.

TABLE V. Energy resulting from electrostatic interaction of the $1f_{7/2}$ protons. The unit of energy is $c=0.76e^2/r_f=[1.10\times10^{-13}/r_f]$ Mev$\approx$0.35 Mev.

Element	Energy
$_{22}$Ti	$1.0c$
$_{23}$V	$2.5c$
$_{24}$Cr	$5.0c$
$_{25}$Mn	$8.1c$
$_{26}$Fe	$12.1c$
$_{27}$Co	$16.6c$

as the interaction due to nuclear forces. However, since the term is small and variations of the term for a group of isotopes are at most 5 percent of the total term, the contribution is listed only for each element. This is done in Table V in units of c, where $c=0.76e^2/r_f$; r_f is the oscillator range parameter. In Sec. III it was estimated that $r_f\approx3\times10^{-13}$ cm for $A=43$; so an average value of c over the shell is $c=0.35$ Mev.

The nuclear part of the interaction of $1f_{7/2}$ particles is given by (11), and it is clear that for isobar differences, $V_n(T-1)-V_n(T)=2Tb(\rho)$. The calculated difference of binding energy is therefore a very simple expression, consisting of a multiple of $b(\rho)$ plus a numerical Coulomb term obtained by using $\epsilon=6.75\times(41/A)^{\frac{1}{3}}$ Mev and $c=0.35$ Mev. The calculated differences are listed in the last column of Table VI.

The experimental binding energy differences are gotten chiefly from beta-decay observations. They are obtained by the equations:

$$\begin{aligned}(\text{B.E.})_{\text{final}}-(\text{B.E.})_{\text{initial}}&=(\text{K.E.})_{\max}\\&\quad+2m_0c^2+({}_0n^1-{}_1\text{H}^1)\text{ for }\beta^+\text{ decay},\\(\text{B.E.})_{\text{final}}-(\text{B.E.})_{\text{initial}}&=(\text{K.E.})_{\max}\\&\quad-({}_0n^1-{}_1\text{H}^1)\text{ for }\beta^-\text{ decay},\end{aligned}\tag{13}$$

where $(\text{K.E.})_{\max}$ is the observed maximum kinetic energy of the beta particle. Some additional binding energy differences are found in the mass spectroscopic data at $A=48$ and 50, the successive beta decays from $_{26}\text{Fe}^{52}\rightarrow{}_{25}\text{Mn}^{52}\rightarrow{}_{24}\text{Cr}^{52}$, and the (p, n) threshold on V^{51}. Unless otherwise noted, the data are taken from references given in the National Bureau of Standards Circular 499. They are listed in the first two columns of Table VI, and the experimental binding energy differences obtained by using $m_0c^2=0.51$ Mev and $({}_0n^1-{}_1\text{H}^1)=0.78$ Mev are given in column three.

TABLE VI. Binding energy differences for isobars in the $1f_{7/2}$ shell. Column two lists the experimental information as well as method and year of observation. Unless noted, data are from National Bureau of Standards Circular 499. Column three lists the experimental binding energy difference, and column four the calculated difference.

Isobars	Maximum K.E. (Mev) method and year of observation[a]	Exp. B.E. diff. (Mev)	Calc. B.E. diff. (Mev)
$\text{Sc}^{43}(\beta^+)\text{Ca}^{43}$	1.12 ± 0.05 a, s (45)	2.92	$6.65-3b(\rho)$
$\text{Ti}^{45}(\beta^+)\text{Sc}^{45}$	1.00 ± 0.02 s (50)	2.80	$6.90-3b(\rho)$
$\text{Ca}^{45}(\beta^-)\text{Sc}^{45}$	0.255 ± 0.005 s (50)	-0.525	$-6.55+5b(\rho)$
$\text{V}^{47}(\beta^+)\text{Ti}^{47}$	1.65 a (49)	3.45	$7.00-3b(\rho)$
$\text{Sc}^{47}(\beta^-)\text{Ti}^{47}$	0.61 a (49)	-0.17	$-6.80+5b(\rho)$
$\text{Cr}^{49}(\beta^+)\text{V}^{49}$	1.45 ± 0.05 a, cc (42)	3.25	$7.25-3b(\rho)$
$\text{Sc}^{49}(\beta^-)\text{Ti}^{49}$	2.4 a (49)	1.6	$-6.70+7b(\rho)$
$\text{Mn}^{51}(\beta^+)\text{Cr}^{51}$	2.0 a (38)	3.8	$7.35-3b(\rho)$
$\text{Cr}^{51}(K)\text{V}^{51}$	Q for $\text{V}^{51}(p, n)\text{Cr}^{51}$ (48)	1.534	$7.15-5b(\rho)$
$\text{Fe}^{52}(\beta^+)\text{Mn}^{52}$	2.5 ± 0.1 s (51)	4.3	$7.60-3b(\rho)$
Ca^{48}—Ti^{48}	Mass spec.[b] (52)	2.7	$-13.15+14b(\rho)$
Ti^{50}—Cr^{50}	Mass spec.[b] (52)	-2.8	$-14.05+10b(\rho)$
Cr^{52}—Fe^{52}	Sum of β^+ and γ energies is 4.76 s (47) a (51)	-8.36	$-14.95+6b(\rho)$

[a] a—absorption; s—spectrometer; cc—cloud chamber.
[b] See reference 25.

By equating the experimental values to the calculated binding energy difference expressions, one obtains points for a curve of b as a function of A. As can be seen from Fig. 3, the points give b a magnitude of about 1.2 Mev, and show a tendency for b to decrease with increasing A. The transitions from $T=1/2$ to $T=3/2$ all have the term $3b$ in the calculated binding energy difference; similarly the $T=0$ to $T=2$ transition contains $6b$. These are the lowest nonvanishing multiples of b that occur in odd-A and even-A transitions respectively, and as will be shown later, the proportionality coefficient would be the same for weak spin-orbit coupling. The points arising from these transitions are the crosses of Fig. 3. The extent to which they scatter about a smooth curve, which is well beyond the average experimental error of about 1 percent, is an indication of the degree of approximation of the model used. The points arising from differences between states of greater T are encircled in Fig. 3. The fact that these points make the scattering no worse is an indication that the proportionality constants of b are given correctly by (11). The significance of these proportionality constants for strong spin-orbit coupling as against weak spin-orbit coupling will be discussed in Part B of this section.

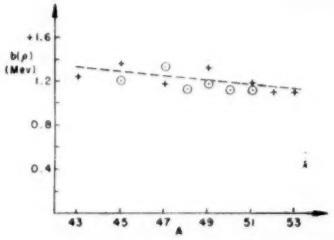

FIG. 3. Plot of $b(\rho)$ as a function of A from the last two columns of Table VI. Broken line is a fitted theoretical curve.

The experimentally determined results for $b(\rho)$ can be used to estimate some nuclear parameters in the theoretical expression. The expressions for $b(\rho)$ in the four central force cases are given in Appendix I; they depend on the parameters in the spatial dependence of the interaction potential A_0, r_0 and on the oscillator parameter r_f in the wave functions. A_0 and r_0 are related by the solution of the deuteron problem with inverse Gaussian potential, while from comparison of oscillator and square-well functions it was found that $r_f\approx3.0\times10^{-13}$ cm. The value of r_0 is expected to lie between 2.0×10^{-13} and 3.0×10^{-13} cm; numerical values of $b(\rho)$ for the four exchange potentials are given in Table VII using these parameters. It is evident that as long as there is a preponderance of potentials involving

space exchange (P_{12}), it is possible to fit the experimental magnitude of $b(\rho)$ with reasonable values of the nuclear parameters. Since all the expressions show a decrease of $b(\rho)$ for increasing r_f and constant r_0, this feature of the experimentally obtained points of Fig. 3 will be present.

For example, the potentials (9) and (10) with $J(r_{12}) = A_0 \exp[-(r_{12}/r_0)^2]$, $A_0 = 35.6$ Mev, $r_0 = 2.25 \times 10^{-13}$ cm will give curves for $b(\rho)$ as a function of mass number that present a reasonable fit to the points of Fig. 3 for:

$$\begin{aligned} &r_f = 3.16(A/53)^{\frac{1}{3}} \times 10^{-13} \text{ cm for (9)}, \\ &\qquad \text{where } A \text{ is the mass number;} \\ &r_f = 2.65(A/53)^{\frac{1}{3}} \times 10^{-13} \text{ cm for (10)}, \\ &\qquad \text{where } A \text{ is the mass number.} \end{aligned} \tag{14}$$

To observe the effect of a spatial dependence having a singularity at the origin, the delta function, $J(r_{12}) = A_\delta \delta(r_{12})$ is treated. In this case, P_{12} is unity, so the two exchange mixtures (9) and (10) coincide. All energies of $1f_{7/2}$ interactions in the delta-function case are proportional to the integral

$$G = 2A_\delta \int_0^\infty R_f^4(r) r^2 dr = 0.865 A_\delta / r_f^3. \tag{15}$$

For the delta-function case the expression $b(\rho) = 0.4G$, which is seen to be proportional to r_f^{-3} and hence inversely proportional to the mass number. The best fit to the experimental points is the curve $b = (57.3/A)$ Mev. The three cases evaluated give substantially the same curve for b as a function of A as is drawn in Fig. 3.

The theoretical binding energy difference resulting from use of the curve of Fig. 3 is generally a value that is small compared to the quantities which contribute to it, since the Coulomb term and the potential energy term have about the same magnitude but opposite sign. These values are listed together with the experimental binding energy differences in Table VIII; the agreement is generally quite good, as would be expected from the agreement in Fig. 3.

B. Symmetry Properties of the Wave Functions

The expression $b(\rho)$, which occurs in the binding energy differences of isobars, has coefficients which can be shown to result from the symmetry properties of the wave functions. The following discussion is based on articles by Hund[19] and Wigner.[20]

The total wave function is antisymmetric to exchange of any two nucleons. Since the isotopic spin is assumed to be a good quantum number, the wave function is separable into the product of an isotopic spin function with a space-spin function. Under the assumption of strong spin-orbit coupling, the space dependence and the ordinary spin dependence are not separable. The symmetry properties of the wave function are

[19] F. Hund, Z. Physik **43**, 788 (1927); **105**, 202 (1937).
[20] E. Wigner, Phys. Rev. **51**, 105 (1937); **51**, 937 (1937).

TABLE VII. Numerical values of the expression $b(\rho)$ for the central force potentials. In both cases $r_f = 3 \times 10^{-13}$ cm, $\rho = r_f/r_0$; in case 1, $A_0 = 42.8$ Mev, $r_0 = 2.0 \times 10^{-13}$ cm; in case 2, $A_0 = 23.1$ Mev, $r_0 = 3.0 \times 10^{-13}$ cm.

Exchange potential	b for $\rho = 1.5$	b for $\rho = 1.0$
1	0.59 Mev	0.41 Mev
P_{12}	1.06 Mev	1.44 Mev
$P_{12}Q_{12}$	1.18 Mev	2.24 Mev
Q_{12}	0.30 Mev	0.20 Mev

designated by the notation:

$\varphi(\{1\ 2\}3)$ is a function antisymmetric to exchange of 1 and 2 and is a function with the symmetry property $A(2+1)$.

$\varphi([1\ 2]3)$ is a function symmetric to the exchange of 1 and 2 and is a function with the symmetry property $S(2+1)$.

The theory of the permutation group says that in order to be able to obtain a completely antisymmetric product wave function, the two components of the product must have adjoint symmetry character. The functions with symmetry properties $A(\lambda_1+\lambda_2)$ and $S(\lambda_1+\lambda_2)$ have adjoint character.

The component wave functions are formed so that they give irreducible representations of the permutation group on n particles, where $\lambda_1+\lambda_2=n$ represents a given partition of n. This means that if one tries to change a wave function of symmetry $A(2+1)$ by permutation and combination to form $A(3)$,

$$\varphi(\{1\ 2\}3) - \varphi(\{3\ 2\}1) - \varphi(\{1\ 3\}2) = \psi(\{1\ 2\ 3\}),$$

one will find that $\psi = 0$. The general statement is that if the λ's of a partition are arranged in order of nonincreasing magnitude, then if the wave function belongs to an irreducible representation, one cannot increase any of the λ's by permutation of particles and combination of terms.

The isotopic spin variable is two-valued; hence a many-particle isotopic spin function cannot be made

TABLE VIII. Comparison of theoretical and experimental binding energy differences.

Isobars	Theor. B.E. differences[a] (Mev)	Exp. B.E. difference (Mev)
$Sc^{41}(\beta^+)Ca^{41}$	$+6.75$	$+6.74$
$Sc^{43}(\beta^+)Ca^{43}$	$+6.65-3.90=+2.75$	$+2.92$
$Ti^{45}(\beta^+)Sc^{45}$	$+6.90-3.80=+3.10$	$+2.80$
$Ca^{45}(\beta^-)Sc^{45}$	$-6.55+6.30=-0.25$	-0.525
$V^{47}(\beta^+)Ti^{47}$	$+7.00-3.65=+3.35$	$+3.45$
$Sc^{47}(\beta^-)Ti^{47}$	$-6.80+6.10=-0.70$	-0.17
$Cr^{49}(\beta^+)V^{49}$	$+7.25-3.55=+3.70$	$+3.25$
$Sc^{49}(\beta^-)Ti^{49}$	$-6.70+8.25=+1.55$	$+1.6$
$Mn^{51}(\beta^+)Cr^{51}$	$+7.35-3.40=+3.95$	$+3.8$
$Cr^{51}(K)V^{51}$	$+7.15-5.70=+1.45$	$+1.534$
$Fe^{53}(\beta^+)Mn^{53}$	$+7.60-3.30=+4.30$	$+4.3$
Ca^{48}—Ti^{48}	$-13.15+16.80=+3.65$	$+2.7$
Ti^{50}—Cr^{50}	$-14.05+11.60=-2.45$	-2.8
Fe^{52}—Cr^{52}	$-14.95+6.70=-8.25$	-8.36

[a] Theoretical values are given to the nearest 0.05 Mev.

antisymmetric in more than two nucleons. This is equivalent to saying that when the isotopic spin function is written in its $S(\lambda_1+\lambda_2+\cdots+\lambda_k)$ form, there can be only two parts, λ_1 and λ_2, to the partition of n. The difference $\lambda_1-\lambda_2$ is twice the isotopic spin quantum number T. Therefore, since the space-spin part of the wave function must have adjoint character if the total wave function is to be antisymmetrized, its symmetry properties are determined by T. This is illustrated in Table IX for the case of seven $1f_{7/2}$ nucleons, that is, mass number 47.

The central interaction potentials involve only the space and spin coordinates, so the symmetry properties of the space-spin functions are the relevant features. With respect to simultaneous permutation of the space and spin coordinates, a given space-spin wave function of n particles ψ_k belongs to an irreducible representation of the permutation group $D(R)$,

$$P_R\psi_k[(X,\sigma)_1,\cdots(X,\sigma)_n] = \sum_{j=1}^{f} D_{jk}(R)\psi_j[(X,\sigma)_1,\cdots(X,\sigma)]. \quad (16)$$

Here P_R is a definite simultaneous permutation of the space (X) and spin (σ) coordinates of the n nucleons; $D(R)$ is the matrix representing this permutation; ψ_j is one of the wave functions representing the group (the ψ_j are an orthonormal set); f is the dimension of the representation (it equals the number of independent wave functions needed to represent the group); $1\leq k, j\leq f$. The potential energy of an interaction using this wave function is

$$V_{kk}=\sum_{\alpha<\beta}^{n}\int\psi_k^*V_{\alpha\beta}\psi_k. \quad (17)$$

By using the group properties as defined in (16) in the same way that Wigner[21] proceeds, one obtains

$$V_{kk}=\frac{n(n-1)}{2f}\sum_{j=1}^{f}\int\psi_j^*V_{12}\psi_j. \quad (18)$$

A representation for a particular group can be chosen so that all of its wave functions are either symmetric or antisymmetric to exchange of the particular coordinates 1 and 2. In this way (18) may be split into

$$V_{kk}=\frac{n(n-1)}{2f}\left[\sum_{j=1}^{s}\int\psi_j^*V_{12}\psi_j+\sum_{j=s+1}^{f}\int\psi_j^*V_{12}\psi_j\right], \quad (19)$$

TABLE IX. Symmetry properties of the component wave functions for seven $1f_{7/2}$ nucleons.

Element	T	Isotopic spin component	Space-spin component
Ca^{47}	7/2	$S(7)$	$A(7)$
Sc^{47}	5/2	$S(6+1)$	$A(6+1)$
Ti^{47}	3/2	$S(5+2)$	$A(5+2)$
V^{47}	1/2	$S(4+3)$	$A(4+3)$

[21] E. Wigner, Phys. Rev. **51**, 947 (1937).

TABLE X. Coefficients of b in the potential energy expression for isobars of mass number 47.

Element	Space-spin symmetry	$\frac{n(n-1)}{2}\frac{2s}{f}b$	Difference
Ca^{47}	$A(7)$	0	$7b$
Sc^{47}	$A(6+1)$	$7b$	$5b$
Ti^{47}	$A(5+2)$	$12b$	$3b$
V^{47}	$A(4+3)$	$15b$	

where the first sum contains all the functions symmetric to exchange of the coordinates of 1 and 2, there being s such functions. Therefore V_{kk} contains two terms, the first of which remains unchanged if the interaction V_{12} is replaced by $V_{12}P_{12}Q_{12}$, whereas the second term will change sign under such replacement.

The result of calculating the $1f_{7/2}$ potential energy contributions is given in Sec. IV, where it was found that all the V_{kk} depend on three expressions D, d and b. For configurations of nucleons of like charge, where the operator $P_{12}Q_{12}$ has the eigenvalue -1, only D and d occur; so these both change sign when V_{12} is replaced by $V_{12}P_{12}Q_{12}$. Since b has no such simple symmetry properties, the second sum must be a linear combination of D and d. There is only one linear combination of D, d, and b which does not change sign under replacement of V_{12} by $V_{12}P_{12}Q_{12}$:

$$S=(-D+5d+18b). \quad (20)$$

Therefore, all the integrals in the first sum of (19) are proportional to S. From the fact that $P_{12}Q_{12}\psi_j=\psi_j$ for all wave functions on the first sum, plus the fact that in the limit of delta-function range dependence $\int\psi_j^*V_{12}P_{12}\psi_j=\int\psi_j^*V_{12}\psi_j$ the proportionality constants can be shown to be independent of the type of exchange. In the limit of infinite range interaction and no exchange, the integrals are all alike,

$$\int\psi_j^*V_\alpha\psi_j=V_\alpha=c_jS,$$

so the proportionality constants are all alike. From the value of S in this limit, one finds $c=1/9$. Thus we can write (19) as

$$V_{kk}=\frac{n(n-1)}{2f}\left[\frac{sS}{9}+\sum_{j=s+1}^{f}\int\psi_j^*V_{12}\psi_j\right]. \quad (19a)$$

Section IV shows that only b occurs in the differences of V_{kk}'s for isobars; so what we seek is the coefficient of b in V_{kk}. Since b occurs only in S, this coefficient is:

$$\frac{n(n-1)}{2f}(2s).$$

The coefficient of b depends on the ratio $2s/f$, which is simply connected to the characters of the repre-

TABLE XI. Coefficients of b' in the potential energy expression under the assumption of separability of space and spin dependence for isobars of mass number 47.

Element	Spatial symmetry	$\frac{n(n-1)}{2}\frac{2sb'}{f}$	Difference
Ca^{47}	$S(2+2+2+1)$	$15b'$	$5b'$
Sc^{47}	$S(3+2+2)$	$20b'$	$4b'$
Ti^{47}	$S(4+2+1)$	$24b'$	$3b'$
V^{47}	$S(4+3)$	$27b'$	

sentation:

$2s-f=X(t)$, the character of a transposition

$f=X(E)$, the dimension of the representation.

The ratio $X(t)/X(E)$ can be obtained[22] from the symmetry properties of the space-spin wave functions, $A(\lambda_1+\lambda_2)$. Murnaghan[23] gives a general formula for the result when the wave functions are in the form $S(\lambda_1+\lambda_2+\cdots+\lambda_k)$:

$$n(n-1)\frac{X(t)}{X(E)}=\sum_{j=1}^{k}\lambda_j(\lambda_j-2j+1). \tag{21}$$

For wave functions in the $A(\lambda_1+\lambda_2+\cdots+\lambda_k)$ form, the sign of the left-hand side of (21) is changed, and with only two λ's the term of V_{kk} which involves b becomes

$$\tfrac{1}{2}n(n-1)(2s/f)b = \tfrac{1}{2}[n(n-1)-\lambda_1(\lambda_1-1)-\lambda_2(\lambda_2-3)]b. \tag{22}$$

Substitution of $\lambda_1+\lambda_2=n$ and $\lambda_1-\lambda_2=2T$ in (22) shows that this term agrees with the term containing b in (11); however, the form (22) shows its origin more clearly. The resulting isobar differences for mass number 47 are listed in Table X.

If instead of assuming strong spin-orbit coupling, one assumes the opposite extreme of negligible spin-orbit coupling, with space-dependent interactions dominant, one has the first approximation[20] in Wigner's supermultiplet theory. Here the wave function is separable into the product of space dependence, spin dependence, and isotopic spin dependence. The symmetry property of the space-dependent component of the wave function is the determining feature in this approximation. The ground states have been classified,[24] and are ^2F for odd-A nuclei, and $^1S_0$ for even-even nuclei. The potential energy differences will again depend on the coefficient $\frac{1}{2}n(n-1)(2s/f)$, where $(2s-f)/f=X(t)/X(E)$. The space wave function can have at most four λ's in the partition and is written in the form $S(\lambda_1+\lambda_2+\lambda_3+\lambda_4)$. From Eq. (21) one obtains

$$\tfrac{1}{2}n(n-1)(2s/f)=\tfrac{1}{2}[n(n-1)+\lambda_1(\lambda_1-1)+\lambda_2(\lambda_2-3)+\lambda_3(\lambda_3-5)+\lambda_4(\lambda_4-7)]. \tag{23}$$

For isobar differences, the coefficient (23) times a function $b'(\rho)$ will be all that is involved[21] in the potential energy differences. The case of mass number 47 is listed in Table XI.

In a Hartree model, the potential energy difference is the only difference in the binding energy of isobars aside from the Coulomb difference. The isobar differences for odd-A and even-even nuclei as given by the two models are summarized in Table XII.

The strong spin-orbit coupling model was compared with experiment in Fig. 3. If the coefficients predicted by the weak spin-orbit coupling model were used instead to plot b' as a function of A, the points for $T=3/2$ and $T=2$ would be unchanged since the coefficients are alike in the two models. However, for greater T's the weak coupling coefficients are smaller; so the encircled points of Fig. 3 would all be raised to values between 1.4 and 1.68 Mev. The points would then be badly scattered, and no smooth dependence of b' on A would give a good fit to the data.

The dependence on the coefficients can be tested without involving b and b' for mass numbers where more than one nonmirror decay is present. By taking ratios of non-Coulomb part of the binding energy differences, the b (or b') cancels. The comparison of the models with experiment is given for the four experimentally measured cases in Table XIII.

The experimental values provide a measure of the degree to which space and spin dependence are separable in the wave function for a Hartree model. The fact that the experimental values lie closer to the values obtained from the approximate functions of the jj model provides a good argument for strong spin-orbit coupling as an approximation preferable to that of weak spin-orbit coupling.

VI. TOTAL BINDING ENERGY OF STABLE NUCLEI

Mass spectroscopic results for nuclei as large as those of the $1f_{7/2}$ shell are generally not so reliable as the results for light nuclei. When comparing the results of various laboratories, the measurements of differences between nuclei are often in much better agreement than the absolute masses. For this reason, it is very fortunate that all the masses in this shell have

TABLE XII. Binding energy differences for isobars, aside from the Coulomb difference, as given by the strong spin-orbit coupling and weak spin-orbit coupling models.

Change of isotopic spin	Strong coupling	Weak coupling
T to $T-1$	$2Tb$	$(T+\frac{3}{2})b'$
T to $T-2$	$(4T-2)b$	$(2T+2)b'$

[22] See reference 3, footnote on p. 98.
[23] F. D. Murnaghan, *The Theory of Group Representation* (Johns Hopkins Press, Baltimore, 1938), p. 140, Eq. (5.6).
[24] B. H. Flowers, Proc. Roy. Soc. (London) **A210**, 497 (1951).

TABLE XIII. Ratios of binding energy differences in the $1f_{7/2}$ shell (Coulomb contribution removed).

Ratio	Exp. value	Strong coupling	Weak coupling
$[Ti^{45}(\beta^+)Sc^{45}/Ca^{45}(\beta^-)Sc^{45}$	0.68	0.60	0.75
$[V^{47}(\beta^+)Ti^{47}/Sc^{47}(\beta^-)Ti^{47}$	0.54	0.60	0.75
$[Cr^{49}(\beta^+)V^{49}/Sc^{49}(\beta^-)Ti^{49}$	0.48	0.43	0.60
$[Mn^{51}(\beta^+)Cr^{51}/Cr^{51}(K)V^{51}$	0.63	0.60	0.75

been measured recently at one laboratory.[25] The calculations had been completed before these results were available, and it was gratifying to discover that agreement with the calculation, particularly in regard to the even-Z isobar differences at mass number 48 and 50, is better for the new data than for that which was previously available.

The experimental binding energies are obtained from the mass spectroscopic data with the following conversion formula:

$$\text{B.E.(Mev)}=0.931[1.008146A+0.000840(A-Z) - \text{mass of neutral atom}], \quad (24)$$

where B.E. is binding energy, A is the mass number, and Z is the charge. The values are listed in Table XIV, and the points are plotted in Fig. 4. The only deviation from a smooth function of mass number A for the binding energy curve is the variation for even and odd isotopes found in the isotopes of Ca, Ti, and Cr. The magnitude of this variation is found to be about 1.7 Mev, in good agreement with the term from the semi-empirical Bohr-Wheeler mass formula, which gives this variation as $33.5A^{-\frac{3}{4}}$ Mev, or 1.8 Mev at $A=49$.

In calculating the total binding energy with Hartree wave functions constructed according to Sec. II, one can separate the contributions as follows:

1. Coulomb interaction of $1f_{7/2}$ protons with themselves and with the other closed shells of protons.
2. Potential energy of interaction of $1f_{7/2}$ nucleons with themselves, exclusive of the Coulomb interaction.
3. Contributions directly proportional to the number of $1f_{7/2}$ nucleons. These include spin-orbit-coupling energy, kinetic energy, and potential energy of interaction with the core nucleons.
4. The total binding energy of the $_{20}Ca^{40}$ core.

The Coulomb contribution is that obtained in Sec. V.

$$\text{Coulomb term (Mev)} = [Z-20][23.28A^{-\frac{1}{3}}]+0.35k, \quad (25)$$

where Z is charge, A mass number, and k is the coefficient of c in Table V. The contribution from nuclear forces among $1f_{7/2}$ nucleons is given by (11). This is based on the assumption that odd-A and even-even nuclei have ground states of $I=7/2$ and $I=0$, respectively.

The remaining binding energy contributions, 3 and 4, while contributing the bulk of the absolute value, are expected to give a smoothly varying function of the mass number A. Calculations of absolute values with product wave functions, done chiefly in the p shell, have been quite unsuccessful, but they have been able to account for the structure of the binding energy curve that is superimposed on a smoothly varying function of A. The procedure of this investigation is to see whether the first two terms can account for the fluctuations of the experimental curve and then determine the uniform function of A needed to give the absolute values of the experimental curve.

The even-odd variation in the binding energy for a given Z is the only irregular dependence on A that is experimentally evident. Among the terms of the calculation for a fixed Z, only the nuclear $1f_{7/2}$ contribution (11) exhibits such behavior. We can rewrite (11) in terms of Z by using the fact that it was assumed that $T=T_z$ for ground states and that $2T_z=A-2Z$. Since $A=n+40$, where n is the number of $1f_{7/2}$ nucleons, (11) becomes

$$V_n=[(Z-20)(n+21-Z)]b + \left[\frac{n-I/(7/2)}{2}\right]D+\left[\frac{n(n-2)+I/(7/2)}{4}\right]d. \quad (11a)$$

The even-odd variation is given by the second difference of Eq. (11a) with Z constant. The small changes in b, D, and d arise from changing the mass number by one are neglected, and in the second difference only the terms involving I or those quadratic in n can contribute.

$$[V_{n+1}-V_n]-[V_n-V_{n-1}] = \frac{d}{2}+\left[\frac{I_{n+1}+I_{n-1}-2I_n}{7/2}\right]\left[\frac{d-2D}{4}\right] = \Delta^2V_n=\left\{\begin{matrix}+D \text{ for odd } n \\ -D+d \text{ for even } n\end{matrix}\right\}. \quad (26)$$

The experimental points within the shell give a nu-

TABLE XIV. Experimental binding energy in Mev.

Nucleus	Binding energy	Nucleus	Binding energy
Ca^{40}	341.9	Ti^{48}	418.7
Ca^{41}	350.2[a]	Ti^{49}	426.6
Ca^{42}	361.7	Ti^{50}	437.6
Ca^{43}	369.7	Cr^{50}	434.8
Ca^{44}	381.1	V^{51}	445.4
Sc^{45}	387.9	Cr^{52}	456.2
Ti^{46}	398.4	Mn^{53}	462.6[b]
Ti^{47}	407.0	Fe^{54}	471.5
Ca^{48}	415.9	Co^{55}	476.5[c]

[a] From $Ca^{41}-Ca^{40}$ mass difference. V. L. Sailor, Phys. Rev. **75**, 1836 (1949).
[b] Related to $Cr^{53}(p, n)Mn^{53}$ threshold. Lovington, McCue, and Preston, Phys. Rev. **85**, 585 (1952).
[c] Related to Mn^{55} by radioactive decay data. All other values taken from reference 25.

[25] Collins, Nier, and Johnson, Phys. Rev. **84**, 717 (1951); **86**, 408 (1952).

merical value for this second difference:

$$\Delta^2 V_n = \left\{ \begin{matrix} +3.3 \text{ Mev for odd } n \\ -3.3 \text{ Mev for even } " \end{matrix} \text{ (error } \pm 0.3) \right\}. \quad (27)$$

This indicates that in order to obtain agreement with experiment, one must have $|d| \ll |D|$, and $D \approx 3.3$ Mev.

So far no particular central force interaction has been used. Before investigating particular potentials, some further properties of d and D will be used to show what properties a potential must have to provide agreement with experiment.

The expressions for D and d are given in Appendix I for the four types of exchange with central forces. These expressions occur in calculating interactions for configurations of identical nucleons; wave functions of such configurations are antisymmetric to simultaneous exchange of space and spin. Therefore, D and d have the property that if the interaction $P_{12}Q_{12}V_{12}$ is used instead of V_{12}, the result is to merely change the sign of D and d. If one uses the coefficients W, M, H, and B to represent the amount of exchange of type 1, P_{12}, $P_{12}Q_{12}$, and Q_{12}, respectively, the general expression for d or D is a linear combination of the expressions listed in the Appendix with these coefficients. Using the further result that from the deuteron problem one expects $W+M=0.8$ and $B+H=0.2$, the general expressions for D and d become

$$d = 0.6 d_W + (M-B)(d_M - d_W), \quad (28)$$
$$D = 0.6 D_W + (M-B)(D_M - D_W).$$

Furthermore, the Appendix shows that $d_M = (-1/2) d_W$, so that

$$d = [0.6 - 1.5(M-B)] d_W. \quad (28a)$$

With the nuclear parameters that were determined from the isobar differences in Sec. V, the magnitudes of D_W, D_M, and d_W are the following:

Finite range	Delta-function range
$D_W \approx 3.8$ Mev	$D_W \approx 6.0$ Mev
$D_M \approx 1.3$ Mev	$D_M \approx 6.0$ Mev
$d_W \approx 2.6$ Mev	$d_W = 0$

From these magnitudes it is clear that in order to satisfy the requirement $|d| \ll |D|$, the coefficient of d_W must be small in the finite range case. This would give $M-B \approx 0.4$ and consequently $D \approx 1.3$ Mev, too small a value for the other requirement, $D \approx 3.3$ Mev, resulting from comparison with experiment. On the other hand, the case of delta-function range gives $d=0$ and $D \approx 3.6$ Mev and is independent of $M-B$. These values will give an even-odd variation term quite similar to observation.

The values resulting from the particular finite range potentials (8), (9), and (10), are the following:

(8) ($M=0.8$, $B=0$) gives $D=0.3$ Mev, $d=-1.5$ Mev;

(9) ($M=0.8$, $B=0.2$) gives $D=0.8$ Mev, $d=-0.8$ Mev;

(10) ($M=0.4$, $B=0.1$) gives $D=1.5$ Mev, $d=+0.4$ Mev.

From these sample cases the indication is that in order to have simultaneous quantitative agreement with isobar differences and with the even-odd variation for isotopes in the binding energy curve, the delta-function limit is the best approximation. This means that the use of a range dependence like the Yukawa potential would improve the agreement of the finite range cases considerably since its results are expected to lie closer

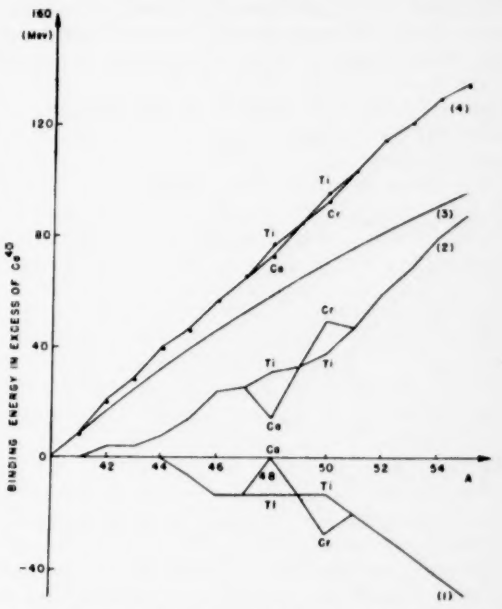

FIG. 4. Binding energy of stable nuclei in the $(1f_{7/2})$ shell: (1) Coulomb contribution; (2) $(1f_{7/2})$ interactions from Eq. (11); (3) $(A-40)$ times the smooth function $W(A)=353A^{-1}$ Mev; (4) Sum of these contributions. The circles are the experimental values.

to those of the delta-function dependence than the inverted Gaussian range dependence.

The even-odd variation discussed above is the only irregular contribution to the binding energy for a given Z. In general, for the nuclei in the shell the Coulomb contribution and the contribution due to the $1f_{7/2}$ interactions cancel each other's irregularities. The contribution 3 directly proportional to the number of $1f_{7/2}$ nucleons can, therefore, be represented by a smooth function of A, namely $(A-40)W(A)$, where $W(A)$ is obtained by fitting the experimental points. The separate contributions and their sum which represents the binding energy in excess of that of Ca^{40} are presented in Fig. 4, for the delta-function case where $W(A) = 8.6(41/A)$ Mev gives a good fit. This dependence on

A is reasonable since one expects the terms which it represents to depend on A to some negative power around unity. For two-thirds of the points agreement is within 0.4 Mev and all are within 1.0 Mev.

VII. *FT* VALUES AND MAGNETIC MOMENTS

A. *ft* Values

The allowed *ft* values in the shell can be calculated for a Gamow-Teller interaction by evaluating the nuclear matrix elements of the operator $\sum_i \sigma^i \tau_x^i$. Here τ_x is the isotopic spin operator which changes the charge variable of a nucleon, and σ is the Pauli spin vector. The transitions are assumed to be between states of $I=7/2$, and the matrix element is averaged over initial states and summed over the final states with different magnetic quantum numbers. The square of the matrix element is listed in the second column of Table XV; the decays are listed by pairing each decay with that of its hole image since their theoretical matrix elements are the same.

The decay $Sc^{41}(\beta^+)Ca^{41}$ is a mirror decay, namely from $T_z=-1/2$ to $T_z=+1/2$. The square of its *GT* matrix element is seen to be from two to ten times as great as those of the nonmirror decays. Experimentally, mirror decays have very low *ft* values and are called super-allowed; if only the GT matrix element were involved, the ratio of squared matrix elements should be about 30:1 to account for the difference between observed *ft* values in allowed and super-allowed transitions. However, the mirror transition can have Fermi interaction as well as the Gamow-Teller interaction contributing to its matrix element, which is not true for the allowed transitions. The matrix element for the Fermi interaction $\sum_i \tau_x^i$ is unity for the mirror transition and zero for all the rest. Therefore, the lack of a difference between calculated allowed and super-allowed transitions comparable to that observed experimentally is the result of the omission of the Fermi interaction and possibly also to lack of cancellation in the matrix element by the many-particle wave functions.

If the calculated GT matrix elements are assumed to be correct, the relative strength of Fermi interaction to GT interaction must be about 20:1 to account for the low *ft* of the super-allowed transition. This is not compatible with recent interpretations[26] which indicate an upper limit of about 1:1 for this ratio.

Therefore, the discrepancy must lie in the calculated GT matrix elements. That this is likely is indicated by the results of Appendix III, where the secular determinant is solved with delta-function interaction in the case of Sc^{43}. While the energy of the resulting ground state differs little from that obtained with the approximate wave function constructed according to Sec. IV, $|M|_{GT}^2$ for the $Sc^{43}(\beta^+)Ca^{43}$ transition drops by 60 percent. The value of the matrix element is thus quite sensitive to the wave function and hence to the type of interaction used when solving the secular determinants; so calculation throughout the shell is not feasible. The fact that the magnitude drops when wave functions resulting from solution of secular determinants are used is expected since these should not have so much similarity as wave functions constructed according to Sec. IV.

A reduction of the calculated $|M|_{GT}^2$ by a factor of about ten is needed to give the magnitude of the observed log *ft*'s for allowed transitions. If a constant reduction factor is assumed and incorporated by fitting the calculated log *ft* for $Sc^{43}(\beta^+)Ca^{43}$, the resulting relationship is

$$\log|M|_{GT}^2 ft = 4.66. \tag{29}$$

Values obtained by using (29) on column 2 of Table XV give column 3. There is still little semblance of any correlation with column 4, so the wave functions of Sec. IV are inadequate for calculating *ft* values. The fact that these wave functions are nevertheless suitable for energy calculations is not surprising since such calculations are an order of magnitude less sensitive to changes in the wave function.

TABLE XV. Comparison of calculated and experimental *ft* values.

Decay	M_{GT}^2	$(\log ft)_{theor}$	$(\log ft)_{exp}$
$Sc^{41}(\beta^+)Ca^{41}$	1.28		3.45
$Sc^{43}(\beta^+)Ca^{43}$	0.57	4.9[a]	4.9
$Fe^{53}(\beta^+)Mn^{53}$	0.57	4.9	4.9
$Ca^{45}(\beta^-)Sc^{45}$	0.46	5.0	5.9
$Cr^{51}(K)V^{51}$	0.46	5.0	5.2
$V^{47}(\beta^+)Ti^{47}$	0.30	5.2	≥ 4.6[b]
$Cr^{49}(\beta^+)V^{49}$	0.30	5.2	≥ 4.5[b]
$Sc^{49}(\beta^-)Ti^{49}$	0.25	5.3	6.0
$Sc^{47}(\beta^-)Ti^{47}$	0.18	5.4	5.6
$Ti^{45}(\beta^+)Sc^{45}$	0.11	5.6	≥ 4.4[b]
$Mn^{51}(\beta^+)Cr^{51}$	0.11	5.6	≥ 5.1[b]

[a] Fitted to experimental value of $Sc^{43}(\beta^+)Ca^{43}$.
[b] Lower limit for log *ft* since branching ratio for *K* capture is unknown.

B. Magnetic Moments

The magnetic moments obtained for the stable nuclei with the many-particle wave functions are listed in the second column of Table XVI. Comparison with the experimental determinations given in the third column shows that the theoretical values are considerably higher. Still, the experimentally observed tendency for the moment to be reduced when going from a nucleus like V^{51}, which has only protons outside closed shells, to Sc^{45}, which has both neutrons and protons outside shells, is given by the model, as has been pointed out by Flowers.[27] As in the case of the beta-decay matrix elements, the magnetic moment is considerably more sensitive to the nuclear wave function than is the energy, so that nuclei having approximate wave functions are affected as is shown in Appendix III.

However, there is no ambiguity in the construction of the wave function for V^{51} whose moment is predicted

[26] G. L. Trigg, Phys. Rev. **86**, 506 (1952); J. M. Blatt, Phys. Rev. **89**, 83 (1953).
[27] B. H. Flowers, Phil. Mag. **43**, 1330 (1952).

to lie on the Schmidt line. There have been proposals[28] that the spin contribution to the magnetic moment is suppressed from its free particle value when a nucleon is in the field of other nucleons. If one follows this suggestion and uses the V^{51} experimental moment to estimate the amount by which the anomalous spin moment of both neutron and proton is suppressed, the results are $\mu_p=2.15\mu_0$ and $\mu_n=-1.27\mu_0$. Magnetic moments calculated with these values are listed in the last column of Table XVI.

TABLE XVI. Magnetic moments for odd-A nuclei in the $1f_{7/2}$ shell.

Nucleus	Calculated[a]	Experimental	Calculated[b]
Ca^{49}	−1.91	...	−1.27
Sc^{45}	+5.11	+4.75[c]	+4.58
Ti^{47}	−1.57		−0.99
		−1.10[d]	
Ti^{49}	−1.67		−1.01
V^{51}	+5.79	+5.15[e]	+5.15

[a] Calculated with $\mu_p=+2.79$, $\mu_n=-1.91$.
[b] Calculated with suppressed moments to fit V^{51}; $\mu_p=+2.15$, $\mu_n=-1.27$.
[c] W. G. Proctor and F. C. Yu, Phys. Rev. **78**, 471 (1950).
[d] Jeffries, Loliger, and Staub, Helv. Phys. Acta **24**, 643 (1951) (isotope uncertain).
[e] W. D. Knight and V. W. Cohen, Phys. Rev. **76**, 1421 (1959).

VIII. CONCLUSIONS

In summary, the following conclusions can be drawn from comparison of the jj-coupling model with experiment in the $1d_{3/2}$ and $1f_{7/2}$ regions.

For identical nucleons, even configurations give the observed order of $I=0$, 2. Odd configurations give the I of the single odd nucleon, although the $(1f_{7/2})^3$ configuration has levels of smaller I that are calculated to lie close to the ground state in energy.

For odd-odd nuclei, the coupling of a single particle with a single hole is given in agreement with experiment. For coupling of two nucleons or two holes, calculation does not always agree with experiment.

For other $1f_{7/2}$ shell nuclei, the wave functions constructed according to the assumptions of Sec. IV seem suitable for obtaining binding energy differences. They can account for the kinks in the binding energy curve of the stable odd-A and even-even nuclei if the range dependence of interaction is closer to the delta function than the Gaussian. They also account for the binding energy differences of isobars within the Hartree model, which the wave functions of the weak spin-orbit coupling model do not.[29] The $1f_{7/2}$ shell is peculiarly suited for such a comparison, since it is the only section of the periodic table where isobars of sufficiently great differences in neutron excess have both neutrons and protons within the same shell. This makes the binding energy difference of neighboring isobars a single, simple quantity, directly related to the symmetry properties of the wave functions.

Although the approximate wave functions are good for energy calculations and give reasonable values for the few measured magnetic moments, they are not adequate for calculation of allowed ft values. The results indicate that while the wave functions formed according to Sec. IV are good first approximations, they are not sufficiently exact for the sensitive test of ft values. Furthermore, if the configuration $(1f_{7/2})_{5/2}^{-3}$, which is the ground state of $_{25}Mn^{55}$, is involved in any of these decays, it would seriously affect the ft calculations. On the other hand, the energy differences would not be seriously affected since the $(1f_{7/2})_{7/2}^{-3}$ configuration which was assumed to be the ground state in the calculations should lie very close to the $(1f_{7/2})_{5/2}^{-3}$ in energy.[29a]

The author wishes to express his gratitude to Professor M. G. Mayer for suggesting the investigation and providing liberal amounts of discussion and guidance during the course of the work.

APPENDIX I. EVALUATION OF INTERACTION INTEGRALS

The potential energy of interaction caused by nuclear forces is obtained by calculating the matrix element for two-body interactions using the many-particle spin-orbit coupled wave functions. This is a sum of integrals involving the individual particle functions with coefficients determined by the wave function of the particular nucleus in question. The individual particle integrals can be integrated over ordinary spin, and are then linear combinations of the fundamental integrals

$$(ab|V|cd)=\int\int u_a^*(1)u_b^*(2)V_{12}u_c(1)u_d(2)d\tau_1 d\tau_2, \quad \text{(A1)}$$

where $u=R_{nl}(r)\Theta_{lm}(\theta)\Phi_m(\varphi)$, the subscripts on the u's referring to the set of quantum numbers n, l, and m. The functions are normalized so that

$$\int_0^\infty R^2r^2dr=1; \quad \int_0^\pi \Theta^2\sin\theta d\theta=1; \quad \int_0^{2\pi}\Phi^2d\varphi=1.$$

The fundamental integrals all involve the spatial dependence of the interaction between pairs of nucleons. This is taken to be the negative Gaussian:

$$J(r_{12})=A_0\exp[-(r_{12}/r_0)^2]$$
$$=A_0\exp[-(r_1^2+r_2^2-2\mu r_1r_2)/r_0^2]. \quad \text{(A2)}$$

[28] F. Bloch, Phys. Rev. **83**, 839 (1951); H. Miyazawa, Progr. Theoret. Phys. (Japan) **6**, 263 (1951); A. de-Shalit, Helv. Phys. Acta **24**, 296 (1951).

[29] E. Wigner (reference 21) accounts for binding energy differences by using a model with potential energy from the Hartree model with negligible spin-orbit coupling and kinetic energy calculated with the statistical model. For the nuclei considered here, the use of two models is not necessary if jj coupling is assumed.

[29a] *Note added in proof:*—Recent experimental data indicate that odd-A nuclei having the configuration $(1f_{7/2})^{-3}$ have a ground state of 5/2 with the state 7/2 a few hundred kilovolts higher, whereas this situation is reversed for the configuration $(1f_{7/2})^3$. The new data also provide closer agreement with the binding energy differences for 7/2 states calculated in Sec. IVA). See L. S. Cheng and M. L. Pool, Phys. Rev. **90**, 886 (1953); B. Crasemann and H. T. Easterday, Phys. Rev. **90**, 1124 (1953); C. D. Jeffries, Phys. Rev. **90**, 1130 (1953) and Bull. Am. Phys. Soc. **5**, 24 (1953).

TABLE XVII. Direct and exchange interaction integrals for $1f_{7/2}$ nucleons. The general expression is $[a_0+a_1x+a_2x^2+a_3x^3]K$, where $x=\rho^4/4(1+\rho^2)$, $K=(A_0/735)(1+\rho^2)^{-9/2}$ and $\rho=r_f/r_0$.

	Wigner interaction				Majorana interaction			
	a_0	a_1	a_2	a_3	a_0	a_1	a_2	a_3
$77D$	735	8820	22 050	14 700	735	8820	22 050	14 700
$75D$	735	6930	14 490	8400	105	3150	10 710	8400
E	0	1890	7560	6300	630	5670	11 340	6300
$73D$	735	5670	11 340	6720	0	1260	6930	6720
E	0	630	4410	4620	525	3780	7560	4620
$71D$	735	5040	10 332	6216	0	378	4914	6216
E	0	0	2268	3444	420	2772	5796	3444
$7\bar{1}D$	735	5040	10 332	6216	0	0	3402	6216
E	0	0	1134	2772	315	2268	4536	2772
$7\bar{3}D$	735	5670	11 340	6720	0	0	1890	6720
E	0	0	0	2100	210	1890	3780	2100
$7\bar{5}D$	735	6930	14 490	8400	0	0	0	8400
E	0	0	0	2100	105	1260	3150	2100
$7\bar{7}D$	735	8820	22 050	14 700	0	0	0	14 700
E	0	0	0	0	0	0	0	0
$55D$	735	6660	16 650	11 820	555	5580	15 570	11 820
$53D$	735	6480	14 580	8520	180	2610	9090	8520
E	0	1440	5220	4980	480	4860	10 260	4980
$51D$	735	6390	12 494	7296	0	1404	5778	7296
E	0	1350	4266	4428	405	3780	6696	4428
$5\bar{1}D$	735	6390	12 492	7296	0	864	3618	7296
E	0	0	1296	2868	330	2610	5796	2868
$5\bar{3}D$	735	6480	14 580	8520	0	0	1890	8520
E	0	0	2430	3540	255	1620	4320	3540
$5\bar{5}D$	735	6660	16 650	11 820	0	0	3240	11 820
E	0	0	0	0	180	1080	1080	0
$33D$	735	7020	15 930	11 340	435	4860	12 690	11 340
$31D$	735	7290	16 362	9456	225	2790	7542	9456
E	0	450	2664	3612	390	4158	10 476	3612
$3\bar{1}D$	735	7290	16 362	9456	0	1008	4464	9456
E	0	1800	6768	5844	345	3132	5886	5844
$3\bar{3}D$	735	7020	15 930	11 340	0	1080	5400	11 340
E	0	0	0	0	300	2160	3240	0
$11D$	735	7740	19 026	13 068	375	4068	10 818	13 068
$1\bar{1}D$	735	7740	19 026	13 068	240	3096	9360	13 068
E	0	0	0	0	360	3672	8208	0

Following the method applied to the case of Coulomb interaction in atomic physics,[30] the interaction is expanded in a series of Legendre polynomials of argument $\mu=\cos\theta$:

$$J(r_{12})=A_0\exp[-(r_1^2+r_2^2)/r_0^2]\sum_k a_k(r_1,r_2)P_k(\mu). \quad \text{(A3)}$$

The fundamental integrals are then linear combinations of Slater integrals with coefficients obtained from the angular part of the integration. These coefficients are the same as for the atomic case and are tabulated in reference 30. For the $1f$ shell, the Slater integrals are the following:

$$F^{(k)}=\int_0^\infty\int_0^\infty R_{1f}^2(r_1)R_{1f}^2(r_2)\exp[-(r_1^2+r_2^2)/r_0^2]\times a_k(r_1,r_2)r_1^2r_2^2dr_1dr_2.$$

The values of k are 0, 2, 4, and 6 with the following a_k:

$$\begin{aligned}
a_0&=(1/y)\sinh y,\\
a_2&=(5/y^3)[(3+y^2)\sinh y-3y\cosh y],\\
a_4&=(9/y^5)[(105+45y^2+y^4)\sinh y\\
&\qquad-(105y+10y^3)\cosh y],\\
a_6&=(13/y^7)[(10395+4725y^2+210y^4+y^6)\sinh y\\
&\qquad-(10395y+1260y^3+21y^5)\cosh y],
\end{aligned} \quad \text{(A4)}$$

where $y=2r_1r_2/r_0^2$.

The radial functions for the $1f$ shell are the harmonic oscillator functions

$$R_{1f}=N_{1f}r^3\exp[-(r/r_f)^2]. \quad \text{(A5)}$$

The Slater integrals are evaluated with these functions, giving the expressions,

$$\begin{aligned}
F^{(0)}&=[105+9(105)x+9(11)(21)x^2\\
&\qquad+9(11)(13)x^3]7K,\\
F^{(2)}&=[0+9(63)x+9(11)(18)x^2\\
&\qquad+9(11)(13)x^3]35K,\\
F^{(4)}&=[0+0+9(11)(11)x^2+9(11)(13)x^3]63K,\\
F^{(6)}&=[0+0+0+9(11)(13)x^3]91K,
\end{aligned} \quad \text{(A6)}$$

where $x=\rho^4/4(1+\rho^2)$, $K=(A_0/735)(1+\rho^2)^{-9/2}$, $\rho=r_f/r_0$.

The integrals desired involve the spin-orbit coupled individual particle functions, and since the integrals are linear combinations of the Slater integrals, they can be expressed as polynomials in x. The formulation in terms of x is convenient since the limiting cases of zero range and infinite range of interaction are immediately evident as x goes respectively to infinity or zero. The integrals for nucleons in the $1f_{7/2}$ shell are given in the form,

$$\begin{aligned}
&\int[7(1)\bar{5}(2)]^*V_{12}[7(1)\bar{5}(2)]d\tau_1d\tau_2\\
&\qquad=7\bar{5}\text{ direct}=7\bar{5}D.\\
&\int[7(1)\bar{5}(2)]^*V_{12}[\bar{5}(1)7(2)]d\tau_1d\tau_2\\
&\qquad=7\bar{5}\text{ exchange}=7\bar{5}E.
\end{aligned} \quad \text{(A7)}$$

Here V_{12} is the two-particle interaction potential, and $7(1)\bar{5}(2)$ means that particle 1 is in the state with z component of angular momentum $m=7/2$ and that particle 2 is in the state $m=-5/2$. The integrals are given for the interactions $V_{12}=J(r_{12})$, the Wigner

[30] E. U. Condon and G. H. Shortley, *The Theory of Atomic Spectra* (Cambridge University Press, Cambridge, 1951), Chap. VI.

interaction, and for $V_{12}=J(r_{12})P_{12}$, the Majorana or space exchange interaction. The integrals for Heisenberg interaction can be obtained from the Wigner integrals since the Heisenberg operator $P_{12}Q_{12}$ merely exchanges particles 1 and 2 in the space-spin function. Thus the direct integral with Heisenberg interaction is the exchange integral of Wigner interaction and vice versa. The same relationship holds between Bartlett (Q_{12}) and Majorana integrals.

The resulting integrals which allow calculation with any type of static central-force interaction are given in Table XVII. There the coefficients of the powers of x in the polynomial $(\alpha_0+\alpha_1x+\alpha_2x^2+\alpha_3x^3)K$ are listed.

The quantities arising in the expression for potential energy within the $1f_{7/2}$ shell (11) can naturally also be expressed as polynomials in x. For the four interactions these are:

Wigner Interaction

$$D_W=(105+1620x+5346x^2+5148x^3)7K,$$
$$d_W=(210+1440x+1980x^2+0)7K,$$
$$b_W=(0+200x+968x^2+1144x^3)7K.$$

Majorana Interaction

$$D_M=(+15+324x+1782x^2+5148x^3)7K,$$
$$d_M=(-105-720x-990x^2+0)7K,$$
$$b_M=(+60+536x+1232x^2+1144x^3)7K. \quad \text{(A8)}$$

Heisenberg Interaction

$$D_H=-D_W,\ d_H=-d_W,$$
$$b_H=(+105+820x+1474x^2+572x^3)7K.$$

Bartlett Interaction

$$D_B=-D_M,\ d_B=-d_M,$$
$$b_B=(0+100x+484x^2+572x^3)7K.$$

APPENDIX II. ENERGY EXPRESSIONS FOR ODD-ODD NUCLEI

The Slater integrals for configurations of $1d_{3/2}$ nucleons and for mixed $1d_{3/2}$ and $1f_{7/2}$ nucleons involve the parameter r_d from the radial $1d$ wave function

$$R_{1d}=N_{1d}r^2\exp[-(r/r_d)^2] \quad \text{(A9)}$$

as well as the parameters r_f, A_0, and r_0 defined in the evaluations of Appendix I.

For $1d_{3/2}$ configurations the Slater integrals are:

$$F^{(0)}=[15+70x+63x^2]K_d,$$
$$F^{(2)}=[0+49x+63x^2]5K_d, \quad \text{(A10)}$$
$$F^{(4)}=[0+0+63x^2]9K_d,$$

where

$$x=\rho_d^4/4(1+\rho_d^2);\quad \rho_d=r_d/r_0;\quad K_d=(A_0/15)(1+\rho_d^2)^{-7/2}.$$

For mixed $1f_{7/2}$ and $1d_{3/2}$ configurations the integrals are:

$$F^{(0)}=[5+30w+33w^2]Q,$$
$$F^{(2)}=[0+21w+33w^2]5Q, \quad \text{(A11)}$$
$$F^{(4)}=[0+0+33w^2]9Q,$$

where

$$w=\frac{1}{4}\left(\frac{2\rho_f^2\rho_d^2}{2+\rho_f^2+\rho_d^2}\right);\ Q=(256A_0/5)(2+\rho_d^2)(w/\rho_f^2\rho_d^2)^{9/2}.$$

$$F^{(1)}=[35/3+42y+33y^2]3C,$$
$$F^{(3)}=[0+27y+33y^2]7C, \quad \text{(A12)}$$
$$F^{(5)}=[0+0+33y^2]11C,$$

where

$$y=\frac{\rho_f^4\rho_d^4}{(\rho_f^2+\rho_d^2)(\rho_f^2+\rho_d^2+2\rho_f^2\rho_d^2)};$$

$$C=(256A_0/5)\rho_d^2(y/\rho_f^2\rho_d^2)^{9/2}.$$

In the limit $\rho_f=\rho_d=\rho$, one obtains the simplification $y=w=x$. The level crossings given in the text are obtained for this particular case.

The expressions for the level order of the various odd-odd nuclei are given in Tables XVIII, XIX, and XX. In this polynomial form it is easy to see the order in the limit of delta-function interaction since in this limit $y=w=x$ and $x\gg1$. The infinite range interaction case is also obvious since here $x, y, w\ll1$.

TABLE XVIII. Energy level order for $1d_{3/2}$ configurations. The expressions are in the form $[\alpha_0+\alpha_1x+\alpha_2x^2](K_d/25)$, where $x=\rho_d^4/4(1+\rho_d^2)$, $\rho_d=r_d/r_0$, and $K_d=(A_0/15)(1+\rho_d^2)^{-7/2}$. The level $I=0$ is set at zero as a reference level.

	$Cl^{36}[(1d_{3/2})(1d_{3/2})]$ and $K^{38}[(1d_{3/2})^{-1}(1d_{3/2})^{-1}]$											
	Majorana			Heisenberg			Wigner			Bartlett		
I	α_0	α_1	α_2	α_0	α_1	α_2	α_0	α_1	α_2	α_0	α_1	α_2
3	330	1930	−1260	750	4970	5040	0	−980	−1260	180	1580	5040
2	−90	−70	−2520	0	1960	2520	0	−1960	−2520	90	70	2520
1	180	280	−1260	750	4970	5040	0	−980	−1260	30	−70	5040
0		0			0			0			0	

	$Cl^{36}[(1d_{3/2})(1d_{3/2})^{-1}]$											
	Majorana			Heisenberg			Wigner			Bartlett		
I	α_0	α_1	α_2	α_0	α_1	α_2	α_0	α_1	α_2	α_0	α_1	α_2
3	750	3470	1260	750	3010	2520	0	980	1260	30	850	2520
2	750	3010	2520	750	2030	1260	0	1960	2520	−60	320	1260
1	600	1820	1260	750	3010	2520	0	980	1260	−120	−800	2520
0		0			0			0			0	

TABLE XIX. Energy level order for $(1d_{3/2}, 1f_{7/2})$ configurations. The level $I=2$ is set equal to zero as a reference level. The expressions for Majorana and Heisenberg interaction are in the form $[\alpha_0+\alpha_1 y+\alpha_2 y^2](C/35)$, where $y=(\rho_f{}^4\rho_d{}^4/\rho_f{}^8+\rho_d{}^8)(\rho_f{}^8+\rho_d{}^8+2\rho_f{}^8\rho_d{}^8)^{-1}$ and $C=(256A_0/5)\rho_d{}^2(y/\rho_f{}^8\rho_d{}^8)^{9/2}$. The expressions for Wigner and Bartlett interaction are in the form $[\beta_0+\beta_1 w+\beta_2 w^2](Q/35)$, where $w=\rho_f{}^8\rho_d{}^8/4+2\rho_f{}^8+2\rho_d{}^8$ and $Q=(256A_0/5)(\rho_d{}^8+2)(w/\rho_f{}^8\rho_d{}^8)^{9/2}$.

$Cl^{38}[(1d_{3/2})(1f_{7/2})]$

	Majorana			Heisenberg			Wigner			Bartlett		
I	α_0	α_1	α_2	α_0	α_1	α_2	β_0	β_1	β_2	β_0	β_1	β_2
5	432	1884	−440	0	60	−1840	0	−280	−440	−120	−1256	−1840
4	−168	84	−1540	0	210	−1540	0	−980	−1540	−70	−1106	−1540
3	72	264	−1100	0	−210	−1540	0	−700	−1100	−30	−746	−1540
2		0			0			0			0	

$K^{40}[(1d_{3/2})^{-1}(1f_{7/2})]$

	Majorana			Heisenberg			Wigner			Bartlett		
I	α_0	α_1	α_2	α_0	α_1	α_2	β_0	β_1	β_2	β_0	β_1	β_2
5	672	2484	440	0	0	−1400	0	280	440	−120	−976	−1400
4	672	2184	1540	0	0	0	0	980	1540	−70	−126	0
3	672	1764	1100	0	−360	−440	0	700	1100	−30	−46	−440
2		0			0			0			0	

APPENDIX III

The nucleus Sc^{43} is treated as an example of the construction of wave functions. This nucleus has one proton and two neutrons in the $1f_{7/2}$ shell so that there are several states with the same total angular momentum I and isotopic spin T. Therefore, the approximate wave function is constructed in accordance with the assumptions discussed in Sec. IV, and an exact wave function is also found by solving a secular determinant. The expectation values of various observables are calculated with the approximate function, and the exact function and the results are compared to check the validity of the approximation method.

The individual particle states are represented by symbols like $7p$ and $\bar{3}n$. The first of these symbols represents the state with z component of angular momentum $m=7/2$ and isotopic spin projection $t_z=-1/2$ (proton); similarly, the second state has $m=-3/2$ and $t_z=1/2$ (neutron). The general wave function for Sc^{43} with $M=\sum m^i=7/2$ and $T_z=\sum t_z{}^i=1/2$ is the linear combination:

$$\begin{aligned}\psi=&A\sum 7p(1)7n(2)\bar{7}n(3)+B_1\sum 7p(1)5n(2)\bar{5}n(3)\\&+B_2\sum 7n(1)5p(2)\bar{5}n(3)+B_3\sum 7n(1)5n(2)\bar{5}p(3)\\&+C_1\sum 7p(1)3n(2)\bar{3}n(3)+C_2\sum 7n(1)3p(2)\bar{3}n(3)\\&+C_3\sum 7n(1)3n(2)\bar{3}p(3)+D_1\sum 7p(1)1n(2)\bar{1}n(3)\\&+D_2\sum 7n(1)1p(2)\bar{1}n(3)+D_3\sum 7n(1)1n(2)\bar{1}p(3)\\&+F_1\sum 5p(1)3n(2)\bar{1}n(3)+F_2\sum 5n(1)3p(2)\bar{1}n(3)\\&+F_3\sum 5n(1)3n(2)\bar{1}p(3)+G\sum 3p(1)3n(2)1n(3)\\&+H\sum 5p(1)5n(2)\bar{3}n(3)+J\sum 5n(1)1p(2)1n(3).\end{aligned}$$

A component $\sum 7p(1)7n(2)\bar{7}n(3)$ represents the sum over all particle permutations in the three individual particle states $7p$, $7n$, and $\bar{7}n$ with appropriate signs to make the function antisymmetric to exchange of any two nucleons.

The arbitrary coefficients are then determined by requiring the desired values $I=7/2$ and $T=1/2$. This means that operating on ψ with $I=I_x+iI_y$ should give zero because of the general equation for angular momenta

$$I^+\psi_{I,M}=[I(I+1)-M(M+1)]^{\frac{1}{2}}\psi_{I,M+1}. \quad \text{(A13)}$$

Similarly, operating with $T^+=T_x+iT_y$ should give zero.

The procedure for obtaining the approximate wave function according to Sec. IV is to set the coefficients F_1, F_2, F_3, G, H, and J equal to zero. Then applying the conditions $I^+\psi=0$ and $T^+\psi=0$ will determine the other coefficients. These are $A=-3$, $B_1=-C_1=D_1$

TABLE XX. Energy level order for $1f_{7/2}$ configurations. The expressions are in the form $[\alpha_0+\alpha_1 x+\alpha_2 x^2+\alpha_3 x^3]K_f$, where $x=\rho_f{}^4/4(1+\rho_f{}^8)$, $\rho_f=r_f/r_0$, $K_f=(A_0/735)(1+\rho_f{}^8)^{-9/2}$. The level $I=0$ is set equal to zero as a reference level.

$Sc^{42}[(1f_{7/2})(1f_{7/2})]$

	Majorana				Heisenberg			
I	α_0	α_1	α_2	α_3	α_0	α_1	α_2	α_3
7	630	6552	9576	21 336	1470	20 160	59 472	50 736
6	−630	−4788	−13 104	−33 936	0	6300	30 492	33 936
5	240	−468	−4464	−27 576	1470	15 480	47 772	44 496
4	−300	−4392	−13 896	−31 824	0	6300	26 928	31 824
3	−30	−576	−9432	−27 144	1470	18 180	49 176	44 928
2	−90	−2628	−17 424	−27 456	0	2520	18 612	27 456
1	−180	−3492	−15 048	−17 160	1470	21 780	66 924	54 912
0		0				0		

	Wigner				Bartlett			
7	0	−2520	−15 372	−21 336	840	11 088	34 524	50 736
6	0	−6300	−30 492	−33 936	630	4788	13 104	33 936
5	0	−7200	−27 072	−27 576	450	4068	20 484	44 496
4	0	−6300	−26 928	−31 824	300	4392	13 896	31 824
3	0	−4500	−25 668	−27 144	180	3960	15 516	44 928
2	0	−2520	−18 612	−27 456	90	2628	17 424	27 456
1	0	−900	−7920	−17 160	30	1044	9900	54 912
0		0				0		

$Sc^{42}[(1f_{7/2})(1f_{7/2})^{-1}]$

	Majorana				Heisenberg			
I	α_0	α_1	α_2	α_3	α_0	α_1	α_2	α_3
7	2940	26 460	58 012	21 336	5880	52 920	116 424	72 072
6	2940	26 460	58 012	33 936	5880	52 920	116 424	67 872
5	2940	26 460	50 992	27 576	5880	52 920	116 424	72 072
4	2940	26 460	54 448	31 824	5880	52 920	109 296	63 648
3	2940	22 896	46 132	27 144	5880	52 920	116 424	72 072
2	2940	22 680	46 132	27 456	5880	45 360	92 664	54 912
1	1680	13 608	28 112	17 160	5880	52 920	116 424	72 072
0		0				0		

	Wigner				Bartlett			
7	0	2520	15 372	21 336	840	13 608	49 896	72 072
6	0	6300	30 492	33 936	630	11 088	43 596	67 872
5	0	7200	27 072	27 576	450	11 268	47 556	72 072
4	0	6300	26 928	31 824	300	10 692	40 824	63 648
3	0	4500	25 668	27 144	180	8460	41 184	72 072
2	0	2520	18 612	27 456	90	5148	36 036	54 912
1	0	900	7920	17 160	30	1944	17 820	72 072
0		0				0		

$=+2$, $B_2=B_3=-C_2=-C_3=D_2=D_3=-1$ with normalizing factor $(27)^{-\frac{1}{2}}$.

If one does not set coefficients equal to zero as in the approximate case, the I^+ and T^+ operators will lead to equations reducing the number of arbitrary constants from 16 to 3. This indicates that there are three states with $I=7/2$, $T=1/2$, which can only be resolved by solving a secular determinant of the matrix elements for nuclear interactions. Three arbitrary wave functions are constructed, consistent with the $I=7/2$, $T=1/2$ requirements and mutually orthogonal. The secular determinant is solved for the case of a two-particle delta-function interaction

$$V_{12}=A_3(0.8+0.2Q_{12})\delta(r_{12}), \qquad \text{(A14)}$$

where Q_{12} is spin exchange. The various physical quantities calculated with the resulting wave functions are given in Table XXI and compared with values obtained by using the approximate wave function.

TABLE XXI. Expectation values with the approximate and exact wave functions for Sc^{43}.

Wave function	$1f_{7/2}$ shell energy	Mag. mom. nm	$\lvert M\rvert_{GT}^2$ for $Ti^{43}(\beta^+)Sc^{43}$	$\lvert M\rvert_{GT}^2$ for $Sc^{43}(\beta^+)Ca^{43}$
ψ (approximate)	2.400 G	+4.08	0.40	0.57
ψ_1	2.516 G	+4.82	0.72	0.24
ψ_2	1.313 G	+1.03		
ψ_3	0.981 G	+0.02		

From Table XXI it is evident that the lowest energy solution of the secular determinant ψ_1 represents a state with about the same energy as the approximate state. However, while the energies agree within 5 percent, the magnetic moments and Gamow-Teller matrix elements for beta decay are considerably different. This indicates the degree of validity in using the approximate wave functions and is satisfactory for energies.

PHYSICAL REVIEW VOLUME 91, NUMBER 6 SEPTEMBER 15, 1953

The Linear Combination in β Decay*

D. C. PEASLEE
Columbia University, New York, New York

(Received April 29, 1953)

Empirical evidence on the shapes of first- and second-forbidden spectra is surveyed to determine the linear combination of invariants in the β-decay interaction. Absence of $1/W$ terms in allowed shape first-forbidden spectra excludes combinations SA and VT. Spectrum shapes for $\Delta I=2$, no, transitions exclude VA and indicate that for negatron emission the relative algebraic sign of the terms is $(S-T)$. These spectra also indicate the need for considerable correction of nuclear matrix element estimates because of the presence of pseudoscalar-coupled forces in the nucleus. Extrapolation of these empirical corrections to the case of RaE shows that the full linear combination should be $[S-T+(1/\delta)P]$, where δ is positive and of order unity. Arguments based on symmetry principles indicate that the correct interaction should in fact be $(S\pm T+P)$, where $\pm$ refers to $\beta^\pm$ emission. The effects of the difference in sign of the T term should in principle be observable. This law for β decay is compared with the decay of the μ meson, and it is found that if the linear combinations are the same, the coupling constants also have identical absolute values. The mean coupling constant is $|f|=1.44\times0.04\times10^{-49}$ erg cm^3. The chief experimental doubt concerns the μ-meson spectrum, which is expected to go through zero at its end point if the β and μ interactions are identical. It appears possible to deduce the combination $(S-T+P)$ uniquely from the postulates that the neutrino field is (1) unique; (2) massless; (3) part of a universal four-particle interaction.

I. INTRODUCTION AND SUMMARY

THE shapes of forbidden β spectra are analyzed to provide information about the linear combination of invariants, $SVTAP$, in the β-decay interaction. It is assumed as a basis throughout that (1) the interaction contains equal parts of Fermi (S, V) and Gamow-Teller (T, A) invariants; and (2) that there is no appreciable ($\lesssim$10 percent) mixture of S and V or of T and A in the interaction. These assumptions are indicated by the most recent analyses of allowed spectra.[1,2]

In forbidden transitions only those spectra involving a mixture of different nuclear matrix elements can give information about the linear combination; by assumption (2) this implies that the only useful spectra are those with a spin change $\Delta I<n+1$, where n is the order of forbiddenness. To extract the parameters λ of the linear combination, it is necessary to have some independent estimate of the ratios of nuclear matrix elements, which always occur in combination with λ. Section II attempts to form such estimates for the general matrix element, extending a procedure previously given[3] for first-forbidden matrix elements and

* Work performed under the research program of the U. S. Atomic Energy Commission.

[1] O. Kofoed-Hansen and A. Winther, Phys. Rev. **86**, 428 (1952).

[2] J. P. Davidson and D. C. Peaslee, Phys. Rev. **91**, 1232 (1953).

[3] T. Ahrens and E. Feenberg, Phys. Rev. **86**, 64 (1952).

making some allowance for pseudoscalar-coupled nuclear forces.[4]

In Sec. III are given simplified expressions for the spectrum shapes of first- and second-forbidden transitions. The low-Z approximation is used in order to obtain perspicuous algebraic forms for the spectrum shapes; since the analysis relies only on order-of-magnitude arguments, the low-Z approximation should not generally vitiate the conclusions. It is found possible to simplify the expressions for the spectrum shape even further by taking only the large terms of order $\alpha Z/2R$. The combinations ST and VA are observed to have the same generic shapes in this lowest-order approximation. They can be differentiated only by using independent estimates of matrix element ratios for second and higher forbidden spectra, or by comparison with spectra like RaE, where the usually dominant terms of order $\alpha Z/2R$ happen to cancel.

Section IV discusses the comparison with empirical data. The allowed shape of most first-forbidden spectra with $\Delta I<2$ clearly arises from the dominance of energy-independent Coulomb terms in the electron wave function, as has been observed.[5] The absence of $1/W$ terms in these first-forbidden transitions of allowed shape definitely rules out the combination SA and provides some evidence against VT. Nothing more can be deduced from these spectra because their allowed shape does not provide any indication of nuclear matrix element ratios.

The second-forbidden spectra with $\Delta I=2$ have nonunique shapes for which only the combinations VA and ST are available on the basis of previous evidence. The combination VA is found to be at variance with the spectrum of Cl^{36}, so that the only remaining possibility is ST. This conclusion is in harmony with recent $\beta-\nu$ correlation experiments[6] in He^6. Further comparison with the $\Delta I=2$, no, shapes indicates that (1) the relative algebraic sign of the terms in negatron decay is given by $S-T$; (2) a reasonable fit cannot be obtained without a considerable correction of the nuclear matrix elements for pseudoscalar-coupled forces.

The spectrum of RaE is considered as the only case that gives evidence on the amount of pseudoscalar interaction P in the linear combination. General arguments based on the rarity of the RaE type spectrum indicate that it should be considered a $0^-\rightarrow 0^+$ transition. The unique shape indicates cancellation of the usually dominant, energy-independent terms. These conclusions are the same as those obtained by a detailed analysis of the spectrum.[7] Extrapolation of the empirical pseudoscalar-coupled force corrections from the second-forbidden spectra to the case of RaE indicates that the linear combination active in this transition is $T-(1/\delta)P$, where δ is a positive number of order unity.

In Sec. V are reviewed the symmetry arguments that bear on the linear combination. The only combination consistent with any symmetry principle and the empirical evidence is $(S-T+P)$. This is taken as the correct form for negatron decay; for positron emission the combination becomes $S+T+P$, and the difference in sign of T should lead to observable effects. This linear combination is uniquely selected by the conditions that (1) the interaction should be antisymmetric in exchange of pairs of equivalent particles, where this does not include all pairs of particles in the interaction; (2) the interaction should be invariant on mass reversal of the massless neutrino field, in the case of μ-meson decay into two neutrinos; and (3) the β-decay interaction is identical with that for μ-meson decay.

In Sec. VI the decay of the isolated μ meson is compared with β decay. It is found that if the linear combination is assumed to be the same for both cases, then the coupling constants have the same magnitudes within allowances for experimental errors. The mean value of the coupling constant in $f(S-T+P)$ is $|f|=1.44\pm0.04$ erg cm^3. The chief point of present experimental doubt is the shape of the μ-meson decay spectrum, which should go to zero at its end point if the β- and μ-decay interactions are indeed identical.

II. NUCLEAR MATRIX ELEMENT RATIOS

The shapes of forbidden spectra with $\Delta I<n+1$ can be used to determine the linear combination only if the ratios of certain nuclear matrix elements can be estimated *a priori*. Arguments of invariance under rotation and reflection show that general relationships exist only between matrix elements with identical selection rules. Fortunately, only such ratios are required in fitting the spectrum shapes. Ratios of matrix elements with different selection rules depend on specific details of the wave functions involved.

A procedure has been given[3] for estimating the ratios of first-forbidden matrix elements. It leads to conclusions at variance with the fit[7] of the RaE spectrum, unless one assumes an unconscionable proportion of P in the linear combination. This dilemma can be resolved[4] in the case of RaE by considering the pseudoscalar nature of nuclear forces. In this section we attempt to obtain approximate ratios for first- and second-forbidden matrix elements, taking pseudoscalar forces into account but otherwise following the spirit of reference 3.

In writing the β-decay operators, a summation $\sum_k$ over all the nucleons of the nucleus will be understood but not written explicitly unless necessary. The β-decay operators concerned are all contained among the

[4] M. Ruderman, Phys. Rev. **89**, 1227 (1953).
[5] H. M. Mahmoud and E. J. Konopinski, Phys. Rev. **88**, 1266 (1952).
[6] B. M. Rustad and S. L. Ruby, Phys. Rev. **89**, 880 (1953); J. S. Allen and W. K. Jentschke, Phys. Rev. **89**, 902 (1953).
[7] A. G. Petschek and R. E. Marshak, Phys. Rev. **85**, 698 (1952).

forms

$$Q\begin{Bmatrix}1\\ \beta\end{Bmatrix}\begin{Bmatrix}1\\ \gamma_5\end{Bmatrix}\begin{Bmatrix}1\\ \boldsymbol{\sigma}\cdot\mathbf{r}\\ R_n\\ \boldsymbol{\sigma}\cdot\boldsymbol{\nabla}R_n\\ \boldsymbol{\sigma}\times\mathbf{r}\cdot\boldsymbol{\nabla}R_n\end{Bmatrix}, \tag{1}$$

where Q changes a neutron into a proton and R_n is a solid harmonic $[r^nY_n(\theta)]$ or equivalent coordinate tensor[8] with $(2n+1)$ independent components. The "relativistic" operators contain the factor γ_5 and depend strongly on the presence or absence of the factor β. The nonrelativistic operators are not much affected by β and will be written without it. The most general relations are those between relativistic and nonrelativistic operators, but there is one fairly general relation between two nonrelativistic operators for an nth-forbidden transition:

$$\int\Psi_f^*Q\boldsymbol{\sigma}\times\mathbf{r}\cdot\boldsymbol{\nabla}R_n\Psi_i=i/h\int\Psi_f^*Q[\boldsymbol{\sigma}\cdot\mathbf{r}\times\mathbf{p},R_n]\Psi_i \tag{2}$$

$$=it\int\Psi_f^*QR_n\Psi_i,$$

where the square bracket is a commutator and the subscripts i and f indicate initial and final nuclear wave functions. For multiparticle transitions or cases where there is considerable Russell-Saunders coupling, the coefficient t can be evaluated only from detailed knowledge of the nuclear wave functions. For the most useful first approximation of transitions between the same subshells in $j-j$ coupling, however,

$$t=(1/h)\{(\boldsymbol{\sigma}\cdot\mathbf{L})_f-(\boldsymbol{\sigma}\cdot\mathbf{L})_i\} \tag{3}$$

$$=\pm n \text{ for odd } A. \tag{3a}$$

The relativistic matrix elements not containing β can be related directly to nonrelativistic elements without explicit introduction of the nuclear forces. For example,

$$\int Q\gamma_5\boldsymbol{\sigma}\cdot\boldsymbol{\nabla}R_n=\frac{-i}{hc}\int[H_0,QR_n]$$

$$=\frac{-i}{hc}\int[H-H_c-H_\nu,QR_n]$$

$$\approx\frac{-i}{hc}\left\{\Delta E-1.2\frac{Ze^2}{R}(1-f_\nu)\right\}\int QR_n, \tag{4}$$

where $H_0=-\boldsymbol{\alpha}\cdot\mathbf{p}c-\beta Mc^2$, again without writing explicitly the summation $\sum_k$. The argument follows that of reference 3: the total energy difference of the two nuclear states is $\Delta E=E_f-E_i$, the Coulomb energy difference for a uniform charge distribution is $1.2\,Ze^2/R$ with R the nuclear radius, and $0<f_\nu<1$ is a fraction representing the extent to which the change in Coulomb energy is counterbalanced by an opposite change in the nuclear symmetry energy. Reference 3 takes $f_\nu\approx\frac{3}{5}$, while a value equivalent to $f_\nu\approx\frac{1}{6}$ is obtained from more explicit calculations[9] with single-particle wave functions and a specific Hamiltonian operator. With atomic units h/m_0c for length, $m_0c^2=\frac{1}{2}$ Mev for energy, Eq. (4) becomes

$$\int Q\boldsymbol{\alpha}\cdot\boldsymbol{\nabla}R_n\approx i\chi\int QR_n,\quad \chi=2.4B(1-f_\nu)-\Delta W, \tag{5}$$

where B is the Coulomb barrier height of the (final) nucleus in Mev and $\Delta W=\Delta E/m_0c^2$. For negatron emission in elements heavy enough to have forbidden spectra, ΔW is frequently negligible relative to the term in B. Equation (5) for $n=1$ is the first Eq. (19) of reference 3.

The only other relativistic operator of possible importance in β decay that does not involve β is $Q\gamma_5$; consider

$$\int[H_0,Q\boldsymbol{\sigma}\cdot\mathbf{r}]=ihc\int Q\gamma_5[\boldsymbol{\sigma}\cdot\boldsymbol{\nabla},Q\boldsymbol{\sigma}\cdot\mathbf{r}]$$

$$=ihc\int Q\gamma_5(3+2i\boldsymbol{\sigma}\cdot\boldsymbol{\nabla}\times\mathbf{r}) \tag{6}$$

$$=ihc\int Q\gamma_5\left(3+\frac{2}{h}\boldsymbol{\sigma}\cdot\mathbf{L}\right).$$

For the operator $\boldsymbol{\sigma}\cdot\mathbf{L}$ in this matrix element we must take, for any individual nucleon that makes a transition, the average value of $\boldsymbol{\sigma}\cdot\mathbf{L}$ for fixed j and $l=j\pm\frac{1}{2}$; this value is $-h$, independent of j and l, so that in general

$$\int Q\gamma_5=\frac{-i}{hc}\int[H_0,Q\boldsymbol{\sigma}\cdot\mathbf{r}]=i\chi\int Q\boldsymbol{\sigma}\cdot\mathbf{r}. \tag{7}$$

This is the second Eq. (19) of reference 3.

In contrast to Eqs. (5) and (7), relativistic operators containing β can be related to nonrelativistic operators only by writing out the matrix elements in nonrelativistic approximation. At this point certain characteristic terms will arise if the nuclear forces are pseudoscalar with pseudoscalar coupling. Consider the operator $\beta\gamma_5$:

$$\int\Psi_f^*Q\beta\gamma_5\Psi_i\approx\int\{\psi_{1f}^*Q\psi_{0i}-\psi_{0f}^*Q\psi_{1i}\}. \tag{8}$$

Here ψ_0 is the product of the large components of the wave function for all nucleons in the nucleus, and ψ_1 differs only by the substitution of the small component for the particle on which $Q\beta\gamma_5$ operates. A nonrela-

[8] E. J. Konopinski and G. E. Uhlenbeck, Phys. Rev. **60**, 308 (1941).

[9] D. L. Pursey, Phil. Mag. **42**, 1193 (1951).

tivistic approximation for ψ_1 is to be obtained from the equation of motion:

$$\sum_k(-\boldsymbol{\alpha}^k\cdot\mathbf{p}^k c-\beta^k Mc^2)\Psi=(E-V-V_p)\Psi, \quad (9)$$

where the pseudoscalar potential is

$$V_p=\tfrac{1}{2}\sum_{j\neq k}T^{jk}V^{jk}(\beta\gamma_5)^j(\beta\gamma_5)^k,$$

$$T^{jk}=\boldsymbol{\tau}^j\cdot\boldsymbol{\tau}^k, \quad V^{jk}=V_0\exp(-\kappa|\mathbf{r}^j-\mathbf{r}^k|)/|\mathbf{r}^j-\mathbf{r}^k|. \quad (10)$$

The "ordinary" potential V does not contain any $\beta\gamma_5$ factors. We write out the component of (9) that corresponds to $(E-V)\psi_1{}^k$:

$$-\boldsymbol{\sigma}^k\cdot\mathbf{p}^k c\psi_0-\sum_{j\neq k}\boldsymbol{\sigma}^j\cdot\mathbf{p}^j c\psi_2{}^{jk}+(A-2)Mc^2\psi_1{}^k=(E-V)\psi_1{}^k$$
$$+\sum_{j\neq k}T^{jk}V^{jk}\psi_1{}^j-\tfrac{1}{2}\sum_{k\neq i\neq j\neq k}T^{ij}V^{ij}\psi_3{}^{ijk}, \quad (11)$$

where no summation is implied on the index k. Here $\psi_n{}^{ijk\cdots}$ is the product of the small component wave functions φ for the n nucleons $ijk\cdots$, times the product of the large components Φ for all other nucleons. Equation (11) reduces to first order in φ by dropping the second and sixth terms, which are small of order φ^2 relative to the otherwise similar first and fifth terms, respectively. Taking $E-V\approx AMc^2$ yields

$$\psi_1{}^k\approx-\frac{1}{2Mc^2}[\boldsymbol{\sigma}^k\cdot\mathbf{p}^k c\psi_0+\sum_{j\neq k}T^{jk}V^{jk}\psi_1{}^j]. \quad (12)$$

Since only terms of first order in φ are preserved, it is consistent to retain only those of first order in V and substitute $\psi_1{}^j\approx(-1/2Mc)\boldsymbol{\sigma}^j\cdot\mathbf{p}^j\psi_0$ on the right-hand side of (12), so that

$$\psi_1{}^k\approx\frac{-1}{2Mc}[\boldsymbol{\sigma}^k\cdot\mathbf{p}^k-\sum_{j\neq k}T^{jk}U^{jk}\boldsymbol{\sigma}^j\cdot\mathbf{p}^j]\psi_0, \quad (13)$$

where $U=V/2Mc^2$.

The matrix element (8) is now, writing the $\sum_k$ explicitly,

$$\langle Q\beta\gamma_5\rangle\approx\frac{-1}{2Mc}\sum_k\int[\boldsymbol{\sigma}^k\cdot\mathbf{p}^k,Q^k]$$
$$+\frac{1}{2Mc}\sum_k\sum_{j\neq k}\int[T^{jk}\boldsymbol{\sigma}^j\cdot\mathbf{p}^j,Q^kU^{jk}]. \quad (14)$$

The first term of (14) is just that obtained without considering pseudoscalar forces and to this approximation vanishes identically. The second term arises from the pseudoscalar potential. Using the fact that $Q=\frac{1}{2}(\tau_x+i\tau_y)$, we obtain

$$[T^{jk}\boldsymbol{\sigma}^j\cdot\mathbf{p}^j,Q^kU^{jk}]=Q^j[\boldsymbol{\sigma}^j\cdot\mathbf{p}^j,U^{jk}]$$
$$+(Q^k\tau_z{}^j-Q^j\tau_z{}^k)[\boldsymbol{\sigma}^j\cdot\mathbf{p}^j,U^{jk}]_+, \quad (15)$$

where the + bracket is an anticommutator. The second term in (15) will be dropped because a summation over τ_z is expected to give a term of order $(N-Z)/A\lesssim 10$ percent relative to the first. The first term of (15) gives a contribution to $\langle Q\beta\gamma_5\rangle$ of

$$\frac{1}{2Mc}\sum_j\sum_{k\neq j}\int[Q^j\boldsymbol{\sigma}^j\cdot\mathbf{p}^j,U^{jk}]. \quad (16)$$

The order-of-magnitude relation between V^{jk} and the nonrelativistic approximation to the two-body pseudoscalar potential is $V^{jk}\sim-(2Mc/\hbar\kappa)^2H^{jk}$. Now $\sum_{k\neq j}H^{jk}$ is that part of the nuclear force on the jth nucleon which is contributed by the two-body pseudoscalar potential. We accordingly write

$$\sum_{k\neq j}U^{jk}=\rho\left(\frac{2M}{\mu}\right)^2\frac{H_\nu{}^j}{2Mc^2}, \quad (17)$$

where μ is approximately the π-meson mass and ρ is an undetermined factor. Here ρ takes care of the fact that the effective potential in the nucleus may not all arise from two-body pseudoscalar forces and also includes the uncertainty in the relation of V^{jk} to H^{jk}. This uncertainty is aggravated because the above discussion depends on the first term of a power series expansion in V_p, and higher terms may be important. We do not expect $|\rho|$ to differ by an order of magnitude from unity, but not much more can be said; it may show appreciable fluctuation from one nucleus to the next, and under these fluctuations may be a gradual trend with A.

Lumping our ignorance in the factor ρ, we have

$$\langle Q\beta\gamma_5\rangle\approx\frac{\rho}{\mu^2c^3}\int[Q\boldsymbol{\sigma}\cdot\mathbf{p},H_\nu]$$
$$=f_\nu\left(\frac{1.2Ze^2}{R}\right)\frac{\rho}{\mu^2c^3}\int Q\boldsymbol{\sigma}\cdot\mathbf{p}. \quad (18)$$

Since we have already taken the pseudoscalar forces into account once, we can evaluate $\int Q\boldsymbol{\sigma}\cdot\mathbf{p}$ to this order by taking for H_0 the nonrelativistic approximation without pseudoscalar forces, $H_0\approx p^2/2M$. Then

$$\int Q\boldsymbol{\sigma}\cdot\mathbf{p}\approx\frac{iM}{\hbar}\int[H_0,Q\boldsymbol{\sigma}\cdot\mathbf{r}]$$
$$\approx\frac{iM}{\hbar}\left\{\Delta E-1.2\frac{Ze^2}{R}(1-f_\nu)\right\}\int Q\boldsymbol{\sigma}\cdot\mathbf{r}, \quad (19)$$

so that, in atomic units,

$$\langle Q\beta\gamma_5\rangle\approx-i\rho\left(\frac{m_0M}{\mu^2}\right)\chi f_\nu 2.4B\int Q\boldsymbol{\sigma}\cdot\mathbf{r}. \quad (20)$$

The procedure leading to (12) may be immediately applied to show that nuclear forces with pseudovector coupling will make a negligible correction to the matrix elements as compared with that from pseudoscalar

coupling. In this case, (13) becomes

$$\psi_1{}^k \approx -(1/2Mc^2)[\boldsymbol{\sigma}^k\cdot\mathbf{p}^k c\psi_0 - \rho H_s\psi_1{}^k] \approx -(1/2Mc^2)[1+\rho H_s/2Mc^2]\boldsymbol{\sigma}^k\cdot\mathbf{p}^k\psi_0, \quad (21)$$

so that

$$\langle Q\beta\gamma_5\rangle \approx -(1/2Mc)\int[\boldsymbol{\sigma}\cdot\mathbf{p}, Q] - (\rho/2Mc)\int[\boldsymbol{\sigma}\cdot\mathbf{p}, QH_s]/2Mc^2. \quad (22)$$

In this case the second term is smaller than (18) by a factor of order $(\mu/2M)^2\sim 5\times 10^{-3}$. Thus pseudovector coupled forces behave like any "ordinary" forces in making no appreciable correction to the lowest order approximation for relativistic matrix elements.

Repeating the above arguments for the operator $Q\beta\gamma_5\boldsymbol{\sigma}\cdot\boldsymbol{\nabla}R_n$ leads to

$$\langle Q\beta\boldsymbol{\alpha}\cdot\boldsymbol{\nabla}R_n\rangle \approx -\frac{1}{2Mc}\sum_k\int Q^k[\boldsymbol{\sigma}^k\cdot\mathbf{p}^k, \boldsymbol{\sigma}^k\cdot\boldsymbol{\nabla}^k R_n{}^k] + \frac{1}{2Mc}\sum_j\sum_{k\neq j}\int[Q^j\boldsymbol{\sigma}^j\cdot\mathbf{p}^j, \boldsymbol{\sigma}^k\cdot\boldsymbol{\nabla}^k R_n{}^k U^{jk}]. \quad (23)$$

Here again the first term is obtained under any nuclear force assumption, and the second is peculiar to pseudoscalar coupling. For the first term we have

$$\int[\boldsymbol{\sigma}\cdot\mathbf{p}, \boldsymbol{\sigma}\cdot\boldsymbol{\nabla}R_n] = 2i\int(\boldsymbol{\sigma}\times\mathbf{p})\cdot\boldsymbol{\nabla}R_n. \quad (24)$$

Consider the quantities

$$a = (-ih/M)(\boldsymbol{\sigma}\times\mathbf{p})\cdot\boldsymbol{\nabla}R_n$$
$$b_m = (\boldsymbol{\sigma}\times\mathbf{r})\cdot\boldsymbol{\nabla}(-(ih/M)\mathbf{p}\cdot\boldsymbol{\nabla})^m R_n. \quad (25)$$

Now using $H_0\approx p^2/2M$ and atomic units, we have

$$\int[H_0, b_m] = -\chi\int b_m = \int\left(\frac{-ih}{M}\boldsymbol{\sigma}\times\mathbf{p}\cdot\boldsymbol{\nabla}\right)\left(\frac{-ih}{M}\mathbf{p}\cdot\boldsymbol{\nabla}\right)^m R_n + \int b_{m+1}. \quad (26)$$

The first term of (26) can be obtained by taking the commutator of a with H_0 m successive times, so that (26) reads

$$-\chi\int b_m = (-\chi)^m\int a + \int b_{m+1}. \quad (27)$$

Equation (27) is a recursion relation in $\int b_m$ subject to the boundary condition that $b_n=0$, since R_n is of degree n in the coordinate on which $\boldsymbol{\nabla}$ operates. The solution is

$$\int b_m = (n-m)(-\chi)^{m-1}\int a, \quad (28)$$

and for the particular case $m=0$,

$$\int(\boldsymbol{\sigma}\times\mathbf{p})\cdot\boldsymbol{\nabla}R_n = -\left(\frac{iM}{h}\right)\left(\frac{\chi}{n}\right)\int(\boldsymbol{\sigma}\times\mathbf{r})\cdot\boldsymbol{\nabla}R_n. \quad (29)$$

The first term of (23) is, accordingly,

$$\langle Q\beta\boldsymbol{\alpha}\cdot\boldsymbol{\nabla}R_n\rangle_0 \approx -\left(\frac{\chi}{n}\right)\int(\boldsymbol{\sigma}\times\mathbf{r})\cdot\boldsymbol{\nabla}R_n = -i\left(\frac{t}{n}\right)\chi\int R_n, \quad (30)$$

by use of (2). For $n=1$ this is the third Eq. (19) of reference 3.

For the second term of (23) we write

$$[\boldsymbol{\sigma}^j\cdot\mathbf{p}^j, \boldsymbol{\sigma}^k\cdot\boldsymbol{\nabla}^k R_n{}^k U^{jk}] = [\tfrac{1}{2}[\boldsymbol{\sigma}^j\cdot\mathbf{p}^j, \times\boldsymbol{\sigma}^k\cdot\boldsymbol{\nabla}^k R_n{}^k]_+, U^{jk}], \quad (31)$$

and then capitalize on the fact that U^{jk} is almost a δ function. Under this approximation, $\boldsymbol{\nabla}^k R_n{}^k = -\boldsymbol{\nabla}^j R_n{}^j$ and the $\sum_{k\neq j}\boldsymbol{\sigma}^k = \mathbf{S}-\boldsymbol{\sigma}^j$, where S is the total spin. Assuming no correlation between $\mathbf{S}$ and $\boldsymbol{\nabla}^j$, we drop the term $\mathbf{S}\cdot\boldsymbol{\nabla}^j$ and have for (31):

$$\sum_{k\neq j}[\boldsymbol{\sigma}^j\cdot\mathbf{p}^j, \boldsymbol{\sigma}^k\cdot\boldsymbol{\nabla}^k R_n{}^k U^{jk}] \approx \sum_{k\neq j}[\mathbf{p}^j\cdot\boldsymbol{\nabla}^j R_n{}^j, U^{jk}]. \quad (32)$$

With (17) the second term of (23) becomes, in atomic units,

$$\frac{\rho}{\mu^2 c^3}\int Q[\mathbf{p}\cdot\boldsymbol{\nabla}R_n, H_s] = f_s\left(\frac{1.2\,Ze^2}{R}\right)\frac{\rho}{\mu^2 c^3}\int Q\mathbf{p}\cdot\boldsymbol{\nabla}R_n = -i\rho\left(\frac{m_0 M}{\mu^2}\right)\chi f_s(2.4B)\int QR_n, \quad (33)$$

since

$$\int\mathbf{p}\cdot\boldsymbol{\nabla}R_n = \frac{iM}{h}\int[H_0, R_n] = \frac{-iM\chi}{h}\int R_n. \quad (34)$$

Thus, finally,

$$\langle Q\beta\boldsymbol{\alpha}\cdot\boldsymbol{\nabla}R_n\rangle \approx -i\chi\left[\frac{t}{n}+\rho\left(\frac{m_0 M}{\mu^2}\right)f_s(2.4B)\right]\int QR_n. \quad (35)$$

Relations (2), (4), (7), (20), and (35) will be used in the analysis of the shapes of forbidden spectra. From this analysis it will appear that the general form of the pseudoscalar corrections is adequate, but that the specific expressions for the coefficients of the pseudoscalar terms cannot be taken too seriously. This is not surprising in view of the many crude approximations made in obtaining these coefficients; they are perhaps better replaced by a single phenomenological parameter with absolute magnitude of order unity.

III. ALGEBRAIC FORMS OF FORBIDDEN SPECTRA

To obtain some insight into the shapes of forbidden spectra that are possible under various linear combinations, we write out the correction factors in low-Z approximation. This procedure has the advantage of showing at once which terms are large and what cancellations must occur among these large terms in order to produce unusual spectral shapes among the remaining small terms. Use of the low-Z formulas means that the cancellation conditions and the spectral shapes resulting from cancellation are given only approximately. Any conclusions based only on order-of-magnitude arguments ought still to be valid, however.

The features of all linear combinations not containing SV or TA mixtures are illustrated by the four choices STP, VA, SAP, VT. The real coefficients λ in these equations are limited by the result from the mirror transitions that $\lambda_F=\pm\lambda_{GT}$. This condition is assumed throughout. To specify the first-forbidden correction factors,[8,10] it is convenient to define the following functions:

$$12x_1=(p^2+K^2),$$

$$y_1(K,a)=[\{B(\lambda+t)-a\}+\tfrac{1}{3}\{(p^2/W)(\lambda+t)+K(\lambda-t)\}]^2+(1/18)[p^2(2\lambda-t)^2+K^2(2\lambda+t)^2]+\tfrac{1}{9}(p^2/W^2)(\lambda+t)^2,$$

$$y_1(K,a,a')=[Bt-a+\tfrac{1}{3}t(p^2/W+K)]^2+[B-a'+\tfrac{1}{3}(p^2/W+K)]^2+(2\lambda/W)[(Bt-a+\tfrac{1}{3}Kt)(B-a'+\tfrac{1}{3}K)-\tfrac{1}{9}K^2t]+(1/18)(p^2+K^2)\times(4+t^2)+\tfrac{1}{9}(p^2/W^2)(1+t^2),$$

$$z_1(K,g,g')=[B-g+\tfrac{1}{3}(p^2/W+K)]^2+g'^2-(2/W)g'(B-g+\tfrac{1}{3}K)+\tfrac{1}{9}(p^2/W^2). \quad (36)$$

Here $B=Ze^2/2R$; and if R is in atomic units, B is numerically equal to the Coulomb barrier height in Mev of the final nucleus, $B\approx Z/A^{\frac{1}{3}}$. The quantities p, W and K are the electron momentum, electron energy, and neutrino energy in m_0c^2 units; and

$$\lambda=\lambda_F/\lambda_{GT}=\pm 1. \quad (37)$$

The other parameters are all real numbers and represent ratios of nuclear matrix elements as follows:

$$\int\boldsymbol{\sigma}\times\mathbf{r}=it\int\mathbf{r},\quad \int\beta\boldsymbol{\alpha}=ia\int\mathbf{r},\quad \int\boldsymbol{\alpha}=ia'\int\mathbf{r},$$
$$(\lambda_P/\lambda_{GT})\int\beta\gamma_5=ig\int\boldsymbol{\sigma}\cdot\mathbf{r},\quad \int\gamma_5=ig'\int\boldsymbol{\sigma}\cdot\mathbf{r}. \quad (38)$$

The factor g includes in its definition the ratio λ_P/λ_{GT}, which is real but of undetermined magnitude. According to the results of the preceding section, the coefficients a, a', g, g' are all of order B.

The first-forbidden correction factors for the four combinations listed above now take the form

$$C_1=\left|\int B_{ij}\right|^2x_1+\left|\int\mathbf{r}\right|^2y_1+\left|\int\boldsymbol{\sigma}\cdot\mathbf{r}\right|^2z_1. \quad (39)$$

Here x is independent of the combination assumed, and y and z are given by the following scheme:

$$\begin{aligned} &STP:\ y_1(-K,a);\ z_1(K,g,0),\\ &VA:\ y_1(K,\lambda a');\ z_1(k,g',0),\\ &SAP:\ y_1(K,0,0);\ z_1(K,g',g),\\ &VT:\ y_1(K,a,a');\ z_1(-K,0,0). \end{aligned} \quad (40)$$

For the second-forbidden correction factors it is convenient to define the functions

$$1080x_2=[(p^2+K^2)^2+(4/3)p^2K^2],$$

$$3y_2(K,a)=p^2\{[\tfrac{1}{2}B(\lambda+\tfrac{1}{2}t)-\tfrac{1}{2}a]+\tfrac{1}{5}(p^2/W)(\lambda+\tfrac{1}{2}t)+\tfrac{1}{3}K(\lambda-\tfrac{1}{2}t)\}^2+K^2\{[B(\lambda+\tfrac{1}{2}t)-\tfrac{1}{2}a]+\tfrac{1}{3}(p^2/W)\times(\lambda+\tfrac{1}{2}t)+\tfrac{1}{5}K(\lambda-\tfrac{1}{2}t)\}^2+(1/150)p^4(3\lambda-t)^2+(1/150)K^4(3\lambda+t)^2+\tfrac{1}{5}p^2K^2+(p^2/W^2)(\lambda+\tfrac{1}{2}t)^2\times[(1/25)p^2+\tfrac{1}{9}K^2],$$

$$3y_2(K,a,a')=p^2\{\eta^2(a';\tfrac{1}{5},\tfrac{1}{3})+(\tfrac{1}{2}t)^2\eta^2(2a/t;\tfrac{1}{5},\tfrac{1}{3})+(2\lambda t/W)[\zeta(a';\tfrac{1}{3})\zeta(2a/t;\tfrac{1}{3})-\tfrac{1}{9}K^2]\}+K^2\{\eta^2(a';\tfrac{1}{3},\tfrac{1}{5})+(\tfrac{1}{2}t)^2\eta^2(2a/t;\tfrac{1}{3},\tfrac{1}{5})+(2\lambda t/W)[\zeta(a';\tfrac{1}{5})\zeta(2a/t;\tfrac{1}{5})-(1/25)K^2]\}+(p^4+K^4)[(9+t^2)/150]+\tfrac{1}{9}p^2K^2+(p^2/W^2)\times(1+t^2/4)[(1/25)p^2+\tfrac{1}{9}K^2]. \quad (41)$$

$$\rho(a;k)=B-\tfrac{1}{2}a+kK,$$
$$\eta(a;j,k)=\zeta(a;k)+jp^2/W,$$

where

$$\int T_{ij}=it\int R_{ij},\quad \int\beta A_{ij}=ia\int R_{ij},$$
$$\int A_{ij}=ia'\int R_{ij}, \quad (42)$$

and the T_{ij}, A_{ij}, R_{ij} are defined in reference 8. The coefficients a, a' are again of order B. In low-Z approximation, the second-forbidden correction factors are then

$$C_2=\left|\int S_{ijk}\right|^2x_2+\left|\int R_{ij}\right|^2y_2, \quad (43)$$

where x_2 is associated with the GT part of any linear combination, and y_2 is given by the following scheme:

$$\begin{aligned} &ST:\ y_2(-K,a),\\ &VA:\ y_2(K,\lambda a'),\\ &SA:\ y_2(-K,0,0),\\ &VT:\ y_2(K,a,a'). \end{aligned} \quad (44)$$

Since the matrix elements of P contribute only a negligible amount to any second-forbidden decay, the

[10] A. M. Smith, Phys. Rev. **82**, 955 (1951).

schemes (44) are independent of P. This was not true of first-forbidden decays, where P contributes appreciably to $\Delta I=0$ transitions. In the applications of (43) below, we consider only transitions with $\Delta I=2$ and drop the term in x_2 as negligibly small.

Some general features of the y_1 and y_2 are at once apparent. For medium-to-heavy nuclei where most forbidden transitions occur, the terms in (36) and (41) involving B are an order of magnitude larger than the remaining terms. Hence to a first approximation the spectrum shapes are given by the terms in B alone. This makes for great simplification in classifying the spectrum shapes. In particular, this simplification shows why most first-forbidden transitions with $\Delta I<2$ have an apparent allowed shape, as has already been pointed out:[5] the dominant terms containing B in (36) have no energy-dependent factors. The same approximation for the second-forbidden spectra leads to a general shape of the form:

$$C_2\sim p^2+v^2K^2,$$

$$v^2=\left[\frac{2B\left(\lambda+\frac{t}{2}\right)-b}{B\left(\lambda+\frac{t}{2}\right)-b}\right]^2, \tag{45}$$

$$\begin{aligned} b&=a && ST,\\ &=\lambda a' && VA,\\ &\approx 0 && SA,\\ &\approx a+\lambda a' && VT. \end{aligned}$$

For the combinations SA and VT the value of b is obtained under the approximation $1/W\approx 1$, which is not unsuitable because all second-forbidden transitions with $\Delta I=2$ have low-energy end points.

In this first approximation where only the leading terms in $\alpha Z/2R$ are retained, certain general features of the combinations are independent of the order of forbiddenness. The $ST(P)$ and VA combinations are indistinguishable in generic form: each contains two constants representing matrix element ratios (t and a or a'), and if we have no prejudices about the values of these parameters, any spectrum can be fitted equally well with $ST(P)$ or VA. The combination $SA(P)$, on the other hand, has only one such parameter (t), and is therefore relatively inflexible for fitting observed spectrum shapes. It will be seen below that this inflexibility is sufficient to rule out the combination $SA(P)$. The combination VT is the most flexible of all, containing three independent parameters (t, a, a'); it would therefore be very difficult in general to exclude this combination by comparison with observed spectral shapes. A fortunate circumstance in the first-forbidden spectra makes it possible to make a fair statistical though not absolute argument against this combination.

The higher terms that do not involve B in the spectrum shapes must be considered only in the event that the terms in B happen just to cancel. In this relatively rare circumstance, the combinations $ST(P)$ and VA will show a real difference in shape, arising from the opposite signs of K in the two cases. Apparently the only known spectrum of this type is the RaE spectrum, where analysis[7] shows that $ST(P)$ is a better fit than VA. It is of interest to note that this necessity of invoking higher terms in the spectrum shape is practically peculiar to first-forbidden transitions. For second- (and presumably for higher) forbidden transitions, the quantity B occurs in several coefficients that multiply simple functions of the energy like p^2 and K^2. These coefficients are not identical in form, so that if one of them vanishes, the others are very likely not to vanish. For example, in the first-forbidden transitions we must use the higher terms in $y_1(K, a)$ if $B(\lambda+t)\approx a$, which is certainly conceivable; in the second-forbidden $y_2(K, a)$ the higher terms will be necessary only if $\lambda+t/2\approx b\approx 0$, which is a much less likely occurrence.

These spectrum shapes, particularly their approximate forms preserving only the large terms, are applied in the next section to observed spectra. The $\Delta I=2$, no, spectra have previously been fitted by using T alone, and it is easy to see why this was possible. This choice corresponds to taking $b=a, \lambda=0$ in (45); and for any value of a that yields a certain v^2 when $\lambda=\pm 1$, we can find another value of a that yields the same v^2 with $\lambda=0$.

IV. COMPARISON WITH OBSERVED SHAPES

First-forbidden spectra with $\Delta I<2$ all have allowed shapes with the exception of RaE, which will be discussed below. These allowed shapes attest to the validity of the first approximation, in which only terms of order B are retained in fitting the spectral shapes. It is impossible from these allowed-shape spectra to distinguish between $ST(P)$ and VA, but the presence of $1/W$ terms in the expression (36) for $SA(P)$ and VT allows us to argue against these combinations.

A number of first-forbidden spectra of apparent allowed shape have been analyzed[2] with a correction factor $C_1=(1+r/W)$. The values of $|r|$ average on the order of 7 percent and are generally within the estimated errors of the determination. The algebraic sign and magnitude of r seem to fluctuate randomly among independent measurements of the same spectrum. We may conclude that there is no evidence at variance with the statement that $r=0$.

This conclusion immediately rules out the combination SA. For the $\Delta I=1$ transitions, only $y_1(K, 0, 0)$ is effective, and

$$r=2\lambda t/(1+t^2)\approx\pm 1, \tag{46}$$

since $\lambda=\pm 1$, and $t=\pm 1$ is the most likely value for a first-forbidden transition with $\Delta I=1$. Of the first-forbidden transitions analyzed in reference 2, the shell model indicates the Pr^{143}, Pm^{147}, Re^{186}, and Au^{198} are

most likely to have $\Delta I=1$; while Be^{139} and Hf^{181} are somewhat uncertain and may or may not have $\Delta I=1$. It is clear, however, that none of the cases most likely to have $\Delta I=1$ give anything approaching $|r|=1$, so the combination SA seems definitely excluded.

The argument is somewhat less positive for VT, the other combination that gives $1/W$ terms in the allowed-shape spectra. Again taking only the $\Delta I=1$ transitions and retaining only terms of order B in (36), we have

$$r=\frac{2\lambda(Bt-a)(B-a')}{[(Bt-a)^2+(B-a')^2]}. \tag{47}$$

This can give $r=0$ in agreement with observation if $a'=B$ or $a=Bt$. The matrix element estimate (35) indicates that $a\neq Bt$; but the estimate (5) shows that $a'\approx\chi$, which is at least of order B. In fact, if $f_v=0.6$ as assumed in reference 3, we have $\chi\approx B$. It is therefore apparent that the nuclear parameters can conspire to give $r\approx 0$ by a fortuitous cancellation in the VT case, while still retaining the allowed shape.[11]

The matrix element estimate (5) is certainly not to be regarded as accurate to the last percent, however: fluctuations are expected in nuclear parameters like f_v and Ze^2/R, and the term ΔW in χ will vary in any case. For example, variations in ΔW alone cause a standard deviation of about 5 percent around a mean value of $\chi/B=1$ for the four $\Delta I=1$ cases of reference 2. If we assume an equivalent, independent deviation in χ/B from other sources and include the factor 2 in (47), we have an expected standard deviation of $\sigma_r\sim 15$ percent about a mean value of $r=0$.

The $\Delta I=1$ transitions in reference 2, weighted according to their errors Δ_r, show a $\sigma_r'\sim 5$ percent about a mean value of -0.02. The probability that four independent elements which should have a fluctuation σ_r actually show by chance a fluctuation $\leq\sigma_r'$ is roughly $p\approx\frac{2}{3}(\sigma_r'/\sigma_r)^{4/3}$ for $\sigma_r'/\sigma_r\ll 1$. If we take $\sigma_r'/\sigma_r\sim 1/3$ as is suggested by the figures in the preceding paragraph, the value obtained for p is on the order of 0.2. We may therefore make a statistical argument that it is quite unlikely (expected chances of order 20 percent) for the linear combination to be VT.

For the second-forbidden transition we again make the simplification of retaining only the terms in (41) of order B^2, since this approximation proves to be so well followed in the first-forbidden cases. We fit the $\Delta I=2$, no, spectra by first plotting $C(W)=[n/(W_0-W)]^2$, where n gives the conventional Kurie plot. According to (45), this $C(W)$ should have a minimum at W_m, where $v^2=W_m/(W_0-W_m)$. Although the experimental minimum is not always very pronounced, it seems more reliable to estimate v^2 in this way than by a least-squares fit, which tends to overemphasize the ends of the spectrum where the data are poorest. Table I lists values† of v^2.

TABLE I. Fits of $\Delta I=2$, no, spectra.

Decay	v^2	Transition	t
Cl^{36} [a]	0.6	$d_{3/2}\rightarrow d_{3/2}$	0
Tc^{99} [a,b]	~ 2	$d_{5/2}\rightarrow g_{9/2}$	+2
I^{129} [c]	$\gtrsim 10$		
Cs^{135} [d]	$\gtrsim 10$	$d_{3/2}\rightarrow g_{7/2}$	−2
Cs^{137} [e]	$\gg 10$		

[a] L. Feldman and C. S. Wu, Phys. Rev. **87**, 1091 (1952).
[b] S. I. Taimuty, Phys. Rev. **81**, 461 (1951).
[c] C. S. Wu and E. der Mateosian (private communication).
[d] Lidofsky, Alperovitch, and Wu, Phys. Rev. **90**, 387 (1953).
[e] L. M. Langer and R. J. D. Moffat, Phys. Rev. **82**, 635 (1951).

Table I also indicates the individual particle transitions according to the shell model and the associated values of the parameter t. As far as the crude arguments below are concerned, Table I contains just three independent cases: Cl^{36} with $t=0$ and $Z=18$ has $v^2<1$; Tc^{99} with $t=+2$ and $Z=44$ has $v^2\gtrsim 1$; and I^{129}, Cs^{135}, Cs^{137} (high-energy transition) all have $t=-2$, $Z\approx 55$, and $v^2\gg 1$. We shall use just these three groups in applying (45) to determine the linear combination. The ideal values of t given in Table I will also be assumed; they are presumably subject to at least the same sort of deviations as found between the magnetic moments and the Schmidt limits, but this should not vitiate the order-of-magnitude considerations below.

The results for first-forbidden spectra indicate that we have only to consider the combinations VA and ST. In allowed-shape, first-forbidden spectra it is impossible to distinguish between these combinations; and the distinction would remain impossible in any order of forbiddenness, if we had no independent means of estimating nuclear matrix element ratios. Because of estimates like those of Sec. II, however, we are able to distinguish VA and ST in the second-forbidden spectra. Consider first VA: Eq. (5) indicates that $a'\sim B$, and inserting this relation in (45), we have

$$v^2\sim 4[(\lambda+t)/t]^2. \tag{48}$$

This should be of order 10 and 1 for $t=2\lambda(=\pm 2)$ and $t=-2\lambda$, respectively, which might agree with Table I if $\lambda=-1$; on the other hand, v^2 should be very large for $t=0$, which is in disagreement with Table I. Hence the spectral shapes provide evidence against VA, corroborating the direct recoil measurements.[6]

For the ST combination we use the matrix element estimate (35), writing it in the form

$$a=-\chi[\tfrac{1}{2}t+\delta], \tag{49}$$

[11] This is just the opposite of the conclusion reached in reference 6 by means of the same arguments. The difference is that reference 6 assumes not only $a'\approx B$ but also $a\approx Bt$, in which case all the first-order terms of $y_1(K,a,a')$ vanish, leaving only the strongly energy-dependent second-order terms. Actually, the matrix element estimate should be $a\approx -Bt$; the error appears to arise from the notation in reference 6, which rather suppresses the roles of λ and t and thus makes it possible to overlook a minus sign.

† *Note added in proof:*—The second-forbidden spectrum of the ground-state β decay of Fe^{60} has been measured by F. R. Metzger (private communication). The spectrum shape indicates $v^2\approx 2$. The most likely shell model assignment is a $p_{3/2}\rightarrow f_{7/2}$ transition with $t=+2$. This case therefore appears to be strictly analogous to Tc^{99}.

where the pseudoscalar correction is regarded as an empirical parameter. The specific form given for δ in (35) depends on too many approximations to be very reliable. From (45) it is clear that $v^2 \approx 1$ when $l \approx -2\lambda$, regardless of the value of a. It is therefore only a question of whether Tc^{99} or the I–Cs group has v^2 closest to unity; and Tc^{99} is obviously the choice. This implies that $\lambda = -\frac{1}{2}l = -1$, or that the combination involves $(S-T)$ for negatron decay.

From (45) we see that v^2 is large (I−Cs) when the denominator approximately vanishes and small (Cl^{36}) when the numerator approximately vanishes. Taking $\lambda = -1$ and the appropriate values of l, these conditions lead to the requirement that

$$a \approx -2B \tag{50}$$

in each case. Comparing with (49) and taking $\chi/B = 1-2$, we have

$$\begin{aligned} &\delta = 1-2 \quad && Cl^{36} \\ &\delta = 2-3 && I-Cs. \end{aligned} \tag{51}$$

The fact that $\delta \neq 0$ is empirical evidence for the necessity of pseudoscalar-coupling corrections to the β-decay matrix elements. It would be impossible to approach cancellation of numerator or denominator in (45) if $\delta = 0$.

The second-forbidden spectrum shapes thus lead to the conclusions that (1) the combination VA is excluded in favor of ST; (2) the relative sign of the terms is $(S-T)$ for negatron emission; (3) nuclear matrix element estimates require substantial corrections for pseudoscalar-coupled forces in the nucleus.

We now return to the first-forbidden spectrum of RaE. This transition has a comparatively long half-life and a non-unique forbidden shape, both of which indicate a cancellation among the large, energy-independent terms in (36). We may argue the choice of the particular expression in (36) as follows: the transition is most likely to be one involving y_1 alone or z_1 alone, because a simultaneous cancellation of the large terms in both y_1 and z_1 is even less likely than the relatively rare cancellation in either one. The quantity y_1 appears alone in all $\Delta I = 1$ transitions, while z_1 appears alone only in $0^- \rightarrow 0^+$ transitions. These latter occur very infrequently,[12] which implies that the rare RaE-type spectrum should be associated with z_1. The previous analysis limits the choice of interaction to STP, and cancellation of the large terms in z_1 implies that

$$g \approx B. \tag{52}$$

This is just the result obtained by detailed analysis[7] of the RaE spectrum. To compare this with the matrix element estimate (20), we write (20) in the form

$$g \approx -(\lambda_P/\lambda_T)\chi\delta. \tag{53}$$

Taking δ to be the same as in (51) and $\chi \approx B$, we obtain

$$-\lambda_P/\lambda_T = 1/\delta \approx (\tfrac{2}{3} \pm \tfrac{1}{3}). \tag{54}$$

The entire empirical argument based on spectrum shapes may now be summarized as follows: the absence of $1/W$ terms in allowed spectra excludes SV and TA; the absence of $1/W$ terms in allowed-shape first-forbidden spectra excludes SA and VT; the non-unique second-forbidden spectra exclude VA and indicate a relative sign $(S-T)$ for negatron emission; and the RaE spectrum indicates that the full linear combination for negatron emission should be

$$[S-T+(1/\delta)P], \tag{55}$$

where δ is a positive number of order unity.

V. SYMMETRY PRINCIPLES

The empirical evidence on the linear combination in β decay is summarized in (55). Because of the difficulty in estimating precisely the contribution of pseudoscalar forces to the nuclear matrix elements, we cannot hope to obtain more than an order of magnitude value of δ from the data. Since it appears impossible to proceed further on an empirical basis, we consider what combinations like (55) may be in accord with various simple symmetry principles.

The general interaction of two Fermi-Dirac fields is

$$\bar{\psi}_1 O \psi_2 \bar{\psi}_3 O \psi_4, \tag{56}$$

where $\bar{\psi} = \psi^{T*}\beta$ is the adjoint function and $O \cdots O$ is a scalar product of any of the five Hermitian relativistic invariants, or a linear combination of these products. The behavior of (56) on permutation of $\bar{\psi}_1$ and $\bar{\psi}_3$ or ψ_2 and ψ_4 has been given.[13] It is convenient to write (56) in terms of the "normal" linear combinations that are eigenvectors under the exchange operation $P = p_{13}$ or p_{24},

$$\begin{aligned} &\Omega_1 = S-T+P, && p=-1; \\ &\Omega_2 = A-V, && p=-1; \\ &\Omega_3 = 2(S-P)-(A+V), && p=-1; \\ &\Omega_4 = 2(S-P)+(A+V), && p=+1; \\ &\Omega_5 = 3S+T+3P, && p=+1. \end{aligned} \tag{57}$$

The eigenvalue of P for each Ω is given in (57).

To generate all possible permutations of (56), it would be necessary to add to P just one further type of permutation operator $P' = p_{12}$ or p_{34}. We cannot find general eigenvalues for P', however, because

$$P'[\bar{\psi}_1 O \psi_2] = \psi_2^T O \bar{\psi}_1^T = (\bar{\psi}_1 O^T \psi_2)^T = \bar{\psi}_1 O^T \psi_2, \tag{58}$$

where the superscript T indicates transpose. There is no general linear relation between O and O^T that is independent of the representation of the Dirac matrices; hence the eigenvalues of P' are dependent on the Dirac

[12] R. W. King (private communication).

[13] M. Fierz, Z. Physik **104**, 553 (1937).

representation, implying that P' has no physical significance.

The only operator like P' for which general eigenvalues exist is P^c, where

$$P^c[\bar{\psi}_1 O\psi_2]=\bar{\psi}_2{}^c O\psi_1{}^c, \tag{59}$$

and ψ^c is the charge conjugate solution[14] defined by

$$\psi^c=C\bar{\psi}^T, \quad \bar{\psi}^c=-\psi^T C^{-1}, \quad C^{-1}\gamma_\mu C=-\gamma_\mu{}^T. \tag{60}$$

This operator is physically suitable because $\bar{\psi}_1 O\psi_2$ and $\bar{\psi}_2{}^c O\psi_1{}^c$ both describe the same physical process. Moreover, the eigenvalues of P^c are independent of the representation, being

$$\begin{aligned} p^c&=-1, \quad O=S, A, P \\ &=+1 \quad O=V, T. \end{aligned} \tag{61}$$

Equations (57) and (61) give the eigenfunctions of P and P^c. There is only one linear combination that is a simultaneous eigenfunction of both operators:[15]

$$\tfrac{1}{2}(\Omega_3-\Omega_2)=S-A-P, \quad p=p^c=-1. \tag{62}$$

Since the combination (62) is excluded for β decay by the experimental data, we may inquire which of the operators P and P^c to abandon first. There is some precedent for requiring the eigenvalue $p=-1$, if the interaction (56) is to hold for equivalent particles in the positions (1,3) or (2,4), since these particles are known to obey anticommutative statistics. On the other hand, the experimental evidence favoring P^c as a valid physical operator is all obtained from interactions with the electromagnetic field, which is not the case described by (56). On this basis the operator P seems to be the more fundamental for (56); the only eigenfunction of P resembling the empirical (55) is Ω_1. We henceforth assume that the true combination in β decay is in fact Ω_1, so that in (55) $\delta\equiv 1$.

The linear combination Ω_1 describes β^- decay when (56) is written in the conventional order:

$$(\bar{\psi}_P O\psi_N)(\bar{\psi}_e O\psi_\nu). \tag{63}$$

To find the corresponding combination Ω_1' that is appropriate the describe β^+ decay, first take the charge conjugate of the right-hand term,

$$\bar{\psi}_e O\psi_\nu=\bar{\psi}_\nu{}^c O'\psi_e{}^c, \tag{64}$$

where O' differs from O by the associated eigenvalue $p^c=\pm 1$. Then insert (64) in (63) and take the complex conjugate of the entire expression, obtaining

$$(\bar{\psi}_N O\psi_P)(\bar{\psi}_\nu{}^c O'\psi_\nu{}^c). \tag{65}$$

According to the eigenvalues (61), the linear combination Ω_1' in (65) that corresponds to Ω_1 in (63) is

$$-\Omega_1'=S+T+P. \tag{66}$$

The minus sign prefixing Ω_1' is unobservable, so that the net result is a change in the relative sign of the T and $(S+P)$ terms in going from β^- to β^+ emission. The effects of this change should in principle be observable.

VI. DECAY OF THE μ MESON

It is of interest to compare the decay of the isolated μ meson into an electron and two neutrinos[16,17] with the law (55) for β decay. In fact, it appears that we can select the combination Ω_1 on the basis of a couple of plausible postulates concerning the neutrino field. In the interest of formal simplicity we consider the equivalent process of annihilation of a μ^+ meson by an electron with the production of two neutrinos. The interaction operator has the form

$$(\bar{\psi}_\nu O\psi_\mu)(\bar{\psi}_\nu O\psi_e). \tag{67}$$

Now if both ψ_ν represent quanta of the same field, we require $p=-1$ to satisfy their anticommutative statistics. This limits the choice of linear combinations for (67) to Ω_1, Ω_2, Ω_3.

We obtain a further selection of the linear combinations by assuming that the unique neutrino field in (67) is strictly massless. This means that (67) should be invariant under mass reversal of the neutrino field. This mass reversal is effected by $\bar{\psi}_\nu\rightarrow\bar{\psi}_\nu\gamma_5$, or hence $O\rightarrow\gamma_5 O$ in (67). This transformation will at most change the sign of (67). The sign changes for the five combinations (57) are, respectively, $m=+, -, -, -, +$. The only combination that has $p=-1$, $m=+1$ is Ω_1.

We can therefore deduce the unique choice Ω_1 for β decay from three postulates:

(1) there is only one type of neutrino field;
(2) this field is massless; (68)
(3) the interaction of four spin $\frac{1}{2}$ fields is "universal."

In the last postulate "universal" means only that β- and μ-meson decay have the same interactions, with proper replacement of equivalent fields. If later developments prove that other four-particle interactions have the same form, we can remove the quotation marks. We can make certain tests of this third postulate by comparing the half-lives for β decay and μ-meson decay, and also by examining the shape of the electron spectrum for μ-meson decay.

The electron spectrum for μ-meson decay has been calculated.[17] It is convenient to express this spectrum in terms of the linear combinations Ω' associated with (65) by writing

$$\sum g_j O_j=\sum f_j\Omega_j', \tag{69}$$

where the g and f are coupling constants. A substitution g_2, $g_5\rightarrow -g_2$, $-g_5$ is necessary to convert the sign conventions of reference 17 to the usual ones. Neglect-

[14] A. Pais and R. Jost, Phys. Rev. **87**, 871 (1952); earlier references are given here.
[15] C. L. Critchfield, Phys. Rev. **63**, 417 (1943).
[16] Tiomno, Wheeler, and Rau, Revs. Modern Phys. **21**, 144 (1949).
[17] L. Michel, Proc. Phys. Soc. (London) **63**, 514 (1950).

ing the electron rest mass, we have for the spectrum formula (45) of reference 17:

$$P(E)dE=\frac{4}{3h(2\pi\hbar^2c^2)^3}\mu E^2dE[a\mu-bE],$$
$$a=3F^2=3(f_1^2+f_2^2+f_3^2+f_4^2+f_5^2), \quad (70)$$
$$b=6f_1^2+6f_2^2+4f_3^2+4f_4^2+2f_5^2,$$

where E is the electron energy and μ is the rest mass energy of the μ meson. Use of the linear combinations Ω' has the advantage of eliminating cross terms in f_if_j from (70). The shape parameter ρ of reference 17 is

$$\rho=\tfrac{3}{2}(1-b/2a)=[f_5^2+\tfrac{1}{2}(f_4^2+f_3^2)]/F^2. \quad (71)$$

The mean life τ for μ-meson decay is given by $1/\tau=\int_0^{\mu/2}P(E)dE$, or hence:

$$f_1^2+f_2^2+2(f_3^2+f_4^2)+3f_5^2=(24h\mu/\tau)[2\pi\hbar^2c^2/\mu^2]^3=2.00\times10^{-98}\ (\text{erg cm}^3)^2, \quad (72)$$

when the experimental values[18,19] $\tau=2.09\times10^{-6}$ sec and $\mu=(209.8\pm2.2)m_0c^2$ are used. We may compare (72) with the value of the interaction constant deduced from β decay. The most detailed estimate published to date[1] is based on mirror-image transitions in light nuclei where the interaction P plays no part. A re-analysis of this problem, using the most recent data, selecting only those cases closest to the ideal one-particle model, and assuming the interaction Ω_1, leads to a constant[12]

$$B_0=(ft)|\Omega_1|^2=2\pi^3h7\ \ln2/(f_1^2m_0^5c^4)=5600\ \text{sec}, \quad (73)$$

where (ft) is the empirical parameter determined in measurements of β-decay lifetimes and m_0 is the electron rest mass. An extra factor of 2 appears in this value for B_0 because the empirical fit in reference 1 was so normalized that $B_0/(ft)=\frac{1}{2}|\Omega_1|^2$. The corresponding value of f_1^2 is

$$f_1^2=2.19\times10^{-98}\ (\text{erg cm}^3)^2. \quad (74)$$

Although the numerical values in (72) and (74) are not identical, the uncertainty in the μ-meson mass introduces an error of about 5 percent into (72), and the scatter of individual (ft) values in determining B makes it reasonable to assign an error on the order of 10 percent to (74). Therefore, if we assume the same linear combination Ω_1 for β and μ decay, the coupling constants are the same within the experimental errors specified. The weighted mean value of the coupling constant is

$$|f_1|=1.44\pm0.04\times10^{-49}\ \text{erg cm}^3. \quad (75)$$

If the μ-meson decay interaction is really Ω_1', the shape factor (71) should be $\rho=0$, indicating a decay electron spectrum that goes to zero at its end point. Present experimental evidence on this question is somewhat conflicting,[20] and an accurate determination of the spectrum near its end point would be of crucial significance in determining whether the β- and μ-decay interactions are identical. It would also be desirable, if possible, to determine the capture rate of μ mesons by individual nucleons to an accuracy comparable with that of (72) and (74), say 10 percent.

The author wishes to express cordial thanks to Prof. C. S. Wu for a number of stimulating discussions and for the opportunity to use unpublished data. He also thanks Dr. M. A. Ruderman and Dr. S. A. Moszkowski for enlightening discussions, and Mr. E. L. Stone for numerical work in obtaining Table I.

[18] Alvarez, Longacre, Ogren, and Thomas, Phys. Rev. **77**, 752 (1950).

[19] Lederman, Booth, Byfield, and Kessler, Phys. Rev. **83**, 685 (1951).

[20] Leighton, Anderson, and Seriff, Phys. Rev. **75**, 1432 (1949); Sagane, Gardner, and Hubbard, Phys. Rev. **88**, 557 (1951); A. Lagarrique and C. Peyrou, J. phys. et radium **12**, 848 (1951); Bramson, Seifert, and Havens, Phys. Rev. **88**, 304 (1952).

Yield of Xe^{133} in the Thermal Neutron Fission of U^{235}†

SEYMOUR KATCOFF AND WILLIAM RUBINSON
Chemistry Department, Brookhaven National Laboratory, Upton, New York

(Received June 9, 1953)

The yield of 5.27-day Xe^{133} in the thermal neutron fission of U^{235} was determined accurately by a method in which the fission rate was measured with a double chamber fission counter, and in which the disintegration rate of the chemically separated Xe was measured by gas phase proportional counting. Five separate determinations gave a mean value of (6.62 ± 0.15) percent, where the indicated error is the 99 : 1 probable error. A considerable number of possible sources of error was investigated in detail and taken into account when making the measurements and calculations.

As by-products of this work, it was determined that: (1) the independent yield of Xe^{133} in U^{235} fission is not greater than 0.1 percent of the chain yield; (2) the independent yield of 9.15-hr Xe^{135} is about 3.5 percent of the total yield of the mass-135 chain; and (3) the half-life of I^{133}, as measured by a procedure which circumvented most of the interference from other nuclides, is 20.8 ± 0.2 hours.

I. INTRODUCTION

UNTIL recently it was felt by those who have measured fission yields radiochemically that the accuracy of such measurements is not better than ±10 percent.[1] The largest part of the error is introduced in the process of getting the disintegration rate from the observed counting rate of a solid radioactive source, usually about 20 mg of a salt spread over a circle of $\sim$15 mm diameter. This error is particularly serious in the case of absolute fission yield measurements. In a relative yield measurement, where the fission yield of a given nuclide is determined relative to that of another fission product, there is usually a partial cancellation of errors in making the correction from counting rate to disintegration rate, so that relative fission yields may be good to ±5 percent.

This state of affairs has become susceptible of considerable improvement due to advances in the techniques of beta counting developed in the last several years. Gas phase counting now enables one to determine beta disintegration rates of radioactive gases with an accuracy of one or two percent, and comparable accuracy can be attained with most solid beta sources by means of 4π counters. These reduced beta-counting errors are now of the same order as fission counting errors, so that the latter must be subjected to a more careful scrutiny if accurate absolute yield measurements are to be made.

We have chosen the gaseous nuclide 5.27-day Xe^{133} as subject for a more accurate determination of an absolute fission yield. This yield, together with published accurate relative fission yields of Xe and Cs isotopes determined mass spectrometrically,[2,3] provides accurate yields for the fission chains of masses 131 through 137. Xe^{133} can also be used as a convenient standard in future radiochemical relative fission yield determinations.

II. THE BASES OF THE YIELD MEASUREMENT

The fission yield of a given nuclide is, by definition, the fraction of fissions that result in the (immediate or ultimate) formation of that nuclide, all possible paths of formation being included (except those arising from secondary effects such as neutron capture by the fission products). A yield measurement requires the determination of the activity of the nuclide produced in a quantity of fissile material that has undergone fission at a known rate for a known time. In an absolute yield measurement, the fission rate is measured by fission counting.

For the case of the Xe^{133} yield in U^{235} fission, the appropriate equations can be developed as follows:

The fission chain of mass 133 is:[4]

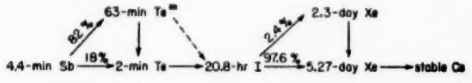

The earlier members of this chain are formed directly in fission to an appreciable extent, without growth from precursors. Pappas[4] showed that about 60 percent of the chain is formed at the 4.4-min Sb (or earlier), about 25 percent starts at 63-min Te, 5 percent at 2-min Te, and 10 percent at 20.8-hr I. In Sec. VI, below, we show that the amount starting at Xe is negligible (<0.1 percent of the chain yield). For the purpose of our

† Research carried out under the auspices of the U. S. Atomic Energy Commission.

[1] See the summary of the Plutonium Project fission yield work by E. P. Steinberg and M. S. Freedman in *Radiochemical Studies: The Fission Products* (McGraw-Hill Book Company, Inc., New York, 1951), Paper No. 219 National Nuclear Energy Series, Plutonium Project Record, Vol. 9, Div. IV.

[2] Macnamara, Collins, and Thode, Phys. Rev. **78**, 129 (1950).

[3] Wiles, Smith, Horsley, and Thode, Can. J. Phys. **31**, 419 (1953).

[4] All data, except the I^{133} half-life, were taken from the most recent compilation, "Table of Isotopes" by Hollander, Perlman, and Seaborg, Revs. Modern Physics **25**, 469 (1953), and from work of A. C. Pappas reported on p. 67 of a Progress Report of the Massachusetts Institute of Technology Laboratory for Nuclear Science and Engineering, May 31, 1951 (unpublished). For the I^{133} half-life the "Table of Isotopes" lists two values: 20.5 hours measured by Bartholomew, Brown, Hawkins, Merrit, and Yaffe, Can. J. Chem. (to be published); and 22.4 hours measured by Pappas. We adopt the value of 20.8 hours obtained in our own measurement, described in Sec. VIII.

calculations, the following simplifications can be introduced without loss of accuracy: the 4.4-min Sb is ignored; the two Te isomers are lumped together as a single activity with a 1.1-hour half-life; 75 percent of the 20.8-hr I grows from a 1.1-hr Te parent; the remaining 25 percent of the I is formed directly in fission (this includes 15 percent which really is not formed directly, but whose path of formation by-passes 63-min Te); when calculating the 2.3-day Xe^{133m} activity and the 5.27-day Xe activity deriving from it, we assume that the entire chain originates at the 20.8-hr I.

Using these simplifying assumptions, we write the following paths of formation for 5.27-day Xe. The relative yield for each path is indicated in parentheses.

(*a*)	Te→I→Xe	(0.976×0.75)
(*b*)	I→Xe	(0.976×0.25)
(*c*)	$I\rightarrow Xe^{m}\rightarrow Xe$	(0.024).

The equations used in the fission yield calculation are adopted from the standard equations of radioactive transformation. For a sample of uranium which had undergone fission at a constant rate f for a time τ, the activities at any subsequent time t, of a primary fission product, its daughter, and grandaughter, are given, respectively, by the following equations:

$$A_1(\tau, t)=fY(1-e^{-\lambda_1\tau})e^{-\lambda_1 t}, \tag{1}$$

$$A_2(\tau, t)=fY\left[\frac{T_1(1-e^{-\lambda_1\tau})}{T_1-T_2}e^{-\lambda_1 t}+\frac{T_2(1-e^{-\lambda_2\tau})}{T_2-T_1}e^{-\lambda_2 t}\right], \tag{2}$$

$$A_3(\tau, t)=fY\left[\frac{T_1^2(1-e^{-\lambda_1\tau})}{(T_1-T_2)(T_1-T_3)}e^{-\lambda_1 t}+\frac{T_2^2(1-e^{-\lambda_2\tau})}{(T_2-T_1)(T_2-T_3)}e^{-\lambda_2 t}+\frac{T_3^2(1-e^{-\lambda_3\tau})}{(T_3-T_1)(T_3-T_2)}e^{-\lambda_3 t}\right]. \tag{3}$$

The subscripts 1, 2, and 3 refer to the parent, daughter, and grandaughter, respectively; λ and T refer to disintegration constants and half-lives, respectively; and Y is the fission yield of the first member of the chain.

The Xe^{133} activities, A_a and A_c, formed by way of paths (*a*) and (*c*) respectively, are both calculated from equations of the form (3), while A_b, the Xe^{133} activity formed by way of path (*b*), is calculated from an equation of the form (2). In our experiments we take $\tau=1.000$ hours (which is close to the actual irradiation times) and $t=253.0$ hours (which is close to the actual times of Xe extraction from the fission product mixtures). With these values of τ and t and the appropriate half-lives and relative path yields given above, the equations for the different paths reduce to:

$$A_a=1.6477\times10^{-3}\,fY\ (0.976)(0.75),$$
$$A_b=1.6334\times10^{-3}\,fY\ (0.976)(0.25),$$
$$A_c=2.2643\times10^{-3}\,fY\ (0.024).$$

The sum of these does not account completely for all the Xe activity observed. A small quantity of 2.3-day Xe^{133m} also contributes to the observed counting rate. Assuming that its counting efficiency is equal to the conversion coefficient of its 0.233-Mev γ ray, i.e., 0.85, its activity from Eq. (2) is:

$$A_d=0.854\times10^{-3}\,fY\ (0.024)(0.85).$$

The sum of the last four equations gives the total of the observed activities of *mass-133* xenons: $1.6763\times10^{-3}\,fY$.

In addition to this, another small contribution is made by 12.0-day Xe^{131m}, a 0.7 percent branch in the decay of 8.1-day I^{131} (whose fission yield is 3 percent). Using the above methods of calculation, we find that this contribution is 0.18 percent of the total observed activity, i.e., $A_{obs}=1.6763\times10^{-3}\,fY\ (1.0018)$. Our final working equation is:

$$Y=595.5(A_{obs}/f)k, \tag{4}$$

where k is a correction factor, close to unity, introduced because the actual times of Xe extraction deviated somewhat from 253 hours. In the different runs, k varied between 1.0003 and 1.0054. (See Table V and Sec. V.)

III. MEASUREMENT OF THE FISSION RATE

A. General Considerations

For an absolute fission yield measurement, we have to measure, by fission counting, the rate of fission in a relatively large quantity of U^{235}, designated the "slug," sealed in a container which prevents loss of fission recoils and permits subsequent complete chemical extraction of the Xe^{133}. This was accomplished as follows.

A small quantity of U^{235}, designated the "foil," whose weight relative to the slug weight was accurately known, was mounted on a platinum backing in a layer so thin that when a fission occurred in it, one of the pair of recoiling fission fragments escaped without serious energy loss and was detected in a fission counter. By placing foil and slug in the same neutron flux in the Brookhaven pile and counting the foil fission rate, we were able to compute the slug fission rate.

For an accurate measurement, it is necessary to investigate a considerable number of possible sources of error. These special investigations will be described in appropriate places below.

B. The Fission Counting Apparatus

This was designed to permit: (1) high fission-counting rates with low counting-rate loss and low background; (2) minimum distortion of the neutron flux distribution

in the neighborhood of slug and foils; (3) insertion deep into the pile to a point of small flux gradient; (4) ease of handling; (5) checks and comparisons of various kinds.

In order to reduce the fission background to the desired limit, the body of the counter was machined from a billet of spectroscopically pure Al (containing less than 5×10^{-3} ppm of U, according to a chemical analysis by Stoenner of this Laboratory[5]), and all other Al used within the counter was 2*S*, plated with $\sim$9 mg/cm^2 of Cr. It may be noted that a counter constructed entirely of 2*S* aluminum would probably show useably low backgrounds if it were chrome-plated, but there is an additional, and by no means negligible, advantage of pure aluminum: its radioactivity decays so rapidly that the counter may be handled with complete safety within a few hours after bombardment.

The counter gas was argon flowed through the counter at atmospheric pressure. The electron collection time was so short ($\sim$3 μsec) in argon that there was a very low probability for the occurrence of pile up pulses as large as fission pulses. By the use of fast amplifiers and scalers, the low counting-rate loss of 0.7 percent per 10^5 fissions/minute was achieved (see Sec. III-D).

The counter proper is shown in Fig. 1. It consisted of two independent pulse ionization chambers housed together, with a $\frac{7}{32}$-in. space between them that just accommodated the fission slug. The use of two independent fission chambers gave checks on the fission counting and provided means for a variety of tests.

The fission foils, $\sim$0.01 μg of U^{235} deposited on a Pt disk 0.002 inches thick and 1 inch in diameter, were mounted on chrome-plated 2*S* aluminum disks, $2\frac{3}{8}$ in. in diameter and $\frac{1}{32}$ in. thick, which made contact with the grounded counter wall. Spaced about 7 mm from these plates were the collecting plates, chrome-plated aluminum, 2 in. in diameter and $\frac{1}{16}$ in. thick, insulated from the counter wall by quartz within the counter and by Teflon elsewhere. Argon was flowed into the counter at a rate of about 15 cc per minute through a long thin 2*S* aluminum tube, and it escaped through leaks left around the insulators, etc.

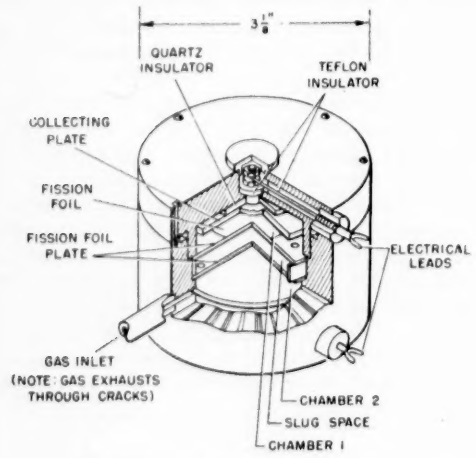

FIG. 1. Double chamber fission counter.

[5] According to R. Stoenner's analyses, 2*S* and 52*S* Al contain 0.5 ppm of U, which is consistent with the backgrounds obtained with another counter constructed of 2*S* Al.

Each of the two fission chambers was provided with its own electrical leads and electronic gear. Fission pulses from a chamber were piped along a 0.010-in. diameter stainless steel wire that ran down the axis of a 15-ft long 2*S* aluminum tube with an effective diameter of about $\frac{5}{8}$ in., the wire being insulated from the tube wall by Teflon spacers placed at intervals of about 15 in. The wire also served to carry voltage to the collector plates from the voltage supply of the amplifier. The two aluminum tubes (one for each chamber) were encased in a larger ($1\frac{5}{16}$-in. diameter) 2*S* aluminum tube, and, for radiation shielding, this tube array was filled with paraffin to within five ft of the counter. In operation, the tube array, together with the gas-flow tube, projected from the pile hole through appropriate radiation shields.

The fission pulses, which were about five-fold attenuated as they passed down the 15-ft tube, were fed into a preamplifier (Atomic Instruments, Model 205B) and amplifier (Atomic Instruments, Model 204C). The amplified pulses were then fed into a very fast scale-of-16 (designed and constructed at our request by the Brookhaven Electronics Division), which, in turn, fed into a commercial scale-of-256, to give an overall scaling factor of 4096. The pulses from the scaler were recorded on Veeder-Root recorders.

Great pains were taken to insure electromagnetic shielding of each of the fission counting systems from each other and from external sources of electromagnetic disturbance. Before each run, the whole counting system was shown to be electrically quiet to a fairly violent test with a special electromagnetic hash generator.

C. Tests on the Counter

Discriminator plateaus of the counter were taken as a function of various variables.

1. *Voltage.*—Good discriminator plateaus were obtained when the voltage across the counter plates was between about 200 and 350 v, as measured with the counter at zero pile power. Below 200 v, the collection of electrons from the fission pulses was not sufficiently rapid, and above 350 v pile up pulses became too prominent. At zero pile power our voltage supply put 270 v across the counter plates, but when the pile was at power for our usual running conditions (5 Mw, nominal), the general radiation intensity made the counter conducting to such an extent that it drew about five microamperes of current, and the voltage dropped to about 240 v.

2. *Amplifier settings.*—Various combinations of gain, time constant, and feedback were tried. The best plateaus were obtained with the following nominal amplifier settings: gain, 32; time constant, 3; feedback, 2. With these settings, the measured over-all amplification factor (preamplifier plus amplifier) was 100 000.

3. *Pile power.*—As the pile power increased, the discriminator plateaus shrank, but they probably remain useable (with some loss of accuracy) at pile powers four or five times greater than the 5 Mw used in all our runs.

4. *Argon flow rate.*—The plateaus were independent of the argon flow rate provided it was greater than about 3 cc per min. Our serious counting was done at flow rates greater than 12 cc per min (about one counter volume in 5 min).

The best discriminator plateaus we obtained (the others were nearly as good as these) are shown in Fig. 2. They were taken under our standard running conditions: flux, $\sim 2\times 10^{11}$ neutrons/cm^2 sec; fission counting rate, $\sim$150 000 counts/min. In taking them, one of the chambers was used to monitor the neutron flux while the plateau was being run on the other chamber, which provides the means of normalizing to the same flux all plateau points of a given chamber. Correction has also been made for the variation of background with discriminator setting (inset of Fig. 2). At discriminator settings corresponding to the middle of the fission counting plateaus, the background counting rates were only about 1.5 percent of the fission counting rates of our standard fission foils (0.007 855 μg of U^{235}).

The plateau slopes were so small that we feel justified in neglecting any plateau slope correction to the observed fission counting rates.

It should be mentioned that the plateaus were the same for different fission foils, and that they were equally good, though displaced slightly, when the electronic gear ordinarily used with one chamber was used with the other.

D. Counting Rate Loss

This was determined by measuring the counting rates of two fission foils of different strengths at two pile powers. Let R denote the observed fission rate of a foil whose true fission rate is f, and assume that the dead-time, δ, of the counter is given by:

$$R=f(1-R\delta).$$

Suppose foil 1 is in chamber 1 of the counter, and foil 2, of greater strength than foil 1, is in chamber 2. Observe their fission counting rates at flux a. Assuming that both chambers have the same dead-time, we have

$$\frac{R_{1a}}{R_{2a}}=\frac{f_{1a}(1-R_{1a}\delta)}{f_{2a}(1-R_{2a}\delta)},$$

where R_{1a} is the observed counting rate of foil 1 at flux a, and similarly for the other symbols. There will be a similar equation for flux b. Since the ratio of the true fission rates of the two foils is independent of the flux, we can solve the two equations pertaining to the two fluxes to get δ in terms of observed fission rates:

$$\delta=\frac{R_{1a}R_{2b}-R_{1b}R_{2a}}{R_{1a}R_{2b}(R_{1b}+R_{2a})-R_{1b}R_{2a}(R_{1a}+R_{2b})}.$$

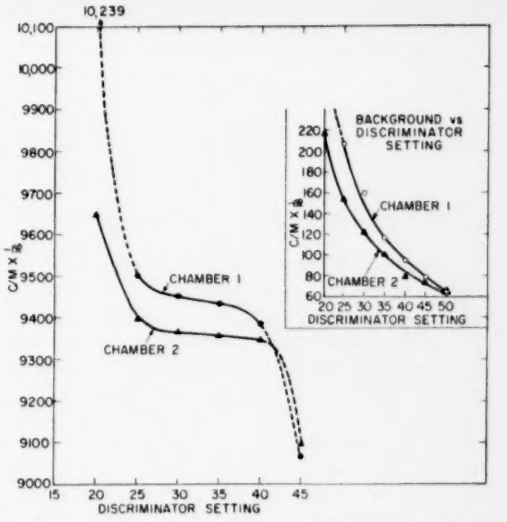

FIG. 2. Discriminator plateaus of fission counter with U^{235} foils under standard run conditions.

In our measurement of δ, foil 2 was six times stronger than foil 1, and the two fluxes were those corresponding to pile powers of 0.5 Mw (where the weak foil fission rate was $\sim$7500 counts/min and the strong foil rate was $\sim$45 000 counts/min), and 5.0 Mw. The value found for δ was 4.3 μsec, which corresponds to a counting-rate loss of 0.72 percent per 10^5 counts/min. The two foils were further compared at pile powers of 1.0, 2.5, and 7.4 megawatts. Between pile powers 0.5 Mw and 7.4 Mw the observed ratio of strong foil rate to weak foil rate dropped 3 percent. Application of the counting-rate loss correction brought the 7.4 Mw ratio to within 0.6 percent of the 0.5 Mw ratio. At 2.5 Mw the observed ratio was 0.9 percent below the observed ratio at 0.5 Mw; by applying the correction this ratio was only 0.2 percent above the ratio at 0.5 Mw.

E. Equality of Neutron Flux at Positions of Slug and Foils

If slug fissions are to be computed with accuracy from the counted foil fissions, slug and foils must be exposed to the same neutron flux. Three perturbing factors must be considered:

1. *Self-shadowing in the slug.*—This was completely negligible in our experiments, where the slug weight was only about 40 μg.

TABLE I. Relative mean specific activities of Cu stacks at different positions in the counter.

Stack No.	Average stack activity 1st measurement	2nd measurement
1	1.000	1.000
2	0.999	1.002
3	1.001	0.998
4	1.003	1.002

2. *Gradients in the neutron flux density in the pile.*—The two fission foils were separated by $\frac{1}{4}$ in. with the slug between them. It was possible for the slug center to be displaced laterally somewhat less than a centimeter from the foil centers. Therefore, the neutron flux must have negligible variation over distances of about a centimeter if slug and foils are to see the same flux. Our bombardments were made with the counter at a point about 12.5 ft deep within a hole of the Brookhaven pile which runs horizontally through an internal thermal column. By observing fission rate *vs* depth of counter in the pile, it was established that at this point the flux variation was certainly less than 0.5 percent per cm over a distance of ~10 cm. It was also shown that rotation of the counter had a negligible effect on the ratio of the fission rates in the two chambers.

3. *Differential neutron shielding of slug and foils.*—The slugs, which consisted of about 40 μg of U^{235} wrapped in several thicknesses of Al foil and sealed in flat quartz cells with walls ~0.5 mm thick, were separated from each of the fission foils by plates of 2*S* aluminum, chromium, and platinum,[6] of thicknesses 0.035, 0.001, and 0.002 in., respectively. From the known cross sections, it was computed that the neutron absorption by all these materials was about 0.6 percent. The extent to which the slug, thus shielded by aluminum foil, quartz, chrome-plated aluminum, and platinum, would see a flux different from that seen by the foils was tested as follows. Twelve copper foils (about 16 mg each), 0.0005 in. thick and 1.5 cm² in area, were each weighed to 0.01 mg. The twelve Cu foils were divided into four stacks of three foils each and, by means of very thin films of Apiezon wax, a stack was fastened to each of two blank platinum disks (substituting for the fission foils) and to each side of a standard quartz cell containing a slug of 4 mg U^{235} (100 times the weight of the standard slug). These were placed in the standard slug and foil positions in the counter and exposed to neutrons in the standard pile position. Several hours after bombardment, the activity of each of the twelve Cu foils was determined twice by measuring the Cu^{64} annihilation radiation with a Lauritsen electroscope. For each of the two activity measurements, the average specific activity of each stack was computed. The normalized results are shown in Table I. We conclude that the neutron flux was the same, within 0.2 percent, at all four positions. This is consistent with a calculation using neutron diffusion theory and assuming that all neutron absorbing material was concentrated in the slug.

Note that in addition to showing the absence of flux distortion due to neutron absorbers in the counter, this experiment also demonstrates the essential absence of neutron flux gradients in the pile, at the position of the counter, over distances of about a centimeter.

F. Foil Preparation and Tests

Uranium enriched to 93.72 percent in U^{235} was made up into a stock solution containing, according to chemical analysis, 39.1 mg U/ml. An aliquot of this stock solution was diluted about 250 000-fold to make a "foil solution" with a U concentration of 0.1565 μg/ml. Dilution was in two steps, the diluent was ~1.5*N* HNO_3 prepared with doubly distilled water, and all dilution vessels were calibrated to better than ±0.2 percent.

In our standard method of fission foil preparation, 50.19 λ (calibrated micropipette) of foil solution was deposited at the center of a smooth clean Pt disk one inch in diameter and 0.002 inch thick.[7] This was followed by a pipette rinse of 1.5*N* HNO_3 (the solution used as diluent in preparing the foil solution), the rinse consisting of a single pipette-full of the acid which was drawn up from, and ejected back onto, a waxed glass slide three or four times[8] before final deposition on the Pt disk. The liquid was evaporated under the heat lamp, and the residue was ignited in a Bunsen flame for about thirty seconds. There remained a faint discoloration which appeared smooth and transparent under the microscope. The Pt disks were finally fixed, by means of a thin film of Apiezon wax, in a depression 0.001 in. deep in a chrome-plated aluminum disk that served as a ground electrode of the fission counter.

Five fission foils, each containing 7.855×10^{-3} μg of 93.72 percent U^{235}, were prepared by the standard method. Two additional foils were prepared by slight variations of this method: one, without final ignition, to test whether ignition affects the escape of fission recoils; and the other, by stippling the foil solution and rinse in small droplets over the surface of the Pt before evaporation and ignition, to test whether possible clumping of the U was great enough to cause loss of fission recoils.

The relative strengths of these seven foils were determined by fission counting them in counter chamber 2

[6] A spectrochemical analysis by M. Slavin of this Laboratory showed the platinum to contain negligible amounts of noble metal impurities.

[7] The Pt foil, obtained from the Baker Platinum Corporation of Newark, New Jersey, was from a rolling with previously unused rollers. It did not have a mirror finish, but appeared smooth and free of pits or scratches under 100× magnification. Prolonged efforts to polish it further by a variety of recommended methods resulted in a mirror finish, but with unacceptable pitting, so it was used as it came from the manufacturer.

[8] We found that this method of repeated rinsing with a single drop gives somewhat more reproducible results than does a single rinse.

against a monitor foil in chamber 1, with results shown in Table II. The relative foil strengths have a standard deviation of 0.47 percent of the mean. In order to insure that no gross error was made in the preparation of the foil solution, another fission foil was made by the standard method, but from a second solution prepared completely independently of the first. Its computed strength relative to a standard foil was 1.215; its observed relative fission counting rate was 1.226.

Finally, to test whether extraneous solids in the foil solution cause loss of fission fragments, two more foils were prepared, the first containing five times, and the second containing ten times, the extraneous solids of a standard foil. This was done by using 5 and 10 times as much HNO_3 solution and rinse. Their observed relative fission counting rates were, respectively, 0.988 and 0.990 of the expected, showing that for our standard foils, no error due to the presence of extraneous solids need be feared.

We conclude from all these results that our standard foils can be trusted to ± 0.5 percent.

The foils used in our five fission yield runs were various pairs selected from foils 23, 24 and 25 (see Table II).

G. Preparation of the Slugs

Two "slug solutions" were prepared independently of each other by diluting aliquots of the U^{235} stock solution described above. Dilutions of 100-fold and 200-fold, respectively, were made with 1*N* HNO_3 as diluent. Four slugs, each containing 37.806 μg of U, were prepared from the 100-fold diluted solution, and one slug, containing 46.971 μg of U, was prepared from the 200-fold diluted solution.

To prepare a slug, 99.91 λ (calibrated micropipette) of a slug solution were deposited at the center of a 6-cm sq of "Reynold's Wrap" aluminum foil. This was followed by a pipette-full of HNO_3 used as a rinse in the manner described under Foil Preparation. The $\sim 200\ \lambda$ of solution plus rinse were evaporated under the heat lamp, following which the edges of the aluminum foil were folded around the resulting dry deposit to give a thin, flat packet, 2 cm sq. The packet was then wrapped in a second 6 cm sq of aluminum foil, so that altogether the slug uranium was enclosed in seven thicknesses (a total of 35 mg/cm^2) of aluminum, several times the maximum range of fission fragments. Finally, the slug was inserted in the open end of a flat quartz cell, 25 mm $\times$30 mm$\times$5.5 mm with walls $\sim$0.5 mm thick; the open end was fuzed shut; the cell was evacuated through a narrow tube and tested for leaks[9] with a Tesla coil; and then the narrow tube was sealed off close to the cell.

H. Slug Bombardment

The slug was bombarded in the space between the two fission foils for an hour at a constant (± 2 percent) neutron flux of $\sim 2\times 10^{11}$ neutrons/cm^2 sec. Foil fission rates were $\sim$150 000 fissions/min. All of the fissions of each of the two foils were recorded. The total of the recorded fissions of each foil was then corrected for background and counting-rate loss, divided by 60 to give the foil fission rate as fissions per min, and multiplied by the ratio of slug weight to foil weight to give the slug fission rate.

The results of the fission counting in five yield measurement runs are shown in Table III. Column 4 gives the slug fission rate computed from the count of the foil in chamber 1 of the counter, and column 5 gives the corresponding fission rate computed from the fission count in chamber 2. Column 6 is included to show the consistency of the results of the two chambers. It is seen that there is a rather systematic difference of about one percent, with chamber 2 giving the higher value. Column 7, the mean of columns 4 and 5, is the slug fission rate datum that enters as f in the yield equation [Eq. (4) of Sec. II].

TABLE II. Relative strengths of fission foils.

Foil	Type	Relative strength
23	standard	1.0000
25	standard	1.0044
VIII	standard	0.9914[a]
IX	standard	0.9934[a]
XI	standard	0.9946[a]
20	not ignited	1.0023
24	stippled	1.0015

[a] Determined indirectly.

IV. MEASUREMENT OF THE Xe^{133} ACTIVITY

A. Xenon Extraction

Seven to ten days after end of bombardment, the quartz cell containing the bombarded slug was fixed vertically between two heavy glass jaws in a dissolver vessel (Fig. 3) which was part of a vacuum system. The air in the dissolver was flushed out by helium, and most of the latter was transferred to an evacuated three liter cylindrical storage bulb. About 140 cc of Xe carrier were accurately measured out in another vessel, and part of it was admitted to the dissolver. Then the lower section of the dissolver was

TABLE III. Fission counting data.

Run	Bombardment time (min)	Slug to foil ratio	Slug fission rate[a] $\times 10^{-6}$ Chamber 1	Slug fission rate[a] $\times 10^{-6}$ Chamber 2	Ratio: Chamber 2 / Chamber 1	Mean slug fission rate $\times 10^{-6}$
U-201	66	4813	8.915	8.842	0.992	8.878
U-202	60	4813	7.435	7.532	1.013	7.483
U-203	55	4813	7.811	7.914	1.013	7.863
U-204	70	4813	8.703	8.776	1.008	8.740
U-205	57	5980	9.354	9.420	1.007	9.387

[a] For convenience in the fission yield calculations, these rates were computed for an assumed standard bombardment time of 1.000 hr. The error so incurred in the yield calculation is vanishingly small.

[9] Preliminary experiments had shown that the presence of small leaks in the quartz cell can result in the escape of as much as half the fission gases.

rotated in the ground joint, breaking the quartz cell between the glass jaws. About 10 ml of 6*N* HCl was admitted to the dissolver, now in communication with the storage bulb, and, while the slug was dissolving, most of the remaining Xe carrier was bubbled through the acid and collected in the storage bulb. A few ml of concentrated HNO_3 were finally added to the dissolver to complete the dissolution, which required about half an hour. During the next hour, the remaining Xe carrier, followed by two liters of He, were bubbled through the solution, now boiling and refluxing, and into the storage bulb, where for the following 16 hr the accumulated gases were thoroughly mixed by heating (heat mantle) at 200° a 40-mm diameter circulation tube connecting the top and bottom of the bulb.

After the mixing period, the gases were passed from the storage bulb through the following series of traps:

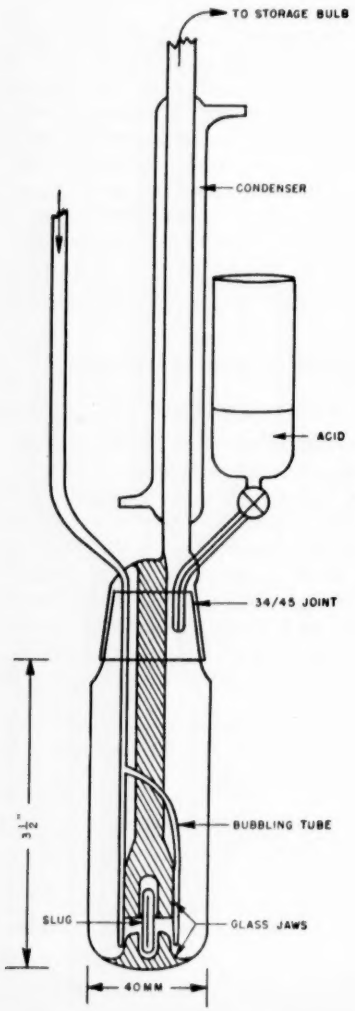

FIG. 3. Slug dissolver vessel.

two traps containing NaOH pellets, the first at 23° and the second at −78°, to remove water and acid vapors; two empty traps at −195°, to freeze out most of the Xe; and a small 80–100 mesh charcoal column at 0° to catch any Xe escaping the −195° traps. At this point any residual Xe in the dissolver was collected by bubbling five more liters of He through the slug solution and passing the resulting gases through all the traps.

The charcoal column was now cooled to −195°, and together with the empty traps containing the frozen Xe at −195°, was pumped free of He. Following this, the charcoal column was warmed to +80° (at which temperature it no longer adsorbs Xe), and the traps containing the frozen Xe were warmed to −78°, whereupon the Xe evaporated, passed through the warm charcoal column, and then through a 50 cm long column of 10–30 mesh Ti metal at 900° (previously outgassed at 1020°) where any remaining non-noble gas impurities were removed. The purified Xe was finally condensed in a bulb at −195°.

The entire Xe extraction process required about 42 hr: 2 hr to dissolve the slug and collect the sweep gases in the storage bulb, 16 hr of gas mixing in the bulb, and 24 hr for the remainder of the procedure. About 95 percent of the original carrier was recovered.

B. Tests on the Xe Extraction Process

No provision had to be made for separating Kr activities from the Xe because the Xe activity was of the order of 10^6 times that of the only long-lived Kr fission product (10-year Kr^{85}) when the counting began, about ten days after the irradiation. By then all of the shorter-lived Kr activities had completely decayed.

In a few preliminary experiments the chemical purity of the carrier Xe before and after being passed through the extraction procedure was determined with a Consolidated-Nier Mass Spectrometer by Mr. A. P. Irsa and Dr. L. Friedman of this Laboratory. All the Xe samples showed the same nitrogen contamination of 0.3 percent, but this may have been an instrumental effect of the spectrometer. In addition, the tank Xe was found to contain 0.2 percent of Kr. Most of this Kr impurity was eliminated by the Xe extraction procedure, necessitating a 0.2 percent correction in computing the chemical recovery of the Xe.

The degree to which Xe activity failed to be swept from the dissolver by our gas sweeping procedure was tested in three auxiliary runs. In the first of these, after an initial sweeping with 140 cc of Xe plus 2 l of He, the slug solution was subjected to a second sweeping with the same amounts of these gases. The second sweeping was found to contain 7 percent of the total Xe activity. The next test was identical with the first, except that the slug solution was boiled more vigorously during the gas sweepings. This time the second sweeping contained 1.5 percent of the Xe activity. In the third test, the initial sweeping was done with 140 cc of Xe plus

four (instead of two) liters of He, and this time the second sweeping contained only 0.5 percent of the total Xe activity. This was considered satisfactory, but as an added safety factor, the slug solution was swept with a total of seven l of He in the fission yield runs.

C. The Xe^{133} Counting

The gas counters were of glass, 2 cm in diameter and 30 cm long, with chemically deposited silver cathodes whose volumes had been measured to within 0.2 percent. They were filled with a portion of the recovered Xe, usually to ~300 mm pressure at 22°, the pressure and temperature being carefully measured. Finally the counter pressure was made up to one atmosphere with pure methane. Under these conditions, the cathode volumes of the counters contained about 23 percent of the original Xe carrier. In calculating the exact percentages, corrections were applied for deviation of the Xe from perfect gas behavior.

Counting was done in the proportional region, with a 5-kv power supply, a non-overloading amplifier, and a scale-of-64 (Atomic Instrument Company, Model 101). Each counter had a zero-slope plateau 100 to 300 v long, centered at about 3000 v. Backgrounds were determined (either before or after the activity measurements) by filling the counters with carrier gas and methane to the usual pressures, and making several measurements during a two week interval. The gases were taken from the same tanks that were used in the runs with activity. The various counters had backgrounds between 70 counts min and 100 counts/min, each one being reliable to ±4 percent.

The Xe from each run was measured into two counters, designated *a* and *b*, each of which was counted ten times, over a period of two weeks, starting about 10 days after irradiation, on each of two electronic circuits, designated 1 and 2. Eight different counters were used for the five runs. Initial counting rates were 12 000 to 24 000 counts per min. In each case the decay followed a 5.3-day half-life very closely during the 2 week counting interval, being little affected by the small amounts of 2.3-day Xe^{133m} and 12.0-day Xe^{131m} also present.

The internal consistency of the Xe counting in a given run was checked as follows.

First we checked whether a given counter showed the same counting rate on the two circuits. The uncorrected decay curves observed with a given counter on the two circuits were drawn separately, and the activities read from each of these curves, at the arbitrarily chosen reference time of 253 hr after end of bombardment, were compared. The ratio of these two activities for counter *a* is shown in column 2, Table IV; column 3 shows the corresponding ratio for counter *b*, results being given for all five runs.

Next, to check whether counters *a* and *b* showed the same specific activity, the counts observed with counter *a* on the two circuits were averaged, and the average, corrected for background and corrected to 100 percent chemical yield, was compared with the corresponding average of counter *b*. The comparison is shown in column 4 of Table IV (the ratios are all greater than one simply because the designation *a* was assigned to the counter of higher counting rate).

TABLE IV. Ratios of the Xe^{133} counting rates of a given counter on two circuits, and ratios of the counting rates of two counters filled with aliquots of Xe^{133} from the same slug.

Run	(counts/min circuit 1)/(counts/min circuit 2) Counter *a*	Counter *b*	(counts/min *a*)/(counts/min *b*)
U-201	0.990	0.998	1.005
U-202	0.994	0.982	1.004
U-203	0.994	0.989	1.004
U-204	0.992	0.993	1.012
U-205	0.996	1.005	1.013
Average	0.993		1.008

The basic Xe activity datum that enters the fission yield calculation in a given run is the mean of the corrected *a* and *b* averages of that run. This gives the disintegration rate of the total Xe in the given slug 253 hr after the end of a 1-hr bombardment. Of this total activity, about 98.8 percent was 5.27-day Xe^{133}, one percent was 2.3-day Xe^{133m}, and the remaining 0.2 percent was 12.0-day Xe^{131m}, as is discussed in detail in Sec. II.

On the basis of past experience [10,11] with similar counters we judge it unnecessary to make wall or end corrections on the observed counting rates. In the work cited, it was shown to a precision of two percent that for two β-ray emitters with maximum energy 0.155 Mev and 1.2 Mev, the observed counting rates (corrected for background) were equal to the disintegration rates of the radioactive gas contained within the cathode volumes of the counters. For example:[11] the A^{41} activity (1.2-Mev β rays) per ml of cathode volume remained constant when the diameter of one series of counters was varied from 1.9 cm to 8.7 cm, and also when the cathode length was varied from 7.0 cm to 75.8 cm in

TABLE V. Data and results for the yield of Xe^{133} from U^{235} fission.[a]

Run	Fissions per minute in slug $\times 10^{-8}$	Time to Xe separation (hours)	Xe activity at $t = 253$ hr (d/m)	Correction factor k	Xe^{133} fission yield (percent)
U-201	8.878	187	98 040	1.0046	6.606
U-202	7.483	235	83 800	1.0003	6.671
U-203	7.863	182	87 140	1.0054	6.635
U-204	8.740	209	97 830	1.0019	6.678
U-205	9.387	192	102 130	1.0039	6.504
Mean					6.62

[a] Standard deviation, σ, for a single determination is 0.95 percent of the mean. The 99:1 probable error for the mean is 2.2 percent of the mean.

[10] W. Bernstein and R. Ballentine, Rev. Sci. Instr. **21**, 158 (1950).

[11] S. Katcoff, Phys. Rev. **87**, 886 (1952).

another set of counters. The standard deviation for individual counters was 1.6 percent of the mean and no trend was indicated with the variation in length or diameter. We assume that the same is true for the 0.345-Mev β rays of Xe^{133}.

V. RESULTS OF THE YIELD MEASUREMENTS

The processed data and the computed fission yield values for Xe^{133} in the thermal neutron fission of U^{235}, as determined in five runs, are shown in Table V. Column 2, which is copied from the last column of Table III, gives the slug fission rates, f. Column 4 gives the total Xe activities, A_{obs}, in the slugs 253 hr after the end of each bombardment, as computed from the observed Xe counting rates. Column 5 shows the factors k which correct for the effect of the difference between the actual extraction times and the assumed time of 253 hr. For example, if the Xe^{133} is extracted 192 hr after the bombardment, an additional small amount, 0.39 percent, grows into the solution from its 20.8-hr I^{133} parent between 192 hr and 253 hr. This must be added to the measured activity. Finally, column 6 shows the Xe^{133} yield values, Y, computed from columns 2, 4 and 5 with the aid of the yield equation (4) derived in Sec. II,

$$Y = 595.5 k A_{obs}/f.$$

The mean value is (6.62 ± 0.15) percent, where the indicated error is the 99:1 probable error. As concerns possible systematic errors, we feel that generous assignments would be one percent in the slug fission rates and two percent in the Xe disintegration rates. Other possible systematic errors, e.g., errors in the nuclear constants of the mass 133 chain, cannot be very significant. We believe it highly unlikely that our measured fission yield is in error by more than 3 percent, which we adopt as our accuracy estimate.

VI. INDEPENDENT YIELD OF Xe^{133} IN U^{235} FISSION

For an accurate measurement of the total fission yield of 5.27-day Xe^{133}, it is necessary to know what fraction of it, if any, is formed directly in fission. This can be determined by separating Xe so soon after a short irradiation of U^{235} that it cannot have grown much from its parent I^{133}, and comparing this activity with that of the Xe separated from the same irradiated U after most of the parent I^{133} has decayed. The Xe^{133} found in the first extract (designated a) results from two sources: direct formation in fission, and growth from I^{133} during the short interval before Xe separation. The amount formed from I^{133} is calculated from the Xe^{133} found in the second extract (designated b), with the aid of Eqs. (2) and (3). The activity of the Xe^{133} in a formed directly in fission is then found by difference.

Let us consider the conditions used in our experiment. The irradiation time was 0.033 hr, extract a was separated 0.34 hour after end of bombardment, and extract b was separated after 253 hr. Using the first two times for τ and t, respectively, Eq. (1) reduces to

$$A_i(0.033, 0.34) = 18.05 \times 10^{-5} f Y_i,$$

where A_i is the activity of 5.27-day Xe^{133} found in extract a which was formed directly in fission, and Y_i is its independent yield. At 253 hr after the bombardment A_i had decayed to

$$A_i(0.033, 253) = 4.52 \times 10^{-5} f Y_i. \quad (5)$$

The activity of 5.27-day Xe^{133} found in extract b after 253 hr is given [from (2) and (3)] by

$$A_g(0.033, 253) = 5.56 \times 10^{-5} f Y_g, \quad (6)$$

where Y_g is, to a very good approximation, the total yield of Xe^{133}. By combining Eqs. (5) and (6) we get the fraction of the total Xe^{133} yield which is formed directly in fission:

$$\frac{Y_i}{Y_g} = 1.23\left(\frac{A_i(0.033, 253)}{A_g(0.033, 253)}\right). \quad (7)$$

In our experimental procedure two identical uranium samples ($\sim 40\ \mu g$ U^{235} in each) were sealed into the usual quartz cells and then irradiated side by side in one of the pile pneumatic tubes for 0.033 hr. Xe extract a was removed from one of these slugs after 0.34 hr, and extract b was swept from the other slug after approximately 253 hr. It was found more convenient to take the two Xe extracts from two identically irradiated slugs instead of from a single slug.[12] This eliminated the possibility of Xe loss during the long decay time.

The standard sweeping and separation procedure (described in Sec. IV-A) was modified somewhat for these independent yield experiments. The slugs were dissolved and swept with Xe carrier and 2 l of helium as rapidly as possible; for extract a this was completed at 0.34 hr after irradiation. In the next 40 min, this mixture was passed through the usual series of traps. No additional helium was used. The Xe of extract a collected at the bottom of the charcoal column was probably contaminated with some short-lived Kr isotopes. Therefore the first 10–15 percent of the Xe desorbed from the column was discarded. The remainder was collected and put into counters in the usual manner.

The Xe of extract b decayed with the usual 5.27-day half-life. Counting of extract a Xe began 24 hr after the

TABLE VI. Activities of Xe at 253 hr after the end of two bombardments to determine the independent yield of 5.27-day Xe^{133} in U fission.

	Run	U-301	U-302
	Total Xe activity	160 dis/min	137 dis/min
Extract a	Xe^{133} grown from I^{133}	183	185
	$A_i(0.033, 253)$	(−23)	(−48)
Extract b	$A_g(0.033, 253)$	56 800	57 400

[12] To a very good approximation, the method of calculation outlined above applies without modification.

irradiation, and the activity decayed initially with the 9.2-hr half-life of Xe^{135} (see next Section). After a few days, when this component had decayed, the remaining activity in each counter, corrected for background, was down to ~100 counts/min, and this decayed with a half-life of ~4.6 days. Since the experimental points of these decay curves were somewhat scattered, the deviation from a 5.27-day half-life is probably within the experimental error.

Data from the two runs of this experiment are summarized in Table VI. All activities are corrected to 100 percent chemical yield and are averages based on the counting of duplicate samples from each extract. The duplicates agree to within a fraction of one percent for extracts *b*. However, for the *a* extracts the duplicates differ by 9 percent in Run U-301 and by 30 percent in Run U-302, differences which are reasonable in view of the low activity of these samples. The activities of Xe^{133} in the *a* extracts which grew from I^{133} were calculated from the Xe activities found in the *b* extracts. This calculation is fairly sensitive to uncertainty in (1) the fraction of I^{133} formed from a 63-min Te precursor; and (2) the times of Xe separation from the solutions. In view of these difficulties it is not surprising that small negative values were obtained for A_i, which are differences between activity values not known with sufficient accuracy. By assuming that 50 dis/min for A_i is the minimum that could have been observed, we calculate from (7) an upper limit of 0.1 percent for the fraction of the mass 133 chain originating at Xe. The independent yield predicted by the postulate of equal charge displacement of the primary fission fragments[13] is 0.04 percent of the total yield. In any case the value is so small that it need not be considered when measuring the total yield of Xe^{133}.

VII. INDEPENDENT YIELD OF 9.15-HR Xe^{135} IN U^{235} FISSION

As a by-product of the experiments reported in the previous section we were also able to measure the independent fission yield of 9.15-hr Xe^{135}. Each of the Xe samples from extracts *a* decayed initially with a 9.2-hr half-life. The portion of this activity produced by decay of its 6.68-hr I^{135} parent is calculated from Eq. (2) and is given by

$$A_g = 1.13\times10^{-5} f Y_g, \tag{8}$$

where A_g is taken at 27.8 hr after the end of the bombardment, and Y_g is the total fission yield of 6.68-hr I^{135}. The fission rate, f, can be evaluated from the amount of 5.27-day Xe^{133} found in extract *b*, taking 6.6 percent[14] for the Xe^{133} fission yield. Then by substituting this value of f into (8) and setting Y_g equal[15] to 0.062, we can calculate A_g. This figure is subtracted from the total observed 9.15-hr Xe^{135} (at 27.8 hr after the irradiation) to get the activity, A_i of the Xe^{135} produced independently. From Eq. (1),

$$A_i(0.033, 27.8) = 3.05\times10^{-4} f Y_i. \tag{9}$$

The independent yield, Y_i, is then calculated from (9) with f the same as before.

TABLE VII. Activities and independent yield of 9.15-hr Xe^{135} from U^{235} fission.

		U-301	U-302
9.15-hr Xe^{135} in extract *a* at 27.8 hours after end of bombardment	Total Xe^{135} activity	23 850 dis/min	19 900 dis/min
	Xe^{135} grown from I^{135}	10 890	11 020
	A_i (0.033, 27.8)	12 960	8 884
Y_i, independent yield of Xe^{135} (percent)		0.27	0.19
Percent of chain yield originating at Xe^{135}		4.2	2.9

The results of these measurements are presented in Table VII. Duplicate samples for activity measurements agreed within 2 percent when correction was made to 100 percent chemical yield. The major cause of the discrepancy between the results from the two runs is probably the ill-defined time of separation of the Xe^{135} from its I^{135} parent. For our final value of the fraction of the total Xe^{135} that is formed independently in U^{235} fission we have 3.5±1.0 percent. Hoagland and Sugarman[16] reported a value of about 5 percent; Brown and Yaffe recently reported[17] a value 2.6±1.0 percent. The curve of Glendenin, Coryell, and Edwards[13] predicts 4 percent.

VIII. HALF-LIFE OF I^{133}

The two values listed in the Table of Isotopes[4] for the half-life of I^{133} (20.5 and 22.4 hr) differ by almost 10 percent. In calculating the Xe^{133} fission yields from our experimental results, yield values differing by 2 percent are obtained depending on which of these I^{133} half-lives is used. Therefore a new half-life determination was made in order to remove this source of error.

The measurement is complicated by the fact that iodine separated from fission products soon after irradiation contains several active isotopes, some of which decay to active Xe daughters. The 6.68-hr I^{135} and its 9.15-hr Xe daughter would interfere very seriously with a measurement of the I^{133} half-life. Fortunately, the I^{135} can be eliminated completely because its Te parent is very short-lived (<2 min) while I^{133} grows from a 1.1-hr Te. Thus it was only necessary to irradiate some uranium for 5 min and isolate Te about 15 min later. This contained 1.1-hr Te^{133} but no Te^{135}. Also present were Te^{131}, Te^{132}, and Te^{134}. The purified Te was allowed to stand for 1.4 hr, and then the iodine activities which grew in were isolated. These consisted of 53-min I^{134} and 21-hr I^{133}, plus small amounts of 2.4-hr I^{132} and

[13] Glendenin, Coryell, and Edwards, Paper 52 of reference 1.

[14] See Sec. V, above.

[15] We use a value of 6.40 percent for the total yield of the mass 135 chain, based on our absolute value of 6.62 percent for the yield of mass 133 and the relative fission yields reported in reference 3. See Table IX, below.

[16] E. J. Hoagland and N. Sugarman, Paper No. 147 of reference 1.

[17] F. Brown and L. Yaffe, Can. J. Chem. **31**, 242 (1953).

TABLE VIII. Data and results of I^{133} half-life determination.

	Run 1			Run 2		
Counter	$\beta-1$	$\beta-4$	$\gamma-1$	$\beta-1$	$\beta-3$	$\gamma-1$
Absorber	130 mg Al/cm²	130 mg Al/cm²	5 g Pb/cm²	100 mg Al/cm²	100 mg Al/cm²	6 g Pb/cm²
Initial counting rate (counts/min)	16 690	9710	9330	3310	4420	1744
Number of I^{133} half-lives observed	11	10	8	10	10	8
Half-life of I^{133} (hr)	20.8	20.9	20.2	20.7	21.0	21.0

8.1-day I^{131}. By allowing the iodine to stand for 24 hr the two shorter-lived isotopes disappeared. Then the iodine was precipitated as AgI and activity measurements were begun.

The only interfering isotopes were the 5.27-day Xe^{133} daughter and 8.1-day I^{131}. These were suppressed by counting the β rays through 100 mg/cm² of Al which removed all of the Xe^{133} β rays and 96 percent of the I^{131} β rays but only 50 percent of the I^{133} radiation. The decay of the γ rays was followed by counting through 5 g/cm² of lead which removed nearly all of the Xe^{133} γ rays, $\frac{3}{4}$ of the I^{131} γ rays, but only $\frac{1}{2}$ of the I^{133} γ rays.

In the chemical procedure the Te was reprecipitated three times as the metal, and the iodine was purified by three cycles of oxidation, extraction with CCl_4, reduction, and extraction with water. One iodine sample was obtained from each of two separate runs. The β rays of each were measured with two different mica window Geiger counters and the γ rays were measured with a NaI crystal scintillation counter. For the first 9 days counts were taken twice daily; then for the next 18 days measurements were made every other day.

The Geiger counter data were corrected for coincidence loss and background, the scintillation counter data only for background.[18] A long-lived tail was subtracted from each of the decay curves to give the exponential decay of the I^{133}. The results are summarized in Table VIII. The six values were averaged, weighting each one by the number of half-lives over which the I^{133} decay was observed. The result is 20.8 $\pm$0.2 hr which agrees fairly well with the value of 20.5 hr found by Bartholomew *et al.*,[4] but it is in marked disagreement with the 22.4 hour value of Pappas.[4] For the fission yield calculations we adopted 20.8 hr.

TABLE IX. Yields of some chains from the thermal neutron fission of U^{235}, expressed in percent of the fissions, as determined by different investigators.

1. Isotope	2[a]	3[b]	4[c]	5[d]
Xe^{131}	2.97	3.28	2.8	3.0
Xe^{132}	4.45	4.92	4.0	4.5
$Xe^{133}Cs$	6.62	7.32[e]	5.0	6.1
Xe^{134}	7.81	8.64	5.5	7.9[f]
Cs^{135}	6.40	7.07[e]	6.0	
Xe^{136}	6.42	7.10	6.0	
Cs^{137}	6.07	6.71[e]	6.1	

[a] Corrected relative values reported by Wiles *et al.* (reference 3) normalized to our value of 6.62 percent for Xe^{133}.
[b] Same as column 2, but normalized to 3.28 percent at Xe^{131}.
[c] Values from smooth yield-mass curve of reference 1 normalized to 6.1 percent at Ba^{140}.
[d] Fission yields of iodine isotopes measured by A. C. Pappas (reference 4) normalized to 6.1 percent at Ba^{140}.
[e] These values are slightly lower than those given in reference 3. See text for explanation.
[f] Yaffe, Day, and Greer, Can. J. Chem. **31**, 48 (1953), reported 6.5 percent for Te^{134}. When the independent yield of I^{134} is added to this, the total I^{134} yield is 8.0 percent (normalized to 6.1 percent at Ba^{140}).

IX. DISCUSSION

Previous values for the fission yield of Xe^{133} are difficult to compare with the value of 6.62 percent found in the present investigation because the former were not measured directly by an absolute method as was the latter. Perhaps the best procedure is to normalize the relative yields measured in the recent mass spectrographic work reported by Wiles *et al.*,[3] to the absolute yield of Xe^{133} determined here. Table IX, column 2, shows these normalized values for mass numbers 131–137. Column 3 is based on the same relative yields as column 2, but the values are normalized to 3.28 percent at mass 131. Apparently this value was adopted by Wiles *et al.*, from the fission yield of I^{131} measured by Bartholomew *et al.*[19] relative to Ba^{140}, whose fission yield[20] was later determined absolutely. The values given in column 3 for masses 133, 135, and 137 are slightly lower than those given in the paper of Wiles *et al.*, to take into account the effect of the 2.3-day Xe^{133m} on the calculation of the 5.27-day Xe^{133} yield from the mass spectrographic work of Macnamara, Collins, and Thode.[21] It is assumed that all of the Cs^{133} is formed from decay of the 5.27-day Xe^{133}. Column 4 of Table IX gives the fission yield values as read from the smooth yield *vs* mass curve for U^{235} fission given in the Plutonium Project Record (PPR).[1] These are normalized to 6.1 percent for Ba^{140}. The last column gives the fission yields determined by Pappas[4] for the iodine isotopes of the given masses, relative to 6.1 percent for Ba^{140}. These values probably apply also to the Xe isotopes of the same mass because the independent yields of the latter are probably very small.

[18] Two of the Geiger counters lost their plateaus when the I^{133} had nearly decayed away. They were replaced with nearly identical counters, apparently without effect on the results.

[19] Bartholomew, Brown, Hawkings, Merritt, and Yaffe, Can. J. Chem. **31**, 120 (1953).
[20] Unpublished work by Bartholomew, Brown, Hawkings, Merritt, Thode, and Yaffe referred to in references 3 and 17.
[21] See reference 2. This work was done before the 2.3-day Xe isomer was discovered.

All values given in Table IX include the effects of delayed neutron emission.

An explanation of the discrepancies shown by Table IX will not be attempted at present because it would be based mostly on speculation. We believe that our fission yield for Xe^{133} is reliable to ± 3 percent of the value given, and we prefer the fission yields of column 2 to the others. The smooth curve of the PPR is not reliable at masses 133–134 because it depends on experiments in which there was very likely incomplete exchange between radioactive fission iodine and carrier iodine.

Experimental investigations recently completed[22] and now in progress[23] in other laboratories, together with the work reported here, should soon result in an accurate and fairly complete yield *vs* mass curve for U^{235} fission products.

ACKNOWLEDGMENTS

We were helped greatly in these experiments by the cooperation of the Electronics Division, the Glass Blowing Shop, and the Pile Operating Crew at Brookhaven. Mr. Ralph White constructed the fission counter and contributed to its design; Mr. A. W. Weinstein and Mr. Roy Anderson did most of the chrome-plating of the aluminum. We are particularly indebted to Mr. D. Clarius of the Electronics Division for his many hours of aid with the fission counting.

[22] A. Turkevich and G. Reed of the Institute for Nuclear Studies at the University of Chicago have recently completed a series of absolute yield determinations in U^{235} fission by the radiochemical method, but they did not cover the range of masses 131 to 137.

[23] L. E. Glendenin and E. P. Steinberg of Argonne National Laboratory have informed us that they are measuring many fission yields mass spectrometrically with the aid of isotopic dilution techniques.

PHYSICAL REVIEW VOLUME 91, NUMBER 6 SEPTEMBER 15, 1953

Chlorine Isotope Separation by Thermal Diffusion*†

A. Z. KRANZ‡ AND W. W. WATSON
Yale University, New Haven, Connecticut

(Received June 8, 1953)

From "two-bulb experiments" the thermal diffusion constant α of HCl has been determined to be $+0.010$ at $T_r = 685°K$ and -0.009 at $T_r = 229°K$. Such a rapid change of α and R_T with temperature and an inversion temperature at or above room temperatures seem to be characteristic of strongly polar molecules. The troublesome "memory effects" of HCl in a mass spectrometer can be eliminated by using a pin-hole leak right in the box of the ion source plus a baking out, flushing and repeated-analysis routine. Some details are given of a 6.8-meter hot-wire thermal diffusion column apparatus, having an equilibrium separation factor of 7, and which has provided fairly large samples of HCl enriched to 94 percent HCl^{35} and 62 percent HCl^{37} for cyclotron beam targets and other experiments.

INTRODUCTION

HYDROGEN chloride is representative of a considerable number of gases whose isotopic components are not easily separated by the method of thermal diffusion. But since isotope separation in quantity is a difficult task by any method and for any of the elements, the relatively simple procedure invented by Clusius and Dickel[1] for cascading the thermal diffusion separation by the thermal syphoning action in vertical columns still seems attractive. HCl was in fact the gas used by Clusius and Dickel in their pioneer experiments in which by employing many meters of column the chlorine isotopes were very well separated. Varying degrees of separation of the Cl isotopes by this method have also been reported by Kennedy and Seaborg[2] and by Shrader.[3]

One of our aims in these experiments has been to improve the experimental factors so as to achieve the greatest possible isotope separation from apparatus of modest size. Ways of optimizing the geometry and operating procedure of thermal diffusion columns have been discussed in a recent paper by one of us.[4] Dickel[5] has also elaborated on the magnitude of the possible improvement in the apparatus factors, granting the inherent low thermodynamic efficiency of the thermal diffusion process. This is a contribution to our continuing effort to improve our knowledge of the thermal diffusion method of separating isotopes.

It was also our desire to collect sufficient quantities of well-separated Cl isotopes for target material in certain nuclear reaction studies. In a second paper we are reporting details of $Cl^{35,37}(\alpha,p)A^{38,40}$ reactions whose

* Part of a dissertation submitted in partial fulfillment of the requirements for the degree of Doctor of Philosophy in Yale University by A. Z. Kranz.

† This work was supported by the U. S. Atomic Energy Commission.

‡ Now at the Atomic Power Division, Westinghouse Electric Corporation, Pittsburgh, Pennsylvania.

[1] K. Clusius and G. Dickel, Z. Phys. Chem. **B44**, 451 (1939).

[2] J. W. Kennedy and G. T. Seaborg, Phys. Rev. **57**, 843 (1940).

[3] E. F. Shrader, Phys. Rev. **69**, 439 (1946).

[4] W. W. Watson, Z. Physik **133**, 272 (1952).

[5] G. Dickel, Naturwiss. **37**, 164 (1950).

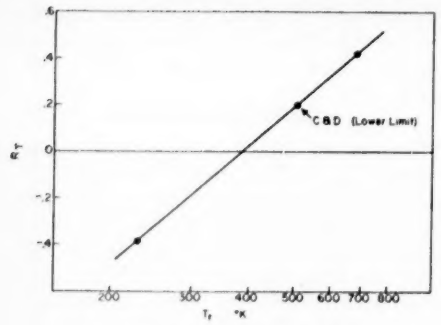

FIG. 1. R_T values as a function of T_r.

interpretation has been aided by the use of these separated isotopes.

THE THERMAL DIFFUSION CONSTANT OF HCl

The predicted separation factor of a thermal diffusion column depends strongly on the value of the thermal diffusion constant α used in the calculations. From viscosity data one can compute that near room temperatures α for HCl is approximately zero,[6] but this quantity does increase with rising temperature. Swartz[7] previously in this laboratory has measured α for HCl at several temperatures, using the two-bulb technique,[8] but he only established that there is a reversal in the sign of α of HCl at about 485°K. In repeating these experiments we have taken great care to minimize the bothersome "memory effect" with HCl in the mass spectrometer.

The hot and cold volumes of our glass two-bulb apparatus were 534 and 106 cm³, respectively. A number of measurements were made at two different pairs of temperatures; the one with the hot-bulb temperature $T_h=800°K$ and the cold-bulb temperature $T_c=600°K$, the other with $T_h=273°K$ and $T_c=194°K$. The mean temperature T_r is computed as $[T_hT_c/(T_h-T_c)]\ln(T_h/T_c)$. For the $T_r=685°$ point the initial HCl gas pressure in the system was 76 cm of Hg, the number of successive Chapman processes carried out was four, and the time for the first process was 15 hours to guarantee equilibrium. For the $T_r=229°$ point the initial pressure was 10 cm of Hg, the number of successive thermal diffusion separations was three, and the equilibrium time for the first one was taken as 17 hours.

The results are summarized in Table I. The quantity C_2^c is the fractional concentration of the heavier isotope in the sample taken from the cold bulb at the end of operations in each case. This was then corrected for the gas in the connecting tube. The normal concentration C_2^0 of Cl^{37} was measured to be 0.2458 ±0.0011. The errors given for C_2^0 and C_2^c are mean deviations of a considerable number of mass spectrometer analyses in each case.

TABLE I. Thermal diffusion constant α for HCl.

T_h	T_c	T_r	C_2^c	α	R_T
800°K	600°K	685°	0.2473±0.0005	+0.010±0.008	+0.42
273°K	194°K	229°	0.2444±0.0004	−0.009±0.007	−0.38

The error in α is large because α depends directly on $C_2^c-C_2^0$. The separations achieved were small and the quantity $C_2^c-C_2^0$ is not much larger than its probable error. Still, the error in each concentration measurement is satisfactorily small, particularly in view of the memory effect.

Figure 1 is a plot of these R_T values *versus* T_r, where R_T is the ratio of α to $\alpha_{e.s.}=(105/118)[(38-36)/(38+36)]$ for elastic-sphere molecules of these masses. The straight line drawn through our two points is justified by the results of similar measurements with other gases,[9] all of which show this linearity. The point at $T_r=507°$ is a lower limit calculated by Jones and Furry[10] from the column operations of Clusius and Dickel with HCl; the excellent agreement is encouraging. We are in agreement with the earlier finding of Swartz that α for HCl does change sign at a temperature well above room temperature, but our value of

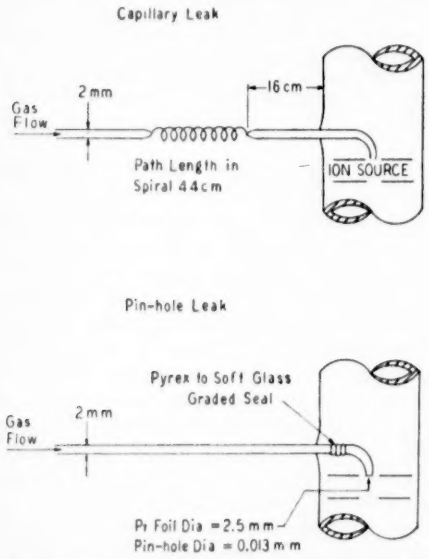

FIG. 2. Gas sample supply to mass spectrometer ion source. Gas flow is at a few mm Hg pressure. Pressure in ion source is about 10^{-3} mm Hg.

[6] R. C. Jones, Phys. Rev. **58**, 11 (1940).
[7] G. B. Swartz, Phys. Rev. **76**, 166 (1949).
[8] A. O. Nier, Phys. Rev. **56**, 1009 (1939).
[9] K. E. Grew and T. L. Ibbs, *Thermal Diffusion in Gases* (Cambridge University Press, Cambridge, 1952), Appendix 6.
[10] R. C. Jones and W. H. Furry, Revs. Modern Phys. **18**, 218 (1946).

the inversion temperature, 385°K, is about a hundred degrees lower than the one he reports.[7]

Since the forces between strongly polar molecules like HCl are certain to be temperature-dependent in a complicated manner, we purposely refrain from a comparison of this R_T *versus* T variation with the predictions of the usual inverse-power models. It is noteworthy, however, that for both of the polar molecules NH_3 and HCl the R_T *versus* T line has a considerably greater slope than those found for nonpolar molecules. The reader is referred to a qualitative explanation of this difference by Watson and Woernley[11] for the NH_3 case.

MEMORY EFFECTS IN THE MASS SPECTROMETER

The analysis of HCl in a mass spectrometer is hindered by serious memory effects. That is, we found that successive analyses of gas samples with changed isotopic abundances yielded nonreproducible and nonpredictable results. Our older instrument is a 60° Nier-type spectrometer, essentially like the one described by Graham, Harkness, and Thode.[12] A capillary leak served to reduce the gas pressure from a few millimeters of Hg in the sampling system to about 10^{-2} mm of Hg in the ion source. The memory effect is attributed to a mixing of the molecules from the previous sample coming off the walls with those of the new sample just entering the ion source. At the pressure in the sampling system this effect is negligible; at the low pressure in the ion source it is serious.

Our principal innovation in overcoming this difficulty was to minimize the surface area in the low pressure region. How this was accomplished is shown in Fig. 2. The capillary was replaced by a pin-hole leak inserted right into the ion source, thereby eliminating all low pressure areas outside of the spectrometer tube.

To prepare the pin-hole leak, a piece of soft-glass tubing was heated above the softening point and touched to a platinum foil. This sealed the platinum to the glass. Then an ordinary sewing needle was sharpened by rubbing a fine stone against its point while it was turning rapidly in a lathe. The point was thus reduced to 0.0005 inch in diameter. The glass tube was then secured in the tail-stock chuck, and the needle was secured in the tool holder of a small lathe. Observing through a traveling microscope, the needle point was pushed into the platinum foil by turning the micrometer feed on the lathe compound. This pin-hole leak was then sealed into the spectrometer tube, using a Pyrex-to-soft-glass graded seal.

The following procedure was adopted for making analyses. After a measurement the spectrometer was pumped out for several hours. During this pump-out time the entire spectrometer tube was heated to about 350°C by an electric furnace. Then a small quantity of the next gas sample was allowed to pass through the pin-hole into the spectrometer. The spectrometer was thus flushed several times. Next the heater was shut off, and the Dewar around the liquid-air trap of the main pump line was filled to the top. This precaution prevented any HCl from backdiffusing into the spectrometer. After an hour's wait for the spectrometer to cool, the sample was fed in and measured, after which the heater was turned on and the flushing and baking repeated. In four hours the next cooling off and subsequent measurement were made.

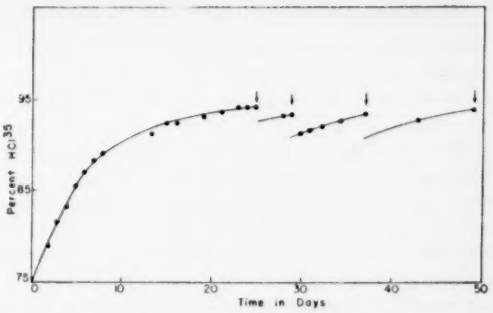

FIG. 3. Rate of rise of concentration of HCl^{35} in reservoir attached to upper end of apparatus.

Following this routine, we have found that the successive analyses of a given sample differ less and less, and finally they are reproducible. It takes from one to three days to complete the analysis of one sample for its Cl isotope abundance ratio, the elapsed time depending on the degree of difference from the previous sample.

There is no simple explanation of this memory effect. It is obviously a matter of surface chemistry, the large dipole moment of the HCl molecule causing it to adhere tenaciously to the walls. The memory effect is negligible for most gases, but for polar molecules careful procedure similar to the one we outline may be necessary for accurate, reproducible isotope abundance measurements.

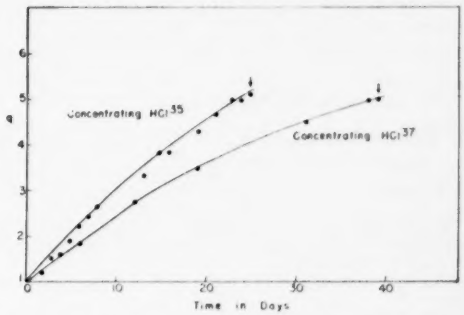

FIG. 4. Rate of increase in separation factor q. Comparison with Fig. 3 illustrates that when the concentration is high, relatively large increases in separation factor are needed to produce small increases in concentration.

[11] W. W. Watson and D. Woernley, Phys. Rev. **63**, 181 (1943).
[12] Graham, Harkness, and Thode, J. Sci. Instr. **24**, 119 (1947).

THERMAL DIFFUSION COLUMN OPERATION

Calculation showed the separation factor q of our hot-wire column to be larger the smaller the diameter of the water-cooled tube and the central wire. Since the column must be absolutely straight and vertical, however, it is not very practical to use glass tubing of diameter less than 8 mm. We have employed two 3.4-meter glass columns of this inner diameter, with the central hot wires of Pt-Ir(10 percent) 0.38 mm in diameter. The two columns were convectively coupled in series by 6-mm tubing. The positive reservoir (where the desired isotope is enriched) was 100 cm³ in volume; the negative reservoir had a volume of 25 liters, which is effectively infinite. The hot wires were operated at 1200°K and the cold walls at 290°K. Pt cross wires spaced at 35-cm intervals served to center the hot wires, and they were kept taut by a small weight (25-g stainless steel pieces), which cannot be large because of the tendency of Pt wire to stretch. Wire extension was accommodated by an accordian-pleated silver foil at the lower end. Total power consumption for the two columns was 454 watts.

Trial runs at different gas pressures with a single column established a fairly sharp maximum q for $p=57$ cm of Hg. Figure 3 shows the approach to equilibrium in the positive reservoir attached to the upper end of the 6.8 meters of column operating at this pressure. The arrows indicate when the contents of the positive reservoir were removed. The fact that the mass spectrometer analyses showed the same rise to equilibrium after each withdrawal of product is taken as evidence that the memory effect has been practically eliminated. A similar curve was obtained for the increase in HCl^{37} content when the end volumes were interchanged. Figure 4 shows the separation factor as a function of time. Note that the rate of rise of the concentration of the heavy isotope is slower. The explanation of this is that more gas must be transported when the concentration is proceeding in this direction.

From these curves we estimate that the equilibrium separation factor would be about 7. The highest concentrations actually collected were 94 percent HCl^{35} and 62 percent HCl^{37}, the samples of each variety totalling about 500 cm³ (NTP). The equilibrium separation factor $q=7$ would mean $\ln q=0.29$ per meter of column, while the top factor of 5 which satisfied us gives $\ln q=0.24$ per meter. For comparison, the best operation reported by Clusius and Dickel indicates their $\ln q$ per meter was 0.23, and Kennedy and Seaborg's data show that they had a $\ln q$ of 0.24 per meter. These results are all about the same, and show that without making a great effort to maximize the efficiency of the columns one can collect by this relatively simple method good-sized samples of fairly well separated isotopes even with gases for which the thermal diffusion constant is close to zero at and near room temperature. Our equilibrium value for $\ln q$ per meter represents a 20 percent improvement over the results of the other investigators, but for better efficiency one should not wait for equilibrium to collect product.

PHYSICAL REVIEW VOLUME 91, NUMBER 6 SEPTEMBER 15, 1953

Energy Levels in A^{38} from the $Cl(\alpha,p)$ Reaction*†

A. Z. KRANZ‡ AND W. W. WATSON
Yale University, New Haven, Connecticut

(Received June 8, 1953)

AgCl targets containing 94 percent Cl^{35}—6 percent Cl^{37} and 62 percent Cl^{37}—38 percent Cl^{35} were bombarded with α particles. The protons resulting were observed at 90° and 0° to the incident beam, and establish excited states in the A^{38} nucleus at 2.13 ± 0.04 and 3.73 ± 0.04 Mev. No groups from A^{40} were observed.

INTRODUCTION

TWO excited states in the A^{38} nucleus have been previously reported in the literature.[1] Pollard and Brasefield[2] studied the (α,p) reaction on natural chlorine targets using ThC′ α particles. They reported levels at 2.6 and 4.3 Mev. Itoh,[3] and Hole and Siegbahn[4] have studied the γ rays accompanying β decay of Cl^{38}. Itoh reports levels in A^{38} at 2.19 and 3.83 Mev, and Hole and Siegbahn find 2.15 and 3.75 Mev for these levels. Langer[5] has studied the β rays from Cl^{38}, and reports levels at 2.04 and 3.70 Mev. By bombarding partially separated Cl isotopes with 7.45 Mev (mean

* Part of a dissertation submitted in partial fulfillment of the requirements for the degree of Doctor of Philosophy in Yale University by A. Z. Kranz.

† This work was supported by the U. S. Atomic Energy Commission.

‡ Now at the Atomic Power Division, Westinghouse Electric Corporation, Pittsburgh, Pennsylvania.

[1] D. E. Alburger and E. M. Hafner, Revs. Modern Phys. **22**, 373 (1950). This review article lists references to earlier work.

[2] E. C. Pollard and C. J. Brasefield, Phys. Rev. **50**, 890 (1936).

[3] J. Itoh, Proc. Phys. Math. Soc. Japan **23**, 605 (1941).

[4] N. Hole and K. Siegbahn, Arkiv. Mat. Astron. Fysik **A33** No. 9 (1946).

[5] L. Langer, Phys. Rev. **77**, 50 (1950).

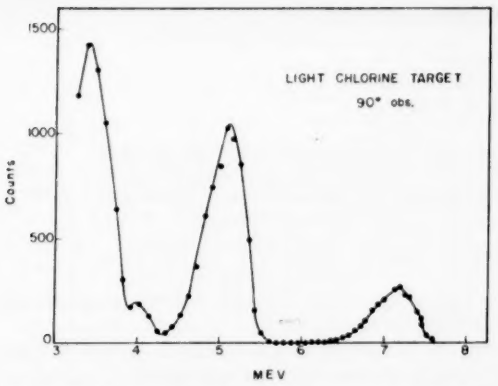

FIG. 1. Yield of protons from $Cl(\alpha,p)$ reaction with chlorine enriched in Cl^{35}.

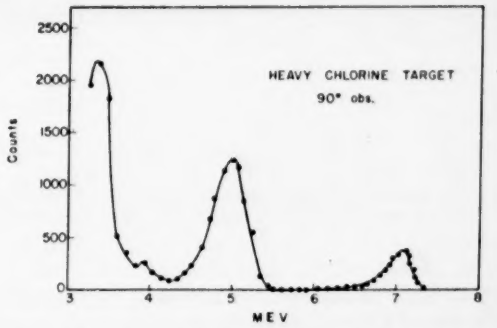

FIG. 2. Yield of protons from $Cl(\alpha,p)$ reaction with chlorine enriched in Cl^{37}.

range) α particles from the Yale 28-inch cyclotron, we hoped to resolve the differences in the older information, and also to get information about the levels in A^{40}.

EXPERIMENTAL METHOD

Protons were observed with a proportional counter at 90° and 0° to the incident α beam. Proton energies were determined by absorption in aluminum; the counting arrangement was such that only those protons ending their range in the proportional counter were recorded. AgCl targets were prepared using partially separated Cl isotopes produced in our thermal diffusion columns.[6] The HCl gas taken from the columns was dissolved in water to produce an 0.05 N solution. A silver disk (0.010 inch thick for 90° observation, 0.001 inches thick for 0° observation) was placed in the solution, and 0.25 mg/cm^2 of Cl plated out as AgCl. The targets stood up very well under the bombardment. Two gas samples were used. The "heavy chlorine" targets were made from gas containing 62 percent HCl^{37} and 38 percent HCl^{35} and the "light chlorine" targets were made from gas containing 94 percent HCl^{35} and 6 percent HCl^{37}.

DISCUSSION

Figure 1 shows the groups observed at 90° observation using the light chlorine target, and Fig. 2 shows the same for the heavy chlorine target. A similar pair of curves were obtained at 0° observation. The fact that changing the concentration of Cl^{37} from 6 percent in the one target to 62 percent in the other did not show a change in the proton spectrum leads us to assign all the groups to A^{38}. In fact, the yield from the heavy chlorine target was less, for a given bombarding current, than the yield from the light chlorine target.

The ground-state Q value was obtained by comparing the mean proton energy from an integral curve with the mean value of the energy of the α beam as measured in an air absorption cell. The excited-state Q values were obtained from differences in the extrapolated ranges. Obtained in this way, the ground-state Q value of A^{38} is 0.81 ± 0.08 Mev, and the Q values for the first and second excited states are -1.32 ± 0.08 and -2.92 ± 0.08 Mev, respectively. These represent levels in the A^{38} nucleus at 0, 2.13 ± 0.04, and 3.73 ± 0.04 Mev.

The agreement with the Q value calculated from the mass data of Li *et al.*,[7] 0.81 ± 0.09, is excellent. The Q value for the ground state of A^{40} as calculated from the mass data is -1.63 ± 0.09 Mev. This group would lie just inside the first excited-state group from A^{38}. It is evident that at our bombarding energy, the cross section for the $Cl^{35}(\alpha,p)A^{38}$ reaction is much higher than that for the $Cl^{37}(\alpha,p)A^{40}$ reaction. The lower ground-state Q value, the smaller cross section, and the fact that Cl^{37} is the less abundant isotope in nature and more difficult to enrich, are all responsible for our inability to observe groups from A^{40}. The low-intensity group at 4 Mev may be due to A^{40}, but it is more likely attributable to an impurity in the target. Probably targets enriched to at least 90 percent in Cl^{37} would be required to observe the proton groups from A^{40} with our α beam.

The authors wish to thank Professor E. C. Pollard for helpful suggestions and discussions.

[6] A. Z. Kranz and W. W. Watson, preceding paper, Phys. Rev. **91**, 1469 (1953).

[7] Li, Whaling, Fowler, and Lauritsen, Phys. Rev. **83**, 512 (1951).

Effects of a Primeval Endowment of U^{236}†

DAVID B. ROSENBLATT
Frankford Arsenal, Philadelphia, Pennsylvania
(Received February 13, 1953)

The effects of a primeval endowment of U^{236} upon theories pertaining to the evolution of the elements, the thermal history of the earth, and geochronology are considered. It is shown that the present thorium to uranium ratio, early volcanism on the earth and on the moon, as well as corrections to the dating of rocks and meteorites may be related to an initial abundance of the isotope, if certain assumptions are made.

RECENT measurements[1,2] indicating that the half-life of U^{236} is approximately 2.4×10^7 yr should be taken into account in formulating theories pertaining to the evolution of the elements, the thermal history of the earth, and geochronology.

A survey of radioactive isotopes shows that known half-lives fall into two classes; (a) those of the same order or longer than the age of the earth, (b) half-lives of insignificant duration on a geological scale. Class (a) contains Th^{232}, U^{238}, Rb^{87}, La^{138}, Sm^{147}, Lu^{176}, and Re^{187}. Also included in this class are U^{235} and K^{40} which possess half-lives of the order of 10^8 or 10^9 yr and, consequently, have been seriously depleted during the earth's 3 or 4 billion years of existence but still persist to a detectable degree. Class (b) contains radioisotopes which occur naturally only by virtue of their constant generation as members in a radioactive series initiated by the decay of one of the substances of class (a), others such as C^{14} or Pu^{239} which are constantly generated by stray neutrons, as well as the artifically produced radioisotopes. U^{236} is unique in belonging to neither class; its half-life relative to the age of the earth is too short to result in a detectable abundance of this isotope in natural uranium, yet it is sufficiently long to insure its existence during the first part of the earth's history. Given an initial endowment of U^{236}, we must consider it to have persisted as a significant entity during the first half-billion years of geological time, for its half-life is not entirely negligible in relation to current estimates of the time interval between the genesis of the elements and the formation of the earth.[3]

The interval between element formation and formation of the earth's atmosphere has been estimated by Katcoff, Schaeffer, and Hastings[4] to be 0.27×10^9 yr and by Suess and Brown[5] to be of the order of 0.4×10^9 yr. Most of the following effects are predicated upon the possibility that these estimates for the interval are too high, or that the earth, as an entity, is appreciably older than its atmosphere.

Owing to the lack of any generally accepted theory concerning the formation of the elements, one cannot postulate an initial endowment of U^{236} in planetary matter with any degree of certainty. However, an initial abundance of U^{235} comparable to that of the main uranium isotope has often been invoked in estimating the age of the earth; there is nothing in the systemics of nuclei to suggest that U^{236}, with an even number of neutrons and protons, and lying closer in mass to the most stable isotope, U^{238}, should have been formed less abundantly than U^{235}. U^{236} is highly fissionable when in a sufficiently excited state; consequently it could only have been formed if the element building process produced the isotopes in their final distribution after the temperature of the nuclei had subsided to low values. Theories which assume that the various nuclides originated as aggregates of neutrons and, subsequently, were transformed through successive beta decay into the naturally occurring isotopes[6] appear to be consistent with an appreciable initial abundance of U^{236}. Although the production of U^{236} in piles is a low yield process, the absorption of a neutron in U^{235} generally imparting sufficient energy to the compound nucleus to result in fission, the opposite would hold for the primeval production through successive beta decay; for in the latter case, the final U^{236} nucleus would not be sufficiently excited to undergo fission. In fact any theory of element building in which the accumulation of the positive charge within the nucleus necessary for the fission process occurs after the universe has passed through the stages of very high density and temperature should result in an original U^{236} endowment in the same way that it leads to a finite abundance for U^{238} and other isotopes for which the values of Z^2/A are not so large as to result in prohibitive rates of spontaneous fission.

Virtually the entire original endowment of U^{236} must have decayed through alpha emission to Th^{232} during the first half-billion years of geological time. Consequently, we should not look for any U^{236} in present analyses of natural uranium, but, instead, should expect to find an enrichment of Th^{232} relative to other nuclides in this portion of the abundance curve of the

† Work done at Brookhaven National Laboratory, Upton, New York, under contract with the U. S. Atomic Energy Commission.
[1] Jaffey, Diamond, Hirsh, and Mech, Phys. Rev. **84**, 785 (1951).
[2] Fleming, Ghiorso, and Cunningham, Phys. Rev. **88**, 642 (1952).
[3] G. Gamow and C. L. Critchfield, *Theory of Atomic Nucleus and Nuclear Energy-Sources* (Oxford University Press, London, 1949), pp. 307 and 309.
[4] Katcoff, Schaeffer, and Hastings, Phys. Rev. **82**, 688 (1951).
[5] H. E. Suess and H. Brown, Phys. Rev. **83**, 1254 (1951).
[6] G. Gamow, Phys. Rev. **70**, 572 (1946).

elements. In Goldschmidt's survey[7] we find that thorium is, indeed, more common throughout the universe than the nearby elements uranium and bismuth. Assuming that, originally, equal numbers of atoms of uranium and thorium were formed, and that uranium consisted chiefly of U^{235}, U^{236}, and U^{238}, in roughly equal quantities, the U^{235} would largely decay to Pb^{207} and the U^{236} would, in its entirety, decay to Th^{232} resulting in a present thorium to uranium ratio of 4, which, even after correction for the partial decay of U^{238}, is still in rough agreement with the value of 3.8 commonly quoted for "average" rocks.

Any appreciable original abundance of U^{236} should have severely affected the early thermal history of the earth. For example, Urey's theory of the formation of the earth by accretion, melting due to radioactive heating, and final cooling[8] would have to be modified and allowance made for two distinct periods of heat production. Due to the relatively enormous disintegration rate of U^{236}, the heat generation in the earth immediately after accretion should have been very great; in fact during the first half-billion years the earth would probably have to be regarded as molten even at the center. As the amount of U^{236} dwindled, temperatures should have dropped to the point where pressure sufficed to insure a semisolid phase at the earth's core. The disintegrations of K^{40} and the $4n+2$, $4n$ and $4n+3$ series should have continued to maintain the molten magma still found at moderate depths.

An original abundance of U^{236} would affect the thermal history of the moon differently owing to the larger surface to volume ratio and lower thermal inertia of the satellite. Heating due to K^{40} and to U^{238}, U^{235}, and Th^{232} and their descendants is insufficient to lead to high internal temperatures, as is demonstrated by the total lack of volcanism on the moon at the present time. However, initially the high disintegration rate of U^{236} may have resulted in formation of the moon's craters. Volcanism on a scale necessary to produce such craters is symptomatic of enormous temperature gradients at a time when the outer crust was already formed. (In the case of the earth no large craters should be expected, for the greater volume to surface ratio and thermal inertia would conserve the heating due to ordinary uranium and thorium thereby maintaining the crust in a molten state after most of the U^{236} had decayed.)

These remarks are based on purely qualitative considerations owing to the difficulty of arriving at reasonable estimates for the thermal conductivities, as well as the roles of convection currents and orogeny, in determining the rate of heat transfer to the surfaces of the earth and the moon during their very early history.

A possible primeval endowment of U^{236} must be taken into account in evaluating methods of geochronology based upon relative abundances of uranium and lead isotopes, as well as those depending upon helium content. For example, Holmes' method leads to certain values for the abundances of the lead isotopes at the time of formation of the earth's crust.[9] Alpher and Herman have shown how to derive these abundances using three basic equations.[10] The equations assume a simple decay of thorium and uranium within the source magma prior to deposition of a lead sample. A primeval endowment of U^{236} would change the form of the third equation by requiring that the simple decay of thorium be replaced by a sharp initial rise, followed by decay. Estimates of the ages of various geological formations and of the age of the earth's crust would not be appreciably affected, since in general a least squares analysis is used which largely eliminates the dependence upon the early abundances of uranium and thorium. On the other hand, the use of present lead isotope ratios in calculating the abundances of Th^{232} and Pb^{208} at the time of origin of the elements would have to be revised. The effect on the former is large and has been discussed earlier in this paper; the effect on the latter would be quite small, but any change would be of interest from the point of view of nuclear shell structure.[11]

Helium age methods as applied to terrestrial samples should not be affected, for such determinations have not been found to be reliable for ages earlier than pre-Cambrian, in any case. However, a primordial abundance of U^{236} would require a modification of helium methods as applied to meteorites, at least in the case of samples whose age is assumed, or found, to exceed 10^9 yr. After subtraction of that part of the He content formed within the meteorite by cosmic rays, as described by Singer,[12] it would be necessary to adjust the remainder so as to allow for emission of one alpha particle in the case of the one out of every four Th^{232} nuclei which had originated as U^{236}. Since only a minority of all the Th^{232} nuclei decay during the life of a meteorite, the correction should be significant.

[7] V. M. Goldschmidt, *Verteilungsgesetze der Elements* (Oslo, 1938).
[8] H. C. Urey, *The Planets* (Yale University Press, New Haven, 1952).
[9] A. Holmes, Nature **157**, 68 (1946).
[10] R. Alpher and R. Herman, Phys. Rev. **84**, 1112 (1951).
[11] R. Alpher and R. Herman, Phys. Rev. **84**, 1113 (1951).
[12] S. F. Singer, Nature **170**, 728 (1952).

Gamma Rays from Interaction of 14-Mev Neutrons with Various Materials

V. E. SCHERRER, R. B. THEUS, and W. R. FAUST
Naval Research Laboratory, Washington, D. C.

(Received April 23, 1953)

Experiments have been performed to observe the pulse-height distribution produced in a single crystal spectrometer by gamma radiation arising from bombardment of various materials with 14-Mev neutrons. Various gamma-ray lines have been identified and estimates made of the total cross section for gamma-ray production.

IN a previous paper,[1] we described some observations of gamma radiation produced by interaction of 14-Mev neutrons with iron. Further results of such experiments are given herein for several elements ranging in atomic weight from carbon to lead.

The experimental apparatus and techniques used were similar to those described in I. Briefly, 14.2-Mev neutrons from the $T^3(d,n)He^4$ reaction bombarded a converter arranged so that whenever a neutron entered the converter the corresponding alpha particle entered the accelerator monitor. The pulse-height distribution from converter gamma rays was observed by a scintillation spectrometer consisting of a single crystal of NaI(Tl) and a twenty-channel pulse-height analyzer. Coincidences between crystal and alpha monitor pulses were used to gate the pulse-height analyzer so that only reactions produced in the converter by neutrons were observed.

Experiments have been performed as described in I to observe pulse-height distributions for carbon, oxygen, aluminum, nickel, copper, cadmium, and lead. Pulse-height distributions were taken with the appropriate converter "in" and "out" of the coincidence neutron beam to obtain source and background data. Generally the source to background ratio was ten to one or greater with the exception noted later. The net counting data, obtained by subtraction of source and background observations are plotted in the accompanying figures in counts per Mev per incident neutron, as a function of secondary electron energy.

Energy calibration of the spectrometer was made as described in I. Gamma-ray energies were estimated directly from this data where available. In the region where pair production is comparable to the Compton process, the gamma-ray energy is 1.02 Mev above the corresponding electron energy, due to the loss of the two 0.51-Mev annihilation quanta.

There appears to be evidence of line or band spectra as indicated by maxima in the pulse-height distribution for all but one of the elements examined. The distributions were analyzed as arising from a continuous gamma-ray spectrum, superimposed upon a line spectrum. We give the results of such analysis by quoting the total gamma-ray production cross section and the cross section for each obvious line.

CARBON

The pulse-height distribution for a carbon converter is given in Fig. 1 in counts per Mev per incident neutron. For comparison, the pulse height distribution in counts per second per Mev obtained from a Po-Be source is also plotted. The similarity of these curves is due to the condition that the residual excited nucleus is C^{12} in both reactions. The 4.45-Mev gamma ray,[2]

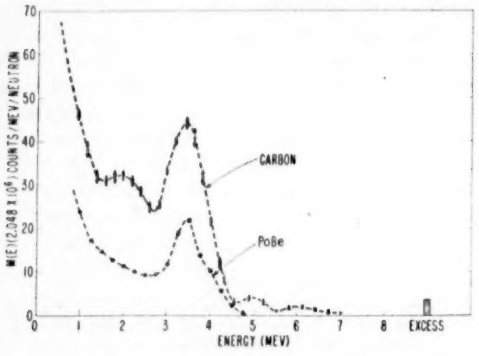

FIG. 1. Pulse-height distribution obtained from carbon and Po-Be gamma rays. Ordinates are counts per Mev per neutron for the carbon curve and counts per sec per Mev for the Po-Be curve.

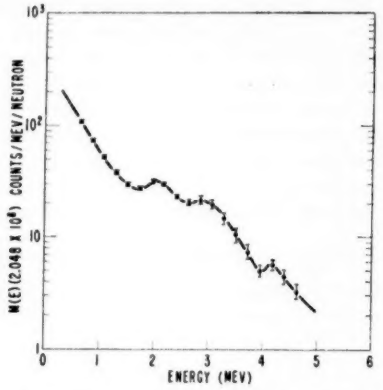

FIG. 2. Pulse-height distribution obtained from oxygen gamma rays.

[1] V. E. Scherrer *et al.*, Phys. Rev. **89**, 1268 (1953); hereafter referred to as I.

[2] J. Terrell, Phys. Rev. **80**, 1076 (1950).

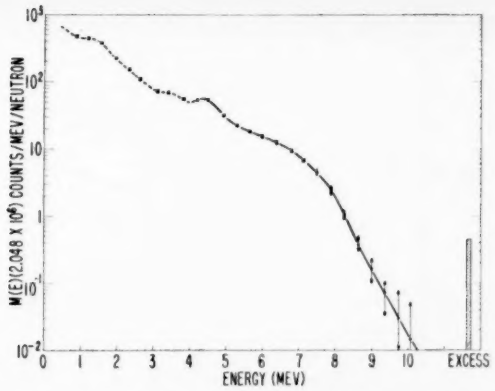

FIG. 3. Pulse-height distribution obtained from aluminum gamma rays.

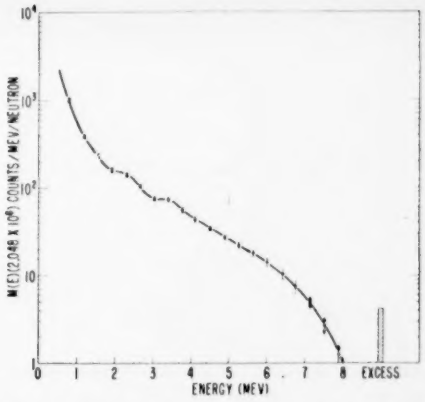

FIG. 5. Pulse-height distribution obtained from copper gamma rays.

which appears at a secondary electron energy of 3.43 Mev due to the loss of the two 0.51-Mev annihilation quanta, is quite evident in both cases. Differences between the curves are probably due to the higher excitation produced by 14-Mev neutrons on carbon as compared with the excitation of the residual nucleus in the reaction $Be^9(\alpha,n)C^{12}$.

An analysis of this pulse-height distribution, following the procedures outlined in I, indicates gamma rays at 2.8, 4.45, 6.0, and 7.0 Mev. The cross section for each line is 0.036, 0.069, 0.002, 0.002 barn, respectively, and the total cross section for gamma-ray production is estimated to be 0.19 barn.

OXYGEN

In these experiments, liquid oxygen in a vacuum flask was placed in the "coincidence neutron beam." Pulse-height distributions were taken both with the flask full and empty to obtain "source" and "background" data. The resulting source to background ratio was of the order of three to one. The pulse-height distribution so obtained is given in Fig. 2. Here there appear to be lines, at 3.0, 3.8, and 5.2 Mev having production cross sections of 0.086, 0.130, and 0.056 barn, respectively. The total cross section for gamma production is estimated to be 0.52 barn.

ALUMINUM

The pulse-height distribution obtained from aluminum is given in Fig. 3, from which it appears that there are maxima at electron energies of 1.5, 3.5, and 4.4 Mev. An analysis of this pulse-height distribution indicates that the production cross section is 1.7 barns while the cross sections are 0.176, 0.024, and 0.054 barn for the 1.7-, 4.5-, and 5.4-Mev gamma rays, respectively. A cross section of 0.0003 barn is estimated for the region above 11 Mev.

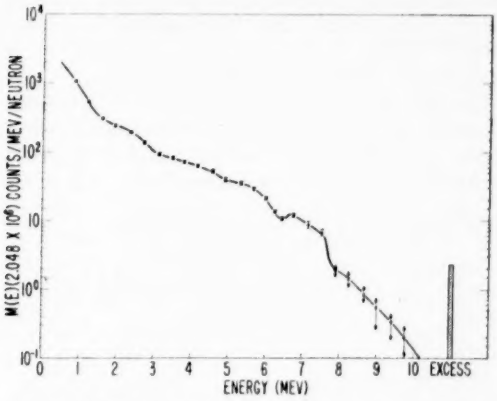

FIG. 4. Pulse-height distribution obtained from nickel gamma rays.

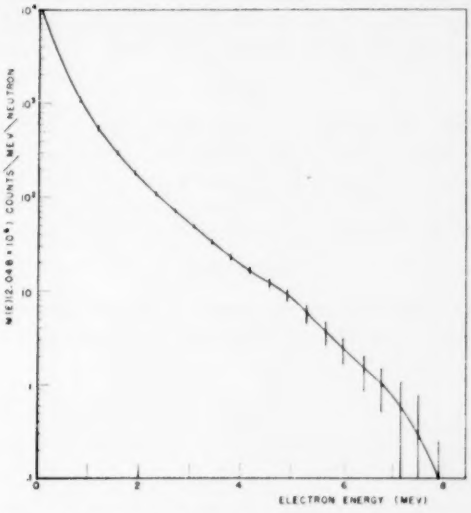

FIG. 6. Pulse-height distribution obtained from cadmium gamma rays.

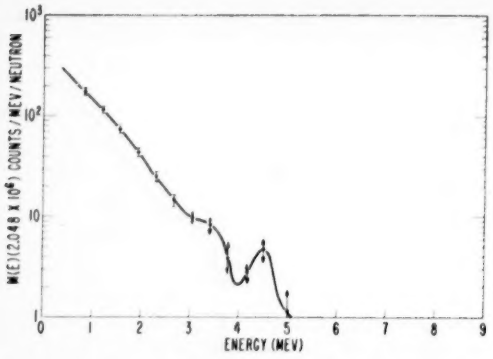

FIG. 7. Pulse-height distribution obtained from lead gamma rays.

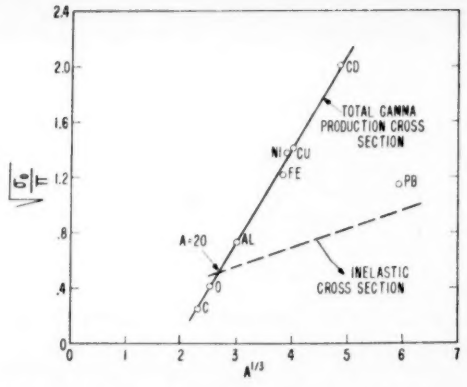

FIG. 8. Gamma-ray production cross section (barns) shown as a function of atomic mass.

NICKEL

The pulse-height distribution for nickel is given in Fig. 4 for which the total cross section is 6 barns. Lines at gamma-ray energies of 2.9, 5.2 Mev, 6.6 Mev, and 8 Mev have cross sections of 0.096, 0.021, 0.032, and 0.01 barn, respectively.

COPPER

A copper converter produced the pulse-height distribution given in Fig. 5. The total cross section for copper is computed as 6.3 barns and the apparent lines at 3.1 and 4.5 Mev have production cross sections of 0.052 and 0.029 barn, respectively. A cross section of 0.007 barn is estimated for the region above 8 Mev.

CADMIUM

The cadmium pulse-height distribution is given in Fig. 6. The total cross section for gamma-ray production is 12.8 barns. There appears to be no definite line structure present, however there appears to be a change of slope at an electron energy of about 4.5 Mev which corresponds to a gamma-ray energy of 5.5 Mev.

LEAD

The lead pulse-height distribution in Fig. 7 indicates two gamma rays in the distribution. It is found that the total cross section for gamma-ray production is about 4.2 barns while the lines at 4.4 Mev and 5.5 Mev have cross sections of 0.048 and 0.017 barn, respectively.

DISCUSSION

Probable errors in the counting data are represented by the vertical lines on the various pulse-height distributions. There are, however, other sources of error present in the cross-section computations that are more serious than the counting statistics. These errors arise from uncertainties in the absorption and scattering of neutrons and gamma rays in the converter and crystal as well as a lack of knowledge of the precise response of the spectrometer at all energies. It is estimated that the probable error in the total production cross section is about ± 25 percent while that associated with the lines is about ± 35 percent.

Gamma-ray production cross sections σ_0 are summarized in Fig. 8 where $(\sigma_0/\pi)^{\frac{1}{2}}$ is plotted against $A^{\frac{1}{3}}$, in which A is the total number of particles in the nucleus. Iron data from I is also included in this curve. For comparison, the inelastic cross section given by Phillips[3] is plotted in the same figure. It is somewhat unexpected that the gamma-ray cross section can be so simply represented. It is presumed that in the case of lead $(n,2n)$ reactions reduce the energy available for gamma-ray production so that the cross section falls below the value expected from extrapolating the curve. Both carbon and oxygen, on the other hand, have gamma-ray production cross sections below the inelastic cross section. Here it is possible that charged particle emission will occur and reduce the energy available for gamma-ray production.

The authors wish to thank Dr. E. H. Krause for his active interest and support, and express their appreciation to Messrs. A. P. Flanick and B. A. Allison for aid in performing the experiments.

[3] D. D. Phillips *et al.*, Phys. Rev. **88**, 600 (1952).

The Energy Levels of Odd-Odd Nuclei*

A. DE-SHALIT
Laboratory for Nuclear Science and Engineering, Massachusetts Institute of Technology, Cambridge, Massachusetts
(Received May 15, 1953)

A derivation of a closed formula for the energy levels of odd-odd nuclei is described, and the plausibility of the Nordheim rule is discussed.

INTRODUCTION

ODD-EVEN nuclei probably constitute the simplest group of nuclei with which the ideas of the shell model can be checked. The reason for this is that the energies involved in exciting the even-even core are believed to be bigger than the separation between adjacent single-particle levels, so that it might be a good approximation to assume that the core remains in its lowest state of total angular momentum zero for the ground states of odd-even nuclei, as well as for their first few excited states.

There is some hope that the situation in odd-odd nuclei is not much more complex than in the odd-even ones. The interaction between a proton and a neutron in nonequivalent orbits is expected to be considerably smaller than the one between two equivalent particles, and may, therefore, be of the order of the separation between single-particle levels or even smaller. Accepting the current interpretation of the odd-even level structure, one is tempted to assume that a state of an odd-odd nucleus is characterized by the angular momenta and parities of the separate proton and neutron groups in addition, of course, to the total angular momentum and parity. One also naturally assigns to the proton and neutron groups those spins and parities as are observed in close-lying odd-even nuclei.

Under these assumptions it was found by Nordheim[1] that the following empirical rules apply to the spin J of the ground states of odd-odd nuclei:

$$J=|j_p-j_n| \text{ if } l_p+j_p+l_n+j_n \text{ is even,}$$
$$|j_p-j_p|<J\lesssim j_p+j_n \text{ if } l_p+j_p+l_n+j_n \text{ is odd,}$$

where $(-1)^l$ and j are, respectively, the parity and spin of the proton and neutron groups (indices p and n).

The present work is an attempt to explain Nordheim's rule by adopting the single-particle model for each of the "subgroups" of neutrons and protons, and assuming further that the interaction between the odd proton and the odd neutron, which is considered as a perturbation on the central field in which they move, is given by the expression:

$$V=[a+b\boldsymbol{\sigma}_n\cdot\boldsymbol{\sigma}_p]\delta(\mathbf{r}_n-\mathbf{r}_p).$$

That a perturbation which depends on the relative coordinates only will probably not yield Nordheim's rule is evident from Racah's results on the energy levels of two nucleons in the jj coupling.[2] It is clear that Nordheim's rule would result for a potential of the type $\boldsymbol{\sigma}_n\cdot\boldsymbol{\sigma}_pV(|\mathbf{r}_n-\mathbf{r}_p|)$ without too severe limitations on $V(x)$. It is, however, still interesting to see how much spin dependent force we should introduce, and whether the different character of the two rules, namely the definite answer of one of them and the rather vague answer of the other, can be understood.

NOTATION

We shall find it very convenient to use a notation introduced by Wigner[3] which exhibits most clearly the symmetry properties of the different coefficients involved in the addition of angular momenta. For convenience we also reproduce here, without proof, some of the relations between these coefficients.[4]

The vector-addition coefficient is denoted by

$$\begin{pmatrix} j_1 & j_2 & j_3 \\ \mu_1 & \mu_2 & \mu_3 \end{pmatrix}. \tag{1}$$

It is related to the usual Clebsch-Gordan coefficient[5] by the relation:

$$\begin{pmatrix} j_1 & j_2 & j_3 \\ \mu_1 & \mu_2 & \mu_3 \end{pmatrix}=\frac{(-1)^{j_2-j_1+\mu_3}}{(2j_3+1)^{\frac{1}{2}}}(j_1j_2j_3-\mu_3|\,j_1\mu_1j_2\mu_2). \tag{2}$$

To prevent confusion we shall call this coefficient a Wigner coefficient. A Wigner coefficient vanishes unless $\mathbf{j}_1+\mathbf{j}_2+\mathbf{j}_3=0$. (This equation should be understood as meaning that the three numbers j_1, j_2, and j_3 satisfy the triangular inequalities, and that in addition $\mu_1+\mu_2+\mu_3=0$.)

The symmetry properties of the Wigner coefficients are given by:

$$\begin{pmatrix} j_1 & j_2 & j_3 \\ \mu_1 & \mu_2 & \mu_3 \end{pmatrix}=\epsilon\begin{pmatrix} j_k & j_l & j_m \\ \mu_k & \mu_l & \mu_m \end{pmatrix}, \tag{3}$$

* This work was assisted by the joint program of the U. S. Office of Naval Research and the U. S. Atomic Energy Commission.

[1] L. W. Nordheim, Phys. Rev. **78**, 294 (1950).

[2] G. Racah, Phys. Rev. **62**, 438 (1942).

[3] E. P. Wigner, "On the Matrices which Reduce the Kronecker Products of Representations of Simply-Reducible Groups" (unpublished). I am indebted to Professor Wigner for making a copy of his manuscript available to me.

[4] See also: Biedenharn, Blatt, and Rose, Revs. Modern Phys. **24**, 249 (1952).

[5] E. U. Condon and G. H. Shortley, *Theory of Atomic Spectra* (Cambridge University Press, Cambridge, 1951).

where ϵ is $+1$ or $(-1)^{j_1+j_2+j_3}$ according to whether (k, l, m) is an even or odd permutation of $(1, 2, 3)$. Also:

$$\begin{pmatrix} j_1 & j_2 & j_3 \\ -\mu_1 & -\mu_2 & -\mu_3 \end{pmatrix} = (-1)^{j_1+j_2+j_3}\begin{pmatrix} j_1 & j_2 & j_3 \\ \mu_1 & \mu_2 & \mu_3 \end{pmatrix}. \quad (4)$$

The orthogonality relations take the forms:

$$\sum_{j_3}(2j_3+1)\begin{pmatrix} j_1 & j_2 & j_3 \\ \mu_1 & \mu_2 & \mu_3 \end{pmatrix}\begin{pmatrix} j_1 & j_2 & j_3 \\ \mu_1' & \mu_2' & \mu_3 \end{pmatrix} = \delta(\mu_1, \mu_1')\delta(\mu_2, \mu_2'), \quad (5a)$$

$$(2j_3+1)\begin{pmatrix} j_1 & j_2 & j_3 \\ \mu_1 & \mu_2 & \mu_3 \end{pmatrix}\begin{pmatrix} j_1 & j_2 & j_3' \\ \mu_1 & \mu_2 & \mu_3' \end{pmatrix} = \delta(\mu_3, \mu_3')\delta(j_3, j_3'), \quad (5b)$$

where the summation convention is applied to double Greek indices.

The Racah coefficients will be denoted by

$$\begin{Bmatrix} j_1 & j_2 & j_3 \\ l_1 & l_2 & l_3 \end{Bmatrix}. \quad (6)$$

They are related to Racah's W^2 by the relation

$$\begin{Bmatrix} j_1 & j_2 & j_3 \\ l_1 & l_2 & l_3 \end{Bmatrix} = (-1)^{j_1+l_1+j_2+l_2}\cdot W(j_1 j_2 l_2 l_1; j_3 l_3). \quad (7)$$

A Racah coefficient vanishes unless:

$$\mathbf{j}_1+\mathbf{j}_2+\mathbf{j}_3=0, \quad \mathbf{l}_1-\mathbf{l}_2+\mathbf{j}_3=0, \quad \mathbf{j}_1+\mathbf{l}_2-\mathbf{l}_3=0, \quad -\mathbf{l}_1+\mathbf{j}_2+\mathbf{l}_3=0.$$

The symmetry properties of the Racah coefficients are

$$\begin{Bmatrix} j_1 & j_2 & j_3 \\ l_1 & l_2 & l_3 \end{Bmatrix} = \begin{Bmatrix} j_k & j_l & j_m \\ l_k & l_l & l_m \end{Bmatrix} = \begin{Bmatrix} l_k & l_l & j_m \\ j_k & j_l & l_m \end{Bmatrix}, \quad (8)$$

where $(k\,l\,m)$ is any permutation of $(1, 2, 3)$. The orthogonality relation for the Racah coefficients is

$$\sum_{j_3}(2j_3+1)(2l_3+1)\begin{Bmatrix} j_1 & j_2 & j_3 \\ l_1 & l_2 & l_3 \end{Bmatrix}\begin{Bmatrix} j_1 & j_2 & j_3 \\ l_1 & l_2 & l_3' \end{Bmatrix} = \delta(l_3, l_3'). \quad (9)$$

In addition they satisfy the following relations:

$$\sum_{l_3}(-1)^{j_3+j_3'+l_3}(2l_3+1) \times\begin{Bmatrix} j_1 & j_2 & j_3 \\ l_1 & l_2 & l_3 \end{Bmatrix}\begin{Bmatrix} j_1 & l_1 & j_3' \\ j_2 & l_2 & l_3 \end{Bmatrix} = \begin{Bmatrix} j_1 & j_2 & j_3 \\ l_2 & l_1 & j_3' \end{Bmatrix}, \quad (10a)$$

$$\sum_k(-1)^{j_1+j_2+j_3+l_1+l_2+l_3+k_1+k_2+k_3+k}(2k+1) \times\begin{Bmatrix} j_1 & k & l_1 \\ l_2 & k_3 & j_2 \end{Bmatrix}\begin{Bmatrix} j_2 & k & l_2 \\ l_3 & k_1 & j_3 \end{Bmatrix}\begin{Bmatrix} j_3 & k & l_3 \\ l_1 & k_2 & j_1 \end{Bmatrix} = \begin{Bmatrix} j_1 & k_2 & j_3 \\ k_1 & j_2 & k_3 \end{Bmatrix}\begin{Bmatrix} l_1 & k_2 & l_3 \\ k_1 & l_2 & k_3 \end{Bmatrix}, \quad (10b)$$

$$\begin{Bmatrix} j_1 & j_2 & j_3 \\ 0 & l_2 & l_3 \end{Bmatrix} = (-1)^{j_1+j_2+j_3}[(2j_2+1)(2j_3+1)]^{-\frac{1}{2}} \times\delta(l_2, j_3)\delta(l_3, j_2). \quad (11)$$

The following relations are satisfied by combinations of Racah and Wigner coefficients:

$$\begin{pmatrix} j_1 & j_2 & j_3 \\ \mu_1 & \mu_2 & \mu_3 \end{pmatrix}\begin{pmatrix} l_1 & l_2 & j_3 \\ \lambda_1 & \lambda_2 & -\mu_3 \end{pmatrix} = \sum_{l_3}(-1)^{j_3+l_3+\mu_1+\lambda_1} \times(2l_3+1)\begin{Bmatrix} j_1 & j_2 & j_3 \\ l_1 & l_2 & l_3 \end{Bmatrix}\begin{pmatrix} l_1 & j_2 & l_3 \\ \lambda_1 & \mu_2 & \lambda_3 \end{pmatrix}\begin{pmatrix} j_1 & l_2 & l_3 \\ \mu_1 & \lambda_2 & -\lambda_3 \end{pmatrix}, \quad (12)$$

$$\begin{Bmatrix} j_1 & j_2 & j_3 \\ l_1 & l_2 & l_3 \end{Bmatrix}\begin{pmatrix} j_1 & j_2 & j_3 \\ \mu_1 & \mu_2 & \mu_3 \end{pmatrix} = (-1)^{l_1+l_2+l_3+\lambda_1+\lambda_2+\lambda_3} \times\begin{pmatrix} j_1 & l_2 & l_3 \\ \mu_1 & \lambda_2 & -\lambda_3 \end{pmatrix}\begin{pmatrix} l_1 & j_2 & l_3 \\ -\lambda_1 & \mu_2 & \lambda_3 \end{pmatrix}\begin{pmatrix} l_1 & l_2 & j_3 \\ \lambda_1 & -\lambda_2 & \mu_3 \end{pmatrix}, \quad (13)$$

$$\begin{pmatrix} j_{11} & j_{12} & j_{13} \\ \lambda_{11} & \lambda_{12} & \lambda_{13} \end{pmatrix}\begin{pmatrix} j_{21} & j_{22} & j_{23} \\ \lambda_{21} & \lambda_{22} & \lambda_{23} \end{pmatrix}\begin{pmatrix} j_{31} & j_{32} & j_{33} \\ \lambda_{31} & \lambda_{32} & \lambda_{33} \end{pmatrix} \times\begin{pmatrix} j_{11} & j_{21} & j_{31} \\ \lambda_{11} & \lambda_{21} & \lambda_{31} \end{pmatrix}\begin{pmatrix} j_{12} & j_{22} & j_{32} \\ \lambda_{12} & \lambda_{22} & \lambda_{32} \end{pmatrix}\begin{pmatrix} j_{13} & j_{23} & j_{33} \\ \lambda_{13} & \lambda_{23} & \lambda_{33} \end{pmatrix} = \sum_j(-1)^{2j}(2j+1)\begin{Bmatrix} j_{11} & j_{12} & j_{13} \\ j_{23} & j_{33} & j \end{Bmatrix}\begin{Bmatrix} j_{21} & j_{22} & j_{23} \\ j_{12} & j & j_{32} \end{Bmatrix} \times\begin{Bmatrix} j_{31} & j_{32} & j_{33} \\ j & j_{11} & j_{21} \end{Bmatrix} = \begin{Bmatrix} j_{11} & j_{12} & j_{13} \\ j_{21} & j_{22} & j_{23} \\ j_{31} & j_{32} & j_{33} \end{Bmatrix}. \quad (14)$$

(14) defines Wigner's nine-j symbol, which is also called an X coefficient (Racah and Fano) or a Schwinger coefficient.[6] It is easy to see from the symmetry properties of the Wigner coefficients that the interchange of any two rows or two columns in a Schwinger coefficient multiples it by the factor

$$(-1)^{j_{11}+j_{12}+j_{13}+j_{21}+j_{22}+j_{23}+j_{31}+j_{32}+j_{33}}.$$

OUTLINE OF THE COMPUTATION

We shall assume that in the zeroth-order approximation the particles are moving in a central field with no interaction between them. The central field, ac-

[6] J. Schwinger, Nuclear Development Associates Report NYO-3071 (unpublished).

cording to this approach, takes care of the major part of the mutual interaction between the nucleons, the remaining part of the interaction being treated as a small perturbation. Limiting our considerations to two particles in the jj-coupling scheme (l_1j_1) and (l_2j_2), the degenerate states of the configuration j_1j_2 will be split by the perturbation, and the first-order correction to the energy of a state with a total angular momentum J will be given by

$$E(j_1j_2, J)=\int\psi^*(j_1j_2JM)V\psi(j_1j_2JM)d\tau. \quad (15)$$

We shall take as our wave function for the state (j_1j_2, JM):

$$\Psi(j_1j_2JM)=(-1)^{j_1-j_2+M}(2J+1)^{\frac{1}{2}} \times\begin{pmatrix} j_1 & j_2 & J \\ \mu_1 & \mu_2 & -M\end{pmatrix}\psi_1(j_1\mu_1)\psi_2(j_2\mu_2). \quad (16)$$

For particles in equivalent states $(j_1=j_2)$ this gives antisymmetric states for even J and symmetric ones for odd J, etc. No τ dependence is assumed, so that this wave function is good only for two distinct particles such as a proton and a neutron, provided they are not considered as two different states of the same entity, i.e., provided the Pauli principle should not be applied to them. This assumption is probably good for the heavier odd-odd nuclei.

Introducing the notation

$$\sigma_0{}^{(0)}=1, \quad \sigma_{-1}{}^{(1)}=-\tfrac{1}{2}(\sigma_x-i\sigma_y),$$
$$\sigma_0{}^{(1)}=\sigma_z, \quad \sigma_{+1}{}^{(1)}=\tfrac{1}{2}(\sigma_x+i\sigma_y),$$

and expanding $V(|\mathbf{r}_1-\mathbf{r}_2|)$ in Legendre polynomials of the angle ω between $\mathbf{r}_1$ and $\mathbf{r}_2$:

$$V(|\mathbf{r}_1-\mathbf{r}_2|)=\sum v_k(|\mathbf{r}_1|, |\mathbf{r}_2|)P_k(\cos\omega), \quad (17)$$

we find that the first-order correction to the energy of the state (j_1j_2, JM) due to a perturbation $\boldsymbol{\sigma}_1{}^{(n)}\cdot\boldsymbol{\sigma}_2{}^{(n)}V(|\mathbf{r}_1-\mathbf{r}_2|)$ can be written in the form

$$E(j_1j_2J)=\sum_k f_{nk}(j_1j_2J)F_k(n_1l_1n_2l_2), \quad (18)$$

where

$$f_{nk}=(2k+1)(j_1j_2JM|\boldsymbol{\sigma}_1{}^{(n)}\cdot\boldsymbol{\sigma}_2{}^{(n)}P_k(\cos\omega)|j_1j_2JM), \quad (19)$$

and

$$F_k=1/(2k+1)\int R_1{}^2(n_1l_1)R_2{}^2(n_2l_2)v_k(r_1, r_2)dr_1dr_2, \quad (20)$$

$R(nl)/r$ being the radial part of the single-particle wave function $\psi(nljm)$.

The integrals f_{nk} can be evaluated exactly since they do not involve any unknown parameters of the central field. This is most easily done by the tensor-operator algebra developed by Racah,[2] and in fact the explicit expression for f_{0k} was given by Racah as early as 1942. We shall here follow a slightly different way which is more convenient for the summations involved in the special case of delta forces.[7]

Following Racah we decompose $P_k(\cos\omega)$ by the addition theorem for spherical harmonics,

$$P_k(\cos\omega)=\sum_\kappa(-1)^\kappa C_\kappa{}^{(k)}(1)C_{-\kappa}{}^{(k)}(2),$$
$$C_\kappa{}^{(k)}(i)=[4\pi/(2k+1)]^{\frac{1}{2}}Y_\kappa{}^{(k)}(\theta_i\varphi_i),$$

and get for (19) the expression:

$$f_{nk}=\sum_{\kappa,\gamma}(2k+1)(j_1j_2JM|\sigma_\gamma{}^{(n)}(1)C_\kappa{}^{(k)}(1) \cdot\sigma_{-\gamma}{}^{(n)}(2)C_{-\kappa}{}^{(k)}(2)|j_1j_2JM)\cdot(-1)^{\gamma+\kappa}. \quad (21)$$

Since both $\sigma^{(n)}$ and $C^{(k)}$ are reduced tensor operators, their product can be reduced into a sum of tensor operators of orders $r(|k-n|\leqslant r\leqslant k+n)$ which are given by

$$T_\rho{}^{(r)}=(-1)^{k+n+\rho}(2r+1)^{\frac{1}{2}}\begin{pmatrix} n & k & r \\ \gamma & \kappa & -\rho\end{pmatrix}\sigma_\gamma{}^{(n)}C_\kappa{}^{(k)}. \quad (22)$$

If we use (5), we obtain

$$f_{nk}=(-1)^{n+k}(2k+1) \times(j_1j_2JM|\textstyle\sum_r(-1)^r\mathbf{T}_1{}^{(r)}\cdot\mathbf{T}_2{}^{(r)}|j_1j_2JM), \quad (23)$$

where $\mathbf{A}\cdot\mathbf{B}$ stands for the scalar product of the tensor operators $\mathbf{A}$ and $\mathbf{B}$.

The matrix elements for the scalar product of tensor operators were given by Racah,[2] and in the present notation one obtains

$$f_{nk}=(-1)^{j_1+j_2+J}\sum_r(-1)^{n+k+r}(2k+1)\begin{Bmatrix} j_1 & j_2 & J \\ j_2 & j_1 & r\end{Bmatrix} \times(j_1\|T_1{}^{(r)}\|j_1)(j_2\|T_2{}^{(r)}\|j_2). \quad (24)$$

By definition,

$$(-1)^{j-\mu}(slj\|T^{(r)}\|s'l'j')\begin{pmatrix} j & r & j' \\ -\mu & \rho & \mu'\end{pmatrix}$$
$$=(slj\mu|T_\rho{}^{(r)}|s'l'j'\mu')=(-1)^{k+n+\rho}(2r+1)^{\frac{1}{2}} \times\begin{pmatrix} n & k & r \\ \gamma & \kappa & -\rho\end{pmatrix}(slj\mu|\sigma_\gamma{}^{(n)}C_\kappa{}^{(k)}|s'l'j'\mu'). \quad (25)$$

If we transform the last matrix element from the $(slj\mu)$ scheme to the $(s\mu_s l\mu_l)$ scheme, and remember that both $\boldsymbol{\sigma}^{(n)}$ and $\mathbf{C}^{(k)}$ are tensor operators with respect to $\mathbf{s}$ and $\mathbf{l}$, respectively, we find that

$$(slj\|T^{(r)}\|s'l'j')=[(2r+1)(2j+1)(2j'+1)]^{\frac{1}{2}} \times(s\|\sigma^{(n)}\|s')(l\|C^{(k)}\|l')\begin{Bmatrix} n & k & r \\ s & l & j \\ s' & l' & j'\end{Bmatrix}. \quad (26)$$

We may note here that due to the symmetry properties of the Schwinger coefficient the diagonal matrix elements of $T^{(r)}$ vanish unless $k+n+r$ is even.

[7] Compare also similar calculations by: M. H. L. Pryce, Proc. Phys. Soc. (London) **A65**, 773 (1952); D. Kurath, Phys. Rev. **87**, 218 (1952); B. Feld and L. Marks (private communication); I. Talmi, Phys. Rev. **90**, 1001 (1953).

From (26) we obtain for (19) the expression

$$f_{nk}=(-1)^{j_1+j_2+J}(2j_1+1)(2j_2+1)(2k+1)\times(s_1\|\sigma^{(n)}\|s_1)(s_2\|\sigma^{(n)}\|s_2)(l_1\|C^{(k)}\|l_1)\times(l_2\|C^{(k)}\|l_2)\sum_r(-1)^{k+n+r}\times\begin{Bmatrix}j_1 & j_2 & J\\ j_2 & j_1 & r\end{Bmatrix}\begin{Bmatrix}n & k & r\\ s_1 & l_1 & j_1\end{Bmatrix}\begin{Bmatrix}n & k & r\\ s_2 & l_2 & j_2\end{Bmatrix}. \quad (27)$$

The sum over r can be performed yielding a relatively simple expression. Since, however, we are interested in the values of the energies for delta interaction, we shall find it easier to evaluate the sum over k first. We also notice that n can assume only two values (since $s=\frac{1}{2}$): 0 and 1; for $n=0$ the summation over k and r reduces to a very simple expression. It is therefore very convenient to sum over n too and obtain the value of $E(j_1j_2, J)$ for $n=1$ by subtracting the contribution of $n=0$.

To proceed with the calculation we note that for

$$V(|\mathbf{r}_1-\mathbf{r}_2|)=\delta(r_1-r_2)\delta(\cos\omega-1)r_1r_2,\qquad v_k(|\mathbf{r}_1|,|\mathbf{r}_2|)=(2k+1)r_1r_2, \quad (28)$$

so that $F_k=F_0$ for every k. $(l\|C^{(k)}\|l)$ was computed by Racah:[2]

$$(l\|C^{(k)}\|l)=(-1)^l(2l+1)\begin{pmatrix}l & l & k\\ 0 & 0 & 0\end{pmatrix}.$$

It is also easy to see that $(s\|\sigma^{(n)}\|s)=[2(2n+1)]^{\frac{1}{2}}$.

If we combine all these results we obtain (expressing E in units of F_0)

$$\tfrac{1}{2}\sum_{n=0,1}E_n(j_1j_2J)=\sum_{n,k,r}(-1)^{j_1+j_2+J+n+2k+r}(2j_1+1)(2j_2+1)\times(2l_1+1)(2l_2+1)(2n+1)(2k+1)(2r+1)\times\begin{pmatrix}l_1 & l_1 & k\\ 0 & 0 & 0\end{pmatrix}\begin{pmatrix}l_2 & l_2 & k\\ 0 & 0 & 0\end{pmatrix}\begin{Bmatrix}j_1 & j_2 & J\\ j_2 & j_1 & r\end{Bmatrix}\times\begin{Bmatrix}n & k & r\\ s_1 & l_1 & j_1\end{Bmatrix}\begin{Bmatrix}n & k & r\\ s_2 & l_2 & j_2\end{Bmatrix}=\sum_{nrk_1k_2}(-1)^{j_1+j_2+J+n+r}\times(2j_1+1)(2j_2+1)(2l_1+1)(2l_2+1)(2n+1)\times(2r+1)\cdot\begin{Bmatrix}j_1 & j_2 & J\\ j_2 & j_1 & r\end{Bmatrix}(-1)^{k_1}(2k_1+1)\times\begin{pmatrix}n & k_1 & r\\ \gamma & 0 & \rho\end{pmatrix}\begin{pmatrix}l_1 & l_1 & k_1\\ 0 & 0 & 0\end{pmatrix}\begin{Bmatrix}n & k_1 & r\\ s_1 & l_1 & j_1\\ s_1 & l_1 & j_1\end{Bmatrix}(-1)^{k_2}\times(2k_2+1)\begin{pmatrix}n & k_2 & r\\ \gamma & 0 & \rho\end{pmatrix}\begin{pmatrix}l_2 & l_2 & k_2\\ 0 & 0 & 0\end{pmatrix}\begin{Bmatrix}n & k_2 & r\\ s_2 & l_2 & j_2\\ s_2 & l_2 & j_2\end{Bmatrix}. \quad (29)$$

The sums over k_1 and k_2 can be carried out separately by using the following relation which is easy to verify:

$$\sum_r(2r+1)\begin{pmatrix}n & k & r\\ \gamma & \kappa & \rho\end{pmatrix}\begin{pmatrix}r & j & j'\\ \rho & \iota & \iota'\end{pmatrix}\begin{Bmatrix}n & k & r\\ s & l & j\\ s' & l' & j'\end{Bmatrix}=\begin{pmatrix}n & s & s'\\ \gamma & \sigma & \sigma'\end{pmatrix}\begin{pmatrix}k & l & l'\\ \kappa & \lambda & \lambda'\end{pmatrix}\begin{pmatrix}s & l & j\\ \sigma & \lambda & \iota\end{pmatrix}\begin{pmatrix}s' & l' & j'\\ \sigma' & \lambda' & \iota'\end{pmatrix}. \quad (30)$$

The sum over n can then be carried out by applying directly the orthogonality relations of the Wigner coefficients, and the sum over r results immediately by the use of the relations involving the Racah coefficients.

The final expression is

$$\tfrac{1}{2}\sum_n E_n(j_1j_2J)=(-1)^{l_1+l_2+j+1}(2j_1+1)(2j_2+1)(2l_1+1)(2l_2+1)\times\begin{pmatrix}j_1 & j_2 & J\\ \alpha_1 & -\alpha_2 & \alpha_2-\alpha_1\end{pmatrix}\begin{pmatrix}j_1 & j_2 & J\\ \alpha_2 & -\alpha_1 & \alpha_1-\alpha_2\end{pmatrix}\times\begin{pmatrix}s_1 & l_1 & j_1\\ \alpha_1 & 0 & -\alpha_1\end{pmatrix}\begin{pmatrix}s_1 & l_1 & j_1\\ \alpha_2 & 0 & -\alpha_2\end{pmatrix}\times\begin{pmatrix}s_2 & l_2 & j_2\\ \alpha_1 & 0 & -\alpha_1\end{pmatrix}\begin{pmatrix}s_2 & l_2 & j_2\\ \alpha_2 & 0 & -\alpha_2\end{pmatrix}. \quad (31)$$

Since both α_1 and α_2 can have only the values $\pm\frac{1}{2}$ and since

$$\begin{pmatrix}\frac{1}{2} & l & j\\ \frac{1}{2} & 0 & -\frac{1}{2}\end{pmatrix}^2=\frac{1}{2(2l+1)},$$

we get

$$\tfrac{1}{2}\sum E_n(j_1j_2J)=\tfrac{1}{2}(2j_1+1)(2j_2+1)\times\left\{\begin{pmatrix}j_1 & j_2 & J\\ \frac{1}{2} & \frac{1}{2} & -1\end{pmatrix}^2-(-1)^{l_1+l_2+J}\begin{pmatrix}j_1 & j_2 & J\\ \frac{1}{2} & -\frac{1}{2} & 0\end{pmatrix}^2\right\}. \quad (32)$$

This expression can be further simplified by means of the relation

$$\begin{pmatrix}j_1 & j_2 & J\\ \frac{1}{2} & \frac{1}{2} & -1\end{pmatrix}^2=\frac{1}{4J(J+1)}\{(2j_1+1)+(-1)^{j_1+j_2+J}\times(2j_2+1)\}\begin{pmatrix}j_1 & j_2 & J\\ \frac{1}{2} & -\frac{1}{2} & 0\end{pmatrix}^2. \quad (33)$$

Noting that

$$\begin{Bmatrix}0 & k & r\\ s & l & j\\ s & l & j\end{Bmatrix}=(-1)^{k+s+l+j}[2(2k+1)]^{-1}\cdot\begin{vmatrix}k & j & j\\ s & l & l\end{vmatrix}\delta(k,r), \quad (34)$$

we get, for $n=0$,

$$E_0(j_1j_2J)=\tfrac{1}{2}(2j_1+1)(2j_2+1)\begin{pmatrix} j_1 & j_2 & J \\ \tfrac{1}{2} & -\tfrac{1}{2} & 0\end{pmatrix}^2 \left[1+\frac{[(2j_1+1)+(-1)^{j_1+j_2+J}(2j_2+1)]^2}{4J(J+1)}\right], \quad (35a)$$

and therefore

$$E_1(j_1j_2J)=\tfrac{1}{2}(2j_1+1)(2j_2+1)\begin{pmatrix} j_1 & j_2 & J \\ \tfrac{1}{2} & -\tfrac{1}{2} & 0\end{pmatrix}^2 \times\left[\frac{[(2j_1+1)+(-1)^{j_1+j_2+J}(2j_2+1)]^2}{4J(J+1)} -(1+2(-1)^{l_1+l_2+J})\right]. \quad (35b)$$

The last two formulas obtain an especially simple form when $j_1=j_2$ and $l_i=l_2$:

$$E_0(j^2J)=\tfrac{1}{2}(2j+1)^2\begin{pmatrix} j & j & J \\ \tfrac{1}{2} & -\tfrac{1}{2} & 0\end{pmatrix}^2 \times\begin{cases}1 & \text{for even } J,\\ [1+(2j+1)^2/J(J+1)] & \text{for odd } J;\end{cases} \quad (36a)$$

$$E_1(j^2J)=\tfrac{1}{2}(2j+1)^2\begin{pmatrix} j & j & J \\ \tfrac{1}{2} & -\tfrac{1}{2} & 0\end{pmatrix}^2 \times\begin{cases}-3 & \text{for even } J,\\ [1+(2j+1)^2/J(J+1)] & \text{for odd } J.\end{cases} \quad (36b)$$

For equivalent nucleons only even-J states are allowed (because of the Pauli principle) and one sees that a potential of the type $[3+\boldsymbol{\sigma}_1\cdot\boldsymbol{\sigma}_2]\delta(\mathbf{r}_1-\mathbf{r}_2)$ yields no interaction in these states corresponding to the fact that $3+\boldsymbol{\sigma}_1\cdot\boldsymbol{\sigma}_2$ vanishes for states symmetric in the coordinates (and therefore antisymmetric in the spins); whereas, $\delta(\mathbf{r}_1-\mathbf{r}_2)$ vanishes for states antisymmetric in the coordinates. For similar reasons, one can see that for these states the Wigner force and the Majorana force $[\frac{1}{4}(1-\boldsymbol{\sigma}_1\cdot\boldsymbol{\sigma}_2)$ for particles of the same charge$]$ give the same results for the energy levels in the delta limit.

NORDHEIM'S RULE

On the basis of the analysis of β transitions in even-A nuclei, Nordheim has deduced the empirical rule for the spins of the ground states of odd-odd nuclei.[1] When the states of the two odd nucleons are l_1j_1 and l_2j_2, this rule can be stated with the help of the Nordheim number $N=l_1+j_1+l_2+j_2$ in the following way:

For even N, $J=|j_1-j_2|$; for odd N, $J>|j_1-j_2|$ and is usually of the order of j_1+j_2.

TABLE I. $|(j_1\tfrac{1}{2}\ j_2-\tfrac{1}{2}|j_1j_2j0)|^2$. The Clebsch-Gordan coefficient is minus or plus the square root of the entry in the table according to whether this entry is, or is not, preceded by an asterisk.

	$j_2\backslash j_1$	1/2	3/2	5/2	7/2	9/2
$J=0$	1/2	1/2	0	0	0	0
	3/2	0	*1/4	0	0	0
	5/2	0	0	1/6	0	0
	7/2	0	0	0	*1/8	0
	9/2	0	0	0	0	1/10
$J=1$	1/2	1/2	1/2	0	0	0
	3/2	1/2	*1/20	*3/10	0	0
	5/2	0	*3/10	1/70	3/14	0
	7/2	0	0	3/14	*1/168	*1/6
	9/2	0	0	0	*1/6	1/330
$J=2$	1/2	0	1/2	1/2	0	0
	3/2	1/2	1/4	*1/14	*9/28	0
	5/2	1/2	*1/14	*4/21	1/42	5/21
	7/2	0	*9/28	1/42	25/168	*5/462
	9/2	0	0	5/21	*5/462	*4/33
$J=3$	1/2	0	0	1/2	1/2	0
	3/2	0	9/20	1/5	*1/12	*1/3
	5/2	1/2	1/5	*4/45	*1/6	1/33
	7/2	1/2	*1/12	*1/6	3/88	3/22
	9/2	0	*1/3	1/33	3/22	12/385
$J=4$	1/2	0	0	0	1/2	1/2
	3/2	0	0	3/7	5/28	*1/11
	5/2	0	3/7	1/7	*15/154	*12/77
	7/2	1/2	5/28	*15/154	*81/616	81/2002
	9/2	1/2	*1/11	*12/77	81/2002	81/385
$J=5$	1/2	0	0	0	0	1/2
	3/2	0	0	0	5/12	1/6
	5/2	0	0	25/63	5/42	*4/39
	7/2	0	5/12	5/42	*75/728	*3/26
	9/2	1/2	1/6	*4/39	*3/26	3/65
$J=6$	1/2	0	0	0	0	0
	3/2	0	0	0	0	9/22
	5/2	0	0	0	25/66	7/66
	7/2	0	0	25/66	25/264	*7/66
	9/2	0	9/22	7/66	*7/66	*16/165
$J=7$	1/2	0	0	0	0	0
	3/2	0	0	0	0	0
	5/2	0	0	0	0	105/286
	7/2	0	0	0	1225/3432	35/429
	9/2	0	0	105/286	35/429	*784/7293
$J=8$	1/2	0	0	0	0	0
	3/2	0	0	0	0	0
	5/2	0	0	0	0	0
	7/2	0	0	0	0	49/143
	9/2	0	0	0	49/143	49/715
$J=9$	1/2	0	0	0	0	0
	3/2	0	0	0	0	0
	5/2	0	0	0	0	0
	7/2	0	0	0	0	0
	9/2	0	0	0	0	3969/12155

We shall now proceed to investigate our results in order to see whether they offer any way of explaining these regularities. It should be emphasized that we do not know as yet any reason to believe that the delta forces give best description of the interactions between nucleons in a nucleus, although they might represent not too bad an approximation.

For pure Wigner forces one gets a dependence of the energy levels on the j's of the interacting particles only

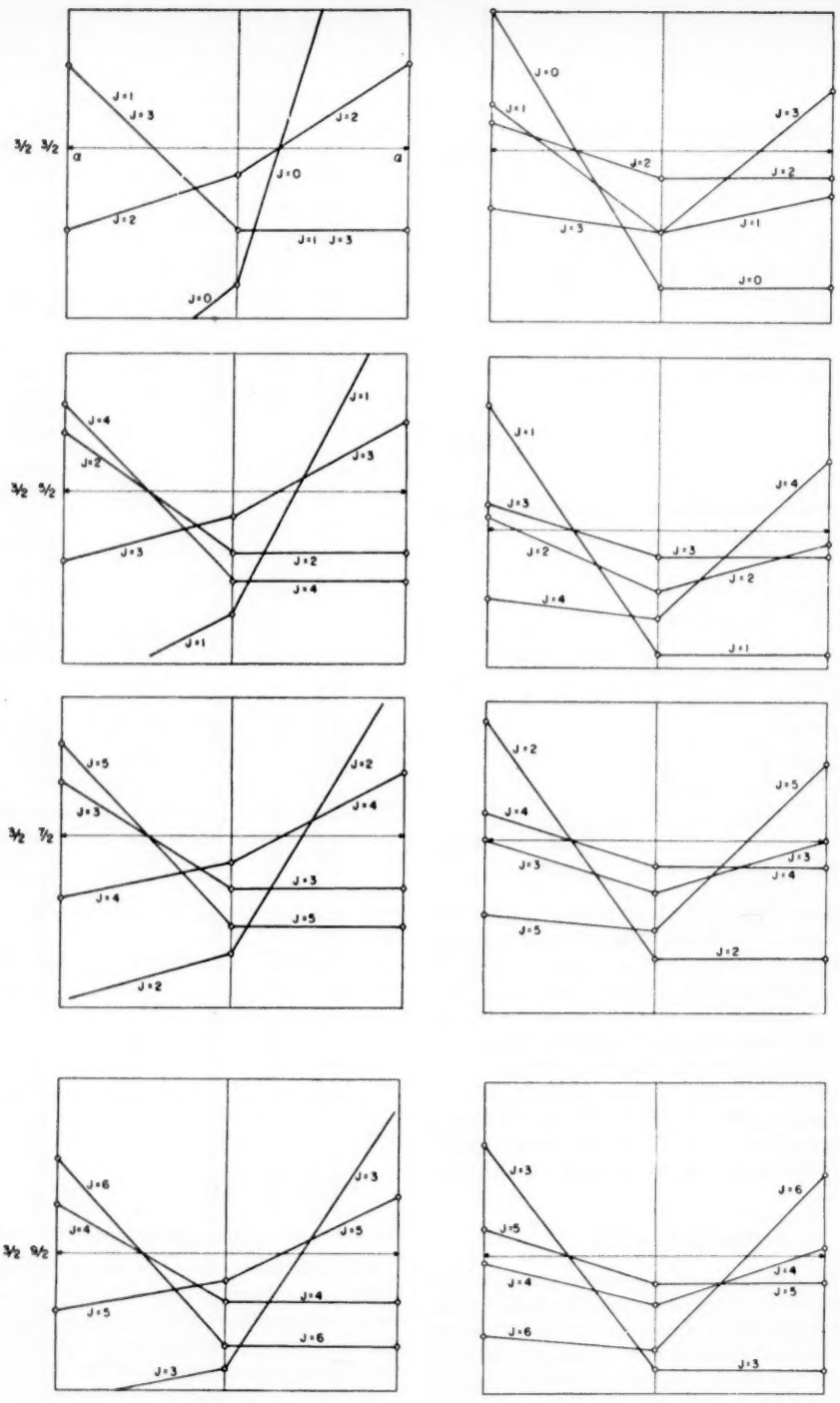

FIG. 1. Energy levels of odd-odd nuclei for a potential $[(1-\alpha)+\epsilon\alpha\sigma_1\cdot\sigma_2]\delta(r_1-r_2)$. Left column—odd Nordheim numbers; right column—even Nordheim numbers. In each figure the right half corresponds to $\epsilon=+1$ and the left half to $\epsilon=-1$. α varies from 0 to 1. The energy scale is arbitrary.

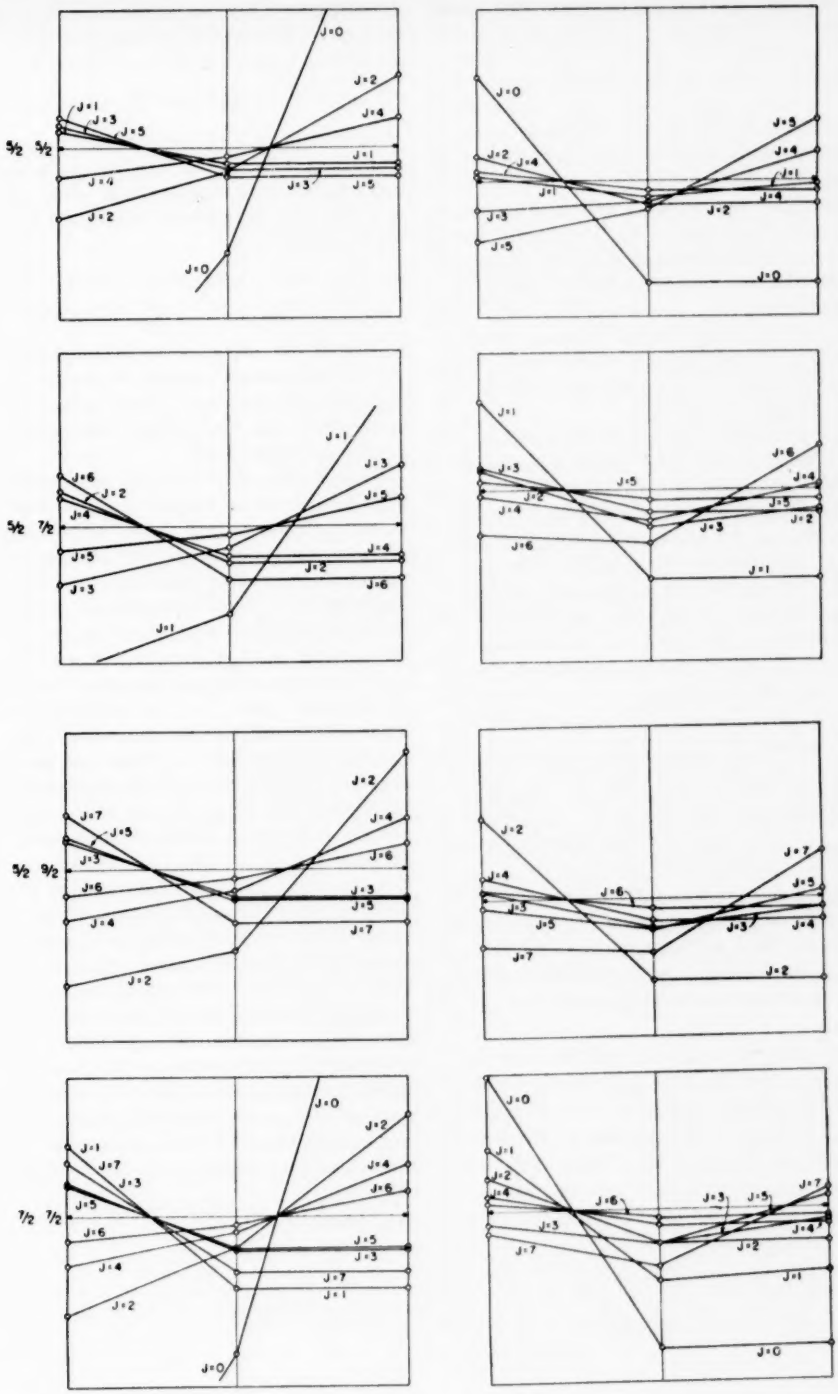

FIG. 1.—*Continued*

(in the jj coupling) and not on their l's. This result is strictly valid for the case of delta interactions, as can be seen from the results of the previous section, but also in other ranges and forms of the potential the dependence on the l's enters only through the usually weak dependence of the F_k on the l's.[2] We, therefore conclude that Nordheim's rule probably cannot be explained on the basis of the Wigner forces alone. A potential which evidently might give results in accordance with Nordheim's rule is $[a+b\boldsymbol{\sigma}_1\cdot\boldsymbol{\sigma}_2]\delta(\mathbf{r}_1-\mathbf{r}_2)$. The energy levels for this potential can be deduced from the results of the previous section. For this purpose we calculated the Clebsch-Gordan coefficients which are involved in the determination of the energy levels. These are given in Table I. In Fig. 1 we have plotted these energy levels for a potential of the form $[(1-\alpha)+\epsilon\alpha\boldsymbol{\sigma}_1\cdot\boldsymbol{\sigma}_2]\delta(\mathbf{r}_1-\mathbf{r}_2)$ with $0\leqslant\alpha\leqslant 1$ and $\epsilon=\pm 1$.

The similarity between the graphs so obtained for different j's is striking, and it is immediately evident that the configurations in question can be divided into two classes according to whether the Nordheim number is odd or even. For $\epsilon=+1$ and starting from $\alpha=0$ (pure Wigner forces) we find that for even N, $J=|j_1-j_2|$ always remains the lowest state even as α increases, and that it is an *isolated* lowest state, i.e., all the other states are clustered at relatively high excitations. For odd N, $J=|j_1-j_2|$ is still the lowest state for $\alpha=0$, but it rises very steeply with α; and even for small values of α, $J=j_1+j_2$ becomes the lowest state. The state $J=j_1+j_2$, however, is no longer isolated as was the state $J=|j_1-j_2|$ for even N, and is relatively close to j_1+j_2-2 and j_1+j_2-4, etc. Thus a weak configuration interaction or a transition to a potential of a finite range could bring one of these close-lying states below $J=j_1+j_2$. We thus see that this simple model can explain Nordheim's rule and its decomposition into "strong" and "weak" rules. It goes a little bit beyond the original formulation of the rule, in as much as it predicts that in the "weak" case the ground state will have an even or odd spin according to whether j_1+j_2 is even or odd.

The spins of very few odd-odd nuclei have been measured directly and the spin assignment for most of them is usually made on the basis of β-decay analysis. This analysis, however, is less reliable in the case of odd-odd nuclei than in the case of odd-even nuclei. Thus, if an odd-odd nucleus with odd neutron in j_n and an odd proton in j_p and total angular momentum J_i undergoes a β decay to the state J_f of the configuration j_p^2 in the daughter nucleus, the matrix element for an allowed transition will be reduced by a factor[5]

$$(2j_n+1)(2J_f+1)|W(j_nJ_ij_pJ_f;\,j_p1)|^2,$$

compared to that of the corresponding single-particle transition. This factor may be quite small and may make an allowed transition look like a first-forbidden one. Also the order of the transition l is determined by the inequalities:

$$|l-1|\leqslant J\leqslant l+1,\quad \pi_i=(-1)^l\pi_f,$$
$$\max(|j_n-j_p|,\,|J_i-J_f|)\leqslant J\leqslant\min(j_n+j_p,\,J_i+J_f);$$

so that if one observes for instance the "unique forbidden" shape one knows only that $\max(|j_n-j_p|,\,|J_i-J_f|)=2$, and one cannot make a definite statement about $|J_i-J_f|$ without some assumption about j_n and j_p, unless $J_f=0$.

Even if one adopts the order of levels for the odd particles from the shell model, an ambiguity arises from an effect similar to that of the pairing energy. It is very probable that the situation in nuclear spectroscopy is such that the energy difference between two adjacent single-particle states (computed for a central field which takes into account most of the mutual interactions of the particles) is small compared to the "extra" interaction between the particles (which is considered as a perturbation upon the central-field approximation). Thus, if the order of levels for the single particles is $j_nj_n'j_n''\cdots j_pj_p'j_p''\cdots$, it does not necessarily mean that the ground state of the configuration (j_nj_p) is lower than that of (j_nj_p') or $(j_n'j_p)$ or even $(j_n'j_p')$, and the assignment of the right configurations for the states of the odd-odd nuclei is not always unique, even if the total spin and parity are known. In principle, the measurements of transition probabilities involving these states could determine their configuration, but so far it has been impossible to get a good enough agreement between calculated and experimental values for transition probabilities even in the "simpler" cases of odd-even nuclei. It seems that the only practical way of obtaining more information concerning the configuration of a certain state in odd-odd nuclei is the measurement of its magnetic moment and eventually its quadrupole moment. This would also enable a check of the refinement proposed here for the Nordheim rule.

[5] Henry Brysk, Phys. Rev. **90**, 365 (1953); A. de-Shalit and M. Goldhaber (unpublished).

The Pairing Effect in Nuclei and Isomerism

ROBERT KATZ
Kansas State College, Manhattan, Kansas
(Received June 5, 1953)

Previous workers have shown from an analysis of the energetics of alpha and beta decay that the pairing energy of protons is greater than that of neutrons. It is here postulated that this effect is responsible for the absence of odd-proton isomers for $50<Z<82$.

THE strong spin-orbit coupling model[1,2] of the nucleus has been remarkably successful in coordinating a number of features of the behavior of odd-A nuclei, with particular regard to the assignment of the spin and parity of both ground and excited states. It has been pointed out by Scharff-Goldhaber[3] that one of the failures of this "shell-structure" theory in its present form has been the relative scarcity of odd-proton isomers for elements with $50<Z<82$, as compared to the relative abundance of odd-neutron isomers for $50<N<82$. The present form of shell structure theory recognizes little difference between protons and neutrons in the availability or population of levels, except perhaps as proposed by Mayer[1] that Coulomb repulsion, tending to concentrate the charge on the outside of the nucleus, would probably put the last odd proton in a state of higher angular momentum than the last odd neutron.

In order to bring the sequence of energy levels obtained from those of a square well by strong spin-orbit coupling into accord with the observed spins of ground states of odd-A nuclei, Mayer[1] found it necessary to assume that "For a given nucleus the pairing energy of the nucleons in the same orbit is *greater* for orbits with larger j." (Note: the italics are mine. R. K.) This assumption implied, for example, that for an odd A nucleus whose odd-nucleon number lay between 50 and 82, the $h_{11/2}$ state would not be occupied as the ground state of the last odd nucleon.

Depending on the magnitude implied by the word *greater*, the $h_{11/2}$ level might not even be found in the excited states of nuclei of odd-nucleon number between 63 and 82, where the pairing energy might be sufficiently large to cause occupancy of all twelve $h_{11/2}$ levels in the shell. Herein appears to be the difference between odd proton and odd neutron nuclei. The abundance of odd neutron isomers lying between $63<N<82$ described by Goldhaber and Hill[4] owe their isomerism to an excited $h_{11/2}$ state which lies within 0.661 Mev of the ground state in the case of Ba^{137}, and considerably closer for most other isomers. If the pairing energy for protons were greater than the pairing energy for neutrons by $\frac{1}{4}$ to $\frac{1}{2}$ Mev in this region, the $h_{11/2}$ state would be populated by $Z=63$. Odd proton isomerism could then be expected only in a region of odd nucleon number where the $h_{11/2}$ level for odd neutron isomers was energetically quite distant from the ground state, as in the case of $_{54}Xe^{135}$ (0.52 Mev) and $_{56}Ba^{137}$ (0.66 Mev). Existing data on odd proton nuclei tend to agree with these observations. The only long-lived odd proton isomer presently known has 79 odd protons ($_{79}Au^{197}$). Recently completed work[5] on $_{63}Eu^{153}$ reveals no excited $h_{11/2}$ state.

By analysis of α and β decay energies, Glueckauf[6] has shown that the pairing energy of protons exceeds that of neutrons in heavy nuclei. The mass defects of isobars of odd mass number when plotted against the neutron excess (N-Z) do not lie on a single smooth parabola but on two parabolas, one for odd Z and one for even Z, separated by about 0.2 Mev. This energy is of the right magnitude to explain the rarity of isomerism in odd proton nuclei.[7]

Kohman[8] has called attention to the relationship between this pairing effect and beta lability, and has offered some possible theoretical explanation of the effect. It is from his paper that the title of the present paper is drawn.

The pairing effect described herein, and the low excitation energy in this region of an even-even core discussed by Scharff-Goldhaber[3] both argue against existence of odd proton isomerism. The extent to which responsibility may be assigned to either effect is presently unknown.

[1] M. G. Mayer, Phys. Rev. **78**, 16, 22 (1950).
[2] Haxel, Jensen, and Suess, Phys. Rev. **75**, 1766 (1949).
[3] G. Scharff-Goldhaber, Phys. Rev. **90**, 587 (1953).
[4] M. Goldhaber and R. D. Hill, Revs. Modern Phys. **24**, 179 (1952).
[5] M. R. Lee and R. Katz (to be published).
[6] E. Glueckauf, Proc. Phys. Soc (London) **61**, 25 (1948).
[7] In this connection see also A. E. S. Green and D. F. Edwards, Phys. Rev. **91**, 46 (1953) for proton and neutron pairing energy differences.
[8] T. P. Kohman, Phys. Rev. **85**, 530 (1952).

Isotope Shift Anomalies and Nuclear Structure

LAWRENCE WILETS,* *Princeton University, Princeton, New Jersey*
DAVID L. HILL,† *Vanderbilt University, Nashville, Tennessee*

AND

KENNETH W. FORD,‡ *Princeton University, Princeton, New Jersey*

(Received June 3, 1953)

When observed isotope shifts in the electronic spectra of the heavy elements have been corrected for electronic structure, the resulting shifts give new insight into nuclear structure. In comparison with the shifts predicted for constant density spherical nuclei, the reduced observed shifts are anomalous (1) in magnitude, being on the average too small by a factor 0.5, (2) in trend with neutron number, showing an oscillation in magnitude, and (3) in the staggering of shifts between even and odd isotopes. The present work shows that the anomaly in magnitude largely disappears when account is taken of the compressibility and polarizability of nuclear matter, as a result of which the nuclear radius is found to vary less rapidly with change in neutron number than is predicted by the average $A^{\frac{1}{3}}$ law. The analysis of experimental data also suggests that nuclear particle density variations are slightly greater than indicated by earlier theoretical estimates. Likewise, the oscillatory trend in isotope shifts ceases to appear anomalous when associated with the regular progression in nuclear shapes as derived from configuration theory, from the analysis of quadrupole moments and the first excited states of even-even nuclei, and from other sources. The general size of the amplitude and the nodal positions of the shift variation are consistent with expectations. Finally, the even-odd staggering in isotope shifts is reasonably to be connected with the staggering to be expected in the progression of nuclear deformations through odd and even isotopes. Thus the over-all pattern of isotope shifts appears to fit together with present ideas and to provide new specific information on nuclear structure.

I. INTRODUCTION

THE atomic electron provides a useful and sensitive probe for the investigation of certain nuclear properties. In addition to the measurement of nuclear magnetic dipole and electric quadrupole moments, atomic spectra yield other information concerning the differences in the electronic interaction among the isotopes of a given element. The resulting displacements in the line spectra are appropriately called isotope shifts.

There are two general effects which give rise to atomic isotope shifts: the finite nuclear mass, and the deviation of the electron-nuclear potential from that of the $1/r$ Coulomb law for a point charge. The latter effect, with which this paper is primarily concerned, is referred to broadly as the field effect and arises from the spatial extension of the nuclear charge distribution.

In Sec. II we consider the field effects for spherical, incompressible nuclei, and present the anomalies which exist. In Secs. III and IV we show how most of the anomalies can be removed in terms of nuclear deformability and compressibility.

The theory of the mass effect has been described by Hughes and Eckart[1] and others.[2] In a coordinate system where the center of mass of an atom is at rest, the momentum of the nucleus must be equal in magnitude and opposite in direction to the resultant momentum of the electrons. The expression for the energy of an atom with a nucleus of finite mass differs from that of an atom with a nucleus of infinite mass by the addition of the term for the kinetic energy of the nucleus,

$$\frac{1}{2M}\left(\sum_i \mathbf{P}_i\right)^2=\frac{1}{2M}\sum_i P_i^2+\frac{1}{2M}\sum_{i\neq j}\mathbf{P}_i\cdot\mathbf{P}_j. \qquad (1)$$

For computational purposes it has been convenient to subdivide the mass effect into the "normal" effect, due to the first term on the right of Eq. (1), and the "specific" effect, due to the second term on the right of Eq. (1). The contribution of normal mass effect to the energy levels can be determined by replacing the electronic mass m by the reduced mass μ in the Hamiltonian. The resulting energy levels are displaced by a factor μ/m with respect to the levels of an atom with an infinite nucleus. This is the only mass effect present in hydrogen and one electron ions. The specific mass effect requires the evaluation of the expectation value of the last term in Eq. (1) and depends upon the particular electron configuration.

The nuclear mass effects decrease with increasing atomic weight and are seldom observed in the spectra of heavy elements. The nuclear field effects, on the other hand, are small among the light elements and dominate among the heavy elements.

II. FIELD EFFECTS FOR SPHERICAL, INCOMPRESSIBLE NUCLEI

A. The Nuclear Volume Effect

Racah,[3] and Rosenthal and Breit[4] investigated the effect of the extended proton distribution in the nucleus.

* Now at the University of California Radiation Laboratory, Livermore, California.

† On leave of absence to Los Alamos Scientific Laboratory, Los Alamos, New Mexico.

‡ Now at Indiana University, Bloomington, Indiana.

[1] D. S. Hughes and C. Eckart, Phys. Rev. **36**, 694 (1930).

[2] J. H. Bartlett, Jr., and J. J. Gibbons, Jr., Phys. Rev. **44**, 538 (1933); J. P. Vinti, Phys. Rev. **56**, 1120 (1939).

[3] G. Racah, Nuovo cimento **8**, 178 (1931).

[4] J. E. Rosenthal and G. Breit, Phys. Rev. **41**, 459 (1932); G. Breit, Phys. Rev. **42**, 348 (1932).

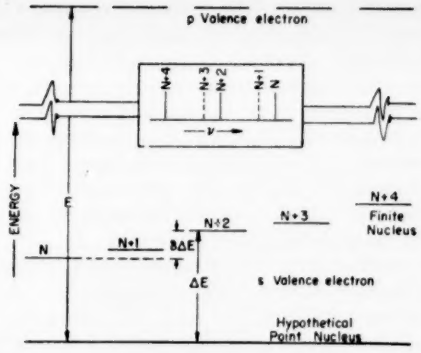

FIG. 1. Schematic representation of energy level displacements. The transition is assumed to involve the change of valence electron from a p state to an s state. The p-state levels for different isotopes are normalized to the same energy. Then the s states for a point nucleus lie also approximately at the same energy. The actual s states lie at progressively higher energies for heavier isotopes. Typically, an odd-N isotope level lies closer to its lower even-N neighbor than to its upper even-N neighbor (even-odd staggering). The energy scale is distorted. In the inset is shown the appearance on a photographic plate of the isotope shift splitting.

The probability density of an s electron in the neighborhood of a point charge as obtained from the Dirac equation is given by

$$P(r)=\frac{2(\rho+1)}{[\Gamma(2\rho+1)]^2}\psi^2(0)\left[\frac{2Zr}{a_H}\right]^{2\rho-2}, \tag{2}$$

where $\rho=(1-Z^2\alpha^2)^{\frac{1}{2}}$, $\psi(0)$ is the nonrelativistic Schrödinger wave function at $r=0$, and a_H is the Bohr radius. The $p_{\frac{1}{2}}$ electron wave function becomes infinite at $r=0$ like the $s_{\frac{1}{2}}$ wave function, but with smaller amplitude; the wave functions for all other electrons are zero at the origin. The principal effects of nuclear structure therefore appear in the energy levels of the s electrons.

If one considers a spherical nucleus of radius a, the electron potential energy is some function $eV(r)$ for $r<a$, and $-Ze^2/r$ for $r>a$. The first-order perturbation of the electronic energy is given by

$$\Delta E=4\pi e\int_0^a P(r)\left[V(r)+\frac{Ze}{r}\right]r^2dr. \tag{3}$$

The sum of these perturbation energies over all s electrons in the atom would give the first-order displacement of the energy level of the atom, but this total displacement is not directly observable. ΔE for an s valence electron gives the displacement in the energy of a photon emitted during the transition of the electron from a p state to an s state, for example. What is generally observed is the difference (shift) in ΔE between the lines of two different isotopes. An exception occurs in the case of x-ray spectra where ΔE is very large and the lines may be calculated accurately. We shall use the term displacement to mean the perturbation energy ΔE, and isotope shift to mean the difference in ΔE between two isotopes of the same element ($\delta\Delta E$). Figure 1 gives a schematic indication of the energy shifts involved.

Two extreme models which might bracket the nuclear proton distribution may be considered (see Fig. 2):

(a) The charge is distributed over the surface of the nucleus. This model is called by Breit the "top slice."

$$V(r)=-Ze^2/a, \quad r<a, \tag{4}$$

$$\Delta E=Ba^{2\rho}/2\rho(2\rho+1), \tag{5}$$

$$\delta\Delta E=\frac{Ba^{2\rho}}{2\rho+1}\frac{\delta a}{a}, \tag{6}$$

where

$$B=8\pi Ze^2\left(\frac{2Z}{a_H}\right)^{2\rho-2}\frac{(\rho+1)}{[\Gamma(2\rho+1)]^2}\psi^2(0),$$

and $\delta\Delta E$ is the energy shift between two isotopes differing in nuclear radius by δa.

(b) The charge is distributed uniformly throughout the nuclear sphere.

$$V(r)=\frac{Ze^2}{a}\left[-\frac{3}{2}+\frac{1}{3}\left(\frac{r}{a}\right)^2\right], \quad r<a, \tag{7}$$

$$\Delta E=\frac{3Ba^{2\rho}}{2\rho(2\rho+1)(2\rho+3)}, \tag{8}$$

$$\delta\Delta E=\frac{3Ba^{2\rho}}{(2\rho+1)(2\rho+3)}\frac{\delta a}{a}. \tag{9}$$

Because the deviation from the unperturbed $1/r$ potential is large inside the nucleus, the first-order perturbation theory is not sufficiently accurate in determining the energy shifts. Rosenthal and Breit[4] have subjected the perturbation treatment to analysis and have found that a factor as small as 0.5 may be required

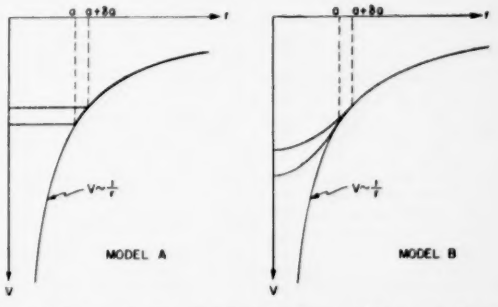

FIG. 2. Schematic diagram of electron potential energy. Model A, charge in shell on outside of nucleus ("top slice"); Model B, charge uniformly distributed through nucleus. The displacement, ΔE, is due to the difference between the actual potential (heavy line) and the $1/r$ potential (light line). The isotope shift, $\delta\Delta E$, is due to the difference in the potentials between isotopes of radius a and $a+\delta a$.

to correct the results predicted by the first-order calculations in some cases. Broch[5] has investigated the shifts by a treatment which avoids perturbation theory, and in the simple case where $V(r)=0$, $r<a$, he shows that a factor $k\approx 2\rho^2/(\rho+1)$ is needed to correct the first order results. Crawford and Schawlow[6] investigated the perturbation theory in the case of thallium ($Z=81$) for both nuclear models. Using Rosenthal and Breit wave functions for the top slice model and a power series solution for the case of uniform charge density, they found that the first-order calculations must be corrected by factors of 0.74 and 0.75. Broch's correction factor for the zero potential model is 0.72. The proximity of the correction factors for such different nuclear models is striking and indicates that Broch's factor k is probably sufficiently good to use generally.

B. Comparison with Experiment

Crawford and Schawlow[6] have compared in detail the experimental results in the isoelectronic sequence Hg II, Tl III, and Pb IV with the theory of the volume effect. They included the correction to the first-order perturbation theory and the contribution of the p electrons. They also took into account the contributions of the inner s electrons. An s valence electron partially shields the inner electrons (and in particular, the inner s electrons) while a p valence electron effectively does not. The effect of shielding on an s electron is to reduce its probability density at the nucleus and so to reduce ΔE. Thus ΔE changes for the inner electrons during a transition and they do contribute to the isotope shift, but with opposite sign than for the valence electron. Crawford and Schawlow found that the inner electrons reduced the shifts by about 20 percent.

The value of $\psi^2(0)$ was obtained from the semi-empirical formula of Fermi and Segrè,[7]

$$\psi^2(0)=\frac{Z_i Z_0^2}{\pi a_H^3 n_0^3}\left(1-\frac{d\sigma}{dn}\right), \tag{10}$$

where Z_i is the effective nuclear charge in the inner region of the orbit and may be set equal to Z, Z_0 is the effective nuclear charge in the outer regions, n_0 is the effective quantum number, and σ is the quantum defect, $n_0=n-\sigma$. The formula was originally derived for alkali metals but has been found to be valid more generally. In a few cases among the heavy elements there are isotopes whose magnetic moments have been

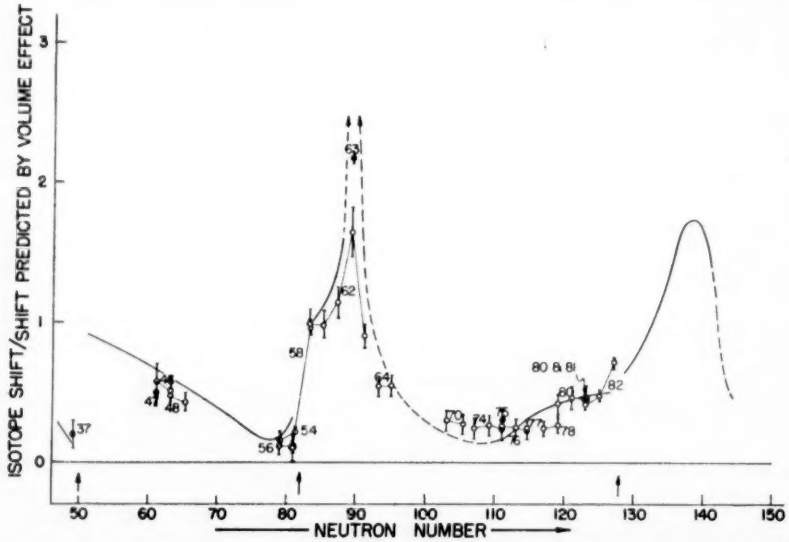

FIG. 3. Comparison of theoretical curve with experimental isotope shifts. The points are taken from Brix and Kopfermann (reference 9) with the exception of the values for Ba and the shift between Ce^{138} and Ce^{140} which were supplied by Dr. O. H. Arrøe in a kind private communication; the cerium datum has not yet been published by Dr. Arrøe. The points are plotted in units of the shifts predicted by the normal volume effect, assuming $a=1.40\times10^{-13}A^{\frac{1}{3}}$ cm. The limits of error indicated (which were generously supplied by Dr. Arrøe) refer only to the error in the spectroscopic measurements and do not include the theoretical uncertainties in the wave function normalization. Points are labeled by the Z value of the element concerned, and are plotted at the average N value of the isotopes measured. The shifts all refer to isotopes differing by two or four in neutron number. Open circles denote even-even nuclei, closed circles, odd-even nuclei. The theoretical curve is the curve of Fig. 5 increased by 0.5, rather than by 1.0, in order to give the best fit to the data. The correction to the volume effect for nuclear compressibility (Sec. IV) may account for the small average relative value ($\sim$0.5) of the experimental isotope shifts. The predicted peak near neutron number 90 is especially well verified. A somewhat broader peak is predicted just below 140 neutrons.

[5] E. K. Broch, Arch. Math. Naturvidenskab **48**, 25 (1945).
[6] M. F. Crawford and A. L. Schawlow, Phys. Rev. **76**, 1310 (1949).
[7] E. Fermi and E. Segrè, Z. Physik **82**, 729 (1933).

measured by induction methods, and the hyperfine structure splittings have been observed spectroscopically. The hfs splittings are proportional to the nuclear magnetic moment and to $\psi^2(0)$ for an s electron, while the value of the magnetic moment obtained from the induction method is independent of the electronic wave functions. The values of $\psi^2(0)$ obtained in this manner are in good agreement with the values given by the Fermi-Segrè formula.

On the basis of uniform charge distribution Crawford and Schawlow found that the observed shifts in the even isotopes of the three elements were very nearly half the values that would be expected from the empirical formula[8] for the nuclear radius, $a=1.5\times10^{-13}A^{\frac{1}{3}}$ cm. The top slice model leads to a greater discrepancy.

Brix and Kopfermann[9] and Humbach[10] have analyzed the experimental data from a large number of elements in a manner similar to that of Crawford and Schawlow. The ratio of the experimental value of the shifts to that predicted by a uniform charge distribution and $a=1.4\times10^{-13}A^{\frac{1}{3}}$ cm is shown in Fig. 3. (The theoretical curve in Fig. 3 is discussed in the next section.) The ratios are plotted as a function of the neutron number and are given in all cases for $\delta N=\delta A=2$. Brix and Kopfermann state that the theoretical values used are probably good to at least 20 percent.

It can be seen from Fig. 3 that the experimental shifts are on the average about half the values predicted by the volume effect, and that there are also considerable variations in the ratios with very large isotope shifts observed in the vicinity of the rare earths.

Schawlow and Townes[11] have investigated data from x-ray spectra where the energy displacement from the point nucleus ΔE can be observed instead of the differential shift between isotopes $\delta\Delta E$. The data are consistent with a nuclear charge distribution which is either uniform or slightly more concentrated toward the surface, and a nuclear radius given by the empirical formula. This suggests that the small value of the observed isotope shifts is a differential effect.

For those elements which have both even and odd isotopes it is observed that the centers of gravity of the energy levels of the odd isotopes are not spaced midway between the levels of the even isotopes, but are rather usually lower than midway (see Fig. 1).

The isotope shift anomalies, then, are these: (1) The observed shifts are on the average smaller by a factor of one-half than is predicted by the volume effect, using a nuclear radius given by $a=1.4\times10^{-13}A^{\frac{1}{3}}$ cm; (2) the shifts vary with the neutron number in a more or less regular manner which appears to be associated with the magic numbers; (3) the energy levels of the odd isotopes are not located midway between the levels of the even isotopes, but are staggered.

C. Nuclear Polarization

Breit, Arfken, and Clendenin[12] have investigated the possible polarization of the nucleus by the atomic electrons The polarization acts in the direction to increase the binding of the electrons and is thus contrary in sense to the volume effect. Only the monopole effect should be large enough to contribute appreciably to the isotope shifts.

The polarization of the nucleus may be interpreted in terms of admixtures to the nuclear ground state of low-lying excited levels, in such a way as to give greater concentration of protons toward the center of the nucleus where the electron probability density is greatest. The size of the effect depends upon the number and spacing of the low-lying excited levels of the nucleus, and might thus be expected to be greater for odd nuclei than for even ones. The authors were looking for an effect half as great as the volume effect in order to account for even-odd staggering. Reasonable approximations appeared to give no more than 20 percent of the needed one-half and rather extreme departures from the central field approximations for an individual nucleon seemed necessary to account for the observed effect.

While the polarization may account in some part for the even-odd staggering, it probably is not important in explaining the small average value of the even shifts. The consistency of the data from x-ray spectra with the predictions of the volume effect indicates that the energy displacement ΔE is due mainly to that effect and that the anomalies in the even shifts may come mainly from differential effects.

D. Non-Coulomb Forces

Havens, Rainwater, and Rabi[13] have reported the observation of an electron-neutron interaction of $V=5300\pm1000$ electron volts, assuming a square well of the classical electron radius $r_e=2.8\times10^{-13}$ cm. An estimate of the effect of this interaction can be obtained by assuming the additional neutrons of a heavior isotope are found primarily near the surface of the nucleus. The ratio of the contribution from this source with that predicted by the volume effect is then given by[14]

$$\frac{\epsilon}{\delta\Delta E}=0.0122(2\rho+1)(2\rho+3)\frac{A^{\frac{1}{3}}}{Z}. \qquad (11)$$

For zinc ($A\sim64$, $Z=30$), which is low in weight for field effect, the ratio is about 0.024; it decreases with increasing atomic weight. Even this is probably an

[8] See, for example, H. A. Bethe, *Elementary Nuclear Theory* (John Wiley and Sons, Inc., New York, 1947), p. 8.
[9] P. Brix and H. Kopfermann, Z. Physik **126**, 344 (1949); Festschr. Akad. Wiss. Göttingen, Math.-Physik. Kl. 17 (1951); Phys. Rev. **85**, 1050 (1952).
[10] Walter Humbach, Z. Physik **133**, 589 (1952).
[11] A. L. Schawlow and C. H. Townes, Science **115**, 284 (1952).
[12] Breit, Arfken, and Clendenin, Phys. Rev. **78**, 390 (1950); Phys. Rev. **77**, 569 (1950).
[13] Havens, Rainwater, and Rabi, Phys. Rev. **82**, 345 (1951).
[14] L. Wilets and L. C. Bradley III, Phys. Rev. **82**, 285 (1951).

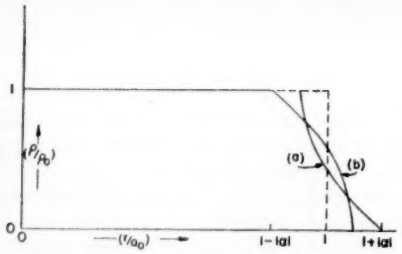

FIG. 4. Average charge density for deformed nucleus. Dashed curve: hypothetical uniform density for spherical nucleus of radius a_0. Curve (a): charge density averaged over all angles for prolate distorted nucleus with maximum radius $a_0(1+\alpha)$, $\alpha>0$. Curve (b): charge density averaged over all angles for oblate distorted nucleus with maximum radius $a_0(1-\alpha/2)$, $\alpha<0$.

overestimate, since as Foldy[15] has pointed out, the reported value of the electron-neutron interaction can be understood almost alone on the basis of the magnetic moment of the neutron. Thus the effects might be expected to cancel for an even number of neutrons and to be given equal weight (equal probability of spin orientation) in determining the center of gravity of the hyperfine structure of an odd isotope.

III. THE NUCLEAR DISTORTION EFFECT

A. Theory

The effect of nuclear distortion on the average nuclear charge distribution seen by an s electron is shown in Fig. 4. The charge distribution is extended radially and the energy displacement, ΔE, is increased for either prolate or oblate deformation. The effect on ΔE is small, but the differential effect measured by the isotope shift may be quite large, since the nuclear deformation may change by a large fraction of itself from one isotope to another, while the nuclear volume does not.[16]

Restricting consideration to cylindrically symmetric ellipsoidal deformations, we write for the nuclear radius,

$$R(\theta)=a_0[1+\alpha P_2(\cos\theta)], \tag{12}$$

where α may be >0 (prolate) or <0 (oblate). Because we deal only with s electrons, there is no loss of generality in choosing the ellipsoid axis along the Z axis. In order to isolate the distortion effect from other effects, it is assumed in the present section that the nucleus has a constant volume, $(4/3)\pi a^3$, and a uniform charge density,

$$\begin{aligned}&\rho_0(r)=Ze[4\pi a^3/3]^{-1}, && r<R(\theta);\\ &\rho_0(r)=0, && r>R(\theta).\end{aligned} \tag{13}$$

The constant volume assumption relates the parameters a_0 and a appearing in Eqs. (12) and (13):

$$a_0=a[1+\tfrac{2}{5}\alpha^2+(2/35)\alpha^3]^{-\frac{1}{3}}. \tag{14}$$

Introducing the notation $m=$ minimum nuclear radius, $M=$ maximum nuclear radius, one obtains for the charge density averaged over all angles in the region $m<r<M$:

$$\text{prolate:}\quad \rho(r)=\rho_0\{1-[(r-m)/(M-m)]^{\frac{1}{2}}\}; \tag{15a}$$

$$\text{oblate:}\quad \rho(r)=\rho_0[(M-r)/(M-m)]^{\frac{1}{2}}. \tag{15b}$$

It is these expressions which are plotted in Fig. 4.

The perturbing energy of interest is the difference between the electron potential energy in the field of a deformed nucleus and in the field of a spherical nucleus of the same charge and volume. Calling this perturbation ΔV, we have, for the case of prolate deformation,

$r<m$,

$$\Delta V_1=-\frac{Ze^2}{a}\left\{\frac{3}{2}[(a_0/a)^2-1]+\frac{3}{10}(a_0/a)^2\alpha^2\right\}; \tag{16a}$$

$m<r<a$,

$$\Delta V_2=-\frac{Ze^2}{a^3}\left\{\frac{4}{35}\frac{(r-m)^{5/2}}{(M-m)^{1/2}}\left[3+4\frac{m}{r}\right]\right\}; \tag{16b}$$

$a<r<M$,

$$\Delta V_3=\Delta V_2-\frac{Ze^2}{a}\left\{\frac{3}{2}-\frac{1}{2}\left(\frac{r}{a}\right)^2-\frac{a}{r}\right\}; \tag{16c}$$

and for oblate deformation,

$r<m$,

$$\Delta V_1=-\frac{Ze^2}{a}\left\{\frac{3}{2}[(a_0/a)^2-1]+\frac{3}{10}(a_0/a)^2\alpha^2\right\}; \tag{17a}$$

$m<r<a$,

$$\Delta V_2=\Delta V_3+\frac{Ze^2}{a}\left\{\frac{3}{2}-\frac{1}{2}\left(\frac{r}{a}\right)^2-\frac{a}{r}\right\}; \tag{17b}$$

$a<r<M$,

$$\Delta V_3=\frac{Ze^2}{a^3}\frac{4}{35}\frac{(M-r)^{5/2}}{(M-m)^{1/2}}\left(3+4\frac{M}{r}\right). \tag{17c}$$

The electronic energy displacement to first order is the diagonal matrix element of ΔV for an s electron, the same for either prolate or oblate deformation. If we define the electron density in the vicinity of the nucleus by

$$\bar{\psi}\psi=Br^{2\rho-2}/4\pi Ze^2 \tag{18}$$

(see Sect. II-A), the extra energy displacement due to nuclear deformation is given by

$$\Delta E_a=Ba^{2\rho}\frac{3}{10}\frac{\alpha^2}{2\rho+1}\left[1+\frac{2}{21}(2\rho+3)\alpha+\cdots\right]. \tag{19}$$

[15] L. L. Foldy, Phys. Rev. **87**, 693 (1952).

[16] Brix and Kopfermann have noted the importance of nuclear deformations in a discussion of the isotope shifts of Sm (reference 9). Shell structure effects from another point of view have been considered by G. Breit, Phys. Rev. **86**, 254 (1952).

The ratio of this displacement to that of the normal volume effect is, to order α^2,

$$\frac{\Delta E_\alpha}{\Delta E_v}=\frac{\rho(2\rho+3)}{5}\alpha^2. \tag{20}$$

If 0.25 is taken to be an upper limit to α, this ratio is less than 0.06. To the accuracy of the α^2 term in Eq. (19), the ratio of the isotope shift due to deformation to the shift due to the normal volume effect is

$$\frac{S_\alpha}{S_v}=\frac{\delta(\Delta E)_\alpha}{\delta(\Delta E)_v}=\frac{3}{10}(2\rho+3)A\left(\frac{\delta(\alpha^2)}{\delta N}\right)_Z. \tag{21}$$

Since the coefficient of α within the bracket of equation (19) is of the order of 0.5, the fractional error of Eq. (21) due to the neglect of higher orders in α is approximately $\frac{1}{2}\alpha$ (with the sign of α). As stated in Sec. II-A, corrections to the first-order perturbation energy are insensitive to the shape of the potential within the nucleus. Therefore the ratio S_α/S_v, calculated using the zero-order electron wave function, should remain very nearly the same if higher-order corrections to the perturbation theory are applied.

One can quickly estimate from Eq. (21) on the basis of known quadrupole moments that the nuclear distortion effect is substantial. Setting $Z=62$, $A=150$, $\delta(\alpha^2)=0.005$. and $\delta N=2$, one finds $S_\alpha/S_v=0.54$. It should be stressed that the α appearing throughout the above derivation is the *intrinsic* nuclear deformation,[17] not the deformation measurable from quadrupole moments. Hence the effect is expected in even-even as well as odd-even nuclei.

In order to predict actual values of isotope shifts expected from the distortion effect, it is required to know the magnitudes of nuclear distortions. There are several sources of information to which we may turn.

(1) *Theory*

The equilibrium shape of the nucleus may be calculated theoretically if the configuration of nucleons outside closed shells is known. In the static approximation (surface motion treated classically), the deformation parameter α is given by[18,19]

$$\alpha=\frac{\bar{T}}{C'}\sum_i\frac{j_i(j_i+1)-3m_i^2}{4j_i(j_i+1)}, \tag{22}$$

where $\bar{T}$ is an interaction energy parameter which is the order of the kinetic energy of the extra nucleons, and C' is the coefficient in the surface potential energy, $V_s=(1/2)C'\alpha^2$, which is around 160 Mev for the heavy elements. The coefficient on the right side of Eq. (22) has approximately the value 0.12 for the heavy elements, varying only slowly with mass number. The m_i are the projections of the vectors $\mathbf{j}_i$ along the axis of the deformed nucleus. There is some evidence[20] that deformations calculated in this way are too large, due to an overestimate of the magnitude of the particle-to-surface interaction, to a breakdown of the idea that the $\mathbf{j}_i$ are quantized along the nuclear axis, or to the approximations employed—considering the P_2 deformation only and working only to first order in α. The more serious practical difficulty preventing an accurate theoretical determination of the nuclear deformation is our ignorance of the detailed nucleon configurations. This is especially true of those nuclei where one expects large deformations and hence large contributions to the isotope shift. It is necessary therefore in our present state of knowledge of nuclear structure, to turn to empirical evidences of the nonspherical shape of the nucleus.

(2) *Quadrupole Moments*

These are generally not measured to high accuracy, so that the differences $\delta(\alpha^2)$ are rather rough. For $A>75$, quadrupole moments are known for pairs of isotopes of the following elements: $_{49}\mathrm{In}^{113,115}$, $_{51}\mathrm{Sb}^{121,123}$, $_{53}\mathrm{I}^{127,129}$, $_{62}\mathrm{Sm}^{147,149}$, $_{63}\mathrm{Eu}^{151,153}$, $_{71}\mathrm{Lu}^{176,177}$, and $_{75}\mathrm{Re}^{185,187}$.

Values of α may be computed from measured quadrupole moments by the formula[20]

$$\alpha=\frac{53.5}{ZA^{\frac{1}{3}}}\frac{(I+1)(2I+3)}{I(2I-1)}Q_{\mathrm{obs}}, \tag{23}$$

where Q_{obs} is in barns. This formula assumes that the nuclear spin is directed along the nuclear axis, and that the total spin vector is strongly coupled to the axis.[21] For this reason it gives a lower limit to the intrinsic nuclear distortion. Other orientations of the spin, or weak coupling of spin to axis, would yield smaller measured quadrupole moments than are assumed in Eq. (23), and hence lead to an underestimate of α. In addition to the few elements mentioned above with known quadrupole moments for pairs of isotopes, there are measured quadrupole moments for single isotopes which contribute information useful for isotope shifts in an indirect way by suggesting that the nuclear deformation varies in a regular way among the elements, reaching minima at the magic numbers and maxima between the magic numbers.

(3) *Energy of the First Excited State of Even-Even Nuclei*

The strong coupling approximation of the collective model of the nucleus[19] yields a simple approximate relation[17,20] between the nuclear deformation and the energy of the first excited state of even-even nuclei:

$$\alpha=10.4A^{-5/6}E_1^{-1/2}, \tag{24}$$

[17] A. Bohr and B. R. Mottelson, Phys. Rev. **89**, 316 (1953).
[18] J. Rainwater, Phys. Rev. **79**, 432 (1950).
[19] A. Bohr, Kgl. Danske Videnskab. Selskab, Mat.-fys. Medd. **26**, No. 14 (1952).
[20] K. W. Ford, Phys. Rev. **90**, 29 (1953).
[21] A. Bohr, Phys. Rev. **81**, 134 (1951).

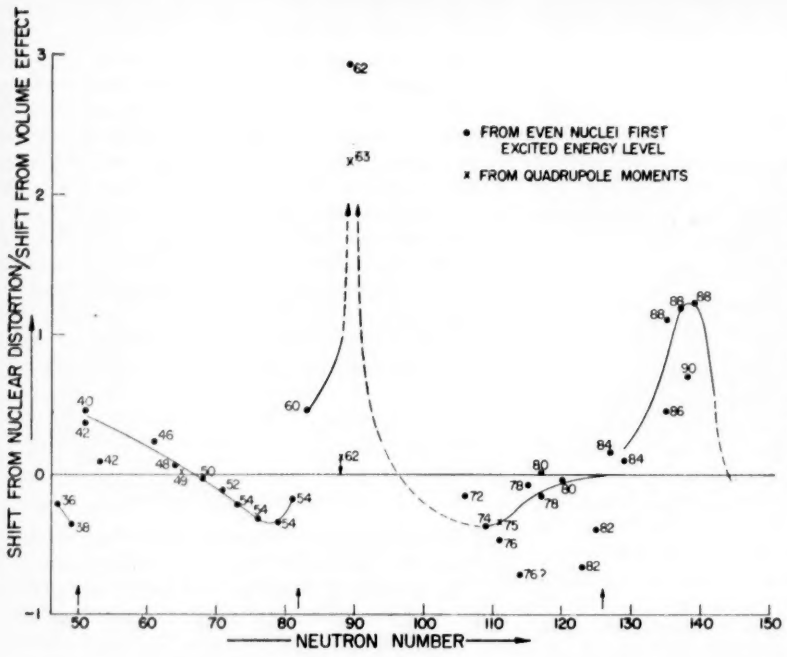
SHIFT FROM NUCLEAR DISTORTION/SHIFT FROM VOLUME EFFECT
• FROM EVEN NUCLEI FIRST EXCITED ENERGY LEVEL
x FROM QUADRUPOLE MOMENTS
NEUTRON NUMBER

FIG. 5. Theoretical curve of isotope shifts due to nuclear deformation in units of the shift predicted by the normal volume effect. Points are predicted isotope shifts and are labeled with the Z value of the elements concerned, and are plotted at the average neutron number of the two isotopes on which each point is based. The particularly low value of the Sm point ($Z=62$) based on quadrupole moments may possibly be explained in terms of mixing of the prolate and oblate forms of deformation. Other special features of the curve are discussed in the text.

where E_1 is in Mev. This simple formula is shown in reference 20 to overestimate the nuclear distortion by a substantial amount, even if all of the parameters of the theory are correct. The error of the formula depends on the detailed nucleon configurations, and can therefore not be estimated with any accuracy.

Our procedure therefore is to normalize Eq. (24) with a single arbitrary parameter to yield agreement with deformations calculated from quadrupole moments in the vicinity of the rare earth elements. The factor of reduction required is 1.7 for α or 3 for α^2. This means of arriving at values of the nuclear deformation is theoretically more tenuous than the more direct evidence of quadrupole moments, but has several advantages: (*a*) the data on the first excited states of even-even nuclei in the region $50<N<126$ are more extensive and more accurate than the quadrupole moment data; (*b*) most of the measured isotope shifts are for even-even nuclei; and (*c*) the isotope shifts and the excited states of even-even nuclei both measure the intrinsic nuclear deformation, independent of spin orientation and independent of possible mixing of states of prolate and oblate deformation.

(4) *Electric Quadrupole Transition Rates in Even-Even Nuclei*

Bohr and Mottelson[17] have given an approximate formula relating the transition rate from first excited state to ground state in even-even nuclei to the intrinsic nuclear deformation. For the few cases of measured transition rate, mostly in the rare earth group, good agreement of calculated deformations is obtained with the trend of values obtained from quadrupole moments, but with deformations obtained from $E2$ transitions being somewhat smaller than those obtained from quadrupole moments. This is consistent with the approximation employed in their formula, which assumes that the surface vibrational part of the wave function is identical in initial and final states. This approximation should lead to an overestimate of the value of the matrix element.

Two other effects can be mentioned which may yield information on nuclear distortions.

(5) *The Regularities in Level Spacing of Single-Particle-Type Energy Levels in the Odd-Even Nuclei*[22]

The single particle energy level positions depend on the nuclear distortion,[23] and the regularities observed in energy level spacings may reflect regularities in the nuclear deformations.

(6) *Alpha Decay*

The nuclear deformation may enhance alpha decay rate[23,24] because of the decreased Coulomb barrier over part of the nuclear surface. In some cases it may also

[22] M. Goldhaber and R. D. Hill, Revs. Modern Phys. **24**, 179 (1952).
[23] D. L. Hill and J. A. Wheeler, Phys. Rev. **89**, 1102 (1953).
[24] J. J. Devaney, Ph.D. dissertation, Massachusetts Institute of Technology, 1950 (unpublished).

contribute to a non-overlap of the initial and final wave functions and thereby inhibit alpha decay.

Neither of the effects (5) and (6) has been analyzed in sufficient detail to yield useful quantitative information on nuclear deformations. Only the effects (2) and (3), and to some extent (4), are based on sufficient experimental data and adequate theoretical grounds to permit a prediction of isotope shifts expected from the nuclear distortion effect.

Figure 5, based on quadrupole moments and on the energies of the first excited states of even-even nuclei, gives the predicted differential isotope shifts caused by nuclear deformation in units of the shift due to the ordinary volume effect. Points are shown where data exist for two or more isotopes of the same element. The trend of the curve is influenced also by the data on single isotopes, e.g., the value of $N=96$ where the curve crosses the horizontal axis. Several special features of the theoretical curve may be noted. Discontinuities appear at the magic numbers, where the predicted shift changes sign. Between magic numbers, the shift also changes sign, but continuously. The positive peak expected between $N=82$ and 126 is higher and narrower than the negative valley in the same shell. Quadrupole moment points were given special weight in drawing the curve. The Pb isotopes were given very little weight because the strong coupling approximation, on which the points due to the even-even nuclei are based, is not expected to be valid in the near vicinity of a double closed shell. Because of the dependence of nuclear deformation on both N and Z, the shifts are not expected to lie accurately along a single curve as a function of N only. The data on which the theoretical curve is based are inadequate for a more detailed prediction, however. The curve should be regarded as a mean prediction along the line of stable elements.

B. Comparison with Experiment

Figure 3 gives the experimental isotope shifts in units of the shift expected from the ordinary volume effect. If only the volume effect plus the distortion effect were effective for isotope shifts, the curve of Fig. 5, increased by one unit, should lie along the experimental points. In fact, such a curve lies too high. In order to fit the data reasonably well, it is required to add to the curve of Fig. 2 a value of only 0.5. The theoretical curve, arbitrarily modified in this way, is given in Fig. 3, and is seen to fit the data rather well, both in shape and in magnitude.

It should be stressed that two arbitrary parameters have gone into the theoretical curve of Fig. 3. The first of these was the normalization of the distortions computed from the energies of the first excited states of even-even nuclei to the distortions computed from quadrupole moments in the rare earth elements. This normalization was required by inadequate knowledge of the detailed nucleon configurations and was in the expected direction—to decrease the distortion found from the even-even nuclei. The second parameter was the shift of the theoretical curve downward everywhere by 0.5. This is equivalent to assuming that all effects other than the volume effect and the distortion effect give a net contribution to the isotope shift half as great as the volume effect and in the opposite direction. It will be shown in Part IV that it may be reasonable to attribute such an effect largely to the finite compressibility of nuclear matter and the consequent variations of nuclear density among the isotopes of a single element. Note that in the theoretical curve of Fig. 3 all of the *variations* of the isotope shifts away from a mean value are attributed to the distortion effect only.

C. Even-Odd Staggering

The nuclear distortion effect may afford also an explanation of the even-odd staggering observed experimentally. There is slight, but by no means conclusive evidence, from the first excited states of even-even nuclei that the even-even nuclei are somewhat more deformed than the odd-even nuclei. Such an effect, in any case, is expected theoretically. Figure 6 shows the square of the nuclear deformation (to arbitrary scale) *vs* number of nucleons in a simple shell of $j=9/2$ particles, calculated according to Eq. (22). If one considers a given element with Z even, then the horizontal scale in Fig. 6 represents the number of neutrons in different isotopes of the element. The α^2 of odd-even isotopes is seen to be less than the average value of α^2 for the neighboring even-even isotopes, which leads to an even-odd staggering in the direction usually observed. A similar result holds for more complicated shells, involving particles in more than one subshell.

Examples of observed even-odd staggering in Ba[25] and in Pb[26] and the possible connection of the staggering

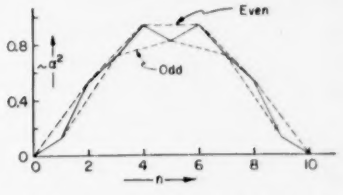

FIG. 6. Nuclear distortions in simple shell of $j=9/2$ particles. Plotted vertically is the quantity

$$\left[\sum_i \frac{j(j+1)-3m_i^2}{4j(j+1)}\right]^2,$$

which in the static approximation is proportional to the square of the nuclear deformation, α^2. Plotted horizontally is the number of nucleons (of a given type) in the shell. The value of α^2 for $n=$ odd is less than the average value of α^2 for the neighboring $n=$ even points. This may afford an explanation of the observed even-odd staggering.

[25] O. H. Arrøe, Ph.D. dissertation, University of Copenhagen, 1951 (Kobenhavn Nordisk Bogtrykkeri, 1951).

[26] Manning, Anderson, and Watson, Phys. Rev. **78**, 417 (1950); K. Murakawa and S. Suwa, J. Phys. Soc. Japan **5**, 382 (1950); F. Geiger, Phys. Rev. **79**, 212 (1950); Brix, von Buttlar, Houtermans, and Kopfermann, Z. Physik **133**, 192 (1952).

with nuclear deformation are illustrated in Fig. 7. Each of these elements possesses an isotope with closed neutron shell. Pb has in addition a closed proton shell, and Ba may have a closed proton subshell ($g_{7/2}$). The deformations, $|\alpha|$, shown in the figure are calculated from the observed isotope shifts assuming (a) that the shift due to the volume effect alone is half of that for an incompressible nucleus with $R=1.4\times10^{-13}A^{\frac{1}{3}}$ cm, and (b) that the deformations for the isotopes with closed neutron shells are negligibly small. The plotted deformations are therefore only qualitatively correct. (In addition, the observed shifts in Ba are subject to considerable uncertainty[25] because of their small value.) To be noted are: (1) The occurrence together of large anomalies in the isotope shift and large even-odd staggering is in agreement with theory. (2) The nuclear deformation effect may reasonably account for much of the observed even-odd staggering, even in the extreme case of barium. There is room, however, for an additional small effect caused by nuclear polarization.[12] It may incidentally be remarked that the large observed anomaly in Ba speaks against a closed proton subshell for all of the Ba isotopes.

IV. FIELD EFFECTS IN THE COMPRESSIBLE NUCLEAR MODEL

In the previous sections we have, for simplicity, discussed the isotope shifts which would follow from nuclei of sharply defined boundaries enclosing uniform charge density. In the present section we shall retain

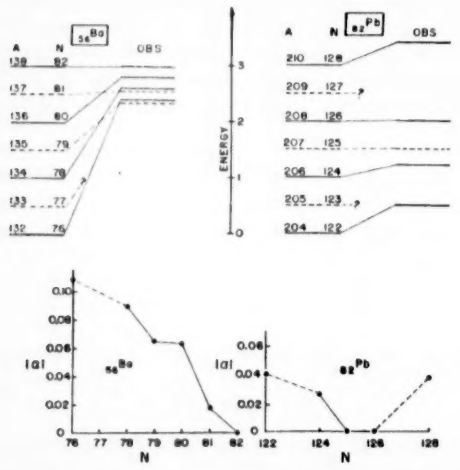

FIG. 7. Nuclear deformations calculated from observed isotope shifts. The energy levels are plotted in units of the energy difference predicted for incompressible nuclei with standard radius $1.4\cdot10^{-13}A^{\frac{1}{3}}$ cm and differing by one neutron. To the left of each diagram are the *presumed* levels in the absence of deformation (half of the standard theoretical value), and to the right are the observed levels, normalized to leave unchanged the level of the nucleus with closed neutron shell. Values of the nuclear deformation plotted below the diagrams are calculated assuming that all of the changes from the left half to the right half of the diagrams are due to the nuclear distortion effect.

the fiction of sharply defined nuclear surface, but subject to this constraint we shall refine our description of the charge distribution. Discarding the assumption of constant mass and charge densities within nuclei, and restricting our discussion initially to spherical nuclei, we shall (1) examine more closely the effect of adding one or more neutrons upon the potential in which the atomic electrons are bound; and so (2) ascertain the isotope shifts to be expected when consideration is given to current estimates of nuclear compressibility and polarizability.

A. Neutron and Proton Densities

The Coulomb repulsion augments the proton density near the nuclear surface relative to the central density; a similar but less pronounced displacement occurs for the neutrons. Wigner,[27] Feenberg,[28] and Swiatecki[29] have computed these particle densities by somewhat different procedures derived from the principle that, for a chosen nuclear radius, the equilibrium neutron and proton densities, n_n and n_p, are given by the variational statement,

$$\delta\int\epsilon(n_n, n_p)d(\text{volume})=0, \tag{25}$$

in which the energy density $\epsilon(n_n, n_p)$ is to be integrated over the nuclear volume. The analytically simple expression for the energy density used by Swiatecki results in particle densities (see Fig. 8) which ascend with monotonically increasing slope toward the nuclear surface, where the densities are truncated to zero value. A similar truncation is used by Feenberg, but in his work the boundary condition is imposed that the particle densities shall intercept the surface at zero slope. The latter method approaches somewhat more closely what is perhaps the actual situation for a heavy nucleus; namely, each particle density rises initially to a maximum, and then falls continuously to reach a negligible value slightly beyond the apparent radius. No satisfactory treatment of particle densities closely resembling this "actuality" exists at present in a form to yield reliable estimates of the small differential effects pertinent to the prediction of isotope shifts. We therefore shall obtain an order of magnitude estimate of how isotope shifts depend on nuclear compressibility, following Feenberg in the treatment of particle densities. The result of this treatment is that the addition of two neutrons increases the nuclear radius by a substantially smaller amount than the increase predicted by the average $A^{\frac{1}{3}}$ law.

The particle densities, which are assumed to vary but slightly from the mean values, $\bar{n}_N$ and $\bar{n}_P$, may be written

$$n_N(r)=\bar{n}_N[1+v_N(x)]; \quad n_P(r)=\bar{n}_P[1+v_P(x)]. \tag{26}$$

[27] E. Wigner, Bicentennial Symposium, University of Pennsylvania, 1940 (unpublished).
[28] E. Feenberg, Phys. Rev. **59**, 593 (1941).
[29] W. J. Swiatecki, Proc. Phys. Soc. (London) **A63**, 1208 (1950).

Here the deviations $v_N(x)$ and $v_P(x)$ are functions of the relative radius $x=r/R$ and may be expanded in terms of the flat-edge polynomials[30] of Feenberg:

$$v_N(x)=a_N v_1(x)+b_N v_2(x),$$
$$v_P(x)=a_P v_1(x)+b_P v_2(x), \tag{27}$$

where the coefficients of expansion are to be determined from (25). In this section we conform to Feenberg's notation, denoting the nuclear radius as R.

B. Isotope Shift

The evaluation of the isotope shift predicted for a nonuniform charge density is simplified by employing an alternate form of Eq. (3) that is an integration of the nuclear charge density, $\rho(r)=en_P(r)$, which determintes $V(r)$, over the effective potential due to the s electron. Then, for a quite general nuclear charge distribution, the first-order perturbation from the field of the finite nucleus is given by

$$\Delta E=[4\pi B/2\rho(2\rho+1)Z]\int_0^\infty n_P(r)r^{2\rho+2}dr. \tag{28}$$

In deriving this expression we have assumed the asymptotic formula (2) to be valid out to a value of r for which the proton density, $n_P(r)$, has fallen to a negligible value. The error introduced by this assumption in both ΔE and $\delta\Delta E$ is less than 0.3 percent for heavy nuclei.

Upon specializing this formula to the present case, with $n_P(r)$ defined by Eqs. (13), (26), and (27), we have

$$\Delta E=\frac{3BR^{2\rho}}{2\rho(2\rho+1)(2\rho+3)}[1+C_a a_P+C_b b_P], \tag{29}$$

with

$$C_a=(2\rho+3)\int_0^1 v_1(x)x^{2\rho+2}dx,$$

$$C_b=(2\rho+3)\int_0^1 v_2(x)x^{2\rho+2}dx.$$

Equation (29) reduces to Eq. (8), as it must, when $v_P(x)$ goes to zero. The isotope shift is now given by

$$\delta(\Delta E)=\frac{3BR^{2\rho}}{(2\rho+1)(2\rho+3)}\left\{[1+C_a a_P+C_b b_P]\frac{\delta R}{R}+\frac{C_a}{2\rho}\delta a_P+\frac{C_b}{2\rho}\delta b_P\right\}, \tag{30}$$

where, as before, the operator δ signifies the difference in the operand values for two isotopes. The term in (30) containing δR as a factor is, as we shall see, the dominant term, representing the contribution to the isotope shift both from the change in average charge density and from the change in surface position. The other two terms give the effect of the relative redistribution of the protons. We now turn to the evaluation of the quantities within the brace of Eq. (30).

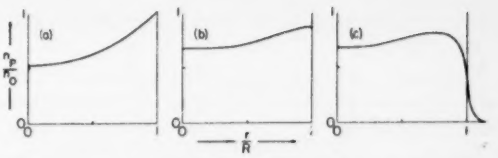

FIG. 8. Proton densities in the nuclear interior, in units of $n_0=3A/8\pi R^3$, plotted for three different models. (a) A rough estimate of the density variation is easily obtained by the method of Swiatecki (reference 29). (b) A somewhat more refined calculation by Feenberg (reference 28) adjusts the density to zero slope at the nuclear surface. (c) A self-consistent treatment of the density variation through the nuclear surface would presumably lead to such a curve as here plotted. In contrast with this estimate, however, is the result deduced by Gombas from a statistical theory of the nucleus (reference 36).

C. Relative Isotopic Radii

Just as, by Eq. (25), the particle distributions are determined which minimize the energy for a fixed radius, so the radius itself is chosen to minimize the total energy. When the potential and kinetic effects of the nuclear surface are ignored, the equilibrium radius is readily found[31] to have the value

$$R=R_0(1+E_c/E_0''). \tag{31}$$

The total Coulomb energy is, in units of $mc^2=0.511$ Mev, adequately given for our purposes by the expression

$$E_c=1.2Z^2A^{-\frac{1}{3}}, \tag{32}$$

and the compressibility coefficient may be written

$$E_0''=KA. \tag{33}$$

The factor K is poorly known, but order of magnitude estimates suggest[31] a value near 100 mc^2 or 150 mc^2. Present information[32] on nuclear radii is not adequate to fix precisely the average dependence on A, but if we accept the conventional estimate that R varies as $A^{\frac{1}{3}}$, then it would follow that R_0 varies as $A^{m/3}$, where m is a number near unity to be found below. R_0 is to be interpreted physically as the radius which the nucleus would take in the absence of Coulomb forces. It then follows (ignoring the A dependence of m) that

$$\frac{1}{R}\frac{\partial R}{\partial N}=\frac{1}{3A}\left[m-\frac{4E_c}{E_0''+E_c}\right],$$
$$\frac{1}{R}\frac{\partial R}{\partial Z}=\frac{1}{3A}\left[m-\frac{4E_c}{E_0''+E_c}\left(1-\frac{3}{2}\frac{A}{Z}\right)\right], \tag{34}$$

[30] As shown in reference 28, the two lowest-order polynomials (above the constant) which are orthonormal in the interval 0 to 1 for the weight factor x^2 and which meet the condition $dv(x)/dx=0$ for $x=0$ and 1, are $v_1(x)=6.1675(1-3.75x^2+2.5x^3)$ and $v_2(x)=11.028(1-13.7879x^2+24.1819x^3-11.2424x^4)$.

[31] E. Feenberg, Phys. Rev. **59**, 149 (1941).

[32] See, for example, J. M. Blatt and V. F. Weisskopf, *Theoretical Nuclear Physics* (John Wiley and Sons, Inc., New York, 1952), p. 15.

of which the former provides the value of $\delta R/R$ required in Eq. (30).

The dependence of nuclear radius on particle number here displayed for the compressible nucleus contrasts with the dependence in the incompressible nucleus:

$$\frac{1}{R}\frac{\partial R}{\partial N}=\frac{1}{R}\frac{\partial R}{\partial Z}=\frac{1}{R}\frac{dR}{dA}=\frac{1}{3A}. \tag{35}$$

Yet the last equality of this chain must, on the average, be satisfied in order to accord with empirical estimates on the average trend of nuclear radii with mass number. This requirement provides a determination of the index m appearing in Eqs. (34). We put

$$\frac{1}{R}\frac{dR}{dA}=\frac{1}{R}\frac{\partial R}{\partial N}\frac{dN}{dA}+\frac{1}{R}\frac{\partial R}{\partial Z}\frac{dZ}{dA}, \tag{36}$$

with dZ/dA and $dN/dA=1-(dZ/dA)$ found from the charge-to-mass stability curve[33] of the nuclides:

$$Z_A=A(1.981+0.01496A^{\frac{2}{3}})^{-1}. \tag{37}$$

It then follows that

$$\frac{3A}{R}\frac{dR}{dA}=1=m-\frac{4E_c}{E_0''+E_c}\left(1-\frac{3}{2}\frac{Z}{A}\frac{dZ}{dA}\right),$$

from which m is computed. The resultant[34] values of the radial derivatives given by Eqs. (34) are listed in Table I, for two different values of the compressibility coefficient E_0''.

TABLE I. The relative differential coefficients for the nuclear radius R as given by the compressible model for two different values of the compressibility coefficient. Also listed are the Coulomb energy E_c in units of mc^2, without correction for the small influence of nonuniform charge density; the index m of the relation $R_0=r_0A^{m/3}$; and the slope dZ/dA from Eq. (37). In an incompressible nuclear model both relative differential ratios are unity.

Z	A	E_c	E_0''	m	dZ/dA	$\frac{3A}{R}\frac{\partial R}{\partial Z}$	$\frac{3A}{R}\frac{\partial R}{\partial N}$
			(a) $E_0''=100Amc^2$				
24	50	179.8	5 000	0.953	0.430	1.248	0.814
44	100	489.1	10 000	0.936	0.394	1.386	0.750
62	150	854.2	15 000	0.928	0.367	1.495	0.713
80	200	1296.9	20 000	0.927	0.346	1.597	0.684
97	250	1773.8	25 000	0.928	0.329	1.688	0.663
			(b) $E_0''=50Amc^2$				
24	50	179.8	2 500	0.908	0.430	1.479	0.640
44	100	489.1	5 000	0.878	0.394	1.737	0.522
62	150	854.2	7 500	0.864	0.367	1.939	0.455
80	200	1296.9	10 000	0.863	0.346	2.126	0.404
97	250	1773.8	12 500	0.865	0.329	2.290	0.368

D. Evaluation of Particle Densities

The evaluation of the expansion coefficients of Eqs. (27) from Eq. (25) then is carried out by a procedure closely resembling Feenberg's.[28] Intermediate to this task is the calculation of partial derivatives of the standard nucleus energy, $E_0(R, N, Z)$, employing the relations (34) and the energy formula

$$E_0/mc^2=2A+[96|N-Z|+38(N-Z)^2/A], \tag{38}$$

in which the coefficient of the quadratic term has been chosen to accord with the same term in the semi-empirical mass formula.[33] The resulting expansion coefficients for the neutron and proton densities are listed in Table II, along with the densities near the surface of neutrons and protons, relative to their densities in the nuclear center.

E. Relevance of Nuclear Compressibility to Isotope Shifts

Having the particle densities we can now compare the isotope shifts predicted by the compressible and the incompressible nuclear model. For the latter, the isotope shift for two nuclides differing by one in mass number is given by (30) to be

$$\left(\frac{\delta(\Delta E)}{\delta N}\right)_{\text{incomp}}=\frac{BR^{2\rho}}{(2\rho+1)(2\rho+3)A}, \tag{39}$$

and the relative size of the isotope shifts in the two models is given by

$$\gamma=\left(\frac{\delta(\Delta E)}{\delta N}\right)_{\text{comp}}\Big/\left(\frac{\delta(\Delta E)}{\delta N}\right)_{\text{incomp}}$$

$$=3A\left\{[1+C_aa_P+C_bb_P]\frac{1}{R}\frac{\delta R}{\delta N}+\frac{C_a}{2\rho}\frac{\delta a_p}{\delta N}+\frac{C_b}{2\rho}\frac{\delta b_p}{\delta N}\right\}. \tag{40}$$

The evaluation of γ outlined in Table III makes it evident that the terms involving a_p, b_p and their derivatives are small and largely canceling in effect, so that the ratio γ is available in good approximation

[33] See, e.g., E. Fermi, *Nuclear Physics* (Notes by Orear, Rosenfeld, and Schluter) (University of Chicago Press, Chicago, 1950).

[34] We note that a simple attempt to introduce surface effects into our theory is of dubious value. If one makes the arbitrary assumption that the effects of the nuclear surface on the kinetic and potential energies of the system may be separated out of the nuclear Hamiltonian, the term proportional to $A^{\frac{2}{3}}$ in the semi-empirical mass formula (reference 33) may be chosen to represent the energy shift involved. Carrying through as before (reference 31) the calculation of how the actual radius is related to the standard radius R_0, one finds

$$R=R_0[1+(E_c-2E_s)/(E_0''+6E_s)], \tag{A}$$

with E_c and E_0'' as above, and $E_s=26A^{\frac{2}{3}}$ in units of mc^2. For nuclei to be stable against fission it is required [N. Bohr and J. A. Wheeler, Phys. Rev. **56**, 426 (1939)] that $E_c<2E_s$, and accordingly by (A) the actual radius is less than the "standard radius," R_0, the contraction by surface tension dominating the expansive Coulomb repulsion. The latter alone was considered in obtaining Eq. (31). On the other hand, the differential ratios derived from (A) have signs and magnitudes similar to the ratios given by (34), as derived from (31). In the present paper we have evaluated the simpler expressions (34) to obtain the differential coefficients required in (25) and (30).

TABLE II. Expansion coefficients for particle densities, and ratios of (density at surface) to (density at center) for protons and neutrons in the compressible nuclear model. Also listed are values (in units $mc^2=0.511$ Mev) of ΔE, the difference in energy between the compressible and incompressible models, a bilinear function of a_P, b_P, a_N, and b_N, which is minimized to determine these coefficients.

Z	N	a_P	b_P	a_N	b_N	ΔE	$n_P(R)/n_P(0)$	$n_N(R)/n_N(0)$
				(a) $E_0''=100Amc^2$				
24	50	−0.01785	0.00274	−0.00977	0.00079	−0.601	1.1217	1.0716
44	100	−0.02833	0.00519	−0.01612	0.00186	−2.618	1.1925	1.1160
62	150	−0.03502	0.00714	−0.02000	0.00277	−5.684	1.2355	1.1414
80	200	−0.04046	0.00887	−0.02322	0.00363	−10.014	1.2699	1.1617
97	250	−0.04457	0.01030	−0.02551	0.00434	−15.140	1.2948	1.1752
				(b) $E_0''=50Amc^2$				
24	50	−0.02075	0.00282	−0.01312	0.00088	−0.695	1.1479	1.1000
44	100	−0.03370	0.00548	−0.02263	0.00221	−3.096	1.2446	1.1738
62	150	−0.04188	0.00764	−0.02874	0.00342	−6.758	1.3044	1.2203
80	200	−0.04835	0.00959	−0.03376	0.00461	−11.897	1.3505	1.2577
97	250	−0.05310	0.01121	−0.03743	0.00563	−17.935	1.3825	1.2838

in the simple form

$$\gamma \simeq \frac{3A}{R}\frac{\delta R}{\delta N}. \tag{41}$$

The values of γ listed in Table III for two possible values of the compressibility reveal how directly the magnitude of the predicted isotope shift depends upon the assumed value of the compressibility coefficient. The trend of γ with A in Table III would be altered to yield more nearly constant values of γ in a theory in which surface effects were properly included, for the effective surface tension is relatively more important in light nuclei. As cited earlier[6,9] and as emphasized by Humbach,[10] the magnitudes of observed isotope shifts are about one-half the values predicted for an incompressible nucleus. In view of the present results, it seems likely that a major part, and perhaps all, of this discrepancy depends upon the neglect of nuclear compressibility.

A reduction in the nuclear radius would of course also reduce the isotope shifts predicted by Eqs. (6), (9), or (30). Recent studies of radiations from the μ-mesonic atom suggest[35] that the nuclear radius has been overestimated; however, similar studies by Schawlow and Townes[11] on radiations from inner electron transitions have confirmed the radius estimates employed in the present paper and seem more reliable as a guide for our analysis of the isotope shifts in *electronic* spectra. This information on x-ray levels also casts doubt on the reality of the Gaussian particle density distribution for heavy elements derived[36] by Gombas in a detailed statistical treatment of the nucleus.

Note added in proof:—Recent observations (to be published) by Hofstadter, Fechter, McIntyre and analyses (to be published) by Schiff of nuclear scattering of fast electrons suggest, however, a proton distribution peaked in the nuclear center, in qualitative agreement with the results of Gombas.

[35] L. N. Cooper and E. M. Henley, Bull. Am. Phys. Soc. **28**, No. 3, 56 (1953).
[36] P. Gombas, Acta ays. Acad. Sci. Hung. **2**, 223 (1952).

The value of E_0'' required to reduce γ to 0.5 is smaller by a factor of 1.5 or 2 than the values of E_0'' estimated[31] with the help of the virial theorem, which, however, are only order-of-magnitude estimates, uncertain by a factor of this size. If we have employed a value for the nuclear radius which is 10 or 15 percent too large, then Feenberg's values for E_0'' are more nearly consistent with the values required by the present analysis of isotope shifts. We should emphasize, moreover, that the artificial method of handling the nuclear surface which we have here adopted renders our treatment of the variations in nuclear radii and particle densities so crude that we can expect nothing better than order-of-magnitude estimates of nuclear compressibility to follow at present from our examination of isotope shifts. The present work does, nevertheless, suggest that the compressibility coefficient E_0'' is smaller than heretofore assumed, and indicates that when a self-consistent treatment of nuclear particle densities is available, the study of isotope shifts will

TABLE III. Calculation of the ratio, γ, of isotope shifts predicted according to Eq. (40) by the compressible and by the incompressible nuclear models. The perturbation coefficients, C_a and C_b, are defined in Eq. (29); and the isotopic variations of the expansion coefficients are defined by such statements as

$$\delta a_P/\delta N = a_P(Z, A+1) - a_P(Z, A).$$

Z	A	C_a	C_b	$10^4\frac{\delta a_P}{\delta N}$	$10^4\frac{\delta b_P}{\delta N}$	$\frac{3A}{R}\frac{\delta R}{\delta N}$	γ
				(a) $E_0''=100Amc^2$			
24	50	−0.7087	0.213	1.543	−0.058	0.814	0.816
44	100	−0.6917	0.200	1.243	−0.095	0.750	0.751
62	150	−0.6659	0.181	0.978	−0.098	0.713	0.713
80	200	−0.6256	0.154	0.809	−0.097	0.684	0.683
97	250	−0.5684	0.120	0.676	−0.092	0.663	0.660
				(b) $E_0''=50Amc^2$			
24	50	−0.7087	0.213	1.710	−0.057	0.640	0.640
44	100	−0.6917	0.200	1.389	−0.097	0.522	0.519
62	150	−0.6659	0.181	1.095	−0.103	0.455	0.449
80	200	−0.6256	0.154	0.899	−0.104	0.404	0.395
97	250	−0.5684	0.120	0.748	−0.099	0.368	0.357

provide one of the most direct and precise methods of measuring nuclear compressibility.

F. Aspherical Nuclei

In aspherical nuclei of deformation α (see Part III) the proton density variation from the average density is enhanced by the approximate factor $(1+\alpha)$ along the principal axis of distortion. This aspherical variation gives a negligible displacement in the *mean* value of predicted isotope shifts. The amplitude of the periodic variation in the ratio of predicted shifts to shifts predicted by the simple volume effect, discussed in Part III, will be augmented by roughly $(1+\frac{1}{3}\langle|\alpha|\rangle_{Av})$. As the average value of the magnitude of intrinsic deformation, $\langle|\alpha|\rangle_{Av}$, is of the order of 0.1, the correction to the amplitude of periodic variation is likewise unimportant.

V. CONCLUSION

In Part II we have noted that when the observed isotope shifts have been adjusted for electronic screening and compared with the isotope shifts predicted for constant density nuclei, after these have been corrected for the deficiency of first-order perturbation theory, three anomalies appear: (1) The average magnitudes of the observed shifts are about one-half the size of the predicted shifts; (2) the observed shifts show a somewhat periodic variation about the predicted shifts, and (3) the shifts between even and odd isotopes are by staggered rather than by equal steps.

In Part III the regular progression of nuclear deformations was reviewed, as deduced mainly from individual particle configuration theory, from observed quadrupole moments, and from the analysis of the first excited states of even-even nuclei. The dependence of isotope shift on nuclear shape was also derived, and the result was then at hand that the estimated progression of nuclear shapes apparently accounts for the regular fluctuations in size of isotope shifts, both as to the amplitude of the fluctuation and in the location of the nodal points. On this basis a prediction, as yet untested, is also made of isotope shift behavior beyond $_{82}$Pb (Fig. 3).

An examination of how nuclear shapes should change between odd and even isotopes likewise provides a reasonable explanation of the observed even-odd staggering of isotope shifts.

In Part IV the influence of nuclear compressibility and polarizability on the size of isotope shifts was investigated and found to alter predictions in a direction to account for the apparent discrepancy in average size of the isotope shifts. The analysis and comparison with experiment suggests that earlier estimates of nuclear compressibility have been too small, although the present treatment is inadequate to provide a reliable measure of the compressibility. A reduction in nuclear radius would also reduce the predicted isotope shift magnitudes but would conflict with x-ray measurements of the inner electron energy levels.

It therefore appears that the general pattern of isotope shifts is consistent with present ideas of nuclear structure, and provides an important source of specific information on the sizes, shapes, and charge distributions of nuclei.

We are grateful to Professor John A. Wheeler for his interest and comments regarding this work.

To Mr. Max Goldstein and Mr. Richard von Holdt, and their co-workers in Group T-1 of the Los Alamos Scientific Laboratory, we are indebted for assistance in the numerical work.

Energy Dependence of the Cross Section for the Reaction $C^{12}(\alpha,\alpha n)C^{11}$†

M. LINDNER AND R. N. OSBORNE
California Research and Development Company, Livermore, California
(Received May 4, 1953)

The cross section *vs* energy curve for the reaction $C^{12}(\alpha,\alpha n)C^{11}$ has been investigated from threshold to 380 Mev.

INTRODUCTION

THORNTON and Senseman[1] determined the energy dependence of the reaction $C^{12}(\alpha,\alpha n)C^{11}$ from threshold to 390 Mev on the 184-inch Berkeley cyclotron using the internal deflected alpha-particle beam. From the shape of the function these investigators concluded that the formation of C^{11} could be described by a single process. With a view to using carbon foils as an alpha-beam monitor, the experiments of these investigators were repeated, and the absolute cross section was established.

EXPERIMENTAL ARRANGEMENT

Polystyrene foils were spaced between aluminum absorbers, and bombarded on the 184-inch cyclotron.

TABLE I. Cross section for $C^{12}(\alpha,\alpha n)C^{11}$.

E	σ(mb)
380	51.0
380	45.0
307	54.0[a]
40	24.5
35	19.5
31	12.5
27	4.0
22	0.5

[a] This value was obtained by direct comparison with an aluminum monitor rather than from absolute electrical measurement.

The C^{11} thus formed was counted under conditions of known geometry on an end-window counter. For cross-section measurements, the absolute disintegration rate was determined on a proportional counter of 100 percent geometry. Two stack runs were made in the external deflected beam of the 184-inch cyclotron and the cross section at 380 Mev established by absolute electrical measurement of the beam intensity. A third stack run was made in the internal deflected helium ion beam of the 184-inch cyclotron. The cross section obtained in the latter case was compared with the previous runs by monitoring the beam with an aluminum foil placed in the stack, the cross section for the Al^{27}-$(\alpha,\alpha 2pn)Na^{24}$ reaction being known.[2] A fourth run was made on the 60-inch Berkeley cyclotron to establish the cross section near the threshold and to minimize the uncertainty in energy inherent in the runs on the 184-inch cyclotron.

The cross sections obtained from electrical measurements of the 184-inch and 60-inch cyclotron beam intensities are given in Table I.

The values at 40 Mev and below were obtained in one bombardment on the 60-inch cyclotron. The energy dependence of the cross section as shown in Fig. 1 was obtained by combining the absolute cross sections (Table I) with the relative cross sections measured by the stacked foil technique. It will be noted that a peak occurs at about 60 Mev and a minimum at about 100 Mev. This observation appears to be in contrast with that of Thornton and Senseman[1] and indicates the formation of C^{11} by more than one energy-dependent reaction.

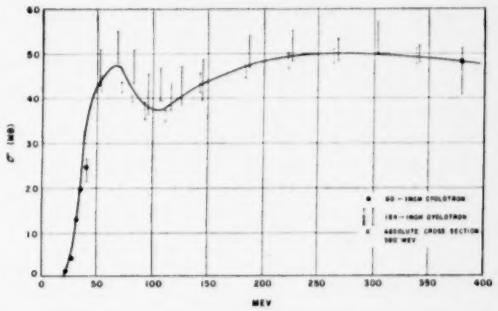

FIG. 1. Energy dependence of the cross section for the reaction $C^{12}(\alpha,\alpha n)C^{11}$.

† This work was performed under a U. S. Atomic Energy Commission contract.

[1] R. L. Thornton and R. W. Senseman, MDDC-1320 (unpublished). Manhattan District Declassified Report.

[2] M. Lindner and R. N. Osborne, U. S. Atomic Energy Commission Report MTA-13 (unpublished); Phys. Rev. **91**, 342 (1953).

Excited States of K^{40}†

W. W. Buechner, A. Sperduto, C. P. Browne, and C. K. Bockelman
Laboratory for Nuclear Science, Massachusetts Institute of Technology, Cambridge, Massachusetts
(Received June 1, 1953)

Using a magnetic spectrograph in conjunction with an electrostatic generator, the region of excitation in K^{40} has been studied up to 1 Mev, using the $K^{39}(d,p)K^{40}$ reaction. Excited states in K^{40} have been found at 0.032, 0.800, and 0.893 Mev, the Q value for the ground-state reaction being 5.576×0.010 Mev.

I. INTRODUCTION

INFORMATION regarding the excited states of potassium 40 has been obtained by Sailor,[1] who studied the $K^{39}(d,p)K^{40}$ reaction, and by Kinsey, Bartholomew, and Walker[2] who investigated the capture gamma rays from potassium when bombarded with slow neutrons. The highest-energy gamma ray which was observed in the latter experiments and which could be attributed to capture in K^{39} was 7.757 ± 0.008 Mev.[2,3] This would indicate a Q value of 5.531 for the ground state of the $K^{39}(d,p)K^{40}$ reaction, in reasonable agreement with the value of 5.48 ± 0.08 Mev, found by Sailor. However, it was pointed out[2] that, if this gamma ray did originate in a transition direct to the ground state of K^{40}, its intensity was considerably higher than would be expected on the basis of shell structure theory. According to this model, the odd proton in K^{39} is $d_{3/2}$, while in the ground state of K^{40}, an odd-odd nucleus, the odd proton and odd neutron are in $d_{3/2}$ and $f_{7/2}$ states, respectively. K^{39} in the ground state has a spin of 3/2 and even parity, and capture of a slow neutron should lead to a compound state in K^{40} with spin 1 or 2 and even parity. Since the ground state of K^{40} has a spin of 4 and odd parity, the gamma ray direct to this state involves a change in parity and would be either electric octopole ($E3$) or magnetic quadrupole ($M2$), depending on whether the capturing state had a spin of 1 or 2 units. In either case, such a gamma ray would be relatively low in intensity. Since the 7.757-Mev radiation was among the most intense of those observed, the suggestion has been made[3] that K^{40} may have a low-lying excited state of spin 2 and odd parity and that the gamma ray is associated with a transition to it rather than the ground state. In this case, the radiation would be of the electric dipole type regardless of whether the spin of the capturing state was 1 or 2. $E1$ gamma rays in this energy range are known to be strongly emitted.[4]

As a result of this suggestion, we have studied the region of excitation in K^{40} up to 1 Mev, using the $K^{39}(d,p)K^{40}$ reaction. In this region, both the gamma-ray measurements and the work of Sailor have shown an excited state at 0.80 Mev.

II. EXPERIMENTAL PROCEDURE

For these measurements, we have used the deuteron beam from a large, vertical, pressure-insulated electrostatic generator constructed for the Laboratory of Nuclear Science by Professor Trump and his associates. We have chosen to call this machine the MIT-ONR generator in order to distinguish it from the various other Van de Graaff generators at the Institute, and we wish to acknowledge our indebtedness to the Office of Naval Research which provided the funds necessary for its construction. We have used this generator for various nuclear investigations for somewhat over a year, and it has operated very successfully in the voltage range from 4 to 8.5 Mev.

After emerging from the generator, the ion beam is deflected by a magnet which can be rotated about a vertical axis so as to direct the beam towards a given portion of the target room. For the present measurements, the deuteron beam was deflected through 90 degrees so as to leave the magnet in a horizontal direction, the radius of curvature in the magnetic field being 60 centimeters. By means of adjustable shims at the entrance and exit faces of the magnet, the beam was focused on a set of defining slits placed 185 centimeters from the exit face of the magnet. The slit jaws were insulated and the currents collected on them were used to control a conventional voltage-stabilizing device using corona directed at the generator terminal. During these experiments, a slit opening of $\frac{1}{2}$ mm was used.

After passing through the exit slits of the 90-degree analyzer, the beam struck a target placed in the gap of a 180-degree annular magnetic spectrograph.[5] This spectrograph has been used in conjunction with another electrostatic generator for a number of previous studies of this type. In its new location, the spectrograph has been aligned so that the plane of the magnet gap is accurately at 90 degrees to the direction of the incident beam. Both visual measurements of the shadows cast by fine wires placed in the beam at the entrance and exit faces of the spectrograph and meas-

† This work has been supported by the joint program of the U. S. Office of Naval Research and the U. S. Atomic Energy Commission.
[1] V. L. Sailor, Phys. Rev. **77**, 794 (1950).
[2] Kinsey, Bartholomew, and Walker, Phys. Rev. **85**, 1012 (1952).
[3] B. B. Kinsey (private communication).
[4] B. B. Kinsey and G. A. Bartholomew, Physica **18**, 1112 (1952).
[5] Buechner, Strait, Stergiopoulos, and Sperduto, Phys. Rev. **74**, 1569 (1948).

urements made on the energies of particles scattered from targets containing nuclei of mass ranging from gold to lithium indicate that, for both proton and deuteron beams with energies between 4 and 8.5 Mev, the 90-degree Q equation for the reaction products can be used without appreciable error.

Power for both the 90-degree deflecting magnet and the 180-degree spectrograph is supplied by stabilized, three-phase, rectifier circuits designed by H. Enge. As measured by nuclear magnetic-resonance fluxmeters, the magnetic field in each analyzer is held constant to approximately 1 part in 100 000. For the field strengths encountered in the present experiments, the signal due to lithium was used.

In these experiments, both the energy of the incident beam and the energies of the reaction products were measured with the spectrograph, the former being determined from observations of the deuterons elastically scattered from various nuclei in the target. Since the values of the proton and lithium magnetic moment have been measured with high precision, it is possible to obtain the particle energies from a direct measurement of the radius of the curvature in the uniform magnetic field. However, a sufficiently accurate and more convenient procedure, using polonium alpha particles, has been employed in these measurements. The details of this calibration procedure and of the conversion of the observed data into nuclear reaction energies have been given in previous publications.[6,7] In the present experiments, the measured deflection of polonium alpha particles from a source placed near the target position has been measured for various values of the magnetic field, the field strengths being determined by the resonance fluxmeter. These measurements were used to determine the distance between the target position and an index mark placed on each plate after it is in position for exposure. The positions of the groups of particles detected on the track plates are measured with respect to the index mark. Since the particles recorded by the spectrograph have approximately the same radius of curvature, the important quantities in the measurements are the relative values of the magnetic fields at which the exposures for the reaction products and for the polonium alpha particles are made, the relative positions of the observed groups on the photographic plates, and the distance between the calibrating alpha-particle source and the position of the beam on the target.

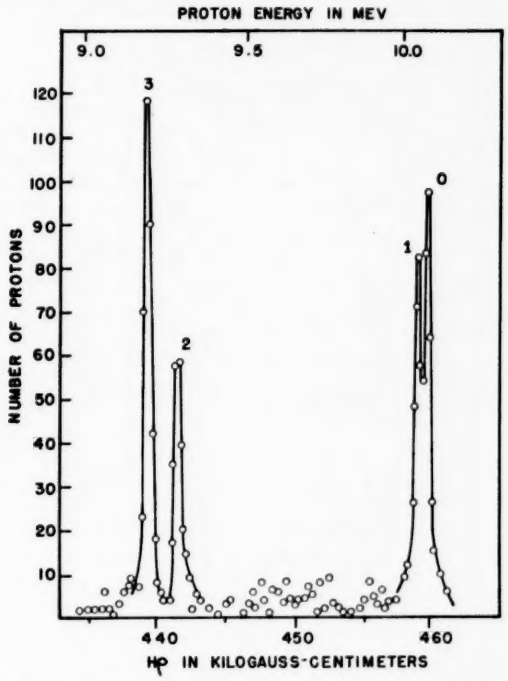

FIG. 1. Proton groups from potassium-iodide target bombarded with 5.00-Mev deuterons.

Since the frequencies corresponding to the various magnetic fields used can be measured to a high precision, the principal uncertainties in the measurements arise from the value used for the Hr of polonium alpha particles and from the uncertainity in the determination of the positions of the observed groups. As in our previous work,[7] we have assumed a value of 3.3159×10^5 gauss-centimeters, accurate to one part in 5000, for polonium alpha particles. In general, the locations of the various groups recorded can be determined to within 0.1 mm, the diameter of the path in the magnetic field being approximately 710 mm. The calibration used in this work has been checked by measuring the Q values of a large number of groups which have previously been determined both in this and in other laboratories. In all cases, the agreement has been highly satisfactory.

The targets used in the present work consisted of thin layers of various potassium-containing compounds evaporated onto very thin commercial gold foil. These foils were stiffened with a thin backing of Formvar. The targets appeared stable for beam currents as high as 0.5 microampere. Targets of KI, KBr, and KCN, both with and without the carbon content enriched in C^{13}, were studied.

III. RESULTS

Studies of the proton energy range corresponding to excitations in K^{40} from the ground state up to 1 Mev were made for deuteron energies of 4.76, 5.00, 5.16, and 5.65 Mev. The results of the 5.00-Mev bombardment of a KI target are shown in Fig. 1. The four proton groups shown were found from each of the targests used and at each of the bombarding energies. The con-

[6] Buechner, Strait, Sperduto, and Malm, Phys. Rev. **76**, 1543 (1949).

[7] Strait, Van Patter, Buechner, and Sperduto, Phys. Rev. **81**, 747 (1951).

TABLE I. $K^{39}(d,p)K^{40}$.

Excitation in K^{40}	Present work	Q values[a] Bartholomew + Kinsey[b]	Sailor[1]
0	5.576±0.010		5.48±0.08
0.032±0.002	5.544±0.010	5.531±0.009	
0.800±0.010	4.776±0.010	4.768±0.008	
0.893±0.010	4.683±0.010		4.67±0.09

[a] 2.226 Mev was used for converting from $K^{39}(n,\gamma)K^{40}$ to $K^{39}(d,p)K^{40}$.
[b] See reference 8.

stancy of the relative intensities of these groups as the target material was varied was used as a check on their assignment to potassium, made on the basis of their shift in energy as the incident deuteron energy was varied. The bombarding energies were purposely kept low in order to bring these groups within the range of the spectrograph. A check on the operation of the spectrograph at these field settings was obtained from measurements on the $C^{13}(d,p)C^{14}$ ground-state group observed from the KCN target enriched in C^{13} and from measurements on the ground state and first excited state from a thin aluminum target. At these bombarding energies, the C^{13} and Al groups occur in the middle of the region shown in Fig. 1. While the precision of the energy measurements made as a function of deuteron energy was not sufficient to determine whether the observed proton groups are due to K^{39} or K^{41}, it is assumed from their intensities and from Sailor's work[1] on normal potassium targets and on targets enriched with K^{41} that the groups originate from $K^{39}(d,p)K^{40}$. The Q values calculated for these groups are tabulated in Table I. Also included are the recent results of Bartholomew and Kinsey,[8] who found in addition to the 7.757-Mev gamma ray another having an energy of 6.994±0.007 Mev, which they ascribed to capture in K^{39}. Also included in the table are the results of Sailor[1] on $K^{39}(d,p)K^{40}$. The excitation energies in K^{40} included in the table are those determined in the present work. One of the advantages of observation at 90 degrees to the incident beam is that, aside from relativistic effects and the effects of the small angle about 90 degrees in which the particles are collected, the energy differences between the groups are independent of the input energy. The energy differences between groups 0 and 1 and between groups 2 and 3 and, hence, the spacings of the corresponding excited states could be determined with a greater precision than could be had by subtraction of the observed Q values.

The Q values listed are each the average of three or more separate determinations, the spread in the individual values in each case being 5 kilovolts or less. Three determinations, agreeing within 1 kev, were used for the spacing of the first level from the ground state. The spacing between the second and third levels was found to be 93±2 kev from four determinations which agreed within 2 kev.

It is clear from the table that, as suggested by Kinsey and his collaborators, the highest-energy gamma ray observed in the $K^{39}(n,\gamma)K^{40}$ reaction proceeds not to the ground state of K^{40} but rather to a low-lying excited state. As has recently been discussed,[8] it is probable that this state has a spin of 2 and odd parity and is analogous to the ground state of K^{42}. Although in both K^{40} and K^{42} the odd proton and odd neutron are in $d_{3/2}$ and $f_{7/2}$ states, respectively, the spin of K^{40} is 4 and K^{42} is 2. It thus appears that, unlike K^{42}, where the total angular momenta of the odd nucleons are antiparallel, the most stable configuration in K^{40} is not the antiparallel condition. It is of interest that the next lowest-energy gamma ray observed in the (n,γ) reaction is associated with the 0.80-Mev level, and no gamma ray was observed which corresponded to a transition to the level at 0.89 Mev.

We have also observed an intense group of lower energy corresponding to a level in K^{40} at approximately 2 Mev. Such a level is indicated both by the gamma-ray work and by the work of Sailor. This group appears to consist of two and possibly three components, but no accurate measurements on it have been made; a similar structure has been found in recent gamma-ray work.[8] In Fig. 1, a considerable background is seen between the pairs of proton groups. This background seems to be mainly due to the gold foil used as a backing material. Elastic-scattering measurements show that there are appreciable amounts of both copper and silver in the gold foil, and such a background has been observed from the foil alone.

[8] G. A. Bartholomew and B. B. Kinsey, Can. J. Phys. (to be published).

PHYSICAL REVIEW VOLUME 91, NUMBER 6 SEPTEMBER 15, 1953

Fluctuations and Irreversible Processes*

L. ONSAGER, *Sterling Chemistry Laboratory, Yale University, New Haven, Connecticut*

AND

S. MACHLUP, *Sloane Physics Laboratory, Yale University, New Haven, Connecticut,*

and

Bell Telephone Laboratories, Murray Hill, New Jersey

(Received May 13, 1953)

The probability of a given succession of (nonequilibrium) states of a spontaneously fluctuating thermodynamic system is calculated, on the assumption that the macroscopic variables defining a state are Gaussian random variables whose average behavior is given by the laws governing irreversible processes.

This probability can be expressed in terms of the dissipation function; the resulting relation, which is an extension of Boltzmann's principle, shows the statistical significance of the dissipation function. From the form of the relation, the principle of least dissipation of energy becomes evident by inspection.

1. INTRODUCTION

THE connection between the theory of irreversible processes and the spontaneous fluctuations of thermodynamic variables of equilibrium systems was discussed in two earlier papers by one of us.[1] There, the fluctuation theory was brought in to prove a theorem for irreversible processes, the reciprocal relations: the symmetry of the matrix of coefficients of the set of linear equations relating thermodynamic "forces" and "fluxes." The connection was made by postulating that the decay of a system from a given nonequilibrium state produced by a spontaneous fluctuation obeys, *on the average*, the (empirical) law for the decay from the same state back to equilibrium, when it has been produced by a constraint which is then suddenly removed.

The present paper will establish a further connection between the two fields, along the lines suggested in Sec. 5 of RRIP II. We add the following to the assumptions made there: that the (fluctuating) thermodynamic variables be *Gaussian* random variables. We are then in a position to calculate the probability that a system, in undergoing spontaneous thermal fluctuation, passes through a given set of thermodynamic states at given instants. Two kinds of coefficients will enter this probability expression: those (s_{ij}) which give the entropy of a given (nonequilibrium) state as a function of the chosen set of thermodynamic variables, and those (R_{ij}) which give the rates of the irreversible processes, i.e., the rates of change of the thermodynamic variables of state when the state itself is known.

The argument proceeds somewhat as follows: if we are interested in only a single instant, the probability of a given state Γ is given by Boltzmann's principle,

$$k \log \text{Prob}(\Gamma) = S(\Gamma) + \text{const}, \qquad (1\text{-}1)$$

which relates the probability of finding the system in the state Γ to the entropy of Γ. If we are interested in two instants widely separated in time, the probability of given states at each instant is equal to the product of the individual probabilities. A long time lapse makes the states statistically independent.[2] Hence the joint probability of the succession is related to the sum of the two entropies. But if the time lapse is not long, the states will be statistically correlated. It is precisely the laws for irreversible behavior which tell us the correlations, by virtue of the postulate connecting these laws with the average course of fluctuations.

These correlations, together with the means (equilibrium values) of the fluctuating variables, are sufficient to determine the joint probability for two instants, by virtue only of the assumption that the fluctuations are Gaussian processes. If we have the correlations for all pairs of instants, the joint probability for any number of instants is determined.

If the thermodynamic variables are properly chosen (see Sec. 2), they also turn out to be Markoffian random variables. This means that the statistics of the future of the system do not depend on its past but only on its present state. The "proper choice" of thermodynamic variables actually implies limitations on the type of systems for which our treatment is valid. The proof of the reciprocal relations (RRIP I and II) was based on the hypothesis of microscopic reversibility, which we retain here. This excludes rotating systems (Coriolis forces) and systems with external magnetic fields. The assumption of Gaussian random variables is also restrictive: Our system must consist of many "sufficiently" independent particles, and equilibrium must be stable at least for times of the order of laboratory measuring times. This is also required in order that

* Much of the work reported in this paper appears in more detail in a dissertation by one of us (S.M.), presented to the Faculty of the Graduate School of Yale University (1952) in partial fulfillment of the requirements for the Ph.D. degree.

[1] L. Onsager, "Reciprocal Relations in Irreversible Processes," Phys. Rev. **37**, 405 (1931); **38**, 2265 (1931). Henceforth referred to as RRIP I and II.

[2] This statement is, of course, charged with meaning, and requires elaborate precautions about ergodicity, etc. It may be said to hold for system which "forget" their initial states in a "reasonably" short time. It is, however, precisely the choice of time scale that matters. In a sufficiently long time, all physical systems "forget."

we can consider our systems as "aged"—left alone long enough to have "forgotten" their initial states.

The mathematics, then, will involve the treatment of stationary Gaussian Markoff processes in a finite number of variables, which is by now standard.[3] What we believe to be original, in this domain, is the introduction of variational expressions of the type of Eq. (4-7) into the description of statistical distributions. The physics—the theory of thermodynamic fluctuations, and the theory of irreversible processes—involves the concepts dealt with in RRIP (see especially II, pp. 2265–2274, also the review article by Casimir[4]), using the methodological foundation for fluctuation theory given by Einstein.[5]

In RRIP, a *dissipation function* was defined, a quadratic form in the "fluxes" which gives the rate of entropy production for irreversible processes. The calculation of the probability for a preassigned succession of thermodynamic states yields a statistical interpretation of the dissipation function.[6]

As is well known, distribution in function space can not be described by a density, but its projection upon any finite number of dimensions can be so described.[7] Accordingly, it makes sense to ask for the probability that a function—or a finite set of functions—assume values within specified limits at an arbitrarily selected finite set of successive instants. We shall arrive at a description of the probability distribution for "fluctuation paths" in terms of an *auxiliary functional*, such that the maximum of this functional, for a given finite set of specifications, determines the appropriate probability density in a space, whose dimensions correspond to the separate specifications of fluctuating functions at each selected instant.

2. IRREVERSIBLE PROCESSES

The irreversible processes we consider are of the type treated in RRIP II: flows of matter, heat, and electricity whose rates are linearly related to the corresponding *thermodynamic forces*—concentration gradients, temperature gradients emf's. The extension to systems with chemical reactions and local relaxation effects usually involves simply a change of language. We are thinking of closed systems, systems displaced from equilibrium and then "released" and allowed to return. But again, the extension to open systems (and steady states) is purely formal.

The thermodynamic *state* of a system will be defined by a set of extensive variables $\alpha_1, \alpha_2 \cdots \alpha_n$, quantities like volume, energy, mass of substance, electric charge. We choose extensive variables because of the conceptual difficulties encountered in speaking of fluctuations of intensive quantities. But defining thermodynamic variables at all for a system not in equilibrium requires some sophistication. The standard device is to assume that the system is built up of small sub-systems, each considered in "local equilibrium." This fails far from equilibrium and in systems undergoing such slow relaxations that the concept of equilibrium itself is hard to define.[8] It should be recalled that the thermodynamic functions (e.g., entropy) can be empirically measured only for states—or sets of sub-system states—which are accessible by reversible manipulations.

One may formulate rules for choosing α variables for which the theory here developed will be applicable:

(1) They must be macroscopic variables, i.e., thermodynamically measurable, and must refer to sub-systems containing a large number of molecules. This is always necessary for thermodynamics.

(2) On a kinetic model, they must be algebraic sums of molecular variables. Their fluctuations will then have Gaussian distributions about the equilibrium values, by virtue of a kind of Central Limit Theorem. The rule also eliminates pathological variables (e.g., nonadditive functions of extensive variables).

(3) They must be even functions of those molecular variables which are odd functions of the time, like molecular velocities. This means that a reversal of the sense of time will not change their values and is necessary for the assumption of microscopic reversibility.

We shall assume that the thermodynamic functions are completely determined by specification of the α's. Rule (3) implies that the kinetic energy of the flows is negligible, since this depends on velocity-type variables. The case in which inertia (and hence kinetic energy) is important—in which time derivatives of the α's enter into the thermodynamic functions—will be treated in a subsequent paper.[9]

Thus the *entropy* is a function of the α's:

$$S = S(\alpha_1 \cdots \alpha_n) = S(\boldsymbol{\alpha}).$$

Its maximum (equilibrium) value is denoted by S_0, and the α's will be redefined to vanish for the equilibrium state:

$$S_0 = S(0, \cdots 0).$$

The tendency of the system to seek equilibrium is measured by the *thermodynamic forces*,

$$X_i = \partial S / \partial \alpha_i, \tag{2-1}$$

[3] See, for instance, M. C. Wang and G. E. Uhlenbeck, Revs. Modern Phys. **17**, 323 (1945) or J. E. Moyal, J. Roy. Statist. Soc. **B11**, 150 (1949), for applications in physics. The recent appearance of J. L. Doob, *Stochastic Processes* (J. Wiley and Sons, New York, 1953) makes unnecessary further reference to the mathematical literature.

[4] H. B. G. Casimir, Revs. Modern Phys. **17**, 343 (1945).

[5] A. Einstein, Ann Physik **33**, 1275 (1910), especially Sec. I, "General Matters Relating to Boltzmann's Principle."

[6] In RRIP II, Sec. 5, a statistical interpretation is suggested in terms of the joint probability for a pair of instants closely spaced in time. An extension of this type of differential expression, using Markoff methods (Fokker-Planck equation), has recently been made by N. Hashitsume, Progr. Theoret. Phys. **8**, 461 (1952).

[7] A. N. Kolmogoroff, *Foundations of the Theory of Probability* (Chelsea Publishing Company, New York, 1950), Chap III, Sec. 4, proves that the set of all finite-dimensional distribution functions uniquely determines the probability functions for all Borel sets in the infinite-dimensional space.

[8] P. W. Bridgman, Revs. Modern Phys. **22**, 56 (1950).

[9] S. Machlup and L. Onsager, following paper [Phys. Rev. **91**, 1512 (1953).

"restoring forces," which evidently vanish with the α's.[10]

The fluxes (of matter, heat, electricity) are measured by the time derivatives of the α's. The essential physical assumption about the irreversible processes is that they are linear; i.e., that the fluxes depend linearly on the forces that "cause" them:

$$\Sigma_j R_{ij}\dot{\alpha}_j = X_i, \quad i=1\cdots n; \tag{2-2}$$

or

$$\Sigma_j L_{ij} X_j = \dot{\alpha}_i, \tag{2-3}$$

where the matrices $\mathbf{L}$ and $\mathbf{R}$ are mutually reciprocal. These equations express, for instance, Ohm's law for electrical conduction, Fourier's law for heat conduction, Fick's law for diffusion, and the extension of these laws to interacting flows, e.g., anisotropic conduction (heat, electricity), thermoelectric effects, thermal diffusion. For systems for which microscopic reversibility holds (to which this work is confined), we have the *reciprocal relations*

$$R_{ij} = R_{ji} \big[\mathbf{R} = \mathbf{R}_{tr}\big], \tag{2-4}$$

where the subscript *tr* means transpose.

The rate of production of entropy is

$$\dot{S} = \Sigma_j (\partial S/\partial \alpha_j)\dot{\alpha}_j = \Sigma_j X_j \dot{\alpha}_j, \text{ by Eq. (2-1)} \tag{2.5}$$

$$= \Sigma_{ij} R_{ij}\dot{\alpha}_i\dot{\alpha}_j, \text{ by Eq. (2-2)} \tag{2-6}$$

$$= \Sigma_{ij} L_{ij} X_i X_j, \text{ by Eq. (2-3)}. \tag{2-7}$$

The quadratic form in the fluxes,

$$\Phi(d\boldsymbol{\alpha}/dt, d\boldsymbol{\alpha}/dt) = \tfrac{1}{2}\Sigma_{ij} R_{ij}\dot{\alpha}_i\dot{\alpha}_j, \tag{2-8}$$

the dissipation function, acts as a potential for the thermodynamic forces. Its specification is therefore equivalent to knowledge of the phenomenological equations. The corresponding function of the forces,

$$\Psi(\mathbf{X}, \mathbf{X}) = \tfrac{1}{2}\Sigma_{ij} L_{ij} X_i X_j, \tag{2-9}$$

has a similar property, but it should be noticed that it is a function of the *state*, whereas the numerically equal $\Phi(d\boldsymbol{\alpha}/dt, d\boldsymbol{\alpha}/dt)$ is a function of its rate of change.

If we expand the entropy in a Taylor series about equilibrium, we have

$$S = S_0 - \tfrac{1}{2}\Sigma_{ij} s_{ij}\alpha_i\alpha_j + \text{higher terms}. \tag{2-10}$$

Neglect of the higher terms means the assumption that fluctuations are Gaussian: for Boltzmann's principle states that the logarithm of the probability of a given fluctuation is proportional to its entropy, or

$$\text{Prob.}\{\boldsymbol{\alpha}\} \propto \exp(S/k) \propto \exp\left[-\left(\frac{1}{k}\tfrac{1}{2}\Sigma_{ij} s_{ij}\alpha_i\alpha_j\right)\right]. \tag{2-11}$$

The thermodynamic forces then become linear restoring forces,

$$X_i = -\Sigma_j s_{ij}\alpha_j, \tag{2-12}$$

and the phenomenological laws (2-2) become

$$\Sigma_j (R_{ij}\dot{\alpha}_j + s_{ij}\alpha_j) = 0. \tag{2-13}$$

3. FLUCTUATIONS

Stochastic Processes

The deterministic Eqs. (2-2) are modified to include fluctuations by the addition of a *random force* term,

$$\Sigma_j R_{ij}\dot{\alpha}_j = X_i + \epsilon_i, \tag{3-1}$$

and thereby become stochastic equations. For the present, the only specification on the statistics of the ϵ's is that they have zero means. Another way of looking at the equations is to call the rhs of (3-1) random forces with means X_i.

We shall be concerned with the path of the α's in time under the "influence" of these random forces. Our aim is to calculate the probability of "any path." We must, therefore, define a probability measure for paths. For simplicity we consider first a single variable α, and ask for the probability of a path $\alpha(t)$ over some finite interval of t. To obtain a nonzero probability, we have to phrase our question: Given a *set* of functions over the given interval, what is the probability that the spontaneously fluctuating variable α is given by a function of this set during the interval? There is a difficulty in specifying the functions: each function is specified by an infinite number of coordinates. If we confine ourselves to well-behaved functions and a finite interval, a denumerable infinity will suffice, e.g., the value of the function at all rational points of t, or all the Fourier coefficients. But the probability of an event which is specified by an infinite number of specifications is always zero, unless the set of specifications is "asymptotically trivial." So we must confine ourselves to specifying a finite number of coordinates.

As far as observation is concerned, this is quite sufficient. For although we may obtain a "continuous record" from a recording instrument, corresponding to an infinite number of observations, every instrument essentially takes a time average over a finite interval, which may be short compared to the relaxation times of the irreversible process, but is always long compared to the mean collision times of the molecules. The essential point is that we must be free to choose which coordinates to specify, i.e., at what instant to perform an observation.

We shall use the following notation: for p instants $t_1 < t_2 \cdots < t_p$ we write the cumulative distribution function (c.d.f.)

$$F_p\begin{pmatrix} \alpha^{(1)} & \alpha^{(2)} & & \alpha^{(p)} \\ & & \cdots & \\ t_1 & t_2 & & t_p \end{pmatrix} = \text{Prob.}\{\alpha(t_k) \le \alpha^{(k)}, k=1\cdots p\}. \tag{3-2}$$

[10] Why this particular definition? It gives Eq. (2-5) the desired form: the rate of dissipation is a sum of products of forces and fluxes. Note that the X's are functions of state, i.e., of the α's.

Such functions must be additive set functions satisfying the usual consistency relations for c.d.f.'s.[11]

We define a stationary process as one whose c.d.f. is invariant against an arbitrary shift of the time axis:

$$F_p\begin{pmatrix}\alpha^{(1)} & \cdots & \alpha^{(p)}\\ t_1 & & t_p\end{pmatrix}=F_p\begin{pmatrix}\alpha^{(1)} & & \alpha^{(p)}\\ t_1+\tau & & t_p+\tau\end{pmatrix}, \text{ for any } \tau. \quad (3\text{-}3)$$

Physically, this describes an *aged* system, a system that has been left alone long enough that any initial conditions have "worn off," or "been forgotten." In dealing with fluctuations, we shall always make this assumption of stationarity. This amounts to a strong form of the statistical interpretation of equilibrium. Thus we consider entropy creation as loss of information: a dissipative system forgets its past.

Pictorially, a function F_p tells the probability that the path $\alpha(t)$ lie below the "barriers" $\alpha^{(1)}\cdots\alpha^{(p)}$ at the corresponding instants $t_1\cdots t_p$. Alternatively, one will ask for the probability that the path pass through narrow "gates" of width $\Delta\alpha^{(k)}$:

$$\sum_{\mu_1\cdots\mu_p=0}^{1}(-)^q F_p\begin{pmatrix}\alpha^{(1)}+\mu_1\Delta\alpha^{(1)} & \cdots & \alpha^{(p)}+\mu_p\Delta\alpha^{(p)}\\ t_1 & \cdots & t^p\end{pmatrix}$$
$$\equiv f_p\begin{pmatrix}\alpha^{(1)}\cdots\alpha^{(p)}\\ t_1\cdots t_p\end{pmatrix}\Delta\alpha^{(1)}\cdots\Delta\alpha^{(p)}, \quad (3\text{-}4)$$

where

$$q=p-\sum_{k=1}^{p}\mu_k.$$

The function f_p is a probability density function (p.d.f.) and will henceforth be used with the tacit assumption that it exists.

Any finite number of gates may be erected, specifying the path to an arbitrary degree of precision in any finite interval.

The conditional probability function for the $(p+1)$th event given the previous p,

$$F_1\left(\begin{matrix}\alpha^{(p+1)}\\ t_{p+1}\end{matrix}\middle|\begin{matrix}\alpha^{(1)}\cdots\alpha^{(p)}\\ t_1\cdots t_p\end{matrix}\right)$$
$$=\text{Prob}\{\alpha(t_{p+1})=\alpha^{(p+1)}|\alpha(t_k)=\alpha^{(k)},\ k=1\cdots p\}, \quad (3\text{-}5)$$

is defined by the relation:

$$F_{p+1}\begin{pmatrix}\alpha^{(1)}\cdots\alpha^{(p+1)}\\ t_1\cdots t_{p+1}\end{pmatrix}$$
$$=\int_{-\infty}^{\alpha^{(1)}}(p\text{-fold})\int_{-\infty}^{\alpha^{(p)}}F_1\left(\begin{matrix}\alpha^{(p+1)}\\ t_{p+1}\end{matrix}\middle|\begin{matrix}x^{(1)}\cdots x^{(p)}\\ t_1\cdots t_p\end{matrix}\right)$$
$$\times dF_p\begin{pmatrix}x^{(1)}\cdots x^{(p)}\\ t_1\cdots t_p\end{pmatrix}. \quad (3\text{-}6)$$

[11] See, for example, Harald Cramèr, *Mathematical Methods of Statistics* (Princeton University Press, Princeton, 1946).

We define a *Markoff process* as one whose conditional probabilities are independent of all but the immediately preceding instant:

$$F_1\left(\begin{matrix}\alpha^{(p+1)}\\ t_{p+1}\end{matrix}\middle|\begin{matrix}\alpha^{(1)} & \cdots & \alpha^{(p)}\\ t_1 & & t_p\end{matrix}\right)=F_1\left(\begin{matrix}\alpha^{(p+1)}\\ t_{p+1}\end{matrix}\middle|\begin{matrix}\alpha^{(p)}\\ t_p\end{matrix}\right). \quad (3\text{-}7)$$

Intuitively: the system has a short memory.

For a Markoff process, Eqs. (3-6) and (3-7) give

$$f_p\begin{pmatrix}\alpha^{(1)} & \cdots & \alpha^{(p)}\\ t_1 & & t_p\end{pmatrix}=f_1\left(\begin{matrix}\alpha^{(p)}\\ t_p\end{matrix}\middle|\begin{matrix}\alpha^{(p-1)}\\ t_{p-1}\end{matrix}\right)$$
$$\times f_1\left(\begin{matrix}\alpha^{(p-1)}\\ t_{p-1}\end{matrix}\middle|\begin{matrix}\alpha^{(p-2)}\\ t_{p-2}\end{matrix}\right)\cdots f_1\left(\begin{matrix}\alpha^{(2)}\\ t_2\end{matrix}\middle|\begin{matrix}\alpha^{(1)}\\ t_1\end{matrix}\right)f_1\left(\begin{matrix}\alpha^{(1)}\\ t_1\end{matrix}\right). \quad (3\text{-}8)$$

For the physical systems considered, the last factor in this product, the one-gate p.d.f., is known from the entropy function by Boltzmann's principle, Eq. (2-11). Thus, in view of the stationarity, all that is needed for the distribution function for an arbitrary number of gates is to evaluate the conditional p.d.f.,

$$f_1\left(\begin{matrix}\alpha^{(2)}\\ t+\tau\end{matrix}\middle|\begin{matrix}\alpha^{(1)}\\ t\end{matrix}\right), \quad (3\text{-}9)$$

which is independent of t: The p-gate problem reduces to the two-gate problem.

All of the above can be extended without modification to the case of several variables.

We shall want to know what form Eqs. (3-1) take for a Markoff process. The result is that the random force terms ϵ_i are purely random "functions"; i.e., values of the ϵ_i at different times are wholly uncorrelated.

$$\langle\epsilon(t)\epsilon(t+\tau)\rangle=0, \quad \tau\neq 0.$$

Such quantities are, to be sure, mathematical freaks: nowhere defined, not even square-integrable, but the seeming difficulties arise only from our inappropriate choice of differential notation, rather than a more rigorous one using finite differences. Only the latter, of course, are accessible to physical observation, since successive measurements cannot be arbitrarily close in time.

A *Gaussian* stochastic process is one whose p.d.f. is a multivariate Gaussian distribution. We shall make the assumption that fluctuations are Gaussian processes. The physical basis for this lies in Rule 2 (Sec. 2) for choosing the α variables: if molecular variables are "sufficiently" independent (weakly coupled), algebraic sums of them will behave as Gaussian random variables. Mathematically, on the other hand, we know that a Gaussian process will always be a good approximation, in the following sense: There is a theorem (Khinchin-Cramèr theorem[12]) which states that for every stochastic (L^2) process, there exists a Gaussian process

[12] A. Khinchin, Math. Ann. **109**, 604 (1933).

which is unitarily equivalent to it, meaning that all first and second moments are equal for the two processes.

The Regression of Fluctuations

The postulate on which the proof of the reciprocal relations theorem (RRIP II) was based may be stated: the average regression of fluctuations from a given nonequilibrium state will obey the same laws as the corresponding irreversible processes.

By the average regression of, say α_i, from the state $\boldsymbol{\alpha}'$ is meant the conditional mean,

$$\langle \alpha_i, t+\tau \,|\, \boldsymbol{\alpha}', t\rangle_{Av} = \int \cdots \int \alpha_i f_1\left(\begin{matrix}\boldsymbol{\alpha} \\ t+\tau\end{matrix}\middle|\begin{matrix}\boldsymbol{\alpha}' \\ t\end{matrix}\right) d\boldsymbol{\alpha}, \quad (3\text{-}10)$$

of α_i at time $t+\tau$ *given* that the state $\boldsymbol{\alpha}$ (the values of all the α's) at time t was $\boldsymbol{\alpha}'$. The postulate asserts that this quantity obeys the phenomenological laws (2-2.)

Intuitively, this states that, as far as the average behavior is concerned, it does not matter whether a state was the result of a spontaneous fluctuation or of an imposed constraint. It may sound "obviously true." Callen and Greene,[13] for instance, do not even dignify it by the term postulate. It is, however, very strong: for a Gaussian process, it can be shown to be equivalent to the Markoff assumption. We can see this intuitively by stating the postulate: the system does not remember how it got to the given state.

The essence of the proof is given by Doob.[14] It is easily shown that the average regressions, together with the one-gate distribution [known from Boltzmann's principle, Eq. (2-11)], completely determine the statistics of a stationary Gaussian process. We have a stationary Gaussian process whose average regressions obey a system of linear differential equations of first order with constant coefficients (2-13). Then the covariance matrix $\mathbf{A}(\tau) \equiv \langle \boldsymbol{\alpha}_{t\tau}(t)\boldsymbol{\alpha}(t+\tau)\rangle$ has the "translation operator" property,

$$\mathbf{A}(\tau_1)\mathbf{A}(\tau_2) = \mathbf{A}(\tau_1+\tau_2), \quad (3\text{-}11)$$

which is a sufficient condition for the process to be Markoffian.

We now have an answer to the question "How do you know you have taken enough variables (enough measurements on the system) for it to be Markoffian?" (Example: a two-mesh *RC* circuit is Markoffian in the two mesh charges, but not in any single variable.) If we accept the Gaussian assumption and the postulate about the average regressions, then the condition that the irreversible behavior of the system be given by equations of the form (2-2) is sufficient for the Markoff property. It is important to realize that this "prediction property" of the phenomenological laws depends on the assumption (Sec. 2) that enough α's have been taken to determine the entropy completely.

[13] H. B. Callen and R. F. Greene, Phys. Rev. **86**, 702 (1952); **88**, 1387 (1952).

[14] Reference 3, V Sec. 8.

4. GAUSSIAN MARKOFF PROCESS

Single Variable

We again consider a single variable α, obeying the equation

$$R\dot{\alpha} + s\alpha = \epsilon \quad (4\text{-}1)$$

(rhs purely random: α is Markoffian). We have for the conditional p.d.f.:

$$f_1\left(\begin{matrix}\alpha^{(2)} \\ t+\tau\end{matrix}\middle|\begin{matrix}\alpha^{(1)} \\ t\end{matrix}\right) = (2\pi)^{-\frac{1}{2}}\frac{s}{k}(1-e^{-2\gamma\tau})^{-\frac{1}{2}} \times \exp\left\{-\frac{1}{2}\frac{s}{k}\frac{[\alpha^{(2)}-e^{-\gamma\tau}\alpha^{(1)}]^2}{(1-e^{-2\gamma\tau})}\right\}, \quad (4\text{-}2)$$

(where $\gamma = s/R$), as is verified by inspection: it gives the right one-gate distribution (2-11, let $\tau\to\infty$) and the right average regression ($\alpha^{(1)}e^{-\gamma\tau}$). The normalization factor will henceforth be omitted to save writing.

This formula, together with Eq. (3-8), constitutes the solution to the problem of finding the probability of any path. The purpose of this paper is to put the formula into a particularly interesting form.

Let us divide the interval $(t, t+\tau)$ into p small, equal sub-intervals, i.e., introduce $p-1$ new gates at instants $t_1 = t$, $t_2 = t+\Delta\tau$, $\cdots$, $t_{p+1} = t+\tau = t+p\Delta\tau$. Then we have

$$f_1\left(\begin{matrix}\alpha^{(p+1)} \\ t_{p+1}\end{matrix}\middle|\begin{matrix}\alpha^{(1)} \\ t_1\end{matrix}\right) = \int (p-1)\text{-fold} \int f_1\left(\begin{matrix}\alpha^{(p+1)} \\ t_{p+1}\end{matrix}\middle|\begin{matrix}\alpha^{(p)} \\ t_p\end{matrix}\right)\cdots \times f_1\left(\begin{matrix}\alpha^{(2)} \\ t_2\end{matrix}\middle|\begin{matrix}\alpha^{(1)} \\ t_1\end{matrix}\right) d\alpha^{(2)}\cdots d\alpha^{(p)}. \quad (4\text{-}3)$$

This is the Chapman-Kolmogoroff relation,[15] valid for all Markoff processes. Evidently there is no limit to the number $(p-1)$ of gates which are "integrated out." It can be made large enough ($\Delta\tau$ small enough) so that the stochastic differential equation (4-1) is well approximated by the stochastic difference equation

$$\alpha^{(k)} - \lambda\alpha^{(k-1)} = y^{(k)}, \quad (4\text{-}4)$$

where $\lambda = 1-\gamma\Delta\tau$ and $y^{(k)} = \epsilon(t_k)\cdot\Delta\tau/R$. Supposing the y's to have Gaussian distributions with mean zero and variance σ_y^2, (4-3) becomes[16]

$$f_1\left(\begin{matrix}\alpha^{(p+1)} \\ t_{p+1}\end{matrix}\middle|\begin{matrix}\alpha^{(1)} \\ t_1\end{matrix}\right) \propto \int (p-1)\text{-fold} \times \int \exp\left\{-\frac{1}{2\sigma_y^2}[(\alpha^{(p+1)}-\lambda\alpha^{(p)})^2 + \cdots + (\alpha^{(2)}-\lambda\alpha^{(1)})^2]\right\} d\alpha^{(1)}\cdots d\alpha^{(p)}. \quad (4\text{-}5)$$

[15] A. Kolmogoroff, Math. Ann. **104**, 415 (1931).

[16] This is stronger than assuming α to be a Gaussian process and is not necessary for the proof of (4-7).

If the integrations are performed in succession, we arrive again at (4-2). We now notice that each integration may be replaced by taking the minimum with respect to the corresponding variable in the exponent, obtaining

$$f_1\begin{pmatrix}\alpha^{(p+1)}\\ t_{p+1}\end{pmatrix}\begin{matrix}\alpha^{(1)}\\ t_1\end{matrix}\Big) \propto \exp -\frac{1}{2\sigma_y^2}\big[(\alpha^{(p+1)}-\lambda\alpha^{(p)})^2+\cdots + (\alpha^{(2)}-\lambda\alpha^{(1)})^2\big]_{\min},$$

with respect to $\alpha^{(2)}, \cdots \alpha^{(p)}$; (4-6)

what has been done is to replace an "average value" by a "most probable value." For Gaussian distributions these are identical.

As p is increased, the sum in the exponent becomes an integral. The value of the integral is specified by the condition that the integral be a minimum subject to given values of α at the end points. Reverting to differential notation, (4-6) becomes

$$f_1\begin{pmatrix}\alpha^{(p+1)}\\ t_{p+1}\end{pmatrix}\begin{matrix}\alpha^{(1)}\\ t_1\end{matrix}\Big) \propto \exp\left\{-\frac{1}{4}\frac{1}{k}\left(\int_{t_1}^{t_{p+1}} R[\dot\alpha(t)+\gamma\alpha(t)]^2dt\right)_{\min}\right\},$$

subject to $\alpha(t_1)=\alpha^{(1)}, \cdots, \alpha(t_{p+1})=\alpha^{(p+1)}$. (4-7)

The direct verification of this formula—seeing that it gives the correct average regression and one-gate p.d.f.—is simpler and more general than the above "synthetic" proof. To find the regressions we again utilize the identity of means and modes of Gaussian distributions. The regression from the value $\alpha^{(1)}$ will therefore be given by the condition

$$f_1\begin{pmatrix}\alpha^{(2)}\\ t_2\end{pmatrix}\begin{matrix}\alpha^{(1)}\\ t_1\end{matrix}\Big) = \max, \qquad (4\text{-}8)$$

where the variation is with respect to $\alpha^{(2)}$. As the integrand in (4-7) is always positive or zero, so is the integral. If it can take the value zero, this is its minimum. But this is possible only if the integrand is everywhere zero, i.e., the condition for a minimum is

$$\dot\alpha+\gamma\alpha=0, \qquad (4\text{-}9)$$

which is recognized as the Eq. (2-13) for the average regression. As the initial condition $\alpha(t_1)=\alpha^{(1)}$ also agrees, (4-7) gives the correct regression.

The one-gate distribution is obtained from the conditional p.d.f. by taking $t_1=-\infty$ and $\alpha^{(1)}=0$. (The aged system certainly was at equilibrium some time long ago.) We want to prove that

$$f_1\begin{pmatrix}\alpha^{(2)}\\ t_2\end{pmatrix}\begin{matrix}0\\ -\infty\end{matrix}\Big) \propto \exp\left[-\frac{1}{k}\frac{1}{2}s(\alpha^{(2)})^2\right]. \qquad (2\text{-}11)$$

Letting $\mathfrak{L}(\alpha, \dot\alpha)=R[\dot\alpha-\gamma\alpha]^2$, the Euler-Lagrange equation for an extreme value of the integral is

$$\frac{d}{dt}\frac{\partial\mathfrak{L}}{\partial\dot\alpha}-\frac{\partial\mathfrak{L}}{\partial\alpha}=0, \qquad (4\text{-}10)$$

or

$$\ddot\alpha-\gamma^2\alpha=0, \qquad (4\text{-}11)$$

whose solution is a superposition of the functions $e^{-\gamma t}$ and $e^{+\gamma t}$. The initial condition at $t=-\infty$ eliminates the exponentially falling solution, that at $t=t_2$ gives $\alpha(t)=\alpha^{(2)}e^{\gamma t}$, and the integral is

$$\tfrac{1}{4}\int_{-\infty}^{t_2} R[\dot\alpha(t)+\gamma\alpha(t)]^2dt_{\min}=\tfrac{1}{2}s(\alpha^{(2)})^2,$$

subject to $\alpha(-\infty)=0$, $\alpha(t_2)=\alpha^{(2)}$ (4-12)

as was to be proved.

Several Variables

The possibility of linearly transforming the α's so as to diagonalize the two matrices **s** and **R** simultaneously, implies that the mathematics is no harder for several variables. It can be shown (see dissertation, footnote *) that in the diagonal representation the random impulse functions ϵ_i [Eq. (3-9)] must be uncorrelated, so that we are dealing with n independent Markoff processes. The extension of (4-7) to several variables will point up the physical significance of the integrand $\mathfrak{L}$.

For independent processes, the joint p.d.f. is simply the product of the single-variable p.d.f.'s. Thus, in the multivariable extension of (4-7), we shall have a sum in the exponent. If the integrand is multiplied out, and the integration performed on the cross term,

$$R[\dot\alpha(t)+\gamma\alpha(t)]^2=R\dot\alpha^2+(1/R)s^2\alpha^2+(d/dt)(s\alpha^2), \qquad (4\text{-}13)$$

(recall $\gamma=s/R$), the sum can be written in terms of the entropy and dissipation functions. For in the diagonal representation, these are sums of squares:

$$S=S_0-\tfrac{1}{2}\Sigma_i s_i\alpha_i^2 \text{ [see (2-10)]}, \qquad (4\text{-}14)$$

$$\Phi(d\boldsymbol{\alpha}/dt, d\boldsymbol{\alpha}/dt)=\tfrac{1}{2}\Sigma_i R_i\dot\alpha_i^2 \text{ [see (2-8)]}, \qquad (4\text{-}15)$$

$$\Psi(X, X)=\tfrac{1}{2}\Sigma_i(1/R_i)X_i^2=\tfrac{1}{2}\Sigma_i(1/R_i)s_i^2\alpha_i^2 \text{ [see (2-9)]}. \qquad (4\text{-}16)$$

Then

$$\Sigma_i R_i[\dot\alpha_i+\gamma\alpha_i]^2=2\Phi(d\boldsymbol{\alpha}/dt, d\boldsymbol{\alpha}/dt)+2\Psi(\mathbf{X}, \mathbf{X}) -2(d/dt)S(\boldsymbol{\alpha}), \qquad (4\text{-}17)$$

and the conditional p.d.f. (4-7) for several variables

becomes

$$f_n\left(\begin{matrix}\boldsymbol{\alpha}^{(2)} & \boldsymbol{\alpha}^{(1)}\\ t_2 & t_1\end{matrix}\right)=\prod_i f_1\left(\begin{matrix}\alpha_i^{(2)} & \alpha_i^{(1)}\\ t_2 & t_1\end{matrix}\right)$$

$$\propto \exp\left\{-\frac{1}{4}\frac{1}{k}\left(\int^{t_2}\left[2\Phi(d\boldsymbol{\alpha}/dt, d\boldsymbol{\alpha}/dt)\right.\right.\right.$$

$$\left.\left.\left.+2\Psi(X, X)-2\frac{d}{dt}S(\boldsymbol{\alpha})\right]dt\right)_{\min}\right\}$$

$$\text{subject to } \boldsymbol{\alpha}(t_1)=\boldsymbol{\alpha}^{(1)},\ \boldsymbol{\alpha}(t_2)=\boldsymbol{\alpha}^{(2)}. \quad (4\text{-}18)$$

In this form, the equation is no longer dependent on the representation chosen, i.e., it is valid also for interacting variables. It must be noticed that Φ is a function of the $\dot{\alpha}$'s, while Ψ, explicitly a function of the X's, is therefore a function of the α's (of the state).

The joint two-gate p.d.f. has a similar appealing form

$$f_{2n}\left(\begin{matrix}\boldsymbol{\alpha}^{(1)} & \boldsymbol{\alpha}^{(1)}\\ t_1 & t_2\end{matrix}\right)=f_n\left(\begin{matrix}\boldsymbol{\alpha}^{(2)} & \boldsymbol{\alpha}^{(1)}\\ t_2 & t_1\end{matrix}\right)f_n(\boldsymbol{\alpha}^{(1)})$$

$$\propto \exp\left[\frac{1}{k}\left\{\tfrac{1}{2}S(\boldsymbol{\alpha}^{(1)})+\tfrac{1}{2}S(\boldsymbol{\alpha}^{(2)})\right.\right.$$

$$\left.\left.-\tfrac{1}{4}\left(\int_{t_1}^{t_2}[2\Phi(d\boldsymbol{\alpha}/dt, d\boldsymbol{\alpha}/dt)+2\Psi(\mathbf{X}, \mathbf{X})]dt\right)_{\min}\right\}\right],$$

$$\text{subject to } \boldsymbol{\alpha}(t_1)=\boldsymbol{\alpha}^{(1)},\ \boldsymbol{\alpha}(t_2)=\boldsymbol{\alpha}^{(2)}. \quad (4\text{-}19)$$

The form also lends itself to the expression of the p.d.f. for any number of gates. Using (4-18) in (3-8), we simply add the integrals in the exponents.

$$f_{pn}\left(\begin{matrix}\boldsymbol{\alpha}^{(1)} & \cdots & \boldsymbol{\alpha}^{(p)}\\ t_1 & & t_p\end{matrix}\right)\propto \exp\left[\frac{1}{k}\left\{\tfrac{1}{2}S(\boldsymbol{\alpha}^{(1)})+\tfrac{1}{2}S(\boldsymbol{\alpha}^{(p)})\right.\right.$$

$$\left.\left.-\tfrac{1}{4}\left(\int_{t_1}^{t_p}[2\Phi(d\boldsymbol{\alpha}/dt, d\boldsymbol{\alpha}/dt)+2\Psi(\mathbf{X}, \mathbf{X})]dt\right)_{\min}\right\}\right]$$

$$\text{subject to } \boldsymbol{\alpha}(t_1)=\boldsymbol{\alpha}^{(1)},\ \boldsymbol{\alpha}(t_2)=\boldsymbol{\alpha}^{(2)},\ \cdots,\ \boldsymbol{\alpha}(t_p)=\boldsymbol{\alpha}^{(p)}. \quad (4\text{-}20)$$

It may be pointed out that the path which makes the integrand a minimum has, in general, discontinuous derivatives at each gate. The separate two-gate paths are just strung end-to-end.

We can make (4-20) particularly simple by permitting integration over an infinite time interval. We assert that

$$\tfrac{1}{4}\int_{-\infty}^{t_1}[2\Phi(d\boldsymbol{\alpha}/dt, d\boldsymbol{\alpha}/dt)+2\Psi(\mathbf{X}, \mathbf{X})]dt_{\min}$$

$$=\tfrac{1}{2}S(\boldsymbol{\alpha}^{(1)})+\text{const} \quad (4\text{-}21)$$

$$\text{subject to } \boldsymbol{\alpha}(-\infty)=0=\text{equilibrium},\ \boldsymbol{\alpha}(t_1)=\boldsymbol{\alpha}^{(1)}.$$

This can be checked directly by working it out (say, in diagonal form). But it can also be seen as follows: the Euler-Lagrange equations (4-10) for an extremum of the integral have double the order of Eqs. (2-13), the phenomenological laws. They are evidently satisfied by the solutions of (2-13), and by the mirror images of these in time ($-t$ replacing t). The former are the "average paths," for which hold Eqs. (2-6) and (2-7). But only the "mirror image" solutions can satisfy the initial conditions of $t=-\infty$ nontrivially. For these

$$2\Phi(d\boldsymbol{\alpha}/dt, d\boldsymbol{\alpha}/dt)+2\Psi(\mathbf{X}, \mathbf{X})=-2\dot{S}, \quad (4\text{-}22)$$

from which (4-21) follows.[17] From symmetry in past and future a similar equation holds for the range of integration (t_p, ∞). If we substitute these into (4-20) we obtain

$$f_p\left(\begin{matrix}\boldsymbol{\alpha}^{(1)} & \cdots & \boldsymbol{\alpha}^{(p)}\\ t_1 & & t_p\end{matrix}\right)\propto \exp\left[-\frac{1}{4}\frac{1}{k}\left(\int_{-\infty}^{\infty}[2\Phi(d\boldsymbol{\alpha}/dt, d\boldsymbol{\alpha}/dt)\right.\right.$$

$$\left.\left.+2\Psi(\mathbf{X}, \mathbf{X})]dt\right)_{\min}\right], \quad (4\text{-}23)$$

$$\text{subject to } \boldsymbol{\alpha}(t_1)=\boldsymbol{\alpha}^{(1)},\ \boldsymbol{\alpha}(t_2)=\boldsymbol{\alpha}^{(2)},\ \cdots,\ \boldsymbol{\alpha}(t_p)=\boldsymbol{\alpha}^{(p)}.$$

A few disconnected remarks may elucidate the physical content of this relation. To form the integrand one must know the form of the dissipation function as well as of the entropy function; the latter is needed in order to give the thermodynamic forces X_i as functions of the state. The path whose probability it is desired to evaluate may be specified as closely as desired, i.e., by any number of gates. Accordingly, the auxiliary functional (4-23) furnishes a complete description of the probability distribution functional. Between gates the path of integration is in a certain sense the "smoothest" path. It is a superposition of decaying and growing exponentials, as required by symmetry in past and future.

The theorem which has been proved is seen to be analogous to the Boltzmann principle. The latter tells the probability of a state in terms of its entropy; this theorem tells the probability of a temporal succession of states in terms of the entropy and dissipation functions.

Incomplete Specification in Some Gates

An important feature of the expression (4-23) is that any variable can be "integrated out" simply by minimizing the exponent with respect to it; i.e., by removing the variable from the set of specifications on the minimum of the integral. For the p.d.f. is Gaussian in all the variables. We can thus invoke the equivalence of means and modes and replace integration over one variable (averaging with respect to it) by maximization of the exponential with respect to it, i.e., taking the minimum of the integral. *Accordingly* (4-23) *is valid as*

[17] This is worked out in II, Sec. 3.

it stands whether or not the state is completely specified at each instant. It therefore describes the statistics of sets of variables which are not necessarily Markoffian, but which are sub-sets of Markoffian sets for which the coefficients of the entropy and dissipation functions are known.

Principle of Least Dissipation

The principle of least dissipation (RRIP I), a generalization of a similar principle in hydrodynamics due to Rayleigh,[18] can be read by inspection from (4-18). Given a state $\boldsymbol{\alpha}$, we ask for the most probable values of the $\dot{\alpha}$'s (and thus for the most probable path of the α's in time). Taking t_2 close to t_1 ($t_2-t_1=\Delta t=$small) we seek the state $\boldsymbol{\alpha}^{(2)}$ which will maximize the exponent. The integral becomes a simple product:

$$-\frac{1}{4}\frac{1}{k}\left[2\Phi(d\boldsymbol{\alpha}/dt,\, d\boldsymbol{\alpha}/dt)+2\Psi(\mathbf{X},\mathbf{X})-2\frac{d}{dt}S(\boldsymbol{\alpha})\right]\Delta t=\max. \tag{4-24}$$

If we remember that the variation is with respect to the $\dot{\alpha}$'s only, we have

$$\dot{S}-\Phi(d\boldsymbol{\alpha}/dt,\, d\boldsymbol{\alpha}/dt)=\max. \tag{4-25}$$

This variational principle is formally equivalent to the phenomenological laws [(2-2), including the reciprocal relations (2-4)].

Spectral Description

It may be useful to recall the connection between this work and that of Callen and his co-workers in the same field.[19] The systems treated are of the same type, and the same physical assumptions are made for them. But while this paper uses a *temporal* description of the course of fluctuations, these other papers use a *spectral* description. The two descriptions correspond to two types of experiment: the temporal to taking successive readings at close intervals, obtaining, for instance, a trace on a moving tape; the spectral to recording by means of a frequency analyzer. Where in the temporal description we postulate linear relations between forces and fluxes, defined by the dissipation matrix $\mathbf{R}$, the spectral description has linear relations between their Fourier transforms, defined by an admittance matrix.

[18] Lord Rayleigh (J. W. Strutt), Phil. Mag. **26**, 776 (1913).

[19] Footnote 13. See also H. Takasi, J. Phys. Soc. Japan **7**, 439 (1952).

PHYSICAL REVIEW VOLUME 91, NUMBER 6 SEPTEMBER 15, 1953

Fluctuations and Irreversible Process. II. Systems with Kinetic Energy*

S. MACHLUP, *Sloane Physics Laboratory, Yale University, New Haven, Connecticut,*

and

Bell Telephone Laboratories, Murray Hill, New Jersey

AND

L. ONSAGER, *Sterling Chemistry Laboratory, Yale University, New Haven, Connecticut*

(Received May 13, 1953).

The results of the previous paper are extended to second-order systems, i.e., systems with inertia. Using a generalized definition of the thermodynamic forces, reciprocal relations for the dissipative coefficients in the equations describing irreversible processes are derived. A dissipation function can again be defined, and it can again be used to express the probability functional for fluctuations.

1. β-TYPE VARIABLES

IN the previous paper of the same principal title[1] the thermodynamic variables treated were limited to those satisfying the hypothesis of microscopic reversibility. The restriction was stated: on a kinetic model, the thermodynamic variables must be algebraic sums of (a large number of) molecular variables, and must be *even* functions of those molecular variables which are odd functions of time (like molecular velocities). Thus a reversal of the sense of time would not change the values of these α variables.

It was assumed that all thermodynamic functions (specifically, the entropy S) were given as functions of the α variables, and that the irreversible processes were "caused" by thermodynamic forces $X_i=\partial S/\partial\alpha_i$. If, however, the kinetic energy of the various flows (e.g., magnetic energy of electric currents) contributes appreciably to the entropy, other variables must be taken into consideration: "velocity" variables, i.e., variables which would change their sign if the sense of time were reversed. Casimir[2] calls them β variables. He points

* Much of the work reported in this paper appears in more detail in a dissertation by one of us (S.M.), presented to the Faculty of the Graduate School of Yale University (1952) in partial fulfillment of the requirements for the Ph.D. degree.

[1] L. Onsager and S. Machlup, preceding paper [Phys. Rev. **91**, 1505 (1953).

[2] H. B. G. Casimir, Revs. Modern Phys. **17**, 343 (1945).

out that for irreversible processes involving both α's and β's, the principle of microscopic reversibility implies that the reciprocal relations have negative signs for the coefficients giving cross phenomena between α and β variables.

The β variables, which arise from the *inertia* of the system, can be expressed as time derivatives of α-type variables. The phenomenological laws for irreversible processes, which would be a set of first-order differential equations in the α and β variables, can thus be written as a set of second-order equations in the α's. (Example: a simple electric circuit containing inductance, capacitance and resistance can be described by two first-order equations in charge and current, or by one second-order equation in charge.)

Phenomenological Laws

Thus, the entropy is now a function of the α's and the $\dot{\alpha}$'s. Both are now the variables of state. We would like to have the phenomenological laws in the form

$$\Sigma_j R_{ij}\dot{\alpha}_j=\xi_i, \quad i=1\cdots n \tag{1-1}$$

again. We can achieve this by defining the thermodynamic forces as

$$\xi_i=\frac{\partial S}{\partial \alpha_i}+\frac{dt}{dt}\frac{\partial S}{\partial \dot{\alpha}_i}. \tag{1-2}$$

The second member of this sum is analogous to a d'Alembert force in mechanics; it is the second-order term in (1-1). The α's are still taken to be zero at equilibrium; the $\dot{\alpha}$'s vanish there by their nature. S_0-S is again a homogeneous quadratic function of all the variables of state, but there are no cross terms between α's and $\dot{\alpha}$'s. For the entropy must not change with a reversal of the sense of time: In the microscopic description, the Hamiltonian is an even function of molecular momenta. One may, therefore, think of the entropy as consisting of a "potential" and a "kinetic" part:

$$S=S_0-\tfrac{1}{2}\Sigma_{ij}s_{ij}\alpha_i\alpha_j-\tfrac{1}{2}\Sigma_{ij}m_{ij}\dot{\alpha}_i\dot{\alpha}_j. \tag{1-3}$$

(The letter m has been chosen because of the analogy to *mass*.) The phenomenological laws (1-1) become

$$\Sigma_j(m_{ij}\ddot{\alpha}_j+R_{ij}\dot{\alpha}_j+s_{ij}\alpha_j)=0, \quad i=1\cdots n, \tag{1-4}$$

or, in matrix notation,

$$m\ddot{\alpha}+R\dot{\alpha}+s\alpha=0. \tag{1-4'}$$

[Henceforth, when appearing without subscript, Greek letters α, ϵ, ξ are vectors, Roman s, m, R, A, B, C are matrices.]

2. LINEAR SECOND-ORDER STOCHASTIC PROCESS

We shall again postulate that the average regressions from a given nonequilibrium state obey the same laws as the corresponding irreversible processes, i.e., the phenomenological laws (1-4). This applies here to the average regressions of the α's *and* the $\dot{\alpha}$'s. If we also assume that the fluctuations are Gaussian stochastic processes, then we arrive, as in I, at the conclusion that they are Markoffian—in the α's and $\dot{\alpha}$'s. Alternatively stated, they are second order stochastic processes in the α's alone. They obey, then, the stochastic differential equations,

$$m\ddot{\alpha}+R\dot{\alpha}+s\alpha=\epsilon, \tag{2-1}$$

with the ϵ's purely random impulses. We need only consider the n equations (1-4) split up into $2n$ first-order equations in the α's and $\dot{\alpha}$'s; then the proof by Doob cited in I, Sec. 3, again becomes applicable.

To prove reciprocal relations for the R matrix, we shall study the second moments and apply microscopic reversibility to them. There are four covariance matrices,

$$\begin{aligned} A(\tau)&=\langle\alpha(t)\alpha_{tr}(t+\tau)\rangle,\\ B(\tau)&=\langle\dot{\alpha}(t)\alpha_{tr}(t+\tau)\rangle,\\ B'(\tau)&=\langle\alpha(t)\dot{\alpha}_{tr}(t+\tau)\rangle,\\ C(\tau)&=\langle\dot{\alpha}(t)\dot{\alpha}_{tr}(t+\tau)\rangle. \end{aligned} \tag{2-2}$$

[Matrix notation: *tr* means *transpose*. If α is a column vector, α_{tr} is a row vector—e.g., $A_{ij}(\tau)=\langle\alpha_i(t)\alpha_j(t+\tau)\rangle$.] These are related as follows:

$$B(\tau)=-B'(\tau), \quad B(\tau)=-\dot{A}(\tau), \quad C(\tau)=\dot{B}(\tau). \tag{2-3}$$

If we multiply 2-1 by $\alpha_{tr}(t-\tau)$ on the right, and take averages, we obtain the matrix equation

$$m(d^2A/d\tau^2)_{tr}+R\dot{A}_{tr}+sA_{tr}=0, \tag{2-4}$$

the right-hand side vanishing because, by hypothesis, the ϵ's are uncorrelated with the α's and $\dot{\alpha}$'s. Similarly, if we multiply by $\dot{\alpha}_{tr}(t-\tau)$,

$$m(d^2B/d\tau^2)_{tr}+R\dot{B}_{tr}+sB_{tr}=0. \tag{2-5}$$

If we use (2-3), these two sets of n^2 simultaneous second-order equations become two sets of $2n^2$ simultaneous first-order equations:

$$\dot{A}_{tr}+B_{tr}=0, \tag{2-6}$$

$$sA_{tr}-m\dot{B}_{tr}-RB_{tr}=0, \tag{2-7}$$

$$\dot{B}_{tr}+C_{tr}=0, \tag{2-8}$$

$$sB_{tr}-m\dot{C}_{tr}-RC_{tr}=0, \tag{2-9}$$

The one-gate distribution function of the α's and $\dot{\alpha}$'s we know from (1-3) by Boltzmann's principle. The second moments of a Gaussian distribution are given by the reciprocal of the matrix defining the quadratic form in the p.d.f. (probability density function):

$$A(0)=ks^{-1}, \tag{2-10}$$

$$B(0)=B'(0)=0, \tag{2-11}$$

(no cross-terms in 1-3)

$$C(0)=km^{-1}. \tag{2-12}$$

These equations give the initial conditions for (2-6) to (2-9). We must be careful about evaluating the covariances at $\tau=0$, since their derivatives need not be continuous there. Specifying approach from positive τ, and substituting (2-11) and (2-12), we obtain from (2-9) a statistical interpretation of the coefficients R_{ij}:

$$\dot{C}_{tr}(0+)=-km^{-1}Rm^{-1}. \tag{2-13}$$

Had we approached $\tau=0$ from negative values, we would have obtained the opposite sign in this equation. The derivatives of the $A_{ij}(\tau)$, which are discontinuous at $\tau=0$ in the case without inertia, now vanish there when the m matrix is positive definite: inertia "smoothes" the correlation between the α's.

Reciprocal Relations

The principle of microscopic reversibility (see RRIP II) requires that the matrix $A(\tau)$ be symmetric; hence, by (2-3), $C(\tau)$ is symmetric. m, as the matrix of a quadratic form, is by nature symmetric. Thus, from (2-13) follow the reciprocal relations for the R_{ij}:

$$R=R_{tr}. \tag{2-14}$$

With R symmetric, a dissipation function,

$$\Phi(\dot{\alpha},\dot{\alpha})=\tfrac{1}{2}\dot{\alpha}_{tr}R\dot{\alpha}, \tag{2-15}$$

can again be defined, having all the properties of the dissipation function of I. For irreversible processes obeying (1-1), the rate of production of entropy is

$$\begin{aligned}\dot{S}&=-\Sigma_{ij}m_{ij}\dot{\alpha}_i\ddot{\alpha}_j-\Sigma_{ij}s_{ij}\alpha_i\dot{\alpha}_j\\&=-\Sigma_{ij}(m_{ij}\ddot{\alpha}_j+s_{ij}\alpha_j)\dot{\alpha}_i=\Sigma_i\xi_i\dot{\alpha}_i\\&=2\Phi(\dot{\alpha},\dot{\alpha})=2\Psi(\xi,\xi),\end{aligned} \tag{2-16}$$

where the function

$$\Psi(\xi,\xi)=\tfrac{1}{2}\xi_{tr}R^{-1}\xi \tag{2-17}$$

is also the natural extension of its counterpart in I.

3. INTEGRAL FORM FOR THE DISTRIBUTION

The probability of a given succession of states can again be expressed in terms of the dissipation function, by means of an auxiliary functional defined for "fluctuation paths." With the convention (1-2), the formula is outwardly the same as for the case without inertia, but of course the terms now have different meanings. The important difference is that a state Γ is now specified by the values of all the α's and all the $\dot{\alpha}$'s. If we begin, as in I, with the two-gate conditional p.d.f., we shall omit any synthetic proof, and assert that it is given by

$$f_{2n}\left(\begin{matrix}\Gamma^{(2)}\\ t_2\end{matrix}\middle|\begin{matrix}\Gamma^{(1)}\\ t_1\end{matrix}\right)\propto\exp\left\{-\frac{1}{4}\frac{1}{k}\left(\int_{t_1}^{t_2}[2\Phi(\dot{\alpha},\dot{\alpha})+2\Psi(\xi,\xi)-2\dot{S}]dt\right)\right\}_{\min},$$

$$\text{subject to } \Gamma(t_1)=\Gamma^{(1)},\ \Gamma(t_2)=\Gamma^{(2)}. \tag{3-1}$$

The proof will consist in showing that the formula leads to the correct (1) average regressions and (2) one-gate p.d.f. (probability density function), since these completely determine a Gaussian process. Actually, this time we must check the average regressions of both α's and $\dot{\alpha}$'s. But we can do this in one stroke by verifying that the equations giving the regressions are indeed the set (1-4) and have the same initial conditions.

In the case without inertia we had the simplification that the R and s matrices could be simultaneously diagonalized, giving n independent equations for the phenomenological laws, and making the entropy and dissipation functions sums of squares. Here, the three matrices R, s, and m cannot, in general, be brought simultaneously to diagonal form, so that all the variables must be handled simultaneously.

From the equality of means and modes for Gaussian distributions, the regressions are given by the condition that (3-1) be maximum with respect to $\Gamma^{(2)}$. Hence,

$$\int_{t_1}^{t_2}[2\Phi(\dot{\alpha},\dot{\alpha})+2\Psi(\xi,\xi)-2\dot{S}]dt_{\min}=\min,$$

$$\text{subject to } \Gamma(t_1)=\Gamma^{(1)},\ \Gamma(t_2)=\Gamma^{(2)}. \tag{3.2}$$

The integrand can be written in such a way as to show its positive definiteness:

$$\begin{aligned}\mathfrak{L}(\alpha,\dot{\alpha},\ddot{\alpha})&\equiv 2\Phi(\dot{\alpha},\dot{\alpha})+2\Psi(\xi,\xi)-2\dot{S}\\&=(\dot{\alpha}-R^{-1}\xi)_{tr}R(\dot{\alpha}-R^{-1}\xi)\\&=(\dot{\alpha}+R^{-1}s\alpha+R^{-1}m\ddot{\alpha})_{tr}R(\dot{\alpha}+R^{-1}s\alpha+R^{-1}m\ddot{\alpha}).\end{aligned} \tag{3-3}$$

Hence the minimum of the integral is zero, which value it takes for

$$\dot{\alpha}-R^{-1}\xi=0, \tag{3-4}$$

or

$$m\ddot{\alpha}+R\dot{\alpha}+s\alpha=0, \tag{3-5}$$

which was to be shown. As the initial conditions $[\Gamma(t_1)=\Gamma^{(1)}]$ also agree, (3-1) is seen to give the right regressions.

The unconditional one-gate distribution will be correct if

$$\int_{-\infty}^{t_2}\mathfrak{L}(\alpha,\dot{\alpha},\ddot{\alpha})dt_{\min}=S(\Gamma^{(2)})+\text{const.} \tag{3-6}$$

$$\text{subject to } \Gamma(-\infty)=\Gamma^0=\text{equilibrium},\ \Gamma(t_2)=\Gamma^{(2)}.$$

The equations for an extreme value of the integral are

$$\frac{d^2}{dt^2}\frac{\partial\mathfrak{L}}{\partial\ddot{\alpha}_i}-\frac{d}{dt}\frac{\partial\mathfrak{L}}{\partial\dot{\alpha}_i}+\frac{\partial\mathfrak{L}}{\partial\alpha_i}=0,\quad i=1\cdots n. \tag{3-7}$$

If we use 3-3, these are factorable, i.e., in matrix notation,

$$(D1+R^{-1}s+D^2R^{-1}m)(D1-R^{-1}s-D^2R^{-1}m)\alpha=0, \tag{3-8}$$

where $D=d/dt$ and $1=$ unit matrix.

The solutions of this equation are superpositions of the solutions of the equations obtained from the factors,

$$(D1+R^{-1}s+D^2R^{-1}m)\alpha=0, \tag{3-9}$$

$$(D1-R^{-1}s-D^2R^{-1}m)\alpha=0. \tag{3-10}$$

(3-9) is the operational form of the phenomenological equations (1-4), while (3-10) can be obtained from these by changing the sign of t. Invoking the initial condition $\Gamma(-\infty)=\Gamma^0$, i.e., $\alpha=0$, $\dot{\alpha}=0$ at $t=-\infty$, (3-9) can have only the trivial (zero) solution, for we see from (2-16),

$$\dot{S}=2\Phi(\dot{\alpha},\dot{\alpha}),$$

that the entropy cannot decrease when the variables obey the phenomenological equations. But the entropy already has its maximum value S_0 at $t=-\infty$, hence all but the trivial solution of (3-9) are excluded. Thus the permitted solutions of (3-8) are solutions of (3-10) [the mirror images of solutions of (3-9)].

We use (3-10) and form the quadratic form,

$$(\dot{\alpha}-R^{-1}s\ddot{\alpha}-R^{-1}m\ddot{\alpha})_{tr}R(\dot{\alpha}-R^{-1}s\alpha-R^{-1}m\ddot{\alpha})=0. \tag{3-11}$$

If we multiply it out and recall the definition of the thermodynamic force ξ(1-2), we have

$$2\Phi(\dot{\alpha},\dot{\alpha})+2\Psi(\xi,\xi)+2\dot{S}=0,$$

whence

$$\mathfrak{L}\equiv 2\Phi+2\Psi-2\dot{S}=-4\dot{S}. \tag{3-12}$$

Integrating $\dot{S}$ over time then gives (3-6). We have shown that (3-1) leads to the correct average regressions and the correct one-gate p.d.f.; it is therefore the correct conditional two-gate p.d.f.

The joint p.d.f. for any number of gates can then be found by the same argument as in I. We have

$$f_{2pn}\begin{pmatrix}\Gamma^{(1)} & \Gamma^{(2)}\cdots\Gamma^{(p)}\\ t_1 & t_2 \quad\quad t_p\end{pmatrix}$$

$$\propto \exp\left\{-\frac{1}{4}\cdot\frac{1}{k}\left(\int_{-\infty}^{\infty}[2\Phi(\dot{\alpha},\dot{\alpha})+2\Psi(\xi,\xi)]dt\right)_{\min}\right\}, \tag{3-13}$$

subject to $\Gamma(t_1)=\Gamma^{(1)}$, $\Gamma(t_2)=\Gamma^{(2)}$, $\cdots$, $\Gamma(t_p)=\Gamma^{(p)}$.

Since the path (now given by α and $\dot{\alpha}$) can be specified to any desired degree of precision (any number of gates), we have again obtained a probability *functional* for fluctuations, in terms of the dissipation function for irreversible processes.

The statement made in I, that the formula is still valid when the state is incompletely specified in one or more gates, is true here as well, and for the same reason: the p.d.f. is Gaussian in all the variables, hence integration over one variable is equivalent to taking the minimum of the integral with respect to that variable. Such a statement is, indeed, necessary in order that (3-13) have a nontrivial meaning when either the s or the m matrix is not positive definite; for in this case the system does not really have $2n$ degrees of freedom. The matrices may be, at worst, positive semidefinite, by the Second Law. The matrix m will certainly be semidefinite when an α variable appears in the entropy function and the corresponding $\dot{\alpha}$ does not. In fact, if all the m_{ij} become zero, (3-13) must reduce to the formula in I (4-23) when we integrate out all the $\dot{\alpha}$ variables, which indeed we must in order to have nonzero probabilities. The s matrix will be semidefinite whenever an $\dot{\alpha}$ variable appears in the entropy function and the corresponding α does not. We have two distinct types of examples of such systems: for a Brownian particle in an infinite (field-free) medium, its position does not enter the entropy function, but its velocity does. Any nontrivial specification of the position leads to zero probability. On the other hand, for an inductive series circuit without capacitance, specification of the electric charge is quite meaningless, although its rate of change, the current, enters the entropy function.

It may be noticed that the roles of the functions $\Phi(\dot{\alpha},\dot{\alpha})$ and $\Psi(\xi,\xi)$ in this paper have changed from those in I. For the systems without kinetic energy of I, the thermodynamic forces $X_i=\partial S/\partial\alpha_i$ are functions of the state Γ. Hence $\Psi(X,X)$ is a function of the state, while $\Phi(\dot{\alpha},\dot{\alpha})$ depends on its change in time. For the systems with kinetic energy considered here, the $\dot{\alpha}$'s belong to the description of the state Γ. On the other hand, the thermodynamic forces $\xi_i=\partial S/\partial\alpha_i+(d/dt)\times(\partial S/\partial\dot{\alpha}_i)$ are not functions of the state alone. Hence $\Phi(\dot{\alpha},\dot{\alpha})$ is a function of the state alone, and $\Psi(\xi,\xi)$ depends on its rate of change in time.

The authors wish to express their appreciation of the friendly hospitality of the Royal Society Mond Laboratory, University of Cambridge, England, during the academic year 1951–1952. Moreover, they gratefully acknowledge a U. S. Atomic Energy Commission Predoctoral Fellowship held by S.M., and a U. S. Government Grant under the Fulbright Act to L.O., which made their stay in Cambridge possible.

Properties of the Salpeter-Bethe Two-Nucleon Equation*

JACK S. GOLDSTEIN
Institute for Advanced Study, Princeton, New Jersey
(Received May 21, 1953)

The relativistic two-nucleon equation of Salpeter and Bethe is examined in the ladder approximation for large binding energy, with an invariant interaction function. The binding energy is considered an adjustable parameter and the coupling constant, $g^2/4\pi$, is taken as the eigenvalue of the problem. As a starting point for this study, the special case of two equal masses and binding energy equal to the total mass is considered. It is found that in this case the equation may be simplified to a remarkable degree. For zero quantum mass, a one-dimensional integral equation in momentum space is obtained, and solved, in closed form. The solutions can also be displayed in closed form in configuration space. Solutions exist corresponding to this binding energy for all positive g^2. Requiring normalizability on a space-like surface in configuration space eliminates solutions for sufficiently small g^2, but a normalizable continuum remains. Arguments are presented to show that this continuum is not due to the choice of binding energy, but is, in fact, characteristic of the invariant equation. It is shown that by introducing a high frequency cutoff into the particle propagators and then going to the limit of infinite cutoff, the remaining continuum is reduced to a single physically sensible solution.

I. INTRODUCTION

THE relativistic two-nucleon equation of Salpeter and Bethe,[1] which has been obtained field-theoretically by Gell-Mann and Low,[2] represents the first completely covariant treatment of bound states in quantum field theory. However, the only applications which have been possible have been in the semirelativistic or nonrelativistic regions; *e.g.*, the mass corrections to the hydrogen fine-structure;[3] the spectrum of positronium;[4] and the partial renormalization of the Dancoff equations.[5] All of these applications have involved the approximation of the SB equation by introducing an instantaneous interaction as the starting point of a perturbation or iteration procedure. It is therefore of considerable interest to study the properties of this equation, and to seek methods of solving it when the interaction is treated covariantly. In fact, it has not previously been shown that solutions to the SB equation exist if no nonrelativistic approximations are made; furthermore, it has not been shown that all of the relativistic solutions, if they exist, have nonzero nonrelativistic limits.

We shall, in this paper, consider the question of existence of solutions, but not the question of existence of the nonrelativistic limits. We shall treat the interaction in a Lorentz-invariant fashion, but we approximate the equation by restricting ourselves to the so-called "ladder" approximation; that is, we retain only the first term in the expansion of the interaction in powers of $g^2/4\pi$, the coupling constant. Salpeter and Bethe[1] have given qualitative arguments for the validity of this procedure when $g^2/4\pi$ is small; however, we will not consider here the validity of the ladder approximation, but only whether it admits solutions if no nonrelativistic approximations are made within it. We shall therefore not restrict ourselves to small values of $g^2/4\pi$, but shall imagine that the interaction is exactly represented by the first term in its expansion.

The existence of solutions to the SB equation, in the ladder approximation, is demonstrated by exhibiting exact solutions for a special case. Treating the binding energy as a fixed parameter and the coupling constant as the eigenvalue of the problem, we consider the case when the binding energy is equal to the total rest mass of the two particles.[6] The equation may then be simplified to a remarkable degree and solved exactly. It is found that solutions exist for all positive values of g^2; imposing the condition that the solutions be normalizable on a space-like surface eliminates solutions for values of g^2 below a certain critical value, but leaves a normalizable continuum of solutions belonging to values of g^2 larger than the critical value. The validity of such a requirement is discussed with reference to the lack of a direct physical interpretation of the solutions.

To show that this continuum does not arise from the choice $E=0$, but rather is due to the high degree of singularity of the kernel, the equation is solved also for $E=0$ and an instantaneous interaction (which reduces the degree of singularity). It is shown that a point spectrum results.

It is then shown that the continuum may be reduced to a point spectrum in an invariant fashion by introducing a high momentum cutoff for the relative momenta and allowing the cutoff to become arbitrarily large. Using this procedure, only one point in the spectrum appears; the solution corresponding to this value of the coupling constant satisfies the suggested normalizability condition.

* Part of this work was performed at Cornell University, and forms part of the author's doctoral thesis.

[1] E. E. Salpeter and H. A. Bethe, Phys. Rev. **84**, 1232 (1951). We shall refer to this equation as the SB equation.

[2] M. Gell-Mann and F. Low, Phys. Rev. **84**, 350 (1951).

[3] E. E. Salpeter, Phys. Rev. **87**, 328 (1952).

[4] R. Karplus and A. Klein, Phys. Rev. **87**, 848 (1952).

[5] M. M. Lévy, Phys. Rev. **88**, 72 (1952); A. Klein, Phys. Rev. **89**, 1158 (1953).

[6] It must be noted that this choice of binding energy implies a system at rest, with zero rest mass; this can only be considered physically if it is interpreted as the limiting case of a nonzero rest mass system.

In so far as is possible, the notation of reference 1 will be used throughout. The time component of the four-vector x will be denoted by x_0, and is real. Three-vectors will be represented in bold-face type; thus, $x=(x_0, \mathbf{x})$. Natural units ($\hbar=c=1$) will be used throughout.

II. PROPERTIES OF THE SALPETER-BETHE EQUATION

In center-of-mass coordinates, the SB equation for bound states may be written, in the ladder approximation, as

$$\Psi(x)=\frac{2ig^2}{(2\pi)^5}\int d^4x' S(x-x')V(x'^2)\Gamma\Psi(x'), \qquad (1)$$

where $V(x^2)$ is the interaction function, assumed to depend only on the proper distance between the particles ($x^2=x_0^2-\mathbf{x}^2$). For a relativistic Yukawa interaction involving quanta of mass κ, this function is given by

$$V(x^2)=\frac{1}{(2\pi)^2}\int e^{-ip\cdot x}\frac{1}{p^2-\kappa^2}d^4p. \qquad (2)$$

The quantity Γ in Eq. (1) is a direct product of two commuting Dirac matrices, describing the transformation properties of the interaction field (i.e., $\Gamma=1$, $\gamma_\mu{}^a\gamma_\mu{}^b$, $\gamma_5{}^a\gamma_5{}^b$, $\gamma_5{}^a\gamma_5{}^b\gamma_\mu{}^a\gamma_\mu{}^b$, for scalar, vector, pseudoscalar, and pseudovector neutral fields, respectively). The kernel $S(x-x')$ is compounded from two S_F functions;[2] it is given by

$$S(x)=\int d^4p e^{-ip\cdot x}\left[\frac{E+p_0+H_a(\mathbf{p})}{(E+p_0)^2-W_a{}^2}\right]\left[\frac{E-p_0+H_b(-\mathbf{p})}{(E-p_0)^2-W_b{}^2}\right]\times\beta_a\beta_b, \qquad (3)$$

where $H_a(\mathbf{p})=\boldsymbol{\alpha}^a\cdot\mathbf{p}+\beta^a m_a$, $W_a{}^2=\mathbf{p}^2+m_a{}^2$, a and b refer to the two particles (assumed distinguishable), and $2E$ represents the total energy of the system. The Dirac matrices labeled a commute with those labeled b; Ψ is a 16-component function, the matrix properties of which will be discussed in detail below. The coordinate x is the relative separation of the particles, and the binding energy of the system is given by $\epsilon_B=2E-m_a-m_b$. We only consider the case when ϵ_B is negative.

The kernel $S(x-x')$ is strongly (quadratically) divergent on the relative light cone, $(x-x')^2=0$. As has been pointed out by Hayashi and Munukata,[7] in calculating the value of $\Psi(x)$ when $x^2=0$ from Eq. (1) the divergence in $S(x-x')$ will coincide with the δ_+-like divergence of $V(x'^2)$. These authors suggest that there may be no solutions to the equation as a result of this property; while this is not true, as we shall show, it seems likely that the character of the equation may be largely determined by this high degree of singularity. It should be noted that if an instantaneous interaction is used, the coincidence of divergences does not occur.

It is easily seen that the divergence in $S(x)$ is independent of the value of E, since it arises from large momenta; hence, this divergence is unaltered when $E=0$. For this reason, therefore, we shall consider E to be a parameter which may equal zero, and shall take $g^2/4\pi$ to be the eigenvalue of Eq. (1). Since one expects, ultimately, to obtain a relation between E and $g^2/4\pi$, it is clearly of no mathematical importance which of these two quantities is taken as the eigenvalue.

We shall show in the next section that it is possible to simplify Eq. (1) to a remarkable degree when $E=0$. As we have mentioned, the problem ceases to have any clear physical meaning at this point in the energy scale, but it seems reasonable to suppose that the mathematical nature of the problem is not seriously altered by this choice, due to the fact that the singular character of the kernel of the equation is independent of E. In the latter part of the paper, we shall attempt to determine to what extent the results are affected by the choice $E=0$, and to what extent they may be considered characteristic of the general problem.

III. SOLUTIONS FOR $E=0$

Equation (1) may be transformed into momentum space, yielding the equation

$$(E\beta_a+p_\mu\gamma_\mu{}^a-m_a)(E\beta_b-p_\mu\gamma_\mu{}^b-m_b)\Phi'(p)=i\lambda'\Gamma\pi^{-2}\int d^4k\frac{1}{(p-k)^2-\kappa^2}\Phi'(k), \qquad (4)$$

where we have put $g^2/4\pi=\lambda'$. We consider first the matrix properties of Φ' and the mode of operation of the γ matrices.

The function Φ' is a 16-component function having the transformation properties of a product of two Dirac free-particle spinors. If the components of Φ' are arranged as the elements of a 4×4 matrix, the rows of which are numbered by the particle a index, and the columns by the particle b index, then the γ matrices operate as follows:[8]

$$\gamma_\mu{}^a\Phi'\equiv\gamma_\mu\Phi', \qquad \gamma_\mu{}^b\Phi'\equiv\Phi'\gamma_\mu{}^+, \qquad (5)$$

where γ_μ is the usual 4×4 Dirac matrix, and $\gamma_\mu{}^+$ is the transpose of γ_μ. Ordinary matrix multiplication is implied. It should be noted that in forming the scalar quantity $\Phi'^*\Phi'$, it is necessary to take the trace of the matrix product.

[7] S. Hayashi and H. Munukata, Prog. Theoret. Phys. **7**, 481 (1952).

[8] L. de Broglie, *Théorie Générale des Particules à Spin (Methode de Fusion)* (Gauthier-Villars. Paris, 1943).

Using this representation of Φ', Eq. (4) becomes

$$(E\beta+p_\mu\gamma_\mu-m_a)\Phi'(p)(E\beta^+-p_\mu\gamma_\mu^+-m_b)$$
$$=i\lambda'\pi^{-2}\int\frac{d^4k}{(p-k)^2-\kappa^2}\rho\Phi'(k)\rho^+, \quad (6)$$

where we have made use of the fact that Γ can, in general, be represented as $\rho_a\rho_b$ with ρ defined according to the transformation properties of the interaction.

The charge conjugate matrix $A=\gamma_1\gamma_3$ has the following property:

$$A\gamma_\mu^+=\gamma_\mu A. \quad (7)$$

Hence, if we define $\Phi=\Phi'A$, it is seen that Φ satisfies

$$(E\beta+p_\mu\gamma_\mu-m_a)\Phi(p)(E\beta-p_\mu\gamma_\mu-m_b)$$
$$=i\lambda'\pi^{-2}\int\frac{d^4k}{(p-k)^2-\kappa^2}\rho\Phi(k)\rho, \quad (8)$$

and, with $E=0$,

$$(p_\mu\gamma_\mu-m_a)\Phi(p)(p_\mu\gamma_\mu+m_b)$$
$$=-i\lambda'\pi^{-2}\int\frac{d^4k}{(p-k)^2-\kappa^2}\rho\Phi(k)\rho. \quad (9)$$

We now put $m_a=m_b$, and assume Φ to be proportional to the unit matrix. We obtain[9]

$$(p^2-m^2)\Phi(p)=-i\lambda\pi^{-2}\int\frac{d^4k}{(p-k)^2-\kappa^2}\Phi(k), \quad (10)$$

where $\lambda=\lambda'\rho^2(\rho^2=1$ for scalar and pseudoscalar interaction, 4 for vector and pseudovector interaction). It is further seen that we may seek a solution to Eq. (10) which is a function of the *single* variable p^2. Such a solution, then, is a scalar under all Lorentz transformations including $\mathbf{p}\rightarrow-\mathbf{p}$, and must correspond to a ^1S state of the system.[10]

Equation (10) may be solved exactly when $\kappa=0$; hence we make this final step, and consider the interaction to take place by means of massless quanta. As we will show, no essential generality is lost by this step. For this case, the kernel of Eq. (10) is the Green's function for the d'Alembertian operator in momentum space; thus, Eq. (10) can be converted into a differential equation in momentum space, directly.

It is desirable, however, to obtain this differential equation somewhat differently; for the less direct method will serve also to replace Eq. (10) by a one-dimensional integral equation. We assume that the function $\Phi(p^2)$ may be written (the justification for this assumption will be provided below):

$$\Phi(p^2)=\int\int_T dxdyg(x,y)(p^2-x^{-1}+y+i\epsilon)^{-2}, \quad (11)$$

where ϵ is a positive infinitesimal constant, and the integration is over some region T in the xy plane. Substituting this expression into Eq. (10), with $\kappa=0$, and expressing all momenta and masses in units of m, we obtain, with $s=p^2$, and suppressing the $i\epsilon$,

$$s(s-1)\int\int_T dxdyg(x,y)(s-x^{-1}+y)^{-2}$$
$$=\lambda\int\int_T dxdyg(x,y)\ln\frac{(x^{-1}-y-s)}{x^{-1}-y}, \quad (12)$$

after the four-dimensional integration is carried out. When the logarithm in Eq. (12) is expressed as a double integral, we obtain

$$s(s-1)\int\int_T dxdyg(x,y)(s-x^{-1}+y)^{-2}$$
$$=\lambda\int_0^s dz\int_z^\infty dt\int\int_T g(x,y)dxdy(t-x^{-1}+y)^{-2}, \quad (13a)$$

or

$$s(s-1)\Phi(s)=\lambda\int_0^s dz\int_z^\infty dt\Phi(t). \quad (13b)$$

Rearranging the order of integration, we obtain

$$s(s-1)\Phi(s)=\lambda\int_0^s t\Phi(t)dt+\lambda s\int_s^\infty\Phi(t)dt. \quad (14)$$

The kernel of this integral equation is just the Green's function for d^2/ds^2; hence, the differential equation mentioned above is

$$\frac{d^2}{ds^2}[s(s-1)\Phi(s)]+\lambda\Phi(s)=0. \quad (15)$$

We may now replace $\Phi(t)$ under the integrals in Eq. (14) by a second derivative; integration by parts then removes the integrals and yields the boundary conditions auxiliary to Eq. (15). These conditions are

$$\lim_{s\rightarrow0}\{s[s(s-1)\Phi(s)]'+s\Phi(s)\}=0, \quad (16a)$$
$$\lim_{s\rightarrow\infty}[s(s-1)\Phi(s)]'=0. \quad (16b)$$

Equation (15) is recognizable as the hypergeometric equation; a solution satisfying conditions (16) is

[9] Equation (10) has been studied by Dr. S. F. Edwards [Phys. Rev. **90**, 284 (1953)] to whom the author is grateful for several useful discussions.

[10] Since no principal quantum member appears in the problem, it is not certain that $\Phi(p^2)$ describes the only ^1S state.

given by[11]

$$\Phi(s)=\int_0^1 t^{\alpha}(1-t)^{-\alpha}(1-[s+i\epsilon]t)^{\alpha-2}dt \tag{17a}$$

$$=B(\alpha,2-\alpha)F(1+\alpha,2-\alpha;2;s+i\epsilon),\quad |s+i\epsilon|\leq 1 \tag{17b}$$

$$=-\frac{1}{\alpha}\left\{\frac{\Gamma(1+\alpha)\Gamma(2\alpha-1)}{\Gamma(\alpha-1)}(-s-i\epsilon)^{-\alpha-1}\times F(1+\alpha,\alpha;2\alpha;[s+i\epsilon]^{-1})+\frac{\Gamma(2-\alpha)\Gamma(1-2\alpha)}{\Gamma(-\alpha)}(-s-i\epsilon)^{\alpha-2}\times F(2-\alpha,1-\alpha;2-2\alpha;[s+i\epsilon]^{-1})\right\},\quad |s+i\epsilon|\geq 1, \tag{17c}$$

where $B(m,n)$ is the beta function, $\Gamma(m)$ the gamma function, F the hypergeometric function, and α is related to λ by $\alpha(1-\alpha)=\lambda$. It is sufficient to restrict $\mathrm{Re}(\alpha)\leq\frac{1}{2}$ to obtain all the solutions.

In order to show that $\Phi(s)$, as defined by Eqs. (17), actually satisfies Eq. (10) with $\kappa=0$, it is only necessary to show that this function may be expressed in the form (11). Using the formula,

$$(x\pm i\epsilon)^{-n}=[B(m,n)]^{-1}\int_0^{\infty}y^{m-1}(x+y\pm i\epsilon)^{-m-n}dy,\quad (m,n>0), \tag{18}$$

valid for all real x, which may be obtained from the definition of the beta function,[12] and putting $m=\alpha$, $n=2-\alpha$, we obtain from Eq. (17a):

$$\Phi(s)=\frac{(-1)^{\alpha-2}}{B(\alpha,2-\alpha)}\int_0^{\infty}dy\int_0^1 dt y^{\alpha-1}t^{2\alpha-2}(1-t)^{-\alpha}\times(s+y-t^{-1}+i\epsilon)^{-2}, \tag{19}$$

which is of the required form.

Since all solutions of Eq. (10) must satisfy Eq. (15), any solutions not of the form (19) must also be hypergeometric functions. If we use well-known integral representations, the most general solution to Eq. (15) may be written down; with the help of formula (18), it is possible to show that no other solutions to Eq. (10) exist.

We have shown, therefore, that the SB equation has solutions belonging to $E=0$ for all positive values of the coupling constant; thus, for any coupling constant, the point $E=0$ is apparently contained in the ^1S energy spectrum, with no constants of the motion to prevent the system from falling into this state. This, of course, contradicts the physical fact that the lowest ^1S state of positronium lies far above $E=0$, and it contradicts the results of the nonrelativistic limit of the SB equation obtained by Salpeter.[3]

It therefore appears that additional regularity conditions must be imposed on the solutions in order to select the physically significant ones. Such conditions can only be obtained from the connection of the solutions to the laws of conservation of charge and energy, since it is only from this connection that the full physical meaning of the solutions can be understood. Unfortunately, this connection has not yet been obtained for the relativistic two-body problem. In the next section we consider imposing the requirement of space-like normalizability on the solutions, but since the interpretation of $\Phi(p^2)$ is incomplete, it must be recognized that there is no real reason to expect this requirement to be sufficient.

We shall find, in fact, that requiring Φ to be normalizable as a probability amplitude does exclude values of λ below a certain critical value, but leaves a normalizable continuum of solutions belonging to values of λ above this critical value.

IV. NORMALIZATION OF THE WAVE FUNCTION

The integrals which arise in carrying out the normalization of the wave function are more easily performed in configuration space. Furthermore, the functions themselves are perhaps more easily understood in this space, and for this reason, we shall first obtain the Fourier transform of the function defined by Eqs. (17).

It is very difficult to obtain these transforms directly, and an easier method exists. If we use the relation,[13]

$$\int e^{ip\cdot x}(p^2-m^2+i\epsilon)^{-2}d^4p=\pi^3 H_0^{(2)}(mR), \tag{20}$$

where $H_0^{(2)}$ is the Hankel function of zero order, second kind, and where $R=(x^2-i\epsilon)^{\frac{1}{2}}$ (positive real if $x^2>0$, negative imaginary if $x^2<0$) we may establish the behavior of the Fourier transform of Eq. (19) for very large imaginary R; that is, Fourier transform of $\Phi(s)$ decreases exponentially in the space-like region. This, of course, is a condition we should have to impose in any event on a bound state solution, but it is important to note that the condition is actually satisfied by the solution $\Phi(s)$.

The Fourier transform, $\Psi(x)$, of $\Phi(p)$ satisfies the following differential equation, which is obtained by transforming Eq. (9). We exhibit the equation for $\kappa\neq 0$ to establish the role played by the quantum rest mass.

$$\left(-i\gamma_\mu\frac{\partial\rightarrow}{\partial x_\mu}-m\right)\Psi(x)\left(-i\gamma_\mu\frac{\partial\leftarrow}{\partial x_\mu}+m\right)=-\frac{2i\lambda\pi\kappa}{R}H_1^{(2)}(\kappa R)\rho\Psi(x)\rho, \tag{21}$$

[11] E. T. Whittaker and G. N. Watson, *Modern Analysis* (Cambridge University Press, Cambridge, 1950).

[12] The author is grateful to Dr. N. Austern and Dr. S. Butler for bringing this useful device to his attention.

[13] J. Schwinger, Phys. Rev. **76**, 790 (1949).

where the arrows imply that the differential operators operate from the left. For $\kappa R \ll 1$ the interaction term reduces to $4\lambda R^{-2}$; hence it is clear that κ only affects the solutions at distances *large* compared to κ^{-1}. The behavior of the solutions near $R=0$ is therefore independent of κ.

Putting $\kappa=0$, and taking Ψ to be a scalar function of R, we obtain

$$\left(\frac{d^2}{dR^2}+\frac{3}{R}\frac{d}{dR}+1+\frac{4\lambda}{R^2}\right)\Psi(R)=0, \tag{22}$$

where we have again expressed all instances in units of m^{-1}. This equation is solved by [14]

$$\Psi(R)=R^{-1}Z_n(R), \tag{23}$$

where Z_n is any Bessel function, and where $n=(1-4\lambda)^{\frac{1}{2}}=1-2\alpha$. The condition that $\Psi(R)$ must be exponentially encreasing in the space-like region implies that

$$\Psi(R)=R^{-1}H_n^{(2)}(R) \tag{24}$$

be the unique solutions.

It should be noted that the behavior of $\Psi(R)$ for very large $|R|$ is virtually independent of n, apart from a phase factor. All of the solutions decay exponentially in the space-like region, and oscillate with slowly decreasing amplitude in the time-like region. However, near $R=0$, $\Psi(R)$ depends quite strongly on n; the behavior is like $R^{-(1+n)}$ for $n\neq 0$, and like $R^{-1}\ln R$ for $n=0$. For n imaginary ($\lambda>\frac{1}{4}$), $\Psi(R)$ oscillates with infinite amplitude and frequency at $R=0$.

The wave function Ψ is defined from field theory as the matrix element of two annihilation operators; as such, it is tentatively suggested that Ψ have the interpretation of probability amplitude whenever the two measurements which are involved commute. This is equivalent to the suggestion that the quantity

$$N=\int \Psi^*(0, \mathbf{r})\Psi(0, \mathbf{r})d^3r \tag{25}$$

should represent the normalization of the wave function on the surface $t=0$, since on this surface the two measurements never interfere.[15]

The integral (25) is performed in Appendix A. The result is finite for $n<\frac{1}{2}$, corresponding to $\lambda>\frac{3}{16}$; on the basis of this normalization condition, then, we are led to reject all solutions corresponding to λ smaller than this quantity as being nonphysical. This is equivalent to the statement that if the coupling is sufficiently weak, it is not possible to obtain a binding this strong without the collapse of the system.

In this connection, a characteristic radius of the state may also be calculated; we define this quantity by

$$\langle r\rangle=N^{-1}\int \Psi^*(0, \mathbf{r})|\mathbf{r}|\Psi(0, \mathbf{r})d^3r. \tag{26}$$

The integral is also carried out in Appendix A, the result being

$$\begin{aligned}\langle r\rangle&=4n\pi^{-1}\cot(n\pi), \quad n<\tfrac{1}{2};\\ &=0, \quad 1\geq n\geq\tfrac{1}{2}.\end{aligned} \tag{27}$$

Thus, the requirement of normalizability does not suffice to reduce the continuous spectrum completely. We shall first examine the source of this difficulty in the next section; subsequently, we shall consider a procedure which does have the effect of reducing the continuum.

V. SOURCE OF THE CONTINUUM

We have shown that for the special case $E=0$, the SB equation has solutions, in the ladder approximation, for all values of the coupling constant. Considerations of normalizability do not suffice to reduce this continuum to a point spectrum, and in any case, such considerations are on an unsure basis, due to the lack of physical interpretation for the solutions. It is therefore of some importance to attempt to isolate the mathematical properties of the SB equation which are responsible for this continuum; that is, we shall attempt to find out to what extent the continuum results from the choice $E=0$, and to what extent it results from the high singularity of the kernel of the equation.

It has been suggested that the nature of the spectrum may be largely determined by the fact that, in coordinate space, the singularity of the interaction on the relative light cone may coincide with the singularity in the function $S(x-x')$, defined by Eq. (3). If this is so, the nature of the spectrum should be altered if the interaction is taken to be instantaneous, for in that case, the two singularities can never coincide. We are therefore led to examine the equation [see Eq. (10)]:

$$(p^2-m^2)\Psi(\mathbf{p}^2, p_0)=-i\lambda\pi^{-2}\int\frac{d^4k}{(\mathbf{p}-\mathbf{k})^2}\Psi(\mathbf{k}^2, k_0), \tag{28}$$

the solution of which describes a ^1S state of a system for which $E=0$ and the interaction is of the instantaneous Coulomb type. If we define a new function,

$$\psi(\mathbf{p}^2)=\int_{-\infty}^{\infty}\Psi(\mathbf{p}^2, p_0)dp_0, \tag{29}$$

[14] E. Jahnke and F. Emde, *Tables of Functions* (Dover Publications, New York, 1945). One may reasonably ask why, when Eq. (22) is so easily solved, the momentum-space treatment is at all necessary. The answer lies in the lack of a definitive set of boundary conditions [such as Eqs. (16)], which are extremely difficult to obtain in coordinate space.

[15] It is tacitly assumed in the field-theoretic derivation of the SB equation (reference 2) that the quantity N is finite. However, it has not been shown that this assumption is essential to the derivation. It is also to be noted that although N is defined by Eq. (25) in a noncovariant way, the result of normalizing over any arbitrary space-like surface can be shown to be finite if N is finite, and infinite otherwise.

we obtain at once the following three-dimensional equation

$$\psi(\mathbf{p}^2)=-i\lambda\pi^{-2}\int_{-\infty}^{\infty}\frac{dp_0}{p_0{}^2-\mathbf{p}^2-m^2}\int d^3k\frac{1}{(\mathbf{p}-\mathbf{k})^2}\psi(\mathbf{k}^2)$$

$$=\frac{\lambda\pi^{-1}}{(\mathbf{p}^2+m^2)^{\frac{1}{2}}}\int d^3k\frac{1}{(\mathbf{p}-\mathbf{k})^2}\psi(\mathbf{k}^2). \tag{30}$$

This equation may be solved by a method suggested by the work of Rubinowicz;[16] the solution is obtained in Appendix B. It is shown there that the only solution of Eq. (30) corresponds to $4\pi\lambda=1$; that solution is given by

$$\psi(\mathbf{p}^2)=[(\mathbf{p}^2+m^2)^{\frac{1}{2}}-m]^{\frac{1}{2}}/[\mathbf{p}^2(\mathbf{p}^2+m^2)]^{\frac{1}{4}}. \tag{31}$$

This example serves to demonstrate that it is extremely plausible to suppose that the continuum actually does arise from the coincidence of the two singularities in question; and if this is the case, it may be expected that the continuum will arise for any value of E, as long as no noncovariant approximations are made.

In the next section we shall examine the effect on the spectrum of reducing the singularity of the function $S(x)$ in a covariant way. We shall find that this procedure enables us to reduce the continuous spectrum to a single physically acceptable solution.

VI. REDUCTION OF THE CONTINUUM

The program to be carried out in this section is the following. We will introduce a factor into Eq. (1) which cuts off the contribution of momenta large compared to some cutoff parameter, say Ω. We will then solve the problem for $E=\kappa=0$ again, and afterwards allow Ω to become arbitrarily large. We will then examine the resulting spectrum.

If we introduce an invariant cutoff factor, $C(p^2-\Omega)$, into Eq. (1), this factor will appear in the integrand of Eq. (3), and multiplying the integral on the right-hand side of Eq. (4), and finally, it will appear in Eq. (14) as follows:

$$s(s-1)\Phi^\Omega(s)=\lambda C(s-\Omega)\left\{\int_0^s t\Phi^\Omega(t)dt+s\int_s^\infty\Phi^\Omega(t)dt\right\}. \tag{32}$$

The superscript on the function Φ^Ω is used to indicate that Φ^Ω differs from Φ in that the former depends on Ω.

We require of the function $C(s-\Omega)$ that it have the property

$$\begin{aligned} C(s-\Omega)&=1, \quad s\ll\Omega;\\ C(s-\Omega)&=0, \quad s\gg\Omega. \end{aligned} \tag{33}$$

In order to construct a problem which may be solved, we shall take $C(s-\Omega)$ to be a step function. It seems likely that the form of the cutoff should be unimportant in the limit, and the results do not appear to depend on the sharpness of the cutoff, provided it is sufficiently sharp. Consequently, we write for $C(s-\Omega)$:

$$C(s-\Omega)=\theta(\Omega-s)=\begin{cases}1, & s<\Omega;\\ 0, & s>\Omega.\end{cases} \tag{34}$$

Consider now the function $\xi(s)$ which is defined as the solution of

$$\begin{aligned} s(s-1)\xi(s)&=\lambda\int_0^s t\xi(t)dt+\lambda s\int_s^\Omega\xi(t)dt, \quad s<\Omega;\\ &=\lambda\int_0^\Omega t\xi(t)dt, \qquad\qquad\qquad s>\Omega. \end{aligned} \tag{35}$$

It is clear that $\Phi^\Omega(s)$ is related to $\xi(s)$ by

$$\Phi^\Omega(s)=\theta(\Omega-s)\xi(s), \tag{36}$$

and therefore we need only solve Eq. (35).

The function $\xi(s)$ satisfies the differential equation (15) for $s<\Omega$, but the boundary condition (16b) now applies at $s=\Omega$ rather than at $s=\infty$. Thus, $\xi(s)$ must satisfy

$$\xi'(\Omega)/\xi(\Omega)=-(2\Omega-1)/\Omega(\Omega-1), \tag{37}$$

as the new boundary condition. Furthermore, for $s<\Omega$, $\xi(s)=\Phi(s)$ as defined by Eqs. (17); and if $\Omega\gg1$, we have

$$\begin{aligned} \xi(\Omega)&=-\frac{1}{\alpha}\left\{\frac{\Gamma(1+\alpha)\Gamma(2\alpha-1)}{\Gamma(\alpha-1)}(-\Omega)^{-\alpha-1}\right.\\ &\qquad\left.+\frac{\Gamma(2-\alpha)\Gamma(1-2\alpha)}{\Gamma(-\alpha)}(-\Omega)^{\alpha-2}\right\}\\ &=-\frac{1}{\alpha}\{C_1(\alpha)\Omega^{-\alpha-1}+C_2(\alpha)\Omega^{\alpha-2}\}. \end{aligned} \tag{38}$$

The definitions of $C_1(\alpha)$ and $C_2(\alpha)$ are apparent. The condition (37) then makes α a function of Ω, as follows (for $\Omega\gg1$):

$$\frac{(\alpha+1)C_1(\alpha)\Omega^{-\alpha-1}-(\alpha-2)C_2(\alpha)\Omega^{\alpha-2}}{C_1(\alpha)\Omega^{-\alpha-1}+C_2(\alpha)\Omega^{\alpha-2}}=2, \tag{39}$$

or

$$\frac{C_1(\alpha)}{C_2(\alpha)}=(-1)^{-2\alpha}\frac{\Gamma(2\alpha)}{\Gamma(2-2\alpha)}=\Omega^{2\alpha-1}\frac{\alpha}{\alpha-1}. \tag{40}$$

The only solution of this equation which is independent of Ω is $\alpha=\frac{1}{2}$; hence we conclude that the only solution which is insensitive to the cut-off procedure is the one for $\lambda=\frac{1}{4}$, i.e., the least divergent (in configuration space, on the relative light cone) of all the solutions.

VII. CONCLUSIONS

We may summarize this work as follows. The SB equation has been considered in the ladder approximation for a relativistic Coulomb interaction, with the

[16] A. Rubinowicz, Prace Mat.-Fiz. **47**, 41 (1949).

following results. Exact solutions have been found corresponding to the binding energy equal to the total mass, ($E=0$), for all positive values of the coupling constant. It is suggested that the existence of a continuous spectrum in the coupling constant is due to the possibility of coincidence of the singularities of the interaction and the particle propagators; to make this suggestion plausible, the SB equation is also considered for $E=0$ with an instantaneous interaction, which removes the possibility of coincidence of the singularities. It is shown that a single-point spectrum results.

It is further shown that if the singularity of the particle propagators is reduced by the introduction of an invariant high momentum cutoff, a single-point spectrum results even with the relativistic Coulomb interaction; this spectrum does not approach a continuum in the limit as the cut-off parameter becomes infinite.

Finally, it is shown that the requirement that the solutions be normalizable on a space-like surface does not suffice to reduce the continuum to a point spectrum; but the solution remaining after the cut-off procedure is carried out is normalizable on a space-like surface.

It has not been conclusively shown, of course, that if Eq. (1) were solved for $E>0$, a continuous spectrum in λ would result; however, the evidence does seem to suggest that the character of the spectrum is determined by the high degree of singularity of the kernel of the equation, and these singularities are independent of E.

This result is of immediate importance if variational procedures are to be used to determine the energy spectrum. For example, we have shown that any analysis which is designed to obtain the lowest-lying ^1S energy level will give $E=0$ as the result, unless extra conditions are imposed which are not already contained in the SB equation. Such a condition has been suggested in this paper; namely, that the solution must be "stable" under the cut-off procedure. It is admittedly very unsatisfactory to introduce such an *ad hoc* procedure into the problem; but the fact that this procedure selects the solution which is least divergent on the light cone suggests, perhaps, that the procedure might be replaced by an additional boundary condition on the light cone. However, any such condition must come directly from the theory when the complete physical interpretation of the solutions is available from the conservation laws.

An attempt has been made, which is not reported here, to obtain approximate solutions for small E (large binding energy) using the solutions for $E=0$ as the starting point of an iteration or perturbation procedure. These methods yield expansions of the wave function in powers of E; but if one may draw an analogy to the Dirac one-particle equation for the hydrogen atom [Eq. (30) suggests that such an analogy may be useful], an expansion of the wave function in powers of E will not be valid near the light cone. Since the eigenvalue problem seems to depend critically on the behavior at small proper distances, it seems plausible to suppose that any method yielding an expansion in powers of E will not be useful in obtaining the spectrum.

The equations describing higher angular momentum states for $E=0$ may be obtained from Eq. (9) as follows. Since Eq. (9) is invariant under Lorentz transformations, one must seek solutions also having that property; thus, one may require that the 4×4 matrix $\Phi(p)$ transform like a scalar, pseudoscalar, vector, etc., corresponding to ^1S, $^3P_0$, ^3S, etc.

I should like to thank Professor E. E. Salpeter for many valuable discussions, and Dr. S. F. Edwards for suggestions which proved extremely helpful. I am grateful to Professor J. R. Oppenheimer and to the faculty of the Institute for Advanced Study for their suggestions and kind hospitality.

APPENDIX

A. Normalization Integrals

We wish to calculate the integral defined by Eq. (25), which is

$$N=\int d^3r^{-2}H_n^{(1)}(ir)H_n^{(2)}(-ir)$$

$$=\frac{16}{\pi}\int_0^\infty K_n^2(r)dr. \tag{A1}$$

This integration may be performed with the help of the following integral representation:[17]

$$K_n^2(r)=\frac{1}{2}\int_0^\infty \exp\left[-\left(\frac{x}{2}+\frac{r^2}{x}\right)\right]K_n(r^2/x)\frac{dx}{x}. \tag{A2}$$

Let $u=r^2/x$, and insert (A2) into (A1):

$$N=\frac{8}{\pi}\int_0^\infty \frac{du}{u}e^{-u}K_n(u)\int_0^\infty dre^{-r^2/2u}$$

$$=\left(\frac{32}{\pi}\right)^{\frac{1}{2}}\int_0^\infty u^{-\frac{1}{2}}du e^{-u}K_n(u). \tag{A3}$$

We now make use of the following integral representation for $K_n(u)$:

$$K_n(u)=\frac{\pi^{\frac{1}{2}}}{\Gamma(n+\frac{1}{2})2^n}u^n\int_0^\infty e^{-u\cosh t}(\sinh t)^{2n}dt, \tag{A4}$$

which gives

$$N=\frac{8}{2^{n+\frac{1}{2}}\Gamma(n+\frac{1}{2})}\int_0^\infty dt(\sinh t)^{2n}\int_0^\infty u^{n-\frac{1}{2}}$$

$$e^{-u(1+\cosh t)}du. \tag{A5}$$

[17] G. N. Watson, *Bessel Functions* (Macmillan and Company, New York, 1944).

The inner integral may be found in tables of Laplace transforms;[18] the result is

$$N=\frac{8}{2^{n+\frac{1}{2}}}\int_0^\infty dt\frac{(\sinh t)^{2n}}{(1+\cosh t)^{n+\frac{1}{2}}}. \tag{A6}$$

The transformation $\cosh t=2x+1$ transforms this integral into the standard beta-function integral, giving

$$N=4\int_0^\infty \frac{x^{n-\frac{1}{2}}}{x+1}=4\Gamma(\tfrac{1}{2}+n)\Gamma(\tfrac{1}{2}-n)=\frac{4\pi}{\cos n\pi}. \tag{A7}$$

The integral is clearly finite only if $\mathrm{Re}(n)<\frac{1}{2}$.

The integral for the radius of the state may also be performed. It is defined by

$$\langle r\rangle=N^{-1}\int d^3rH_n^{(1)}(ir)rH_n^{(2)}(-ir)$$

$$=\frac{4\cos n\pi}{\pi^2}\int_0^\infty rdrK_n^2(r). \tag{A8}$$

Using the integral representation of Eq. (A2), we obtain

$$\langle r\rangle=\frac{2\cos n\pi}{\pi^2}\int_0^\infty\frac{du}{u}e^{-u}K_n(u)\int_0^\infty rdr\exp(-r^2/2u)$$

$$=\frac{2\cos n\pi}{\pi^2}\int_0^\infty due^{-u}K_n(u). \tag{A9}$$

This integral is also to be found in tables of Laplace transforms. The result is

$$\langle r\rangle=(4n/\pi)\cot(n\pi). \tag{A10}$$

B. Solution for Instantaneous Interaction

The equation which is to be solved [Eq. (30) of the text] is

$$(\mathbf{p}^2+m^2)^{\frac{1}{2}}\psi(\mathbf{p}^2)=\lambda\pi^{-1}\int d^3k\frac{1}{(\mathbf{p}-\mathbf{k})^2}\psi(\mathbf{k}^2). \tag{B1}$$

We use a method suggested by Rubinowicz' momentum-space treatment of the Dirac equation for the hydrogen atom.[16] Carrying out the integration over angles in Eq. (1), we obtain (with $m=1$)

$$(1+p^2)^{\frac{1}{2}}\psi(p)=\lambda\int_0^\infty\frac{k}{p}dk\psi(k)\int_{-1}^1\frac{dx}{t-x}$$

$$=2\lambda\int_0^\infty\frac{k}{p}dk\psi(k)Q_0(t), \tag{B2}$$

where $t=(p^2+k^2)/2pk$, and where we have written p for $|\mathbf{p}|$. Q_0 is the zero-order Legendre function of the second kind. We use the following integral representation of that function:[17]

$$Q_0\left(\frac{p^2+k^2}{2pk}\right)=\pi(pk)^{\frac{1}{2}}\int_0^\infty J_{\frac{1}{2}}(sp)J_{\frac{1}{2}}(sk)ds, \tag{B3}$$

which gives

$$(1+p^2)^{\frac{1}{2}}\psi(p)=2\pi\lambda p^{-\frac{1}{2}}\int_0^\infty J_{\frac{1}{2}}(sp)ds$$

$$\cdot\int_0^\infty k^{\frac{1}{2}}dkJ_{\frac{1}{2}}(sk)\psi(k). \tag{B4}$$

We then assume that $\psi(p)$ may be written

$$\psi(p)=p^{-\frac{1}{2}}\int_0^\infty f(x)J_{\frac{1}{2}}(px)xdx, \tag{B5}$$

which is equivalent to assuming that $\psi(p)$ has a Fourier transform. If we insert (B5) into (B4), we obtain

$$(1+p^2)^{\frac{1}{2}}\int_0^\infty f(x)J_{\frac{1}{2}}(px)xdx=2\pi\lambda\int_0^\infty J_{\frac{1}{2}}(sp)ds$$

$$\times\int_0^\infty kdkJ_{\frac{1}{2}}(sk)\cdot\int_0^\infty f(x)J_{\frac{1}{2}}(kx)xdx. \tag{B6}$$

Because of the Hankel inversion theorem, we may write

$$\int_0^\infty kJ_{\frac{1}{2}}(sk)dk\int_0^\infty xf(x)J_{\frac{1}{2}}(xk)dx=f(s), \tag{B7}$$

which yields

$$(1+p^2)^{\frac{1}{2}}\int_0^\infty xf(x)J_{\frac{1}{2}}(px)dx=2\pi\lambda\int_0^\infty f(x)J_{\frac{1}{2}}(px)dx. \tag{B8}$$

We now make use of the following two integral formulas:[18]

$$\int_0^\infty e^{-t}J_{\frac{1}{2}}(pt)dt=[(1+p^2)^{\frac{1}{2}}-1]^{\frac{1}{2}}p^{-\frac{1}{2}}(1+p^2)^{-\frac{1}{4}},$$

$$\int_0^\infty e^{-t}J_{\frac{1}{2}}(pt)\frac{dt}{t}=2[(1+p^2)^{\frac{1}{2}}-1]^{\frac{1}{2}}p^{-\frac{1}{2}}, \tag{B9}$$

which enables us to write

$$(1+p^2)^{\frac{1}{4}}=\frac{1}{2}\int_0^\infty e^{-t}J_{\frac{1}{2}}(pt)\frac{dt}{t}\Big/\int_0^\infty e^{-t}J_{\frac{1}{2}}(pt)dt, \tag{B10}$$

or

$$\int_0^\infty e^{-t}J_{\frac{1}{2}}(pt)\frac{dt}{t}\int_0^\infty J_{\frac{1}{2}}(xp)xf(x)dx$$

$$=4\pi\lambda\int_0^\infty e^{-t}J_{\frac{1}{2}}(pt)dt\int_0^\infty J_{\frac{1}{2}}(xp)f(x)dx. \tag{B11}$$

[18] W. Magnus and F. Oberhettinger, *Special Functions of Mathematical Physics* (Chelsea Publishing Company, New York, 1949).

Multiply both sides of Eq. (B11) by pdp and integrate over p,

$$\int_0^\infty e^{-t}\frac{dt}{t}\int_0^\infty pdpJ_{\frac{1}{2}}(pt)\int_0^\infty xf(x)J_{\frac{1}{2}}(px)dx$$

$$=4\pi\lambda\int_0^\infty e^{-t}dt\int_0^\infty pdpJ_{\frac{1}{2}}(pt)\int_0^\infty f(x)J_{\frac{1}{2}}(px)dx. \quad \text{(B12)}$$

If we use the Hankel inversion formula once more, we obtain

$$\int_0^\infty e^{-t}\frac{dt}{t}f(t)=4\pi\lambda\int_0^\infty e^{-t}\frac{dt}{t}f(t),$$

or

$$4\pi\lambda=1. \quad \text{(B13)}$$

This solution is evidently given by

$$\psi(p)=p^{-\frac{1}{2}}\int_0^\infty e^{-t}dtJ_{\frac{1}{2}}(pt)$$

$$=[(1+p^2)^{\frac{1}{2}}-1]^{\frac{1}{2}}p^{-1}(1+p^2)^{-\frac{1}{4}}, \quad \text{(B14)}$$

and apart from possible degenerate solutions also belonging to $4\pi\lambda=1$, is the only solution having a Fourier transform.

PHYSICAL REVIEW VOLUME 91, NUMBER 6 SEPTEMBER 15, 1953

The Fredholm Theory of the S Matrix

J. HAMILTON
Christ's College, Cambridge, England
(Received May 26, 1953)

The equation for the interaction representation transformation operator is put into integral form and the Fredholm theory of integral equations is used to give an explicit expression for the solution. No extension of the circle of convergence of the S matrix seems possible in the general case.

INTRODUCTION

THE Fredholm theory of linear integral equations has recently been used by Salam and Matthews[1] to study the convergence of the S-matrix expansion for the scattering of an electron in an external time dependant electromagnetic field. The Fredholm solution is expressed as the ratio of two infinite series, both of which have an infinite radius of convergence in terms of the coupling constant, provided that the square of the kernel of the equation is integrable. Salam and Matthews deduce that in general the iterative expansion of the S matrix is convergent, when the quantum fluctuations of the electromagnetic field are ignored.

The Fredholm solution of an integral equation (with a suitably bounded kernel) is identical with the iterative solution in the region in which the latter converges, and if the iterative solution has a finite radius of convergence the Fredholm method gives a continuation of the solution outside this radius of convergence. It seems reasonable to enquire to what extent the Fredholm method can be used to extend the convergence of the S matrix when both the electron and the photon fields are quantized and no external electromagnetic field is present. In view of the good reasons for believing that the iterative solution has zero radius of convergence in terms of the coupling constant,[2] any extension would be of considerable value.

It is necessary to write the equation giving the interaction representation transformation operator $S(t)$ in integral form, and to apply the Fredholm method to this equation. As the integral equation has a q-number kernel it is immediately obvious that the usual theory of the convergence of the Fredholm solution[3] need not be valid. However, it is possible to give an explicit expression for the Fredholm solution. This expression shows that the integral equation method actually has no advantage in the general S-matrix case; and it is easy to see that this fact is closely related to the unitary character of the matrix $S(t)$. It seems to be impossible to derive any benefit from using the integral-equation method once the quantum fluctuations of the electromagnetic field are included.

THE INTEGRAL EQUATION

The operator $S(t)$ satisfies the differential equation

$$ih\partial S(t)/\partial t=\lambda H_R(t)S(t),$$

[1] A. Salam and P. T. Matthews, Phys. Rev. **90**, 690 (1953). The author is grateful for being able to see the typescript of this paper.

[2] F. J. Dyson, Phys. Rev. **85**, 631 (1952); C. A. Hurst, Proc. Cambridge Phil. Soc. **48**, 625 (1952); W. Thirring, Helv. Phys. Acta **26**, 33 (1953); A. Petermann, Arch. Sci. **6**, 5 (1953).

[3] E. T. Whittaker and G. N. Watson, *Modern Analysis* (Cambridge University Press, Cambridge, 1940), 4th edition, Chap. XI.

where $\lambda H_R(t)$ is the spatial integral of the interaction Hamiltonian (expressed in interaction representation variables), and λ is the coupling constant. This equation can be written

$$S(t)=S(-T)-\frac{i}{\hbar}\int_{-T}^{t}\lambda H_R(t)S(t)dt, \quad (-T<t<T), \quad (1)$$

and after integration the limit $T\to\infty$, $S(-T)\to I$ will be imposed. Dividing up the time interval $(-T, T)$ into intervals $(-T, -T+\delta)$, $(-T+\delta, -T+2\delta)$, $\cdots(T-\delta, T)$ where δ/T is small, Eq. (1) can be written as a set of simultaneous linear matrix equations,

$$\begin{aligned}
&S(-T+\delta)+(i/\hbar)\lambda\delta H_R(-T+\delta)S(-T+\delta)=S(-T),\\
&S(-T+2\delta)+(i/\hbar)\lambda\delta H_R(-T+\delta)S(-T+\delta)\\
&\qquad+(i/\hbar)\lambda\delta H_R(-T+2\delta)S(-T+2\delta)=S(-T), \quad (2)\\
&\cdots\cdots\cdots\cdots\cdots\cdots\cdots\cdots\\
&S(T)+(i/\hbar)\lambda\delta H_R(-T+\delta)S(-T+\delta)+\cdots\\
&\qquad+(i/\hbar)\lambda\delta H_R(T)S(T)=S(-T).
\end{aligned}$$

Each line of the set (2) represents as many equations as there are free particle states of the system. Following the usual form of the Fredholm theory[3] it is clear that the discriminant $D(\lambda)$ of the Eqs. (2) is a determinant of the form

$$D(\lambda)=\begin{array}{c|cccccc|c}
 & (-T+\delta) & (-T+2\delta) & (-T+3\delta) & \cdots & \cdots & (T) & \\
\hline
 & \cdots & & & & & & \\
 & \cdots & 0 & 0 & 0 & \cdots & 0 & (-T+\delta)\\
 & \cdots & & & & & & \\
\hline
 & \cdots & \cdots & & & & & \\
 & \cdots & \cdots & 0 & 0 & \cdots & 0 & (-T+2\delta)\\
 & \cdots & \cdots & & & & & \\
\hline
 & \cdots & \cdots & \cdots & & & & \\
 & \cdots & \cdots & \cdots & 0 & \cdots & 0 & (-T+3\delta)\\
 & \cdots & \cdots & \cdots & & & & \\
\hline
 & \cdots & \cdots & \cdots & \cdots & \cdots & \cdots & \cdots\\
\hline
 & \cdots & \cdots & \cdots & \cdots & \cdots & \cdots & \cdots\\
\hline
 & \cdots & \cdots & \cdots & \cdots & \cdots & & \\
 & \cdots & \cdots & \cdots & \cdots & \cdots & 0 & (T)\\
 & \cdots & \cdots & \cdots & \cdots & \cdots & &
\end{array} \quad (3)$$

In the above the time variables have been labeled while the subsets consisting of the free-particle variables have not been indicated. The square block of terms at the intersection of the $(-T+r\delta)$ rows and columns form the matrix

$$I+(i/\hbar)\lambda\delta H_R(-T+r\delta),$$

while blocks of terms $(i/\hbar)\lambda\delta H_R(-T+s\delta)$, $(s<r)$ lie to the left of it, and blocks of zeros lie to the right.

It follows that

$$\begin{aligned}
D(\lambda)&=\det[I+(i/\hbar)\lambda\delta H_R(-T+\delta)]\\
&\quad\times\det[I+(i/\hbar)\lambda\delta H_R(-T+2\delta)]\cdots\\
&\quad\times\det[I+(i/\hbar)\lambda\delta H_R(T)]\\
&=\det\{[I+(i/\hbar)\lambda\delta H_R(-T+\delta)]\\
&\quad\times[I+(i/\hbar)\lambda\delta H_R(-T+2\delta)]\cdots\\
&\quad\times[I+(i/\hbar)\lambda\delta H_R(T)]\}\\
&=\det\Big[I+\frac{i\lambda}{\hbar}\int_{-T}^{T}H_R(t_1)dt_1\\
&\quad+\Big(\frac{i\lambda}{\hbar}\Big)^2\int_{-T}^{T}dt_1\int_{-T}^{t_1}dt_2H_R(t_2)H_R(t_1)+\cdots\Big].
\end{aligned}$$

Taking the limit $T\to\infty$, $S(-T)\to I$ gives

$$D(\lambda)=\det[S^*(\infty)], \quad (4)$$

where $S(\infty)$ is the usual perturbation theory expansion of the S matrix,[4] and the asterisk denotes the Hermitian conjugate. It follows in the usual way that the Fredholm solution of (1) is

$$S(\infty)\cdot D(\lambda)/D(\lambda) \quad (5)$$

the numerator being the power series in λ obtained by multiplying the series for $S(\infty)$ and $D(\lambda)$. Any extension of the radius of convergence resulting from using (5) will clearly depend on the form of $D(\lambda)$. As $S(\infty)$ is a

[4] F. J. Dyson, Phys. Rev. **75**, 486 (1949).

unitary matrix it follows that $\det[S(\infty)]$ should be of the form $\exp(i\phi)$ where ϕ is real. The expansion of ϕ as a power series in λ will be derived below, but it is clear that with $D(\lambda)=\exp(-i\phi)$ Eq. (5) cannot improve on the convergence of $S(\infty)$. If $D(\lambda)$ has no zeros it cannot remove any singularities that may be present in $S(\infty)$.

THE DISCRIMINANT

From Eq. (4) it follows that one factor of $D(\lambda)$ is $\langle S^*(\infty)\rangle_{\text{vac}}$, the vacuum expectation value of $S^*(\infty)$. This has been shown by Feynman[5] to be of the form

$$\langle S(\infty)\rangle_{\text{vac}}=\exp(\tfrac{1}{2}h_2+\tfrac{1}{4}h_4+\tfrac{1}{6}h_6+\cdots), \qquad (6)$$

where h_{2n} is the sum of the vacuum contributions from all *connected* graphs with $2n$ vertices. All the h_{2n} are pure imaginary in the absence of an external electromagnetic field.

The remaining factor of $D(\lambda)$ will be found by evaluating the free particle state contribution to $\det[S(\infty)]$. The over-all energy momentum conservation leads to (infinite) constants which are identical in the numerator and the denominator of Eq. (5), and can be omitted. Free particle states will be denoted by $\alpha, \beta, \gamma, \cdots$. Suppose that the elements of an infinite determinant are $\delta_{rs}-\mu k_{rs}$; $r, s=1, 2, 3, \cdots$, where δ_{rs} is the Kronecker delta function and μk_{rs} are complex numbers such that the determinant converges. Then it is easy to see that

$$\det(\delta_{rs}-\mu k_{rs})=\exp[-(\mu\sum_r k_{rr}+\tfrac{1}{2}\mu^2\sum_{r,s}k_{rs}k_{sr} +\tfrac{1}{3}\mu^3\sum_{r,s,t}k_{rs}k_{st}k_{tr}+\cdots)]. \qquad (7)$$

It is convenient to use the division of the S-matrix elements into parts representing processes having real intermediate states (i.e., real graph parts) and parts representing processes having purely virtual intermediate states (i.e., virtual graph parts). Following Gupta and the author,[6] it is clear that

$$[S(\infty)]_{\alpha\beta}=\delta_{\alpha\beta}+G_{\alpha\beta}+\tfrac{1}{2}\sum_\gamma G_{\alpha\gamma}G_{\gamma\beta} +\frac{1}{2^2}\sum_{\gamma,\epsilon}G_{\alpha\gamma}G_{\gamma\epsilon}G_{\epsilon\beta}+\cdots, \qquad (8)$$

where $G_{\alpha\beta}$ is the sum of all virtual graph parts connecting the free particle states α and β. In (8) the summations over γ, ϵ, $\cdots$ are to be taken over all possible free particle states. The virtual graph parts $G_{\alpha\beta}$ are anti-Hermitian, i.e., $G_{\alpha\beta}{}^*=-G_{\alpha\beta}$.[6]

[5] R. P. Feynman, Phys. Rev. **76**, 749 (1949).
[6] S. N. Gupta, Proc. Cambridge Phil. Soc. **47**, 454 (1951); J. Hamilton, Proc. Cambridge Phil. Soc. **48**, 640 (1952).

Substitution of (8) in (7) yields

$$\det[S(\infty)]=\langle S(\infty)\rangle_{\text{vac}}\cdot\exp(A_1\sum_\alpha G_{\alpha\alpha}+A_2\sum_{\alpha,\beta}G_{\alpha\beta}G_{\beta\alpha} +A_3\sum_{\alpha,\beta,\gamma}G_{\alpha\beta}G_{\beta\gamma}G_{\gamma\alpha}+\cdots),$$

where

$$A_{n+1}=\frac{1}{2^n}-\frac{1}{2}\binom{n}{1}\frac{1}{2^{n-1}}+\frac{1}{3}\binom{n}{2}\frac{1}{2^{n-2}}-\cdots+(-1)^n\frac{1}{n+1}$$
$$=\frac{1}{2^{n+1}}\int_0^2(1-x)^n dx=\begin{cases}0, & n \text{ odd};\\ 1/2^n(n+1), & n \text{ even}.\end{cases}$$

Hence

$$\det[S(\infty)]=\langle S(\infty)\rangle_{\text{vac}} \cdot\exp\left(\sum_\alpha G_{\alpha\alpha}+\frac{1}{3}\cdot\frac{1}{2^2}\sum_{\alpha,\beta,\gamma}G_{\alpha\beta}G_{\beta\gamma}G_{\gamma\alpha}+\cdots\right). \qquad (9)$$

As the terms containing the product of an even number of $G_{\alpha\beta}$ have vanished, the argument of the exponential in (9) is pure imaginary. The discussions of convergence mentioned above[2] suggest that this series for $i\phi$ is divergent. Salam and Matthews[1] found that in the external-field case the terms corresponding to (9) could be written in the form $\exp(-\xi+i\phi)$, where ξ, ϕ are real and $\xi>0$. ξ is closely related to the cross section for the production of electron pairs by the external field, and it has no analog in the present, more complete theory.

Finally, it is worth noting that the Cayley form of the S matrix[7] can be used to express the results concisely. Writing $K_{\alpha\beta}=iG_{\alpha\beta}$ Eq. (8) can be written formally

$$S=(1-\tfrac{1}{2}iK)/(1+\tfrac{1}{2}iK),$$

where K is the (Hermitian) Cayley matrix. Then (9) can be written

$$D(\lambda)=\langle S^*(\infty)\rangle_{\text{vac}}\,\text{exp trace}\,2[(\tfrac{1}{2}iK)+\tfrac{1}{3}(\tfrac{1}{2}iK)^3+\cdots]$$
$$=\langle S^*(\infty)\rangle_{\text{vac}}\,\text{exp trace}\,\log\left(\frac{1+\frac{1}{2}iK}{1-\frac{1}{2}iK}\right)$$
$$=\langle S^*(\infty)\rangle_{\text{vac}}\,\text{exp trace}\,\log S^*(\infty).$$

I am indebted to Dr. Abdus Salam for his comments and for pointing out the last formula.

Note added in proof:—The renormalization of Eq. (5) can be investigated along the lines indicated by Salam and Matthews (see reference 1).

[7] S. N. Gupta (see reference 6); J. Schwinger, Phys. Rev. **74**, 1439 (1948).

Many-Body Forces and Nuclear Saturation*†

S. D. DRELL AND KERSON HUANG‡
Department of Physics and Laboratory of Nuclear Science, Massachusetts Institute of Technology, Cambridge, Massachusetts
(Received June 10, 1953)

Nuclear saturation is studied with many-body interactions derived from pseudoscalar meson theory with pseudoscalar coupling. All parameters appearing in this calculation are fixed on the basis of the work of Lévy, who has shown that leading terms in a perturbation deduction of the two-body interaction are well fitted to reproduce the experimental data. The leading term in the n-body potential depends only on the interparticle distances and is repulsive (attractive) for n odd (even). The energy of the nucleus is calculated with potentials up through five-body interactions and with neglect of Coulomb and surface effects. Saturation properties derived from these considerations are in accord with experience. Antisymmetrization of the nuclear wave function reduces the many-body interaction energies considerably by inhibiting the close approach of many particles. Thus the Pauli exchange terms are found to reduce the five-body interaction energy by 76 percent and to give a rapid convergence for the expansion in n-body forces.

I. INTRODUCTION

ONE of the outstanding problems of nuclear structure is the explanation of the saturation of nuclear forces in complex nuclei. The main facts involved in this problem are the saturation of nuclear density and the saturation of binding energy. The first refers to the fact that the density of nuclear matter seems to be very roughly independent of mass number A, for all but the lightest nuclei. Observed nuclear radii equal, approximately,

$$R_0 = 1.4A^{\frac{1}{3}} \times 10^{-13} \text{ cm} = A^{\frac{1}{3}}/\mu,$$

with μ^{-1} defined as the meson Compton wavelength. Saturation of nuclear binding energy refers to the fact that the average binding energy per nucleon is roughly independent of A and approximately equal to 8 Mev.

These saturation features limit the choice of acceptable theories of nuclear forces. For example, purely attractive forces between pairs of nucleons (Wigner forces) are excluded.[1]

In 1932, Heisenberg[2] borrowed the concept of exchange forces from molecular theory and applied it to the nucleon-nucleon interaction problem. With the introduction of such forces as these, which are attractive or repulsive depending on the symmetry of the interacting nucleon pairs, it has proved possible to account for nuclear stability in terms of static, central, two-body potentials of short range. Combinations of ordinary and exchange forces consistent both with the saturation requirements and with observations on deuterons, α particles, and nucleon-nucleon scattering have been given during the 1930's by Wigner, Breit, Feenberg, Kemmer, Volz, and others.[3]

Recently, however, the study of the n-p and p-p scattering cross sections in the energy region up to 300 Mev has cast some doubt upon the role of exchange forces as the main reason of saturation. The analysis by Christian and Hart[4] seems to reveal a mixture of ordinary and exchange forces (Serber force) inconsistent with the saturation requirements.[5] It must be said, however, that this analysis is based upon rather incomplete experimental data; and the result, therefore, cannot be taken to exclude definitely the explanation of saturation by two-body exchange forces.

It has often been recognized and remarked that the limitation of considerations within the framework of two-body, velocity-independent interactions was too restrictive. Primakoff and Holstein[6] and Wheeler[7] have discussed extensions of the basis of considerations to include many-body and velocity-dependent forces. Also the development of meson theories of nuclear forces has suggested that, especially, the many-body forces should play an important role in nuclear matter. The interaction between mesons and nucleons is strong enough so that meson exchanges will be frequent between more than two neighboring nucleons, and this phenomenon leads to many-body forces.

The present status of meson theory is too uncertain to permit us to draw any quantitative conclusions, let alone to rely upon them. In this paper we consider the pseudoscalar meson theory with pseudoscalar coupling

* This work was assisted in part by the joint program of the U. S. Office of Naval Research and the U. S. Atomic Energy Commission.

† Part of a Doctoral thesis submitted by K. Huang to the Physics Department at the Massachusetts Institute of Technology.

‡ E. I. duPont de Nemours Fellow.

[1] J. M. Blatt and V. F. Weisskopf, *Theoretical Nuclear Physics* (J. Wiley and Sons, New York, 1952), Chap. III. In the following, we refer to this book as B.W.

[2] W. Heisenberg, Z. Physik **77**, 132 (1932).

[3] G. Breit and E. P. Wigner, Phys. Rev. **53**, 998 (1938). For a comprehensive bibliography of the literature on this subject, see L. Rosenfeld, *Nuclear Forces* (North Holland Publishing Company, Amsterdam, 1948), Chap. XI.

[4] R. S. Christian and E. W. Hart, Phys. Rev. **77**, 441 (1950).

[5] This question is discussed in reference 1, Chap. IV. More recently E. Lomon and H. Feshbach [Bull. Am. Phys. Soc. **28**, No. 3, 30 (1953)] have shown that the scattering data can also be analyzed with forces which give odd-state repulsions that are absent from a Serber mixture.

[6] H. Primakoff and T. Holstein, Phys. Rev. **55**, 218 (1939); L. Janossy, Proc. Cambridge Phil. Soc. **35**, 616 (1939); N. N. Svartholm, thesis, Lund, 1945 (unpublished).

[7] J. A. Wheeler, Phys. Rev. **52**, 1083 (1937).

as a guide with which to explore some possible forms which many-body forces may assume, and we study the implications of these forces for the saturation problem.

We are using a very primitive approach in the evaluation of the meson theory. Perturbation theory is employed and only the leading terms, in powers of the meson-nucleon coupling constant $G^2/4\pi$ multiplied by the meson-nucleon mass ratio μ/M are considered, although it has been shown that other terms contribute also and may change the results considerably.[8] The two-body interaction emerging from this calculation is identical with the one derived by Lévy,[9] and it seems to be well fitted to reproduce the two-body experimental data. We then choose for our work the same coupling constant as Lévy has used.

We note especially one feature of the Lévy two-body force: Outside of a repulsive core of radius $r_c=0.38/\mu$, it contains a strongly attractive short-ranged Wigner force and two longer-ranged forces, one proportional to $(\boldsymbol{\sigma}_1\cdot\boldsymbol{\sigma}_2)(\boldsymbol{\tau}_1\cdot\boldsymbol{\tau}_2)$, the other to $(\boldsymbol{\tau}_1\cdot\boldsymbol{\tau}_2)S_{12}$, where S_{12} is the tensor operator. The combination of these terms reproduces a characteristic feature of the two-body interaction; namely, that the range of the tensor force is longer than the range of the central force. The strongly attractive short-ranged Wigner force comes from the exchange of meson pairs, and it is this exchange, when applied to more than two nucleons, which gives rise to the leading terms of the many-body forces. We are aware that this primitive evaluation of the pseudoscalar meson theory neglects terms which may be important and, indeed, not negligible. However, we plan to use it as a first exploration of the many-body forces and to make use of the fact that it gives us a set of many-body interactions without the introduction of any new adjustable constants. It is hoped that their orders of magnitude, shapes, and nonexchange properties are guessed correctly by this procedure.

One of the most striking properties of these many-body forces is their alternation in sign. The potentials between odd (even) numbers of nucleons are repulsive (attractive). The average distance between nucleons at which the forces act decreases with increasing number, and at the same time the Pauli exclusion principle makes it more difficult for the nucleons to approach close to one another. These features are the main reasons for the saturating effects of the many-body forces. In fact, the repulsive three-body forces contribute most decisively to the potential energy and prevent the nucleus from collapsing.

Another effect of possible importance derives from the many-body forces. The marked position correlation between nucleons resulting from strong, short-ranged two-body forces is difficult to harmonize with the shell theory model of a nucleon moving in an average potential hole. The introduction of many-body repulsive interactions will tend to weaken the correlation between nucleons and bring the two viewpoints into closer accord.

The program of this paper is to study the effect of many-body forces upon the energies of complex nuclei in their lowest states. We use the results of the pseudoscalar meson theory as a characteristic example of such forces, without implying their correctness.

The pioneering work of this nature is that of Wentzel[10] in 1942. He discussed these questions on the basis of a meson scalar pair theory and by treating the nucleus as an infinitely large source of uniform finite density. His methods and results will be discussed in Sec. IV.

We should mention here another recently developed approach to an understanding of nuclear saturation from the point of view of nonlinear meson theory. Schiff[11] has studied the possible forms of nonlinearities which may be introduced into the meson equations, in a classical field treatment, and which predict saturation. The effective mesic self-repulsion introduced by the nonlinearity is the primary agent preventing collapse of the nucleus in this approach.

II. OUTLINE AND SUMMARY

A brief outline and summary of our calculations are presented in this section. Lévy's difficult and important analysis of the low-energy properties of the two-nucleon system provides the point of departure for the present work. Lévy has applied the methods of Tamm[12] and Dancoff[13] to calculate an effective two-body interaction with the pseudoscalar meson theory through terms of order $(G^2/4\pi)(\mu/2M)^2$, $(G^2/4\pi)^2(\mu/2M)^2$, and $(G^2/4\pi)^2(\mu/2M)^3$, where $(G^2/4\pi)$ is the meson-nucleon coupling constant and μ and M are the meson and nucleon masses, respectively. Lévy argued that, for internucleon separations $r\gtrsim(M\mu)^{-\frac{1}{2}}$, terms of these orders in the coupling constant and mass ratio are of major importance in determining the potential shape and depth.[9] For separations $r\lesssim(M\mu)^{-\frac{1}{2}}$ a complete analysis was not possible, but Lévy developed arguments from the field theory indicating a strong repulsion in this range. With choice of $G^2/4\pi=10$ and of the radius of the repulsive core $r_c=0.38/\mu$, the Lévy potential has been impressively successful in matching the data for n-p and p-p systems with energies up through 40 Mev.

[8] We elaborate on this point in Sec. III, which is concerned with the deduction of the interaction potentials from the meson field theory.

[9] M. M. Lévy, Phys. Rev. **88**, 725 (1952). We consider just the two leading and important terms V_2 and $V_4^{(a)}$ in Lévy's work. Algebraic errors in his calculation of the correction terms, independently noticed by A. Klein, Phys. Rev. **89**, 1158 (1953), destroy the validity of his convergence arguments. This is discussed more fully in Sec. III.

[10] G. Wentzel, Helv. Phys. Acta **15**, 111 (1942); **25**, 569 (1952).

[11] L. I. Schiff, Phys. Rev. **83**, 1 (1951); B. J. Malenka, Phys. Rev. **86**, 68 (1952); D. Finkelstein, Ph.D. thesis, Massachusetts Institute of Technology, 1953 (unpublished).

[12] I. Tamm, J. Phys. (U.S.S.R.) **9**, 449 (1945).

[13] S. M. Dancoff, Phys. Rev. **78**, 382 (1950).

Guided by Lévy's success and viewpoint, and adopting his parameters, we derive the interaction potential from pseudoscalar meson theory for n-body interactions. The leading term for an n-body interaction is proportional to λ^n with λ defined by $\lambda=(G^2/4\pi)(\mu/2M)$, is repulsive or attractive according as n is odd or even, and is a function of the magnitudes of the interparticle separations only. These potentials are identical with those of Wentzel's scalar pair theory,[10] as is readily shown with the Dyson[14] or Foldy[15] transformation. In our calculations of the energies, we consider those potential terms which are proportional to λ^2 and to $\lambda\mu/M$ for the two-body interaction, and to λ^n for n-body interactions ($n>2$). We then determine the nuclear potential energies by taking expectation values of these interaction potentials with a completely antisymmetrized wave function of A particles confined to a box of radius $R=\eta R_s$. In order to determine, firstly, whether the three-body repulsion derived from the pseudoscalar theory is qualitatively sufficient to prevent collapse of heavy nuclei and, secondly, under what conditions it is possible to make a convergent expansion of the interactions in a series of n-body forces, we approximate the wave function for each of the A nucleons by plane waves for *all* internucleon separations greater than r_c. Within the repulsive cores, the wave function is taken to vanish. The potential energy per nucleon for two- plus three-body interactions resulting from this calculation shows a minimum of depth 30 Mev at a nuclear radius of $R=1.0R_s$. If we include the contribution of four plus five-body interactions, we find only a slight shift in the minimum to a depth of 32 Mev at a radius $R=1.1R_s$. It is of interest to note just briefly here the primary reason for the smallness of the effect of many-body interactions for $n>3$. As n increases, the range of the many-body potentials decreases, and at the same time the Pauli exclusion principle makes it more difficult for the n bodies to approach close to one another.

For the kinetic energies of the nuclear particles, we refer to a calculation of Lenz[16] in 1929. Point nucleons obeying the Pauli exclusion principle have the usual Fermi kinetic energy due to the filling of free particle energy levels. The requirement that the wave function vanish whenever any two nucleons approach within a separation of r_c, the hard core radius, of one another increases the wave function curvature and, hence, the kinetic energy above the Fermi value. With Lenz's approximate result for this increase, we write for the kinetic energy,

$$T=T_F(1+0.82/\eta), \tag{1}$$

where T_F denotes the Fermi energy. If Eq. (1) is added to the potential energy, there emerges finally an expression for the total energy per nucleon with a minimum of depth 12-Mev at a radius $R=1.15R_s$. Since surface and Coulomb effects have been neglected in the calculations outlined above, the 12-Mev binding energy per nucleon that we obtain is to be compared with the volume binding energy term in the von Weizsacker semiempirical formula.[17] Feenberg's[18] analysis gives approximately 14-Mev per nucleon for this.

Once it is established that the three-body force of pseudoscalar theory used in this calculation can qualitatively explain nuclear saturation, and that an expansion in n-body forces has meaning, it becomes desirable to improve the quantitative value of our results with more realistic wave functions. If the step-function correlation form discussed above is applied literally in the calculation of the kinetic energy, it yields an infinitely large result because of its discontinuity at the edge of the hard core. One can construct trial functions that go to zero continuously at the core and can then perform a variational calculation for the minimum value of the kinetic plus potential energy. Jastrow[19] has suggested a function in the form of a Slater determinant for the A free-particle states multiplied by $\frac{1}{2}A(A-1)$ symmetric correlation terms, one for each pair. The correlation term for each pair is identical in form and is taken to fall smoothly to zero for interparticle separations $r\leq r_c$. The parameters that determine the shape of a correlation term then are varied and the minimum energy found. Calculations of this type have been carried through and yield reasonable saturation as above. The correlation term corresponding to the minimum energy is essentially constant for $r>r_c$, indicating no marked tendency for nucleons to cluster or to anticluster. This result suggests that many-body repulsive forces may be of importance in harmonizing the two different viewpoints of the meson theory, which predicts strong internucleon interactions, and of the shell theory, which is based on the independent particle model. Further discussion on the calculations and results is presented in the following sections.

III. POTENTIALS

The interaction potentials are derived from the pseudoscalar meson theory in this section. The problem of two interacting nucleons is analyzed, first in order to illustrate the method of our calculations, and to show clearly the approximations inherent in the work.

We write for the interaction term in the Hamiltonian for nucleons and charge-symmetric pseudoscalar mesons with pseudoscalar coupling,

$$H'=iG\sum_{\alpha=1}^{3}\int\bar{\psi}\gamma_5\tau_\alpha\varphi_\alpha\psi d\tau, \tag{2}$$

where ψ and $\bar{\psi}=\psi^*\gamma_4$ are the quantized nucleon field amplitudes; φ_α, with $\alpha=1, 2, 3$, are the amplitudes of

[14] F. J. Dyson, Phys. Rev. **73**, 929 (1948).
[15] L. L. Foldy, Phys. Rev. **84**, 168 (1951).
[16] W. Lenz, Z. Physik **56**, 778 (1929).
[17] Reference 1, Chap. VI.
[18] E. Feenberg, Revs. Modern Phys. **19**, 239 (1947).
[19] R. Jastrow (private communication).

FIG. 1. Feynman diagrams for two-body interactions of order $(G^2/4\pi)(\mu/M)^2$, $(G^2/4\pi)^2(\mu/M)^2$, and $(G^2/4\pi)^2(\mu/M)^3$.

the meson field; and τ_a are the usual two-by-two isotopic spin (charge) matrices. We perform now the canonical transformation introduced by Dyson[14] to a new representation in which the velocity-independent aspects of the nucleon motion are more readily identified. This transformation is discussed by Lepore[20] and by Drell and Henley,[21] in whose work it is explicitly carried through in closed form. Keeping only the leading terms in G/M, the effects of which will be included in the calculations presented here, we write for the effective interaction Hamiltonian,

$$H_{\text{eff}}=(G^2/2M)\int\bar{\psi}\psi\varphi^2 d\tau + (G/2M)\int(\bar{\psi}\tau_a\sigma\psi)\cdot(\nabla\varphi_a)d\tau. \quad (3)$$

The first term of Eq. (3) is recognized as the scalar pair term of Wentzel's theory, and the second one as the usual gradient coupling term. These two terms are the only ones that need be considered in order to derive n-body interaction potentials of order λ^n, $\lambda^{n-1}(\mu/M)$, and $\lambda^n(\mu/M)$, with $\lambda\equiv(G^2/4\pi)(\mu/2M)$.

With the interaction Hamiltonian cast in this representation, one can immediately apply adiabatic perturbation theory in the limit of fixed delta-function sources, for interparticle distances $r\gtrsim(M\mu)^{-1}$. The Feynman diagrams of the processes considered for two-body interactions appear in Fig. 1. The direct result is

$$\begin{aligned}V^{2\text{-body}}&=V_2+V_4^{(a)}+V_4^{(c)}\\&=-\left(\frac{G}{2M}\right)^2\frac{2\tau_1\cdot\tau_2}{2(2\pi)^3}\int d\mathbf{q}(\boldsymbol{\sigma}_1\cdot\mathbf{q})(\boldsymbol{\sigma}_2\cdot\mathbf{q})\frac{e^{i\mathbf{q}\cdot\mathbf{r}}}{\omega_q^2}\\&\quad-\left(\frac{G^2}{2M}\right)^2\frac{2\cdot6}{4(2\pi)^6}\int\int d\mathbf{p}d\mathbf{q}\frac{e^{i(\mathbf{p}+\mathbf{q})\cdot\mathbf{r}}}{\omega_p\omega_q(\omega_p+\omega_q)}\\&\quad-\left(\frac{G^2}{2M}\right)\left(\frac{G}{2M}\right)^2\frac{6}{4(2\pi)^6}\int d\mathbf{p}d\mathbf{q}(\mathbf{p}\cdot\mathbf{q})\frac{e^{i(\mathbf{p}+\mathbf{q})\cdot\mathbf{r}}}{\omega_p\omega_q}\\&\quad\times\left[\frac{1}{\omega_p\omega_q}+\frac{1}{\omega_q(\omega_q+\omega_p)}+\frac{1}{\omega_p(\omega_q+\omega_p)}\right]\\&=\tfrac{1}{3}\lambda(\mu/2M)(\tau_1\cdot\tau_2)\{\boldsymbol{\sigma}_1\cdot\boldsymbol{\sigma}_2+S_{12}[1+3/(\mu r)\\&\quad+3/(\mu r)^2]e^{-\mu r}/r\}-(3\lambda^2/\mu r^2)\{(2/\pi)K_1(2\mu r)\\&\quad-(\mu/M)[1+(1/\mu r)]^2e^{-2\mu r}\},\end{aligned} \quad (4)$$

where $S_{12}=(3/r^2)(\boldsymbol{\sigma}_1\cdot\mathbf{r})(\boldsymbol{\sigma}_2\cdot\mathbf{r})-\boldsymbol{\sigma}_1\cdot\boldsymbol{\sigma}_2$ is the tensor force operator, $\omega_q=(q^2+\mu^2)^{\frac{1}{2}}$, and $K_1(x)$ is the Hankel function of the first kind, with imaginary argument.[9] The last term $V_4^{(c)}$ in Eq. (4) differs from the corresponding term of order $\lambda^2\mu/M$ in Lévy's potential[9] (denoted as $V_4^{(b)}$). Whereas Lévy's $V_4^{(b)}$ was attractive and of minor importance and indicated the convergence of his procedure, the $V_4^{(c)}$ in Eq. (4) is repulsive, of comparable magnitude with $V_4^{(a)}$, which it largely cancels, and indicates the danger in neglecting terms of higher order[9,22] in μ/M. The terms in Eq. (4) appear in Fig. 2, from which it is clear that the above expression for $V^{2\text{-body}}$ cannot fit known properties of the two-nucleon system. It remains, however, as shown by Lévy that a potential of the form

$$V^{2\text{-body}}=\begin{cases}V_2+V_4^{(a)}, & r>r_c,\\ \infty, & r<r_c,\end{cases} \quad (5)$$

is spectacularly successful in describing the low-energy two-nucleon interaction. As a basis for further discussion, we adopt here the attitude that only the leading order terms in the pseudoscalar meson theory calculations are to be taken literally. We cannot give a rigorous argument to support the validity of this assumption, as we have no convergent procedure for calculating the many higher-order graphs that contribute. Thus, as shown by Lévy in his paper, there are radiative corrections to the lowest-order graphs in Fig. 1 that give large contributions.[22,23] Special classes

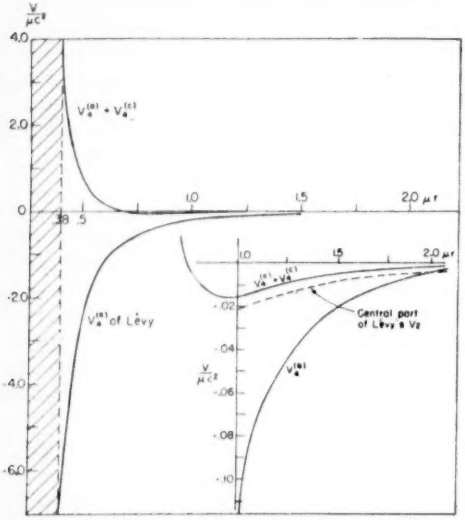

FIG. 2. The two-body interaction potential as expressed by Eq. (4). The dotted curve in the inset represents the contribution of the central part of V_2 for the deuteron ground state.

[20] J. V. Lepore, Phys. Rev. **88**, 750 (1952).
[21] S. D. Drell and E. M. Henley, Phys. Rev. **88**, 1053 (1952).
[22] A. Klein, Bull. Am. Phys. Soc. **28**, No. 3, 36 (1953).
[23] M. Ruderman, Phys. Rev. **90**, 183 (1953).

of these have been summed,[24] but the general problem remains unsolved. However, this approach gives a two-body potential, Eq. (5), that "works," and it permits us to derive many-body potentials consistent with it.

The leading term responsible for the three-body interaction is of order λ^3, corresponding to the pair term of Eq. (3) operating at each vertex. The diagram for the process appears in Fig. 3. The interaction potential is obtained readily with the identical methods as applied in the two-body case. It is, for interparticle distances $\mathbf{r}_{12}$, $\mathbf{r}_{23}$, and $\mathbf{r}_{31}$,

$$V^{3\text{-body}}=\left(\frac{G^2}{2M}\right)^3\frac{2\cdot 24}{8(2\pi)^9}\int\int\int d\mathbf{p}d\mathbf{q}d\mathbf{k}$$
$$\times\frac{e^{i(\mathbf{p}\cdot\mathbf{r}_{12}+\mathbf{q}\cdot\mathbf{r}_{23}+\mathbf{k}\cdot\mathbf{r}_{31})}}{\omega_p\omega_q\omega_k}\left[\frac{1}{(\omega_p+\omega_q)(\omega_p+\omega_k)}\right.$$
$$\left.+\frac{1}{(\omega_q+\omega_p)(\omega_q+\omega_k)}+\frac{1}{(\omega_k+\omega_p)(\omega_k+\omega_q)}\right]$$
$$=-\left(\frac{G^2}{2M}\right)^3\left(\frac{3}{2\pi^6}\right)(r_{12}r_{23}r_{31})^{-1}\int\int\int_0^\infty dpdqdk$$
$$\times(p\sin pr_{12})(q\sin qr_{23})(k\sin kr_{31})$$
$$\times\left[\frac{1}{\omega_p(\omega_q{}^2-\omega_p{}^2)(\omega_k{}^2-\omega_p{}^2)}\right.$$
$$+\frac{1}{\omega_q(\omega_p{}^2-\omega_q{}^2)(\omega_k{}^2-\omega_q{}^2)}$$
$$\left.+\frac{1}{\omega_k(\omega_p{}^2-\omega_k{}^2)(\omega_q{}^2-\omega_k{}^2)}\right].$$

The singularities introduced in the process of rationalizing the energy denominators are simply and unambiguously handled by assigning small, numerically ordered imaginary masses to the mesons: *viz.*, $\omega_p\rightarrow(p^2+\mu^2+i\epsilon_p)^{\frac{1}{2}}$. We find readily

$$V^{3\text{-body}}=\left(\frac{\lambda}{\mu}\right)^3\left(\frac{24}{\pi}\right)(r_{12}r_{23}r_{31})^{-1}$$
$$\times\int_0^\infty(k/\omega)\sin[k(r_{12}+r_{23}+r_{31})]dk$$
$$=12\lambda^3\left(\frac{2}{\pi}\right)\frac{K_1[\mu(r_{12}+r_{23}+r_{13})]}{\mu^2r_{12}r_{23}r_{31}}. \qquad (6)$$

Thus we see that the leading contribution to the three-body interaction is repulsive, spin and charge independent, and a function of the three interparticle distances only. The three-body terms of order $\lambda^2\mu/M$ and $\lambda^3\mu/M$, which arise when a pair of mesons is absorbed by a nucleon, one at a time, via the gradient coupling term in Eq. (3), are calculated in a similar manner. They are discussed in Appendix A and shown not to affect our saturation considerations because of their angular properties. It is, of course, not consistent to introduce them here since we have neglected the analogous term in the two-body analysis, $V_4{}^{(c)}$ in Eq. (4), in order to fit the data on the low-energy 2-nucleon system.

[24] Brueckner, Gell-Mann, and Goldberger, Phys. Rev. **90**, 476 (1953).

FIG. 3. Feynman diagram for the three-body interaction resulting from the pair term operating at each vertex.

The general n-body interaction potential for $n\leqslant 5$ has been deduced directly as above and expressed as a sum over the $(n-1)!/2$ possible perimeters of a K_1 function of a perimeter divided by the product of the n legs forming the perimeter. An argument extending this result for all n is given in Appendix (B). The expression obtained is

$$V^{n\text{-body}}=-(3\mu/\pi)(-2\lambda)^n\sum_{i=1}^{(n-1)!/2}\frac{K_1(p_i)}{l_{i1}l_{i2}\cdots l_{in}}, \qquad (7)$$

with p_i equal to μ times the ith perimeter, and $l_{i\alpha}$ equal to μ times the αth leg of the ith perimeter. Thus, for $n=4$, there are three possible perimeters, as illustrated in Fig. 4 together with the corresponding graphs. We notice that the even-body forces are attractive and the odd ones are repulsive.[25]

Wentzel[10] has given a very elegant procedure for obtaining the n-body interactions with the scalar pair theory, in which he takes the limit of fixed sources but makes no assumptions as to the magnitude of the coupling parameter. For interparticle distance greater than the radius of the Lévy-Jastrow[26] repulsive core, his results are of the same form as Eq. (7), but have

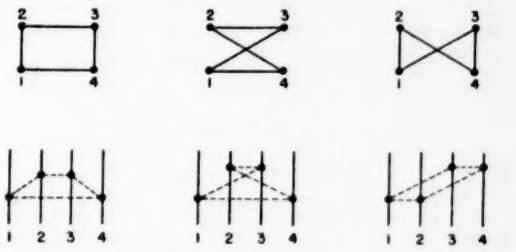

FIG. 4. The three distinct perimeters of a four-body configuration and their corresponding Feynman graphs for interactions via the pair term.

[25] This sign alternation has its formal origin in our calculations in the fact that the n-body potential is obtained by nth-order perturbation theory, with each of the $(n-1)$ energy denominators negative in sign.

[26] R. Jastrow, Phys. Rev. **79**, 389 (1950); **81**, 165 (1951).

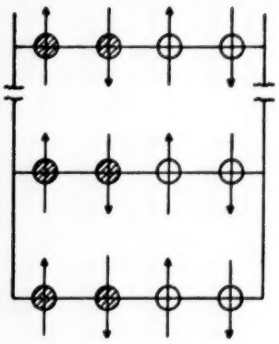

FIG. 5. Schematic picture of filled energy levels for a nucleus containing equal numbers of protons and neutrons, with one-half of each having spin up and spin down.

smaller effective coupling constants which reduce to the results of Eq. (7) in the perturbation limit of his calculations.

For want of a rigorous procedure, we accept the semiphenomenological, semifield theoretic potentials of Eqs. (4), (5), (6), and (7) as describing the interactions of nucleons.

IV. ENERGIES

In this section we apply the above model to a calculation of potential and kinetic energies as a function of the density of nuclear matter. Our initial goal is to establish that the three-body repulsion, Eq. (6), with Lévy's constants, is qualitatively sufficient to prevent collapse of nuclear matter to very high densities, and that an expansion in n-body forces, as given by Eq. (7), converges in the sense that, for normal nuclear densities, all n-body interactions with $n>5$ contribute negligibly.

To this end we calculate first the average value of the potential operator,

$$\langle V\rangle=\int\Psi^*V\Psi d\mathbf{r}_1\cdots d\mathbf{r}_A\Big/\int\Psi^*\Psi d\mathbf{r}_1\cdots d\mathbf{r}_A, \quad (8)$$

where Ψ is the ground-state wave function for a nucleus of mass number A and is taken to be a Slater determinant of free-particle states satisfying periodic boundary conditions[27] in a box of radius $R=\eta R_s$ and volume $v=(4\pi/3)R^3$, multiplied by a symmetric function of the position coordinates of the A particles,

$$\Psi=\frac{1}{(A!)^{\frac{1}{2}}}\begin{vmatrix}\varphi_1(1)&\cdots&\varphi_1(A)\\ \cdot&&\cdot\\ \varphi_A(1)&\cdots&\varphi_A(A)\end{vmatrix}\theta(\mathbf{r}_1\cdots\mathbf{r}_A), \quad (9)$$

with

$$\varphi_i(j)=v^{-\frac{1}{2}}e^{i\mathbf{k}_i\cdot\mathbf{r}_j}\chi_i(\sigma_j)\nu_i(\tau_j). \quad (10)$$

$\chi_i(\sigma_j)$ is a two-row spinor fixing the jth spin state of the ith particle. For spin up, it is $\binom{1}{0}$ and for spin down $\binom{0}{1}$. $\nu_i(\tau_j)$ is the analogous quantity fixing the nucleon charge in isotopic spin space. $\theta(\mathbf{r}_1\cdots\mathbf{r}_A)$ is an arbitrary symmetric function of the A nucleon position coordinates. We introduce position correlations between the A particles in order to satisfy the boundary condition that the wave function vanish whenever any two nucleons approach within $r_c=0.38/\mu$ of one another. This boundary condition expresses the repulsive core nature of the interaction potentials. We consider in these calculations a special form of $\theta(\mathbf{r}_1\cdots\mathbf{r}_A)$ that takes into account pairwise correlations of the nucleons only.[19] This form is

$$\theta(\mathbf{r}_1\cdots\mathbf{r}_A)=\sum_{i<j=1}^{A}f(r_{ij}), \quad (11)$$

with $r_{ij}\equiv|\mathbf{r}_i-\mathbf{r}_j|$. In order to attain the initial goal specified at the beginning of this section, we choose first for $f(r_{ij})$ a simple step function,

$$f(r_{ij})=\begin{cases}1, & r_{ij}>r_c\\ 0, & r_{ij}<r_c.\end{cases} \quad (12)$$

A variational calculation of the nuclear energy based on a two parameter trial form for $f(r_{ij})$ is presented in Sec. V.

Three assumptions underlie our calculation of the nuclear potential energy, Eq. (8), with the wave function expressed in Eqs. (9) to (12). Firstly, we neglect nuclear surface effects and calculate the "volume" potential energy of the nucleons. Formally, this implies treating the nucleus as a region of average particle density $A/v=(3/4\pi)\mu^3/\eta^3$ extending over all space. With this assumption the tensor interaction term in Eq. (4) and the angle dependent three-body potentials as deduced in Appendix A average to zero and do not influence our results. Secondly, we neglect Coulomb interactions between protons. The nucleus is then treated as composed of $A/2$ protons and $A/2$ neutrons, uniformly distributed, and equal numbers of each having spin up and spin down. For $A\gg1$, a negligible error is introduced in the cases of those nuclei with extra nucleons outside of the filled levels indicated in Fig. 5. Thirdly, we neglect the influence of the correlation function, Eqs. (11) and (12) on the orthogonality properties of the free-particle states. In the absence of a repulsive core ($r_c\to0$), the free-particle states, Eq. (10), are orthogonal in the nuclear "well." For repulsive cores of volume small in comparison with the average volume per nucleon in nuclear matter we expect the deviations of these states from orthogonality to be unimportant. Corrections resulting from such deviations are here neglected. An argument justifying their neglect is presented in Appendix C wherein are also discussed the analogous normalization corrections.

Two-Body Forces

For two-body interactions, Eq. (8) reduces in the standard way, with the above approximations, to[28]

[27] The effect of various boundary conditions on the kinetic energy has been studied by G. M. Volkoff, Phys. Rev. **62**, 126 (1942).

[28] See Rosenfeld's book, reference 3; Chap. XI.

$$\langle V^{2\text{-body}}\rangle=\binom{A}{2}\frac{(A-2)!}{A!}\sum_{i,j=1}^{A}\int d\mathbf{r}_1 d\mathbf{r}_2\varphi_i^*(1)\varphi_j^*(2)\times V(12)\begin{vmatrix}\varphi_i(1) & \varphi_i(2)\\ \varphi_j(1) & \varphi_j(2)\end{vmatrix} f^2(r_{12}). \quad (13)$$

The factor multiplying the integral expresses the number of interacting pairs among A nucleons times the number of possible state assignments (permutations) of the remaining $(A-2)$ particles, for each interacting pair, divided by the normalization constant appearing in Eq. (9).

In order to carry out products of spin and isotopic spin matrices in Eq. (13), we consider separately the two relevant terms of Eqs. (4) and (5). In the case of $V_4^{(a)}$, which is a spin and charge independent Wigner attraction, we obtain,[1,29] with neglect of $1\ll A$,

$$\sum_{i,j=1}\varphi_i^*(1)\varphi_j^*(2)[\varphi_i(1)\varphi_j(2)-\varphi_j(1)\varphi_i(2)]=v^{-2}\{A^2-\tfrac{1}{4}\sum_{i,j}e^{-i(\mathbf{k}_i-\mathbf{k}_j)\cdot(\mathbf{r}_1-\mathbf{r}_2)}\}=(A/v)^2\{1-\tfrac{1}{4}[3j_1(k_M r_{12})/(k_M r_{12})]^2\}, \quad (14)$$

where $j_1(x)$ is a spherical Bessel function, and $k_M=1.52\mu/\eta$ is the momentum of the highest filled energy level for the free-particle states in the nuclear well. The factor $\frac{1}{4}$ multiplying the exchange density term expresses the fact that, to leading order in $A\gg 1$, $\frac{5}{8}$ of the pairs are antisymmetric in their space coordinates, and $\frac{3}{8}$ are symmetric. This factor results directly in the sum in Eq. (14), since states with different spin and/or isotopic spin are mutually orthogonal, and one-fourth of the nucleons are in each group of spin-up protons, spin-down protons, spin-up neutrons, and spin-down neutrons. For the central part of V_2, we have

$$\sum_{i,j=1}^{A}\varphi_i^*(1)\varphi_j^*(2)(\boldsymbol{\sigma}_1\cdot\boldsymbol{\sigma}_2)(\boldsymbol{\tau}_1\cdot\boldsymbol{\tau}_2)\times[\varphi_i(1)\varphi_j(2)-\varphi_j(1)\varphi_i(2)]=v^{-2}\{0-(9/4)\sum_{i,j}e^{-i(\mathbf{k}_i-\mathbf{k}_j)\cdot(\mathbf{r}_1-\mathbf{r}_2)}\}=-(9/4)(A/v)^2[3j_1(k_M r_{12})/(k_M r_{12})]^2. \quad (15)$$

The expression then for the potential energy of nuclear matter resulting from two-body interactions is

$$\langle V^{2\text{-body}}\rangle=(3/8\pi)A(\mu/\eta)^3\int_{r>r_c}d\mathbf{r}\times\left\{-(6/\pi)\lambda^2\frac{K_1(2\mu r)}{\mu r^2}[1-\tfrac{1}{4}D^2(k_M r)]-\tfrac{3}{4}\lambda(\mu/2M)(e^{-\mu r}/r)D^2(k_M r)\right\}, \quad (16)$$

where we introduce the notation

$$D(k_M r)\equiv 3j_1(k_M r)/k_M r,$$

and change coordinates in accord with the stated approximations,

$$\int d\mathbf{r}_1 d\mathbf{r}_2 w(r_{12})f^2(r_{12})=v\int_{r>r_c}d\mathbf{r}\,w(r). \quad (17)$$

Introducing dimensionless variables $x=\mu r$, $\alpha=k_M/\mu$, and $b=\mu r_c$, and integrating the classical density term, we obtain

$$\langle V^{2\text{-body}}\rangle=-\left(\frac{3A\mu}{2\eta^3}\right)\left\{\left(\frac{6}{\pi}\right)\lambda^2\left[\tfrac{1}{2}K_0(2b)-\tfrac{1}{4}\int_b^\infty dxK_1(2x)D^2(\alpha x)\right]+\tfrac{3}{4}\lambda\left(\frac{\mu}{2M}\right)\int_b^\infty dxxe^{-x}D^2(\alpha x)\right\}. \quad (18)$$

A graph of this expression for the two-body potential energy appears in Fig. 6, where we have used Lévy's parameters $G^2/4\pi=10$, and $r_c\mu=b=0.38$. At normal nuclear density ($\eta=1$), the exchange density term in the Wigner interaction potential, $V_4^{(a)}$, reduces the contribution from the classical term by 19 percent.

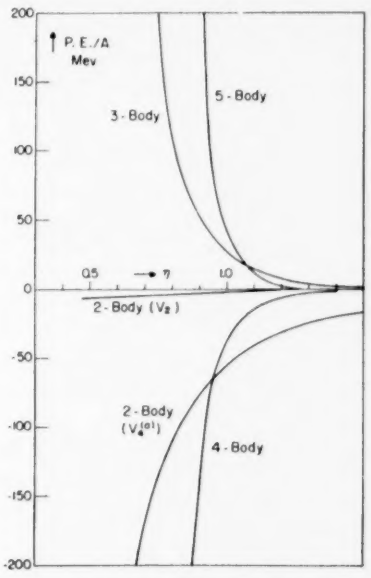

FIG. 6. Potential energy contributions, plotted as a function of η, as calculated from Eq. (18) for two-body interactions ($V_4^{(a)}$ and V_2), from Eq. (21) for three-body interactions, from Eq. (26) for four-body interactions, and from the corresponding expression for five-body interactions.

[29] E. P. Wigner and F. Seitz, Phys. Rev. **43**, 804 (1933); E. Feenberg, Phys. Rev. **60**, 204 (1941).

Three-Body Forces

For three-body interactions, Eq. (8) reduces to

$$\langle V^{3\text{-body}}\rangle=\binom{A}{3}\frac{(A-3)!}{A!}$$
$$\times\sum_{i,j,k=1}^{A}\int d\mathbf{r}_1 d\mathbf{r}_2 d\mathbf{r}_3\varphi_i^*(1)\varphi_j^*(2)\varphi_k^*(3)V(123)$$
$$\cdot\begin{vmatrix}\varphi_i(1) & \varphi_i(2) & \varphi_i(3)\\ \varphi_j(1) & \varphi_j(2) & \varphi_j(3)\\ \varphi_k(1) & \varphi_k(2) & \varphi_k(3)\end{vmatrix} f^2(\mathbf{r}_{12})f^2(\mathbf{r}_{13})f^2(\mathbf{r}_{23}),\quad(19)$$

in analogy with Eq. (13). For Wigner-type three-body interactions as in Eq. (6), the spin and isotopic spin matrix products may be worked out directly, giving

$$\sum_{i,j,k=1}^{A}\varphi_i^*(1)\varphi_j^*(2)\varphi_k^*(3)\begin{vmatrix}\varphi_i(1) & \varphi_i(2) & \varphi_i(3)\\ \varphi_j(1) & \varphi_j(2) & \varphi_j(3)\\ \varphi_k(1) & \varphi_k(2) & \varphi_k(3)\end{vmatrix}$$
$$=(A/v)^3\{1-\tfrac{1}{4}D^2(k_M r_{12})-\tfrac{1}{4}D^2(k_M r_{23})-\tfrac{1}{4}D^2(k_M r_{31})$$
$$+(2/16)D(k_M r_{12})D(k_M r_{23})D(k_M r_{31})\}.\quad(20)$$

The first four terms in Eq. (20) represent the classical density and the double exchange density for the interchange of any two of the interacting trio. The last term represents the two symmetric permutations of the three nucleons among themselves, the factor $\frac{1}{16}$ expressing the relative probability that all three of them have the same spin-isotopic spin quantum numbers, just as in the discussion for two-body interactions. The integrations in the above expressions are simplified by noting that

$$\int d\mathbf{r}_1 d\mathbf{r}_2 d\mathbf{r}_3 w(r_{12}, r_{23}, r_{31})f^2(r_{12})f^2(r_{23})f^2(r_{31})$$
$$=v\int_{(r_{12},\,r_{23},\,r_{31})>r_c} d\mathbf{r}_{12}d\mathbf{r}_{13}w(r_{12}, r_{23}, r_{31})$$
$$=8\pi^2 v\int_{r_c}^{\infty}r_{12}dr_{12}\int_{r_c}^{\infty}r_{13}dr_{13}$$
$$\times\int_{>|r_c,\,|r_{12}-r_{13}|}^{r_{12}+r_{13}}r_{23}dr_{23}w(r_{12}, r_{23}, r_{31}),$$

in accord with our stated approximations. Utilizing the symmetry in the three-particle separations r_{12}, r_{23}, and r_{31}, we obtain, in dimensionless form

$$\langle V^{3\text{-body}}\rangle=(3A\mu/4\eta^6)(24/\pi)\lambda^3$$
$$\times\int_b^\infty dx\int_b^\infty dy\int_{>|b,\,|x-y|}^{x+y}dzK_1(x+y+z)$$
$$\cdot\{1-\tfrac{3}{4}D^2(\alpha x)+\tfrac{1}{8}D(\alpha x)D(\alpha y)D(\alpha z)\}.\quad(21)$$

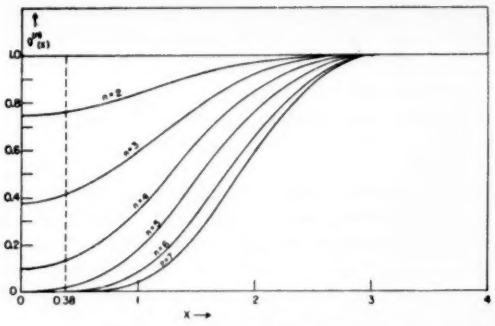

FIG. 7. The relative probability for n nucleons to be separated by a distance $x=\mu r$, for $n=2$ through 7. These curves are calculated for normal nuclear density $\eta=1$.

The following integral representation,[30] which decomposes a K_1 function of a sum of arguments into a product of factors of each argument, facilitates analysis of the integrals in Eq. (21):

$$K_1(a_1+a_2+\cdots+a_n)$$
$$=\int_1^\infty\frac{tdt}{(t^2-1)^{\frac{1}{2}}}e^{-a_1 t}e^{-a_2 t}\cdots e^{-a_n t}.\quad(22)$$

There results for the classical term

$$\int_b^\infty dx\int_b^\infty dy\int_{>|b,\,|x-y|}^{x+y}dzK_1(x+y+z)$$
$$=\int_1^\infty\frac{tdt}{(t^2-1)^{\frac{1}{2}}}\frac{e^{-3bt}}{t^3}(1-\tfrac{3}{4}e^{-bt})$$
$$=0.121\quad(\text{for}\quad b=0.38).\quad(23)$$

The double exchange term reduces to

$$-\tfrac{3}{4}\int_b^\infty dx\int_b^\infty dy\int_{>|b,\,|x-y|}^{x+y}dzK_1(x+y+z)D^2(\alpha x)$$
$$=-\frac{3\pi}{8}\left\{\int_b^\infty D^2(\alpha x)P(x)dx-\int_{2b}^\infty D^2(\alpha x)Q(x)dx\right\},$$

with

$$P(x)\equiv F(x+2b)-F(2x+2b),$$
$$Q(x)\equiv F(x+2b)-F(2x)+(2b-x)(2/\pi)K_0(2x),$$
$$F(x)\equiv(2/\pi)\int_x^\infty K_0(y)dy.$$

At normal nuclear density, it subtracts away 42 percent of the classical term. The triple exchange term can be evaluated only by approximate numerical procedures[31]

[30] W. Magnus and F. Obberhettinger, *Special Functions of Mathematical Physics* (Chelsea, New York, 1949).

[31] A more detailed discussion is presented in K. Huang, Ph.D. thesis, Massachusetts Institute of Technology, 1953 (unpublished).

and is found to equal 6 percent of the classical term for $\eta=1$. Antisymmetrization of the wave function thus reduces the three-body interaction energy by 36 percent at normal nuclear density; correspondingly, the two-body energy is reduced by 19 percent. The calculated results for Eq. (21) are plotted in Fig. 6 as a function of η.

Four- and Five-Body Forces

Increasing complexities enter into the calculations of higher-body forces. Additional exchange density terms appear and also the available integration volume for interacting hard spheres becomes more difficult to express and handle. The physical effect of the additional exchange terms resulting from the Pauli principle is to decrease the relative probability of finding many nucleons close to one another. We show this by calculating the probability distribution for n particles,

$$g^{(n)}(\mathbf{r}_1\cdots\mathbf{r}_n)$$

$$=v^n\int d\mathbf{r}_{n+1}\cdots d\mathbf{r}_A\Psi^*\Psi\Big/\int d\mathbf{r}_1\cdots d\mathbf{r}_A\Psi^*\Psi. \quad (24)$$

For two nucleons, $g^{(2)}(r_{12})$ is given in Eq. (14), multiplied there by $(A/v)^2$. The expression for $g^{(3)}(r_{12}, r_{23}, r_{31})$ appears in Eq. (20), multiplied there by $(A/v)^3$. The corresponding $g^{(n)}$ for higher n values are deduced from Eq. (24) in precisely the same manner. The result for $n=4$ is given below, with $a_{ij}\equiv k_M r_{ij}$,

$$\begin{aligned}g^{(4)}=1&-\tfrac{1}{4}\sum_{i<j=1}^{4}D^2(a_{ij})\\&+(2/16)\sum_{i<j<p=1}^{4}D(a_{ij})D(a_{jp})D(a_{pi})\\&-(2/64)\{D(a_{12})D(a_{23})D(a_{34})D(a_{41})\\&+D(a_{13})D(a_{34})D(a_{42})D(a_{21})\\&+D(a_{13})D(a_{32})D(a_{24})D(a_{41})\}\\&+(1/16)\{D^2(a_{12})D^2(a_{34})+D^2(a_{13})D^2(a_{24})\\&\qquad+D^2(a_{14})D^2(a_{23})\}. \quad (25)\end{aligned}$$

In Fig. 7 we graph the probability distributions $g^{(n)}(r)$, for $n=2$ through $n=7$, with all arguments $r_{ij}\equiv r\equiv x/\mu$. For $n=3$ this corresponds to arranging the three nucleons in an equilateral triangle of side r; for $n=4$, they form an equilateral tetrahedron. For $n>4$, there is no geometrical configuration with all $r_{ij}=r$. Figure 7 just indicates that the relative probability for finding nucleons close to one another decreases with increasing n. We see from Eq. (25) that $g^{(4)}$ reduces to $\frac{3}{32}$ in the limit of zero interparticle distances. All $g^{(n)}$ for $n>4$ vanish in this limit, in consequence of the exclusion principle and of the fact that there are but four spin and charge states for nucleons. We see from Fig. 7 that, for $n\geq 4$ the effective "Pauli repulsion" is of greater "range" and importance than the repulsive potential core.[32]

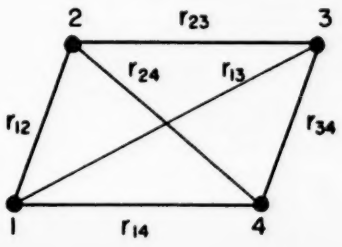

FIG. 8. Notation for four-body interaction integrals.

There is an additional factor weighting against close approach of n nucleons in the energy integrals. In going from the n to the $(n+1)$ body interactions, we see by Eq. (7) that the singularity in the potential for zero-particle separations increases by but one power of r, whereas the additional nucleon introduces one more volume element $d\mathbf{r}\propto r^2dr$ into the integral. Thus, for example, in the absence of a repulsive core, the two-body energy diverges, whereas the energies for all $n>2$ are finite.

On the basis of these observations we can make the calculation of four- and five-body interaction energies tractable by neglecting the repulsive potential cores and thereby vastly simplifying the integrals. We obtain then for $n=4$, by Eqs. (7)–(12), (25), and by symmetry of the potential in the coordinates,

$$\langle V^{4\text{-body}}\rangle=-\lambda^4\frac{48\mu}{\pi}\frac{3A^4}{4!v^4}\int d\mathbf{r}_1d\mathbf{r}_2d\mathbf{r}_3d\mathbf{r}_4\times\frac{K_1[\mu(r_{12}+r_{23}+r_{34}+r_{41})]}{\mu^4r_{12}r_{23}r_{34}r_{41}}g^{(4)}. \quad (26)$$

We can carry through the above integrals analytically for the first two terms in Eq. (25), corresponding to the classical density and the double exchange density describing the interchange of any pair. To do this, we use Eq. (22) and note that (see Fig. 8) for integrands that do not depend on r_{24},

$$\begin{aligned}\int d\mathbf{r}_1d\mathbf{r}_2d\mathbf{r}_3d\mathbf{r}_4&=v\int d\mathbf{r}_{12}d\mathbf{r}_{23}d\mathbf{r}_{14}\\&\to 2v(2\pi)^3\int_0^\infty r_{12}dr_{12}\int_0^\infty r_{23}dr_{23}\int_0^\infty r_{14}dr_{14}\\&\quad\times\int_{|r_{12}-r_{23}|}^{r_{12}+r_{23}}dr_{13}\int_{|r_{13}-r_{14}|}^{r_{13}+r_{14}}r_{34}dr_{34}. \quad (27)\end{aligned}$$

The resulting contribution to $\langle V^{4\text{-body}}\rangle$ of the first two

[32] We wish to thank Dr. E. P. Gross for an illuminating discussion on this point.

terms of $g^{(4)}$, labeled U^{4b}, is

$$U^{4b}=-\lambda^4\frac{81A\mu}{2\pi\eta^9}\int_1^\infty\frac{tdt}{(t^2-1)^{\frac{1}{2}}}\int_0^\infty dx\int_0^\infty dy\int_0^\infty dz \times\int_{|x-y|}^{x+y}dw\int_{|w-z|}^{w+z}due^{-(x+y+z+u)t}[1-\tfrac{3}{2}D^2(\alpha x)]$$

$$=-\lambda^4\frac{27A\mu}{\pi\eta^9}\int_1^\infty\frac{tdt}{t^3(t^2-1)^{\frac{1}{2}}}\int_0^\infty dx\times(\tfrac{1}{2}xt+x^2t^2)e^{-2xt}[1-\tfrac{3}{2}D^2(\alpha x)]$$

$$=-\lambda^4\frac{27A\mu}{4\pi\eta^9}\left\{1+\frac{27(1-\alpha^2)}{4\alpha^4}-\frac{27}{2\alpha^3}(1+\alpha^2)^{\frac{1}{2}}\tanh^{-1}\left(\frac{\alpha}{(1+\alpha^2)^{\frac{1}{2}}}\right)+\frac{27}{4\alpha^6}(1+2\alpha^2)\left[\tanh^{-1}\left(\frac{\alpha}{(1+\alpha^2)^{\frac{1}{2}}}\right)\right]^2\right\}.$$

For $\eta=1$, the double exchange term subtracts 83.3 percent of the classical term. The third term in $g^{(4)}$, describing symmetric permutations of three interacting nucleons, can be integrated after making exponential fits to the D functions,[31] and it yields 21 percent of the classical density term for $\eta=1$. The remaining, or "quartet," exchange terms present further difficulties, in that some of them involve both diagonals r_{13} and r_{24} of Fig. 8 simultaneously so that the reduction to Eq. (27) cannot be completely effected. It has proved possible to calculate these terms only approximately. However, their contribution is small,[31] being about 3.4 percent of the classical term for $\eta=1$. The net result of the exchange terms for four-body interactions is a reduction of the classical term by 59 percent at $\eta=1$.

The calculation of the five-body energy proceeds along a parallel if more arduous path. The exchange densities give a 76 percent reduction in this case for $\eta=1$.

The potential energies for up through $n=5$ body interactions are presented in Figs. 6 and 9 as functions of the nuclear radius. In analyzing these curves, we observe the following: For $\eta\gtrsim1.5$, corresponding to nuclear densities of less than 30 percent of normal, the potential energy is due entirely to two-body interactions. At such densities it is relatively improbable to have three (or more) nucleons in a cluster of perimeter $\sim1/\mu$ so that the many-body interactions contribute very little to the energy. In the region $1.3\lesssim\eta\lesssim1.5$, three-body forces become important also. On the basis of two- and three-body forces alone, the potential energy per nucleon has a minimum of -30 Mev at $\eta=1.0$. When four- and five-body interactions are included, the minimum alters but slightly to -32 Mev at $\eta=1.1$.

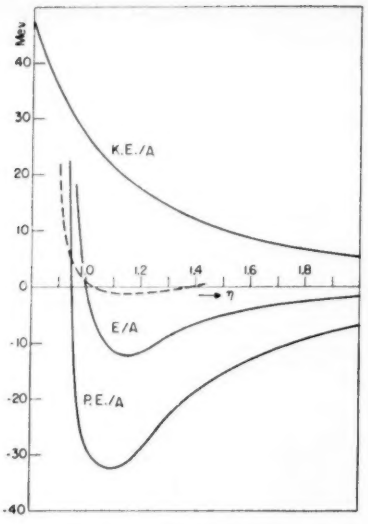

FIG. 9. Potential, kinetic, and total energy per nucleon as a function of η. The potential energy includes up through five-body interactions and is calculated for $G^2/4\pi=10$ and $r_c=0.38/\mu$. The kinetic energy is obtained from Eq. (29) expressing the Fermi plus Lenz contributions. The total energy has a minimum of depth 12 Mev per nucleon at $\eta=1.15$. The dashed curve is the total energy per nucleon calculated with $G^2/4\pi=15$ for the V_2 interaction, and $G^2/4\pi=7.5$ for all other interactions. It has a minimum of depth 2 Mev per nucleon at $\eta=1.15$.

Our aim in this calculation of the four- and five-body interaction energies has been only to demonstrate that their effect is quite small at normal nuclear density. We attach no significance to their numerical contributions as we have found it necessary to approximate in a relatively rough manner the "quartet" and "quintet" exchange terms and to neglect the repulsive potential cores. This neglect of the repulsive cores overestimates both of their contributions, and in particular, overestimates the four-body contribution more, as is evident from Fig. 7.

With regard to the higher-body forces, one can adopt either of two attitudes. In that the basis for the potentials used in these calculations is semiphenomenological, we can limit ourselves entirely to two- and three-body forces. In that the basis is semifield theoretic, however, we can accept and investigate all higher-body forces as appearing in Eq. (7). We have already seen that the four- and five-body interactions affect the energy minimum but slightly and indicate a rapid convergence for the series of n-body interactions for nuclear radii $\eta\gtrsim1$. We can also see from Fig. 6 that this series oscillates wildly for $\eta\lesssim1$. However, the contributions of two- to A-body forces can be summed approximately for high densities ($\eta\ll1$). Wentzel[10] has deduced this directly with the meson scalar pair theory, which gives potentials of the form Eq. (7). In his calculation nucleons are treated as fixed sources uniformly distributed within an infinite nucleus. The

repulsive potential core is simulated in Wentzel's calculation by a high-momentum cutoff for the meson field, given by the reciprocal Compton wavelength of the nucleon. In that the nucleons are treated as static sources, the Pauli principle does not operate. For a nucleus in the collapsed state ($\eta \ll 1$), however, it is well known that the exchange density contributions to the energy vanish. Thus we see by Eq. (15) that the interaction energy for a $(\sigma_1\cdot\sigma_2)(\tau_1\cdot\tau_2)$ potential vanishes in the collapsed state. Whereas the exchange density reductions we calculated for the two- and three-body Wigner interactions were, respectively, 19 percent and 36 percent at $\eta=1$, they are only 9.5 percent and 15 percent at $\eta=0.5$.

In Appendix B, we outline a procedure for summing up the energy contributions with potentials of the form of Eq. (7) and with neglect of the Pauli exchange terms. The point to be made here is that the energy is positive and increasing with decreasing η, for $\eta \ll 1$. We can conclude that $n>3$ body forces given by Eq. (7) are relatively unimportant at the potential energy minimum deduced from consideration of two- and three-body forces. For high nuclear densities, they contribute significantly and operate so as to oppose collapse. However, for moderately high density, i.e., $\eta \lesssim 1$, both the Pauli exchange terms and the higher-body forces are important. In this region we can only accept the indication of our calculations including the five-body forces that the potential energy curve is monotonically rising with decreasing η.

Kinetic Energy

Having calculated the potential energy of the neutrons and protons in the nucleus, we come next to a discussion of their kinetic energy. The sum of these two quantities gives us then the total energy.

The well-known Fermi kinetic energy for a gas of A noninteracting point nucleons ($A/2$ protons and $A/2$ neutrons) of mass M confined to a spherical box of radius R is[1]

$$T_F = 0.695A^{5/3}/MR^2 = 14.7A/\eta^2 \text{ Mev}. \quad (28)$$

For the nuclear model under discussion here, the kinetic energy is greater than the Fermi energy because of the additional curvature introduced in the nucleon wave functions by the repulsive core boundary condition. This additional kinetic energy was calculated by Lenz[16] who considered the problem of noninteracting hard spheres. With the approximation of hard sphere radius small in comparison with interparticle separation Lenz obtained[33]

$$T = T_F\left(1+\frac{2.16b}{\eta}\right) = 14.7A\left(\frac{1}{\eta^2}+\frac{0.82}{\eta^3}\right) \text{ Mev}. \quad (29)$$

[33] An interpolation formula has been given by F. London, Proc. Roy. Soc. (London) **153**, 576 (1935), which is applicable for arbitrary interparticle separations. Applied to our case it yields a 12 percent increase above Lenz's result.

Lenz's result, and in particular its density variation, can be qualitatively understood as follows. The kinetic energy for a point nucleon of wavelength $\lambda = R/n$ is $2\pi^2n^2/MR^2$. For a nucleon of radius r_c, the wavelength shortens to $(R-r_c)/n$, the numerator here representing the available linear dimension after exclusion of the interior of the nucleon. For a nucleus of A nucleons, with $A^{\frac{1}{3}}$ along a diameter, the wavelength reduces to $(R-A^{\frac{1}{3}}r_c)/n = (R/n)(1-b/\eta)$, and the kinetic energy increases to $T_F(1-b/\eta)^{-2} \approx T_F(1+2b/\eta)$. We remark here that comparison of Eqs. (18) and (29) readily shows that the nucleus would tend to collapse under the influence of two-body forces alone. The coefficient of the leading η^{-3} term is negative with $G^2/4\pi = 10$ and $b=0.38$. If we add the kinetic energy of Lenz, Eq. (29) to the potential energy, we obtain Fig. 9 for the total nuclear energy as a function of η. The curve shows a minimum at $\eta=1.15$ corresponding to a binding energy of 12 Mev per nucleon. The dotted curve indicated in the same figure is calculated for an alternative choice of the coupling constants which Jastrow[34] has found to give an equally satisfactory account of low-energy two-body interactions. We obtain the dotted curve if we set $G^2/4\pi = 15\epsilon$, where $\epsilon=1$ for the two-body $(\sigma_1\cdot\sigma_2)(\tau_1\cdot\tau_2)$ interaction, and $\epsilon=0.5$ for all other terms; $b=0.38$ is used as a compromise between the two triplet and singlet repulsive core radii proposed by Jastrow. With these parameters the stable radius is given by $\eta=1.15$, and the binding energy minimum corresponds to 2 Mev per nucleon.

In summary, the qualitative deductions of this section are twofold. A three-body repulsion of the form in Eq. (6), as suggested by pseudoscalar meson theory, prevents nuclear collapse and indicates nuclear saturation properties in accord with experience. The expansion in a series of many-body interactions rapidly converges for normal nuclear densities. This convergence is due chiefly to the Pauli exclusion principle, which serves to inhibit close approach of many nucleons.

Finally, we note just briefly that a system of nucleons interacting through the potentials discussed in this section is stable against lining up of the spins of the particles. This is because the kinetic energy increases by a factor of roughly four for the state in which all spins are parallel, whereas the change in the potential energy is considerably smaller since the dominating interactions are Wigner potentials.

V. VARIATIONAL CALCULATION

In this section we present a brief account of a variational calculation of the total energy based on more realistic wave functions. With saturation and convergence of the n-body expansion qualitatively established on the basis of our previous calculations, it is desirable to deduce more quantitatively significant numbers for the saturation radius and binding energy.

[34] R. Jastrow, *Proceedings of the Third Annual Rochester Conference* (Interscience Publishers, Inc., New York, 1953), p. 77.

Aside from this, however, there is an additional problem of considerable importance on which a variational calculation can shed some light. This is the degree of position correlation between the nucleons, as expressed by $f(r_{ij})$, which corresponds to the minimum value of the total energy. The great success of the shell theory based on the independent-particle model of the nucleus argues against strong correlations. The results of this calculation support this picture.

A two-parameter continuous trial form is introduced for the correlation function:

$$f_T(r)=\begin{cases}(1-r_c/r)[1+ae^{-\beta\mu(r-r_c)}], & r>r_c;\\ 0, & r<r_c.\end{cases} \tag{30}$$

The parameters a and β are varied and the energy minimum determined. The radial dependence of f_T^2 is shown in Fig. 10 for various values of (a,β). We see for $(a,\beta)=(2.5, 1)$ that there is a strong positive correlation between pairs, whereas for $a=0$, the probability of forming a pair is low. For parameters in the range $(a,\beta)=(1, 2)$ the correlation is weak; *viz*, the nucleon wave functions vanish at each other's core, but exhibit no strong tendence to cluster with or to avoid their neighbors, for $r>r_c$.

The potential energies for two- and three-body interactions have been calculated with Eq. (30). For two-body interactions this amounts to recalculating Eq. (16) with

$$\int_{r>r_c}^{\infty} d\mathbf{r}\rightarrow\int d\mathbf{r} f_T^2(r).$$

For three-body interactions, Eq. (21) is altered by

$$\int_b^\infty dx\int_b^\infty dy\int_{>|b,|x-y||}^{x+y} dz$$

$$\rightarrow\int_b^\infty dx f_T^2(x)\int_b^\infty dy f_T^2(y)\int_{>|b,|x-y||}^{x+y} dz f_T^2(z).$$

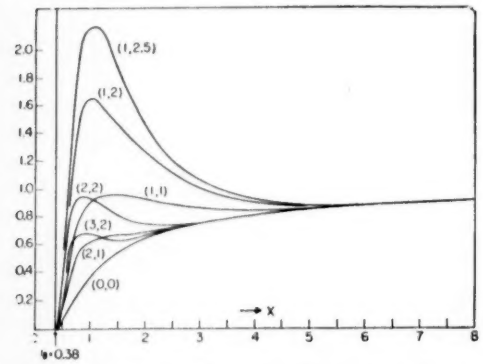

FIG. 10. The square of the correlation function of Eq. (30) plotted as a function of $x=\mu r$ for different sets of parameters a and β. The individual curves are labeled by the corresponding pair (β, a).

These integrations are then carried through numerically.

For the kinetic energy we calculate directly

$$T=-\frac{1}{2M}\frac{\sum_{i=1}^{A}\int\Psi^*\Delta_i\Psi d\mathbf{r}_1\cdots d\mathbf{r}_A}{\int\Psi^*\Psi d\mathbf{r}_1\cdots d\mathbf{r}_A}$$

$$=T_F-(A^2/2Mv)\int d\mathbf{r} f_T(r)\Delta f_T(r)[1-\tfrac{1}{4}D^2(k_M r)], \tag{31}$$

consistent with the approximations explicitly stated in the preceding section. The second term of Eq. (31) represents the increase in kinetic energy due to the position correlation of the nucleons.

The calculations with the trial form of Eq. (30) indicate the existence of an energy minimum for approximate parameter values $a=1$, $\beta=2$. The method of calculation has been to determine the energy as a function of η for various sets of (a,β). For $a=1$ and $\beta=2$, the energy has a minimum at $\eta=0.95$ corresponding to a binding energy of roughly 4 Mev per nucleon. Though this result can be presented only in numerical form, its physical implications are clear. The two-body attractive forces favor strong position correlation of nucleons, corresponding to large values of a and small values of β as indicated in Fig. 10. However, the three-body repulsive forces operate in the opposite direction, since their positive contribution to the nuclear energy decreases with smaller a and larger β. Also the kinetic energy opposes strong positive correlation which increases the wave function curvature. The kinetic energy increase expressed by Eq. (31) varies roughly in proportion to a^2/β. The compromise effected by these antipodal tendencies falls at $a=1$, $\beta=2$. The graph of f_T^2 in Fig. 10 shows that for this set of parameter values no marked correlation of nucleon coordinates is evident for r greater than the repulsive core radius. We interpret this result as evidence in favor of the independent particle model.

VI. CONCLUSION

To summarize, we have deduced many-body potentials from the pseudoscalar meson theory with pseudoscalar coupling. Guided by Lévy's success in fitting low-energy properties of the two-body system and by his parameters, we have kept only the potentials of leading order in an expansion in powers of $(G^2/4\pi)(\mu/2M)$. It is quite possible that further developments in field theory will show that the terms we have studied are of lesser importance than others neglected in our analysis or that there are different effective values of $G^2/4\pi$ for the many-body potentials we have studied. Indeed, Wentzel's[10] calculations with the scalar

pair theory predict a considerable reduction in the strength of these terms.[24] At present, however, it is impossible to say to what extent a complete covariant calculation in the framework of the renormalization program will remove the damping found by Wentzel.

However, if we accept the potentials in Eqs. (4), (5), (6), and (7) as a semiphenomenological working basis for our calculations, we find that the many-body forces, and in particular the three-body repulsion, provide a satisfactory qualitative understanding of nuclear saturation. The effect of the Pauli exclusion principle in these calculations has been to reduce considerably the contributions of $n>3$ body Wigner forces for nuclei at normal density.

In that the binding energies are obtained as relatively small differences of larger potential and kinetic energy contributions, their numerical values are to be understood primarily as order of magnitude indications. However, the resulting saturation radii are more accurately determined in this work since the position of the energy minimum is fixed to a large extent by the minimum in the curve of the two- plus three-body potential energies. This is because the kinetic energy is a considerably smoother function of $\eta=R/R_s$ than is the potential energy. We can best illustrate this point by comparing the step function calculation of Sec. IV with the variational calculation of Sec. V. The continuous correlation form of Eq. (30) with $a=1$, $\beta=2$ reduces the potential energy contribution by a factor of roughly two in comparison with the step function result. This potential reduction serves to decrease the magnitude of the binding energy from 12 Mev to 4 Mev per nucleon while altering $\eta_{\min}$ from 1.15 to 0.95.

The energy minimum for the variational calculation is obtained with a trial form f_T showing no marked correlation of the nucleon coordinates. This result suggests that many-body repulsive forces may aid in harmonizing the shell theory and its underlying independent particle model with the meson theory and its prediction of strong internucleon interactions.

Further variational calculations are now in progress with more flexible trial forms. Energies deduced by such variational procedures must necessarily lie above the true eigenvalue so that one can in this way establish only an upper limit on the energy for a given choice of effective coupling constants for the n-body interactions. Better wave functions serve to lower the upper limit and to bring it closer to the true value.[35]

ACKNOWLEDGMENT

It is a pleasure to acknowledge our great indebtedness to Professor Victor F. Weisskopf for his initiating and continuing stimulus and contributions to this work.

[35] Additional information which may be culled from these calculations includes a minimal value for the ratio of the effective coupling constant for the three-body interaction to the two-body constant which is consistent with saturation.

FIG. 11. Feynman diagrams for three-body interactions.

APPENDIX A

We outline here the various contributions[36] to three-body interactions of orders $\lambda^2\mu/M$ and $\lambda^3\mu/M$. The Feynman graphs of the processes are drawn in Fig. 11.

The potentials are deduced from Eq. (3) in the adiabatic perturbation limit as discussed in Sec. III. All possible permutations and time orderings of process (a) contribute to the one pair interaction of order $\lambda^2\mu/M$. The result is

$$V_{3a}=\frac{G^4}{(2M)^3}\frac{2\boldsymbol{\tau}_2\cdot\boldsymbol{\tau}_3}{(2\pi)^6}\int\int d\mathbf{p}d\mathbf{q}(\boldsymbol{\sigma}_2\cdot\boldsymbol{\nabla}_2)(\boldsymbol{\sigma}_3\cdot\boldsymbol{\nabla}_3)\frac{e^{i\mathbf{p}\cdot\mathbf{r}_{12}+i\mathbf{q}\cdot\mathbf{r}_{13}}}{\omega_p^2\omega_q^2}$$

$$+\text{symmetric terms in (1, 2) and (1, 3)}$$

$$=\lambda^2(\mu^2/M)\Big[(\boldsymbol{\tau}_2\cdot\boldsymbol{\tau}_3)\frac{(\boldsymbol{\sigma}_2\cdot\mathbf{r}_{12})(\boldsymbol{\sigma}_3\cdot\mathbf{r}_{13})}{r_{12}r_{13}}\Big(1+\frac{1}{\mu r_{12}}\Big)$$

$$\times\Big(1+\frac{1}{\mu r_{13}}\Big)\frac{e^{-\mu r_{12}}}{\mu r_{12}}\frac{e^{-\mu r_{13}}}{\mu r_{13}}+\text{symmetric terms}\Big].$$

Two pair terms of the form illustrated by process (b) contribute an interaction of order $\lambda^3\mu/M$ which has the form

$$V_{3b}=\frac{G^6}{(2M)^4}\frac{12}{(2\pi)^9}\int\int\int d\mathbf{p}d\mathbf{q}d\mathbf{k}$$

$$\times(\boldsymbol{\nabla}_{12}\cdot\boldsymbol{\nabla}_{23}+\boldsymbol{\nabla}_{13}\cdot\boldsymbol{\nabla}_{32}+\boldsymbol{\nabla}_{21}\cdot\boldsymbol{\nabla}_{13})\frac{e^{i\mathbf{p}\cdot\mathbf{r}_{12}+i\mathbf{q}\cdot\mathbf{r}_{23}+i\mathbf{k}\cdot\mathbf{r}_{21}}}{\omega_p^2\omega_q^2\omega_k^2}$$

$$=\lambda^3(6\mu^2/M)(1/\mu^2)(\boldsymbol{\nabla}_{12}\cdot\boldsymbol{\nabla}_{23}+\boldsymbol{\nabla}_{13}\cdot\boldsymbol{\nabla}_{32}+\boldsymbol{\nabla}_{21}\cdot\boldsymbol{\nabla}_{13})$$

$$\times(e^{-\mu r_{12}}/\mu r_{12})(e^{-\mu r_{13}}/\mu r_{13})(e^{-\mu r_{23}}/\mu r_{23}).$$

Irreducible graphs of type c, a typical one of which appears in the time ordered Fig. 11(c), contribute a

[36] Similar potentials together with Eq. (7) for $n=3$ and 4 have been deduced independently by A. Klein [Phys. Rev. **90**, 1101 (1953)] in the framework of the Tamm-Dancoff formalism.

potential, of order $\lambda^3\mu/M$, which we write in the form

$$V_{3c}=\frac{G^3}{(2M)^4}\frac{3}{(2\pi)^9}(\boldsymbol{\tau}_2\cdot\boldsymbol{\tau}_3)(\boldsymbol{\sigma}_2\cdot\boldsymbol{\nabla}_{23})(\boldsymbol{\sigma}_3\cdot\boldsymbol{\nabla}_{23})$$
$$\times\left\{\int d\mathbf{k}\frac{e^{i\mathbf{k}\cdot\mathbf{r}_{23}}}{\omega_k{}^2}\int d\mathbf{q}d\mathbf{p}\frac{e^{i(\mathbf{p}+\mathbf{q})\cdot\mathbf{r}_{12}}}{\omega_p\omega_q(\omega_p+\omega_q)^2}\right.$$
$$\left.+\int d\mathbf{k}\frac{e^{i\mathbf{k}\cdot\mathbf{r}_{23}}}{\omega_k{}^3}\int\int d\mathbf{q}d\mathbf{p}\frac{e^{i(\mathbf{p}+\mathbf{q})\cdot\mathbf{r}_{12}}}{\omega_p\omega_q(\omega_p+\omega_q)}\right\}$$
$$+\text{symmetric terms}$$
$$=\lambda^3(6\mu^2/\pi^2M)(1/\mu^2)(\boldsymbol{\tau}_2\cdot\boldsymbol{\tau}_3)(\boldsymbol{\sigma}_2\cdot\boldsymbol{\nabla}_{23})(\boldsymbol{\sigma}_3\cdot\boldsymbol{\nabla}_{23})$$
$$\times\left\{(e^{-\mu r_{23}}/\mu r_{23})(1/\mu^2r_{12}{}^2)\int_{\mu r_{12}}^{\infty}xK_0{}^2(x)dx\right.$$
$$\left.+K_0(\mu r_{23})K_1(2\mu r_{12})/\mu^2r_{12}{}^2\right\}$$
$$+\text{symmetric terms.}$$

Interactions V_{3a} and V_{3b} average to zero in our nuclear model. Interaction V_{3c} reduces to two terms, a tensor interaction which averages to zero plus a $(\boldsymbol{\sigma}_a\cdot\boldsymbol{\sigma}_b)(\boldsymbol{\tau}_a\cdot\boldsymbol{\tau}_b)$ term which was evaluated with the methods discussed in Sec. III and shown to give a three-body repulsive energy amounting to less than 5 percent of Eq. (21).

APPENDIX B

In the limit of high nuclear density, all exchange effects are negligible. The n-body probability density function $g^{(n)}$ then reduces to unity, and the n-body potential energy is given simply by the "classical term,"

$$\langle V^{n\text{-body}}\rangle\underset{\eta\to 0}{\longrightarrow}C^{(n)},$$
$$C^{(n)}=(A/v)^n(1/n!)\int d\mathbf{r}_1\cdots d\mathbf{r}_nV^{n\text{-body}}\prod_{i<j}f^2(r_{ij}),\quad\text{(B1)}$$

where we replace $\binom{A}{n}$ by $A^n/n!$ for $A\to\infty$. The sum of $C^{(n)}$ from $n=3$ to ∞ can be carried out, if we neglect the repulsive core. (The two-body term is omitted because it diverges in the absence of core.) With this approximation we can then compare our result with that indicated by Wentzel.[10] The identity of these results then demonstrates the validity of $V^{n\text{-body}}$ deduced in Eq. (7).

We have evaluated this sum directly by establishing a recursion relation by means of term-by-term integration of Eq. (B1). We indicate here a more elegant procedure.[37]

[37] We wish to thank Mr. W. Frank for helpful discussions on this method.

Using Eq. (22), we can manipulate $C^{(n)}$ into the form

$$C^{(n)}=(-1)^{n+1}(2\mu/\pi)\frac{(3\lambda)^n}{n\eta^{3(n-1)}}\int_1^{\infty}\frac{tdt}{(t^2-1)^{\frac{1}{2}}}$$
$$\times\int_{(n)0}\exp\{-(x_2+x_n+a_1+a_2+\cdots+a_n)t\},$$

where

$$x_k\equiv\mu|\mathbf{r}_k-\mathbf{r}_1|,\quad a_k\equiv\mu|\mathbf{r}_{k+2}-\mathbf{r}_{k+1}|.$$

The integration limits are given by

$$\int_{(n)0}=\int_0^{\infty}dx_2\int_0^{\infty}dx_3\cdots$$
$$\times\int_0^{\infty}dx_n\int_{|x_2-x_3|}^{x_2+x_3}da_1\cdots\int_{|x_{n-1}-x_n|}^{x_{n-1}+x_n}da_{n-2}$$
$$=2^{n-2}\int_0^{\infty}dxe^{-xt}(-G_t)^{n-2}F(x,t),$$

where $F(x,t)\equiv e^{-xt}$ and G_t is an integral operator such that for any function $\beta(x,t)$,

$$G_t\beta(x,t)=\tfrac{1}{2}\int_0^{\infty}dy\beta(y,t)g_t(x,y),$$

with

$$g_t(x,y)\equiv-\int_{|x-y|}^{x+y}e^{-at}da=-\frac{1}{t}\begin{cases}e^{-xt}\sinh(yt), & x>y\\ e^{-yt}\sinh(xt), & y>x.\end{cases}$$

We see that $g_t(x,y)$ is a Green's function satisfying

$$\{d^2/dx^2-t^2\}g_t(x,y)=\delta(x-y),$$
$$g_t(x,y)=g_t(y,x),\quad\text{(B2)}$$
$$g_t(0,y)=g_t(\infty,y)=0.$$

By manipulation with Eq. (B2), we can show that, for the special form $F(x,t)=e^{-xt}$, we have

$$(G_t)^nF(x,t)=\frac{1}{n!}\left[\frac{d}{d(t^2)}\right]^ne^{-xt}.$$

Hence, if γ is a constant, and if we set $z\equiv t^2$, we obtain

$$\sum_{n=0}^{\infty}(\gamma G_t)^nF(x,t)=\sum_{n=0}^{\infty}\frac{\gamma^n}{n!}\left(\frac{d}{dz}\right)^n\exp(-xz^{\frac{1}{2}})$$
$$=\exp[-(t^2+\gamma)^{\frac{1}{2}}x].\quad\text{(B3)}$$

With the help of Eq. (B3), we obtain after a number of elementary integrations,

$$\left(\frac{1}{A}\right)\sum_{n=3}^{\infty}C^{(n)}=\left(\frac{\mu\eta^3}{8\pi}\right)\{\tfrac{1}{2}(1+\gamma)^2\ln(1+\gamma)-\tfrac{1}{2}\gamma-\tfrac{3}{4}\gamma^2\},$$

where $\gamma=6\lambda/\eta^3$. Exactly the same expression may be obtained by the method indicated by Wentzel.[10]

APPENDIX C

In this Appendix we discuss corrections to the orthogonality and normalization of the free-particle states introduced by the correlation function in Eqs. (9) to (12). Our aim here is to justify the reduction of Eq. (8) to Eqs. (13) and (19).

We develop here the argument for two-body interactions only, the generalization for n-body potentials being immediate.

We rewrite then Eq. (8) in the form for

$$V=\sum_{i<j}V(ij)\rightarrow\binom{A}{2}V(12),$$

$$\langle V\rangle=\binom{A}{2}\left|\int d\mathbf{r}_1\cdots d\mathbf{r}_A\Psi^*\Psi\right|^{-1}\times\int d\mathbf{r}_1\cdots d\mathbf{r}_A\sum_{(\alpha)}\sum_{(\beta)}S^{(\alpha)}S^{(\beta)}\times\{\varphi_{\alpha_1}^*(1)\varphi_{\alpha_2}^*(2)V(12)\varphi_{\beta_1}(1)\varphi_{\beta_2}(2)\}\times\{\varphi_{\alpha_3}^*(3)\varphi_{\beta_3}(3)\}\cdots\times\{\varphi_{\alpha_A}^*(A)\varphi_{\beta_A}(A)\}\prod_{i<j}f^2(r_{ij}),\tag{C1}$$

where we have expanded the Slater determinants with the following notations: (α) is a set of integers $(\alpha_1\cdots\alpha_A)$ representing a permutation of $(1, 2, \cdots, A)$, and $S^{(\alpha)}\equiv S^{\alpha_1\alpha_2\cdots\alpha_A}$ is the Levi-Civita tensor density of rank A, with the values ±1 for even (odd) permutations of the indices. We introduce the definition

$$X_{\alpha_1\alpha_2\beta_1\beta_2}(12)=\sum_{(\alpha)(\beta)}{}'S^{(\alpha)}S^{(\beta)}\int d\mathbf{r}_3\cdots d\mathbf{r}_A\times\{\varphi_{\alpha_3}^*(3)\varphi_{\beta_3}(3)\}\cdots\times\{\varphi_{\alpha_A}^*(A)\varphi_{\beta_A}(A)\}\prod{}'f^2(r_{ij}),\tag{C2}$$

where $\sum'$ represents sum over all permutations for fixed $(\alpha_1, \alpha_2, \beta_1, \beta_2)$ and $\prod'$ represents a product of all $f^2(r_{ij})$, excluding $f^2(r_{12})$. Equation (C1) is then written in the form

$$\langle V\rangle=\binom{A}{2}\frac{\int d\mathbf{r}_1d\mathbf{r}_2\sum_{\alpha_1\alpha_2\beta_1\beta_2}\{\varphi_{\alpha_1}^*(1)\varphi_{\alpha_2}^*(2)V(12)\varphi_{\beta_1}(1)\varphi_{\beta_2}(2)\}f^2(r_{12})X_{\alpha_1\alpha_2\beta_1\beta_2}(12)}{\int d\mathbf{r}_1d\mathbf{r}_2\sum_{\alpha_1\alpha_2\beta_1\beta_2}\{\varphi_{\alpha_1}^*(1)\varphi_{\alpha_2}^*(2)\varphi_{\beta_1}(1)\varphi_{\beta_2}(2)\}f^2(r_{12})X_{\alpha_1\alpha_2\beta_1\beta_2}(12)}.\tag{C3}$$

In terms of Eq. (C3) we formulate our problem as follows. We wish to demonstrate that, accurate to terms of order $\lesssim(1/10)(k_Mr_c)^2\approx0.03/\eta^2$, $X_{\alpha_1\alpha_2\beta_1\beta_2}(12)$ is independent of the particle coordinates and equal to $+c$ for $\alpha_1=\beta_1, \alpha_2=\beta_2$; $-c$ for $\alpha_1=\beta_2, \alpha_2=\beta_1$; 0 otherwise, where c is some constant. Once this result is established, Eq. (C3) reduces to Eq. (13) and our goal is achieved. This result is evidently rigorously valid in the absence of a repulsive core, since $f(r_{ij})\rightarrow1$ and

$$(1/v)\int d\mathbf{r}_je^{-i(\mathbf{k}_a-\mathbf{k}_b)\cdot\mathbf{r}_j}=\delta_{ab}.$$

With $r_c\neq0$, and $v_c\equiv(4\pi/3)r_c^3$, however, we write

$$f^2(r_{ij})\equiv1-U(r_{ij}),\quad U(r_{ij})\equiv\begin{cases}1, & r_{ij}<r_c,\\ 0, & r_{ij}>r_c,\end{cases}\tag{C4}$$

and note that

$$(1/v^2)\int d\mathbf{r}_id\mathbf{r}_je^{-i(\mathbf{k}_a-\mathbf{k}_b)\cdot(\mathbf{r}_i-\mathbf{r}_j)}f^2(r_{ij})=\delta_{ab}-(v_c/v)j_1(k_{ab}r_c)/k_{ab}r_c\approx\delta_{ab}-(v_c/v)(1-(1/10)k_{ab}^2r_c^2+\cdots),\tag{C5}$$

since in general the argument of the spherical Bessel function is small, its maximum value being $k_Mr_c=0.57/\eta$, so that, therefore, $(1/10)(k_{ab}r_c)^2<0.03/\eta^2$. Similarly, we observe, for $k_a\neq k_b\neq k_c\neq0$,

$$v^{-3}\int d\mathbf{r}_id\mathbf{r}_jd\mathbf{r}_pe^{i\mathbf{k}_a\cdot\mathbf{r}_{ij}+i\mathbf{k}_b\cdot\mathbf{r}_{jp}+i\mathbf{k}_c\cdot\mathbf{r}_{pi}}f^2(\mathbf{r}_{ij})f^2(\mathbf{r}_{jp})f^2(\mathbf{r}_{pi})=v^{-3}\int d\mathbf{r}_id\mathbf{r}_jd\mathbf{r}_pe^{i\mathbf{k}_a\cdot\mathbf{r}_{ij}+i\mathbf{k}_b\cdot\mathbf{r}_{jp}+i\mathbf{k}_c\cdot\mathbf{r}_{pi}}\times\{U(r_{ij})U(r_{jp})+U(r_{jp})U(r_{pi})+U(r_{pi})U(r_{ij})-U(r_{ij})U(r_{jp})U(r_{pi})\}\approx3(v_c/v)^2(1-5/32).\tag{C6}$$

From Eqs. (C5) and (C6) we can immediately generalize for all permutations of $(\alpha_3\cdots\alpha_A)$ and $(\beta_3\cdots\beta_A)$ leaving $(\alpha_1, \alpha_2)=(\beta_1, \beta_2)$ or (β_2, β_1) that

$$X_{\alpha_1\alpha_2\alpha_1\alpha_2}(12)=-X_{\alpha_1\alpha_2\alpha_2\alpha_1}(12)\approx\text{constant}\approx(A-2)!\prod_{m=1}^{A-1}[1-m(v_c/v)]\times\left[1+\binom{A-2}{2}\frac{1}{4}\frac{(v_c/v)}{1-(v_c/v)}+\cdots\right].\tag{C7}$$

The form of Eq. (C7) is understood as follows. The first term in the brackets is contributed by the "classical" term with $\alpha_i=\beta_i$, for all $i\geqslant 3$. The factor $(A-2)!$ represents the number of possible permutations of the $A-2$ particles in this set. The products of factors $\prod[1-m(v_c/v)]$ just represents the excluded volume effect calculated to first order in v_c/v for each factor; *viz.*,

$$\int d\mathbf{r}_1\cdots d\mathbf{r}_A \prod_{i<j=1}^{A} f^2(r_{ij})$$

$$\approx\{1-(A-1)v_c/v\}\int d\mathbf{r}_2\cdots d\mathbf{r}_A \prod_{i<j=2}^{A} f^2(r_{ij})$$

$$\approx \prod_{m=1}^{A-1}[1-m(v_c/v)].$$

The second term in the brackets in Eq. (C7) results from an interchange among any of the $\binom{A-2}{2}$ pairs that can be constructed such that $\alpha_i=\beta_j$, $\alpha_j=\beta_i$. Only $\frac{1}{4}$th of the possible pairs are not orthogonal in spin or isotopic spin space and these contribute according to Eq. (C5), with a plus sign because of the relation

$$s^{\cdots\alpha_i\cdots\alpha_j\cdots}s^{\cdots\alpha_j\cdots\alpha_i\cdots}=-1.$$

In this same manner, one can explicitly calculate further terms in Eq. (C7). As above, we find that to leading order they are constants independent of the argument r_{12} and the indices (α,β). The magnitude of the constants is unimportant since $\langle V\rangle$ is expressed in Eq. (C3) as a ratio.

It remains to be shown now that, for the class of permutations with

$$\alpha_1=\beta_1,\quad \alpha_2\neq\beta_2,\quad \text{or}\quad \alpha_2=\beta_2,\quad \alpha_1\neq\beta_1, \tag{C8}$$

there results a negligibly small contribution to Eq. (C3). This conclusion is readily established formally. We just indicate the argument as follows. The second term in Eq. (C7) expresses contributions of the $\binom{A-2}{A}\approx A^2/2$ pairs with $\alpha_i=\beta_j$, $\alpha_j=\beta_i$, for $3\leqslant i<j$. However for the class of permutations in Eq. (C8), there are only $2(A-2)$ such pairs that can be formed; i.e., there are $2(A-2)$ ways in which to form pairs with $\alpha_1=\beta_1$, $\alpha_2=\beta_j$, $\alpha_j=\beta_2$, or with $\alpha_2=\beta_2$, $\alpha_1=\beta_j$, $\alpha_j=\beta_1$, for $j\geqslant 3$, and with all other $\alpha_p=\beta_p$. Thus the contribution to X of the pairs in the class of Eq. (C8) is small of order $1/A$ and can be neglected in Eq. (C3). The same conclusion follows directly for triple exchanges, in the class of Eq. (C8), of form $\alpha_1=\beta_1$, $\alpha_2=\beta_j$, $\alpha_j=\beta_k$, $\alpha_k=\beta_2$, for $j\neq k\geqslant 3$ in comparison with the $\binom{A-2}{3}\approx A^3/6$ triple exchanges of form $(\alpha_1,\alpha_2)=(\beta_1,\beta_2)$, $(\alpha_j,\alpha_k,\alpha_p)=(\beta_k,\beta_p\beta_j)$, which contribute to the next term in Eq. (C7).

The same reasoning extends simply to the cases corresponding to permutations described by

$$(\alpha_1,\alpha_2,\alpha_n,\alpha_m)=(\beta_n,\beta_m,\beta_1,\beta_2).$$

The Wave Function of a Relativistic System

F. J. DYSON*
Laboratory of Nuclear Studies, Cornell University, Ithaca, New York
(Received June 11, 1953)

Three methods of handling problems in relativistic quantum mechanics are discussed. One is the Tamm-Dancoff method, one is the Bethe-Salpeter method, and the third is a new method intermediate between the other two. The connections between the three methods are investigated. It is shown that the new method provides a kind of bridge between the 3- and 4-dimensional points of view. The new method is illustrated with applications to simple examples.

I. INTRODUCTION

THE purpose of this paper is to clarify the physical meaning of a wave function in relativistic quantum mechanics. The subject is full of obscurities and unsolved problems, most of which will not be discussed here. Only some facts will be pointed out, which it is hoped will stimulate further thought on these questions.

A relativistic system can be described from two points of view, 3 dimensional and 4 dimensional. In the 3-dimensional point of view, the wave function describes completely the configuration of the system at a particular time. The typical example of this point of view is the formalism of Tamm[1] and Dancoff.[2] In the 4-dimensional point of view, the wave function describes the probability amplitude for finding particle 1 at position 1 and time 1, particle 2 at position 2 and time 2, and so on. This is the point of view of Bethe and Salpeter.[3] Each point of view fails to include important aspects of the situation. The 3-dimensional picture conceals the relativistic invariance, and thereby makes practical calculations much more complicated. The 4-dimensional picture is manifestly relativistic, but the wave function does not give a complete description of the system in the sense of elementary quantum mechanics. The physical meaning of the 4-dimensional wave function is quite unclear.[4] Worst of all, there still exists no exact method[5] of relating the two wave functions to one another so as to make use of the advantages of both in the same problem.

This paper is concerned mainly with establishing connections between the 3- and 4-dimensional wave functions. The connection is made via a new formulation of the Tamm-Dancoff method which was briefly explained in a recent letter.[6] Section V deals with the important unsolved problem of the correct normalization conditions to be imposed on the 4-dimensional wave function. The later sections discuss the wave equations of relativistic systems and the boundary conditions which should go with them.

II. DEFINITIONS

We consider for definiteness a system of two quantized spinor fields $\psi^P(x)$ and $\psi^N(x)$ representing protons and neutrons, interacting with a neutral pseudoscalar meson field $\phi(x)$. The operators $\psi(x)$, $\phi(x)$ are Heisenberg operators defined at a space-time point x and are relativistically covariant. The actual state of the system is denoted by Ψ, a constant state vector in the Heisenberg representation. The vacuum state of the interacting fields is Ψ_0. We suppose that Ψ is a state consisting of one proton and one neutron in interaction, but not necessarily bound together.

The 4-dimensional wave function of the 2-particle state Ψ is, according to Gell-Mann and Low,[7] defined as the matrix element

$$\psi_{\alpha\beta}(x, y) = (\Psi_0{}^* T(\psi^P{}_\alpha(x), \psi^N{}_\beta(y))\Psi), \tag{1}$$

where T represents the chronological product as defined by Wick.[8] This wave function is a 16-component spinor and is a function of the two independent space-time points x and y. In particular, x and y may be taken to be two space points $\mathbf{r}$ and $\mathbf{r}'$ at the same time $t=0$. Then $\psi_{\alpha\beta}(x, y)$ specializes to

$$\psi_{\alpha\beta}(\mathbf{r}, \mathbf{r}') = (\Psi_0{}^* \psi^P{}_\alpha(\mathbf{r}) \psi^N{}_\beta(\mathbf{r}')\Psi). \tag{2}$$

We may identify the Heisenberg operator $\psi^P{}_\alpha(\mathbf{r})$ at $t=0$ with the time-independent operator which describes the proton field in the Schrödinger representation. Likewise $\psi^N{}_\beta(\mathbf{r}')$ is a neutron field operator in the Schrödinger representation. With this identification the state vector of the actual state in the Schrödinger representation is

$$\Psi \exp(-iEt), \tag{3}$$

* Now at the Institute for Advanced Study, Princeton, New Jersey.

[1] I. Tamm, J. Phys. (U.S.S.R.) **9**, 449 (1945).
[2] S. M. Dancoff, Phys. Rev. **78**, 382 (1950).
[3] E. E. Salpeter and H. A. Bethe, Phys. Rev. **84**, 1232 (1951).
[4] J. Goldstein (to be published).
[5] A big step in the understanding of the relation between 3- and 4-dimensional wave functions was taken by E. E. Salpeter, Phys. Rev. **87**, 328 (1952) and M. M. Lévy, Phys. Rev. **88**, 72, 725 (1952). But these authors deal only with systems in which the interactions are almost instantaneous and the particles can be considered to be at rest as a first approximation.
[6] F. J. Dyson, Phys. Rev. **90**, 994 (1953).
[7] M. Gell-Mann and F. Low, Phys. Rev. **84**, 350 (1951).
[8] G. C. Wick, Phys. Rev. **80**, 268 (1950).

supposing the actual state to have a given total energy E. The Schrödinger state vector of the vacuum state is

$$\Psi_0 \exp(-iE_0 t), \tag{4}$$

where E_0 is the vacuum energy. We are using natural units so that $h=c=1$.

The Schrödinger operator $\psi^P{}_\alpha(\mathbf{r})$ may be represented as a superposition of plane waves obeying periodic boundary conditions in a finite box of volume V, thus

$$\psi^P{}_\alpha(\mathbf{r}) = V^{-\frac{1}{2}} \sum_k \sum_u u_\alpha b_{ku} \exp(i\mathbf{k}\cdot\mathbf{r}), \tag{5}$$

where k is summed over the normal frequencies of the box and u is summed over the 4 spinors satisfying the Dirac equation for given k. For each k the u are normalized by

$$(u^* u') = \delta_{uu'}. \tag{6}$$

The b_{ku} are proton absorption operators and antiproton creation operators, and satisfy the anticommutation rules

$$[b_{ku}, b_{k'u'}{}^*]_+ = \delta_{uu'}\delta_{kk'}. \tag{7}$$

The neutron field is similarly

$$\psi^N{}_\alpha(\mathbf{r}) = V^{-\frac{1}{2}} \sum_k \sum_u u_\alpha d_{ku} \exp(i\mathbf{k}\cdot\mathbf{r}), \tag{8}$$

and the b_{ku} anticommute with the d_{ku}.

The meson field in the Schrödinger representation is

$$\phi(\mathbf{r}) = \sum_k (2V\omega_k)^{-\frac{1}{2}}(a_k + a_{-k}{}^*) \exp(i\mathbf{k}\cdot\mathbf{r}),$$

with

$$[a_k, a_{k'}{}^*] = \delta_{kk'}, \quad \omega_k = (\mu^2 + k^2)^{\frac{1}{2}}. \tag{9}$$

Finally the interaction between the fields in the Schrödinger representation is

$$H' = G\int (\psi^{P*}(\mathbf{r})\gamma\psi^P(\mathbf{r}) + \psi^{N*}(\mathbf{r})\gamma\psi^N(\mathbf{r}))\phi(\mathbf{r})\,d_3\mathbf{r} \tag{10}$$

$$= G\sum_k \sum_{k'} (2V\omega_k)^{-\frac{1}{2}}(a_k + a_{-k}{}^*) \sum_u \sum_v (u^*\gamma v) \times (b_{k'u}{}^* b_{k'-k,v} + d_{k'u}{}^* d_{k'-k,v}), \tag{11}$$

where γ is written for the Dirac matrix $i\beta\gamma_5$.

Let N be a set of occupation numbers for the noninteracting fields. Thus, N is a set of integers $(N_1, N_2, \cdots)$, one corresponding to each state of a free proton, antiproton, neutron, antineutron or meson. Let $A(N)$ be the product of the absorption operators b_{ku}, $b_{ku}{}^*$, d_{ku}, $d_{ku}{}^*$, and a_k, which annihilate the particles represented by N. Let $C(N)$ be the product of the corresponding creation operators. Then the normalized state vector of the state in which the particle occupation numbers have the values N is

$$\Phi(N) = [\Pi(N)]^{-\frac{1}{2}} C(N)\Phi_0, \tag{12}$$

where Φ_0 is the vacuum state of the noninteracting fields, and

$$\Pi(N) = (N_1!)(N_2!)(N_3!)\cdots. \tag{13}$$

The $\Phi(N)$ form a complete orthonormal set of states for the system of fields. The 3-dimensional wave function of the system in the state Ψ is given according to Tamm[1] and Dancoff[2] by the set of amplitudes

$$\alpha(N) = (\langle\Phi(N)\rangle^*\Psi) = [\Pi(N)]^{-\frac{1}{2}}(\Phi_0{}^* A(N)\Psi). \tag{14}$$

The $\alpha(N)$ define the state Ψ completely in the sense of elementary quantum mechanics. We denote by $\beta(N)$ the Tamm-Dancoff amplitudes for the interacting vacuum state Ψ_0,

$$\beta(N) = [\Pi(N)]^{-\frac{1}{2}}(\Phi_0{}^* A(N)\Psi_0). \tag{15}$$

Thus

$$\Psi = \sum_N \alpha(N)\Phi(N), \quad \Psi_0 = \sum_N \beta(N)\Phi(N). \tag{16}$$

There is no clear relation between the 4- and 3-dimensional wave functions (1) and (14). Substituting from (5) and (8) into (2),

$$\psi_{\alpha\beta}(\mathbf{r}, \mathbf{r}') = V^{-1} \sum_k \sum_{k'} \sum_u \sum_{u'} u_\alpha u_\beta' \times \exp(i\mathbf{k}\cdot\mathbf{r} + i\mathbf{k}'\cdot\mathbf{r}')(\Psi_0{}^* b_{ku} d_{k'u'}\Psi). \tag{17}$$

Thus $\psi(\mathbf{r}, \mathbf{r}')$ is a linear combination of the coefficients $(\Psi_0{}^* b_{ku} d_{k'u'}\Psi)$, which are a special case of the coefficients

$$a(N, N') = [\Pi(N)\Pi(N')]^{-\frac{1}{2}}(\Psi_0{}^* C(N) A(N')\Psi). \tag{18}$$

We take the $a(N, N')$ as an alternative 3-dimensional wave function[9] of the state Ψ. We will call the theory using $\alpha(N)$ the "old Tamm-Dancoff formalism," and the theory using $a(N, N')$ the "new Tamm-Dancoff formalism."

III. PHYSICAL MEANING OF THE WAVE FUNCTIONS

The meaning of the old Tamm-Dancoff wave function $\alpha(N)$ is clear. It is just the probability amplitude for finding the free particles specified by N, if the system is first put into the state Ψ, and the field interaction is then instantaneously switched off.

The physical meaning of the wave function $a(N, N')$ cannot be expressed so directly. Intuitively we can say, by looking at Eq. (18), that $a(N, N')$ is related to the probability amplitude for ending in the true vacuum state Ψ_0, if we start in the state Ψ and instantaneously annihilate the particles N' and create the particles N. Thus $a(N, N')$ describes the probability in the state Ψ of finding N' particles more, and N particles less, than are to be found in the vacuum of the interacting fields. A less exact but briefer way of expressing it, is to say that $a(N, N')$ is the probability of finding N' plus particles and N minus particles in the state Ψ. A "minus particle" is defined as one which is absent in Ψ but present in the comparison state Ψ_0.

A great advantage of this introduction of minus particles is that it enables us to handle the positive and negative energy solutions of the Dirac equation together. Using the old wave function $\alpha(N)$, one is forced at every stage to separate the proton states from the antiproton states and write a separate equation for each. This makes the old Tamm-Dancoff method ex-

[9] The notation here differs from that of reference 6 by a numerical factor.

tremely cumbersome when applied to processes involving pair creation and annihilation. On the other hand, the one-proton component of the new wave function $a(N, N')$ is

$$a_1(ku) = (\Psi_0^* b_{ku} \Psi), \tag{19}$$

where b_{ku} is an annihilation operator for a proton when u is a positive-energy spinor. The same expression (19) also represents, when u is a negative-energy spinor, the minus-one-antiproton component of the wave function since b_{ku} is then an antiproton creation operator. We may always take the one-proton and the minus-one-antiproton parts of the wave function together in the equations. That is to say, we may proceed as if the Dirac hole theory had not been invented, as if the proton were actually allowed to occupy states of both positive and negative energy. The hole theory has to be taken into account only at one place in the calculations; when Eq. (18) is used to define $a(N, N')$ we must make sure that the creation operators $C(N)$ are written to the left of the annihilation operators $A(N')$.

Similarly the component,

$$a_1'(ku) = (\Psi_0^* b_{ku}^* \Psi), \tag{20}$$

of $a(N, N')$ represents both the one-antiproton and the minus-one-proton part of the wave function. In this way a physical interpretation is found for the negative-energy components of the wave function $\psi_{\alpha\beta}(\mathbf{r}, \mathbf{r}')$ in Eq. (17). This two-particle wave function represents the amplitude for finding in Ψ either one proton and one neutron, one proton minus one antineutron, one neutron minus one antiproton, or minus one antiproton minus one antineutron. The general 4-dimensional wave function $\psi(x, y)$ has no such simple interpretation, when x and y are separated by a time-like interval. But at least we have now an understanding of the meaning of $\psi(x, y)$ for equal times, including positive and negative energy components on an equal footing.

IV. CONNECTION BETWEEN THE WAVE FUNCTIONS

We have now established a direct connection between the 4-dimensional wave function and the 3-dimensional amplitudes $a(N, N')$. It remains to work out the connections between the $a(N, N')$ and the $\alpha(N)$ and $\beta(N)$. Substituting from (12) and (16) into (18),

$$a(N, N') = \sum_{N_1} \sum_{N_2} \beta^*(N_1)\alpha(N_2) \times [\Pi(N)\Pi(N')\Pi(N_1)\Pi(N_2)]^{-\frac{1}{2}} \times (\Phi_0^* A(N_1)C(N)A(N')C(N_2)\Phi_0). \tag{21}$$

The expectation value in (21) is zero unless there exists a set of nonnegative occupation numbers

$$M = N_2 - N' = N_1 - N, \tag{22}$$

and is then equal to

$$\Pi(N_2)\Pi(N_1)[\Pi(M)]^{-1}. \tag{23}$$

We define a symbolic binomial coefficient

$$\binom{N_1}{N} = \Pi(N_1)[\Pi(N)\Pi(N_1 - N)]^{-1}, \tag{24}$$

and then (21) becomes

$$a(N, N') = \sum_M \beta^*(N+M)\alpha(N'+M) \times \binom{N+M}{M}^{\frac{1}{2}} \binom{N'+M}{M}^{\frac{1}{2}}. \tag{25}$$

This gives the formal definition of the $a(N, N')$ in terms of old Tamm-Dancoff wave functions.

The inverse of the relation (25) is

$$\beta^*(N_1)\alpha(N_2) = \sum_M (-1)^M a(N_1+M, N_2+M) \times \binom{N_1+M}{M}^{\frac{1}{2}} \binom{N_2+M}{M}^{\frac{1}{2}}, \tag{26}$$

where $(-1)^M$ means $(-1)^{\sum M}$ and $\sum M$ is the sum of the occupation numbers M. To verify (26), substitute back (25) into (26). The result is

$$\beta^*(N_1)\alpha(N_2) = \sum_M \sum_{M'} (-1)^M \beta^*(N_1+M+M')\alpha(N_2+M+M') \binom{N_1+M+M'}{N_1}^{\frac{1}{2}} \binom{N_2+M+M'}{N_2}^{\frac{1}{2}} \binom{M+M'}{M}. \tag{27}$$

But it is easily proved that, keeping $M+M'$ fixed and summing over M,

$$\sum_M (-1)^M \binom{M+M'}{M} = 0, \tag{28}$$

except when $M+M'=0$. Therefore the right side of Eq. (27) reduces to the term $M=M'=0$ and is equal to the left side. This verifies Eq. (26). In consequence of Eq. (26) the amplitudes $a(N, N')$ include a complete, and indeed redundant, determination of the $\alpha(N)$ and $\beta(N)$. Therefore, the $a(N, N')$ in principle provide a complete description of the states Ψ and Ψ_0 and determine all measurable properties of these states.

V. NORMALIZATION AND CONVERGENCE CONDITIONS

The old Tamm-Dancoff wave function, being defined directly as a probability amplitude, must be normalized by the conditions

$$\sum_N |\alpha(N)|^2 = \sum_N |\beta(N)|^2 = 1. \tag{29}$$

In a particular theory the sums (29), which are really multiple integrals, may or may not converge. If they diverge then the $\alpha(N)$ and $\beta(N)$ cannot rigorously be defined, and the whole Tamm-Dancoff picture makes no exact sense. It is likely that this is the case for the

field theories now in general use. Nevertheless the method of renormalization can be incorporated into the Tamm-Dancoff formalism,[10] and probably some kind of "renormalized" $\alpha(N)$ can be defined for which the integrals (29) become convergent. We may say that if the Tamm-Dancoff point of view finally makes sense in this context, Eq. (29) will remain as the correct normalization condition for the $\alpha(N)$.

We now discuss the appropriate normalization condition for the $a(N, N')$. Let z be any positive number, and write z^M for $z^{\frac{1}{2}M}$ as in Eq. (26). From Eq. (25) we derive

$$\sum_N \sum_{N'} z^{N+N'} |a(N, N')|^2 = \sum_N \sum_{N'} \sum_M \sum_{M'} \beta^*(N+M)\alpha(N'+M) \times \beta(N+M')\alpha^*(N'+M') z^{N+N'} \binom{N+M}{M}^{\frac{1}{2}} \binom{N'+M}{M}^{\frac{1}{2}} \binom{N+M'}{M'}^{\frac{1}{2}} \binom{N'+M'}{M'}^{\frac{1}{2}}. \quad (30)$$

Using Cauchy's inequality, the right side of (30) does not exceed $X^{\frac{1}{2}}Y^{\frac{1}{2}}$, where

$$X = Y = \sum_N \sum_{N'} \sum_M \sum_{M'} |\alpha(N'+M)|^2 \times |\beta(N+M')|^2 z^{N+N'} \binom{N'+M}{M} \binom{N+M'}{M'} = \sum_{N_1} \sum_{N_2} |\alpha(N_1)|^2 |\beta(N_2)|^2 (z+1)^{N_1+N_2}, \quad (31)$$

by the binomial theorem. Thus for every z,

$$\sum_N \sum_{N'} z^{N+N'} |a(N, N')|^2 \leq (\sum_N (z+1)^N |\alpha(N)|^2) \times (\sum_N (z+1)^N |\beta(N)|^2). \quad (32)$$

The same argument applied to (26) gives

$$\sum_N \sum_{N'} (z+1)^{N+N'} |a(N, N')|^2 \geq (\sum_N z^N |\alpha(N)|^2)(\sum_N z^N |\beta(N)|^2). \quad (33)$$

The inequalities (32) and (33) show that there is a close connection between the normalization integrals for the $\alpha(N)$ and the $a(N, N')$. In particular, suppose a theory is such that *the old Tamm-Dancoff amplitude for finding more than 85 particles simultaneously present in the state Ψ or in Ψ_0 is strictly zero.* (Here 85 is chosen only as an example of a large but finite number.) Then the right side of Eq. (32) converges for all z if it converges for $z=0$. In this case the normalization condition,

$$\sum_N \sum_{N'} |a(N, N')|^2 = \text{finite}, \quad (34)$$

may be imposed, and the sum (34) will automatically converge provided that (29) is convergent.

[10] M. Cini, Nuovo cimento **10**, 526 and 614 (1953) has shown how to renormalize the Tamm-Dancoff theory. See remarks in Sec. VII below.

In practice the Tamm-Dancoff method necessarily requires that the amplitudes $\alpha(N)$ be calculated with a cut-off theory, in which all the amplitudes involving more than say Q particles are set equal to zero by definition. It is taken as a fundamental hypothesis that, if Q is sufficiently large, the results of the calculation will be insensitive to the value of Q and will tend to a limit as Q tends to infinity. If this hypothesis fails then again the Tamm-Dancoff point of view makes no sense. Therefore, we must always suppose in practice that we are working with a cut-off theory with some finite value of Q. This being so, the previous argument applies, and we may take (34) as a practical normalization condition for the $a(N, N')$ which will always be valid in circumstances where the Tamm-Dancoff method itself is valid.

If $\alpha(N)$ and $\beta(N)$ are set equal to zero for $\sum N > Q$, the $a(N, N')$ defined by (25) will also be zero for $\sum N > Q$ or $\sum N' > Q$, and Eqs. (25) and (26) will still be consistent. Thus, the old Tamm-Dancoff formalism with cutoff is equivalent to a theory in which a cutoff is applied directly to the amplitudes $a(N, N')$ involving more than Q particles.

Supposing that we are not content with the above arguments and wish to obtain a rigorous normalization condition for the $a(N, N')$ independent of cutoff, then Eq. (32) is just not strong enough to deduce anything nontrivial from (29) alone. In order that (34) should hold, we must assume

$$\sum_N 2^N |\alpha(N)|^2 < \infty, \quad \sum_N 2^N |\beta(N)|^2 < \infty. \quad (35)$$

Thus the normalization condition (34) will apply, provided that the expectation values of 2^N in the states Ψ and Ψ_0 are finite. More generally, a practical normalization condition for the $a(N, N')$ will result from Eq. (32), provided that the expectation values of z^N in the states Ψ and Ψ_0 are finite for some $z > 1$. In practice it is very likely that these conditions will be fulfilled in cases where Eq. (29) holds. In any case, the order of magnitude of the Tamm-Dancoff amplitudes for large N is so hard to estimate accurately that there is practically no likelihood of being able to distinguish between (35) and (29). Therefore again we may conclude that (34) is a correct normalization condition for the $a(N, N')$ in all cases to which the Tamm-Dancoff point of view is applicable.

From (34) we may derive in turn a normalization condition for the wave function $\psi_{\alpha\beta}(\mathbf{r}, \mathbf{r}')$ defined by (2). Using Eqs. (17), (6), and (34), we find

$$\int\int d_3\mathbf{r} d_3\mathbf{r}' \sum_\alpha \sum_\beta |\psi_{\alpha\beta}(\mathbf{r}, \mathbf{r}')|^2 = \text{finite}. \quad (36)$$

It is convenient to take (36) equal to 1, although $\psi(\mathbf{r}, \mathbf{r}')$ is not strictly a probability amplitude. The space integrations in (36) extend over the whole space, since the volume V of the normalization box can be made to tend to infinity without introducing any dif-

ficulties. Equation (36) gives important information about the normalization of the 4-dimensional wave function $\psi(x, y)$, although it still does not throw any light on the behavior of the function for x and y separated by a time-like interval. At least Eq. (36) is a necessary condition for the 4-dimensional wave function to have a physical meaning.

VI. AN ELEMENTARY EXAMPLE

To illustrate the preceding sections in a simple way, consider a neutral scalar meson field $\phi(x)$ interacting with a classical source. Let the interaction be

$$H'=\sum_k \rho(k)(a_k+a_k^*), \tag{37}$$

where $\rho(k)$ is a given function of k. As is well known,[11] the stationary states of this system can be found explicitly. Let S be the anti-Hermitian operator

$$S=\sum_k \tau(k)(a_k^*-a_k), \quad \tau(k)=\omega_k^{-1}\rho(k). \tag{38}$$

A complete set of stationary states of the system is

$$\Psi(N)=\exp(-S)\Phi(N), \tag{39}$$

with $\Phi(N)$ given by Eq. (12). Let Ψ be the state in which just one real meson is present with momentum $\boldsymbol{p}$. The old Tamm-Dancoff amplitudes of Ψ and Ψ_0 are

$$\alpha(N)=[\Pi(N)]^{-\frac{1}{2}}(\Phi_0^* A(N)\exp(-S)a_p^*\Phi_0), \tag{40}$$

$$\beta(N)=[\Pi(N)]^{-\frac{1}{2}}(\Phi_0^* A(N)\exp(-S)\Phi_0). \tag{41}$$

An elementary calculation gives[11]

$$\beta(N)=[\Pi(N)]^{-\frac{1}{2}}\exp\{-\tfrac{1}{2}\sum_k[\tau(k)]^2\}\times\Pi_k[-\tau(k)]^{N(k)}, \tag{42}$$

$$\alpha(N)=\beta(N)[\tau(p)-(N(p)/\tau(p))]. \tag{43}$$

The necessary and sufficient condition that the old Tamm-Dancoff wave functions be normalizable is that the sum

$$\sum_k[\tau(k)]^2=\sum_k \omega_k^{-2}[\rho(k)]^2 \tag{44}$$

be convergent.

For the same state Ψ, the wave function $a(N, N')$ is

$$\begin{aligned} a(N,N')&=(\Pi(N)\Pi(N'))^{-\frac{1}{2}}(\Phi_0\exp(S)C(N)A(N')\\ &\quad\times\exp(-S)a_p^*\Phi_0)\\ &=(\Pi(N)\Pi(N'))^{-\frac{1}{2}}[-N'(p)/\tau(p)]\\ &\quad\times\Pi_k[-\tau(k)]^{N(k)+N'(k)}. \end{aligned} \tag{45}$$

This gives immediately

$$\begin{aligned} &\sum_N\sum_{N'}|a(N,N')|^2\\ &\quad=\{1+[\tau(p)]^2\}\exp\{2\sum_k[\tau(k)]^2\}. \end{aligned} \tag{46}$$

Hence Eq. (34) also is satisfied if, and only if, the series (44) converges. Thus, in this example, the normalization condition (34) for the $a(N, N')$ is precisely equivalent to the condition (29) for the old Tamm-Dancoff wave function to be definable.

[11] See R. J. Glauber, Phys. Rev. **84**, 395 (1951).

VII. EQUATIONS OF MOTION

The Schrödinger equation for the old Tamm-Dancoff wave function is

$$(E-E_M)\alpha(M)=\sum_N(\Phi^*(M)H'\Phi(N))\alpha(N), \tag{47}$$

where E_M is the sum of the energies of the free particles specified by M. The corresponding equation for the $a(N, N')$ is

$$\begin{aligned} &(\epsilon+E_N-E_{N'})a(N,N')\\ &\quad=[\Pi(N)\Pi(N')]^{-\frac{1}{2}}(\Psi_0^*[C(N)A(N'),H']\Psi), \end{aligned} \tag{48}$$

where $\epsilon=E-E_0$. The $a(N, N')$ were originally introduced in order to avoid difficulties with the vacuum energy, which arise with Eq. (47) but not with Eq. (48). This aspect of the $a(N, N')$ has been already discussed,[6] and no more will be said about it here.

It is important to distinguish between two possible methods of solving Eqs. (47) and (48). The first method is the Tamm-Dancoff method proper, as discussed in Sec. V. All amplitudes $\alpha(N)$ or $a(N, N')$ involving more than Q particles are set equal to zero, and the result is a finite set of coupled linear integral equations for the $\alpha(N)$ or $a(N, N')$ involving not more than Q particles. The finite set of integral equations is then to be solved, numerically or otherwise, without any further approximations. The only hypothesis made in this method is that the $\alpha(N)$ or $a(N, N')$ for sufficiently large numbers of particles are unimportant. The second method is the method of Lévy[5] and Klein.[12] In this method we single out the components of the wave function involving the smallest possible number of particles for the given system. Thus, for the state Ψ of one proton and one neutron, we single out the $\alpha(M)$ in which M denotes one proton and one neutron and no other particles, and we call this lowest-order part of the wave function α_{11}. Similarly, we single out the components a_{11} of the $a(N, N')$ representing one proton (or minus one antiproton) and one neutron (or minus one antineutron), which are just the components appearing in $\psi_{\alpha\beta}(\boldsymbol{r}, \boldsymbol{r}')$ according to Eq. (17). Equations (47) and (48) are then converted into integral equations for the α_{11} or a_{11} alone, successively eliminating all the rest of the $\alpha(N)$ and $a(N, N')$ by substituting from one equation into another. The result of the elimination is a linear integral equation for the α_{11} or a_{11}, in which the kernel appears as a power-series expansion in the coupling constant G. The integral equation is in principle exact, if the substitution process could be carried to completion. In practice the series for the kernel has to be broken off at some finite power of G. So the Lévy-Klein method is based on the assumed convergence of the power-series expansion of the kernel, a much stronger hypothesis than that used by the Tamm-Dancoff method.

Klein has shown[12] by actual calculation that the power series for the kernel diverges badly, even if one considers only those meson exchange processes in

[12] A. Klein, Phys. Rev. **90**, 1101 (1953).

which ultraviolet divergences of the self-energy type do not occur. For this reason the Lévy-Klein method must be considered unworkable, and we must in future rest our hopes on the Tamm-Dancoff method. Unfortunately the solution of the Tamm-Dancoff equations becomes a formidable task as soon as the Lévy-Klein expansion is abandoned. There is no evidence showing whether or not the solutions converge as the number of particles considered increases, because nobody has ever solved the equations taking into account more than a very few components of the wave function.

The 4-dimensional wave function $\psi(x, y)$ satisfies the Bethe-Salpeter equation,[3] which is again a linear integral equation with a kernel which is expressed as a power-series expansion in G. This equation is open to the same objections that were raised against the Lévy-Klein treatment of Eqs. (47) and (48). Only in this case the situation is worse, because there is no known way of expressing the equation in any form other than the series expansion. There exist no 4-dimensional equations analogous to (47) and (48) from which the Bethe-Salpeter equation might be derived. Up to now the 4-dimensional theory has been inextricably tied up with the power-series expansion.

Whichever form of the equations of motion is chosen, in order to solve the equations it is necessary to use the method of renormalization to eliminate self-energy and other divergences. The renormalization is at present only possible in terms of a power-series expansion in G. Thus, Lévy[5] renormalized the power-series expansion of the Bethe-Salpeter kernel, and he found an approximate connection between that kernel and the kernel of the integral equation for the old Tamm-Dancoff wave function α_{11}. In this way he could obtain a divergence-free integral equation for α_{11}, using an expansion in powers of G and various other approximations. More recently Cini[10] has succeeded in writing the old Tamm-Dancoff Eqs. (47) in a covariant form, and so he is able to renormalize directly the kernel of the integral equation for α_{11}. But Cini's method is still based on the power-series expansion; he can renormalize the Lévy-Klein treatment of the Eqs. (47), but he cannot yet renormalize the Tamm-Dancoff treatment.

The method of Cini can be used with Eq. (48) just as well as with Eq. (47). Also, since the $a(N, N')$ is much more closely related than the $\alpha(N)$ to the 4-dimensional wave function, it seems likely that it will be easier to renormalize the Tamm-Dancoff treatment for Eq. (48) than for Eq. (47). It remains an outstanding task for the future to avoid the series expansions and to renormalize Eq. (48) directly.

VIII. THE ONE-PARTICLE SYSTEM

In this section we illustrate the use of Eq. (48) by setting up the equations for a state Ψ consisting of a single proton. In this case the lowest-order component of $a(N, N')$ is the one-proton wave function $(\Psi_0 b_{pu}\Psi)$. It is convenient to use instead of this wave function the related quantity,

$$\psi_\alpha(p)=\sum_u(\Psi_0{}^* b_{pu}\Psi)u_\alpha, \tag{49}$$

which is a Dirac spinor, the sum being taken over the 4 solutions u of the Dirac equation for a free particle of momentum p. We write

$$E_p=(M^2+p^2)^{\frac{1}{2}}, \tag{50}$$

and let

$$\eta(p)=E_p{}^{-1}(\alpha\cdot p+\beta M) \tag{51}$$

be the Dirac operator whose eigenvalues are $+1$ for the positive energy states and -1 for the negative energy states of momentum p. The equation (48) for $\psi_\alpha(p)$ is then

$$[\epsilon-\eta(p)E_p]\psi_\alpha(p)=\sum_u(\Psi_0{}^*[b_{pu}, H']\Psi)u_\alpha. \tag{52}$$

Using (11) and (7), the right side of (52) becomes

$$G\sum_k(2V\omega_k)^{-\frac{1}{2}}\sum_v(\gamma v)_\alpha(\Psi_0{}^* b_{p-k,v}(a_k+a_{-k}{}^*)\Psi). \tag{53}$$

Equation (52) couples the one-proton wave function $\psi_\alpha(p)$ only to the one-proton-one-meson wave function

$$\psi_\alpha{}^+(p, k)=\sum_v(\Psi_0{}^* b_{pv}a_k\Psi)v_\alpha, \tag{54}$$

and to the one-proton-minus-one-meson wave function

$$\psi_\alpha{}^-(p, k)=\sum_v(\Psi_0{}^* a_{-k}{}^* b_{pv}\Psi)v_\alpha. \tag{55}$$

With these notations, Eq. (52) becomes

$$[\epsilon-\eta(p)E_p]\psi(p)=G\sum_k(2V\omega_k)^{-\frac{1}{2}} \times[\gamma\psi^+(p-k, k)+\gamma\psi^-(p-k, k)]. \tag{56}$$

The equation (48) for $\psi^+(p-k, k)$ is

$$[\epsilon-\eta(p-k)E_{p-k}-\omega_k]\psi^+(p-k, k) =\sum_v(\Psi_0{}^*[a_k b_{p-k,v}, H']\Psi)v. \tag{57}$$

Equation (57) couples the one-proton-one-meson wave function to the one-proton wave function and to various components $a(N, N')$ involving 3 particles. To obtain the first approximation of the Tamm-Dancoff method,[13] we set all the 3-particle amplitudes equal to zero. To do this we must arrange the commutator in (57) as a sum of terms written in normal form[8] with creation operators standing to the left of absorption operators, and then keep only the term which involves a single b_{pu} operator. This gives for the right side of (57)

$$G(2V\omega_k)^{-\frac{1}{2}}\Lambda^+(p-k)\gamma\psi(p), \tag{58}$$

with

$$\Lambda^+(p)=\tfrac{1}{2}[1+\eta(p)], \quad \Lambda^-(p)=\tfrac{1}{2}[1-\eta(p)]. \tag{59}$$

Because of the Λ^+ in (58), Eq. (57) becomes

$$(\epsilon-E_{p-k}-\omega_k)\psi^+(p-k, k) =G(2V\omega_k)^{-\frac{1}{2}}\Lambda^+(p-k)\gamma\psi(p). \tag{60}$$

[13] The Tamm-Dancoff treatment in this first approximation gives the same results as the Lévy-Klein treatment with the interaction kernel calculated to order G^2. The two methods become different only in the next approximation.

Similarly, the equation for $\psi^-(p-k, k)$ is

$$(\epsilon+E_{p-k}+\omega_k)\psi^-(p-k, k) = G(2V\omega_k)^{-\frac{1}{2}}\Lambda^-(p-k)\gamma\psi(p). \quad (61)$$

Substituting Eqs. (60) and (61) into Eq. (56), and letting $V\to\infty$, we derive an integral equation for $\psi(p)$ alone,

$$(\epsilon-\alpha\cdot p-\beta M)\psi(p)=(G^2/16\pi^3)\left\{\int d_3k(\omega_k)^{-1} \times\gamma[\epsilon-\eta(p-k)(E_{p-k}+\omega_k)]^{-1}\gamma\right\}\psi(p). \quad (62)$$

Equation (62) gives the second-order self-energy of a proton interacting with the meson field. The Dirac operator multiplying $\psi(p)$ on the right side is the self-energy operator. This operator in general has matrix elements between positive and negative energy components of $\psi(p)$. Thus, Eq. (62) is a set of 4 coupled equations and will have four independent solutions $\psi(p)$, two with a positive eigenvalue ϵ and two with a negative ϵ. The positive ϵ is the energy of a proton of momentum p, including self-energy, and the negative ϵ is minus the energy of an antiproton of momentum p.

It is noteworthy that Eq. (62) differs from the corresponding equation obtained using the old Tamm-Dancoff wave function $\alpha(N)$. The form of the energy denominators is here symmetrical between positive and negative energy intermediate states, whereas in the equation for $\alpha(N)$ the negative intermediate states give denominators of a quite different and unsymmetrical form. The denominators in Eq. (62) are much closer to those which appear in the covariant 4-dimensional perturbation theory. This removes one of the major difficulties found by Lévy[5] and Klein[12] in connecting the Bethe-Salpeter equation with the 3-dimensional treatment.

IX. THE TWO-PARTICLE SYSTEM

We now use the method of Sec. VIII to construct from Eq. (48) the wave equation for the neutron-proton system, setting equal to zero all components $a(N, N')$ involving 4 or more particles. We define the 2-particle wave function

$$\psi_{\alpha\beta}(p, q)=\sum_u\sum_v(\Psi_0{}^*b_{pu}d_{qv}\Psi)u_\alpha v_\beta. \quad (63)$$

This is just the momentum transform of the configuration-space wave-function (17). Similarly we write

$$\psi^+{}_{\alpha\beta}(p, q, k)=\sum_u\sum_v(\Psi_0{}^*b_{pu}d_{qv}a_k\Psi)u_\alpha v_\beta, \quad (64)$$

$$\psi^-{}_{\alpha\beta}(p, q, k)=\sum_u\sum_v(\Psi_0{}^*a_{-k}{}^*b_{pu}d_{qv}\Psi)u_\alpha v_\beta. \quad (65)$$

The equation (48) for $\psi(p; q)$ is

$$[\epsilon-\eta^1(p)E_p-\eta^2(q)E_q]\psi(p, q) = G\sum_k(2V\omega_k)^{-\frac{1}{2}}[\gamma^1\psi^+(p-k, q, k) +\gamma^1\psi^-(p-k, q, k)+\gamma^2\psi^+(p, q-k, k) +\gamma^2\psi^-(p, q-k, k)], \quad (66)$$

where the indices 1, 2 denote Dirac matrices operating on the first and second spinor suffix of ψ, respectively. The equation for $\psi^+(p-k, q, k)$, dropping the 4-particle components, is

$$[\epsilon-\eta^1(p-k)E_{p-k}-\eta^2(q)E_q-\omega_k]\psi^+(p-k, q, k) = G(2V\omega_k)^{-\frac{1}{2}}[\Lambda^{+1}(p-k)\gamma^1\psi(p, q) +\Lambda^{+2}(q)\gamma^2\psi(p-k, q+k)]. \quad (67)$$

Similarly,

$$[\epsilon-\eta^1(p-k)E_{p-k}-\eta^2(q)E_q+\omega_k]\psi^-(p-k, q, k) = G(2V\omega_k)^{-\frac{1}{2}}[\Lambda^{-1}(p-k)\gamma^1\psi(p, q) +\Lambda^{-2}(q)\gamma^2\psi(p-k, q+k)]. \quad (68)$$

Substituting from (67) and (68) into (66), we find the two-particle wave equation

$$[\epsilon-(\alpha^1\cdot p+\beta^1M)-(\alpha^2\cdot q+\beta^2M)]\psi(p, q) = (G^2/16\pi^3)\int d_3k(\omega_k)^{-1}[K\psi(p, q) +L\psi(p-k, q+k)]. \quad (69)$$

The kernel K gives the effect of the self-energies of the two particles,

$$K=\gamma^1[\epsilon-\eta^1(p-k)(E_{p-k}+\omega_k)-\eta^2(q)E_q]^{-1}\gamma^1 +\gamma^2[\epsilon-\eta^2(q+k)(E_{q+k}+\omega_k)-\eta^1(p)E_p]^{-1}\gamma^2. \quad (70)$$

The kernel L gives the interaction between the particles resulting from exchange of a single meson,

$$L=\gamma^1[\epsilon-\eta^1(p-k)E_{p-k}-\eta^2(q)(E_q+\omega_k)]^{-1}\gamma^2 +\gamma^2[\epsilon-\eta^2(q+k)E_{q+k}-\eta^1(p)(E_p+\omega_k)]^{-1}\gamma^1. \quad (71)$$

Again we see that Eq. (69) differs from the two-body equation derived from the old Tamm-Dancoff method. The energy denominators in Eq. (71) are similar to those which appear in the Bethe-Salpeter equation and are symmetrical between positive and negative energies.

To make use of Eq. (69), it is necessary to use the Cini method of renormalization[10] to eliminate the divergent parts from the self-energy kernel K. The resulting equation is free of divergences and suitable for practical calculations. By separating the center-of-mass motion and considering a state with a definite angular momentum, we can reduce the equation to a one-dimensional integral equation for a 16-component function of one real variable. The number of components can be reduced by making further use of the symmetry properties of the equation. In any case, a one-dimensional integral equation of this kind can be solved numerically without a prohibitive amount of work. We are, therefore, in a position to explore quantitatively the behavior of the wave function $\psi_{\alpha\beta}(r, r')$ of a relativistic 2-body system, without assuming the velocities of the particles to be nonrelativistic and without assuming the negative-energy components of the wave function to be small.

The solutions of Eq. (69) will divide into four classes, characterized by the way in which they behave for small G. The first class tends as $G\to 0$ to a state of one free proton and one free neutron. The second class tends to one free proton minus one free antineutron, the third to one free neutron minus one antiproton, the fourth to minus one antiproton minus one antineutron. It is possible that for large G these classes of solutions will no longer be clearly distinguishable. However, in studying the two-body system we are only interested in the solutions of the first class. The other 3 classes represent systems in which real particles are present in the comparison state Ψ_0, so that Ψ_0 for these solutions is not the vacuum state. We have never used, in the whole analysis leading to Eq. (69), the information that Ψ_0 is the vacuum state. The fact that Ψ_0 is the vacuum state is an additional boundary condition which we impose on Eq. (69), restricting the allowed solutions to those of the first class.

A practical difficulty in the use of Eq. (69) is the fact that the energy denominators in Eq. (71) may vanish. When

$$\epsilon - E_{p-k} - E_q - \omega_k = 0, \tag{72}$$

the energy of the system is sufficiently large to allow production of a real meson. In this case the wave function $\psi^+(p-k, q, k)$ has a singularity where (72) is satisfied, representing an out-going wave of created mesons. This singularity appears in the integral Eq. (69) as a Dirac δ_+ function, in consequence of the assumed boundary condition that the free mesons form an outgoing wave. The integration over the δ_+ function then has a well-defined meaning and does not introduce any ambiguity. The type of vanishing energy denominator typified by Eq. (72) is handled here in exactly the same way as in nonrelativistic scattering theory.

However, another type of singularity in Eq. (71) occurs when

$$\epsilon + E_{p-k} - E_q - \omega_k = 0. \tag{73}$$

This corresponds to a singularity in $\psi^+(p-k, q, k)$ at the point where one neutron and one meson and minus-one antiproton are present. Such a singularity could exist only if a real antiproton were present in the comparison state Ψ_0. So again we use the fact that Ψ_0 is the vacuum state as an extra boundary condition, implying that there is no δ-function singularity in $\psi^+(p-k, q, k)$ where Eq. (73) is satisfied. This means that the integrations over vanishing energy denominators in Eq. (69) are always to be taken as Cauchy principal values, except in the case where they are of the form (72) and are associated with real particle creation.

The appearance of the "spurious" vanishing energy denominators in Eq. (69) is a defect of the new Tamm-Dancoff method, which may considerably complicate the practical use of the method. But it is clear that this defect is also inherent in the Bethe-Salpeter equation. The Bethe-Salpeter equation is also derived formally without using the fact that Ψ_0 in Eq. (1) is the vacuum state. Hence the fact that Ψ_0 is the vacuum state must be used as a boundary condition in order to obtain the physically meaningful solutions of the equation. Only because there is no known method of solving the Bethe-Salpeter equation except in a quasi-static approximation, this need for additional boundary conditions has hitherto been concealed.

Note added in proof:—W. M. Visscher (Cornell thesis, 1953, to be published) has calculated the finite part of the self-energy kernel (70) which remains after mass-renormalization. He used the Cini method, adapted to this problem as explained in an earlier letter [F. J. Dyson, Phys. Rev. **91**, 421 (1953)].

PHYSICAL REVIEW VOLUME 91, NUMBER 6 SEPTEMBER 15, 1953

A New Form for the Statistical Postulate of Quantum Mechanics

NORBERT WIENER AND ARMAND SIEGEL
Massachusetts Institute of Technology, Cambridge, Massachusetts
(Received May 15, 1953)

A new type of representation of the wave function of quantum mechanics, and a new form of the statistical interpretation of the wave function, are presented. The variable in the new representation is a mapping of points of differential space, closely related to Hilbert space, but having an associated measure for suitably defined sets of points in it. In the new statistical interpretation, an eigenvalue of every observable defined in the system is associated with each point in differential space. This can be done in such a way that, for each observable, the measure (=probability) of the set of all differential-space points belonging to a given set of eigenvalues is equal to the quantum-mechanical probability, calculated in the usual way (Born statistical postulate), that an experiment will yield an eigenvalue in this set. Thus we obtain an interpretation of quantum mechanics in terms of probability densities or probabilities instead of probability amplitudes.

I. INTRODUCTION

THE statistical interpretation of the wave function, introduced by Born,[1] consists of the following postulate: If $\varphi(q)$ is the wave function in a representation in which any operator $\mathbf{q}$ (having eigenvalues q) is diagonal, the probability that the corresponding observable q will be found on measurement to lie in the range q_1 to q_2 is

$$\int_{q_1}^{q_2} |\varphi(q)|^2 dq, \tag{1}$$

if $\mathbf{q}$ has a continuous eigenvalue spectrum with an analogous expression for discrete spectra. Since the entity in terms of which the dynamics of the system is expressed, through the time-dependent Schrödinger equation, is the wave function $\varphi(q)$ and not the probability density $|\varphi(q)|^2$, actual physical probabilities—i.e., frequencies of occurrence of given events—play a noncentral role in the conventional quantum theory.[2]

In this paper we propose an explicit statistical postulate distinct from that of Born, which is equivalent to the Born postulate so far as final results are concerned, but which has the effect of altering the structure of quantum mechanics in such a way that the dynamics is capable of being formulated as a time-rate of change of probabilities.

II. MATHEMATICAL APPARATUS

We first put the wave function into a representation such that its change with time, under any time-independent Hamiltonian,[3] is a measure-preserving point transformation of its argument. The mathematical techniques involved have been fully described in the literature.[4] However, in order to make the basic ideas readily accessible to those unfamiliar with them we shall give here a full, but nonrigorous, account of all the underlying mathematics.

We have first to consider Wiener's mathematical generalization of the Brownian motion. We are actually not concerned with the literal, physical Brownian motion, but with a set of functions having statistical properties very similar to those of the set of functions (describing the displacement of a Brownian particle in its dependence on the time) that would be obtained if we selected a large number of paths of such particles at random from a given solution.

Imagine a fluid containing a large number of particles undergoing Brownian motion. Describe the path of each particle as a function of time. The ensemble of all these functions has rather easily describable statistical properties when considered on a comparatively gross scale; this is due to the *randomness* (again on a gross scale) of the impacts to which the Brownian particles are continually subjected, this randomness being reflected in a corresponding randomness of the paths. With a finer scale of description, however, a nonrandom element begins to appear. This is, of course, due primarily to the nonvanishing mass of the Brownian particle, which gives it the ability at least partially to maintain its direction and velocity through a series of not too large a number of molecular impacts.

Wiener postulates a set of functions which is an abstraction from the ensemble of physical Brownian motion paths. Roughly speaking, the abstraction consists mainly of retaining the randomness of the "displacements" under *indefinite* subdivision of the paths. Wiener's set also contains discontinuous functions, which of course would not exist at all in the physical Brownian motions; but all such functions, relative to the whole set, constitute a set of zero probability—in the

[1] M. Born, Z. Physik **37**, 863 (1926).

[2] We speak here in terms of the Schrödinger picture. In the Heisenberg picture, where the dynamics is applied to the operators representing physical observables rather than to the wave function, probabilities are (at least formally) still further removed from any role in the dynamic part of the theory. The operators are here entirely independent of the probabilities, which vary with the initial conditions of the problem.

[3] This is not an essential restriction, provided we may regard any system with a time-dependent Hamiltonian as part of a larger, isolated system having a time-independent Hamiltonian. The former case then involves an inessential alteration in the proposed statistical interpretation.

[4] R. E. A. C. Paley and N. Wiener, *Fourier Transforms in the Complex Domain* (American Mathematical Society, New York, 1934), Chap. 9; N. Wiener, Acta Math. **55**, 117–258 (1930), Sec. 13; N. Wiener, J. Math. and Phys. **2**, 131 (1923).

terminology of measure theory, "almost all" the Brownian motions are continuous. The statistical properties possessed as an approximation by the physical Brownian motions become *exact* for Wiener's set, i.e., they subsist even under indefinitely minute scrutiny of the "paths."

From now on, we shall refer to the generalized set of functions referred to above simply as "Brownian motion functions." Whenever we refer to the *physical* Brownian motion, we shall explicitly include the additional adjective.

We now proceed to give a partly heuristic, quantitative account of the statistical properties of the set of Brownian motion functions. Consider a one-dimensional Brownian motion taking place in a discrete "time" described by the variable x, which can take on the equally spaced values $0, 1/N, 2/N, \cdots 1 (N = \text{integer})$. (This variable is not destined to play the role of time in the theory we shall ultimately describe, hence we avoid using the symbol t for it. It is, however, the analog of the time of the physical Brownian motion.) The "displacement" is a real function $X(\alpha, x)$. Here α is a parameter whose value singles out a particular function from the whole set. Wiener has shown that a set of real numbers α from zero to one is sufficient for this purpose, for Brownian motions not only in one dimension, but in any finite number of dimensions. We shall not prove this here, although we shall describe and utilize certain important properties of this mapping of the functions on the unit interval.

Let

$$\begin{aligned} X_j(\alpha) &= X(\alpha, j/N), \qquad (j=0, 1, \cdots N), \\ \Delta_j(\alpha) &= X_{j+1}(\alpha) - X_j(\alpha), \quad (j=0, 1, \cdots N-1). \end{aligned} \tag{2}$$

We now postulate that the "number"[5] of Brownian motions, in the whole set, having its jth increment Δ_j (for any given value of j) in the range $a<\Delta_j<b$, is proportional to

$$\frac{1}{(2\pi/N)^{\frac{1}{2}}} \int_a^b \exp\left(-\frac{\Delta^2}{2/N}\right) d\Delta,$$

independently of what ranges may be fixed simultaneously for the Δ's having other values of j. In other words, each Δ_j has a Gaussian distribution of values from $-\infty$ to $+\infty$, centered at zero, with mean square $1/N$, and statistically independent of all other increments; we shall say that the increments have *independent Gaussian distributions*. This will be recognized as the same as the gross statistical behavior of the increments of displacement in the physical Brownian motion: In the physical Brownian motion the independence of increments results from the large-scale lack of influence of all prior states of motion on the motion of the particle at any given moment, the increment in a given time interval thus being given entirely by the integrated molecular impulses received during that interval; while the Gaussian distribution can be shown from general probability laws to result from the fact that the individual molecular impulses are random in nature.

It can readily be shown that, with the above distribution for the elementary increments of the process, the distribution of the increment for an arbitrary multiple of the elementary "time interval" $1/N$ will obey the same Gaussian law, and will always have its mean square equal to the reciprocal of the length of the interval. We could multiply $1/N$ in the elementary distribution law by any constant, and have an analogous proportionality of the mean-square increment for arbitrary intervals; but for our present purposes such a coefficient need not be included explicitly.

Since the distribution law given above is normalized to unity, it may be used in the sense of a probability, i.e., the probability that $a \leqq \Delta_j(\alpha) \leqq b$ for α chosen at random is

$$\Pr\{a \leqq \Delta_j(\alpha) \leqq b\} = \frac{1}{(2\pi/N)^{\frac{1}{2}}} \int_a^b \exp\left(-\frac{\Delta^2}{2/N}\right) d\Delta. \tag{3}$$

In the above assertion, the basic property of the mapping of Brownian motions on the parameter α, which has not been given up to now, is implicitly assumed: The set of Brownian motions is *uniformly* distributed over the interval $0 \leqq \alpha \leqq 1$, i.e., the probability of a given subset is equal to the Lebesgue measure of the corresponding set of α's. If, moreover, the distribution law for the increments within each of the elementary "time" intervals $1/N$ is normalized to unity, as above, it is easy to show that the distribution law for any interval equal to an integer multiple of the basic interval is also normalized to unity.

Since the distributions of the Δ_j are mutually independent, it is a simple matter to obtain the probability that a randomly chosen Brownian motion will have all of its increments within a given set of ranges,

$$\begin{aligned} &\Pr\{a_1 \leqq \Delta_1(\alpha) \leqq b_1, \quad a_2 \leqq \Delta_2(\alpha) \leqq b_2, \\ &\qquad \cdots, \quad a_{N-1} \leqq \Delta_{N-1}(\alpha) \leqq b_{N-1}\} \\ &= \left(\frac{2\pi}{N}\right)^{-\frac{1}{2}(N-1)} \int_{a_1}^{b_1} \int_{a_2}^{b_2} \cdots \int_{a_{N-1}}^{b_{N-1}} \exp\left(-\frac{\Delta_1^2}{2/N} \right. \\ &\qquad \left. -\frac{\Delta_2^2}{2/N} - \cdots - \frac{\Delta_{N-1}^2}{2/N}\right) d\Delta_1 d\Delta_2 \cdots d\Delta_{N-1}. \end{aligned} \tag{4}$$

This is equal to the measure of the set of α's for which $X(\alpha, x)$ satisfies the given inequalities.

The set of Brownian motions in a continuous "time" variable x varying from 0 to 1 may now be characterized in its statistical properties by going to the limit $N \to \infty$ in

[5] Actually, measure rather than number. The "number" here involved is infinite. It must thus be dealt with quantitatively in terms of measure, just as the "number" of points in a line segment is dealt with in terms of the measure of the segment—a segment being, of course, an example of a simple type of set for which the measure is given merely by its length.

the above equations. This gives the measure of any set of Brownian motions all of whose X *vs* x graphs lie between those of any two given Brownian motions, or the measure of any sum of (a denumerable number of) such sets.

The general reasoning so far given can be readily extended to any range of the x variable, including an infinite range, without any essential changes.

The multidimensional Brownian motion is a simple generalization of the one-dimensional case. X will in this case have a number of components, all functions of one time variable x. The increments of any component are independent of one another as well as of those of the other components; the measure of a set is given by an obvious generalization of the method already given, based on the independence of all increments. As already mentioned, a measure-preserving mapping onto the interval (0, 1) is still possible.

An important special case of multidimensional Brownian motion, which is particularly important to us, is the *complex* Brownian motion. Here X is a complex number, a function of the real variable x and the parameter α. The increments of its real and imaginary parts are all independent of one another.

The usefulness for us of the set of Brownian motions lies in the fact that it is capable of giving a measure for a set of functions. If a function is thought of as a vector in function space in the usual way, namely, if the variable x in the function $f(x)$ is considered as a component index, i.e., $f(x_0)$ is the x_0th component, etc., of the representative vector, then one might expect to have a measure of certain simple sets of functions, simply by using a volume element in the function space. This expectation is, of course, not borne out, because a volume element in a space of an infinite number of dimensions can only be equal to zero or infinity. The statistical weighting technique used with the Brownian motions, on the other hand, gives a manageable definition of measure for a set of functions.

This measure is made visualizable in another kind of space, the "differential space." Imagine all the increments Δ_j divided by the increment $\Delta x=1/N$. Then the set

$$\frac{\Delta_1(\alpha)}{\Delta x}, \quad \frac{\Delta_2(\alpha)}{\Delta x}, \quad \cdots, \quad \frac{\Delta_{N-1}(\alpha)}{\Delta x}$$

is a set of difference quotients which approaches, in the limit $N\to\infty$, the values of the derivative of $X(\alpha, x)$. (Since almost all of the $X(\alpha, x)$ are nondifferentiable, most of the difference quotients will approach infinity; but one may imagine the derivative as obtained by termwise differentiation of an expansion of $X(\alpha, x)$ in an orthogonal series of continuous functions.) The ordinary function-space representation of the derivative of $X(\alpha, x)$ has components equal to the above difference quotients, in the limit $N\to\infty$, $\Delta x\to 0$. Again, a set of finite components may be obtained, in a nonrigorous sense of course, by a Fourier transformation of $X(\alpha, x)$ followed by termwise differentiation: Let the range of x be from 0 to 1, and expand $X(\alpha, x)$. In terms of the orthogonal set $e^{2\pi inx}$,

$$X(\alpha, x)=\sum_{n=-\infty}^{\infty} a_n e^{2\pi inx},$$

$$dX(\alpha, x)/dx=\sum 2\pi ina_n e^{2\pi inx}.$$

Thus $dX(\alpha, x)/dx$ is represented in Hilbert space by the components $2\pi ina_n$ with respect to the orthogonal axes given by the functions $e^{2\pi inx}$. The norm of dX/dx, $\sum|2\pi ina_n|^2$, will not converge, of course, except for a set of α of measure zero, hence dX/dx is undefined, strictly speaking.

Differential space, referred to above, is not quite the same as the function space of the derivative; it is defined as the space in which a function is represented by its *differentials* ("limits" of the increments Δ_j) as coordinates, rather than by the values of its derivative. This makes the norm of the vector almost always finite, since

$$\lim_{N\to\infty}\sum_{j=0}^{N-1}|\Delta_j|^2$$

is the quadratic variation of the function, which is finite for almost all of the Brownian functions as a result of their definition.

If now we select a large number of Brownian motions at random, and imagine the fine dust formed by their representative points in differential space, we would find a Gaussian distribution of the density of this dust, centered at the origin, as we moved out along any axis. The number of dust particles in a given region of the differential space is proportional to the measure (in physical terms, probability) assigned to this region by going to the limit $N\to\infty$ in Eq. (4), or the counterpart of Eq. (4) for a Brownian motion of whatever number of components may be involved. This in turn is the measure assigned to the functions satisfying the inequalities given in the curly brackets on the left-hand side of Eq. (4).

The mean squares of all increments are kept equal to one another in the limiting process $N\to\infty$, and therefore the density of the "dust" in differential space is hyperspherically symmetrical. Considering for a moment a real Brownian motion, this corresponds to the fact that in Eq. (4) the exponent of the Gaussian function is proportional to the squared magnitude of the differential-space vector. Hence any rotation of the axes in differential space, or any rigid rotation of all vectors in the space, would leave this exponent invariant, and we would have the result that the independent Gaussian distribution of differential-space components of the set of real Brownian motions is invariant to such rotations, i.e., to any real orthogonal transformation of these

functions. It is, in fact, readily apparent that such transformations transform the set into itself.

In the case of complex Brownian motions, the Gaussian exponent is equal to the sum of the squares of the real and imaginary parts of the complex increments in the limit $N\to\infty$, or the sum of the quadratic variations of the real and imaginary parts of the Brownian function. In this case, the analog of the rigid rotation in the real case is a unitary transformation; hence a unitary transformation of the differential-space vector conserves the independent Gaussian distributions of the differentials and transforms the set of complex Brownian motions into itself.

Consider now a subdivision of the interval (0, 1) of definition of the x variable of the Brownian motion labeled as follows:

$$x_0=0, \quad x_1=1/N, \quad x_2=2/N, \quad \cdots, \quad x_N=1,$$

and a matrix depending on the two indices x_i, y_m, having matrix elements $\varphi(x_i, y_m)$. These satisfy the unitarity conditions,

$$\begin{aligned}\sum_{y_m} \bar{\varphi}(x_i, y_m)\varphi(x_j, y_m)&=\delta_{ij},\\ \sum_{x_i} \bar{\varphi}(x_i, y_m)\varphi(x_i, y_n)&=\delta_{mn}.\end{aligned} \tag{5}$$

The quantity

$$\psi(\alpha, y_m)=\sum_{i=0}^{N} \bar{\Delta}_i(\alpha)\varphi(x_i, y_m) \tag{6}$$

then has the meaning of a component, namely, the mth of the vector representing the αth Brownian motion in the differential space (of Brownian functions of the discrete time variable x) with respect to a new set of axes labeled by the indices y_m; or alternatively, as a component of the vector obtained by rotating the original Brownian motion vector. In the case of a unitary transformation represented by a function $\varphi(x, y_m)$ which is continuous in x, the counterpart of Eq. (6) is the Stieltjes integral

$$\psi(\alpha, y_m)=\int d\bar{X}(\alpha, x)\varphi(x, y_m). \tag{7}$$

Because the Stieltjes integral is not rigorously defined for all Brownian motions $X(\alpha, x)$, since not all are of bounded variation, it is necessary to state that (7) is to be interpreted only in a formal sense. The right-hand side of Eq. (7) obtains its rigorous definition through integration by parts

$$\psi(\alpha, y_m)=-\int \bar{X}(\alpha, x)d\varphi(x, y_m). \tag{8}$$

As a result of the interpretation given $\psi(\alpha, y_m)$ in the case of discrete x, immediately following Eq. (6), we would expect that the distribution of the values of the real and imaginary parts of $\psi(\alpha, y_m)$, obtained by letting α range through all its values, is Gaussian and independent of the values of the similarly distributed real and imaginary parts of all $\psi(\alpha, y_n)$ for which $n\neq m$. This is indeed the case; the proof is given in the references cited, and we shall not repeat it here.

The functions $\psi(\alpha, y_m)$ may be interpreted in another way: They are the coefficients in the formal expansion of $d\bar{X}(\alpha, x)/dx$ in terms of the orthogonal set of functions $\varphi(x, y_m)$. If for $\varphi(x, y_m)$ we take the exponential function $e^{2\pi imx}$ (the interval of x being from 0 to 1), the term-by-term integration of the series gives the expansion of $\bar{X}(\alpha, x)$ in terms of these functions. Going back to Eq. (7), with $\varphi(x, y_m)$ an arbitrary orthogonal set other than the complex exponentials, the expansion of $X(\alpha, x)$ in complex exponentials may be used in this equation to yield a formal proof of a second basic property of the functions $\psi(\alpha, y_m)$: They are a *normal orthogonal set in* α, if the $\varphi(x, y_m)$ are normal and orthogonal in x,

$$\begin{aligned}\int_0^1 \bar{\psi}(\alpha, y_m)\psi(\alpha, y_n)d\alpha&=\int \bar{\varphi}(x, y_m)\varphi(x, y_n)dx\\ &=\delta_{mn}.\end{aligned} \tag{9}$$

Hence the quantities $\Delta_i(\alpha)$ are in a generalized sense also representatives of a unitary transformation between the discrete "axes" represented by the letters i and the continuous variable α; and the improper functions $d\bar{X}(\alpha, x)/dx$ represent a generalized unitary transformation between the two continuous variables x and α. Hence $\psi(\alpha, y_m)$ has a double meaning: It may be regarded as (a) the representative of $\varphi(x, y_m)$ transformed from the variable x to α, or (b) the representative of the formal derivative $d\bar{X}(\alpha, x)/dx$ transformed from the variable x to y_m. The independence of the $\psi(\alpha, y_m)$ follows from (b), and their orthogonality follows from (a); but it should be noted that, even if the $\varphi(x, y_m)$ are a complete set in the variable x, the $\psi(\alpha, y_m)$ are not a complete set in α.

III. THE WAVE FUNCTION IN THE "α REPRESENTATION"

We now consider x as the spatial variable of a normalizable wave function $\varphi(x, t)$, where t represents the time.

Let

$$\psi(\alpha, t)=\int d\bar{X}(\alpha, x)\varphi(x, t). \tag{10}$$

We shall call this the "wave function in the α representation." The use of the term "representation" is justified by the remarks above to the effect that $d\bar{X}(\alpha, x)/dx$ behaves like a unitary transformation representative. This is an extension of the usual meaning of a representation, since α is equivalent to an infinity of ordinary variables of the type of the spatial variable x and,

although $d\bar{X}(\alpha, x)/dx$ behaves, as we saw above, like the representative of a unitary transformation, it completely lacks the symmetry that would be expected between α and x in an ordinary unitary transformation.

Suppose now that $\varphi(x, t)$ transforms with time according to the equation

$$\varphi(x, t)=\int u(x, x'; t)\varphi(x', 0)dx', \tag{11}$$

where $u(x, x'; t)$ is a unitary kernel. If (11) is substituted into (10), the result can be formally altered according to the following steps:

$$\begin{aligned}\psi(\alpha, t)&=\int d\bar{X}(\alpha, x)\int u(x, x'; t)\varphi(x', 0)dx'\\&=\int dx'\left[\int d\bar{X}(\alpha, x)u(x, x'; t)\right]\varphi(x', 0)\\&=\int d\bar{X}(T^t\alpha, x')\varphi(x', 0).\end{aligned} \tag{12}$$

The first line shows the result of direct substitution. The second is obtained by interchanging the order of the integrations. The quantity

$$dx'\int d\bar{X}(\alpha, x)u(x, x'; t) \tag{13}$$

can be seen, by a reasoning analogous to that given in connection with Eq. (7), to be the formal expression for the x' component in differential space of a vector obtained from that having components $d\bar{X}(\alpha, x)$ by a "rotation"—i.e., a unitary transformation in differential space.[6] Hence $dx'\int d\bar{X}(\alpha, x)u(x, x'; t)$ is the x' component of a new Brownian motion, and the transformation merely rotates the entire differential space. From this it follows that the set of Brownian motions is transformed into itself. This transformation is denoted in the third line of Eq. (12) by the operator T^t; $T^t\alpha$ is the new value of α obtained from the rotation of the Brownian function having parameter α by the unitary kernel $u(x, x'; t)$. As suggested by the hyperspherical symmetry of the distribution in differential space, this rotation sends a given region of differential space into another region with preservation of measure. Crudely speaking, the "number" of Brownian motions in the original region and the transformed region is unaltered by the transformation; the rigorous statement of this fact is that for all α belonging to a given measurable set on the interval $0\leqq\alpha\leqq 1$ the measure of the set of the corresponding $T^t\alpha$ is equal to that of the original set.

[6] The formal parallelism between Eqs. (7) and (13) is established by associating ξ_m with x' and $\varphi(x, \xi_m)$ with $u(x, x'; t)dx'$; the differential in the latter quantity is necessary in doing this because x' is a continuous variable while ξ_m is discrete.

Comparing the third line of Eq. (12) with Eq. (10), we see that

$$\psi(\alpha, t)=\psi(T^t\alpha, 0), \tag{14}$$

i.e., *the change with time in $\psi(\alpha, t)$ is in general a measure-preserving point transformation on the argument α.* Such a result is impossible for the wave function in any of the usual representations of quantum mechanics. It would contradict the characteristic spreading-out in time of wave functions in representations such that operators diagonal in them do not commute with the Hamiltonian, and would be similarly inconsistent with the mode of change with time [through exponentials $\exp(iEt/\hbar)$] of wave functions in representations such that the diagonal operators do commute with the Hamiltonian.

The transformation $\psi(\alpha, 0)\rightarrow\psi(\alpha, t)=\psi(T^t\alpha, 0)$ may be "visualized" in differential space as follows: $\psi(\alpha, 0)$ associates with each point α in this space a complex number $\psi(\alpha, 0)$. The time-transformation brought about by the dynamics in time t corresponds to a "rigid rotation" of the generalized contours in differential space that characterize this function, i.e., to a rotation of the structure of complex numbers that are values of $\psi(\alpha, 0)$ for the different points α.

IV. IDENTIFICATION OF DIFFERENTIAL-SPACE POINTS WITH INDIVIDUAL SYSTEMS

With quantum dynamics in the form of a transformation of points in differential space into one another, the final step that we want to make is the identification of these points with individual systems having well-defined values of all observable quantities. This section is devoted to establishing an algorithm for this purpose, which takes the form of a new statistical interpretation for the wave function, as promised in the introductory section.

Consider an observable $\mathfrak{R}$ to which corresponds an operator $\mathbf{R}$ acting on the variable x of the wave function $\varphi(x)$. Suppose at first that $\mathbf{R}$ has only discrete eigenvalues R_1, R_2, $\cdots$ corresponding to eigenfunctions $\chi_1(x)$, $\chi_2(x)$, $\cdots$, i.e.,

$$\mathbf{R}\chi_1(x)=R_1\chi_1(x), \quad \mathbf{R}\chi_2(x)=R_2\chi_2(x), \quad \cdots. \tag{15}$$

We suppose the $\chi_i(x)$ normalized and orthogonal. Expand the wave function in terms of the $\chi_i(x)$,

$$\varphi(x)=\sum_{i=1}^{\infty} a_i\chi_i(x). \tag{16}$$

Now let

$$\xi_i(\alpha)=\int d\bar{X}(\alpha, x)\chi_i(x). \tag{17}$$

Then, integrating term by term, we get

$$\psi(\alpha)=\int d\bar{X}(\alpha, x)\varphi(x)=\sum_{i=1}^{\infty} a_i\xi_i(\alpha). \tag{18}$$

We now consider each $\xi_i(\alpha)$ as a random variable, a function in turn of the random variable α. As we have seen (end of Sec. II), the distributions of the real and imaginary parts of $\xi_i(\alpha)$ are mutually independent of one another and of those of all other $\xi_j(\alpha)$ and are Gaussian in form, i.e., the relative probability that any $\mathrm{Re}\xi_i(\alpha)$ or $\mathrm{Im}\xi_i(\alpha)$ lies between a and b is

$$\frac{1}{(2\pi)^{\frac{1}{2}}}\int_a^b \exp(-y^2/2)dy, \tag{19}$$

independently of what ranges may be fixed simultaneously for the other part of the same ξ_i and the real and imaginary parts of the others.

We now assign an eigenvalue of $\mathbf{R}$ to any given value of α in the following way: Divide $\psi(\alpha)$ into two parts, say

$$\psi(\alpha)=\psi_{11}(\alpha)+\psi_{12}(\alpha), \tag{20}$$

$$\psi_{11}(\alpha)=\sum_{i=1}^{n_1} a_i\xi_i(\alpha), \quad \psi_{12}(\alpha)=\sum_{i=n_1+1}^{\infty} a_i\xi_i(\alpha). \tag{21}$$

Since ψ_{11} and ψ_{12} are orthogonal, the distributions of their real and imaginary parts are independent and Gaussian. The mean square of $\mathrm{Re}\psi_{11}$, $\langle(\mathrm{Re}\psi_{11})^2\rangle$, equals that of $\mathrm{Im}\psi_{11}$, and similarly for $\mathrm{Re}\psi_{12}$ and $\mathrm{Im}\psi_{12}$. Hence the mean square is

$$\sigma_{11}=\langle(\mathrm{Re}\psi_{11})^2\rangle=\langle(\mathrm{Im}\psi_{11})^2\rangle=\tfrac{1}{2}\langle|\psi_{11}|^2\rangle$$
$$=\tfrac{1}{2}\int_0^1|\psi_{11}(\alpha)|^2d\alpha=\tfrac{1}{2}\int|\chi_{11}(x)|^2dx=\tfrac{1}{2}\sum_{i=1}^{n_1}|a_i|^2 \tag{22}$$

$$\frac{\displaystyle\iiiint_{(u^2+v^2\geq x^2+y^2)} \exp\left(-\frac{u^2+v^2}{2\sigma_{11}}\right)\exp\left(-\frac{x^2+y^2}{2\sigma_{12}}\right)dudvdxdy}{\displaystyle\int_{-\infty}^{\infty}\int_{-\infty}^{\infty}\int_{-\infty}^{\infty}\int_{-\infty}^{\infty}\exp\left(-\frac{u^2+v^2}{2\sigma_{11}}\right)\exp\left(-\frac{x^2+y^2}{2\sigma_{12}}\right)dudvdxdy}$$
$$=\frac{4}{\sigma_{11}\sigma_{12}}\int_0^{\infty}\exp\left(-\frac{t}{2\sigma_{12}}\right)dt\int_t^{\infty}\exp\left(-\frac{s}{2\sigma_{11}}\right)ds=\frac{\sigma_{11}}{\sigma_{11}+\sigma_{12}}=2\sigma_{11}=\sum_{i=1}^{n_1}|a_i|^2, \tag{24}$$

which is equal to the relative probability according to the Born postulate that the measured value of $\mathfrak{R}$ lie in the set S_{11}. The probability that $R(\alpha)$ is in S_{12} is obviously $2\sigma_{12}$, and the sum of the two probabilities is 1.

At any later step, moreover, we shall obtain a set of probabilities for $R(\alpha)$ lying in the ranges defined at this step (there will be at this step 2^n ranges in the subdivision of the total infinite range of R) having the following property: The relative probabilities of the two ranges obtained by subdivision of any single one of the ranges of the previous step are proportional to the Born probabilities. Since the absolute probabilities of the two ranges obtained in the first step agree with the Born probabilities, it follows that those of the second step also agree, and so on, as may be shown by mathematical induction.

We are evidently at liberty to choose the indices defining the successive subdivisions in any way we wish. In particular, with normalizable wave functions the eigenfunctions can be numbered and n_1 chosen so that the probability of S_{12} is as small as we wish, and the set S_{11} is simultaneously finite. This choice insures that, after some finite number of dichotomies for each α, the set of all α that are still not assigned an $\mathbf{R}$ eigenvalue is of measure as small as we wish, i.e., that the still unassigned $\mathbf{R}$ eigenvalues are of correspondingly small probability.

The case where $\mathbf{R}$ has continuous eigenvalues, i.e., for $\mathrm{Re}\psi_{11}$ and $\mathrm{Im}\psi_{11}$, and

$$\sigma_{12}=\langle(\mathrm{Re}\psi_{12})^2\rangle=\langle(\mathrm{Im}\psi_{12})^2\rangle=\tfrac{1}{2}\sum_{i=n_1+1}^{\infty}|a_i|^2 \tag{23}$$

for $\mathrm{Re}\psi_{12}$ and $\mathrm{Im}\psi_{12}$. We shall take $\varphi(x)$ normalized, hence

$$\int_0^1|\psi(\alpha)|^2d\alpha=\int[|\psi_{11}(\alpha)|^2+|\psi_{12}(\alpha)|^2]d\alpha$$
$$=2(\sigma_{11}+\sigma_{12})=1.$$

We now determine which is bigger, $|\psi_{11}(\alpha)|$ or $|\psi_{12}(\alpha)|$. If the first, we take R to lie in the set $R_1,\cdots R_{n_1}$, which we shall call S_{11}; otherwise, in the remaining set S_{12}. This completes the first step in an infinite dichotomic process, consisting of steps similar to the above, whereby the choice of an R belonging to α is successively narrowed down, leading in the limit to a unique value (except for a set of α of measure zero) of R, which we shall call $R(\alpha)$. In the next step, we take ψ_{11} or ψ_{12}—depending on which was chosen in the first step—and proceed with it exactly as we did in the first step, dividing it into two parts, finding which is of bigger modulus, and assigning $R(\alpha)$ to the corresponding range; and so on.

We now wish to know, first, the *probability* of $R(\alpha)$ lying in S_{11} or S_{12}. Since the real and imaginary parts of $\psi_{11}(\alpha)$ and $\psi_{12}(\alpha)$ are all mutually independent, the probability that $|\psi_{11}(\alpha)|\geq|\psi_{12}(\alpha)|$, i.e. $|\psi_{11}(\alpha)|^2\geq|\psi_{12}(\alpha)|^2$, is

where

$$\varphi(x)=\int_{-\infty}^{\infty}\chi(x,R)a(R)dR, \tag{25}$$

$\chi(x,R)$ satisfying the orthogonality and normalization conditions

$$\int\bar{\chi}(x,R)\chi(x,R')dx=\delta(R-R'),$$

$$\int\bar{\chi}(x,R)\chi(x',R)dR=\delta(x-x'),$$

is treated along the same lines as the discrete case, by exploiting the formal parallel between $a(R)$ and a_i, and between $\chi(x,R)$ and $\chi_i(x)$. Specifically, we proceed as follows:

Let

$$\psi(\alpha)=\int d\bar{X}(\alpha,x)\varphi(x), \tag{26}$$

as before. Then

$$\psi(\alpha)=\int_{-\infty}^{\infty}a(R)dR\int d\bar{X}(\alpha,x)\chi(x,R) \tag{27a}$$

$$=\int_{-\infty}^{\infty}d\bar{\xi}(\alpha,R)a(R), \tag{27b}$$

where

$$d\bar{\xi}(\alpha,R)=dR\int d\bar{X}(\alpha,x)\chi(x,R). \tag{28}$$

Now put

$$\psi_{11}(\alpha)=\int_{-\infty}^{A_1}d\bar{\xi}(\alpha,R)a(R), \tag{29a}$$

$$\psi_{12}(\alpha)=\int_{A_1}^{\infty}d\bar{\xi}(\alpha,R)a(R). \tag{29b}$$

These two quantities have, like the like-named quantities in the discrete case, independent Gaussian distributions for their real and imaginary parts, and are orthogonal to one another. The mean squares of the real and imaginary parts of, respectively, ψ_{11} and ψ_{12}, are

$$\sigma_{11}=\tfrac{1}{2}\int_{-\infty}^{A_1}|a(R)|^2dR,\quad \sigma_{12}=\tfrac{1}{2}\int_{A_1}^{\infty}|a(R)|^2dR, \tag{30}$$

i.e., again the usual quantum-mechanical probabilities for finding a value of R in the ranges indicated by the limits of integration. From here on, the calculation is the same as in the discrete case: One assigns to a given α the range $(-\infty, A_1)$ or $(A_1, +\infty)$, depending on whether $|\psi_{11}(\alpha)|$ or $|\psi_{12}(\alpha)|$ is the greater. The measures of the two sets of values of α corresponding to these ranges will be $2\sigma_{11}$ and $2\sigma_{12}$, respectively (if $\varphi(x)$ is normalized), agreeing with the quantum-mechanical probabilities for these two ranges. Successive steps in the sequence of dichotomies are modeled on the first one, exactly as in the case of discrete eigenvalues.

Although we have in the above development given a privileged status, so to speak, to the variable x, formally speaking x and R are really on the same footing. This is readily apparent from the completely parallel form of Eqs. (26) and (27b): $\xi(\alpha,R)$ is a complex Brownian motion in R, and $X(\alpha,x)$ and $\xi(\alpha,R)$ may be thought of as representatives, in terms of different variables, of a single element of an ensemble of abstract elements represented by points in differential space. Using Dirac's bra and ket notation, it is possible to demonstrate this equivalence in a formal way. We take advantage of the fact already shown that $d\bar{X}(\alpha,x)/dx$ and $d\bar{\xi}(\alpha,R)/dR$ behave to some extent like unitary transformation coefficients; let us then denote them by $\langle\alpha|x\rangle$ and $\langle\alpha|R\rangle$, respectively, although it must be borne in mind that this notation is not completely justified in view of the lack of symmetry between the α variable and the ordinary variables of quantum theory. Let us put

$$\chi(x,R)=\langle x|R\rangle,$$
$$\varphi(x)=\langle x|\varphi\rangle,$$
$$a(R)=\langle R|\varphi\rangle,$$

and

$$\psi(\alpha)=\langle\alpha|\varphi\rangle.$$

The first equation is of standard type. The second and third are the ordinary consequences, expressed in the Dirac notation, of the assumption that the state vector of the system is $|\varphi\rangle$. The fourth equation has the same interpretation as the second and third, once one accepts the treatment of α as on the same footing as x or R as is implied by the very use of the symbols $\langle\alpha|x\rangle$ and $\langle\alpha|R\rangle$. Equations (25), (26), (27a), and (27b) may now be written

$$\langle x|\varphi\rangle=\int\langle x|R\rangle dR\langle R|\varphi\rangle, \tag{25'}$$

$$\langle\alpha|\varphi\rangle=\int\langle\alpha|x\rangle dx\langle x|\varphi\rangle \tag{26'}$$

$$=\int\int\langle\alpha|x\rangle dx\langle x|R\rangle dR\langle R|\varphi\rangle \tag{27'a}$$

$$=\int\langle\alpha|R\rangle dR\langle R|\varphi\rangle. \tag{27'b}$$

In order to go from (27'a) to (27'b) directly, one has to assume

$$\langle\alpha|R\rangle=\int\langle\alpha|x\rangle dx\langle x|R\rangle, \tag{28'}$$

which is entirely consistent with the previous identifications and corresponds to (28).

When **R** has a discrete spectrum, the situation is formally not changed, and we shall not trouble to write

down all the equations corresponding to (25′) to (27′b). The transformation equations

$$\langle\alpha|R_i\rangle=\xi_i(\alpha)=\int\langle\alpha|x\rangle dx\langle x|R_i\rangle,$$

$$\langle\alpha|x\rangle=d\bar{X}(\alpha,x)/dx=\sum_i\langle\alpha|R_i\rangle\langle R_i|x\rangle,$$

where

$$\langle x|R_i\rangle=\chi_i(x),$$

reveal that $\xi_i(\alpha)$ is the ith increment of a Brownian motion in the *discrete* "time" variable R which takes on the values $R_1, R_2, \cdots$.

We can now give a concise general statement of the new statistical postulate for quantum mechanics: Given a division of the (continuous or discrete) set of eigenvalues of a quantum-mechanical operator into two non-overlapping subsets,[7] and a normalizable state vector $|\varphi\rangle$. The state vector is projected onto the two subspaces of Hilbert space corresponding to the two subsets of eigenvalues, and the "wave functions" in the α representation for these two projections are evaluated. The "wave function" having the larger modulus is then selected and its subspace divided in turn into two non-overlapping sub-subspaces. The "wave functions" in α representing the projections on these smaller subspaces are again compared in modulus, the larger selected, and so on. At each stage the eigenvalue of R that we seek is assigned to the subset corresponding to the subspace chosen, and its range thus narrowed down, in the limit, to a single number $R(\alpha)$. At each stage, moreover, it can be shown that the relative probability of the two subsets of eigenvalues involved is equal to that given by the Born postulate; the total probability of all subsets is one, so that the absolute probability of any subset, with this normalization, also agrees with that of the Born postulate.

In this way we may obtain a function $R(\alpha)$ for each observable $\mathfrak{R}$, such that

$$\int_0^1 R(\alpha)d\alpha=\langle\mathfrak{R}\rangle, \tag{34}$$

where $\langle\mathfrak{R}\rangle$ is the quantum-mechanical expectation value. Since the set of such functions for all observables also gives the probabilities for any defined ranges of values of any observables, we have a postulate entirely equivalent to the Born postulate. Moreover, we now have quantum dynamics expressed as a transformation of the same random variable α as that which furnishes, via the measure of appropriate subsets, the probability basis of the theory. This conclusion, stated only briefly here, will be discussed more fully in a subsequent paper.

V. NONUNIQUENESS OF $R(\alpha)$. THE POLYCHOTOMIC METHOD

The particular way in which the Hilbert space is divided at each stage of the succession of dichotomies is evidently entirely arbitrary. This means that the R value assigned to a given α is correspondingly arbitrary. For example, if at any stage R is found to be in a given subset of eigenvalues, the extension at this stage of the subspace corresponding to this subset at the expense of the other subspace might well throw R into the other subset, even though it has become smaller; and by the very nature of the dichotomous process, R cannot at any later stage re-enter the region from which it was thus ejected.

A brief calculation will show that the division of the subspace at each stage of the sequence into more than two parts will not work; for example, if one divides the subspace into *three* parts and assigns R to the subset of eigenvalues for which the projection of the wave function is the largest in modulus of the three, the relative probabilities of the three subsets do not satisfy Born's postulate.

It is interesting to note that this limitation can be removed by an alteration of the method in a different respect, as follows (for the sake of illustration, we treat first the case of discrete eigenvalues): We choose as $R(\alpha)$ the eigenvalue R_k for which $|\xi_k(\alpha)/a_k|$ (see Eq. (18)) is the *smallest of the entire set* of these quantities; the probability that $|\xi_k(\alpha)/a_k|$ is the smallest of all the $|\xi_i(\alpha)/a_i|$ is just $|a_k|^2$, as given by Born's postulate. To prove this, consider first a wave function for which only n coefficients a_i fail to vanish, and let these be named $a_1, a_2, \cdots a_n$. We first find the probability that

$$|\xi_n/a_n|<|\xi_{n-1}/a_{n-1}|<\cdots<|\xi_1/a_1|,$$

which we shall call for brevity

$$\Pr\{n<n-1<\cdots<1\}.$$

The quantities $|\xi_i(\alpha)/a_i|$ have mutually independent Gaussian distributions of their real and imaginary parts, with mean squares $\frac{1}{2}|a_i|^2$. Let $A_i=|a_i|^2$. Then

$$\Pr\{n<n-1<\cdots<1\}=\frac{\int_0^\infty e^{-A_nu_n}du_n\int_{u_n}^\infty e^{-A_{n-1}u_{n-1}}du_{n-1}\cdots\int_{u_2}^\infty e^{-A_1u_1}du_1}{\int_0^\infty e^{-A_nu_n}du_n\int_0^\infty e^{-A_{n-1}u_{n-1}}du_{n-1}\cdots\int_0^\infty e^{-A_1u_1}du_1}$$

$$=\frac{A_n}{A_1+\cdots+A_n}\cdot\frac{A_{n-1}}{A_1+\cdots+A_{n-1}}\cdots\frac{A_2}{A_1+A_2}. \tag{35}$$

[7] If the eigenvalues are discrete, no further characterization is necessary. If they are continuous, the subsets must be measurable.

The probability that $|\xi_n/a_n|$ is the smallest of all, $\Pr\{n<n-1, n-2, \cdots, 1\}$, is the sum of the above over all permutations of $A_1, A_2, \cdots A_{n-1}$. To carry out this summation, we note that since (35) must hold for any n,

$$\Pr\{n-1<n-2<\cdots<1\} = \frac{A_{n-1}}{A_1+\cdots+A_{n-1}} \frac{A_{n-2}}{A_1+\cdots+A_{n-2}} \cdots \frac{A_2}{A_1+A_2}; \quad (36)$$

hence

$$\Pr\{n<n-1<\cdots<1\} = \frac{A_n}{A_1+\cdots+A_n} \Pr\{n-1<n-2<\cdots<1\}, \quad (37)$$

and for the sum of the permutations we obtain

$$\Pr\{n<n-1, n-2, \cdots, 1\} = \sum_{\substack{\text{perm. of} \\ A_1, \cdots, A_{n-1}}} \Pr\{n<n-1<\cdots<1\} = \frac{A_n}{A_1+\cdots+A_n} \sum_{\substack{\text{perm. of} \\ A_1, \cdots, A_{n-1}}} \Pr\{n-1<n-2<\cdots<1\} = \frac{A_n}{A_1+\cdots+A_n}, \quad (38)$$

which is the Born probability of the eigenvalue R_n. Since the numbering of the eigenvalues is arbitrary, the theorem holds for any of the R_i in the set $R_1, R_2, \cdots R_n$. It holds, moreover, for any value of n, and therefore holds in the limit $n\to\infty$.

It is not necessary to carry the breakdown all the way to individual eigenvalues; we can assign $R(\alpha)$ merely to one or another subset of the set of n eigenvalues, with the correct probability for each subset as follows: If the n eigenvalues are to be divided into n' subsets, they may be renumbered in such a way as to make the indices consecutive in each group; then one has a set of numbers $1\leqq k_1<k_2\cdots<k_{n'-1}<n$ such that the particular inequality satisfied by i from the set

$$\begin{aligned} 1&\leqq i\leqq k_1, \\ k_1&< i\leqq k_2, \\ &\cdots \\ k_{n'-1}&< i\leqq n, \end{aligned}$$

determines the subset to which R_i belongs. Let

$$\begin{aligned} b_1&=(\sum_1^{k_1}|a_i|^2)^{\frac{1}{2}}, \\ b_2&=(\sum_{k_1+1}^{k_2}|a_i|^2)^{\frac{1}{2}}, \\ &\cdots \\ b_{n'}&=(\sum_{k_{n'-1}+1}^{n}|a_i|^2)^{\frac{1}{2}}; \end{aligned}$$

then

$$\begin{aligned} \xi_1'&=\frac{1}{b_1}\sum_1^{k_1} a_i\xi_i, \\ \xi_2'&=\frac{1}{b_2}\sum_{k_1+1}^{k_2} a_i\xi_i, \\ &\cdots \\ \xi_{n'}'&=\frac{1}{b_{n'}}\sum_{k_{n'-1}+1}^{n} a_i\xi_i, \end{aligned}$$

is a set of orthonormal functions such that

$$\psi(\alpha)=\sum_{i=1}^{n'} b_i\xi_i'(\alpha). \quad (39)$$

Then the preceding method may be used, with b_i replacing a_i, ξ_i' replacing ξ_i, and n' replacing n. This determines $R(\alpha)$ only as belonging to one or another of the n' sets, but gives the correct probability $|b_i|^2$ for the ith set, for any i.

The method for continuous eigenvalues is modeled on that for groups of discrete eigenvalues. If

$$\psi(\alpha)=\int_{-\infty}^{\infty} d\bar{\xi}(\alpha, R)a(R), \quad (40)$$

we break up the infinite range of integration into n' subsets; for simplicity, let these be intervals, although they need only be measurable, nonoverlapping subsets. Then we choose a set of numbers $r_1<r_2<\cdots r_{n'-1}$, corresponding to $k_1, k_2, \cdots k_{n'}$. If

$$\begin{aligned} b_1&=\left(\int_{-\infty}^{r_1}|a(R)|^2dR\right)^{\frac{1}{2}}, \\ b_2&=\left(\int_{r_1}^{r_2}|a(R)|^2dR\right)^{\frac{1}{2}}, \\ &\cdots \\ b_{n'}&=\left(\int_{r_{n'-1}}^{\infty}|a(R)|^2dR\right)^{\frac{1}{2}}, \end{aligned}$$

then

$$\begin{aligned} \xi_1&=\frac{1}{b_1}\int_{-\infty}^{r_1} d\bar{X}(\alpha, R)a(R), \\ \xi_2&=\frac{1}{b_2}\int_{r_1}^{r_2} d\bar{X}(\alpha, R)a(R), \\ &\cdots \\ \xi_{n'}&=\frac{1}{b_{n'}}\int_{r_{n'-1}}^{\infty} d\bar{X}(\alpha, R)a(R), \end{aligned}$$

is a set of orthonormal functions such that

$$\psi(\alpha)=\sum_{i=1}^{n} b_i\xi_i(\alpha), \quad (41)$$

and the real and imaginary parts of the ξ_i's have independent Gaussian distributions with mean squares equal to $\frac{1}{2}$. Then the method of discrete eigenfunctions can be applied, determining $R(\alpha)$ to within one of the n subsets, with the correct probability $|b_i|^2$ for the ith subset.

The general method presented in this section, which we will call the polychotomic method, has certain advantages over the dichotomic method. First, it has

the advantage, so far as manipulation of its results is concerned, of yielding a result at one step. Second, for a given subdivision of the total set of eigenvalues, it gives a unique result, unlike the dichotomic method. In particular, when a discrete set of eigenvalues is divided up into individual eigenvalues, it gives a unique assignment of eigenvalues to values of α, except for those values of α for which two or more $|\xi_i(\alpha)/a_i|$ are smaller than all others but equal to one another, but these values of α form a set of measure zero and can be neglected. On the other hand, it does not yield a unique $R(\alpha)$ in the continuous case: A sequence of finer and finer subdivisions, each yielding a range for $R(\alpha)$ by the polychotomic method, will not give convergence to a unique single value of $R(\alpha)$ in the limit. The dichotomic method, on the other hand, does in the limit converge to a single value of $R(\alpha)$ for almost all values of α, for any given sequence of dichotomies.

The polychotomic method, on the other hand, can be used in a way analogous to the dichotomic method; this is because, using the polychotomic method with subsets of eigenvalues, one can take a set of α for which all R values belong to one of the subsets of R and make more precise assignments of R values within the subset, by a further polychotomy or sequence of polychotomies of arbitrary type. In particular, the mode of fixing upon a subset of R eigenvalues (to be associated with an α) characteristic of the polychotomic method could if desired be used with a sequence of dichotomies (to avoid confusion, such a procedure might be dubbed a dicho-polychotomy). Thus the polychotomic method is a generalization of the dichotomic method. A fixed succession of finer and finer dicho-polychotomies will converge for almost all α values. Here every finer division is a subdivision of the coarser divisions which precede it.

VI. CONCLUDING REMARKS

At this point, we wish to call attention to the fact that it was only for the sake of simplicity that we presented the preceding material as if x or R were single variables. No essential change is required if one has a system of more than one degree of freedom, in which case x and R stand for sets of more than one variable, some of which may even be discrete while others are continuous. The Brownian motion functions $X(\alpha, x)$ or $\eta(\alpha, R)$ are then still single complex numbers, but functions of several variables—complex Brownian motions of a multidimensional "time." Integrals like $\int d\bar{X}(\alpha, x)\varphi(x)$ are multidimensional. The set of values of α is still the unit interval. Where in the case of a single variable the division of $\psi(\alpha)$ into two parts is a division of the line into two subsets, a division of the multidimensional space of eigenvalues into subsets takes its place when x or R stands for more than one variable

It should be emphasized that the purpose of our theory is simply to achieve an interpretation of quantum mechanics in terms of probability densities, and not to reconcile quantum concepts with classical ones. The method rests on the identification of observables with operators in Hilbert space, and achieves quantization purely as a result of this assumption, which has basic, not derived, status.

The following simple example will suffice to show the nonclassical nature of the observables in our theory: By the method we have given, simultaneous values of position q and momentum p can be assigned to almost all values of α. Consider, on the other hand, the operator for p^2+q^2; its eigenvalues are quantized, and the value obtained for this observable, for a given α, will not in general coincide with the sum of the squares of the position and momentum variables belonging to this value of α. Thus our method does not restore the classical meaning of observables. In fact, it would seem reasonable to picture the process of determining an eigenvalue to go with an α value as the mathematical counterpart of "forcing" the system into an eigenstate by the measuring process. This "forcing" is closely associated with the uncontrollable disturbance of the system, emphasized by Bohr, which necessarily accompanies measurement of an observable when the system is not in an eigenstate of that observable.

Closely associated with the preceding considerations is the lack of invariance of the individual eigenvalues tied to values of α under transformations of the associated variables. If, for example, the zero point of the scale of $\mathbf{R}$ eigenvalues is translated an amount R_0, i.e., the wave function $a(R)$ is transformed into $a(R+R_0)$, the value of R belonging to an individual α, say $R(\alpha)$, does not go into $R(\alpha)-R_0$ (unless, of course, the state is an eigenstate of $\mathbf{R}$). It is, however, trivially evident—from the fact that our postulate is equivalent to the Born postulate—that the *distribution function* of $R(\alpha)$ is correctly displaced by an amount R_0, and this is all we can reasonably expect, given the essential impossibility of a classical type of assignment of R values to individual systems.

In this connection, we wish further to point out that, since the operator formalism of relativistic (Dirac) quantum mechanics is subsumed under that of nonrelativistic quantum mechanics, the application of our method to Dirac particles is straightforward. On the other hand, the preceding remarks show that, although distributions of relativistic dynamic variables in differential space transform covariantly under Lorentz transformations, given the correct transformations of the wave functions, the individual values attached to points in differential space do not do so (except, again, for eigenstates of the variable concerned). Here again it is impossible to attribute any meaning to these individual values independent of the act of measurement. No contradiction can come from this, since the verification of covariance of momentum and energy of a single particle would imply at least two measurements of the components in two different Lorentz frames, and since the disturbance due to a quantum-mechanical measurement prevents the second quantity measured from ever being "the same" as the first.

Letters to the Editor

PUBLICATION of brief reports of important discoveries in physics may be secured by addressing them to this department. The closing date for this department is five weeks prior to the date of issue. No proof will be sent to the authors. The Board of Editors does not hold itself responsible for the opinions expressed by the correspondents. Communications should not exceed 600 words in length and should be submitted in duplicate.

Production of Sodium Airglow Excitation by Imprisonment of Resonance Radiation*

A. FODERARO AND T. M. DONAHUE
University of Pittsburgh, Pittsburgh, Pennsylvania
(Received July 6, 1953)

SERIOUS difficulties hamper the understanding of the emission of the sodium D lines in the night airglow on a photochemical basis. In substance the trouble arises from the indications at twilight that sodium in very low concentration is in equilibrium with the atmosphere at least up to 100 km, whereas nocturnal measurements place the airglow layer at 250 km where the concentration of sodium as well as of possible reactants would be far too low to account for the D line intensity observed.[1]

It should be pointed out that a resonance photon, originating somewhere in a sodium layer containing as many atoms as the twilight measurements imply, has a very good chance of being reabsorbed before it leaves the layer. In fact, calculation shows that in a spherical shell of sodium at 300°K, 100 km thick and containing 10^{11} atoms per cm^2 column, a photon radiated into the upward hemisphere of directions at the base of the layer has a total probability of 0.84 of being captured before it escapes through the top of the layer. As a consequence it appears possible, on the basis of calculations so far completed, to account for the observed concentration of excited atoms on the night side of the earth by transport of imprisoned resonance radiation from the sunlit side.

The theory of imprisonment of resonance quanta developed by Holstein[2] adapted to the present problem of sodium photons with Doppler line shape is simplified considerably in principle compared to the problems he treated because only a steady-state distribution fed by a constant source need be sought. The density of excited atoms in the "dark" region of the atmosphere is then

$$n(\mathbf{r}) = \int n(\mathbf{r}')G(\mathbf{r}, \mathbf{r}')d\mathbf{r}',$$

where $G(\mathbf{r}, \mathbf{r}')$ is the probability that a photon emitted at $\mathbf{r}'$ be absorbed at $\mathbf{r}$. Holstein demonstrates how $G(\mathbf{r}, \mathbf{r}')$ may be calculated for various types of line shapes.

Here, unfortunately, the region of integration and the boundary conditions are extremely complex, and recourse must be had to special methods of attacking the problem which will be explained in detail elsewhere.

The results obtained so far indicate that transport of excitation into the unilluminated region is very important for a layer of the type described above, or indeed under conditions which would have to be assumed to account for the excitation on any other basis. Unaided by reflections from the surface and from clouds, the imprisoned photons would, however, be attenuated too rapidly for layers reasonably thin—less than 100 km. But reflection is certain to be appreciable. Perhaps 0.4 of the photons striking the surface of the earth or clouds, would, on the average, be reflected. This, plus the gradual shrinking of the volume of the zones toward the antisolar point into which the radiation travels, appears to be capable of giving a rather constant average density of photons on the night side of the earth. Diurnal fluctuations, as well as the seasonal variation with a maximum in the summer, we believe to be mainly the result of the variations in surface reflectivity, particularly significant changes in cloud and snow cover, and partly perhaps the result of changes in the width of the trapping layer because of variable ionization.

Experiments to test these ideas are in progress. It should perhaps also be suggested here that imprisonment might be of great importance in explaining the excitation of resonance lines of atmospheric constituents other than sodium. Certainly it ought to be considered in connection with the deduction of layer heights and twilight concentrations when resonance photons are involved.

* This work was supported in part by the U. S. Air Force Cambridge Research Center.
[1] D. R. Bates and M. Nicolet, J. Geophys. Research **55**, 235 (1950).
[2] T. Holstein, Phys. Rev. **72**, 1212 (1947); **83**, 1159 (1951).

Optical Properties of Indium Antimonide

M. TANENBAUM AND H. B. BRIGGS
Bell Telephone Laboratories, Murray Hill, New Jersey
(Received July 28, 1953)

RECENT investigators have reported rather divergent values for the forbidden energy gap ΔE in the semiconducting compound indium antimonide InSb. Welker[1] has quoted a value of 0.53 ev and Breckenridge, Hosler, and Oshinsky[2] have reported an activation energy for intrinsic conduction of *ca* 0.4 ev. Both of these values were obtained from measurements of the conductivity as a function of temperature T. They contain the assumptions that the effective masses of electrons and holes are unity, that the carrier mobilities vary as $T^{-\frac{3}{2}}$, and that ΔE is independent of temperature over the investigated temperature range.

The analysis of infrared transmission spectra permits an independent determination of an upper limit for ΔE. However, when we turned to infrared transmission to determine ΔE, we encountered a rather anomalous behavior.

The preparation of indium antimonide and the growth of single crystals have been described earlier.[3,4] Our first samples were prepared from commercial grade 99.8 percent antimony and 99.95 percent indium. This polycrystalline material was stoichiometric to within two parts per thousand and its resistivity was about 10^{-4} ohm cm. The transmission spectrum of a 0.010-inch slice is shown by curve A of Fig. 1. It is characterized by a long-wavelength

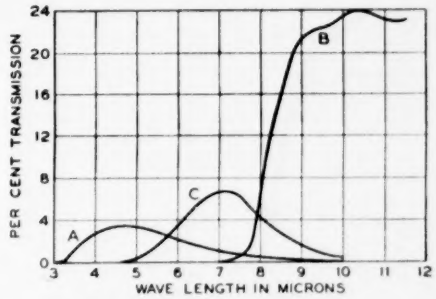

FIG. 1. Infrared transmission of InSb.

limit of absorption near 3.2 microns. This would correspond to an optical gap of 0.39 ev.

In order to increase the resistivity of the compound, it was necessary to refine both the antimony and the compound itself. Zone refining techniques[5] were employed, and material was obtained with a resistivity of about 7×10^{-3} ohm cm. This appears to be the intrinsic resistivity of InSb at room temperature. The transmission spectrum of a typical 0.007-inch slice of a single crystal of this material is shown by curve B in Fig. 1. The long-wavelength limit of absorption now lies at 7.0 microns, corresponding to an optical gap of 0.18 ev. Refining has moved the limit of absorption out 3.8 microns or 0.21 ev.

X-ray diffraction studies have revealed no readily apparent differences in the crystal structure of the two materials characterized by curves *A* and *B*. Similarly, annealing below the melting point does not affect the position of the limit of absorption. It would therefore seem that the transmission between 3.2 and 7.0 microns is caused by some impurity which is removed by zone refining. Although this proposal is somewhat unusual, there is other evidence to support it. Material, whose transmission is at first of the type in curve *A*, can be converted to material similar to *B* by sufficient zone refining. In addition, by sampling the material between zone refining cycles, the long-wavelength limit of absorption was observed to progress from 3.2 to 7.0 microns. Curve *C* is the transmission curve of a 0.007-inch slice of such a partially refined sample. Its resistivity was 2.5×10^{-1} ohm cm. Similarly, if a heavily refined bar is examined along its length, it is observed that the limit of absorption moves to shorter wavelengths as one proceeds from the pure to the impure end of the bar. Thus, it appears that the intrinsic limit of absorption lies at 7.0 microns, and the anomalous transmission from 3.2 to 7.0 microns is caused by an impurity with distribution coefficient less than unity.

Selective doping should reveal the nature of the impurity responsible for this behavior, and experiments have been performed in which material with an intrinsic limit of absorption at 7.0 microns is doped with lead, nickel, arsenic, excess indium, and excess antimony. These five agents were chosen since chemical analysis has shown them to be the most abundant impurities in the 3.2-micron material. Doping with up to 0.05 percent lead, arsenic, indium, or antimony produced no observable shift in the long-wavelength limit of absorption. However, an equal amount of nickel caused a shift of about one micron. By adding 0.1 percent of nickel, the long-wavelength limit has been moved to 5 microns. Thus it seems that nickel is at least partially responsible for the anomalous transmission between 3 and 7 microns.

If a single crystal of InSb with a long-wavelength limit of absorption at 7.0 microns at room temperature is cooled to 77°K, the long-wavelength limit shifts to 4.5 microns corresponding to an optical gap of 0.28 ev. Assuming that the change in energy gap is essentially linear over this temperature range, this corresponds to a temperature coefficient for the energy gap of -4×10^{-4} ev/degree K. This coefficient is in excellent agreement with the electrical properties of InSb if the effective mass of the charge carriers is assumed to be 0.083.[4]

We wish to thank R. F. C. Cummings who assisted with the experimental measurements.

[1] H. Welker, Z. Naturforsch. **7a**, 744 (1952); **8a**, 248 (1953).
[2] Breckenridge, Hosler, and Oshinsky, Phys. Rev. **91**, 243 (1953).
[3] G. L. Pearson and M. Tanenbaum, Phys. Rev. **90**, 153 (1953).
[4] M. Tanenbaum and J. P. Maita, Phys. Rev. **91**, 1009 (1953).
[5] W. G. Pfann, Trans. Am. Inst. Mining Met. Engrs. **194**, 747 (1952)

Magnetic Self-Focusing of Auroral Protons

W. H. Bennett and E. O. Hulburt
Naval Research Laboratory, Washington, D. C.
(Received July 30, 1953)

THE recent beautiful experiments of Meinel[1] on spectra of the aurora show that protons are entering the upper atmosphere at the commencement of an auroral display. From the Doppler spreading to the violet which he observed in H_α, Meinel concluded that the primary protons enter auroral zones with velocities probably greater than 3×10^9 cm sec^{-1}. These speeds are in accord with the original Birkland-Störmer[2] theory of a charged stream of solar particles bent into auroral zones by the earth's magnetic field. The observations therefore throw doubt on criticisms[3] of the theory which argued that such charged streams could not exist as streams because of spreading due to the electrostatic repulsion of the charges.

It is the purpose here to bring to attention an effect which has not been considered in auroral stream theories, namely, the magnetic self-focusing action of ionized streams which was worked out in some detail in 1934.[4] Calculations of this focusing action show that a stream of protons and electrons ejected from the sun in a wide angle cone will rapidly focus itself into a stream having a diameter of the same order as the diameter of an auroral display. Such a stream will be bent into the auroral zones in agreement with the calculations of Störmer. The amount of focusing into the stream depends on the rate of emission of the particles from the sun and on the density of the ionization (which we assume to be electrostatically neutral) in the region between the sun and the earth. Quantitative estimates appear reasonable and will be published. The bearing of the focusing action on corpuscular theories of magnetic storms is being considered.

[1] A. B. Meinel, Astrophys. J. **113**, 50–4 (1951).
[2] C. Störmer, Videnskapsselskapets Skrifter. I. Mat-naturv. Kl., Kristiania, Nos. 1, 10, 14 (1913).
[3] F. A. Lindeman, Phil. Mag. **38**, 669 (1919); S. Chapman and V. C. A. Ferraro, Terr. Mag. **36**, 77 (1931).
[4] W. H. Bennett, Phys. Rev. **45**, 890 (1934).

Anisotropic Resistivities of Selenium Crystals at High Frequencies

H. W. Henkels and J. Maczuk
Moore School of Electrical Engineering, University of Pennsylvania, Philadelphia, Pennsylvania
(Received June 22, 1953)

THE electrical properties of liquid and hexagonal selenium have been presented in four reports.[1–4] The temperature dependence of the resistivity of the crystals grown in a melt[2] was measured at 200 Mc/sec with the same care as described in that report to avoid contributions of end contact resistance and capacitative shunting of the specimens (Boella or Howe effects). The dark resistivities of representative crystals in a rough vacuum are compared with simultaneous dc values in Fig. 1. The dc curves

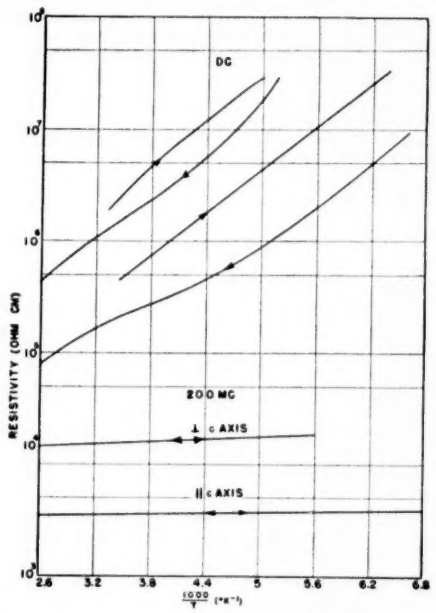

FIG. 1. Anisotropic resistivities of selenium crystals at high temperatures.

behave as previously described.[2] There was, however, no hysteresis in the ac measurements. Data for a number of crystals are presented in Table I. The ratio 3.5 of the average value of $\rho\perp c$

to the average value of $\rho\|c$ agrees well with the measurements on one crystal (crystal 22) for which $\rho\perp c/\rho\|c$ is 4, as also obtained in dc measurements. Temperature coefficients (i.e., φ in $\rho=\rho_0 e^{q\varphi/kT}$, where q=electronic charge) are given in the last column of the table. The best values are considered to be those for crystal 22 which were constant from a temperature of 147°K to 435°K. Some crystals were heated to the melting point with no changes in the coefficients. The data of Schaller[5] from measurements of crystals condensed from the vapor are given in the lower portion of the table. The kink that occurs at room temperature has been noted and studied in a distinct type of microcrystalline specimen.[6] None of the crystals we studied exhibited this behavior, so it is attributed to defects in the crystals deposited from the vapor.

The anisotropy ratio of some crystals deposited from the vapor have been reported to be of the order of ten. (Lower values of the order noted above have been personally communicated to the author.) From photomicrographic examinations we expect that crystals deposited from the vapor are less perfect. Moreover, the kink observed by Schaller indicated additional defects[6] not found in our crystals. It seems natural to expect larger differences in properties perpendicular to the c axis since the lattice constant in this direction is the one sensitive to structural changes.

TABLE I. Room temperature resistivities and temperature coefficients (i.e., φ in $\rho=\rho_0 e^{q\varphi/kT}$, where q=electronic charge) for conduction perpendicular and parallel to the c axis.

Crystal No.	$\rho\|c$ axis (ohm-cm)	$\rho\perp c$ axis (ohm-cm)	φ (ev)
4	···	$1.2-2.1\times10^{4}$	0.018
6	5.4×10^{3}	···	0.007
8	$4.1-5.7\times10^{3}$	···	0.009
20	5.0×10^{3}	···	···
22	$3.6-3.9\times10^{3}$	1.5×10^{4}	0.0045 (|c) 0.0066 ($\perp c$)
27	···	1.9×10^{4}	···
Average	4.8×10^{3}	1.7×10^{4}	
Schaller[5]	$1\sim1\times10^{4}$	···	0.005 under 300°K 0.21 over 300°K
	$2\sim1\times10^{4}$	···	0.038 under 300°K 0.18 over 300°K

The value of 3.5 or 4 for the anisotropy ratio justifies the use of the relations for thermoelectric power in isotropic materials in determining the order of the carrier densities. This use, in conjunction with the development of a general model to explain the dc properties of crystals and the behaviors of microcrystalline specimens, is made in reference 6. This value is smaller than might be expected for the chain-like structure of hexagonal selenium and indicates considerable cross coupling between chains.

Using then the average values of acceptor densities found in selenium crystals and the exhausted condition of these acceptors indicated by the data in the table, an upper limit on the extrinsic activation energy for holes is 0.15 ev. Measurements will shortly be extended to lower temperatures.

The theoretically small dependence of mobility on temperature cannot be distinguished within the precision of the measurement of thermoelectric power and in view of possible residual effects of internal barriers even at 200 Mc/sec. At 50°C the mobility parallel to the c axis is 5–17 cm²/volt sec ($n=1$–3×10^{14}/cm³); at 180°C this mobility is 33 cm²/volt sec, the temperature dependence reflecting the behavior of the thermoelectric power. Since the material does not become intrinsic below the melting point, an upper limit of effective mass can be determined.

[1] H. W. Henkels, J. Appl. Phys. **21**, 725 (1950).
[2] H. W. Henkels, J. Appl. Phys. **22**, 916 (1951).
[3] H. W. Henkels, J. Appl. Phys. **22**, 1265 (1951).
[4] H. W. Henkels and J. Maczuk, J. Appl. Phys. **24**, 1056 (1953).
[5] H. Schaller, Ph.D. dissertation Prague, 1944 (unpublished).
[6] H. W. Henkels and J. Maczuk, J. Appl. Phys. (to be published).

Some Predicted Effects of Temperature Gradients on Diffusion in Crystals

W. SHOCKLEY
Bell Telephone Laboratories, Inc., Murray Hill, New Jersey
(Received July 14, 1953)

SINCE the discovery of the Kirkendall effect,[1] it has been appreciated that the mass transport associated with diffusion caused by interstitial atoms or by vacancies may be used to distinguish experimentally between these mechanisms on one hand and interchange mechanisms on the other. The analysis of the Kirkendall effect does not, however, permit distinguishing experimentally between vacancies and interstitials.[2]

Various experiments have been proposed which in principle can distinguish between vacancies and interstitials. In general, these involve quenching a specimen so that a high density of defects may be trapped at a lower temperature. The effects of this high density have, in general, been below the range of detection.

In this communication, it is proposed that observable effects can be produced by dealing with specimens with temperature gradients. If the density ρ_d of defects has the value $\rho_d(T)$ characteristic of the local temperature $T(x, y, z)$, then the temperature gradient will give rise to a corresponding defect gradient. A diffusion current of defects will exist under steady-state conditions. This current will produce mass transport through the lattice towards high temperature for vacancies and towards low temperature for interstitials.

Figure 1 illustrates one example of an effect to be expected for vacancy diffusion currents. A specimen containing a tilt type grain boundary is made in the form of a wire and heated by passing current through it lengthwise. Vacancies generated at edge dislocations then diffuse from the hotter center to the cooler outside with the resultant motion of dislocations shown in (a). This results in the non-uniform distribution of dislocations shown in (b) which is equivalent to (a) plus (c). The stress distribution due to (c) places the center of the specimen under a compressive stress τ_2 and the outside under tensile stress τ_1. These stresses tend to reduce the vacancy density near the center and increase it near the outside. To a first approximation, the steady state will be reached when the vacancy density is uniform along the grain boundary, and this leads to

$$\tau_2-\tau_1\doteq(E/v)\Delta T/T,$$

where E is the activation energy of forming a vacancy, v the atomic volume, and ΔT and T the difference and average value of the temperature, respectively. From this, one concludes that strains of the order of 10^{-3} might readily be produced. In addition to observing the strains, it may be possible to observe dislocation displacements in the grain boundary for small angle grain boundaries.[3]

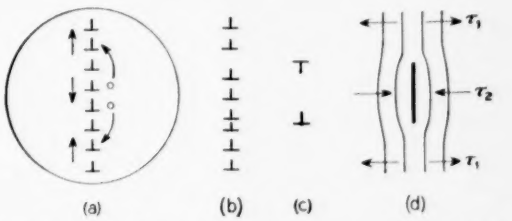

FIG. 1. Predicted effect of temperature gradient provoked diffusion of vacancies upon a grain boundary.

Figure 2 illustrates a modification of the Kirkendall effect in which the temperature gradient of Fig. 1 replaces the concentration gradient as a driving force for defects. Motion (b) of the markers should be produced by interstitial atoms and (c) by vacancies. Combined with data on self diffusion, the effect of

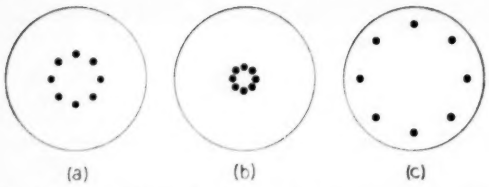

FIG. 2. Predicted effect of a radial temperature gradient upon markers. (a) Initial condition; (b) effect produced by interstitial diffusion; (c) effect produced by vacancy diffusion.

Fig. 2 should make possible a determination of both vacancy density and jump frequency in a pure metal.

Figure 3 represents a predicted effect for a plate, (b) corresponding to interstitials and (c) to vacancies.

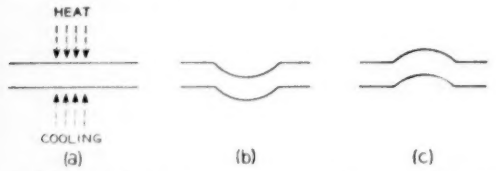

FIG. 3. Predicted effect of a linear temperature gradient (a), for interstitial diffusion (b), and vacancy diffusion (c).

It should be noted that stress gradients due to differential thermal expansion accompany temperature gradients. Effect (b) of Fig. 3 could arise after cooling from this cause. However, the defect flows continue in time and should thus be separable from the thermal expansion effects. This conclusion is particularly clear for Fig. 2.

[1] A. D. Smigelkas and E. O. Kirkendall, Trans. Am. Inst. Mining Met Engrs. **171**, 130 (1947).
[2] F. Seitz, Acta Metallurgica **1**, 355 (1953), particularly Sec. II references.
[3] Vogel, Pfann, Corey, and Thomas, Phys. Rev. **90**, 489 (1953).

Radiation Damage and Rate Processes

J. W. MARX
Department of Mining and Metallurgical Engineering, University of Illinois, Urbana, Illinois
(Received July 22, 1953)

IN several recent investigations,[1-3] electrical resistance changes have been employed as a measure of the damage incurred in the low-temperature cyclotron irradiation of pure metals, and a resistivity index has been used to follow the kinetics of the resulting thermal recovery processes. In the interpretation[4] of this data the lattice defects were considered to be overwhelmingly of the Frenkel type, i.e., interstitial-vacancy, or $i-v$, pairs.[5]

Pulse-annealing studies showed that the low-temperature (below $-150°$C) thermal recovery processes were characterized by activation energies as small as 0.2 ev in Cu, Ag, and Au.[2,3] A later investigation also resulted in a minimum estimate of 0.2 ev for the low-temperature recovery in Cu.[3] The very excellent isothermal annealing data obtained during this latter study showed that the low-temperature recovery processes were not uniquely resolved, indicating that the recombination of $i-v$ pairs in various states of predissociation[6] might provide a reasonable recovery mechanism in this region, an alternative suggested by previous investigators.[2] At about $-40°$C a reasonably unique 0.68-ev process was observed to emerge from the unresolved background. This process was ascribed[3] to the migration of vacancies, although there seems to be no convincing discrimination against interstitial motion in the data themselves.[7]

It is important to note that the low-temperature reactions should be first-order reactions if the reacting entity is presumed to be the predissociated pair. When the excess concentration of predissociated pairs was exhausted, the annihilations would be governed by the random migration of the individual i or v defects, and the process should then revert to a second-order reaction.

Using the recoverable resistivity increment r as a reaction index, for an idealized second-order reaction one would expect to find that $dr/dt=Mr^2$, where M is an isothermal constant. When this criterion was applied to the 0.68-ev process, it was observed that $dr/dt=Mr^{2.5}$. Stipulating that the apparent higher order could not be the result of residual low-temperature processes, that author[3] rationalized the discrepancy in terms of elastic strain considerations.

The present writer would like to point out that the data may not actually require such interpretation. The preceding work,[3] and some other studies of solid state reactions, involves the tacit assumption that the N_j reactants are homogeneously distributed through the specimen volume V_0. While the resistivity increment may be a fair measure of the *gross* defect concentration $C_j=N_j/V_0$, it provides little information concerning the *microscopic* concentration $c_j=dN_j/dV$. Yet it is precisely this microscopic concentration that determines the velocity of any unique process of the second, or higher, order in inhomogeneous mixtures.

The distinction between homogeneous and inhomogeneous mixtures is best illustrated by considering two idealized second-order cases. Assume that the thermodynamic potential barrier ΔG is not a function of the c_j, so that the factor $\exp(-\Delta G/RT)$ may be included in an isothermal proportionality constant K. In the first case, N interstitials and N vacancies are uniformly distributed through a specimen of macroscopic volume V_0 at a given instant t_0, so that $c_i=c_v=C_0$. The resistivity increment r then decays at a rate

$$(dr/dt)_t=K\int^{V_0} c_i c_v dV=KC_0^2V_0=Mr^2. \quad (1)$$

In the second case, the same N defects are thoroughly mixed and then concentrated within n microscopic, nonoverlapping subvolumes V_m contained within the original macroscopic volume V_0. For simplicity, the microscopic concentration has the constant value $c_i=c_v=c_m$ inside each subvolume. Since the gross defect concentration has not been changed, the resistivity increment will be the same for both cases, i.e., $r'=r$ at $t=t_0$. The decay rate for this case is

$$(dr'/dt)_{t_0}=Kn\int^{V_m} c_i c_v dV=Knc_m^2V_m=(c_m/C_0)t_0Mr^2. \quad (2)$$

The reaction rate is thus not uniquely determined for a given resistivity, but may be arbitrarily accelerated by localized concentration of the reactants.

If case (2) is superimposed on case (1), so that two different, nonzero concentrations exist within the same sample, an elementary extension of the preceding analysis shows that the order of the reaction will appear fictitiously high for the latter inhomogeneous case, an artefact resulting logically from the inhomogeneity itself. In general, whenever two or more reactants are mixed and the mixture distributed in *varying* concentrations throughout the specimen volume, the apparent order of even a rigorously unique reaction will appear higher the greater the inhomogeneity.

Idealized though it is, the simple model chosen for the inhomogeneous example affords a rough picture of a nucleon-damaged metal for small flux densities. For larger fluxes, the subvolumes V_m, which correspond to microscopic damage spots localized about each primary interstitial atom ejection[4,5] could be expected to overlap. After the excess of predissociated pairs has been annihilated, either by microcataclysms triggered by the passage of a nucleon through an existing damage spot, or by low-temperature thermal recovery, some individual defects remain. There is no reason to believe that these would be distributed in microscopic uniformity for the fluxes under discussion, although a uniform distribution might be approached at very large flux densities. Similarly, the reactants involved in plastic deformation damage recovery could also be expected to exist in localized concentrations.

Therefore, it seems possible that the elastic strain calculation previously invoked[3] to explain the relation $dr/dt = Mr^{2.5}$ may be, at least in part, a gratuitous complication. In any case, the effect due to lowering of the energy barriers by elastic strains would simply aggravate that which would normally be expected from the inhomogeneity itself. For if ΔG is a diminishing function of c, the factor $\exp(-\Delta G/RT)$ must be inserted into the integrand of Eq. (1) or its counterpart, and this would have the effect of heavily weighting the inhomogeneity contribution.

For illustrative purposes nucleon damage and recovery have been considered here solely in terms of the formation and annihilation of $i-v$ pairs. The existence of residual defects that persist at high temperatures shows that this model can be only partly correct. Either other defects are produced along with the $i-v$ pairs during irradiation, or the coalescence of vacancies and/or interstitials competes with the annihilation process to produce stable aggregates.

The writer would like to extend thanks to Professor J. S. Koehler for detailed information concerning particle ranges, and to Dr. C. E. Dixon for the privilege of seeing the manuscript previously referred to,[7] prior to its publication. This critique was incidental to the work sponsored by the U. S. Atomic Energy Commission.

[1] Martin, Austerman, Eggleston, McGee, and Tarpinian, Phys. Rev. **81**, 664 (1951).
[2] Marx, Cooper, and Henderson, Phys. Rev. **88**, 106 (1952).
[3] A. W. Overhauser, Phys. Rev. **90**, 393 (1953).
[4] J. S. Koehler, AEC Progress Report, Feb. 1, 1952 (unpublished).
[5] F. Seitz, Phil. Mag. **43**, Suppl. No. 1, 60 (1952).
[6] J. Frenkel, *Kinetic Theory of Liquids* (Oxford University Press, London, 1947).
[7] Brinkman, Dixon, and Meecham (to be published).

Antiparallel Dipole Arrangement in Tungsten Trioxide

RYUZO UEDA AND JINZO KOBAYASHI
Department of Applied Physics, Waseda University, Tokyo, Japan
(Received July 20, 1953)

ALTHOUGH tungsten trioxide WO_3 is reported to have ferroelectric or antiferroelectric properties,[1] no definite structural mechanism has been proposed to account for this behavior. The detailed crystal structure analysis of WO_3 has been carried out from a study of its Patterson function. The structure given by Braekken[2] is shown to be incorrect in dipole arrangement.

The single crystal used (0.1×0.2×0.01 mm) is composed of two domains, twinned on the (110) plane.[3] Each domain contains a number of repeated twins (180° domains) of submicroscopic dimensions. We have successfully completed the structure determination at room temperature by using only reflections from a similar kind of twin component. The unit cell is monoclinic with the lattice constants: $a=7.274\pm0.002$A, $b=7.501\pm0.001$A, $c=3.824\pm0.003$A, and $\beta=89°56'$. The space group is $P\,2_1/a$, and $Z=4$. The atomic coordinates and interatomic W−O distances are as follows:

W:	$\frac{1}{4}+x$, $\frac{1}{4}+y$, z.	$x=0.006$, $y=-0.021$, $z=0.053$.
O_I:	$\frac{1}{4}$, y, 0.	$y=0.03$.
O_{II}:	0, $\frac{1}{4}$, 0.	
O_{III}:	$\frac{1}{4}$, $\frac{1}{4}+y$, $\frac{1}{4}$.	$y=0.03$,

and

$$W-O_I=1.87\text{A}, \quad W-O_{III}\ (\text{above})=1.71\text{A},$$
$$W-O_{II}=1.83\text{A}, \quad W-O_{III}\ (\text{below})=2.11\text{A}.$$

The angle $W-O_{II}-W$ differs from 180° by about 12°, which will be important in connection with the dielectric properties of this substance.[4] The sites of the oxygen atoms, which are too light to give considerable contributions to the x-ray reflections, have been derived mainly from spatial considerations.[5]

It is to be stressed from the above results that the dipole arrangement in WO_3 is very similar to that of $NaNbO_3$ which has recently been analyzed by Vousden.[6] In both structures, the dipoles parallel to the x direction are arranged in alternate senses, while the ones perpendicular to it are put in the same sense (Fig. 1). The dipoles in Braekken's structure, however, are arranged alternately in both directions. The dipole orientations obtained above will also give WO_3 antiferroelectric properties, similar to those of $NaNbO_3$.

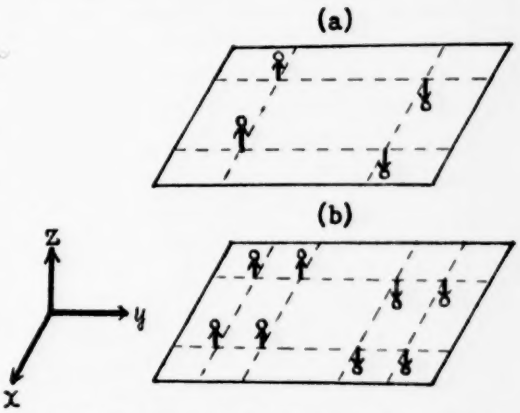

FIG. 1. The dipole arrangement in WO_3 and $NaNbO_3$. The arrows show the directions of displacement of the metal ions. (a) WO_3 (present work), (b) $NaNbO_3$ (Vousden). The axes are referred to the original perovskite structure.

A detailed description of the work will be published elsewhere shortly.

[1] B. T. Matthias, Phys. Rev. **76**, 430 (1949); C. Kittel, Phys. Rev. **82**, 729 (1951).
[2] H. Braekken, Z. Krist. **78**, 484 (1931).
[3] R. Ueda and T. Ichinokawa, Phys. Rev. **80**, 1106 (1950).
[4] H. D. Megaw, Acta Cryst. **5**, 739 (1952).
[5] A. Magnéli, Acta Cryst. **4**, 447 (1951).
[6] P. Vousden, Acta Cryst. **4**, 545 (1951).

Microwave Observation of the Collision Frequency of Holes in Germanium

T. S. BENEDICT
Bell Telephone Laboratories, Murray Hill, New Jersey
(Received July 7, 1953)

IT has been shown in a previous letter[1] that the inertial effects of the electrons in n-type germanium may be studied through a microwave measurement of the dielectric constant as a function of temperature. The working equations[2] for the dielectric constant and conductivity, based on a free carrier model with relaxation time independent of energy, derived in reference 1 are

$$\kappa=\kappa_0-\frac{Ne^2\tau^2}{\epsilon_0 m^*[1+(\omega\tau)^2]} \tag{1}$$

and

$$\sigma=\frac{Ne^2\tau}{m^*[1+(\omega\tau)^2]}, \tag{2}$$

where κ_0 is the dielectric constant associated with carrier free germanium, N is the number of carriers per unit volume, m^* is the effective mass, τ is the relaxation time, and ω the microwave angular frequency.

Measurements of the dielectric constant and conductivity have now been made in p-type germanium in order to determine m^* and τ for the holes.

The samples were prepared by doping intrinsic germanium with sufficient gallium to make the carrier contribution to the dielectric constant appreciable. Measurements were made of the attenuation and phase shift due to transverse slabs 0.016 and 0.032 in. thick

with 1.24 cm microwaves. The results for the hole contribution to the dielectric constant $\Delta\kappa$ are given in Fig. 1. The value used for κ_0 was 16.[1] The solid curves are the theoretical curves based on Eq. (1) plotted for various values of m^*.

Some recent calculations[2] of Herring of the hole contribution to the dielectric constant assume a Maxwellian distribution

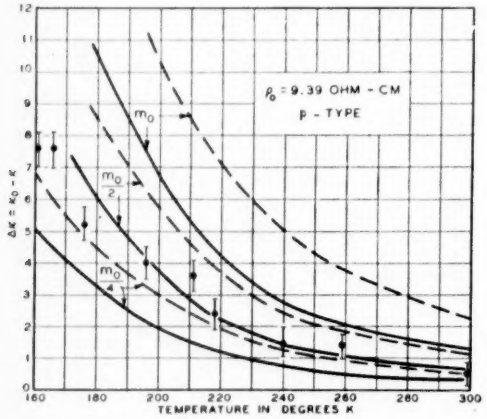

FIG. 1. Plot of $\Delta\kappa = \kappa_0 - \kappa$ *vs* absolute temperature for germanium ($\rho_0 = 9.39$ ohm-cm).

of velocities for the holes, an energy dependent relaxation time, and energy surfaces of the type suggested by Herman and Callaway,[4,5] and by Shockley.[6] These calculations give for $\omega\tau < 1$ the following simple formula:

$$\kappa = \kappa_0 - \frac{Ne^2}{m^*\epsilon_0} \Big/ \left[\left(\frac{e}{m^*}\right)^2 \frac{1}{\mu_0\mu_H} + \omega^2\right].$$

It is seen that this formula is essentially the same as that used in the previous work[1] for electrons except that the square of the drift mobility has been replaced by the product of the drift mobility (μ_0) and Hall mobility (μ_H). This change if applied to electrons makes very little difference in the effective mass since $\mu_H/\mu_0 \cong 1.03$; however, for holes[7] the value of μ_H/μ_0 varies from 1.30 to 1.70 giving a large variation from the energy independent τ theory. The dashed curves shown in Fig. 1 are those predicted by Herring's

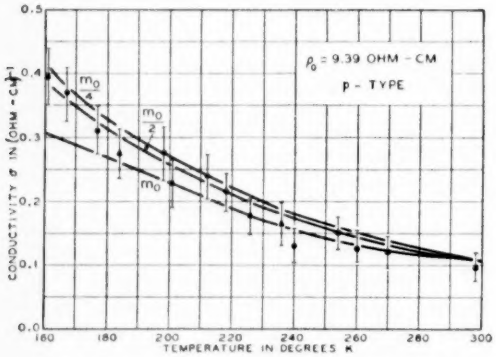

FIG. 2. Plot of σ *vs* absolute temperature for germanium ($\rho_0 = 9.39$ ohm-cm).

theory and it is seen that a good fit to the theory can be obtained by setting m^* equal to about $(0.30 \pm 0.13)m_0$.

The conductivity data are shown in Fig. 2. It is seen that they also are consistent with the theoretical curves based on Eq. (2), further indicating that the free carrier model is adequate in the present case. The conductivity data are consistent with the mass deduced from the dielectric measurements but are not in themselves good enough to yield an effective mass.

The measurements were carried out for samples whose room temperature resistivities varied from 5 ohm-cm to 15 ohm-cm and the measurements are consistent with the effective mass given above independent of resistivity and temperature over the regions described. The relaxation time based on Eqs. (1) and (2) is then given by $\tau = 3.6 \times 10^{-7} T^{-2.3}$ sec.

The author wishes to thank W. Shockley for many helpful discussions concerning this work, M. B. Prince for furnishing the drift mobility data required in calculating the theoretical curves, and Herring for allowing the author to use his results in the analysis of the data priort o publication.

[1] T. S. Benedict and W. Shockley, Phys. Rev. **89**, 1152 (1953).
[2] Equations (1) and (2) are written in mks units.
[3] C. Herring (to be published).
[4] F. Herman and J. Callaway, Phys. Rev. **89**, 518 (1953).
[5] F. Herman, Phys. Rev. **88**, 1210 (1952).
[6] W. Shockley, Phys. Rev. **90**, 491 (1953).
[7] F. J. Morin and J. P. Maita (to be published).

Electrical Conductivity of Mechanically Disturbed Germanium Surfaces

EDWARD N. CLARKE AND ROBERT L. HOPKINS
Sylvania Electric Products, Bayside, New York
(Received July 20, 1953)

THE mechanically disturbed germanium surface has been of interest in the study of surface electron-hole recombination,[1] in the study of contact potentials,[2] and in the study of rectification and thermoelectric effects.[3,4]

If the germanium surface is mechanically disturbed as by grinding, polishing, or sandblasting, we have, in effect, a surface

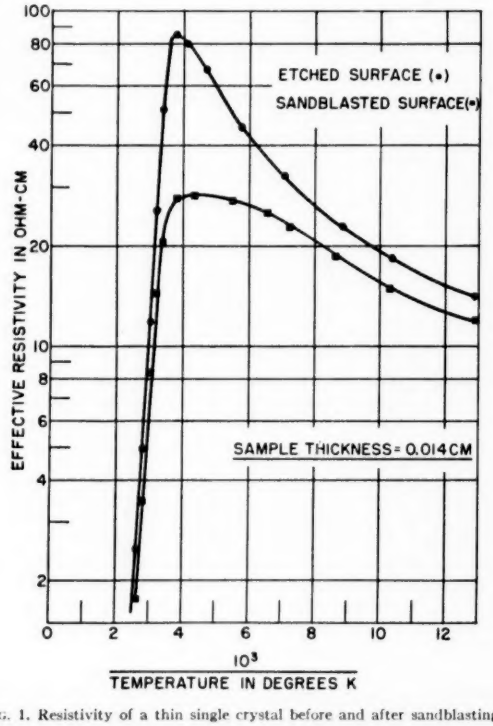

FIG. 1. Resistivity of a thin single crystal before and after sandblasting.

layer in parallel with the bulk crystal. A comparison of resistance before and after surface treatment will allow determination of the surface layer resistance. The change in going from one surface to the other is amplified by using a thin crystal. By effective resistivity we shall mean that of the composite crystal, surface plus volume. Figure 1 shows a plot of effective resistivity of a thin (0.014-cm) germanium single crystal over the temperature range 78°K to 385°K, for the crystal with surfaces etched (upper curve) and with one surface sandblasted (lower curve). It is seen that sandblasting produces a surface layer of relatively high conductivity. It is to be noted that even at the highest temperature, the resistivity with a sandblasted surface is lower than that with an etched surface, implying that there exists a large concentration of extrinsic carriers in the surface layer.

The surface layer thickness is determined by etching the surface slowly with a calibrated etchant and watching the effective resistivity return to its original etched surface value. The thickness of this particular disturbed layer is about 0.7×10^{-4} cm. With this thickness, the average disturbed surface layer resistivity can be calculated. Its variation with temperature is shown in Fig. 2.

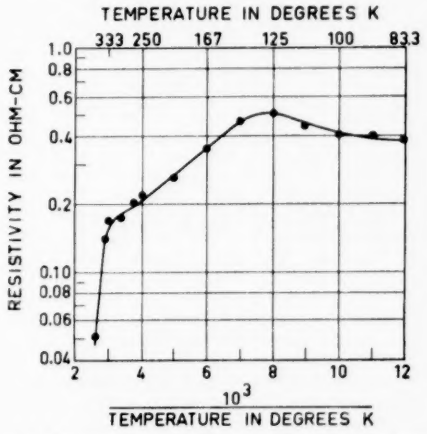

FIG. 2. Resistivity of the mechanically disturbed surface layer.

There are three distinct regions. In the range 345°K to 385°K the slope corresponds to an activation energy of 0.4 ev, and in the range 143°K to 300°K, to 0.022 ev. From 83°K to 125°K there is a small negative slope. The value 0.4 ev must be considered a preliminary one because it is based upon only two temperatures for each surface and is thus only roughly reproducible with a given sandblasting procedure. The value 0.022 ev does appear to be fairly reproducible with a given sandblasting procedure.

Thermoelectric measurements with a hot point probe[2] indicate that the mechanically disturbed surface layer is p type, at least in the region near room temperature. Thus, it is tentatively assumed that the activation energies 0.4 and 0.022 ev represent two acceptor levels (although the levels are probably at higher positions than indicated by these values). It is further suggested that the high-lying level represents the centers responsible for the high rate of recombination of electrons and holes at these surfaces. A surface energy level model proposed by Bardeen and Brattain[2] is being examined in the light of the present measurements. The effective Hall coefficient of these thin single crystals is decreased by as much as a factor of eight when one surface is sandblasted. The data are being analyzed in order to determine the Hall coefficient of the disturbed layer.

Other methods for disturbing the germanium surface, including polishing with rouge and water on felt show similar effects, although the absolute value of surface resistance depends upon the details of the method.

The disturbed surface can be annealed by heating at high temperatures, and Fig. 3 shows the surface layer resistivity of a different sample increasing with annealing time at 488°C in helium. (A surface layer thickness of 10^{-4} cm is assumed.) The experimental accuracy is such that it can be said only that the surface layer resistivity returns to some value greater than 10 ohm-cm after 21 minutes. The curve is particularly interesting in

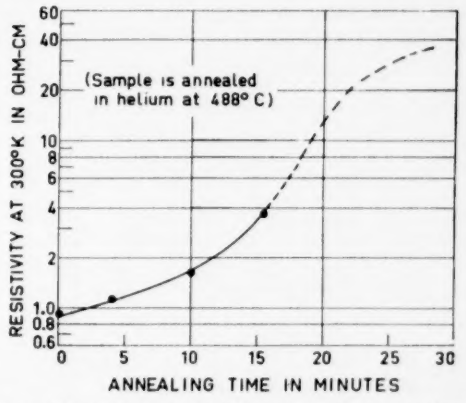

FIG. 3. Resistivity of the mechanically disturbed surface layer as a function of annealing time.

that it shows a faster annealing rate becoming operative only after annealing has proceeded for ten minutes. We are reminded of the plastic deformation of germanium[5,6] which requires an "incubation time" before the external stress becomes effective. However, other effects such as the reaction of germanium with surface impurities might alter the shape of the annealing curve.

[1] Navon, Bray, and Fan, Proc. Inst. Radio Engrs. **40**, 1342 (1952).
[2] W. H. Brattain and J. Bardeen, Bell System Tech. J. **32**, 1 (1953).
[3] J. W. Granville and C. A. Hogarth, Proc. Phys. Soc. (London) **B64**, 488 (1951).
[4] C. A. Hogarth and J. W. Granville, Proc. Phys. Soc. (London) **B64**, 992 (1951).
[5] C. J. Gallagher, Phys. Rev. **88**, 721 (1952).
[6] F. Seitz, Phys. Rev. **88**, 722 (1952).

The Heat Capacities of Superconducting and Normal Tantalum*

R. D. WORLEY, M. W. ZEMANSKY,† AND H. A. BOORSE‡
Pupin Physics Laboratories, Columbia University, New York, New York
(Received July 30, 1953)

THE heat capacities of tantalum below 5°K were first measured by Keesom and Désirant,[1] and again by Mendelssohn[2] and Désirant[3] in 1941. As part of the program for measuring heat capacities in this laboratory, we have repeated these measurements using the same apparatus and technique described in preliminary reports on niobium[4] and vanadium.[5] Two samples of tantalum were used, the first with a mass of 3.029 moles and density of 16.09 g/cm³ (somewhat below the value given in the *International Critical Tables*), and the second with a mass of 0.5545 mole and density of 16.65 g/cm³. Both samples contained more than 99.9 percent tantalum, less than 0.03 percent iron, and less than 0.03 percent carbon. No estimate of gaseous impurities was given. The samples were annealed by the supplier, the Fansteel Metallurgical Corporation, by heating in high vacuum to a temperature of about 1000°C. Heat capacities were measured in the temperature range 1.8°K to 5.1°K, a total of 295 determinations being made on sample I and 216 on sample II.

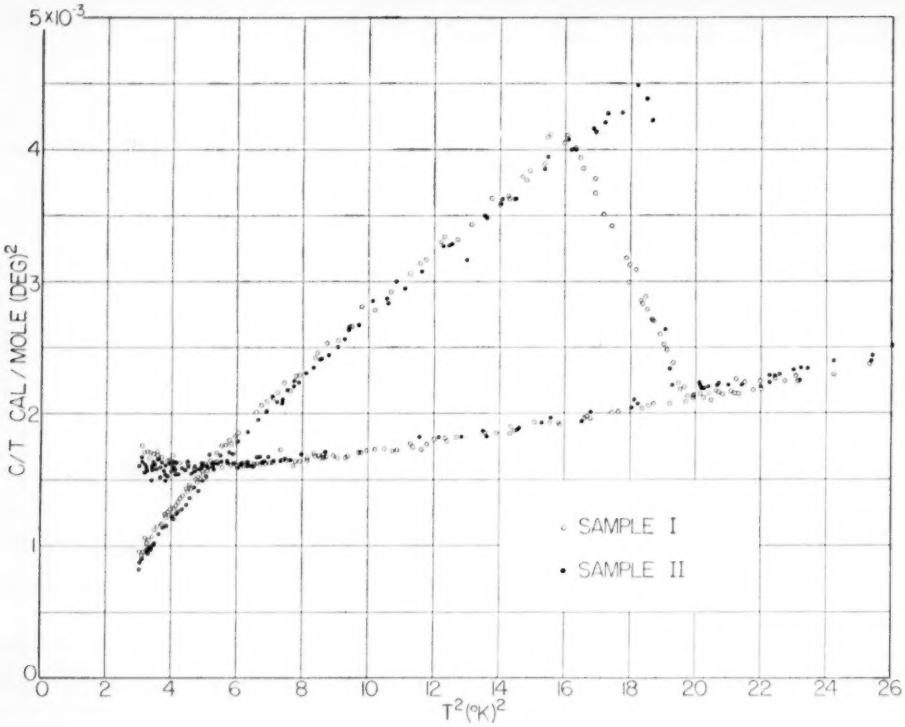

FIG. 1. The heat capacities of superconducting and normal tantalum.

In the absence of a magnetic field, sample I was observed to start the transition from the superconducting to the normal phase at 4.01°K and to complete it at 4.42°K. The width of the transition for sample II was much narrower, extending from 4.36°K to 4.40°K.

To maintain the normal phase at temperatures below the zero-field transition temperature, magnetic fields of from 3000 to 5000 gauss were applied. At these field strengths and at temperatures from 3°K to 5°K, as well as above the transition temperature in zero field, the molar heat capacity was found to vary with the temperature according to the usual relation

$$C_n = \gamma T + (464.4/\Theta^3)T^3. \tag{1}$$

γ and Θ were obtained from a plot of C/T *versus* T^2 by the method of least squares. A tabulation of our results, together with the results of the earlier investigations, is given in Table I.

Below 3°K the heat capacities exceed the values given by Eq. (1), the departure being as much as 20 percent at the lowest temperatures reached. This anomalous behavior was found to be independent of the magnetic field at field strengths above 3000 gauss for sample I and above 1200 gauss for sample II. A similar anomaly has been observed for two samples of vanadium in the same temperature range.

In the superconducting phase the heat capacity of tantalum, like that of niobium and of vanadium, failed to show a simple T^3 dependence on temperature.

Experimental results for both samples are shown in Fig. 1.

The results obtained with sample II were compared with Koppe's[6,7] calculation and with those of Marcus and Maxwell[8] based on the α model by plotting C_s^{el}/C_n^{el} against the reduced temperature T/T_0, where T_0 is the zero-field transition temperature. This plot differs from that used in reference 7 in that the ordinate has been divided by T/T_0. On a plot of this type Koppe's relation is very nearly linear above $T/T_0=0.4$. The ratio C_s^{el}/C_n^{el} was obtained from the experimental results in three ways: (a) by neglecting the departure of C_n from Eq. (1), (b) by assuming that the electronic contribution to C_n is γT and that the anomaly is due to the lattice, and (c) by assuming that the lattice heat capacity is $(464.4/\Theta^3)T^3$ and that the anomaly is due to the normally conducting electrons. None of these three interpretations yielded satisfactory agreement with the theoretical predictions.

A complete account of these experiments and similar experiments on vanadium will be published in *The Physical Review*.

TABLE I. Calorimetric measurements on tantalum.

	Density g/cm³	Purity %	T_0 °K	γ 10^{-4} cal/mole-deg²	Θ °K
This article Sample I	16.69	99.9+	4.01 – 4.42	13.1	225
This article Sample II	16.65	99.9+	4.36 – 4.40	12.1	213
Keesom and Désirant (1941)	16.566	99.9+	3.96 – 4.16	14.1	246.5
Mendelssohn and Désirant (1941)	...	99.95	4.38 ± 0.02	...	...

* Assisted by the U. S. Office of Naval Research and Linde Air Products Company.
† City College of New York, New York, New York.
‡ Barnard College, Columbia University, New York, New York.
[1] W. H. Keesom and M. Désirant, Physica **8**, 273 (1941).
[2] K. Mendelssohn, Nature **148**, 316 (1941).
[3] M. Désirant, *Report of International Conference on Fundamental Particles and Low Temperatures* (Physical Society, London, 1947), Vol. 2, p. 124.
[4] Brown, Zemansky, and Boorse, Phys. Rev. **86**, 134 (1952).
[5] Worley, Zemansky, and Boorse, *Proceedings of the Schenectady Cryogenics Conference*, 128 (1952).
[6] H. Koppe, Ann. Physik **1**, 405 (1947).
[7] Worley, Zemansky, and Boorse, Phys. Rev. **87**, 1142 (1952).
[8] P. M. Marcus and E. Maxwell, National Bureau of Standards Report 2496, 1952 (unpublished).

A Possible Mechanism for $1/f$ Noise Generation in Semiconductor Filaments*

LEON BESS
Lincoln Laboratory, Massachusetts Institute of Technology, Cambridge, Massachusetts
(Received June 17, 1953)

IN describing the mechanism to be proposed here for $1/f$ noise generation in semiconductor filaments, it is first of all assumed that the low-frequency noise is caused by random fluctuations in the number of mobile charges (i.e., holes and electrons). This explains the fact that noise power seems to vary as the square of the current through the semiconductor. The fluctuations of mobile charges are, in turn, assumed to be due to the random creation and annihilation of trapping centers.[1] For reasons that will appear later, it will be assumed that these trapping centers are all on the surface of the material. The physical model which describes this random creation and annihilation process will be as follows. A lattice atom or impurity atom at the surface of the material is knocked out of its equilibrium position (by a source which will not be specified) and starts to diffuse throughout the surface. The motion will then be a sort of Brownian movement about the equilibrium position O. It is assumed that the diffusion must be confined to the surface (i.e., it takes place only over two dimensions). From the theory of Brownian motion the diffusion atom at any time t after its release will on the average be within a circle whose center is at O and whose radius $\bar{r}$ is determined by

$$\bar{r}^2=4D(t+t_0). \tag{1}$$

D is the diffusion constant. The vacancy O is assumed to act as a trapping center for a hole or electron until its diffusing atom or another diffusing atom gets captured in it. At the instant of atom capture the trapped hole or electron is released to become a mobile charge again. Thus, during the time O was unoccupied there was one less mobile charge. With a constant current through the sample, this would have produced a square pulse at the output voltage, whose length is the time O was unoccupied.

It is assumed that the trapping centers are being created randomly at a more or less constant average rate. Their rate of annihilation is dependent upon the intensity of diffusing atoms (and, therefore, the number of trapping centers present); thus, after a while there will be an equilibrium condition where the average density of diffusing atoms and trapping centers will be constant. This is the condition with which we will be concerned here.

The output voltage will then be a sum of randomly occurring square pulses of varying lengths. If the probability of any one pulse width being between s and $s+ds$ is $g(s)ds$, then it can be shown that the correlation function $R(t)$ of the output voltage will be

$$\begin{aligned} R(t)&=K\int_t^\infty (s-t)g(s)ds \\ &=K\int_t^\infty \rho(s)ds, \end{aligned} \tag{2}$$

where

$$\rho(s)\equiv\int_s^\infty g(u)du,$$

and K is the average number of pulses per unit length of time.

The power spectrum $G(\omega)$ for output will then be

$$\begin{aligned} G(\omega)&=K\int_0^\infty\left[\int_t^\infty \rho(s)ds\right]\cos\omega t dt \\ &=(K/\omega)\int_0^\infty \rho(t)\sin\omega t dt. \end{aligned} \tag{3}$$

Now $\rho(t)$ can also be shown to be the probability that an unoccupied trapping center is still unoccupied after a time t, after having been created at $t=0$. $\rho(t)$ is to be determined from the following relation:

$$-(d\rho/dt)=[(\bar{N}\sigma_c\bar{v})+\big((\sigma_c\bar{v})/(\pi\delta\bar{r}^2)\big)]\rho, \tag{4}$$

where σ_c is the capture cross section, $\bar{v}$ is the average velocity of the diffusing atom, δ is the thickness of the surface layer, and $\bar{N}$ is the average density of the diffusing atoms from other vacancies at the position of a given vacancy. Equation (4) expresses the fact that a trapping center can be annihilated in two ways. The first way (given by the second term on the r.h.s. of the equation) is by having its own diffusing atom come back and be recaptured. The second way (denoted by the first term) is by capturing a diffusing atom from another trapping center.

If (1) is substituted in (4) and the boundary condition $\rho(0)=1$ is used, $\rho(t)$ can be obtained specifically and has the form,

$$\rho(t)=[t_0/(t+t_0)]^n\exp(-t/T), \tag{5}$$

where

$$T\equiv(\bar{N}\sigma_c\bar{v})^{-1}, \tag{6a}$$

$$n\equiv(\sigma_c\bar{v})/(4\pi\delta D). \tag{6b}$$

$G(\omega)$ can be obtained by substituting (5) into (3), with the result that

$$\begin{aligned} G(\omega)&=\frac{K\pi t_0{}^nF(n,\theta)}{[\omega^2+(1/T)^2]^{(2-n)/2}} \quad \text{when} \quad \omega<1/t_0, \\ &=1/[\omega^2+(n/t_0)^2] \quad \text{when} \quad \omega>1/t_0, \end{aligned} \tag{7a}$$

where $\theta\equiv\tan^{-1}(\omega T)$ and

$$F(n,\theta)\equiv\frac{\sin(1-n)\theta}{\Gamma(n)[\sin n\pi][\sin\theta]}. \tag{7b}$$

When $1/T<\omega<1/t_0$, (7a) shows that $G(\omega)$ varies as $1/\omega^m$, where $m=2-n$. Thus $G(\omega)$ has the observed $1/\omega$ dependence if $n=1$. Experimental data indicate that m may vary from 0.8 to 1.5, so n can vary from 0.5 to 1.2.

A crude estimate of n will now be made in terms of the physical parameters which are involved. From the theory of diffusion, it can be shown that D and $\bar{v}$ can have the following forms:[2,3]

$$D=\tfrac{1}{2}\bar{f}a^2, \tag{8a}$$

$$\bar{v}=\bar{f}a. \tag{8b}$$

In the above equation $\bar{f}$ is the average jump frequency and a is the separation between adjacent potential wells. It should also be noted at this point that $\sigma_c=\delta\lambda_c$, where λ_c is a mean capture length. Thus with the aid of (8a) and (8b), n from (6b) can be brought into the following simple form:

$$n=\lambda_c/(\pi a). \tag{9}$$

If n is to be of the order of unity, λ_c must be of the order of πa ($=10^{-7}$ cm), a value which is not too unreasonable physically.

* The research in this document was supported jointly by the U. S. Army, Navy, and Air Force under contract with the Massachusetts Institute of Technology.

[1] The general picture up to this point is similar to noise models of other investigators. See, for example, G. G. Macfarlane, Proc. Phys. Soc. (London) **B63**, 807 (1950); J. M. Richardson, Bell System Tech. J. **29**, 117 (1950).

[2] See, for example, A. H. Cottrell, *Theoretical Structural Metallurgy* (Longmans Green, New York, 1948), pp. 190–5.

[3] Equation (8a) was derived on the assumption that the jumps can take place in any direction.

Infrared Absorption Induced by Static Electric Fields

M. F. CRAWFORD AND I. R. DAGG
McLennan Laboratory, University of Toronto, Toronto, Canada
(Received July 13, 1953)

CONDON[1] showed theoretically in 1932 that vibrational modes normally infrared inactive could be rendered active by a static electric field. He estimated the magnitude of the effect and concluded that, although the absorption would be small, it should be observable under suitable experimental conditions.

The rotation-vibration spectrum of hydrogen induced by a static electric field has been observed and initial results are reported in this letter.

The absorption cell was that used in the investigation of pressure-induced absorption.[2] The light guide also served as a parallel

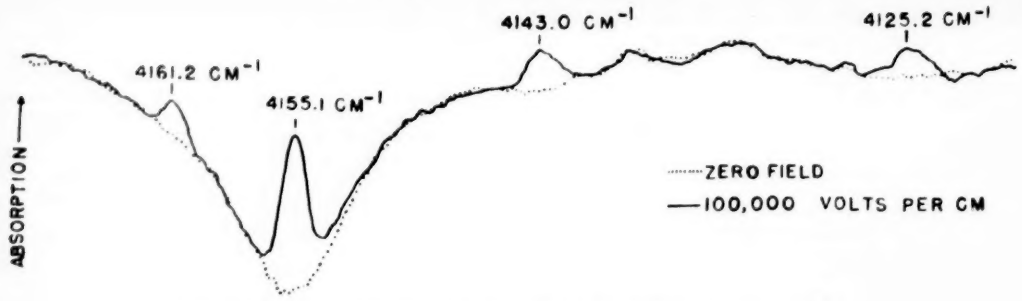

FIG. 1. Field induced components of the Q branch of the 1←0 vibrational transition of H_2.

plate condenser. The two side walls were polished strips of aluminum 85 cm long by 1.75 cm wide; the top and bottom were strips of Plexiglass which separated the metal walls by 1.4 mm. One plate of this condenser was connected to an insulated terminal in the wall of the absorption cell. The other plate was in electrical contact with the wall. Hydrogen pressures up to 2000 lb per square inch were used. The absorption was measured with a Littrow type grating spectrometer using a PbS photoconductive cell as a detector.

The absorption induced by the static electric field is observed superimposed on the pressure-induced absorption,[3] but the two effects are readily distinguished from each other because their half-widths are radically different. The dotted curve of Fig. 1 shows a contour of a portion of the Q branch of the pressure-induced absorption of hydrogen. The sharp maximum of transmission at 4155 cm^{-1} arises from the splitting of the Q branch. The continuous curve of Fig. 1 shows the contour obtained when the potential difference between the plates of the light guide was 14 000 volts, other conditions remaining the same. It is apparent that the application of the electric field has produced four sharp absorption lines. These are components of the Q branch of the fundamental rotation-vibration band. A comparison of the frequencies of these lines with the frequencies of the Q branch components of the Raman spectrum of hydrogen[4] is given in Table I.

TABLE I. Observed transitions.

Transition $\Delta v=1-0$ $\Delta J=0$	Frequency, (cm^{-1}); static field (density =82.9 amagat[a])	Frequency, (cm^{-1}); Raman spectrum (density =5 amagats)
0–0	4161.2	4161.28
1–1	4155.1	4155.48
2–2	4143.0	4143.55
3–3	4125.2	4125.88

[a] The density in amagats is defined as the ratio of the density of the gas under experimental conditions to the density of the gas at one atmosphere pressure and zero °C.

The static field frequencies are slightly smaller; the differences apparently are significant since they increase with J and with density.

In principle the matrix element of the mean value of the polarizability for the 1–0 vibrational transition, α_{01}, and the matrix element of the anisotropy γ_{01} can be evaluated from the integrated absorption coefficients. The integrated absorption coefficients as yet are not sufficiently accurate to warrant an estimate of γ_{01}. However, the coefficient of the 1–1 component of the Q branch has been measured sufficiently well to allow a first determination of α_{01}. It has been established experimentally that the absorption coefficient is proportional to the square of the field strength. Thus a specific absorption coefficient can be defined and for the 1–1 component is 5.53×10^{-29} cm^{-1}, per cm path, per molecule per cm^3, per (esu of potential per cm)^2. The matrix element determined from this value is $\alpha_{01}=1.2(5)\times10^{-25}$ cm^3.[5] Corrections have been applied for polarization produced in the incident light flux by the quartz prism of the monochromator and for the small effect of the matrix element of the anisotropy. The result is intermediate to the value obtained from the ratio of Raman to Rayleigh scattering, 1.05×10^{-25} cm^3,[6] and the theoretical value, 1.393×10^{-25} cm^3.[7] By using polarized light and a more efficient grating, more accurate determinations of α_{01} and γ_{01} should be possible.

These results definitely establish the field-induced absorption predicted by Condon. The effect has several interesting and potentially important applications.

[1] E. U. Condon, Phys. Rev. **41**, 759 (1932).
[2] Welsh, Crawford, and Locke, Phys. Rev. **76**, 580 (1949).
[3] Crawford, Welsh, MacDonald, and Locke, Phys. Rev. **80**, 469 (1950); Chisholm, MacDonald, Crawford, and Welsh, Phys. Rev. **88**, 957 (1952).
[4] C. Cumming, Ph.D. thesis, University of Toronto (unpublished).
[5] The calculation will be given in a subsequent publication.
[6] Stansbury, Crawford, and Welsh, Can. J. Phys. (to be published).
[7] Ishiguro, Arai, Mizushima, and Kotani, Proc. Phys. Soc. (London) **A65**, 178 (1952).

Bleaching of CaF_2 Crystals Colored by X-Rays*

ALEXANDER SMAKULA
Laboratory for Insulation Research, Massachusetts Institute of Technology, Cambridge, Massachusetts
(Received July 15, 1953)

SYNTHETIC and natural CaF_2 crystals colored by x-rays exhibit absorption bands: 5800, 4000, 3350, and 2250A.[1] The increase of absorption below 2100A indicates at least one more band. The same absorption is produced by weak, additive coloration.[2] A theoretical explanation of the nature of these bands is still lacking.

A study of thermal and light bleaching of colored alkali halides contributed much to the understanding of color centers in those

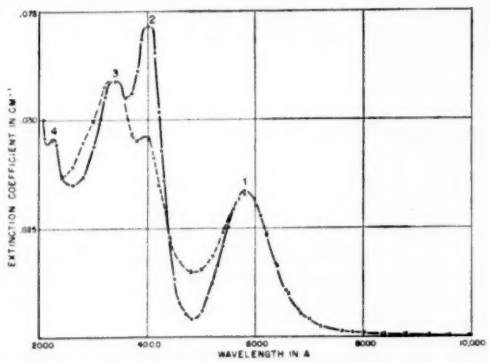

FIG. 1. Bleaching of colored CaF_2 crystal by light absorbed by band 2; — — before bleaching, – – × – – after bleaching.

crystals. According to Barile,[3] colored CaF_2 can be bleached thermally but not by light at room temperature. It will be shown in the present note that colored CaF_2 can be bleached by light at room temperature also. However, the bleaching process seems to be quite different from that in alkali halides.

All experiments were carried out on synthetic crystals (Harshaw Chemical Company). For bleaching, a Hg lamp with proper Corning glass filters was used. Figure 1 (—·— curve) shows the absorption of CaF_2 colored by x-rays with bands marked 1 to 4, respectively. The bands are very stable at room temperature; after 3 weeks no bleaching could be detected. An exposure to light absorbed only by band 1 does not bleach this band after one hour exposure. If, however, the light absorbed by band 2 is used, a strong decrease of band 2 was observed after 5 minutes exposure (Fig. 1). The other bands remained unaffected. Simultaneously with the destruction of band 2, a new band appears with a peak at 4850A (Fig. 1). Band 2 can be restored either by heat or by light absorbed by band 1. In this case the new band at 4850A disappears, but band 1 remains unaffected. Figure 2 shows the bleaching

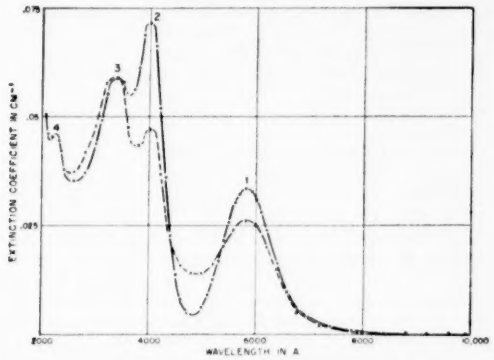

FIG. 2. Bleaching of colored CaF_2 crystal by light absorbed by bands 1 and 2 simultaneously; —·— before bleaching, – – × – – after bleaching.

of bands 1 and 2 and formation of a new band at 4850A if light is used which is absorbed by band 1 and 2 simultaneously. Both bands can be restored either thermally or by irradiation in band 1.

The following tentative explanation of the absorption bands is proposed. Since the bands can be formed either by x-rays or by additive coloration, they correspond to trapped electrons. Since band 1 cannot be bleached by light it may be ascribed to an excitation to a level several tenths of an electron volt below the conduction band. Band 2 may correspond to a transition to the conduction band or very close to it. This band and its transformation into a band at 4850A resembles very much the F and M bands in alkali halides. The peculiar bleaching intercombination between band 1 and 2 requires a further experimental study before it will be possible to give an explanation.

* Sponsored by the U. S. Office of Naval Research, the U. S. Army Signal Corps, and the U. S. Air Force.

[1] A. Smakula, Phys. Rev. **77**, 408 (1950).
[2] F. Lüty, Z. Physik **134**, 596 (1953).
[3] S. Barile, J. Chem. Phys. **20**, 297 (1952).

Thermalization of Positrons in Metals

R. L. GARWIN
Watson Scientific Laboratory, Columbia University, New York, New York
(Received July 21, 1953)

BELL and Graham,[1] in a very thorough investigation of the time distribution of positron annihilation in solids, find a lifetime for positrons in metals of $1.5\pm0.3\times10^{-10}$ sec, independent of the particular metal used; and a complex decay with two time components for not very crystalline material. Their discussion quotes DeBenedetti *et al.*[2] who calculated a thermalization time for positrons in metals of 3×10^{-10} sec, and they presume the positrons to decay before thermalization.

It is the purpose of this note to point out that the thermalization time of positrons in a metal is $\sim10^{-14}$ sec and that the calculation of Appendix I[2] refers to monatomic insulators rather than to metals. Appendix I[3] computes the thermalization time in a metal by considering only the excitation of lattice vibrations after a positron has reached an energy so low that it can no longer cause interband electronic transitions. In a metal, however, it can still transfer energy to the degenerate electrons (here considered in the free electron approximation) by ordinary Coulomb scattering. Indeed, the positron of 0.1-volt energy loses energy to an electron of energy 5 volts almost as fast as to an electron at rest.

This situation arises in the following manner:

Consider a metal of conduction electron density N, Fermi energy $E_F=(\hbar^2/2m)(3N/8\pi)^{\frac{2}{3}}$, and a positron of energy $E\ll E_F$. We shall work at the absolute zero of temperature, although the results obtained are not sensitive to temperature. It is clear that the positron cannot gain kinetic energy in a collision with an electron, for the electron would then have a decreased energy for which all states are filled. These collisions are forbidden by the Pauli principle. But if there is a collision such that the positron loses energy to an electron of energy within $\frac{1}{2}E$ of E_F, this collision is not restricted by the Pauli principle since all states above E_F are empty. Such a collision between free particles cannot occur in one dimension, since the electrons either give energy to the positrons or are moving away from them so that no collisions take place. But in two dimensions the collision is possible. Figure 1 shows a possible collision between an electron of 5-volt energy and a positron of 3-volt energy in which the positron transfers 2.5 ev. to the electron Energy and momentum are, of course, conserved. Indeed, the process can be conceived as a relatively small angle scattering of

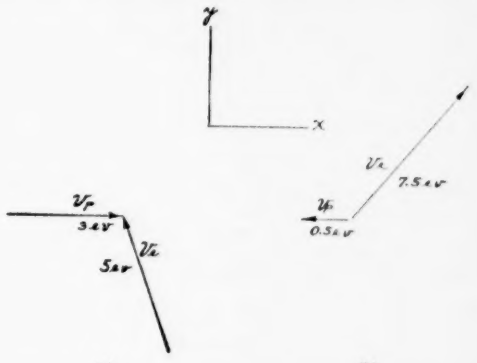

FIG. 1. The collision of a positron of energy 3 ev with an electron of energy 5 ev results in the transfer of 2.5 ev to the electron. (a) Velocities before collision. (b) Velocities after collision.

the electron by the positron. About one-fourth of the free electron-positron scatterings resulting in a momentum transfer $<(2mE)^{\frac{1}{2}}$ lead to a loss of energy by the positron. The average energy lost in such a scattering may be taken as $\frac{1}{2}E$ and the cross section is then $\sim\pi e^4/EE_F$. The number of collisions per second by electrons of energy between E_F and $E_F-\frac{1}{2}E$ is

$$(N)\left(\frac{2E}{6E_F}\right)\left(\frac{2E_F}{m}\right)^{\frac{1}{2}}\left(\frac{\pi e^4}{EE_F}\right),$$

the first two factors being the number of conduction electrons per cc between E_F and $E_F-\frac{1}{2}E$, the third the velocity of these electrons, and the fourth the cross section. The rate of positron energy

loss is then given by the collision rate times the energy lost per collision and is $(\sqrt{2}\pi e^4 N/6m^{\frac{1}{2}})EE_F^{-\frac{1}{2}}$. For a metal with $N=5\times10^{22}$/cc, $E_F\sim8\times10^{-12}$ ergs and a positron of low energy loses energy at a rate of $E\times3\times10^{15}$ sec^{-1}. The loss rate can be written $E\times(16\pi^2/9)\times(me^4/h^3)$ and is thus independent of the electron density so long as the Fermi energy is much greater than the positron energy. The collision cross section, above, is rather unrealistically large because of shielding by the free electrons. It appears unreasonable to imagine it reduced more than a factor of 100, though, still leaving the slowing-down time $\sim10^{-12}$ sec. In a semiconductor, in particular, one could easily detect 10^{16} electrons/cc by their efficacy in thermalizing positrons.

How then can one explain the negative results of Madansky and Rasetti[3] in not finding thermal positrons diffusing from the surface of condensed material? It seems probable that the emergence of thermal positrons is not observed because thermal (or epithermal) positronium comes out instead, being energetically favored over thermal positrons by $E_B-\varphi e$, where E_B is the binding energy of positronium ($=6.8$ ev) and φ is the work function of the metal. More probably the competition is not with thermal positrons but with positrons of energy eV, where V is the "inner potential" ($\equiv\varphi+E_F$), and the energy difference favoring positronium is closer to $E_B-\varphi+V=E_B+E_F$. Even in the singlet state thermal positronium travels $(1.25\times10^{-10})\times10^7=1.3\times10^{-3}$ cm before decaying, so it could be observed by a collimated system as annihilation radiation emitted from vacuum close to the surface. Triplet positronium would be observable to a distance of several centimeters.

The results of Bell and Graham with metals are explained, then, as immediate thermalization followed by capture (accelerated by the Auger effect involving the conduction electrons) to form positronium. Exchange collisions with electrons on the Fermi surface convert any triplet state to singlet, and so the decay is very rapid. If this were all that occurred, however, the lifetime would be lengthened by a factor four since the system would spend three-fourths of its time in the nondecaying triplet state, there being no effective energy difference between them. There is still, therefore, a slight puzzle with metals. The results with nonmetals indicate that some positrons are preserved either free or as triplet positronium, decaying probably not by conversion to singlet (in an insulator), but by annihilation with an electron of appropriate spin from a neighboring molecule.

While it is still not certain what processes are effective, it appears that positrons are thermalized in metals in times $\sim10^{-15}$ sec, and that the Auger effect is important in the formation of positronium. It is suggested that work be done on the annihilation of positrons in semiconductors of varying conductivity and that one should look for thermal positronium emerging from the surface of materials in which positrons are stopping.

[1] R. E. Bell and R. L. Graham, Phys. Rev. **90**, 644 (1953).
[2] DeBenedetti, Cowan, Konneker, and Primakoff, Phys. Rev. **77**, 205 (1950).
[3] L. Madansky and F. Rasetti, Phys. Rev. **79**, 397 (1950).

Some K-Particle Mass Measurements*

D. M. Ritson†
Physics Department, University of Rochester, Rochester, New York
(Received July 21, 1953)

In a recent publication, Crussard *et al.*[1] have reported mass values for six K mesons absorbed in photographic emulsions of $950m_e\pm40m_e$. Reported below are measurements made on three K particles with a new technique of measuring gap density as a function of residual range in electron sensitive photographic emulsion. The term "gap density" was first defined by Hodgson[2] to be the fractional length of a track unoccupied by grains. To determine mass values, it is assumed that singly charged particles of the same velocity, but differing mass, will produce tracks in photographic emulsions of identical gap density. Then if the ranges at which the velocities are equal are known, the ratio of the masses equals the ratio of the ranges.

To provide a simple precise method of measurement a motor drive was attached to the stage of a Bausch-Lomb scattering microscope (these microscopes permit tracks to be rotated parallel to the stage movements) in such a way that a track was driven past a hairline at the rate of 100μ in 4 minutes. The observer was provided with two counters driven by a common pulser. One counter ran continuously; the other, when the observer pressed a button. The observer pressed a button whenever the hairline was over a portion of track unoccupied by grains. The ratio of the readings of the two counters gave the gap density.

To make a mass measurement on a given particle, one or more reference protons were selected (protons being differentiated from deuterons on the basis of scattering range measurements) running at similar depth in the emulsion to the track being measured. The variation of gap density d with range R was roughly determined and found to be proportional to $R^{0.52\pm0.05}$. The gap density of the K particle was measured for 200μ and then the gap density of the reference protons at the same depth and approximately twice the range (chosen to make the gas density almost identical) was measured for 200μ.

Suppose the gap density of the K particle was d_K and range R_K, and of the proton was d_p and R_p, then using the previously determined variation of d with R, the mass of the K particle m_K relative to the mass of the proton m_p is

$$m_K/m_p=(R_K/R_p)(d_p/d_K)^2.$$

It is possible for the absolute value of d to drift with time by the order of 10 percent, but the ratio, d_p/d_K is repeatable to better than 4 percent. The procedure outlined above was repeated over the whole range of the K particle above 1000μ. Comparison of gap densities on the ranges below 1000μ is affected by differences in the scattering of K particles and protons. If care is taken to randomize the procedure, the accuracy obtainable on a given track should be limited only by the length of track available, and, of course, by the degree of fading on the plates which have been used. The method outlined above seems to be of similar precision with the photoelectric method, of greater simplicity, and less affected by local changes in optical quality occasioned by surface scratches or other factors.

Three K particles were observed in balloon flight exposures; K_1, observed in a stack of stripped emulsions, was 4.5 mm long and came from a star consisting of 14 evaporation prongs and two minimum tracks (probable energy on the order of 5 Bev). K_2 and K_3 (3 mm long) were loaned to us by Dr. P. Barrett of Cornell for measurement using the above method. The origins of these two particles were not observed. In all three cases, the secondary particles were too short to be identified but had ionizations of the order of $I_{\min}$. The mass values determined were

$$K_1=970\pm100m_e \text{ (standard deviation)},$$
$$K_2=1020\pm100m_e \text{ (standard deviation)},$$
$$K_3=870\pm100m_e \text{ (standard deviation)}.$$

The results are quite consistent with the assumption of a single mass value $950\pm60m_e$ and add additional weight to the conclusions reached by Crussard *et al.*[1] that the masses of the majority of K particles observed in emulsions in balloon flights are about $950m_e$ and are within the accuracy of the experiments indistinguishable from the mass of the τ meson.

The author is very grateful to Dr. P. Barrett of Cornell for providing two examples of K mesons for measurement and to Professor M. F. Kaplon for discussion during the course of the work.

* This research was supported in part by the U. S. Air Force under a contract monitored by the Office of Scientific Research, Air Research and Development Command.
† Now at Massachusetts Institute of Technology, Cambridge, Massachusetts.
[1] Crussard, Leprince-Ringuet, Morellet, Orkin-Lecourtois, and Trembley, Phys. Rev. **90**, 1127 (1953).
[2] P. E. Hodgson, Phil. Mag. **41**, 725 (1950).

The Absorption Mean Free Path of the High-Energy Nucleonic Component of Cosmic Radiation*

M. F. KAPLON, J. Z. KLOSE, D. M. RITSON, AND W. D. WALKER
University of Rochester, Rochester, New York
(Received July 27, 1953)

TWO similar emulsion cloud chambers[1] consisting of 24 alternate 3-mm lead plates and 250μ G-5 emulsions were exposed to the cosmic radiation. One stack was exposed for 30 days at 10 700 feet at Echo Lake, Colorado with the planes of the emulsions and lead plates at an angle of 45° with the vertical, the other was exposed for 6 hours at 90 000 feet at White Sands, New Mexico with the planes of the emulsions and lead plates horizontal. These two emulsion cloud chambers were used to obtain flux measurements of the nuclear interacting component of the cosmic radiation for energies $\gtrsim 10^{12}$ ev; the data obtained was used to determine the absorption mean free path in the atmosphere (λ) for this energy region.

Since the emulsion cloud chamber is not a unidirectional detector, a Gross transformation must be used in evaluating the data. Five nuclear interactions were observed in a systematic survey of 106 cm^2 of emulsion in the mountain stack, and fifteen such interactions were observed in a systematic survey of 45 cm^2 of emulsion in the high-altitude stack. In each case the survey was made in an emulsion midway in the stack. The solution of the Gross transformations for λ was obtained by forming a ratio of the transformation expressions for each plate assembly. Since the energy selection characteristics of these two stacks are the same, the ratio is not dependent upon the energy of the interactions if the energy spectrum is independent of depth. Energy determinations of the interactions were made by methods previously used for this type of exposure.[1] The expression involving the Gross transformations of the two stacks is

$$\frac{N_{sc}(X_c)}{N_{sm}(X_m)}=\frac{N_0A_cT_c\left[1-\exp\left(-\frac{t_c}{\lambda_1}\right)\right]2\pi \times\int_{\theta_{\min}}^{\pi/2}\sin\theta\cos\theta d\theta\exp\left(-\frac{X_c}{\lambda\cos\theta}\right)}{N_0A_mT_m\left[1-\exp\left(-\frac{t_m}{\lambda_1\cos\alpha}\right)\right]2\pi\sin\alpha \times\int_0^{\theta_{\max}}\sin\theta\cos\theta d\theta\exp\left(-\frac{X_m}{\lambda\cos\theta}\right)}.$$

In the expression all quantities with subscript c refer to the high-altitude stack, and all those with subscript m refer to the mountain stack. $N_{sc}(X_c)$ and $N_{sm}(X_m)$ represent the number of interactions observed in the two stacks at effective atmospheric depths X_c and X_m, respectively. N_0 is the primary interacting flux at the top of the atmosphere, the A's refer to the area of plate scanned for showers, and the T's are the times of exposure of the two stacks. t_c and t_m are the depths in the stacks of the point of observation, λ_1 represents the interaction mean free path of the combination of materials of the stacks, and $\alpha=45°$, the angle with the vertical of the mountain stack. θ is the zenith angle of the incoming interacting particle, and $\theta_{\min}$ and $\theta_{\max}$ are limits imposed by the minimum observable track length in the plates. Solution of this expression with $\theta_{\min}=15°$ and $\theta_{\max}=45°$ gives $\lambda=129\pm15$ grams/cm^2. The errors were determined from the statistical fluctuations in $N_{sc}(X_c)$ and $N_{sm}(X_m)$. Taking into account the possibility of a transition effect by means of a simple diffusion equation, it was found that the mean value of the absorption mean free path could not be less than $\sim$115 grams per cm^2.

The result for λ obtained here agrees with the majority of previous results obtained by other experimenters at lower energies.[2] (Contradictory results are given by Gottlieb[3] and Stinchcomb[4]). Our result taken with the generally accepted results at lower energies indicates that the absorption mean free path in the atmosphere is independent of energy from $\sim10^9$ ev to $\sim10^{12}$ ev. Our result is inconsistent with the value calculated by Milford and Foldy[5] assuming completely inelastic nucleon collisions. Greisen and Walker[6] have suggested that a possible interpretation of such a long mean free path is that the fundamental act in the high-energy nucleonic component cascade is rather elastic.

Substituting the value of λ obtained here in the Gross transformation for the high-altitude stack, a value of the primary nucleonic flux at the top of the atmosphere of $N_0=0.22\pm0.075$ per meter^2 per second per steradian was obtained. This result is in good agreement with that given by Kaplon and Ritson[1] for a somewhat higher energy. For a distribution of nucleons $\propto\cos^6\theta$, the integral primary flux of nucleons at mountain altitude was determined to be $N_0=0.0009\pm0.0004$ per meter^2 per second per steradian. For comparison the integral primary flux of nucleons determined at mountain altitude assuming an isotropic distribution of nucleons was $N_0=0.0004\pm0.0002$ per meter^2 per second per steradian. (This represents a lower limit on N_0 at mountain altitude.)

The authors are indebted to the Aero Medical Field Laboratory, Holloman Air Force Base and to Professor Mario Iona of the University of Denver for assistance in obtaining successful exposures. They would also like to thank Miss Barbara Hull for her assistance in scanning the plates.

* This research was supported in part by the United States Air Force under a contract monitored by the Office of Scientific Research, Air Research and Development Command.

[1] M. F. Kaplon and D. M. Ritson, Phys. Rev. **88**, 386 (1952).
[2] B. Rossi, Revs. Modern Phys. **20**, 537 (1948); John Tinlot, Phys. Rev. **74**, 1197 (1948); M. A. Clark, Phys. Rev. **87**, 87 (1952); H. K. Ticho, Phys. Rev. **88**, 236 (1952).
[3] M. B. Gottlieb, Phys. Rev. **82**, 349 (1951).
[4] T. G. Stinchcomb, Phys. Rev. **83**, 422 (1951).
[5] F. J. Milford and L. L. Foldy, Phys. Rev. **81**, 13 (1951).
[6] K. Greisen and W. D. Walker, Phys. Rev. **90**, 915 (1953).

Many-Nucleon Forces

GREGOR WENTZEL
Institute for Nuclear Studies, University of Chicago, Chicago, Illinois
(Received July 13, 1953)

IN pseudoscalar meson theory (*PS* coupling), the saturation character of nuclear forces is accounted for by the cooperative action of many-body forces.[1] In particular, the repulsive 3-, 5-, 7-, $\cdots$ body forces keep the nucleus from collapsing into a very small volume. These nuclear interactions result mainly from matrix elements describing virtual nucleon-pair creation and annihilation processes, and, therefore, they can also be derived, and more easily so, from the equivalent (pseudo-) scalar pair theory,[2] if one grants a nonrelativistic treatment of the nucleons and adopts, accordingly, a "cutoff" in the interaction with high-energy mesons.

Considering the importance of the saturation problem, it may be worth while to outline a short derivation of the many-body potentials from the scalar pair theory, at the same time pointing out the approximations involved.

Let $\mathbf{x}_s$ ($s=1, 2, \cdots, n$) be the (fixed) locations of n nucleons. The normal modes of the meson field oscillators are then obtained by solving the eigenvalue problem of the quadratic form

$$\Sigma_k\omega_k^2|q_k|^2+\lambda V^{-1}\Sigma_s\left|\Sigma_k u_k q_k e^{i\mathbf{k}\cdot\mathbf{x}_s}\right|^2,$$

($\omega_k^2=\mu^2+k^2$; u_k=form-factor; λ=coupling parameter G^2/M; V=normalization volume). The corresponding linear equations are

$$(\zeta-\omega_k^2)q_k=\lambda V^{-1}u_k^*\Sigma_s e^{-i\mathbf{k}\cdot\mathbf{x}_s}\Sigma_{k'}u_{k'}q_{k'}e^{i\mathbf{k}'\cdot\mathbf{x}_s}.$$

They are solved by setting

$$q_k=\lambda V^{-1}(\zeta-\omega_k^2)^{-1}u_k^*\Sigma_s e^{-i\mathbf{k}\cdot\mathbf{x}_s}c_s,$$

with the n coefficients c_s subjected to the n linear equations:

$$\Sigma_t c_t\left[\delta_{st}-\lambda V^{-1}\Sigma_k(\zeta-\omega_k^2)^{-1}|u_k|^2e^{i\mathbf{k}\cdot(\mathbf{x}_s-\mathbf{x}_t)}\right]=0. \quad (1)$$

The eigenvalues ζ are the roots of the $n\times n$ determinant $\varphi_n(\zeta)$ of (1).

The potential energy of the system, in the absence of free mesons, is the zero-point energy of the field oscillators, minus its vacuum

value ($n=0$, or $\lambda=0$),

$$E_n=\tfrac{1}{3}(\Sigma\zeta^{-1}-\Sigma_k\omega_k).$$

The factor 3 takes account of the three charge states of the π meson in a charge-symmetric theory. As has been shown in I, E_n may be written as a contour integral,

$$E_n=-3(8\pi i)^{-1}\int d\zeta\zeta^{-1}\ln\varphi_n(\zeta),$$

where the path of integration in the ζ plane encircles all roots ζ (and all ω_k^2). [The identity of the determinant $\varphi_n(\zeta)$ with the function called $\varphi(\zeta)$ in I, Eqs. (2) and (3), is easily proved: $\varphi_n\Delta_0=\Delta$.] If all nucleons are removed to infinite distances, E_n reduces to nE_1, i.e., the self-energy of the n isolated nucleons. Subtracting this, we get the potential energy proper,

$$U_n=E_n-nE_1=-3(8\pi i)^{-1}\int d\zeta\zeta^{-1}\ln[\varphi_n(\zeta)\varphi_1^{-n}(\zeta)]. \quad (2)$$

Note that, according to (1), $\varphi_n\varphi_1^{-n}$ is an $n\times n$ determinant $\|\beta_{st}\|$ with

$$\beta_{ss}=1;\ \beta_{st}=\beta_{ts}=-\lambda\varphi_1^{-1}(\zeta)(2\pi)^{-3}\times\int d^3\mathbf{k}(\zeta-\omega_k^2)^{-1}|u_k|^2e^{i\mathbf{k}\cdot(\mathbf{x}_s-\mathbf{x}_t)}\ (s\neq t) \quad (3)$$

(in the limit $V\to\infty$).

As long as all nucleon distances are large compared with the "nucleon radius" a (the cut-off momentum $\Lambda\sim a^{-1}$ is assumed $\gg\mu$), three approximations can be made (see I for details):

(a) In the $\mathbf{k}$-space integral in (3), $|u_k|^2$ can be replaced by 1.

(b) The factor $\varphi_1^{-1}(\zeta)$ in (3) can be replaced by its value at the point $\zeta=\mu^2$. The error thereby introduced in the contour integral (2) is negligible. The energy U_n then depends only on the "effective coupling strength,"

$$\lambda_A=\lambda\varphi_1^{-1}(\mu^2), \quad (4)$$

which, actually, is smaller than λ and tends to zero in the limit $a\to 0$, or $\Lambda\to\infty$.

(c) The off-diagonal elements of the matrix β are $\ll 1$ in magnitude, and the logarithm of the determinant in (2) can be expanded into powers of β_{st} (or λ_A).

Take, as an example, $n=3$,

$$U_3=-3(8\pi i)^{-1}\int d\zeta\zeta^{-1}\ln[1-(\beta_{12}^2+\beta_{13}^2+\beta_{23}^2)+2\beta_{12}\beta_{23}\beta_{31}].$$

Neglecting terms $\sim\lambda_A^4$, one sees that U_3 comprises, as leading terms, the two-body potentials of the 3 pairs (1,2), (1,3), (2,3), and, next, the three-body potential

$$W_3=-3(4\pi i)^{-1}\int d\zeta\zeta^{-1}\beta_{12}\beta_{23}\beta_{31}. \quad (5)$$

With the approximations (a) and (b), the $\mathbf{k}$ and ζ integrals are easily evaluated,

$$W_3=3(64\pi^4)^{-1}\mu K_1(\mu[r_{12}+r_{23}+r_{31}])\lambda_A^3(r_{12}r_{23}r_{31})^{-1}. \quad (6)$$

Similarly, for $n=4$, one finds the sum of the 6 pair potentials and of the 4 triplet potentials, supplemented by various terms $\sim\lambda_A^4$. Among these one recognizes the 4-body potential

$$W_4=3(4\pi i)^{-1}\int d\zeta\zeta^{-1}[\beta_{12}\beta_{23}\beta_{34}\beta_{41}+\beta_{13}\beta_{34}\beta_{42}\beta_{21}+\beta_{14}\beta_{42}\beta_{23}\beta_{31}]. \quad (7)$$

In addition, there are terms involving products like β_{12}^4 and $\beta_{12}^2\beta_{13}^2$ which represent corrections to the two- and three-body potentials.[3] (Terms like $\beta_{13}^2\beta_{34}^2$ cancel.) Note that a product $\Pi_i\beta_{s_it_i}$ in the expansion of the logarithm in (2) gives rise to the potential

$$3(2\pi)^{-1}\mu K_1(\mu\textstyle\sum_i r_{s_it_i})\prod_i(\lambda_A/4\pi r_{s_it_i}). \quad (8)$$

It is then a mere combinatorial problem to write down the general n-nucleon potential; the answer need not be restated here [see I, Eqs. (22), (23); also Drell and Huang, reference 1, Eq. (7)[4]]. But a final remark concerning volume integrals may be of interest. Using the definition (3) and the approximations (a), (b), one finds immediately

$$\int d^3\mathbf{x}_3\beta_{13}\beta_{23}=\lambda_A\partial\beta_{12}/\partial\zeta=-\lambda_A\partial\beta_{12}/\partial(\mu^2).$$

[The regions where $r_{13}\lesssim a$, or $r_{23}\lesssim a$, do not contribute appreciably to this integral.] Hence

$$\int d^3\mathbf{x}_3W_3=\lambda_A\partial W_2(\mathbf{x}_1,\mathbf{x}_2)/\partial(\mu^2),$$
$$\int d^3\mathbf{x}_4W_4=\lambda_A\partial W_3(\mathbf{x}_1,\mathbf{x}_2,\mathbf{x}_3)/\partial(\mu^2), \quad (9)$$

and so forth. After $n-1$ volume integrations (and ζ integration by Cauchy's theorem)

$$\int d^3\mathbf{x}_2\cdots\int d^3\mathbf{x}_nW_n=(-1)^{n-1}\tfrac{3}{4}[\tfrac{1}{2}\times\tfrac{2}{3}\times\cdots\times(n-\tfrac{2}{3})]\times\lambda_A^n(2\pi)^{-3}\int d^3\mathbf{k}\omega_k^{-2n+1}\quad(n\geqslant 3). \quad (10)$$

These formulas prove useful in computations of nuclear energies, including surface energies resulting from many-body forces.

[1] G. Wentzel, Helv. Phys. Acta **25**, 569 (1952); S. D. Drell and K. Huang, Phys. Rev. **91**, 1527 (1953).
[2] G. Wentzel, Helv. Phys. Acta **15**, 111 (1942), to be quoted as I.
[3] These terms also appear in the energy of a nucleon lattice, as calculated in I, Eq. (22); there they are formally listed among the 4-body terms. The two-body term (from β_{12}^4) is listed by A. Klein, Phys. Rev. **90**, 1101 (1953), Eq. (48). The three-body terms (like $\beta_{12}^2\beta_{13}^2$), which have the effect of weakening the repulsive potential W_3, may well be equally important.
[4] Drell and Huang use the symbol λ for the pure number $\lambda\mu/8\pi$ (our notation). They ignore higher-order effects, in particular those which reduce λ to λ_A.

The Energy Spectrum of Particles from Stars*

R. W. Waniek and Taiichiro Ohtsuka
Cyclotron Laboratory, Harvard University, Cambridge, Massachusetts
(Received April 14, 1953)

THE range distribution of particles from stars was observed in Ilford G5 plates, 200 microns thick, exposed to a high-energy neutron beam (about 90 Mev) by methods already described.[1]

In previous work, the range distributions have been inferred from the distributions of the projected range. In our case the actual range for each prong was determined. The critical factor entering this determination is the shrinkage factor. Several plates of the same batch were exposed to a well-collimated alpha beam of thorium C' particles entering the emulsion at a predetermined angle of 45°. Measurements were also carried out with extremely thin x-ray beams which penetrated through the whole emulsion and gave information as to the uniformity of the shrinkage. The shrinkage factor was then determined by the change in inclination. Changes in the shrinkage factor due to the aging of the plates and varying humidity conditions of the scanning room were also

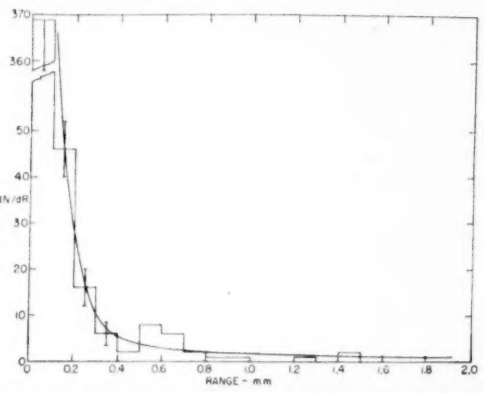

FIG. 1. Plate 11 G5 at 0°. Range histogram of all prong events (0–2 mm).

checked. A reasonable estimate of the variation of the shrinkage factor attributable mainly to changes in humidity was taken as 20 percent which is probably an overestimate. Thus the percentage error involved in the range determination δR, assuming the shrinkage factor as the predominant source of error, can be determined from the following equation:

$$\delta R/R = (d^2S^2/R)\cdot(\delta S/S),$$

where d is the vertical component of the track, S is the shrinkage factor, and $\delta S/S$ is 20 percent. This results, for instance, in an uncertainty of roughly 20 percent at the peak of the range distribution.

Figure 1 shows the range spectrum of the particles from all types of stars (1-prong to 5-prong events; total number of stars equal to 400) from the plate exposed at 0°.[1,2]

The detailed spectrum between 5 and 200 microns is given in Fig. 2 (particles with range under 5 microns were not included).

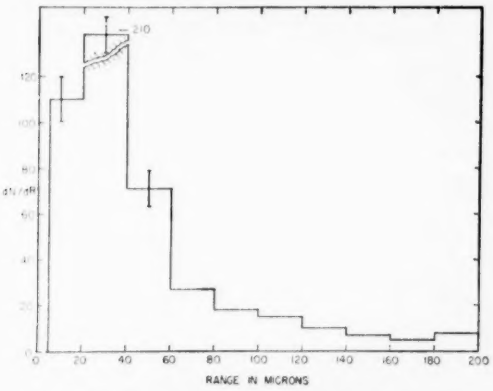

FIG. 2. Plate 11 G5 at 0°. Range histogram of all prong events (0–200 microns).

The spectra have been corrected for escape in the conventional manner.[3]

In recently developed plates in which the shrinkage was eliminated with various techniques, the shape of the spectrum was essentially unaffected. In Figs. 1 and 2 no discrimination is introduced between the different types of particles. We carried out some additional work in the discrimination of protons from alpha particles (deuterons and tritons could not be discriminated from protons). The peak of the range distribution of the alpha particles was found to coincide approximately with the one of the proton distribution. The alpha particles amounted to about 12 percent of the total number of prongs. The peak would correspond in the case of the protons to an energy of about 2.5 Mev and in the case of the alpha particles to about 6 Mev. These values are definitely much lower than the average Coulomb barrier of the heavy nuclei component of the emulsion (approximately 8 Mev for protons and 16 Mev for alphas); however, they would correspond to the average Coulomb barrier of the light nuclei component. Assuming no unusual behavior of the nucleus, one would surmise that the majority of our events originate in the light nuclei of the emulsion. From consideration of the composition and the geometrical cross section alone, about 70 percent of the events should be ascribed to the heavy nuclei. Blau's measurement at 300 Mev favors the heavy nuclei even more (82 percent heavy nuclei and 18 percent light nuclei for stars with two or more prongs).[4]

It is not feasible to distinguish between stars originating in light and heavy nuclei, unless one uses special techniques. Experiments along this line are now under way. One can, however, set a lower limit to the number of stars originating in light nuclei by selecting stars with at least one prong having an energy below the Coulomb barrier of the heavy nuclei. In carrying out this analysis we found that for 1- and 2-prong stars at least 80 percent of the stars are attributable to light nuclei, whereas for 3-prong stars the fraction increases to about 95 percent. The 4- and 5-prong stars are almost completely the result of light nuclei. More conclusive results are expected upon completion of our experiments with wire-embedded emulsions.

The range histogram has also been plotted for different spatial angles (Fig. 3). There was no appreciable variation in the position

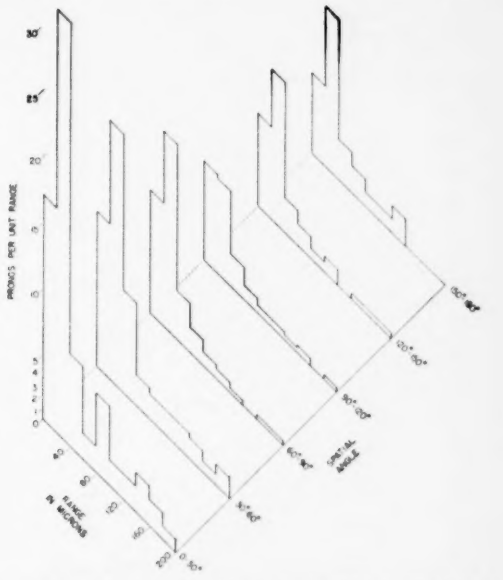

FIG. 3. Plate 11 G5 at 0°. Range histogram at different spatial angles (30° intervals) from all prong events.

of the peak of the range spectrum at different angles. However, the intensity of the peak varies in such a fashion as to exhibit a forward asymmetry.

Acknowledgments are due Matthew J. Hurley and Junzaburo Iwata for their assistance in the scanning and in the analysis of the data.

* Assisted by the joint program of the U. S. Office of Naval Research and the U. S. Atomic Energy Commission.

[1] R. W. Waniek and T. Ohtsuka, Phys. Rev. **89**, 882 (1953).
[2] R. W. Waniek and T. Ohtsuka, Phys. Rev. **89**, 1307 (1953).
[3] F. C. Champion and C. F. Powell, Proc. Roy. Soc. (London) **A183**, 64 (1944).
[4] M. Blau and A. R. Oliver, Phys. Rev. **87**, 182 (1952).

The Reaction $Li^6(\alpha,\gamma)B^{10}$

D. H. WILKINSON AND G. A. JONES
Cavendish Laboratory, Cambridge, England
(Received July 23, 1953)

WE have investigated the reaction $Li^6(\alpha,\gamma)B^{10}$ with alpha particles of up to 1.5 Mev. Within the range of excitation in B^{10} so produced (4.45−5.35 Mev), states are known at 4.77, 5.11, and 5.16 Mev[1] from the reactions $Be^9(d,n)B^{10}$ [2] and $B^{10}(p,p')B^{10}$.[3] We observe the lowest state ($\omega\Gamma\sim0.15$ ev, where Γ is the smaller of Γ_α and Γ_γ) at 4.75±0.02 Mev and the highest at 5.162×0.008 Mev ($\omega\Gamma\sim0.2$ ev); the latter measurement agrees well with those of Bonner and Butler[2] (5.165±0.006 Mev) and Bockelman *et al.*[3] (5.159±0.010 Mev). We do not observe the middle level ($\omega\Gamma<\sim0.007$ ev); we believe it to be (2−) and its absence due to an isotopic spin discouragement of the $E1$ transitions.[4] [Ajzenberg[2] has suggested (1−) or (2−) for one or other element of the 5.11−5.16-Mev doublet.]

We have determined the decay schemes with the aid of NaI(Tl) crystals and display them in Fig. 1. The measured gamma-ray

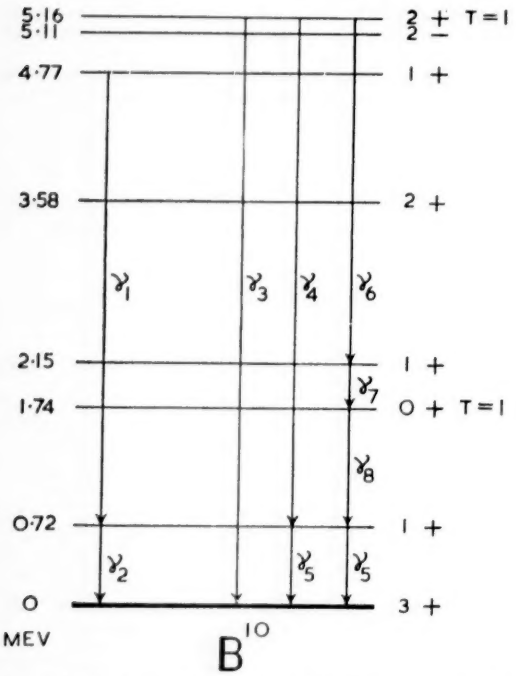

FIG. 1. Level scheme of B^{10} showing the gamma rays observed in the present investigation. The spin and parity assignments for the top three states are those suggested here; the rest are taken from Ajzenberg and Lauritsen (reference 1).

energies are shown in Table I where the "expected energies" are taken from the work of Bockelman *et al.*,[3] and Rasmussen *et al.*[5] (No corrections have been made for Doppler shift—our own observations were made in poor geometry at 0° to the alpha-particle beam.)

The relative intensities of the gamma rays coming from the 2.15-Mev level have been determined with the aid of the results of Rasmussen *et al.*,[5] Pruitt, Hanna, and Swartz,[6] and Ajzenberg.[2]

The 5.16-Mev state we believe to be the $(2+)$ $T=1$ companion of the 3.37-Mev state of Be^{10};[4] its formation is not a serious violation of the isotopic spin rules. This assignment is supported by the observed decay scheme which is most reasonably explained by $J=2$ (though $J=1$ is not excluded); negative parity is unlikely because all our observed initial gamma rays would then be isotopic-spin forbidden $E1$ transitions, but with a discouragement factor of less than 10 which is improbably low. The $T=1$ assignment is also supported by the fact that this state emits gamma rays in successful competition with alpha particles[7] as would be expected of a $T=1$ but not a $T=0$ level.

TABLE I. Measured and expected γ-ray energies. Relative intensity refers to the strength of the transition relative to the sum of all transitions from the initial level in question.

Gamma ray	Relative intensity	Measured energy (Mev)	Expected energy (Mev)
$^{1}\gamma_1$	1	4.02 ±0.04	4.054 ±0.010
γ_2	1	0.703 ±0.010	0.717 ±0.001
γ_3	0.05	5.25 ±0.10	5.159 ±0.010
γ_4	0.25	4.49 ±0.05	4.442 ±0.010
γ_6	0.77	0.716 ±0.010	0.717 ±0.001
γ_8	0.70	2.99 ±0.03	3.007 ±0.014
γ_7	0.25	0.413 ±0.010	0.414 ±0.001
γ_8	0.25	1.017 ±0.010	1.022 ±0.002

The 4.77-Mev state we believe to be $(1+)$. The decay scheme favors $J=0$ or 1; $(0+)$ we cannot form and odd parity is again unlikely because a $(1-)$ state would decay predominantly by an allowed $E1$ transition to the 1.74-Mev $(0+)$ $T=1$ state while the $(0-)$ assignment would again imply anun expectedly small isotopic-spin discouragement factor for the then forbidden $E1$ transition to the first excited state.

[1] F. Ajzenberg and T. Lauritsen, Revs. Modern Phys. **24**, 321 (1952).
[2] F. Ajzenberg, Phys. Rev. **88**, 298 (1952); T. W. Bonner and J. W. Butler, Phys. Rev. **83**, 1091 (1951).
[3] Bockelman, Browne, Sperduto, and Buechner, Phys. Rev. **90**, 340 (1953).
[4] G. A. Jones and D. H. Wilkinson, Phys. Rev. **90**, 722 (1953).
[5] Rasmussen, Hornyak, and Lauritsen, Phys. Rev. **76**, 581 (1949).
[6] Pruitt, Hanna, and Swartz, Phys. Rev. **87**, 534 (1952).
[7] Chao, Lauritsen, and Rasmussen, Phys. Rev. **76**, 582 (1949).

Positive π-Meson Production by Negative π Mesons*

W. F. FRY
Department of Physics, University of Wisconsin, Madison, Wisconsin
(Received July 27, 1953)

A STACK of Ilford G-5, 600- and 1000-micron thick plates was exposed in the 220-Mev negative π-meson beam of the University of Chicago cyclotron. The plates were arranged with the emulsion of one plate in contact with the adjacent plate so that the tracks could be followed through both plates. Two methods of area scanning were employed. Initially the plates were searched for each π-meson interaction. A total of 4160 meson interactions were found and studied. 12 $\pi-\mu$ decays were observed along with 123 negative π-meson stars. Of the 123 mesons, 20 were observed to originate from high-energy π-meson interactions. Additional plates have been scanned for slow meson tracks only, with a low magnification. By this method 292 negative π-meson stars and 24 $\pi-\mu$ decays have been found. Of these 292 negative π mesons, 51 were observed to originate from a high-energy π-meson interaction. In two cases the π-meson track from the $\pi-\mu$ decay originated from a high-energy meson interaction. In 21 of the $\pi-\mu$ decays, the μ meson stopped in the emulsion. In each case the range of the μ meson was normal and a decay electron track was observed from the end of the μ-meson track. Since the probability of decay in flight of a negative π meson is very small[1] ($<10^{-3}$) and since the range of the μ-meson track was normal, it was assumed that the π mesons which decay into μ mesons were positively charged. This assumption was further substiantiated by the subsequent decay of each of the μ mesons (only 36±2 percent of th enegative μ mesons, which stop in a photographic emulsion, decayed into an electron).[2]

A projection drawing of event 1 is shown in Fig. 1. The incident π-meson track (track 1) is parallel with the other meson tracks and has the same grain density and multiple scattering as the other tracks. Since the π mesons were magnetically analyzed twice, it is assumed that in this case the incident meson was also negatively charged. Track 2 is 200 microns long and is 1.2±0.2 times minimum ionizing. It is assumed that the particle which produced the track was a π meson of about 50 Mev. The π-meson track 3 is 250 microns long and ends in the emulsion. The μ-meson track from the π-meson decay leaves the emulsion after about 500 microns. A short recoil track is observed which indicates that the target nucleus was a light nucleus. The event is interpreted as the inelastic scattering, of a negative π meson with the production of a positive π meson,

$$\pi^- + p \text{ (in nucleus)} \rightarrow \pi^- + n + \pi^+. \qquad (1)$$

There is no evidence for the formation of a ζ^0 meson.

A projection drawing of event 2 is shown in Fig. 2. Track 1 is the track of the incident π meson. Track 2 is 8 microns long and the result of a charged nuclear particle. Track 3 was produced by a proton of 4.4 Mev. Track 4 leaves the surface of the emulsion after 2100 microns and exhibits the multiple scattering of a π meson of a velocity which corresponds to the observed grain density. This meson track has been followed into the adjacent plate and ends

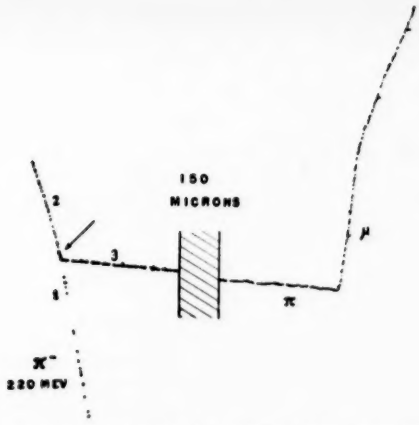

FIG. 1. A projection drawing of a negative π-meson interaction in a photographic emulsion. A positive π meson (track 3) was produced in the collision with a light nucleus.

after 2900 microns. The μ-meson track from the $\pi-\mu$ decay is 610 microns long. A decay electron is observed from the end of the μ-meson track. The event is interpreted as the production of a positive π meson by a negative π meson by a double charge exchange reaction:

$$\begin{aligned}\pi^-+p\ (\text{in a nucleus})&\rightarrow\pi^0+n,\\ \pi^0+p\ (\text{in the same nucleus})&\rightarrow\pi^++n.\end{aligned}\qquad(2)$$

A very crude estimate of the probability per nuclear interaction of positive π-meson production by negative π mesons can be made from the number of π^- meson stars and $\pi-\mu$ decays. A π meson of energy less than about 20 Mev from an interaction will on the average stop in the stack of plates. A lower limit of the probability that a positive π meson of energy less than about 20 Mev will be produced in an interaction is estimated from the ratio of the number of π^+ to π^- times the probability of finding a π^- meson of energy less than 20 Mev from an interaction,

$$(36/415)\times(20/4160)\cong 4\times 10^{-4}.$$

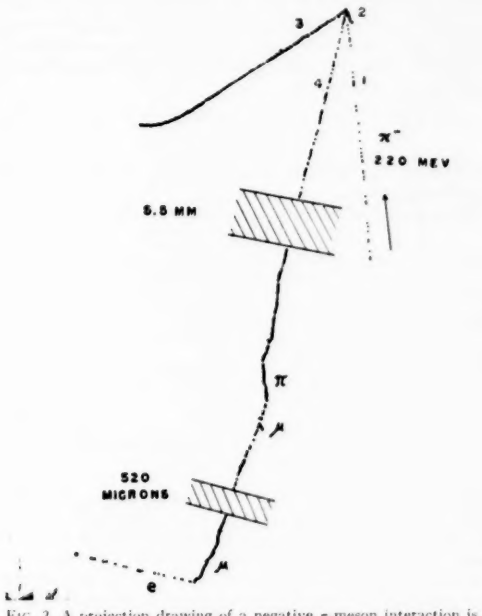

FIG. 2. A projection drawing of a negative π-meson interaction is shown above. A positive π meson (track 4) was produced in the collision.

The author is grateful to Professor H. L. Anderson for the use of the facilities of the University of Chicago cyclotron. The author is indebted to Mr. A. Rosenfeld and Mr. J. Orear for their assistance with the exposures and for many helpful discussions. Many discussions with Dr. G. Takeda were helpful.

* Supported in part by the Research Committee of the graduate school from funds supplied by the Wisconsin Alumni Research Foundation.

[1] W. F. Fry, Phys. Rev. **91**, 130 (1953); **84**, 385 (1951). W. F. Fry and George R. White, Phys. Rev. **90**, 207 (1953).
[2] W. F. Fry, Nuovo cimento **10**, 490 (1953); Phys. Rev. **85**, 676 (1952).

Far Ultraviolet Radiation from the Cornell Synchrotron*

P. L. HARTMAN AND D. H. TOMBOULIAN
Cornell University, Ithaca, New York
(Received July 17, 1953)

THE existing experimental studies[1-3] of the properties of the radiation due to transversely accelerated high-energy electrons have been confined to the visible and near ultraviolet regions of the spectrum. An attempt was therefore made to extend the region of observation to the vacuum ultraviolet. Since a grazing incidence spectrograph was available and could readily be modified for this purpose, it was decided to omit the observations in the Schumann region and to proceed directly with the exploration of the soft x-ray region (50A to 500A). The spectrograph was equipped with a lightly ruled 30 000-line grating whose radius of curvature was 154 cm. The grazing angle of incidence was set at 4.5° with a resulting calculated short-wavelength limit of 30A.

The spectrograph slit housing was connected to a porthole in the synchrotron "donut" by sections of tubing containing a vacuum gate-valve provided with a retractable quartz window. The latter was used only in the initial determination of the height and direction of the visible beam prior to positioning of the spectrograph. The valve served to isolate the spectrograph chamber from the "donut" of the synchrotron while the spectrograph was being pumped out. Upon evacuation of the spectrograph, the gate-valve was opened, allowing the radiation to pass through the evacuated interconnecting tube and fall directly upon the slit of the spectrograph.

The radiation is emitted tangentially from the electron orbit and is confined to a narrow cone centered on the instantaneous direction of the motion of the electron. The angular opening of the cone is of the order of 1/600 radian for a 300-Mev electron. This property demands that great care be exercised in aligning the axis of the spectrograph (line joining mid-points of grating and slit) with the axis of the cone of radiation. This adjustment was carried out by first observing through a theodolite the image of a visible spot of light at the orbit as reflected by a mirror placed opposite the quartz window located at the end of the porthole tube. The axial direction of the radiation in space was thus established and the spectrograph was slid into position so that its optical axis fell into coincidence with the direction of the light beam. The latter adjustment was also accomplished with the now fixed mirror and theodolite by sighting through them at two reference points fixed in the body of the spectrograph. The reference points were previously so located as to define the axis of the spectrograph. The final alignment was further verified by the use of a photocell placed within the spectrograph so as to detect the light from the central image when the usual trap for the central image was moved out of the way. The various runs reported here were exploratory in nature and were designed to determine whether the radiation could be detected within reasonable exposure times and, if so, to gain qualitative information concerning the intensity distribution and

the possible existence of a short-wavelength limit to the continuous spectrum.[4] Hence, in all the exposures but one, the electrons were accelerated to the peak energy of the synchrotron (310 Mev) so that the spectrum corresponds to the integral of the instantaneous power spectrum over an acceleration cycle. In one run, by turning off the rf voltage early in the acceleration cycle, the maximum energy was lowered to 220 Mev. The exposure times, under the particular operating conditions of the synchrotron, were of the order of 30 minutes except for the low-energy run. With Ilford QI plates, good photographic densities were obtained with the above exposure times.

The following observations are derived by inspection of the photographic records dealing with various runs at the peak energy.

a. A strong continuum is present in the soft x-ray region, which for 310-Mev electrons appears to extend at least down to the instrumental short-wavelength cutoff which is observed to set in at about 55A.

b. The photographic negatives over the 50 to 400A spectral range show no marked density variations, with no sudden drop over the short-wavelength region available under the particular conditions of detection.

c. When thin metallic foils of Be and Al are introduced into the path of the undispersed radiation, the characteristic K and $L_{2,3}$ absorption edges of Be and Al, respectively, are strongly recorded in two orders. (The Be K edge is located at 110A, while the $L_{2,3}$ edge of Al is at 170A.)

d. For the 220-Mev run, the microphotometer trace shows a gradual but definite increase in density, from about 60A on, and attains a peak in the vicinity of 170A, diminishing gradually towards longer wavelengths.

The height of the recorded continuous spectrum here is much smaller than the height of images of line spectra photographed with the same highly astigmatic spectrograph. This characteristic is probably the result of the fact that the space distribution of the radiation is very different from that of conventional light sources.

Various tests have definitely established the absence of fogging of the spectral plates by gamma rays or other sources such as the light from the injector filament. An attempt will be made to carry out a photometric reduction of the plates in order to obtain more quantitative information concerning the spectral energy distribution, at least over that part of the spectrum involving no overlap of the various orders of the instrument.

It is a pleasure to acknowledge the generous assistance of many members of the staff of the Nuclear Laboratory. We also wish to thank the director, Dr. R. R. Wilson, for his continued interest in the problem.

* This work was supported by the Office of Ordnance Research, U. S. Army.

[1] Elder, Langmuir, and Pollock, Phys. Rev. **74**, 52 (1948).
[2] P. Hartman and D. Tomboulian, Phys. Rev. **87**, 233 (1952).
[3] D. Corson, Phys. Rev. **90**, 748 (1953).
[4] J. Schwinger, Phys. Rev. **75**, 1912 (1949).

The Theory of Coulomb Excitation of Nuclei

K. ALDER* AND A. WINTHER
Institute for Theoretical Physics, University of Copenhagen, Copenhagen, Denmark
(Received July 28, 1953)

THE possibility of exciting nuclear states by the electric field of impinging charged particles has been discussed by several authors. We shall here follow the formulation of the theory of the Coulomb excitation process as given by Ter-Martirosyan.[1,2]

The feasibility of performing experiments of this type has recently been demonstrated,[3] and we here report numerical results of use in the application of the theory to the interpretation of the experiments.

The basis for the theory is that the trajectory of the impinging particle can be described by classical mechanics. This is possible if

$$\kappa = 2Z_1Z_2e^2/\hbar v \gg 1 \tag{1}$$

and if the particle loses only a small fraction of its energy in the collision. In the expression (1), Z_1 and Z_2 refer to the charge numbers of the projectile and the target nucleus respectively, and v means the relative velocity.

Usually one will bombard with energies below the Coulomb barrier to ensure that no nuclear interaction takes place, and thus $\kappa \gg 1$ is fulfilled. As the excitation probability is small, one may use quantum-mechanical perturbation theory to find the cross section. The perturbation energy is

$$V(t) = \sum_{p=1}^{A} \frac{Z_1 e_p^3}{|\mathbf{r}_p - \mathbf{r}(t)|}, \tag{2}$$

where $\mathbf{r}_p$ are the coordinates and e_p the charges of the nucleons in the target nucleus, and $\mathbf{r}(t)$ is the coordinate of the projectile in the classical hyperbolic orbit. It is now convenient to expand (2) in multipole components. One gets in this way an expression for the excitation probability as a sum over multipole components. Each term will be proportional to the square of the usual nuclear matrix element for emission of electric 2^n-pole radiation and a definite function $S^{(n)}$ of the orbit of the projectile.

Particularly well suited for Coulomb excitation are the rotational states in rather heavy nuclei for which the quadrupole component of the nuclear matrix elements are especially big.[4] Also the conditions for the semi-classical treatment are well satisfied here.

By taking n equal to 2 and performing an integration over the different orbits, one gets

$$\sigma_{\text{inel}} = \frac{4\pi^2}{25} \cdot \frac{m}{Z_2^2 e^2 \hbar} E B_e(2) g_2(\xi) \tag{3}$$

for the total inelastic cross section for excitation by the electric quadrupole field. The reduced mass is denoted by m, and E is the kinetic energy in the center-of-mass system. The energy-independent quantity

$$B_e(2) = \sum_{\mu, M_f} |\langle i| \sum_{p=1}^{A} e_p r_p^2 Y_{2,\mu}(\theta_p, \varphi_p) |f\rangle|^2 \tag{4}$$

is the reduced transition probability for the electric quadrupole excitation from the initial state i to the final state f with the magnetic quantum number M_f. Further, the $Y_{2,\mu}$ are the normalized spherical harmonics depending on the polar angles θ_p, φ_p of the nucleons in the target nucleus. The function $g_2(\xi)$ depends on the energy through the variable

$$\xi = \frac{\Delta E}{2E} \frac{Z_1 Z_2 e^2}{\hbar v}, \tag{5}$$

which measures the ratio of the collision time to the nuclear period, ΔE being the nuclear excitation.

The function $g_2(\xi)$ is given by

$$g_2(\xi) = \sum_{\mu} \int_1^{\infty} |S_\mu^{(2)}|^2 \epsilon d\epsilon, \tag{6}$$

where ϵ is the eccentricity of the orbit, and where the non-vanishing components of $S^{(2)}$ are

$$S_0^{(2)} = \int_{-\infty}^{\infty} \exp[i\xi(\epsilon \sinh\omega + \omega)] \frac{1}{(\epsilon \cosh\omega + 1)^2} d\omega,$$

$$S_{\pm 2}^{(2)} = -\sqrt{\tfrac{3}{8}} \int_{-\infty}^{\infty} \exp[i\xi(\epsilon \sinh\omega + \omega)] \times \frac{[\cosh\omega + \epsilon \mp i(\epsilon^2 - 1)^{\frac{1}{2}} \sinh\omega]^2}{(\epsilon \cosh\omega + 1)^4} d\omega. \tag{7}$$

These integrals have been evaluated numerically, and the resultant function g_2 is given in Fig. 1.

The yield of γ quanta following the Coulomb excitation provides a measure of the cross section for the excitation. The direction of these quanta is, however, correlated with the direction of the incident particles and the angle in which the exciting projectile is scattered. If one measures only the angle of emission of the γ rays

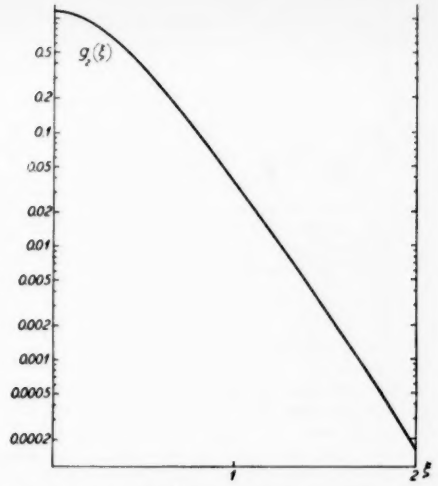

FIG. 1. The function $g_2(\xi)$ plotted on a logarithmic scale, for $0<\xi<2$.

with respect to the incident particles, one obtains an angular distribution which is very similar to the angular correlation between two γ's in cascade. It turns out that the distribution function is

$$W(\theta)=1+B_2a_2(\xi)P_2(\cos\theta)+B_4a_4(\xi)P_4(\cos\theta), \tag{8}$$

which should be compared with the angular correlation in the $\gamma-\gamma$ cascade,

$$I_i \xrightarrow{E2} I_f \xrightarrow{\gamma} I_{ff},$$

given by

$$W'(\theta)=1+B_2P_2(\cos\theta)+B_4P_4(\cos\theta). \tag{9}$$

The I's are the spins of the target nucleus, the Coulomb excited state, and the final state after the γ-emission, respectively. The first γ-transition, being an electric quadrupole radiation, corresponds to the electric quadrupole excitation. The coefficients B_K are given, e.g., by Biedenharn and Rose.[6]

The energy-dependent coefficients a_k are determined by

$$a_2(\xi)=\int_1^\infty\left[S_2{}^2-S_0{}^2+S_{-2}{}^2+\sqrt{6}S_0(S_2+S_{-2})\left(1-\frac{2}{\epsilon^2}\right)\right]\epsilon d\epsilon \times\left\{\int_1^\infty[S_2{}^2+S_0{}^2+S_{-2}{}^2]\epsilon d\epsilon\right\}^{-1},$$

$$a_4(\xi)=\int_1^\infty\left[\frac{3}{32}S_2{}^2+\frac{9}{16}S_0{}^2+\frac{3}{32}S_{-2}{}^2+\frac{5\sqrt{6}}{16}S_0(S_2+S_{-2})\left(1-\frac{2}{\epsilon^2}\right)+\frac{35}{16}S_2S_{-2}\left(1-\frac{8}{\epsilon^2}+\frac{8}{\epsilon^4}\right)\right]\epsilon d\epsilon\times\left\{\int_1^\infty[S_2{}^2+S_0{}^2+S_{-2}{}^2]\epsilon d\epsilon\right\}^{-1}.$$

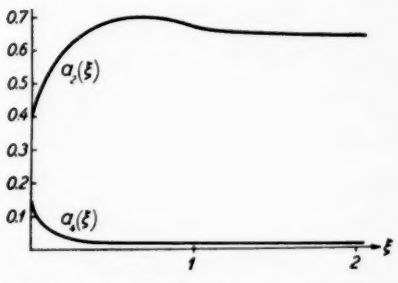

FIG. 2. The angular distribution coefficients $a_2(\xi)$ and $a_4(\xi)$ in the region $0<\xi<2$.

The result of a numerical calculation of these functions is shown in Fig. 2.

As it is seen from this figure, a_4 is so small that P_4 will give almost no contribution. The P_2 term may however be quite big. In the important case of the excitation of the lowest state in even-even nuclei, where $I_i=I_{ff}=0$ and $I_f=2$, the anisotropy amounts to 30 percent. In the case of Ta^{181}, studied by Huus and Zupančič,[3] where $I_i=I_{ff}=7/2$ and $I_f=9/2$, the anisotropy is however only about 0.5 percent.

A more detailed discussion of the theory of Coulomb excitation is being prepared.

* Theoretical Study Group, European Council for Nuclear Research. On leave from Physikalisches Institut der Eidgenössischen Technischen Hochschule, Zürich, Switzerland.

[1] K. A. Ter-Martirosyan, J. Exptl. Theor. Phys. (U.S.S.R.) **22**, 284 (1952).
[2] We have followed the notation used in a review of reference 1 given by A. Bohr and B. Mottelson, Kgl. Danske Videnskab. Selskab, Mat.-fys. Medd. **27**, No. 16 (1953).
[3] T. Huus and C. Zupančič, Kgl. Danske Videnskab. Selskab, Mat.-fys. Medd. **28**, No. 1 (1953); C. McClelland and C. Goodman, Phys. Rev. **91**, 760 (1953).
[4] A. Bohr and B. Mottelson, Phys. Rev. **89**, 316 (1953); Phys. Rev. **90**, 717 (1953).
[5] L. C. Biedenharn and M. E. Rose, Revs. Modern Phys. (to be published).

$Li^7(\gamma,p)He^6$ Cross Section*

B. L. TUCKER AND E. C. GREGG
Case Institute of Technology, Cleveland, Ohio
(Received June 15, 1953)

THE (γ,p) reaction in Li^7 produces β-active He^6. This activity gives a convenient measure of the photonuclear reaction. The β half-life of 0.9 sec allows a typical yield curve to be obtained by a scintillation counter gated to operate during the betatron's dead time. Normalization of the curve was made by direct comparison with copper under the same geometry. The cross section was derived from the yield curve by the photon-difference method.

Figure 1 shows the experimental setup. Stilbene was adopted as a scintillator to avoid a troublesome neutron-capture activity in the NaI crystal previously employed. The discriminator was set on the 625-kev cesium conversion line. Identical geometry with

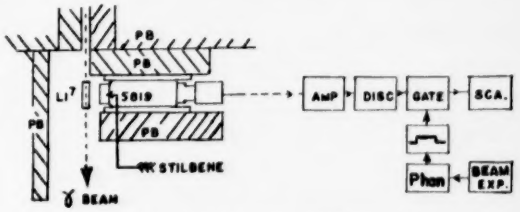

FIG. 1. Experimental arrangement.

comparable self-absorption was obtained by using a laminated copper sample of the same weight as the lithium disk.

The usual self-absorption and discriminator corrections were applied to each yield curve. Then the copper cross section $[Cu^{63}(\gamma,n)Cu^{62}]$ of Katz *et al.*[1] was used to calibrate the absolute scale.

The beam transmission monitor was checked against copper at 13, 15, and 17 Mev and was found to be energy-independent. Under apparently constant betatron trapping conditions, the monitor reading showed no variation with beam energy between 9 and 17 Mev, with only a 5 percent decline at 18 Mev and a 12 percent decline at 19 Mev. These variations were incorporated in the calculated cross section and in the probable errors.

A contaminating neutron-induced 5-min acitivity in the copper was separated by observing the decay of the copper activity over several half-lives.

The only troublesome competing activity in Li^7 would be neutron capture resulting in radioactive Li^8, which has a β decay

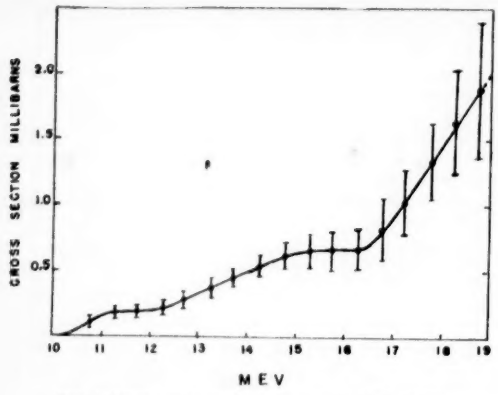

FIG. 2. Cross section *vs* photon energy for $Li^7(\gamma,p)He^6$.

with the same half-life as He^6. However, the neutron-capture cross section of Li^7 is sufficiently low to be negligible.

The indicated probable errors in Fig. 2 do not include a possible 15 percent error in the absolute scale depending upon the error in the Saskatchewan values.[2]

The cross-section curve shown in Fig. 2 is in essential disagreement with the values of Titterton and Brinkley.[3] Using Illford emulsions they observed 118 complete (γ,p) events and obtained a cross section rising to a sharp symmetrical maximum at 15.7 Mev.

* This work was performed under the auspices of the U. S. Atomic Energy Commission.

[1] L. Katz and A. G. W. Cameron, Can. J. Research **29**, 518 (1951).
[2] R. N. H. Haslam *et al.*, Can. J. Phys. **31**, 216 (1953).
[3] E. W. Titterton and T. A. Brinkley, Proc. Phys. Soc. (London) **A66**, 194 (1953).

Errata

The Nuclear Moments of Ta^{181}, B. M. BROWN AND D. H. TOMBOULIAN [Phys. Rev. **88**, 1158 (1952)]. R. E. Trees[1] has been kind enough to call to the author's attention an error in the value of the matrix element $[\Sigma_i\langle 3\cos^2\theta_i-1\rangle_W]_{M=J}$ which was computed in estimating the quadrupole moment of Ta^{181} from hyperfine-structure measurements[2] of the Ta II ground state $^5F_1$. The factor preceding the parenthesis [Eq. (6) of reference 2] should read 4/875. Unfortunately, 8/875 was used in the estimation of the quadrupole moment. With this correction, one arrives at the unusual value $q=11.8\times10^{-24}$ cm^2 for the quadrupole moment. The large discrepancy between this value and that reported by Schmidt[3] forces a re-evaluation of the approximations made in estimating the moment. As yet this has not been carried out. The factors which can be responsible for this discrepancy are (1) the experimentally determined value of B, the quadrupole coupling factor, (2) the angular average mentioned above, and (3) the radial average $\langle 1/r_d{}^3\rangle$. The worst view of the experimental error in the hyperfine-structure measurement will allow perhaps a spread of ±15 percent in the quadrupole moment. The factors mentioned in (2) and (3) depend upon the coupling in the electronic structure. Russell-Saunders coupling was assumed in making these averages on the evidence of the interval rule agreement shown by the two lowest intervals of the ^5F multiplet and the fact that the level whose hyperfine-structure was measured has the g value expected from Russell-Saunders coupling. The disturbing evidence (besides the discrepancy now evident) is the intermixing of the terms of the three low-lying configurations of Ta II and the ratio $(\zeta_d\text{Ta II}/\zeta_d\text{Ta I})$. ζ_d is the d-electron fine-structure splitting factor. This ratio is approximately 1.3 for Ta. For other elements which ionize from the configuration d^ns^2 to d^ns this ratio deviates only slightly from unity. Among the elements tested are several which show better Russell-Saunders coupling than Ta. Trees[4] gives further evidence in support of deviation from Russell-Saunders coupling as a possible reason for the discrepancy. The author wishes to thank Dr. Trees for calling attention to the error and making his paper available to him in advance of publication.

[1] R. E. Trees (private communication).
[2] B. M. Brown and D. H. Tomboulian, Phys. Rev. **88**, 1158 (1952).
[3] T. Schmidt, Z. Physik **121**, 63 (1943).
[4] R. E. Trees (to be published).

Radioactive Charging through a Dielectric Medium, E. G. LINDER AND P. RAPPAPORT [Phys. Rev. **91**, 202 (1953)]

AND

Two-Particle Potential from the Bethe-Salpeter Equation, WILHELM MACKE [Phys. Rev. **91**, 195 (1953)]. Figure 1 of these two Letters were inadvertently interchanged.

Decay of Re^{188} and the Lifetimes of Os^{186m} and Os^{188m}, C. C. MCMULLEN AND M. W. JOHNS [Phys. Rev. **91**, 418 (1953)]. The authors would like to withdraw the statements made concerning the lifetimes of the excited states in Os^{186} and Os^{188} which subsequent experiments have shown to be unreliable.

Gyromagnetic Ratios of Microcrystalline and Macrocrystalline Materials, S. J. BARNETT [Phys. Rev. **90**, 315 (1953)]. In the second line of the fifth paragraph, "(5–80) Permalloy" should be "(4–79) Permalloy." In the next line, "Permalloy" should be "Permalloy (80 percent Ni, 20 percent Fe)." Also, in Footnote 3, "A. S. Kenny" should be "G. S. Kenny."

Directional Effects in the Electric Breakdown of Ionic Crystals, ELMER L. OFFENBACHER AND HERBERT B. CALLEN [Phys. Rev. **90**, 401 (1953)]. The authors regret the omission of acknowledgment of support of the reported research by the U. S. Office of Naval Research.

Interference Terms of the Electron-Neutrino Angular Correlation, MASATO MORITA [Phys. Rev. **90**, 1005 (1953)]. The following corrections should be made in the equations in the left hand column of page 1006:

In the equation for $\mathfrak{W}_{1ST}$, the end of the first line should be $\{L_1-M_0\}$ instead of $\{L_0-M_0\}$. In the equation for $\mathfrak{W}_{1VT}$, the last term should be $+\{\mathfrak{M}^*(\boldsymbol{\alpha})\mathfrak{M}(\beta\boldsymbol{\alpha})+\text{c.c.}\}L_0^-$ instead of $-\{\mathfrak{M}^*(\boldsymbol{\alpha})\mathfrak{M}(\beta\boldsymbol{\alpha})+\text{c.c.}\}L_0^-$. In the equation for $\mathfrak{W}_{1AP}$, the last term should be $+\{\mathfrak{M}^*(\gamma_5)\mathfrak{M}(\beta\gamma_5)+\text{c.c.}\}L_0^-$ instead of $-\{\mathfrak{M}^*(\gamma_5)\mathfrak{M}(\beta\gamma_5)+\text{c.c.}\}L_0^-$.

In addition, in the third last sentence of the Letter, the phrase "tensor interaction" should be replaced by "allowed tensor interaction."

Calculation of Nuclear Binding Energies with Single-Particle Oscillator Wave Functions, ERWIN H. KRONHEIMER [Phys. Rev. **90**, 1003 (1953)]. In Eq. (4) the lower limit of the integral should be 0. In the fourth line of Eq. (5), "$(2l+1-2g-2s)!!$" should read "$2L+1-2g-2s)!!$". In the expression for $\phi_l\{L_1, L_2, k;\ 1\}$, the term "$(2g-2p+2m)$" should appear as the argument of the C-function, not as a factor.

The β Decay of Li^8, D. STP. BUNBURY [Phys. Rev. **90**, 1121 (1953)]. In this letter it was stated that the author's calculations of the theoretical $(\beta-\alpha)$ angular correlation in the decay of Li^8 were in disagreement with those of J. W. Gardner [Phys. Rev. **82**, 283 (1951)]. An error has since been found in these calculations and the revised results are now in agreement with Gardner's.

Author Index to Volume 91

References with (A) are to abstracts of papers presented at meetings of the American Physical Society, and those with (T) designate title only; references with (L) are to Letters to the Editor; references with (E) are to Errata.

Abragam, A. and K. Kambe. Dipolar broadening of quadrupole resonance line width in zero applied field—894
Acquista, N. (see Mann, D. E.)—464(A)
Adair, R. K. (see Fields, R. E.)—441(A)
Adam, J. S. (see Butler, J. P.)—1219
Adams, R. V. (see Whetten, N. R.)—432(A)
Ajzenberg, Fay, C. M. Braams, and W. W. Buechner. Neutrons from proton bombardment of Be^9—463(A)
—— **and W. W. Buechner.** Neutrons from proton bombardment of Be^9—674
Akers, Lawrence K. and Ernest A. Jones. Raman spectrum, force constants, and calculated thermodynamic properties of GeF_4—236(A)
Albers-Schönberg, H., K. Alder, O. Braun, E. Heer, and T. B. Novey. Effect of electric quadrupole interaction on γ-γ directional correlation in Cd^{111}—1287(L)
——, **E. Heer, T. B. Novey, and R. Rüetschi.** Effect of the electric quadruple interaction on the γ-γ directional correlation in Cd^{111}. II—199(L)
Albert, R. D. and E. R. Gaerttner. Neutron capture resonances using (n,γ) scintillation detector—451(A)
Albrecht, H. O. and C. E. Mandeville. Phosphorescence of and energy storage in Ag-activated NaCl—471(A)
—— (see Mandeville, C. E.)—219(A); 470(A); 566
Alder, K. and A. Winther. Theory of Coulomb excitation of nuclei—1578(L)
—— (see Albers-Schönberg, H.)—1287(L)
Aldrich, L. T. Natural variations in abundance of isotopes—442(T)
Alers, P. B. and R. T. Webber. Magnetoresistance of Bi crystals at low temperatures—1060
Alfrey, Turner, Jr. Opening remarks—225(T)
Allen, G. Band structures of one-dimensional crystals with square well potentials—531
—— **and Rolf Landauer.** Energy-band crossings for periodic square well potentials—471(A)
Allen, K. W. (see Almqvist, E.)—1022(L)
Allison, B. A. (see Scherrer, V. E.)—768(L)
Allison, Samuel K. Break-up energy of Be^8—882
Allred, J. C., A. H. Armstrong, and L. Rosen. Interactions of 14-Mev neutrons with protons and deuterons—90
Almqvist, E., K. W. Allen, J. T. Dewan, and T. P. Pepper. $He^3(He^3,p)Li^5$ and $T(He^3,p)He^5$—1022(L)
Almy, G. M. (see Butler, W. A.)—58
Alpher, R. A., J. W. Follin, Jr., and R. C. Herman. Initial conditions in expanding universe and element synthesis—479(A)
—— **and R. J. Rubin.** Transmission of sound pulse through shock wave—1030(A)
Althaus, E. J. and R. D. Sard. Cloud-chamber study of neutron production by sea-level cosmic rays, with particular reference to μ mesons stopped in Pb—373
Altshuler, Saul. Exchange scattering of electron by H atom—1167
Ames, D. P., M. E. Bunker, L. M. Langer, and B. M. Sorenson. Disintegration of Sr^{91} and Y^{91m}—68
Amster, Adolph B. and Quentin Van Winkle. Nucleoprotein monolayers—211(A)
Anderson, G. W., P. S. Freier, and J. E. Naugle. Time and directional study of primary heavy nuclei—431(A)
Anderson, H. L., E. Fermi, R. Martin, and D. E. Nagle. Angular distribution of pions scattered by H—155
Anderson, James L. Green's functions in S-matrix theory—479(A)
Anderson, Kinsey and John R. Winckler. High-altitude cosmic-ray investigation by means of Čerenkov counter. I. Instrumentation details—431(A)
—— (see Winckler, John R.)—431(A)
Anderson, R. L. (see Hunter, L. P.)—1315
Andrew, E. R. Nuclear magnetic resonance modulation correction—425(L)
Angell, C. E. and J. P. Perry. Total cross sections for 37-Mev pions in H—468(A)
—— (see Perry, J. P.)—1289(L)
Annis, M. (see Wilkins, H. C.)—480(A)
Anslow, Gladys A. and Irene S. White. Correlation of infrared and uv spectra of associated alcohols—241(A)
Anthony, D. J., B. Waldman, and W. C. Miller. Elastic scattering of 1.7-Mev electrons—439(A)
Armstrong, A. H. (see Allred, J. C.)—90
Arnowitt, R. Bound states of meson-nucleon system—459(A)
Aronofsky, J. S. Effect of gas slip on unsteady flow of gas through porous media—1032(A)
Artman, J. O. and P. E. Tannenwald. Measurement of permeability tensor in ferrites—1014(L)
Asaro, Frank and I. Perlman. Patterns in α spectra of even-even nuclei—763(L)
Ashkin, Julius and Seymour H. Vosko. Graphical method for obtaining phase shifts from experimental data on meson-nucleon scattering—1248
Austern, N., S. T. Butler, H. McManus, and W. T. Sharp. Angular distributions from (n,p) nuclear reactions—453(A)
Averbach, B. L. (see Warren, B. E.)—233(A)
Azumi, K. Magnetostriction in Fe-Co alloys—434(A)

Babcock, M. L., D. F. Holshouser, and H. Von Foerster. Diode characteristic of hollow cathode—755(L)
Bach, D. R. and P. V. C. Hough. (d,t) reactions and triton wave function—463(A)
Bacher, R. F. Caltech synchrotron and some experiments with high-energy photons—477(T)
Bailey, L. Evan (see Heckman, Harry H.)—1237
Balasubrahmanyam, V. K. (see Rao, A. S.)—764(L)
Balazs, N. L. Energy-momentum tensor of electromagnetic field inside matter—240(A); 408
Baldock, Russell, John R. Sites, L. O. Gilpatrick, and Howard E. Carr. Mass spectrometer analysis of UO_2F_2 in UF_4—242(A)
Ballam, J., D. R. Harris, A. L. Hodson, R. Ronald Rau, George T. Reynolds, S. B. Treiman, and M. L. Vidale. Kinetic energies of V_1^0 particles—1019(L); Momenta of V^0 particles—446(A)
Band, William. Low-temperature diamagnetism of electrons in cylinder—249
Bandtel, Kenneth C., Wilson J. Frank, and Richard Madey. Photoproduction of π^- mesons from D—487(A)
—— (see Frank, Wilson J.)—487(A)
—— (see Godfrey, Charles)—487(A)
Baranger, M. Stark shift and broadening due to electrons—436(A)
Barbour, J. P. (see Dyke, W. P.)—1043
Barkas, Walter H. Analysis of high-energy nuclear disintegrations—477(T)
—— (see Smith, F. M.)—765(L)
Barnes, C. B. (see Heer, C. V.)—412(L)
Barnes, R. G., P. J. Bray, and N. J. Harrick. Spin-orbit and spin-spin interactions in H_2—475(A)

—— (see Bray, P. J.)—475(A)
Barnes, S. W. Pion-nucleon scattering—466(T)
Barnett, C. F. Characteristics of Allen-type electron multiplier—224(A)
Barnett, S. J. Gyromagnetic ratios of microcrystalline materials, erratum—1580(E)
Barr, E. Scott. Sharp shadows as "images"—226(A)
Barr, T. A., Jr. Values of diffusion coefficients for some chain polymers computed from anomalous osmotic pressure data—211(A)
Barrett, P. H. Decay of heavy mesons in nuclear emulsion—446(A)
Barschall, H. H. (see Walt, M.)—441(A)
Bartoe, W. F. (see Protzman, T. F.)—211(A)
Baskir, E. (see Oxley, C. L.)—419(L)
Bass, J. Space and time spectra in homogeneous turbulence—1031(A)
Bassi, P., G. Clark, and B. Rossi. Time delays in air showers—432(A)
Batta, M. E. γ rays from 14-Mev neutron bombardment of C, O, Al, Fe, and Pb—441(A)
Batzel, R. E., W. W. T. Crane, and G. D. O'Kelley. Excitation function for $Al^{27}(d,\alpha p)Na^{24}$ reaction—939
Bauer, Ernst and Ta-You Wu. Origin of ionization in E layer of ionosphere—458(A)
Bauer, S. H. (see Widom, B.)—240(A)
Beams, J. W. Studies of tensile strengths and adhesion of metals by means of high centrifugal fields—239(T)
—— (see Morton, H. S., Jr.)—449(A)
—— (see Robeson, A.)—493(A)
Bearden, J. A., M. D. Earle, J. M. Minkowski, and J. S. Thomsen. Present status of fundamental atomic constants—482(A)
Beck, C. K. Raleigh research reactor—226(T)
Becker, E. W., R. Misenta, and O. Stehl. Difference in viscosity of ortho- and para-deuterium at low temperatures—414(L)
Becker, M., M. Cutler, T. Firle, R. Shulman, and W. Spitzer. Lifetime of minority carriers in localized crystal regions—491(A)
Becker, R. A. (see Shore, F. J.)—1203
Becker, R. L. (see Fields, R. E.)—441(A)
Becker, W. M. and K. Lark-Horovitz. Ge films—230(A)
Beckman, Olof, Torben Huus, and Črtomir Zupančič. Excitation curves for α particles from B^{11} bombarded with protons—606
Beer, A. C. (see Willardson, R. K.)—243(A)
Beers, Yardley and Samuel Weisbaum. Uhf rotational line of HDO—1014(L)
Beiser, Arthur. Zenith angle variation of cosmic-ray meson intensity—446(A)
Belinfante, Frederick J. Deficiency of phenomenological theory of Lamb shift—1285(L)
—— Intrinsic magnetic moment of particle of spin 3/2—477(A)
—— (see Swihart, J. C.)—500(A)
Belmont, E. (see Lehovec, K.)—492(A)
Belser, Richard B. Effect of sputtering rate on resistivity and "aging" of sputtered Ag films—221(A)
—— Versatile radiation oven—246(A)
—— **and Robert J. Raudebaugh.** Structure and aging of thin metal films—449(A); 499(A)
—— (see Raudebaugh, Robert J.)—449(A)
Benade, A. H. Mean life of μ^- mesons stopped in Fe—971
Bendel, W. L. (see Shore, F. J.)—1203
Benedict, T. S. Microwave observation of collision frequency of holes in Ge—1565(L)
—— **and W. Shockley.** Carrier contribution to dielectric constant of Ge—207(A)
Benesch, William and Tait Elder. Relative optical collision diameters from pressure broadening of individual infrared absorption lines—308
Bengston, J. and R. M. Thaler. Phase-shift analysis of high-energy p-p scattering—454(A)
—— (see Thaler, R. M.)—454(A)
Bennett, F. D. (see Bergdolt, V. E.)—1033(A)
Bennett, W. H. and E. O. Hulburt. Magnetic self-focusing of auroral protons—1562(L)
Bent, R. D., T. W. Bonner, and R. F. Sipple. γ rays from disintegration of C^{13} by deuterons—472(A)
Bergdolt, V. E. and F. D. Bennett. Preliminary drag measurements in pressurized range—1033(A)
Bergmann, Peter G. Generalized canonical ensemble in quantum mechanics—477(A)
—— **and Alice C. Thomson.** Generalized statistical mechanics and Onsager relations—180
Bergstein, J. and R. D. Birkhoff. Performance of 125-kv accelerator and spectrometer—223(A)
Berko, Stephan and Frank L. Hereford. Deflection of high-energy electrons in magnetized Fe—1127
Berkowitz, A. E. and A. D. Franklin. Approach to saturation in diluted ferromagnetic powders—206(A)
Berlincourt, Ted G. Relation between de Haas-van Alphen effect and magnetoresistance in Bi—1277(L)
—— **and M. C. Steele.** Method for measuring magnetic moments of superconductors—215(A)
Bernstein, W. (see Schwartz, Robert B.)—883
—— (see Weiss, M. M.)—483(A)
Bershader, Daniel. Shock-tube studies of transient boundary layers in compressible flow—470(A)
—— (see Bradley, L. C.)—469(A)
Bersohn, R. (see Weneser, J.)—1257
Bertaut, E. F. Electric field and energy in dipole lattices—415(L)
Bess, Leon. Possible mechanism for $1/f$ noise generation in semiconductor filaments—1569(L)
Betchov, R. Asymmetry of turbulent functions—470(A)
—— Stability of isotropic turbulence—1031(A)
Bethe, H. A., L. Maximon, and F. Low. Bremsstrahlung at high energies—417(L)
—— (see Cole, F. T.)—481(A)
Biggerstaff, J. A. (see Lafferty, D. L.)—223(A)
Billington, D. S. (see Cleland, J. W.)—238(A)
Biondi, Manfred A. Diffusion cooling of electrons in ionized gases—437(A)
Bird, George R. and Richard C. Mockler. Microwave spectrum of unstable molecule C—S—222(A)
Birkhoff, R. D. (see Bergstein, J.)—223(A)
—— (see Kalil, F.)—505
Birks, J. B. and M. E. Szendrei. Absolute scintillation efficiency of anthracene—197(L)
Birnbaum, Milton, Erich Harth, Leo Seren, and Ralph Tobin. (γ,n) thresholds of Cu^{63} and Ag^{109} based on (γ,n) thresholds of N^{14}, O^{16}, and C^{13}—474(A)
—— (see Harth, Erich)—474(A)
—— (see Seren, Leo)—474(A)
Birnbaum, W. (see Smith, F. M.)—765(L)
Biswas, S. N. Approximate solution of Heitler's integral equation—1026(L)
Bitter, F., H. Plotkin, B. Richter, A. Teviotdale, and J. E. R. Young. Magnetic scanning method for investigating hfs and isotope shift—421(L)
Blackadar, A. K. Second law of eddy thermodynamics—1031(A)
Blanchard, C. H. (see Spencer, L. V.)—240(A)
Blatt, John M. and M. H. Kalos. Ground state of deuteron with tensor forces—444(A)
—— (see Kalos, I. M. H.)—444(A)
—— (see Lustig, Harry)—453(A)

Blau, M., A. R. Oliver, and J. E. Smith. Neutron and meson stars induced in light elements of emulsion—949
Bleakney, W. (see Weimer, D.)—1032(A)
Blewett, J. P. (see Courant, E. D.)—202(L)
Blewitt, T. H. Deformation of Cu single crystals at 300° and 78°K—1115
——, **R. R. Coltman, R. E. Jamison, and J. K. Redman.** Stress-strain curves of Cu single crystal at 4.2°K—448(A)
——, **J. K. Redman, and F. A. Sherrill.** Deformation of Cu crystals at 78°K and 300°K—236(A)
—— (see Coltman, R. R.)—236(A)
—— (see Jamison, R. E.)—237(A)
—— (see Redman, J. K.)—448(A)
Bloch, Ingram and Yü-Chang Hsieh. Nuclear shell structure as many-body phenomenon—240(A)
Block, M. M., S. Passman, and W. W. Havens, Jr. Phenomenological interpretation of π^+ meson production by protons on C—210(A)
Bloembergen, N. (see Willenbrock, F. K.)—1281(L)
Bloom, S. D. and C. O. Muehlhause. Design of high-efficiency low-background fast neutron detector—494(A)
—— (see Toppel, B. J.)—473(A)
Bludman, Sidney. Hard-core interpretation of reaction $p + d \rightarrow \pi^+ + t$—487(A)
Bobb, Franklin C. (see Tipton, Isabel H.)—214(A)
Boch, A. L. and E. D. Hudson. Cyclotron efficiency and power distribution measurements—224(A)
Bockelman, C. K. (see Braams, C. M.)—474(A)
—— (see Buechner, W. W.)—1502
Bodansky, D., A. Sachs, and J. Steinberger. Differential cross sections for scattering of 48-Mev π^+ mesons in H—467(A)
Boehm, F. (see Wu, C. S.)—319
Bollinger, Lowell M., G. E. Thomas, and R. R. Palmer. Application of liquid scintillation neutron detector to time-of-flight spectroscopy—452(A)
—— (see Palmer, R. Ronald)—450(A)
—— (see Thomas, G.)—452(A)
Bömmel, H. and J. L. Olsen. Velocity of sound in superconducting Pb and Sn—1017(L)
Bonet, J. V. and A. V. Bushkovitch. Calculation of diamagnetic and paramagnetic susceptibility of N_2—433(A)
Bonner, T. W. (see Bent, R. D.)—472(A)
—— (see Cook, C. F.)—441(A)
Boorse, H. A. (see Worley, R. D.)—1567(L)
Booth, E. C. (see Rasetti, F.)—315; 1192
Borowitz, Sidney (see Mostov, Philip M.)—465(A)
Borst, L. B. (see Kunstadter, J. W.)—594
Bowen, Dwain B. Debye temperature of Cu_3Au—220(A)
Bowers, Raymond. Thickness of saturated He II film—1016(L)
Bowers, W. A. Application of Thomas-Fermi method to calculation of certain molecular vibration frequencies—242(A)
Bowman, J. C., S. Hayes, and R. Smoluchowski. X-ray study of graphitization—244(A)
Boyd, B. A. (see Domenicali, C. A.)—220(A)
Boyer, R. F. Relations between crystallization and second-order transition—225(T)
Bozorth, R. M. (see Williams, H. J.)—1107
Braams, C. M., C. K. Bockelman, C. P. Browne, and W. W. Buechner. Inelastic scattering of protons from Ca^{40}—474(A)
—— (see Ajzenberg, F.)—463(A)
Brabant, J. M., L. W. Cochran, and R. S. Caswell. Average energy of β rays of P^{32} and Ag^{111}—210(A)
Brachman, Malcolm K. and Roland E. Meyerott. Electron distributions for opacity calculations—437(A)
Bradley, L. C., C. C. Van Voorhis, and D. Bershader. Phosphorescence method for study of surface temperatures in supersonic flow field—469(A)
Braid, T. H. Neutron capture γ rays with scintillation spectrometer—442(A)
Braun, O. (see Albers-Schönberg, H.)—1287(L)
Bray, P. J. and R. G. Barnes. Nuclear shielding in H_2 and D_2—475(A)
—— (see Barnes, R. G.)—475(A)
Bray, Ralph and B. R. Gossick. Effect of transit time on Ge rectifier behavior—1011(L)
—— **and F. van der Maesen.** Thick p-n junctions in Ge—231(A)
Breckenridge, Robert G. Semiconducting intermetallic compounds—461(T)
—— **and William R. Hosler.** Electrical properties of TiO_2 semiconductors—793
——, **W. R. Hosler, and W. Oshinsky.** Electrical properties of InSb—243(A)
Breit, G. (see Thaler, R. M.)—454(A)
Breneman, Edward J. and Dudley Williams. Molecular rotation in liquids—465(A)
Brice, M. K. (see Cork, J. M.)—76; 497(A)
Bridge, H. S., H. Courant, H. DeStaebler, Jr., and B. Rossi. Recent experimental results on S particles—1024(L)
——, **C. Peyrou, B. Rossi, and R. Safford.** V^0 particles in multi-plate cloud chamber—362
Briggs, G. R., S. Singer, and W. K. Jentschke. α-α scattering at 21.8 and 22.9 Mev (proportional counter)—438(A)
Briggs, H. B. and R. C. Fletcher. Absorption of infrared light by free carriers in Ge—1342
—— (see Tanenbaum, M.)—1561(L)
Brooks, Harvey. Cohesive energy of alkali metals—1027(L)
—— 1952 NRC Conference on nature and properties of surfaces of solids—239(T)
Brown, Alexander and F. T. Reding. Infrared study of crystallization of polyethylene—226(A)
Brown, B. M. and D. H. Tomboulian. Nuclear moments of Ta^{181}, erratum—1580(E)
Brown, Fielding and George T. Reynolds. Cosmic-ray star production rates in gases—444(A)
Brown, Frank B., Jr., and A. V. Masket. Star clustering in nuclear emulsions—210(A)
Brown, H. N. (see Shore, F. J.)—1203
Brown, James B. He film flow—489(A)
Brown, R. J. S., K. F. Famularo, H. D. Holmgren, and D. M. Van Patter. Differential cross sections for elastic scattering of 1.0- to 3.25-Mev deuterons by He^4—438(A)
Brown, W. L. n-type surface conductivity on p-type Ge—518
—— **and R. C. Fletcher.** Annealing of bombardment damage in Ge: Experimental—237(A)
—— (see Fletcher, R. C.)—237(A)
Browne, C. P. (see Braams, C. M.)—474(A)
—— (see Buechner, W. W.)—1502
Brueckner, K. A. Radiative corrections to nuclear forces in pseudoscalar theory—761(L)
——, **J. Gell-Mann, and M. L. Goldberger.** Damping of virtual nucleon-pair formation in pseudoscalar meson theory—460(A)
—— (see Chappelear, J.)—480(A)
—— (see Watson, K. M.)—460(A)
Buck, Warren L. (see Swank, Robert K.)—495A; 927
Buder, E. E., J. J. Ruddick, and A. H. Weber. Photoemission of W in region of predicted Schottky deviations—561
Bueche, A. M. Reinforcement of silicone rubber—211(T)

Buechner, W. W., A. Sperduto, C. P. Browne, and C. K. Bockelman. Excited states of K^{40}—1502
—— (see Ajzenberg, Fay)—463(A); 674
—— (see Braams, C. M.)—474(A)
—— (see Sperduto, A.)—473(A)
Bunbury, D. StP. β decay of Li^8, erratum—1580(E)
Bunker, M. F., R. J. Prestwood, and J. W. Starner. Scintillation study of As^{77} and Br^{77}—1021(L)
—— (see Ames, D. P.)—68
—— (see Knight, J. D.)—889
Bunn, C. W. Molecular structure and crystallizability of polymers—225(T)
—— Recent work on structures of crystalline polymers—225(T)
Burke, Edward W. Isotope shift in B III—457(A)
Burkhardt, James L. Dipole photonuclear reactions and independent particle model—420(L)
Burrus, C. A. (see Trambarulo, R.)—222(A)
Burson, S. B. and W. C. Jordan. Argonne Laboratory scintillation coincidence spectrometer—498(A)
—— (see Jordan, W. C.)—497(A)
Burstein, Eli. Optical and photoconductive investigations of impurity levels in Ge and Si—213(T)
—— (see Lax, Melvin)—208(A); 492(A)
—— (see Sclar, N.)—215(A)
Burton, R. L. (see Cobbs, W. H., Jr.)—225(A)
Bushkovitch, A. V. (see Bonet, J. V.)—433(A)
—— (see Herbst, R. F.)—442(A)
Buskirk, A. V., L. R. Etter, C. J. Karzmark, R. H. Rediker, and R. W. Thompson. Magnetic cloud-chamber observations of V particles. I. Apparatus and reduction of data—445(A)
—— (see Thompson, R. W.)—446(A)
Butler, J. P. and J. S. Adam. Radiations of Ra^{227}—1219
Butler, S. T. Stripping and three-body system—488(T)
—— (see Austern, N.)—453(A)
—— (see Friedman, M. H.)—465(A)
Butler, W. A. and G. M. Almy. Photoprotons from Mo^{100} and Mo^{92}—58
Byatt, William J. Calculating approximate cross sections for electron scattering—240(A)
Byram, E. T., T. Chubb, H. Friedman, and N. Gailar. Lyman-α radiation in solar spectrum—1278(L)

Cabrera, N. Role of nucleation-theory in crystal growth—232(T)
Caldwell, W. C. (see Johnson, R. G.)—466(A)
Callen, Herbert B. Thermodynamics of irreversible processes—239(T)
—— (see Dank, M.)—229(A)
—— (see Harrison, Sol E.)—205(A)
—— (see Offenbacher, Elmer L.)—1580(E)
Cameron, A. G. W. and M. M. Hoffman. Angular and energy distributions of photoprotons from Al and Ta—473(A)
Cameron, J. R. (see Eppling, F. J.)—438(A)
Campbell, E. C. and F. Nelson. Chemical separation of 0.82-sec Pb^{207m} from Bi^{207}—499(A)
Campbell, R. B. (see Franklin, A. D.)—205(A)
Campbell, W. H. and J. I. Hopkins. Terphenyl-B liquid neutron detector—224(A)
Carlson, B. C. (see Gerhart, J. B.)—455(A)
Carlson, R. O. (see Fabricand, B. P.)—1403
—— (see Lee, Charles A.)—1395
Carlton, A. G. Optimum filter design for incompletely specified filter and noise processes—438(T)
Carmichael, B. M., M. B. Sampson, and O. E. Johnson. Inelastic scattering of alphas from N^{14}—473(A)
Carr, Howard E. Negative ions in gaseous phase—209(T)
—— (see Baldock, Russell)—242(A)
Carroll, Thomas J. Propagation of short radio waves well beyond horizon—458(A)
Carter, R. S., H. Palevsky, and V. W. Myers. Absorption cross section of Au and B for thermal and cold neutrons—450(A)
—— (see Myers, V. W.)—451(A)
Cartwright, W. F., C. Richman, M. N. Whitehead, and H. A. Wilcox. Production of positive pions by 341-Mev protons on protons—677
—— (see Oxley, C. L.)—419(L)
Case, K. M. and H. Mendlowitz. Measurement of gyromagnetic ratio for free electron: precession and depolarization—475(A)
—— (see Moldauer, P.)—459(A)
Caswell, R. S. (see Brabant, J. M.)—210(A)
Caulk, H. M. (see Davis, L. R.)—431(A)
Chandrasekhar, S. Thermal instability in hydrodynamics and hydromagnetics—488(T)
—— Thermonuclear reactions with light nuclei in stars—488(T)
——, **Donna Elbert, and Gerhard Herzberg.** Shift of 1^1S state of He—1172
Chang, Hung-Chi. Electric conduction at metal-semiconductor and metal-solution interfaces—214(A)
—— (see Morris, L. W.)—215(A)
Chappelear, J. and K. A. Brueckner. Photoproduction of mesons in D—480(A)
Charney, Jule. Use of high-speed computing machines in meteorological predictions—488(T)
Chase, C. E. Ultrasonic measurements in liquid He—489(A)
Chase, D. M. (see Rohrlich, F.)—454(A)
Chatterjee, Santimay and Ajit Kumar Saha. γ-γ angular correlation measurements—200(L)
Cheo, Peter (see Loh, H. Y.)—221(A)
Chiba, R. (see Takemoto, S.)—1024(L)
Chilton, A. B., J. N. Cooper, and J. C. Harris. Stopping power of several elements for protons—495(A)
Chou, C. N. Energy spectra of cosmic-ray photons and electrons from plastic scintillation counter measurements—433(A)
Chraplyvy, Zeno V. Approximate two-body relativistic wave equations—478(A)
—— Reduction of relativistic two-particle wave equations to approximate forms—388
Christian, R. S. and J. L. Gammel. Elastic scattering of protons and neutrons by deuterons—100
Christian, Russell H. and John M. Walsh. Experimental method to determine equation-of-state data for solids by shock-wave measurements—1030(A)
Chubb, T. (see Byram, E. T.)—1278(L)
Clark, A. E., R. A. Grandey, S. K. Kao, and L. Mann. Elastic scattering in nuclear emulsions—467(A)
Clark, G. (see Bassi, P.)—432(A)
Clark, L. B., Sr. Transparent, nonmetallic, electrically conducting film applications—471(A)
Clarke, Edward N. Oxygen-induced surface conductivity on Ge—756(L)
—— **and Robert L. Hopkins.** Electrical conductivity of mechanically distributed Ge surfaces—1566(L)
Clarke, R. L. (see Paul, E. B.)—463(A)
Cleland, J. W., D. S. Billington, and J. H. Crawford, Jr. Low-temperature fast-neutron bombardment of Cu-Be alloy—238(A)
—— (see Crawford, J. H., Jr.)—243(A)
Clement, J. D. (see Okazaki, A.)—440(A)
Clotfelter, B. E. Hall effect in flowing ion clouds—436(A)

Cobbs, W. H., Jr., S. B. Cole, and R. L. Burton. Orientation in polymeric films by infrared and x-ray techniques—225(A)
Cochran, J. F. (see Mapother, D. E.)—216(A)
Cochran, L. W. (see Brabant, J. M.)—210(A)
—— (see Jenkins, G. L.)—210(A); 915
Coester, F. Influence of extranuclear fields on γ-γ directional correlations—452(A)
Cohen, Bernard L. Ga^{64}—74
—— Statistical theory of nuclear reactions—241(A)
——, **R. V. Neidigh, and E. Newman.** Measurement of angular distributions of nuclear reaction products with internal cyclotron beam—486(A)
—— (see Newman, E.)—486(A)
Cohn, Hans O., L. R. Etter, and R. W. Thompson. Cluster-count determination of specific ionization of cloud-chamber tracks—445(A)
Cole, F. T. and H. A. Bethe. Capture of μ mesons in matter—481(A)
Cole, S. B. (see Cobbs, W. H., Jr.)—225(A)
Collins, F. C. Time lag in spontaneous nucleation due to non-steady-state effects—232(T)
Collins, R. J. and H. Y. Fan. Infrared absorption in n-type Ge—230(A)
—— (see Kaiser, W.)—230(A); 1380
Collins, T. L., W. H. Johnson, Jr., and A. O. Nier. Second minimum in packing fraction curve at 40 neutrons—482(A)
Coltman, R. R. and T. H. Blewitt. Effect of fast-neutron bombardment on diffusion in Cu_3Au—236(A)
—— (see Blewitt, T. H.)—448(A)
—— (see Redman, J. K.)—448(A)
Conwell, Esther M. Electrical properties of n-type Ge—208(A)
Cook, C. F. and T. W. Bonner. Scattering of 14–18 Mev neutrons in light elements—441(A)
Cook, Charles J., Emerson Jones, Jr., and Theodore Jorgensen, Jr. Range-energy relations of 10–250 kev protons and He ions in various gases—1417
Cool, R. L. (see Piccioni, O.)—433(A)
Cooper, C. Dewey. Near uv absorption spectrum of p-difluorobenzene vapor—241(A)
Cooper, J. N. (see Chilton, A. B.)—495(A)
Cooper, L. N. and E. M. Henley. μ-mesic atom—480(A)
Coor, T. (see Hornyak, W. F.)—463(A)
Corey, H. E. (see Vogel, F. L.)—230(A)
Cork, J. M., J. M. LeBlanc, W. H. Nester, and M. K. Brice. Nuclear levels in Cs^{131}—76; Radioactive decay of Ba^{131}—497(A)
—— (see Jordan, W. C.)—497(A)
Couling, L. and R. Smoluchowski. Anisotropy of grain boundary diffusion—245(A)
Coulliette, J. H. (see McCay, M. S.)—213(A)
Courant, E. D. Field inhomogeneities in alternating gradient synchrotron—456(A)
——, **M. S. Livingston, H. S. Snyder, and J. P. Blewett.** Origin of strong-focusing principle—202(L)
Courant, H. (see Bridge, H.)—1024(L)
Cowan, D. A. (see Gursky, Herbert)—209(A)
Cox, Everett F. Degeneration of shock wave into sound—1030(A)
Cox, J. T., P. B. Peyton, Jr., and Walter Gordy. Zeeman effect in microwave spectra of CH_3F and CH_3CCD—222(A)
Crane, H. R., R. W. Pidd, and W. H. Louisell. Method of measuring gyromagnetic ratio of free electron—475(A)
—— (see Louisell, W. H.)—475(A)
Crane, W. W. T. (see Batzel, R. E.)—939
Crawford, Frank S., Jr., and M. Lynn Stevenson. $p + p \rightarrow d + \pi^+$ cross section at 340 Mev and 327 Mev—468(A)
Crawford, George W. Measurement of thickness of thin films by employing electron microscope shadowcasting technique—214(A)
Crawford, J. H., Jr., J. W. Cleland, D. K. Holmes, and J. C. Pigg. Thermally unstable disorder in p-type Ge produced by fast neutron bombardment—243(A)
—— (see Cleland, J. W.)—238(A)
Crawford, M. F. and I. R. Dagg. Infrared absorption induced by static electric fields—1569(L)
Crittenden, E. C., Jr., and H. Dieckamp. Change of elastic constants resulting from annealing of Cu and Al cold worked at $-196°C$—232(A)
Croft, George T. and Foster C. Nix. de Haas-van Alphen effect in Sn-Sb alloys—212(A)
Crowell, A. D. (see Soller, T.)—1058
Cummins, William E. Forces and moments acting on body in time-varying potential stream—1029(T)
Cunningham, J. A. Multichannel pulse-height analyzer using storage tube—437(A)
Cutler, M. (see Becker, M.)—491(A)
Czyzak, S. J. (see Wessel, Walter)—986

Dagg, I. R. (see Crawford, M. F.)—1569(L)
Dailey, B. P. (see Solimene, N.)—464(A)
Dalgarno, A. Three-body scattering problems—198(L)
Daly, Richard T., Jr., and Jerrold R. Zacharias. Doppler effects in atomic-beam magnetic-resonance method—476(A)
Damm, C. C. and Lincoln G. Smith. Doublet measurements with mass synchrometer—482(A)
—— (see Smith, Lincoln G.)—481(A)
Danforth, W. E. (see Weinreich, O. A.)—231(A)
Danielson, G. C. (see Gardner, W. R.)—220(A)
—— (see Shaw, William C.)—208(A)
Dank, M. and H. B. Callen. Iteration-variation calculation of electronic structure of diamond—229(A)
Danos, Michael and Stanley Geschwind. Broadening of microwave absorption lines due to wall collisions—1159
Darden, S. E. (see Fields, R. E.)—441(A)
Darin, S. R. (see Taylor, G. R.)—211(A)
Darling, B. T. and P. R. Zilsel. Theory of finite displacement operators and fundamental length—1252
Dash, J. G. (see Goldstein, L.)—490(A)
—— (see Sommers, H. S., Jr.)—489(A)
Daunt, J. G. (see Heer, C. V.)—412(L)
—— (see Horowitz, M.)—1099
Davidson, J. P. Spectrum and half-life of κ meson—1020(L)
—— **and D. C. Peaslee.** Cross terms in allowed shape β spectra—1232
—— **and D. C. Peaslee.** $1/W$ terms in allowed β spectra—442(A)
Davies, E. B. (see Stoner, R. G.)—1032(A)
Davis, L. R., H. M. Caulk, and C. Y. Johnson. Intensity of primary protons and α particles—431(A)
Davis, Luther, Jr., Lawrence Rubin, and W. D. Straub. Recording of temperature-dependent electrical properties of semiconductors—490(A)
Davis, R. H. (see Eppling, F. J.)—438(A)
Davis, V. (see DeCarvalho, H. G.)—224(A)
Davisson, J. W. Electrical breakdown path orientation in alkali halide crystals—228(A)
—— (see Sclar, N.)—215(A)
Day, Harold R. Irradiation-induced photoconductivity in MgO—238(A); 822
Day, Robert B. (see Huus, Torben)—599
Dayton, B. and D. Willard. Decay of V^0 particle into two mesons—348

Dazai, T. (see Takemoto, S.)—1024(L)
DeBenedetti, S. (see Leipuner, L.)—198(L)
DeBretteville, A., Jr. Threshold field and free energy for antiferroelectric-ferroelectric phase transition in $PbZrO_3$—213(A)
Debye, Peter P. Hall effect and conductivity of Ge containing As or Ga as impurities—208(A)
DeCarvalho, H. G., V. Davis, and W. Tesh. Gradation development method for nuclear emulsions—224(A)
Dehmelt, H. G. Nuclear quadrupole resonance in rhombic S and quadrupole moments of S^{33} and S^{35}—313
de Klerk, D. and R. P. Hudson. Adiabatic demagnetization of chromium methylamine alum—278
DeLollis, N. J. (see Ehrlich, P.)—218(A)
DePasquali, G. (see Eby, F. S.)—495(A)
der Mateosian, E. and C. S. Wu. Decay and β spectrum of I^{129}—497(A)
de-Shalit, A. Energy levels of odd-odd nuclei—1479; Ground state of odd-odd nuclei—443(A)
—— (see Mihelich, J. W.)—78; 498(A)
Deshotels, W. J. and A. H. Weber. Effect of strong electrostatic fields on resistance of W wires—448(A)
DeStaebler, H., Jr. (see Bridge, H.)—1024(L)
Deutsch, R. W. Secondary particles resulting from high-energy bombardment—485(A)
Devaney, Joseph J. Theory of α decay—587
Deverall, G. V., K. W. Meissner, and G. J. Zissis. Hfs of resonance lines of In^{115}—297
Dewan, J. T. (see Almqvist, E.)—1022(L)
DeWire, J. (see Wolfe, B.)—446(A)
DeWitt, T. W. (see Padden, F. J.)—217(A)
—— (see Zapas, L. J.)—217(A)
Dexter, D. L. Small-angle scattering of x-rays from cold-worked crystals—448(A)
—— **and W. R. Heller.** Quantum theory of polarizability of idealized crystal—273
Dicke, R. H. (see Hawkins, W. B.)—1008(L)
Dieckamp, H. (see Crittenden, E. C., Jr.)—232(A)
Dienes, G. J. Variable activation energy and motion of lattice defects—1283(L)
—— **and D. A. Kleinman.** Nature of radiation damage in diamond—238(A)
Dillinger, J. R. (see Knudsen, W. C.)—489(A)
Ditzenberger, J. A. (see Fuller, C. S.)—193(L)
Divatia, Ajay S. (see Eppling, F. J.)—438(A)
Dixon, C. E. and C. J. Meechan. Hardness change in Cu irradiated with 1.25-Mev electrons—237(A)
Dobischek, Dietrich, Harold Jacobs, and John Freely. Mechanism of self-sustained electron emission from MgO—804
Dolan, W. W. Current density tables for field emission theory—510
——, **W. P. Dyke, and J. K. Trolan.** Field emission initiated vacuum arc. II. Resistively heated emitter—1054
Dolecek, R. L. Adiabatic magnetization of superconducting sphere—216(A); 490(A)
Domenicali, C. A. and B. A. Boyd. Thermoelectric power and electrical resistivity of dilute solid solution of Si in Cu—220(A)
Donahoe, F. J. Field and temperature dependence of de Haas-van Alphen effect in Zn alloy single crystals—212(A)
Donahue, D. J. (see Jones, K. W.)—879
Donahue, T. M. (see Foderaro, A.)—1561(L)
Douglas, C. A. Atmospheric transmission of light—459(T)
Douglas, R. A. (see Galonsky, A.)—439(A)
—— (see Haeberli, W.)—438(A)
—— (see Jones, K. W.)—482(A); 879
Doyle, Barbara (see Hutchinson, Franklin)—493(A)
—— (see Setlow, Richard)—494(A)
Drawbaugh, Donald (see Dresden, M.)—478(A)
Drell, S. D. and Kerson Huang. Many-body forces and nuclear saturation—1527
——, **K. Huang, and V. F. Weisskopf.** Many-body forces and nuclear saturation—460(A)
Dresden, M. and Donald Drawbaugh. Modified random walk problems—478(A)
Dresner, Lawrence. Spin-orbit coupling in pseudoscalar meson theory—201(L)
Duckworth, Henry E. (see Hogg, Benjamin G.)—1289(L)
DuMond, Jesse W. M. (see Hoyt, Harry C.)—1027(L)
Dunbar, D. N. F., H. K. Reynolds, W. A. Wenzel, and W. Whaling. Stopping cross section of gases for protons and deuterons—496(A)
Dungey, J. W. Origin of cosmic rays—766(L)
Dunlap, W. C., Jr. Acceptor states of Au in Ge—208(A)
—— Electrical properties of Au-Ge alloys—1282(L)
Dyke, W. P., J. K. Trolan, E. E. Martin, and J. P. Barbour. Field emission initiated vacuum arc. I. Experiments on arc initiation—1043
—— (see Dolan, W. W.)—1054
Dyson, F. J. Mass-renormalization with Tamm-Dancoff method—421(L)
—— Scattering of mesons by protons—499(T)
—— Wave function of relativistic system—1543

Earle, M. D. (see Bearden, J. A.)—482(A)
Easterday, Harry T. Radioactivity of Cu^{67}—653
Eatherly, W. P. Theoretical and experimental studies of electronic phenomena in graphite—239(T)
—— (see Rodeback, G. W.)—237(A)
Eby, F. S., W. K. Jentschke, and G. DePasquali. Response of NaI(Tl) scintillation crystals as function of Tl concentration—495(A)
Eckart, Carl. Relation between time-averages and ensemble-averages in statistical dynamics of continuous media—784
Edwards, David F. (see Green, Alex E. S.)—46; 443(A)
Eggen, D. T. and M. J. Laubenstein. Displacement energy for radiation damage in Cu—238(A)
Ehrlich, P. and N. J. DeLollis. Dielectric relaxation in styrene-acrylonitrile copolymer during and after its polymerization—218(A)
Eiland, P. F. (see Pepinsky, R.)—229(A)
Elbert, Donna (see Chandrasekhar, S.)—1172
Elder, Tait (see Benesch, William)—308
Elkind, M. M. and A. Sperduto. Energy levels of B^{11} and B^{12} by (d,p) reaction—463(A)
—— (see Sperduto, A.)—473(A)
Elliott, J. F., S. Legvold, and F. H. Spedding. Magnetic properties of Gd metal—28
Elliott, N. and M. Wolfsberg. Magnetic susceptibility of Wurster's blue between 65° and 356°K—435(A)
Engler, Nicholas A. (see Green, Alex E. S.)—40
Eppling, F. J., J. R. Cameron, R. H. Davis, Ajay S. Divatia, A. I. Galonsky, E. Goldberg, and R. W. Hill. Elastic scattering of protons—438(A)
Epstein, P. S. Absorption of sound in fogs and emulsions—458(A)
Epstein, Saul T. Causal interpretation of quantum mechanics—985
Erickson, R. A. and L. D. Roberts. Apparatus for magnetic measurements at low temperatures—216(A)
—— (see Roberts, L. D.)—488(A)
Eshelby, J. D. Tentative theory of metallic whisker growth—755(L)
Etter, L. R. (see Buskirk, A. V.)—445(A)
—— (see Cohn, Hans O.)—445(A)
—— (see Thompson, R. W.)—446(A)
Ewald, A. H. Solubility of solids in gases—215(A)
Ewald, A. W. Preparation of gray Sn filaments—244(A)

Fabricand, B. P., R. O. Carlson, C. A. Lee, and I. I. Rabi. Molecular beam investigation of rotational transitions. II. Rotational levels of KBr and their hfs—1403
—— (see Lee, Charles A.)—1395
Fader, W. J. (see Sperduto, A.)—473(A)
Fainberg, Joseph (see Schein, Marcel)—479(A); 973
Fairbank, Henry A. (see King, J. C.)—489(A)
Fairbank, W. M. (see Soller, T.)—1058
Famularo, K. F. and G. C. Phillips. Accurate determinations of nuclear reaction energies—1195
—— (see Brown, R. J. S.)—438(A)
—— (see Phillips, G. C.)—462(A)
Fan, H. Y. Infrared absorption in elementary semiconductors—213(T)
—— (see Collins, R. J.)—230(A)
—— (see Forster, J. H.)—229(A)
—— (see Gebbie, H. A.)—230(A)
—— (see Kaiser, W.)—230(A); 1380
—— (see Navon, D.)—491(A)
Fano, U. and L. V. Spencer. Energy spectrum resulting from electron slowing-down—240(A)
Farquhar, R. M. (see Russell, R. D.)—1223
Faust, W. R. (see Scherrer, V. E.)—768(L); 1476
Fechter, H. R. (see Hofstadter, R.)—422(L); 439(A)
Feld, Bernard T. Role of nucleon isobar in high-energy interactions—454(A)
Ferguson, A. J. and H. E. Gove. Resonances in $S^{32}(p,p)S^{32}$—439(A)
Fermi, Enrico. Nucleon polarization in pion-proton scattering—947
—— (see Anderson, H. L.)—155
—— (see Martin, R. L.)—467(A)
Ferry, John D. Relaxation distribution functions of polymers and their concentrated solutions and gels—218(T)
——, **Lester D. Grandine, Jr., and Edwin R. Fitzgerald.** Relaxation distribution function of polyisobutylene in transition from rubberlike to glasslike behavior and its dependence on temperature—217(A)
—— (see Fitzgerald, Edwin R.)—217(A)
Feshbach, Herman, C. E. Porter, and V. F. Weisskopf. Theory of total neutron cross sections—453(A)
—— (see Lomon, Earle)—454(A)
Feynman, R. P. Atomic theory of λ transition in He—1291; Atomic theory of liquid He near 0°K—1301
Fields, R. E., R. K. Adair, R. L. Becker, and S. E. Darden. Total n-p cross section at 1 Mev—441(A)
Fillnow, R. H., E. K. Halteman, and G. F. Mechlin. X-ray and metallurgical studies on neutron-irradiated Cu_3Au—236(A)
Fink, Richard W. and Edwin O. Wiig. Radiations of neutron-deficient Ba and Ce nuclides—194(L)
Finn, George. Evaporation of Cu from Ge—754(L)
Fireman, E. L. Measurement of (n,H^3) cross section in N and its relationship to T production in atmosphere—922
Firle, T. (see Becker, M.)—491(A)
Fisher, John C. Applications of dislocation theory to plastic deformation—205(T)
—— Strength of solid solution alloys—232(A)
Fisher, L. H. (see Kachickas, G. A.)—775
Fitzgerald, Edwin R., Lester D. Grandine, Jr., and John D. Ferry. Dynamic mechanical properties of polyisobutylene—217(A)
—— (see Ferry, John D.)—217(A)
Fleeman, Jerome. Effect of neutron irradiation on phase change in Sn—237(A)
Fletcher, R. C., W. L. Brown, and S. Machlup. Annealing of bombardment damage in Ge: Theoretical—237(A)
—— (see Briggs, H. B.)—1342
—— (see Brown, W. L.)—237(A)
Fletcher, W. H. (see Parker, F. W.)—235(A)
—— (see Shelton, R. D.)—235(A)
Flory, P. J. Equilibrium theory of crystallization—225(T)
Flowers, J. W. (see Shreckengost, R. C.)—224(A)
Floyd, J. J. (see Kunstadter, J. W.)—594
Foderaro, A. and T. M. Donahue. Production of sodium airglow excitation by imprisonment of resonance radiation—1561(L)
Foland, W. D. (see Tipton, Isabel H.)—214(A)
Foley, H. M. (see Sessler, A. M.)—444(A)
Follin, J. W., Jr. (see Alpher, R. A.)—479(A)
Foner, Simon. Hall effect in pure Ti, V, and Cr—447(A)
—— **and Emerson M. Pugh.** Hall effect in ordered and disordered Ni_3Mn—220(A); Hall effects of Co-Ni alloys and of Armco iron—20
Fonger, William H. Cosmic radiation intensity time variations and their origin. II. Energy dependence of 27-day variations—351
Foote, H. L., Jr. Low-energy neutron resonance scattering—450(A)
—— (see Sailor, V. L.)—450(A)
Foote, R. S. and Ben Petree. Operation of electromagnetic electron beam extractor—456(A)
—— (see Koch, H. W.)—455(A)
Ford, Kenneth W. (see Wilets, Lawrence)—1488
Forro, M. Method for determination of maximum energy of weak β emitters—483(A)
Forster, J. H., H. Y. Fan, and K. Lark-Horovitz. Deuteron irradiation of Ge near liquid N temperature—229(A)
Fosdick, Lloyd D. and Hubert M. James. New approximation method for order-disorder problems—1131
Fourie, D. J. Photoelectric effect of thin Bi films—803
Fowler, E. C., W. B. Fowler, R. P. Shutt, A. M. Thorndike, and W. L. Whittemore. Diffusion cloud chamber study of pion interactions in H and He—135
Fowler, J. L., C. H. Johnson, and J. R. Risser. Angular distribution of neutrons scattered from N—441(A)
Fowler, W. A. Experimental results on nuclear reactions in stars—456(T)
—— **and R. G. Thomas.** Analysis of $N^{15}(p,\alpha)C^{12}$ excitation function—473(A)
—— (see Warters, W. D.)—917
Fowler, W. B., R. P. Shutt, A. M. Thorndike, and W. L. Whittemore. Multiple pion production in n-p collisions observed at the cosmotron—758(L)
——, **R. P. Shutt, A. M. Thorndike, and W. L. Whittemore.** Pions and protons from target bombarded by 2.3-Bev protons in cosmotron—479(A)
——, **R. P. Shutt, A. M. Thorndike, and W. L. Whittemore.** Production of V_1^0 particles by π^- mesons in H—1287(L)
—— (see Fowler, E. C.)—135
Francis, Norman C. and Kenneth M. Watson. Elastic scattering of particles by atomic nuclei—454(A)
Frank, Wilson J., Kenneth C. Bandtel, Richard Madey, and Burton J. Moyer. Angular distribution of process $p + d \rightarrow t + \pi^+$—487(A)
—— (see Bandtel, Kenneth C.)—487(A)
—— (see Godfrey, Charles)—487(A)
Franklin, A. D., R. B. Campbell, and J. A. Weinman. Measurement of particle size of ultrafine ferromagnetic powders—205(A)
—— (see Berkowitz, A. E.)—206(A)
Frauenfelder, H. (see Lawson, J. S., Jr.)—484(A); 649
Frazer, B. C. Phase transition in $ND_4D_2AsO_4$—246(A)
—— **and Ray Pepinsky.** Phase transition in CsH_2AsO_4—212(A)
Frederikse, H. P. R. Thermoelectric power in Ge single crystals—491(A)

Freely, John (see Dobischek, Dietrich)—804
Freeman, A. J. Effective nuclear charges for atoms from self-consistent field calculations—1410
Freier, P. S. (see Anderson, G. W.)—431(A)
Freistadt, Hans. Electromagnetic mass in Darling's theory of elementary particles—478(A)
Fremlin, J. H. Nuclear reactions with cyclotron-accelerated He^3—488(T)
French, J. B. and Y. Shimamoto. Theory of multipole radiation—898
Fried, B. D. and R. J. Riddell, Jr. Tomonaga approximation—460(A)
Friedlander, G., Elizabeth Wilson, A. Ghiorso, and I. Perlman. Genetic relationships of 0.8-sec Pb^{207m} isomer—498(A)
—— (see Miller, J. M.)—485(A)
—— (see Welker, Joan P.)—484(A)
Friedman, H. (see Byram, E. T.)—1278(L)
Friedman, M. H. and S. T. Butler. Bose-Einstein condensation of imperfect gas—465(A)
Friedman, Murray. Influence of host in determining radiation sensitivity of bacterial virus—494(A)
Friedrich, L. W. and V. P. Jacobsmeyer. Electrical properties of elementary B—492(A)
Frisch, Harry L. Equipartition principle of generalized canonical ensembles—477(A); 791
—— (see Willis, Charles)—465(A)
Froehlich, Fritz E. and Kurt Sitte. Mean free path for shower production by high-energy π mesons—433(A)
Froman, Darol, James Kenney, and Victor H. Regener. Collision lengths of neutral, penetrating-shower-producing cosmic radiation in light and heavy water—707
Frost, Albert D., Charles R. Mingins, and Lawrence A. Howard. Electric wave filter combining piezoelectric divided electrode units—471(A)
Frost, R. T. and S. S. Hanna. $Li^6(d,t)Li^5(p)He^4$ reaction—462(A)
Frost, Robert H. and Carl E. Nielsen. Specific probable ionization of electrons observed with Wilson cloud chamber—864
Fry, W. F. Nuclear capture of μ^- mesons in photographic emulsions—481(T)
—— π^+ meson production by π^- mesons—1576(L)
—— Unusual π-μ decays in photographic emulsions—130
—— (see John, W.)—1234
Fuller, C. S. and J. A. Ditzenberger. Diffusion of Li into Ge and Si—193(L)
Fultz, Dave. Experiments in fluid mechanics for meteorological purposes—488(T)
Fung, Si-Chang and A. Turkevich. Production of Cu radioactivity in interaction of negative pions and muons with Zn—480(A)
Furst, Milton and Hartmut Kallmann. Fluorescence, phosphorescence, and photostimulation of NaCl (AgCl) with high-energy irradiation—1356; Fluorescent light yields with α, β, and γ radiations—766(L)
Fusfeld, Herbert I. Comparison of resistivity and density changes in cold-worked brass—233(A)
Fuson, Nelson, Marie-Louise Josien, and Conrade C. Hinds. Infrared analysis of associated O—H and O—D stretching vibrations of simple carboxylic acids—234(A)
—— (see Josien, Marie-Louise)—235(A)

Gaerttner, E. R. (see Albert, R. D.)—451(A)
—— (see Yeater, M. L.)—451(A)
Gailar, N. (see Byram, E. T.)—1278(L)
Galonsky, A. I., W. Haeberli, E. Goldberg, and R. Douglas. Inelastic scattering of protons by Ne—439(A)
—— (see Eppling, F. J.)—438(A)
—— (see Haeberli, W.)—438(A)
Gammel, J. L. (see Christian, R. S.)—100
Gardner, W. R. and G. C. Danielson. Electron density in sodium tungsten bronze—220(A)
Garrett, R. E., F. L. Hereford, and B. W. Sloope. Inelastic scattering of d-d neutrons—441(A)
Garth, R. C. (see Hughes, D. J.)—1423
Garwin, R. L. Thermalization of positrons in metals—1571(L)
Gasiorowicz, S. Phenomenological study of meson-nucleon scattering—481(A)
Geballe, Ronald (see Harrison, Melvin A.)—1
Gebbie, H. A., M. Nisenoff, and H. Y. Fan. Photoconductivity and carrier traps in Ge—230(A)
Geisler, A. H. (see Wilson, V. C.)—494(A)
Geller, M. (see von Hippel, A.)—568
Gell-Mann, Murray and M. L. Goldberger. Formal theory of scattering—398
—— **and Valentine L. Telegdi.** Consequences of charge independence for nuclear reactions involving photons—169
—— (see Brueckner, K. A.)—460(A)
Gerhart, J. B., R. Sherr, and B. C. Carlson. Annihilation of fast positrons in flight—455(A)
—— (see Sherr, R.)—909
Gerjuoy, E. Theory of (d,p) reactions—453(A); 645
Geschwind, Stanley (see Danos, Michael)—1159
Ghiorso, A. (see Friedlander, G.)—498(A)
Ghosh, S. N. (see Trambarulo, R.)—222(A)
Gibbons, J. H. and Henry W. Newson. Neutron resonances in Bi, Tl, and Pb—209(A)
Gibbs, Julian H. Ferroelectricity in rochelle salt—447(A)
Gifford, Frank, Jr. Turbulent diffusion from volume source with nonuniform initial distribution—1031(A)
Gilleo, M. A. Photoemission from Ag into AgCl, KBr, NaCl, and new bands of photosensitivity in AgCl—534
Gillon, L. P. (see Mihelich, J. W.)—498(A)
Gilmore, F. R. Compressibility and thermal effects in cavitation—1029(T)
Gilpatrick, L. O. (see Baldock, Russell)—242(A)
Givin, H. H. (see Jenkins, G. L.)—210(A)
Glaser, Donald A. Bubble chamber tracks of penetrating cosmic-ray particles—762(L); Possible bubble chamber for study of ionizing events—496(A)
Glasser, R. G. (see Schein, Marcel)—479(A); 973
Glauber, Roy J. Potential scattering at high energies—459(A)
Glick, Harvey L. and W. F. Witzig. Resistivity of Cu_3Au during neutron irradiation—236(A)
Godfrey, Charles, Kenneth C. Bandtel, Wilson J. Frank, and Richard Madey. Production of tritons in d-d collisions—487(A)
Goertz, Matilda (see Williams, H. J.)—1107
Gokhale, G. S. (see Rao, A. S.)—764(L)
Goldberg, E. (see Eppling, F. J.)—438(A)
—— (see Galonsky, A.)—439(A)
—— (see Haeberli, W.)—438(A)
Goldberg, M. D. and J. A. Harvey. Coherent cross sections of Fe and Ni—451(A)
Goldberger, M. L. (see Brueckner, K. A.)—460(A)
—— (see Gell-Mann, M.)—398
Goldemberg, J. (see Montalbetti, R.)—659
Goldgraber, Howard D. Configuration interaction in Mo II—456(A)
Goldhaber, Gerson and S. Goldhaber. Inelastic scattering of negative pions—467(A)
Goldhaber, S. (see Goldhaber, Gerson)—467(A)
Goldman, J. E. (see Urquhart, Helen M. A.)—435(A)
Goldowski, N. Is it possible to teach physics to humanities students?—227(A)

Goldschmidt-Clermont, Y., L. S. Osborne, and A. W. Winston. Angular distribution of mesons from 320-Mev photons on protons—468(A)
Goldstein, Jack S. Properties of Salpeter-Bethe two-nucleon equation—461(A); 1516
Goldstein, L., H. S. Sommers, Jr., and J. G. Dash. Transmission of slow neutrons by liquid He—490(A)
Good, R. H., Jr. (see Miller, S. C., Jr.)—174
Good, W. M. Nuclear reactions with He^3 nuclei—226(T)
——, **W. E. Kunz, and C. D. Moak.** $He^3 + He^3$ reaction—462(A)
—— (see Kunz, W. E.)—676
Goodenough, J. B. Nucleation centers for domains of reverse magnetization—434(A)
Goodman, Clark (see Guernsey, Janet B.)—440(A)
—— (see Kay, Robert)—472(A)
—— (see Kiehn, R. M.)—66
—— (see McClelland, Clyde L.)—760(L)
Goodrich, M., J. S. Levinger, and W. Payne. Bremsstrahlung from P^{32} betas—455(A); 1225
—— (see Payne, W.)—497(A)
Gopalakrishnan, K. (see Tomlinson, E. P.)—484(A)
Gordy, Walter M. 1- to 2-mm wave spectroscopy—209(T)
—— (see Cox, J. T.)—222(A)
—— (see Hill, Robert M.)—222(A)
—— (see Mockler, Richard C.)—222(A)
—— (see Trambarulo, R.)—222(A)
—— (see Venkateswarlu, Putcha)—222(A)
Gossett, C. R. (see Phillips, G. C.)—462(A)
Gossick, B. R. Post-injection barrier emf of p-n junctions—1012(L)
—— (see Bray, R.)—1011(L)
Gouza, J. J. (see Protzman, T. F.)—211(A)
Gove, H. E. and E. B. Paul. Yield and angular distribution of γ rays from $B^{11}(p,\gamma)C^{12}$—463(A)
—— (see Ferguson, A. J.)—439(A)
Grad, Harold. Validity of Boltzmann equation—1031(T)
Graham, Irven C., David Pomeroy, W. C. McGarvey, and John G. Randall. Biophysical study of burns—214(A)
Grandey, R. A. (see Clark, A. E.)—467(A)
Grandine, Lester D., Jr. (see Ferry, John D.)—217(A)
—— (see Fitzgerald, Edwin R.)—217(A)
Green, Alex E. S. and David F. Edwards. Discontinuities in nuclear mass surface—46; 443(A)
—— **and Nicholas A. Engler.** Mass surfaces—40
Green, Farno L. Electromagnetic shims for focusing in fixed-frequency cyclotron—223(A)
Green, Louis C., Marjorie M. Mulder, and Paul C. Milner. Correlation energy in ground state of He I—35
Green, M. (see Keck, P. H.)—472(A)
Greenberg, J. Mayo. Scattering approximations for transparent nucleus model—454(A)
Gregg, E. C. (see Tucker, B. L.)—1579(L)
Gregory, Christopher. Construction of conservation equations for nonlocal field theories—770(L)
Grimes, D. M., L. W. Orr, and M. H. Winsnes. Reversible susceptibility in ferrimagnetic materials—435(A)
Gropp, Armin H. (see Letaw, Harry, Jr.)—235(A)
Grosof, Gerard M. (see Weinreich, Gabriel)—195(L)
Gross, E. P. Electron motion in polar crystals—228(A)
—— (see von Hippel, A.)—568
Grosse, A. V. (see Javan, A.)—222(A)
Grunwald, Ernest (see Marshall, Henry P.)—214(A)
Guernsey, Janet B. and Clark Goodman. Total neutron cross section of liquid A—440(A)
Gugelot, P. C. and H. A. Lauter. Inelastic scattering of 18.3-Mev protons—486(A)
Guinier, A. Possibilities of x-ray small-angle scattering for study of crystal imperfections—239(T)
Gursky, Herbert, Barbara Winnemore, and D. A. Cowan. Ranger study of Po-Be neutron spectrum—209(A)
Gursky, Judith Cassidy and P. K. S. Wang. Determination of x-ray spectrum from absorption measurements by Laplace transformation—239(A)
Gutowsky, H. S. and B. R. McGarvey. Nuclear magnetic resonance in Th compounds—81
Gutzwiller, Martin. Quantum electrodynamics in space of constant curvature—478(A)

Haeberli, W., A. Galonsky, E. Goldberg, and R. Douglas. Elastic scattering of protons by Ne—438(A)
—— (see Galonsky, A.)—439(A)
Hagstrum, Homer D. Electron ejection from Ta by He^+, He^{++}, and He_2^+—543
Hahn, Beat. Scintillations produced by α particles in CsI—772(L)
Hahn, T. M. (see Jenkins, G. L.)—210(A); 915
—— (see Lafferty, D. L.)—223(A)
Hall, R. W. (see Maxwell, L. R.)—206(A)
Halpern, J. and E. V. Weinstock. Photodisintegration of deuteron at 20 Mev—934
—— (see Weinstock, E. V.)—461(A)
Halteman, E. K. (see Fillnow, R. H.)—236(A)
Hamilton, J. Fredholm theory of S matrix—1524
Handley, T. H. (see Jones, W. H.)—486(A)
—— (see Newman, E.)—486(A)
Hanna, S. S. (see Frost, R. T.)—462(A)
—— (see Pruitt, J. S.)—463(A)
—— (see Shafroth, S. M.)—483(A)
Hansen, K. F. (see Kiehn, R. M.)—66
Hanson, H. P. and H. W. Schrader. Measurements of K edge jump ratios with linear motion x-ray spectrometer—457(A)
Harbottle, Garman. Half-life of Tl^{204}—1234
Harrick, N. J. (see Barnes, R. G.)—475(A)
Harris, D. R. (see Ballam, J.)—446(A); 1019(L)
Harris, J. C. (see Chilton, A. B.)—495(A)
Harris, S. P., C. O. Muehlhause, D. Rose, H. P. Schroeder, G. E. Thomas, Jr., and S. Wexler. Thermal n-p capture—125
Harrison, Melvin A. and Ronald Geballe. Simultaneous measurement of ionization and attachment coefficients—1
Harrison, Sol E. and Herbert B. Callen. Electronic interactions in ferromagnetic metals—205(A)
Hart, Edward W. Yield point strain—232(A)
Harth, Erich, Leo Seren, Milton Birnbaum, and Ralph Tobin. Thresholds for reactions $Cu^{63}(\gamma,n)Cu^{62}$ and $Ag^{109}(\gamma,n)Ag^{108}$—474(A)
—— (see Birnbaum, Milton)—474(A)
—— (see Seren, Leo)—474(A)
Hartman, P. L. and D. H. Tomboulian. Far uv radiation from Cornell synchrotron—1577(L)
Harvey, J. A. (see Goldberg, M. D.)—451(A)
Haskin, D. M. (see Schein, Marcel)—479(A); 973
Hastings, Samuel (see Lehnert, Richard)—1032(A)
Havas, Peter. Classical equations of motion of point particles—997
—— (see Mehl, Clarence R.)—393
Havens, W. W., Jr. (see Block, M. M.)—210(A)
—— (see Melkonian, E.)—450(A)
Hawkins, W. B. and R. H. Dicke. Polarization of Na atoms—1008(L)
Hayes, S. and R. Smoluchowski. Small-angle x-ray scattering in proton-irradiated diamond—244(A)
—— (see Bowman, J. C.)—244(A)
Haynes, C. W. and R. Smoluchowski. Grain boundary self-diffusion in body-centered lattice—245(A)
Haynes, J. R. (see Smith, Charles S.)—491(A)

Haynes, Sherwood K. (see Kerr, Robert J.)—214(A)
Heckman, Harry H. and L. Evan Bailey. Large-angle scattering of π^- mesons in Al, Cu, and Pb—1237
Heckman, R. C. and H. Sponer. Near uv vapor spectrum of thianaphthene—242(A)
Heer, C. V., C. B. Barnes, and J. G. Daunt. Magnetic refrigerator for maintaining temperatures below 1°K—412(L)
Heer, E. (see Albers-Schönberg, H.)—199(L); 1287(L)
Heikes, Robert R. Magnetic properties of pyrrhotite—212(A)
Hein, R. A. (see Steele, M. C.)—490(A)
Heindl, C. (see Sheer, C.)—449(A)
Heller, W. R. (see Dexter, D. L.)—273
Hemmendinger, Arthur. Interactions of T and He^3 with light nuclei below 5 Mev—488(T)
Hemstreet, H. W. and J. M. Reynolds. Electrical resistance of graphite at low temperatures—242(A)
—— (see Reynolds, J. M.)—1152
Henisch, H. K. Transistor experiments on binary Pb compounds—213(T)
Henkels, H. W. and J. Maczuk. Anisotropic resistivities of Se crystals at high frequencies—1562(L)
Henley, E. M. and M. A. Ruderman. Nuclear forces from extended sources—480(A)
—— (see Cooper, L. N.)—480(A)
Henry, Warren E. Magnetic saturation and apparent molecular fields of $MnCl_2 \cdot 4H_2O$—435(A)
Henshaw, D. G. and D. G. Hurst. Neutron diffraction by liquid He—1222
——, **D. G. Hurst, and N. K. Pope.** Neutron diffraction by liquid O_2, N_2, and A—472(A)
Herbst, R. F. and A. V. Bushkovitch. Pauli form of β decay matrix elements—442(A)
Hereford, Frank L. Polarized photons—226(T)
—— (see Berko, Stephan)—1127
—— (see Garrett, R. E.)—441(A)
Herlin, Melvin A. (see Rogers, D. H.)—489(A)
—— (see Waldron, S.)—447(A)
Herman, Frank. Energy band structure of diamond and Ge crystals—491(A)
Herman, R. C. (see Alpher, R. A.)—479(A)
Hertzberg, Abraham and William E. Smith. C.A.L. hypersonic test facility—1029(A)
—— **and W. Squire.** Shock tube for studying chemical kinetics—469(A)
Herzberg, Gerhard (see Chandrasekhar, S.)—1172
Heydenburg, N. P. and G. M. Temmer. α-particle scattering in N—439(A)
Heyman, R. J., A. Sherman, and T. Schiffman. Pressure multiplication in reentrant corners—1032(A)
Hill, David L. (see Wilets, Lawrence)—1488
Hill, F. K. Boundary layer hypersonic flow—1029(A)
Hill, R. D. Auger electron intensities—770(L)
—— (see Swan, J. B.)—424(L)
Hill, R. W. (see Eppling, F. J.)—438(A)
Hill, Robert M. and Walter Gordy. Temperature dependence of line breadths of O_2—222(A)
Hinds, Conrade C. (see Fuson, Nelson)—234(A)
Hines, R. L. Excitation function for $Mn^{55}(\gamma,3n)Mn^{52}$—474(A)
Hobstetter, John. Nucleation of solid-solid transitions—232(T)
Hodson, A. L. (see Ballam, J.)—446(A); 1019(L)
Hoerni, Jean A. and James A. Ibers. Complex amplitudes for electron scattering by atoms—1182
Hoffmann, Banesh. Similarity theory of relativity and Dirac-Schrödinger theory of electrons—751
Hoffman, M. M. (see Cameron, A. G. W.)—473(A)
Hofstadter, R., H. R. Fechter, and J. A. McIntyre. Electron scattering from nuclei at high energies—439(A)
——, **H. R. Fechter, and J. A. McIntyre.** Scattering of high-energy electrons and method of nuclear recoil—422(L)
Hogan, C. L. Electromagnetic phenomena in ferrites—461(T)
Hoge, Harold J. Series method for comparison of resistances—493(A)
Hogg, Benjamin G. and Henry E. Duckworth. Evidence for region of extra nuclear stability between 82- and 126-neutron shells—1289(L)
Holmes, D. K. (see Crawford, J. H., Jr.)—243(A)
Holmgren, H. D. (see Brown, R. J. S.)—438(A)
Holshouser, D. F. (see Babcock, M. L.)—755(L)
Holstein, T. Electromagnetic absorptivity of metals at low temperatures—490(A)
Honig, Richard E. Mass spectrometric study of sublimation of graphite—465(A)
Hopkins, J. I. (see Campbell, W. H.)—224(A)
—— (see Porter, P. T.)—209(A)
Hopkins, Robert L. (see Clarke, Edward N.)—1566(L)
Hornyak, W. F. and T. Coor. Capture γ rays from proton bombardment of Be—463(A)
Horowitz, M. and J. G. Daunt. Electronic and lattice specific heats in W, Mo, and Re—1099
Hosler, William R. (see Breckenridge, Robert G.)—243(A); 793
Hough, P. V. C. (see Bach, D. R.)—463(A)
Howard, Lawrence A. (see Frost, Albert D.)—471(A)
Howard, Louis N. and J. Samuel Smart. Specific heat discontinuity in antiferromagnets and ferrites—17
Howland, J. J., Jr. (see Welker, Joan P.)—484(A)
Hoyt, Harry C. and Jesse W. M. DuMond. γ radiation following decay of I^{131}—1027(L)
Hsiao, C. A. and V. L. Telegdi. Mechanism of reaction $O^{16} + h\nu \rightarrow 4He^4$—473(A)
Hsieh, Yü-Chang (see Bloch, Ingram)—240(A)
Huang, Kerson (see Drell, S. D.)—460(A); 1527
Huddlestone, R. H. Compton scattering on nucleons—461(A)
Hudson, D. E. (see Johnson, R. G.)—466(A)
—— (see Shaw, William C.)—208(A)
Hudson, E. D. (see Boch, A. L.)—224(A)
Hudson, R. P. (see de Klerk, D.)—278
Huebner, W. F. (see Phelps, John)—496(A)
Hughes, D. J., R. C. Garth, and J. S. Levin. Fast-neutron cross sections and nuclear level density—1423
—— (see Kato, W. Y.)—450(A)
—— (see Palevsky, H.)—451(A)
Hughes, Raymond H. Isotope shift in arc spectrum of Li—457(A)
Hughes, Vernon W., Gardiner Tucker, Emlyn Rhoderick, and Gabriel Weinreich. Magnetic moment of He atom in metastable triplet state—828
—— **and Gabriel Weinreich.** Effect of nuclear structure on hfs of He^3—196(L)
—— (see Perl, William)—842
—— (see Weinreich, Gabriel)—195(L)
Huibregtse, E. J. and L. P. Hunter. Current carrier lifetimes deduced from Hall coefficient and resistivity measurements—208(A)
—— (see Hunter, L. P.)—1315
Hulburt, E. O. (see Bennett, W. H.)—1562(L)
Hunter, L. P. Current carrier mobility ratio in semiconductors—207(A); 579
——, **E. J. Huibregtse, and R. L. Anderson.** Current carrier lifetimes deduced from Hall coefficient and resistivity measurements—1315

—— (see Huibregtse, E. J.)—208(A)
Huntington, H. B. Mobility of interstitial atoms in face-centered metal—1092
——, G. A. Shirn, and E. S. Wajda. Activation entropies for diffusion mechanisms—246(A)
Hurley, J. P. (see Whittle, C. E.)—498(A)
Hurst, D. G. (see Henshaw, D. G.)—472(A); 1222
Hutchinson, Franklin and Barbara Doyle. Inactivation of bovine serum albumin with low-voltage electrons—493(A)
—— (see Phelps, John)—496(A)
Hutchison, Thomas S. Precipitation effects in Cu-Fe alloys—449(A)
—— (see Reekie, James)—490(A)
Huus, Torben and Robert B. Day. γ radiation from B^{11} bombarded by protons—599
—— (see Beckman, Olof)—606

Ibers, James A. (see Hoerni, Jean A.)—1182
Inn, Edward C. Y. Photoionization of molecules in vacuum uv—1194
—— (see Watanabe, K.)—436(A); 1155
Innes, Frederick R. Matrix elements of spin-spin interaction—31
Iwersen, Eric, W. S. Koski, and Franco Rasetti. Triton-induced activities in Mg and Al—1229

Jaccarino, V. (see King, J. G.)—209(A); 476(A)
Jacobs, Donald H., Milton E. Pugh, and Seymour Scholnick. High-accuracy, high-speed shaft position digitalizer—492(A)
Jacobs, Harold (see Dobischek, Dietrich)—804
Jacobsmeyer, V. P. (see Friedrich, L. W.)—492(A)
Jakobson, M. J., A. G. Schulz, and R. S. White. Production of charged photomesons from He. H-He ratios—695
James, Hubert M. (see Fosdick, Lloyd D.)—1131
Jamison, R. E. and T. H. Blewitt. Deformation characteristics of reactor-irradiated Cu single crystals at 78°K and 300°K—237(A)
—— (see Blewitt, T. H.)—448(A)
Jarmie, Nelson, Gordon W. Repp, and R. Stephen White. Positive photomesons from H at 0°—1023(L)
—— (see White, R. Stephen)—468(A)
Jastram, P. S. (see Robinson, J. E.)—498(A)
—— (see Whittle, C. E.)—498(A)
Jastrow, Robert. Low-energy properties of nucleon-nucleon interaction—749
—— Saturation of nuclear forces—460(A)
Jaumot, Frank E., Jr., and Leonard Muldawer. Strain and crystallite size in experimental Fe powders—232(A)
—— (see Sanville, W. W.)—220(A)
—— (see Sutcliffe, Charles H.)—221(A)
Javan, A., G. Silvey, C. H. Townes, and A. V. Grosse. Quadrupole moments of Mn^{55}, Re^{185}, and Re^{187}—222(A)
Jeffries, C. D. and P. B. Sogo. Nuclear magnetic moment of Cr^{53} and Sr^{87}—1286(L)
Jelatis, J. G. (see von Hippel, A.)—568
Jen, C. K. Zeeman effect in microwave spectroscopy—458(T)
Jenkins, G. L., L. W. Cochran, H. H. Givin, J. L. Ryan, T. M. Hahn, and B. D. Kern. Angular distribution of 12-Mev γ rays from proton bombardment of B—210(A); G. L. Jenkins, L. W. Cochran, B. D. Kern, and T. M. Hahn—915
Jenkins, T. (see Luckey, D.)—468(A)
Jentschke, W. K. (see Briggs, G. R.)—438(A)
—— (see Eby, F. S.)—495(A)
—— (see Kerman, R. O.)—438(A)
—— (see Lawson, J. S., Jr.)—484(A)
John, W. and W. F. Fry. π^- and μ^- meson-induced fission—1234
Johns, M. W. (see McMullen, C. C.)—418(L); 1580(E)
Johnson, C. H. (see Fowler, J. L.)—441(A)
—— (see Trail, Carroll C.)—474(A)
Johnson, C. Y. (see Davis, L. R.)—431(A)
Johnson, Edgar G. and Alfred O. Nier. Angular aberrations in sector-shaped electromagnetic lenses for focusing beams of charged particles—10
Johnson, F. F. (see Tittman, J.)—452(A)
Johnson, J. B. and K. G. McKay. Secondary electron emission of crystalline MgO—582
Johnson, John L. and J. L. McHale. Calculation of half-widths of one-body resonances—87
—— (see McHale, J. L.)—452(A)
Johnson, O. E. (see Carmichael, B. M.)—473(A)
Johnson, R. G., W. C. Caldwell, D. E. Hudson, and F. H. Spedding. Mass spectrometric positive ion technique for determining phase transition temperatures and heats of transformation in metals—466(A)
Johnson, T. H. Research program of AEC—442(T)
Johnson, V. A. and K. Lark-Horovitz. Theory of thermoelectric power in semiconductors—230(A)
Johnson, W. H., Jr. (see Collins, T. L.)—482(A)
Jones, Emerson, Jr. (see Cook, Charles J.)—1417
Jones, Ernest A. (see Akers, Lawrence K.)—236(A)
Jones, G. A. (see Wilkinson, D. H.)—1575(L)
Jones, K. W., D. J. Donahue, M. T. McEllistrem, R. A. Douglas, and H. T. Richards. Break-up energy of Be^8—879
——, M. T. McEllistrem, R. A. Douglas, and H. T. Richards. Comparison of nuclear and γ-ray absolute energy scales—482(A)
Jones, Lawrence W. and Kent M. Terwilliger. Photoneutron production excitation functions to 320 Mev—699
Jones, Royce J. Oak Ridge 44-in. cyclotron—223(A)
Jones, W. H., J. H. Paehler, T. H. Handley, and A. Timnick. Yield distribution in proton fission of U—486(A)
Jordan, W. C., J. M. Cork, and S. B. Burson. Decay scheme for $_{66}Dy^{165m}$ (1.25 min) and $_{66}Dy^{165}$ (2.3 hr)—497(A)
—— (see Burson, S. B.)—498(A)
Jorgensen, Theodore, Jr. (see Cook, Charles J.)—1417
Josien, Marie-Louise, Nelson Fuson, and Essie M. Shelton. Infrared study of influence of molecular structure on carbonyl band in polycyclic quinones—235(A)
—— (see Fuson, Nelson)—234(A)

Kachickas, G. A. and L. H. Fisher. Formative time lags of uniform field breakdown in A—775
Kahn, Bernd and W. S. Lyon. K^{42} decay—1212
Kaiser, H. F. Electron cyclotrons (microtrons) for X- and K-band operation—456(A)
—— Relativistic particle cyclotron with electrostatic focusing—499(A)
Kaiser, W., R. J. Collins, and H. Y. Fan. Infrared absorption in p-type Ge—230(A); 1380
Kalil, F. and R. D. Birkhoff. Straggling distributions for electrons in passing through thin foils—505
Kallmann, Hartmut (see Furst, Milton)—766(L); 1356
Kalos, M. H. and J. M. Blatt. Ground state of deuteron with tensor forces—444(A)
—— (see Blatt, J. M.)—444(A)
Kambe, K. (see Abragam, A.)—894
Kandel, R. J. Ionization and dissociation of nitromethane by electron impact—436(A)
Kane, R. P. (see Sarabhai, V.)—688
Kao, S. K. (see Clark, A. E.)—467(A)

Kaplon, M. F., J. Z. Klose, D. M. Ritson, and W. D. Walker. Absorption mean free path of high-energy nucleonic component of cosmic radiation—1573(L)
Karzmark, C. J. (see Buskirk, A. V.)—445(A)
—— (see Thompson, R. W.)—446(A)
Kasper, J. S. (see Wilson, V. C.)—494(A)
Kastner, J. and G. N. Whyte. Half-life of Co^{60}—332
Katcoff, Seymour and William Rubinson. Yield of Xe^{133} in thermal neutron fission of U^{235}—1458
Kato, W. Y., Marilyn J. Stafne, J. S. Levin, and D. J. Hughes. Neutron resonances in Ag—450(A)
Katz, L. (see Montalbetti, R.)—659
Katz, Robert. Pairing effect in nuclei and isomerism—1487
Kay, Robert, Hans Mark, and Clark Goodman. Angular distribution of neutrons from $C^{14}(p,n)N^{14}$—472(A)
Keck, Paul H., M. Green, and M. L. Polk. Shapes of floating liquid zones between solid rods—472(A)
—— **and Wendell Van Horn.** Surface tension of liquid Si and Ge—243(A); 512
Keesom, P. H. and N. Pearlman. Atomic heat of Ge below 4°K—215(A); 1347; Heat capacity of KCl below 4°K—1354
Keffer, Frederic. Dipolar anisotropy in cubic ferromagnetic crystals—206(A)
Keister, G. L. (see Schmidt, F. H.)—483(A)
Keller, F. L. and A. H. Nielsen. Infrared spectrum and molecular constants of DBr—235(A)
Keller, W. E. (see Sommers, H. S., Jr.)—489(A)
Kendall, J. M. Compressible flow of viscous fluid in capillary connected to closed vessel—470(A)
Kenney, James (see Froman, Darol)—707
Kerman, R. O., R. Nilson, and W. K. Jentschke. α-α scattering at 21.6, 22.4, and 22.8 Mev (nuclear plate)—438(A)
Kern, B. D. (see Jenkins, G. L.)—210(A); 915
—— (see Lafferty, D. L.)—223(A)
Kerner, Edward H. Excitation of molecular rotations and vibrations in inelastic scattering processes—1174
Kerr, Robert J., Sherwood K. Haynes, and George R. Meneely. Study with NaI scintillation spectrometer of methods of estimating I^{131} contained in human thyroid—214(A)
Kevane, C. J., S. Legvold, and F. H. Spedding. Hall effect in Y, La, Ce, Pr, Nd, Gd, Dy, and Er—1372
Kiehn, R. M., Clark Goodman, and K. F. Hansen. Total neutron cross sections of Cl and C—66
Kikuchi, Ryoichi. Quantum statistical mechanics of ferromagnetism—205(A)
Kim, Y. B. Energy distribution of neutral mesons produced in cosmic-ray stars—445(A)
King, D. T. (see Seeman, Nathan)—446(A)
King, J. C. and Henry A. Fairbank. λ-point shift in He^3—He^4 mixtures—489(A)
King, J. G. and V. Jaccarino. Hfs and nuclear moment ratios of stable Br isotopes—209(A)
——, **H. H. Stroke, and V. Jaccarino.** Hfs of I—476(A)
Kip, A. F., C. Kittel, R. A. Levy, and A. M. Portis. Electronic structure of F centers: Hyperfine interactions in electron spin resonance—1066
—— (see Portis, A. M.)—207(A)
Kirkaldy, J. S. (see Westcott, C. H.)—495(A)
Kittel, Charles. Electronic structure of F centers—219(A)
—— Theory of conduction-electron spin resonance—239(T)
—— (see Kip, A. F.)—1066
Klein, Abraham. Construction of potentials in quantum field theory—1285(L); Convergence of adiabatic nuclear potential—460(A); 740
Klein, D. (see Oxley, C. L.)—419(L)
Klein, J. A. and A. H. Nethercot, Jr. Microwave spectrum of DI at 1.5-mm wavelength—1018(L)
Kleinman, D. A. (see Dienes, G. J.)—238(A)
Klema, E. D. and F. K. McGowan. γ-γ angular correlation in Ni^{60}—616
Kloepper, Robert M. Angular correlation of Ni^{60} γ-γ cascade—1026(L)
Klose, J. Z. (see Kaplon, M. F.)—1573(L)
Kmetko, E. A. Electrical properties of carbon bisulfate compounds—243(A)
—— (see Mrozowski, S.)—234(A)
Knight, J. D., M. E. Bunker, B. Warren, and J. W. Starner. Radiations of U^{240} and Np^{240}—889
Knight, W. D. Nuclear resonance line shapes at high rf fields—206(A)
Knipe, R. H. Molecular orbital treatment of contribution of π electrons to electric dipole moments of some phenyl halides—242(A)
Knudsen, W. C. and J. R. Dillinger. Linear velocity of He II film—489(A)
Kobayashi, Jinzo (see Ueda, Ryuzo)—1562(L)
Koch, H. W. X-ray spectrometer for nuclear-energy studies with betatron—477(T)
—— **and R. S. Foote.** Direct measurement of nuclear absorption of x-rays—455(A)
Koehler, J. S. Theory of initial stress strain curves in face-centered metals—233(A)
—— Work hardening in substitutional alloys—448(A)
Koehler, W. C. and E. O. Wollan. Slow-neutron scattering cross sections for rare earth nuclides—597
Koenigsberg, Ernest. Conductivity of thin films in longitudinal magnetic field—8
Kohn, Walter (see Rostoker, Norman)—234(A)
Kolsky, H. G. Low-energy properties of n-p system—459(A)
Korobkin, Irving. Heat transfer on hemispherical body in supersonic flow—469(A)
Koski, W. S. (see Iwersen, Eric)—1229
Koster, G. F. (see Slater, J. C.)—205(A); 1323
Kranz, A. Z. and W. W. Watson. A^{38} energy levels from $Cl(\alpha,p)$—1472
—— **and W. W. Watson.** Cl isotope separation by thermal diffusion—1469
Krishnan, K. G. (see Mihelich, J. W.)—498(A)
Krogstad, R., W. Nelson, and S. T. Stephenson. X-ray absorption fine structure with polarized x-rays—457(A)
Kroll, N. M. (see Weneser, J.)—1257
Krone, Ralph W. (see Reardon, William A.)—334; 442(A)
Kronheimer, Erwin H. Calculation of nuclear binding energies with single-particle oscillator wave functions, erratum—1580(E)
Kruse, U. E. (see Malenka, B. J.)—1165
—— (see Ramsey, N. F.)—1162
Kuhlthau, A. R. Viscous drag measurements on rarefied gas using high-rotational speed techniques—1029(A)
Kundu, D. N. H^3 and He^3 reactions with medium-heavy nuclei—488(T)
—— **and M. L. Pool.** Inverse Oppenheimer-Phillips process in $Cu^{65}(He^3,\alpha)$—417(L)
—— (see Pool, M. L.)—462(A)
Kunstadter, J. W., J. J. Floyd, and L. B. Borst. Long-lived delayed neutrons from fission—594
Kunz, W. E. Cross section of $He^3(H^2,H^1)He^4$ reaction from 100–800 kev He^3 energy—462(A)
——, **C. D. Moak, and W. M. Good.** Energy levels in Be^8 from $Li^6(He^3,p)Be^8$—676
Kupperian, J. E., Jr., and E. D. Palmatier. Ionization energy losses of relativistic μ mesons in gases—1186
Kurath, Dieter. Application of jj-coupling model to moderately light nuclei—1430

Kursunöglu, Behram. Relativistic two-body equation—478(A)
Kurzweg, H. H. Physical problems encountered in high-speed flight—459(T)

Lafferty, D. L., J. A. Biggerstaff, B. D. Kern, and T. M. Hahn. High-current 120-kev positive ion accelerator—223(A)
Lamphere, R. W. Fission cross section of U^{234}—210(A); 655
Landauer, Rolf and John Swanson. Diffusion currents in Hall effect in semiconductors—207(A); 555
—— (see Allen, G.)—471(A)
Lander, J. J. Auger peaks in energy spectra of secondary electrons from various materials—1382
Landon, H. H. (see Sailor, V. L.)—450(A)
Langer, L. M., N. H. Lazar, and R. J. D. Moffat. Disintegration of Sb^{124}—338; 485(A)
—— (see Ames, D. P.)—68
—— (see Lazar, N.)—498(A)
—— (see Moffat, R. J. D.)—485(A)
Langmuir, D. B. Interpretation of "dc etch" phenomena—447(A)
Lark-Horovitz, K. (see Becker, W. M.)—230(A)
—— (see Forster, J. H.)—229(A)
—— (see Johnson, V. A.)—230(A)
Laubenstein, M. J. (see Eggen, D. T.)—238(A)
Lauritsen, C. C. (see Warters, W. D.)—917
Lauter, H. A. (see Gugelot, P. C.)—486(A)
Lawson, J. S., Jr., and H. Frauenfelder. Correction for finite angular resolution in directional correlation measurements—649
——, **H. Frauenfelder, and W. K. Jentschke.** Measurement of directional correlation of Ni^{60} γ-γ cascade—484(A)
Lax, Melvin and Eli Burstein. Broadening of impurity levels in Si—208(A)
—— **and Eli Burstein.** Lattice absorption in diamond: One-dimensional model—492(A)
Lazar, N. H., R. J. D. Moffat, and L. M. Langer. Disintegration of W^{185}—498(A)
—— (see Langer, L. M.)—338
—— (see Moffat, R. J. D.)—485(A)
Lazarus, D. (see Sonder, E.)—245(A)
—— (see Tomizuka, T.)—245(A)
Leaderman, Herbert. Rheology of polyisobutylene III. Approximation methods in linear viscoelasticity theory: Wiechert function calculations—217(A)
LeBlanc, J. M. (see Cork, J. M.)—76; 497(A)
Leddicotte, G. W. (see Reynolds, S. A.)—333
Lee, Charles A., B. P. Fabricand, R. O. Carlson, and I. I. Rabi. Molecular beam investigation of rotational transitions. I. Rotational levels of KCl and their hfs—1395
—— (see Fabricand, B. P.)—1403
Legvold, S. (see Elliott, J. F.)—28
—— (see Kevane, C. J.)—1372
Lehnert, Richard. Reynolds number effect on spheres at supersonic speeds—1033(A)
—— **and Samuel Hastings.** Spin effects on base-pressure—1032(A)
Lehovec, Kurt. Electronic energy states of impurities in nonmetallic crystals—228(A)
—— **and E. Belmont.** Preparation of junctions in single crystals by surface melting—492(A)
Leinhardt, T. E. (see Reynolds, J. M.)—1152
Leipuner, L., R. Siegel, and S. DeBenedetti. Polarization of three-photon annihilation radiation—198(L)
Leivo, W. J. Density change in proton-irradiated KCl—245(A)
—— (see Vaughan, W. H.)—245(A)
Leprince-Ringuet, L. Some unusual cases of heavy mesons (K and V_0) observed in photographic emulsions—466(T)
Letaw, Harry, Jr., and Armin H. Gropp. Infrared spectrum of amide group—235(A)
Levin, J. S. (see Hughes, D. J.)—1423
—— (see Kato, W. Y.)—450(A)
Levinger, J. S. (see Goodrich, M.)—455(A); 1225
Levy, R. A. (see Kip, A. F.)—1066
Lew, Hin. Hfs and nuclear moments of Pr^{141}—619
—— (see Wessel, Günter)—476(A)
Lewis, H. W. Search for Hall effect in superconductor—216(A)
——, **B. E. Simmons, and E. Merzbacher.** Production of characteristic x-rays by protons—943
Libby, W. F. T in nature—442(T)
Linder, E. G. and P. Rappaport. Radioactive charging through dielectric medium—202(L); erratum—1580(E)
Lindner, Manfred. New nuclides produced in Cl spallation—642
—— **and R. N. Osborne.** Cross section for $Al^{27}(a,a2pn)Na^{24}$ from threshold to 380 Mev—342
—— **and R. N. Osborne.** Energy dependence of cross section for $C^{12}(a,an)C^{11}$—1501
Linlor, W. I. and B. Ragent. Time-of-flight instrumentation for 100-Mev neutrons—440(A)
—— (see Ragent, B.)—440(A)
Linz, Arthur, Jr. Electrical properties of $SrTiO_3$—753(L)
Lippmann, B. A. Complementarity in angular momentum states—1213
Livingston, M. S. (see Courant, E. D.)—202(L)
Loeb, Arthur L. Free-energy model for hysteresis loop—434(A)
Loebner, E. E. Thermoelectric power of carbons—243(A)
Logan, R. A. Thermally-induced acceptors in single crystal Ge—757(L)
Loh, H. Y. and Peter Cheo. Change of optical constants of fresh thin Cu and Ag films on exposure to air—221(A)
Lomon, Earle and Herman Feshbach. n-p scattering—454(A)
London, Fritz. Theory of liquid He—209(T)
Lord, J. J. Emulsion chamber studies of high-energy cosmic-ray interactions—432(A)
—— (see Weaver, A. B.)—466(A)
Lord, Norman W. Effects of heat treatment on lattice perfection—472(A)
—— Kinetics of disorder-order transformation in Cu_3Au—221(A)
Louisell, W. H., R. W. Pidd, and H. R. Crane. Experimental measurement of gyromagnetic ratio for free electron—475(A)
—— (see Crane, H. R.)—475(A)
Lovell, Robert James. Analysis of infrared spectrum of CF_3COCl—235(A)
Low, Francis E. and David Pines. Mobility of slow electrons in polar crystals—193(L)
—— (see Bethe, H. A.)—417(L)
Luckey, D., T. Jenkins, and R. R. Wilson. Photomeson production from H and deuterium at 90° and 30°—468(A)
—— (see Palfrey, T. R.)—468(A)
Lukasiewicz, J. Shock compression in ducts and diffusers—1032(A)
Lummis, Frances L. and Richard L. Petritz. Noise in p-n junction rectifiers. II. Experiment—231(A)
Lundquist, Stig. Stability of orbits in strong-focusing synchrotron—981
Lustig, Harry and John M. Blatt. New method for calculation of nuclear phase-shifts from cross-section measurements—453(A)

Lynch, Frank J. and Clarence L. Wesenberg. Very high resistance measurement—493(A)
Lyon, W. S. (see Kahn, Bernd)—1212

Ma, S. T. Power-series expansion of unitary operator $U(t,t_0)$—392
Macdonald, J. Ross. New model for Debye dispersion equations—412(L)
Machlup, Stefan. Nyquist and Einstein relations derived from scattering model—240(A)
—— **and L. Onsager.** Fluctuations and irreversible process. II. Systems with kinetic energy—1512
—— (see Fletcher, R. C.)—237(A)
—— (see Onsager, L.)—1505
Mack, Rex C., J. J. Neuer, and M. L. Pool. $Eu^{147, 148, 149, \text{and } 150}$—497(A); Radioactive Eu^{150} and Gd^{150}—903
Macke, Wilhelm. Two-particle potential from Bethe-Salpeter equation—195(L); Erratum—1580(E)
MacLeod, David W. (Mingins, Charles R.)—471(A)
Maczuk, J. (see Henkels, H. W.)—1562
Madey, Richard. Short resolution time and short "dead" time coincidence counting equipment—486(A)
—— (see Bandtel, Kenneth C.)—487(A)
—— (see Frank, Wilson J.)—487(A)
—— (see Godfrey, Charles)—487(A)
Mador, I. L., J. J. Markham, and R. T. Platt, Jr. Band width of F centers in KBr—219(A); 1277(L)
—— (see Markham, J. J.)—219(A)
—— (see Platt, R. T., Jr.)—219(A)
Mahlman, H. A. (see Reynolds, S. A.)—333
Maita, J. P. (see Tanenbaum, M.)—1009(L)
Malenka, B. J., U. E. Kruse, and N. F. Ramsey. Electric scattering of polarizable deuteron—1165
—— (see Ramsey, N. F.)—1162
Mandelkern, Leo. Kinetics of crystallization—225(T)
—— (see Roberts, Donald E.)—225(A)
Mandeville, C. E. and H. O. Albrecht. Storage of energy in Ag-activated KCl—219(A); 566; Storage of energy in KCl-Tl and NaCl-Tl—470(A)
—— (see Albrecht, H. O.)—471(A)
—— (see Saraf, B. L.)—1216
Mann, D. E., N. Acquista, and Earle K. Plyler. Vibrational spectra of $F_2C{:}CF_2$ and $Cl_2C{:}CCl_2$—464(A)
Mann, L. (see Clark, A. E.)—467(A)
Mapother, D. E. and J. F. Cochran. Super-conducting transition in Al—216(A)
Marcus, Paul M. Theory of pressure effects on superconducting transition temperatures—216(A)
—— **and E. Maxwell.** Two-fluid models of superconductivity with application to isotope effects—1035
Mark, Hans (see Kay, Robert)—472(A)
Markham, Jordan J., R. T. Platt, Jr., and I. L. Mador. Bleaching properties of F centers in KBr at 5°K—219(A)
—— (see Mador, Irving L.)—219(A); 1277(L)
—— (see Platt, R. T., Jr.)—219(A)
Markovitz, H. (see Padden, F. J.)—217(A)
Marmo, Frederick (see Watanabe, K.)—436(A); 1155
Marshall, Henry P. and Ernest Grunwald. Molar activity coefficients of electrolytes from conductivity data—214(A)
Marshall, J., L. Marshall, and V. A. Nedzel. Total cross sections of 408-Mev protons for H and light elements—767(L)
Marshall, John H. Liquid A ionization chamber measurement of shape of β-ray spectrum of K^{40}—905
Marshall, L. (see Marshall, J.)—767(L)
Martin, Donald C. Graduate training for high school physics teachers and cooperation between college and high school physics departments—227(A)
Martin, E. E. (see Dyke, W. P.)—1043
Martin, J. A. Radioisotope production in ORNL 86-in. cyclotron—224(A)
Martin, R. L., E. Fermi, and D. E. Nagle. Scattering of 169- and 192-Mev pions by H—467(A)
—— (see Anderson, H. L.)—155
Marton, L., J. Arol Simpson, and J. A. Suddeth. Electron interferometer—437(A)
—— (see Simpson, J. Arol)—437(A)
—— (see Suddeth, J. A.)—437(A)
Marx, J. W. Radiation damage and rate processes—1564(L)
Masket, A. V. (see Brown, Frank B., Jr.)—210(A)
Matland, C. G. Natural lifetime of Cd 5^3P_1 state—436(A)
Matthias, B. T. Superconducting compounds—413(L)
Maurer, R. J. (see Teegarden, K.)—219(A)
Maximon, L. (see Bethe, H. A.)—417(L)
Maxwell, E. (see Marcus, Paul M.)—1035
Maxwell, L. R. Trivalent substitutions in ferrites—461(T)
——, **S. J. Pickart, and R. W. Hall.** Thermomagnetic investigations of Ni ferrite-aluminates—206(A)
Mayburg, S. and L. Rotondi. Thermal acceptors in vacuum heat-treated Ge—1015(L)
Mazenko, J. J. (see Schwertz, F. A.)—491(A)
McAfee, K. B. (see McKay, K. G.)—1079
McCay, M. S. and J. H. Coulliette. Motion of ions in perpendicular hf electric fields—213(A)
—— (see Morrison, Ray M.)—227(A)
McClelland, Clyde L. and Clark Goodman. Excitation of heavy nuclei by electric field of low-energy protons—760(L)
McClure, G. W. Upper limit on fraction of positive particles emanating from two β emitters—483(A)
—— (see Porter, W. C.)—495(A)
McCorkle, W. C. (see Tipton, Isabel H.)—214(A)
McCusker, C. B. A., N. A. Porter, and B. G. Wilson. Production of mesons above 10 Bev—384
—— **and F. C. Roesler.** Extreme energy interactions in heavy nuclei—769(L)
—— **and F. C. Roesler.** Interpretation of $0+xp$ type stars in photographic emulsions—769(L)
—— (see Roesler, Frank C.)—690
McDonald, E. W. and D. C. Ralph. 10-Mc rf ion source—223(A)
McDonald, Frank B. Cloud-chamber study of particles in primary cosmic radiation—432(A)
McEllistrem, M. T. (see Jones, K. W.)—482(A); 879
McGarvey, B. R. (see Gutowsky, H. S.)—81
McGarvey, W. C. (see Graham, Irven C.)—214(A)
McGowan, F. K. (see Klema, E. D.)—616
McGuire, T. R. Magnetic resonance absorption in Ni ferrite-aluminates—206(A)
McHale, J. L. and John L. Johnson. Half-widths and level shifts of one-body resonances—452(A)
—— (see Johnson, John L.)—87
McIntyre, J. A. (see Hofstadter, R.)—422(L); 439(A)
McKay, K. G. and K. B. McAfee. Electron multiplication in Si and Ge—1079
—— (see Johnson, J. B.)—582
McManus, H. (see Austern, N.)—453(A)
McMichael, B. D. (see Mrozowski, S.)—234(A)
McMickle, R. H., R. W. Schiessler, and W. Webb. Compressions to 150 000 psi for series of high molecular weight liquid hydrocarbons—466(A)
McMullen, C. C. and M. W. Johns. Decay of Re^{188} and lifetimes of Os^{186m} and Os^{188m}—418(L); Erratum—1580(E)
McNown, John S. Recent investigations at Iowa Institute of Hydraulic Research—1029(T)
McReynolds, Andrew W. Inelastic scattering of thermal neutrons in Pb—1368

Meadows, J. W. Excitation functions for proton-induced reactions with Cu—885
Mechlin, G. F. (see Fillnow, R. H.)—236(A)
Meckler, Alvin. Electronic energy levels of O_2—242(A)
Meechan, C. J. (see Dixon, C. E.)—237(A)
Mehl, Clarence R. and Peter Havas. Classical scattering of neutral mesons—393
Meissner, K. W. (see Deverall, G. V.)—297
Melkonian, E., W. W. Havens, Jr., and L. J. Rainwater. Doppler effect on neutron resonance levels—450(A)
Melnick, Donald A. and Leo J. Neuringer. Adsorbed O in ZnO photoconductivity—229(A)
Melvin, M. Avramy. Energy-momentum tensor in general stream electrodynamics—241(A)
Mendlowitz, H. (see Case, K. M.)—475(A)
Mendoza, E. Minimum in electrical resistance of metals at low temperatures—239(T)
Meneely, George R. (see Kerr, Robert J.)—214(A)
Meneghetti, David (see Sidhu, S. S.)—435(A)
Menyuk, Norman. Magnetization reversal of square-loop polycrystalline materials by domain growth—434(A)
Merz, Walter J. Double hysteresis loop of $BaTiO_3$ at Curie point—513
Merzbacher, E. (see Lewis, H. W.)—943
—— (see Newson, H. W.)—241(A)
Meshkov, Sydney. Theory of complex spectra—871
Metzger, F. R. and W. B. Todd. Lower limit for lifetime of 665-kev excited state of Mo^{95}—1286(L)
Meyerott, Roland E. Approximate Hartree type wave function and matrix elements for K and L shells of atoms and ions—456(A)
—— (see Brachman, Malcolm K.)—437(A)
Middleton, A. E. (see Willardson, R. K.)—243(A)
Mihelich, J. W. Successive neutron capture in Ta—427(L); Erratum—1580(E)
—— **and A. de-Shalit.** Decay of Au^{197m}—78
——, **L. P. Gillon, K. G. Krishnan, and A. de-Shalit.** Neutron-deficient isotopes of Hg—498(A)
Miller, J. M. and G. Friedlander. Nuclear reactions produced in Brookhaven cosmotron—485(A)
Miller, P. H. Infrared absorption and photoconductivity in Te—213(T)
Miller, S. C., Jr., and R. H. Good, Jr. WKB-type approximation to Schrödinger equation—174
Miller, W. C. (see Anthony, D. J.)—439(A)
Milner, Paul C. (see Green, Louis C.)—35
Mingins, Charles R., Robert W. Perry, and David W. MacLeod. Effects of grooves in piezoelectric filter plates—471(A)
—— (see Frost, Albert D.)—471(A)
Minkowski, J. M. (see Bearden, J. A.)—482(A)
Minshall, Stanley. Separation of shock wave into elastic and plastic waves, and measurement of pressure of elastic wave—1030(A)
Misenta, R. (see Becker, E. W.)—414(L)
Miskel, J. A. (see Perlman, M. L.)—899
Mitchell, F. H. Experiment with transistors for elementary electronics laboratory course—227(A)
Mittelman, Phillip S. Radiations from Zr^{95}—484(A)
Mize, J. P. and D. J. Zaffarano. β-ray spectra of C^{14} and Ni^{63}—210(A)
Mizushima, Masataka. Frequencies of microwave absorption lines of O_2—222(A)
—— Theory of rotational spectra of allene type molecules—464(A)
Moak, C. D. $H^3 + He^3$ reactions—462(A)
—— (see Kunz, W. E.)—676
Mockler, Richard C. and Walter Gordy. Microwave spectrum of $(CH_3)_2SiCl$—222(A)
—— (see Bird, George R.)—222(A)
—— (see Venkateswarlu, Putcha)—222(A)
Moffat, R. J. D. (see Langer, L. M.)—338
—— (see Lazar, N.)—498(A)
Moldauer, P. and K. M. Case. Equivalence theorems—459(A)
Mollo-Christensen, E. Separated solutions of linearized equation for unsteady transonic flow—1030(A)
Montalbetti, R., L. Katz, and J. Goldemberg. Photoneutron cross sections—659
Moore, J. (see Sheer, G.)—449(A)
Morita, Masato. Interference terms of the electron-neutrino angular correlation, erratum—1580(E)
Morowitz, Harold J. Information content of living systems—492(A)
Morris, L. W. and Hung-Chi Chang. Continuous flow cell for investigation of polarization at metal-solution interface—215(A)
Morrish, A. H. Grain density in tracks of 117- and 222-Mev π^- mesons in emulsions—423(L)
—— 210-Mev negative pion interactions—468(A)
Morrison, Ray M. and M. S. McCay. Incentive grading for basic laboratory reports—227(A)
Morton, H. S., Jr., and J. W. Beams. Tensile strength and adhesion of thin films of Ag—449(A)
Moses, Harry E. Exchange scattering in three-body problem—185
—— **and Ta-You Wu.** Dissociation and recombination of O_2 in upper atmosphere assuming three-body recombinations—458(A); 1408
Moshinsky, Marcos. Poles of S matrix for resonance reactions—984
Mostov, Philip M. and Sidney Borowitz. Radiation effects and rotational-translational relaxation time constant—465(A)
Mousuf, A. K. (see Russell, R. D.)—1223
Moyer, Burton J. (see Frank, Wilson J.)—487(A)
Mrozowski, S., B. D. McMichael, and E. A. Kmetko. New detector for infrared—234(A)
Muehlhause, Carl O. Gas scintillation counters—495(A)
—— (see Bloom, S. D.)—494(A)
—— (see Harris, S. P.)—125
Muldawer, Leonard (see Jaumot, Frank E., Jr.)—232(A)
Mulder, Marjorie M. (see Green, Louis C.)—35
Myers, V. W., R. S. Carter, and H. Palevsky. Total neutron cross sections of heavy water and glass at long wavelengths—451(A)
—— (see Carter, R. S.)—450(A)

Nagel, E. (see Wu, C. S.)—319
Nagle, D. E. (see Anderson, H. L.)—155
—— (see Martin, R. L.)—467(A)
Naugle, J. E. (see Anderson, G. W.)—431(A)
Navon, D. and H. Y. Fan. Carrier traps in Ge at low temperatures—491(A)
Nedzel, A. V. (see Marshall, J.)—767(L)
—— Total cross sections for 400-Mev neutrons—440(A)
Neidigh, R. V. (see Cohen, B. L.)—486(A)
Nelson, F. (see Campbell, E. C.)—499(A)
Nelson, W. (see Krogstad, R.)—457(A)
Nester, W. H. (see Cork, J. M.)—76; 497(A)
Nethercot, A. H., Jr. (see Klein, J. A.)—1018(L)
Neuer, J. J. (see Mack, Rex C.)—497(A); 903
Neuringer, Leo J. (see Melnick, Donald A.)—229(A)
Newell, Gordon F. Vibration spectrum of simple cubic lattice—227(A)
Newman, E., B. L. Cohen, and T. H. Handley. (p,pn) and (p,an) excitation functions—486(A)
—— (see Cohen, B. L.)—486(A)

Newman, Roger. Optical studies of injected carriers. I. Infrared absorption in Ge—1311; II. Recombination radiation in Ge—1313
Newson, Henry W. and E. Merzbacher. Magic numbers and statistical model of nucleus—241(A)
—— (see Gibbons, J. H.)—209(A)
Nichols, J. B. X-ray and infrared studies on extent of crystallization—225(T)
Nielsen, A. H. (see Keller, F. L.)—235(A)
—— (see Parker, F. W.)—235(A)
—— (see Shelton, R. D.)—235(A)
Nielsen, Carl E. (see Frost, Robert H.)—864
Nier, Alfred O. (see Collins, T. L.)—482(A)
—— (see Johnson, Edgar G.)—10
Nilson, R. (see Kerman, R. O.)—438(A)
Nisenoff, M. (see Gebbie, H. A.)—230(A)
Nix, Foster C. (see Croft, George T.)—212(A)
—— (see Sanville, W. W.)—220(A)
Novey, T. B. (see Albers-Schönberg, H.)—199(L); 1287(L)
Nowick, A. S. and A. E. Roswell. Decay of vacancies frozen into alloy by quenching—221(A)
Nozick, Seymour (see Winkler, Stanley)—492(A)

O'Dell, Francis W., Maurice M. Shapiro, and Bertram Stiller. Pellicle stacks in nuclear research—496(A)
Offenbacher, Elmer L. and Herbert B. Callen. Directional effects in the electric breakdown of ionic crystals, erratum—1580(E)
Ohtsuka, Taiichiro (see Wanick, R. W.)—445(A); 1574(L)
Okazaki, A., R. B. Walton, and J. D. Clement. Total cross sections of Nd, Er, and Hf for fast neutrons—440(A)
O'Kelley, G. D. (see Batzel, R. E.)—939
Oliver, A. R. (see Blau, M.)—949
Olsen, J. L. (see Bömmel, H.)—1017(L)
Onsager, L. and S. Machlup. Fluctuations and irreversible processes—1505
—— (see Machlup, S.)—1512
Orear, Jay. Scattering of 120-Mev π^- mesons by H—467(A)
—— (see Weaver, A. B.)—466(A)
Oriani, R. A. Thermodynamic activities in Fe-Ni alloys—465(A)
O'Rourke, R. C. Absorption of light by trapped electrons—265
Orr, L. W. (see Grimes, D. M.)—435(A)
Osborne, L. S. (see Goldschmidt-Clermont, Y.)—468(A)
Osborne, M. F. M. (see Steele, M. C.)—1281(L)
Osborne, R. N. (see Lindner, M.)—342; 1501
Osgood, T. H. Responsibilities and training of physics teachers—226(T)
Oshinsky, W. (see Breckenridge, R. G.)—243(A)
Overhauser, Albert W. Influence of impurities on diffusion in solids—246(A)
—— Polarization of nuclei in metals—476(A)
Oxley, C. L., W. F. Cartwright, J. Rouvina, E. Baskir, D. Klein, J. Ring, and W. Skillman. Double scattering of high-energy protons by H and C—419(L)

Padden, F. J., H. Markovitz, and T. W. DeWitt. Dynamic properties of concentrated polymer solutions—217(A)
Paehler, J. H. (see Jones, W. H.)—486(A)
Pai, Shih I. Hypersonic viscous flow over insulated flat plate at large angle of attack—1029(A)
Palevsky, H., N. G. Sjöstrand, and D. J. Hughes. Neutron detectors for Brookhaven fast chopper—451(A)
—— (see Carter, R. S.)—450(A)
—— (see Myers, V. W.)—451(A)
Palfrey, T. R., D. Luckey, and R. R. Wilson. Photomeson production from H and deuterium at 180°—468(A)
Palmatier, E. D. Ionization energy losses of μ mesons in gases—210(T)
—— (see Kupperian, J. E., Jr.)—1186
Palmer, R. Ronald and Lowell M. Bollinger. Neutron transmission measurements of Cd, Gd, and Hg using Argonne fast chopper—450(A)
—— (see Bollinger, L. M.)—452(A)
Parker, F. W., A. H. Nielsen, and W. H. Fletcher. Infrared grating spectrum of CH_3CN vapor—235(A)
Passman, S. (see Block, M. M.)—210(A)
Paul, E. B. and R. L. Clarke. Yield of α particles from $B^{11}(p,\alpha)Be^8$—463(A)
—— (see Gove, H. E.)—463(A)
Payne, W. and M. Goodrich. γ rays in decay of Ba^{131}—497(A)
—— (see Goodrich, M.)—455(A); 1225
Pearlman, N. (see Keesom, P. H.)—215(A); 1347; 1354
Pearlstein, E. A. Changes in conductivity of NaCl produced by bombardment with 360-Mev protons—244(A)
Pearson, G. L. (see Tanenbaum, M.)—244(A)
Peaslee, D. C. j-j coupling for $A \lesssim 50$—443(A)
—— Linear combination of invariants in β decay—1447
—— Speculation on V-spin—446(A)
—— (see Davidson, J. P.)—442(A); 1232
Peckham, D. C. (see Stoner, R. G.)—1032(A)
Pellam, J. R. Recent experiments on second sound in liquid He II—481(T)
Pepinsky, Ray and P. F. Eiland. Computations of three-dimensional structure factors on S-FAC—229(A)
—— (see Frazer, B. C.)—212(A)
—— (see Schwartz, Robert B.)—812
—— (see Shirane, Gen)—212(A)
Pepper, T. P. (see Almqvist, E.)—1022(L)
Pereira, A. W. (see Rao, A. S.)—764(L)
Perl, William. Relativistic contributions to magnetic moment of n-electron atoms—852
—— **and Vernon Hughes.** Relativistic contributions to magnetic moment of $^3S_1$ He—842
Perlman, I. (see Asaro, Frank)—763(L)
—— (see Friedlander, G.)—498(A)
Perlman, M. L. and J. A. Miskel. Average charge on daughter atoms produced in decay of A^{37} and Xe^{131m}—899
—— (see Schwartz, Robert B.)—883
Perry, J. P. and C. E. Angell. Scattering of 40-Mev π^+ mesons by H—1289(L)
—— (see Angell, C. E.)—468(A)
Perry, Robert W. (see Mingins, Charles R.)—471(A)
Petree, Ben (see Foote, R. S.)—456(A)
Petritz, Richard L. Noise in p-n junction rectifiers and transistors. I. Theory—231(A)
—— (see Lummis, Frances L.)—231(A)
Peyrou, C. (see Bridge, H. S.)—362
Peyton, P. B., Jr. (see Cox, J. T.)—222(A)
Pfann, W. G. (see Vogel, F. L.)—230(A)
Phelps, Arthur V. Metastable atoms in afterglow of low-pressure He discharge—436(A)
Phelps, John, W. F. Huebner, and Franklin Hutchinson. Stopping powers of thin compound foils—496(A)
Phillips, G. C., K. F. Famularo, and C. R. Gossett. Absolute magnetic analysis of reaction energies of $Li^6(d,\alpha)He^4$, $Li^7(p,\alpha)He^4$, and $C^{12}(d,\alpha)B^{11}$—462(A)
—— (see Famularo, K. F.)—1195
Phillips, J. A. Equilibrium proton charge ratios from charge exchange in various materials—455(A)

Piccioni, O. and R. L. Cool. Altitude variation and transition effects of air showers—433(A)
Pickart, J. (see Maxwell, L. R.)—206(A)
Pidd, R. W. (see Crane, H. R.)—475(A)
—— (see Louisell, W. H.)—475(A)
Pigg, J. C. (see Crawford, J. H., Jr.)—243(A)
Pines, David (see Low, Francis E.)—193(L)
Pinnick, H. T. Crystallite size and diamagnetic susceptibility of carbons—228(A)
Plass, Gilbert N. Contribution of 15-micron CO_2 band to earth's radiation balance—458(A)
Platt, J. B. π-mesic atom—499(T)
Platt, Reuel T., Jr., I. L. Mador, and J. J. Markham. Production of F, M, and R centers in NaCl at room temperature—219(A)
—— (see Mador, Irving L.)—219(A); 1277(L)
—— (see Markham, J. J.)—219(A)
Plotkin, H. (see Bitter, F.)—421(L)
Plyler, Earle K. (see Mann, D. E.)—464(A)
Polk, M. L. (see Keck, P. H.)—472(A)
Pollard, Ernest (see Powell, W. F.)—494(A)
—— (see Schiffer, J. P.)—474(A)
Pomeroy, David. Teaching of biophysics—226(A)
—— (see Graham, Irven C.)—214(A)
Pond, T. A. Annihilation of positrons in solids—455(A)
Pool, M. L. and D. N. Kundu. He^3 reactions in Cu and Si—462(A)
—— (see Kundu, D. N.)—417(L)
—— (see Mack, Rex C.)—497(A); 903
Pope, N. K. (see Henshaw, D. G.)—472(A)
Porter, C. E. (see Feshbach, H.)—453(A)
Porter, N. A. (see McCusker, C. B. A.)—384
Porter, P. T. and J. I. Hopkins. α-particle straggling in thin foils—209(A)
Porter, W. C. and G. W. McClure. Observation of positive ion flux in GM counter—495(A)
Portis, A. M. Electronic structure of F centers: Saturation of electron spin resonance—1071
—— **and A. F. Kip.** Saturation of paramagnetic resonance from color centers in alkali halides—207(A)
—— (see Kip, A. F.)—1066
Powell, W. F. and Ernest Pollard. Radiation sensitivity of enzymes in intact cells—494(A)
Pratt, G. W., Jr. Eigenfunctions of S^z by spin-operator method—212(A)
Preston, R. S. (see Whetten, N. R.)—432(A)
Prestwood, R. J. (see Bunker, M. E.)—1021(L)
Primakoff, H. μ^- meson nuclear capture in H and D—480(A)
Prince, M. B. Experimental confirmation of relation between pulse drift mobility and charge carrier drift mobility in Ge—271
—— Temperature variation of drift mobilities of minority carriers in semiconductors—208(A)
Pringsheim, Peter. Reversible bleaching of absorption band of diamond—220(A); 551
Protzman, T. F., J. J. Gouza, and W. F. Bartoe. Stress crazing thresholds of methyl methacrylate polymers—211(A)
Pruitt, J. S., S. S. Hanna, and C. D. Swartz. Neutrons from $Be^9(d,n)B^{10}$—463(A)
Pugh, Emerson M. (see Foner, Simon)—20; 220(A)
Pugh, Milton E. (see Jacobs, Donald H.)—492(A)
Purcell, E. M. (see Reif, F.)—631

Quimby, S. L. and Paul M. Sutton. Computation of mean Debye temperature of cubic crystals from elastic constants—1122

Rabi, I. I. (see Fabricand, B. P.)—1403
—— (see Lee, Charles A.)—1395
Ragent, B. and W. I. Linlor. Total neutron cross section of Pb from 30 to 150 Mev—440(A)
—— (see Linlor, W. I.)—440(A)
Rainwater, L. J. (see Melkonian, E.)—450(A)
Ralph, D. C. (see McDonald, E. W.)—223(A)
Ramsey, Norman F. Electron coupled interactions between nuclear spins in molecules—303
——, **B. J. Malenka, and U. E. Kruse.** Polarizability of the deuteron—1165
—— (see Malenka, B. J.)—1162
Randall, John G. (see Graham, Irven C.)—214(A)
Rao, A. S., V. K. Balasubrahmanyam, G. S. Gokhale, and A. W. Pereira. High-altitude measurements of intensity of cosmic radiation at magnetic latitudes 3°N and 19°N—764(L)
Rappaport, P. (see Lindner, E. G.)—202(L); 1580(E)
Rasetti, Franco and E. C. Booth. γ-ray spectrum of As^{77}—1192; of ionium (Th^{230})—315
—— (see Iwersen, Eric)—1229
Rau, R. Ronald (see Ballam, J.)—446(A); 1019(L)
Raudebaugh, Robert J. and Richard B. Belser. Structure and aging of thin metal films—449(A)
—— (see Belser, Richard B.)—449(A); 499(A)
Read, W. T. Recent advances in dislocation theory—205(T)
Reardon, William A., Ralph W. Krone, and Robert Stump. Neutron capture γ rays—442(A); in Cd, Co, and Cl—334
Reboul, T. Todd. Luminescent effects in chemically pure ZnO—229(A)
Redfield, Alfred G. Electronic Hall effect in NaCl—753(L)
—— Hall mobility in insulation photoconductors—244(A)
Rediker, R. H. (see Buskirk, A. V.)—445(A)
—— (see Thompson, R. W.)—446(A)
Reding, F. P. (see Brown, Alexander)—226(A)
Redlich, Martin G. Preferred ratios of energies of excited states of nuclei—328
Redman, J. K., R. R. Coltman, and T. H. Blewitt. Activation energy for recovery of reactor-irradiated Cu crystals—448(A)
—— (see Blewitt, T. H.)—236(A); 448(A)
Reekie, James and Thomas S. Hutchison. Structure of liquid He—490(A)
Reff, Israel. Nuclear photostar production—150
Regener, Victor H. (see Froman, Darol)—707
Reif, F. and E. M. Purcell. Nuclear magnetic resonance in solid H—631
Reilly, Edith F. Electrostatic energy matrices of configuration f^4—876
Rense, William A. Intensity of Lyman-α line in solar spectrum—299
Repp, Gordon W. (see Jarmie, Nelson)—1023(L)
—— (see White, R. Stephen)—468(A)
Reynolds, George T. (see Ballam, J.)—446(A); 1019(L)
—— (see Brown, Fielding)—444(A)
Reynolds, H. K. (see Dunbar, D. N. F.)—496(A)
Reynolds, H. L. and A. Zucker. Range-energy relation of N ions in emulsion—496(A)
Reynolds, J. M., H. W. Hemstreet, and T. E. Leinhardt. Electrical resistance of graphite at low temperatures—1152
—— (see Hemstreet, H. W.)—242(A)
Reynolds, S. A., G. W. Leddicotte, and H. A. Mahlman. γ radiation from As^{77}—333
Rhoderick, Emlyn (see Hughes, Vernon)—828
Ribe, F. L. $Li^6(n,\alpha)H^3$ cross section as function of neutron energy—462(A)
Rice, O. K. Thermodynamics of stationary He films—209(T)

Richards, H. T. (see Jones, K. W.)—482(A); 879
Richman, C. (see Cartwright, W. F.)—677
Richter, B. (see Bitter, F.)—421(L)
Riddell, R. J., Jr. Number of Feynman diagrams—461(A); 1243
—— (see Fried, B. D.)—460(A)
Rider, John A. Polarization in liquids of intermediate conductivity—214(A)
Ridgway, S. L. (see Tomlinson, E. P.)—484(A)
Rieke, Foster F. (see Silber, Leo M.)—434(A)
Ring, J. (see Oxley, C. L.)—419(L)
Risser, J. R. (see Fowler, J. L.)—441(A)
Ritland, H. N. Density changes in glass during heat treatment—228(A)
Ritson, D. M. K-particle mass measurements—1572(L)
—— (see Kaplon, M. F.)—1573(L)
Roberts, B. W. Neutron diffraction study of BiMn alloy—435(A)
—— (see Wilson, V. C.)—494(A)
Roberts, Donald E. and Leo Mandelkern. Melting transition of natural rubber—225(A)
Roberts, Donald M. Polarization correlation of Nd^{144} γ cascade—497(A)
Roberts, L. D. and R. A. Erickson. Temperature scale in liquid He region—488(A)
—— (see Erickson, R. A.)—216(A)
Robeson, A., N. Snidow, and J. W. Beams. Improved equilibrium ultracentrifuge—493(A)
Robinson, J. E., C. E. Whittle, and P. S. Jastram. Branching ratio in Re^{186}—498(A)
Robinson, W. H. Response of anthracene crystals to monoenergetic soft x-rays—457(A)
Rodeback, G. W. and W. P. Eatherly. Electron mean free path of damaged Cu in terms of electrical resistivity and thermoelectric power—237(A)
Roesler, Frank C. and C. B. A. McCusker. Anisotropic distribution of secondaries in extreme energy cosmic-ray stars—690
—— (see McCusker, C. B. A.)—769(L); 769(L)
Rogers, D. H. and Melvin A. Herlin. Thermomechanical effect in liquid He II to 0.9°K—489(A)
Rohrlich, F. and D. M. Chase. Elastic scattering of protons by nuclei—454(A)
Rose, D. (see Harris, S. P.)—125
Rose, M. E. Analysis of angular correlation and angular distribution data—610
—— Angular correlation in allowed β transitions—197(L)
Rose, Marian. Cylindrical Couette flow—469(A)
Rosen, L. (see Allred, J. C.)—90
Rosenblatt, David B. Effects of primeval endowment of U^{238}—1474
Rosenstock, Herbert B. Lattice vibrations in graphite—233(A)
Ross, Donald. Characteristics of two-dimensional turbulent boundary layers—1031(A)
Rossi, B. (see Bassi, P.)—432(A)
—— (see Bridge, H. S.)—362; 1024(L)
Rostoker, Norman and Walter Kohn. New treatment of energy bands—234(A)
Roswell, A. E. (see Nowick, A. S.)—221(A)
Roth, W. L. (see Wilson, V. C.)—494(A)
Rotondi, L. (see Mayburg, S.)—1015(L)
Rouvina, J. (see Oxley, C. L.)—419(L)
Ruark, Arthur E. Classical neutron model—227(A)
Rubin, Lawrence (see Davis, Luther, Jr.)—490(A)
Rubin, R. J. (see Alpher, R. A.)—1030(A)
Rubinson, William (see Katcoff, Seymour)—1458
Ruddick, J. J. (see Buder, E. E.)—561
Ruderman, M. A. (see Henley, E. M.)—480(A)
Rüetschi, R. (see Albers-Schönberg, H.)—199(L)
Russell, R. D., H. A. Shillibeer, R. M. Farquhar, and A. K. Mousuf. Branching ratio of K^{40}—1223
Ryan, J. L. (see Jenkins, G. L.)—210(A)

Sachs, A. (see Bodansky, D.)—467(A)
Saénz, A. W. Changes in electrical, thermal, and thermoelectrical properties of monovalent metals by lattice distortions—1142
Safford, R. (see Bridge, H. S.)—362
Saha, Ajit Kumar (see Chatterjee, Santimay)—200(L)
Sailor, V. L. Parameters for slow neutron resonance in Rh—53
——, **H. H. Landon, and H. L. Foote, Jr.** Neutron resonances in rare earths—450(A)
Salkovitz, E. I. and A. I. Schindler. Brillouin zone structures of alloys. I. Implications of present theories—234(A)
—— (see Schindler, A. I.)—234(A); 1320
Salpeter, E. E. Repulsive core and charge independence—994
Salzman, G. and A. H. Taub. Rigid motion in special relativity—477(A)
Sampson, M. B. (see Carmichael, B. M.)—473(A)
—— (see Steigert, F. E.)—439(A)
Sanderson, J. A. Recent advances in atmospheric optics—459(T)
Sandoval, Manuel. Magnetic properties of sun and their relation to cosmic radiation—466(T)
Sanville, W. W., Foster C. Nix, and Frank E. Jaumot, Jr. Dilatometric study of order-disorder transformation in Cu-Au alloys—220(A)
Sarabhai, V. and R. P. Kane. Effects at Godhavn and lower latitudes of changes in energy and composition of solar cosmic rays—688
Saraf, B. L., J. Varma, and C. E. Mandeville. Radiations from As^{77} and Ge^{77}—1216
—— (see Varma, J.)—484(A)
Sard, R. D. (see Althaus, E. J.)—373
Sartain, Carl C. Electrolysis of water: Experiment in atomic physics—227(A)
Satten, R. A. Crystalline electric field in NdBr—471(A)
Sawada, Shozo. Thermal and electrical properties and crystal structure of tungsten oxide at high temperatures—1010(L)
Schaaf, S. A. Frictional phenomena in rarefied air—1031(T)
Schardt, A. W. (see Welker, Joan P.)—484(A)
Schein, Marcel, Joseph Fainberg, D. M. Haskin, and R. G. Glasser. High-energy pairs of particles from nuclear interactions—479(A); Production of high-energy electron pairs by negative pions in nuclear collisions—973
—— (see Yngve, Victor H.)—432(A)
Scherrer, V. E., W. L. Smith, B. A. Allison, and W. R. Faust. γ radiation from inelastic scattering of 2.7-Mev neutrons—768(L)
——, **R. B. Theus, and W. R. Faust.** γ rays from interaction of 14-Mev neutrons with various materials—1476
Schiessler, R. W. (see McMickle, R. H.)—466(A)
Schiffer, J. P. and Ernest Pollard. Limiting Q value for $K^{39}(\alpha,p)Ca^{42}$—474(A)
Schiffman, T. (see Heyman, R. J.)—1032(A)
Schindler, A. I. and E. I. Salkovitz. Brillouin zone investigation of Mg alloys. I. Hall effect and conductivity—1320
—— **and E. I. Salkovitz.** Brillouin zone structures of alloys. II. Hall constant data of dilute Mg alloys—234(A)
—— (see Salkovitz, E. I.)—234(A)
Schmidt, F. H. and G. L. Keister. Branching ratio and γ-ray order in decay of Sc^{46}—483(A)
Scholnick, Seymour (see Jacobs, Donald H.)—492(A)
Schrader, H. W. (see Hanson, H. P.)—457(A)

Schroeder, H. P. (see Harris, S. P.)—125
Schulz, A. G. (see Jakobson, M. J.)—695
Schwartz, Robert B., M. L. Perlman, and W. Bernstein. Radiations from Rb^{86} and Rb^{86m}—883
—— (see Wheeler, G. W.)—485(A)
Schwarzschild, A. (see Wu, C. S.)—483(A)
Schwertz, F. A. and J. J. Mazenko. Nonlinear semiconductor resistors—491(A)
Schwinger, Julian. Theory of quantized fields—713; 728
Sclar, N., E. Burstein, W. J. Turner, and J. W. Davisson. Low-temperature "breakdown" effect in Ge—215(A)
Scott, Allen B. (see Smith, William A.)—219(A)
Seeman, Nathan, D. T. King, and Maurice M. Shapiro. Charged ξ mesons—446(A)
Segrè, Emilio. Mesons and fission—499(T)
Seitz, F. Current status of F-center problem in alkali halides—218(T)
Senitzky, I. R. Interaction between classical electron and quantized electromagnetic field—1309
Seren, Leo, Milton Birnbaum, Erich Harth, and Ralph Tobin. Effect of magnetic flux amplitude on flux integrator energy control of betatron—474(A)
—— (see Birnbaum, Milton)—474(A)
Sessler, A. M. and H. M. Foley. Contributions to hyperfine spectrum of He^3 resulting from nuclear structure—444(A)
Setlow, Richard and Barbara Doyle. Effect of temperature and uv radiation on dry catalase—494(A)
Shafroth, S. M. and S. S. Hanna. Coincidence studies of B^{10} γ rays—483(A)
Shapiro, Maurice M. Nuclear emulsions in high-energy physics—481(T)
—— (see O'Dell, Francis W.)—496(A)
—— (see Seeman, Nathan)—446(A)
—— (see Stiller, Bertram)—496(A)
Sharp, W. T. (see Austern, N.)—453(A)
Shaw, T. M. and J. J. Windle. Dielectric dispersion of polar polymers at microwave frequencies—218(A)
Shaw, William C., D. E. Hudson, and G. C. Danielson. Mobilities of carriers in crystalline B—208(A)
Sheer, C., J. Moore, and C. Heindl. Measurement of resonant neutron scattering cross sections—449(A)
Shelton, Essie M. (see Josien, Marie-Louise)—235(A)
Shelton, R. D., A. H. Nielsen, and W. H. Fletcher. Infrared absorption spectrum of SO_2—235(A)
Sherman, A. (see Heyman, R. J.)—1032(A)
Sherr, R. and J. B. Gerhart. Experimental evidence for Fermi interaction in β decay of O^{14} and C^{10}—909
—— (see Gerhart, J. B.)—455(A)
Sherrill, F. A. (see Blewitt, T. H.)—236(A)
Shillibeer, H. A. (see Russell, R. D.)—1223
Shimamoto, Y. (see French, J. B.)—898
Shirane, Gen and Ray Pepinsky. Phase transitions in antiferroelectric $PbHfO_3$—212(A); 812
Shirn, G. A. (see Huntington, H. B.)—246(A)
Shockley, William. Dislocations and edge states in diamond crystal structure—228(A)
—— Electrons and holes in electric and magnetic fields—213(T)
—— Some predicted effects of temperature gradients on diffusion in crystals—1563(L)
—— (see Benedict, T. S.)—207(A)
Shore, F. J., W. L. Bendel, H. N. Brown, and R. A. Becker. Radiations from Zr^{89}—1203
Shreckengost, R. C., D. C. Swanson, and J. W. Flowers. Differential pulse-height discriminator—224(A)
Shufler, S. L. (see Zapas, L. J.)—217(A)
Shulman, R. (see Becker, M.)—491(A)
Shutt, R. P. (see Fowler, E. C.)—135
—— (see Fowler, W. B.)—479(A); 758(L); 1287(L)
Sidhu, S. S. and David Meneghetti. Neutron diffraction study of antiferromagnetic structure of pyrrhotite, FeS_x—435(A)
Siegel, Armand (see Wiener, Norbert)—1551
Siegel, R. (see Leipuner, L.)—198(L)
Silber, Leo M. and Foster F. Rieke. Faraday effect in metals at microwave frequencies—434(A)
Silverman, Albert. Photoproduction of neutral mesons in H and D—499(T)
—— (see Wolfe, B.)—446(A)
Silvey, G. (see Javan, A.)—222(A)
Simmons, B. E. (see Lewis, H. W.)—943
Simon, Albert. Production of polarized particles in nuclear reactions—226(T)
—— **and T. A. Welton.** Production and detection of polarized particles in nuclear reactions—453(A)
Simon, J. (see Zernow, L.)—233(A)
Simpson, J. Arol, J. A. Suddeth, and L. Marton. Observations in electron interferometer and their interpretation—437(A)
—— (see Marton, L.)—437(A)
—— (see Suddeth, J. A.)—437(A)
Singer, S. (see Briggs, G. R.)—438(A)
Sipple, R. F. (see Bent, R. D.)—472(A)
Sites, John R. and Bernard L. Strehler. Molecular weight of organic compounds by mass spectrometry—242(A)
—— (see Baldock, Russell)—242(A)
Sitte, Kurt and Don L. Stierwalt. Development of extensive showers in atmosphere—433(A)
—— (see Frochlich, Fritz E.)—433(A)
Sjöstrand, N. G. (see Palevsky, H.)—451(A)
Skillman, W. (see Oxley, C. L.)—419(L)
Sladek, Ronald J. New thermal resistivity maximum in superconducting alloys—1280(L)
Slater, J. C. Generalized self-consistent field method—528
——, **H. Statz, and G. F. Koster.** Two-electron example of ferromagnetism—205(A); 1323
Slifkin, L. (see Sonder, E.)—245(A)
—— (see Tomizuka, T.)—245(A)
Sloope, B. W. (see Garrett, R. E.)—441(A)
Smakula, Alexander. Bleaching of CaF_2 crystals colored by x-rays—1570(L)
Smart, J. Samuel (see Howard, Louis N.)—17
Smith, Charles S. and J. R. Haynes. Piezoresistance effect in Ge—491(A)
Smith, Cyril L. Inactivation of desoxyribonucleic acid by bombardment with deuterons and electrons—493(A)
Smith, F. M., W. Birnbaum, and Walter H. Barkas. Measurements of meson masses and related quantities—765(L)
Smith, H. M., Jr. (see Walbridge, N. L.)—1031(A)
Smith, J. E. (see Blau, M.)—949
Smith, Lincoln G. and C. C. Damm. Present status of mass synchrometer—481(A)
—— (see Damm, C. C.)—482(A)
Smith, R. O. (see Wildhack, W. A.)—213(A)
Smith, Thor L. Calculation of extrusion behavior of viscoelastic materials from relaxation distribution function—218(A)
Smith, W. L. (see Scherrer, V. E.)—768(L)
Smith, W. V. and R. G. Barnes. Electric field gradient of atomic p electrons—457(A)
Smith, William A. and Allen B. Scott. Electron energy levels in F centers—219(A)
Smith, William E. (see Hertzberg, Abraham)—1029(A)
Smoluchowski, R. Change of metallic conductivity through change in thermal scattering—245(A)

—— Phenomena of plastic flow—205(T)
—— (see Bowman, J. C.)—244(A)
—— (see Couling, L.)—245(A)
—— (see Hayes, S.)—244(A)
—— (see Haynes, C. W.)—245(A)
—— (see Vaughan, W. H.)—245(A)
Snidow, N. (see Robeson, A.)—493(A)
Snyder, H. S. (see Courant, E. D.)—202(L)
Sogo, P. B. (see Jeffries, C. D.)—1286(L)
Solimene, N. and B. P. Dailey. Rotational spectrum and molecular structure of CH_3SH—464(A)
Soller, T., W. M. Fairbank, and A. D. Crowell. Rapid separation of He^3 from He^4 by "heat flush" method—1058
Solomon, George E.—1030(A)
Sommers, H. S., Jr., W. E. Keller, and J. G. Dash. Heat of mixing of He^3 in He^4—489(A)
—— (see Goldstein, L.)—490(A)
Sonder, E., L. Slifkin, and D. Lazarus. Diffusion of Sb in Ag—245(A)
Sorenson, B. M. (see Ames, D. P.)—68
Spedding, F. H. (see Elliott, J. F.)—28
—— (see Johnson, R. G.)—466(A)
—— (see Kevane, C. J.)—1372
Spencer, L. V. and C. H. Blanchard. Spin-relativistic effects in multiple scattering of electrons—240(A)
—— (see Fano, U.)—240(A)
Sperduto, A., W. W. Buechner, M. M. Elkind, and W. J. Fader. Energy levels in N^{15}—473(A)
—— (see Buechner, W. W.)—1502
—— (see Elkind, M. M.)—463(A)
Spitzer, W. (see Becker, M.)—491(A)
Spohr, D. A. (see Webber, R. T.)—414(L)
Sponer, H. (see Heckman, R. C.)—242(A)
Sprague, G. and D. H. Tomboulian. Quadrupole moments of stable Sb nuclei—476(A)
Squire, W. (see Hertzberg, A.)—469(A)
Stafne, Marilyn J. (see Kato, W. Y.)—450(A)
Starner, J. W. (see Bunker, M. E.)—1021(L)
—— (see Knight, J. D.)—889
Statz, H. (see Slater, J. C.)—205(A); 1323
St. Clair, Byron W. Delayed neutrons in cosmic-ray stars—445(A)
Steele, M. C. and R. A. Hein. Superconductivity of Ti—490(A)
—— **and M. F. M. Osborne.** Penetration depth of superconductors—1281(L)
—— (see Berlincourt, Ted G.)—215(A)
Steffen, Rolf M. Reduction of $E1$ matrix element in mixed $E1+M2$ transition of Sr^{90}—443(A)
Stehl, O. (see Becker, E. W.)—414(L)
Steigert, F. E. and M. B. Sampson. Energy dependence of differential elastic scattering cross section of α-particles in He—439(A)
Steinberger, J. (see Bodansky, D.)—467(A)
Stephenson, S. T. (see Krogstad, R.)—457(A)
Sternheimer, R. M. Energy loss of fast-charged particle by Čerenkov radiation—256
Stevenson, M. Lynn (see Crawford, Frank S.)—468(A)
Stewart, John Q. Subject of social physics—493(A)
Stierwalt, Don L. (see Sitte, Kurt)—433(A)
Stiller, Bertram and Maurice M. Shapiro. Relativistic rise in ionization loss in nuclear emulsions—496(A)
—— (see O'Dell, Francis W.)—496(A)
Stix, T. H. Heavy nuclei in primary cosmic radiation—431(A)
Stoner, R. G., E. B. Davies, and D. C. Peckham. Shock refraction—1032(A)
Strandberg, M. W. P. (see Tate, P.)—464(A)
Straub, W. D. (see Davis, Luther, Jr.)—490(A)
Strehler, Bernard L. (see Sites, John R.)—242(A)
Stroke, H. H. (see King, J. G.)—476(A)
Stump, Robert (see Reardon, William A.)—334; 442(A)
Sturcken, E. F. and A. H. Weber. Internal conversion coefficients on Nb^{95} and Zn^{65} (actually Mo^{95} and Cu^{65})—484(A)
Suddeth, J. A., L. Marton, and J. Arol Simpson. Construction and operation of electron interferometer—437(A)
—— (see Marton, L.)—437(A)
—— (see Simpson, J. Arol)—437(A)
Sutcliffe, Charles H. and Frank E. Jaumot, Jr. Short-range order in Cu-Au alloy—221(A)
Sutton, Paul M. Variation of elastic constants of crystalline Al with temperature between 63°K and 773°K—816
—— (see Quimby, S. L.)—1122
Swan, J. B. and R. D. Hill. Internal conversion in L subshells—424(L)
Swank, Robert K. and Warren L. Buck. Plastic scintillators—495(A); Scintillation process in plastic solid solutions—927
Swann, W. F. G. Charged density distribution *versus* semi-permanent polarization as basis for electret behavior—447(A)
Swanson, D. C. Van de Graaff electrostatic generator—223(A)
—— (see Shreckengost, R. C.)—224(A)
Swanson, John (see Landauer, Rolf)—207(A); 555
Swartz, C. D. (see Pruitt, J. S.)—463(A)
Swihart, J. C. and F. J. Belinfante. Special-relativistic linear theory of gravitation—500(A)
Szendrei, M. E. (see Birks, J. B.)—197(L)

Takemoto, S., T. Dazai, and R. Chiba. Angular distributions of protons from $Na^{23}(d,p)Na^{24}$—1024(L)
Talmi, Igal. Matrix elements of β decay in jj-coupling—122
—— **and E. P. Wigner.** Evidence concerning spin-orbit forces from β decay—443(A)
Tanenbaum, M. and H. B. Briggs. Optical properties of InSb—1561(L)
—— **and J. P. Maita.** Hall effect and conductivity of InSb single crystals—1009(L)
—— **and G. L. Pearson.** Magneto-resistance effect in InSb—244(A)
Tannenwald, P. E. (see Artman, J. O.)—1014(L)
Tate, P. and M. W. P. Strandberg. Stark effect in high temperature microwave spectroscopy—464(A)
Taub, A. H. (see Salzman, G.)—477(A)
Tauber, G. E. and Ta-You Wu. Spin and magnetic moment of Li^6 nucleus—443(A)
Taylor, G. R. and S. R. Darin. Dependence of photoelastic properties of GR-S on degree of cross linking—211(A)
Teegarden, K. and R. J. Maurer. Photo-conductivity and V centers—219(A)
Telegdi, Valentine L. (see Gell-Mann, Murray)—169
—— (see Hsiao, C. A.)—473(A)
Temmer, G. M. (see Heydenburg, N. P.)—439(A)
ter Haar, D. Vapor pressure and entropy of liquid He^3—1018(L)
Terwillinger, Kent (see Jones, Lawrence W.)—699
Tesh, W. (see DeCarvalho, H. G.)—224(A)
Tessman, Jack R. Antiferroelectrics in applied field—447(A)
Teviotdale, A. (see Bitter, F.)—421(L)
Thaler, R. M., J. Bengston, and G. Breit. Effect of $^3P_2-{}^3F_2$ coupling on p-p scattering—454(A)
—— (see Bengston, J.)—454(A)
Theus, R. B. (see Scherrer, V. E.)—1476
Thomas, E. E. (see Vogel, F. L.)—230(A)

Thomas, G. E., Jr., and L. Bollinger. Construction and properties of liquid scintillation neutron counters—452(A)
—— (see Bollinger, L. M.)—452(A)
—— (see Harris, S. P.)—125
Thomas, L. H. Stability of plane Poiseuille flow—780
Thomas, R. G. Reduced widths in stripping processes—453(A)
—— (see Fowler, W. A.)—473(A)
Thompson, R. W., A. V. Buskirk, L. R. Etter, C. J. Karzmark, and R. H. Rediker. Magnetic cloud-chamber observations of V particles. II. V^0 particles—446(A)
—— (see Buskirk, A. V.)—445(A)
—— (see Cohn, Hans O.)—445(A)
Thomsen, John S. Logical relations among principles of statistical mechanics and thermodynamics—477(A); 1263
—— (see Bearden, J. A.)—482(A)
Thomson, Alice C. (see Bergmann, Peter G.)—180
Thorndike, A. M. (see Fowler, E. C.)—135
—— (see Fowler, W. B.)—479(A); 758(L); 1287(L)
Timnick, A. (see Jones, W. H.)—486(A)
Tinlot, J. H. Charge-exchange pion-nucleon scattering—466(T)
Tipton, Isabel H., W. D. Foland, Franklin C. Bobb, and W. C. McCorkle. Spectrographic analysis of human tissue—214(A)
Tittman, J. and F. F. Johnson. Moderation of Ra-Be neutrons in limestone—452(A)
Tobin, Ralph (see Birnbaum, Milton)—474(A)
—— (see Harth, Erich)—474(A)
—— (see Seren, Leo)—474(A)
Todd, W. B., Jr. (see Metzger, F. R.)—1286(L)
—— (see Varma, J.)—484(A)
Tomboulian, D. H. Absorption of P in neighborhood of $L_{2,3}$ edge—457(A)
—— (see Brown, B. M.)—1580(E)
—— (see Hartman, P. L.)—1577(L)
—— (see Sprague, G.)—476(A)
Tomizuka, T., L. Slifkin, and D. Lazarus. Diffusion of Cd in single crystals of Ag—245(A)
Tomlinson, E. P., S. L. Ridgway, and K. Gopalakrishnan. Conversion coefficients and spectrum shapes from Sb^{124}—484(A)
Toppel, B. J. and S. D. Bloom. $A^{36}(n,\alpha)S^{33}$ reaction—473(A)
Townes, C. H. Some recent developments in microwave spectroscopy—209(T)
—— (see Javan, A.)—222(A)
Tracy, James F. Scattering and absorption of π^+ mesons by Al—960
Trail, Carroll C. and C. H. Johnson. (p,n) thresholds of nuclei with $49 \leq A \leq 75$—474(A)
Trambarulo, R., S. N. Ghosh, C. A. Burrus, Jr., and W. Gordy. Microwave spectrum and molecular properties of O_3—222(A)
Treiman, S. B. Cosmic-ray albedo—432(A); 957
—— (see Ballam, J.)—446(A); 1019(L)
Trice, James B. Measurement of neutron energy distribution in ORNL graphite reactor—224(A)
Trolan, J. K. (see Dolan, W. W.)—1054
—— (see Dyke, W. P.)—1043
Truesdell, C. Precise hydrodynamical theory of absorption and dispersion of ultrasonic waves—1031(T)
Tucker, B. L. and E. C. Gregg. $Li^7(\gamma,p)He^6$ cross section—1579(L)
Tucker, Gardiner (see Hughes, Vernon)—828
Turkevich, A. (see Fung, Si-Chang)—480(A)
Turnbull, David. Nucleation in condensed systems—232(T)
Turner, W. J. (see Sclar, N.)—215(A)
Tweet, A. G. Small-angle scattering of x-rays from He I and He II—488(A)

Ueda, Ryuzo and Jinzo Kobayashi. Antiparallel dipole arrangement in WO_3—1562(L)
Uram, Earl M. Characteristics of axisymmetric turbulent boundary layers in adverse pressure gradient—1032(A)
Urquhart, Helen M. A. Single crystal magnetostriction constants of Fe-Co alloys—434(A)
—— **and J. E. Goldman.** Antiferromagnetostriction—435(A)

van der Maesen, F. (see Bray, Ralph)—231(A)
Van Horn, Wendell (see Keck, Paul H.)—243(A); 512
van Kampen, N. G. Causality condition and S matrix for nonrelativistic particles—459(A); 1267
Van Patter, D. M. (see Brown, R. J. S.)—438(A)
van Roosbroeck, W. Transport of added current carriers in homogeneous semiconductor—282
Van Voorhis, C. C. (see Bradley, L. C.)—469(A)
Van Winkle, Quentin (see Amster, Adolph B.)—211(A)
Varma, J., B. L. Saraf, and W. B. Todd, Jr. Angular correlation of γ rays of Sr^{90}—484(A)
—— (see Saraf, B. L.)—1216
Varnerin, L. J., Jr. Neutralization of ions and ionization of atoms near metal surfaces—859
Vaughan, W. H., W. J. Leivo, and R. Smoluchowski. Mechanical properties of proton-irradiated alkali halides—245(A)
Veenendaal, A. L. (see Wapstra, A. H.)—426(L)
Venkateswarlu, Putcha, Richard C. Mockler, and Walter Gordy. Microwave spectrum and structure of $HGeCl_3$—222(A)
Vidale, M. L. (see Ballam, J.)—446(A); 1019(L)
Villars, F. Collective modes of motion in nuclei—443(A)
Vineyard, George H. Second-order scattering correction in neutron and x-ray diffraction—239(A)
Vinti, John P. Theory of penetration of γ rays through thin barriers—345
Vogel, F. L. Dislocations in low-angle crystal boundaries—461(T)
——, **W. G. Pfann, H. E. Corey, and E. E. Thomas.** Dislocations in low-angle boundaries in Ge single crystals—230(A)
Volkin, Howard C. Effect of capture on slowing-down length of neutrons in hydrogenous mixtures—425(L)
Volkov, A. B. Magnetic moment deviations from Schmidt limits via admixed states—444(A)
von Dardel, G. and A. W. Waltner. Precision determination of n-p capture cross section—1284(L)
Von Foerster, H. (see Babcock, M. L.)—755(L)
von Hippel, A., E. P. Gross, J. G. Jelatis, and M. Geller. Photocurrent, space-charge build-up, and field emission in alkali halide crystals—568
Vosko, Seymour H. (see Ashkin, Julius)—1248

Wacker, Paul F. Matrix formulation of molecular orbital, Heitler-London, and configurational interaction computations—465(A)
Wahl, John S. Energy distributions of fission fragments—486(A)
Wajda, E. S. (see Huntington, H. B.)—246(A)
Walbridge, N. L., H. M. Smith, Jr., and L. A. Woodward. Production and measurement of surface ripples—1031(A)
Waldman, B. (see Anthony, D. J.)—439(A)
Waldron, S. and Melvin A. Herlin. Measurement of thermal diffusivity of Mg at low temperatures by variable state techniques—447(A)
Wales, M. Sedimentation rates in dilute and moderately-concentrated polymer solutions—211(A)
Walker, R. W. (see Whetten, N. R.)—432(A)

Walker, W. D. (see Kaplon, M. F.)—1573(L)
Wall, Nathan Sanders. $Bi^{209}(d,p)B^{210}$ Q value—485(A)
Walsh, Hohn M. (see Christian, Russell H.)—1030(A)
Walt, M. and H. H. Barschall. Angular distributions of elastically-scattered 1-Mev neutrons—441(A)
Walter, Lloyd W. Pressure and temperature distribution on circular cylinder in supersonic cross flow—470(A)
Waltner, A. W. (see von Dardel, G.)—1284(L)
Walton, R. B. (see Okazaki, A.)—440(A)
Wang, P. K. S. (see Gursky, Judith Cassidy)—239(A)
Wangsness, Roald K. g values of Ni ferrite-aluminates—206(A)
—— Sublattice effects in magnetic resonance—1085
Waniek, R. W. and T. Ohtsuka. Energy distribution of neutron stars—445(A)
—— **and Taiichiro Ohtsuka.** Energy spectrum of particles from stars—1574(L)
Wannier, Gregory H. Radiationless trapping of charge carriers in solids—207(A)
Wapstra, A. H. and A. L. Veenendaal. Decay of Mg^{28}—426
Warekois, E. (see Warren, B. E.)—233(A)
Warren, B. (see Knight, J. D.)—889
Warren, B. E., B. L. Averbach, and E. Warekois. X-ray measurements of cold-worked α-brass—233(A)
Warters, W. D., W. A. Fowler, and C. C. Lauritsen. Elastic scattering of protons by Li—917
Watanabe, K., Frederick Marmo, and Edward C. Y. Inn. Photoionization of NO—436(A); 1155
Watanabe, Satosi. Connection between fusion theory of bosons and non-local field theory—771(L)
Watson, Kenneth M. and K. A. Brueckner. Nuclear forces in pseudoscalar meson theory—460(A)
—— (see Francis, Norman C.)—454(A)
Watson, W. W. (see Kranz, A. Z.)—1469; 1472
—— (see Wheeler, G. W.)—485(A)
Weaver, A. B., J. J. Lord, and Jay Orear. Scattering of 43-Mev π^+ mesons by H—466(A)
Webb, W. (see McMickle, R. H.)—466(A)
Webber, R. T. Thermal conductivity of supra-conducting metals—481(T)
—— **and D. A. Spohr.** Thermal resistivity of superconducting Hg in intermediate state—414(L)
—— (see Alers, P. B.)—1060
Webeler, R. (see Welber, B.)—448(A)
Weber, A. H. (see Buder, E. E.)—561
—— (see Deshotels, W. J.)—448(A)
—— (see Sturcken, E. F.)—484(A)
Weidner, R. T. and C. A. Whitmer. Shape of exchange narrowed paramagnetic resonance lines—1279(L)
Weimer, D., W. Bleakney, and D. R. White. Inexpensive Mach Zehnder interferometer—1032(A)
Weinberg, A. M. Progress in reactor physics and reactor technology—226(T)
Weinman, J. A. (see Franklin, A. D.)—205(A)
Weinreich, Gabriel, Gerard M. Grosof, and Vernon W. Hughes. Hfs of metastable triplet state of He^3—195(L)
—— (see Hughes, Vernon)—196(L); 828
Weinreich, O. A. and W. E. Danforth. Electrical conduction and thermoelectric power in thorium oxide crystals—231(A)
Weinstock, E. V. and J. Halpern. Photodisintegration of deuteron at 20 Mev—461(A)
—— (see Halpern, J.)—934
Weisbaum, Samuel (see Beers, Yardley)—1014(L)
Weiss, M. M. and W. Bernstein. Degradation of Co^{60} γ rays in infinite water medium—483(A)
Weisskopf, V. F. (see Drell, S. D.)—460(A)
—— (see Feshbach, H.)—453(A)
Welber, B. and R. Webeler. Anomaly in heat content of metal in fatigued state—448(A)
Welker, Joan P., A. W. Schardt, J. J. Howland, Jr., and G. Friedlander. Metastable states of Ge^{73}—484(A)
Welton, T. A. (see Simon, A.)—453(A)
Weneser, J. Inner bremsstrahlung and magnetic moment of neutrino—1025(L)
——, **R. Bersohn, and N. M. Kroll.** Fourth-order radiative corrections to atomic energy levels—1257
Wentzel, Gregor. Many-nucleon forces—1573(L)
Wenzel, W. A. (see Dunbar, D. N. F.)—496(A)
Wert, C. A. Ordering in alloy system Mg-Cd—221(A)
Wesenberg, Clarence L. (see Lynch, Frank J.)—493(A)
Wessel, Günter and Hin Lew. Hfs of Ag with aid of universal ionizer for atomic beams—476(A)
Wessel, Walter and S. J. Czyzak. Interpretation and generalization of Dirac's theory of electron—986
Westcott, C. H. and J. S. Kirkaldy. Corrections for dead-time of counters in coincidence systems—495(A)
Westervelt, D. R. Z centers in alkali halides—218(A)
Wexler, S. (see Harris, S. P.)—125
Weyl, Peter K. Energy loss of H, He, N, and Ne ions in gases—289
Whaling, W. (see Dunbar, D. N. F.)—496(A)
Wheeler, G. W., R. B. Schwartz, and W. W. Watson. (d,p) reactions with separated Kr isotopes—485(A)
Whetten, N. R., R. S. Preston, R. V. Adams, and R. W. Walker. Cloud-chamber investigation of nuclear interactions—432(A)
White, D. R. (see Weimer, D.)—1032(A)
White, Irene S. (see Anslow, Gladys A.)—241(A)
White, R. Stephen, Gordon W. Repp, and Nelson Jarmie. Positive photomesons from H at 0°—468(A)
—— (see Jakobson, M. J.)—695
—— (see Jarmie, Nelson)—1023(L)
White, Robert L. Quadrupole coupling of deuteron in DCCCl and DCN—1014(L)
Whitehead, M. N. (see Cartwright, W. F.)—677
Whitmer, C. A. (see Weidner, R. T.)—1279(L)
Whittemore, W. L. (see Fowler, E. C.)—135
—— (see Fowler, W. B.)—479(A); 758(L); 1287(L)
Whittle, C. E., J. P. Hurley, and P. S. Jastram. β-γ correlations in decay of Re^{186}—498(A)
—— (see Robinson, J. E.)—498(A)
Whyte, G. N. (see Kastner, J.)—332
Widom, B. and S. H. Bauer. Energy exchange in molecular collisions—240(A)
Wiedling T. Metastable state of V^{52}—767(L)
Wiener, Norbert and Armand Siegel. New form for statistical postulate of quantum mechanics—1551
Wigner, E. P. (see Talmi, I.)—443(A)
Wiig, Edwin O. (see Fink, Richard W.)—194(L)
Wilcox, H. A. (see Cartwright, W. F.)—677
Wildhack, W. A. and R. O. Smith. Effect of centrifugal force field on response of vibrating mass-spring system—213(A)
Wilets, Lawrence, David L. Hill, and Kenneth W. Ford. Isotope shift anomalies and nuclear structure—1488
Wilkins, H. C. and M. Annis. Interaction cross section of μ mesons with nuclei—480(A)
Wilkinson, D. H. and G. A. Jones. $Li^6(\alpha,\gamma)B^{10}$—1575(L)
Willard, D. (see Dayton, B.)—348
Willardson, R. K., A. C. Beer, and A. E. Middleton. Electrical properties of AlSb—243(A)
Willenbrock, F. K. and N. Bloembergen. Paramagnetic resonance in N- and P-type Si—1281(L)
Williams, Dudley (see Breneman, Edward J.)—465(A)
Williams, H. J., R. M. Bozorth, and Matilda Goertz. Mechanism of transition in magnetite at low temperatures—1107

Willis, Charles and Harry L. Frisch. Vapor-liquid transitions in closed system—465(A)
Wilson, B. G. (see McCusker, C. B. A.)—384
Wilson, Elizabeth (see Friedlander, G.)—498(A)
Wilson, R. R. (see Luckey, D.)—468(A)
—— (see Palfrey, T. R.)—468(A)
Wilson, V. C., B. W. Roberts, W. L. Roth, J. S. Kasper, and A. H. Geisler. Double crystal neutron spectrometer—494(A)
Wimett, T. F. d-p magnetic moment ratio—499(A)
—— Nuclear resonance line structure in HD and molecular shielding in HD, H_2, and D_2—476(A)
Winckler, John R. and Kinsey Anderson. High-altitude cosmic-ray investigation by means of Čerenkov counter. II. Experimental results—431(A)
—— (see Anderson, Kinsey)—431(A)
Windle, J. J. (see Shaw, T. M.)—218(A)
Winkler, Eva M. Design and calibration of total-temperature probes for use at high supersonic speeds and elevated temperatures—469(A)
Winkler, Stanley and Seymour Nozick. Noise in storage tubes—492(A)
Winnemore, Barbara (see Gursky, Herbert)—209(A)
Winsnes, M. H. (see Grimes, D. M.)—435(A)
Winston, A. W. (see Goldschmidt-Clermont, Y.)—468(A)
Winther, A. (see Alder, K.)—1578(L)
Witmer, Enos E. Excitation energies of nuclei as rational multiples of electron mass—500(A)
—— Nuclear masses as rational multiples of electron mass—482(A)
Witzig, W. F. (see Glick, Harvey L.)—236(A)
Wolfe, B., J. DeWire, and A. Silverman. Particle selection using crystal telescope—446(A)
Wolff, P. A. Plasma waves in metals—233(A)
Wolfsberg, Max. Configurational interaction in molecular orbital theory and relative energies of polar and nonpolar functions—464(A)
—— (see Elliott, N.)—435(A)
Wollan, E. O. (see Koehler, W. C.)—597
Wood, Lawrence A. Crystallization in butadiene-styrene copolymers—225(A)
Woodward, L. A. (see Walbridge, N. L.)—1031(A)
Woodward, William. Photodisintegration of deuteron—456(T)
Worley, R. D., M. W. Zemansky, and H. A. Boorse. Heat capacities of superconducting and normal Ta—1567(L)
Wright, G. T. Scintillation response of organic phosphors—1282(L)
Wrinch, Dorothy. Fourier transforms of shells and intensities from crystalline proteins—471(A)
Wu, C. S., F. Boehm, and E. Nagel. Radiations from RaD and RaE—319
—— **and A. Schwarzschild.** β spectrum of C^{14}—483(A)
—— (see der Mateosian, E.)—497(A)
Wu, Ta-You (see Bauer, Ernst)—458(A)
—— (see Moses, Harry E.)—458(A); 1408
—— (see Tauber, G. E.)—443(A)

Yagoda, Herman. Observations on stars and heavy primaries recorded in emulsions during flight of Viking rocket—445(A)
Yeater, M. L. and E. R. Gaerttner. Neutron time-of-flight spectrometer with betatron source—451(A)
Yngve, Victor H. and Marcel Schein. Time variation of cosmic-ray heavy nuclei—432(A)
Yntema, G. B. Magnetoresistance of Mg, Cu, Sb, and Al at liquid He temperatures—1388
Yokota, Ryosuke. Thermoluminescence of quartz and fused quartz colored by x-ray irradiation—1013(L)
Young, J. E. R. (see Bitter, F.)—421(L)
Yukawa, Hideki. Structure and mass spectrum of elementary particles. I. General considerations—415(L); II. Oscillator model—416(L)

Zacharias, Jerrold R. (see Daly, Richard T., Jr.)—476(A)
Zaffarano, D. J. (see Mize, J. P.)—210(A)
Zapas, L. J., S. L. Shufler, and T. W. DeWitt. Dynamic properties of unvulcanized GR-S—217(A)
Zarwyn, Berthold. Generalized theory of Mach reflection of shock waves—470(A)
Zemansky, M. W. (see Worley, R. D.)—1567(L)
Zernow, L. and J. Simon. Plastic behavior of polycrystalline metals at very high strain rates—233(A)
Zilsel, P. R. He II: Bose-Einstein condensation and two-fluid model—216(A)
—— (see Darling, B. T.)—1252
Zimm, B. H. Statistical mechanics of polymer chains in solution—232(T)
Zissis, G. J. (see Deverall, G. V.)—297
Zucker, A. (see Reynolds, H. L.)—496(A)
Zumino, Bruno. True vacuum and dressed particles in quantum field theory—478(A)
Zupančič, Črtomir (see Beckman, Olof)—606

Analytic Subject Index to Volume 91

References with (A) are to abstracts of papers presented at meetings of the American Physical Society; references with (L) are to Letters to the Editor; references with (E) are to Errata. Items are listed under the following categories:

Acoustics
Astrophysics
Atomic and Molecular Beams
Atomic Mass and Abundance
Atomic Structure and Spectra
Biophysics
Chemical Effects and Properties
Constants, Standards, Units
Cosmic Radiation
Crystalline State
Dielectrics and Dielectric Properties
Diffraction
Diffusion
Elasticity and Plasticity
Electrical Conductivity and Resistance
Electrical Discharges
Electrical Properties
Electromagnetic Theory and Electrodynamics
Electrons and Positrons
Elementary Particle Interactions
Errata
Field Theory
Films, Properties
Fluid Dynamics
Gamma Rays
Gases
Geophysics
Helium, Liquid
Imperfections in Solids
Ionization
Ions
Ions and Electrons, Mobility
Liquids
Luminescence
Magnetic Properties
Magnetic Resonance
Mathematical Methods
Mechanics
Mesons
Methods and Instruments
Microwaves
Miscellaneous
Molecular Aggregates
Molecular Structure and Spectra
Neutrino
Noise
Nuclear Fission
Nuclear Moments and Spin
Nuclear Photoeffects
Nuclear Reactions, General
Nuclear Reactions Induced by α Particles and He^3
Nuclear Reactions Induced by Deuterons and Tritons
Nuclear Reactions Induced by Mesons
Nuclear Reactions Induced by Neutrons
Nuclear Reactions Induced by Protons
Nuclear Spectra
Nuclear Structure Theory
Optical Properties
Proceedings of the American Physical Society
Quantum Electrodynamics
Quantum Mechanics
Radiation
Radioactivity
Range and Energy Loss of Particles
Relativity and Gravitation
Scattering, General
Scattering of α Particles
Scattering of Deuterons
Scattering of Electrons and Positrons
Scattering of Mesons
Scattering of Neutrons
Scattering of Protons
Semiconductors
Spectra, General
Statistical Mechanics and Thermodynamics
Superconductivity
Thermal Properties
X-Rays

Absorption of Radiation (see **Radiation**)

Acoustics

Absorption of sound in fogs and emulsions, P. S. Epstein—458(A)

Degeneration of shock wave into sound, Everett F. Cox—1030(A)

Transmission of sound pulse through shock wave, R. A. Alpher and J. R. Rubin—1030(A)

Ultrasonic measurements in liquid He, C. E. Chase—489(A)

Velocity of sound in superconducting Pb and Sn, H. Bommel and J. L. Olsen—1017(L)

Adsorption (see **Gases**)

Aerodynamics (see **Fluid Dynamics**)

Afterglow (see **Electrical Discharges**)

Alloys (see **Crystalline State**)

Annihilation (see **Electrons and Positrons**)

Antiferroelectric Phenomena (see **Dielectrics and Dielectric Properties**)

Antiferromagnetism (see **Magnetic Properties**)

Arcs (see **Electrical Discharges**)

Astrophysics

Initial conditions in expanding universe and element synthesis, R. A. Alpher, J. W. Follin, Jr., and R. C. Herman—479(A)

Intensity of Lyman-α line in solar spectrum, William A. Rense—299

Lyman-α radiation in solar spectrum, E. T. Byram, T. Chubb, H. Friedman, and N. Gailar—1278(L)

Magnetic self-focusing of auroral protons, W. H. Bennett and E. O. Hulburt—1562(L)

Atmosphere (see **Geophysics**)

Atomic and Molecular Beams

Doppler effects in atomic beam magnetic resonance method, Richard T. Daly, Jr., and Jerrold R. Zacharias—476(A)

Hfs and nuclear moment ratios of stable Br isotopes, J. G. King and V. Jaccarino—209(A)

Hfs and nuclear moments of Pr^{141}, Hin Lew—619

Hfs of Ag with aid of universal ionizer for atomic beams, Günter Wessel and Hin Lew—476(A)

Hfs of I, J. G. King, H. H. Stroke, and V. Jaccarino—476(A)

Hfs of metastable triplet state of He^3, Gabriel Weinreich, Gerard M. Grosof, and Vernon W. Hughes—195(L)

Hfs of resonance lines of In^{115}, G. V. Deverall, K. W. Meissner, and G. J. Zissis—297

Magnetic moment of He atom in metastable triplet state, Vernon Hughes, Gardiner Tucker, Emlyn Rhoderick, and Gabriel Weinreich—828

Molecular beam investigation of rotational transitions. I. Rotational levels of KCl and their hfs, Charles A. Lee, B. P. Fabricand, R. O. Carlson, and I. I. Rabi—1395; II. Of KBr, B. P. Fabricand, R. O. Carlson, C. A. Lee, and I. I. Rabi—1403

Atomic Mass and Abundance

Doublet measurements with mass synchrometer, C. C. Damm and Lincoln G. Smith—482(A)

Evidence for region of extra nuclear stability between 82- and 126-neutron shells, Benjamin G. Hogg and Henry E. Duckworth—1289(L)

Nuclear masses as rational multiples of electron mass, Enos E. Witmer—482(A)

Second minimum in packing fraction curve at 40 neutrons, T. L. Collins, W. H. Johnson, Jr., and A. O. Nier—482(A)

Atomic Structure and Spectra
Approximate Hartree type wave function and matrix elements for K and L shells of atoms and ions, R. E. Meyerott—456(A)
Auger electron intensities, R. D. Hill—770(L)
Configuration interaction in Mo II, Howard D. Goldgraber—456(A)
Contributions to hyperfine spectrum of He^3 resulting from nuclear structure, A. M. Sessler and H. M. Foley—444(A)
Correlation energy in ground state of He I, Louis C. Green, Marjorie M. Mulder, and Paul C. Milner—35
Deficiency of phenomenological theory of Lamb shift, Frederik J. Belinfante—1285(L)
Effect of nuclear structure on hfs of He^3, Vernon Hughes and Gabriel Weinreich—196(L)
Effective nuclear charges for atoms from self-consistent field calculations, A. J. Freeman—1410
Electric field gradient of atomic p electrons, W. V. Smith and R. G. Barnes—457(A)
Electrostatic energy matrices of configuration f^4, Edith F. Reilly—876
Fourth-order radiative corrections to atomic energy levels, J. Weneser, R. Bersohn, and N. M. Kroll—1257
Hfs of metastable triplet state of He^3, Gabriel Weinreich, Gerard M. Grosof, and Vernon W. Hughes—195(L)
Hfs of resonance lines of In^{115}, G. V. Deverall, K. W. Meissner, and G. J. Zissis—297
Intensity of Lyman-α line in solar spectrum, William A. Rense—299
Isotope shift anomalies and nuclear structure, Lawrence Wilets, David L. Hill, and Kenneth W. Ford—1488
Isotope shift in arc spectrum of Li, Raymond H. Hughes—457(A)
Isotope shift in B III, Edward W. Burke—457(A)
Lyman-α radiation in solar spectrum, E. T. Byram, T. Chubb, H. Friedman, and N. Gailar—1278(L)
Magnetic moment of He atom in metastable triplet state, Vernon Hughes, Gardiner Tucker, Emlyn Rhoderick, and Gabriel Weinreich—828
Magnetic scanning method for investigating hfs and isotope shift, F. Bitter, H. Plotkin, B. Richter, A. Teviotdale, and J. E. R. Young—421(L)
Matrix elements of spin-spin interaction, Frederick R. Innes—31
μ mesic atom, L. N. Cooper and E. M. Henley—480(A)
Natural lifetime of Cd 5^3P_1 state, C. G. Matland—436(A)
Nuclear moments of Ta^{181}, erratum, B. M. Brown and D. H. Tomboulian—1580(E)
Polarization of Na atoms, W. B. Hawkins and R. H. Dicke—1008(L)
Production of Na airglow excitation by imprisonment of resonance radiation, A. Foderaro and T. M. Donahue—1561(L)
Quadrupole moments of stable Sb nuclei, G. Sprague and D. H. Tomboulian—476(A)
Relativistic contributions to magnetic moment of n-electron atoms, William Perl—852
Relativistic contributions to magnetic moment of $^3S_1$ He, William Perl and Vernon Hughes—842
Shift of 1^1S state of He, S. Chandrasekhar, Donna Elbert, and Gerhard Herzberg—1172
Stark shift and broadening due to electrons, M. Baranger—436(A)
Theory of complex spectra, Sydney Meshkov—871

Aurora (see **Astrophysics; Geophysics**)

Barkhausen Effect (see **Magnetic Properties**)

Biophysics
Biophysical study of burns, Irven C. Graham, David Pomeroy, W. C. McGarvey, and John G. Randall—214(A)
Effect of temperature and ultraviolet radiation on dry catalase, Richard Setlow and Barbara Doyle—494(A)
Fourier transforms of shells and intensities from crystalline proteins, Dorothy Wrinch—471(A)
Inactivation of desoxyribonucleic acid by bombardment with deuterons and electrons, Cyril L. Smith—493(A)
Study with NaI scintillation spectrometer of methods of estimating I^{131} contained in human thyroid, Robert J. Kerr, Sherwood K. Haynes, and George R. Meneely—214(A)

Boson Theory (see **Field Theory**)

Bremsstrahlung (see **Radiation**)

Broadening of Spectral Lines (see **Atomic Structure and Spectra; Molecular Structure and Spectra; Spectra, General**)

Capture Cross Sections (see **Electrons and Positrons; Nuclear Reactions; Radiation**)

Chemical Effects and Properties
Compressions to 150 000 psi for series of high molecular weight liquid hydrocarbons, R. H. McMickle, R. W. Schiessler, and W. Webb—466(A)
Electrolysis of water: experiment in atomic physics, Carl C. Sartain—227(A)
Mass spectrometer analysis of UO_2F_2 in UF_4, Russell Baldock, John R. Sites, L. O. Gilpatrick, and Howard E. Carr—242(A)
Mass spectrometric positive ion technique for determining phase transition temperatures and heats of transformation in metals, R. G. Johnson, W. C. Caldwell, D. E. Hudson, and F. H. Spedding—466(A)
Molar activity coefficients of electrolytes from conductivity data, Henry P. Marshall and Ernest Grunwald—214(A)
Polarization in liquids of intermediate conductivity, John A. Rider—214(A)
Shock tube for studying chemical kinetics, A. Hertzberg and W. Squire—469(A)
Solubility of solids in gases, A. H. Ewald—215(A)
Vapor-liquid transitions in closed system, Charles Willis and Harry L. Frisch—465(A)

Chemical Reactions (see **Chemical Effects and Properties**)

Chemiluminescence (see **Luminescence**)

Cold Emission (see **Electrical Properties**)

Colloids (see **Chemical Effects and Properties; Molecular Aggregates**)

Compton Effect (see **Radiation**)

Conductivity, Electrical (see **Electrical Conductivity and Resistance**)

Conductivity, Thermal (see **Thermal Properties**)

Constants, Standards, Units
Comparison of nuclear and γ-ray absolute energy scales, K. W. Jones, M. T. McEllistrem, R. A. Douglas, and H. T. Richards—482(A)
Present status of fundamental atomic constants, J. A. Bearden, M. D. Earle, J. M. Minkowski, and J. S. Thomsen—482(A)
Temperature scale in liquid He region, L. D. Roberts and R. A. Erickson—488(A)

Cosmic Radiation
Absorption mean free path of high-energy nucleonic component, M. F. Kaplon, J. Z. Klose, D. M. Ritson, and W. D. Walker—1573(L)

Cosmic Radiation (Continued)
Altitude variation and transition effects of air showers, O. Piccioni and R. L. Cool—433(A)
Anisotropic distribution of secondaries in extreme energy cosmic-ray stars, Frank C. Roesler and C. B. A. McCusker—690
Bubble-chamber tracks of penetrating particles, Donald A. Glaser—762(L)
Charged τ mesons, Nathan Seeman, D. T. King, and Maurice M. Shapiro—446(A)
Cloud-chamber investigation of nuclear interactions, N. R. Whetten, R. S. Preston, R. V. Adams, and R. W. Walker—432(A)
Cloud-chamber study of particles in primary cosmic radiation, Frank B. McDonald—432(A)
Cluster-count determination of specific ionization of cloud-chamber tracks, Hans O. Cohn, L. R. Etter, and R. W. Thompson—445(A)
Collision lengths of neutral, penetrating-shower-producing cosmic radiation in light and heavy water, Darol Froman, James Kenney, and Victor H. Regener—707
Cosmic-radiation intensity time variations and their origin. II. Energy dependence of 27-day variations, William H. Fonger—351
Cosmic-ray albedo, S. B. Treiman—432(A); 957
Cosmic-ray star production rates in gases, Fielding Brown and George T. Reynolds—444(A)
Decay of heavy mesons in nuclear emulsion, P. H. Barrett—446(A)
Decay of V^0 particle into two mesons, B. Dayton and D. Willard—348
Delayed neutrons in cosmic-ray stars, Byron W. St. Clair—445(A)
Development of extensive showers in atmosphere, Kurt Sitte and Don L. Stierwalt—433(A)
Effects at Godhavn and lower latitudes of changes in energy and composition of solar cosmic rays, V. Sarabhai and R. P. Kane—688
Emulsion chamber studies of high-energy cosmic-ray interactions, J. J. Lord—432(A)
Energy distribution of neutral mesons produced in cosmic-ray stars, Y. B. Kim—445(A)
Energy distribution of neutron stars, R. W. Waniek and T. Ohtsuka—445(A)
Energy spectra of cosmic-ray photons and electrons from plastic scintillation counter measurements, C. N. Chou—433(A)
Energy spectrum of particles from stars, R. W. Waniek and Taiichiro Ohtsuka—1574(L)
Extreme energy interactions in heavy nuclei, C. B. A. McCusker and F. C. Roesler—769(L)
Heavy nuclei in primary cosmic radiation, T. H. Stix—431(A)
High-altitude cosmic-ray investigation by means of Čerenkov counter. I. Instrumentation details, Kinsey Anderson and John R. Winckler—431(A); II. Experimental results, John A. Winckler and Kinsey Anderson—431(A)
High-altitude measurements of intensity of cosmic radiation at magnetic latitudes 3°N and 19°N, A. S. Rao, V. K. Balasubrahmanyam, G. S. Gokhale, and A. W. Pereira—764(L)
Intensity of primary protons and α particles, L. R. Davis, H. M. Caulk, and C. Y. Johnson—431(A)
Interpretation of $0+xp$ type stars in photographic emulsions, C. B. A. McCusker and F. C. Roesler—769(L)
K-particle mass measurements, D. M. Ritson—1572(L)
Kinetic energies of V_1^0 particles, J. Ballam, D. R. Harris, A. L. Hodson, R. Ronald Rau, George T. Reynolds, S. B. Treiman, and M. Vidale—1019(L)
Magnetic cloud-chamber observations of V particles. I. Apparatus and reduction of data, A. V. Buskirk, L. R. Etter, C. J. Karzmark, R. H. Rediker, and R. W. Thompson—445(A); II. V^0 particles, R. W. Thompson, A. V. Buskirk, L. R. Etter, C. J. Karzmark, R. H. Rediker—446(A)
Mean free path for shower production by high-energy π mesons, Fritz E. Froehlich and Kurt Sitte—433(A)
Momenta of V^0 particles, J. Ballam, D. R. Harris, A. L. Hodson, R. Ronald Rau, George T. Reynolds, S. B. Treiman, and M. L. Vidale—446(A)
Neutron and meson stars induced in light elements of emulsion, M. Blau, A. R. Oliver, and J. E. Smith—949
Neutron production by sea-level cosmic rays, with particular reference to μ mesons stopped in Pb, E. J. Althaus and R. D. Sard—373
Observations on stars and heavy primaries recorded in emulsions during flight of Viking rocket, Herman Yagoda—445(A)
Origin of cosmic rays, J. W. Dungey—766(L)
Production of mesons above 10 Bev, C. B. A. McCusker, N. A. Porter, and B. G. Wilson—384
Recent experimental results on S particles, H. Bridge, H. Courant, H. DeStaebler, Jr., and B. Rossi—1024(L)
Speculation on V spin, D. C. Peaslee—446(A)
Star clustering in nuclear emulsions, Frank B. Brown, Jr., and A. V. Masket—210(A)
Time and directional study of primary heavy nuclei, G. W. Anderson, P. S. Freier, and J. E. Naugle—431(A)
Time delays in air showers, P. Bassi, G. Clark, and B. Rossi—432(A)
Time variation of cosmic-ray heavy nuclei, Victor H. Yngve and Marcel Schein—432(A)
Zenith angle variation of cosmic-ray meson intensity, Arthur Beiser—446(A)

Cosmology (see **Astrophysics; Relativity and Gravitation**)
Critical Potentials (see **Atomic Structure and Spectra; Molecular Structure and Spectra**)
Cross Section (see **Electrons and Positrons; Nuclear Reactions; Radiation; Scattering**)
Crystal Counters (see **Methods and Instruments**)
Crystalline State (see also **Electrical Properties; Imperfections in Solids; Magnetic Properties; Semiconductors; etc.**)
Absorption of light by trapped electrons, R. C. O'Rourke—265
Activation energy for recovery of reactor-irradiated Cu crystals, J. K. Redman, R. R. Coltman, and T. H. Blewitt—448(A)
Activation entropies for diffusion mechanisms, H. B. Huntington, G. A. Shirn, and E. S. Wajda—246(A)
Anisotropy of grain boundary diffusion, L. Couling and R. Smoluchowski—245(A)
Annealing of bombardment damage in Ge: Theoretical, R. C. Fletcher, W. L. Brown, and S. Machlup—237(A); Experimental, W. L. Brown and R. C. Fletcher—237(A)
Anomaly in heat content of metal in fatigued state, B. Welber and R. Webeler—448(A)
Antiparallel dipole arrangement in WO_3, Ryuzo Ueda and Jinzo Kobayashi—1562(L)
Band structures of one-dimensional crystals with square well potentials, G. Allen—531
Band width of F centers in KBr, I. L. Mador, J. J. Markham, and R. I. Platt, Jr.—219(A); 1277(L)
Bleaching of CaF_2 crystals colored by x-rays, Alexander Smakula—1570(L)
Bleaching properties of F centers in KBr at 5°K, J. J. Markham, R. I. Platt, Jr., and I. L. Mador—219(A)

Brillouin zone investigation of Mg alloys. I. Hall effect and conductivity, A. I. Schindler and E. I. Salkovitz—1320
Brillouin zone structures of alloys. I. Implications of present theories, E. I. Salkovitz and A. I. Schindler—234(A)
Change of elastic constants resulting from annealing of Cu and Al cold worked at −196°C, E. C. Crittenden, Jr., and H. Dieckamp—232(A)
Changes in electrical, thermal, and thermoelectrical properties of monovalent metals by lattice distortions, A. W. Sáenz—1142
Cohesive energy of alkali metals, Harvey Brooks—1027(L)
Comparison of resistivity and density changes in cold-worked brass, Herbert I. Fusfeld—233(A)
Computation of mean Debye temperature of cubic crystals from elastic constants, S. L. Quimby and Paul M. Sutton—1122
Computations of three-dimensional structure factors on S-FAC, R. Pepinsky and P. F. Eiland—229(A)
Crystalline electric field in NdBr, R. A. Satten—471(A)
Crystallite size and diamagnetic susceptibility of carbons, H. T. Pinnick—228(A)
Debye temperature of Cu_3Au, Dwain B. Bowen—220(A)
Decay of vacancies frozen into alloy by quenching, A. S. Nowick and A. E. Roswell—221(A)
Deformation characteristics of reactor-irradiated Cu single crystals at 78°K and 300°K, R. E. Jamison and T. H. Blewitt—237(A)
Deformation of Cu crystals at 78°K and 300°K, T. H. Blewitt, J. K. Redman, and F. A. Sherrill—236(A); T. H. Blewitt—1115
Density change in proton-irradiated KCl, W. J. Leivo—245(A)
Diffusion of Cd in single crystals of Ag, T. Tomizuka, L. Slifkin, and D. Lazarus—245(A)
Dilatometric study of order-disorder transformation in Cu-Au alloys, W. W. Sanville, Foster C. Nix, and Frank E. Jaumot, Jr.—220(A)
Dislocations and edge states in diamond crystal structure, W. Shockley—228(A)
Displacement energy for radiation damage in Cu, D. T. Eggen and M. J. Laubenstein—238(A)
Effect of neutron irradiation on phase change in Sn, Jerome Fleeman—237(A)
Effects of heat treatment on lattice perfection, Norman W. Lord—472(A)
Effects of temperature gradients on diffusion in crystals, W. Shockley—1563(L)
Electric field and energy in dipole lattices, E. F. Bertaut—415(L)
Electrical breakdown path orientation in alkali halide crystals, J. W. Davisson—228(A)
Electron density in sodium tungsten bronze, W. R. Gardner and G. C. Danielson—220(A)
Electron distributions for opacity calculations, Malcolm K. Brachman and Roland E. Meyerott—437(A)
Electron energy levels in *F* centers, William A. Smith and Allen B. Scott—219(A)
Electron mean free path of damaged Cu in terms of electrical resistivity and thermoelectric power, G. W. Rodeback and W. P. Eatherly—237(A)
Electron motion in polar crystals, E. P. Gross—228(A)
Electronic and lattice specific heats in W, Mo, and Re, M. Horowitz and J. G. Daunt—1099
Electronic energy states of impurities in nonmetallic crystals, Kurt Lehovec—228(A)
Electronic structure of *F* centers, C. Kittel—219(A)
Energy band crossings for periodic square well potentials, G. Allen and Rolf Landauer—471(A)
Energy band structure of diamond and Ge crystals, Frank Herman—491(A)
Evaporation of Cu from Ge, George Finn—754(L)
Experimental method to determine equation of state data for solids by shock wave measurements, Russell H. Christian and John M. Walsh—1030(A)
Generalized self-consistent field method, J. C. Slater—528
Grain boundary self-diffusion in body-centered lattice, C. W. Haynes and R. Smoluchowski—245(A)
Gyromagnetic ratios of microcrystalline materials, erratum, S. J. Barnett—1580(E)
Hall effect in ordered and disordered Ni_3Mn, Simon Foner and Emerson M. Pugh—220(A)
Hall effects of Co-Ni alloys and of Armco iron, Simon Foner and Emerson M. Pugh—20
Hardness change in Cu irradiated with 1.25-Mev electrons, C. E. Dixon and C. J. Meechan—237(A)
Influence of impurities on diffusion in solids, Albert W. Overhauser—246(A)
Interpretation of "dc etch" phenomena, D. B. Langmuir—447(A)
Irradiation-induced photoconductivity in MgO, Harold R. Day—238(A); 822
Iteration variation calculation of electronic structure of diamond, M. Dank and H. B. Callen—229(A)
Kinetics of disorder-order transformation in Cu_3Au, Norman W. Lord—221(A)
Lattice absorption in diamond: one-dimensional model, Melvin Lax and Eli Burstein—492(A)
Lattice vibrations in graphite, Herbert B. Rosenstock—233(A)
Low temperature fast neutron bombardment of Cu-Be alloy, J. W. Cleland, D. S. Billington, and J. H. Crawford, Jr.—238(A)
Magnetoresistance of Bi crystals at low temperatures, P. B. Alers and R. T. Webber—1060
Mass spectrometric positive ion technique for determining phase transition temperatures and heats of transformation in metals, R. G. Johnson, W. C. Caldwell, D. E. Hudson, and F. H. Spedding—466(A)
Mass spectrometric study of sublimation of graphite, Richard E. Honig—465(A)
Mechanical properties of proton-irradiated alkali halides, W. H. Vaughan, W. J. Leivo, and R. Smoluchowski—245(A)
Mobility of interstitial atoms in face-centered metal, H. B. Huntington—1092
Mobility of slow electrons in polar crystals, Francis E. Low and David Pines—193(L)
Nature of radiation damage in diamond, G. J. Dienes and D. A. Kleinman—238(A)
Neutron diffraction study of antiferromagnetic structure of pyrrhotite, FeS_x, S. S. Sidhu and David Meneghetti—435(A)
Neutron diffraction study of BiMn alloy, B. W. Roberts—435(A)
New approximation method for order-disorder problems, Lloyd D. Fosdick and Hubert M. James—1131
New treatment of energy bands, Norman Rostoker and Walter Kohn—234(A)
Nyquist and Einstein relations derived from scattering model, Stefan Machlup—240(A)
Ordering in alloy system Mg-Ce, C. A. Wert—221(A)
Phase transition in $ND_4D_2AsO_4$, B. C. Frazer—246(A)
Photoconductivity and *V* centers, K. Teegarden and R. J. Maurer—219(A)
Plasma waves in metals, P. A. Wolff—233(A)
Plastic behavior of polycrystalline metals at very high strain rates, L. Zernow and J. Simon—233(A)

Crystalline State (Continued)
Precipitation effects in Cu-Fe alloys, Thomas S. Hutchison—449(A)
Production of F', M, and R centers in NaCl at room temperature, R. T. Platt, Jr., I. L. Mador, and J. J. Markham—219(A)
Quantum theory of polarizability of idealized crystal, D. L. Dexter and W. R. Heller—273
Radiation damage and rate processes, J. W. Marx—1564(L)
Reversible bleaching of absorption band of diamond, Peter Pringsheim—220(A); 551
Shapes of floating liquid zones between solid rods, P. H. Keck, M. Green, and M. L. Polk—472(A)
Short-range order in Cu-Au alloy, Charles H. Sutcliffe and Frank E. Jaumot, Jr.—221(A)
Strain and crystallite size in experimental Fe powders, Frank E. Jaumot, Jr., and Leonard Muldawer—232(A)
Strength of solid solution alloys, John C. Fisher—232(A)
Structure and aging of thin metal films. I, Robert J. Raudebaugh and Richard B. Belser—449(A); II, Richard B. Belser and Robert J. Raudebaugh—449(A); III. Richard B. Belser and Robert J. Raudebaugh—499(A)
Tentative theory of metallic whisker growth, J. D. Eshelby—755(L)
Theory of initial stress strain curves in face-centered metals, J. S. Koehler—233(A)
Thermal and electrical properties and crystal structure of tungsten oxide at high temperatures, Shozo Sawada—1010(L)
Thermalization of positrons in metals, R. L. Garwin—1571(L)
Thermodynamic activities in Fe-Ni alloys, R. A. Oriani—465(A)
Two-electron example of ferromagnetism, J. C. Slater, H. Statz, and G. F. Koster—205(A); 1323
Variable activation energy and motion of lattice defects, G. J. Dienes—1283(L)
Vibration spectrum of simple cubic lattice, Gordon F. Newell—227(A)
Work hardening in substitutional alloys, J. S. Koehler—448(A)
X-ray and metallurgical studies on neutron-irradiated Cu_3Au, R. H. Fillnow, E. K. Halteman, and G. F. Mechlin—236(A)
X-ray measurements of cold-worked α brass, B. E. Warren, B. L. Averbach, and E. Warekois—233(A)
X-ray study of graphitization, J. C. Bowman, S. Hayes, and R. Smoluchowski—244(A)
Yield point strain, Edward W. Hart—232(A)
Z centers in alkali halides, D. R. Westervelt—218(A)

Diamagnetism (see **Magnetic Properties**)

Dielectrics and Dielectric Properties
Antiferroelectrics in applied field, Jack R. Tessman—447(A)
Antiparallel dipole arrangement in WO_3, Ryuzo Ueda and Jinzo Kobayashi—1562(L)
Carrier contribution to dielectric constant of Ge, T. S. Benedict and W. Shockley—207(A)
Charged density distribution *vs* semipermanent polarization as basis for electret behavior, W. F. G. Swann—447(A)
Directional effects in the electric breakdown of ionic crystals, erratum, Elmer L. Offenbacher and Herbert B. Callen—1580(E)
Double hysteresis loop of $BaTiO_3$ at Curie point, Walter J. Merz—513
Effects of grooves in piezoelectric filter plates, Charles R. Mingins, Robert W. Perry, and David W. MacLeod—471(A)
Electric field and energy in dipole lattices, E. F. Bertaut—415(L)
Electric wave filter combining piezoelectric divided electrode units, Albert D. Frost, Charles R. Mingins, and Lawrence A. Howard—471(A)
Electrical breakdown path orientation in alkali halide crystals, J. W. Davisson—228(A)
Electrical properties of TiO_2 semiconductors, Robert G. Breckenridge and William R. Hosler—793
Ferroelectricity in rochelle salt, Julian H. Gibbs—447(A)
Mechanism of self-sustained electron emission from MgO, Dietrich Dobischek, Harold Jacobs, and John Freely—804
New model for Debye dispersion equations, J. Ross Macdonald—412(L)
Phase transition in CsH_2AsO_4, B. C. Frazer and Ray Pepinsky—212(A)
Phase transition in $ND_4D_2AsO_4$, B. C. Frazer—246(A)
Phase transitions in antiferroelectric $PbHfO_3$, Gen Shirane and Ray Pepinsky—212(A); 812
Radioactive charging through dielectric medium, E. G. Linder and P. Rappaport—202(L); erratum—1580(E)
$SrTiO_3$ electrical properties, Arthur Linz, Jr.—753(L)
Threshold field and free energy for antiferroelectric ferroelectric phase transition in $PbZrO_3$, A. DeBretteville, Jr.—213(A)

Diffraction (see also **Scattering**)
Complex amplitudes for electron scattering by atoms, Jean A. Hoerni and James A. Ibers—1182
Double crystal neutron spectrometer, V. C. Wilson, B. W. Roberts, W. L. Roth, J. S. Kasper, and A. H. Geisler—494(A)
Electron interferometer, L. Marton, J. Arol Simpson, and J. A. Suddeth—437(A); Construction and operation, J. A. Suddeth, L. Marton, and J. Arol Simpson—437(A); Observations and interpretation, J. Arol Simpson, J. A. Suddeth, and L. Marton—437(A)
Neutron diffraction by liquid He, D. G. Henshaw and D. G. Hurst—1222; By liquid O_2, N_2, and A, D. G. Henshaw, D. G. Hurst, and N. K. Pope—472(A)
Neutron diffraction study of antiferromagnetic structure of pyrrhotite, FeS_x, S. S. Sidhu and David Meneghetti—435(A)
Neutron diffraction study of BiMn alloy, B. W. Roberts—435(A)
Second-order scattering correction in neutron and x-ray diffraction, George H. Vineyard—239(A)

Diffusion (see also **Fluid Dynamics**)
Activation entropies for diffusion mechanisms, H. B. Huntington, G. A. Shirn, and E. S. Wajda—246(A)
Anisotropy of grain boundary diffusion, L. Couling and R. Smoluchowski—245(A)
Cl isotope separation by thermal diffusion, A. Z. Kranz and W. W. Watson—1469
Diffusion currents in semiconductor Hall effect, Rolf Landauer and John Swanson—207(A); 555
Diffusion of Cd in single crystals of Ag, T. Tomizuka, L. Slifkin, and D. Lazarus—245(A)
Diffusion of Li into Ge and Si, C. S. Fuller and J. A. Ditzenberger—193(L)
Diffusion of Sb in Ag, E. Sonder, L. Slifkin, and D. Lazarus—245(A)
Effect of fast-neutron bombardment on diffusion in Cu_3Au, R. R. Coltman and T. H. Blewitt—236(A)
Effects of temperature gradients on diffusion in crystals, W. Shockley—1563(L)

Grain boundary self-diffusion in body-centered lattice, C. W. Haynes and R. Smoluchowski—245(A)
Influence of impurities on diffusion in solids, Albert W. Overhauser—246(A)
Interpretation of "dc etch" phenomena, D. B. Langmuir —447(A)
Turbulent diffusion from volume source with nonuniform initial distribution, Frank Gifford, Jr.—1031(A)
Values of diffusion coefficients for some chain polymers computed from anomalous osmotic pressure data, T. A. Barr, Jr.—211(A)

Discharge of Electricity in Gases (see **Electrical Discharges**)

Disintegration and Excitation of Nucleus (see **Nuclear Reactions**)

Dynamics (see **Mechanics**)

Elasticity and Plasticity
Change of elastic constants resulting from annealing of Cu and Al cold worked at −196°C, E. C. Crittenden, Jr., and H. Dieckamp—232(A)
Deformation characteristics of reactor-irradiated Cu single crystals at 78°K and 300°K, R. E. Jamison and T. H. Blewitt—237(A)
Deformation of Cu crystals at 78°K and 300°K, T. H. Blewitt, J. K. Redman, and F. A. Sherrill—236(A); T. H. Blewitt—1116
Dependence of photoelastic properties of GR-S on degree of cross linking, G. R. Taylor and S. R. Darin—211(A)
Hardness change in Cu irradiated with 1.25-Mev electrons, C. E. Dixon and C. J. Meechan—237(A)
Plastic behavior of polycrystalline metals at very high strain rates, L. Zernow and J. Simon—233(A)
Stress-strain curves of Cu single crystal at 4.2°K, T. H. Blewitt, R. R. Coltman, R. E. Jamison, and J. K. Redman—448(A)
Tensile strength and adhesion of thin films of Ag, H. S. Morton, Jr., and J. W. Beams—449(A)
Theory of initial stress-strain curves in face-centered metals, J. S. Koehler—233(A)
Variation of elastic constants of crystalline Al with temperature between 63°K and 773°K, Paul M. Sutton—816
Work hardening in substitutional alloys, J. S. Koehler—448(A)
Yield point strain, Edward W. Hart—232(A)

Electrical Breakdown (see **Dielectrics and Dielectric Properties; Electrical Discharges**)

Electrical Conductivity and Resistance (see also **Semiconductors; Superconductors**)
Adsorbed O in ZnO photoconductivity, Donald A. Melnick and Leo J. Neuringer—229(A)
Of AlSb, R. K. Willardson, A. C. Beer, and A. E. Middleton—243(A)
Anisotropic resistivities of Se crystals at high frequencies, H. W. Henkels and J. Maczuk—1562(L)
Brillouin zone investigation of Mg alloys. I. Hall effect and conductivity, A. I. Schindler and E. I. Salkovitz—1320
Brillouin zone structures of alloys. I. Implications of present theories, E. I. Salkovitz and A. I. Schindler—234(A); II. Hall constant data of dilute Mg alloys, A. I. Schindler and E. I. Salkovitz—234(A)
Of carbon bisulfate compounds, E. A. Kmetko—243(A)
Change of metallic conductivity through change in thermal scattering, R. Smoluchowski—245(A)
Changes in conductivity of NaCl produced by bombardment with 360-Mev protons, E. A. Pearlstein—244(A)
Comparison of resistivity and density changes in cold-worked brass, Herbert I. Fusfeld—233(A)
Conductivity of thin films in longitudinal magnetic field, Ernest Koenigsberg—8
Continuous flow cell for investigation of polarization at metal-solution interface, L. W. Morris and Hung-Chi Chang—215(A)
Current carrier lifetimes deduced from Hall coefficient and resistivity measurements, E. J. Huibregtse and L. P. Hunter—208(A); L. P. Hunter, E. J. Huibregtse, and R. L. Anderson—1315
Debye temperature of Cu_3Au, Dwain B. Bowen—220(A)
Deformation of Cu crystals at 78°K and 300°K, T. H. Blewitt, J. K. Redman, and F. A. Sherrill—236(A); T. H. Blewitt—1115
Diffusion currents in Hall effect in semiconductors, Rolf Landauer and John Swanson—207(A); 555
Effect of sputtering rate on resistivity and "aging" of sputtered Ag films, Richard B. Belser—221(A)
Effect of strong electrostatic fields on resistance of W wires, W. J. Deshotels and A. H. Weber—448(A)
Electric conduction at metal-semiconductor and metal-solution interfaces, Hung-Chi Chang—214(A)
Electrical properties of TiO_2 semiconductors, Robert G. Breckenridge and William R. Hosler—793
Electrical resistance of graphite at low temperatures, H. W. Hemstreet and J. M. Reynolds—242(A); J. M. Reynolds, H. W. Hemstreet, and T. E. Leinhardt—1152
Electron density in sodium tungsten bronze, W. R. Gardner and G. C. Danielson—220(A)
Electron mean free path of damaged Cu in terms of electrical resistivity and thermoelectric power, G. W. Rodeback and W. P. Eatherly—237(A)
Electronic Hall effect in NaCl, Alfred G. Redfield—753(L)
Of elementary B, L. W. Friedrich and V. P. Jacobsmeyer —492(A)
Hall effect and conductivity of Ge containing As or Ga as impurities, Peter P. Debye—208(A)
Hall effect and conductivity of InSb single crystals, M. Tanenbaum and J. P. Maita—1009(L)
Hall effect in flowing ion clouds, B. E. Clotfelter—436(A)
Hall effect in ordered and disordered Ni_3Mn, Simon Foner and Emerson M. Pugh—220(A)
Hall effect in pure Ti, V, and Cr, Simon Foner—447(A)
Hall effect in Y, La, Ce, Pr, Nd, Gd, Dy, and Er, C. J. Kevane, S. Legvold, and F. H. Spedding—1372
Hall effects of Co-Ni alloys and of Armco iron, Simon Foner and Emerson M. Pugh—20
Hall mobility in insulation photoconductors, Alfred Redfield—244(A)
Of InSb, R. G. Breckenridge, W. R. Hosler, and W. Oshinsky—243(A)
Irradiation-induced photoconductivity in MgO, Harold R. Day—238(A); 822
Low-temperature fast-neutron bombardment of Cu-Be alloy, J. W. Cleland, D. S. Billington, and J. H. Crawford, Jr.—238(A)
Magnetoresistance in InSb, M. Tanenbaum and G. L. Pearson—244(A)
Magnetoresistance of Bi crystals at low temperatures, P. B. Alers and R. T. Webber—1060
Magnetoresistance of Mg, Cu, Sb, and Al at liquid He temperatures, G. B. Yntema—1388
Mechanically-disturbed Ge surfaces, Edward N. Clarke and Robert L. Hopkins—1566(L)
Molar activity coefficients of electrolytes from conductivity data, Henry P. Marshall and Ernest Grunwald—214(A)
Of *n*-type Ge, Esther M. Conwell—208(A)
Nyquist and Einstein relations derived from scattering model, Stefan Machlup—240(A)

Electrical Conductivity and Resistance (Continued)
Photoconductivity and carrier traps in Ge, H. A. Gebbie, M. Nisenoff, and H. Y. Fan—230(A)
Photoconductivity and V centers, K. Teegarden and R. J. Maurer—219(A)
Photocurrent, space-charge buildup, and field emission in alkali halide crystals, A. von Hippel, E. P. Gross, J. G. Jelatis, and M. Geller—568
Piezoresistance effect in Ge, Charles S. Smith and J. R. Haynes—491(A)
Polarization in liquids of intermediate conductivity, John A. Rider—214(A)
Preparation of gray Sn filaments, A. W. Ewald—244(A)
Relation between de Haas-van Alphen effect and magnetoresistance in Bi, Ted G. Berlincourt—1277(L)
Resistivity of Cu_3Au during neutron irradiation, Harvey L. Glick and W. F. Witzig—236(A)
Search for Hall effect in superconductor, H. W. Lewis—216(A)
Series method for comparison of resistances, Harold J. Hoge—493(A)
Thermoelectric power and electrical resistivity of dilute solid solution of Si in Cu, C. A. Domenicali and B. A. Boyd—220(A)
Very high-resistance measurement, Frank J. Lynch and Clarence L. Wesenberg—493(A)
Electrical Discharges
Diffusion cooling of electrons in ionized gases, Manfred A. Biondi—437(A)
Field emission initiated vacuum arc. I. Experiments on arc initiation, W. P. Dyke, J. K. Trolan, E. E. Martin, and J. P. Barbour—1043; II. Resistively heated emitter, W. W. Dolan, W. P. Dyke, and J. K. Trolan—1054
Formative time lags of uniform field breakdown in A, G. A. Kachickas and L. H. Fisher—775
Hall effect in flowing ion clouds, B. E. Clotfelter—436(A)
Metastable atoms in afterflow of low-pressure He discharge, Arthur V. Phelps—436(A)
Simultaneous measurement of ionization and attachment coefficients, Melvin A. Harrison and Ronald Geballe—1
Electrical Properties (see also **Dielectrics and Dielectric Properties; Electrical Conductivity and Resistance; Semiconductors; Superconductors**)
Of AlSb, R. K. Willardson, A. C. Beer, and A. E. Middleton—243(A)
Of Au-Ge alloys, W. C. Dunlap, Jr.—1282(L)
Auger peaks in energy spectra of secondary electrons from various materials, J. J. Lander—1382
Of carbon bisulfate compounds, E. A. Kmetko—243(A)
Changes in electrical, thermal, and thermoelectrical properties of monovalent metals by lattice distortions, A. W. Sáenz—1142
Current carrier lifetimes deduced from Hall coefficient and resistivity measurements, E. J. Huibregtse and L. P. Hunter—208(A); L. P. Hunter, E. J. Huibregtse, and R. L. Anderson—1315
Current density tables for field emission theory, W. W. Dolan—510
Directional effects in the electric breakdown of ionic crystals, erratum, Elmer L. Offenbacher and Herbert B. Callen—1580(E)
Electrical conduction and thermoelectric power in thorium oxide crystals, O. A. Weinreich and W. E. Danforth—231(A)
Electron ejection from Ta by He^+, He^{++}, and He_2^+, Homer D. Hagstrum—543
Electron mean free path of damaged Cu in terms of electrical resistivity and thermoelectric power, G. W. Rodeback and W. P. Eatherly—237(A)
Of InSb, R. G. Breckenridge, W. R. Hosler, and W. Oshinsky—243(A)
Mechanism of self-sustained electron emission from MgO, Dietrich Dobischek, Harold Jacobs, and John Freely—804
Neutralization of ions and ionization of atoms near metal surfaces, L. J. Varnerin, Jr.—859
Photocurrent, space-charge buildup, and field emission in alkali halide crystals, A. von Hippel, E. P. Gross, J. G. Jelatis, and M. Geller—568
Photoelectric effect of thin Bi films, D. J. Fourie—803
Photoemission from Ag into AgCl, KBr, NaCl, and new bands of photosensitivity in AgCl, M. A. Gilleo—534
Photoemission of W in region of predicted Schottky deviations, E. E. Buder, J. J. Ruddick, and A. H. Weber—561
Quantum theory of polarizability of idealized crystal, D. L. Dexter and W. R. Heller—273
Secondary electron emission of crystalline MgO, J. B. Johnson and K. G. McKay—582
$SrTiO_3$ electrical properties, Arthur Linz, Jr.—753(L)
Theory of thermoelectric power in semiconductors, V. A. Johnson and K. Lark-Horovitz—230(A)
Thermoelectric power and electrical resistivity of dilute solid solution of Si in Cu, C. A. Domenicali and B. A. Boyd—220(A)
Thermoelectric power in Ge single crystals, H. P. R. Frederikse—491(A)
Thermoelectric power of carbons, E. E. Loebner—243(A)
Of TiO_2 semiconductors, Robert G. Breckenridge and William R. Hosler—793
Electrodynamics (see **Electromagnetic Theory and Electrodynamics**)
Electrolysis (see **Chemical Effects and Properties**)
Electromagnetic Theory and Electrodynamics
Angular aberrations in sector-shaped electromagnetic lenses for focusing beams of charged particles, Edgar G. Johnson and Alfred O. Nier—10
Electron interferometer, L. Marton, J. Arol Simpson, and J. A. Suddeth—437(A); Construction and operation, J. A. Suddeth, L. Marton, and J. Arol Simpson—437(A); Observations and interpretation, J. Arol Simpson, J. A. Suddeth, and L. Marton—437(A)
Energy-momentum tensor in general stream electrodynamics, M. Avramy Melvin—241(A)
Energy-momentum tensor of electromagnetic field inside matter, N. L. Balazs—240(A); 408
Magnetic self-focusing of auroral protons, W. H. Bennett and E. O. Hulburt—1562(L)
Motion of ions in perpendicular electric fields, M. S. McCay and J. H. Coulliette—213(A)
Electron Diffraction (see **Diffraction; Scattering of Electrons and Positrons**)
Electron Optics (see **Electromagnetic Theory and Electrodynamics**)
Electronic Tubes (see **Methods and Instruments**)
Electrons and Positrons (see also **Electromagnetic Theory and Electrodynamics; Elementary Particle Interactions; Scattering of Electrons and Positrons**)
Annihilation of fast positrons in flight, J. B. Gerhart, R. Sherr, and B. C. Carlson—455(A)
Annihilation of positrons in solids, T. A. Pond—455(A)
Gyromagnetic ratio of free electron, H. R. Crane, R. W. Pidd, and W. H. Louisell—475(A); W. H. Louisell, R. W. Pidd, and H. R. Crane—475(A); Precession and depolarization, K. M. Case and H. Mendlowitz—475(A)
Polarization of three-photon annihilation radiation, L. Leipuner, R. Siegel, and S. DeBenedetti—198(L)

Production of high-energy electron pairs by negative pions in nuclear collisions, Marcel Schein, Joseph Fainberg, D. M. Haskin, and R. G. Glasser—973
Thermalization of positrons in metals, R. L. Garwin—1571(L)

Electrons, Mobility (see **Ions and Electrons, Mobility**)
Electrons, Scattering of (see **Scattering of Electrons and Positrons**)
Electrons, Secondary (see **Electrical Properties**)
Electrons, Thermionic (see **Electrical Properties**)
Electro-Optical Effects (see **Optical Properties**)
Electrostriction (see **Dielectrics and Dielectric Properties**)

Elementary Particle Interactions
Angular distribution of pions scattered by H, H. L. Anderson, E. Fermi, R. Martin, and D. E. Nagle—155
Bound states of meson-nucleon system, R. Arnowitt—459(A)
Classical scattering of neutral mesons, Clarence R. Mehl and Peter Havas—393
Convergence of higher-order adiabatic potentials, Abraham Klein—460(A)
Damping of virtual nucleon-pair formation in pseudoscalar meson theory, K. A. Brueckner, J. Gell-Mann, and M. L. Goldberger—460(A)
Differential cross sections for scattering of 48-Mev π^+ mesons in H, D. Bodansky, A. Sachs, and J. Steinberger—467(A)
Diffusion cloud-chamber study of pion interactions in H and He, E. C. Fowler, W. B. Fowler, R. P. Shutt, A. M. Thorndike, and W. L. Whittemore—135
Effect of $^3P_2 - {}^3F_2$ coupling on p-p scattering, R. M. Thaler, J. Bengston, and G. Breit—454(A)
Equivalence theorems, P. Moldauer and K. M. Case—459(A)
Graphical method for obtaining phase shifts from experimental data on meson-nucleon scattering, Julius Ashkin and Seymour H. Vosko—1248
Interactions of 14-Mev neutrons with protons and deuterons, J. C. Allred, A. H. Armstrong, and L. Rosen—90
Low-energy properties of n-p system, H. G. Kolsky—459(A)
Low-energy properties of nucleon-nucleon interaction, Robert Jastrow—749
Many-body forces and nuclear saturation, S. D. Drell, K. Huang, and V. F. Weisskopf—460(A); S. D. Drell and Kerson Huang—1527
Many-nucleon forces, Gregor Wentzel—1573(L)
μ^--meson nuclear capture in H and D, H. Primakoff—480(A)
Multiple pion production in n-p collisions observed at the cosmotron, W. B. Fowler, R. P. Shutt, A. M. Thorndike, and W. L. Whittemore—758(L)
n-p scattering, Earle Lomon and Herman Feshbach—454(A)
Nuclear forces from extended sources, E. M. Henley and M. A. Ruderman—480(A)
Nuclear forces in pseudoscalar meson theory, K. M. Watson and K. A. Brueckner—460(A)
Nucleon polarization in pion-proton scattering, Enrico Fermi—947
$p + p \rightarrow d + \pi^+$ cross section at 340 Mev and 327 Mev, Frank S. Crawford, Jr., and M. Lynn Stevenson—468
Phase-shift analysis of high-energy p-p scattering, J. Bengston and R. M. Thaler—454(A)
Phenomenological study of meson-nucleon scattering, S. Gasiorowicz—481(A)
Precision determination of the n-p capture cross section, G. von Dardel and A. W. Waltner—1284(L)
Production of positive pions by 341-Mev protons on protons, W. F. Cartwright, C. Richman, M. N. Whitehead, and H. A. Wilcox—677
Production of V_1^0 particles by π^- mesons in H, W. B. Fowler, R. P. Shutt, A. M. Thorndike, and W. L. Whittemore—1287(L)
Radiative corrections to nuclear forces in pseudoscalar theory, K. A. Brueckner—761(L)
Scattering of 40-Mev positive pions by H, J. P. Perry and C. E. Angell—1289(L)
Scattering of 43-Mev positive pions by H, A. B. Weaver, J. J. Lord, and J. Orear—466(A)
Scattering of 120-Mev negative pions by H, J. Orear—467(A)
Scattering of 169- and 192-Mev pions by H, R. L. Martin, E. Fermi, and D. E. Nagle—467(A)
Speculation on V spin, D. C. Peaslee—446(A)
Spin-orbit coupling in pseudoscalar meson theory, Lawrence Dresner—201(L)
Structure and mass spectrum of elementary particles. I. General considerations, Hideki Yukawa—415(L); II. Oscillator model, Hideki Yukawa—416(L)
Thermal n-p capture, S. P. Harris, C. O. Muehlhause, D. Rose, H. P. Schroeder, G. E. Thomas, Jr., and S. Wexler—125
Total cross sections for 37-Mev pions in H, C. E. Angell and J. P. Perry—468(A)
Total cross sections of 408-Mev protons for H and light elements, J. Marshall, L. Marshall, and V. A. Nedzel—767(L)
Total n-p cross section at 1 Mev, R. E. Fields, R. K. Adair, R. L. Becker, and S. E. Darden—441(A)
Two-particle potential from Bethe-Salpeter equation, Wilhelm Macke—195(L); Erratum—1580(E)

Elements (see **Atomic Mass and Abundance**)
Energy Loss of Particles (see **Range and Energy Loss of Particles**)
Energy States of Atoms (see **Atomic Structure and Spectra**)
Energy States of Molecules (see **Molecular Structure and Spectra**)
Energy States of Nucleus (see **Nuclear Reactions; Nuclear Spectra; Nuclear Structure Theory**)
Equations of State (see **Chemical Effects and Properties**)

Errata
β decay of Li^8, D. StP. Bunbury—1580(E)
Calculation of nuclear binding energies with single-particle oscillator wave functions, Erwin H. Kronheimer—1580(E)
Decay of Re^{188} and lifetimes of Os^{186m} and Os^{186m}, C. C. McMullen and M. W. Johns—1580(E)
Directional effects in electric breakdown of ionic crystals, Elmer L. Offenbacher and Herbert B. Callen—1580(E)
Gyromagnetic ratios of microcrystalline materials, S. J. Barnett—1580(E)
Interference terms of electron-neutrino angular correlation, Masato Morita—1580(E)
Nuclear moments of Ta^{181}, B. M. Brown and D. H. Tomboulian—1580(E)
Radioactive charging through dielectric medium, E. G. Linder and P. Rappaport—1580(E)
Two-particle potential from the Bethe-Salpeter equation, Wilhelm Macke—1580(E)

Errors of Measurement (see **Methods and Instruments**)
Evaporation (see **Liquids**)
Excitation of Atoms (see **Atomic Structure and Spectra**)

Excitation of Molecules (see **Molecular Structure and Spectra**)
Excitation of Nucleus (see **Nuclear Reactions; Nuclear Spectra; Nuclear Structure Theory**)
Explosion Phenomena (see **Fluid Dynamics**)

Faraday Effect (see **Optical Properties**)
Ferroelectric Phenomena (see **Dielectrics and Dielectric Properties**)
Ferromagnetism (see **Magnetic Properties**)
Field Emission (see **Electrical Properties**)
Field Theory (see also **Quantum Electrodynamics**)
Bound states of meson-nucleon system, R. Arnowitt—459(A)
Classical equations of motion of point particles, Peter Havas—997
Compton scattering on nucleons, R. H. Huddlestone—461(A)
Connection between fusion theory of bosons and nonlocal field theory, Satosi Watanabe—771(L)
Construction of conservation equations for nonlocal field theories, Christopher Gregory—770(L)
Construction of potentials in quantum field theory, Abraham Klein—1285(L)
Convergence of adiabatic nuclear potential, Abraham Klein—460(A); 740
Damping of virtual nucleon-pair formation in pseudoscalar meson theory, K. A. Brueckner, J. Gell-Mann, and M. L. Goldberger—460(A)
Energy-momentum tensor in general stream electrodynamics, M. Avramy Melvin—241(A)
Equivalence theorems, P. Moldauer and K. M. Case—459(A)
Intrinsic magnetic moment of particle of spin 3/2, F. J. Belinfante—477(A)
Low-energy properties of n-p system, H. G. Kolsky—459(A)
Low-energy properties of nucleon-nucleon interaction, Robert Jastrow—749
Many-body forces and nuclear saturation, S. D. Drell, K. Huang, and V. F. Weisskopf—460(A); S. D. Drell and Kerson Huang—1527
Many-nucleon forces, Gregor Wentzel—1573(L)
Mass-renormalization with Tamm-Dancoff method, F. J. Dyson—421(L)
Nuclear forces from extended sources, E. M. Henley and M. A. Ruderman—480(A)
Nuclear forces in pseudoscalar meson theory, K. M. Watson and K. A. Brueckner—460(A)
Number of Feynman diagrams, R. J. Riddell, Jr.—471(A); 1243
Poles of S matrix for resonance reactions, Marcos Moshinsky—984
Properties of Salpeter-Bethe two-nucleon equation, Jack S. Goldstein—461(A); 1516
Radiative corrections to nuclear forces in pseudoscalar theory, K. A. Brueckner—761(L)
Repulsive core and charge independence, E. E. Salpeter—994
S matrix and causality condition. II. Nonrelativistic particles, N. G. van Kampen—1267
Similarity theory of relativity and Dirac-Schrödinger theory of electrons, Banesh Hoffman—751
Spin-orbit coupling in pseudoscalar meson theory, Lawrence Dresner—201(L)
Structure and mass spectrum of elementary particles. I. General considerations, Hideki Yukawa—415(L); II. Oscillator model, Hideki Yukawa—416(L)
Theory of quantized fields, Julian Schwinger—713; 728
Tomonaga approximation, B. D. Fried and R. J. Riddell, Jr.—460(A)
True vacuum and dressed particles in quantum field theory, Bruno Zumino—478(A)
Two-particle potential from Bethe-Salpeter equation, Wilhelm Macke—195(L); Erratum—1580(E)
Wave function of relativistic system, F. J. Dyson—1543
Films, Properties
Change of optical constants of fresh thin Cu and Ag films on exposure to air, H. Y. Loh and Peter Cheo—221(A)
Conductivity of thin films in longitudinal magnetic field, Ernest Koenigsberg—8
Effect of sputtering rate on resistivity and "aging" of sputtered Ag films, Richard B. Belser—221(A)
Ge films, W. M. Becker and K. Lark-Horovitz—230(A)
He film flow, James B. Brown—489(A)
Linear velocity of He II film, W. C. Knudsen and J. R. Dillinger—489(A)
Measurement of thickness of thin films by employing electron microscope shadow-casting technique, George W. Crawford—214(A)
Orientation in polymeric films by infrared and x-ray techniques, W. H. Cobbs, Jr., S. B. Cole, and R. L. Burton—225(A)
Photoelectric effect of thin Bi films, D. J. Fourie—803
Structure and aging of thin metal films. I, Robert J. Raudebaugh and Richard B. Belser—449(A); II. Richard B. Belser and Robert J. Raudebaugh—449(A); III, Richard B. Belser and Robert J. Raudebaugh—499(A)
Tensile strength and adhesion of thin films of Ag, H. S. Morton, Jr., and J. W. Beams—449(A)
Transparent, nonmetallic, electrically conducting film applications, L. B. Clark, Sr.—471(A)
Fine Structure (see **Atomic Structure and Spectra**)
Fission of Nucleus (see **Nuclear Fission**)
Fluctuation Phenomena (see **Noise**)
Fluid Dynamics
Asymmetry of turbulent functions, R. Betchov—470(A)
Boundary layer hypersonic flow, F. K. Hill—1029(A)
C.A.L. hypersonic test facility, Abraham Hertzberg and William E. Smith—1029(A)
Characteristics of axisymmetric turbulent boundary layers in adverse pressure gradient, Earl M. Uram—1032(A)
Characteristics of two-dimensional turbulent boundary layers, Donald Ross—1031(A)
Compressible flow of viscous fluid in capillary connected to closed vessel, J. M. Kendall—470(A)
Cylindrical Couette flow, Marian Rose—469(A)
Degeneration of shock wave into sound, Everett F. Cox—1030(A)
Drag measurements in pressurized range, V. E. Bergdolt and F. D. Bennett—1033(A)
Effect of gas slip on unsteady flow of gas through porous media, J. S. Aronofsky—1032(A)
Experimental method to determine equation of state data for solids by shock-wave measurements, Russell H. Christian and John M. Walsh—1030(A)
Generalized theory of Mach reflection of shock waves, Berthold Zarwin—470(A)
Heat transfer on hemispherical body in supersonic flow, Irving Korobkin—469(A)
Hypersonic viscous flow over insulated flat plate at large angle of attack, Shih I. Pai—1029(A)
Mach Zehnder interferometer, D. Weimer, W. Bleakney, and D. R. White—1032(A)
Phosphorescence method for study of surface temperatures in supersonic flow field, L. C. Bradley, C. C. Van Voorhis, and D. Bershader—469(A)
Pressure and temperature distribution on circular cylinder in supersonic cross flow, Lloyd W. Walter—470(A)

Pressure multiplication in re-entrant corners, R. J. Heyman, A. Sherman, and T. Schiffman—1032(A)
Production and measurement of surface ripples, N. L. Walbridge, H. M. Smith, Jr., and L. A. Woodward—1031(A)
Reynolds number effect on spheres at supersonic speeds, Richard Lehnert—1033(A)
Second law of eddy thermodynamics, A. K. Blackadar—1031(A)
Separated solutions of linearized equation for unsteady transonic flow, E. Mollo-Christensen—1030(A)
Separation of shock wave into elastic and plastic waves, and measurement of pressure of elastic wave, Stanley Minshall—1030(A)
Shock compression in ducts and diffusers, J. Lukasiewicz—1032(A)
Shock refraction, R. G. Stoner, E. B. Davies, and D. C. Peckham—1032(A)
Shock tube for studying chemical kinetics, A. Hertzberg and W. Squire—469(A)
Shock-tube studies of transient boundary layers in compressible flow, Daniel Bershader—470(A)
Space and time spectra in homogeneous turbulence, J. Bass—1031(A)
Spin effects on base pressure, Richard Lehnert and Samuel Hastings—1032(A)
Stability of isotropic turbulence, R. Betchov—1031(A)
Stability of plane Poiseuille flow, L. H. Thomas—780
Total-temperature probes for use at high supersonic speeds and elevated temperatures, Eva M. Winkler—469(A)
Transmission of sound pulse through shock wave, R. A. Alpher and R. J. Rubin—1030(A)
Turbulent diffusion from volume source with nonuniform initial distribution, Frank Gifford, Jr.—1031(A)
Viscous drag measurements on rarefied gas using high rotational speed technique, A. R. Kuhlthau—1029(A)

Fluorescence (see **Luminescence**)

Friction (see **Mechanics**)

Galvanomagnetic Effect (see **Magnetic Properties**)

Gamma Rays (see also **Nuclear Reactions; Nuclear Spectra**)
Degradation of Co^{60} γ rays in infinite water medium, M. M. Weiss and W. Bernstein—483(A)
Theory of penetration of γ rays through thin barriers, John P. Vinti—345

Gases
Adsorbed O in ZnO photoconductivity, Donald A. Melnick and Leo J. Neuringer—229(A)
Bose-Einstein condensation of imperfect gas, M. H. Friedman and S. T. Butler—465(A)
Effect of gas slip on unsteady flow of gas through porous media, J. S. Aronofsky—1032(A)
Solubility of solids in gases, A. H. Ewald—215(A)

Geophysics
Contribution of 15-micron CO_2 band to earth's radiation balance, Gilbert N. Plass—458(A)
Dissociation and recombination of O_2 in upper atmosphere assuming three-body recombinations, Harry E. Moses and Ta-You Wu—458(A); 1408
Effects of primeval endowment of U^{235}, David B. Rosenblatt—1474
Origin of ionization in E layer of ionosphere, Ernst Bauer and Ta-You Wu—458(A)
Production of sodium airglow excitation by imprisonment of resonance radiation, A. Foderaro and T. M. Donahue—1561(L)
Propagation of short radio waves well beyond the horizon, Thomas J. Carroll—458(A)

Glasses (see **Molecular Aggregates**)

Gravitation (see **Relativity and Gravitation**)

Gyromagnetization (see **Magnetic Properties**)

Hall Effect (see **Electrical Conductivity and Resistance**)

Heat Capacity (see **Thermal Properties**)

Heat Conduction (see **Thermal Properties**)

Heat of Dissociation and Formation (see **Molecular Structure and Spectra**)

Heat of Fusion (see **Thermal Properties**)

Heat of Vaporization (see **Thermal Properties**)

Helium, Liquid
Atomic theory of λ transition in He, R. P. Feynman—1291
Atomic theory of liquid He near 0°K, R. P. Feynman—1301
He film flow, James B. Brown—489(A)
He II: Bose-Einstein condensation and two-fluid model, P. R. Zilsel—216(A)
Heat of mixing of He^3 in He^4, H. S. Sommers, Jr., W. E. Keller, and J. G. Dash—489(A)
λ-point shift in $He^3 - He^4$ mixtures, J. C. King and Henry A. Fairbank—489(A)
Linear velocity of He II film, W. C. Knudsen and J. R. Dillinger—489(A)
Neutron diffraction by liquid He, D. G. Henshaw and D. G. Hurst—1222
Rapid separation of He^3 from He^4 by "heat flush" method, T. Soller, W. M. Fairbank, and A. D. Crowell—1058
Small-angle scattering of x-rays from He I and He II, A. G. Tweet—488(A)
Structure of liquid He, James Reekie and Thomas S. Hutchison—490(A)
Temperature scale in liquid He region, L. D. Roberts and R. A. Erickson—488(A)
Thermomechanical effect in liquid He II to 0.9°K, D. H. Rogers and Melvin A. Herlin—489(A)
Thickness of saturated He II film, Raymond Bowers—1016(L)
Transmission of slow neutrons by liquid He, L. Goldstein, H. S. Sommers, Jr., and J. G. Dash—490(A)
Ultrasonic measurements in liquid He, C. E. Chase—489(A)
Vapor pressure and entropy of liquid He^3, D. ter Haar—1018(L)

High-Voltage Tubes and Machines (see **Methods and Instruments**)

Hydrodynamics (see **Fluid Dynamics**)

Hyperfine Structure (see **Atomic Structure and Spectra; Molecular Structure and Spectra; Nuclear Moments and Spin**)

Imperfections in Solids (see also **Crystalline State; Electrical Conductivity and Resistance; Luminescence; Semiconductors**)
Activation energy for recovery of reactor-irradiated Cu crystals, J. K. Redman, R. R. Coltman, and T. H. Blewitt—448(A)
Activation entropies for diffusion mechanisms, H. B. Huntington, G. A. Shirn, and E. S. Wajda—246(A)
Adsorbed O in ZnO photoconductivity, Donald A. Melnick and Leo J. Neuringer—229(A)
Anisotropy of grain boundary diffusion, L. Couling and R. Smoluchowski—245(A)
Annealing of bombardment damage in Ge: Theoretical, R. C. Fletcher, W. L. Brown, and S. Machlup—237(A); Experimental, W. L. Brown and R. C. Fletcher—237(A)

Imperfections in Solids (Continued)
Anomaly in heat content of metal in fatigued state, B. Welber and R. Webeler—448(A)
Band width of F centers in KBr, I. L. Mador, J. J. Markham, and R. T. Platt, Jr.—219(A); 1277(L)
Bleaching of CaF_2 crystals colored by x-rays, Alexander Smakula—1570(L)
Bleaching properties of F centers in KBr at 5°K, J. J. Markham, R. T. Platt, Jr., and I. L. Mador—219(A)
Broadening of impurity levels in Si, M. Lax and E. Burstein—208(A)
Change of elastic constants resulting from annealing of Cu and Al cold worked at −196°C, E. C. Crittenden, Jr., and H. Dieckamp—232(A)
Change of metallic conductivity through change in thermal scattering, R. Smoluchowski—245(A)
Changes in conductivity of NaCl produced by bombardment with 360-Mev protons, E. A. Pearlstein—244(A)
Changes in electrical, thermal, and thermoelectrical properties of monovalent metals by lattice distortions, A. W. Sáenz—1142
Comparison of resistivity and density changes in cold-worked brass, Herbert I. Fusfeld—233(A)
Debye temperature of Cu_3Au, Dwain B. Bowen—220(A)
Decay of vacancies frozen into alloy by quenching, A. S. Nowick and A. E. Roswell—221(A)
Deformation of Cu single crystals at 78°K and 300°K, T. H. Blewitt, J. K. Redman, and F. A. Sherrill—236(A); R. E. Jamison and T. H. Blewitt—237(A); T. H. Blewitt—1115
Density change in proton-irradiated KCl, W. J. Leivo—245(A)
Diffusion of Cd in single crystals of Ag, T. Tomizuka, L. Slifkin, and D. Lazarus—245(A)
Diffusion of Li into Ge and Si, C. S. Fuller and J. A. Ditzenberger—193(L)
Diffusion of Sb in Ag, E. Sonder, L. Slifkin, and D. Lazarus—245(A)
Dilatometric study of order-disorder transformation in Cu-Au alloys, W. W. Sanville, Foster C. Nix, and Frank E. Jaumot, Jr.—220(A)
Dislocations and edge states in diamond crystal structure, W. Shockley—228(A)
Dislocations in low-angle boundaries in Ge single crystals, F. L. Vogel, W. G. Pfann, H. E. Corey, and E. E. Thomas—230(A)
Displacement energy for radiation damage in Cu, D. T. Eggen and M. J. Laubenstein—238(A)
Effect of fast-neutron bombardment on diffusion in Cu_3Au, R. R. Coltman and T. H. Blewitt—236(A)
Effect of neutron irradiation on phase change in Sn, Jerome Fleeman—237(A)
Effects of heat treatment on lattice perfection, Norman W. Lord—472(A)
Effects of temperature gradients on diffusion in crystals, W. Shockley—1563(L)
Electrical properties of AlSb, R. K. Willardson, A. C. Beer, and A. E. Middleton—243(A)
Electrical properties of carbon bisulfate compounds, E. A. Kmetko—243(A)
Electron energy levels in F centers, William A. Smith and Allen B. Scott—219(A)
Electron mean free path of damaged Cu in terms of electrical resistivity and thermoelectric power, G. W. Rodeback and W. P. Eatherly—237(A)
Electronic energy states of impurities in nonmetallic crystals, Kurt Lehovec—228(A)
Electronic structure of F centers, C. Kittel—219(A)
Electronic structure of F centers: hyperfine interactions in electron spin resonance, A. F. Kip, C. Kittel, R. A. Levy, and A. M. Portis—1066; Saturation of electron spin resonance, A. M. Portis—1071
Evaporation of Cu from Ge, George Finn—754(L)
Grain boundary self-diffusion in body-centered lattice, C. W. Haynes and R. Smoluchowski—245(A)
Hall effect in ordered and disordered Ni_3Mn, Simon Foner and Emerson M. Pugh—220(A)
Hardness change in Cu irradiated with 1.25-Mev electrons, C. E. Dixon and C. J. Meechan—237(A)
Influence of impurities on diffusion in solids, Albert W. Overhauser—246(A)
Irradiation-induced photoconductivity in MgO, Harold R. Day—238(A); 822
Kinetics of disorder-order transformation in Cu_3Au, Norman W. Lord—221(A)
Low-temperature fast-neutron bombardment of Cu-Be alloy, J. W. Cleland, D. S. Billington, and J. H. Crawford, Jr.—238(A)
Mechanical properties of proton-irradiated alkali halides, W. H. Vaughan, W. J. Leivo, and R. Smoluchowski—245(A)
Mobility of interstitial atoms in face-centered metal, H. B. Huntington—1092
Nature of radiation damage in diamond, G. J. Dienes and D. A. Kleinman—238(A)
New approximation method for order-disorder problems, Lloyd D. Fosdick and Hubert M. James—1131
Ordering in alloy system Mg-Cd, C. A. Wert—221(A)
Phosphorescence of and energy storage in Ag-activated NaCl, H. O. Albrecht and R. E. Mandeville—471(A)
Photoconductivity and V centers, K. Teegarden and R. J. Maurer—219(A)
Photoemission from Ag into AgCl, KBr, NaCl, and new bands of photosensitivity in AgCl, M. A. Gilleo—534
Plastic behavior of polycrystalline metals at very high strain rates, L. Zernow and J. Simon—233(A)
Production of F', M, and R centers in NaCl at room temperature, R. T. Platt, Jr., I. L. Mador, and J. J. Markham—219(A)
Radiation damage and rate processes, J. W. Marx—1564(L)
Radiationless trapping of charge carriers in solids, Gregory H. Wannier—207(A)
Resistivity of Cu_3Au during neutron irradiation, Harvey L. Glick and W. F. Witzig—236(A)
Reversible bleaching of absorption band of diamond, Peter Pringsheim—220(A); 551
Saturation of paramagnetic resonance from color centers in alkali halides, A. M. Portis and A. F. Kip—207(A)
Short-range order in Cu-Au alloy, Charles H. Sutcliffe and Frank E. Jaumot, Jr.—221(A)
Small-angle scattering of x-rays from cold-worked crystals, D. L. Dexter—448(A)
Small-angle x-ray scattering in proton-irradiated diamond, S. Hayes and R. Smoluchowski—244(A)
Storage of energy in Ag-activated KCl, C. E. Mandeville and H. O. Albrecht—219(A); 566
Strain and crystallite size in experimental Fe powders, Frank E. Jaumot, Jr., and Leonard Muldawer—232(A)
Strength of solid solution alloys, John C. Fisher—232(A)
Stress-strain curves of Cu single crystals at 4.2°K, T. H. Blewitt, R. R. Coltman, R. E. Jamison, and J. K. Redman—448(A)
Tentative theory of metallic whisker growth, J. D. Eshelby—755(L)
Theory of initial stress-strain curves in face-centered metals, J. S. Koehler—233(A)

Thermally unstable disorder in *p*-type Ge produced by fast-neutron bombardment, J. H. Crawford, Jr., J. W. Cleland, D. K. Holmes, and J. C. Pigg—243(A)
Thermoelectric power and electrical resistivity of dilute solid solution of Si in Cu, C. A. Domenicali and B. A. Boyd—220(A)
Thermoluminescence of quartz and fused quartz colored by x-ray irradiation, Ryosuke Yokota—1013(L)
Variable activation energy and motion of lattice defects, G. J. Dienes—1283(L)
Work hardening in substitutional alloys, J. S. Koehler—448(A)
X-ray and metallurgical studies on neutron-irradiated Cu_3Au, R. H. Fillnow, E. K. Halteman, and G. F. Mechlin—236(A)
X-ray measurements of cold-worked α brass, B. E. Warren, B. L. Averbach, and E. Warekois—233(A)
X-ray study of graphitization, J. C. Bowman, S. Hayes, and R. Smoluchowski—244(A)
Yield point strain, Edward W. Hart—232(A)
Z centers in alkali halides, D. R. Westervelt—218(A)

Inelastic Scattering (see **Nuclear Reactions; Scattering**)

Instruments (see **Methods and Instruments**)

Internal Conversion (see **Nuclear Spectra**)

Ionization (see also **Electrical Discharges; Range and Energy Loss of Particles**)
Cluster-count determination of specific ionization of cloud-chamber tracks, Hans O. Cohn, L. R. Etter, and R. W. Thompson—445(A)
Ionization and dissociation of nitromethane by electron impact, R. J. Kandel—436(A)
Neutralization of ions and ionization of atoms near metal surfaces, L. J. Varnerin, Jr.—859
Origin of ionization in *E* layer of ionosphere, Ernst Bauer and Ta-You Wu—458(A)
Photoionization of molecules in vacuum uv, Edward C. Y. Inn—1194
Photoionization of NO, K. Watanabe, Frederick Marmo, and Edward C. Y. Inn—436(A)
Production of characteristic x-rays by protons, H. W. Lewis, B. E. Simmons, and E. Merzbacher—943
Relativistic rise in ionization loss in nuclear emulsions, Bertram Stiller and Maurice M. Shapiro—496(A)
Simultaneous measurement of ionization and attachment coefficients, Melvin A. Harrison and Ronald Geballe—1
Specific probable ionization of electrons observed with Wilson cloud chamber, Robert H. Frost and Carl E. Nielsen—864

Ionization Potentials of Atoms (see **Atomic Structure and Spectra**)

Ionization Potentials of Molecules (see **Molecular Structure and Spectra**)

Ions (see also **Electrical Discharges**)
Electron ejection from Ta by He^+, He^{++}, and He_2^+, Homer D. Hagstrum—543
Energy loss of H, He, N, and Ne ions in gases, Peter K. Weyl—289
Hall effect in flowing ion clouds, B. E. Clotfelter—436(A)
Motion of ions in perpendicular electric fields, M. S. McCay and J. H. Coulliette—213(A)
Neutralization of ions and ionization of atoms near metal surfaces, L. J. Varnerin, Jr.—859
Positive ion flux in GM counter, W. C. Porter and G. W. McClure—495(A)

Ions and Electrons, Mobility (see also **Semiconductors**)
Current carrier mobility ratio in semiconductors, L. P. Hunter—207(A); 579
Experimental confirmation of relation between pulse drift mobility and charge carrier drift mobility in Ge, M. B. Prince—271
Mobilities of carriers in crystalline B, William C. Shaw, D. E. Hudson, and G. C. Danielson—208(A)
Mobility of slow electrons in polar crystals, Francis E. Low and David Pines—193(L)
Temperature variation of drift mobilities of minority carriers in semiconductors, M. B. Prince—208(A)

Isobars (see **Atomic Mass and Abundance**)

Isomers, Molecular (see **Molecular Structure and Spectra**)

Isomers, Nuclear (see **Nuclear Spectra**)

Isotopes (see **Atomic Mass and Abundance; Radioactivity**)

Kerr Effect (see **Optical Properties**)

Kinetic Theory of Gases (see **Gases**)

Liquid Helium (see **Helium, Liquid**)

Liquids
Compressions to 150 000 psi for series of high molecular weight liquid hydrocarbons, R. H. McMickle, R. W. Schiessler, and W. Webb—466(A)
Difference in viscosity of *ortho-* and *para*-deuterium at low temperatures, E. W. Becker, R. Misenta, and O. Stehl—414(L)
Molar activity coefficients of electrolytes from conductivity data, Henry P. Marshall and Ernest Grunwald—214(A)
Molecular rotation in liquids, Edward J. Breneman and Dudley Williams—465(A)
Neutron diffraction by liquid O_2, N_2, and A, D. G. Henshaw, D. G. Hurst, and N. K. Pope—472(A)
Polarization in liquids of intermediate conductivity, John A. Rider—214(A)
Surface tension of liquid Si and Ge, Paul H. Keck and Wendell Van Horn—243(A); 512
Vapor-liquid transitions in closed system, Charles Willis and Harry L. Frisch—465(A)

Luminescence
Absolute scintillation efficiency of anthracene, J. B. Birks and M. E. Szendrei—197(L)
Fluorescence, phosphorescence, and photostimulation of NaCl (AgCl) with high-energy irradiation, Milton Furst and Hartmut Kallmann—1356
Fluorescent light yields with α, β, and γ radiations, Milton Furst and Hartmut Kallmann—766(L)
Luminescent effects in chemically pure ZnO, T. Todd Reboul—229(A)
Phosphorescence method for study of surface temperatures in supersonic flow field, L. C. Bradley, C. C. Van Voorhis, and D. Bershader—469(A)
Phosphorescence of and energy storage in Ag-activated NaCl, H. O. Albrecht and C. E. Mandeville—471(A)
Plastic scintillators, R. K. Swank and W. L. Buck—495(A)
Response of anthracene crystals to monoenergetic soft x-rays, W. H. Robinson—457(A)
Response of NaI(Tl) scintillation crystals as function of Tl concentration, F. S. Eby, W. K. Jentschke, and G. DePasquali—495(A)
Reversible bleaching of absorption band of diamond, Peter Pringsheim—220(A); 551
Scintillation process in plastic solid solutions, Robert K. Swank and Warren L. Buck—927
Scintillation response of organic phosphors, G. T. Wright—1282(L)
Scintillations produced by α particles in CsI, Beat Hahn—772(L)

Luminescence (Continued)
Storage of energy in Ag-activated KCl, C. E. Mandeville and H. O. Albrecht—219(A); 566
Storage of energy in KCl-Tl and NaCl-Tl, C. E. Mandeville and H. O. Albrecht—470(A)
Thermoluminescence of quartz and fused quartz colored by x-ray irradiation, Ryosuke Yokota—1013(L)

Magnetic Fields (see **Electromagnetic Theory and Electrodynamics**)

Magnetic Properties
Adiabatic demagnetization of chromium methylamine alum, D. de Klerk and R. P. Hudson—278
Antiferromagnetostriction, Helen M. A. Urquhart and J. E. Goldman—435(A)
Apparatus for magnetic measurements at low temperatures, R. A. Erickson and L. D. Roberts—216(A)
Approach to saturation in diluted ferromagnetic powders, A. E. Berkowitz and A. D. Franklin—206(A)
Calculation of diamagnetic and paramagnetic susceptibility of N_2, J. V. Bonet and A. V. Bushkovitch—433(A)
Crystallite size and diamagnetic susceptibility of carbons, H. T. Pinnick—228(A)
Deflection of high-energy electrons in magnetized Fe, Stephan Berko and Frank L. Hereford—1127
de Haas-van Alphen effect in Sn-Sb alloys, George T. Croft and Foster C. Nix—212(A)
Dipolar anisotropy in cubic ferromagnetic crystals, Frederic Keffer—206(A)
Electronic interactions in ferromagnetic metals, Sol E. Harrison and Herbert B. Callen—205(A)
Field and temperature dependence of de Haas-van Alphen effect in Zn alloy single crystals, F. J. Donahoe—212(A)
Free-energy model for hysteresis loop, Arthur L. Loeb—434(A)
Gyromagnetic ratios of microcrystalline materials, erratum, S. J. Barnett—1580(E)
Low-temperature diamagnetism of electrons in cylinder, William Band—249
Magnetic properties of Gd metal, J. F. Elliott, S. Legvold, and F. H. Spedding—28
Magnetic saturation and apparent molecular fields of $MnCl_2 \cdot 4H_2O$, Warren E. Henry—435(A)
Magnetic susceptibility of Wurster's blue between 65° and 356°K, N. Elliott and M. Wolfberg—435(A)
Magnetization reversal of square-loop polycrystalline materials by domain growth, Norman Menyuk—434(A)
Magnetostriction in Fe-Co alloys, K. Azumi—434(A)
Measurement of permeability tensor in ferrites, J. O. Artman and P. E. Tannenwald—1014(L)
Mechanism of transition in magnetite at low temperatures, H. J. Williams, R. M. Bozorth, and Matilda Goertz—1107
Method for measuring magnetic moment of superconductors, Ted G. Berlincourt and M. C. Steele—215(A)
Neutron diffraction study of antiferromagnetic structure of pyrrhotite, FeS_x, S. S. Sidhu and David Meneghetti—435(A)
Neutron diffraction study of BiMn alloy, B. W. Roberts—435(A)
Nucleation centers for domains of reverse magnetization, J. B. Goodenough—434(A)
Particle size of ultrafine ferromagnetic powders, A. D. Franklin, R. B. Campbell, and J. A. Weinman—205(A)
Of pyrrhotite, Robert R. Heikes—212(A)
Quantum statistical mechanics of ferromagnetism, Ryoichi Kikuchi—205(A)
Relation between de Haas-van Alphen effect and magnetoresistance in Bi, Ted G. Berlincourt—1277(L)
Reversible susceptibility in ferrimagnetic materials, D. M. Grimes, L. W. Orr, and M. H. Winsnes—435(A)
Single crystal magnetostriction constants of Fe-Co alloys, Helen M. A. Urquhart—434(A)
Specific heat discontinuity in antiferromagnets and ferrites, Louis N. Howard and J. Samuel Smart—17
Thermomagnetic investigations of Ni ferrite-aluminates, L. R. Maxwell, S. J. Pickart, and R. W. Hall—206(A)
Two-electron example of ferromagnetism, J. C. Slater, H. Statz, and G. F. Koster—205(A); 1323

Magnetic Resonance (see also **Nuclear Moments and Spin**)
d-p magnetic moment ratio, T. F. Wimett—499(A)
Dipolar broadening of quadrupole resonance line width in zero applied field, A. Abragam and K. Kambe—894
Doppler effects in atomic beam magnetic resonance method, Richard T. Daly, Jr., and Jerrold R. Zacharias—476(A)
Electronic structure of F centers, C. Kittel—219(A)
Electronic structure of F centers; hyperfine interactions in electron spin resonance, A. F. Kip, C. Kittel, R. A. Levy, and A. M. Portis—1066; Saturation of electron spin resonance, A. M. Portis—1071
g values of Ni ferrite-aluminates, Roald K. Wangsness—206(A)
Hfs and nuclear moment ratios of stable Br isotopes, J. G. King and V. Jaccarino—209(A)
Hfs of Ag with aid of universal ionizer for atomic beams, Günter Wessel and Hin Lew—476(A)
Hfs of I, J. G. King, H. H. Stroke, and V. Jaccarino—476(A)
Magnetic resonance absorption in Ni ferrite-aluminates, T. R. McGuire—206(A)
Nuclear magnetic moment of Cr^{53} and Sr^{87}, C. D. Jeffries and P. B. Sogo—1286(L)
Nuclear magnetic resonance in solid H, F. Reif and E. M. Purcell—631
Nuclear magnetic resonance in Th compounds, H. S. Gutowsky and B. R. McGarvey—81
Nuclear magnetic resonance modulation correction, E. R. Andrew—425(L)
Nuclear quadrupole resonance in rhombic S and quadrupole moments of S^{33} and S^{35}, H. G. Dehmelt—313
Nuclear resonance line shapes at high rf fields, W. D. Knight—206(A)
Paramagnetic resonance in N- and P-type Si, F. K. Willenbrock and N. Bloembergen—1281(L)
Polarization of nuclei in metals, Albert W. Overhauser—476(A)
Saturation of paramagnetic resonance from color centers in alkali halides, A. M. Portis and A. F. Kip—207(A)
Sublattice effects in magnetic resonance, Roald K. Wangsness—1085

Magneto-Optical Effects (see **Optical Properties**)

Magnetoresistance (see **Electrical Conductivity and Resistance**)

Magnetostriction (see **Magnetic Properties**)

Mass Defects (see **Atomic Mass and Abundance**)

Mass Spectroscopy (see **Atomic Mass and Abundance; Methods and Instruments**)

Mathematical Methods
Approximate solution of Heitler's integral equation, S. N. Biswas—1026(L)
Matrix formulation of molecular-orbital, Heitler-London, and configurational interaction computations, Paul F. Wacker—465(A)
Methods for calculating approximate cross sections for electron scattering, William J. Byatt—240(A)

Measurements (see **Methods and Instruments**)

Mechanics
Effect of centrifugal force field on response of vibrating mass-spring system, W. A. Wildhack and R. O. Smith—213(A)
Mechanics, Quantum-Atomic Structure and Spectra (see **Atomic Structure and Spectra**)
Mechanics, Quantum—General (see **Quantum Mechanics**)
Mechanics, Quantum—Molecular Structure and Spectra (see **Molecular Structure and Spectra**)
Mechanics, Quantum—Nuclear (see **Nuclear Structure Theory**)
Mechanics, Quantum—of Solid Bodies (see **Crystalline State**)
Mechanics, Statistical (see **Statistical Mechanics and Thermodynamics**)
Meson Field Theory (see **Field Theory**)
Mesons (see also **Cosmic Radiation; Elementary Particle Interactions; Nuclear Reactions Induced by Mesons; Scattering of Mesons**)
Angular distribution of mesons from 320-Mev photons on protons, Y. Goldschmidt-Clermont, L. S. Osborne, and A. W. Winston—468(A)
Angular distribution of process $p + d \rightarrow t + \pi^+$, Wilson J. Frank, Kenneth C. Bandtel, Richard Madey, and Burton J. Moyer—487(A)
Bound states of meson-nucleon system, R. Arnowitt—459(A)
Charged ζ mesons, Nathan Seeman, D. T. King, and Maurice M. Shapiro—446(A)
Classical scattering of neutral mesons, Clarence R. Mehl and Peter Havas—393
Decay of heavy mesons in nuclear emulsion, P. H. Barrett—446(A)
Decay of V^0 particle into two mesons, B. Dayton and D. Willard—348
Energy distribution of neutral mesons produced in cosmic-ray stars, Y. B. Kim—445(A)
Grain density in tracks of 117- and 222-Mev π^- mesons in emulsions, A. H. Morrish—423(L)
Hard core interpretation of reaction $p + d \rightarrow \pi^+ + t$, Sidney Bludman—487(A)
K-particle mass measurements, D. M. Ritson—1572(L)
Kinetic energies of V_1^0 particles, J. Ballam, D. R. Harris, A. L. Hodson, R. Ronald Rau, George T. Reynolds, S. B. Treiman, and M. Vidale—1019(L)
Magnetic cloud-chamber observations of V particles. I. Apparatus and reduction of data, A. V. Buskirk, L. R. Etter, C. J. Karzmark, R. H. Rediker, and R. W. Thompson—445(A); II. V^0 particles, R. W. Thompson, A. V. Buskirk, L. R. Etter, C. J. Karzmark, and R. H. Rediker—446(A)
Mean life of μ^- mesons stopped in Fe, A. H. Benade—971
Meson masses and related quantities, F. M. Smith, W. Birnbaum, and Walter H. Barkas—765(L)
Momenta of V^0 particles, J. Ballam, D. R. Harris, A. L. Hodson, R. Ronald Rau, George T. Reynolds, S. B. Treiman, and M. L. Vidale—446(A)
μ-mesic atom, L. N. Cooper and E. M. Henley—480(A)
Multiple pion production in n-p collisions observed at the cosmotron, W. B. Fowler, R. P. Shutt, A. M. Thorndike, and W. L. Whittemore—758(L)
Neutron and meson stars induced in light elements of emulsion, M. Blau, A. R. Oliver, and J. E. Smith—949
$p + p \rightarrow d + \pi^+$ cross section at 340 Mev and 327 Mev, Frank S. Crawford, Jr.—468(A)
Phenomenological interpretation of π^+-meson production by protons on C, M. M. Block, S. Passman, and W. W. Havens, Jr.—210(A)
Photomeson production from H and D at 90° and 30°, D. Luckey, T. Jenkins, and R. R. Wilson—468(A); at 180°, T. R. Palfrey, D. Luckey, and R. R. Wilson—468(A)
Photoproduction of mesons in D, J. Chappelear and K. A. Brueckner—480(A)
Photoproduction of π^- mesons from D, Kenneth C. Bandtel, Wilson J. Frank, and Richard Madey—487(A)
Pions and protons from target bombarded by 2.3-Bev protons in cosmotron, W. B. Fowler, R. P. Shutt, A. M. Thorndike, and W. L. Whittemore—479(A)
Positive π-meson production by π^- mesons, W. F. Fry—1576(L)
Positive photomesons from H at 0°, R. Stephen White, Gordon W. Repp, and Nelson Jarmie—468(A); Nelson Jarmie, Gordon W. Repp, and R. Stephen White—1023(L)
Production above 10 Bev, C. B. A. McCusker, N. A. Porter, and B. G. Wilson—384
Production of charged photomesons from He. H-He ratios, M. J. Jakobson, A. G. Schulz, and R. S. White—695
Production of positive pions by 341-Mev protons on protons, W. F. Cartwright, C. Richman, M. N. Whitehead, and H. A. Wilcox—677
Production of V_1^0 particles by π^- mesons in H, W. B. Fowler, R. P. Shutt, A. M. Thorndike, and W. L. Whittemore—1287(L)
Recent experimental results on S particles, H. Bridge, H. Courant, H. DeStaebler, Jr., and B. Rossi—1024(L)
Spectrum and half-life of κ meson, J. P. Davidson—1020(L)
Unusual π-μ decays in photographic emulsions, W. F. Fry—130
V^0 particles in multi-plate cloud chamber, H. S. Bridge, C. Peyrou, B. Rossi, and R. Safford—362
Zenith angle variation of cosmic-ray meson intensity, Arthur Beiser—446(A)
Metals (see **Crystalline State**)
Metastable Atoms (see **Atomic Structure and Spectra**)
Metastable Molecules (see **Molecular Structure and Spectra**)
Meteorology (see **Geophysics**)
Methods and Instruments
Absolute scintillation efficiency of anthracene, J. B. Birks and M. E. Szendrei—197(L)
Angular aberrations in sector-shaped electromagnetic lenses for focusing beams of charged particles, Edgar G. Johnson and Alfred O. Nier—10
Apparatus for magnetic measurements at low temperatures, R. A. Erickson and L. D. Roberts—216(A)
Application of liquid scintillation neutron detector to time-of-flight spectroscopy, L. M. Bollinger, G. E. Thomas, and R. R. Palmer—452(A)
Argonne Laboratory scintillation coincidence spectrometer, S. B. Burson and W. C. Jordan—498(A)
Bubble chamber for study of ionizing events, Donald A. Glaser—496(A)
Bubble-chamber tracks of penetrating cosmic-ray particles, Donald A. Glaser—762(L)
C.A.L. hypersonic test facility, Abraham Hertzberg and William E. Smith—1029(A)
Characteristics of Allen-type electron multiplier, C. F. Barnett—224(A)
Cl isotope separation by thermal diffusion, A. Z. Kranz and W. W. Watson—1469
Computations of three-dimensional structure factors on S-FAC, R. Pepinsky and P. F. Eiland—229(A)

Methods and Instruments (Continued)

Continuous flow cell for investigation of polarization at metal-solution interface, L. W. Morris and Hung-Chi Chang—215(A)

Corrections for dead time of counters in coincidence systems, C. H. Westcott and J. S. Kirkaldy—495(A)

Cyclotron efficiency and power distribution measurements, A. L. Boch and E. D. Hudson—224(A)

Differential pulse-height discriminator, R. C. Shreckengost, D. C. Swanson, and J. W. Flowers—224(A)

Diode characteristic of hollow cathode, M. L. Babcock, D. F. Holshouser, and H. Von Foerster—755(L)

Double crystal neutron spectrometer, V. C. Wilson, B. W. Roberts, W. L. Roth, J. S. Kasper, and A. H. Geisler—494(A)

Effect of magnetic flux amplitude on flux integrator energy control of betatron, Leo Seren, Milton Birnbaum, Erich Harth, and Ralph Tobin—474(A)

Effects of grooves in piezoelectric filter plates, Charles R. Mingins, Robert W. Perry, and David W. MacLeod—471(A)

Electric wave filter combining piezoelectric divided electrode units, Albert D. Frost, Charles R. Mingins, and Lawrence A. Howard—471(A)

Electromagnetic electron beam extractor, R. S. Foote and Ben Petree—456(A)

Electromagnetic shims for focusing in fixed-frequency cyclotron, Farno L. Green—223(A)

Electron cyclotrons (microtrons) for X- and K-band operation, H. F. Kaiser—456(A)

Electron interferometer, L. Marton, J. Arol Simpson, and J. A. Suddeth—437(A); Construction and operation, J. A. Suddeth, L. Marton, and J. Arol Simpson—437(A); Observations and interpretation, J. Arol Simpson, J. A. Suddeth, and L. Marton—437(A)

Equilibrium ultracentrifuge, A. Robeson, N. Snidow, and J. W. Beams—493(A)

Experiment with transistors for elementary electronics laboratory course, F. H. Mitchell—227(A)

Experimental method to determine equation-of-state data for solids by shock-wave measurements, Russell H. Christian and John M. Walsh—1030(A)

Field inhomogeneities in alternating gradient synchrotron, E. D. Courant—456(A)

Gas scintillation counters, Carl O. Muehlhause—495(A)

Gradation development method for nuclear emulsions, H. G. DeCarvalho, V. Davis, and W. Tesh—224(A)

Graphical method for obtaining phase shifts from experimental data on meson-nucleon scattering, Julius Ashkin and Seymour H. Vosko—1248

High-accuracy, high-speed shaft position digitalizer, Donald H. Jacobs, Milton E. Pugh, and Seymour Scholnick—492(A)

High-altitude cosmic-ray investigation by means of Cerenkov counter. I. Instrumentation details, Kinsey Anderson and John R. Winckler—431(A); II. Experimental results, John R. Winckler and Kinsey Anderson—431(A)

High-current 120-kev positive ion accelerator, D. L. Lafferty, J. A. Biggerstaff, B. D. Kern, and T. M. Hahn—223(A)

High-efficiency low-background fast-neutron detector, S. D. Bloom and C. O. Muehlhause—494(A)

Liquid scintillation neutron counters, G. Thomas and L. Bollinger—452(A)

Mach Zehnder interferometer, D. Weimer, W. Bleakney, and D. R. White—1032(A)

Magnetic cloud-chamber observations of V particles. I. Apparatus and reduction of data, A. V. Buskirk, L. R. Etter, C. J. Karzmark, R. H. Rediker, and R. W. Thompson—445(A)

Magnetic refrigerator for maintaining temperatures below 1°K, C. V. Heer, C. B. Barnes, and J. G. Daunt—412(L)

Magnetic scanning method for investigating hfs and isotope shift, F. Bitter, H. Plotkin, B. Richter, A. Teviotdale, and J. E. R. Young—421(L)

Mass spectrometric positive ion technique for determining phase transition temperatures and heats of transformation in metals, R. G. Johnson, W. C. Caldwell, D. E. Hudson, and F. H. Spedding—466(A)

Mass synchrometer, Lincoln G. Smith and C. C. Damm—481(A)

Measurement of thickness of thin films by employing electron microscope shadow-casting technique, George W. Crawford—214(A)

Method for determination of maximum energy of weak β emitters, M. Forro—483(A)

Method for measuring magnetic moments of superconductors, Ted G. Berlincourt and M. C. Steele—215(A)

Method of measuring gyromagnetic ratio of free electron, H. R. Crane, R. W. Pidd, and W. H. Louisell—475(A); W. H. Louisell, R. W. Pidd, and H. R. Crane—475(A)

Multichannel pulse-height analyzer using storage tube, J. A. Cunningham—437(A)

Neutron detectors for Brookhaven fast chopper, H. Palevsky, N. G. Sjostrand, and D. J. Hughes—451(A)

Neutron energy distribution in ORNL graphite reactor, James B. Trice—224(A)

Neutron time-of-flight spectrometer with betatron source, M. L. Yeater and E. R. Gaerttner—451(A)

New detector for infrared, S. Mrozowski, B. D. McMichael, and E. A. Kmetko—234(A)

Noise in storage tubes, Stanley Winkler and Seymour Nozick—492(A)

Nuclear magnetic resonance modulation correction, E. R. Andrew—425(L)

Oak Ridge 44-in. cyclotron, Royce J. Jones—223(A)

Origin of strong focusing principle, E. D. Courant, M. S. Livingston, H. S. Snyder, and J. P. Blewett—202(L)

Particle selection using crystal telescope, B. Wolfe, J. DeWire, and A. Silverman—446(A)

Pellicle stacks in nuclear research, Francis W. O'Dell, Maurice M. Shapiro, and Bertram Stiller—496(A)

Performance of a 125-kv accelerator and spectrometer, J. Bergstein and R. D. Birkhoff—223(A)

Phosphorescence method for study of surface temperatures in supersonic flow field, L. C. Bradley, C. D. Van Voorhis, and D. Bershader—469(A)

Plastic scintillators, R. K. Swank and W. L. Buck—495(A)

Positive ion flux in G-M counter, W. C. Porter and G. W. McClure—495(A)

Preparation of gray Sn filaments, A. W. Ewald—244(A)

Preparation of junctions in single crystals by surface melting, K. Lehovec and E. Belmont—492(A)

Radioisotope production in ORNL 86-in. cyclotron, J. A. Martin—224(A)

Rapid separation of He^3 from He^4 by "heat flush" method, T. Soller, W. M. Fairbank, and A. D. Crowell—1058

Recording of temperature-dependent electrical properties of semiconductors, Luther Davis, Jr., Lawrence Rubin, and W. D. Straub—490(A)

Relativistic particle cyclotron with electrostatic focusing, H. F. Kaiser—499(A)

Response of NaI(Tl) scintillation crystals as function of Tl concentration, F. S. Eby, W. K. Jentschke, and G. DePasquali—495(A)
Scintillation process in plastic solid solutions, Robert K. Swank and Warren L. Buck—927
Scintillations produced by α particles in CsI, Beat Hahn—772(L)
Series method for comparison of resistances, Harold J. Hoge—493(A)
Shapes of floating liquid zones between solid rods, P. H. Keck, M. Green, and M. L. Polk—472(A)
Short resolution time and short "dead" time coincidence counting equipment, Richard Madey—486(A)
Stability of orbits in strong-focusing synchrotron, Stig Lundquist—981
10-Mc rf ion source, E. W. McDonald and D. C. Ralph—223(A)
Terphenyl-*B* liquid neutron detector, W. H. Campbell and J. I. Hopkins—224(A)
Time-of-flight instrumentation for 100-Mev neutrons, W. I. Linlor and B. Ragent—440(A)
Total-temperature probes for use at high supersonic speeds and elevated temperatures, Eva M. Winkler—469(A)
Transparent, nonmetallic, electrically conducting film applications, L. B. Clark, Sr.—471(A)
Van de Graaff electrostatic generator, D. C. Swanson—223(A)
Versatile radiation oven, Richard B. Belser—246(A)
Very high-resistance measurement, Frank J. Lynch and Clarence L. Wesenberg—493(A)

Microwaves (see also **Atomic Structure and Spectra; Magnetic Resonance; Molecular Structure and Spectra; Nuclear Moments and Spin**)
Broadening of microwave absorption lines due to wall collisions, Michael Danos and Stanley Geschwind—1159
Microwave observation of collision frequency of holes in Ge, T. T. Benedict—1565(L)
Stark effect in high-temperature microwave spectroscopy, P. Tate and M. W. P. Strandberg—464(A)

Miscellaneous
Graduate training for high school physics teachers and cooperation between college and high school physics departments, Donald C. Martin—227(A)
Incentive grading for basic laboratory reports, Ray M. Morrison and M. S. McCay—227(A)
Information content of living systems, Harold J. Morowitz—492(A)
Is it possible to teach physics to humanities students?, N. Goldowski—227(A)
Subject of social physics, John Q. Stewart—493(A)

Mobility of Ions and Electrons (see **Ions and Electrons, Mobility**)

Molecular Aggregates
Calculation of extrusion behavior of viscoelastic materials from relaxation distribution function, Thor L. Smith—218(A)
Crystallization in butadiene-styrene copolymers, Lawrence A. Wood—225(A)
Density changes in glass during heat treatment, H. N. Ritland—228(A)
Dependence of photoelastic properties of GR-S on degree of cross linking, G. R. Taylor and S. R. Darin—211(A)
Dielectric dispersion of polar polymers at microwave frequencies, T. M. Shaw and J. J. Windle—218(A)
Dielectric relaxation in styrene-acrylonitrile copolymer during and after its polymerization, P. Ehrlich and N. J. DeLollis—218(A)
Dynamic mechanical properties of polyisobutylene, Edwin R. Fitzgerald, Lester D. Grandine, Jr., and John D. Ferry—217(A)
Dynamic properties of concentrated polymer solutions, F. J. Padden, H. Markovitz, and T. W. DeWitt—217(A)
Dynamic properties of unvulcanized GR-S, L. J. Zapas, S. L. Shufler, and T. W. DeWitt—217(A)
Infrared study of crystallization of polyethlene, Alexander Brown and F. T. Reding—226(A)
Melting transition of natural rubber, Donald E. Roberts and Leo Mandelkern—225(A)
Nucleoprotein monolayers, Adolph B. Amster and Quentin Van Winkle—211(A)
Orientation in polymeric films by infrared and x-ray techniques, W. H. Cobbs, Jr., S. B. Cole, and R. L. Burton—225(A)
Relaxation distribution function of polyisobutylene in transition from rubber-like to glass-like behavior and its dependence on temperature, John D. Ferry, Lester D. Grandine, Jr., and Edwin R. Fitzgerald—217(A)
Rheology of polyisobutylene. III. Approximation methods in linear viscoelasticity theory: Wiechert function calculations, Herbert Leaderman—217(A)
Sedimentation rates in dilute and moderately concentrated polymer solutions, M. Wales—211(A)
Stress crazing thresholds of methyl methacrylate polymers, T. F. Protzman, J. J. Gouza, and W. F. Bartoe—211(A)
Values of diffusion coefficients for some chain polymers computed from anomalous osmotic pressure data, T. A. Barr, Jr.—211(A)

Molecular Beams (see **Atomic and Molecular Beams**)

Molecular Structure and Spectra
Analysis of infrared spectrum of CF_3COCl, Robert James Lovell—235(A)
Application of Thomas-Fermi method to calculation of certain molecular vibration frequencies, W. A. Bowers—242(A)
Broadening of microwave absorption lines due to wall collisions, Michael Danos and Stanley Geschwind—1159
Configurational interaction in molecular orbital theory and relative energies of polar and nonpolar functions, Max Wolfsberg—464(A)
Correlation of infrared and ultraviolet spectra of associated alcohols, Gladys A. Anslow and Irene S. White—241(A)
Dissociation and recombination of O_3 in upper atmosphere assuming three-body recombinations, Harry E. Moses and Ta-You Wu—458(A); 1408
Electron-coupled interactions between nuclear spins in molecules, Norman F. Ramsey—303
Electronic energy levels of O_2, Alvin Meckler—242(A)
Energy exchange in molecular collisions, B. Widom and S. H. Bauer—240(A)
Excitation of molecular rotations and vibrations in inelastic scattering processes, Edward H. Kerner—1174
Frequencies of microwave absorption lines of O_2, Masataka Mizushima—222(A)
Infrared absorption induced by static electric fields, M. F. Crawford and I. R. Dagg—1569(L)
Infrared absorption spectrum of SO_2, R. D. Shelton, A. H. Nielsen, and W. H. Fletcher—235(A)
Infrared analysis of associated O-H and O-D stretching vibrations of simple carboxylic acids, Nelson Fuson, Marie-Louise Josien, and Conrade C. Hinds—234(A)
Infrared grating spectrum of CH_3CN vapor, F. W. Parker, A. H. Nielsen, and W. H. Fletcher—235(A)
Infrared spectrum and molecular constants of DBr, F. L. Keller and A. H. Nielsen—235(A)

Molecular Structure and Spectra (Continued)
Infrared spectrum of amide group, Harry Letaw, Jr., and Armin H. Gropp—235(A)
Infrared study of influence of molecular structure on carbonyl band in polycyclic quinones, Marie-Louise Josien, Nelson Fuson, and Essie M. Shelton—235(A)
Ionization and dissociation of nitromethane by electron impact, R. J. Kandel—436(A)
Matrix formulation of molecular orbital, Heitler-London, and configurational interaction computations, Paul F. Wacker—465(A)
Microwave spectrum and molecular properties of O_3, R. Trambarulo, S. N. Ghosh, C. A. Burrus, Jr., and W. Gordy—222(A)
Microwave spectrum and structure of $HGeCl_3$, Putcha Venkateswarlu, Richard C. Mockler, and Walter Gordy—222(A)
Microwave spectrum of $(CH_3)_3SiCl$, Richard C. Mockler and Walter Gordy—222(A)
Microwave spectrum of DI at 1.5-mm wavelength, J. A. Klein and A. H. Nethercot, Jr.—1018(L)
Microwave spectrum of unstable molecule CS, George R. Bird and Richard C. Mockler—222(A)
Molecular beam investigation of rotational transitions. I. Rotational levels of KCl and their hfs, Charles A. Lee, B. P. Fabricand, R. O. Carlson, and I. I. Rabi—1395; II. Of KBr, B. P. Fabricand, R. O. Carlson, Charles A. Lee, and I. I. Rabi—1403
Molecular orbital treatment of contribution of π electrons to electric dipole moments of some phenyl halides, R. H. Knipe—242(A)
Molecular rotation in liquids, Edward J. Breneman and Dudley Williams—465(A)
Molecular weight of organic compounds by mass spectrometry, John R. Sites and Bernard L. Strehler—242(A)
Near uv absorption spectrum of *p*-difluorobenzene vapor, Dewey C. Cooper—241(A)
Near uv vapor spectrum of thianaphthene, R. C. Heckman and H. Sponer—242(A)
Nuclear resonance line structure in HD and molecular shielding in HD, H_2, and D_2, T. F. Wimett—476(A)
Nuclear shielding in H_2 and D_2, P. J. Bray and R. G. Barnes—475(A)
Photoionization of NO, K. Watanabe, Frederick Marmo, and Edward C. Y. Inn—436(A); 1155
Photoionization of molecules in vacuum uv, Edward C. Y. Inn—1194
Quadrupole coupling of deuteron in DCCCl and DCN, Robert L. White—1014(L)
Quadrupole moments of Mn^{55}, Re^{185}, and Re^{187}, A. Javan, G. Silvey, C. H. Townes, and A. V. Grosse—222(A)
Raman spectrum, force constants, and calculated thermodynamic properties of GeF_4, Lawrence K. Akers and Ernest A. Jones—236(A)
Relative optical collision diameters from pressure broadening of individual infrared absorption lines, William Benesch and Tait Elder—308
Rotational spectrum and molecular structure of CH_3SH, N. Solimene and B. P. Dailey—464(A)
Spin-orbit and spin-spin interactions in H_2, R. G. Barnes, P. J. Bray, and N. J. Harrick—475(A)
Stark effect in high-temperature microwave spectroscopy, P. Tate and M. W. P. Strandberg—464(A)
Temperature dependence of line breadths of O_2, Robert M. Hill and Walter Gordy—222(A)
Theory of rotational spectra of allene-type molecules, M. Mizushima—464(A)
Uhf rotational line of HDO, Yardley Beers and Samuel Weisbaum—1014(L)
Vibrational spectra of $F_2C{:}CF_2$ and $Cl_2C{:}CCl_2$, D. E. Mann, N. Acquista, and Earle K. Plyler—464(A)
Zeeman effect in microwave spectra of CH_3F and CH_3CCD, J. T. Cox, P. B. Peyton, Jr., and Walter Gordy—222(A)

Moments, Nuclear (see **Nuclear Moments and Spin**)

Moments of Molecules (see **Molecular Structure and Spectra**)

Neutrino (see also **Nuclear Spectra; Radioactivity**)
Inner bremsstrahlung and magnetic moment of neutrino, J. Weneser—1025(L)
Interference terms of electron-neutrino angular correlation, erratum, Masato Morita—1580(E)

Neutron Diffraction (see **Diffraction; Scattering of Neutrons**)

Neutrons (see **Elementary Particle Interactions**)

Noise
Noise in *p-n* junction rectifiers and transistors. I. Theory, Richard L. Petritz—231(A); II. Experiment, Francis L. Lummis and Richard L. Petritz—231(A)
Noise in storage tubes, Stanley Winkler and Seymour Nozick—492(A)
Nyquist and Einstein relations derived from scattering model, Stefan Machlup—240(A)
Possible mechanism for $1/f$ noise generation in semiconductor filaments, Leon Bess—1569(L)

Nuclear Fission
Energy distributions of fission fragments, John S. Wahl—486(A)
Long-lived delayed neutrons from fission, J. W. Kunstadter, J. J. Floyd, and L. B. Borst—594
π^- and μ^- meson-induced fission, W. John and W. Fry—1234
U^{234} fission cross section, R. W. Lamphere—210(A); 655
Yield distribution in proton fission of U, W. H. Jones, J. H. Paehler, T. H. Handley, and A. Timnick—486(A)
Yield of Xe^{133} in thermal neutron fission of U^{235}, Seymour Katcoff and William Rubinson—1458

Nuclear Forces (see **Elementary Particle Interactions; Field Theory; Nuclear Structure Theory**)

Nuclear Induction (see **Magnetic Resonance; Nuclear Moments and Spin**)

Nuclear Isomers (see **Nuclear Spectra; Radioactivity**)

Nuclear Moments and Spin
d-p magnetic moment ratio, T. F. Wimett—499(A)
Dipolar broadening of quadrupole resonance line width in zero applied field, A. Abragam and K. Kambe—894
Effect of electric quadrupole interaction on γ-γ directional correlation in Cd^{111}, H. Albers-Schönberg, E. Heer, T. B. Novey, and R. Rüetschi—199(L); H. Albers-Schönberg, K. Alder, O. Braun, E. Heer, and T. B. Novey—1287(L)
Electric field gradient of atomic *p* electrons, W. V. Smith and R. G. Barnes—457(A)
Electron-coupled interactions between nuclear spins in molecules, Norman F. Ramsey—303
Hfs and nuclear moment ratios of stable Br isotopes, J. G. King and V. Jaccarino—209(A)
Hfs and nuclear moments of Pr^{141}, Hin Lew—619
Magnetic moment deviations from Schmidt limits via admixed states, A. B. Volkov—444(A)
Nuclear magnetic moment of Cr^{53} and Sr^{87}, C. D. Jeffries and P. B. Sogo—1286(L)
Nuclear magnetic resonance in Th compounds, H. S. Gutowsky and B. R. McGarvey—81
Nuclear moments of Ta^{181}, erratum, B. M. Brown and D. H. Tomboulian—1580(E)

Nuclear quadrupole resonance in rhombic S and quadrupole moments of S^{33} and S^{35}, H. G. Dehmelt—313
Polarization of nuclei in metals, Albert W. Overhauser—476(A)
Quadrupole coupling of deuteron in DCCCl and DCN, Robert L. White—1014(L)
Quadrupole moments of Mn^{55}, Re^{185}, and Re^{187}, A. Javan, G. Silvey, C. H. Townes, and A. V. Grosse—222(A)
Quadrupole moments of stable Sb nuclei, G. Sprague and D. H. Tomboulian—476(A)
Spin and magnetic moment of Li^6 nucleus, G. E. Tauber and Ta-You Wu—443(A)

Nuclear Photoeffects
Angular and energy distributions of photoprotons from Al and Ta, A. G. W. Cameron and M. M. Hoffman—473(A)
Angular distribution of mesons from 320-Mev photons on protons, Y. Goldschmidt-Clermont, L. S. Osborne, and A. W. Winston—468(A)
Consequences of charge independence for nuclear reactions involving photons, Murray Gell-Mann and Valentine L. Telegdi—169
$Cu^{63}(\gamma,n)Cu^{62}$ and $Ag^{109}(\gamma,n)Ag^{108}$ reaction thresholds, Erich Harth, Leo Seren, Milton Birnbaum, and Ralph Tobin—474(A)
Dipole photonuclear reactions and independent particle model, James L. Burkhardt—420(L)
Direct measurement of nuclear absorption of x-rays, H. W. Koch and R. S. Foote—455(A)
(γ,n) thresholds of Cu^{63} and Ag^{109} based on (γ,n) thresholds of N^{14}, O^{16}, and C^{12}, Milton Birnbaum, Erich Harth, Leo Seren, and Ralph Tobin—474(A)
$Li^7(\gamma,p)He^6$ cross section, B. L. Tucker and E. C. Gregg—1579(L)
$Mn^{55}(\gamma,3n)Mn^{52}$ excitation function, R. L. Hines—474(A)
Nuclear photostar production, Israel Reff—150
$O^{16}+h\nu \rightarrow 4$ He^4 reaction mechanism, C. A. Hsiao and V. L. Telegdi—473(A)
Photodisintegration of deuteron at 20 Mev, E. V. Weinstock and J. Halpern—461(A); J. Halpern and E. V. Weinstock—934
Photoneutron cross sections, R. Montalbetti, L. Katz, and J. Goldemberg—659
Photoneutron production excitation functions to 320 Mev, Lawrence W. Jones and Kent M. Terwilliger—699
Photoproduction of mesons in D, J. Chappelear and K. A. Brueckner—480(A)
Photoproduction of μ^- mesons from D, Kenneth C. Bandtel, Wilson J. Frank, and Richard Madey—487(A)
Photoprotons from Mo^{100} and Mo^{92}, W. A. Butler and G. M. Almy—58
Production of charged photomesons from He. H-He ratios, M. J. Jakobson, A. G. Schulz, and R. S. White—695

Nuclear Reactions, General (see also **Elementary Particle Interactions; Scattering**)
Accurate determinations of nuclear reaction energies, K. F. Famularo and G. C. Phillips—1195
Be^8 breakup energy, Samuel K. Allison—882; K. W. Jones, D. J. Donahue, M. T. McEllistrem, R. A. Douglas, and H. T. Richards—879
Consequences of charge independence for nuclear reactions involving photons, Murray Gell-Mann and Valentine L. Telegdi—169
Cosmic-ray star production rates in gases, Fielding Brown and George T. Reynolds—444(A)
Coulomb excitation of nuclei, K. Alder and A. Winther—1578(L)
Delayed neutrons in cosmic-ray stars, Byron W. St. Clair—445(A)
Energy distribution of neutral mesons produced in cosmic-ray stars, Y. B. Kim—445(A)
Energy spectrum of particles from stars, R. W. Waniek and Taiichiro Ohtsuka—1574(L)
Excitation energies of nuclei as rational multiples of electron mass, Enos E. Witmer—500(A)
Half-widths and level shifts of one-body resonances, J. L. McHale and John L. Johnson—452(A)
Inverse Oppenheimer-Phillips process in $Cu^{65}(He^3,\alpha)$, D. N. Kundu and M. L. Pool—417(L)
Neutron and meson stars induced in light elements of emulsion, M. Blau, A. R. Oliver, and J. E. Smith—949
Observations on stars and heavy primaries recorded in emulsions during flight of Viking rocket, Herman Yagoda—445(A)
Production and detection of polarized particles in nuclear reactions, A. Simon and T. A. Welton—453(A)
Reduced widths in stripping processes, R. G. Thomas—453(A)
Role of nucleon isobar in high-energy interactions, Bernard T. Feld—454(A)
Statistical theory of nuclear reactions, Bernard L. Cohen—241(A)

Nuclear Reactions Induced by α Particles and He^3 (see also **Scattering of α Particles**)
A^{38} energy levels from $Cl(\alpha,p)$, A. Z. Kranz and W. W. Watson—1472
$Al^{27}(\alpha,\alpha 2pn)Na^{24}$ cross section from threshold to 380 Mev, M. Lindner and R. N. Osborne—342
Be^8 energy levels from $Li^6(He^3,p)Be^8$, W. E. Kunz, C. D. Moak, and W. M. Good—676
$C^{12}(\alpha,\alpha n)C^{11}$ cross section, energy dependence, M. Lindner and R. N. Osborne—1501
H^3+He^3 reactions, C. D. Moak—462(A)
$He^3(He^3,p)Li^5$ and $T(He^3,p)He^5$, E. Almqvist, K. W. Allen, J. T. Dewan, and T. P. Pepper—1022(L)
He^3 reactions in Cu and Si, M. L. Pool and K. N. Kundu—462(A)
He^3+He^3 reaction, W. M. Good, W. E. Kunz, and C. D. Moak—462(A)
Inelastic scattering of alphas from N^{14}, B. M. Carmichael, M. B. Sampson, and O. E. Johnson—473(A)
$Li^8(\alpha,\gamma)B^{10}$, D. H. Wilkinson and G. A. Jones—1575(L)
Limiting Q value for $K^{39}(\alpha,p)Ca^{42}$, J. P. Schiffer and Ernest Pollard—474(A)
Ranger study of Po-Be neutron spectrum, Herbert Gursky, Barbara Winnemore, and D. A. Cowan—209(A)

Nuclear Reactions Induced by Deuterons and Tritons (see also **Scattering of Deuterons**)
Absolute magnetic analysis of reaction energies of $Li^6(d,\alpha)He^4$, and $C^{13}(d,\alpha)B^{11}$, G. C. Phillips, K. F. Famularo, and C. R. Gossett—462(A)
$Al^{27}(d,\alpha p)Na^{24}$ excitation function, R. E. Batzel, W. W. T. Crane, and G. D. O'Kelley—939
Angular distributions of protons from $Na^{23}(d,p)Na^{24}$, S. Takemoto, T. Dazai, and R. Chiba—1024(L)
$Bi^{209}(d,p)B^{210}$ Q value, Nathan Sanders Wall—485(A)
Coincidence studies of B^{10} γ rays, S. M. Shafroth and S. S. Hanna—483(A)
Cross section of $He^3(H^3,H^1)He^4$ reaction from 100–800 kev He^3 energy, W. E. Kunz—462(A)
(d,p) reactions with separated Kr isotopes, G. W. Wheeler, R. B. Schwartz, and W. W. Watson—485(A)
(d,t) reactions and triton wave function, D. R. Bach and P. V. C. Hough—463(A)
Energy levels of B^{11} and B^{12} by (d,p) reaction, M. Elkind and A. Sperduto—463(A)
γ rays from disintegration of C^{13} by deuterons, R. D. Bent, T. W. Bonner, and R. F. Sipple—472(A)

Nuclear Reactions (Continued)
K^{40} excited states, W. W. Buechner, A. Sperduto, C. P. Browne, and C. K. Bockelman—1502
$Li^6(d,t)Li^5(p)He^4$ reaction, R. T. Frost and S. S. Hanna—462(A)
N^{15} energy levels, A. Sperduto, W. W. Buechner, M. M. Elkind, and W. J. Fader—473(A)
Neutrons from $Be^9(d,n)B^{10}$, J. S. Pruitt, S. S. Hanna, and C. D. Swartz—463(A)
Production of tritons in *d-d* collisions, Charles Godfrey, Kenneth C. Bandtel, Wilson J. Frank, and Richard Madey—487(A)
Reduced widths in stripping processes, R. G. Thomas—453(A)
Secondary particles resulting from high-energy bombardment, R. W. Deutsch—485(A)
Theory of (d,p) reactions, E. Gerjuoy—453(A); 645
Triton-induced activities in Mg and Al, Eric Iwersen, W. S. Koski, and Franco Rasetti—1229

Nuclear Reactions Induced by Mesons (see also **Elementary Particle Interactions; Mesons; Scattering of Mesons**)
Capture of μ mesons in matter, F. T. Cole and H. A. Bethe—481(A)
Diffusion cloud-chamber study of pion interactions in H and He, E. C. Fowler, W. B. Fowler, R. P. Shutt, A. M. Thorndike, and W. L. Whittemore—135
High-energy pairs of particles from nuclear interactions, Marcel Schein, Joseph Fainberg, D. M. Haskin, and R. G. Glasser—479(A)
Inelastic scattering of negative pions, Gerson Goldhaber and S. Goldhaber—467(A)
Interaction cross section of μ mesons with nuclei, H. C. Wilkins and M. Annis—480(A)
Mean free path for shower production by high-energy π mesons, Fritz E. Frochlich and Kurt Sitte—433(A)
Mean life of μ^- mesons stopped in Fe, A. H. Benade—971
μ^- meson nuclear capture in H and D, H. Primakoff—480(A)
Neutron production by μ mesons stopped in Pb at sea level, E. J. Althaus and R. D. Sard—373
Nucleon polarization in pion-proton scattering, Enrico Fermi—947
π^- and μ^- meson-induced fission, W. John and W. F. Fry—1234
Positive π-meson production by π^- mesons, W. F. Fry—1576(L)
Production of Cu radioactivity in interaction of negative pions and muons with Zn, Si-Chang Fung and A. Turkevich—480(A)
Production of high-energy electron pairs by negative pions in nuclear collisions, Marcel Schein, Joseph Fainberg, D. M. Haskin, and R. G. Glasser—973
Production of V_1^0 particles by π^- mesons in H, W. B. Fowler, R. P. Shutt, A. M. Thorndike, and W. L. Whittemore—1287(L)
Scattering and absorption of π^+ mesons by Al, James F. Tracy—960
Scattering of 120-Mev negative pions by H, Jay Orear—467(A)
Scattering of 169- and 192-Mev pions by H, R. L. Martin, E. Fermi, and D. E. Nagle—467(A)
Total cross sections for 37-Mev pions in H, C. E. Angell and J. P. Perry—468(A)
210-Mev negative pion interactions, A. H. Morrish—468(A)

Nuclear Reactions Induced by Neutrons (see also **Elementary Particle Interactions; Scattering of Neutrons**)
$A^{36}(n,\alpha)S^{33}$ reaction, B. J. Toppel and S. D. Bloom—473(A)
Absorption cross section of Au and B for thermal and cold neutrons, R. S. Carter, H. Palevsky, and V. W. Myers—450(A)
Angular distributions from (n,p) nuclear reactions, N. Austern, S. T. Butler, H. McManus, and W. T. Sharp—453(A)
Application of liquid scintillation neutron detector to time-of-flight spectroscopy, L. M. Bollinger, G. E. Thomas, and R. R. Palmer—452(A)
Doppler effect on neutron resonance levels, E. Melkonian, W. W. Havens, Jr., and L. J. Rainwater—450(A)
Energy distribution of neutron stars, R. W. Waniek and T. Ohtsuka—445(A)
Fast neutron cross sections and nuclear level density, D. J. Hughes, R. C. Garth, and J. S. Levin—1423
γ radiation from inelastic scattering of 2.7-Mev neutrons, V. E. Scherrer, W. L. Smith, B. A. Allison, and W. R. Faust—768(L)
γ rays from 14-Mev neutron bombardment of C, O, Al, Fe, and Pb, M. E. Battat—441(A)
γ rays from interaction of 14-Mev neutrons with various materials, V. E. Scherrer, R. B. Theus, and W. R. Faust—1476
Inelastic scattering of *d-d* neutrons, R. E. Garrett, F. L. Hereford, and B. W. Sloope—441(A)
Interactions of 14-Mev neutrons with protons and deuterons, J. C. Allred, A. H. Armstrong, and L. Rosen—90
$Li^6(n,\alpha)H^3$ cross section as function of neutron energy, F. L. Ribe—462(A)
Low-energy neutron resonance scattering, H. L. Foote, Jr.—450(A)
Multiple pion production in n-p collisions observed at the cosmotron, W. B. Fowler, R. P. Shutt, A. M. Thorndike, and W. L. Whittemore—758(L)
(n,H^3) cross section in N and relationship to T production in atmosphere, E. L. Fireman—922
Neutron-capture γ-rays in Cd, Co, and Cl, W. A. Reardon, R. W. Krone, and R. Stump—334; 442(A)
Neutron capture γ rays with scintillation spectrometer, T. H. Braid—442(A)
Neutron capture resonances using (n,γ) scintillation detector, R. D. Albert and E. R. Gaerttner—451(A)
Neutron resonances in Ag, W. Y. Kato, Marilyn J. Stafne, J. S. Levin, and D. J. Hughes—450(A)
Neutron resonances in Bi, Tl, and Pb, J. H. Gibbons and Henry W. Newson—209(A)
Neutron resonances in rare earths, V. L. Sailor, H. H. Landon, and H. L. Foote, Jr.—450(A)
Neutron transmission measurements of Cd, Gd, and Hg using Argonne fast chopper, R. Ronald Palmer and Lowell M. Bollinger—450(A)
Parameters for slow neutron resonance in Rh, V. L. Sailor—53
Precision determination of n-p capture cross section, G. von Dardel and A. W. Waltner—1284(L)
Resonant neutron scattering cross sections, C. Sheer, J. Moore, and C. Heindl—449(A)
Scattering of 14–18-Mev neutrons in light elements, C. F. Cook and T. W. Bonner—441(A)
Successive neutron capture in Ta, J. W. Mihelich—427(L)
Thermal n-p capture, S. P. Harris, C. O. Muehlhause, D. Rose, H. P. Schroeder, G. E. Thomas, Jr., and S. Wexler—125
Total cross sections for 400-Mev neutrons, V. Alexander Nedzel—440(A)
Total cross sections of Nd, Er, and Hf for fast neutrons, A. Okazaki, R. B. Walton, and J. D. Clement—440(A)
Total n-p cross section at 1 Mev, R. E. Fields, R. K. Adair, R. L. Becker, and S. E. Darden—441(A)
Total neutron cross section of liquid A, Janet B. Guernsey and Clark Goodman—440(A)

Total neutron cross section of Pb from 30 to 150 Mev, B. Ragent and W. I. Linlor—440(A)
Total neutron cross sections of Cl and C, R. M. Kiehn, Clark Goodman, and K. F. Hansen—66
Total neutron cross sections of heavy water and glass at long wavelengths, V. W. Myers, R. S. Carter, and H. Palevsky—451(A)
Total neutron cross sections, theory, H. Feshbach, C. E. Porter, and V. F. Weisskopf—453(A)

Nuclear Reactions Induced by Protons (see also **Elementary Particle Interactions; Scattering of Protons**)
Absolute magnetic analysis of reaction energies of $Li^7(p,\alpha)He^4$, G. C. Phillips, K. F. Famularo, and C. R. Gossett—462(A)
Accurate determinations of nuclear reaction energies, K. F. Famularo and G. C. Phillips—1195
Analysis of $N^{15}(p,\alpha)C^{12}$ excitation function, W. A. Fowler and R. G. Thomas—473(A)
Angular distribution of neutrons from $C^{14}(p,n)N^{14}$, Robert Kay, Hans Mark, and Clark Goodman—472(A)
Angular distribution of process $p+d\rightarrow t+\pi^+$, Wilson J. Frank, Kenneth C. Bandtel, Richard Madey, and Burton J. Moyer—487(A)
Angular distribution of 12-Mev γ rays from proton bombardment of B, G. L. Jenkins, L. W. Cochran, H. H. Givin, J. L. Ryan, T. M. Hahn, and B. D. Kern—210(A); G. L. Jenkins, L. W. Cochran, B. D. Kern, and T. M. Hahn—915
Angular distributions of nuclear reaction products with internal cyclotron beam, B. L. Cohen, R. V. Neidigh, and E. Newman—486(A)
Be^8 breakup energy, Samuel K. Allison—882; K. W. Jones, D. J. Donahue, M. T. McEllistrem, R. A. Douglas, and H. T. Richards—879
Capture γ rays from proton bombardment of Be, W. F. Hornyak and T. Coor—463(A)
Comparison of nuclear and γ-ray absolute energy scales, K. W. Jones, M. T. McEllistrem, R. A. Douglas, and H. T. Richards—482(A)
Coulomb excitation of nuclei, K. Alder and A. Winther—1578(L)
Excitation curves for α particles from B^{11} bombarded with protons, Olof Beckman, Torben Huus, and Črtomir Zupančič—606
Excitation functions for proton-induced reactions with Cu, J. W. Meadows—885
Excitation of heavy nuclei by electric field of low-energy protons, Clyde L. McClelland and Clark Goodman—760(L)
Extreme energy interactions in heavy nuclei, C. B. A. McCusker and F. C. Roesler—769(L)
γ radiation from B^{11} bombarded by protons, Torben Huus and Robert B. Day—599
Half-widths and level shifts of one-body resonances, J. L. McHale and John L. Johnson—452(A)
Hard core interpretation of reaction $p+d\rightarrow\pi^++t$, Sidney Bludman—487(A)
Inelastic scattering of 18.3-Mev protons, P. C. Gugelot and H. A. Lauter—486(A)
Inelastic scattering of protons from Ca^{40}, C. M. Braams, C. K. Bockelman, C. P. Browne, and W. W. Buechner—474(A)
Interpretation of $0+xp$ type stars in photographic emulsions, C. B. A. McCusker and F. C. Roesler—769(L)
Neutrons from proton bombardment of Be^9, F. Ajzenberg, C. M. Braams, and W. W. Buechner—463(A); Fay Ajzenberg and W. W. Buechner—674
Nuclear reactions produced in Brookhaven cosmotron, J. M. Miller and G. Friedlander—485(A)
(p,n) thresholds of nuclei with $49\leq A\leq 75$, Carroll C. Trail and C. H. Johnson—474(A)
$p+p\rightarrow d+\pi^+$ cross section at 340 Mev and 327 Mev, Frank S. Crawford, Jr., and M. Lynn Stevenson—468(A)
(p,pn) and $(p,\alpha n)$ excitation functions, E. Newman, B. L. Cohen, and T. H. Handley—486(A)
Phenomenological interpretation of π^+ meson production by protons on C, M. M. Block, S. Passman, and W. W. Havens, Jr.—210(A)
Pions and protons from target bombarded by 2.3-Bev protons in cosmotron, W. B. Fowler, R. P. Shutt, A. M. Thorndike, and W. L. Whittemore—479(A)
Production of positive pions by 341-Mev protons on protons, W. F. Cartwright, C. Richman, M. N. Whitehead, and H. A. Wilcox—677
Secondary particles resulting from high-energy bombardment, R. W. Deutsch—485(A)
Total cross sections of 408-Mev protons for H and light elements, J. Marshall, L. Marshall, and V. A. Nedzel—767(L)
Yield and angular distribution of γ rays from $B^{11}(p,\gamma)C^{12}$, H. E. Gove and E. B. Paul—463(A)
Yield distribution in proton fission of U, W. H. Jones, J. H. Paehler, T. H. Handley, and A. Timnick—486(A)
Yield of α particles from reaction $B^{11}(p,\alpha)Be^8$, E. B. Paul and R. L. Clarke—463(A)

Nuclear Scattering (see **Scattering**)

Nuclear Spectra (see also **Nuclear Isomers; Nuclear Reactions; Radioactivity**)
A^{39} energy levels from $Cl(\alpha,p)$, A. Z. Kranz and W. W. Watson—1472
α decay, theory, Joseph J. Devaney—587
α-γ correlations in Re^{186} decay, C. E. Whittle, J. P. Hurley, and P. S. Jastram—498(A)
Analysis of angular correlation and angular distribution data, M. E. Rose—610
Angular correlation in allowed β transitions, M. E. Rose—197(L)
Angular correlation of γ rays of Sr^{88}, J. Varma, B. L. Saraf, and W. B. Todd, Jr.—484(A)
Angular correlation of Ni^{60} γ-γ cascade, Robert M. Kloepper—1026(L)
Angular distribution of 12-Mev γ rays from proton bombardment of B, G. L. Jenkins, L. W. Cochran, H. H. Given, J. L. Ryan, T. M. Hahn, and B. D. Kern—210(A); G. L. Jenkins, L. W. Cochran, B. D. Kern, and T. M. Hahn—915
Argonne Laboratory scintillation coincidence spectrometer, S. B. Burson and W. C. Jordan—498(A)
As^{77} and Br^{77} scintillation study, M. E. Bunker, R. J. Prestwood, and J. W. Starner—1021(L)
As^{77} and Ge^{71} radiations, B. L. Saraf, J. Varma, and C. E. Mandeville—1216
As^{77} γ radiation, S. A. Reynolds, G. W. Leddicotte, and H. A. Mahlman—333
As^{77} γ-ray spectrum, F. Rasetti and E. C. Booth—1192
Au^{179m} decay, J. W. Mihelich and A. de-Shalit—78
Ba^{131} decay, J. M. Cork, J. M. LeBlanc, W. H. Nester, and M. K. Brice—497(A)
Ba^{131} decay γ rays, W. Payne and M. Goodrich—497(A)
Be^8 energy levels from $Li^6(He^3,p)Be^8$, W. E. Kunz, C. D. Moak, and W. M. Good—676
Bremsstrahlung from P^{32} betas, M. Goodrich, J. S. Levinger, and W. Payne—455(A); 1225
C^{14} and Ni^{63} β-ray spectra, J. P. Mize and D. J. Zaffarano—210(A)
C^{14} β spectrum, C. S. Wu and A. Schwarzschild—483(A)
Capture γ rays from proton bombardment of Be, W. F. Hornyak and T. Coor—463(A)
Coincidence studies of B^{10} γ rays, S. M. Shafroth and S. S. Hanna—483(A)

Nuclear Spectra (Continued)
Complementarity in angular momentum states, B. A. Lippmann—1213
Correction for finite angular resolution in directional correlation measurements, J. S. Lawson, Jr., and H. Frauenfelder—649
Cross terms in allowed shape β spectra, J. P. Davidson and D. C. Peaslee—1232
Cs^{131} nuclear levels, J. M. Cork, J. M. LeBlanc, W. H. Nester, and M. K. Brice—76
Cu^{67} radioactivity, Harry T. Easterday—653
Directional correlation of Ni^{60} γ-γ cascade, J. S. Lawson, Jr., H. Frauenfelder, and W. K. Jentschke—484(A)
$_{66}Dy^{165m}$ (1.25-min) and $_{66}Dy^{165}$ (2.3-hr) decay scheme, W. C. Jordan, J. M. Cork, and S. B. Burson—497(A)
Effect of electric quadrupole interaction on γ-γ directional correlation in Cd^{111}, H. Albers-Schönberg, E. Heer, T. B. Novey, and R. Rüetschi—199(L); H. Albers-Schönberg, K. Alder, O. Braun, E. Heer, and T. B. Novey—1287(L)
Energy levels of odd-odd nuclei, A. de-Shalit—1479
$Eu^{147-150}$, Rex C. Mack, J. J. Neuer, and M. L. Pool—497(A)
Eu^{150} and Gd^{150}, Rex C. Mack, J. J. Neuer, and M. L. Pool—903
Evidence concerning spin-orbit forces from β decay, I. Talmi and E. P. Wigner—443(A)
Experimental evidence for Fermi interaction in β decay of O^{14} and C^{10}, R. Sherr and J. B. Gerhart—909
Ga^{64}, Bernard L. Cohen—74
γ-γ angular correlation measurements, Santimay Chatterjee and Ajit Kumar Saha—200(L)
γ radiation from B^{11} bombarded by protons, Torben Huus and Robert B. Day—599
γ radiation from inelastic scattering of 2.7-Mev neutrons, V. E. Scherrer, W. L. Smith, B. A. Allison, and W. R. Faust—768(L)
γ rays from disintegration of C^{13} by deuterons, R. D. Bent, T. W. Bonner, and R. F. Sipple—472(A)
γ rays from 14-Mev neutron bombardment of C, O, Al, Fe, and Pb, M. E. Battat—441(A)
γ rays from interaction of 14-Mev neutrons with various materials, V. E. Scherrer, R. B. Theus, and W. R. Faust—1476
Ge^{79} metastable states, Joan P. Welker, A. W. Schardt, J. J. Howland, Jr., and G. Friedlander—484(A)
Genetic relationships of 0.8-sec Pb^{207m} isomer, G. Friedlander, Elizabeth Wilson, A. Ghiorso, and I. Perlman—498(A)
I^{129} decay and β spectrum, E. der Mateosian and C. S. Wu—497(A)
I^{131} γ radiation, Harry C. Hoyt and Jesse W. M. DuMond—1027(L)
Influence of extranuclear fields on γ-γ directional correlations, F. Coester—452(A)
Interference terms of the electron-neutrino angular correlations, erratum, Masato Morita—1580(E)
Internal conversion coefficients on Nb^{95} and Zn^{65} (actually Mo^{95} and Cu^{65}), E. F. Sturcken and A. H. Weber—484(A)
Internal conversion in L subshells, J. B. Swan and R. D. Hill—424(A)
j-j coupling for $A \lesssim 50$, D. C. Peaslee—443(A)
K^{40} excited states, W. W. Buechner, A. Sperduto, C. P. Browne, and C. K. Bockelman—1502
K^{42} decay, Bernd Kahn and W. S. Lyon—1212
Li^8 β decay, D. StP. Bunbury—1580(E)
Linear combination of invariants in β decay, D. C. Peaslee—1447
Liquid A ionization chamber measurement of shape of β-ray spectrum of K^{40}, John H. Marshall—905
Lower limit for lifetime of 665-kev excited state of Mo^{97}, F. R. Metzger and W. B. Todd—1286(L)
Matrix elements of β decay in jj coupling, Igal Talmi—122
Metastable state of V^{52}, T. Wiedling—767(L)
Mg^{28} decay, A. H. Wapstra and A. L. Veenendall—426
N^{15} energy levels, A. Sperduto, W. W. Buechner, M. M. Elkind, and W. J. Fader—473(A)
Neutron-capture γ rays in Cd, Co, and Cl, W. A. Reardon, R. W. Krone, and R. Stump—334; 442(A)
Neutron capture γ rays with scintillation spectrometer, T. H. Braid—442(A)
Neutron-deficient isotopes of Hg, J. W. Mihelich, L. P. Gillon, K. G. Krishnan, and A. de-Shalit—498(A)
New nuclides produced in Cl spallation, Manfred Lindner—642
Ni^{60} γ-γ angular correlation, E. D. Klema and F. K. McGowan—616
$1/W$ terms in allowed β spectra, J. P. Davidson and D. C. Peaslee—442(A)
Pairing effect in nuclei and isomerism, Robert Katz—1487
Patterns in α spectra of even-even nuclei, Frank Asaro and I. Perlman—763(L)
Polarization correlation of Nd^{144} γ cascade, Donald M. Roberts—497(A)
Preferred ratios of energies of excited states of nuclei, Martin G. Redlich—328
Of Ra^{227}, J. P. Butler and J. S. Adam—1219
RaD and RaE radiations, C. S. Wu, F. Boehm, and E. Nagel—319
Radiations of neutron-deficient Ba and Ce nuclides, Richard W. Fink and Edwin O. Wiig—194(L)
Rb^{86} and Rb^{86m} radiations, Robert B. Schwartz, M. L. Perlman, and W. Bernstein—883
Re^{186} branching ratio, J. E. Robinson, C. E. Whittle, and P. S. Jastram—498(A)
Re^{188} decay and lifetimes of Os^{180m} and Os^{188m}, C. C. McMullen and M. W. Johns—418(L); Erratum—1580(E)
Reduction of $E1$ matrix element in mixed $E1 + M2$ transition of Sr^{89}, Rolf M. Steffen—443(A)
Sb^{124} decay, conversion coefficients and spectrum shapes, E. P. Tomlinson, S. L. Ridgway, and K. Gopalakrishnan—484(A)
Sb^{124} disintegration, L. M. Langer, N. H. Lazar, and R. J. D. Moffat—338; 485(A)
Sc^{46} decay, branching ratio and γ-ray order, F. H. Schmidt and G. L. Keister—483(A)
Sr^{91} and Y^{91m} disintegration, D. P. Ames, M. E. Bunker, L. M. Langer, and B. M. Sorenson—68
Successive neutron capture in Ta, J. W. Mihelich—427(L)
Th^{230} γ-ray spectrum, F. Rasetti and E. C. Booth—315
Theory of multipole radiation, J. B. French and Y. Shimamoto—898
U^{240} and Np^{240} radiations, J. D. Knight, M. E. Bunker, B. Warren, and J. W. Starner—889
W^{185} disintegration, N. Lazar, R. J. D. Moffat, and L. M. Langer—498(A)
Zr^{89} radiations, F. J. Shore, W. L. Bendel, H. N. Brown, and R. A. Becker—1204
Zr^{95} radiations, Phillip S. Mittelman—484

Nuclear Structure Theory (see also **Nuclear Reactions; Nuclear Spectra**)
Application of jj-coupling model to moderately light nuclei, Dieter Kurath—1430
Calculation of nuclear binding energies with single-particle oscillator wave functions, erratum, Erwin H. Kronheimer—1580(E)
Classical neutron model, Arthur E. Ruark—227(A)
Collective modes of motion in nuclei, F. Villars—443(A)
Contributions to hyperfine spectrum of He^3 resulting from nuclear structure, A. M. Sessler and H. M. Foley—444(A)

Dipole photonuclear reactions and independent particle model, James L. Burkhardt—420(L)
Discontinuities in nuclear mass surface, Alex E. S. Green and David F. Edwards—46; 443(A)
Effect of nuclear structure of hfs of He^3, Vernon Hughes and Gabriel Weinreich—196(L)
Energy levels of odd-odd nuclei, A. de-Shalit—1479
Evidence concerning spin-orbit forces from β decay, I. Talmi and E. P. Wigner—443(A)
Evidence for region of extra nuclear stability between 82- and 126-neutron shells, Benjamin G. Hogg and Henry E. Duckworth—1289(L)
Fast-neutron cross sections and nuclear level density, D. J. Hughes, R. C. Garth, and J. S. Levin—1423
Ground state of deuteron with tensor forces, J. M. Blatt and M. H. Kalos—444(A); M. H. Kalos and J. M. Blatt—444(A)
Ground state of odd-odd nuclei, A. de-Shalit—443(A)
Hard-core interpretation of reaction $p + d \rightarrow \pi^+ + t$, Sidney Bludman—487(A)
Isotope shift anomalies and nuclear structure, Lawrence Wilets, David L. Hill, and Kenneth W. Ford—1488
j-j coupling for $A \lesssim 50$, D. C. Peaslee—443(A)
Magic numbers and statistical model of nucleus, H. W. Newson and E. Merzbacher—241(A)
Magnetic moment deviations from Schmidt limits via admixed states, A. B. Volkov—444(A)
Many-body forces and nuclear saturation, S. D. Drell, K. Huang, and V. F. Weisskopf—460(A); S. D. Drell and K. Huang—1527
Many-nucleon forces, Gregor Wentzel—1573(L)
Mass surfaces, Alex E. S. Green and Nicholas A. Engler—40
Matrix elements of β decay in jj coupling, Igal Talmi—122
Nuclear forces from extended sources, E. M. Henley and M. A. Ruderman—480(A)
Nuclear shell structure as many-body phenomenon, Ingram Bloch and Yü-Chang Hsieh—240(A)
$1/W$ terms in allowed β spectra, J. P. Davidson and D. C. Peaslee—442(A)
Pairing effect in nuclei and isomerism, Robert Katz—1487
Pauli form of β-decay matrix elements, R. F. Herbst and A. V. Bushkovitch—442(A)
Polarizability of the deuteron, N. F. Ramsey, B. J. Malenka, and U. E. Kruse—1162
Repulsive core and charge independence, E. E. Salpeter—994
Role of nucleon isobar in high-energy interactions, Bernard T. Feld—454(A)
Saturation of nuclear forces, Robert Jastrow—460(A)
Spin and magnetic moment of Li^6 nucleus, G. E. Tauber and Ta-You Wu—443(A)
Spin-orbit coupling in pseudoscalar meson theory, Lawrence Dresner—201(L)

Optical Instruments (see **Methods and Instruments**)
Optical Properties (see also **Luminescence**)
Absorption of infrared light by free carriers in Ge, H. B. Briggs and R. C. Fletcher—1342
Absorption of light by trapped electrons, R. C. O'Rourke—265
Band width of F centers in KBr, I. L. Mador, J. J. Markham, and R. T. Platt, Jr.—219(A); 1277(L)
Bleaching of CaF_2 crystals colored by x-rays, Alexander Smakula—1570(L)
Bleaching properties of F centers in KBr at 5°K, J. J. Markham, R. T. Platt, Jr., and I. L. Mador—219(A)
Change of optical constants of fresh thin Cu and Ag films on exposure to air, H. Y. Loh and Peter Cheo—221(A)
Electron distributions for opacity calculations, Malcolm K. Brachman and Roland E. Meyerott—437(A)
Faraday effect in metals at microwave frequencies, Leo M. Silber and Foster F. Rieke—434(A)
Infrared absorption in n-type Ge, R. J. Collins and H. Y. Fan—230(A)
Infrared absorption in p-type Ge, W. Kaiser, R. J. Collins, and H. Y. Fan—230(A); 1380
Of InSb, M. Tanenbaum and H. B. Briggs—1561(L)
Optical studies of injected carriers. I. Infrared absorption in Ge, Roger Newman—1311; II. Recombination radiation in Ge, Roger Newman—1313
Production of F', M, and R centers in NaCl at room temperature, R. T. Platt, Jr., I. L. Mador, and J. J. Markham—219(A)
Reversible bleaching of absorption band of diamond, Peter Pringsheim—220(A); 551
Sharp shadows as "images", Scott E. Barr—226(A)
Z centers in alkali halides, D. R. Westervelt—218(A)

Pair Production (see **Electrons and Positrons**)
Phosphors and Phosphorescence (see **Luminescence**)
Photoconductivity (see **Electrical Conductivity and Resistance**)
Photodisintegration (see **Nuclear Photoeffects**)
Photoelasticity (see **Elasticity and Plasticity**)
Photoelectric Effect (see **Electrical Properties**)
Photography and Photographic Emulsions (see **Methods and Instruments**)
Photometry (see **Methods and Instruments**)
Photons (see **Radiation**)
Photovoltaic Effect (see **Electrical Properties**)
Piezoelectric Effect (see **Dielectrics and Dielectric Properties**)
Polymers (see **Molecular Aggregates**)
Positrons (see **Electrons and Positrons**)
Probability (see **Mathematical Methods**)
Proceedings of the American Physical Society
North Carolina Meeting, Durham and Chapel Hill, North Carolina, March 26–28, 1953 [Bull. Am. Phys. Soc. **28**, No. 2 (1953)]—203
Washington Meeting, Washington, D. C., April 30, May 1–2, 1953 [Bull. Am. Phys. Soc. **28**, No. 3 (1953)]—429
Division of Fluid Dynamics Meeting, State College, Pennsylvania, July 1–3, 1953—1029
Protons (see **Elementary Particle Interactions**)

Quantum Electrodynamics (see also **Field Theory**)
Angular distribution of mesons from 320-Mev photons on protons, Y. Clermont-Goldschmidt, L. S. Osborne, and A. W. Winston—468(A)
Bremsstrahlung at high energies, H. A. Bethe, L. Maximon, and F. Low—417(L)
Deficiency of phenomenological theory of Lamb shift, Frederik J. Belinfante—1285(L)
Fourth-order radiative corrections to atomic energy levels, J. Weneser, R. Bersohn, and N. M. Kroll—1257
Fredholm theory of S matrix, J. Hamilton—1524
Green's functions in S-matrix theory, James L. Anderson—479(A)
Interaction between classical electron and quantized electromagnetic field, I. R. Senitzky—1309
Mass renormalization with Tamm-Dancoff method, F. J. Dyson—421(L)
Number of Feynman diagrams, R. J. Riddell, Jr.—461(A); 1243
Poles of S matrix for resonance reactions, Marcos Moshinsky—984
Quantum electrodynamics in space of constant curvature, Martin Gutzwiller—478(A)

Quantum Electrodynamics (Continued)
Relativistic contributions to magnetic moment of n-electron atoms, William Perl—852
Relativistic contributions to magnetic moment of $^3S_1$ He, William Perl and Vernon Hughes—842
S matrix and causality condition. II. Nonrelativistic particles, N. G. van Kampen—1267
True vacuum and dressed particles in quantum field theory, Bruno Zumino—478(A)
Quantum Mechanics
Approximate two-body relativistic wave equations, Z. V. Chraplyvy—478(A)
Causal interpretation of quantum mechanics, Saul T. Epstein—985
Eigenfunctions of S^2 by spin-operator method, G. W. Pratt, Jr.—212(A)
Electromagnetic mass in Darling's theory of elementary particles, Hans Freistadt—478(A)
Generalized canonical ensemble in quantum mechanics, Peter G. Bergman—477(A)
Generalized self-consistent field method, J. C. Slater—528
Interpretation and generalization of Dirac's theory of electron, Walter Wessel and S. J. Czyzak—986
New form for statistical postulate of quantum mechanics, Norbert Wiener and Armand Siegel—1551
Power-series expansion of unitary operator $U(t,t_0)$, S. T. Ma—392
Reduction of relativistic two-particle wave equations to approximate forms, Zeno V. Chraplyvy—388
Relativistic two-body equation, Behram Kurşunoğlu—478(A)
Similarity theory of relativity and Dirac-Schrödinger theory of electrons, Banesh Hoffman—751
Theory of finite displacement operators and fundamental length, B. T. Darling and P. R. Zilsel—1252
Wave function of relativistic system, F. J. Dyson—1543
WKB-type approximation to Schrödinger equation, S. C. Miller, Jr., and R. H. Good, Jr.—174
Quenching of Radiation (see **Radiation**)

Radar (see **Methods and Instruments; Radiation**)
Radiation
Approximate solution of Heitler's integral equation, S. N. Biswas—1026(L)
Bremsstrahlung at high energies, H. A. Bethe, L. Maximon, and F. Low—417(L)
Bremsstrahlung from P^{32} betas, M. Goodrich, J. S. Levinger, and W. Payne—455(A); 1225
Compton scattering on nucleons, R. H. Huddlestone—461(A)
Contribution of 14-micron CO_2 band to earth's radiation balance, Gilbert N. Plass—458(A)
Degradation of Co^{60} γ rays in infinite water medium, M. M. Weiss and W. Bernstein—483(A)
Electromagnetic absorptivity of metals at low temperatures, T. Holstein—490(A)
Energy loss of fast charged particle by Čerenkov radiation, R. M. Sternheimer—256
Far uv radiation from Cornell synchrotron, P. L. Hartman and D. H. Tomboulian—1577(L)
Infrared absorption in p-type Ge, W. Kaiser, R. J. Collins, and H. Y. Fan—230(A); 1380; R. J. Collins and H. Y. Fan—230(A)
Inner bremsstrahlung and magnetic moment of neutrino, J. Weneser—1025(L)
Photoionization of molecules in vacuum uv, Edward C. Y. Inn—1194
Photoionization of NO, K. Watanabe, Frederick Marmo, and Edward C. Y. Inn—436(A); 1155
Polarization of Na atoms, W. B. Hawkins and R. H. Dicke—1008(L)
Polarization of three-photon annihilation radiation, L. Leipuner, R. Siegel, and S. DeBenedetti—198(L)
Production of sodium airglow excitation by imprisonment of resonance radiation, A. Foderaro and T. M. Donahue—1561(L)
Propagation of short radio waves well beyond the horizon, Thomas J. Carroll—458
Theory of penetration of γ rays through thin barriers, John P. Vinti—345
Versatile radiation oven, Richard B. Belser—246(A)
Radio Waves (see **Radiation**)
Radioactivity (see also **Nuclear Spectra**)
α decay, theory, Joseph J. Devaney—587
Average charge on daughter atoms produced in decay of A^{37} and Xe^{131m}, M. L. Perlman and J. A. Miskel—899
Chemical separation of 0.82-sec Pb^{207m} from Bi^{207}, E. C. Campbell and F. Nelson—499(A)
Co^{60} half-life, J. Kastner and G. N. Whyte—332
Effects of primeval endowment of U^{238}, David B. Rosenblatt—1474
$Eu^{147-150}$, Rex C. Mack, J. J. Neuer, and M. L. Pool—497(A)
Eu^{150} and Gd^{150}, Rex C. Mack, J. J. Neuer, and M. L. Pool—903
Ga^{64}, Bernard L. Cohen—74
Genetic relationships of 0.8-sec Pb^{207m} isomer, G. Friedlander, Elizabeth Wilson, A. Ghiorso, and I. Perlman—498(A)
K^{40} branching ratio, R. D. Russell, H. A. Shillibeer, R. M. Farquhar, and A. K. Mousuf—1223
K^{42} decay, Bernd Kahn and W. S. Lyon—1212
Method for determination of maximum energy of weak β emitters, M. Forro—483(A)
Mg^{28} decay, A. H. Wapstra and A. L. Veenendaal—426
New nuclides produced in Cl spallation, Manfred Lindner—642
P^{32} and Ag^{111} β rays, average energy, J. M. Brabant, L. W. Cochran, and R. S. Caswell—210(A)
Radiation damage and rate processes, J. W. Marx—1564(L)
Radiations of Ra^{227}, J. P. Butler and J. S. Adam—1219
Radioactive charging through dielectric medium, E. G. Linder and P. Rappaport—202(L); erratum—1580(E)
Radioisotope production in ORNL 86-in. cyclotron, J. A. Martin—224(A)
Re^{186} branching ratio, J. E. Robinson, C. E. Whittle, and P. S. Jastram—498(A)
Re^{188} decay and lifetimes of $Os^{188(n)}$ and $Os^{188(m)}$, C. C. McMullen and M. W. Johns—418(L); 1580(E)
Sc^{46} decay, branching ratio and γ-ray order, F. H. Schmidt and G. L. Keister—483(A)
Study with NaI scintillation spectrometer of methods of estimating I^{131} contained in human thyroid, Robert J. Kerr, Sherwood K. Haynes, and George R. Meneely—214(A)
Tl^{204} half-life, Garman Harbottle—1234
Upper limit on fraction of positive particles emanating from two emitters, G. W. McClure—483(A)
Raman Spectra (see **Molecular Structure and Spectra**)
Range and Energy Loss of Particles (see also **Scattering**)
α-particle straggling in thin foils, P. T. Porter and J. I. Hopkins—209(A)
Cluster-count determination of specific ionization of cloud-chamber tracks, Hans O. Cohn, L. R. Etter, and R. W. Thompson—445(A)
Effect of capture on slowing-down length of neutrons in hydrogenous mixtures, Howard C. Volkin—425(L)

Energy loss of fast charged particle by Čerenkov radiation, R. M. Sternheimer—256
Energy loss of H, He, N, and Ne ions in gases, Peter K. Weyl—289
Energy spectrum resulting from electron slowing-down, U. Fano and L. V. Spencer—240(A)
Grain density in tracks of 117- and 222-Mev π^- mesons in emulsions, A. H. Morrish—423(L)
Ionization energy losses of relativistic μ mesons in gases, J. E. Kupperian, Jr., and E. D. Palmatier—1186
Moderation of Ra-Be neutrons in limestone, J. Tittman and F. F. Johnson—452(A)
Range-energy relation of N ions in emulsion, H. L. Reynolds and A. Zucker—496(A)
Range-energy relations of 10–250-kev protons and He ions in various gases, Charles J. Cook, Emerson Jones, Jr., and Theodore Jorgensen, Jr.—1417
Relativistic rise in ionization loss in nuclear emulsions, Bertram Stiller and Maurice M. Shapiro—496(A)
Specific probable ionization of electrons observed with Wilson cloud chamber, Robert H. Frost and Carl E. Nielsen—864
Stopping cross section of gases for protons and deuterons, D. N. F. Dunbar, H. K. Reynolds, W. A. Wenzel, and W. Whaling—496(A)
Stopping power of several elements for protons, A. B. Chilton, J. N. Cooper, and J. C. Harris—495(A)
Stopping powers of thin compound foils, John Phelps, W. F. Huebner, and Franklin Hutchinson—496(A)
Straggling distributions for electrons in passing through thin foils, F. Kalil and R. D. Birkhoff—505
Thermalization of positrons in metals, R. L. Garwin—1571(L)

Recombination (see **Molecular Structure and Spectra**)

Rectifiers (see **Electrical Conductivity and Resistance; Semiconductors**)

Relativity and Gravitation

Approximate two-body relativistic wave equations, Z. V. Chraplyvy—478(A)
Relativistic two-body equation, Behram Kurşunoğlu—478(A)
Rigid motion in special relativity, G. Salzman and A. H. Taub—477(A)
Similarity theory of relativity and Dirac-Schrödinger theory of electrons, Banesh Hoffmann—751
Special-relativistic linear theory of gravitation, J. C. Swihart and F. J. Belinfante—500(A)

Resistance, Electrical (see **Electrical Conductivity and Resistance**)

Resonance Radiation (see **Radiation**)

Scattering, General (see also **Diffraction; Nuclear Reactions; Range and Energy Loss of Particles**)

Approximate solution of Heitler's integral equation, S. N. Biswas—1026(L)
Causality condition and S matrix for nonrelativistic particles, N. G. van Kampen—459(A)
Elastic scattering of particles by atomic nuclei, Norman C. Francis and Kenneth M. Watson—454(A)
Energy exchange in molecular collisions, B. Widom and S. H. Bauer—240(A)
Exchange scattering in three-body problem, Harry E. Moses—185
Excitation of molecular rotations and vibrations in inelastic scattering processes, Edward H. Kerner—1174
Formal theory of scattering, M. Gell-Mann and M. L. Goldberger—398
New method for calculation of nuclear phase shifts from cross-section measurements, Harry Lustig and John M. Blatt—453(A)
Nuclear forces from extended sources, E. M. Henley and M. A. Ruderman—480(A)
Potential scattering at high energies, Roy J. Glauber—459(A)
Scattering approximations for transparent nucleus model, J. Mayo Greenberg—454(A)
Three-body scattering problems, A. Dalgarno—198(L)

Scattering of α Particles

α-α scattering at 21.6, 22.4, and 22.8 Mev (nuclear plate), R. O. Kerman, R. Nilson, and W. K. Jentschke—438(A)
α-α scattering at 21.8 and 22.9 Mev (proportional counter), G. R. Briggs, S. Singer, and W. K. Jentschke—438(A)
α-particle scattering in N, N. P. Heydenburg and G. M. Temmer—439(A)
Energy dependence of differential elastic scattering cross section of α particles in He, F. E. Steigert and M. B. Sampson—439(A)

Scattering of Atoms and Molecules (see **Atomic and Molecular Beams**)

Scattering of Deuterons

Differential cross sections for elastic scattering of 1.0- to 3.25-Mev deuterons by He^3, R. J. S. Brown, K. F. Famularo, H. D. Holmgren, and D. M. Van Patter—438(A)
Elastic scattering of particles by atomic nuclei, Norman C. Francis and Kenneth M. Watson—454(A)
Electric scattering of polarizable deuteron, B. J. Malenka, U. E. Kruse, and N. F. Ramsey—1165
Polarizability of the deuteron, N. F. Ramsey, B. J. Malenka, and U. E. Kruse—1162

Scattering of Electrons and Positrons

Calculation of approximate cross sections for electron scattering, William J. Byatt—240(A)
Complex amplitudes for electron scattering by atoms, Jean A. Hoerni and James A. Ibers—1182
Deflection of high-energy electrons in magnetized Fe, Stephan Berko and Frank L. Hereford—1127
Elastic scattering of 1.7-Mev electrons, D. J. Anthony, B. Waldman, and W. C. Miller—439(A)
Electron scattering from nuclei at high energies, R. Hofstadter, H. R. Fechter, and J. A. McIntyre—439(A)
Energy spectrum resulting from electron slowing-down, U. Fano and L. V. Spencer—240(A)
Exchange scattering of electron by H atom, Saul Altshuler—1167
Scattering of high-energy electrons and method of nuclear recoil, R. Hofstadter, H. R. Fechter, and J. A. McIntyre—422(L)
Spin-relativistic effects in multiple scattering of electrons, L. V. Spencer and C. H. Blanchard—240(A)
Straggling distributions for electrons in passing through thin foils, F. Kalil and R. D. Birkhoff—505

Scattering of Mesons (see also **Mesons; Nuclear Reactions Induced by Mesons**)

Angular distribution of pions scattered by H, H. L. Anderson, E. Fermi, R. Martin, and D. E. Nagle—155
Classical scattering of neutral mesons, Clarence R. Mehl and Peter Havas—392
Differential cross sections for scattering of 48-Mev π^+ mesons in H, D. Bodansky, A. Sachs, and J. Steinberger—467(A)
Elastic scattering in nuclear emulsions, A. E. Clark, R. A. Grandey, S. K. Kao, and L. Mann—467(A)
Graphical method for obtaining phase shifts from experimental data on meson-nucleon scattering, Julius Ashkin and Seymour H. Voskó—1248
Inelastic scattering of negative pions, Gerson Goldhaber and S. Goldhaber—467(A)

Scattering of Mesons (Continued)
Ionization energy losses of relativistic μ mesons in gases, J. E. Kupperian, Jr., and E. D. Palmatier—1186
Large-angle scattering of π^- mesons in Al, Cu, and Pb, Harry H. Heckman and L. Evan Bailey—1237
Nucleon polarization in pion-proton scattering, Enrico Fermi—947
Phenomenological study of meson-nucleon scattering, S. Gasiorowicz—481(A)
Scattering and absorption of π^+ mesons by Al, James F. Tracy—960
Scattering of 40-Mev positive pions by H, J. P. Perry and C. E. Angell—1289(L)
Scattering of 43-Mev positive pions by H, A. B. Weaver, J. J. Lord, and J. Orear—466(A)
Scattering of 120-Mev negative pions by H, Jay Orear—467(A)
Scattering of 169- and 192-Mev pions by H, R. L. Martin, E. Fermi, and D. E. Nagle—467(A)
210-Mev negative pion interactions, A. H. Morrish—468(A)

Scattering of Neutrons
Angular distributions of elastically scattered 1-Mev neutrons, M. Walt and H. H. Barschall—441(A)
Angular distribution of neutrons scattered from N, J. L. Fowler, C. H. Johnson, and J. R. Risser—441(A)
Coherent cross sections of Fe and Ni, M. D. Goldberg and J. A. Harvey—451(A)
Effect of capture on slowing-down length of neutrons in hydrogenous mixtures, Howard C. Volkin—425(L)
Elastic scattering of protons and neutrons by deuterons, R. S. Christian and J. L. Gammel—100
γ radiation from inelastic scattering of 2.7-Mev neutrons, V. E. Scherrer, W. L. Smith, B. A. Allison, and W. R. Faust—768(L)
Inelastic scattering of alphas from N^{14}, B. M. Carmichael, M. B. Sampson, and O. E. Johnson—473(A)
Inelastic scattering of d-d neutrons, R. E. Garrett, F. L. Hereford, and B. W. Sloope—441(A)
Inelastic scattering of thermal neutrons in Pb, Andrew W. McReynolds—1368
Low-energy neutron resonance scattering, H. L. Foote, Jr.—450(A)
Measurement of resonant neutron scattering cross sections, C. Sheer, J. Moore, and C. Heindl—449(A)
Moderation of Ra-Be neutrons in limestone, J. Tittman and F. F. Johnson—452(A)
n-p scattering, Earle Lomon and Herman Feshbach—454(A)
Neutron diffraction by liquid He, D. G. Henshaw and D. G. Hurst—1222; By liquid O_2, N_2, and A, D. G. Henshaw, D. G. Hurst, and N. K. Pope—472(A)
Scattering of 14–18-Mev neutrons in light elements, C. F. Cook and T. W. Bonner—441(A)
Second-order scattering correction in neutron and x-ray diffraction, George H. Vineyard—239(A)
Slow neutron scattering cross sections for rare earth nuclides, W. C. Koehler and E. O. Wollan—597
Transmission of slow neutrons by liquid He, L. Goldstein, H. S. Sommers, Jr., and J. G. Dash—490(A)

Scattering of Protons
Double scattering of high-energy protons by H and C, C. L. Oxley, W. F. Cartwright, J. Rouvina, E. Baskir, D. Klein, J. Ring, and W. Skillman—419(L)
Effect of $^3P_2-{}^3F_2$ coupling on p-p scattering, R. M. Thaler, J. Bengston, and G. Breit—454(A)
Elastic scattering in nuclear emulsions, A. E. Clark, R. A. Grandey, S. K. Kao, and L. Mann—467(A)
Elastic scattering of protons by Li, W. D. Warters, W. A. Fowler, and C. C. Lauritsen—917
Elastic scattering of protons by Ne, W. Haeberli, A. Galonsky, E. Goldberg, and R. Douglas—438(A)
Elastic scattering of protons by nuclei, F. Rohrlich and D. M. Chase—454(A)
Elastic scattering of protons by O^{16}, J. E. Eppling, J. R. Cameron, R. H. Davis, Ajay S. Divatia, A. I. Galonsky, E. Goldberg, and R. W. Hill—438(A)
Elastic scattering of protons and neutrons by deuterons, R. S. Christian and J. L. Gammel—100
Equilibrium proton charge ratios from charge exchange in various materials, J. A. Phillips—455(A)
Half-widths of one-body resonances, John L. Johnson and J. L. McHale—87
Inelastic scattering of 18.3-Mev protons, P. C. Gugelot and H. A. Lauter—486(A)
Inelastic scattering of protons by Ne, A. Galonsky, W. Haeberli, E. Goldberg, and R. Douglas—439(A)
Inelastic scattering of protons from Ca^{40}, C. M. Braams, C. K. Bockelman, C. P. Browne, and W. W. Buechner—474(A)
New method for calculation of nuclear phase-shifts from cross-section measurements, Harry Lustig and John M. Blatt—453(A)
Phase-shift analysis of high-energy p-p scattering, J. Bengston and R. M. Thaler—454(A)
Range-energy relations of 10–250-kev protons and He ions in various gases, Charles J. Cook, Emerson Jones, Jr., and Theodore Jorgensen, Jr.—1417
Resonances in $S^{32}(p,p)S^{32}$, A. J. Ferguson and H. E. Gove—439(A)

Scattering of Radiation (see **Radiation; X-Rays**)
Scintillation Counters (see **Methods and Instruments**)
Secondary Emission (see **Electrical Properties**)
Semiconductors
Absorption of infrared light by free carriers in Ge, H. B. Briggs and R. C. Fletcher—1342
Acceptor states of Au in Ge, W. C. Dunlap, Jr.—208(A)
Broadening of impurity levels in Si, M. Lax and E. Burstein—208(A)
Carrier contribution to dielectric constant of Ge, T. S. Benedict and W. Shockley—207(A)
Carrier traps in Ge at low temperatures, D. Navon and H. Y. Fan—491(A)
Current carrier lifetimes deduced from Hall coefficient and resistivity measurements, E. J. Huibregtse and L. P. Hunter—208(A); L. P. Hunter, E. J. Huibregtse, and R. L. Anderson—1315
Current carrier mobility ratio in semiconductors, L. P. Hunter—207(A); 579
Deuteron irradiation of Ge near liquid N temperature, J. H. Forster, H. Y. Fan, and K. Lark-Horovitz—229(A)
Diffusion currents in Hall effect in semiconductors, Rolf Landauer and John Swanson—207(A); 555
Diffusion of Li into Ge and Si, C. S. Fuller and J. A. Ditzenberger—193(L)
Dislocations in low-angle boundaries in Ge single crystals, F. L. Vogel, W. G. Pfann, H. E. Corey, and E. E. Thomas—230(A)
Effect of transit time on Ge rectifier behavior, R. Bray and B. R. Gossick—1011(L)
Electrical conduction and thermoelectric power in thorium oxide crystals, O. A. Weinreich and W. E. Danforth—231(A)
Electrical conductivity of mechanically disturbed Ge surfaces, Edward N. Clarke and Robert L. Hopkins—1566(L)
Electrical properties of AlSb, R. K. Willardson, A. C. Beer, and A. E. Middleton—243(A)

Electrical properties of Au-Ge alloys, W. C. Dunlap, Jr. —1282(L)
Electrical properties of elementary B, L. W. Friedrich and V. P. Jacobsmeyer—492(A)
Electrical properties of InSb, R. G. Breckenridge, W. R. Hosler, and W. Oshinsky—243(A)
Electrical properties of *n*-type Ge, Esther M. Conwell—208(A)
Electron multiplication in Si and Ge, K. G. McKay and K. B. McAfee—1079
Energy band structure of diamond and Ge crystals, Frank Herman—491(A)
Evaporation of Cu from Ge, George Finn—754(L)
Experiment with transistors for elementary laboratory course, F. H. Mitchell—227(A)
Experimental confirmation of relation between pulse drift mobility and charge carrier drift mobility in Ge, M. B. Prince—271
Ge films, W. M. Becker and K. Lark-Horovitz—230(A)
Hall effect and conductivity of Ge containing As or Ga as impurities, Peter P. Debye—208(A)
Hall effect and conductivity of InSb single crystals, M. Tanenbaum and J. P. Maita—1009(L)
Infrared absorption in *n*-type Ge, R. J. Collins and H. Y. Fan—230(A)
Infrared absorption in *p*-type Ge, W. Kaiser, R. J. Collins, and H. Y. Fan—230(A)
Lattice absorption in diamond: one-dimensional model, Melvin Lax and Eli Burstein—492(A)
Lifetime of minority carriers in localized crystal regions, M. Becker, M. Cutler, T. Firle, R. Shulman, and W. Spitzer—491(A)
Low-temperature "breakdown" effect in Ge, N. Sclar, E. Burstein, W. J. Turner, and J. W. Davisson—215(A)
Magnetoresistance in InSb, M. Tanenbaum and G. L. Pearson—244(A)
Microwave observation of collision frequency of holes in Ge, T. S. Benedict—1565(L)
Mobilities of carriers in crystalline B, William C. Shaw, D. E. Hudson, and G. C. Danielson—208(A)
n-type surface conductivity on *p*-type Ge, W. L. Brown —518
Noise in *p-n* junction rectifiers and transistors, I. Theory, Richard L. Petritz—231(A); II. Experiment, Francis L. Lummis and Richard L. Petritz—231(A)
Nonlinear semiconductor resistors, F. A. Schwertz and J. J. Mazenko—491(A)
Optical properties of InSb, M. Tanenbaum and H. B. Briggs—1561(L)
Optical studies of injected carriers. I. Infrared absorption in Ge, Roger Newman—1311; II. Recombination radiation in Ge, Roger Newman—1313
Oxygen-induced surface conductivity on Ge, Edward N. Clarke—756(L)
Photoconductivity and carrier traps in Ge, H. A. Gebbie, M. Nisenoff, and H. Y. Fan—230(A)
Piezoresistance effect in Ge, Charles S. Smith and J. R. Haynes—491(A)
Possible mechanism for $1/f$ noise generation in semiconductor filaments, Leon Bess—1569(L)
Post-injection barrier emf of *p-n* junctions, B. R. Gossick 1012(L)
Preparation of junctions in single crystals by surface melting, K. Lehovec and E. Belmont—492(A)
Radiationless trapping of charge carriers in solids, Gregory H. Wannier—207(A)
Recording of temperature dependent electrical properties of semiconductors, Luther Davis, Jr., Lawrence Rubin, and W. D. Straub—490(A)
Surface tension of liquid Si and Ge, Paul H. Keck—243(A); 512
Temperature variation of drift mobilities of minority carriers in semiconductors, M. B. Prince—208(A)
Theory of thermoelectric power in semiconductors, V. A. Johnson and K. Lark-Horovitz—230(A)
Thermal acceptors in vacuum heat-treated Ge, S. Mayburg and L. Rotondi—1015(L)
Thermally-induced acceptors in single crystal Ge, R. A. Logan—757(L)
Thermally unstable disorder in *p*-type Ge produced by fast neutron bombardment, J. H. Crawford, Jr., J. W. Cleland, D. K. Holmes, and J. C. Pigg—243(A)
Thermoelectric power in Ge single crystals, H. P. R. Frederikse—491(A)
Thick *p-n* junctions in Ge, Ralph Bray and F. van der Maesen—231(A)
Transport of added current carriers in homogeneous semiconductor, W. van Roosbroeck—282

Shock Waves (see **Fluid Dynamics**)
Solid State (see **Crystalline State**)
Solutions (see **Liquids**)
Sound (see **Acoustics**)
Spallation (see **Nuclear Reactions**)
Spark Discharge (see **Electrical Discharges**)
Specific Heat (see **Thermal Properties**)
Spectra, Atomic (see **Atomic Structure and Spectra**)
Spectra, General

New detector for infrared, S. Mrozowski, B. D. McMichael, and E. A. Kmetko—234(A)
Stark shift and broadening due to electrons, M. Baranger —436(A)

Spectra, Molecular (see **Molecular Structure and Spectra**)
Spectra, Nuclear (see **Nuclear Spectra**)
Spectroscopy Technique (see **Methods and Instruments**)
Spinor Fields (see **Field Theory**)
Standards (see **Constants, Standards, Units**)
Stark Effect (see **Atomic Structure and Spectra**)
Statistical Mechanics and Thermodynamics

Atomic theory of λ transition in He, R. P. Feynman—1291
Atomic theory of liquid He near 0°K, R. P. Feynman—1301
Bose-Einstein condensation of imperfect gas, M. H. Friedman and S. T. Butler—465(A)
Equipartition principle of generalized canonical ensembles, Harry L. Frisch—477(A); 791
Fluctuations and irreversible processes, L. Onsager and S. Machlup—1505; II. Systems with kinetic energy, S. Machlup and L. Onsager—1512
Generalized canonical ensemble in quantum mechanics, Peter G. Bergmann—477(A)
Generalized statistical mechanics and Onsager relations, Peter G. Bergmann and Alice C. Thomson—180
Logical relations among principles of statistical mechanics and thermodynamics, John S. Thomsen—477(A); 1263
Modified random walk problems, M. Dresden and Donald Drawbaugh—478(A)
Quantum statistical mechanics of ferromagnetism, Ryoichi Kikuchi—205(A)
Radiation effects and rotational-translational relaxation time constant, Philip M. Mostov and Sidney Borowitz —465(A)
Relation between time averages and ensemble averages in statistical dynamics of continuous media, Carl Eckart —784
Second law of eddy thermodynamics, A. K. Blackadar—1031(A)
Thermodynamic activities in Fe-Ni alloys, R. A. Oriani —465(A)

Statistical Mechanics and Thermodynamics (Continued)
Vapor-liquid transitions in closed system, Charles Willis and Harry L. Frisch—465(A)
Statistical Methods (see **Mathematical Methods**)
Superconductivity
Adiabatic magnetization of superconducting sphere, R. L. Dolecek—216(A); 490(A)
Heat capacities of superconducting and normal Ta, R. D. Worley, M. W. Zemansky, and H. A. Boorse—1567(L)
Method for measuring magnetic moments of superconductors, Ted. G. Berlincourt and M. C. Steele—215(A)
New thermal resistivity maximum in superconducting alloys, Ronald J. Sladek—1280(L)
Penetration depth of superconductors, M. C. Steele and M. F. M. Osborne—1281(L)
Pressure effects on superconducting transition temperatures, theory, Paul M. Marcus—216(A)
Search for Hall effect in superconductor, H. W. Lewis—216(A)
Superconducting compounds, B. T. Matthias—413(L)
Superconducting transition in Al, D. E. Mapother and J. F. Cochran—216(A)
Thermal resistivity of superconducting Hg in intermediate state, R. T. Webber and D. A. Spohr—414(L)
Of Ti, M. C. Steele and R. A. Hein—490(A)
Two-fluid models of superconductivity with application to isotope effects, Paul M. Marcus and E. Maxwell—1035
Velocity of sound in superconducting Pb and Sn, H. Bömmel and J. L. Olsen—1017(L)
Supersonics (see **Fluid Dynamics**)

Thermal Conductivity (see **Thermal Properties**)
Thermal Diffusion (see **Diffusion**)
Thermal Expansion (see **Thermal Properties**)
Thermal Properties
Anomaly in heat content of metal in fatigued state, B. Welber and R. Webeler—448(A)
Atomic heat of Ge below 4°K, P. H. Keesom and N. Pearlman—215(A); 1347
Changes in electrical, thermal, and thermoelectrical properties of monovalent metals by lattice distortions, A. W. Sáenz—1142
Dilatometric study of order-disorder transformation in Cu-Au alloys, W. W. Sanville, Foster C. Nix, and Frank E. Jaumot, Jr.—220(A)
Electronic and lattice specific heats in W, Mo, and Re, M. Horowitz and J. G. Daunt—1099
Heat capacities of superconducting and normal Ta, R. D. Worley, M. W. Zemansky, and H. A. Boorse—1567(L)
Heat capacity of KCl below 4°K, P. H. Keesom and N. Pearlman—1354
Heat transfer of hemispherical body in supersonic flow, Irving Korobkin—469(A)
Mass spectrometric study of sublimation of graphite, Richard E. Honig—465(A)
New thermal resistivity maximum in superconducting alloys, Ronald J. Sladek—1280(L)
Specific heat discontinuity in antiferromagnets and ferrites, Louis N. Howard and J. Samuel Smart—17
Thermal and electrical properties and crystal structure of tungsten oxide at high temperatures, Shozo Sawada—1010(L)
Thermal diffusivity of Mg at low temperatures by variable state techniques, S. Waldron and Melvin A. Herlin—447(A)
Thermal resistivity of superconducting Hg in intermediate state, R. T. Webber and D. A. Spohr—414(L)
Thermal Radiation (see **Radiation**)
Thermionic Emission (see **Electrical Properties**)
Thermodynamics (see **Statistical Mechanics and Thermodynamics**)
Thermoelectric Effect (see **Electrical Properties**)
Thermoluminescence (see **Luminescence**)
Thermomagnetic Effect (see **Magnetic Properties**)
Total Cross Sections (see **Electrons and Positrons; Nuclear Reactions**)
Transmutation (see **Nuclear Reactions**)

Uncertainty Principle (see **Quantum Mechanics**)
Units (see **Constants, Standards, Units**)

Vacuum Tubes (see **Methods and Instruments**)
Van der Waals Forces (see **Molecular Structure and Spectra**)
Viscosity (see **Liquids**)

Wave Mechanics (see **Quantum Mechanics**)
Work Function (see **Electrical Properties**)

X-Rays
Absorption of P in neighborhood of $L_{2,3}$ edge, D. H. Tomboulian—457(A)
Antiparallel dipole arrangement in WO_3, Ryuzo Ueda and Jinzo Kobayashi—1562(L)
Auger electron intensities, R. D. Hill—770(L)
Determination of x-ray spectrum from absorption measurements by Laplace transformation, Judith Cassidy Gursky and P. K. S. Wang—239(A)
Direct measurement of nuclear absorption of x-rays, H. W. Koch and R. S. Foote—455(A)
Measurements of K-edge jump ratios with linear motion x-ray spectrometer, H. P. Hanson and H. W. Schrader—457(A)
Production of characteristic x-rays by protons, H. W. Lewis, B. E. Simmons, and E. Merzbacher—943
Response of anthracene crystals to monoenergetic soft x-rays, W. H. Robinson—457(A)
Second-order scattering correction in neutron and x-ray diffraction, George H. Vineyard—239(A)
Small-angle scattering of x-rays from cold-worked crystals, D. L. Dexter—448(A); from He I and He II, A. G. Tweet—488(A); in proton-irradiated diamond, S. Hayes and R. Smoluchowski—244(A)
X-ray absorption fine structure with polarized x-rays, R. Krogstad, W. Nelson, and S. T. Stephenson—457(A)
X-ray study of graphitization, J. C. Bowman, S. Hayes, and R. Smoluchowski—244(A)

CONTENTS

THE PHYSICAL REVIEW SECOND SERIES, VOLUME 91, NO. 6 SEPTEMBER 15, 1953

Atomic Theory of the λ Transition in Helium . . . . . R. P. Feynman 1291
Atomic Theory of Liquid Helium Near Absolute Zero . . . . . R. P. Feynman 1301
Interaction between Classical Electron and Quantized Electromagnetic Field . . . . . I. R. Senitzky 1309
Optical Studies of Injected Carriers. I. Infrared Absorption in Germanium . . . . . Roger Newman 1311
Optical Studies of Injected Carriers. II. Recombination Radiation in Germanium . . . . . Roger Newman 1313
Current Carrier Lifetimes Deduced from Hall Coefficient and Resistivity Measurements . . . . . L. P. Hunter, E. J. Hollerguer, and P. L. Anderson 1315
Brillouin Zone Investigation of Mg Alloys. I. Hall Effect and Conductivity . . . . . A. I. Schindler and E. I. Salkovitz 1320
Two-Electron Example of Paramagnetism . . . . . J. C. Slater, H. Statz, and G. F. Koster 1323
Absorption of Infrared Light by Free Carriers in Germanium . . . . . H. B. Briggs and R. C. Fletcher 1342
Atomic Heat of Germanium below 4°K . . . . . P. H. Keesom and N. Pearlman 1347
Heat Capacity of KCl below 4°K . . . . . P. H. Keesom and N. Pearlman 1354
Fluorescence, Phosphorescence, and Photoconduction of NaCl(AgCl) with High-Energy Excitation . . . . . Milton Forst and Hartmut Kallmann 1356
Inelastic Scattering of Thermal Neutrons in Lead . . . . . Andrew W. McReynolds 1368
Hall Effect in Yttrium, Lanthanum, Cerium, Praseodymium, Neodymium, Gadolinium, Dysprosium, and Erbium . . . . . C. J. Kevane, S. Legvold, and F. H. Spedding 1379
Infrared Absorption in P-Type Germanium . . . . . W. Kaiser, R. J. Collins, and H. Y. Fan 1380
Auger Peaks in the Energy Spectra of Secondary Electrons from Various Materials . . . . . J. J. Lander 1387
Magnetoresistance of Mg, Cu, Sb, and Al at Liquid Helium Temperatures . . . . . G. E. Yntema 1388
Molecular Beam Investigation of Rotational Transitions. I. The Rotational Levels of KCl and Their Hyperfine Structure . . . . . Charles A. Lee, E. P. Fabricand, R. O. Carlson, and I. I. Rabi 1395
Molecular Beam Investigation of Rotational Transitions. II. The Rotational Levels of KBr and Their Hyperfine Structure . . . . . E. P. Fabricand, R. O. Carlson, C. A. Lee, and I. I. Rabi 1398
Self-Consistent Calculation of the Dissociation of Oxygen in the Upper Atmosphere. II. Three-Body Recombinations . . . . . Harry E. Moses and Te-You Wu 1402
Effective Nuclear Charges for Atoms from Self-Consistent Field Calculations . . . . . A. J. Freeman 1410
Range-Energy Relations of 10- to 250-Mev Protons and Helium Ions in Various Gases . . . . . Charles J. Cook, Emerson Jones, Jr., and Theodore Jorgensen, Jr. 1417
Fast Neutron Cross Sections and Nuclear Level Density . . . D. J. Hughes, R. C. Garth, and J. S. Levin 1423
Application of the jj-Coupling Model to Moderately Light Nuclei . . . . . Dieter Kurath 1430
Linear Combination in β Decay . . . . . D. C. Peaslee 1447
Yield of Xe^{135} in the Thermal Neutron Fission of U^{235} . . . . . Seymour Katcoff and William Rubinson 1450
Chlorine Isotope Separation by Thermal Diffusion . . . . . A. Z. Kranz and W. W. Watson 1462
Energy Levels in A^{37} from the $Cl^{37}(\alpha,p)$ Reaction . . . . . A. Z. Kranz and W. W. Watson 1472
Effects of a Primeval Endowment of U^{236} . . . . . David B. Rosenblatt 1474
Gamma Rays from Interaction of 14-Mev Neutrons with Various Materials . . . . . V. E. Scherrer, R. B. Theus, and W. R. Faust 1476
Energy Levels of Odd-Odd Nuclei . . . . . A. de-Shalit 1479
Pairing Effect in Nuclei and Ionization . . . . . Robert Matz 1487
Isotope Shift Anomalies and Nuclear Structure . Lawrence Wilets, David L. Hill, and Kenneth W. Ford 1489
Energy Dependence of the Cross Section for the Reaction $C^{12}(\alpha,\alpha\gamma)C^{12}$. M. Lindner and R. N. Osborne 1501
Excited States of K^{40} . . . . . W. W. Buechner, A. Sperduto, C. P. Browne, and C. K. Rockinson 1502
Fluctuations and Irreversible Processes . . . . . L. Onsager and S. Machlup 1505
Fluctuations and Irreversible Processes. II. Systems with Kinetic Energy . . S. Machlup and L. Onsager 1512
Properties of the Salpeter-Bethe Two-Nucleon Equation . . . . . Jack S. Goldstein 1516
Predictive Theory of the S Matrix . . . . . J. Hamilton 1524
Many-Body Forces and Nuclear Saturation . . . . . S. D. Drell and Kerson Huang 1532
Wave Function of a Relativistic System* . . . . . F. J. Dyson 1543
New Form for the Statistical Postulate of Quantum Mechanics . . Norbert Wiener and Armand Siegel 1551

(continued on cover three)

LANCASTER PRESS, INC., LANCASTER, PA.